Handbook on the Physics and Chemistry of Rare Earths volume 4

Non-Metallic Compounds – II

Edited by: Karl A. Gschneidner, Jr. and LeRoy Eyring
ISBN: 978-0-444-85216-8

North Holland Publishing Company (1979)

PREFACE

Karl A. GSCHNEIDNER, Jr., and LeRoy EYRING

These elements perplex us in our rearches [sic], *baffle us in our speculations, and haunt us in our very dreams. They stretch like an unknown sea before us – mocking, mystifying, and murmuring strange revelations and possibilities.*

Sir William Crookes (February 16, 1887)

Today, about a decade short of two centuries after Lt. C.A. Arrhenius discovered the rare earths, we are witnessing a rapid growth in our knowledge of this family of 17 elements. In the five years, 1971 through 1975, we have learned as much about the rare earths as in the previous 25 years. In an attempt to assess the current state of the art (1976) the editors, with the encouragement of the publishers and other fellow scientists, have invited experts in various areas to write comprehensive, broad, up-to-date, and critical reviews. Some of the subjects were chosen because they are mature and still quite active; others because they are essential as background information and for reference; and some topics because they are relatively new and exciting areas of research. Unfortunately there are a few areas which have not been included in the four volumes either because they could not be covered adequately at present or because the appropriate authors were unavailable. Perhaps a future volume could remedy this and bring other rapidly expanding topics up-to-date.

A goal of these volumes is to attempt to combine and integrate as far as practical the physics and the chemistry of these elements. The strategy has been to divide the work into four volumes, the first two dealing primarily with metallic materials and the other two with non-metallic substances. The interaction of these disciplines is important if our knowledge and understanding is to advance quickly and broadly. Historically there are several important instances where one discipline had a great influence on the advancement of the science of rare earths. From the time of Arrhenius' discovery in Ytterby, Sweden until the last naturally occurring rare earth was discovered (lutetium in 1907) the chemistry of the rare earths was hopelessly confused, but the theoretical work of Niels Bohr and the experimental studies of H.G.J. Moseley (both physicists) in 1913–1914 showed that there were 15 lanthanide elements to be expected plus the two closely related metals scandium and yttrium. The discovery of ferromagnetism in gadolinium by G. Urbain,

P. Weiss and F. Trombe in 1935 stirred much excitement and was a foreshadow of the activities of the past twenty years. All of this, however, might not have been were it not for the efforts of two groups of chemists headed by G.E. Boyd at the Oak Ridge National Laboratory and F.H. Spedding at the Ames Laboratory who in the late 1940's developed the ion exchange techniques for separating rare earths. The method developed by the latter group is still being utilized by many industrial firms for preparing high purity rare earth materials. In the 1960's and 1970's several important discoveries—rare earth phosphors, cracking catalysts, rare earth-cobalt permanent magnets, etc. have made significant practical impacts and stimulated much research, but the extent of these are difficult to judge and put into their proper perspective at this time. Hopefully, these four volumes, and any which may follow will make a major contribution to our progress in understanding these exotic and fascinating elements.

In writing these chapters the authors have been asked to use the term "rare earths" to include Sc, Y and the elements La through Lu, and the term "lanthanides" when referring to only the elements La through Lu. The editors have attempted to enforce this usage rigorously when editing the various chapters. Furthermore, we have encouraged the authors to use the SI units as far as practicable to bring the subject matter into accord with current scientific and technical practice.

CONTENTS

VOLUME 1: METALS

VOLUME 2: ALLOYS AND INTERMETALLICS

VOLUME 3: NON-METALLIC COMPOUNDS - I

VOLUME 4: NON-METALLIC COMPOUNDS – II

Handbook on the Physics and Chemistry of Rare Earths, edited by K.A. Gschneidner, Jr. and L. Eyring

Chapter 31

SULFIDES, SELENIDES AND TELLURIDES

Jean FLAHAUT
Laboratorie de Chimie Minérale Structurale, Associé au CNRS No. 200, Faculté des Sciences Pharmaceutiques et Biologiques de Paris Luxembourg, Université Rene Descartes, 4, Avenue de l'Observatoire, 75270 Paris Cedex 06, France

Contents

The rare earths form a very large number of binary sulfides, selenides and tellurides, which belong to various crystal types. Moreover, in the field of the ternary compounds, there are plenty of compounds having special crystal types. A large part of this paper will be devoted to these latter compounds.

The binary compounds, for which almost all the crystal structures are known, are now well studied from different physical points of view. In the case of the ternary compounds, for which a complete knowledge is not yet obtained in spite of a lot of work, only the structural aspect will be considered here – except for some optic, magnetic and electrical studies. The present paper will be especially concerned with the structural aspect of the rare earth chalcogenides.

1. General considerations

The important evolution of the crystallochemical behavior of the R elements from lanthanum to lutetium, leads to a distinct trend in the composition and crystal structures of their compounds. Here, we shall consider two main aspects: the valence and the coordination of the R atoms in their chalcogenides.

Concerning the *valence* of the rare earth atom in the chalcogenides, we observed no tetravalence, and an increasing importance of divalence. For instance, CeO_2 is a diamagnetic compound containing Ce(IV) while Ce_2S_4 is a paramagnetic derivative corresponding to Ce(III), in which 2 of the 4 sulfur atoms are in the form of a disulfide $(S–S)^{2-}$ group. It is possible that in some fluorosulfides or oxysulfides of cerium, Ce(IV) does exist, but some additional work is necessary to confirm this behavior, which would be favored by the high electronegativity of the second anion.

In contrast, the divalent state is stabilized by the low electronegativity of the anions, with increasing stability as the anion electronegativity decreases. For instance, in the case of europium, for which the normal oxide is Eu_2O_3, the corresponding Eu_2S_3 sulfide does not exist. The normal sulfide is Eu(II)S, which is easily obtained by action of H_2S on trivalent europium compounds (oxide, carbonate, etc). However the trivalence of europium is manifest in some chalcogenides, which may all be considered as ternary or quaternary compounds.

(1) *Compounds containing only Eu(III).* There is necessarily a second strongly electronegative anion, or a second weakly electronegative cation. E.g.:

Eu_2O_2S and Eu_2O_2Se (but not Eu_2O_2Te)

EuSF (but not EuSeF)

EuSCl (?) (but not EuSBr or EuSI)

$EuMS_2$ with M = Li, Na, K, Rb (not Cs) and also TlI.

(2) *Compounds containing mixtures of Eu(II) and Eu(III).*

Eu_3S_4 (or Eu_2(III)Eu(II)S_4), easily dissociated by heat into EuS

$Eu_5Sn_3S_{12}$ (or Eu_2(III)Eu_3(II)Sn_3(IV)S_{12})

$Eu_4Sn_2S_9$(or Eu_2(III)Eu_2(II)Sn_2(IV)S_9).

These two last compounds, recently discovered, are especially stable, and some other similar compounds certainly exist in other series.

In the case of selenides and tellurides, only divalent Eu is known in the binary chalcogenides. Among the ternary chalcogenides, almost all the compounds are formed by Eu(II), but some rare derivatives of Eu(III) are known, and especially Eu_2O_2Se and $NaEuSe_2$. However, the selenides have not been so extensively studied as the sulfides.

With ytterbium, we observe a similar behavior, but with a greater stability of the III state. The only oxide is Yb_2O_3; the oxide YbO is only known for certain in solid solutions with another oxide such as CaO. The normal sulfide is still Yb_2S_3, but it is easily dissociated by heat into Yb_3S_4 (or Yb_2(III)Yb(II)S_4); moreover, the compound Yb(II)S is well known. Finally, only one binary

telluride is known, Yb(II)Te. In the II state, ytterbium is very similar to calcium, and gives exactly the same ternary chalcogenides.

With thulium, for which the III state is still more stable, this trend manifests itself in an even more curious way. TmS and TmSe are semi-metallic compounds, derived from Tm(III), while TmTe is a derivative of Tm(II) (Bucher et al., 1975).

The second characteristic we have to consider is the coordination of the R elements in their compounds. First of all, we notice that a large proportion of the structures have flat cells (thickness of about 4 Å for sulfides), probably because the rare earths have a strong tendency to the prismatic environment, and the thickness of the cells corresponds to the height of the prisms. The study of the environment of the R elements in these flat cells is relatively easy. Two kinds of sulfur (or selenium) coordination polyhedra are formed around the rare earth. One kind is related to the triangular prism, and the other is derived from the octahedron.

In the case of the triangular prism, additional X chalcogen atoms are in the equatorial plane of the prism, in front of the lateral sides (mono, di or tricapped prisms). According to whether there are 1, 2 or 3 X atoms, the coordination is 7, 8 or 9 (never 6 with the R elements). In most of the cases, the R–X equatorial distances are larger than the other six (to the apices of the prism). Even, in some cases, the equatorial distances for some X atoms are so large that it is difficult to decide whether or not these atoms should be included in the coordination. It is for this reason that Besançon (1979) is presently developing a process to calculate the rare earth coordination from their Voronoj polyhedra. The values obtained give a better view of the real environment of the rare earth. For instance, in La_2SnS_5 in which there are three relatively large equatorial La–S distances, the coordination can be arbitrarily chosen as 6 or as 9. The calculation gives 8.52. For Sm_2SnS_5 in which there are two smaller Sm–S equatorial distances and a third one which is larger than the preceding ones, the coordination would appear to be 8. The calculation gives 8.33, in good agreement with the value of La_2SnS_5 and with the great similarity of the two structures (see section 8), which are probably isotypic. These prisms are characteristic of the light lanthanides, the coordination progressively decreasing going from lanthanum to gadolinium.

The second type of environment of the R elements is the octahedron. In the flat cells, it is always oriented in such a way that the pseudo square formed by the four X atoms and containing the R atom is parallel to the short axis of the flat cells. This means that the two other R–X bonds are before and after this square, parallel to the base of the cell. This octahedron is the only environment of Yb(III), Lu and also Sc. But for the other R elements of the second part of the R family (Gd to Tb), a characteristic modification of the octahedron is observed, one apex being substituted by two contiguous X atoms, in front of the square (fig. 1). These two X atoms are very close to one another: 3.20 to 3.40 Å in the case of sulfur, while the normal distance between contiguous but not bonded S atoms is 3.60 to 3.90 Å. Another distortion from the octahedron is the

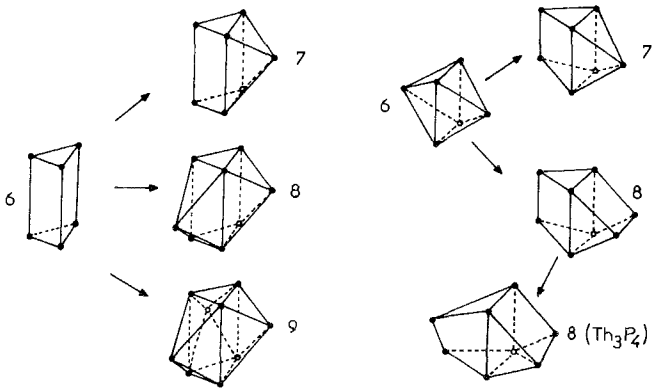

Fig. 31.1. Coordination polyhedra of the rare earths in their chalcogenides. They are related to the triangular prism (left) or to the octahedron (right).

removal of the R atom from the plane of the square toward the doubled apex (see for instance fig. 31.1).

We shall classify these environments in an abbreviated form as 7- or 8- or 9-prismatic and 6- or 7-octahedral. But it is evident that the 7-prismatic and 7-octahedral environments are very similar. They are easily distinguished in the flat cells in reference to their orientation relative to the short axis. In the larger cell, an easy distinction is made from the short S–S distance, which is characteristic of the 7-octahedral environment.

The characteristic interatomic distances $(R–X)_n$, for X = S or Se, were evaluated for the 6 and 8 coordinations, by Poix (1970).

In the following sections, we shall describe the main characteristics of the rare earths chalcogenides, with references to works after 1965. Older works are described, for instance, in Flahaut (1968, 1972) and Flahaut et al. (1968). Should it happen that some of these results are used, their references are not given.

2. Binary sulfides and selenides (RX_n) and tellurides (RTe and R_2Te_3–R_3Te_4)

The crystal structures of the binary sulfides and selenides are for the most part presently well known. However, some phases still remain unsolved, especially the polychalcogenides of all the R elements, and subchalcogenides of the heavy R elements. In these cases the structural studies are often complicated by the simultaneous appearance of twins and superstructures for some nonstoichiometric compositions.

The R–X systems contain many phases. Some phase diagrams have been described even though their study is difficult because of the high melting points of the R_2X_3 compounds and of the sub-chalcogenides. The following phase diagrams of the sulfide and selenide systems have been described:

La–S (in the La_2S_3–LaS_2 region) Loganova et al. (1975);
La–Se Jarembash et al. (1965b, 1969);
Eu–S Eliseev et al. (1974);
Eu–Se Eliseev et al. (1975b);
Er–Se Haase et al. (1965);
Yb–S Eliseev et al. (1975d, 1976a).

2.1. *R_2X_3 compounds (X = S, Se, Te)*

The R_2X_3 sulfides, selenides and tellurides exhibit a large number of crystal types which are related to the important evolution of the environments of the R elements from La to Lu. Moreover, the generally low symmetry of these environments (except for Yb^{3+} and Lu^{2+} which are inside octahedra) involves complicated structures and frequent polymorphism. Figure 31.2 introduces the nomenclature previously recommended.

Because the selenides and the tellurides have exactly the same structures (at similar cationic radius/anionic radius ratio), the binary R_2Te_3 tellurides will be studied here together with the sulfides and selenides, instead of in section 14.

The crystal chemistry of the rare earth sulfides was described by Guittard et al. (1966), Flahaut et al. (1965a), White et al. (1965a), Flahaut et al. (1968), Sleight et al. (1968). Greek letters were assigned by Flahaut et al. to each of the five structures of the R_2S_3 compounds, because of the many polymorphs in which they occur. For example,

for La_2S_3 $\alpha \rightleftarrows \beta \rightleftarrows \gamma$;
for Gd_2S_3 $\alpha \rightleftarrows \delta \rightleftarrows \gamma$;
for Yb_2S_3 $\sigma \rightleftarrows \epsilon$.

The corresponding Roman letters were used by Sleight et al. because they provide special reference to the structural types. We shall use both systems where appropriate.

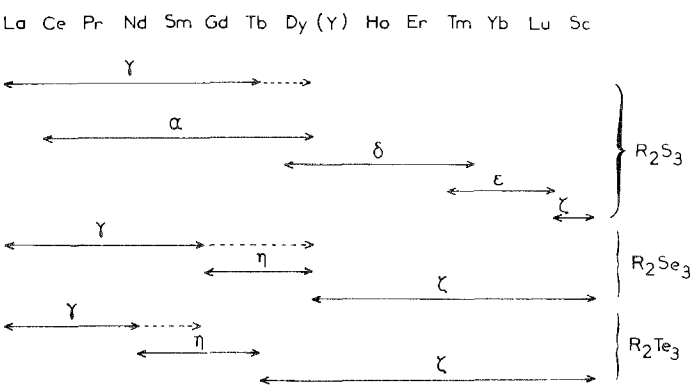

Fig. 31.2. Structural types and polymorphism of rare earth chalcogenides of R_2X_3 formula.

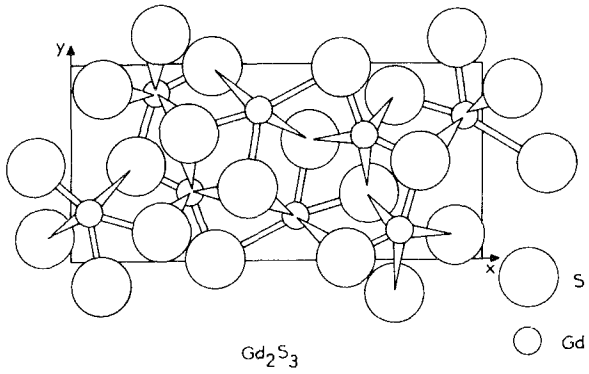

Fig. 31.3. Orthorhombic cell of Gd_2S_3 (α or A type): $a = 7.339$ Å, $b = 15.223$ Å, $c = 3.932$ Å, $z = 4$.

We begin by discussing the five crystal types which are typical of the R_2S_3 sulfides. Then we shall see the structures common to the sulfides, selenides and tellurides.

Gd_2S_3 or La_2S_3-type (α or A). The orthorhombic *Pnma* cell is flat (fig. 31.3). The rare earth atom sites are of two kinds, 8-prismatic and 7-octahedral (Prewitt et al., 1968; Besançon et al., 1969; Eliseev et al., 1972b). It is exactly stoichiometric and is stable at low temperature (Grizik et al., 1977). The following transitions appear at higher temperatures (Besançon, 1973):

$$\alpha\ La_2S_3 \rightleftarrows \beta\ La_2S_3 \simeq 900°C$$
$$\alpha\ Nd_2S_3 \rightleftarrows \gamma\ Nd_2S_3 \simeq 1180°C$$

Eliseev et al. (1975a) observed at low temperature several modifications of this structure, which they called α', α'', α'''.

β-type. This type was previously attributed to the R_2S_3 sulfides of the light lanthanides. Then Carré et al. (1970), Besançon (1973) and Besançon et al. (1969, 1970, 1973) showed that the Pr derivative has the composition $Pr_{10}S_{14}O$. In its structure, tetragonal $I4_1/acd$, the oxygen atom has a special position at the center of a regular tetrahedron of Pr atoms. The rare earth atoms have various environments: 7-octahedral (RS_7), (RS_7O) and (RS_8), this last being similar to the environment of the metal in the Th_3P_4 type structure. These oxysulfides exist from La to Sm (Besançon, 1973).

It is possible to substitute the O by an S atom, in a solid solution $R_{10}S_{14}O_{1-x}S_x$. The extent of the homogeneity range decreases from La to Sm. Only in the case of the La derivative is the complete substitution of O by S observed, and the β variety of La_2S_3 obtained. It is stable between about 900 and 1300°C (Besançon et al., 1971, 1973).

A high pressure modification of β-La_2S_3 has been described (Vereshchagin et al., 1975).

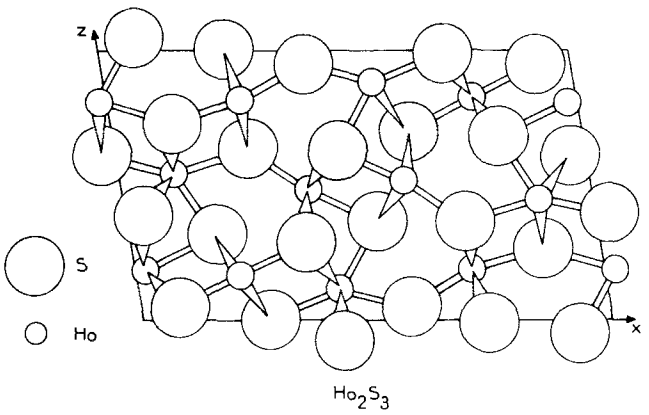

Fig. 31.4. The monoclinic cell of Ho_2S_3 (δ or D type): a = 17.50 Å, b = 4.002 Å, c = 10.15 Å, β = 99.40°; z = 6.

Ho_2S_3-type (δ *or D*). The monoclinic $P2_1/m$ cell is flat, and contains 6 formulas (fig. 31.4). The R atoms have 7-octahedral and 6-octahedral coordination, in equal proportions (White et al., 1967). So this type is characteristic of the sulfides of the second part of the family, and of yttrium.

In case of $\alpha \rightleftarrows \delta$ dimorphism, the δ type is stable at high temperatures. In case of $\delta \rightleftarrows \gamma$ dismorphism, the situation is opposite, and moreover the γ form can be slightly sub-stoichiometric. For Dy_2S_3, the transition temperature is 1160°C (Loireau-Lozac'h, 1977).

By high-pressure high-temperature treatment, a new monoclinic $P2_1/m$ variety is obtained from δ Tm_2S_3 (Range et al., 1976a).

Al_2O_3-type (ϵ *or E*). This rhombohedral structure exists only for Yb and Lu sulfides (Flahaut et al., 1965a). The structure of Lu_2S_3, recently solved by Range et al. (1975a), confirms the earlier work. The rare earth is not exactly at the center of the S-octahedron (which is more precisely a trigonal antiprism), but is displaced along the ternary axis toward a trigonal face of the octahedron in such a way that three Lu–S bonds are shorter (2.642 Å) than the other three (2.730 Å). A study of Eliseev et al. (1975c) does not seem in agreement with the preceding results.

Tl_2O_3-type (σ). This structure is observed only (Patrie, 1969) in the low temperature varieties of the Tm and Yb sulfides. Therefore, these two elements have the same structural type in their oxides and sulfides. The cubic cell contains 16 formulas. The R atoms, inside severely distorted triangular prisms, are 6-coordinated.

The preceding types are only present in the R_2S_3 sulfides. In contrast, the following types are simultaneously present for R_2X_3 compounds with X = S, Se and Te.

Th_3P_4 type (γ or C). This type is observed in the high temperature varieties of the R_2S_3 sulfides, and is the only form of the R_2Se_3 selenides and R_2Te_3 tellurides for the light lanthanides. The body-centered cubic cell, $I\bar{4}3d$, contains 16/3 R_2X_3 formulas, or 4 $R_{8/3}X_4$ formulas. Vacancies exist on the metal sites, and have a disordered arrangement.

The R atoms are octocoordinated with an unusual environment, which is also observed in the "β" type. It is a triangular dodecahedron, which can be regarded as formed by the superposition of two tetrahedra, a flat one and an elongated one. The structure, first established by Zachariasen (1948) for Ce_3S_4, was then studied for La_3Se_4 and Gd_2Se_3 (Holtzberg et al., 1965), La_2Te_3 (Cox et al., 1966), and Ce_2S_3 (Atoji, 1971). In each case, the only positional parameter of the S atoms in the structure, has a value of about 0.075, not far from the ideal value of 0.083. This value indicates that the bonding is mainly covalent (Carter, 1965).

By high pressure (77 kbars) high temperature (2000°C) treatment, Eatough et al. obtained the Th_3P_4-type for all the elements up to lutetium, in the R_2S_3 sulfide series (1969) and in the R_2Se_3 selenides series (1969, 1970).

By filling up the vacancies, continuous solid solutions are obtained from the R_2X_3 (or $R_{8/3}\square_{1/3}X_4$) to the R_3X_4 composition. For the R_2X_3 composition the ionic charges are equilibrated and the compounds have a very high resistivity. Later the non-equilibrium of the ionic charges results in metallic behavior.

Large domains exist for all the light trivalent lanthanides. For elements which lie on the limits of stability of this structural type, the homogeneity ranges become narrow and are localised in intermediate compositions, which are shown by dotted lines in table 31.1 (Guittard et al., 1966).

The compound Ho_2S_3, which usually has a δ-type structure, can be obtained by arc melting in the γ-form, probably resulting in a sulfur deficient composition (Verkhovets et al., 1971).

In the case of Sm and Eu, the behavior is very different from this, resulting from the great stability of their 2+ state in the chalcogenides. The Sm_3S_4 and Eu_3S_4 compounds are semiconductors. The Eu_2S_3 compound does not exist, and

TABLE 31.1
Crystal structures of R_2S_3 sulfides.

La	Ce	Pr	Nd	Sm	Eu	Gd	Tb	Dy	(Y)	Ho	Er	Tm	Yb	Lu	(Sc)
				γ											
		β													
				α											
										δ					
												ϵ			
												τ			
														ψ	

Dashed line: non-stoichiometric phases; α: orthorhombic Gd_2S_3-type; β: tetragonal $Pr_{10}S_{14}O$-type; γ: cubic Th_3P_4-type; δ: monoclinic Er_2S_3-type; ϵ: rhombohedral Al_2O_3-type; ψ: orthorhombic Sc_2S_3-type; τ: cubic Tl_2O_3-type.

there is only a very narrow homogeneity range near Eu_3S_4. For samarium, the homogeneity range goes from Sm_3S_4 to Sm_2S_3, by substitution of Sm(II) by $\frac{2}{3}Sm(III) + \frac{1}{3}\square$; the variation of the a-parameter is very marked.

In Sm_3S_4 and Eu_3S_4, ordering of the di and trivalent cations occurs at sufficiently low temperature. Mössbauer studies (Berkooz et al., 1968), an electrical transition near 175 K (Bransky et al., 1970), differential thermal analysis, magnetic data and X-ray studies (Davis et al., 1970) all show up this ordering which causes a tetragonal distortion of the cubic cell ($c/a = 1.004$), at 168 K for Eu_3S_4.

Moreover, such distortions of the unit cells appear at low temperature, between 20 and 100 K, for all the R_3S_4 compounds of purely trivalent R elements (Dernier et al., 1975).

Carter (1972) established a tetragonal model of ordered cationic vacancies in the $R_{3-x}X_4$ compounds from considerations involving the stereohedral metal sites or Wigner–Seitz cells, and tested it by Madelung constant calculations.

The vibrational spectra of the R_2S_3 sulfides were described by Barnier et al. (1976b).

Some thermal properties of the Th_3P_4-type compounds were determined

– *specific heat* between 12 and 300 K, *standard entropy* and *enthalpy* and *free energy* of formation:

La_2S_3 Paukov et al. (1969)
Nd_2S_3 Nogteva et al. (1969b)
La_2Te_3 Nogteva et al. (1969a), Tikhonov et al. (1975a,b)
Nd_2Te_3 Paukov et al. (1968)
R_3Te_4 (R = La to Nd) Tikhonov et al. (1971)

– *standard enthalpy of formation* by calorimetry:

La_2Te_3 Sharifov et al. (1967)

– *thermal expansion*:

La_3Te_4 Eliseev et al. (1967b).

The electrical and magnetic properties of the Th_3P_4-type compounds were studied in many cases. A review was made by Holtzberg et al. (1966). Interest in these substances is twofold. First of all, the $R_{3-x}(III)\square_xX_4$ compounds ($0 \leq x \leq \frac{1}{3}$) change continuously from metal to insulator with increasing vacancy concentration, leading to a variety of cooperative effects (superconductivity and ferromagnetism). Second, the random distribution of vacancies at the metal sites leads to fluctuating repulsive potentials and tailing of the conduction band in which the electronic states are localized.

Ferromagnetism is observed only in the R_3X_4 compounds as shown by Holtzberg et al. (1964). It was studied by Holtzberg et al. (1965) and Starovoitov et al. (1969), for Ce_3X_4, by Novikov et al. (1970), for Ce_3X_4 and Nd_3X_4, by Bucher et al. (1975) for Pr_3X_4 and by Andrianov et al. (1975) for Gd_2S_3 and Gd_3S_4. The Curie temperatures are considerably lower in Pr_3X_4 than in corresponding Ce_3X_4 and Nd_3X_4.

The R_2X_3 compounds are paramagnetic, and are antiferromagnetic at very low temperature, with Néel temperatures generally below 4 K.

Superconducting properties have been found in La_3S_4 and La_3Se_4 by Bozorth et al. (1965) and Guthrie et al. (1965), and in La_3Te_4 by Zhuze et al. (1966). They were studied by Seiden (1968) and Holtzberg et al. (1968). The critical temperatures T_c are, from Holtzberg et al.:

La_3S_4 8.12 K, La_3Se_4 7.63 K, and La_3Te_4 4.61 K.

Bucher et al. (1975) obtained similar values. Moreover, they showed that the substitution of lanthanum by yttrium or praseodymium revealed a rapid drop in the superconducting transition temperature and the electronic specific heat.

The action of high pressures produces a considerable increase in T_c of La_3S_4, whereas the T_c of La_3Se_4 shows a maximum at about 10 kbar, and the T_c of La_3Te_4 shows a small linear decrease with pressure. These differences are parallel to the variation of the temperature of the cubic $\rightleftarrows$ tetragonal transition (Shelton et al., 1975).

The electric and thermal transport properties of single crystals of Nd_2S_3, Gd_2S_3 and Dy_2S_3 were described by Taher et al. (1973a,b, 1974).

The Debye temperatures in the La_3Te_4–La_2Te_3 system were determined by Tikhonov et al. (1975a).

In order to explain the paramagnetic properties of $Ce_{3-x}S_4$, the concept of localization of electronic states in the conduction band was proposed by Cutler and Mott (1969). It was extended to $Gd_{3-x}S_4$, to explain the electric and magnetic properties observed in this ferromagnetic semi-conductor (von Molnar et al., 1972; Penney et al., 1974).

The s–f exchange interactions in Gd-doped $La_{3-x}S_4$ were described by Solomons et al. (1974).

U_2S_3-type (η). This flat orthorhombic *Pbnm* cell is only observed for three selenides (Gd to Dy) and four tellurides (Pr to Gd) (Flahaut et al., 1965a). Moreover, Range et al. (1975b) have obtained this structural type for sulfides (Ho to Lu and Y), by high-pressure high-temperature treatment, and quenching to ambient conditions.

The structure of Dy_2Se_3, refined from single crystal data by Range et al. (1976b), confirms the U_2S_3 structural type. The coordination polyhedra of the R atoms have two different types, 7-octahedral and 7-prismatic.

Sc_2S_3-type (ϕ *or* F). This type results in the ordering of cations and vacancies in the NaCl array, with the appearance of an orthorhombic Fddd superstructure (Dismukes and White, 1964). The only sulfide is Sc_2S_3. Among selenides and tellurides, this type is the normal one of the R elements of the second part of the lanthanide family. The octahedron of X atoms around the R atom is regular in the tellurides, slightly distorted in the selenides and Sc_2S_3 (White et al., 1965a; Flahaut et al., 1965b).

Sc_2Te_3-type. This structure really belongs to a series of polytypes resulting in different arrangements of layers along a six-fold (or three-fold) axis. The first

known structure of this series (White et al., 1965b) involves the following close packing of anions

$$[A\,C\,A\,C\,B\,A\,B\,A\,C\,B\,C\,B]_3$$

The lattice is rhombohedral $R3m$. The scandium atoms occupy the octahedral sites situated between each layer of tellurium. One layer of cations in two is completely full, while the other has only $\frac{1}{3}$ of its sites occupied in a disordered way. A nonstoichiometric $Sc_{7/3}Te_3$ telluride is described in the same crystal structure with a partial filling of the vacant sites (White et al., 1965b).

It is noteworthy that the two structures of the scandium derivatives, Sc_2X_3, are both related to close packed structures of the general MX types, in which vacancies appear on the metal sites. It is a consequence of the affinity of scandium (also Yb(III) and Lu) for regular octahedral sites. This behavior is observed in the lower chalcogenides as well.

2.2. *Polysulfides and polyselenides*

Polysulfides and polyselenides are very similar, but strongly differ from the Te-rich tellurides (section 14). The RX_2 composition is usually attributed to these compounds. In many cases, however, nonstoichiometries occur either from a deficiency or an excess of sulfur, and by a deficiency of selenium. It seems, from recent studies, that large homogeneity ranges do not exist, but rather different super-structures corresponding to narrow composition ranges.

For the polysulfides, (see table 31.2) all the proposed structures have the anti-Fe_2As structure (tetragonal cell, $P4/nmm$ with $a_0 \simeq 4$ Å and $c_0 \simeq 8$ Å) or are super-structures of this type. But, except for YbS_2 and LaS_2, the unit cells of the super-structures were described from powder X-ray diagrams, and their structures are not known exactly.

The simplest tetragonal structure, of the anti-Fe_2As type, with parameters a_0 and c_0, was observed with single crystals obtained from iodine vapor transport (Eliseev et al., 1971, 1972a,b). In the earlier studies, it appeared that the RS_2 compounds of the light lanthanides had cells of $2a_0$, $2a_0$, c_0, which seemed nearly cubic, but actually had lower symmetry, perhaps tetragonal. S-deficient compounds had pseudo-tetragonal cells, $\simeq 2a_0$, $\simeq 2a_0$, c_0, which certainly have lower symmetry and different cells (Flahaut et al., 1959; Ring and Tercotzky, 1964; Eliseev et al., 1976b).

The polysulfides of plutonium PuS_2 and PuS_{2-x}, obtained in single crystals by Marcon et al. (1966a,b), have to be considered here because they are isomorphous with the Ce derivatives. Whereas PuS_{2-x} has the tetragonal anti-Fe_2As structure, the PuS_2 compound is a super-structure of it, with $2a_0$, $2a_0$, c_0 cell, and appears nearly cubic.

Recently, the crystal structure of stoichiometric La_2S_4 was described by Dugué et al. (1978). It is a super-structure, with distortion, of the anti-Fe_2As type: the orthorhombic $Pnma$ cell is $a = 2a_0$, $b = 2c_0$, $c = a_0$. The structure is formed, as for all the polysulfides and polyselenides of the light lanthanides, by alternating sheets

TABLE 31.2
Formulas and proposed structures of the polysulfides (P = powder studies, C = crystal studies of the cells).

Formulas	References	X-ray materials	Cells	Space groups or type	Parameters		
RS_2							
(La–Nd)	Flahaut et al. (1959)	P	pseudocubic		$2a_0$	$2a_0$	c_0
$RS_{1.89-1.94}$							
(Sm, Dy and Y)	Flahaut et al. (1959)	P	tetrag.		$2a_0$	$2a_0$	c_0
$LaS_{1.94}$	Ring and Tecotzky (1964)	P	orthorh.		$2a_0$	$\simeq 2a_0$	$2c_0$
$LaS_{1.80-1.75}$	Ring and Tecotzky (1964)	P	tetrag.		$2a_0$	$2a_0$	$2c_0$
$RS_{1.7}$							
(Pr to Ho and Y)	Ring and Tecotzky (1964)	P	tetrag.		$2a_0$	$2a_0$	c_0
PuS_2	Marcon et al. (1966, 1968)	C	tetrag.		$2a_0$	$2a_0$	c_0
PuS_{2-x}	Marcon et al. (1966, 1968)	C	tetrag.	Fe_2As	a_0	a_0	c_0
NdS_{2-x}	Eliseev et al. (1971)	C	tetrag.	Fe_2As	a_0	a_0	c_0
NdS_{2+x}	Uspenkaya et al. (1972)	C	orthorh.	*Pmmm* or $Pnm2_1$	4.085	4.071	9.244
$NdS_{2\pm x}$	Eliseev et al. (1972)	P	tetrag.	$P\bar{4}b2$	$2a_0$	$2a_0$	c_0
La_2S_4	Dugué et al. (1978)	C	orthorh.	*Pnma*	$2a_0$	$2c_0$	a_0
YbS_2	Teske (1974)	C	monocl.		–	–	–

TABLE 31.3
Formulas and proposed structures for the polyselenides (P = powder studies, C = crystal studies of the cells).

Formulas	References	X-ray materials	Cells	Space groups and type	Parameters		
RSe_2 (La–Nd)	Benacerraf et al. (1959)	P	tetrag.	–	$2a_0$	$2a_0$	c_0
$ErSe_2$	Haase et al. (1965)	C	α: orthor β: orthor	*Cmma* *Immm*	16.22 4.06	15.80 5.57	11.88 13.16
RSe_{2-x} ($0 < x < 0.2$) R = La–Sm	Eliseev et al. (1966a,b)	C	tetrag.	Fe_2As	a_0	a_0	c_0
R_4Se_7 (R = La–Sm)	Eliseev et al. (1967a)	C	monocl.	$P2_1/a$	$2a_0$	$2a_0$ $\beta = 90°$	c_0
$CeSe_2$	Marcon et al. (1968)	C	monocl.	$P2_1/a$	$2a_0$	a_0 $\beta = 90°$	c_0
Er_4Se_7	Guittard et al. (1967)	P	idem α $ErSe_2$ of Haase et al.	–	$2c_0$	$4a_0$	$3c_0$
$LaSe_2$	Benazeth et al. (1975)	C	triclin.	x	$2a_0$	$2a_0$ $\alpha = \beta = \gamma = 90°$	c_0
$LaSe_{1.95}$	Benazeth et al. (1975)	C	monocl.	$P2_1b$	$2a_0$	a_0 $\gamma = 90°$	c_0
$LaSe_{1.90}$	Benazeth et al. (1975)	C	monocl.	$P2_1$	$a_0\sqrt{5}$	$a_0\sqrt{5}$ $\gamma = 90°$	$2c_0$

of $(LaS)_n$ composition, and layers of $(S)_n$. In the sheets, the sulfur atoms are isolated, and probably are S^{2-} anions. In the layers, the sulfur atoms form disulfide, S_2^{2-}, anions with a short S–S distance (2.104 Å).

The vibrational spectra of RS_2 (R = La–Gd) are described by Golovin et al. (1975).

By high pressure high temperature treatment, Webb et al. (1970b) found the pseudo-cubic forms, normally observed for only the light lanthanides, for all the R elements. By use of the same high pressures, but at more elevated temperatures, tetragonal cells ($\simeq 2a_0$, $\simeq 2a_0$, c_0) occur. They are similar to the cells of the S-deficient polysulfides of the light lanthanides obtained in the usual way. In a similar treatment Yanagisawa et al. (1973) obtained under 35 kbar and 1000°C, a CeS_2 compound, the powder diagram of which seems to suggest an orthorhombic cell ($2a_0$, $2c_0$, a_0), and similar to that of La_2S_4 found by Dugué et al. (1978).

Teske (1974) has described the structure of YbS_2 from single crystals obtained from high pressure treatment. The monoclinic cell observed is not related to the preceding schemes; all the sulfur atoms are in S_2^{2-} pairs, and this compound seems to be a disulfide of divalent Yb.

For the polyselenides, (see table 31.3) the structural characteristics are similar to the polysulfides. But, in this case, the sub-structure of the anti-Fe_2As type has a c_0/a_0 ratio which is always smaller than 2 and the pseudo-cubic superstructure has not been observed. First of all, Benacerraf et al. (1959) have described the polyselenides RSe_2 (R = La to Sm) as a pseudo-tetragonal superstructure $a = 2a_0$, $c = c_0$.

Then Marcon et al. (1968a,b), from a single crystal study, have shown that the structure of $CeSe_2$ is monoclinic $P2_1/a$, with $a = 2a_0$, $b = a_0$, $c = c_0$, $\beta = 90°$.

The polyhedron of Se around Ce is highly distorted, relative to the anti-Fe_2As type. But the main characteristic of this structure is the presence of Se_2^{2-} pairs, with a short Se–Se distance (2.47 Å) and isolated Se^{2-} anions. Marcon et al. (1968) propose that the simple cell of the anti-Fe_2As type, observed in some cases, results from an arrangement of Se_2^{2-} and Se^{2-} anions, which can occur from a deficient Se-content. This remark seems to be confirmed by Eliseev et al. (1966a,b), who obtain Se-deficient RSe_{2-x} compounds with $0 < x < 0.2$. Eliseev et al. (1967a) also obtained Se deficient compounds, to which they attribute the composition R_4Se_7 (La to Sm). From single crystal work, the cell is found to be a monoclinic, $P2_1/a$, super-structure of the anti-Fe_2As type, with $a = 2a_0$, $b = 2a_0$, $c = c_0$, $\beta = 90°$.

Haase et al. (1965) described an $ErSe_2$ polyselenide, which has two varieties, with a reversible transition at 890°C. Guittard et al. (1967) in their study of the Er–Se system only observed the low temperature form to which they give the composition Er_4Se_7.

The existence of different super-structures related to different compositions is shown in a recent study of Benazeth et al. (1975) from single crystals obtained in various preparations from $LaSe_2$ to $LaSe_{1.88}$. Three phases are observed. For $LaSe_2$ the cell has a shape similar to that of Eliseev et al. but is triclinic. Near $LaSe_{1.95}$ the cell is monoclinic like that of Marcon et al. for $CeSe_2$. Finally,

$LaSe_{1.90}$ appears to be a new phase with a large monoclinic cell containing two $La_{10}Se_{19}$ formulas not previously observed. All these phases are super-structures of the Fe_2As type.

More recently, Benazeth et al. (1977) solved the first two structures which appear to be two different twinnings of the same monoclinic $2a_0$, a_0, c_0 structure. So, in agreement with some other work which shows a strong relation between different kinds of twinning and the composition of a nonstoichiometric phase, these two apparently different phases have exactly the same structure but correspond to different compositions and consequently to different c_0/a_0 ratios which are the source of the different kinds of twinning.

By high-pressure high-temperature treatment, Webb et al. (1970a) obtained tetragonal RSe_2 polyselenides with R = Tm, Yb, Lu.

2.3. *Lower chalcogenides (X = S, Se, Te)*

In this chapter we have to consider the only derivatives in which the rare earths are purely trivalent, and these have a metallic behavior. The properties of the Eu monochalcogenides are described in ch. 19, and chalcogenides which have valence changes are covered in ch. 20. Moreover, we have previously described the R_3X_4 compounds of the Th_3P_4 type.

The only crystal types yet to be described are Y_5S_7, Er_3Se_4, and the NaCl-type. However, in order to give a general view of the R–X systems, we shall describe the Yb_3S_4 and Yb_3Se_4 types.

Y_5S_7-type. This structural type is only observed in sulfides from Tb to Tm and Y. The flat cell is monoclinic $C2/m$. Three of the Y atoms have an octahedral environment, and the other two are 7-prismatic coordinated. These compounds are always semi-metals (Adolphe, 1965).

Yb_3S_4-type. Ytterbium is the only R element to form this kind of compound, but this structure is well-known in numerous MR_2S_4 compounds (section 5, A′ type). The orthorhombic *Pnma* cell contains 4 formulas (fig. 31.5). The Yb(III) atoms are

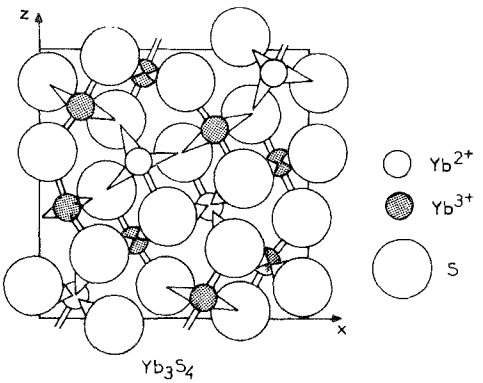

Fig. 31.5. The orthorhombic cell of Yb_3S_4: a = 12.71 Å, b = 3.80 Å, c = 12.88 Å, z = 4.

situated in slightly distorted octahedra. The Yb(II) atoms are 7-prismatic coordinated (Chevalier et al., 1967).

Solid solutions of $Yb_{3+x}S_4$ are obtained from $YbS_{1.48}$ to $YbS_{1.33}$. They are formed by substitution of $3Yb^{2+}$ by $2Yb^{3+} + \square$, and the vacancies are localised exclusively in the prismatic sites.

Yb_3Se_4 type. This type is derived from the NaCl structure and is the upper limit of a range of homogeneity which, starting from YbSe, results from the progressive replacement of $3Yb^{2+}$ by $2Yb^{3+} + \square$. At the beginning, the cubic lattice is first maintained, but at a composition corresponding to $YbSe_{1.1}$ a rhombohedral distortion appears which increases until the composition $YbSe_{1.33}$ (or Yb_3Se_4) has been reached (Souleau et al., 1969). A similar phenomenon is encountered in the YbSe–R_2Se_3 and CaSe–R_2Se_3 systems (section 5).

The heavy lanthanides form semi-metallic R_3Se_4 compounds (Dy to Lu and Y). Their structures appear to be very similar to that just described with scarcely a noticeable rhombohedral distortion from the NaCl structure (Guittard et al., 1968b).

Monochalcogenides RX (X = S, Se, Te)

All these compounds have the NaCl structure. From a general point of view their parameters change regularly from one lanthanide to another. Their magnetic properties and their metallic behavior depend on the presence of one conduction electron per RX formula related to the presence of the rare earths in their trivalent state.

The monochalcogenides of Sm, Eu and Yb, and also YbTe, have lattice parameters which are larger than those of the neighboring compounds formed by typically trivalent rare earths. They are semiconductors or insulators and have no metallic luster. The rare earth is in a divalent state. The monochalcogenides of Eu are described in ch. 19. Moreover, the Sm, Eu and Yb monochalcogenides show a pressure induced semi-conductor to metal transition due to electron delocalization. This phenomenon is presented in ch. 20. Consequently, we shall only describe the monochalcogenides of trivalent lanthanides.

Preparation of monochalcogenides in a single crystal form was studied extensively by Holtzberg (1971).

Monosulfides show homogeneity ranges resulting from sulfur deficiency, RS_{1-x}. They undergo a regular decrease of the lattice parameter with increasing R concentration, especially from neodymium. The lower limit of these domains is usually $RS_{0.75}$. But, with lutetium the homogeneity range extends to both sides of the stoichiometric composition (Guittard, 1965; Bruzzone et al., 1965). With selenides a similar behavior is observed; in Gd_xSe_{1-x} the homogeneity range is $0.52 > x > 0.44$ (Holtzberg et al., 1972). In this case, the lattice parameter decreases linearly with decreasing Gd content.

The RX monochalcogenides have a paramagnetic behavior corresponding to R^{3+} ions, except at low temperatures (Adamjan et al., 1966, 1967; Loginov et al., 1969; Smolenskii et al., 1966). An antiferromagnetic ordering appears at lower

temperatures. For example, the following Neél temperatures were shown by specific heat measurements (Bucher et al., 1975):

TbS	49 K	TbSe	52 K	TbTe	63 K
TmS	5.2 K	TmSe	1.85 K	TmTe	0.21 K.

In the Gd_xSe_{1-x} solid solution described above, the Néel temperature varies from 20 to 60 K with increasing Gd or electron concentration (Holtzberg et al., 1972).

The study of this magnetic ordering was carried out at 4.2 K, by Schobinger-Papamantellos et al. (1974). It appears to be a type II antiferromagnetic ordering, similar to FeO and MnO, which leads to rhombohedral symmetry of the magnetic structure. However, a first order tetragonal lattice distortion at the Néel temperature was shown to occur with the following compounds: NdS (Golosovski et al., 1973), NdS, DyS and ErS (Tao et al., 1974, NdS, NdSe and NdTe (Hulliger et al., 1975). A non-collinear magnetic structure with two propagation vectors was observed on NdS (Golosovski). A second phase-transition between antiferromagnetic arrangements is observed in NdSe and NdTe, at lower temperature and in zero magnetic field (Hulliger).

The electrical and thermoelectric properties were determined over a large range of temperatures and for several compositions, and the conduction mechanisms were analyzed (see for instance Daunov et al., 1975; Beckenbaugh et al., 1975; Vasilev et al., 1975). Parallel to this, optical properties were studied (Guntherodt et al., 1974; Eastman et al., 1974). The s–f exchange interactions were evaluated from the electronic resonance spectra (Urban et al., 1974).

The thermal and thermodynamic properties of the monochalcogenides were collected and analysed by Westrum (1968) and Smirnov (1972). Measurements of thermal capacities and thermal conductivities were made respectively by Bucher et al. (1970) and Khusnutdinova et al. (1971).

The dissociation energies of some monosulfides were determined by effusion methods and by mass spectrometry of their vapors (Cater et al., 1965; Coppens et al., 1967; Smoes et al., 1969; Stretz et al., 1975). The thermodynamic properties of the gaseous monosulfides were deduced.

3. Ternary systems R–R′–X (X = S, Se)

Two kinds of compounds must be considered.

First, the intermediate phases are formed by the typically trivalent rare earths, (R(III)), (R′(III)), X. Two cases will be distinguished;

those phases which belong to the R_2X_3–R'_2X_3 binary systems (in 3.1),

and those phases having a smaller content of the X element (in 3.2).

Second, the ternary phases containing a divalent R element (Sm(II), Eu(II), Yb(II)) and a trivalent R element, R(III). The crystal properties of the $(R(II))(R'(III))_2X_4$ compounds formed in this case are very similar to those of the $(M(II))(R(III))_2X_4$ compounds in which M(II) = Ca, Sr, Ba or Pb. Therefore, their crystal properties will be described in section 5.

3.1. *Intermediate phases containing two trivalent R elements*

3.1.1. *The $(R(III))_2X_3$–$(R'(III))_2X_3$ systems*

A general view of the structural aspects of the sulfide systems was published by Carré et al. (1973a).

In the R_2S_3–R'_2S_3 systems, at temperatures of 1000–1100°C, the intermediate phases observed are:

Solid solutions. They have either the α or δ type structures of the binary sulfides. They extend, by a continuous range of homogeneity, from R_2S_3 to R'_2S_3 when the R and R′ sulfides have the same crystal type. This behavior is noted as α_c or δ_c in Table 31.4. They have a limited range of homogeneity when the constituents R and R′ sulfides have different crystal types. This behavior is noted as α_1 or δ_1 in table 31.4. (We restrict this notation to the cases in which the $RR'S_3$ composition is included in the homogeneity range.)

The crystal structure of the "$CeDyS_3$" term of the α-type solid solution shows the Ce in the VIII-coordinated site and the Dy in the VII-coordinated site (Rodier et al., 1977b).

Definite compounds. There are compounds with two general formulas $RR'S_3$ and RR'_3S_6. The $RR'S_3$ compounds have four distinct crystal types (Vo Van et al.,

TABLE 31.4
Crystal types of the $RR'S_3$ compounds, at 1000°C.

R \ R′	La	Ce	Pr	Nd	Sm	Gd	Tb	Dy	(Y)	Ho	Er	Tm	Yb	Lu	Sc
La	α	α_c	α_c	α_c	α_c	α_c	α_c	G	G	G	G	G	I	I	I
Ce		α	α_c	α_c	α_c	α_c	α_c	α_1	G	G	G	G	H	H	I
Pr			α	α_c	α_c	α_c	α_c	α_c	α_1	α_1	G	G	H	H	I
Nd				α	α_c	α_c	α_c	α_c	α_1	α_1	α_1	G	H	H	I
Sm					α	α_c	α_c	α_c	α_1	α_1	α_1	α_1	F	F	I
Gd						α	α_c	α_c	x	x	x	F	F	F	I
Tb							α	α_c	x	x	x	x	F	F	I
Dy								α	δ_c	δ_c	δ_c	δ_c	δ_1	δ_1	I
(Y)									δ	δ_c	δ_c	δ_c	δ_1	δ_1	I
Ho										δ	δ_c	δ_c	δ_1	δ_1	I
Er											δ	δ_c	δ_1	δ_1	I
Tm												δ	δ_1	δ_1	–
Yb													ϵ	ϵ_c	–
Lu														ϵ	–

α_c and δ_c = solid solutions of the α or δ types, continuous from R_2S_3 to R'_2S_3.
α_1 and δ_1 = solid solutions of the α or δ types, with a limited region of homogeneity, including the $RR'S_3$ composition.
x = mixture of phases at the $RR'S_3$ composition.
F, G, H, I = crystal types of the $RR'S_3$ compounds.
At the bottom of each column, α, δ, ϵ represent the crystal types of the R_2S_3 sulfides, at 1000°C.

TABLE 31.5
RR'_3S_6 compounds of the F type.

R \ R'	Dy	(Y)	Ho	Er	Tm	Yb	Lu
La	F	F	F	F	F	F	F
Ce	–	F	F	F	F	F	F
Pr	–	F	F	F	F	F	F
Nd	–	F	F	F	F	F	F
Sm	–	–	–	–	?	F	?
Gd	–	–	–	–	F	F	F
Tb	–	–	–	–	–	F	F

1970a). They are designated by the letters F, G, H and I in table 31.4. Their structures were established from single crystals of the following compounds:

F $CeYb_3S_6$ (Rodier et al., 1973, 1974, 1976c)
G $CeTmS_3$ (Rodier, 1973)
H $NdYbS_3$ (Carré et al., 1974)
I $YScS_3$ (Rodier et al., 1970).

Other RR'_3S_6 compounds also have the F-type structure of $CeYb_3S_6$ (table 31.5) (Rodier et al., 1976c).

At elevated temperatures (about 1400°C), continuous solid solutions of the cubic Th_3P_4 structure appear between γ–R_2S_3 and γ–R'_2S_3 sulfides of this same type. Moreover, the phases G and H are no longer stable and only the I and F phases persist (Vo Van et al., 1971).

In these structures (except for the I-type and the γ-solid solutions) the cells are flat (about 4Å thick), and the environments of the R elements have the characteristic features and the same orientations relative to the short axis of the cells, which are described in section 1.

The effect of high temperatures and high pressures on some $RR'S_3$ compounds was studied. Upon quenching, $GdYbS_3$ (F-type) gives, with increasing pressure, three phases, the cubic Th_3P_4 type, the orthorhombic Gd_2S_3 or α-type, and the orthorhombic U_2S_3 or η-type (Clark et al., 1975). In a similar way $DyYbS_3$ (δ-type R_2S_3 sulfide) gives the cubic Th_3P_4 type and the U_2S_3 type (Clark et al., 1976).

3.2. *Structural studies of the definite compounds*

$CeYb_3S_6$ type or F type. The monoclinic cell has the space group $P2_1/m$ (Fig. 31.6). There are four kinds of metal sites and the crystallographic formula is $(VIIIp)_2(VIIo)_2(VIo)_2(VI'o)_2S_{12}$ (Rodier et al., 1974). The VIII prismatic sites are always occupied by light rare earths, and the VI octahedral sites by heavy rare earths. But, depending on the nature of the elements, the VII octahedral sites

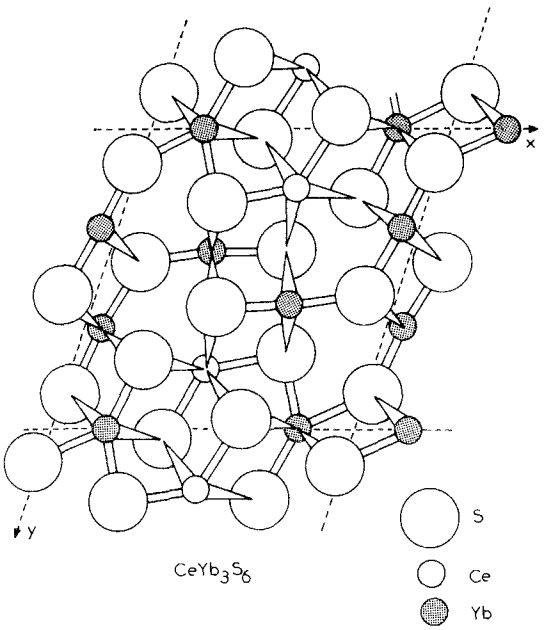

Fig. 31.6. Monoclinic cell of $CeYb_3S_6$(F-type): $a = 10.93$ Å, $b = 11.20$ Å, $c = 3.940$ Å, $\gamma = 108.8°$.

can be occupied by light rare earths R (formula $RR'S_3$) or by heavy rare earths R' (formula RR'_3S_6) (Rodier et al., 1976c). Moreover, in the special case of Er_3ScS_6 (Rodier et al., 1972) a disordered arrangement of both elements Er and Sc in the VI octahedral sites, with different relative proportions on the two kinds of sites, gives a third possibility (table 31.6).

$CeTmS_3$ type or G type. The monoclinic cell, space group $P2_1/m$, contains eight formulas (fig. 31.7). Four kinds of metal sites are present: $(VIIIp)_4(VIIp)_4(VIIo)_3(VIo)_4S_{24}$ (Rodier, 1973). In spite of the many possibilities of various kinds of occupancy by atoms of a different nature, only one kind of compound of chemical formula $RR'S_3$ is obtained. In this case, the prismatic

TABLE 31.6
The three kinds of occupancy of the sites of the monoclinic cell $CeYb_3S_6$-type.

Formulas	$(VIIIp)_2$	$(VIIo)_2$	$(VIo)_2$	$(VI'o)_2$
RR'_3S_6	R = La to Nd	R' = Ho to Lu and Y		
$RR'S_3$	R = Sm to Tb		R' = Tm to Lu	
$Er_{2.92}Sc_{1.08}S_6$	R = Er		0.52 Er +0.48 Sc	0.39 Er 0.61 Sc

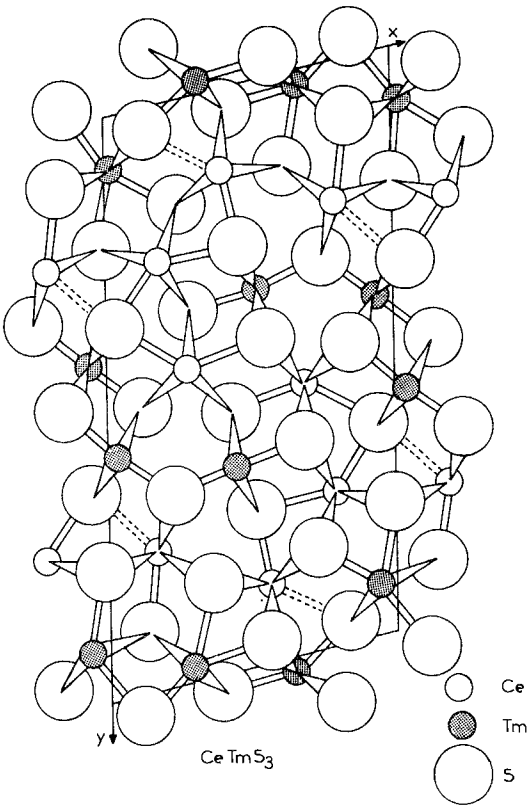

Fig. 31.7 Monoclinic cell of $CeTmS_3$ (G-type): $a = 11.09$ Å, $b = 21.42$ Å, $c = 3.98$ Å, $\gamma = 102.95°$.

sites are occupied by light lanthanides (La to Nd) and the octahedral sites by heavy lanthanides (Dy to Tm and Y). We see here a characteristic feature of the lanthanides in their sulfides. When two sites of coordination number 7 are present in a structure with two different environments, the light lanthanides choose the prismatic environment and the heavy lanthanides choose the environment related to the octahedron.

$NdYbS_3$ type or H type. The cell is orthorhombic $B22_12$ (fig. 31.8). Two kinds of metallic sites are present in equal proportion, and the crystallographic formula is $(VIIIp)_4(VIo)_4S_{12}$. (Carré et al., 1974). The only possible chemical formula is $RR'S_3$. Because of the high coordination and the prismatic character of the first sites, they may only be occupied by the lighter lanthanides (Ce to Nd). The VI octahedral sites contain exclusively the last two lanthanides Yb and Lu.

$YScS_3$ type or I type. This orthorhombic cell $Pna2_1$ is the only one not flat. This structure (Rodier et al., 1970) is very similar to the preceding one. It has the same kinds of sites, it corresponds to the same general formula, and it contains approximately the same R elements. But, the VIII prismatic site is larger than

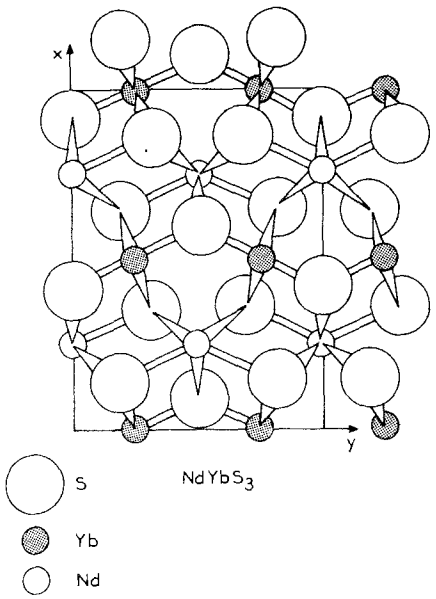

Fig. 31.8. Orthorhombic cell of $NdYbS_3$ (H-Type): $a = 12.54$ Å, $b = 9.66$ Å, $c = 3.85$ Å, $z = 4$.

the corresponding site of the H-type, and only lanthanum is able to occupy it. The VI octahedral site is, as before, occupied by ytterbium or lutetium.

In the case of the scandium derivatives, this element is on the octahedral sites, and a large number of R elements accept the VIII prismatic coordination (from La to Er) (Rodier et al., 1969).

3.3. *Ternary intermediate phases* $(R, R')X_x$ *formed between subsulfides or subselenides* $(R(III))X_x$ *with* $1.33 \leq x \leq 1.50$

In the ternary diagram R–R'–X, some studies were made on sulfides (Vo Van et al., 1968, 1969) and selenides (Guittard et al., 1971). The following phases were observed:

Homogeneity surfaces of the Th_3P_4*-type.* They are formed between the two binary solid solutions R_2S_3–R_3S_4 and R'_2S_3–R'_3S_4 of the same type (Vo Van et al., 1968). In the case of the La–Er–Se system the homogeneity surface has a limited extension, because the Th_3P_4 type does not exist in the binary Er–Se system (Guittard et al., 1971).

Solid solutions of the Y_5S_7*-type.* The only systems which have been studied are those formed between the Er_5S_7 compound of the Y_5S_7 type, and the R_5S_7 compositions which, for the first rare earths, belong to the homogeneity region R_2S_3–R_3S_4 of the Th_3P_4-type. Beyond Er_5S_7, the monoclinic solid solutions are relatively narrow, and cease in the neighborhood of the composition REr_4S_7 (Vo Van et al., 1969).

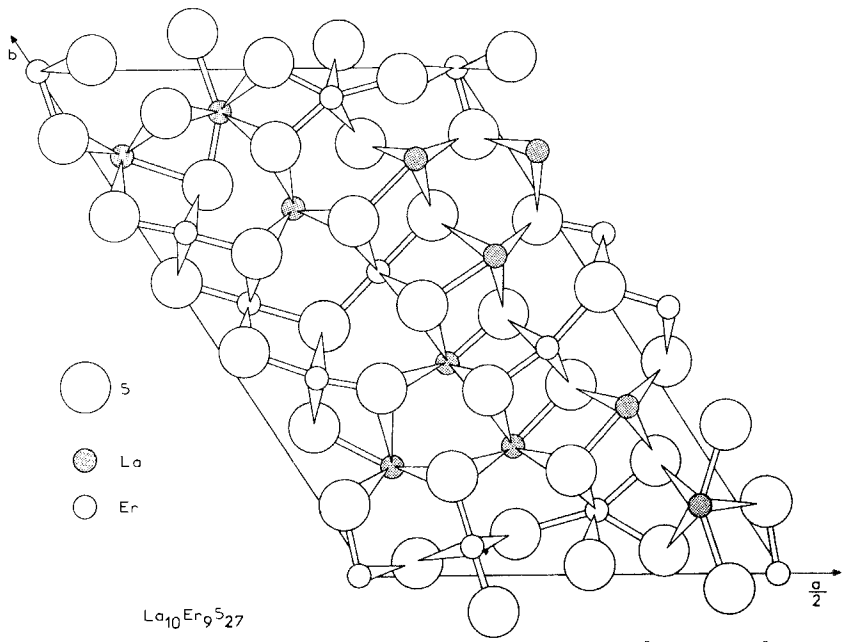

Fig. 31.9 Asymmetric content of the monoclinic cell of $La_{10}Er_9S_{27}$: $a = 29.71$ Å, $b = 21.83$ Å, $c = 3.94$ Å, $\gamma = 122.0°$, $z = 2$.

Although binary selenides have no compounds of the Y_5S_7-type, the ternary $LaEr_4Se_7$ has this crystal type (Guittard et al., 1971).

Moreover, Rodier et al. (1972) have described the structure of a compound of formula $Er_3Sc_2S_7$, in which there is a disordered arrangement of the two cations in the two kinds of metal sites of the Y_5S_7 type structure.

Compounds of the $La_{10}Er_9S_{27}$-type. The monoclinic cell has the space group $B2/m$ and contains two formulas (fig. 31.9). Ten different metal sites are present (Carré et al., 1973b):

$$(\mathrm{VIIIp})_4(\mathrm{VIII'p})_4(\mathrm{VIIp})_4(\mathrm{VII'p})_4(\mathrm{VII''p})_4(\mathrm{VIIo})_4(\mathrm{VIo})_4(\mathrm{VI'o})_4(\mathrm{VI''o})_4(\mathrm{VI'''o})_2\mathrm{X}_{54}.$$

Or, combining the equivalent positions one has $(\mathrm{VIIIp})_8(\mathrm{VIIp})_{12}(\mathrm{VIIo})_4(\mathrm{VIo})_{14}\mathrm{X}_{54}$.

The prismatic sites are occupied by lanthanum, and the octahedral sites by erbium atoms. The occupancy of the 7-coordinated sites follows the same rule as for $CeTmS_3$ – the light rare earths are in the prismatic sites, the heavy rare earths have environments which are related to the octahedron. This kind of compound has been observed for R = La to Nd and for R' = Er, but other possibilities probably exist (Vo Van et al., 1968).

Compounds of the $Ce_4Lu_{11}S_{22}$ type. This large monoclinic cell, space group $B2/m$, contains two formulas (fig. 31.10). Eight kinds of metal positions are observed (Rodier et al., 1975):

$$(\mathrm{VIIIp})_4(\mathrm{VIII'p})_4(\mathrm{VIIo})_4(\mathrm{VIo})_4(\mathrm{VI'o})_4(\mathrm{VI''o})_4(\mathrm{VI'''o})_4(\mathrm{VI''''o})_2\mathrm{X}_{44}$$

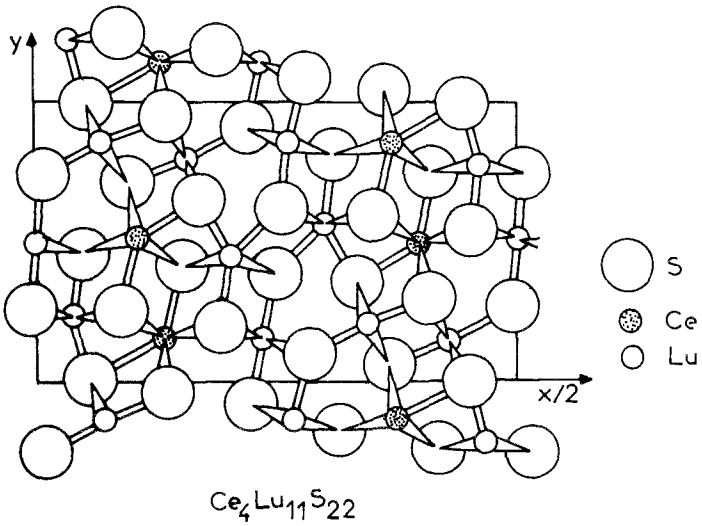

Fig. 31.10. Asymmetric content of the monoclinic cell of $Ce_4Lu_{11}S_2$. $a = 38.60$ Å, $b = 11.21$ Å, $c = 3.91$ Å, $\gamma = 91.3°$, $z = 2$.

Or, combining the equivalent positions one has $(VIIIp)_8(VIIo)_4(VIo)_{18}X_{44}$.

The 8-coordinated prismatic positions are occupied by cerium atoms, and the positions which are related to the octahedron are occupied by lutetium atoms. In fact, the two kinds of sites are very different and only one type of occupation is possible. The light lanthanides are on the prismatic sites and the heavy lanthanides are on the other sites.

This structure is especially interesting because of its relationship to the $CeYb_3S_6$ structure (F-type). It is possible to obtain the large $Ce_4Lu_{11}S_{22}$ array by a shear mechanism of every two cells of the $CeYb_3S_6$ array, along the ***b*** axis. This mechanism explains why the two kinds of structures are observed for the same R elements, and are often simultaneously present in the same sample when the $CeYb_3S_6$ type compounds are prepared under reducing conditions.

In all the phases which are described in this subsection, electrical equilibrium between the cations and anions is not realized, and the electrical conductivity appears to be metallic.

3.4. *Conclusions*

The large number of structures observed in the R–R′–X systems shows a very important evolution of the nature of the environment of the rare earths going from lanthanum to lutetium and a relatively strict affinity of each rare earth for a special type of environment.

4. Ternary systems IA–R–X and Tl(I)–R–X (X = S, Se, Te)

All the compounds presently known have the general formula MRX_2. In spite of the large dimensional change from the first to the last element of the IA group

TABLE 31.7

Structural types of the MRX_2 compounds (M(I) = Li, Na, K, Rb, Cs and Tl(I)).

	La	Ce	Pr	Nd	Sm	Eu	Gd	Tb	Dy	(Y)	Ho	Er	Tm	Yb	Lu	(Sc)	References
$LiRS_2$	O	O	A	A	A	A	A	A	A	A	B	B	?	?	?	?	Ballestracci (1965)
$NaRS_2$	A	A	A	A,B	B	B	B	B	B	B	B	B	?	?	?	?	Ballestracci and (1965a) Bertaut
$NaRSe_2$	A,B	B	B	B	B	AB[x]	B	B	B	B	B	B	?	?	?	?	Ballestracci and (1965a) Bertaut
$K RS_2$	B	B	B	B	B	B	B	B	B	B	B	B	?	B	?	?	Ballestracci (1965); Bronger et al. (1973)
$RbRS_2$	B	B	B	B	B	B	B	B	O	—	—	—	—	—	—	—	Bronger et al. (1973)
$CsRS_2$	B	B	O	—	—	—	—	—	—	—	—	—	—	—	—	—	Bronger et al. (1973)
$Tl(I)RS_2$	O	O	O	O	B	B	B	B	B	B	B	B	B	B	B	B	Kabré et al. (1974)
$Tl(I)RSe_2$	O	O	B	B	B	O	B	B	B	B	B	B	B	B	B	?	Kabré et al. (1974)
$Tl(I)RTe_2$	O	O	B	B	B	O	B	B	B	B	B	B	B	O	B	?	Kabré et al. (1974)

A: NaCl type.

B: $NaFeO_2$ type.

O: Two phases for the MRS_2 composition.

x: probably selenium deficient compound.

of the periodic table, only two crystal types are known, the cubic NaCl-type, and the rhombohedral $NaFeO_2$-type. These two types are closely related and the cell of the second is a distortion of the face-centered cube by decreasing or more frequently increasing the length of one of the ternary axes. In the NaCl-type, the two metal atoms have a disordered arrangement on the same metal sites. On the other hand in the $NaFeO_2$-type, the metal atoms are ordered, each being in planes perpendicular to the ternary axis which alternatively contain the R atoms and the IA atoms (or Tl(I)).

Table 31.7 shows, in the case of the parallel series $NaRX_2$ and $TlRX_2$, that the crystallographic character of the sulfides and those of the selendides are very similar. (See also Hoppe, 1968; Tromme, 1971). No information exists for the selenides formed with Li, K, Rb and Cs.

In the case of the tellurides, the only compounds described are formed with thallium (Kabré et al., 1972; 1974). They exist from Pr to Lu, with the exception of Eu and Yb and are of the rhombohedral $NaFeO_2$-type, as are the sulfides and the selenides.

The crystal structure of compounds of the $NaFeO_2$-type has been solved from single crystal determinations: for $KCeS_2$ by Plug et al. (1976) and for $TlErS_2$ by Kabré et al., (1974). In this last case, the thallium atom, which is in the center of a trigonal antiprism (nearly an octahedron), has six neighboring sulphur atoms at 3.16Å. Therefore, the stereochemical behavior of the non-bonded pair $6s^2$ of monovalent thallium is not observed. The erbium atom is in the center of a nearly regular octahedron, with six equal Er–S distances (2.76Å).

It is noteworthy that, in these two structures, the coordination of the rare earth is always 6. This value, unusual for the first lanthanides in their chalcogenides, explains the absence of the MRX_2 compounds for the light lanthanides from La to Nd in the case of M = Tl, and for La and Ce in the case of M = Li. But the very weak electronegativity of the other IA elements stabilizes this low coordination (as does the very strong electronegative character of the anions of the fluorine compounds).

5. Ternary sulfides and selenides of R(III) and divalent elements IIA, Pb and R(II)

In this section are gathered divalent elements which have the same structural behavior in their compounds. We shall see that Pb is very similar to Sr, and the divalent rare earths very similar to the alkaline earth elements. Specifically we associate Sm(II) and Eu(II) with Sr, and Yb(II) with Ca. Finally magnesium has, in this group, the most singular behavior. No information exists about Be derivatives.

5.1. *Mg derivatives*

For these compounds we find the crystal types described in section 10 for the Mn derivatives. In the case of the sulfides we observe for the light lanthanides

TABLE 31.8

Crystal structures of the $M(II)R(III)_2S_4$ compounds (and of the high temperature forms of R_2S_3).

	La	Ce	Pr	Nd	Sm(III)	Gd	Tb	Dy	Ho	Er	Tm	Yb(III)	Lu	Y
R_2S_3	γ	γ	γ	γ	γ	γ	γ	δ	δ	δ	δ	ϵ	ϵ	δ
$Yb(II)R_2S_4$	T	T	T	T	T	T	T	T	A'T	A'A	A'A	A'	A'	A'T
CaR_2S_4	T	T	T	T	T	T	T	T	A'T	A'A	A'A	A'A	A'A	A'A
$Eu(II)R_2S_4$	T	T	T	T	T	T	T	T	B	B	B	B	B	B
$Sm(II)R_2S_4$	T	T	T	T	T	T	T	T	B	B	B	B	B	B
PbR_2S_4	T	T	T	T	T	T	(T)	(T)	B	B	B	B	B	B
SrR_2S_4	T	T	T	T	T	T	B	B	B	B	B	B	B	B
BaR_2S_4	T	T	T	B,T	B	B	B	B	B	B	B	B	B	B

For the MR_2S_4 compounds:
T: cubic Th_3P_4-type
A: orthorhombic Er_2MnS_4-type
A': orthorhombic Yb_3S_4-type
B: orthorhombic $CaFe_2O_4$-type

For the R_2S_3 compounds:
γ: cubic Th_3P_4-type
δ: monoclinic Y_2S_3-type
ϵ: rhombohedral Al_2O_3 α-type

In the case of dimorphism, the first indicated form is stable at low temperature, and the second one is stable at high temperature.

TABLE 31.9
Crystal structures of the $M(II)(R(III))_2Se_4$ compounds.

	La	Ce	Pr	Nd	Sm(III)	Gd	Tb	Dy	Ho	Er	Tm	Yb(III)	Lu	Y
R_2Se_3	γ	γ	γ	γ	γ	η	η	η	φ	φ	φ	φ	φ	φ
$Yb(II)R_2Se_4$	(T)	O	O	O	O	O	O	O	A',R	A',R	A',R	R	R	A',R
CaR_2Se_4	(T)	(T)	(T)	(T)	(T)	(T)	(T)	(R)	A',R	R	R	R	R	A',R
$Eu(II)R_2Se_4$	T	T	T	T	T	(T)	(T)	B	B	B	B	B	B	B
$Sm(II)R_2Se_4$	T	T	T	T	T	T	B	B	B	B	B	B	B	B
PbR_2Se_4	T	T	T	T	T	(T)	(T)	X	X	B	B	B	B	X
SrR_2Se_4	T	T	T	T	T	T	B	B	B	B	B	B	B	B
BaR_2Se_4	T	T	T	B, T	B	B	B	B	B	B	B	B	B	B

For the MR_2Se_4 compounds:
O: no compound
T: cubic Th_3P_4-type (sol. sol. R_2X_3–MR_2X_4)
R: rhombohedral Yb_3Se_4-type (sol. sol. from YbSe or CaSe)
B: orthorhombic $CaFe_2O_4$-type
A': orthorhombic Yb_3S_4-type
X: unknown structure

For the R_2Se_3 compounds:
γ: cubic Th_3P_4-type
η: orthorhombic U_2S_3-type
φ: orthorhombic Sc_2S_3-type

( ): two phases, but the indicated solid solution stops not far from this composition.

(La to Gd), solid solutions of the cubic Th_3P_4-type, which extend from R_2S_3 to compositions generally in the neighborhood of $n = 0.10$ ($n = Mg/(Mg + R)$). Compounds of definite composition do not exist (Flahaut et al., 1965).

For the heavy lanthanides and for Y, several kinds of compounds exist:

solid solutions of the NaCl-type, which are extensive specially for the heavy lanthanides and for Y (Patrie et al., 1965).

R_2MgS_4 compounds of the Er_2MnS_4 orthorhombic type, observed with R = Tb to Tm, and Y (Patrie et al., 1966).

R_2MgS_4 compounds of the spinel type observed for R = Tm, Yb, Lu and Sc (Patrie et al., 1965). A transition to the Th_3P_4-type is observed by high pressure high-temperature treatment (Hirota et al., 1976).

R_4MgS_7 compounds of the Ho_4FeS_7 structural type occurring for R = Dy to Tm and Y (Adolphe et al., 1968).

See, for example, the similar systems formed by MnS in fig. 31.25.

In the case of selenides, only the R_2MgSe_4 compounds from Ho to Lu and for Y and Sc have the spinel structure. (Guittard et al., 1964).

5.2. *Ca and Yb(II) derivatives*

The systems formed between CaX and R_2X_3 compounds for X = S, Se, and Te are shown schematically in tables 31.8 and 31.9, which show the arrangement of the phases as a function of the composition at a temperature of 1200°C. Three types of intermediate compounds are observed.

(1) *Solid solutions of the* Th_3P_4*-type* for the light lanthanides. These solid solutions are of wider composition with the sulfides and exist from compositions R_2S_3 to CaR_2S_4. Their width decreases going to the selenides (Golabi et al., 1965b) and to the tellurides, (Pardo et al., 1969). There are no CaR_2X_4 compounds in these last two cases.

(2) *Solid solutions formed from the CaX* compounds by addition of R_2X_3 chalcogenides of the heavy lanthanides (fig. 11) have especially large composition ranges. They are least in the case of the sulfides, with a maximum composition in R of about 48 at%. They are face-centered cubic for Sm, Gd, Dy, Er and Y and show a transition to a rhombohedral distortion in the cases of Yb and Lu, at a R concentration of about 30 at% (Patrie et al., 1965, 1967).

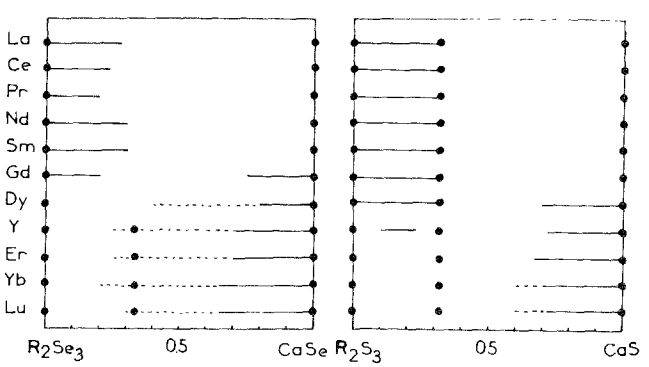

Fig. 31.11. Phases and homogeneity ranges in the R_2S_3–CaS and R_2Se_3–CaSe systems.

For the selenides (Golabi et al., 1965a,b) the solid solutions often exceed the CaR_2X_4 compositions (R = Ho to Lu and Y). With a smaller R content their structure is exactly face-centered cubic, like the CaSe compounds. But for contents of about 30 at% R, a rhombohedral distortion appears, which progressively increases with the R content. These distortions are greatest for the CaR_2Se_4 compositions. In these homogeneity ranges the CaR_2Se_4 compositions have a particular individuality shown by an extremum of the α angle of the rhombohedron.

(3) *CaR_2X_4 compounds.* In the sulfide systems there are two varieties. One is orthorhombic of the Yb_3S_4-type at low temperatures (for Ho to Lu and Y) and the other is orthorhombic of the Er_2MnS_4 type at high temperature (from Er to Lu and Y) (Patrie et al., 1967). The crystal structure of $CaLu_2S_4$ of the first type is described by Rodier et al., (1977a). In the selenide systems, we have just seen that the CaR_2Se_4 (R = Ho to Lu and Y) compounds correspond to an extremum of the rhombohedral distortion of the solid solution (Golabi et al., 1965a,b).

The $CaCe_2S_4$ compound, the only sulfide of this series to be cathodoluminescent, has a yellow emission which is of practical importance (Yim et al., 1973).

The structural behavior of the telluride system (section 14) is closely related to that of the selenides (Pardo et al., 1969).

The structures of the divalent ytterbium intermediate phases in the systems YbX–R_2X_3 are nearly identical to those of the systems formed by calcium. For the sulfides of the YbR_2S_4-type there is a cubic Th_3P_4-type (for La to Ho), and an orthorhombic Yb_3S_4-type (for Ho to Lu and Y) (Vo Van et al., 1966). For the selenides there are solid solutions of the Th_3P_4-type with the light lanthanides, and solid solutions of the NaCl-type which become rhombohedral in the neighborhood of the YbR_2Se_4 compositions (Ho to Lu and Y). Moreover, at low temperature "YbR_2Se_4" nonstoichiometric phases of the Yb_3S_4-type exist (Ho to Tm) (Souleau et al., 1969).

5.3. *Sr, Ba, Pb, Mn(II) and Eu(II) derivatives*

Compounds of the formula MR_2X_4 have the structural types given in tables 31.8 and 31.9. For the Th_3P_4 structural type, solid solutions exist continuously between R_2X_3 and MR_2X_4. Therefore, these last compounds are only observed for the light lanthanides. The compounds formed by the other elements have the orthorhombic $CaFe_2O_4$ structural type.

References to these systems are the following:

Sr and Ba sulfides	Flahaut et al. (1965a, 1965c)
	Patrie et al. (1965)
Pb sulfide	Patrie et al. (1969b)
Sm(II) sulfide	Vo Van et al. (1966, 1969)
Eu(II) sulfide	Vo Van et al. (1966, 1969)
	Hulliger et al. (1966a)
	Lugscheider et al. (1970)

Pb selenide	Patrie et al. (1969b)
Sr and Ba selenides	Patrie et al. (1964)
	Golabi et al. (1965a)
	Flahaut et al. (1965c)
Eu(II) selenide	Hulliger et al. (1966a)
	Souleau et al. (1968).

Solid solutions of the NaCl-type formed by sulfides R_2S_3 of the light lanthanides in SrS have been obtained in a flux of Li_2S and in an atmosphere of H_2S. It seems that these solid solutions, which do not exist in the absence of flux, are possible because of the substitution of rare earth for the calcium and the lithium (Banks and Ward, 1949; Yakel et al. 1949).

The magnetic properties of the compounds EuR_2S_4 and EuR_2Se_4 have been studied by Hulliger et al. (1965), (1966a,b) by Gorochov et al. (1969) and by Lugscheider et al. (1970), (1971). All these compounds are paramagnetic, and have magnetic ordering only below 4 K. Hulliger et al. found EuY_2X_4 and $EuGd_2X_4$ to be ferromagnetic, and $EuTb_2X_4$, $EuLu_2X_4$ and $EuSc_2X_4$ to be metamagnetic. In all cases, only the Eu sublattice seems to be ordered. Lugscheider et al. found all the EuR_2S_4 compounds to be antiferromagnetic below 4 K.

Coordination of the elements. In these compounds, the rare earths have their usual coordination from 8 to 6. The magnesium is six coordinated (MnY_2S_4 and Ho_4FeS_7-types) or four-coordinated (spinel) as usual. In the solid solutions of the Th_3P_4-type Mg has an unusual 8-coordinated environment, which explains the small extent of the homogeneity range.

The other divalent elements are 8-coordinated (Th_3P_4 and $CaFe_2O_4$ types), 7-coordinated (Yb_3S_4 and Er_2MnS_4 types) or 6-coordinated (NaCl type solid solutions). It is observed in this case that the coordination of the divalent element changes as a function of the coordination of the rare earths elements with which it is combined.

6. Ternary systems R–Cu–X and R–Ag–X (X = S, Se)

In these systems, the sulfides are very similar to the selenides. In contrast, the tellurides are quite different and will be discussed in section 14.

6.1. *The Cu_2X–R_2X_3 (X = S, Se) systems*

These have been studied by Ballestracci et al. (1965a,b), Julien-Pouzol et al. (1968c, 1970, 1972), Dismukes et al. (1971), and Aliev et al. (1972, 1973) when X is S and by Julien-Pouzol (1968a,b,c, 1972) and Aliev et al. (1975) when X is Se.

The distribution of the observed phases is shown in (fig. 31.12), as a function of the composition (n = Cu/(R + Cu)). Five structural types are identified.

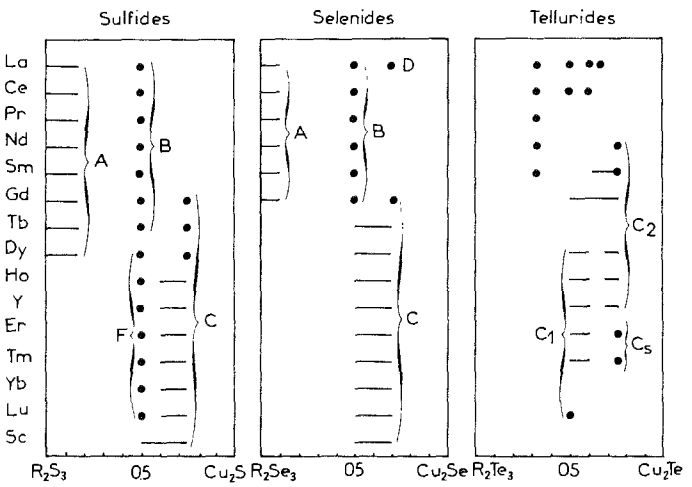

Fig. 31.12. Crystal types in the R_2X_3–Cu_2X systems. A: Th_3P_4 type, B: monoclinic unknown structure, C: solid solutions of the hexagonal $Er_{2/3}Cu_2S_2$ type, C_1: $ScCuS_2$ type, C_2: $Er_{2/3}Cu_2S_2$ type, C_s: orthorhombic superstructure of the C-type, D: orthorhombic $Cu_{13}La_5Se_{14}$, F: orthorhombic structure.

Solid solutions of the cubic Th_3P_4-type. These are formed from the R_2X_3 chalcogenides of this type. The homogeneity ranges are large in the sulfides, up to the compositions CuR_5S_8, for which the metal positions are filled. In the selenides as is usual, these homogeneity ranges are narrower (Julien-Pouzol et al., 1968a, 1972).

Monoclinic $CuRX_2$. These compounds, formed by the light lanthanides, from La to Tb for the sulfides and from La to Gd for the selenides have the space group $P2_1/b$. The structure is unknown (Julien-Pouzol et al., 1968c, 1972).

Orthorhombic $CuRS_2$. These compounds only occur in the sulfides, and are characteristic of the elements of the second part of the rare earth family (from Ho to Lu, and for Y). They have the space group $P2_12_12_1$. The structure is unknown, but seems closely related to the $AgErSe_2$-type (Julien-Pouzol et al., 1970, 1972).

Orthorhombic $La_5Cu_{13}Se_{14}$. This compound is only observed in the La_2Se_3–Cu_2Se system (Julien-Pouzol et al., 1972).

Solid solutions of the trigonal C type. These are characteristic of the heavy lanthanides, yttrium and scandium, and are observed in all the systems R_2X_3–Cu_2X for X = S, Se, Te (and also in the R_2Te_3–Ag_2Te systems). Typically, homogeneity ranges exist from $CuRX_2$ ($n = 0.50$) to $Cu_2R_{2/3}X_2$ ($n = 0.75$).

The structure of $Cu_2Er_{2/3}S_2$ was determined by Ballestracci et al. (1965b,c) from powder diagrams. In the trigonal $P\bar{3}$ cell, which contains one formula, the

atomic positions are:

$\frac{2}{3}$ Er in	1(a)	0	0	0			
2 Cu	2(d)	$\frac{1}{3}$	$\frac{2}{3}$	0.365,	$\frac{2}{3}$	$\frac{1}{3}$	0.635
2 S	2(d)	$\frac{1}{3}$	$\frac{2}{3}$	0.745,	$\frac{2}{3}$	$\frac{1}{3}$	0.255

The copper atoms have a tetrahedral coordination, and the R atom has a nearly regular octahedral environment of sulphur atoms (fig. 31.13). The $\frac{2}{3}$Er has a disordered arrangement in the 1(a) position, but without a single crystal study it is not possible to be sure of the absence of superstructure.

More recently, the structure of $CuScS_2$ was described by Dismukes et al. (1971), from single crystal determinations. The structure is nearly the same as the preceding one, but the copper atom occupies only one of the 2(d) sites. The space group is then: $P3m1$, and the atomic positions are:

Sc	1(a)	0	0	0
Cu	1(b)	$\frac{1}{3}$	$\frac{2}{3}$	0.4126
S(1)	1(b)	$\frac{1}{3}$	$\frac{2}{3}$	0.7760
S(2)	1(b)	$\frac{1}{3}$	$\frac{2}{3}$	0.2542.

At the present time, we may consider two alternatives for the solid solutions. First, a completely disordered one, for which each extremity of the homogeneity range has a disordered arrangement of copper on its positions, or of R on its positions:

$(Cu\square)RS_2$ and $Cu_2(R_{2/3}\square_{1/3})S_2$,

For the intermediate compositions, the two series of metal sites are simultaneously partially vacant, but contain only one kind of element:

$(Cu_{2-x}\square_x)(R_{(2+x)/3}\square_{(1-x)/3})S_2$,

The second possibility involves the ordered phases $CuRS_2$ and Cu_3RS_3, the first having the structural type of $CuScS_2$ and the second being a superstructure of this trigonal array. For the intermediate compositions the ordered vacant sites are progressively occupied by the supplementary atoms. It can be represented,

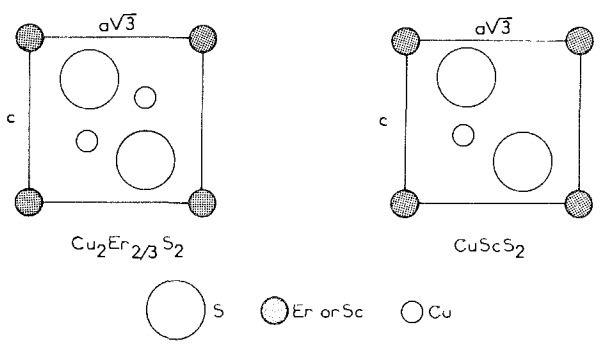

Fig. 31.13. Structures of the trigonal cells of $Cu_2Er_{2/3}S_2$ and $CuScS_2$, along the 100 planes.

for example:

$$Cu_3(Cu_{1-x}\square_x)_3R_2(R_x\square_{1-x})S_6.$$

In this case, it is possible to pass progressively from an ordered structure to a disordered one. Other alternatives are possible, and some further work is necessary on this subject.

Apparently, in the system Ag_2Te–R_2Te_3 (Pardo et al., 1973, section 14) the same two possibilities of solid solutions exist depending upon the nature of the rare earth, a disordered one for the system Gd_2Te_3–Ag_2Te, and a partially ordered one for the other rare earths.

6.2. *The Ag_2X–R_2X_3 (X = S, Se) systems*

Four families of phases have been observed (fig. 31.14) by Ballestracci [1966a,b), Julien-Pouzol et al. (1973) for the S compounds and by Julien-Pouzol et al. (1968b, 1969, 1973) for Se compounds.

Solid solutions of the Th_3P_4-type. These are nearly the same as in the Cu_2X–R_2X_3 systems (Ballestracci, 1966a; Julien-Pouzol et al., 1973).

$AgRX_2$ compounds of the $AgYbS_2$-type. This type was described by Ballestracci (1966b), from a powder diagram analysis. The tetragonal cell has the space group $I4_1md$.

The ytterbium atoms are inside nearly regular octahedra of sulphur. The silver atoms have strongly distorted octahedral environments with one of the six S

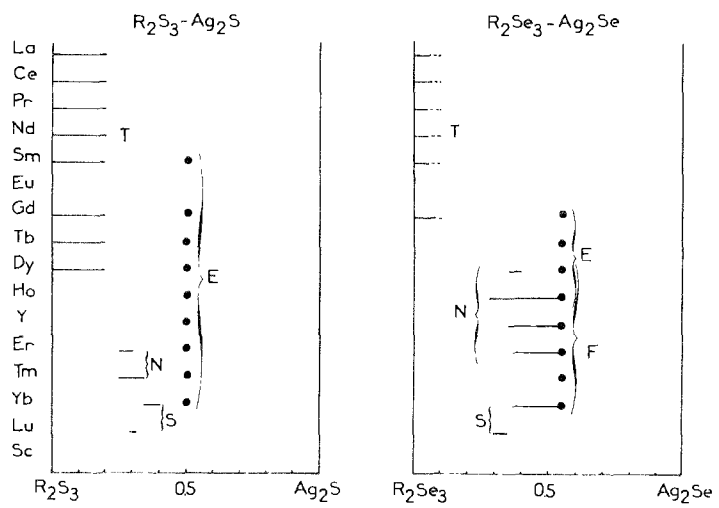

Fig. 31.14. Crystal types in the R_2X_3–Ag_2X systems. T: Th_3P_4 type, E: $AgYbS_2$ type, F: $AgErSe_2$ type, N: NaCl type solid solutions, S: tetragonal superstructure of the N type.

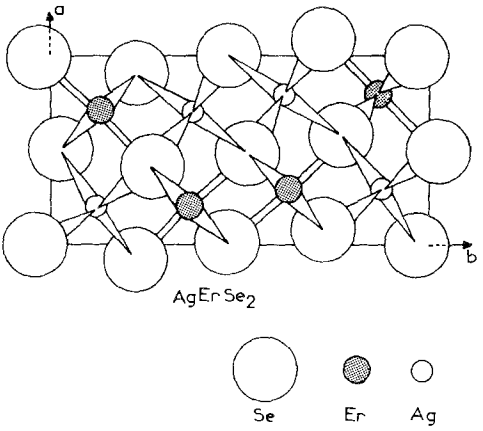

Fig. 31.15. Structure of the $AgErSe_2$, orthorhombic: $a = 6.876$ Å, $b = 13.786$ Å, $c = 4.175$ Å.

atoms very far from the Ag atom, and probably not bonded. Ballestracci observed a monoclinic distortion of this structure with the other rare earth sulfides, but this observation needs supportive studies with single crystals. Four compounds of this type are observed in the selenides series, from Gd to Ho. They are tetragonal (Julien-Pouzol et al., 1969, 1973).

$AgRSe_2$ compounds of the $AgErSe_2$-type. This structure was established, from a single crystal study, by Julien-Pouzol et al. (1977) (fig. 31.15). The flat orthorhombic cell, $P2_12_12_1$, contains four formulas. The erbium atoms are at the center of nearly regular octahedra of selenium. The silver atoms are inside flat tetrahedra, with four nearly equal Ag–S distances. These tetrahedra form open chains along the Oz direction and constitute channels in which it might be possible for the silver ions to move. These compounds are ionic conductors. They are only known in the selenides series, from Dy to Lu, and for Y and Sc (Julien-Pouzol et al., 1969, 1973).

Phases of the NaCl type. These phases were described, for the $AgRS_2$ compositions (R = Er to Lu), by Ballestracci (1967). In fact, they are nonstoichiometric phases observed for Er and Tm in the sulfide systems, and for Dy and Er and Y in the selenide systems (Julien-Pouzol et al., 1973). They occur in the Ag_2X rich region of the system, and in some cases they approach the $AgRX_2$ composition.

Superstructures of the NaCl-type. These phases are only observed for the heavy rare earths (Julien-Pouzol et al., 1973). They form homogeneity ranges similar to the preceding ones. Moreover, in the Yb–Ag–X ternary systems, the possibility of a valence change in ytterbium from 3 to 2 affords a large homogeneity surface including the $Ag_2Yb_5X_8$ composition. For this composition, a tetragonal superstructure of the NaCl type is observed, with $a' = a\sqrt{2}$ and $c = 2a$. Some additional work is necessary to define this structure precisely.

6.3. *Remarks concerning the coordination of the cations*

The known structures in these systems concern the heavy rare earths exclusively. In these cases, the rare earth atoms have their usual octahedral environment. The copper atoms always are inside tetrahedra ($CuScS_2$, $Cu_2Er_{2/3}S_2$). However, the big question concerns the Th_3P_4-type solid solutions, for which the metal atoms only have one kind of 8-coordinated site. It does not seem possible that copper atoms can accept this environment. We are obliged to admit that these atoms are displaced inside the large polyhedron of eight S atoms, in order to be bonded to only three or four S atoms (as in $La_6Cu_2Si_2S_{14}$, where the copper is shifted toward the center of a triangular face of the octahedron, section 9.2).

The silver atoms accept tetrahedral ($AgErSe_2$), five-coordinated ($AgYbS_2$) or octahedral (NaCl phases) environments. For the Th_3P_4-type solid solutions the preceding remarks are still of value.

7. Ternary compounds formed by rare earths and IIB elements

7.1. *The R_2S_3–ZnS systems*

Most of the R_2S_3–ZnS systems do not contain definite intermediate compounds. The R_2ZnS_4 compounds are only obtained for the heavy lanthanides (R = Tm to Yb). They are orthorhombic, Er_2MnS_4-type (Yim et al., 1973).

The Sc_2ZnS_4 compound is a spinel (probably normal). Its electrical and optical properties have been studied on single crystals, pure and doped with various elements. It shows a band gap in the visible ($E_g = 2.1$ eV), and its electrical conductivity, which usually is very small, is strongly increased by doping with elements like Ag, Cr or Ga. In these cases, it becomes an n-type semiconductor. It does not show cathodoluminescence (Yim et al., 1973).

7.2. *The R_2S_3–CdS systems*

The following intermediate phases are observed.

Solid solutions of the Th_3P_4-type. These are formed from R_2S_3 sulfides of this type, although their extent is not well-known. It is possible that they go to the compositional limit R_2CdS_4. However, Yim et al. (1973) observed only the Th_3P_4-type for the La_2CdS_4 phase, and obtained non-identified phases or mixtures of phases for the subsequent elements up to Dy.

Compounds R_2CdS_4 of the spinel type. These are known for the sulfides with R = Dy to Lu and for Y and Sc (Fujii, 1972; Yim et al., 1973). They are normal spinel, as shown for Yb_2CdS_4 (Holtzberg, 1963) and Tm_2CdS_4 (Suchow and Stemple 1964). Electrical (Yim et al., 1973) and optical properties (Suchow, Stemple, 1964; Yim et al., 1973) were especially studied. Infrared fluorescence (at 1.97 μm) is observed at 6 K for Tm_2CdS_4 and for various compositions of the spinel

homogeneity range formed between In_2S_3 and Tm_2CdS_4 (Suchow and Stemple (1964). Single crystals of Sc_2CdS_4 were doped with various elements. The electrical conductivity is greatly increased in some cases with the formation of p-type (Cr) or n-type (Ga) semiconductors.

Compounds R_4CdS_7 of the Ho_4FeS_7-type. These are observed for the sulfides with R = Dy to Er, and Y (Adolphe et al., 1968).

7.3. *The R_2Se_3–CdSe systems*

The compounds R_2CdSe_4 have the normal spinel structure, from Dy to Lu, and for Y (Holtzberg, 1963; Fuji, 1972). The magnetic properties of Yb_2CdSe_4 and their interpretation in terms of their crystal field are described by Pokrzywnicki et al. (1974).

8. Ternary sulfides and selenides formed by IIIB or IVB elements with R elements

The structures of the ternary compounds formed by R sulfides (or selenides) with M = IIIB or IVB sulfides (or selenides) are closely related to each other.

The elements Al, Ga, Si, and Ge are always inside MX_4 tetrahedra of S or Se atoms. In the known structures, these tetrahedra are independent from one another. On the other hand, in the corresponding ternary compounds formed by IA or IIA elements instead of the R trivalent elements, these MX_4 tetrahedra generally have common apices, and constitute chains and cycles. The R elements favor the insulation of the MX_4 tetrahedra in the ternary compounds.

The elements In and Sn in ternary compounds with the rare earths occur only in their upper oxidation states, In(III) and Sn(IV). Their environment is no longer tetrahedral but octahedral. The $[MX_6]$ octahedra are linked to each other by common edges and constitute chains through the network. In contrast, in compounds formed by IA or IIA elements instead of R elements, the In or Sn are always found inside tetrahedra $[MX_4]$.

This influence of the R elements on the atomic environments of the M elements in ternary compounds, that is, insulation of the tetrahedra and a passage to a higher coordination of the M elements, is related to a decrease in the ionic character of the R–X bond relative to the IA or IIA–X bonds. There is a concomitant increase of the ionic character of the M–X bond.

In contrast to the preceding cases Tl or Pb only exist in ternary compounds with their lower valencies, Tl(I) and Pb(II). These compounds, of general formulae $TlRX_2$ and PbR_2X_4, have classical structures, rhombohedral $NaFeO_2$-type and cubic Th_3P_4-type or orthorhombic $CaFe_2O_4$-type respectively. These compounds have been described in sections 4 and 5.

8.1. *Description of the systems*

The R_2S_3–SiS_2 systems. Three types of compounds are known at present.

Rhombohedral $R_4Si_3S_{12}$, which really is an $R_4(SiS_4)_3$ orthothiosilicate, has the $La_4Ge_3S_{12}$ structural type, R = Ce to Gd (Perez et al., 1969). Hexagonal $R_6Si_{2.5}S_{14}$ has the structure of the $R_6B_2C_2X_{14}$ family (section 9), R = Gd to Dy and Y (Michelet et al., 1970).

The R_2S_3–GeS_2 and GeS systems. The phase diagram of the La_2S_3–GeS_2 system has been described by Sarkisov et al. (1968, 1970). Two congruent compounds are present, $La_2Ge_2S_7$ (m.p. 1071°C) and La_2GeS_5 (m.p. 1105°C). The first involves a phase transition at 845°C. Actually, from the structural studies of Michelet et al. (1966, 1969a, 1970, 1975), Mazurier et al. (1973, 1974), Collin et al. (1973a) there are the three following phases in this system, $La_6Ge_{2.5}S_{14}$ which is only stable at high temperature in a disordered form, $La_4Ge_3S_{12}$ and La_2GeS_5.

For the other rare earths, the following compounds are also observed: $R_6Ge_{2.5}S_{14}$, where R = La to Ho and Y (Michelet et al., 1969a) which probably undergoes an order–disorder transition, except for the La sulfide; $R_4Ge_3S_{12}$, where R = La to Gd (Michelet et al., 1966); R_2GeS_5, where R = La (Michelet et al., 1970) and probably Ce (Beskrovnaya et al., 1971).

In the R_2S_3–GeS systems (Gus'kova et al., 1973a, 1975), the R_2GeS_4 thiogermanites exist for R = La to Gd. They disproportionate at about 600°C. Their structure is unknown.

In the ternary R–Ge–S systems (Michelet et al., 1969a), solid solutions exist between the $R_6Ge_{2.5}S_{14}$ and $R_6Ge_3S_{14}$ compositions with the same hexagonal $R_6B_2C_2X_{14}$ structure (section 9). A general view of the structural aspects of the preceding compounds has been presented by Michelet et al. (1975).

The R_2Se_3–$GeSe_2$ systems. Some R_2Se_3–$GeSe_2$ phase diagrams have been studied by Russian teams, La_2Se_3–$GeSe_2$ by Rustamov et al. (1973), and Pr_2Se_3–$GeSe_2$ by Alieva et al. (1973) and Beskrovnaya et al. (1973). A general view of the systems formed with La, Ce and Pr is given by Nasibov et al. (1975a). In these systems, which are very similar, three compounds are observed, R_2GeSe_5, $R_2Ge_2Se_7$ and $R_2Ge_3Se_9$. The first two involve phase transitions.

Recently, the La_2Se_3–$GeSe_2$ system was studied again (Loireau et al., 1977b). Two compounds were characterized. One of them, $La_6Ge_{2.5}Se_{14}$, belongs to the hexagonal $R_6B_2C_2X_{14}$ hexagonal family (section 9). The other, $La_2Ge_2Se_7$, seems only stable between 950 and 1000°C.

The ternary La_2Se_3–$GeSe_2$–Ga_2Se_3 system is described by Loireau-Lozac'h et al. (1977b).

The R_2S_3–SnS_2 and SnS systems. These have been studied by Gus'kova et al. (1973b), Mel'chenko et al. (1973) and Guittard et al. (1976a). Compounds of the general formula R_2SnS_5 exist from La to Dy with two very similar crystal types, but with different crystal type for Y.

The R_2Se_3–$SnSe_2$ and SnSe systems. The phase diagrams of the systems R_2Se_3–$SnSe_2$ have been described for R = La to Sm (Rustamov et al., 1971); Nasibov et

al., 1972, 1975b). They were found to be very similar to each other, and contain compounds of the general formulas R_2SnSe_5 and $R_2Sn_2Se_9$. However, the existence of the intermediate compounds is denied by Guittard et al. (1976a).

The R_2X_3–Al_2X_3 systems ($X = S, Se$). The La_2S_3–Al_2S_3 phase diagram is described by Guittard et al. (1976b). The hexagonal compound $La_6Al_{10/3}S_{14}$ undergoes an order–disorder transition (section 9). One other compound of probable composition $LaAl_3S_6$ exists only in a short interval of temperature. Glasses are obtained with a large range of compositions by fast cooling of the melts. The temperature of the glassy transition is relatively high at about $T_g = 550°C$. These glasses crystallize when heated, with intermediate formation of three metastable phases.

The $R_6Al_{10/3}S_{14}$ compounds, previously described as having the composition $RAlS_3$, are observed for R = La to Ho and Y, and the $R_6Al_{10/3}Se_{14}$ compounds for R = La to Ho (Patrie et al., 1969a).

The R_2X_3–Ga_2X_3 systems ($X = S, Se$). Russian workers have described the following phase diagrams:

Nd_2S_3–Ga_2S_3	Kejserukhskaya et al. (1970, 1972),
La_2Se_3–Ga_2Se_3	Efendiev et al. (1964a),
Ce_2Se_3–Ga_2Se_3	Efendiev et al. (1964d),
Nd_2Se_3–Ga_2Se_3	Efendiev et al. (1964c),
Sm_2Se–Ga_2Se_3	Efendiev et al. (1964b).

In all these cases, intermediate isostructural $RGaX_3$ compounds were observed (Karaev et al., 1966a). Their electrical properties were studied by Samsonov et al. (1967, 1968) and (Babaev et al., 1970). Actually, these compounds have the $R_6Ga_{10/3}X_{14}$ formula, and have the hexagonal structure of $Ce_6Al_{10/3}S_{14}$. Therefore, a new description of the phase diagrams R_2S_3–Ga_2S_3, for R = La, Ce, Nd, Er and Y (Loireau-Lozac'h et al., 1977a) and R_2Se_3–Ga_2Se_3 for R = La, Nd, Gd and Y (Lozac'h et al., 1973a) has been presented, which is in strong disagreement with the previous reports.

Finally, the following series of compounds has been identified (Lozac'h et al., 1973a,b; Loireau-Lozac'h et al., 1977a):

$R_6Ga_{10/3}S_{14}$, R = La to Tb and Y is hexagonal $Ce_6Al_{10/3}S_{14}$-type (Patrie et al., 1969a) with order–disorder transitions;

$RGaS_3$, R = La and Ce, of unknown structure;

$R_{10/3}Ga_6S_{14}$, R = La and Ce, is melilite-type (Lozac'h et al., 1973b);

R_3GaS_6, R = Dy to Er and Y, orthorhombic Er_3GaS_6-type (Lozac'h et al., 1971);

$R_6Ga_{10/3}Se_{14}$, R = La to Gd (Patrie et al., 1969a);

$RGaSe_3$, R = Gd to Ho, of unknown structure.

In some cases, glasses are obtained by quenching the melts from 1100–1200°C. These glasses crystallize when heated, with the formation of intermediate

phases. Their vitreous transition is about $T = 650°C$ (Loireau et al., 1976). Their vibrational properties are described by Lucazeau et al. (1977). They have strong fluorescent properties (Reisfeld et al., 1977a,b).

For the selenides, glasses are only obtained in the ternary system La_2Se_3–Ga_2Se_3–$GeSe_2$ (Loireau-Lozac'h et al., 1977b).

The R_2X_3–In_2X_3 systems ($X = S, Se$). Five series of intermediate phases have been identified (Guittard et al., 1978a) in the sulfide systems:

$RInS_3$ (?) is orthorhombic, with unknown structure, R = La to Nd;
R_3InS_6 is orthorhombic of the La_3InS_6-type, R = La to Nd;
R_3InS_6 is orthorhombic of the Sm_3InS_6-type, R = Sm to Tb
$R_3In_5S_{12}$ is monoclinic of the $Tb_3In_5S_{12}$-type, R = Sm to Tb.

From Dy to Tm, there are no intermediate compounds but only narrow solid solutions of the spinel-type from In_2S_3. With Yb, the homogeneity range is larger and exists from In_2S_3 to $YbInS_3$ (Abdullaev et al., 1968). Finally, with yttrium an orthorhombic compound $YInS_3$ has been described (Karaev et al., 1966b).

In the selenide systems which have not been extensively studied, only the $La_6In_{10/3}Se_{14}$ compound has been identified. It exists only with lanthanum for dimensional reasons (section 9) (Patrie et al., 1969a).

8.2. *Crystal structures of some special crystal types*

Compounds related to the $R_6B_2C_2X_{14}$ family. This hexagonal family will be discussed in greater detail in the next section. Three series of compounds are directly related to this type.

1. *$R_6Al_{10/3}S_{14}$ ($R = La$ to Ho and Y), $R_6Al_{10/3}Se_{14}$ ($R = La$ to Ho); $R_6Ga_{10/3}S_{14}$ ($R = La$ to Tb), $R_6Ga_{10/3}Se_{14}$ ($R = La$ to Gd) and the single indium derivative $La_6In_{10/3}Se_{14}$ (Patrie et al., 1969a).* These compounds, prepared at high temperatures and quenched, have the structure described for $Ce_6Al_{10/3}S_{14}$, or $Ce_6(Al_{4/3}\square_{2/3})\ Al_2S_{14}$, in which the Al atoms occupy, in a disordered way, the B sites of the general formula (de Saint-Giniez et al., 1968). When they are slowly cooled, an hexagonal superstructure appears ($a = a_0\sqrt{3}$, $c = 2c_0$), which certainly results in an ordering of the Al or Ga atoms and the vacancies on the B sites of the general formula. But this ordered structure has not yet been described.

2. *$R_6Si_{2.5}S_{14}$ ($R = Gd$ to Dy and Y) and $R_6Ga_{2.5}S_{14}$ ($R = La$ to Ho and Y) (Michelet et al., 1969a).* These compounds correspond to the $R_6[B_{0.5}\square_{1.5}]C_2X_{14}$ general formula. Recently, an order–disorder transition similar to the preceding one was observed (Guittard et al., 1976b). The structure of the ordered arrangement was first described for $Dy_6Ge_{2.5}S_{14}$ as a hexagonal superstructure, space group $P3$ ($a = a_0\sqrt{3}$, $c = 2c_0$), by Collin et al. (1973b). The structure of the disordered a_0, c_0 hexagonal cell was recently described by Bakakin et al. (1974) for $Pr_6Ge_{2.5}S_{14}$.

3. *$R_6Ge_3S_{14}$ ($R = La$ to Sm), (Michelet et al., 1969a).* These compounds are only

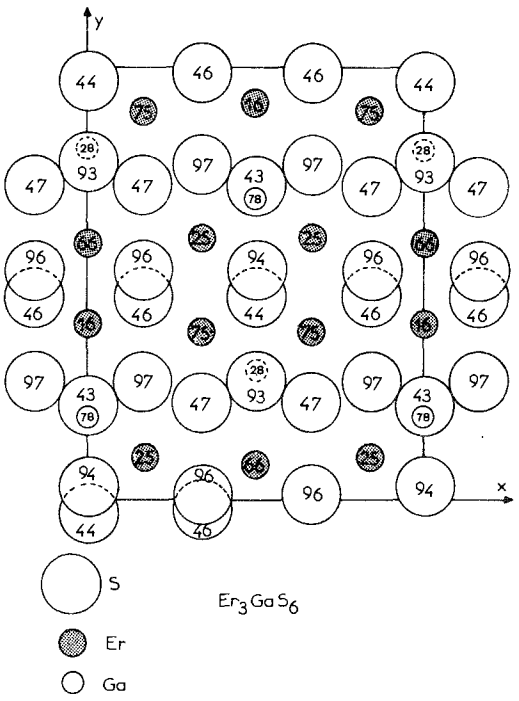

Fig. 31.16. Orthorhombic cell of Er_3GaS_6: $a = 10.36$ Å, $b = 13.12$ Å, $c = 6.40$ Å, $z = 4$.

known with the simple (a_0, c_0) hexagonal cell, corresponding to the disordered arrangement of germanium on the B sites, in agreement with the general formula $R_6(B\square)C_2X_{14}$.

In fact, there is a homogeneity range from $R_6Ge_{2.5}S_{14}$ to $R_6Ge_3S_{14}$, in which the Ge atoms which occupy the B sites are tetravalent and divalent respectively for the extreme compositions, and have mixed valencies for the intermediate compositions. The C sites are exclusively occupied by tetravalent germanium.

Er_3GaS_6-type, (*Jaulmes et al.*, 1973). The cell is orthorhombic, space group $Cmc2_1$. The Ga atoms are inside nearly regular tetrahedra (Ga–S distances 3×2.25 Å and 2.30 Å) which are independent of one another. The Er atoms have 7-prismatic coordination. The prisms are linked together by common triangular faces or common edges, and form a sheet parallel to the a, c plane. Two parallel sheets are linked by Ga tetrahedra (fig. 31.16).

Sm_3InS_6-type, (*Messin et al.*, 1977). The cell is orthorhombic, space group *Pnnm*. The In atoms are inside nearly regular octahedra of S atoms which share two of their opposite edges and form chains parallel to the c axis. The three Sm atoms have two kinds of environments, two of them have 8-prismatic coordination and the third has 7-octahedral coordination (fig. 31.17).

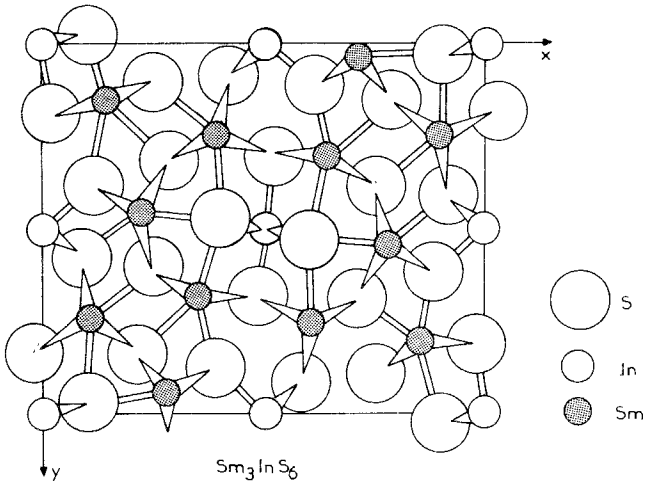

Fig. 31.17. Orthorhombic cell of Sm_3InS_6: $a = 16.51$ Å, $b = 13.63$ Å, $c = 3.901$ Å, $z = 4$.

La_3InS_6-type, (*Carré et al.*, 1978). The cell is very similar to the preceding one, but has a different space group: $P2_12_12$. The structure only differs in the environment of half the In atoms, whose coordination is no more octahedral but tetrahedral, resulting in a translation of the corresponding In atom toward a bridge of the octahedron of Sm_3InS_6. The tetrahedra are independent from one another.

The R atoms keep the same environment in the two structures.

$Tb_3In_5S_{12}$-type, (*Carré*, 1977). The monoclinic cell has space group $P2_1/m$. The In atoms have two kinds of environments with four octahedral and one tetrahedral sites. The R atoms have the same environments as in the two preceding structures (fig. 31.18).

$La_4Ge_2S_{12}$-type, (*Mazurier et al.*, 1974). This compound is rhombohedral, space group $R3c$. The Ge atoms are inside nearly regular tetrahedra of sulphur atoms, which are independent of one another. The La atoms have two different sites in prismatic environments with additional equatorial La–S bonds. The La(1) atom seems to be 9-coordinated with three long equatorial bonds. The La(2) atom is 7-coordinated, because two of the three equatorial La–S distances are too large to be true bonds. This structure can be regarded as formed by $[GeS_4]^{4-}$ anions and La^{3+} cations, and is characteristic of the orthothiogermanates.

La_2GeS_5-type, (*Mazurier et al.*, 1973). This compound is monoclinic, space group $P2_1/a$ (fig. 31.19). The coodinations of the atoms are similar to those discussed above. The La atoms are inside triangular prisms of S atoms, with two or three more S atoms in the equatorial plane of the prism. The La and S atoms constitute sheets, parallel to the a, c plane, which have the [LaS] composition

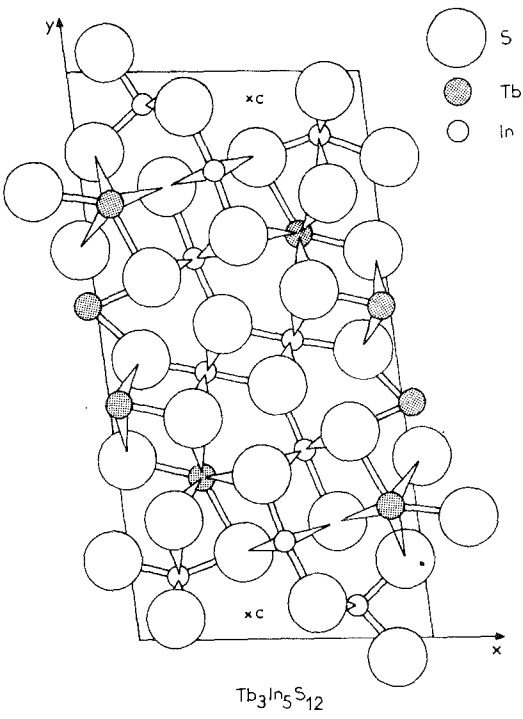

Fig. 31.18. Monoclinic cell of $Tb_3In_5S_{12}$: $a = 10.998$ Å, $b = 21.26$ Å, $c = 3.897$ Å, $\gamma = 96.3°$, $z = 2$.

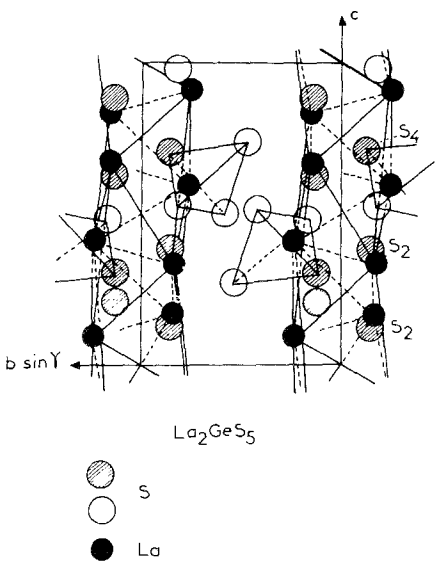

Fig. 31.19. Structure of La_2GeS_5. The shaded S atoms belong to the [LaS] sheets. The Ge atoms are not shown: they are inside the 2 central tetrahedra.

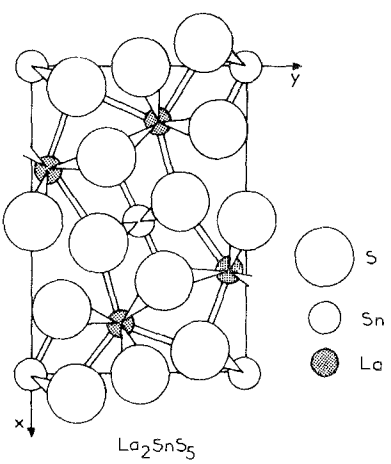

Fig. 31.20. Orthorhombic cell of La_2SnS_5: $a = 11.22$ Å, $b = 7.92$ Å, $c = 3.96$ Å, $z = 2$.

and bear some resemblance to the hexagonal sheets observed in the RXY compounds with two anions such as SmSI described in section 15. The GeS_4 tetrahedra are between the sheets, and share one S atom with only one of the sheets.

La_2SnS_5 and Sm_2SnS_5-types. These compounds (fig. 31.20) are extremely similar, and differ only in the coordination of the R atoms. They are orthorhombic, space group *Pbam*. The Sn atoms have an octahedral environment. The octahedra are bound together, as are the octahedra $[InS_6]$ in Sm_3InS_6, and constitute independent chains parallel to the *c* axis. The R atoms are inside tricapped trigonal prisms. In the case of La_2SnS_5, two of the three equatorial La–S distances are relatively long, but are nevertheless considered to correspond to true bonds yielding a coordination number of 9 for La (Jaulmes, 1974). In the case of Sm_2SnS_5, one of the equatorial Sm–S distances becomes so large that it is no longer considered a bond giving a coordination number of 8 to Sm (Guittard et al., 1976a). Thus, in the different R_2SnS_5 compounds, from R = La to Dy, although the structures are nearly identical, there is a significant change in the environments of the rare earths. The problem is to know whether or not the change is continuous or discontinuous and further structural work is necessary. From a consideration of the Guinier diagrams, it seems that a discontinuity exists between Nd and Sm suggesting that the La, Ce, Pr and Nd derivatives are of the La_2SnS_5-type, and that the Sm, Gd, Tb and Dy derivatives are of the Sm_2SnS_5-type.

9. Quaternary compounds

Two groups of quaternary compounds are well known:
– those formed by 3 metal and one non-metal atoms: tetragonal RBC_3S_7 compounds of the melilite type; hexagonal $R_6B_2L_2X_{14}$ (X = S, Se) compounds of the $Ce_6Al_{10/3}S_{14}$-type; monoclinic $R_2B_3Sn_3S_{12}$ compounds of the $Eu_5Sn_3S_{12}$ type.
– those formed by 2 metal and 2 non-metal atoms: $RBOS_2$ (with B = Sb, Bi, Cr‴, Ga, . . .) of different crystal structures; $(RO)_2Ga_{10/3}S_{14}$, tetragonal. They are two cations oxysulfides.

9.1. *The RBC_3S_7 compounds*

Compounds of the RBC_3O_7 general formula have been described by Russian workers, especially for the light rare earths, with B = Ca, Sr or Ba and C = Al or Ga (Toropov et al., 1970; Ismatov, 1970a,b,c; Ismatov et al., 1970). Similar compounds were observed for sulfides but more limited in extent (Lozac'h et al., 1973b): $RCaAl_3S_7$, R = La to Nd; $RSrAl_3S_7$, R = only La; $RCaGa_3S_7$, R = only La; $RSrGa_3S_7$, R = La and Ce; $REu''Ga_3S_7$, R = La and Ce.

These compounds are obtained by the way of glasses (prepared by quenching the melts), which are then heated at temperatures slightly above the crystallization temperatures.

In the tetragonal cell of these compounds, rare earths and alkaline earths occupy an 8-coordinated position in a disordered way (an Archimedian antiprism of non-metal atoms), while the Al or Ga atoms are in two kinds of tetrahedral sites. This structure was first described for melilite, a mineral of the composition $(Ca, Na)_2(Mg, Al, Si)_3O_7$.

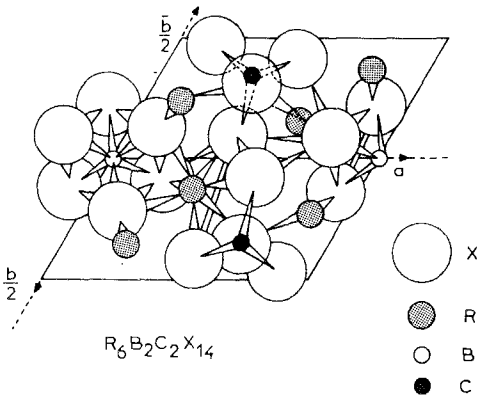

Fig. 31.21. Hexagonal lattice of the $R_6B_2C_2X_{14}$ compounds. Two half orthorhombic equivalent cells are joined in order to show the octahedral B environment.

Vacancy compounds result from the preceding structures by substitution of alkaline earths by rare earths, $R_{5/3}Ga_3S_7$ with R = La and Ce (see section 8).

9.2. *The $R_6B_2C_2X_{14}$ and related compounds*

These were first described by Guittard et al. (1968a). General views of these compounds were published by Flahaut et al. (1970) and Collin et al. (1973a) (fig. 31.21). Many compounds of this general formula are presently known (table 31.10). Moreover, in many cases the necessity of equality between cationic and anionic charges requires the existence of vacancies. These vacancies are always on the B sites and the deficient compounds presently known have the compositions $R_6(B_n\square_{2-n})C_2X_{14}$ with $n = \frac{1}{2}, \frac{2}{3}, 1$ and $\frac{4}{3}$ (table 31.11).

The cell is hexagonal, space group $P6_3$. The crystal structure was first described from $Ce_6Al_{10/3}S_{14}$ (de Saint-Giniez et al., 1968), and later with $La_6MnSi_2S_{14}$ (Michelet et al., 1969b; Collin et al., 1970a), $La_6Cu_2Si_2S_{14}$ (Collin et al., 1971b). $La_6Sn_{0.5}Si_2S_{14}$, $Dy_6Ge_{2.5}S_{14}$ or $Dy_6Ge_{0.5}Ge_2S_{14}$, $La_6In_{2/3}Si_2S_{14}$ (Collin et al., 1973b) and $Pr_6Ge_{2.5}S_{14}$ (Bakakin et al., 1974).

It appears that, in all cases, disordered arrangements of vacancies and atoms on the B sites occur in samples obtained at sufficiently high temperatures and quenched. But, superstructures have been observed in samples cooled slowly or prepared at appropriate temperatures. Three kinds of superstructures are known:

$$\left.\begin{matrix}La_6Sn_{0.5}Si_2S_{14}\\ Dy_6(Ge_{0.5})Ge_2S_{14}\end{matrix}\right\} \quad a = a_0\sqrt{3} \quad c = 2c_0 \text{ space group } P3;$$

$$La_6(In_{2/3})Si_2S_{14} \quad a = a_0\sqrt{3} \quad c = 3c_0 \text{ space group } P6_3;$$

$$La_6(Ga_{4/3})Ga_2S_{14} \quad a = a_0\sqrt{3} \quad c = 2c_0.$$

The superstructures have been solved in the first two cases (Collin et al., 1973b).

In the hexagonal sub cell a_0, c_0 the R atom is in a triangular prism of X atoms with two additional X atoms in the equatorial plane of the prism. One of the R–X

TABLE 31.10.
Saturated $R_6B_2C_2X_{14}$ compounds.

R site	B site	C site	Formulas	References
Ln(III)	Cu(I), Ag(I)	Si(IV)	$Ln_6Cu_2Si_2S_{14}$	(a) Guittard et al. (1968a, 1970)
			$Ln_6Ag_2Si_2S_{14}$	(a) Guittard et al. (1970)
		Ge(IV)	$Ln_6Cu_2Ge_2S_{14}$	(a) Guittard et al. (1970)
			$Ln_6Ag_2Ge_2S_{14}$	(b) Guittard et al. (1970)
		Sn(IV)	$Ln_6Cu_2Sn_2S_{14}$	(c) Collin et al. (1972)
	Mg(II)	Al(III)	$Ln_6M(II)_2Al_2S_{14}$	(b) Collin et al. (1970a,b)
	Ti(II)–Ni(II)			
	Zn(II) Cd(II)	Ga(II)	$Ln_6Mn_2Ga_2S_{14}$	(c, d) Collin et al. (1972)
Y(III)	Ti(III)–Cr(III)			
	Sb(III) Bi(III)			
	Sc(III)	Be(II)	$Ln_6M(III)_2Be(II)_2S_{14}$	(b) Collin et al. (1972)
	Yb(III) Lu(III)			
	In(III)			
Eu(II)–(III)	Ti(III)–(II)	Si(IV)	$Eu_2Ti_2M(IV)_2S_{14}$	(b) Collin (1971)
		Ge(IV)		
		Sn(IV)		
Eu(II)	Ti(III)	P(V)	$Eu_2M(III)_2P_2S_{14}$	(b) Collin (1971)
Sr(II)	V(III)		$Sr_2M(III)_2P_2S_{14}$	
	Cr(III)			

a: the corresponding selenides exist. b: no corresponding selenides. c: no information about possible selenides. d: similar compounds exist with other B(II) elements, but they are not described.

TABLE 31.11.
Vacancy compounds $R_6B_nC_2X_{14}$.

Saturated formulas	n value	Corresponding deficient formulas	Studied structures
$Ln_6B(I)_2C(IV)_2X_{14}$	1	$Ln_6(B(II)\square)C(IV)_2X_{14}$	$Nd_6Ge_3S_{14}$ $La_6MnSi_2S_{14}$
	$\frac{2}{3}$	$Ln_6(B(III)_{2/3}\square_{4/3})C(IV)_2X_{14}$	$Ln_6In_{2/3}Si_2S_{14}$
	$\frac{1}{2}$	$Ln_6(B(IV)_{1/2}\square_{3/2})C(IV)_2X_{14}$	$La_6Sn_{1/2}Si_2S_{14}$ $Dy_6Ge_{2.5}S_{14}$
$Ln_6B(II)_2C(III)_2X_{14}$	$\frac{4}{3}$	$Ln_6(B(III)_{4/3}\square_{2/3})C(III)_2X_{14}$	$Ce_6Al_{10/3}S_{14}$
	1	$Ln_6(B(IV)\square)C(III)_2X_{14}$	$La_6SnAl_2S_{14}$
$Ln_6B(III)_2C(II)_2X_{14}$	$\frac{3}{2}$	$Ln(B(IV)_{3/2}\square_{1/2})C(II)_2X_{14}$	No known compound

equatorial distances is nearly parallel to the c_0 axis, and the other is oblique. Their relative value is therefore strongly dependent on c_0/a_0. For relatively small values of c_0/a_0, the coordination of the R atom is 8, characteristic of light rare earths. For relatively large values of c_0/a_0, the interatomic distance R–X which is parallel to the c_0 axis is too long for a bond, and hence the coordination is only 7, characteristic of the heavy rare earths.

The B site is on the hexagonal axis inside a trigonal antiprism of X atoms, which can be viewed as a slightly distorted octahedron. Elements which usually have an octahedral environment in their compounds (Mg, 3d elements) occupy the center of the antiprism. Elements which usually have lower coordinations (e.g. 4 for Si, Ge(IV) or Sn(IV); 3 for Al or Ga; or 2 for Ag or Cu) are not at the center, but are displaced along the hexagonal axis in order to shorten 3 of the B–X interatomic distances and to lengthen the other three. For instance, for Al in $Ce_6Al_{10/3}S_{14}$ the Al–S interatomic distances are 3 at 2.24 Å and 3 at 2.09 Å (fig.

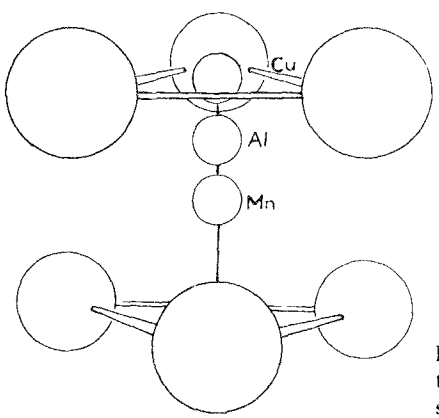

Fig. 31.22. Relative dispositions of the B cations inside the B octahedral sites of the hexagonal $R_6B_2C_2X_6$ structure.

31.22). The limiting case is observed for Cu atom which is exactly in the plane of the three S atoms at the base of the antiprism in $La_6Cu_2Si_2S_{14}$. The three short Cu–S distances are 2.27 Å while the three long ones are 3.61 Å and do not correspond to bonds. Therefore, according to the position of the atom inside the antiprism along the 6-fold axis, the coordination goes from 6 to 3. The possibility of this variation in coordination explains the large number of compounds of this structural type.

The C site is on the 3-fold axis, inside a tetrahedron of X atoms. These sites are exclusively occupied by elements which usually are 4-coordinated in their compounds, and mainly form covalent bonds (especially for Al, Ga, Si, Ge and SnIV).

Some elements can simultaneously occupy the B and C sites: Al, Ga, In, Si and Ge. In this case, ternary compounds are formed, (section 8). These are: $R_6Al_{10/3}X_{14}$, $R_6Ga_{10/3}X_{14}$, (X = S, Se) (Patrie et al., 1969a), $R_6Si_{2.5}S_{14}$, $R_6Ge_{2.5}S_{14}$, $R_6Ge_3S_{14}$, $R_6Ge_3Se_{14}$ (Michelet et al., 1969a; Guittard et al., 1970).

9.3. *$R_2B_3Sn_3S_{12}$ compounds*

These compounds have structures of the $Eu_5Sn_3S_{12}$ type (Jaulmes et al., 1977a) (fig. 31.23), orthorhombic $Pm2_1b$, in which the europium has the two valences 2 and 3, specifically $Eu(III)_2Eu(II)_3Sn(IV)_3S_{12}$ (section 13). It is possible to substitute a trivalent rare earth for Eu(III), and a divalent element for Eu(II) if they have the same crystallochemical behavior especially Sr and Pb:

$R_2(III)Eu(II)_3Sn_3S_{12}$	for La to Yb and Y;
$R_2(III)Sr_3Sn_3S_{12}$	for La to Yb and Y;
$R_2(III)Pb_3Sn_3S_{12}$	for La to Gd.

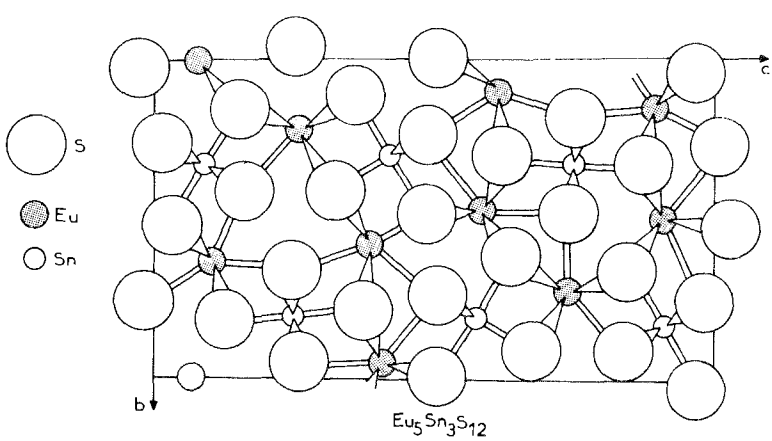

Fig. 31.23. Orthorhombic $Pm2_1b$ cell of $Eu_5Sn_3S_{12}$: $a = 3.924$ Å, $b = 11.509$ Å, $c = 20.219$ Å.

The trivalent rare earths are in one 8-prismatic and in one special 7-coordinated site. The divalent elements, europium (II), strontium or lead, are in 7- or 8-coordinated prisms. The tin IV occupies two nearly octahedral sites and one 5-coordinated triangular bipyramidal site. Other possibilities exist for the filling of the sites with the formation of superstructures.

9.4 *Two cations oxysulfides*

In the La_2O_2S–Ga_2S_3 system (Guittard et al., 1977), 3 intermediate compounds are present: $(LaO)_4Ga_{8/3}S_6$ tetragonal, $LaGaOS_2$ orthorhombic and $LaGa_3OS_5$. The structure of the first compound shows the presence of (LaO) sheets, which alternate with gallium sulfide sheets. In this case, oxygen atoms are only bonded to the lanthanum atoms, and gallium atoms are only bonded to the sulfur atoms. In contrast, the structure of $LaGaOS_2$ (Jaulmes, 1978) is not a sheet structure, and the O and S atoms are bonded to the two metal atoms, without preferential bonding.

In the R_2O_2S–Sb_2S_3 or Bi_2S_3 systems only exist one intermediate compound (RO)BiS_2 (R = La to Pr) or (RO)SbS_2 (R = La to Nd) (Pardo et al. 1976). Two different crystal types are observed; one of them is described for (CeO)BiS_2 (Ceolin et al., 1976): it is a sheet structure, with alternating sheets of (CeO) and sheets of bismuth sulfide.

Glasses are obtained in the R_2O_2S–Ga_2S_3 systems, especially with R = La (Guittard et al., 1978b). Similar glasses can be prepared with a third sulfide; in the case of Ag_2S, the glasses are ionic conductors (Carcaly et al., 1978).

10. Ternary sulfides and selenides of the rare earths and the 3d elements

The 3d elements, from which we exclude scandium studied in the section 3 with the rare earths, exhibit primarily the two oxidation states +2 and +3 in their ternary chalcogenides. The +2 oxidation state is the more frequent from Cr to Ni and is the only one in the case of Mn and Ni. The +2 state is observed as tabulated below.

R_4MS_7 where R = La to Nd and M = Co, Ni (Collin et al., 1974b) is tetragonal of La_4NiS_7 type. Where R = Y and Dy to Yb and M = Cr, Mn, Fe (Adolphe et al., 1968; Patrie et al., 1969c) it is monoclinic of the Ho_4FeS_7 type; (table 31.12). This last type is also observed in the Dy_4MSe_7 selenides where M = Cr, Mn, Fe (Souleau et al., 1966).

$R_8M_3S_{15}$ or $R_{32.66}M_{11}S_{60}$ where R = La and Ce and M = Cr, Mn, Fe is monoclinic of the $La_{32.66}Mn_{11}S_{60}$ type (Colin et al., 1974a).

R_2MS_4 where R = Tm to Lu and Sc and M = Mn and Fe (Patrie et al., 1964) is a direct spinel and where R = Tb to Yb and M = Mn, Fe (Patrie et al., 1966) it is an orthorhombic Er_2MnS_4 type; or where R = Ho to Yb and Y and M = Cr (Tomas et al., 1976a) it is an orthorhombic Er_2CrS_4 type. The spinel

TABLE 31.12
R_4MS_7 compounds of the Ho_4FeS_7-type (identical to the Y_5S_7-type)

	Gd	Tb	Dy	(Y)	Ho	Er	Tm	Yb	Lu	Ref.
R_5S_7 compounds		+	+	+	+	+	+			
R_4VS_7			+		+	+	+			b
R_4CrS_7				+	+	+	+			a
R_4MnS_7			+	+	+	+	+	+		a
R_4FeS_7				+	+	+	+	+		a
R_4MgS_7			+	+	+	+	+			a
R_4CdS_7				+	+	+	+			a

a: Adolphe et al. (1968); b: Patrie et al. (1969c).

type is also observed for selenides where R = Lu, Y, Sc and M = Mn only (Guittard et al., 1966).

$R_2M_2S_5$ where R = La and Ce and M = Cr, Mn, Fe (Patrie et al., 1968) is orthorhombic of $La_2Fe_2S_5$ type.

The +3 oxidation state is most often observed in the chromium derivatives. The $RCrS_3$ sulfides were described by Takahashi et al. (1973) and the $RCrSe_3$ selenides by Nguyen et al. (1971).

With iron, the +3 state is only known in $LaFeS_3$ (Takahashi et al., 1971). In some cases, intermediate oxidation states are observed. For instance, in the $La_2Fe_2S_5$ structure all the iron is in the +2 state. However, Fe^{3+} ions and vacancies in the iron sites appear in the nonstoichiometric $La_2Fe_{1.87}S_5$ and $La_2Fe_{1.76}S_5$ compounds (Besrest et al., 1977, 1978).

Very little information exists about ternary derivatives of titanium and vanadium.

10.1. *Description of the various systems*

10.1.1. *R–Ti–X and R–V–X systems*

There has been no structural study made on the phases observed in these systems which often have complicated structures. For the trivalent state of titanium or vanadium some phases have been pointed out, but the description of the networks should be reexamined. $LaTiX_3$ where X = S, Se and $LaVX_3$ where X = S, Se are probably monoclinic (Donohue, 1975). $R_6Ti_4S_{15}$ where R = La to Gd and $R_6V_4S_{15}$ where R = La to Gd are probably also monoclinic (Patrie et al., 1969c).

Phases in which titanium or vanadium are in the divalent state have well-known crystal types. There are, for example, R_4VS_7 of the Ho_4FeS_7 type (table

31.12) and Yb_2TiS_4 and Yb_2VS_4 of the Yb_3S_4 type, whose magnetic properties seem to show mixtures of II and III valences for the two metal elements (Patrie et al., 1969c).

10.1.2. *R_2S_3–CrS systems*

The chromium 2+ ion has a t_{2g}^3, e_g^1 electronic configuration for an octahedral environment in low field. It therefore presents a Jahn–Teller effect with distortion of the CrS_6 octahedron, two of the opposite Cr–S bounds being longer than the other four. This Jahn–Teller distortion is observed only for a sufficiently high proportion of Cr(II) ions relative to the other metal atoms. It exists in the R_2CrS_4 compounds which present a distortion of the CrS_6 octahedron relative to the Er_2MnS_4 crystal type, (Tomas et al., 1976b) but it is not observed in the R_4CrS_7 compounds which have the Ho_4FeS_7 crystal type. The phases presently known are indicated in fig. 31.24.

R_2CrS_4 compounds. They exist from Ho to Yb, and for yttrium (Tomas et al., 1976a). Their X-ray diagrams are very similar to those of the Er_2MnS_4-type with which they were first confused (Patrie et al., 1966).

$La_{32.66}Cr_{11}S_{60}$. This compound, only known with La, has the $La_{32.66}Fe_{11}S_{60}$ structural type (Collin et al., 1974a).

R_4CrS_7 compounds. They exist from Ho to Tm and for Y (Adolphe et al., 1968). No solid solutions were observed (see for example the description of the CrS–Y_2S_3 system (Flahaut et al., 1962)).

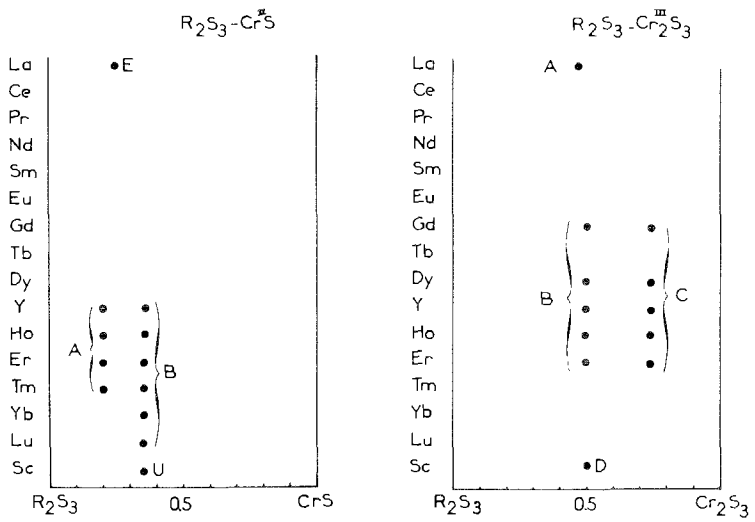

Fig. 31.24. Crystal types in the R_2S_3–CrS systems. A: Er_4MnS_7 type, B: Er_2CrS_4 type, E: $La_{2.66}Cr_{11}S_{60}$, U: Sc_2CrS_4. Crystal types in the R_2S_3–Cr_2S_3 systems, A: $LaCrS_3$ type, B: monoclinic $RCrS_3$ compounds, C: RCr_3S_6 compounds, D: $ScCrS_3$ type.

10.1.3. R_2S_3–Cr_2S_3 systems

$RCrS_3$ compounds. They seem to exist for all the rare earths, but not all are described (Takahashi et al., 1971, 1973). $LaCrS_3$ has a special monoclinic structure which was solved by Kato et al. (1977). $DyCrS_3$ has an unknown orthorhombic structure. $YCrS_3$, $GdCrS_3$, $HoCrS_3$ and $ErCrS_3$ have the same monoclinic structure, called the $YCrS_3$ structure, which is also unknown. The optical absorption of these compounds was described in the range 0.15–1.7 eV. In all cases, a sharp absorption edge was found at 1.20–1.30 eV at room temperature.

The $ScCrS_3$ compound has a rhombohedral structure which is a distortion of the NaCl array (Dismukes et al., 1970).

RCr_3S_6 compounds. They exist for yttrium and from Gd to Er (Takahashi et al., 1974). Their optical properties were described by Ametani (1974) but their structure is still unknown.

10.1.4. R_2Se_3–$CrSe$ systems

The only compound which has been described is Dy_4CrSe_7. Other phases do not appear (Souleau et al., 1966).

10.1.5. R_2Se_3–Cr_2Se_3 systems

$RCrSe_3$ compounds. Only one series of isostructural compounds (from La to Nd) exists. Their crystal structure was described for $CeCrSe_3$ (Nguyen et al., 1969, 1971). The magnetic and electrical properties of polycrystalline samples and single crystals were described by McKinzie et al. (1971) and by Gorochov et al. (1971, 1973). All these compounds are antiferromagnetic with Néel temperatures between 160 K for $LaCrSe_3$ and 180 K for $NdCrSe_3$, but the magnetic behavior is a relatively complicated one. Above the Néel point the positive Weiss constants indicate ferromagnetic intrachain Cr–Se–Cr interactions. As the temperature is lowered through the Néel point, longer antiferromagnetic Cr–Se–Se–Cr interactions between the chains become dominant. At still lower temperatures, there may be a canting of the spins which would give rise to a weak ferromagnetism. The resistivity and Hall effect show these compounds to be extrinsic semiconductors at room temperature.

10.1.6. R_2S_3–MnS systems

Six series of phases have been identified, most of them being also observed with Mg (section 5.1, fig. 31.25).

Solid solutions of the Th_3P_4-type. These solutions have nearly the same extent as in the MgS–R_2S_3 systems. They never attain the composition R_2MnS_4 corresponding to the complete filling of the metal positions (Flahaut et al., 1965c).

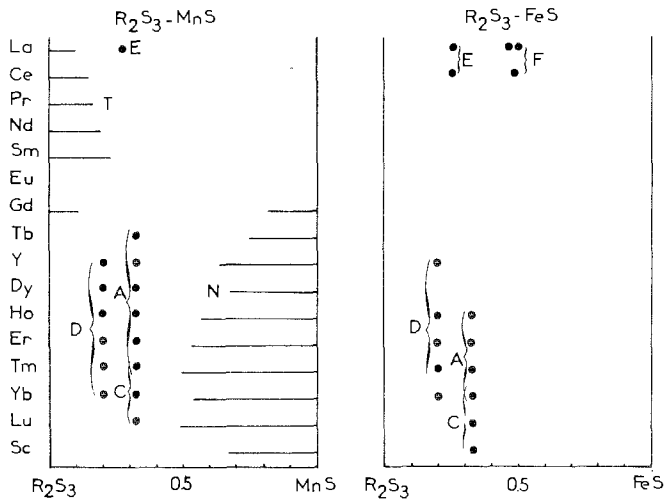

Fig. 31.25. Crystal types in the R_2S_3–MnS and R_2S_3–FeS systems, A: Y_2MnS_4 type B: Er_2CrS_4 type, C: spinel type, D: Ho_4FeS_7 type, E: $La_{32.66}Mn_{11}S_{60}$, F: $La_2Fe_2S_5$ and non-stoichiometric related super-structures, N: NaCl type, T: Th_3P_4 type.

Solid solutions of the NaCl-type. Manganese is the only 3d element having a sulfide of the NaCl-type, and it is able to form solid solutions with the R_2S_3 sulfides. The homogeneity ranges are especially large for the heavy rare earths, and nearly identical to those observed for MgS. In the case of Sc_2S_3 a discontinuity in the variation of the parameter is probably due to a superstructure (Barthélémy, 1971). In these solid solutions, the exchange interactions characteristic of pure MnS decrease very rapidly as a function of the R_2S_3 content (Barthélémy, 1971).

R_2MnS_4 compounds. They have two crystal types, orthorhombic of the Er_2MnS_4 type from Tb to Tm and for Y (Patrie et al., 1966) and cubic normal spinel from Tm to Lu and Sc (Patrie et al., 1964). The spinel Yb_2MnS_4 was studied extensively by Longo et al. (1967). The transition from the spinel to a new cubic Th_3P_4-type is achieved by high pressure in the cases of Tm_2MnS_4 and Yb_2MnS_4, as in the corresponding derivatives of magnesium (Hirota et al., 1976).

The magnetic properties of the R_2MnS_4 compounds have been studied by Barthélémy (1971). They have a normal paramagnetic behavior up to about 10 K, except for the compounds formed by non-magnetic rare earths Y_2MnS_4, Lu_2MnS_4 and Sc_2MnS_4, which are antiferromagnetic at low temperature. The exchange interactions of Sc_2MnS_4 are described by Wojtowicz et al. (1969).

In the solid solution $Mn_xMg_{1-x}Y_2S_4$, anomalous behavior of the magnetic properties are explained by the disordered distribution of Mn, Mg and Y on the same octahedral sites (Heikens et al., 1973).

R_4MnS_7 compounds. They exhibit the Ho_4FeS_7 structural type where R = Dy to Yb and Y (Adolphe et al., 1968). Their magnetic properties were studied by Barthélémy (1971).

$La_{32.66}Mn_{11}S_{60}$ compound. It is the only representative of this structure in these systems (Collin et al., 1974a).

10.1.7. *R_2Se_3–MnSe systems*

The only selenides which exist in these systems are:

(1) *Dy_4MnSe_7* of the Ho_4FeS_7-type. (The other rare earths only give mixtures of constituent selenides.) (Souleau et al., 1966).

(2) *R_2MnSe_4* of the spinel type for R = Yb, Lu and Sc (Guittard et al., 1966). For the other R elements unidentified ternary compounds probably exist.

10.1.8. *R_2S_3–FeS systems*

These are very similar to the R_2S_3–MnS systems so far as the nature of the intermediate phases are concerned. Indeed, for the heavy lanthanides we observe R_2FeS_4 compounds of the Er_2MnS_4-type for R = Ho to Yb, the spinel type for R = Y, Lu and Sc, and R_4FeS_7 compounds of the Ho_4FeS_7-type for R = Ho to Yb and Y. Likewise, for the light lanthanides we observe phases of the $La_{32.66}Mn_{11}S_{60}$-type with La and Ce. There is, however, an absence of the Th_3P_4-type solid solutions with light lanthanides, and of the NaCl-type solid solutions with heavy lanthanides and yttrium (Patrie et al., 1969c) (fig 31.25).

In addition, there exist new phases $La_2Fe_2S_5$ and $Ce_2Fe_2S_5$ (Patrie et al., 1968) and nonstoichiometric phases which were studied with lanthanum derivatives $La_2Fe_{2-x}S_5$ with $x = 0.13$ and 0.24. These nonstoichiometric compounds are superstructures of $La_2Fe_2S_5$ in which part of the iron sites are partially vacant while some of the iron atoms become trivalent (Besrest, 1975; Besrest et al., 1977, 1978), (fig. 31.26). $La_2Fe_2S_5$ is antiferromagnetic at low temperature, with a Néel point of 11 K (Collin et al., 1973d). Its magnetic structure was determined at 4.2 K. It shows superexchange interactions between Fe^{2+} ions located in the chains. The nearest neighbor chains are uncoupled but coupling between next nearest neighbour chains is realized through super–super exchange interactions of the type Fe–S–S–Fe, or possibly more complex paths including La^{3+} (Plumier et al., 1974).

10.1.9. *R_2S_3–Fe_2S_3 systems*

A hexagonal compound was described by Takahashi et al. (1971) for the $LaFeS_3$ composition. However, a structural study of Collin (1978) concludes that this phase belongs to the $R_6B_2C_2X_{14}$ hexagonal family (section 9) and really has the $La_6Fe_{10/3}S_{14}$ composition. In this case, the two tetrahedral C sites are fully occupied by Fe^{3+} ions, and the two octahedral B sites are partially occupied in a disordered way by $\frac{4}{3}Fe^{3+}$ ions, in agreement with the general rule.

10.1.10. *R–Co–X and R–Ni–X systems*

The compound $LaCoS_3$, in which the Co has the surprising +3 oxidation state, was described by Takahashi et al. (1971). Collin et al. (1974b) have obtained the

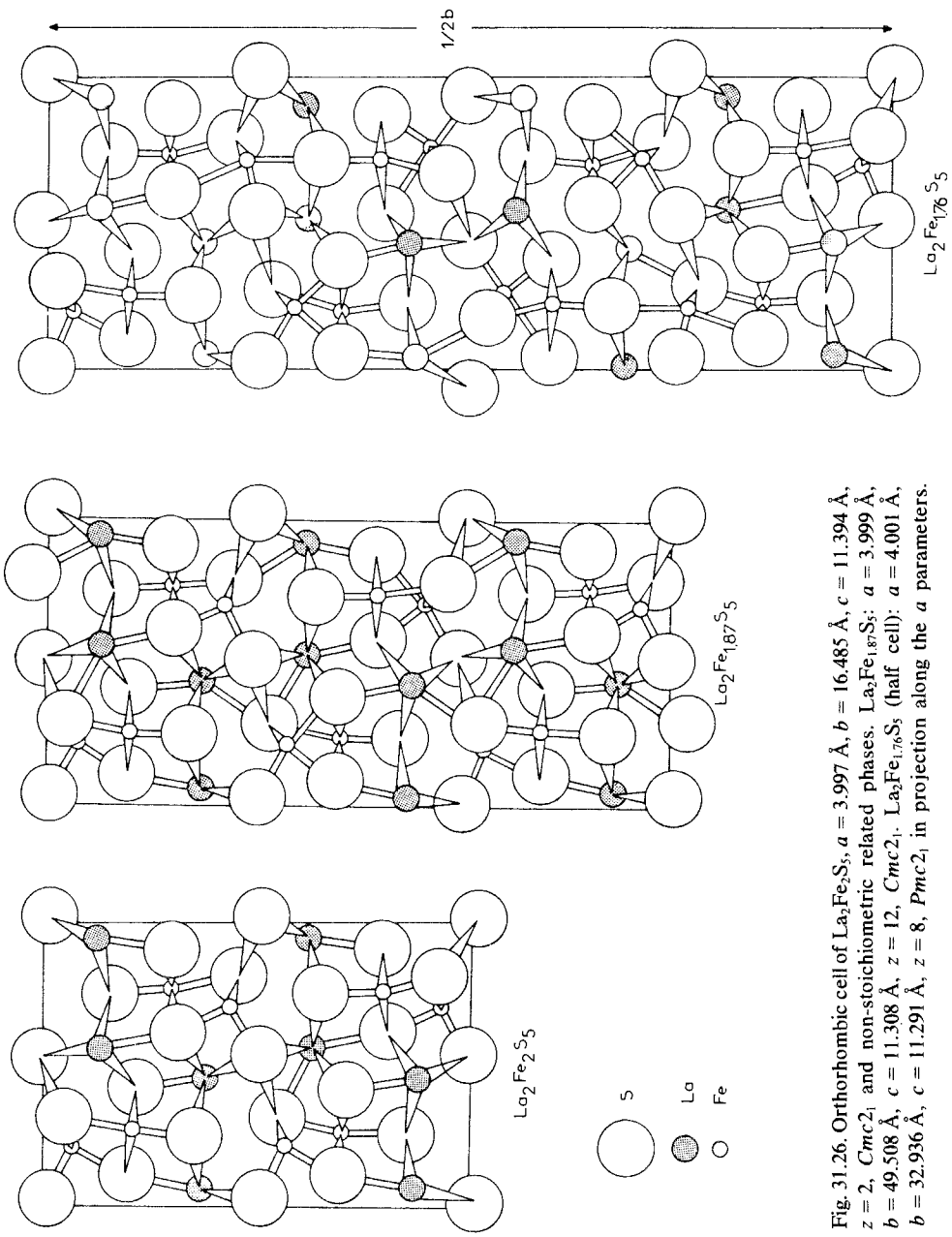

Fig. 31.26. Orthorhombic cell of $La_2Fe_2S_5$, $a = 3.997$ Å, $b = 16.485$ Å, $c = 11.394$ Å, $z = 2$, $Cmc2_1$ and non-stoichiometric related phases. $La_2Fe_{1.87}S_5$: $a = 3.999$ Å, $b = 49.508$ Å, $c = 11.308$ Å, $z = 12$, $Cmc2_1$. $La_2Fe_{1.76}S_5$ (half cell): $a = 4.001$ Å, $b = 32.936$ Å, $c = 11.291$ Å, $z = 8$, $Pmc2_1$ in projection along the a parameters.

tetragonal compounds R_4CoS_7 for R = La and R_4NiS_7 where R = La to Nd in which the transition element is normally divalent.

10.2. *Description of the structural types*

The so-called "spinels". Patrie et al. (1964) first described R_2MnS_4 spinels and R_2FeS_4 spinels (R = Yb, Lu and Sc). Riedel et al. (1977) published a study of polycrystalline spinel $Fe_{1+x}Yb_{2-x}S_4$, with $0 \leq x \leq 0.4$. From Mossbaüer spectra it appears that xFe is trivalent. From X-ray powder studies, the tetrahedral site is occupied by iron only, and the octahedral site by a mixture of Fe and Yb. Recently, Tomas et al. (1978) found from single-crystal X-ray and Mössbauer studies, that the tetrahedral site is not fully filled by Fe atoms, and that Yb atoms and some of the Fe atoms occupy 2 series of octahedral sites. The occupancy factors are: tetrahedral site 8a: 0.8 Fe, normal octahedral site 16d: 0.8 Yb + 0.09 Fe, octahedral site 16c: 0.13 Yb + 0.01 Fe.

$LaCrS_3$ type. The large triclinic cell contains 64 formula units. The structure consists of alternating layers of LaS and CrS_2. The LaS layers have a NaCl-like atomic arrangement. The CrS_2 layers have a CdI_2 like intralayer structure. The two kinds of layers are stacked without strict commensurability between them (Kato et al., 1977).

$LaCrSe_3$-type. The orthorhombic *Pnam* structure is identical with that of NH_4CdCl_3 (fig. 31.27). The Cr atoms are inside nearly regular tetrahedra which share opposite edges to form zig-zag chains parallel to the short axis of the cell. These chains are separated by $CrSe_9$ polyhedra, formed by tricapped trigonal prisms (Nguyen et al., 1971).

$La_{32.66}Mn_{11}S_{60}$-type. This formula is contained in a monoclinic cell of space group *Bm*. There are 28 positions for lanthanum in this cell, of which 12 are only partially filled (occupancy factors 0.63 to 0.82). Their coordination is 7–8. Eight manganese atoms are inside distorted octahedra. On the other hand, six other very special positions at very short distances from one another (1.95–1.96 Å) are, in groups of three, in the same cavity formed by 12 S atoms. These positions are half filled by the Mn atoms. Here is the first example of clusters of 3d elements with metal–metal bonds. The same structure was observed with the iron derivative (Collin et al., 1974a).

Er_2MnS_4-type. This structure, previously described by way of Y_2MnS_4 (Chevalier, 1968), was solved later with better accuracy from a crystal of Er_2MnS_4. The cell is orthorhombic, space group $Cmc2_1$. The metal atoms have two kinds of positions, one is a 7-coordinated site (7-prismatic) which contains one of the two Er atoms of the formula. The second type consists of two 6-coordinated sites (octahedral) containing a mixture in equal proportions of the second Er atom and the Mn atom in a disordered arrangement

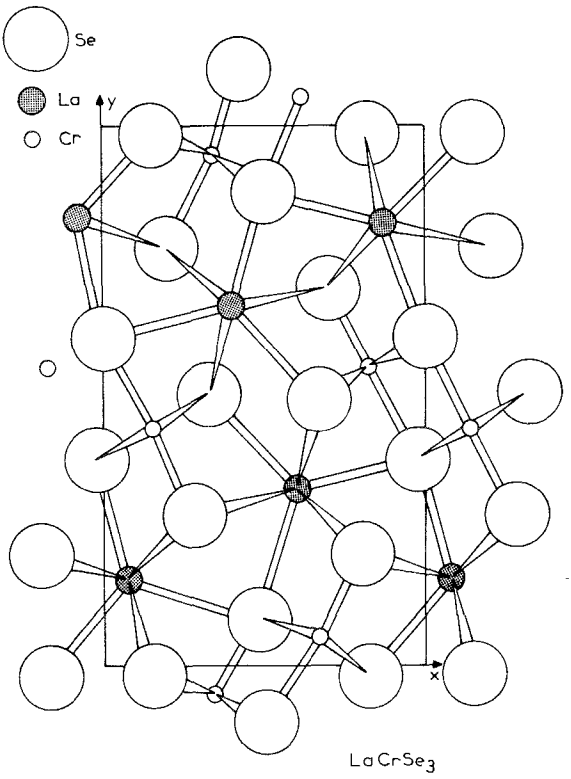

Fig. 31.27. Orthorombic cell of $LaCrSe_3$. $a = 8.08$ Å, $b = 13.74$ Å, $c = 3.95$ Å, $z = 4$.

Er_2CrS_4-type. This structure is very similar to the preceding one. It is the consequence of the ordered distribution of the Er and Cr atoms on the octahedral sites. The orthorhombic $Pb2_1a$ cell, which results from this order, is twice as large. Whereas the ErS_6 octahedron is nearly regular, the CrS_6 octahedron is very distorted, with a lengthening of two opposite Cr–S distances, and a relatively large variation of the length of the other four bounds (Tomas et al., 1976b). This distortion, and the ordering, are the consequences of the Jahn–Teller effect of Cr(II) in a weak field.

$La_2Fe_2S_5$-type and related vacancy structures. The cell of $La_2Fe_2S_5$ is orthorhombic $A2_1am$. The La atoms are in two very similar positions (7- or 8-coordinated, in mono or dicapped trigonal prisms). The Fe(II) atoms have two extremely different environments; the first is tetrahedral, the second one is octahedral. The FeS_4 and FeS_6 polyhedra are contiguous, and share a common edge. They constitute zig-zag chains, parallel to the c-axis, formed by the two alternating Fe sites. Four similar chains go through each cell, and are connected by LaS_{7-8} polyhedra (Collin et al., 1971a; Besrest et al., 1977).

Two non-stoichiometric vacancy compounds have been isolated, $La_2Fe_{1.87}S_5$

and $La_2Fe_{1.76}S_5$. Their cells remain orthorhombic, and result from the preceding by having multiples of the b parameter (fig. 31.26).

$La_2Fe_2S_5$	$La_2Fe_{1.87}S_5$	$La_2Fe_{1.76}S_5$
$a = 11.406$ Å	$a' = a$	$a'' = a$
$b = 16.492$ Å	$b' = 3b$	$b'' = 2b$
$c = 3.996$ Å	$c' = c$	$c'' = c$
$A2_1am$	$A2_1am$	$P2_1am$

The structure of $La_2Fe_{1.87}S_5$ has nearly the same general array as $La_2Fe_2S_5$ except that one octahedral and one tetrahedral Fe sites are partially vacant, with respective occupancy factors of 0.82 and 0.80. One of the tetrahedral Fe exchanges an additional bond with a fifth neighboring S atom, and simultaneously brings together the neighboring octahedral Fe atom of the same chain (Fe_{octa}–$Fe_{tetra} = 2.82$ Å) (Besrest et al., 1977).

In the structure of $La_2Fe_{1.76}S_5$ the modifications are more obvious. Only one of the iron chains remains saturated; the other three have partial vacancies, two on the octahedral Fe sites, one on the tetrahedral Fe sites, with respective ratios of occupancy of 0.80, 0.74 and 0.39. The "tetrahedral" sites are the most modified, because all of the Fe atoms which occupy them become five-coordinated by bonding with the neighboring fifth sulfur atom. But, whereas, the "tetrahedral" Fe located near a partially vacant site of octahedral Fe draws near the sulfur, the tetrahedral Fe located in the neighborhood of a saturated octahedral Fe draws away from it (Besrest et al., 1978).

Ho_4FeS_7-type. This compound is isostructural with Y_5S_7 (section 1). In the monoclinic $C2/m$ cell, there are three kinds of positions for the metal atoms. The first, with a multiplicity 4 and 7-coordination is exclusively occupied by Ho. The others are 6-coordinated (nearly regular octahedra) containing the two metal atoms in a disordered way in the proportion of three Ho to one Fe. One of these positions has the multiplicity 2, and contains 30% of the Fe atoms, while the second has the multiplicity 4 and contains 35% of the Fe atoms (Adolphe et al., 1965, 1968).

So, we find once more for this structure, as for Er_2MnS_4, the disordered arrangement of heavy rare earths and the 3d elements Cr, Mn, and Fe, which is only possible on the octahedral sites.

La_4NiS_7-type. The tetragonal cell of this compound, I_4/mmm, shows a superstructure $a' = 4a$, $c' = c$, for which the space group is not known. The structure was solved from reflections of the sub-structure only, because the reflections of the superstructure are too weak to be determined. This structure is related to that of K_2NiF_4. The La atoms are 7- or 8-coordinated. The Ni atoms are 6- or 7-coordinated but with 2 or 3 long bonds (Collin et al., 1974b).

$ScCrS_3$-type. The very large rhombohedral cell contains 12 formulas. It is a superstructure (×18) of a rhombohedral sub-cell which is simply related to the

NaCl structure. It is likely that the distortion and the superstructure result from the ordering of the metal atoms and vacancies on the cationic sites of NaCl (Dismukes et al., 1970).

11. Ternary sulfides and selenides formed by rare earths and 4d and 5d elements

Donohue et al. (1974b) described the R_2MX_5 families:

R_2HfS_5, R = La to Lu, Eu and Yb excepted;
R_2ZrS_5, R = La to Lu, Eu and Yb excepted;
R_2HfSe_5, R = La to Gd (?);
R_2ZrSe, R = La to Tb.

The synthesis of these compounds, in sealed ampoules, is only possible in the presence of a small quantity of iodine. These compounds are orthorhombic, U_3S_5-type, like the corresponding compounds formed by M = U or Th (Jeitschko et al., 1975). They have a high electrical resistivity, except for the Sm derivatives, for which the relatively low electrical resistivity is probably related to a non-stoichiometry due to the presence of a small proportion of divalent ions.

Compounds RMX_3 exist with M = Nb and Ta, for X = S and Se, but they have not been so extensively studied. All show metallic electrical conductivity. Their structures are unknown (Donohue, 1975).

The $EuNb_2S_4$ compound was described by Berkooz et al. (1970). Really, it is an insertion compound of divalent europium in NbS_2, having a composition near $Eu_{1/6}NbS_2$ (Jellinek, 1971). It is hexagonal and has no ferromagnetic transition.

The insertion compounds $R_xMo_6S_8$ have been obtained for all the R elements (Fisher et al., 1975). They crystallize in a rhombohedral lattice, like $PbMo_{6.35}S_8$ (Chevrel et al., 1971). These compounds have narrow homogeneity ranges, with x approximately equal to 1 for the light rare earths, and to 1.2 for the heavy rare earths. More extended solid solutions are observed for Pr, Nd, Eu and Yb. The magnetic moments correspond to the presence of trivalent ions, with the exceptions of Eu, which is divalent, and Yb, for which the magnetic moment is strongly dependent on the x value. Magnetic ordering does not appear in the samples, down to 1.3 K.

These compounds are superconductors. Most of them have transition temperatures, T_c below 1 K, however, some occur at higher temperatures (about 7 K for the La derivative and 8.5 K for the Yb derivative). These compounds are superconductors in spite of the presence of magnetic ions. This characteristic shows that the exchange interaction between the superconducting electrons and the R ions is very weak, and supports the idea that the d-electrons of Mo are primarily responsible for the superconducting properties.

In an attempt to reduce this interaction further, the $R_xMo_6Se_6$ series was synthesized (Shelton et al., 1976). Almost all these compounds are superconductors above 5 K (except Ce and Eu derivatives) and the transition temperatures are higher than those found in the sulfides. The lanthanum compound possesses

the third highest transition temperature among the $M_xMo_6X_8$ phases reported to date.

In the $PbMo_6S_{8-x-y}Se_xTe_y$ and $Mo_6S_{8-x-y}Se_xTe_y$ systems, Chevrel et al. (1975) pointed out a strong correlation between T_c and the lattice parameters especially the rhombohedral angle α. In the $Sn_{1.2-x}Er_xMo_6S_8$ system, Fradin et al. (1976) verified that there is a cell size that optimizes T_c, but in this case the angle is constant as Er is substituted for Sn.

12. Systems U (or Th)–R–X

Some of the phases which exist in the systems U–S (Picon and Flahaut, 1958) and U–Se (Khodadad, et al. 1965) have great structural similarities with rare earth chalcogenides. Moreover, in the trivalent state, uranium has nearly the same dimensions and the same environment as neodymium. However, the U_2S_3 sulfide (Zachariasen, 1949) is not isomorphous with Nd_2S_3 and only some selenides and tellurides of intermediate rare earths have the type (cf. table 31.8, η phases). The U_3S_4 sulfide does not exist, and only the U_3Se_4 selenide has the Th_3P_4 type structure of the light lanthanides.

In spite of these differences, the similarities are the source of large homogeneity ranges in the ternary systems R–U–X. There are not as yet complete descriptions of these systems. Figures 31.28 and 31.29, prepared from literature

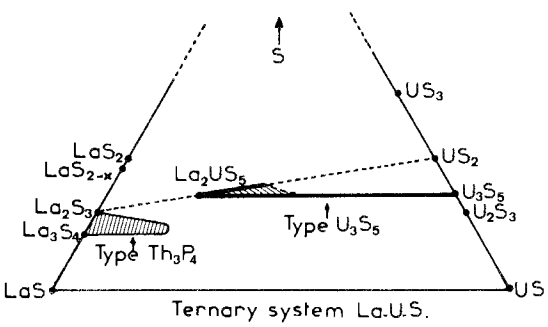

Fig. 31.28. Ternary system La–U–S.

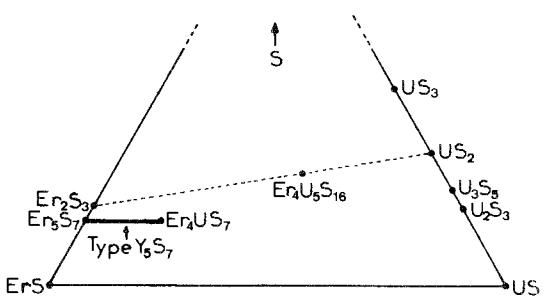

Fig. 31.29. Ternary system Er–U–S.

data, although incomplete, suggest the existence of large homogeneity domains between the UX and RX compounds.

In some of these intermediate compounds, uranium has the normal valency of four or perhaps the valency 3 (in ScU_3S_6). It is more difficult to know its valency in compounds and solid solutions where it has the apparent oxidation state +2 (solid solutions of the Th_3P_4 and Y_5S_7 types).

$R(III)_2U(IV)S_5$ compounds and solid solutions of the U_3S_5 type. The R_2US_5 compounds are observed from La to Gd (Vo Van et al., 1975). They are orthorhombic, space group *Pnma*, of the U_3S_5 type (described by Potel et al., 1972; Moseley et al., 1972). The structure was solved for Sm_2US_5 (Vo Van et al., 1975).

The Sm atom has an 8-prismatic environment, the same as the trivalent U atom of U_3S_5, and the interatomic distances Sm–S and U(III)–S are equal. The U atom has the same 7-octahedral environment as the U(IV) atom in U_3S_5. As is usual in this kind of polyhedron, the two sulphur atoms which substitute at one apex of the octahedron are at a very short distance from one another (3.21 Å).

Continuous solid solutions are formed from these compounds to U_3S_5, $(R_{1-x}(III)U_x(III))_2U(IV)S_5$, with $0 \leqslant x \leqslant 1$. Partial solid solutions are observed from these compounds on the R_2US_5–US_2 section. There are vacancies in the R(III) site represented as $(R(III)_{2-x}U(IV)_{(3/4)x}\square_{(1/4)x})U(IV)S_5$, with $0 \leqslant x \leqslant 1.09$ for R = La. In the case of lanthanum, which was especially studied, the domains are represented in fig. 31.28.

The compounds $R(II)U(IV)_2S_5$ of the U_3S_5 type. The RU_2S_5 compositions belong to the R_2US_5–U_3S_5 systems alluded to above. For the exclusively trivalent rare earths dealt with in the preceding paragraph, these compositions are written R(III)U(III)U(IV)S_5. For Eu and Sm, valence changes represented by R(III) + U(III) → R(II) + U(IV) occur because their divalent states are more stable than the trivalent state of uranium.

Valences of both II and III exist in the samarium sulfides. Thus, the reaction of U_3S_5 with $Sm(III)_2U(IV)S_5$ involves the progressive transformation of Sm(III) into Sm(II), to give the final composition $Sm(II)U(IV)_2S_5$ in which all the samarium is divalent (Vo Van et al., 1975).

In the case of the europium, for which the trivalent state is not very stable in the sulfides, the compound $Eu(III)_2U(IV)S_5$ does not exist. Only $Eu(II)U(IV)_2S_5$ is known (Brochu et al., 1970, 1972) and the solid solution is formed only between $Eu(II)U(IV)_2S_5$ and U_3S_5. Finally the two compounds $Sm(II)U(IV)_2S_5$ and $Eu(II)U(IV)_2S_5$ have a special position in the phase diagram (Vo Van et al., 1975).

The compounds $R_4U(IV)_5S_{16}$ and $R_4Th_5S_{16}$. These two series of isostructural compounds, located on the R_2S_3–US_2 or –ThS_2 sections, only exist for the heavy lanthanides from Tb to Lu and for Y. They are orthorhombic, space group *B*2, *Bm* or *B*2/*m* but their structure is unknown (Vo Van et al., 1974).

$Yb_{10.8}U_{3.7}S_{22}$ compound. This compound is isostructural with $Ce_4Lu_{11}S_{22}$ (Rodier et al., 1975). The two metals are simultaneously present with two oxidation states, +3 and +4 for uranium and +2 and +3 for ytterbium. The environments are as follows: 8-prismatic for U(III), 7-octahedron for U(IV), 7-prismatic for Yb(II) and 6-nearly regular octahedral for Yb(III). The crystallographic formula is $0.90(U(III))_20.94(U(IV))_20.92(Yb(II))_2(Yb(III))_60.95(Yb(III))_3$ and four sites are partially vacant (Rodier et al., 1976b).

$ScU(III)_3S_6$ compound. This compound is orthorhombic, space group *Pnnm*. The uranium occupies three kinds of sites: 8-prismatic, 7- or 8-prismatic and 7-octahedral. The scandium is in slightly distorted octahedra (Rodier et al., 1976a).

Solid solutions and $R(III)_2UX_4$ compounds of the Th_3P_4 type. They have been studied in the case of the sulfides along the sections R_2S_3–US and R_3S_4–"U_3S_4", this latter composition really is a mixture of U_2S_3 and US (Demoncy et al., 1970). The widest range of homogeneity is observed in the ternary R–U–S systems for Ce and Pr, where it attains the composition $n = 0.30$ ($n = U/(U+R)$).

In the case of the selendides and tellurides, these domains have been studied only on the R_2X_3–UX binary systems. They are broader than for the sulfides, and attain the $R(III)_2UX_4$ composition, for R = La to Nd. But it is likely that continuous homogeneity ranges exist from R_3X_4 to U_3X_4, of the same type, and contain the R_2UX_4 compounds (Demoncy et al., 1970).

Solid solutions and $R(III)_4US_7$ compounds of the Y_5S_7 type. These compounds, obtained from Ho to Tm and for Y, are isostructural with the R_5S_7 compounds formed by the same R elements. Continuous homogeneity ranges probably exist between these two kinds of compounds, but they have not been observed (Demoncy et al., 1970).

In these two series of solid solutions, and in the R_2UX_4 and R_4US_7 compounds, the uranium valency is not well defined, and it is probable that these compounds have semi-metallic properties.

13. Ternary compounds formed by divalent rare earth elements

In the rare earth family, the stability of the divalent state, relative to the trivalent state, follows the order EuII $\gg$ SmII > YbII. Therefore, the Eu derivatives are observed more frequently because EuX compounds have no oxidation or reduction behavior against chalcogenides of multivalent elements in their maximal valency. For instance, SnS_2 combines with EuS but it is reduced to SnS by SmS or YbS sulfides. In this case, the compound Eu_2SnS_4 exists but the compounds Sm_2SnS_4 or Yb_2SnS_4 are unknown. In a similar way, SmS reduces MgS and cannot form solid solutions with it; but SmS does not reduce CaS, SrS or BaS, which are more stable than MgS, and forms solid solutions with them (Vo Van et al., 1970b).

13.1. *Compounds with the IIA elements*

The SmS–MS and EuS–MS systems (M = Mg, Ca, Sr, Ba). Continuous solid solutions exist between these sulfides which have the same NaCl-type. With Sm, it is necessary to prepare them above 900°C, because SmS disproportionates at low temperature into Sm_3S_4 and Sm, and in this case MSm_2S_4 derivatives of Sm(III) appear. Moreover, MgS is reduced at high temperature, and this sulfide cannot form solutions with SmS (Vo Van et al., 1970b).

13.2. *Compounds with the IIIA elements in their trivalent state*

SmR_2X_4, EuR_2X_4 and YbR_2X_4. See section 5.3.

13.3. *Compounds with the 3d elements*

$EuTi_2S_4$ and EuV_2S_4. These compounds have the same crystal structure as the high temperature variety of $EuCr_2S_4$ (Nguyen, 1971). They have a paramagnetic behavior between 80 and 800 K (Gorochov et al., 1969).

$EuCr_2S_4$ and $EuCr_2Se_4$. These compounds seem to be dimorphoic, but Nguyen (1971) gives slightly different compositions for the two varieties. The "low temperature variety" is hexagonal $P6$, isostructural with $PbCr_2S_4$ (Omloo et al., 1968, 1971; Gorochov et al., 1969; Nguyen, 1971), but this structure is unknown. For the "high temperature variety", the crystal network is still unknown. These compounds are semiconductors (Gorochov et al., 1969). The "low temperature varieties" of the two compounds are ferrimagnetic with $T_N = 150$ K for the selenide (Gorochov et al., 1969) and $T_N = 68$ K for the sulfide (Lugscheider et al., 1971).

EuS–FeS system. No intermediate compound is observed in the phase diagram (Meyer et al., 1973).

13.4. *Compounds with the IIIB elements*

$EuAl_2X_4$, $EuGa_2X_4$ and $EuIn_2X_4$ (X = S, Se). These compounds have the same crystal type, orthorhombic $PbGa_2Se_4$-type, but this structure is not yet known (Eholié et al., 1971; Donohue et al., 1974a; Aliev et al., 1976). The phase diagram of the EuS–Ga_2S_3 system shows the congruent melting of $EuGa_2S_4$ at 1215°C (Barnier et al., 1976a). All these compounds are paramagnetic between 80 and 800 K. They have p-type semiconductivity (Aliev et al., 1976).

13.5. *Compounds with the IVB elements*

Eu_2SiS_4 and Eu_2GeS_4. These compounds are monoclinic, like Sr_2GeS_4 (Michelet, 1972).

Eu–Sn–S system. Two intermediate phases are known: $Eu_3Sn_2S_7$ and $Eu_5Sn_3S_{12}$. They are formed by tetravalent tin.

$Eu_3Sn_2S_7$. It belongs to the EuS–SnS_2 system. The flat orthorhombic *Pbam* cell contains two formulas. Each tin atom is inside a tetrahedron of sulfur atoms. It is however strongly displaced towards one face. As a result it is in front of a fifth S atom, but at a relatively large distance. The coordination of tin is therefore between four and five.

The Eu atoms have two kinds of eight-coordinated environments. The first is a tetragonal prism, a form which is unknown for the trivalent rare earths. The second is a triangular prism with two additional bonds in the equatorial plane (coordination 8-prismatic) (Jaulmes et al., 1977b).

$Eu_5Sn_3S_{12}$. This compound does not belong to the system EuS–SnS_2 because Eu has the two valences 2 and 3: $(Eu(II))_3(Eu(III))_2(Sn(IV))_3S_{12}$. In this sense, it is a quaternary compound (fig. 31.23).

Two Sn atoms are inside nearly regular octahedra. The third is five-coordinated but its arrangement differs from that in $Eu_3Sn_2S_7$. The sulfur polyhedra form chains through the structure, parallel to the short axis. The three Eu(II) atoms have a 8-triangular prismatic coordination. The two Eu(III) atoms have varied environments: 8-prismatic as in the preceding case, but with shorter Eu–S bonds, and 7-octahedral (Jaulmes et al., 1977a). This structure figures centrally in new families of quaternary compounds (9–3).

13.6. *Compounds with the VB elements*

$EuSb_2X_4$ and $EuBi_2X_4$ (X = S, Se, Te). The synthesis and the crystallographic study are described by Rustamov et al. (1977).

14. Binary tellurides

We shall describe here the binary tellurides which are different from the binary sulfides and selenides, and the properties studied in the R–Te systems.

14.1. *Phase diagrams*

The *phase diagrams* of various R–Te systems have been described:

La–Te	Ramsey et al. (1965a), Eliseev et al. (1965b)
Ce–Te	Chukalin et al. (1967a,b);
Pr–Te	Jarembash et al. (1970);
Nd–Te	Jarembash et al. (1965a), Lin et al. (1965), Abrikosov et al. (1965), Zinchenko et al. (1966, 1967);
Eu–Te	Sadovskaya et al. (1970);

Gd–Te Zargarjan et al. (1967);
Dy–Te Abrikosov et al. (1970);
Ho–Te Jarembash et al. (1974);
Er–Te Haase et al. (1965);
Tm–Te Eliseev et al. (1976a).

The first four systems are very similar and contain the following phases: RTe, cubic NaCl-type; R_3Te_4–R_2Te_3, solid solution of the Th_3P_4-type; R_4Te_7, tetragonal; RTe_{2-x}, tetragonal Fe_2As-type in which $0 \leqslant x \leqslant 0.2$; R_2Te_5, R_4Te_{11} and RTe_3, closely related compounds which have elongated pseudo-tetragonal cells.

With Gd, Dy, and Ho, the phases seem very similar to those preceding, except for the R_2Te_3, which has another crystal type and is exactly stoichiometric. However, some discrepancies exist concerning the compositions of the Te-rich phases, which are due to the absence of complete structural studies.

In the case of the Eu–Te system, only the compounds EuTe, Eu_3Te_4, Eu_4Te_7 and Eu_3Te_7 are observed.

The sesquitelluride R_2Te_3, R_3Te_4 and the lower tellurides RTe were discussed in section 2 because of their close structural and physical relationship with the corresponding sulfides and selenides.

In contrast, the higher tellurides have special characteristics which will be discussed here. Some references concerning physical properties of R–Te systems are as follows (see also section 2):

thermoelectric and electrical properties
La–Te system, Ramsey et al. (1965b)
Nd–Te system, Abrikosov et al. (1967)
Er–Te system, Haase et al. (1966);
thermal expansion
La–Te system, Eliseev et al. (1967b);
thermodynamic properties
La–Te system, Somov et al. (1973);
magnetic properties
Pr–Te system, Chechernikov et al. (1967)
Nd–Te system, Pechennikov et al. (1967)
Dy–Te system, Pechennikov et al. (1970)
Sm–Te system, Lashkarev et al. (1971)
Er–Te system, Hoggins et al. (1968);
Mössbauer effect
Sm–Te system, Aleksandrov et al. (1971).

14.2. *Higher binary tellurides*

All these compounds apparently have structures which are closely related to the Fe_2As structural type of the RTe_2 compounds.

RTe_2 compounds. These compounds were first described by Pardo et al. (1965). Their crystal structures were confirmed by structural studies from Eliseev et al. (1965a) on $CeTe_2$ and Wang et al. (1966) on $NdTe_2$ (fig. 31.30).

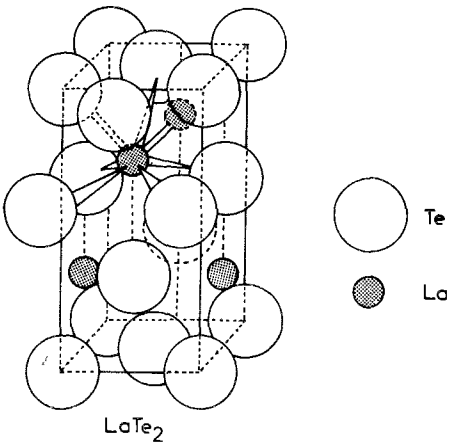

Fig. 31.30. Tetragonal cell of the Fe_2As type of $LaTe_2$.

From Wang et al. (1966) the interatomic distances in $NdTe_2$ are: Te(a)–Te(a) 3.187 Å; Te(a)–Te(b) 4.036 Å; Te(b)–Te(b) 4.009 Å; Te–Nd 3.26 to 3.38 Å. These values show the very special behavior of the Te(a) contained in the basal plane of the cell. These Te atoms are at very short distances from one another and form very compact layers of Te, in which they are directly bonded by covalency. In contrast, the Te(b) are at large distances from the other Te atoms and are not bonded together; they are only bonded to the five R atoms which surround them.

Each R atom is at the center of a 9-apices polyhedron. Because of this large coordination, this structural type is only observed from La to Dy. But high pressure (100 kbars) high temperature (1200°C) treatments give RTe_{2-x} compounds for all the lanthanides and for Y (Cannon et al., 1970).

A non-stoichiometry exists in each case, to about $RTe_{1.8}$ (Wang et al., 1966). The vacancies of tellurium only occur in the basal plane of the cell.

The thermoelectric and electrical properties of $LaTe_2$ and its solid solutions were studied by Ramsey et al. (1963, 1965a). The specimens of $LaTe_2$ studied are degenerate semi-conductors of p-type. However, single crystals of $LaTe_2$ (Eliseev and Kuznecov, 1965a) and $NdTe_2$ (Andrellos and Bro, 1962) are n-type under certain conditions of temperature. Really, these compounds are very sensitive to the influence of impurities. The solid solution $LaTe_{2-x}$, which probably has n-type conductivity when pure, can be changed to p-type by introduction of various impurities, especially oxgen, and also metals like Sb (Narasimhan et al., 1968). The magnetic properties of $PrTe_{1.9}$ are described by Chechernikov et al. (1967).

R_4Te_7 compounds. These compounds exist from La to Dy. Their structure, which is not yet known, is apparently closely related to RTe_2, as suggested by their X-ray diagrams. Their cells seem to be tetragonal $P4/mbm$ (Eliseev et al., 1966c) except for La_4Te_7 (Kuznecov, 1972).

R_2Te_5 compounds. These compounds exist from La to Ho, and for Y, except for Eu. From powder studies, they have very elongated orthorhombic pseudo-

tetragonal cells. A structural model was proposed, based on similarities with the crystal structures of RTe_2 and RTe_3 (Pardo et al., 1965, 1967a). The cell consists of two blocks of two superimposed RTe_2 unit cells placed one upon another. A double layer of Te atoms appear between the blocks, as in RTe_3.

RTe_3 compounds. These compounds, first observed by Carter (1965) for $CeTe_3$ and by Ramsey et al. (1965a) for $LaTe_3$, exist for Y and from La to Tm, except for Eu (Pardo et al., 1965, 1967a). The crystal structure, described by Norling et al. (1966) for $NdTe_3$ is orthorhombic pseudo-tetragonal, space group *Bmmb*. The structure may be viewed as a stacking of two $NdTe_2$ blocks of the Fe_2As-type; a double layer of Te atoms is between each block.

$LaTe_3$ (Ramsey et al., 1965b) and $ErTe_3$ (Haase et al., 1966) are degenerate semiconductors of p-type. By stacking different kinds of blocks of the Fe_2As-type, it would be possible a priori to obtain various kinds of formulas especially R_3Te_8 and R_4Te_{11}. The latter appears in the phase diagrams of the Russian workers without structural description. Structural research needs to be done, but twinning and very easy cleavages make it hard to obtain good crystals.

15. Ternary compounds containing rare earths, tellurium and a third element

15.1. *Ternary compounds with two anions*

Presently five series are known.

The solid solutions formed between the R_2S_3 sulfides and the R_2Te_3 tellurides were studied in a few cases. For the light lanthanides they have the Th_3P_4 structural type. For the heavy rare earths (R = Er, Tm and Lu) these solid solutions have the structural type of the sesquitellurides, orthorhombic Sc_2S_3 (Ghémard, 1976: Ghémard et al., 1971a, 1978a,b).

The oxytellurides $(RO)_2Te$, tetragonal from La to Dy (Pardo et al., 1965; Kent et al., 1962; Obolonchik et al., 1966; Raccah et al., 1967) and orthorhombic from Er to Lu (Pardo et al., 1967b). The magnetic properties of some of these compounds were studied by Lashkarev et al. (1967).

The sulfotellurides $(RS)_2Te_{1+x}$, from Tb to Tm and for Y. These compounds have a large homogeneity range ($0 \leqslant x \leqslant 0.13$ for Dy, for instance) and present an order–disorder transition from a low temperature monoclinic form to a high temperature orthorhombic form, the first being a superstructure of the other (Ghémard, 1976; Ghémard et al., 1971a, 1978a,b).

We shall show in section 16 that the (RO) or (RS) groups form sheets of pseudo-tetragonal arrangements of distorted tetrahedra $[R_4O]$ or $[R_4S]$. Between the sheets are double layers (for $(RO)_2Te$) or single layers (for $(RS)_2Te$) of tellurium atoms.

The hydrotellurides (RH_x)Te, from La to Pr. These phases are hydrogen deficient. They are tetragonal, probably of the PbFCl-type (Carter, 1961).

15.2. *Ternary compounds with two cations*

Ternary compounds containing tellurium, rare earth and a second metal were studied in the following cases.

Cu_2Te–R_2Te_3 systems. These systems were studied by Pardo et al. (1971, 1972) and Agaev et al. (1973, 1974) (fig. 31.12). Many new phases are observed in the case of the light rare earths, but their structures remain unknown. For the heavy rare earths, from Gd to Lu and for Y, trigonal phases $RCuTe_2$ appear similar to those observed for the corresponding sulfides and selenides. A continuous homogeneity range exists to the composition $GdCu_3Te_3$ only for Gd (or between $n = 0.5$ and $n = 0.75$ with $n = Cu/(Cu + R)$ atomic), as for the selenides. With the subsequent rare earths, the homogeneity ranges are narrower and stop at about $n = 0.60$. They probably have the $ScCuS_2$ structure. A second series of phases appears near the composition $n = 0.70$–0.75 for Tb, Dy and Ho. They are closely related to the preceding and probably are hexagonal superstructures. Finally for Er and Tm, the compounds RCu_3Te_3 have orthorhombic cells which are distortions of the hexagonal cells of the preceding phases. In these studies, complementary single crystal work is necessary.

Ag_2Te–R_2Te_3 systems. Three types of phases are observed near the $RAgTe_2$ composition (Pardo et al., 1973). From Dy to Tm and for Y, the compounds are of two varieties. One is a tetragonal unknown structure which is stable at low temperature, and the other a trigonal $ScCuS_2$-type structure stable at high temperature without a homogeneity range. In the special case of Gd, both varieties are present, but the trigonal one probably has a disordered arrangement and gives a large homogeneity range (between $n = 0.50$ and 0.75). Lutetium has only a trigonal $LuAgTe_2$ compound.

$CaTe$–R_2Te_3 systems. They are very similar to the corresponding systems of selenides (section 5, fig. 31.11) (Pardo et al., 1969).

With the light lanthanides from La to Sm, only solid solutions of the Th_3P_4 type exist. These solid solutions do not attain the CaR_2Te_4 composition. With the heavy lanthanides Dy to Lu and yttrium, there are two categories known. At low temperatures the CaR_2Te_4 compounds are of the rhombohedral Yb_3Se_4-type. At high temperatures large homogeneity ranges (only studied for Er) exist from CaTe, cubic NaCl-type, to $n = Ca/(Ca + Yb) = 0.65$ in which there is a rhombohedral distortion. The distortion has its maximum value for the composition CaR_2Te_4, like in the selenide system (section 5).

Ga_2Te_3–R_2Te_3 systems. Only Ga_2Te_3–Sm_2Te_3 was studied. An intermediate $SmGaTe_3$ compound exists (Karaev et al., 1965).

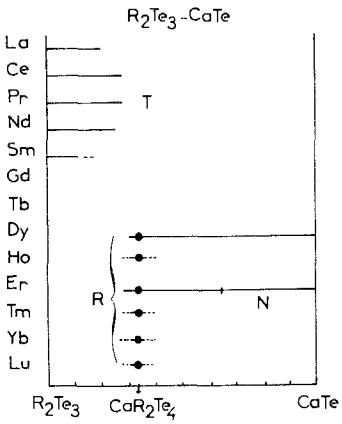

Fig. 31.31. Crystal types in the R_2Te_3–CaTe systems: T: type Th_3P_4, R: rhombohedral solid solutions, distortion of the NaCl type N.

Tl_2Te–R_2Te_3 systems. In agreement with the corresponding selenide systems (section 4), these contain intermediate $TlRTe_2$ compounds which are rhombohedral of the $NaFeO_2$-type, where R = Pr to Lu and Y, but not Eu and Yb (Kabré et al., 1972, 1974).

PbTe–R_2Te_3–R_3Te_4 systems. Aloman et al. (1968, 1971) describe R_2PbTe_4 compounds, which form Th_3P_4-type solid solutions with R_2Te_3 and R_3Te_4. However, the existence of these compounds has not been confirmed by other studies (Patrie et al., 1969b).

$LaTe_2$–$LaSb_2$ system. A large solid solution exists from $LaTe_2$ to the composition limit $LaSb_{1.5}Te_{0.5}$, in which the substitution of Te by Sb creates an orthorhombic distortion of the tetragonal structure of $LaTe_2$ (Wang et al., 1967). This substitution decreases the resistivity, and degenerate p-type semi-conductors are obtained. The thermoelectric power first increases then decreases as the material becomes more metallic (Narasimhan et al., 1968).

MTe–EuTe systems. Several systems were studied to follow the influence of substitution of Eu by other metals, M, upon magnetic interactions and the electronic properties of EuTe (see ch. 20). Studies of SnTe–EuTe have been made by Mathur et al. (1971) and of PbTe–EuTe by Suryanarayanan et al. (1968).

16. Ternary compounds with two anions

Ternary compounds formed by rare earths and two non-metals, in which one of them is a chalcogen, have been widely investigated. A review was made by Dagron et al. (1971) of halogeno-sulfides and by Flahaut (1976) of [RS] sheet compounds.

We can distinguish two classes of compounds. First, those which are solid

solutions formed from the binary constituent compounds and which have the crystal structure of the binary compounds, and secondly, those which have special crystal types.

16.1. *Solid solutions*

They are formed from the binary compounds by substitution of S or Se by a second non-metal, frequently arsenic, silicon, germanium, or tellurium. Such a choice of elements is evidence of the covalent character of the bonding in the rare earth sulfides and selenides.

The following homogeneity ranges have been described.

$RS_{1-x}M_x$, with $M = As$, Si, Ge. With As, the homogeneity range extends continuously from RS to RAs to give compounds which have the same NaCl-type structure. With Si and Ge, the domain stops at $x = 0.33$ (Ghémard et al., 1971b).

R_2S_3–R_3S_4 – $R_2S_{3-x}Te_x$. This homogeneity surface in the R–Te–S ternary system has the Th_3P_4 structural type.

R_2S_3–R_3S_4 – R_3AsS_3. This homogeneity surface in the R–As–S ternary system also has the Th_3P_4 structural type (Céolin et al., 1971). These two series of solid solutions are formed only by the light R elements.

$R_2Te_{3-x}S_x$ solid solutions. These solid solutions of the orthorhombic Sc_2S_3-type tellurides of the heavy rare earths and yttrium have a wide composition range (x attains 1.95 for Er, Tm and Lu) (Ghémard et al., 1972).

16.2. *Ternary compounds*

Their crystal structures, which are different from those of the binary compounds, are listed in table 13. In many cases the rare earths and one of the two non-metals, X, form sheets of general formula $(RX)_n^{n+}$, the second non metal Z being between these sheets in a single or double layer. Some exceptions of this general arrangement are known, however, especially in the series of polytypes RSeF with R = Y or the heavy rare earths.

16.2.1. *Sheet compounds*

The (RX) sheets have three kinds of arrangements.

16.2.1.1. *The R and X atoms have planar coordinations.* These are only known when X is a small atom like fluorine and Z a large atom like Se. But two kinds of coordinations are observed for R atoms.

First, in the RX planes, the R and X atoms have the same *triangular* coordination. This type of structure is only observed for the largest rare earths.

TABLE 31.13

Ternary two anions compounds – References of the second column are concerned with the description of compounds. References of the third column are concerned with the description of crystal structures.

Formulas	Elements concerned		Crystal types
$(RO)_2S$	La–Lu and Y [1, 17, 48]	hex.	Ce_2O_2S [10]
$(R_{10}S_{14})O$	La–Sm [22, 23]	tetrag.	$Pr_{10}S_{14}O$ [21]
$(RO)_2Se$	La–Lu and Y [8, 9, 20]	hex.	Ce_2O_2S [10]
$(RO)_2Te$	La–Dy [29, 31]	tetrag.	Nd_2O_2Te [32]
	Ho–Lu and Y [30]	orthorh.	unknown
$(RO)_2S_2$	La–Nd (Ce excepted) [2]	tetrag.	$Pr_2O_2S_2$ [11]
$(RO)_4Se_3$	La–Yb (Eu excepted) [41]	orthorh.	$La_4O_4Se_3$ [43]
(RF)S	La–Er and Y [3, 4]	tetrag.	PbFCl [3]
	Tm–Lu and Y [3, 4]	hex.	β YSF [12]
(RF)Se	La [35]	hex.	α LaSeF [33]
	La–Gd, (Eu excepted) [35]	tetrag.	PbFCl
	Dy–Yb [36]; Polytypes:	orthorh.	2 O [37]
	(see also 44)		6 O [38]
			14 O [46]
		monocl.	4 M [39]
			8 M [47]
			10 M [45]
	Ho–Lu and Y [28]	rhomb.	YbSeF
		hex.	YSF β [12]
R_2SeF_4	La–Nd [35]	rhomb.	Ce_2SeF_4 [34]
(RS)Cl	La–Pr (Eu excepted) [5]	orthorh.	CeSI [15]
	Dy–Lu and Y	orthorh.	FeOCl [16]
(RS)Br	La–Pr [3, 5, 6]	orthorh.	CeSI [15]
	Pr–Tb (Eu excepted) [3, 6]	monocl.	NdSBr [13]
	Dy–Lu and Y [3, 6]	orthorh.	FeOCl [18]
(RS)I	La and Ce [3, 4, 5]	orthorh.	CeSI [15]
	Ce–Sm [3, 4]	rhomb.	SmSI [14]
	Gd–Lu and Y [3, 4]	hexag.	unknown
$(RS)_2Te_{1+x}$	Tb–Tm and Y [27]	orthorh.	$(TbS)_2Te$ [26]
		monocl.	$(DyS)_2Te_{1+x}$ [26, 49]
$(RS)_2As_{2-x}$	La–Tm (Eu excepted) [7, 40]	monocl.	CeAsS [19]
R_2SiS_5	La–Nd [24]	monocl.	La_2GeS_5 [25]
R_2GeS_5	La [24] and Ce [42]	monocl.	La_2GeS_5 [25]

[1] Flahaut et al. (1958). [2] Khodadad et al. (1965). [3] Dagron et al. (1971). [4] Dagron et al. (1969). [5] Dagron (1966). [6] Dagron et al. (1970). [7] Céolin et al. (1972). [8] Benacerraf et al. (1959). [9] Guittard et al. (1966). [10] Zachariasen (1949). [11] Ballestracci (1967). [12] Rysanek et al. (1973). [13] Savigny et al. (1973a). [14] Savigny et al. (1973b). [15] Etienne (1969). [16] Sfez et al. (1973). [17] Collin et al. (1965). [18] Collin et al. (1973c). [19] Sfez et al. (1972). [20] Eick (1960). [21] Carré et al. (1970). [22] Besançon (1973). [23] Besançon et al. (1973). [24] Michelet et al. (1970). [25] Mazurier et al. (1973). [26] Ghémard (1976). [27] Ghémard et al. (1971a). [28] Dagron (1976). [29] Pardo et al. (1965). [30] Pardo et al. (1967b). [31] Kent et al. (1962). [32] Raccah et al. (1967). [33] Nguyen (1973a). [34] Nguyen (1973b). [35] Dagron (1971). [36] Dagron (1972). [37] Nguyen (1973c). [38] Nguyen et al. (1975a). [39] Nguyen et al. (1975b). [40] Céolin et al. (1977). [41] Khodadad et al. (1967). [42] Beskrovnaya et al. (1971). [43] Dugué et al. (1970). [44] Van Dyck et al. (1976). [45] Nguyen et al. (1977a). [46] Nguyen et al. (1979). [47] Nguyen et al. (1977b). [48] Eick (1958). [49] Ghémard et al. (1978a,b).

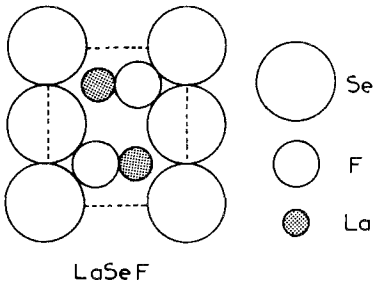

Fig. 31.32. Crystal structure of LaSeF: content of the 110 plane of the hexagonal cell, $a = 4.217$ Å, $c = 8.188$ Å, $P6_3/mmc$, $z = 2$.

It has been known for a long time for bastnaësite (in this case the second anion is a CO_3 group). In the case of the chalcogenides, for example, in α *LaSeF* studied by Nguyen (1973a) (fig. 31.32) the Se atoms alternate with (LaF) planes. Further in Ce_2SeF_4 (fig. 31.33) studied by Nguyen (1973b), the tysonite-like groups alternate with α LaSeF like groups. In this way, there are two kinds of environments for the fluorine atoms – tetrahedral in the tysonite-like groups, triangular in the α LaSeF-like groups.

Second, in the RX planes the F atoms have the same *triangular* environment of R atoms, and the R atoms have a *hexagonal* environment of F atoms. This kind of arrangement is only observed with Y and the smaller rare earths. Two structures are known, which are closely related to one another, the first having a hexagonal – A B A B – arrangement of its groups, and the second having a rhombohedral – A B C – arrangement. Hexagonal β–YSF (Rysanek et al., 1973, fig. 31.34) is an example of the first and rhombohedral $YbSeF_{1-x}O_{x/2}$ (Nguyen et al., 1979) is an example of the second. This compound is widely nonstoichiometric with an x value of about 0.9.

These two structures are indicated as 2H and 3R terms of a new series of

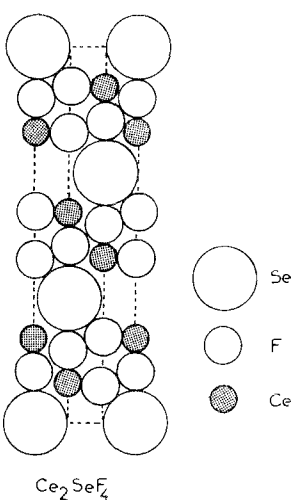

Fig. 31.33. Rhombohedral $R\bar{3}m$ cell of Ce_2SeF_4. The equivalent hexagonal cell is represented along the 110 plane. $a_h = 4.144$ Å, $c_h = 23.09$ Å, $z = 3$.

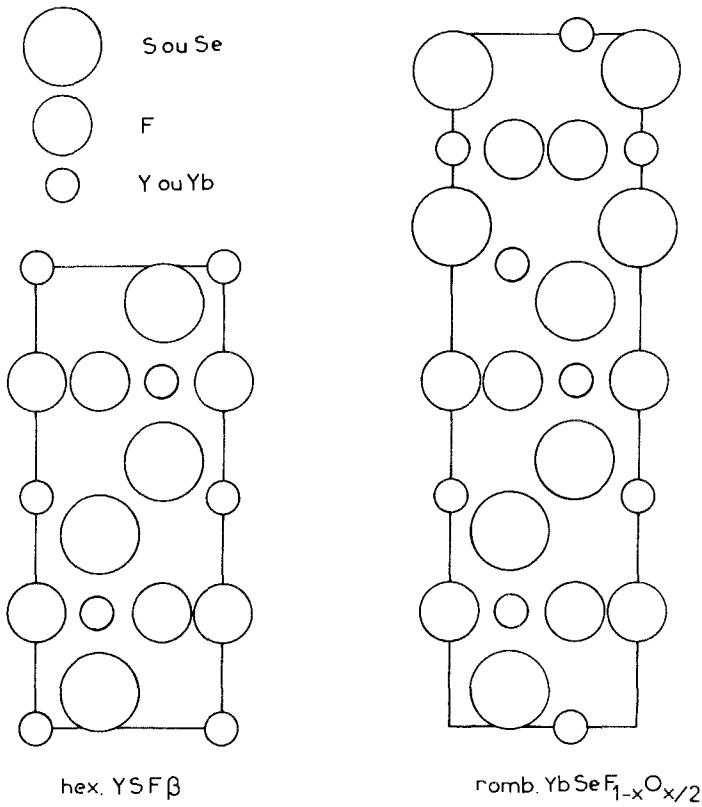

Fig. 31.34. Structures of YSF_{β} (hex.) and YbSeF (rhomb.). Content of the 110 planes.

polytypes formed by the fluoroselenides RSeF of the heavy lanthanides (Dagron, 1976). A 33R term is also known.

16.2.1.2. *The X atoms have a tetrahedral environment of R atoms.* The $[R_4X]$ tetrahedra share their four apices with four neighboring tetrahedra, so the mean formula of the sheet is $[RX]_n^{n+}$.

The X atoms which are associated with the R atoms in these sheets are the smaller, or the more electronegative, of the two non-metals. For example, the known families of this type are:

(RO) sheets $(RO)_2S$, $(RO)_2SE$, $(RO)_2Te$, $(RO)_2S_2$, $(RO)_4Se_3$ (fig. 31.35);
(RF) sheets (RF)S, (RF)Se;
(RS) sheets (RS)Cl, (RS)Br, (RS)I, $(RS)_2Te_{1+x}$.

Two kinds of arrangements of these tetrahedra are possible (fig. 31.36).
(1) A hexagonal arrangement such as occurs in SmSI (Savigny et al., 1973b), rhombohedral (fig. 31.37) and $(CeO)_2S$ (Zachariasen, 1949) hexagonal. The cor-

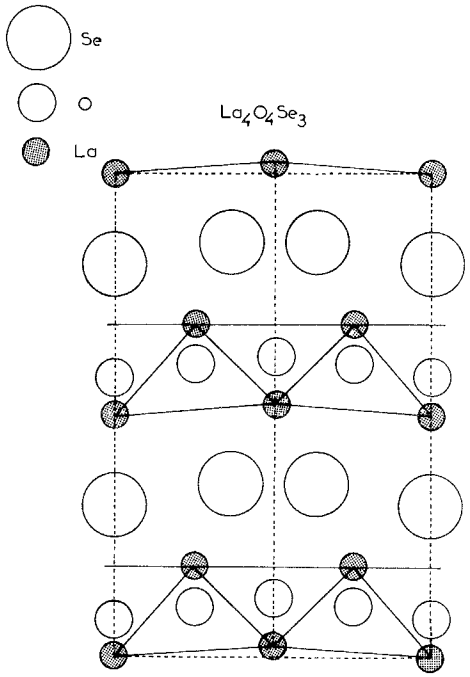

Fig. 31.35. Sheet structure of $(LaO)_4Se_3$, orthorhombic: $a = 13.23$ Å, $b = 8.59$ Å, $c = 4.101$ Å.

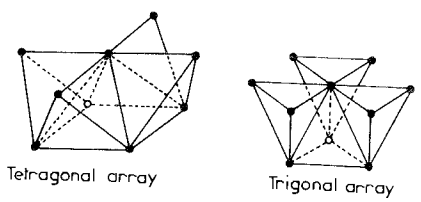

Fig. 31.36. The two fundamental arrangements of $[R_4O]$ tetrahedra.

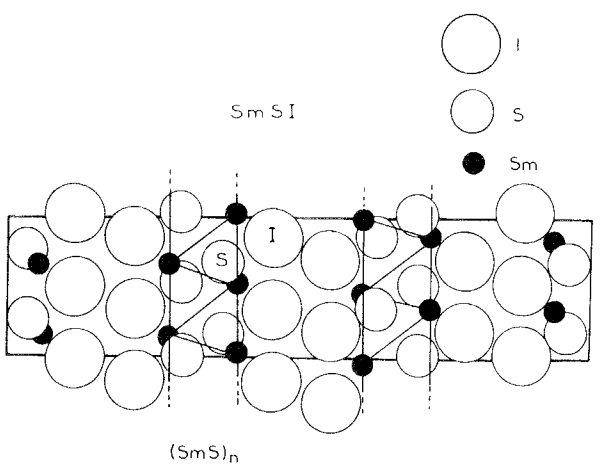

Fig. 31.37. Rhombohedral structure of SmSI, represented by the 110 plane of the hexagonal equivalent cell. $a_h = 4.54$ Å, $c_h = 32.69$ Å.

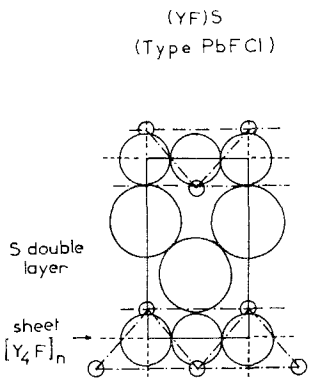

Fig. 31.38. Sheet structure of the PbFCl type of YSF. Tetragonal cell, $a = 3.77$ Å, $c = 6.80$ Å.

responding hexagonal arrangement is not known for the other rare earth compounds.

A strong distortion of this hexagonal arrangement is observed in the La_2GeS_5-type (Mazurier et al., 1973), in which the (RS) sheets alternate with $[GeS_4]$ tetrahedra. But each $[GeS_4]$ tetrahedron shares one S atom with the neighboring sheet; this is the reason why the formula is not $(LaS)_2GeS_4$ (see section 8.2).

(2) A tetragonal arrangement occurs in PbFCl, a classical structure determined for α-YSF by Dagron et al. (1971), and observed only for (RF)S and (RF)Se compounds (fig. 31.38). This tetragonal sheet is also observed in $(NdO)_2Te$ (Raccah et al., 1967) and the oxytellurides of light R elements.

In the case of the (RS) sheets, however, distortions in the tetragonal array occur and the following structural types have been described:

FeOCl, orthorhombic (as shown in ErSCl by Sfez et al., 1973) and in LuSBr by Collin et al., 1973c);

CeSI, orthorhombic (Etienne, 1969);

NdSBr, monoclinic (Savigny et al., 1973a) (fig. 31.39);

$(TbS)_2Te$, which occurs at low temperatures in a monoclinic form (fig. 31.40) as in $(DyS)_2Te_{1.5}$, and an orthorhombic form at high temperature, as shown in $(TbS)_2Te$ (Ghémard, 1976, 1978a,b). Wide non-stoichiometry is observed in this case (Ghémard et al., 1971a).

In all the preceding structures, the sheets of $[R_4X]$ tetrahedra – hexagonal, tetragonal or with lower symmetries – are separated from one another by double layers of the Z anions. The only exception is the Te atoms in the $(TbS)_2Te$ structural type, which are in a single layer, with a disordered arrangement and a partial formation of Te_2 pairs.

16.2.1.3. *The X atoms have a pentahedral environment of R atoms.* The R atoms in this case are inside square-based pyramids $[R_5X]$, which share their apices with five neighboring pyramids (four in one way and the fifth in the opposite

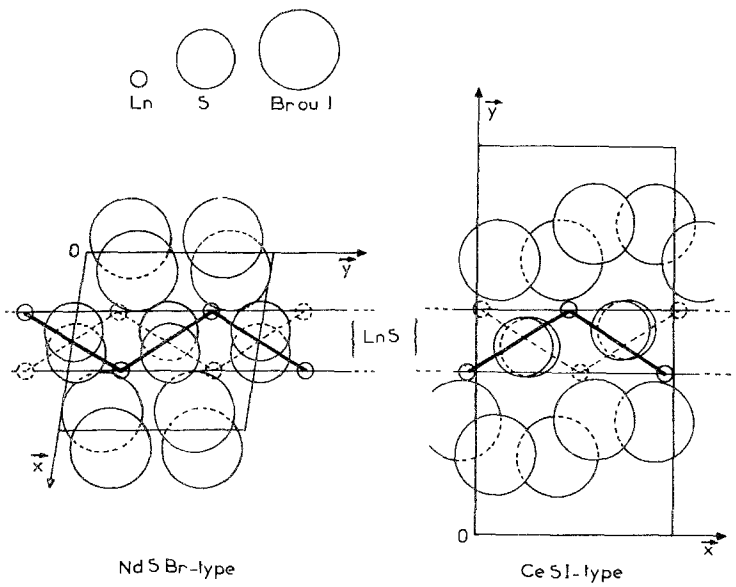

Fig. 31.39. Sheet structure of the closely related monoclinic NdSBr-type and orthorhombic CeSI type.NdSBr: $a = 6.94$ Å, $b = 6.91$ Å, $c = 7.05$ Å, $\gamma = 99.28°$, $z = 4$. CeSI: $a = 7.35$ Å, $b = 14.42$ Å, $c = 7.06$ Å, $z = 8$.

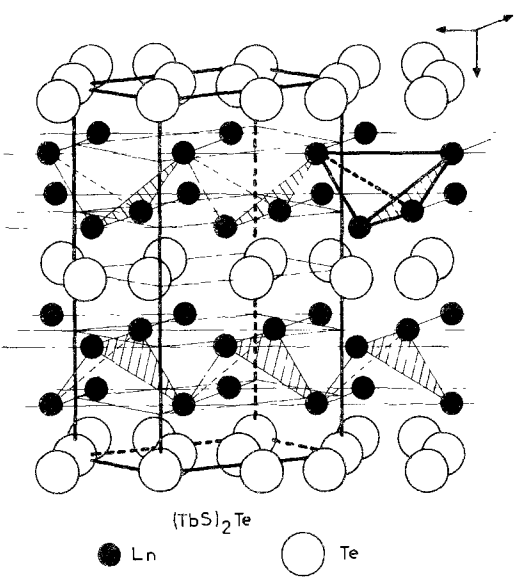

Fig. 31.40. Sheet structures of $(LnS)_2Te_{1+x}$. The S atoms are not shown: they are inside the $(Ln)_4$ tetrahedra. For $(TbS)_2Te$: $a = 4.18$ Å, $b = 5.32$ Å, $c = 13.68$ Å, $z = 2$.

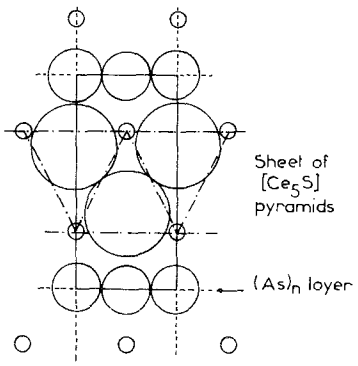

Fig. 31.41. The tetagonal cell of the anti-Fe_2As type. The (CeS)As compound is a slight monoclinic distortion of this type.

way), and constitute sheets of (RX) composition. Between these sheets is a single layer of the second Z non-metal. This structure is that of the anti-Fe_2As-type (Flahaut, 1974) (fig. 31.41). It is observed, with a slight monoclinic distortion, in the $(CeS)_2As_{2-x}$ type of the arseniosulfides of the rare earths, which are widely nonstoichiometric. The As atoms are bonded by covalency to each other in their plane, and form a planer macromolecule. Thus this structure is formed by the superposition of $(CeS)_n^{n-}$ planes (Sfez et al., 1972; Céolin et al., 1972).

16.2.2. *The RSeF polytypes*

The RSeF fluoroselenides of the heavy rare earths and yttrium form two series of closely related polytypes – the first one being orthorhombic, O, the second one monoclinic, M. Their cells have the same a_0 and c_0 parameters (fig. 42) and differ only in the third parameter b_n, which is a multiple of the b_0 parameter of the fundamental cell. For example, $b_n = \frac{1}{2}nb_0$ for the orthorhombic cells in which $n = 6$ or 14 in the known examples, and $b_n = \frac{1}{2}nb_0/\sin\gamma$ for the monoclinic cells where with $n = 4$, 6, 8, 10, 12 or 14. The γ angle is given by the relation $\tan\gamma = 2a_0/3nb_0$ (Dagron, 1972).

One of the important characteristics of these polytypes is the possibility of obtaining each of them in a pure structural form (Dagron, 1972, 1976).

The structure of the fundamental orthorhombic type was described for YSeF (Nguyen, 1973c). It has the 2 O symbol, because it involves two alternating blocks (fig. 31.43). These blocks, designated by S and T really are structurally equivalent, and result from one another by a glide plane parallel to *a*, *b*. Therefore, the arrangement of the 2 O polytype has the symbol $[ST]_n$.

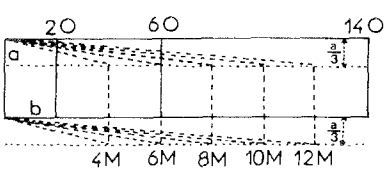

Fig. 31.42. Cells of orthorhombic (O) and monoclinic (M) polytypes. The *c* axis is perpendicular to the figure plane.

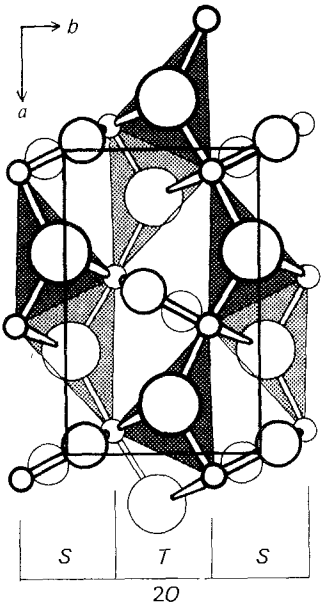

Fig. 31.43. Orthorhombic cell of the 2 O polytype of YSeF, $a = 9.91$ Å, $b = 6.31$ Å, $c = 4.080$ Å, $z = 4$.

The structures of the other polytypes depend on the arrangements of the S and T blocks. If the S and T blocks are in equal numbers, the cells are orthorhombic, O. In all the known cases, there is an SSS triad associated with a TTT triad and with a variable number of ST pairs. There are no ST pairs in the 6 O, but two pairs occur in the 10 O.

If the S and T blocks are in unequal numbers the cells are monoclinic M. There is always an SSS (or TTT) triad associated with an odd number of alternating S and T blocks.

The following structures are known presently from X-ray diffraction studies:

4 M [SSS T]$_n$	(Nguyen et al., 1975b, fig. 31.44);
6 O [SSS TTT]$_n$	(Nguyen et al., 1975a, fig. 31.45);
8 M [SSS TS TS T]$_n$	(Nguyen et al., 1977b)
10 M [SSS TS TS TST]$_n$	(Nguyen et al., 1977a);
14 O [SSS TSTS TTT STST]$_n$	(Nguyen et al., 1979).

A study from Van Dyck et al. (1976a,b), by electron diffraction and microscopy, confirms these arrangements, and shows other polytypes having the following arrangements:

6 M [SSS TS T]$_n$
12 M [SSS TS TS TS TS T]$_n$;
14 M [SSS TS TS TS TS TST]$_n$

In addition the electron microscopic study also shows some special arrangements, for instance, a monoclinic polytype formed by regular alternating units of

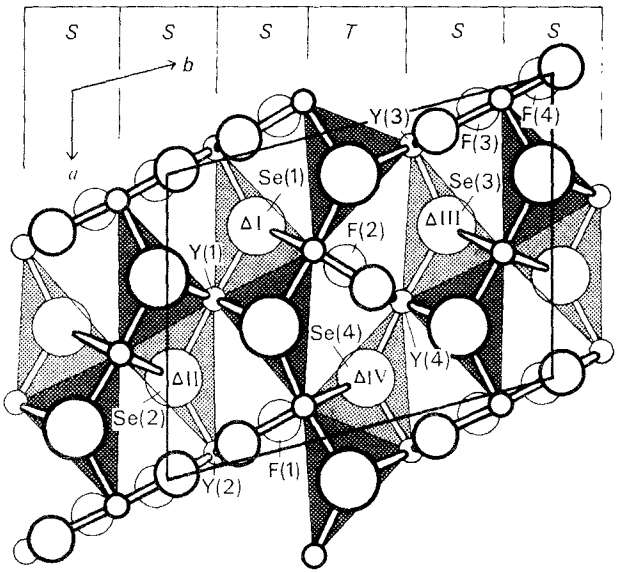

Fig. 31.44. Structure of the monoclinic 4 M polytype of YSeF, $a = 9.96$ Å, $b = 13.00$ Å, $c = 4.106$ Å, $\gamma = 104.92$ Å, $z = 8$.

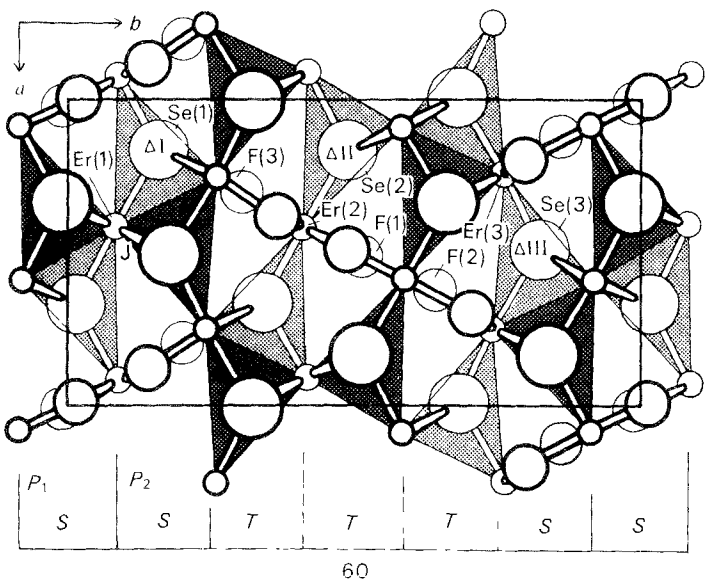

60

Fig. 31.45. Structure of the orthorhombic 6 O polytype of ErSeF, $a = 9.90$ Å, $b = 18.70$ Å, $c = 4.095$ Å, $z = 12$.

10 M and 12 M. Moreover, stacking faults appear in some cases with, for example, exchange of a triad SSS for an alternating arrangement STS.

Recent studies on 8 M, 10 M and 14 O polytypes show the central block of the SSS triad to be strongly non-stoichiometric, fluorine being substituted for by oxygen (Nguyen et al., 1977a,b, 1979).

Finally, it should be noted that this series of polytypes is closely related to another series of polytypes which was described in 16. 2.1.1. Note that the structure of $YbSeF_{1-x}O_{x/2}$ really is an infinite arrangement of the same kind of blocks, $[S]_n$ or $[T]_n$.

References*

Abdullaev, M. Ju., B.N. Ivanovamin and Z.Sh. Karaev, 1968, Azerbajdzh. Khim. Zh. 138.

Abrikosov, N.Kh. and V. Sh. Zargarjan, 1965, Izvest. Akad. Nauk SSSR, neorg. Mater. **1**, 1462.

Abrikosov, N.Kh., V.Sh. Zargarjan, 1967, Izvest. Akad. Nauk SSSR, neorg. Mater. **3**, 280.

Abrikosov, N. Kh., K.A. Zinchenko and A.A. Eliseev, 1970, Izvest. Akad. Nauk, SSSR, neorg. Mater. **6**, 720.

Adamjan, V.E. and G.M. Loginov, 1966, Zh. eksper. teor. Fiz. SSSR **51**, 1044.

Adamjan, V.E. and G.M. Loginov, 1967, Izvest. Akad. Nauk, Arm. SSR., Fiz. **2**, 132.

Adolphe, C., 1965, Ann. Chim., France **10**, 271.

Adolphe, C. and P. Laruelle, 1968, Bull. Soc. Fr. Mineral. Cristallogr. **91**, 219.

Agaev, A.B., U.M. Aliev and T.Kh. Azimov, Azerb. Gos. Univ., Ser. Khim., Nauk **1**, 17.

Agaev, A.B., U.M. Aliev and T.Kh. Azimov, 1974, Azerb. Khim. Zh. **1**, 146.

Aleksandrov, A.Yu., S.P. Ionov, A.K. Karabekov, E.I. Jarembash, 1971, Izvest. Akad. Nauk, SSSR, neorg. Mater. **7**, 1922.

Aliev, 1977, Zh. neorg. Khim., SSSR **22**, 540.

Aliev, U.M., R.S. Gamidov and G.G. Gusejnov, 1972, Izvest. Akad. Nauk, SSSR, neorg. Mater. **8**, 1855.

Aliev, U.M., R.S. Gamidov, G.G. Gusejnov and M.A. Alidzhanov, 1973, Izvest. Akad. Nauk, SSSR., neorg. Mater. **9**, 843.

Aliev, O.M., P.G. Rustamov, 1975, Izvest, Akad. Nauk, SSSR, neorg. Mater. **11**, 2072.

Aliev, O.M., T.Kh. Kurbanov, P.G. Rustamov, M.A. Alidzhanov, S.M. Salmanov, 1976, Izvest. Akad. Nauk, SSSR., neorg. Mater. **12**, 1944.

Alieva, M.M., I.O. Nasibov and P.G. Rustamov, 1973, Akad. Nauk Azerbajdzh. SSR, Dokl., SSSR **28**, 21.

Aloman, A., 1968, Rev. roumaine Sci. tech., Metal. **13**, 185.

Aloman, A.A., S.S. Gorelik, V.M. Maloveckaja, V.I. Buzanov, 1971, Izvest. vyssh. uchebn, Zaved., cvetn. Metallurg., SSSR. **14**, 73.

Ametani, K., 1974, Bull. Chem. Soc. Japan **49**, 2238.

Andrianov, D.G., G.P. Borodulenko, A.A. Grisik, S.A. Drozdov and V.I. Fistul, 1975, Fiz. Tverd. Tela (Leningrad) **17**, 1831.

Atoji, M., 1971, J. Chem. Phys. **54**, 3226.

Babaev, S.Kh., Z.Sh. Karaev and A.G. Rustamov, 1970, Izvest. Akad. Nauk, Azerbajdzh. SSR, Fiz. tekh. mat. Nauk, SSSR **56**.

Bakakin, V.V., E.N. Ipatova and L.P. Solov'eva, 1974, Zh. Strukt. khim. **15**, 460.

Ballestracci, R., 1965, Bull. Soc. fr. Mineral. Cristallogr. **88**, 207.

Ballestracci, R., 1967, Mat. Res. Bull. **2**, 473.

Ballestracci, R. and E.F. Bertaut, 1965a, Bull. Soc. fr. Mineral. Cristallogr. **88**, 136.

Ballestracci, R. and E.F. Bertaut, 1965b, C.R. Acad. Sci., Paris **261**, 5064.

Ballestracci, R. and E.F. Bertaut, 1965c, Bull. Soc. fr. Mineral. Cristallogr. **88**, 575.

Ballestracci, R., 1966a, C.R. Acad. Sci., Paris, Ser. C **262**, 1155.

Ballestracci, R., 1966b, C.R. Acad. Sci., Paris, Ser. C **262**, 1253.

Barnier, S. and M. Guittard, 1976a, C.R. Acad. Sci., Paris, Ser. C **282**, 461.

Barnier, S. and G. Lucazeau, 1976b, J. Chim. Phys. **73**, 580.

Barthélémy, E., 1971, Thèse de 3ème Cycle, Paris.

Beckenbaugh, W., J. Evers, G. Guntherodt, E. Kaldis and P. Wachter, 1975, J. Phys. chem. Solids **36**, 239.

Benazeth, S., D. Carré, M. Guittard and J. Flahaut, 1975, C.R. Acad. Sci., Paris, Ser. C **280**, 1021.

Benazeth, S., D. Carré and P. Laruelle 1977, J. Phys. Col. C7, suppl. No.12, **38**, C7-112.

Berkooz, O., M. Malamud and S. Shtrikman, 1968, Solid. State Comm. **6**, 185.

*This list contains references published after 1964. For references published in or before 1964 consult Flahaut (1968) and Flahaut and Laruelle (1968).

Andrellos, J.C. and P. Bro, 1962, Solid State Electronics 5, 414.

Banks, E. and Ward, R., 1949, J. Electrochem. Soc. 96, 297.

Benacerraf, A. L. Domange and J. Flahaut, 1959, Compt. rend. 248, 1672.

Berkooz, O. and E. Hermon, 1970, Mat. Res. Bull. **5**, 193.
Besançon, P., 1973, J. Solid State Chem. **7**, 232.
Besançon, P., 1979, J. Solid State Chem., (in press.);
Besançon, P. and P. Laruelle, 1969, C.R. Acad. Sci., Paris, Ser. C **268**, 48.
Besançon, P., D. Carré, M. Guittard, M.C. Monnier and J. Flahaut, 1970, C.R. Acad. Sci., Paris, Ser. C **271**, 679.
Besançon, P. and M. Guittard, 1971, C.R. Acad. Sci., Paris, Ser. C **273**, 1348.
Besançon, P., D. Carré and P. Laruelle, 1973, Acta Cryst. **B29**, 1064.
Beskrovnaya, R.A., G.N. Kustova and V.V. Serrebrennikov, 1971, Izvest. Akad. Nauk, SSSR., neorg. Mater. **7**, 1078.
Beskrovnaya, R.A., I.G. Kamaeva, V.V. Serrebrennikov and T.P. Alekseeva, 1973, Tekh. Progr. Dostizh. Nauki Khim. Prom. **149**.
Besrest, F., 1975, Thèse de 3ème Cycle, Paris.
Besrest, F. and G. Collin, 1977, J. Solid. State Chem. **21**, 161.
Besrest, F. and G. Collin, 1978, J. Solid State Chem. **24**, 301.
Bozorth, R.M., F. Holtzberg and S. Mathfessel, 1965, Phys. Rev. Letters **14**, 952.
Bransky, I., N.M. Tallan and A.Z. Hed, 1970, J. Appl. Phys. **41**, 1787.
Brochu, R., J. Padiou and J. Prigent, 1970, C.R. Acad. Sci., Paris, Ser. C **270**, 809.
Brochu, R., J. Padiou and J. Prigent, 1972, C.R. Acad. Sci., Paris Ser. C **274**, 959.
Bronger, W., R. Elter, E. Maus and T. Schmitt, 1973, Rev. Chim. Min. **10**, 147.
Bruzzone, G. and G.L. Olcese, 1965, Colloque Intern. sur les propriétés des dérivés semimétal. Orsay. Edit. CNRS. 1967, Paris, 387.
Bucher, E., A.C. Gossord, K. Anders, J.P. Maita and A.S. Cooper, 1970, 8th Rare Earth Res. Conf. **1**, 74.
Bucher, E., K. Anders, F.J. di Salvo, J.P. Maita, A.C. Gossard, A.S. Cooper and G.W. Hull, 1975, Phys. Rev. **B11**, 500.
Cannon, J.F. and H.T. Hall, 1970, Inorg. Chem. **9**, 1639.
Carcaly, C., J. Flahaut, M. Guittard and M.P. Pardo, 1978, Mat. Res. Bull. **13**, 407.
Carré, D., 1977, Acta Cryst. **B33**, 1163.
Carré, D., P. Laruelle and P. Besançon, 1970, C.R. Acad. Sci., Paris, Ser. C **270**, 537.
Carré, D., J. Flahaut, P. Khodadad, P. Laruelle, N. Rodier and Vovan Tien, 1973a, J. Solid. State Chem. **7**, 321.
Carré, D. and P. Laruelle, 1973b, Acta Cryst. **B29**, 70.
Carré, D. and P. Laruelle, 1974, Acta Cryst. **B30**, 952.
Carré, D., M. Guittard and C. Adolphe, 1978, Acta Cryst., in press.
Carter, F.L., 1965, in Rare Earth Research III, Gordon and Breach, New York, 495.
Carter, F.L., 1972, J. Solid State Chem. **5**, 300.
Cater, E.D., T.E. Lee, E.W. Johnson, E.G. Rauh and H.A. Fick, 1965, J. Phys. Chem. **69**, 2684.
Céolin, R. and P. Khodadad, 1971, C.R. Acad. Sci., Paris, Ser. C **272**, 1769.
Céolin, R. P. Khodadad and G. Sfez, 1972, C.R. Acad. Sci., Paris, Ser. C **274**, 1731.
Céolin, R. and N. Rodier, 1976, Acta Cryst. **B32**, 1476.
Céolin, R., N. Rodier and P. Khodadad, 1977, J. Less-Common Met. **53**, 137.
Chechernikov, V.I., A.V. Pechennikov, E.I. Jarembash and E.S. Vigileva, 1967, Izvest. Akad. Nauk, SSSR, neorg. Mater. **3**, 169.
Chevalier, R., 1968, Thèse de 3ème Cycle, Paris.
Chevalier, R., P. Laruelle and J. Flahaut, 1967, Bull. Soc. fr. Mineral. Cristallogr. **40**, 564.
Chevrel, R., M. Sergent and J. Prigent, 1971, J. Solid State Chem. **3**, 515.
Chevrel, R., M. Sergent and O. Fischer, 1975, Mat. Res. Bull. **10**, 1169.
Chukalin, V.I. and E.I. Jarembash, 1967a, Izvest. Akad. Nauk, SSSR, neorg. Mater. **3**, 1269.
Chukalin, V.I., E.I. Jarembash and A.I. Vilenskij, 1967b, Izvest. Akad. Nauk SSSR, neorg. Mater. **3**, 1538.
Clark, J.B. and K.J. Range, 1975, Z. Naturforsch. **B 30**, 896.
Clark, J.B. and K.J. Range, 1976, Z. Naturforsch. **B 31**, 275.
Collin, G., 1971, Thèse Doctorat ès Sciences, Paris.
Collin, G. and J. Loriers, 1965, C.R. Acad. Sci., Paris, Ser. C **260**, 5043.
Collin, G. and P. Laruelle, 1970a, C.R. Acad. Sci., Paris **270**, 410.
Collin, G. and J. Flahaut, 1970b, C.R. Acad. Sci., Paris **270**, 488.
Collin, G. and P. Laruelle, 1971a, Bull. Soc. fr. Mineral. Crist. **94**, 113.
Collin, G. and P. Laruelle, 1971b, Bull. Soc. fr. Mineral. Crist. **94**, 175.
Collin, G. and J. Flahaut, 1972, Bull. Soc. Chim. France, 2207.
Collin, G., J. Etienne, J. Flahaut, M. Guittard and P. Laruelle, 1973a, Rev. Chim. Min. (Paris) **10**, 225.
Collin, G., J. Etienne and P. Laruelle, 1973b, Bull. Soc. fr. Mineral. Cristallogr. **96**, 12.
Collin, G., C. Dagron and F. Thévet, 1973c, Bull. Soc. Chim. France, 418.
Collin, G., E. Barthélémy and O. Gorochov, 1973d, C.R. Acad. Sci., Paris, Ser. C **277**, 775.
Collin, G. and P. Laruelle, 1974a, Acta Cryst. B **30**, 1134.
Collin, G. and J. Flahaut, 1974b, J. Solid State Chem. **9**, 352.
Collin, G., 1978, To be published.
Coppens, P., S. Smoes and J. Drowart, 1967, Trans. Faraday, Soc. **63**, 2140.
Cox, W.L., H. Steinfink and W.F. Bradley, 1966, Inorg. Chem. **5**, 318.
Cutler, M. and N.F. Mott, 1969, Phys. Rev. **181**, 1336.
Dagron, C., 1966, C.R. Acad. Sci., Paris, Ser. C **262**, 1575.
Dagron, C., 1971, C.R. Acad. Sci., Paris, Ser. C **273**, 352.
Dagron, C., 1972, C.R. Acad. Sci., Paris, Ser. C **275**, 817.

Dagron, C., 1976, C.R. Acad. Sci., Paris, Ser. C **283**, 743.
Dagron, C. and F. Thévet, 1969, C.R. Acad. Sci., Paris, Ser. C **268**, 1867.
Dagron, C. and F. Thévet, 1970, C.R. Acad. Sci., Paris, Ser. C **271**, 677.
Dagron, C. and F. Thévet, 1971, Ann. Chim. **6**, 67.
Daunov, M.I., A.A. Grizik, N.M. Ponomarev and E.V. Schmidt, 1975, Izvest. Akad. Nauk, SSSR, neorg. Mater. **11**, 1129.
Davis, H.H., I. Bransky, N.M. Tallan, 1970, J. Less-Common Metals **22**, 193.
Demoncy, Ph. and P. Khodadad, 1970, Ann. Chim. **5**, 341.
Dernier, P.D., E. Bucher and L.D. Longinotti, 1975, J. Solid State Chem. **15**, 203.
de Saint Giniez, D., P. Laruelle and J. Flahaut, 1968, C.R. Acad. Sci., Paris, Ser. C **267**, 1029.
Dismukes, J.P., R.T. Smith and J.G. White, 1970, Z. Kristallogr. **132**, 272.
Dismukes, J.P., R.T. Smith and J.G. White, 1971, J. Phys. Chem. Solids **32**, 913.
Donohue, P.C., 1975, J. Solid State Chem., **12**, 80.
Donohue, P.C. and J.E. Hanlon, 1974a, J. Electrochem. Soc. **121**, 137.
Donohue, P.C. and W. Jeitschko, 1974b, Mat. Res. Bull. **9**, 1333.
Dugué, J., C. Adolphe and P. Khodadad, 1970, Acta Cryst. B **26**, 1627.
Dugué J., D. Carré and M. Gwittard, 1978, Acta Cryst. **B34**, 403.
Eastman, D.E., F. Holtzberg, J. Freeouf and M. Erbudak, 1974, AIP Conf. Proc. N 18 pt. 2. 1030.
Eatough, N.L., A.W. Webb and H.T. Hall, 1969, Inorg. Chem. **8**, 2069.
Eatough, N.L. and H.T. Hall, 1970, Inorg. Chem. **9**, 417.
Efendiev, G.Kh., Z.Sh. Karaev and I.O. Nasibov, 1964a, Azerbajdzh. Khim. Zh., 103.
Efendiev, G.Kh., Z.Sh. Karaev and I.O. Nasibov, 1964b, Azerbajdzh. Khim. Zh., 125.
Efendiev, G.Kh., Z.Sh. Karaev and I.O. Nasibov, 1964c, Azerbajdzh. Khim. Zh., 111.
Efendiev, G.Kh., Z.Sh. Karaev and I.O. Nasibov, 1964d, Izvest. Akad. Nauk SSSR **28**, 1103.
Eholié, R., O. Gorochov, M. Guittard, A. Mazurier and J. Flahaut, 1971, Bull. Soc. Chim. 747.
Eick, H.A., 1958, J. Am. Chem. Soc. **80**, 43.
Eick, H.A., 1960, Acta Cryst. **13**, 161.
Eliseev, A.A. and V.G. Kuznecov, 1965a, Izvest. Akad. Nauk SSSR, neorg. Mater. **1**, 696.
Eliseev, A.A., E.I. Jarembash, V.G. Kuznecov, L.I. Antonova, I.P. Stojancova, 1965b, Izvest. Akad. Nauk SSSR, neorg. Mater. **1**, 1027.
Eliseev, A.A. and E.I. Jarembash, 1966a, Izvest. Akad. Nauk SSSR, neorg. Mater. **2**, 1156.
Eliseev, A.A. and E.I. Jarembash, 1966b, Izvest. Akad. Nauk SSSR, neorg. Mater. **2**, 1367.
Eliseev, A.A., V.G. Kuznecov, E.I. Jarembash; E.S. Vigileva, L.I. Antonova and K.A. Zinchenko, 1966c, Izvest. Akad. Nauk SSSR, neorg. Mater. **2**, 2241.
Eliseev, A. A. and E.I. Jarembash, 1967a, Izvest. Akad. Nauk SSSR, neorg. Mater. **3**, 1487.
Eliseev, A.A., V.G. Kuznecov and E.I. Jarembash, 1967b, Izvest. Akad. Nauk SSSR, neorg. Mater. **3**, 1267.
Eliseev, A.A., S.I. Uspenskaya and A.A. Federov, 1971, Russ. J. Inorg. chem., **16**, 768 – Zh. neorg. chem., SSSR **16**, 1485.
Eliseev, A.A., S.I. Uspenskaya and T.A. Kalganova, 1972a, Russ. J. Inorg. Chem. **17**, 1222 – Zh. neorg. Khim. SSSR **17**, 2340.
Eliseev, A.A., S.I. Uspenskaya, A.A. Federov and V.A. Tolstova, 1972b, Zh. strukt. Khim., SSSR **13**, 77.
Eliseev, A.A., O.A. Sadovskaya and Nguyen Van Tyam, 1974, Izvest. Akad. Nauk SSSR, neorg. Mater. **10**, 2134.
Eliseev, A.A., A.A. Grizik, V.A. Tolstova and G.P. Borodulenko, 1975a, Zh. Neorg. Khim. **20**, 1159.
Eliseev, A.A., O.A. Sadovskaya and Nguyen Van Tyam, 1975b, Izvest. Akad. Nauk SSSR, neorg. Mater. **11**, 424.
Eliseev, A.A., A.A. Grizik, G.M. Kuz'micheva and G.P. Borodulenko, 1975c, Zh. Neorg. Khim. **20**, 1738.
Eliseev, A.A., G.M. Kuz'micheva, E.A. Pisarev, G.P. Borodulenko and A.A. Grizik, 1975d, Zh. Neorg. Khim. **20**, 1167.
Eliseev, A.A., K.A. Zinchenko, V.M. Zemlyanukhia and Nguyen Van Tyam, 1976a, Zh. Neorg. Khim. **21**, 2603.
Eliseev, A.A., G.M. Kuz'micheva and Le Van Khuan, 1976b, Zh. Neorg. Khim., SSSR **21**, 3167.
Etienne, J., 1969, Bull. Soc. fr. Mineral. Cristallogr. **92**, 134.
Etienne, J., 1973, Bull. Soc. fr. Mineral. Cristallogr. **96**, 37.
Fischer, O., A. Treyvaud, R. Chevrel and M. Sergent, 1975, Solid State Comm. **17**, 721.
Flahaut, J., 1968. Chimie cristalline des combinaisons ternaires soufrées, séléniées et tellurées formées par les éléments des terres rares – in "Progress in Science and Technology of the Rare Earths". **3**, 209–283 (Pergamon Press).
Flahaut, J., 1972, "Transition metal chalcogenides", in "Biennal Review of Chemistry" **10**, 185–241, M.T.P., (Butterworths and Cie).
Flahaut, J., 1974, J. Solid State Chem. **9**, 124.
Flahaut, J., 1976, Ann. Chim. **1**, 27.
Flahaut, J., L. Domange, M. Guittard and M.P. Pardo, 1965a, Bull. Soc. Chim. France, **226**.
Flahaut, J., P. Laruelle, M.P. Pardo and M. Guittard, 1965b, Bull. Soc. Chim. France, 1399.
Flahaut, J., M. Guittard, M. Patrie, M.P. Pardo, S.M. Golabi and L. Domange, 1965c, Acta Cryst. **19**, 14.
Flahaut, J. and P. Laruelle, 1968. Chimie cristalline des sulfures, séléniures et tellurures binares des éléments des terres rares – in

Dismukes, J.P. and J.G. White, 1964, Inorg. Chem. 3, 1220.
Flahaut, J., M. Guittard and M. Patrie, 1958, Bull. Soc. Chim. France, p. 990.
Flahaut, J., M. Guittard and M. Patrie, 1959, Bull. Soc. Chim. France, p. 1917.

"Progress in Science and Technology of the Rare Earths". **3**, 151–208 (Pergamon Press).
Flahaut, J. and P. Laruelle, 1970, in "The Chemistry of Extended Defects in Non-Metallic Solids" (North-Holland, Amsterdam) 109–123.
Fradin, F.Y., J.W. Downey and T.E. Klippert, 1976, Mat. Res. Bull. **11**, 993.
Furrer, A. and E. Warming, 1974, J. Phys., C. **7**, 3365.
Fujii, H., 1972, J. Sci. Hiroshima Univ., A **36**, 67.
Ghémard, G., 1976, Bull. Soc. Chim. France, 1007.
Ghémard, G., C. Souleau and J. Etienne, 1971a, C.R. Acad. Sci., Paris, Ser. C **272**, 468.
Ghémard, G., C. Souleau and M. Chaigneau, 1971b, Bull. Soc. Chim. France, 3120.
Ghémard, G., C. Souleau and J. Flahaut, 1972, C.R. Acad. Sci., Paris, Ser. C **274**, 1817.
Ghémard, G. and J. Etienne, 1978a, Acta Cryst., in press.
Ghémard, G., J. Schiffmacher and J. Etienne, 1978b, Acta Cryst., in press.
Godlewski, E., S. Jaulmes, J. Etienne, 1978, Acta Cryst., to be published.
Golabi, S.M., J. Flahaut and L. Domange, 1965a, C.R. Acad. Sci., Paris **260**, 6385.
Golabi, S.M., J. Flahaut and L. Domange, 1965b, Rev. Hautes Temp. et Réfract. **2**, 263.
Golosovski, I.V. and V.P. Plakhty, 1973, Phys. Status Solidi b **56**, 61.
Golovin, Yu. M., K.I. Petrov, E.M. Loginova, A.A. Grizik and N.M. Ponomarev, 1975, Zh. neorg. Khim., SSSR **20**, 283.
Gorochov, O., Vovan Tien, Nguyen Huy Dung, E. Barthélémy and J. Flahaut, 1969, Colloque Eléments Terres Rares, Edit. CNRS, 1970, 157, T.2.
Gorochov, O., E. Barthélémy and Nguyen Huy Dung, 1971, C.R. Acad. Sci., Paris, Ser. C **273**, 368.
Gorochov, O. and H. McKenzie, 1973, J. Solid State Chem. **7**, 400.
Goryachev, Yu. M., T.G. Kutnenok, 1972, High Temperature–High Pressures, vol. 4, 663.
Grizik, A.A., G.P. Borodulenko, 1977, Zh. neorg. Khim. **22**, 542.
Guittard, M., 1965, C.R. Acad. Sci., Paris **261**, 2109.
Guittard, M., J. Flahaut and L. Domange, 1966, Acta Cryst. **21**, 832.
Guittard, M. and J. Flahaut, 1967, C.R. Acad. Sci., Paris **264**, 1951.
Guittard, M., M. Julien-Pouzol, P. Laruelle and J. Flahaut, 1968a, C.R. Acad. Sci., Paris, Ser. C **267**, 767.
Guittard, M. and J. Flahaut, 1968b, Bull. Soc. Chim. France, 4759.
Guittard, M. and M. Julien-Pouzol, 1970, Bull. Soc. Chim. France, 2467.
Guittard, M. and A.M. Lozac'h, 1971, Bull. Soc. Chim. France, 751.
Guittard, M., M. Julien-Pouzol and S. Jaulmes, 1976a, Mat. Res. Bull. **11**, 1073.
Guittard, M., P.H. Fourcroy and J. Flahaut, 1976b, Ann. Chim. **1**, 47.
Guittard, M., M.P. Pardo and A.M. Loireau-Lozac'h, 1977, C.R. Acad. Sci., Paris, Ser. C **284**, 37.
Guittard, M., D. Carré and T.S. Kabré, 1978a, Mat. Res. Bull. **13**, 279.
Guittard, M., A.M. Loireau-Lozac'h, M.P. Pardo and J. Flahaut, 1978b, Mat. Res. Bull. **13**, 317.
Guntherodt, G. and P. Wachter, 1974, AIP Conf. Proc., N 18 Pt 2, 1034.
Gus'kova, V.P. and V.V. Serebrennikov, 1973a, Tr. Tomsk. Gos. Univ. **240**, 132, and **249**, 137.
Gus'kova, V.P. and V.V. Serebrennikov, 1973b, Tr. Tomsk. Gos. Univ. 249, 168.
Gus'kova, V.P., V.V. Serebrennikov and G.E. Snopkov, 1975, Zh. neorg. Khim, SSSR **20**, 2058.
Guthrie, G.L. and R.L. Palmer, 1965, Phys. Rev. Letters **15A**, 8.
Haase, D.J., H. Steinfink and E.J. Weiss, 1965, Inorg. Chem. **4**, 541.
Haase, D.J. and H. Steinfink, 1966, J. Appl. Phys. **37**, 2246.
Heikens, H.H. and C.F. van Bruggen, 1973, 4th Conference on the Transition Elements – Genève.
Hirota, K., N. Kinomura, S. Kume and M. Koizumi, 1976, Mat. Res. Bull. **11**, 227.
Hoggins, J. and H. Steinfink, 1968, Inorg. Chem. **7**, 826.
Holtzberg, F., 1971, Mat. Res. Symp. Solid State Chem., Gaithersburg. 100.
Holtzberg, F., Y. Okaya and N. Stemple, 1965, Americ. Cryst. Association Meeting, Gatlinberg, Tenn.
Holtzberg, F., and S. Methfessel, 1966, J. Appl. Phys. **37**, 1433.
Holtzberg, F., P.E. Seiden and S. von Molnar, 1968, Phys. Rev. **168**, 408.
Holtzberg, F., D.C. Cronemeyer, T.R. McGuire and S. von Molnar, 1972, Nat. Bur. Stand. (U.S.), Spec. Publ. No. 364, 637.
Hoppe, R., 1968, Z. anorg. allgem. Chem. **357**, 202.
Hulliger, F., and O. Vogt, 1965, Physics Letters **17**, 238.
Hulliger, F. and O. Vogt, 1966a, Physics Letters **21**, 138.
Hulliger, F. and O. Vogt, 1966b, Helv. Phys. Acta **34**, 199.
Hulliger, F., M. Landolt, R. Schmelczer and I. Zarbach, 1975, Solid State Comm. **17**, 751.
Ismatov, A.A., 1970a, Uzbek. Khim. Zh. SSSR, neorg. Khim. **14**, 17.
Ismatov, A.A., 1970b, Zh. Neorg. Khim. SSSR, **15**, 3371.
Ismatov, A.A., 1970c, Izvest. Akad. Nauk SSSR, Neorg. Mater. **6**, 178.
Ismatov, A.A., V.A. Kolesova and M.M. Pirjeitko, 1970, Izvest. Akad. Nauk SSSR, Neorg. Mater. **6**, 1361.
Jarembash, E.I., A.A. Eliseev and K.A. Zinchenko, 1965a, Izvest. Akad. Nauk SSSR, Neorg. Mater. **1**, 60.

Holtzberg, F., 1963, Acta Cryst. 16A, 44.

Jarembash, E.I., E.S. Vigileva, A.A. Eliseev and A.A. Rechicova, 1965b, Izvest. Akad. Nauk SSSR, Neorg. Mater. **1**, 330.
Jarembash, E.I., E.S. Vigileva, R.R. Kagramanova and L.Kh. Kravchenko, 1969, Izvest. Akad. Nauk SSSR, Neorg. Mater. **5**, 260.
Jarembash, E.I. and E.S. Vigileva, 1970, Izvest. Akad. Nauk SSSR, Neorg. Mater. **6**, 1572.
Jarembash, E.I., E.S. Vigileva, A.A. Eliseev, A.V. Zachatskaya, T.G. Aminov and M.A. Chernitsyna, 1974, Izvest. Akad. Nauk SSSR, Neorg. Mater. **10**, 1409.
Jaulmes, S., 1974, Acta Cryst. **B30**, 2283.
Jaulmes, S., 1978, Acta Cryst., in press.
Jaulmes, S. and P. Laruelle, 1973, Acta Cryst. **B29**, 352.
Jaulmes, S. and M. Julien-Pouzol, 1977a, Acta Cryst. **B33**, 1191.
Jaulmes, S. and M. Julien-Pouzol, 1977b, Acta Cryst. **B33**, 3898.
Jeitschko, W. and P.C. Donohue, 1975, Acta Cryst. **B31**, 1890.
Jellinek, F., 1971, Mat. Res. Bull. **6**, 169.
Julien-Pouzol, M., M. Guittard and J. Flahaut, 1968a, Bull. Soc. Chim. France, 533.
Julien-Pouzol, M. and M. Guittard, 1968b, Bull. Soc. Chim. France 2293.
Julien-Pouzol, M., M. Guittard and C. Adolphe, 1968c, C.R. Acad. Sci., Paris, Ser. C **267**, 823.
Julien-Pouzol, M. and M. Guittard, 1969, C.R. Acad. Sci. Paris, Ser. C **269**, 316.
Julien-Pouzol, M., M. Guittard and A. Mazurier, 1970, C.R. Acad. Sci., Paris, Ser. C **271**, 1317.
Julien-Pouzol, M. and M. Guittard, 1972, Ann. Chim. **7**, 253.
Julien-Pouzol, M. and M. Guittard, 1973, Ann. Chim. **8**, 139.
Julien-Pouzol, M. and P. Laruelle, 1977, Acta Cryst. **B33**, 1510.
Kabré, S., M. Julien-Pouzol and M. Guittard, 1972, C.R. Acad. Sci., Paris, Ser. C **275**, 1367.
Kabré, S., M. Julien-Pouzol and M. Guittard, 1974, Bull. Soc. Chim. France, 1881.
Karaev, Z.Sh., A.M. Gamidov and M.I. Murguzov, 1965, Azerb. Khim. Zh. 110.
Karaev, Z.Sh., I.O. Nasibov and Sh.S. Alieva, 1966a, Izvest. Akad. Nauk SSSR, Neorg. Mater. **2**, 1322.
Karaev, Z.Sh., L.G. Kejserukhskaya, Sh.A. Alieva and A.M. Gamidov, 1966b, Azerbajdzh., Khim. Zh., 112.
Kato, K., I. Kawada and T. Takahashi, 1977, Acta Cryst. **B33**, 3437.
Kejserukhskaya, L.G., N.P. Luzhnaya and Z.Sh. Karaev, 1970, Neorg. Mater. **6**, 1869.
Kejserukhskaya, L.G., N.P. Luzhnaya and Z.Sh. Karaev, 1972, Azerbajdzh. Khim. Zh., SSSR, 159.
Kent, R.A. and H.A. Eick, 1962, Inorg. Chem. **1**, 956.
Kharitonov, Yu.A., N.L. Smirnova and N.V. Belov, 1966, Zh. strukt., Khim., SSSR **7**, 889.
Khodadad, P., Tek Tat, J. Flahaut and L. Domange, 1965, C.R. Acad. Sci., Paris, Ser. C **260**, 2235.
Khodadad, P., J. Dugué and C. Adolphe, 1967, C.R. Acad. Sci., Paris, Ser. C **265**, 379.
Khusnutdinova, V., V.S. Oskotskii, I.A. Smirnov and V.M. Sergeeva, 1971, Phys. Status Solidi **B48**, 353.
Kuznecov, V.G., A.A. Eliseev and G.N. Novitskaya, 1972, Congrès Minsk, 119.
Lashkarev, G.V. and A.V. Savickij, 1967, Fiz. Tverd. Tela. SSSR **9**, 1883
Lashkarev, G.V., E.I. Jarembash, A. Karabekov and N.P. Giletskii, 1971, Phys. Status Solidi **B44**, K 41.
Lin, W., H. Steinfink and E.J. Weiss, 1965, Inorg. Chem. **5**, 877.
Loganova, E.M., A.A. Grizik, N.M. Ponomarev and A.A. Eliseev, 1975, Izvest. Akad. Nauk SSSR, neorg. Mater. **11**, 749.
Loginov, G.M., A.T. Starovojtov and A.V. Golubkov, 1969, Fiz. tverd. Tela. SSSR **11**, 3637.
Loireau-Lozac'h, A.M., 1977, Thèse Doctorat ès Sciences, Paris VI.
Loireau-Lozac'h, A.M., M. Guittard and J. Flahaut, 1976, Mat. Res. Bull. **11**, 1489.
Loireau-Lozac'h, A.M., M. Guittard and J. Flahaut, 1977a, Mat. Res. Bull. **12**, 881.
Loireau-Lozac'h, A.M. and M. Guittard, 1977b, Mat. Res. Bull. **12**, 887.
Longo, J.M. and P.M. Raccah, 1967, Mat. Res. Bull. **2**, 541.
Lozac'h, A.M., S. Jaulmes and M. Guittard, 1971, C.R. Acad. Sci., Paris **272**, 1123.
Lozac'h, A.M. and M. Guittard, 1973a, Bull. Soc. Chim. France, 6.
Lozac'h, A.M., M. Guittard and J. Flahaut, 1973b, Mat. Res. Bull. **8**, 75.
Lucazeau, G., S. Barnier and A.M. Loireau-Lozac'h, 1977, Mat. Res. Bull. **12**, 437.
Lugscheider, W., H. Pink, K. Weber and W. Zinn, 1970, Z. angew. Phys. **30**, 36.
Lugscheider, W., H. Pink, K. Weber and W. Zinn, 1971, J. Phys. Colloq. **32**, 731.
McKinzie, H., O. Gorochov, Nguyen Huy Dung and C. Dagron, 1971, C.R. Acad. Sci., Paris, Ser. **B**, **273**, 1040.
Marcon, J.P. and R. Pascard, 1966a, C.R. Acad. Sci., Paris, Ser. C **262**, 1679.
Marcon, J. and R. Pascard, 1966b, J. Inorg. nucl. Chem. **28**, 2551.
Marcon, J. and R. Pascard, 1968a, Rev. Int. Hautes Temp. Réfract. **5**, 51.
Marcon, J.P. and R. Pascard, 1968b, C.R. Acad. Sci., Paris, Ser. C **266**, 270.
Mathur, M.P., D.W. Deis, C.K. Jones, A. Patterson and W.J. Carr, 1971, J. Appl. Phys. **42**, 1693.
Mazurier, A. and J. Etienne, 1973, Acta Cryst., **B29**, 817.
Mazurier, A. and J. Etienne, 1974, Acta Cryst., **B30**, 752.
Mel'chenko, G.G. and V.V. Serebrennikov, 1973, Zh. Neorg. Khim. **18**, 2572.
Messin, D., D. Carré and P. Laruelle, 1977, Acta Cryst. **B33**, 2540.
Meyer, A. and H. Pink, 1973, J. less Common Metals, 30, 314.
Michelet, A., 1972, Thèse Doctorat ès Sciences, Paris.

Michelet, A., P. Laruelle and J. Flahaut, 1966, C.R. Acad. Sci., Paris, Ser. C **262**, 753.
Michelet, A. and J. Flahaut, 1969a, C.R. Acad. Sci., Paris, Ser. C **268**, 326.
Michelet, A. and J. Flahaut, 1969b, C.R. Acad. Sci., Paris, **269**, 1203.
Michelet, A., G. Perez, J. Etienne and M. Darriet-Duale, 1970, C.R. Acad. Sci., Paris, Ser C **271**, 513.
Michelet, A., A. Mazurier, G. Collin, P. Laruelle and J. Flahaut, 1975, J. Solid. State Chem. **13**, 65.
Moseley, P.T., D. Brown and B. Whittaker, 1972, Acta Cryst. **B28**, 1816.
Narasimhan, K.S.V.L. and H. Steinfink, 1968/9, Mater. Sci. Eng. **3**, 309.
Nasibov, I.O., T.I. Sultanov, P.G. Rustamov, Z.Sh. Karaev, and A.D. Nazarov, 1972, Azerbajdzh. Khim. Zh. SSSR **1**, 99.
Nasibov, I.O., P.G. Rustamov, M.M. Alieva and M.I. Mourgusov, 1975a, in "Préparations et étude des propriétés des combinaisons des métaux des terres rares." Edit. Akad. Sci., SSR Ukraine, Kiev, 104.
Nasibov, I.O., P.G. Rustamov, Z.Sh. Karaev, T.U. Sultanov and M.I. Mourgusov, 1975b, in "Préparations and studies of properties of rare earth metals compounds." Edit. Akad. Sci., SSR Ukraine, Kiev, 129.
Nguyen Huy-Dung, 1971, Thèse Doctorat ès Sciences, Paris.
Nguyen Huy-Dung, 1973a, Bull. Soc. fr. Mineral. Crist. **96**, 41.
Nguyen Huy-Dung, 1973b, Bull. Soc. fr. Mineral. Crist. **96**, 44.
Nguyen Huy-Dung, 1973c, Acta Cryst. **B29**, 2095.
Nguyen Huy-Dung, J. Etienne and J. Flahaut, 1969, C.R. Acad. Sci., Paris, Ser. C **269**, 120.
Nguyen Huy-Dung, J. Etienne and P. Laruelle, 1971, Bull. Soc. Chim. France, 2433.
Nguyen Huy-Dung, C. Dagron and P. Laruelle, 1975a, Acta Cryst. **B31**, 514.
Nguyen Huy-Dung, C. Dagron and P. Laruelle, 1975b, Acta Cryst. **B31**, 519.
Nguyen Huy-Dung and P. Laruelle, 1977a, Acta Cryst. **B33**, 1444.
Nguyen Huy-Dung and P. Laruelle, 1977b, Acta Cryst. **B33**, 3360.
Nguyen Huy-Dung and P. Laruelle, 1979, Acta Cryst. (in press).
Nogteva, V.V., I.E. Paukov and E.I. Jarembash, 1969a, Zh. fiz. Khim., SSSR **43**, 2118.
Nogteva, V.V., I.E. Paukov and E.I. Jarembash, 1969b, Zh. fiz. Khim., SSSR **43**, 2344.
Norling, B.K. and H. Steinfink, 1966, Inorg. Chem. **5**, 1488.
Novikov, V.I. and S.S. Shalyt, 1970, Fiz. Tverd. Tela **12**, 3252.
Obolonchik, V.A., G.V. Lashkarev and V.G. Denijanchuk, 1966, Izvest. Akad. Nauk SSSR, Neorg. Mater. **2**, 100.
Omloo, W.P., F. Jellinek, 1968, Rec. Trav. Chim. Pays-Bas, **87**, 545.
Omloo, W.P., J.C. Bommerson, H.H. Heikens, H. Risselda, M.B. Vellinga, C.F. Van Bruggen, C. Haas and F. Jellinek, 1971, Phys. Status Solidi, appl. Res. **5**, 349.
Pardo, M.P., O. Gorochov, J. Flahaut and L. Domange, 1965, C.R. Acad. Sci., Paris **260**, 1666.
Pardo, M.P. and J. Flahaut, 1966, C.R. Acad. Sci., Paris, Ser. C **262C**, 1058.
Pardo, M.P. and J. Flahaut, 1967a, Bull. Soc. Chim., 3658.
Pardo, M.P. and J. Flahaut, 1967b, C.R. Acad. Sci., Paris, Ser. C **265**, 1254.
Pardo, M.P. and J. Flahaut, 1969, Bull. Soc. Chim. France, 6.
Pardo, M.P. and J. Flahaut, 1971, Bull. Soc. Chim. France, 3411.
Pardo, M.P. and J. Flahaut, 1972, Bull. Soc. Chim. France, 2189.
Pardo, M.P., M. Julien-Pouzol and J. Flahaut, 1973, C.R. Acad. Sci., Paris, Ser. C **276**, 599.
Pardo, M.P., R. Céolin and M. Guittard, 1976, C.R. Acad. Sci., Paris, Ser. C **283**, 735.
Patrie, P., 1969, Bull. Soc. Chim., France, 1600.
Patrie, M., J. Flahaut and L. Domange, 1965, Rev. Hautes Temp. et Réfract. **2**, 187.
Patrie, M. and R. Chevalier, 1966, C.R. Acad. Sci., Paris, Ser. C **263**, 1061.
Patrie, M. and J. Flahaut, 1967, C.R. Acad. Sci., Paris, Ser. C **264**, 395.
Patrie, M., Nguyen Huy-Dung and J. Flahaut, 1968, C.R. Acad. Sci., Paris, Ser. C **266**, 1575.
Patrie, M. and M. Guittard, 1969a, C.R. Acad. Sci., Paris, Ser. C **268**, 1136.
Patrie, M., M. Guittard and J. Flahaut, 1969b, Bull. Soc. Chim. France, 3832.
Patrie, M., H.D. Nguyen, N. Rodier, N. Nikolova, M. Lepeltier and J. Flahaut, 1969c, Colloque Eléments Terres Rares, Paris-Grenoble, 1970. Edit. CNRS, 451.
Paukov, I.E., V.V. Nogteva and E.I. Jarembash, 1968, Zh. fiz. Khim., SSSR **42**, 998.
Paukov, I.E., V.V. Nogteva and E.I. Jarembash, 1969, Zh. fiz, Khim., SSSR **43**, 2351.
Pechennikov, A.V., V.I. Chechernikov, E.I. Jarembash, K.A. Zinchenko, 1967, Izvest. Akad. Nauk SSSR, Neorg. Mater. **3**, 1086.
Pechennikov, A.V., V.A. Kuprijanov, V.I. Chechernikov, N.Kh. Abrikosov, K.A. Zinchenko, 1970, Izvest. Akad. Nauk SSSR, Neorg. Mater. **6**, 1528.
Penney, T., F. Holtzberg, L.J. Tao, S. von Molnar, 1974, AIP Conf. Proc. N 18, 908.
Perez, G. and M. Duale, 1969, C.R. Acad. Sci., Paris, Ser. C. **269**, 984.
Perez, G., M. Darriet-Duale and P. Hagenmuller, 1970, J. Solid. State Chem., **2**, 42.
Plug, C.M. and G.C. Vershoor, 1976, Acta Cryst. **32**, 1856.
Plumier, R., M. Sougi and G. Collin, 1974, Solid. State Comm. **14**, 971.
Poix, P., 1970, C.R. Acad. Sci., Paris, Ser. C **270**, 1852.
Pokrzywnicki, S., A. Czopnik, B. Wróbel and L. Pawlak, 1974, Phys. Status Solidi (b) **64**, 685.
Potel, M., R. Brochu, J. Padiou and D. Grandjean, 1972, C.R. Acad. Sci., Paris, Ser. C **275**, 1419.
Prewitt, C.T. and A.W. Sleight, 1968, Inorg. Chem. **7**, 1090.
Picon, M. and J. Flahaut, 1958, Bull. Soc. Chim. France, p. 772.

Raccah, P.M., J.M. Longo and H.A. Eick, 1967, Inorg. Chem. **6**, 1471.
Ramsey, T.H., H. Steinfink and E.J. Weiss, 1965a, Inorg. Chem. **5**, 1154.
Ramsey, T.H., H. Steinfink and E.J. Weiss, 1965b, J. Appl. Phys. **36**, 548.
Range, K.J. and R. Leeb, 1975a, Z. Naturforsch. **30b**, 637.
Range, K.J. and R. Leeb, 1975b, Z. Naturforsch. **30b**, 889.
Range, K.J. and R. Leeb, 1976a, Z. Naturforsch. **31b**, 311.
Range, K.J. and R. Leeb, 1976b, Z. Naturforsch. **31b**, 685.
Reisfeld, R. and A. Bornstein, 1977a, Chem. Phys. Letters **47**, 194.
Reisfeld, R., A. Bornstein, J. Flahaut, M. Guittard and A.M. Loireau-Lozac'h, 1977b, Chem. Phys. Letters **47**, 408.
Riedel, E., R. Karl and R. Rackwitz, 1977, Mat. Res. Bull. **12**, 599.
Rodier, N., 1973, Bull. Soc. fr. Mineral. Cristallogr. **96**, 350.
Rodier, N., P. Laruelle and J. Flahaut, 1969, C.R. Acad. Sci., Paris, Ser. C **269**, 1391.
Rodier, N. and P. Laruelle, 1970, C.R. Acad. Sci., Paris, Ser. C **270**, 2127.
Rodier, N. and P. Laruelle, 1972, Bull. Soc. fr. Mineral, Cristallogr. **95**, 548.
Rodier, N. and P. Laruelle, 1973, Bull. Soc. fr. Mineral Cristallogr. **96**, 30.
Rodier, N. and Vovan Tien, 1974, C.R. Acad. Sci., Paris, Ser. C. **279**, 817.
Rodier, N. and Vovan Tien, 1975, Bull. Soc. fr. Mineral Cristallogr. **98**, 30.
Rodier, N. and Vo Van Tien, 1976a, Acta Cryst. **B32**, 2705.
Rodier, N. and Vo Van Tien, 1976b, Bull. Soc. fr. Mineral. Cristallogr. **99**, 8.
Rodier, N., Vo Van Tien and M. Guittard, 1976c, Mat. Res. Bull. **11**, 1209.
Rodier, N. and Vo Van Tien, 1977a, C.R. Acad. Sci., Paris, Ser. C **284**, 909.
Rodier, N. Vo Van Tien, 1977b, C.R. Acad. Sci., Paris, Ser. C **285**, 133.
Rustamov, P.G., Z.Sh. Karaev, I.O. Nasibov, T.I. Sultanov and R.S. Gamidov, 1971, Azerbadjdzh. Khim. Zh. SSSR **3**, 97.
Rustamov, P.G., I.O. Nasibov and M.M. Alieva, 1973, Izvest. Akad. Nauk SSSR, Neorg. Mater. **9**, 1900.
Rustamov, P.G., Eh. M. Godzhaev, M.S. Guseinov, O.M. Aliev, 1977, Zh. neorg. Khim. **22**, 540.
Rysanek, N. and O. Loye, 1973, Acta Cryst. **B29**, 1567.
Sadovskaya, O.A., and E.I. Jarembash, 1970, Izvest. Akad. Nauk SSSR, Neorg. Mater. **6**, 1252.
Samsonov, G.V., Yu.B. Paderno, Z.Sh. Karaev, M.I. Murguzov, V.P. Fedorchenko, I.O. Nasibov, 1967, Azerbajdzh. Khim., Zh. 43.
Samsonov, G.V., Yu.B. Paderno, M.I. Murguzov and V.P. Fedorchenko, 1968, Izvest. Akad. Nauk SSSR., Neorg. Mater. **4**, 1225.
Sarkisov, E.S., R.A. Lidin and Yu.M. Khazaĭnov, 1968, Izvest. Akad. Nauk SSSR, Neorg. Mater. **4**, 2033.
Sarkisov, E.S., R.A. Lidin and V.V. Shum, 1970, Izvest. Akad. Nauk SSSR, Neorg. Mater. **6**, 2054.
Savigny, N., C. Adolphe, A. Zalkin and D.H. Templeton, 1973a, Acta Cryst. **B29**, 1532.
Savigny, N., P. Laruelle and J. Flahaut, 1973b, Acta Cryst. **B29**, 345.
Schobinger-Papamantellos, P.P. Fischer, A. Niggli, E. Kaldis and V. Hildebrand, 1974, J. Phys. C **7**, 2023.
Seiden, P.E., 1968, Phys. Rev. **168**, 403.
Sfez, G. and C. Adolphe, 1972, Bull. Soc. fr. Mineral. Crist. **95**, 553.
Sfez, G. and C. Adolphe, 1973, Bull. Soc. fr. Mineral. Crist. **96**, 37.
Sharifov, K.A., Z.Sh. Karaev and T.Kh. Azizov, 1967, Izvest. Akad. Nauk SSSR, Neorg. Mater. **3**, 719.
Shelton, R.N., A.R. Moodenbaugh, P.D. Dernier and B.T. Mattias, 1975, Mat. Res. Bull. **10**, 1111. ^h
Shelton, R.N., R.W. McCallum and H. Adrian, 1976, Phys. Letters, A. **56A**, 213.
Sleight, A.W. and C.T. Prewitt, 1968, Inorg. Chem.**7**, 2282.
Smirnov, I.A., 1972, Phys. Status Solidi **14**, 363.
Smirnov, I.A., L.S. Parfenieva and V.M. Sergeieva, 1972, Phys. Status Solidi, **14**, 1050.
Smirnov, I.A., L.S. Parfenieva and V.M. Sergeieva, 1973, Izvest. Akad. Nauk SSSR, Neorg. Mater. **9**, 485.
Smoes, S., P. Coppens, C. Bergman and J. Drowart, 1969, Trans. Faraday Soc. **65**, 682.
Smolenskii, G.A., V.P. Zhuza, V.E. Adamyan and G.M. Loginov, 1966, Phys. Status Solidi **18**, 873.
Solomons, F.W., E. Antonides, D. Stoppels and G.A. Sawatzky, 1974, Solid State Comm. **15**, 1467.
Somov, A.P., A.V. Nikolskaya, Ya.I. Gerasimov, 1973, Izvest. Akad. Nauk SSSR, Neorg. Mater. **9**, 575.
Souleau, C., M. Guittard and M. Wintenberger, 1966, Bull. Soc. Chim. France, 1644.
Souleau, C. and M. Guittard, 1968, Bull. Soc. Chim. France, 3632.
Souleau, C., M. Guittard and P. Laruelle, 1969, Bull. Soc. Chim. France, 9.
Starovoitov, A.T., V.I. Oshogin, G.M. Loginov and V.M. Sergeyeva, 1969, Zh. Eksp. Teor. Fiz.**57**, 791.
Stretz, L.A. and E.D. Cater, 1975, High. Tem. Sc. **7**, 204.
Suryanarayanan, R. and C. Paparoditis, 1968, J. Phys., Colloq., 46.
Taher, S.M.A., J.B. Gruber and L.C. Olsen, 1973a, Bull. Amer. Phys. Soc. **18**, 354.
Taher, S.M.A. and J.B. Gruber, 1973b, Bull. Amer. Phys. Soc. **18**, 1606.
Taher, S.M.A., J.B. Gruber and L.C. Olsen, 1974, J. Chem. Phys. **60**, 2050.
Takahashi, T., T. Oka, O. Yamada and K. Ametani, 1971, Mater. Res. Bull. **6**, 173.
Ring, S.A. and M. Tecotzky, 1964, Inorg. Chem. 3, 182.
Suchow, L. and N.R. Stemple, 1964, J. Electrochem. Soc 111, 191.

Takahashi, T., S. Osaka and O. Yamada, 1973, J. Phys. Chem. Solids **34**, 1131.
Takahashi, T., K. Ametani and O. Yamada, 1974, J. Cryst. Growth **24**, **25**, 151.
Tao, L.J., J.B. Torrance and F. Holtzberg, 1974. Solid State Comm. **15**, 1025.

Teske, C.L., 1974, Naturforsch. **B29**, 16.
Tikhomirova, L.M., A.A. Eliseev and E.I. Jarembash., 1970, Izvest. Akad. Nauk SSSR, Neorg. Mater. **6**, 994.
Tikhonov, V.V., M.V. Romanova, I.A. Smirnov and V.M. Sergeeva, 1971, Fiz. Tverd. Tela, SSSR **13**, 2023.
Tikhonov, V.V., V.N. Bystrova, R.G. Mitarova and I.A. Smirnov, 1975a, Fiz. Tverd. Tela, SSSR **17**, 1225.
Tikhonov, V.V., R.G. Mitarov and I.A. Smirnov, 1975b, Zh. Fiz. Khim. **49**, 3008.
Tomas, A., M. Guittard, R. Chevalier and J. Flahaut, 1976a, C.R. Acad. Sci., Ser. C **282**, 587.
Tomas, A., R. Chevalier, P. Laruelle and B. Bachet, 1976b, Acta Cryst. **B32**, 3287.
Tomas, A. and M. Guittard, 1977, Mat. Res. Bull. **12**, 1043.
Tomas, A., R. Chevalier and P. Laruelle, 1978, Acta Cryst., in press.
Toropov, N.A. and A.A. Ismatov, 1970, Izvest. Akad. Nauk SSSR, Neorg. Mater. **6**, 590.
Tromme, M., 1971, C.R. Acad. Sci., Paris, Ser. C **273**, 849.
Urban, P., G. Sperlich and R. Neuhaüser, 1974, Solid State Comm. **14**, 591.
Uspenskaya, S.I. and A.A. Eliseev, 1972, Russ. J. Inorg. Chem. **17**, 1344, Zh. Neorg. Khim., SSSR **17**, 2569.
Van Dyck, D., J. Van Landuyt, S. Amelinckx, Nguyen Huy-Dung, C. Dagron, 1976a, C.R. Acad. Sci., Paris, Ser. C **282**, 233.
Van Dyck, D., J. Van Landuyt, S. Amelinckx, C. Dagron and Nguyen Huy-Dung, 1976b, J. Solid State Chem. **19**, 179.
Vasilev, L.N., I.N. Kulikova, L.S. Parfeneva, N.N. Stepanov, E.V. Shadrichev, 1975, Fiz. Tverd. Tela **17**, 2928.
Vereshchagin, L.F., A.A. Eliseev, G.M. Kuz'micheva, V.V. Evdokimova, N.I. Novokshonov, O.P. Fialkovskii, 1975, Zh. Neorg. Khim. **20**, 1466.
Verkhovets, M.N., V.V. Sokolov and A.A. Kamarzin, 1971, Izvest. sibir. Otdel. Akad. Nauk SSSR, Khim. Nauk **3**, 122.
Von Molnar, S., F. Holtzberg, T.R. McGuire and T.J.A. Popma, 1972, AIP Conf. Proc. N 5, 869.
Vo Van Tien, J. Flahaut and L. Domange, 1966, C.R. Acad. Sci., Ser. C, Paris **262**, 278.
Vo Van Tien and P. Khodadad, 1968, Bull. Soc. Chim. France, 1859.
Vo Van Tien and P. Khodadad, 1969, Bull. Soc. Chim. France, 30.
Vo Van Tien, D. Carré and P. Khodadad, 1970a, C.R. Acad. Sci., Paris, Ser. C **271**, 1571.
Vo Van Tien and P. Khodadad, 1970b, Bull. Soc. Chim. France, 2888.
Vo Van Tien and P. Khodadad, 1971, Bull. Soc. Chim. France, 3454.
Vo Van Tien and M. Guittard, 1974, C.R. Acad. Sci., Paris, Ser. C **279**, 849.
Vo Van Tien, M. Guittard, J. Flahaut and N. Rodier, 1975, Mat. Res. Bull. **10**, 547.
Wang, R., H. Steinfink and W.F. Bradley, 1966, Inorg. Chem. **5**, 142.
Wang, R., H. Steinfink and A. Raman, 1967, Inorg. Chem. **6**, 1298.
Webb, A.W. and H.T. Hall, 1970a, Inorg. Chem. **9**, 843.
Webb, A.W. and H.T. Hall, 1970b, Inorg. Chem. **9**, 1084.
Westrum, E.F., 1968, Progr. Sci. Technol. Rare Earths **3**, 459.
White, J.G. and J.P. Dismukes, 1965a, Inorg. Chem. **4**, 970.
White, J.G. and J.P. Dismukes, 1965b, Inorg. Chem. **4**, 1760.
White, J.G., P.N. Yocom and S. Lerner, 1967, Inorg. Chem. **6**, 1872.
Wojtowicz, P.J., L. Darcy and M. Rayl, 1969, J. Appl. Phys. **40**, 1023.
Yanagisawa, Y. and S. Kume, 1973, Mat. Res. Bull. **8**, 1241.
Yim, W.M., A.K. Fan and E.J. Stofko, 1973, J. Electroch. Soc. **120**, 441.
Zargarjan, V.Sh. and N.Kh. Abrikosov, 1967, Izvest. Akad. Nauk SSSR, Neorg. Mater. **3**, 769.
Zhuze, V.P., S.S. Shalyt, V.A. Noskin and V.M. Sergeeva, 1966, Zh. eksper. teor. Fiz. Pis'ma Redakc., SSSR **3**, 217.
Zinchenko, K.A., N.P. Luzhnaja and E.I. Jarembash, 1966, Izvest. Akad. Nauk SSSR, Neorg. Mater. **2**, 1747.
Zinchenko, K.A., E.I. Jarembash, A.A. Eliseev, N.P. Luzhnaja and L.A. Chernjaev, 1967, Izvest. Akad. Nauk SSSR, Neorg. Mater. **3**, 29.

Yakel, H.L., E. Banks, and R. Ward, 1949, J. Electrochem. Soc. 96, 304.
Zachariasen, W.H., 1948, Acta Crystallogr. 1, 265.

Handbook on the Physics and Chemistry of Rare Earths, edited by K. A. Gschneidner, Jr. and L. Eyring

Chapter 32

HALIDES

John M. HASCHKE
Rockwell International, Rocky Flats Plant,
PO Box 464, Golden, Colorado 80401, USA

Contents

Symbols

Å = Angstrom units
Cp_T = Heat capacity at temperature T
D°_T = Dissociation energy at temperature T
eu = Entropy units (cal/deg mole)
ΔG°_{fT} = Free energy of formation at temperature T
ΔH°_{fT} = Enthalpy of formation at temperature T
J = Total angular momentum quantum number
M = Metal other than rare earth
R' = Gas constant
S°_T = Standard entropy at temperature T
X = Halide
Z = Number of formula units per cell

1. Introduction

1.1. *An historical perspective*

The historical development of the chemistry of the rare earth halides is similar to that of most elements in that the halides were some of the first compounds to be prepared. Pioneering work was done by Moissan, Matignon and Bourion near

the beginning of this century and was followed about thirty years later by a second flurry of activity in the reports of Klemm and Jantsch and their coworkers. Near the middle of the century, interest was again rekindled after a second period of inactivity. The renewed efforts were in part due to the need for separating the lanthanide elements from spent nuclear fuel mixtures. An important part of this work was the development of methods for the preparation of large quantities of the metals by reduction of the fluorides and chlorides (Spedding and Daane, 1952; Daane and Spedding, 1953). The development of these procedures has obviously been very important in the growth of rare earth metallurgy, but it also seemed to coincide with an uninterrupted interest in the chemistry and fundamental properties of the rare earth halides. The availability of high purity rare earth oxides has undoubtedly contributed to this activity. During the next ten to fifteen years, interest in the chemistry and fundamental properties of the rare earth halides grew steadily and the state of the art is described in two important reviews (Thoma, 1966; Brown, 1968). During the past decade, the level of activity has increased substantially with the investigation of both new aspects of halide chemistry as well as careful reexamination of previous results. This work is an attempt to complement the earlier reviews by focussing attention on recent results, on how they have altered the understanding of fundamental properties and hopefully to draw attention to those topics which need additional investigation.

Several areas of halide chemistry have recently been active or significantly altered by recent results. The area of preparative methods has been surprisingly active and has expanded to include crystal growth procedures. Substantial progress has been made in the definition and refinement of structural properties and in the expansion of thermodynamic data. Other important areas of progress include the identification and characterization of both novel reduced halides and interesting gas phase species.

Interest in the halides has also been enhanced by a variety of recently developed uses and potential uses for the halides. A thorough discussion of rare earth halide applications is beyond the scope of this review, but a brief mention of several interesting and important topics should be made. In addition to their use in metallurgical procedures, the halides have found numerous applications as heterogeneous catalysts for fluorination and chlorination of hydrocarbons and as host materials for luminescence studies and for the investigation of spectral, magnetic and crystal field parameters of ions. Certain trifluorides are transparent over wide spectral ranges, have high radiation and thermal stability and have found application as optical materials for lasers. Halides doped with other lanthanides have been found to act as filters for the vacuum ultraviolet region. The band width varies with dopant level. Various halides and mixed halides are finding uses as hosts for upconversion phosphors (Wright et al., 1973; Pierce and Hong, 1973). The use of a lanthanide trichloride quantum counter for thermal imaging has also been described (Herrington et al., 1975). The lanthanide halides have recently been employed both as primary irradiators and as additives for spectral balance in high intensity discharge lamps (Zollweg et al., 1975). The

trifluorides are ionic conductors (Kummer and Millberg, 1969) and because of their insolubility in aqueous solution have found important applications as selective ion electrodes. The properties of halide thin films (Tiller et al., 1973) have been described; potential applications are as optical coatings and in electrical devices. The molten halides have potential for use as fluxes in electroslag melting of active metals such as titanium and zirconium, and because of their ability to dissolve the rare earth metals they show promise as solvent systems for preparative reactions.

1.2. *A survey of the halides and their properties*

If the binary rare earth halides are classified according to composition, three convenient categories are found: the trihalides (RX_3), the tetrahalides (RX_4) and the reduced halides (RX_x, $x < 3$). The trihalides are known for all the rare earth elements except europium. The triiodide of europium is unstable and has not been prepared. The various physical property measurements that have been reported for anhydrous EuI_3 cannot be correct. The trihalides of promethium have been prepared and characterized (Weigel and Scherrer, 1967; Weigel, 1969). The chemistry of these materials is similar to that of the adjacent lanthanide halides; the somewhat specialized procedures for these materials will not be included in this review and the reader is referred to these sources. For the tetrahalides, only the tetrafluorides of cerium praseodymium and terbium are known. Reports for $CeCl_4$ appear in the literature, but its existence has not been substantiated and these references must be discounted. The dihalides have long been known for those elements, Sm, Eu, and Yb, which have stable divalent states; however, dihalides have been characterized for a surprisingly large number of lanthanides. Other reduced halides include the sesquichloride of gadolinium, Gd_2Cl_3, and an extensive series of intermediate halides with $2 < x < 3$.

Marked differences are observed between the properties of the halides. The trifluorides are stable in air at room temperature and are non-hydroscopic. They are sparingly soluble in water with solubility product constants which vary from 10^{-19} for lanthanum to 10^{-15} for lutetium (DaDilva and Queimado, 1973). In liquid HF, the solubilities are less than 4×10^{-4} mole/ℓ (Ikrami et al., 1972). At high temperatures the trifluorides react with oxygen and moisture to form the oxide fluorides, ROF, which are stable in air at temperatures greater than 1000°C. Conversion of the fluorides to the oxides may be achieved by heating in steam at 1000°C (Stezowski and Eick, 1970).

In contrast, the anhydrous trichlorides, tribromides and triiodides and the reduced halides are extremely air sensitive materials and are rapidly hydrated or hydrolyzed in air. The triiodides are especially moisture sensitive and deliquesce. Unlike the trifluorides, the other trihalides are very soluble in water at 25°C. Solubilities of the trichlorides vary from 3.89 moles/ℓ for lanthanum, to a minimum of 3.57 moles/ℓ at terbium and back up to 4.10 moles/ℓ at lutetium with pH values of the saturated solutions in the range 1.0–2.0 (Spedding et al., 1974a). At high temperatures, the trichlorides, tribromides and triiodides also

react with water or oxygen to form the oxide halides, ROX. Like the oxide fluorides, the lighter oxide chlorides are stable in air at 1000°C. The heavier oxide chlorides, the oxide bromides and the oxide iodides are readily converted to the oxides by ignition in air at 1000°C. Equilibrium measurements have been made for the reactions $RCl_3 + \frac{1}{2}O_2 \rightarrow ROCl + Cl_2$ at elevated temperatures (Baev and Novikov, 1965). In general the reactivity of the halides increases down the halide group. At high temperatures, they are known to react with silicon dioxide to form silicon tetrahalides (Corbett, 1973). The iodides are particularly reactive, and in somewhat similar high temperature processes act as reducing agents in reactions with metal phosphates, (Haschke, 1976a). The products include lanthanide oxide silicates, elemental iodine and high yields of phosphorus triiodide, which has previously been prepared only by direct combination of the elements.

2. The trihalides

2.1. *Preparative methods*

The large number of recent publications on preparative methods suggests that this is an important aspect of halide chemistry. High purity materials with low levels of anionic contamination are naturally desired for property measurements. The trihalides occupy a position of special importance because they are employed as starting materials for the preparation of essentially all the tetrahalides and reduced halides. High quality anhydrous halides are commercially available, but care must be exercised in their procurement (Haschke, 1975a). The reactivity of the chlorides, bromides and iodides to atmospheric moisture virtually necessitates that they be prepared in the laboratory. Preparative procedures have been described in several comprehensive reviews (Taylor, 1962; Kiss, 1963; Brown, 1968). Additional reviews have appeared for the fluorides (Carlson and Schmidt, 1961; Bratsanova, 1971) and for the chlorides, bromides and iodides (Block and Campbell, 1961; Johnson and Mackenzie, 1970). In the present review, an attempt will be made to evaluate the various methods.

The important preparative methods for the trihalides may be included in one of the following categories: (a) preparation from the rare earth metals, (b) preparation from other halides by metathetical processes, and (c) preparation from the oxides. Since the hydrated halides are readily prepared from the oxides, their dehydration is considered as a special case of category (c). A variety of additional preparative methods appears in the literature, and many of these are described in the reviews mentioned above. The starting materials are frequently so unusual and the procedures so complex that they are of little synthetic value.

Preparation of the trihalides from the metals has generally been confined to the chlorides, bromides and iodides. Two variations of the procedure are the reaction of the metal with either the gaseous hydrohalic acid or with halogen

vapor (Druding and Corbett, 1961). Reaction between the hydrohalic acid and metallic containers such as Mo and W is prevented by controlling the partial pressure of H_2 in the reaction zone. Rigorous purification of the gas stream is necessary, but impurities which are inherent in the metal are unavoidable. Analytical data for commercially available rare earth metals of 99.9% purity show the presence of several mole percent of dissolved gases such as nitrogen and oxygen (Bush et al., 1971).

Several different types of metathetical reactions have been employed. The reactions of HBr and HI with the trichlorides have been described (Taylor, 1962), but these procedures are complicated by the hydroscopic nature of both reactants and products, and they seem to be of minor importance. The exchange reaction between the mercuric halides and the rare earth metals (Asprey et al., 1960) is a useful procedure for preparing laboratory quantities of the trihalides (X = Cl, Br, I). Carter and Murray (1972) have employed two variations of this procedure to produce the trihalide, RX_3, plus either Hg or HgX depending on the $R:HgX_2$ ratio of the reactants. The reaction mixtures, which are easily prepared by weighing, are heated in glass ampoules at 300°C, and the Hg or HgX products are separated from the rare earth halide by distillation. The products frequently contain traces of mercury and like other reactions employing the metals are subject to inherent contamination. Tribromides and triiodides have also been prepared by exchange reactions using the rare earth oxides (Taylor, 1962). The oxides are heated with either AlX_3 or a mixture of Al and X_2 (X = Br, I).

Preparative procedures which employ the oxides as starting materials have several advantages. The methods are particularly attractive because oxides are available in high purity at lower unit cost than any other starting materials. The trifluorides are readily prepared by the reaction of anhydrous HF with the oxides at 700°C (Carlson and Schmidt, 1961). Large quantities of product may be obtained by this procedure, but kinetic problems arise from the formation of a thick product layer on the unreacted oxide. These difficulties have been overcome by mechanical mixing and the use of a fluidized bed. A variation of this fluorination process employs the reaction of the oxide with excess ammonium fluoride or ammonium bifluoride at 200–300°C and sublimation of the residual reagent at higher temperatures. The analogous reactions with the other ammonium halides are substantially incomplete even after repeated additions of excess reagent (Taylor, 1962). A somewhat surprising variation of the latter method is the reaction of ammonium fluoride with oxide, hydroxide or carbonate under hydrothermal conditions in a process which may parallel the geological formation of tysonite (Haschke, 1975b). The oxides may also be fluorinated with gaseous F_2, but the experimental problems limit the use of this method. Direct halogenation of the oxides are incomplete for the other halogens and in general do not proceed past the formation of the oxide halide.

A large number of chlorinating agents have been employed for conversion of the oxides at temperatures between 400 and 800°C. These methods, which have been extensively reviewed by Taylor (1962), include the use of carbon tetrachloride, thionyl chloride, disulfur dichloride, disulfur dichloride plus chlorine

mixtures and phosgene. Extra precaution is necessary because several of these methods involve toxic substances such as phosgene, a product of the carbon tetrachloride reaction. In general these methods are limited to small quantities of product because of kinetic inhibition. The reagents and carrier gases must be rigorously purified. Analogous procedures are not applicable to other halides, and these methods appear to be of rather limited importance.

Dehydration of the dehydrated trihalides is a final method for oxide conversion. The hydrated trichlorides, tribromides and triiodides, $RX_3 \cdot xH_2O$, are obtained by dissolution of the oxides in aqueous hydrohalic acid and condensation by warming and desiccation (Ashcroft and Mortimer, 1968; Brown et al., 1968). The hydrated trifluorides are prepared by dissolution of the oxide in HNO_3 or HCl and precipitation with aqueous HF. The filtered trifluoride may be dehydrated by heating slowly to 600°C in an inert gas stream or in vacuum (Strizhkov et al., 1972). Products obtained by heating in air are contaminated with oxide fluoride (Batsanova, 1971). Thermal decomposition studies of the hydrated trichlorides, cf. section 5.1, have shown that the oxide chlorides are readily formed, but careful dehydration under N_2 flow has apparently been successful for the chlorides (Ashcroft and Mortimer, 1968). Tribromides have also been prepared by careful vacuum dehydration, but the lutetium products were contaminated with oxide bromide (Brown et al., 1968). In general simple dehydration becomes increasingly difficult with increasing atomic number of both the lanthanide and the halide.

The dehydration process is greatly enhanced by the presence of a high halide activity. The trifluorides and trichlorides have been prepared by thermal dehydration under a flow of the purified hydrogen halide (Taylor, 1962). An adaptation of this method involves dehydration in the presence of a high concentration of the respective ammonium halide (Taylor and Carter, 1962). This method has been applied to the fluorides (Greis and Petzel, 1974), the chlorides (Cox and Fong, 1973), the bromides (Haschke and Eick, 1970a) and the iodides (Kutscher and Schneider, 1971). An intimate mixture of the hydrated halide and a multifold molar ratio of ammonium halide is obtained by condensation of an aqueous solution. The mixture is dehydrated at low temperature and high vacuum with cryogenic trapping. The ammonium halide is sublimed at higher temperatures. Early work indicated that large quantities of product were swept away by escaping gases, but this occurs only if the temperature is increased too rapidly. The vacuum system should be designed so that the ammonium halide will transport to its final deposition point in one step. The ammonium halides have high temperature phase transitions with large molar volume changes and attempts to chase the deposit by movement of the hot zone may fracture a glass vacuum system. Of all the methods only this one is applicable to all the trihalides. The fluorides, chlorides and bromides and the iodides of the lighter elements are high quality products. Even with the careful procedures outlined by Kutscher and Schneider (1971), the heavier iodides are contaminated with oxygen and must be purified by distillation.

Although high quality products are obtained by several of the above methods,

the preparation of high purity halides requires that additional precautions be taken. The first concerns the choice of container material. Quartz and other silicate glasses are convenient, but at high temperatures react with the halides, especially the iodides, according to the following reaction (Corbett, 1973):

$$2RX_3(s, \ell) + SiO_2(s, \ell) \rightarrow 2ROX(s) + SiX_4(g)$$

A variety of oxide silicates and halide silicates such as the $Yb_3(SiO_4)_2Cl$ phase characterized by Ayasse and Eick (1973) are also possible products. Tantalum, tungsten and molybdenum appear to be suitable high temperature container materials and problems are encountered only in the presence of HX or X_2. Consequently these materials are not suitable for containment of trihalides which decompose to RX_2 and X_2 at high temperatures (Haschke and Eick, 1970b). In the absence of lanthanide metal, graphite containers are also satisfactory and have been employed for vaporization studies. Some confusion seems to have arisen from the reports of Block and Campbell (1961). The carbon contamination described by these authors results from the preparative techniques, not from the miscibility of carbon in the halides. Graphite has been found (Kirshenbaum and Cahill, 1960) to react slightly (less than 0.1%) with several trifluorides at 2200°C, but SmF_3 is reduced to the difluoride at 1700°C. A second essential for preparation of high purity halides is purification by vacuum distillation. Oxygen contamination is eliminated because the oxide halides vaporize incongruently with formation of the gaseous trihalides and the nonvolatile oxides (Haschke and Eick, 1970b; Work and Eick, 1973). Procedures and apparatus for vacuum distillation have been described by Block and Campbell (1961) and Carter and Murray (1972). Purification of the trifluorides by a molten salt process has also been described by Carlson and Schmidt (1961).

Another aspect of preparative procedures is the growth of large single crystals. Trifluoride crystals have been obtained by the Stockbarger and Stober techniques (Jones and Shand, 1968) and similar procedures employing the Bridgman-Stockbarger method have been described for the chlorides and bromides (Cox and Fong, 1973). Problems are encountered with $EuCl_3$ and the tribromides of Sm, Eu and Yb because of thermal decomposition. Crystals of $EuCl_3$ have been grown by the Bridgman method in sealed tubes containing a chlorine atmosphere (Mroczkowski, 1970). Schaefer and Karbinski (1974) have described a chemical transport method for growth of certain RF_3 and RCl_3 crystals at 500–600°C and a high partial pressure of Al_2Cl_6. The transport species may be molecules of the type RAl_3Cl_{12}.

A final comment concerns the thermal instability of several trihalides and the adjustments which must be made in the procedures for their preparation. Early work demonstrated that several of the trihalides such as $SmBr_3$ and SmI_3 were thermally unstable (Jantsch and Skalla, 1930); however, these findings have not received adequate attention. The triiodides of Sm, Eu and Yb are unstable with respect to their diiodides at temperatures of most preparative methods. Asprey et al. (1964) have prepared SmI_3 and YbI_3 by reaction of the diiodides with iodine at 30 atm and 500°C, and Kutscher and Schneider (1971) have prepared SmI_3 by

low temperature dehydration. Asprey et al. (1964) were unable to prepare EuI_3 from the diiodide and iodine at 100 atm and 600°C. The author has observed that hydrated EuI_3 loses iodine at 100°C, and since trivalent europium is so easily reduced by iodide, it is doubtful that a simple preparative method will be successful. Europium tribromide has been obtained by the reaction of the dihalide with bromine (Haschke and Eick, 1970a); the bromine pressure in equilibrium with the dibromide and tribromide is 1 atm at 400°C, Haschke (1973). Data for $EuCl_3$ (Sommers, 1976) show that samples prepared in vacuum at 350°C have a substantially substoichiometric composition, $EuCl_{2.989\pm0.003}$. After the product was heated at 360°C under 1 atm of chlorine, the composition was found to be $EuCl_{2.999\pm0.002}$. Similar tendencies toward slight substoichiometry might be expected for SmI_3 and $YbBr_3$ at relatively low temperatures.

2.2. *Structural properties*

Although systematics and similarities in the chemical properties of the trihalides have long been recognized, such is not the case for their structural properties. Six different structure types are known for the trihalides at room temperature; their stability ranges and other data are presented in table 32.1. As one might expect, a regular decrease in cation coordination number is observed with increasing atomic number. Lattice parameters for all the trihalides are given by Brown (1968). High precision parameters have recently been reported for the trifluorides by Greis and Petzel (1974). Several of the structures are frequently designated as other types; UCl_3- and $Y(OH)_3$-type, YCl_3- and $AlCl_3$-type and BiI_3- and $FeCl_3$-type are used interchangeably in the literature.

The lanthanide trihalides structures are known to exhibit a high frequency of nine-coordinate-cation geometries (Karraker, 1970) but only recently has an

TABLE 32.1
Structural data for the rare earth trihalides, RX_3.

Structure type (space group)	LaF_3 ($P\bar{3}c1$)	YF_3 (Pnma)	UCl_3 ($P6_3/m$)	$PuBr_3$ (Cmcm)	YCl_3 (C2/m)	BiI_3 ($R\bar{3}$)
F	La–Pm	Sm–Lu, Y	–	–	–	–
Cl	–	–	La–Gd	Tb	Dy–Lu, Y	–
Br	–	–	La–Pr	Nd–Eu	–	Gd–Lu, Y
I	–	–	–	La–Nd	–	Sm–Lu[a], Y
X/R^{3+} Range[b]	1.28–1.39	1.41–1.60	1.63–1.93	1.96–2.17	1.99–2.13	2.08–2.55
Cation coord. No.	11(9)	9	9	8	6	6

[a]EuI_3 is unknown. [b]Data for isostructural actinide compounds are included, Brown et al. (1968).

attempt been made to correlate the structural data (Haschke, 1976b). It is interesting that the anions and cations of most trihalide structures are bilevel, i.e., in one crystallographic direction all the anions and cations are found at one of two levels in the structure. The high coordinate structure types (LaF_3, YF_3, UCl_3, $PuBr_3$) may be derived from the anti-NiAs-type structure by removal of two-thirds of the metal layers. These structures are therefore closely related to a structure with closest packing of cations and have space groups which are subgroups of the highest symmetry space group, $P6_3/mmc$, of anti-NiAs. In addition, these structures are all interrelated by displacive processes involving slight displacements of the ions. The remaining structure types (YCl_3, BiI_3) are based on closest packed arrangements of cations in which the metals occupy layers of octahedral sites.

Definition of the LaF_3-type or tysonite structure has had a complicated historical development. The original work of Oftedal (1929) showed a substructure-superstructure relationship and resulted in the assignment of a hexagonal ($P6_3/mcm$, $Z = 6$) supercell, but later work by Schlyter (1953) showed no superstructure and led to the assignment of a bimolecular hexagonal ($P6_3/mmc$) cell. Recent independent results by Mansmann (1965) and Zalkin et al. (1966) on high quality crystals verify the superstructure and show a trigonal space group, $P\bar{3}c1$. A third independent X-ray study (Rango et al., 1966) gives atomic coordinates in close agreement with these results, but is based on a different space group, $P6_3cm$. Both space groups are subgroups of $P6_3/mmc$, and attempts to resolve the discrepancy in symmetry by spectroscopic methods have not been successful (Bratsanova, 1971); however, the $P6_3cm$ symmetry could arise from twinning of a trigonal system. The subcell structure proposed by Schlyter is projected on $(11\bar{2}0)$ of the hexagonal cell in fig. 32.1. The centered orthorhombic equivalent of the hexagonal cell is outlined. Heavy and light circles indicate ions at fractional coordinates of 0 and $\frac{1}{2}$, respectively, along the projection axis; the bilevel nature of the structure is obvious. Large circles indicate anions and small circles indicate cations. Since most trihalide structures

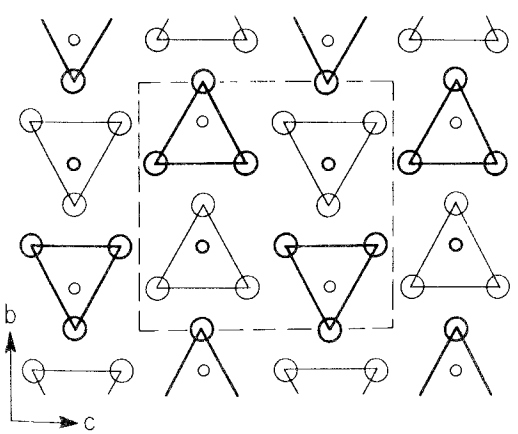

Fig. 32.1. The disordered LaF_3-type structure ($P6_3/mmc$) projected on $(11\bar{2}0)$. (See text for identification of symbols.)

have this bilevel feature, these identification symbols will be employed throughout this section. The metals occupy pentacapped trigonal prisms and are therefore eleven-coordinate. Since two fluorides are at somewhat greater distances (3.01 Å) than the other nine (2.41–2.61 Å), the cations have also been described as nine-coordinate. The structure of disordered LaF_3, which is derived directly from anti-NiAs without loss of crystallographic symmetry (Haschke, 1976b) may also be represented by layers of RX_2 and X (cf. fig. 32.2) which are residual layers from the anti-NiAs structure. Projection of ordered LaF_3 in the same orientation in fig. 32.3 shows that the superstructure arises primarily from the ordering of anions in the X layers. Two-thirds of the X anions are displaced slightly within the layers and result in a tripling of the orthorhombic cell along the projection axis and in a hexagonal supercell that is a three-fold multiple of the subcell.

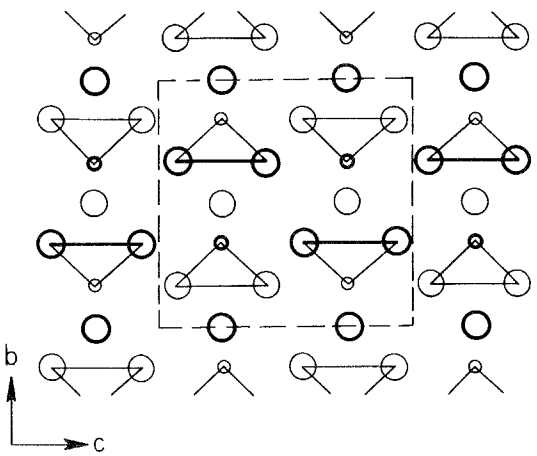

Fig. 32.2. A $(11\bar{2}0)$ projection of disordered LaF_3 in which alternating RX_2 (triangles) and X (free circles) layers are shown normal to [010].

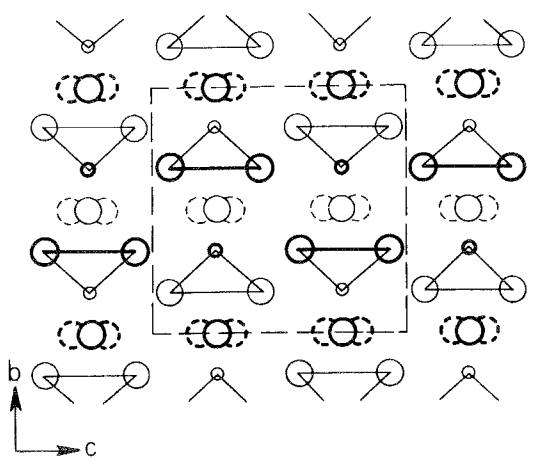

Fig. 32.3. The ordered LaF_3-type structure ($P\bar{3}c1$) projected on (100) of the centered orthorhombic equivalent.

The other high-coordinate trihalide structures in table 32.1 are related to the disordered LaF_3 structure by displacive processes (Haschke, 1976b). The YF_3-type structure (Zalkin and Templeton, 1953) is projected on (001) of the orthorhombic cell in fig. 32.4. The metal and fluoride positions are both slightly distorted from the bilevel values of the LaF_3 structure (cf. fig. 32.1). The fractional coordinates along the projection axis are indicated by the numbers in the diagram. Although the anion to cation radius ratio is substantially increased, the cation coordination number is maintained at nine by this distortion. The UCl_3-type structure (Zachariasen, 1948) is projected on (0001) of the hexagonal cell in fig. 32.5. The cation coordination polyhedra are again tricapped trigonal prisms and the ions are rigorously bilevel. The space group of UCl_3 is a direct

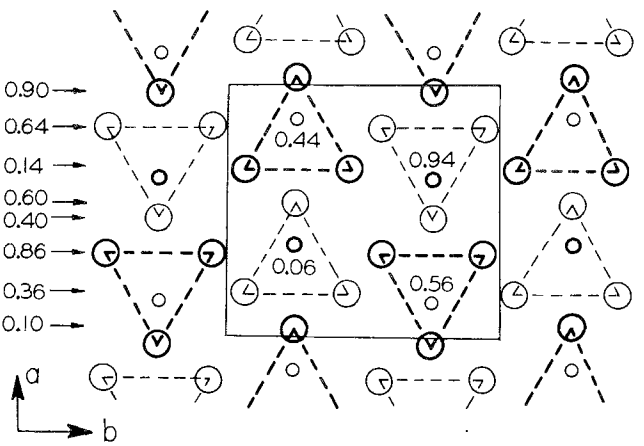

Fig. 32.4. The YF_3-type structure (Pnma) projected on (001).

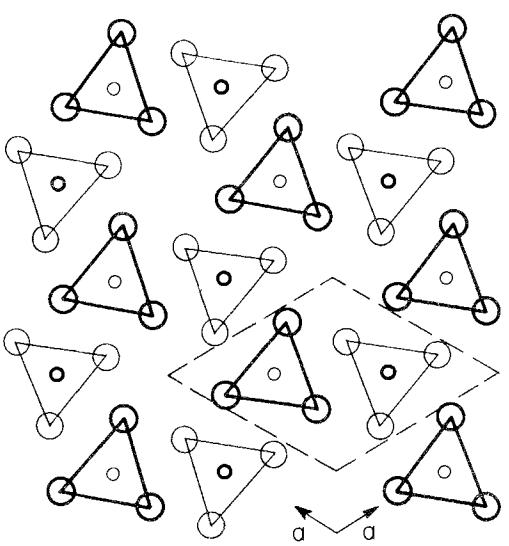

Fig. 32.5. The UCl_3-type structure ($P6_3/m$) projected on (0001).

subgroup of that for disordered LaF_3, and the two structures may be interchanged by a simple displacive process (Haschke, 1976b). The UCl_3 is unusual in that a regular nine-coordinate cation geometry is maintained at even higher anion to cation radius ratios than for the YF_3 structure. The structure is also interesting because of vacant channels of anions running through the structure normal to the projection plane. These channels provide potential sites for the accommodation of two additional cations per unit cell. If cation occupancy occurs half-way between the two layers of anions, the cations are six-coordinate (essentially octahedral); if occupancy occurs at the same level as the anions, they are nine-coordinate (tricapped trigonal prismatic). The UCl_3 structure may also be described by alternating layers of RX_2 and X as shown in fig. 32.6. The RX_2 layers are composed of $[M_2X_4]$ units like those of LaF_3, but the arrangement of units within the layers are different (Haschke, 1975c). The orthorhombic $PuBr_3$ structure (Zachariasen, 1948) is projected on (100) in fig. 32.7. Comparison of this structure with that of disordered LaF_3 in fig. 32.1 shows a remarkable similarity. The space group of $PuBr_3$ is also a direct subgroup of that for disordered LaF_3. A simple distortion of the X layers from their planar alignment (cf. fig. 32.2) produces the $PuBr_3$ structure and reduces the effective cation coordination number to eight. The stability of these anti-NiAs-related structures is consistent with the apparent stability of the RX_2 layers in which the metals achieve six-coordinate arrangements in essentially two dimensions and which permit the attainment of high coordination numbers in three dimensions.

The structures observed at high anion to cation radius ratios are derived from closest packed anion arrays. The YCl_3- and BiI_3-type structures (Wyckoff, 1964) differ primarily in the type of closest packing. A projection of the monoclinic YCl_3 structure on (010) in fig. 32.8 shows that the anion rearrangement is a slight distortion of cubic closest packing. The octahedral sites, which are viewed along

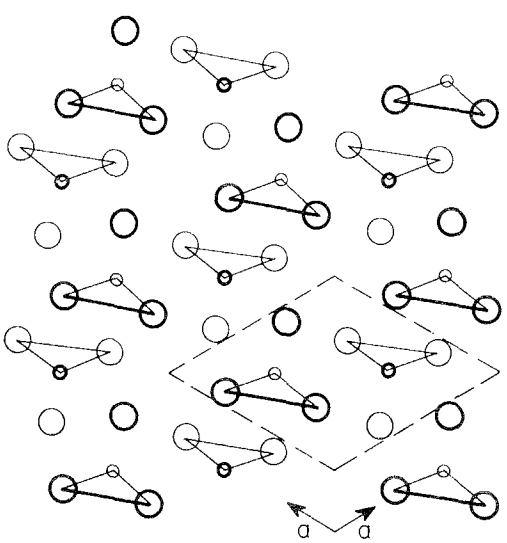

Fig. 32.6. A (0001) projection of UCl_3 in which alternating RX_2 (triangles) and X (free circles) layers are shown normal to [100].

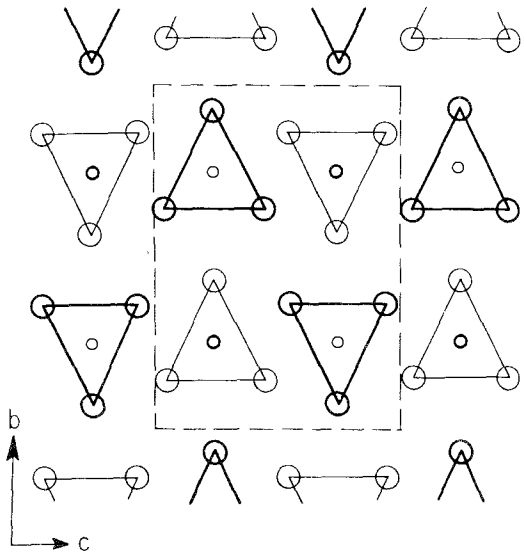

Fig. 32.7. The $PuBr_3$-type structure (Cmcm) projected on (100).

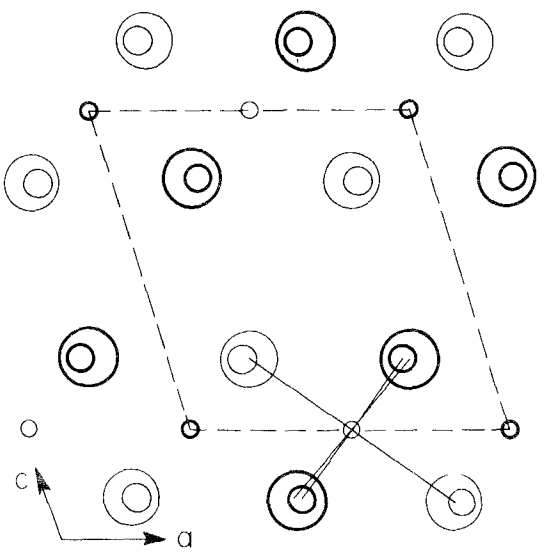

Fig. 32.8. The YCl_3-type structure (C2/m) projected on (010).

their two-fold axes, lie in layers coplanar with (001). Alternate layers are vacant, and one-third of the octahedral sites in the occupied layers are also vacant, but the ordering of vacancies is not shown by the projection. A partial projection of the rhombohedral BiI_3-type structure on $(11\bar{2}0)$ of the hexagonal cell in fig. 32.9 shows that the anions occupy nearly perfect hexagonal closest packed positions. Alternate layers of octahedral sites are vacant and two-thirds occupied by cations. The ordering of metals in the layers, which is again not shown by the

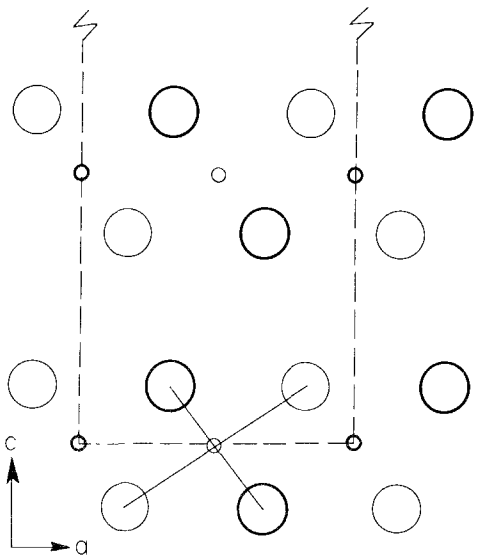

Fig. 32.9. The BiI_3-type structure ($R\bar{3}$) projected on ($11\bar{2}0$) of the hexagonal cell. (One-half of the cell is shown.)

projection, gives rise to the long hexagonal c parameter and the rhombohedral symmetry of the structure.

An important aspect of rare earth halide structural chemistry not shown by table 32.1 is polymorphism. Its occurrence is expected along the interfaces of the various structural types, and because of the displaced structural relationships is to be expected for additional trihalides. Structural transitions are known for trifluorides, trichlorides and triiodides, but not for tribromides. The high temperature X-ray diffraction data of Thoma and Brunton (1966) show that the LaF_3-type trifluorides melt without structural change; however, an ordered-disordered transition is expected at high temperatures. High temperature modifications are observed for the YF_3-type trifluorides (Sm–Lu, Y). A maximum in the transition temperature coincides with a minimum in the melting points near Ho, and the stability range for the high temperature form of HoF_3 is only 73°C. The lighter trifluorides (Sm–Ho) have LaF_3-type modifications, but a different high temperature form exists for the heavier trifluorides (Er–Lu, Y). More recent work of Jones and Shand (1968) shows that YF_3-type HoF_3 can be grown directly from the melt. High temperature calorimetric data for the trifluorides (Spedding and Henderson, 1971; Spedding et al., 1974b) do not show a transition for either TbF_3, DyF_3 or HoF_3. The observed shattering of these crystals indicates that the transition occurs, but that it is too close to the melting point to be resolved by DTA or drop calorimetric measurements. Pastor and Robins (1974) have proposed a revised high temperature phase diagram which shows that SmF_3 and EuF_3 have high temperature LaF_3 modifications, but that the heavier trifluorides melt without transition. These workers ascribe the differences in transition temperatures to sample purity and suggest that earlier samples were contaminated by hydroxide which stabilizes the high temperature

structure. Data are not presented for the heavy trifluorides (Er–Lu) and additional work is necessary to resolve this question.

The YF_3-type to LaF_3-type transition of the trifluorides is consistent with the displacive relationships of the two structures. Transformation of the metastable LaF_3-type EuF_3 to the YF_3-type at temperatures as low as 50°C (Greis and Petzel, 1974) can readily be explained. The observed distortions of the LaF_3-type trifluorides with decrease in cationic radius (Bratsanova, 1971) suggest that the interface between the LaF_3 and YF_3 structures is not sharp. X-ray data for the high temperature forms of the heavy trifluorides have been assigned to the α-UO_3-type structure (Sobolev and Fedorov, 1973). A projection of the α-UO_3 structure (Zachariasen, 1948) on (100) of the centered orthorhombic equivalent of the unimolecular hexagonal cell is presented in fig. 32.10. The space group of α-UO_3 is a direct subgroup of that for disordered LaF_3, and the two structures are related by a displacive process (Haschke, 1976c). The anions in α-UO_3 are in a rather highly distorted cubic closest packed array. One-third of the octahedral sites in all the cation layers are occupied by metals. The up and down alternation of the metal columns is like that in LaF_3 and related phases. The existence of a displacive relationship and the tendency toward formation of closest packed anion structures at high anion:cation radius ratios are consistent with the proposed α-UO_3-type structures.

Polymorphism is also observed for the trichlorides. Harris and Veale (1965) obtained a mixture of UCl_3- and $PuBr_3$-type $GdCl_3$ by condensation of the vapor on a water-cooled surface. DTA data for the mixture show a sharp exotherm at 100°C, and the authors conclude that the $PuBr_3$-type trichloride is the stable form below 100°C. Low temperature (Sommers, 1976) and high temperature (Dworkin and Bredig, 1971a) heat capacity data show no evidence for a trans-

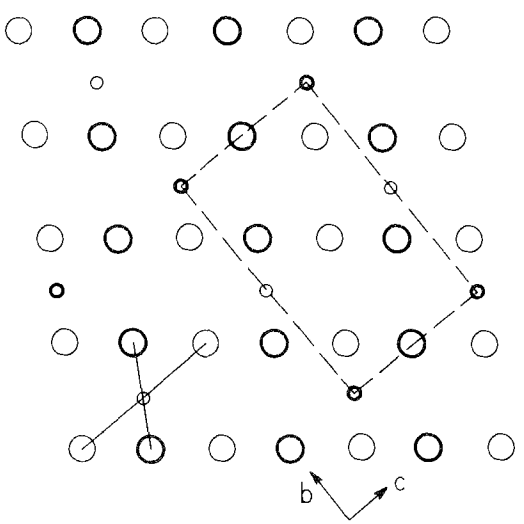

Fig. 32.10. The α-UO_3-type structure ($P\bar{3}ml$) projected on (100) of the centered orthorhombic equivalent.

ition, and it appears that the $PuBr_3$-type phase is a metastable product formed by condensation of the vapor. $PuBr_3$-type $TbCl_3$ (Forrester et al., 1964) is the only trichloride for which a high temperature transition is observed (Dworkin and Bredig, 1971a), but the high temperature structure has not been identified. Dimorphism has also been reported for $DyCl_3$ by Bommer and Hohmann (1941a) who found β and γ forms which were subsequently identified as $PuBr_3$- and YCl_3-type structures, respectively. Enthalpy of solution data showed that the $PuBr_3$-type phase is more stable than the YCl_3 form by approximately 3 kcal/mole, but the methods for preparing or interconverting the two forms are not described. During gas phase hydrolysis experiments, Weigel and Vishnevsky (1969) obtained $DyCl_3$ products which gave two sets of equilibrium data consistent with the earlier report. The YCl_3 form was readily identified, but the X-ray diffraction data for the second phase could not be assigned to a $PuBr_3$-type structure, and its method of preparation could not be defined. Heat capacity data show no evidence for a thermal transition and additional investigation of $DyCl_3$ is necessary. NMR data for $PrCl_3$ in an applied magnetic field shows that a spike at 0.42 K in the heat capacity is not a magnetic transition, and the formation of a low-symmetry trichloride phase has been proposed (Hessler and Carlson, 1971).

Phase transitions have been observed for several triiodides (Druding and Corbett, 1961; Mee and Corbett, 1965; Corbett et al., 1966; Johnson and Corbett, 1969; Kutscher and Schneider, 1971; Dworkin and Bredig, 1971a), but structural data are not available. The lighter $PuBr_3$-type triiodides (La–Pr) melt without transition, but the isostructural NdI_3 phase is dimorphic. Transitions are observed for the lighter BiI_3-type triiodides (Sm, Gd-Ho, Y), but not for Er.

Several of the structure types found for the halides are observed for other important monovalent anion systems such as the trihydroxides and trihydrides and derivatives of these structures are observed for a variety of ternary phases (Haschke, 1975c and 1976b). Other monovalent anions, Y, are accommodated in $PuBr_3$- and UCl_3-type RX_3 phases by replacement of the X layers. The resulting RX_2Y compositions are structural derivatives of the parent trihalide structures. These observations and the phase equilibria and crystal growth habits of the ternary derivatives support the conclusion that several of the trihalide structures are accurately described by alternation of RX_2 and X layers, but additional work is clearly necessary.

2.3. *Thermodynamic properties*

The determination of thermodynamic properties for the trihalides has been a particularly active area of investigation and the availability of data has been greatly enhanced. Several compilations of thermochemical data are available. Available experimental data and estimated values are found in the early reference works of Wicks and Block (1963) and Feber (1965). Since data are still unavailable for many halides, the value of these compilations has remained. Thermodynamic data are reviewed by Novikov and Baev (1964) and the thermodynamic and magnetic properties are extensively reviewed by Westrum

(1968). Selected thermochemical data are reported by Thoma (1966) and Brown (1968). Data for the fluorides are given by Batsanova (1971) and numerous compilations and original references are cited by Meyers (1975). The compilation by Schumm et al. (1973) is an important source of critically evaluated data the halides is condensed, solution and gaseous phases at 298 K. Enthalpies of formation are reported for the anhydrous trichlorides, and triiodides and for a large number of trifluorides, but data are not available for the tribromides. Free energy of formation, heat capacity and entropy values are also reported for some trihalides. In the absence of experimental data, this source is useful for evaluating and adjusting estimated values of earlier compilations. Thermochemical functions have been compiled for the gaseous species RX_3, RX_2 and RX (X = F, Cl, Br, I) from 298–3000 K (Krasnov and Danilova, 1969), but the values based on estimated molecular constants. Because of the extensive literature in this area, this review will concentrate on most recent work. The thermochemistry of vapor species and vaporization processes and of hydrated halides is discussed in sections 2.3 and 5.1.

Determination of the basic thermodynamic properties of the rare earth trifluorides remains incomplete. This is in part due to experimental difficulties, and only one direct calorimetric measurement has been reported. The enthalpy of formation, ΔH°_{f298}, of YF_3 (-410.7 ± 0.8 kcal/mole) has been measured by fluorine bomb calorimetry (Rudzitis et al., 1965). In an expansion of earlier work, Polyachenok (1967) has obtained values for several trifluorides (La, Pr, Nd, Gd, Er) by an equilibrium exchange reaction: $RCl_3(\ell) + AlF_3(\ell) \rightarrow RF_3(\ell) + AlCl_3(g)$. Solid state emf data have been reported by Skelton and Patterson (1973) for the trifluorides of Nd, Gd, Dy and Er. Similar measurements have been described by Rezukhina et al. (1974) for the trifluorides of La, Pr and Y. The ΔH°_{f298} values are 5–10 kcal/mole more negative than values reported earlier.

Enthalpies of formation of the trichlorides are given in several reports. The initial solution calorimetric measurements of Bommer and Hohmann (1941a) have been repeated in part by Spedding and Flynn (1954), Stuve (1964), (1965), (1967a) and (1967b) and most recently by Krestkov et al. (1972). The enthalpies of solution are generally in good agreement, but substantial variations (5–10 kcal/mole) are observed in ΔH°_{f298} values. The differences obviously arise from the data employed in the reduction cycle. The ΔH°_{f298} values listed by Schumm et al. (1973) vary regularly (-256 to -238 kcal/mole) from $LaCl_3$ to $TbCl_3$, but increase to -240 kcal/mole for $HoCl_3$ before decreasing regularly to -226 kcal/mole for $LuCl_3$. The discontinuity coincides with the structural change from the closely related UCl_3- and $PuBr_3$-type phases to the cubic closest packed YCl_3-type phases. The -239 kcal/mole value for β($PuBr_3$-type)-$DyCl_3$ and the -236 kcal/mole value for γ(YCl_3-type)-$DyCl_3$ are inconsistent with the trends established by adjacent trichlorides, and the need for additional investigation of these phases is reemphasized. The measurements of Krestkov et al. (1972) include the determination of the temperature dependence of the enthalpy of solution for several trichlorides; the values are more negative by approximately 15 kcal at 100°C than at 0°C. Other data for the condensed phases include the

measurement of densities and molar volumes of several molten trichlorides (Cho et al., 1972).

Although experimental thermochemical data are virtually nonexistent for the tribromides, data for the triiodides are extensive. The enthalpy of formation of $EuBr_3$ has been determined (Haschke, 1973), but should be reevaluated when additional data become available for $EuBr_2$. The ΔH°_{f298} values for the triiodides (Schumm et al., 1973) which are apparently based on the calorimetric data of Bommer and Hohmann (1941b), decrease regularly from -159 kcal/mole for LaI_3 to -131 kcal/mole for LuI_3. A discontinuity at the point of structural change from the $PuBr_3$- to the BiI_3-type structure is not observed. Enthalpies and free energies of formation and entropies of the solid triiodides have been derived by Hirayama et al. (1975) from vaporization and mass spectrometric studies. The ΔH°_{f298} values for the lighter iodides are in close agreement with the above values, but differences of approximately 10 kcal/mole exist for HoI_3, ErI_3 and TmI_3. The ΔH°_{f298} values listed by Lishenko et al. (1973) are intermediate between those of the above reports, and a pronounced discontinuity in the values coincides with the structural change occurring between NdI_3 and SmI_3. The origin of the differences for the heavy triiodides is not understood, but it may well be related to difficulties encountered in preparing these materials in high purity.

The thermodynamic data of the condensed trihalides has been greatly expanded by recent measurements of high and low temperature heat capacities. Drop calorimetry has been employed by Spedding and Henderson (1971) and Spedding et al. (1974b) for determining the high temperature heat capacities of the rare earth trifluorides. Heat capacity equations, enthalpy and entropy increments and free energy functions are tabulated from 400–1900 K. Data for EuF_3 are limited to a maximum of 1500 K because of reduction by the tantalum container. The transition temperatures, melting points and enthalpies of transition, ΔH°_{tr}, and enthalpies of fusion, ΔH°_{fus}, are reported. The values of $\Delta H_{tr} + \Delta H_{fus}$ are 12–13 kcal/mole across the series. Similar measurements are reported for the trichlorides, tribromides and triiodides by Dworkin and Bredig (1963a,b, 1971a), and the corresponding thermodynamic functions are reported for 298–1300 K. Data are available for all the trichlorides except those of Pm, Sm, Eu, and Yb. For the UCl_3- and $PuBr_3$-type trihalides, $\Delta H^\circ_{tr} + \Delta H^\circ_{fus} = 11$–13 kcal/mole. Similar values for the YCl_3-type trichlorides and BiI_3-type tribromides and triiodides are in the range 7–11 kcal/mole. These data emphasize the differences between the anti-NiAs-related structures and the closest-packed-anion structures and are consistent with ΔH°_{f298} values in which discontinuities of 3–5 kcal/mole are observed.

A limited number of low temperature heat capacity measurements have been described. The adiabatic calorimetric measurements of Westrum and Beale (1961) are the only data available for the trifluorides. Similar heat capacity measurements have recently been reported for the lighter lanthanide trichlorides (La–Gd) in the range 5–350 K (Sommers, 1976), and for $EuBr_3$ in the range 5–340 K (Deline et al., 1975). Heat capacities, enthalpy and entropy increments

and free energy functions are tabulated. The Schottky contributions are in agreement with values calculated from spectroscopic data. Excellent agreement is observed between the low and high temperature data for the trichlorides. Heat capacity measurements for trichlorides of Ce, Pr, Nd and Sm and the tribromide of Ce in the range 0.3–4.2 K show maxima at or below 1 K (Colwell et al., 1969). These data and results of NQR and magnetic susceptibility measurements indicate the occurrence of cooperative magnetic interactions and are consistent with the formation of antiferromagnetic linear chains.

The recent heat capacity measurements have greatly expanded the number of halides for which standard entropy values, S°_{298}, are known. However, methods for estimating entropies remain important. Values have been estimated for fluorides (Petzel and Greis, 1972), chlorides (Hariharan et al., 1972), bromides (Haschke and Eick, 1970c), and iodides (Hirayama et al., 1975), using the method of Latimer (1951) and the modifications of Westrum (1967). The procedure, which involves combination of lattice contributions of the anion and cation with the magnetic contribution of the lanthanide ion has been examined by Sommers (1976) using experimental S°_{298} data for the trichlorides. The magnetic contributions equal $R' \ln(2J + 1)$ eu for all the trivalent lanthanides except Eu, for which the population of low lying levels must be considered and a value of 3.5 eu is recommended. If the experimental S°_{298} of $LaCl_3$ is employed as a reference, the lattice contribution of chloride is 5.9 eu, a value which is 1.0 eu lower than that projected by Latimer. The experimental and estimated S°_{298} values for the trihalides are in excellent agreement if the revised cation contributions of Westrum (1967) are employed. A similar analysis of experimental S°_{298} values for the trifluorides (Westrum and Beal, 1961; Rezukhina et al., 1974), indicate that the lattice contribution of fluoride should also be revised downward to 3.1 eu The S°_{298} data for $EuBr_3$ (Deline et al., 1975), suggest that the projected lattice contribution for bromide may also be too high, but additional data are needed before revised bromide and iodide values can be recommended.

2.4. *Vaporization and the vapor phase*

Numerous mass spectrometric investigations of the vaporization reactions of condensed rare earth trihalides have shown that they are congruent processes and that at low partial pressures the primary vapor species is the monomeric gas, RX_3. Mass spectra of equilibrium trifluoride (Zmbov and Margrave, 1968), trichloride (Hastie et al., 1968), and triiodide (Hirayama and Castle, 1973) species effusing from a Knudsen source generally show intense peaks of RX_2^+ and low relative intensities of RX_3^+, RX^+ and R^+. Incongruent processes are observed for the trihalides of Sm, Eu and Yb. Formation of the dihalides is observed in some cases, but intermediate compounds, RX_x, $(2 < x < 3)$ are formed in the case of $SmBr_3$ (Jantsch and Skalla, 1930), $YbCl_3$ (Fishel and Eick, 1971), SmF_3 (Biefeld, 1974), EuF_3 (Petzel and Greis, 1972) and YbF_3 (Biefeld and Eick, 1975). ESCA data for condensed effusates of the trifluorides (McCreary and Thorn, 1974a) show that EuF_3 and YbF_3 and to lesser extents SmF_3 and TmF_3 are dissociated

to RF_2 and F_2 in the vapor phase. Although the trihalides are generally stable in equilibrium, the observations of Lishenko et al. (1973) indicate that this is not the case for nonequilibrium conditions. At 1400 K and 10^{-6} atm, the triiodides are unstable with respect to the elements and can be used for preparing metallic films.

Determination of molecular structures of the gaseous trihalides has been a difficult problem. The RX_3 molecules were generally assumed to be planar, D_{3h}, and early electron diffraction data confirmed this conclusion. Subsequent IR spectra of matrix isolated rare earth trifluorides reopened this question. The data of Hauge et al. (1971) have been interpreted on the basis of nonplanar, C_{3v}, geometries. Similar data of Wesley and DeKoch (1971) have been assigned to D_{3h} symmetry; however, PrF_3 was found to be nonplanar. Electric field deflection studies of the trifluorides (Kaiser et al., 1972a) are inconclusive. Several of the trifluorides appear to be polar and others nonpolar. Gas phase IR data for the trichlorides (Selivanov et al., 1973) show only the asymmetric frequencies, ν_3; evidence for ν_1 modes could not be found. The more recent electron diffraction results of Giritcheva et al. (1974) show that the rare earth trihalides are pyramidal. The reported X–R–X bond angles, with uncertainties of $\pm 2°$, are: ScF_3 (109°), $LuCl_3$ (111°), $LaBr_3$ (115°), $GdBr_3$ (114°) and $LuBr_3$ (114°). The IR spectra of ScF_3 and $LuCl_3$ have been assigned and unobserved frequencies calculated. Since planar molecules are expected only if the bonding is ionic, the calculations of Meyers (1975) are of particular importance. Comparison of experimental atomization energies with those calculated by an ionic model shows that the total bond energy cannot be accounted for by ionic interaction.

Another interesting aspect of rare earth trihalide vaporization processes is the formation of dimeric molecules, R_2X_6. The existence of the diamer was first observed (McKinley, 1965) in the mass spectrum of YCl_3. The diamer fragments $Y_2Cl_5^+$, $Y_2Cl_4^+$ and $Y_2Cl_3^+$ were observed along with fragments of the monomer, and enthalpy changes were measured for both vaporization processes. Similar results were reported for lanthanide trichlorides by Novikov and Gavrycherkov (1967) and Hastie et al. (1968). The latter authors give estimated enthalpies of diamerization for the rare earth trichlorides and observe that La_2Cl_6 constitutes about 1% of the vapor at 0.1 torr (1030 K). Extrapolation of the data to the boiling point (2085 K) shows that the gas phase is approximately 85% diamer. Skinner and Searcy (1971) determined that R_2F_6 fragments were not observed in earlier work because of masking by monomer fragments and that La_2F_6 is 1% of the vapor at 1575 K. The thermodynamics of vaporization and diamerization are reported for the La and Ce fluorides by Roberts and Searcy (1972). Recent data (Hirayama et al., 1976) show that La_2I_6 also constitutes approximately 1% of the vapor at the melting point (995 K).

Substantial efforts have been devoted to the determination of the equilibrium partial pressures and the thermodynamics of vaporization of the trihalides. The first systematic investigation of vapor pressures of the trifluorides is the series of mass spectrometric measurements of Margrave and coworkers (Zmbov and Margrave, 1966; Kent et al., 1966; Besenbruck et al., 1967; Zmbov and

Margrave, 1967), and results for all the lanthanides and yttrium are described by Zmbov and Margrave (1968). In general the enthalpies of sublimation at 298 K are reported to vary between 95 and 111 kcal/mole across the lanthanide series; however, substantially higher values (115–120 kcal/mole) are given for the trifluorides of Dy, Ho, Er and Y. Substantial variations are observed in the entropies of sublimation, which range from 36 eu for YbF_3 to 52 eu for ErF_3. Vaporization data reported by Suvorev et al. (1966) and torsion effusion measurements for several of the lighter trifluorides are described by Searcy and coworkers (Lim and Searcy, 1966; Mar and Searcy, 1967; Skinner and Searcy, 1968; Roberts and Searcy, 1972). Second and third law enthalpies of sublimation at 298 K for LaF_3, CeF_3 and PrF_3 are in good agreement assuming D_{3h} symmetry for the gaseous trifluorides. Langmuir data show that the vaporization coefficients for (0001) of the LaF_3-type trifluorides is 0.90–0.95. Simultaneous mass loss and mass spectrometric studies are described in the more recent reports of McCreary and Thorn (1973a,b, 1974b,c). Results of the two methods are in close agreement. High precision pressure equations and enthalpy and entropy values are reported. Values of DyF_3, HoF_3 and ErF_3 and those of Biefeld and Eick (1976) for TmF_3 differ substantially from those of previous reports. Biefeld (1974) and Biefeld and Eick (1975) have shown that SmF_3 and YbF_3 vaporize incongruently by the following net reaction: $RF_3(s) \rightarrow 0.95\ RF_3(g) + 0.05\ RF_{2.40}(s) + 0.03\ F(g)$; i.e., 95% of the trifluoride vaporizes by the congruent process. The enthalpy and entropy of the hypothetical congruent sublimation of YbF_3 are appreciably higher than reported previously. The observations of Petzel and Greis (1972) indicate that EuF_3 also vaporizes incongruently by a similar process, but reduction by the container cannot be excluded.

Equilibrium pressure data have also been reported for the trichlorides, tribromides and triiodides. As expected, the relative vapor pressures of the trihalides at a given temperature follow the sequence $RF_3 < RCl_3 < RBr_3 < RI_3$. Initial pressure measurements for the lighter lanthanide trihalides (R = La–Nd, X = Cl, Br, I) are described in a report by Schimazaki and Niwa (1962). Comprehensive measurements of trichloride pressures are described in the effusion study of Moriarty (1963) and the boiling point measurements of Polyachenok and Novikov (1963a). The enthalpy values of the first study in the range 30–80 kcal/mole across the lanthanide series; those of the last study vary regularly from 84 kcal/mole for $LaCl_3$ to 74 kcal/mole for $LuCl_3$. Hastie et al. (1968) describe mass spectrometric measurements for selected trichlorides and note that higher temperature data of Polyachenok and Novikov could be altered by high partial pressures of diamer. Recent mass spectrometric values for $NdCl_3$ and $GdCl_3$, 70 and 65 kcal/mole respectively (Ciach et al., 1973), are consistent with this possibility. A limited number of measurements have been reported for the tribromides (Weigel and Trinkl, 1970; Makhmadmurodov et al., 1975; Dudchik et al., 1975). Vaporization data for the triiodides have been extensively studied by Hirayama and coworkers using mass spectrometric and mass effusion methods (Hirayama and Camp, 1972; Hirayama and Castle, 1973; Hirayama et

al., 1975; Hirayama et al., 1976). The enthalpies of sublimation at 298 K vary regularly from 76 kcal/mole for LaI_3 to 69 kcal/mole for EuI_3. Comments on the data reduction cycles of the triiodides have been made by Gupta (1976). Equilibrium data have also been reported for the incongruent vaporization of $SmCl_3$, $EuCl_3$ and $YbCl_3$ (Polyachenok and Novikov, 1964), and sublimation of $EuBr_3$ (Haschke, 1973). The vaporization processes for these trihalides are $RX_3(s, \ell) \rightarrow RX_2(s, \ell) + \frac{1}{2}X_2(g)$.

3. Tetrahalides

3.1. *Preparative methods*

Of numerous attempts to prepare tetrahalides, the efforts have only been successful for Ce, Pr and Tb. Reaction of the trifluoride or the metals with fluorine at 300–500° is applicable to CeF_4 and TbF_4 (Cunningham et al., 1954); however, other fluorinating agents such as XeF_2 have recently been employed (Spitsyn et al., 1973, 1974). All attempts to prepare other tetrafluorides by these methods have not been successful. The tetrafluorides of Pr and Nd cannot be obtained from the trifluorides at 350°C and 330 atm fluorine pressure (Kaiser et al., 1972b). The only successful method for preparing PrF_4 (Soriano et al., 1966; Asprey et al., 1967), involves the preparation of a complex alkali metal fluoride of tetravalent praseodymium (Na_2PrF_6 or $Na_7Pr_6F_{31}$) and extracting the NaF with anhydrous hydrofluoric acid. The tetrafluoride product is obtained as an insoluble residue. Other methods employing oxides of Ce and Tb have also been described. Asker and Wylie (1964) have prepared CeF_4 by reaction of CeO_2 with fluorine at 500°C. Bratsanova et al. (1973) have employed ClF_3 for fluorination of CeO_2 and $TbO_{1.75}$. Attempts to dehydrate $CeF_4 \cdot xH_2O$ under gaseous HF have not been successful (Asker and Wylie, 1964).

The experimental conditions required for preparation of the tetrafluorides place restraints on the possible container materials. Nickel and monel are satisfactory, but it is necessary that the surfaces be passivated by fluorination.

3.2. *Properties of the tetrafluorides*

The tetrafluorides are white solids which are only slightly soluble in water, but decompose slowly to form trifluorides. The cerium compound which is appreciably more stable than those of praseodymium and terbium, reacts with moist air above 500°C to form CeO_2 and HF. Additional properties of the tetrafluorides are described by Bratsanova (1971).

The tetrafluorides have monoclinic (C2/c) UF_4 (or ThF_4)-type structures (Zachariasen, 1949; Larson et al., 1964), with twelve formula units per cell. The metals are eight coordinate and occupy slightly distorted antiprismatic sites. The structure may be described by alternation of RF^{3+} and $R_2F_{11}^{3-}$ layers parallel to (100), but unlike the trihalide structures it does not appear to be a derivative of

anti-NiAs. Lattice parameters for the tetrafluorides are tabulated by Brown (1968).

The high temperature and vapor phase properties of the tetrafluorides are partially characterized. The order of thermal stability is $PrF_4 < TbF_4 < CeF_4$. The CeF_3–CeF_4 system has been investigated by thermal, X-ray and optical analyses and by mass effusion studies (Asker and Wylie, 1964). At temperatures below 550°C, the tetrafluoride apparently sublimes congruently, but at higher temperatures the process is incongruent and results in formation of reduced compositions. The tetrafluoride melts incongruently at 830–835°C with formation of a slightly substoichiometric liquid, $CeF_{3.95}$, plus fluorine rich vapor. A simple eutectic is observed at $CeF_{3.8}$ and 808°C; no evidence is found for intermediate fluoride phases. Mass spectrometric and electric-deflection experiments have been employed for further characterization of the vaporization process and the vapor phase at temperatures up to 940°C (Kaiser et al., 1972b). Congruent vaporization of CeF_4 to monomeric gas is indicated by these data. The fragmentation pattern includes all cerium-containing species except the parent ion. Slight decomposition of the phase is confirmed by a low fluorine pressure at high temperatures. The appearance of nickel fluoride at high temperatures indicates reduction by the container. Although a low partial pressure of the tetrafluoride is observed for TbF_4, fluorine loss is substantial at low temperatures, and complete decomposition is rapid at 940°C. Loss of fluorine from PrF_4 occurs at very low temperatures and no evidence for tetrafluoride vapor is found. Gaseous CeF_4 appears to have a nonpolar geometry. A small refocussing of the molecular beam could arise from a slight asymmetry or from a vibrationally induced moment of a tetrahedral molecule.

Thermochemical data for the tetrafluorides are limited. The estimated molar enthalpy (−442 kcal) and free energy of formation of CeF_4 are approximately 40 kcal more negative than those of CeF_3 (Wicks and Block, 1963). In comparison, the estimated molar free energy of PrF_4 is only one kcal more negative than that of PrF_3 (Britton, 1954). These data are obviously consistent with the observed properties of the tetrafluorides, but additional work is clearly needed.

4. The reduced halides

4.1. *A survey of the reduced halides*

A particularly active area of halide chemistry has been the investigation of the reduced halide systems. Dihalides of Sm, Eu and Yb have been known for years, but thorough examination of their properties has only recently been undertaken. Some of the most interesting reduced halides have been observed in the metal-rich chloride, bromide and iodide systems of normally trivalent rare earths. Numerous intermediate phases, $RX_x (2 < x < 3)$, dihalides, RX_2, and several sesquihalides, R_2X_3, are known in the solid state. The gaseous dihalides

and monohalides have also been characterized. Although the existence of anomalous dihalides was predicted on the basis of thermodynamic estimates (Holleck, 1938; Brewer et al., 1950), these systems have been investigated only during the last fifteen years. A substantial fraction of the phase studies of these anomalous systems has been conducted by Corbett and coworkers and are described in recent reviews (Corbett, 1973, 1976). Early work is also described in a review by Novikov and Polyachenok (1964). Although there is some basis for dividing the reduced halides into either common or uncommon categories, there is a continuum from very stable to marginally stable phases. The more easily studied stable compounds provide a convenient reference point for understanding the properties of phases of lower stability, and an attempt will be made to unify the chemistry of the reduced phases.

The general stability trends of the reduced halides are indicated by the survey of experimental results for rare earth systems in table 32.2. The rather extensive list of phase studies is given in table 32.3. Several trends are evident (Corbett, 1973). As one would expect, the stability of the dihalides increases from fluoride to iodide. Condensed difluorides have been characterized for only three rare earths, but iodides are known for ten elements. Investigations of bromide systems are incomplete and the number of stable dibromides may exceed the number of dichlorides. A less obvious trend occurs across the rare earth series with substantially lower tendencies toward divalency for Y, La, Ce, Gd, Tb, Er and Lu. Except for Er, the trend is a dual periodicity with maxima in stability at Eu and Yb. Thermodynamics of dihalide stability are described by the free energy of the disproportionation reaction: $3RX_2(s) \rightarrow 2RX_3(s) + R(s)$. The tendency toward disproportionation is consistent with fusion characteristics; the stable $EuCl_2$ phase melts congruently, but the marginally stable $NdCl_2$ phase melts incongruently (Druding and Corbett, 1961).

Examination of the experimental methods listed in table 32.3 shows that two methods, thermal and X-ray analysis, have most frequently been employed for characterization of the reduced halides. These methods provide invaluable data, but it has become increasingly clear that single crystal X-ray structure determinations are necessary for accurate definition of compositions. Properties of the liquidus and of the solid–liquid interface are uniquely defined by thermal

TABLE 32.2
Survey of rare earth elements forming solid reduced halides.

X	M_2X_3	RX_2	$RX_x (2 < x < 3)$	None
F	*	Sm, Eu, Yb	Sm, Eu, Tm, Yb	La, Ce, Nd
Cl	Sc, Gd	Nd, Sm, Eu, Dy, Tm, Yb	Pr, Nd, Sm, Dy, Ho, Tm, Yb	Y, La, Ce, Er, Lu
Br	Sc	Nd, Sm, Eu, Dy, Tm, Yb	Pr, Sm	La, Ce
I	*	La, Ce, Pr, Nd, Sm, Eu, Gd Dy, Tm, Yb	Sc, La, Ce, Pr	Y, Tb, Ho, Er

*Sesquihalides or other subhalides not known.

TABLE 32.3
Investigations of reduced rare earth halide systems.

System	Methods	Reference(s)
La, Ce, Nd–F	thermal analysis	Dworkin and Bredig (1971b)
Sm–F	X-ray	Catalano et al. (1969)
	X-ray	Stezowski and Eick (1970)
	thermal analysis, equilibration	Bedford and Catalano (1970)
	thermal analysis ($Sm–SmF_2$)	Dworkin and Bredig (1971b)
	X-ray, vaporization	Biefeld (1974)
Eu–F	X-ray	Catalano et al. (1969)
	thermal analysis, equilibration	Bedford and Catalano (1970)
	X-ray	Tanguy et al. (1972)
	X-ray	Petzel and Greis (1972)
Yb–F	X-ray	Catalano et al. (1969)
	thermal analysis, equilibration	Bedford and Catalano (1970)
	thermal analysis ($Yb–YbF_2$)	Dworkin and Bredig (1971b)
	X-ray, vaporization	Biefeld and Eick (1975)
Y–Cl	thermal analysis	Polyachenok and Novikov (1963b)
	thermal analysis	Corbett et al. (1966)
	thermal analysis	Dworkin and Bredig (1973)
La–Cl	thermal analysis	Keneshea and Cubicciotti (1961)
Ce–Cl	thermal analysis	Mellors and Senderoff (1959)
Pr–Cl	thermal analysis	Druding et al. (1963)
	thermal analysis, vaporization	Novikov and Polyachenok (1963)
Nd–Cl	thermal analysis	Druding and Corbett (1961)
	thermal analysis, vaporization	Novikov and Polyachenok (1963)
Sm–Cl	thermal analysis	Polyachenok and Novikov (1963b)
Gd–Cl	thermal analysis	Mee and Corbett (1965)
Dy–Cl	thermal analysis	Corbett and McCollum (1966)
Ho–Cl	thermal analysis	Loechner and Corbett (1975)
Er–Cl	thermal analysis	Corbett et al. (1966)
Tm–Cl	thermal analysis, X-ray	Caro and Corbett (1969)
Yb–Cl	X-ray	Fishel and Eick (1971)
La, Ce, Pr–Br	thermal analysis	Sallach and Corbett (1963)
Sm–Br	X-ray	Haschke (1976d)
Eu–Br	X-ray, vaporization	Haschke (1973)
Y–I	thermal analysis	Corbett et al. (1966)
La, Ce, Pr–I	thermal analysis	Corbett et al. (1962)
	thermal analysis	Mironov et al. (1974)
Nd–I	thermal analysis	Druding and Corbett (1961)
	thermal analysis	Mironov et al. (1974)
Gd–I	thermal analysis	Mee and Corbett (1965)
Tb, Dy, Ho–I	thermal analysis	Johnson and Corbett (1969)
Er–I	thermal analysis	Corbett et al. (1966)

analysis. Results of thermal analyses and other physical property measurements of R–RX_3 melts have been extensively reviewed by Corbett (1973). The formation of dipositive ions, R^{2+}, in solutions of R in RX_3 melts is clearly demonstrated by conductivity measurements (Dworkin and Bredig, 1961; Bronstein et al., 1962; Dworkin et al., 1962; Dworkin et al., 1963), vapor pressure isotherms (Novikov and Polyachenok, 1963), and emf data (Bronstein, 1969). The level of reduction, i.e., the stability of the R^{2+} ion, is directly indicated by the extent of the solution reaction $2RX_3(\ell) + R(s, \ell) \rightarrow 3RX_2$ (soln). The degree of reaction is proportional to the composition (mole % metal) of the melt in equilibrium with the metal (Corbett, 1973). The increase in stability of R^{2+} from fluoride to iodide is demonstrated by the La solubility, which is approximately 0.3% in LaF_3 (Dworkin and Bredig, 1971b), 9% in $LaCl_3$ (Keneshea and Cubicciotti, 1961), 14% in $LaBr_3$ (Sallach and Corbett, 1963) and 33% (quantitative reduction to the diiodide) in LaI_3 (Corbett et al., 1962). Analysis of Born-Haber cycles for disproportionation of the dihalides to the trihalides plus metal show that the stability variations across the series are accounted for by the third ionization potential and the enthalpy of sublimation of the metal (Corbett, 1973); however, an alternate approach correlates the solubility with the enthalpy of sublimation of the metal (Topol, 1965).

Several of the solid reduced iodides, LaI_2, CeI_2, PrI_2, GdI_2 and $ScI_{2.17}$, exhibit metal-like electrical conductivity (Corbett, 1973). The colors of these compounds vary from black to bronze. Resistivity measurements and magnetic susceptibility data for LaI_2 (Corbett et al., 1967) are consistent with the metallic formulation, $La^{3+}(I^-)_2e^-$, and in this respect these diiodides are like the metallic lanthanide dicarbides, $R^{3+}(C_2^{2-})e^-$, and monosulfides, $R^{3+}(S^{2-})e^-$. Since metallic phases are observed only for the diiodides, it appears that iodine orbitals are involved with low lying 5d orbitals of the metals in formation of the conduction bands.

4.2. *Preparative methods*

The preparative procedures are one area in which marked differences are observed between the so-called common and anomalous reduced halides. The need for a very strong reducing agent limits the available methods to metal reduction of the trihalides in all cases except Sm, Eu and Yb. High purity starting materials obviously must be employed and the use of sealed tantalum containers is necessary. Procedures and precautions of these preparative techniques have been thoroughly discussed by Corbett (1966) and (1973). The matathetical reaction of metal with a stoichiometric amount of HgI_2 has been employed for preparation of DyI_2 and TmI_2 (Asprey and Kruse, 1960; Baernighausen and Warkentin, 1973).

A variety of preparative methods have been described for the dihalides of Sm, Eu and Yb. Because of thermal instability of the trihalides in vacuum, SmI_2, $EuBr_2$, EuI_2 and YbI_2 are obtained by the preparative procedures usually employed for the trihalides. The commonly used methods for these lanthanides are reviewed by DeKock and Radtke (1970) and include reduction of the

trihalides by the respective metals, by hydrogen or by other metals such as zinc and by reaction of the metal in liquid ammonia. Although EuF_2 may be prepared by hydrogen reduction at 1000°C (Petzel and Greis, 1972), the difluorides of Sm and Yb are more difficult to prepare and usually involve the reaction of metal and trifluoride in sealed tantalum containers which prevent the loss of metal by vaporization (Stezowski and Eick, 1970). Since the difluorides have wide regions of composition variation, RF_{2+x}, cf. ch. 32, section 4.5.1, preparation of stoichiometric difluorides is frequently difficult. This problem is easily overcome by an equilibration procedure employing a double effusion cell (Petzel and Greis, 1973). One compartment of the Mo cell contains excess rare earth metal and opens into the second compartment containing trifluoride and a second opening to high vacuum. Since substoichiometry does not occur in these systems, the difluorides are obtained by equilibration at 700–900°C. Procedures for hydrogen or hydrogen plus ammonia reduction of the trihalides are reviewed by Doell and Klemm (1939) and are effective in all cases except for the difluorides of Sm and Yb. Reduction of the trihalides with Zn (Polyachenok and Novikov, 1963c; Johnson and Mackenzie, 1970) has been modified into a one-step dehydration and reduction procedure by DeKock and Radtke (1970). Zinc dihalide is included in a hydrated trihalide-ammonium halide mixture, cf. ch. 32, section 2.1, and zinc is added to the dried product. The combined mixture is dehydrated, melted at 350°C for reduction and heated to higher temperatures for complete removal of the ammonium and zinc halides. The dihalides (X = Cl, Br, I) of Eu and Yb are also obtained by reaction of ammonium halide with liquid ammonia solutions of the metal (Howell and Pytlewski, 1969). The ammoniated dihalide products are readily decomposed in vacuum at 200°C.

In general, the same precautions regarding crucible materials must be observed for the dihalides as for the trihalides, cf. ch. 32, section 2.1. Although noble metal containers were employed in much of the early work, platinum is particularly unsuited because of the formation of stable R–Pt alloys (Brewer et al., 1950; Bedford and Catalano, 1970). Several of the dihalides melt and vaporize congruently, cf. ch. 32, section 4.4.3, and can be purified by sublimation or distillation and single crystals can be grown from the melts. The majority of the reduced halides are thermally unstable and preparation of high purity samples is difficult.

4.3. *The sesquihalides*

As indicated by the data in table 32.2, unusual R_2X_3 compositions are observed for normally trivalent rare earths which have low stabilities of dipositive ions in their trihalide melts. A sesquihalide phase was first reported for the Gd–Cl system (Mee and Corbett, 1965) and subsequently for the Sc–Cl and Sc–Br systems (McCollum and Corbett, 1968; McCollum et al., 1973). In the Sc–I system, a substantially higher composition, $ScI_{2.17}$, is the only phase observed. Initial data for the gadolinium phase, which forms long black-grey needles, showed it to be $GdCl_{1.58\pm0.06}$; however, a more recent single crystal X-ray study

established the sesquihalide composition (Lokken and Corbett, 1973). The sesquihalides are the only reduced phases observed in the respective systems, and all melt incongruently. The existence of $ScCl_2$ and $ScCl_{2.67}$ reported by Polyachenok and Novikov (1963d) is not confirmed. Resistance measurements on the needle-shaped crystals show a salt-like conductivity. The magnetic moment (Greiner et al., 1966) is in close agreement with that for the $4f^7$ configuration of Gd(III), and it appears that all electrons above this core are paired. Curie–Weiss behavior is observed above 80 K and the onset of antiferromagnetic ordering occurs at 50 K. Possible factors affecting the formation of the sesquihalides are suggested by the systematics of occurrence; the phase is observed only for metal ions with filled or half-filled cores and occupied d orbitals with appreciable radial extension (Corbett, 1973).

The structure of Gd_2Cl_3 is very unusual. The X-ray determination of Lokken and Corbett (1973) shows that the phase is monoclinic with space group Cm, $Z = 8$, $a = 15.237$, $b = 3.896$, $c = 10.179$ Å and $\beta = 117.66°$. A projection of the structure on (010) in fig. 32.11 shows that the anions and cations are rigorously bilevel like those of the lanthanide trihalides, cf. ch. 32, section 2.2, and the same identification symbols are employed. The Gd–Cl distances (2.72–2.88 Å) are similar to those found in $GdCl_3$. The most peculiar structural feature is the occurrence of vacant channels of distorted edge-shared metal octahedra normal to the projection plane. The Gd–Gd distances, which range from 3.35 Å along certain octahedral edges to 3.90 Å along the projection axis, indicate that metal–metal interaction is strong within the octahedra, but negligible along the projection axis. The structure may also be described by alternation of complex

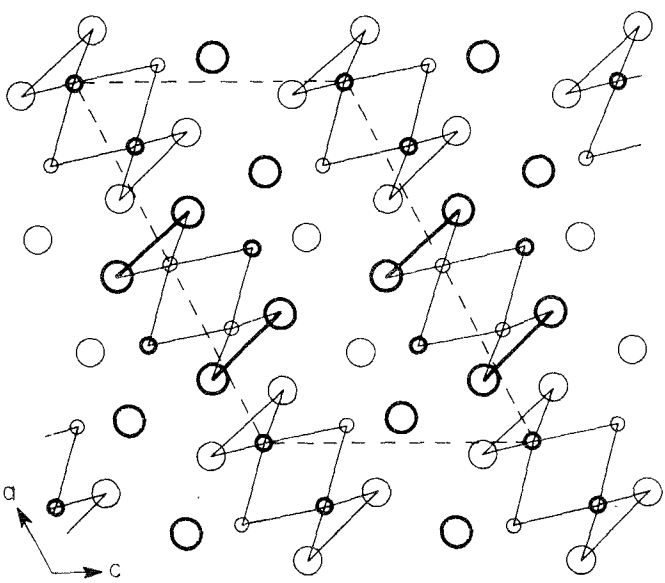

Fig. 32.11. The Gd_2Cl_3 structure (Cm) projected on (010).

cationic layers with simple chloride layers parallel to (001) and like many of the trihalide structures is closely related to anti-NiAs (Haschke, 1976b). The Cm space group is a subgroup of $P6_3/mmc$ and the structure is obtained from anti-NiAs by systematically removing one-third of the metal layers. The edge-shared metal octahedra appear as residual fragments of the hexagonal closest packed metal array of anti-NiAs and are similar to those found in closest packed metals and other metal-rich phases. The complex cationic layers are composed of $[R_2X_4]$ channels (Haschke, 1975c), which are intergrown with the channels of metal octahedra. The structure is very similar to that of $Y_3(OH)_5OCl_2$ (Klevtsova et al., 1967). Rapid crystal growth in the direction of $[R_2X_4]$ channels is characteristic of structural derivatives of anti-NiAs, and the acicular crystal habit of Sc_2Cl_3 and Sc_2Br_3 suggests that they might be structurally related to Gd_2Cl_3.

4.4. *The dihalides*

4.4.1. *Structural properties*

The dihalides are the best characterized group of reduced halides, and, in turn, their structural properties are the best characterized aspect of their chemistry. Diffraction data have been reported for all the dihalides listed in table 32.2, and their structure types have been identified. The investigation and interpretation of dihalide structures have been greatly advanced by the contributions of Baernighausen and coworkers. The crystal chemistry of the dihalides has been reviewed by Baernighausen et al. (1971). The nine known structural types of the dihalides are presented table 32.4 with corresponding RX_2 phases. As with the trihalides, cf. ch. 32, section 2.2, the cation coordination numbers decrease regularly in the series fluoride to iodide. A second similarity is found in the structural relationships of the phases; structures with high coordination numbers are derived from two different closest-packed metal arrays while those with low coordination are based on closest packing of cations. Since definitive crystallographic data have only recently been obtained and are in part unpublished (Baernighausen, 1976a), selected values are presented in table 32.5.

Examination of the nine structural types shows that they are conveniently placed in three categories: derivatives of anti-NiAs, derivatives of CaF_2 and derivatives of closest packed anion arrays. Like many of the trihalide structures and the Gd_2Cl_3 structure, the space group of $PbCl_2$ is a subgroup of that for anti-NiAs, and the $PbCl_2$-type structure is readily derived from the arsenide structure by removing one-half of the metal layers (Haschke, 1976b). A projection of the orthorhombic $PbCl_2$-type structure (Baernighausen, 1973), on (010) in fig. 32.12 shows that the ions are rigorously bilevel. The cations are nine coordinate, and the structure may be described either by RX_2 layers (Haschke, 1976b,c) or by edge sharing of trigonal prisms similar to those found in nine-coordinate RX_3 structures. The edge sharing shown in fig. 32.12 is consistent with the observation that $PbCl_2$- and UCl_3-type structures are related by crystallographic shear (Hyde et al., 1974).

TABLE 32.4
Structural data for rare earth dihalides, RX_2.

Structure type	$PbCl_2$	CaF_2	$CuTi_2$	$SrBr_2$
F	Eu	Sm, Eu, Yb	–	–
Cl	Nd, Sm, Eu	–	–	Dy
Br	Nd, Sm	–	–	Sm, Eu
I	–	–	La, Ce, Pr	Nd
Cation coord. No.	9	8	8	8

Structure type	EuI_2	SrI_2	$CaCl_2$	$CdCl_2$	CdI_2
F	–	–	–	–	–
Cl	–	Tm, Yb	–	–	–
Br	–	Dy, Tm, Yb	Yb	–	–
I	Sm, Eu	Eu	–	Pr, Dy	Tm, Yb
Cation coord. No.	7	7	6	6	6

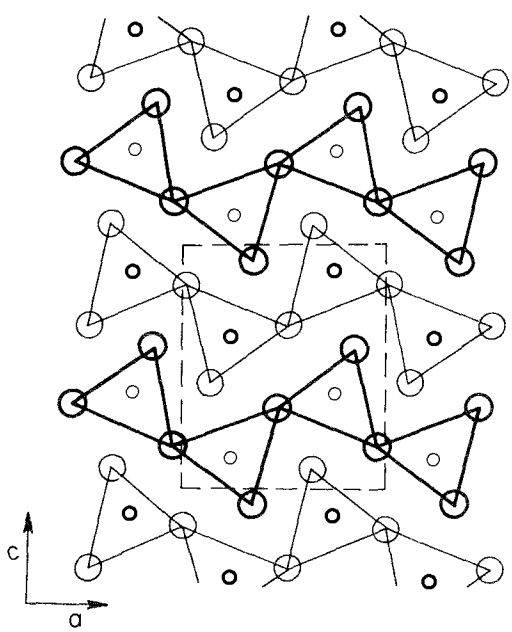

Fig. 32.12. The $PbCl_2$-type structure (Pnma) projected on (010).

TABLE 32.5
Selected crystallographic data for the rare earth dihalides.

RX_2	a(Å)	b(Å)	c(Å)	References
$PbCl_2$-type, Space group Pnma, Z = 4				
EuF_2	6.324	3.802	7.435	Seifert (1968)
$NdCl_2$	7.609	4.554	9.080	Baernighausen (1976a)
$SmCl_2$	7.556	4.517	8.993	Baernighausen (1973)
$EuCl_2$	7.538	4.511	8.965	Baernighausen (1973)
$NdBr_2$	8.026	4.785	9.585	Baernighausen (1976a)
$SmBr_2$	7.977	4.754	9.506	Baernighausen (1973)
CaF_2-type, Space group Fm3m, Z = 4				
SmF_2	5.871			Petzel and Greis (1973)
EuF_2	5.842			Petzel and Greis (1973)
YbF_2	5.599			Petzel and Greis (1973)
$CuTi_2$-type, Space group I4/mmm, Z = 2				
LaI_2	3.922		13.97	Warkentin and Baernighausen (1976)
CeI_2	3.888		13.95	Warkentin and Baernighausen (1976)
PrI_2	3.864		13.94	Warkentin and Baernighausen (1976)
$SrBr_2$-type, Space group P4/n, Z = 10				
$DyCl_2$	10.775		6.643	Baernighausen (1976a)
$SmBr_2$	11.593		7.100	Baernighausen (1973)
$EuBr_2$	11.566		7.094	Haschke (1973)
NdI_2	12.573		7.678	Baernighausen (1976a)
EuI_2-type, Space group $P2_1/c$, Z = 4				
SmI_2	7.616	8.281	7.901	Baernighausen (1976a)
	$\beta = 97.96°$			
EuI_2	7.621	8.245	7.894	Baernighausen (1976a)
	$\beta = 98.01°$			
SrI_2-type, Space group Pbca, Z = 8				
$TmCl_2$	13.176	6.975	7.710	Hariharan (1973)
$YbCl_2$	13.150	6.693	6.942	Fishel and Eick (1971)
$DyBr_2$	13.989	7.476	7.175	Baernighausen (1976a)
$TmBr_2$	13.813	7.380	7.100	Baernighausen (1976a)
$YbBr_2$	13.786	7.358	7.088	Baernighausen (1976a)
EuI_2	15.14	8.22	7.86	Baernighausen (1976a)
$CaCl_2$-type, Space group Pnnm, Z = 2				
$YbBr_2$	6.602	6.923	4.370	Baernighausen (1976a)
$CdCl_2$-type, Space group $R\bar{3}$, Z = 1 (data listed for hexagonal cell)				
PrI_2	4.25		22.43	Warkentin and Baernighausen (1976)
DyI_2	4.61		20.86	Baernighausen and Warkentin (1973)
CdI_2-type, Space group $P\bar{3}m1$, Z = 1				
TmI_2	4.520		6.967	Asprey and Kruse (1960)
YbT_2	4.503		6.972	Asprey and Kruse (1960)

The structural correlations of Baernighausen et al. (1971) and Baernighausen (1975) have demonstrated that the $SrBr_2$-, EuI_2-, SrI_2- and $CaCl_2$-type structures are derivatives of the CaF_2-type (fluorite) structure. The space groups of all these structure types are subgroups of the highest symmetry Fm3m space group of CaF_2. The existence of close structural relationships is readily demonstrated by structural projections of the type shown in fig. 32.13 (Baernighausen, 1975). The cubic eight-fold coordination of CaF_2 is indicated by its (100) projection in which the cubic closest packed metals appear at two levels, $\frac{1}{4}$ and $\frac{3}{4}$, along the projection axis. This bilevel cation arrangement is again indicated by use of heavy and light circles. The anion positions, 0 and $\frac{1}{2}$ along the projection axis, are indicated by the intersection points of the square nets. These nets are coincident in the fluorite projection, but in general this is not the case and the two levels are distinguished by use of solid and dashed lines. All derivatives of the CaF_2 structure have essentially bilevel cations which are found between anion nets similar to those of fluorite. Rigorous planarity of the anion nets is not observed in the derivative structures; however, the distortions are usually so small that the structural features are readily demonstrated by the projections.

The tetragonal $CuTi_2$-(or $MoSi_2$-)type structure observed for the metallic diiodides of La, Ce and Pr by Warkentin and Baernighausen (1976) is similar to a CaC_2-type in which the anions are not bonded, but may also be described as a derivative of fluorite. The tetragonal cation arrangement is distorted from the face centered cubic arrangement of fluorite by a substantial displacement of the anion layers, which are shifted relative to the metals and split into a doubled layer. These distortions reduce the anion repulsions and simultaneously maintain a cubic cation coordination. The $MoSi_2$ structure is characterized by a large splitting of the anion layer, a large c/a ratio (3.6) and an eight-fold cation coordination. The diiodides appear to have a structure more like that of $CuTi_2$ in

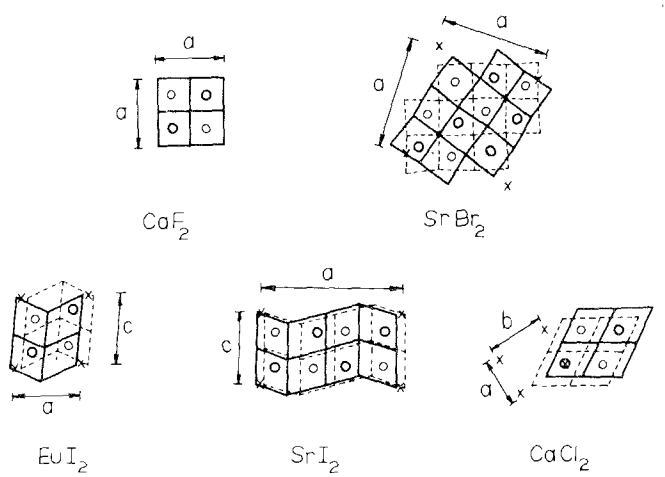

Fig. 32.13. The fluorite and fluorite-related structures of the dihalides. (See text for identification of symbols.)

which the layer splitting is somewhat smaller, c/a is 2.6 and the cation coordination number of 8 + 2. The metal-iodine distances are consistent with those of the trivalent cations and support the formulation $R^{3+}(I^-)_2e^-$ suggested by Corbett et al. (1967).

The correct $SrBr_2$-type structure has only recently been described. The initial single crystal structure determination for $SrBr_2$ (Kammermans, 1939) showed an orthorhombic cell similar to that of $PbCl_2$. Powder diffraction data showed that the dibromides of Sr, Sm and Eu are isostructural (Doell and Klemm, 1939). Combination of these reports led to the assignment of the orthorhombic structure to the rare earth phases. Subsequent powder diffraction data (Sass et al., 1963; Haschke and Eick, 1970a) showed that the orthorhombic structures were those of the dibromide monohydrates. The tetragonal structure derived from the powder measurements was confirmed and refined by the single crystal study of Smeggil and Eick (1971). The (001) projection of the $SrBr_2$-type structure in fig. 32.13 shows that it is closely related to fluorite. Displacement of one anion net relative to the other gives essentially square antiprismatic cation coordination (Baernighausen et al., 1971). Four-fifths of the antiprismatic sites are highly distorted, and the cation coordination may be described either as seven- or eight-fold. This distortion of fluorite permits the coordination number to remain unchanged at higher anion to cation radius ratios. The non-metallic $SrBr_2$-type neodymium iodide is reported to have a substoichiometric composition, $NdI_{1.95}$ (Druding and Corbett, 1961), but the mechanism for composition variation is not known.

The seven-coordinate monoclinic EuI_2-type and orthorhombic SrI_2-type structures (Baernighausen and Schultz, 1969; Reitschel and Baernighausen, 1969), and the six-coordinate orthorhombic $CaCl_2$-type structure (Wyckoff, 1963), are observed at higher anion to cation radius ratios. Examination of the structural projections in fig. 32.13 shows that they are also closely related to fluorite. Comparison of the anion nets in EuI_2 and SrI_2 demonstrate that they are displaced differently in the two structures; these structures are related by an intracellular twinning mechanism (Baernighausen et al., 1971). The SrI_2 (or CeSI)-type structure has been found for the dichlorides of Dy, Tm and Yb (Beck and Baernighausen, 1971; Baernighausen et al., 1974). The true cell is a two-fold multiple of that assigned in earlier work. The orthorhombic $CaCl_2$-type structure of $YbBr_2$ (Beck and Baernighausen, 1971; Baernighausen et al., 1974) may be considered either as a derivative of a closest packed anion array or as a derivative of fluorite. The relationship to fluorite (Baernighausen, 1975) is clearly seen in fig. 32.13.

The $CdCl_2$- and CdI_2 (or $Cd(OH)_2$)-type structures of the heavy diiodides are readily derived from closest packing of anions (Wyckoff, 1963). The anions are cubic closest packed in $CdCl_2$ and hexagonal closest packed in CdI_2 and consequently the structures are closely related to those of YCl_3 (cf. fig. 32.8) and BiI_3 (cf. fig. 32.9). The alternate layers of octahedral sites are completely occupied by cations instead of two-thirds occupied as in the trihalides. The $ScI_{2.17}$ phase also has the CdI_2-type structure (McCollum and Corbett, 1968), and

it has been suggested that the composition is achieved via random cation vacancies.

The extensive structural relationships of the dihalides suggest the possibility of dimorphism and of displacive transitions. The known occurrences of dimorphism are indicated by double entries in table 32.4. In all cases, EuF_2, $SmBr_2$, SmI_2, EuI_2 and $YbBr_2$, the cation coordination number of the two structures are equal or differ by only one. The CaF_2- to $PbCl_2$-type transition, which is observed for EuF_2 at 112 kbar and 850°C (Seifert, 1968), is consistent with the existence of a displacive relationship between the two structure types (Haschke, 1975d). Although a high temperature phase transition is observed for $SrBr_2$ (Dworkin and Bredig, 1963a), the unusual dimorphism of $SmBr_2$ does not appear to be a thermal transition. In one case (Baernighausen, 1973) the $PbCl_2$-type phase was obtained by distillation of the $SrBr_2$-type dibromide, and in the other (Haschke, 1976d), the $PbCl_2$- and $SrBr_2$-type phases were found only on the metal-rich and bromine-rich sides of the dibromide composition, respectively. The $PbCl_2$-type phase exists in equilibrium with the $SrBr_2$-type phases and is apparently stabilized by a high metal activity which could arise from preferential loss of bromine in an incongruent vaporization process. The dimorphism observed for PrI_2 (Warkentin and Baernighausen, 1976) is somewhat surprising because of the change in coordination number from eight or ten to six. However, the metallic nature of one or both of these phases complicates comparisons with other systems. A thermal arrest observed just below the melting point of $NdCl_2$ (Druding and Corbett, 1961) may indicate a thermal transition. Beck and Baernighausen (1971) have suggested that the low temperature cubic form of YbI_2 (Howell and Pytlewski, 1969) is CsCl-type NH_4I.

4.4.2. *Thermodynamic properties*

A substantial amount of thermochemical data have been reported for the dichlorides, but as with the trihalides, only estimated values are available for many dihalides (Wicks and Block, 1963; Feber, 1965; Johnson, 1969). A limited amount of data is reported for the condensed and gaseous dihalides (Schumm et al., 1973) and estimated values for a large number of gaseous dihalides are available (Krasnov and Danivola, 1969).

The enthalpies of formation, ΔH°_{f298}, available for the dichlorides have been obtained primarily from calorimetric data. Solution microcalorimetry measurements are described for $SmCl_2$ and $YbCl_2$ (Machlan et al., 1955), but incomplete oxidation of europium prevented similar measurements for $EuCl_2$. Solution data for $EuCl_2$ have subsequently been reported by Stubblefield et al. (1965) and most recently by Morss and Haug (1973). The most recent ΔH°_{f298} value (−197 kcal/mole) is substantially more negative than the −193 kcal/mole result of the earlier work and is in good agreement with the −196 kcal/mole value obtained from vaporization data by Hariharan and Eick (1972a). Other ΔH°_f values for the dichlorides include those of $SmCl_2$ (−195 kcal/mole) and $YbCl_2$ (−191 kcal/mole) (Schumm et al., 1973), and those of $NdCl_2$ (−169 kcal/mole)

and $TmCl_2$ (−170 kcal/mole) (Morss and McCue, 1975). This $NdCl_2$ value differs from the calorimetric result (−163 kcal/mole) obtained by Polyachenok and Novikov (1963e), but is in exact agreement with their earlier tensimetric value (Novikov and Polyachenok, 1963). The recent ΔH°_{f298} values (Morss and McCue, 1975) are of importance in demonstrating that the enthalpies for $3RX_2 \rightarrow 2RX_3 + R$ are +9 kcal and +37 kcal for $NdCl_2$ and $TmCl_2$ at 298 K, and in supplementing earlier calculations of dihalide stabilities (Johnson, 1969). Solution microcalorimetric methods have recently been employed by Morss and Fahey (1976) for redetermining the enthalpy of formation of $SmCl_2$ (−191.7 kcal/mole) and for measuring the value for $DyCl_2$ (−236.50 kcal/mole). These data include a remeasurement of the enthalpy of formation of $Dy^{3+}(aq)$ and complete the R^{2+}–R^{3+} (R = Nd, Sm, Eu, Dy, Tm, Yb) reduction potentials which were partially described by Morss and McCue (1975).

Other thermochemical data include a recently reported ΔH°_{f298} for SmF_2 (−231 kcal/mole) (Khanaev et al., 1975), and values which have been obtained for the condensed and gaseous dihalides and gaseous monohalides from high temperature investigations, cf. section 4.4.3. Measured enthalpies of vaporization, dissociation and formation are reported; derived thermal functions for the gases and estimated heat capacities and entropies of the solids are included in several reports. Free energy changes determined for $RCl_3 \rightarrow RCl_2 + \frac{1}{2}Cl_2$ (R = Sm, Eu, Yb) by electrochemical measurements in alkali metal chloride melts (Johnson and Mackenzie, 1969) are in good agreement with earlier tensimetric values of Polyachenok and Novikov (1964). Heat capacities have not been measured for either the high or low temperature regions. An S°_{298} of $EuBr_2$ (33 eu) is obtained from the calorimetric value for the tribromide (Deline et al., 1975), and from its entropy of vaporization (Haschke, 1973).

4.4.3. *Vaporization and the vapor phase*

The vaporization process and vapor species of several dihalide systems have been investigated. Vaporization reactions and other high temperature properties of RX_2 phases are determined largely by their thermodynamic stabilities. Those halides which are obtained without use of the rare earth metal as a reducing agent are generally stable with respect to disproportionation and are congruently melting and vaporizing. The metallic diiodides are congruently melting, but their vaporization reactions have not been characterized. Substantial contributions toward understanding the vaporization properties of the dihalides have been made by Eick and coworkers. Mass spectrometric studies of equilibrium vapors from effusion sources have shown that the monomeric dihalides are the only vapor species for several RX_2(X = Cl, Br, I) phases. The fragmentation patterns of dichlorides (Hastie et al., 1968), dibromides (Haschke and Eick, 1970c) and diiodides (Hariharan and Eick, 1972b) include RX_2^+, RX^+ and R^+ ions. No evidence for diameric R_2X_4 species has been observed. Dihalide partial pressures, which are substantially lower than those of the stable trihalides, have been measured for the congruently vaporizing dihalides shown in table 32.6. These

reports include equilibrium vapor pressure measurements, mass spectrometric data and thermodynamic functions for the condensed and gaseous phases. The results are consistent except in the case of $EuBr_2$; its enthalpy and entropy of sublimation appear to be low and consequently the extrapolated boiling point is too high.

Several of the dihalides are known to vaporize incongruently, but the behavior of others is unclear. The equilibrium measurements of Biefeld (1974) and Biefeld and Eick (1975) have demonstrated that unlike EuF_2, SmF_2 and YbF_2 vaporize incongruently to form $RF_{2.40}$ solids plus metal rich vapors. The trichloride is the only vapor species observed in the vaporization of $NdCl_2$ (Polyachenok and Novikov, 1963b). Reports that $YbCl_2$ and $YbBr_2$ (Jantsch et al., 1931) and $SmBr_2$ and SmI_2 (Jantsch and Skalla, 1930) and SmI_2, EuI_2 and YbI_2 (Lishenko et al., 1973), disproportionate to RX_3 and R on heating to 800–900°C are in part inconsistent with effusion studies showing congruent processes. It is rather peculiar that several RX_3 phases disproportionate to RX_2 plus $\frac{1}{2}X_2$ at low temperatures, and the RX_2 product then disproportionates to RX_3 and R at higher temperatures. The calculations of Johnson (1969) clearly indicate that $YbCl_2$ should not disproportionate. The exact experimental arrangements are not always clear, and differences between equilibrium and nonequilibrium conditions are expected to be very important in cases of marginal stability. Furthermore, the observations of Brewer et al. (1950) emphasize that the apparent decomposition processes might be promoted by reaction between the sample and container.

TABLE 32.6
Thermodynamic data[a] for congruently vaporizing dihalides

RX_2	SmI_2	EuF_2	$EuCl_2$
$\Delta H^\circ_{298}[RX_2(s) \rightarrow RX_2(g)]$	72	101	85
$\Delta S^\circ_{298}[RX_2(s) \rightarrow RX_2(g)]$	43	49	48
b.p.(K)	1932	2487	2335
$D^\circ_0[MX_2(g)]$	171	263	210
$\Delta H^\circ_{f298}[MX_2(s)]$	−141	−284	−196
Reference	Hirayama et al. (1974)	Petzel and Greis (1972)	Hariharan and Eick (1972a)

RX_2	$EuBr_2$	EuI_2	$YbCl_2$
$\Delta H^\circ_{298}[RX_2(s) \rightarrow RX_2(g)]$	71	75	85
$\Delta S^\circ_{298}[RX_2(s) \rightarrow RX_2(g)]$	37	48	48
b.p.(K)	2530	2048	2306
$D^\circ_0[MX_2(g)]$	(202)[b]	156	−194
$\Delta H^\circ_{f298}[MX_2(s)]$	−178	−138	−185[c]
Reference	Haschke and Eick (1970c)[d]	Hariharan and Eick (1972b)	Hariharan et al. (1972)

[a]Units of enthalpy and entropy are kcal/mole and cal/deg mole (eu), respectively. [b]Estimated value from Feber (1965). [c]Calorimetric value of Machlan et al. (1955). [d]See Recent Developments section for new $EuBr_2$ data.

High temperature mass spectrometric studies of the rare earth halide systems have verified earlier reports of the gaseous subfluorides, RF_2 and RF (Zmbov and Margrave, 1968). The equilibrium vapor from an effusion source containing HoF_3 and Ho include HoF_2 and HoF. The analogous Sm, Eu, Gd, Dy and Er fluorides have been studied by isomolecular exchange reactions with the Ho species. The vapor from the $Nd + BaF_2$ system (Zmbov and Margrave, 1966) and the $Y + YF_3$ system also include these subfluorides. Ionization potential, bond dissociation energies and enthalpies of formation of the subfluorides are reported and are included in the compilation of Schumm et al. (1973).

The structural chemistry of the gaseous dihalides is of special interest because of the similarities with alkaline earth species, which are known to have nonlinear geometries. As with the trihalides, the dihalides have been investigated both by spectroscopic and electric-deflection techniques; however, the results are much more conclusive. The IR measurements for matrix isolated EuF_2 and $EuCl_2$ (Hastie et al., 1971), resulted in assignment of the stretching frequencies for $EuCl_2$ and determination of the Cl–Eu–Cl angle as $135 \pm 8°$. The estimated F–Eu–F angle is $110 \pm 15°$. On the basis of similar measurements (DeKock et al., 1972) assigned the spectra and calculated the force constants for the difluorides and dichlorides of Sm, Eu and Yb. The following X–R–X angles are reported: SmF_2 (110°), YbF_2 (140°), $SmCl_2$ (130°), $EuCl_2$ (130°) and $YbCl_2$ (140°). The deflection experiments of Kaiser et al. (1972a) confirm that the gaseous difluorides are polar molecules.

4.5. *The intermediate halides*

4.5.1. *Phase equilibria*

The intermediate phases, RX_x ($2.0 < x < 3.0$), are an extensive area of halide chemistry. Although their existence is to be anticipated because of stable divalent and trivalent halides and was suggested by early work, they have only recently been identified by the phase studies listed in table 32.3 (cf. section 4.1). The intermediate phases are conveniently grouped in two categories, the intermediate fluorides and the intermediate chlorides, bromides and iodides.

Intermediate fluorides are known for only four elements, Sm, Eu, Tm and Yb Phase equilibria in these systems have been described by Catalano et al. (1969). The Sm and Eu systems appear to be similar; diagrams for the Tm and Yb systems are incomplete. Fluorite-type difluorides are reported for all systems, and a fluorite-type solid solution, RF_x, with $2.00 \leq x \leq 2.25$, and a second single-phased region with $2.25 \leq x \leq 2.45$ are described for Sm and Eu. The results clearly show that earlier reports of stable metal-rich fluorides ($x \leq 2.00$) are incorrect. The work of Stezowski and Eick (1970) demonstrates that the Sm system is more complex. The observed SmF_x phases include a fluorite solid solution for $2.00 \leq x \leq 2.14$, a pseudo-tetragonal phase at $x = 2.35$ and a rhombohedral phase of variable composition for $2.41 \leq x \leq 2.46$. The higher composition phases are both closely related to fluoride, and additional weak reflections

for the tetragonal phase suggest long range ordering of the anions. Density data are consistent with interstitial anion substitution in a fluorite structure. Analogies between the SmF_2–SmF_3 and the UO_2–UO_3 systems are apparent, and the phases are possible members of the series Sm_nF_{3n-6} ($6 \leq n \leq 11$). The thermal analysis data of Bedford and Catalano (1970) are not definitive for the Sm–F system, but the phase diagrams for Sm, Eu and Yb all show the formation of a high temperature phase at $2.7 \leq x \leq 2.8$. A series of line phases are indicated for the Eu–F system in the range $2.00 \leq x \leq 2.45$. The data for the Yb–F system show a solid solution in the range $2.00 \leq x \leq 2.18$ and phases at $x = 2.25$ and $2.38 \leq x \leq 2.45$. An X-ray investigation of the Eu–F system (Tanguy et al., 1972), shows a solid solution for $2.00 \leq x \leq 2.14$, a tetragonal phase at $x = 2.25$ and a rhombohedral phase for $2.33 \leq x \leq 2.40$. The Sm, Eu and Yb systems are obviously very similar. The relationship of the tetragonal and rhombohedral cells to fluorite is proposed. A higher composition limit, $x = 2.19$, is observed for EuF_x by Petzel and Greis (1972); however, variations in the composition limits reported for the fluorite-type solutions appear to be functions of the reaction temperatures and annealing procedures. Vaporization and X-ray data of the Yb–F system (Biefeld and Eick, 1975) show fluorite, tetragonal and rhombohedral phases like those of the Sm and Eu systems.

Equilibria in the Tm–F system remain somewhat unclear. Recent studies indicate that metal reduction to the difluoride is incomplete. Greis (1976) reports a cubic intermediate ($x = 2.37$) with a lattice parameter ($a = 5.604$ Å) in close agreement with that ($a = 5.597$ Å) reported earlier for TmF_2 (Catalano et al., 1969). The results of Biefeld and Eick (1976) also indicate incomplete reduction and formation of a pseudo-rhombohedral intermediate similar to those of the other R–F systems.

A large number of RX_x intermediate phases are also observed for the chlorides, bromides and iodides. The preparation, equilibria and some properties of these materials are extensively reviewed by Corbett (1973). Unlike the intermediate fluorides, these phases appear to have narrow composition ranges and are therefore similar to the praseodymium and terbium oxides and to the so-called Magneli phases of the transition metal oxides. Other similarities are found in the systematics of their compositions (Haschke, 1976d), which correspond closely with members of the homologous series R_nX_{2n+1}. Halide compositions defined by this series are presented in table 32.7; references are cited in table 32.3. Observed compositions near $RX_{2.40}$ ($LaI_{2.42}$, $PrBr_{2.38}$, $NdCl_{2.37}$) and $RX_{2.29}$ ($NdCl_{2.286}$) and $RX_{2.18}$ ($SmBr_{2.182}$) cannot readily be assigned to this series. However, the phases correspond closely to the $n = 5$, 7 and 11 members of the R_nX_{2n+2} series. The $2n + 1$ series is the even-integer subset of the $2n + 2$ series which therefore accounts for all the observed compositions. As with the intermediate oxides, the systematic intermediate halides are expected to have structures that are related to those of a terminal halide. Structural models for derivation of these intermediates have been proposed (Caro, 1972; Hyde et al., 1974; Haschke, 1976d), and recent structural data have verified the general concepts of these proposals, cf. ch. 32, section 4.5.2.

TABLE 32.7
Intermediate halide compositions defined by the homologous series R_nX_{2n+1}

n	Theoretical X:R	Reported compositions
1	3.000	RX_3 phases
2	2.500	$PrI_{2.5}$
3	2.333	$PrCl_{2.31}$, $NdCl_{2.33}$
4	2.250	$NdCl_{2.25}$, $NdCl_{2.27}$
5	2.200	$DyCl_{2.200}$, $HoCl_{2.200}$, $SmBr_{2.200}$
6	2.167	$DyCl_{2.167}$, $YbCl_{2.167}$, $SmBr_{2.167}$
7	2.143	none
8	2.125	none
9	2.111	$TmCl_{2.11}$
10	2.100	$TmCl_{2.10}$
11	2.091	$TmCl_{2.090}$
12	2.080	$TmCl_{2.080}$
13	2.077	$TmCl_{2.074}$
15	2.067	$TmCl_{2.067}$
25	2.050	$TmCl_{2.040}$
∞	2.000	RX_2 phases

As the data in table 32.7 indicate, several of the R–X equilibrium diagrams are very complex. Thermal analysis data, cf. table 32.3, show that in general the intermediate phases melt incongruently. The Tm–Cl system (Caro and Corbett, 1969), is obviously the most complex of the known systems. In addition to the binary phases listed in table 32.7, several mixed-metal phases have also been described. These include the face centered cubic $(Nd, Ce)Cl_{2.20}$ and the $(Nd, Ce)Cl_{2.37}$ compositions in which divalent cerium is observed (Druding and Corbett, 1961). The $PrCl_{2.37}$ phase, which decomposes below 594°C, is stabilized at low temperatures by substitution of Nd (Druding et al., 1963).

Thermodynamic data for the intermediate halides are limited. The only available measurements are for the intermediate fluorides, $SmF_{2.40}$ and $YbF_{2.40}$ (Biefeld, 1974; Biefeld and Eick, 1975). Both phases vaporize congruently according to the reaction $RF_{2.40}(s, \ell) \rightarrow 0.06\ RF_2(g) + 0.40\ RF_3(g)$. Investigation of the Eu–F and Tm–F systems (Petzel and Greis, 1972; Biefeld and Eick, 1976), show that EuF_2 and TmF_3 are the only congruently vaporizing phases in the respective systems.

4.5.2. *Structural properties*

Complete structural data, which have recently been obtained for several of the intermediate halides, confirm the assignment of homologous series compositions and demonstrate close structural relationships to the dihalides. The structures of monoclinic ($P2_1/m$) Dy_5Cl_{11} (Baernighausen, 1976b) and of monoclinic ($C2/c$) Yb_6Cl_{13} (Lueke and Eick, 1976), are derivatives of fluorite. As suggested by Caro

and Corbett (1969) they are similar to those of the homologous series rare earth oxide fluorides R_nX_{2n+1} (X = O + F) (Mann and Bevan, 1972; Bevan and Mann, 1975), and are therefore additional examples of the so-called "vernier" phases described by Hyde et al. (1974). The Dy_5Cl_{11} structure, which is only slightly distorted from orthorhombic symmetry, is projected on (001) in the upper part of fig. 32.14. Comparison of the metal positions and the intervening anion nets with those of fluorite and the fluorite-related dihalides (cf. ch. 32, section 4.4.1 and fig. 32.13) demonstrates their similarity. The metal array and the rectangular anion net are very similar to those of fluorite, and their periodicities along [010] are equal but different from those of the triangular anion net. The cation coordination changes gradually from seven- to eight-fold along [010] and gradually back to seven-fold before the anion arrays invert at the center of the cell. The seven-coordinate regions have RX_2 composition. Insertion of the extra anion layer at the eight-coordinate metals produces a layer of RX_3 composition. Since the extra anion layer appears in every fifth metal layer, the phase clearly corresponds to the $n = 5$ member of the R_nX_{2n+1} homologous series. The structural refinement permits identification of the di- and tri-valent cations which appear in both seven- and eight-coordinate sites.

The structure and composition of the intermediate ytterbium chloride phase (Fishel and Eick, 1971), have been determined by single crystal X-ray methods with the iso-structural mixed-metal phase, Yb_5ErCl_{13} (Lueke and Eick, 1976). Although the standard space group is C2/c, selection of a body centered equivalent (I2/a) facilities comparison with the Dy_5Cl_{11} structure. Seven- and eight-coordinate cations also arise from differences in the periodicity of metal and triangular anion arrays, but the higher coordination occurs in every sixth metal layer. The phase is therefore the $n = 6$ member of the R_nX_{2n+1} series. The layering sequence of the known series members is correctly predicted by the

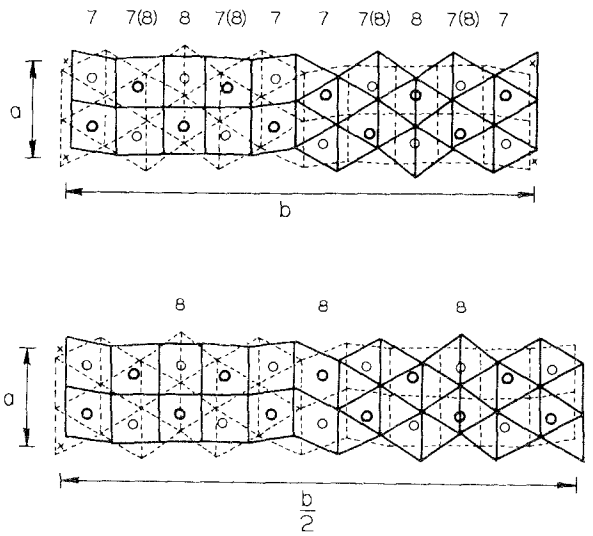

Fig. 32.14. The monoclinic Dy_5Cl_{11}-type structure (above) and the closely related monoclinic $Sm_{11}Br_{24}$-type structure (below).

structural model of Caro (1972) and additional series members are expected to arise from similar differences in periodicity of layers.

Identification of these intermediate phases by crystallographic methods has permitted the correct assignment of compositions for isostructural phases. Lattice parameters of the monoclinic $RX_{2.200}$ and $RX_{2.167}$ phases are presented in table 32.8. Both compositions have been observed for the Dy–Cl system (Baernighausen, 1976b). Other $RX_{2.200}$ phases which have been identified from powder diffraction data include Ho_5Cl_{11} (Loechner and Corbett, 1975), and $SmBr_{2.172}$ (Haschke, 1976d). Likewise, the phases reported as $YbCl_{2.26}$ (Fishel and Eick, 1971), and as $SmBr_{2.129}$, Haschke (1976d), are $RX_{2.167}$ compositions.

The apparent stabilities of intermediate halides R_nX_{2n+1} with $n = 5$ and $n = 6$ can in part be understood by consideration of anion packing (Baernighausen, 1976b). The rectangular anion net is similar to the anion nets of fluorite, and the triangular net is essentially a closest packed array. The width of five anion rows in the fluorite arrangement is only slightly less than that of six anion rows in a closest packed arrangement. These intermediate halides may be described as fluorite structures in which extra anions are accommodated by closest packing of half the anion layers. Compensation for the slight difference in width of five fluorite rows and six closest packed rows is made by their inversion at $\frac{1}{2}b$ in the structures. Because it is composed of five half-cells of fluorite and five inverted half-cells of fluorite, the Dy_5Cl_{11} structure is conveniently described as a 5–5′ arrangement. In a similar way, the Yb_6Cl_{13}-type structure is a 6–6′ arrangement.

A third R–X phase with a composition between $SmBr_{2.200}$ and $SmBr_{2.167}$ is observed in the Sm–Br system. The phase originally reported as $SmBr_{2.140}$ (Haschke, 1976d), has been identified as $Sm_{11}Br_{24}$ ($SmBr_{2.182}$) by evaluation of powder X-ray diffraction data (Baernighausen and Haschke, 1978). The diffraction pattern is similar to that of Sm_5Br_{11}; the $P2_1/n$ space group is a direct subgroup of $P2_1/m$ and examination of the (001) projection of half the unit cell in fig. 32.14 shows that the structure is very similar to that of Dy_5Cl_{11} shown in the upper part of the figure. Although the composition corresponds to the $n = 11$

TABLE 32.8
Crystallographic data for intermediate halide phases.

Phase	Space group	a(Å)	b(Å)	c(Å)	Monoclinic angle (deg)
Dy_5Cl_{11}	$P2_1/m$	7.110	34.68	6.634	$\beta = 90.23$
Ho_5Cl_{11}[a]	$P2_1/m$	7.210	34.57	6.603	$\beta = 90.19$
Sm_5Br_{11}	$P2_1/m$	7.652	37.21	7.121	$\beta = 90.26$
Dy_6Cl_{13}	I2/a[b]	7.096	41.40	6.667	$\gamma = 91.38$
Yb_5ErCl_{13}	I2/a	7.004	41.00	6.537	$\gamma = 91.25$
Yb_6Cl_{13}	I2/a	6.958	40.98	6.539	$\gamma = 91.19$
Sm_6Br_{13}	I2/A	7.649	44.44	7.139	$\gamma = 91.30$
$Sm_{11}Br_{24}$	$P2_1/n$	7.652	81.62	7.130	$\beta = 90.19$
Pr_2I_5	$P2_1/m$	8.655	4.317	16.80	$\beta = 120.48$

[a]Loechner et al. (1976). [b]The standard space group is C2/c.

member of a $2n + 2$ homologous series, its structure is most accurately described as a coherent intergrowth of unit-cell-wide layers of the Dy_5Cl_{11}- and Yb_6Cl_{13}-type structures. In terms of fluorite half-cells, the sequence along [010] is 5-6-6′-5′, 5-6-6′-5′, ... The 81.62 Å repeat distance corresponds to 22 half-cells of fluorite. In light of this interpretation of the $Sm_{11}Br_{24}$ structure, a strong case cannot be made for the existence of a unique R_nX_{2n+2} series.

The structure of another intermediate halide, Pr_2I_5, has been described by Warkentin and Baernighausen (1976). The results are especially interesting because the structural principle is different from that of the fluorite-related phases. Lattice parameters for the monoclinic cell ($Z = 2$) are given in table 32.8. The structure has an unusual layered arrangement in which all the cation coordination polyhedra are monocapped trigonal prisms. The average metal–iodine distance (3.22 Å) is in the range expected for trivalent praseodymium. The structure is related to both the $PuBr_3$-type PrI_3 and $CdCl_2$-type PrI_2 structures and is closely modeled by intergrowth of a layer of the dihalide structure with a layer of the trihalide structure along [001].

Elucidation of the structural properties and phase equilibria of the intermediate phases are clearly an emerging area of halide chemistry. Many of the known structures are fluorite-related and powder data for other intermediate halides (Druding and Corbett, 1961), indicate that they too are fluorite derivatives. It is possible that many of the intermediate halides, including the fluorite-related fluorides, are structurally related members of homologous series. Because of the long periodicities of the intermediate halide structures, they should be amenable to investigation by lattice imaging techniques.

5. The hydrated halides

5.1. *The hydrated trihalides*

Hydrated trihalides, $RX_3 \cdot xH_2O$ are known for all the halide systems. Some properties of these compounds have been briefly discussed in relation to their use in preparation of the anhydrous phases (cf. ch. 32, section 2.1). Reported phases include the $RF_3 \cdot xH_2O$ ($x \leq 1$), $RCl_3 \cdot xH_2O$ ($x \leq 7$), $RBr_3 \cdot xH_2O$ ($x \leq 8$) and $RI_3 \cdot xH_2O$ ($x \leq 9$). As expected, x values decrease with decreasing cationic radius, e.g., trichloride heptahydrates are known only for the lighter lanthanides. The insoluble hydrated fluorides are obtained by precipitation of the trivalent lanthanides with aqueous HF. The other hydrated halides are more difficult to prepare because of their high solubility and their tendency to supersaturate on evaporation. The chlorides and bromides are obtained by cooling solutions saturated with trihalide and hydrohalic acid and by condensation of the solutions by desiccation. Difficulties encountered in preparation of the hydrated iodides apparently account for their limited characterization.

Thermal decomposition reactions of the hydrated halides have been extensively investigated because of their preparative potentiality. Dehydration methods are, however, of limited utility because of the hydrolysis reaction:

$RX_3 \cdot xH_2O(s) \rightarrow ROX(s) + 2HX(g) + (x-1)H_2O$. The water content of the trifluorides varies with the preparative conditions and dehydration in air proceeds with the formation of small amounts of oxide fluoride (Wendlandt and Love, 1959). Quantitative removal of the water is achieved by thermal dehydration under inert gas or in vacuum (Strizhkov et al., 1972). Water loss down to $x = 0.5$ is gradual and occurs at low temperatures; higher temperatures (500–600°C) are necessary for complete dehydration. The reactions of $RCl_3 \cdot xH_2O$ ($x = 6, 7$) phases have been extensively studied by thermal analysis methods (Wendlandt, 1957, 1959; Wendlandt and Baer, 1959; Powell and Burkholder, 1960; Haeseer and Matthes, 1965; Ashcroft and Mortimer, 1968; Illin et al., 1972). In general, the results show step-wise water loss with formation of the monohydrate intermediate, $RCl_3 \cdot H_2O$; however, variations are observed with heating rate and atmosphere. In air the terminal products at 1000°C vary from ROCl to R_2O_3 across the series. Products in inert atmospheres approach the RCl_3 composition, but rigorous exclusion of oxygen is difficult. DSC measurements under nitrogen (Ashcroft and Mortimer, 1968), show three intermediate hydrates ($x = 3, 2, 1$) for the lighter lanthanides and two ($x = 4, 1$) for the heavy elements plus formation of RCl_3 terminal products. Illin et al. (1972) report additional intermediate hydrates ($x = 5, 4, 3, 1$) for the Sm system, but were unable to obtain pure trichloride. Thermal decomposition of the $RBr_3 \cdot xH_2O$ ($x = 6, 7$) phases in air is similar to that of the hydrated chlorides (Mayer and Solotov, 1965). Products of the light lanthanide hydrates are $RBr_3 \cdot H_2O$, RBr_3 and ROBr. The product sequence for the heavier elements includes an RBr_3–ROBr mixture, ROBr and R_2O_3.

The structural properties of the hydrated halides are partially characterized. The LaF_3-type (tysonite) structure is reported for the hydrated trifluorides of the lighter elements (La–Sm) (Batsanova and Lukina, 1972). The lattice parameters are identical to, but less precise than those of the anhydrous trifluorides. Since measured densities of the hydrated products are substantially lower than those of the anhydrous trifluorides, it has been suggested that the water is accommodated by formation of anion and cation vacancies. Similar conclusions have been reached by analysis of the thermal decomposition data (Strizhkov et al., 1972). The initial mass loss at low temperature may correspond to adsorbed water, but the residual fraction, $x = 0.5$, is difficult to remove and suggests that water molecule occupies a definite lattice site in a defect structure. The hemihydrate appears to have a stable composition, but its crystallization in an undistorted LaF_3-type structure seems rather unusual. Lattice parameters for highly crystalline LaF_3 samples prepared under hydrothermal conditions (600°C, 100 atm H_2O pressure) agree with those reported for the anhydrous trifluorides (Haschke, 1975b); thermal analysis data show that the water and hydroxide contents of the products are below detectable limits (Haschke, 1976e). The X-ray and density observations and the variability of x suggest precipitation products may be mixtures of crystalline anhydrous and amorphous hydrated trifluorides. The need for additional work is obvious.

The structures of the hydrated trichlorides have been determined by single

crystal methods. The $RCl_3 \cdot 6H_2O$ structure is monoclinic (P2/n, Z = 2) and contains complex species $[RCl_2(H_2O)_6]$ (Marezio et al., 1961). The eight-coordinate complexes are held together by hydrogen bonds to chlorides of adjacent groups. Although earlier reports indicated that the $RCl_3 \cdot 7H_2O$ structure has orthorhombic or monoclinic symmetry, recent work has demonstrated that the phase is triclinic and readily forms monoclinic twins (Brouty and Herpin, 1972). The full refinement shows that the heptahydrate structure ($P\bar{1}$, Z = 2) has the nine-coordinate complex $[LaCl_2(H_2O)_7]$ and is topotactically related to the hexahydrate structure (Bakakin et al., 1974). This relationship accounts for the fact that $RCl_3 \cdot xH_2O$ phases frequently have x-values between six and seven. These structures are apparently stable for both the hydrated chlorides and bromides. Lattice parameters and other properties are reported for $RCl_3 \cdot 6H_2O$ (Graeber et al., 1966) and $RBr_3 \cdot 6H_2O$ (Brown et al., 1968) phases.

A substantial amount of thermochemical data are reported for the solid hydrated trihalides. Enthalpies of formation, ΔH°_{f298}, of several trifluoride hemihydrates and ΔH°_{f298}, ΔG°_{f298}, S°_{298} and Cp_{298} values for most trichloride hexahydrates and heptahydrates are tabulated (Schumm et al., 1973). Heat capacity measurements (5–300 K) for trichloride hexahydrates are reported by Spedding et al. (1972); enthalpy and entropy increments and free energy functions are reported. Magnetic contributions are 80–85% of the $R \ln(2J + 1)$ values. The results are in good agreement with those derived by Hinchley and Cobble (1970), who provide an extensive review of earlier work in their compilation of thermochemical data. Enthalpies of dehydration, which vary between 90 and 95 kcal/mole for $RCl_3 \cdot xH_2O$ ($x = 6 - 7$), have been obtained from DSC measurements (Ashcroft and Mortimer, 1968). Equilibrium measurements for the high temperature processes, $RCl_3(s) + H_2O(g) \rightarrow ROCl(s) + 2HCl(g)$, have also been reported (Koch et al., 1952; Koch and Cunningham, 1953, 1954; Weigel and Haug, 1961; Weigel and Vishnevsky, 1969, 1970; Weigel and Wishnevsky, 1972, 1973).

Thermodynamic and physicochemical properties of aqueous trihalide solutions have been extensively investigated. Enthalpies of formation values for several RX_2^+ (X = F, Cl; 1 molal) and for essentially all RCl_3 systems between 1 molal and infinite dilution are given by Schumm et al. (1973). Numerous additional properties of aqueous trichloride systems have been described by Spedding and coworkers. These include enthalpies of dilution (Spedding et al., 1966a), partial molar heat capacities (Spedding and Jones, 1966; Spedding et al., 1975), molal volumes (Spedding et al., 1966b; Spedding et al., 1974c), viscosities (Spedding and Pikal, 1966; Spedding et al., 1974d), conductances (Spedding et al., 1974a), and densities and thermal expansion data (Gildseth et al., 1975; Habenschuss and Spedding, 1976). The solutions obey the Debye-Hueckel limiting law and the viscosity measurements suggest a change in the number of coordinated water molecules near the middle of the lanthanide series. Raman data indicate complete dissociation into R^{3+} and Cl^- in dilute solutions, but outer-sphere ion pair complexes are apparently formed at high concentrations (Munday and Spedding, 1973). Conductance, transference and activity coefficient measure-

ments have been described for dilute trichloride and tribromide solutions of terbium (Spedding et al., 1974e). Various properties of the aqueous systems are reviewed by Habenschuss and Spedding (1974) and Rard and Spedding (1974).

5.2. *Other hydrated halides*

Hydrated phases are known for both the tetrahalides and the dihalides, but neither has been extensively characterized. Cerium tetrafluoride monohydrate, $CeF_4 \cdot H_2O$, has been prepared by several procedures (Asker and Wylie, 1964). The product of digesting CeO_2 in concentrated aqueous HF solution at 100–130° is $CeF_{4.0} \cdot 1.0H_2O$, while that obtained by reaction of the dioxide with anhydrous HF is $CeF_{4.0} \cdot 0.8H_2O$. Powder X-ray diffraction data are reported; the structure is unknown and different from that of the anhydrous tetrafluoride.

Hydrated dihalides similar to those of the alkaline earth phases have been described. The dihydrate, $EuCl_2 \cdot 2H_2O$, is precipitated from concentrated HCl solution (Moeller, 1973). The dihalide monohydrates, $RX_2 \cdot H_2O$ (X = Br, I), have been obtained for samarium and europium by vapor phase hydration of the anhydrous phases (Haschke and Eick, 1970a; Haschke, 1976a,d). They have orthorhombic (Pnma, Z = 4) $BaCl_2 \cdot H_2O$-type (Vajnstejn and Pinsker, 1951) or $SrBr_2 \cdot H_2O$-type (Kammermans, 1939), structures. A topotactic relationship of the structure to $PbCl_2$ and other RX_2 structure types (Haschke, 1976b) accounts for the facile formation of crystalline products and the observed irregularities in lattice parameters. Further hydration of the dibromide monohydrate results in oxidation of the metal and formation of the tribromide hexahydrates.

6. Mixed metal halides

6.1. *A survey of the mixed metal halides*

A large number of mixed metal or complex fluorides have been characterized for the rare earths. In part, these systems have been extensively studied because of their interesting optical, electrical and magnetic properties and because of their potential as host materials for ions of spectroscopic interest. The M(I)X–R(III)X_3, the M(I)X–R(IV)X_4 and the M(II)X_2–R(III)X_3 (M(I)–alkali metal, M(II) alkali earth or divalent rare earth) systems have been most extensively investigated; however, a limited number of M(III)X_3–R(III)X_3 and M(IV)X_4–R(III)X_3 systems have been described. The mixed metal halides have interesting complex vapor species and several of the solid phases have structures which are closely related to those of binary halides. Phase equilibria of mixed metal systems have been determined primarily by thermal and X-ray diffraction analyses. The preparative procedures and many properties of the mixed halides have been reviewed by Brown (1968) and the mixed fluorides have been reviewed by Batsanova (1971).

6.2. *The* M(I)X–R(III)X_3 *systems*

Five well-defined mixed fluoride compositions are found in the alkali metal fluoride-rare earth fluoride systems. These compounds and the rare earth elements forming the respective phases are presented in table 32.9. The complex fluorides have been reviewed by Thoma (1973). Investigations for all the rare earth systems are complete for lithium (Thoma et al., 1961, 1970) and for sodium (Thoma et al., 1965). The stability limits of several compositions correlate well with the radius ratio of the alkali metal and rare earth ions, and the occurrence of these phases was predicted on this basis in early work by Thoma (1962). Adjusted limiting radius ratios derived from experimental results are given by Brown (1968) and Vedrine et al. (1975). The 1:1 complex, MRF_4, is obviously a very stable composition. Phases not shown in table 32.9 include the high temperature solid solutions which exist between the $NaRF_4$ and $Na_5R_9F_{32}$ (R = Pr–Lu, Y) compositions (Thoma et al., 1965). Stability of the 5:9 complex increases across the series, and the phase plus an intermediate composition are stable for Lu at 25°C. Appreciable substoichiometry of $NaRF_4$ is also observed for the heavier lanthanides. Several reports of a 1:7 complex, MR_7F_{22}, appear in the literature; however, Pierce and Hong (1973) suggest that these phases are actually one of the oxide fluorides described by Mann and Bevan (1972).

A substantial amount of structural data are available for the mixed metal fluorides. Thermal analysis data indicate high and low temperature forms of the K_3RF_6 phases. Bode and Voss (1957) have characterized the tetragonal (I4/mm) Rb_3TlF_6-type structures for both K_3YF_6 and $CsYF_6$. A second form is the monoclinic ($P2_1/n$) Na_3AlF_6-type (cryolite) structure which has recently been described for the K_3RF_6 phases of Y (Borzenkova et al., 1971), Dy (Ardashnikova et al., 1974), and Yb (Labeau et al., 1974).

A variety of structure types are known for the MRF_4 phases. Single crystal data have verified that the isostructural $LiRF_4$ phases have the $CaWO_4$-type (scheelite) structure (Thoma et al., 1970). The $NaRF_4$ phases are more complex in that one high temperature and two lower temperature forms are known. Two hexagonal structures with similar lattice parameters, but different space groups ($P\bar{6}$ and $P6_3/m$), are described by Burns (1965). The structure of the lower

TABLE 32.9
Phases in the alkali metal-rare earth metal-fluoride systems, M(I)–R(III)–F.

Composition	MF:RF_3	Li	Na	K	Rb	Cs
M_3RF_6	3:1	u[a]	u	Ce, Gd–Yb[b], Y	La–Lu[b], Y	La–Lu[b], Y
M_2RF_5	2:1	u	u	Gd–Yb[b], Y	Sm, Gd	–
MRF_4	1:1	Eu–Lu, Y	La–Lu, Y	La–Yb[b], Y	La–Sm[b]	–
MR_2F_7	1:2	u	u	Ce, Gd–Yb[b], Y	Sm, Gd	Sm, Gd
MR_3F_{10}	1:3	u	u	Dy–Lu, Y	Sm–Dy	–

[a]u: Composition is unobserved; a dash indicates that no reports are available. [b]All members of the group have not been reported, but their existence is expected.

symmetry $NaNdF_4$-type form is projected on (0001) in fig. 32.15. Comparison of this projection with fig. 32.5 (cf. ch. 32, section 2.2) demonstrates that this structure is a derivative of UCl_3 (Haschke, 1976b). The $NaRX_4$ composition is obtained by ordered placement of Na^+ on one-fourth of the R^{3+} sites and on one-half of the vacant octahedral sites of the UCl_3 structure. Although the positions of Na^+ ions on rare earth sites are not identified in fig. 32.15, those near the octahedral sites ($z = \frac{3}{4}$ along the projection axis) appear as small crossed circles. The $NaNdF_4$ and UCl_3 cells are outlined by dashes and dots, respectively. A random occurrence of $P\bar{6}$ and $P6_3/m$ space groups is observed across the lanthanide series. The direct subgroup-supergroup relationship of these space groups clearly indicates that the two forms are related by an order–disorder transition involving the randomized placement of sodium on the rare earth sites and the two octahedral sites (Haschke, 1976b). Furthermore, substoichiometry of the phase is readily achieved by additional substitutional and interstitial placement of sodium. The high temperature α forms have CaF_2-type (fluorite) structures and can be obtained by quenching (Hund, 1950). Lattice parameters for the hexagonal phases are compiled by Brown (1968).

Low and high temperature forms are also known for the KRF_4 phases. Earlier reports assigned the so-called β_1 forms to the Na_2ThF_6-type structure (cf. ch. 32, section 6.3), but they appear to have the hexagonal $NaNdF_4$-type structure. The β forms have the orthohombic (Pnma) $KCeF_4$-type structure projected on (010) in fig. 32.16 (Brunton, 1969a). The potassium positions are indicated by crossed circles. Examination of the structure shows that it has only bilevel ions and is derived from coherent intergrowth of one-unit-cell-wide slabs of UCl_3-type RF_3 with slightly distorted half-unit-cell-wide slabs of CsCl-type MF (Haschke, 1976b). Both metals occupy tricapped trigonal prismatic coordination sites like those found in the trihalide structures (cf. section 2.2). Hexagonal cells unlike that of $NaNdF_4$ have been assigned to the KRF_4 phases of Y (Borzenkova et al.,

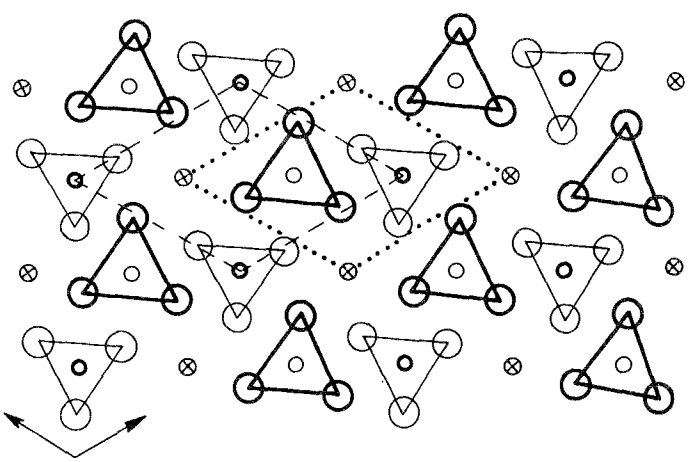

Fig. 32.15. The $NaNdF_4$-type structure ($P\bar{6}$) projected on (0001).

1971) and Dy (Andashnikova et al., 1974), and a third hexagonal cell is reported for $KYbF_4$ (Labeau et al., 1974). The high temperature α forms of KRF_4 are also CaF_2-type. Structural data for the 1:1 complexes of Rb and Cs have not been reported.

The formation of a high temperature solid solution between the $NaRF_4$ and $Na_5R_9F_{32}$ compositions suggest that these materials are structurally related. A cubic superstoichiometric ($Na_{1-3x}Y_{1+x}F_4$) phase was first described by Hund (1950) and an analogous observation has recently been reported for the K–Y–F system (Borzenkova et al., 1971). Single crystal data for the low temperature form of $Na_5R_9F_{32}$ shows a large orthorhombic (Cmmm) cell, e.g. for R = Dy, $a = 5.547$, $b = 39.23$ and $c = 7.845$ Å (Thoma et al., 1965). The structure has not been reported, but the presence of a fluorite substructure and long-range anion ordering is clearly present. The lattice parameters are remarkably similar to those of the intermediate halides and oxide fluorides that are members of R_nX_{2n+1} homologous series (section 4.5) and the composition corresponds closely to those of $M_7R_8F_{33}$ or $M_5R_7F_{26}$, the $n = 5$ and 6 members of the M_nF_{2n+1} (M = Na + R) series. Vernier phases are known for altervalent anion (oxide-fluoride) and other cation [R(II)–R(III)] systems and might be expected for R(I)–R(III) systems as well. The plausibility of this suggestion is enhanced by the fact that the ionic radii of Na^+ and R^{3+} are equal near the middle of the lanthanide series. The miscibility range may arise from closely spaced vernier phases, but the occurrence of a simple solid solution $Na_{1-3x}R_{1+x}F_4$ ($0 \leq x \leq 1$) cannot be excluded and additional work is clearly needed.

Data for the 1:2 complexes, MR_2F_7, are not definitive. Thermal dimorphism is observed. The high temperature form K and Rb phases plus the low temperature

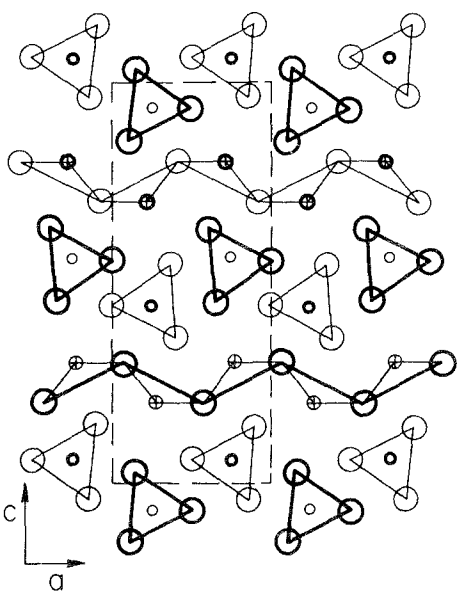

Fig. 32.16. The $KCeF_4$-type structure (Pnma) projected on (010).

Cs phases are orthorhombic ($Pna2_1$) (Labeau et al., 1974; Vedrine et al., 1975). Tetragonal and monoclinic forms have been described by Ardashnikova (1974). All the 1:3 complexes, MR_3F_{10}(M = K, Rb), are cubic (Vedrine et al., 1975). The crystal structure of KY_3F_{10} (Pierce and Hong, 1973), reveals a close relationship to fluorite with ordering of K^+ at the coordinate (0, 0, 0) and Y^{3+} at $(\frac{1}{2}, \frac{1}{2}, 0)$ in the CaF_2-type subcell. Four extra anions are inserted regularly in alternate subcells so that the contents of one subcell is $KY_3F_8^{2+}$ and that of the next is $KY_3F_{12}^{2-}$. The composition corresponds to the $n = 2$ member of the M_nF_{2n+1} (M = K + R) series; the regular substitution of extra fluoride in the fluorite structure is reminiscent of that for the intermediate halides (cf. section 4.5). Tetragonal and hexagonal forms of the 1:3 complexes have been reported (Shaimuradov et al., 1974; Ardashnikova, 1974), but their relationship to the cubic form is not clear. The tentative report of NaY_3F_{10} (Zalkin and Templeton, 1953), has not been confirmed by later work.

The mixed metal phases of the MX–RX_3 (M = alkali metal, X–Cl, Br, I) systems are presented in table 32.10. Early work and new data for the chloride systems are described by Drobot et al. (1968). Additional results for the chlorides and data for the bromides and iodides are described by Kutscher and Schneider (1974). Investigations for all the rare earths are complete only for the NaCl and KCl systems. The absence of data for the lithium halide systems may indicate that intermediate phases are not formed; data for the Rb systems are limited (Drobot et al., 1968). Comparison of the compositions in table 32.10 with those of the fluorides in table 32.9 show the formation of identical compositions except

TABLE 32.10
Phases in the alkali metal–rare earth metal–chloride, bromide and iodide systems

Composition ($MX:RX_3$)	X	Na	K	Cs
M_3RX_6	Cl	Eu–Lu, Y	La–Lu, Y	La–Sm, Y
(3:1)	Br	Gd	–	La–Sm
	I	Sm–Gd	Pr–Er	La–Er
M_2RX_5	Cl	Sm, Eu	La–Tb	u
(2:1)	Br	u[a]	–	u
	I	u	La–Nd	u
MR_2X_7	Cl	Tb	Sm, Eu, Tb, Ho	Sm
(1:2)	Br	u	–	Pr–Gd
	I	u	u	u
MR_3X_{10}	Cl	Dy	La, Gd, Dy, Er, Y	Y
(1:3)	B	u	–	u
	I	u	u	u

[a]u: Composition not observed in systems which have been investigated; a dash indicates that no reports are available.

for one case. The 1:1 complex, which occurs most frequently for the fluoride systems, is not observed for the other halides. Several phases with unusual ratios, 7:1, 1:4 and 1:9 are reported for isolated rare earths. In the Cs system, the 3:2 ratio, $Cs_3R_2F_9$, is observed for R = Pr – Er. The systematics of these systems are discussed both by Drobot et al. (1968) and Kutscher and Schneider (1974).

Several properties of the molten $MX–RX_3$ systems have been described. The enthalpies of mixing for several chloride, bromide and iodide systems have been measured (Papatheodorou and Kleppa, 1974; Papatheodorou and Ostvold, 1974; Dienstbach and Blachnik, 1975). Interaction parameters have been determined. The bonding forces appear to be mainly ionic. Existence of the RX_6^{3-} complex is indicated, and its stability appears to increase with increasing size of M^+ and with decreasing size of R^{3+} and X^-. Distribution coefficients of the trihalides in alkali halide melts have been measured by Ferris et al. (1972). Enthalpies of fusion of several complex chlorides have also been measured (Blacknik and Schneider, 1971). The data for the 3:1 complex also suggest formation of RCl_6^{3-} ions in the melt. Electrical conductivities are also reported for the chloride melts (Foerthermann and Schneider, 1969; Foerthermann et al., 1969). In addition to RCl_6^{3-}, the formation of $R_2Cl_7^-$ and $R_3Cl_{10}^-$ species is indicated. Raman data for the molten $KCl–LaCl_3$ system show the existence of a highly symmetric species (Maroni et al., 1974).

Complex halide vapors in equilibrium with the melts have been characterized by mass spectrometric and spectroscopic methods. Early reports of gaseous $MRCl_4$ (M–Li, Na, K, Cs) species are reviewed by Novikov and Gavryucherkov (1967). Enthalpies and entropies of dissociation to gaseous MCl and RCl_3 are presented. Equilibrium partial pressures of $MRCl_4$ for several chloride systems have been measured (Austin et al., 1970). Enthalpies of mixing and activities of melt components have been obtained. Vapor-species of the chloride (Ciach et al., 1973) and iodide systems (Hirayama and Castle, 1973; 1974) have also been characterized. Equilibria in the $Cs–CeI_3$ system have been extensively studied and thermodynamic data for gaseous $CsCeI_4$ are derived. Absorption spectra show that $CsRI_4$ is the dominant species in the vapor phase of the $CsI–RI_3$ systems (Liu and Zollweg, 1974).

6.3. *The* $M(I)X–R(IV)X_4$ *systems*

Because stable tetravalent rare earth halides are formed only for the fluorides of Ce, Pr and Tb, the number of $MX–MX_4$ complexes is much lower than for the $MX–MX_3$ systems. Early reports of stable complex fluorides of Nd(IV) and Dy(IV) have not been confirmed. The complex tetravalent fluorides are predicted by radius ratio correlations (Thoma, 1962) and are reviewed by Brown (1968). An extensive investigation by Delaigue and Cousseins (1972) has greatly expanded the data for the cerium systems. Seven complex fluorides and the corresponding metal systems are shown in table 32.11. As expected, these phases are similar to the corresponding complexes of the actinides (Brown, 1968).

TABLE 32.11
Phases in the alkali metal–rare earth metal–fluoride systems, M(I)F–R(IV)–F.

Composition	MF:RF_4	Li	Na	K	Rb	Cs
M_3RF_7	3:1	u[a]	Ce, Pr, Tb	Ce, Pr, Tb	Ce, Pr, Tb	Ce, Pr, Tb
M_2RF_6	2:1	u	Ce, Pr	Ce, Pr	Ce, Pr	Ce
$M_7R_6F_{31}$	7:6	u	Ce, Pr	Ce	Ce, Pr	u
MRF_5	1:1	Ce	u	Tb	Ce	Ce, Pr, Tb
MR_2F_9	1:2	u	u	Ce	u	u
MR_4F_{17}	1:4	Ce	u	u	u	u
MR_6F_{19}	1:6	u	u	u	Ce	Ce

[a]u: Composition is unobserved; however, all systems have not been thoroughly examined.

The crystal chemistry of the MF–RF_4 complexes is the only property that has been extensively characterized. Structural data are reviewed by Brown (1968) and X-ray diffraction data are reported by Delaigue et al. (1972). The 3:1 complexes of Na are tetragonal ($I4/mmm$) and those of K, Rb and Cs are cubic ($Fm3m$). Hexagonal and orthorhombic symmetries have been reported for the 2:1 Na complexes of Ce and Pr, respectively. The 2:1 K complexes have the hexagonal ($P\bar{6}2m$) K_2UF_6-type structure (Zachariasen, 1948; Brunton, 1969b), which is projected on (0001) in fig. 32.17. Comparison of this structure with those of UCl_3 and $NaNdF_4$ (cf. figs. 32.5 and 32.15) shows that they are very similar. The K_2UF_6 structure is derived from UCl_3 by ordering of potassium (crossed circles) on half of the cation sites and on half of the nine-coordinate interstitial sites (cf. ch. 32, section 2.2). The tricapped trigonal prismatic coordination polyhedra of R^{4+} are substantially smaller than those of K^+. The 7:6 complexes have the rhombohedral ($R\bar{3}$) $Na_7Zr_6F_{31}$-type structure (Burns, 1968). The 1:2 complexes are probably isostructural with orthorhombic ($Pnma$) KU_2F_9 (Brunton, 1969c).

6.4. *The* M(II)X_2–R(III)X_3 *systems*

Investigation of the mixed MX_2–MX_3 systems has been confined largely to

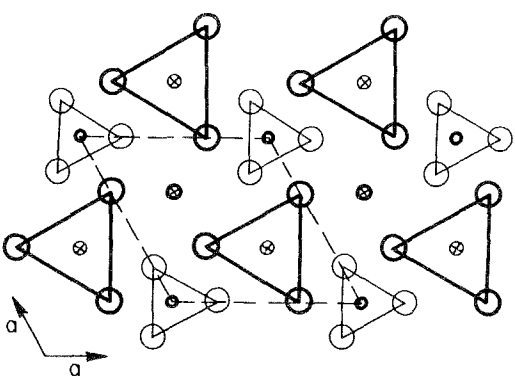

Fig. 32.17. The β-K_2UF_6-type structure ($P\bar{6}2m$) projected on (0001).

fluoride systems of the alkaline earths; however, other divalent metal systems and several chloride systems have also been described. Early reports for the fluoride systems are reviewed by Bratsanova (1971). In general, two types of mixed metal fluorides are observed. The phases are structurally related either to MF_2 or to MF_3; the formulations commonly employed, $M_{1-x}R_xF_{2+x}$ and $M_yR_{1-y}F_{3-y}$ $(y = 1 - x)$, reflect these relationships. For convenience, only the $M_{1-x}R_xF_{2+x}$ formulation will be employed here. A survey of the fluoride systems (M = Ca, Sr, Br and Cd) is given by Garashina and Sobolev (1971). As might be expected, different behavior is observed for the CaF_2 systems with the LaF_3- and the YF_3-type trifluorides (cf. ch. 32, section 2.2). All the rare earths, however, form similar fluorite-type solid solutions $Ca_{1-x}R_xF_{2+x}$ $(x > 0)$ at high dihalide contents, but the maximum values of x decrease from approximately 0.6 to 0.3 across the lanthanide series. The elements with LaF_3-type trifluorides (La–Nd) form hexagonal $Ca_{1-x}R_xF_{2+x}$ solid solutions in the composition range $0.85 \leq x \leq 1$. The elements with YF_3-type trifluorides (Sm–Lu, Y) form two phases of variable composition. An hexagonal LaF_3-type phase is observed near the $Ca_2R_5F_{19}$ composition $(x = 0.715)$. The hexagonal Er–Lu and Y phases show a pronounced superstructure relationship at high x values. Orthorhombic YF_3-type phases are formed near $x = 1$. Results for the SrF_2–EuF_3 system (Tanguy et al., 1972), the SrF_2–YF_3 system (Nafziger et al., 1973), the EuF_2–YF_3 system (Banks and Nimroff, 1974), and the CaF_2–YF_3 system (Seiranian et al., 1974), are consistent with the earlier work for the Ca systems; however, differences are observed in the composition limits of the phases. Fluorite phases are reported for the SmF_2–NdF_3 and SmF_2–PrF_3 systems, but the higher composition regions have not been characterized, Catalano et al. (1969). Mixed phases are not observed in the MgF_2–YF_3 system which only forms a simple eutectic (Nafziger et al., 1973). Stabilization of the LaF_3-type structures for YF_3-type trifluorides by substitution of MF_2 was proposed by Mansmann (1965) and has been investigated for the SrF_2–EuF_3 and EuF_2–GdF_3 systems by Greis and Petzel (1974). For the Sr–Eu and Eu–Gd systems, the LaF_3-type phase is observed for $0.700 \leq x \leq 0.951$ and $0.680 \leq x \leq 0.935$, respectively; the YF_3-type phase is formed at all higher compositions. The hexagonal to orthorhombic transition points correlate well with radius ratio predictions. Other phases include the stoichiometric 1:2 and 1:1 complexes, BaR_2F_8 and $BaRF_5$ (R = Er–Lu, Y) (Bratsanova, 1971). A quarternary phase, $BaCaR_2F_{10}$ (R = Dy–Lu), with a cubic structure closely related to that of YR_3F_{10} (cf. ch. 32, section 6.2) has recently been described (Valon et al., 1976).

Investigations of the mixed MCl_2–RCl_3 systems are limited in number. Equilibrium diagrams are presented for the Mg, Sr and Ba systems of several rare earths (R = La, Nd, Sm, Gd, Eu) (Vogel and Schneider, 1972). Observed phases include Sr_3NdCl_9, Ba_2LaCl_7 and Ba_3NdCl_9. X-ray data for the Sr_4DyCl_{11} phase (Baernighausen, 1976b), show that it is isostructural with monoclinic Dy_5Cl_{11}, the $n = 5$ member of the R_nX_{2n+1} homologous series (cf. ch. 32, section 4.5). Mass spectrometric analysis of the equilibrium vapor of the $MgCl_2$–RCl_3 systems indicates that mixed metal chloride species are not formed (Ciach et al., 1973).

6.5. *Other mixed metal halide systems*

Additional mixed halides are observed for MX_3–RX_3 and MX_4–RX_3 systems, but the extent of these investigations is indeed limited. As expected, the trihalides form extensive solid solutions with the isostructural rare earth and actinide trihalides. The fluoride phases and their application in extraction of trivalent rare earth fission products are reviewed by Bratsanova (1971). The mixed systems between rare earth trifluorides with LaF_3- and YF_3-type structures are more complex (Krudryavtseva et al., 1973). Examination of the LaF_3–RF_3 (R = Sm, Gd, Y, Er) systems shows the formation of LaF_3-type $La_{1-x}R_xF_3$ solid solutions for which the maximum value of x decreases from 0.6 for Sm to 0.3 for Er. These limits are substantially higher than the limiting compositions for growth of strain-free single crystals (Jones and Shand, 1968). Examination of the LaF_3–YF_3 system shows extensive miscibility at LaF_3-rich compositions, eutectic formation and limited miscibility at YF_3-rich compositions (Nafzinger et al., 1973).

Although condensed MCl_3–RCl_3 phases have not been characterized, their occurrence in the vapor phase is known. Mass spectrometric data for the equilibrium vapor of the $EuCl_3$–$LuCl_3$ system shows the presence of $EuLuCl_6$, which coexists with higher partial pressures of monomeric RX_3 and diameric R_2X_6 (Hastie et al., 1968). Vaporization studies of solid $NdCl_3$ in the presence of gaseous Al_2Cl_6 has been conducted in the temperature range 225–625°C (Oye and Gruen, 1969). The apparent vapor pressure of $NdCl_3$ is increased by a factor of 10^7 to total pressures of 1–7 atm across the temperature range. The formation of gaseous Al_3NdCl_{12} and Al_4NdCl_{15} is indicated by visible spectra of the gas phase.

Characterization of MX_4–RX_3 systems is perhaps least complete. Early coprecipitation studies which show the formation of extensive solid solutions in the MF_4–RF_3 (M = Zr, Ce, Th, U) systems are reviewed by Bratsanova (1971). Since subsequent investigation of the CeF_4–CeF_3 system (cf. section 3.2) has shown limited miscibility and the absence of intermediate phases, the precipitation products are in part metastable materials. Recent investigation of the ZrF_4–RF_3 systems show that two intermediate phases of variable composition are formed (Poulain et al., 1972). In the ZrF_4–SmF_3 system, a monoclinic phase is observed between $SmZrF_7$ and $SmZr_2F_{11}$ (50–66 mole % ZrF_4) and an orthorhombic phase occurs near $SmZr_4F_{19}$ (66–85 mole % ZrF_4). Lattice parameters are reported for similar phases formed by all the rare earths. Refinement of the monoclinic ($P2_1$) $SmZrF_7$-type structure shows that it contains both ZrF_6 and SmF_8 polyhedra and that it may be described as a derivative of ReO_3 (Poulain et al., 1973), since extra anions are introduced by interruption of the corner-shared octahedral array in regularly-spaced layers. Luminescence studies with $NdZrF_7$ and (Y, Er, Yb)ZrF_7 show that visible fluorescence is induced by both UV and IR excitation. Consequently, these phases are new materials for spectral upconversion (Lucas et al., 1974).

7. Mixed halogen halides

Investigation of the mixed halogen systems of the rare earths is a relatively new area of halide chemistry. Interest in these materials has been enhanced by their potential for application as luminescent materials and as spectroscopic host materials with novel site symmetries. Most of the work has dealt with the halide systems of divalent europium. The Eu–F–Cl system has been simultaneously described by Lambrecht et al. (1974) and Brixner and Bierlein (1974). The EuFCl phase, which is obtained by fusion of the binary halides, has the tetragonal (P4/mmm) PbFCl-type structure with $a = 4.137$, $c = 6.984$ Å. Single crystals are obtained from the melts and the phase forms solid solutions with the isostructural ROF phases. Magnetic data indicate Curie law dependence (Lambrecht et al., 1974). Diffraction data and fluorescence spectra are reported by Brixner and Bierlein (1974). Luminescence spectra of quaternary $M(II)_{1-x}Eu_xFCl$ phases are described by Tanguy et al. (1974). Crystallographic and luminescence data have also been described for congruently melting PbFCl-type EuFBr (Brixner, 1976).

Several different compositions in the Eu–Cl–Br system have been obtained by dehydration of $EuCl_3 \cdot xH_2O$ in the presence of NH_4Br (Clink, 1974). As with the binary europium bromide system (cf. section 2.1), the dehydration process proceeds with complete reduction of the europium by bromide and formation of orthorhombic $EuCl_xBr_{2-x}$ phases. A single crystal selected from an $x = 0.46$ composition has the orthorhombic (Pnma) $PbCl_2$-type structure with $a = 7.880$, $b = 4.611$, $c = 9.198$ Å (cf. section 4.4). The four- and five-coordinate anion cites are occupied respectively by Cl and Br. The R-value is minimized at $x = 0.50$, but the orthorhombic phase is apparently formed over a substantial portion of the $EuCl_2$–$EuBr_2$ system.

Although spectroscopic properties have been measured for trihalides doped with low levels of a second halide, phase studies are limited to the mixed halides of lanthanum (Beda, 1975; Haschke, 1976e). A cursory study of the LaF_3–$LaCl_3$ systems indicates that intermediate phases are not formed and that miscibility levels are low; however, complete solid solution is observed in the $LaCl_3$–$LaBr_3$ system. The terminal trihalides both have UCl_3-type structures and adherence to Vegard's law is expected. Terminal phases in the $LaCl_3$–LaI_3 system have UCl_3- and $PuBr_3$-type structures, respectively, and a mixed halide intermediate is formed. Phases observed at the 450°C section include a UCl_3-type solid solution, $LaCl_{3-x}I_x$, with a maximum of x near 0.3, a phase with a limited composition range at $La_8Cl_{18}I_6$, and a $PuBr_3$-type $LaCl_xI_{3-x}$ phase near the triiodide composition. Single crystal data for $La_8Cl_{18}I_6$ show a hexagonal structure with $a = 15.36$, $c = 4.457$ Å. A pronounced UCl_3-type substructure suggests that the halides are ordered on the anion sites. Crystallographic data for $LaCl_xI_{3-x}$ clearly shows that chloride substitution in the $PuBr_3$-type structure occurs in the RX_2^+ layers (cf. section 2.2) while the intervening anion layers are occupied only by iodide.

8. Recent developments

8.1. Reduced halides

The synthesis of rare earth monochloride phases (Simon et al., 1976) is probably the most interesting recent development in halide chemistry. GdCl and TbCl have been prepared by reaction of the respective trichlorides and metals at 800°C in sealed tantalum containers. Earlier workers have apparently not observed these phases because of slow reaction rates. The graphite-colored monochlorides are air sensitive and have the ZrCl-type structure (Adolphson and Corbett, 1976). The structure refinement is equal in monoclinic, C2, and rhombohedral, $R\bar{3}m$, space groups. The presence of a short two-fold axes in the monoclinic cells is characteristic of those halide structures that may be derived from the anti-NiAs structure (cf. sections 2.2, 4.3, 4.4.1). The monochloride structure is clearly related to that of Gd_2Cl_3 (cf. section 4.3). Condensation of the layers of metal octahedra in the sesquihalide structure leads to the layers of edge-shared metal octahedra in the monohalide structure. This relationship is consistent with symmetry constraints; C_2 is a direct subgroup of Cm, the space group of the Gd_2Cl_3-type structure. However, it is interesting that the higher-symmetry $R\bar{3}m$ space group is a supergroup of Cm and a subgroup the high-symmetry $P6_3/mmc$ space group of anti-NiAs. The existence of this relationship and the presence of layers of closest-packed metals in the monochloride structure lends support for the proposal that many structure types of the halides are derivatives of a hexagonal-closest-packed metal array. Additional work on these reduced halides is clearly needed.

Synthesis of CaF_2-type difluorides of normally trivalent rare earths (La, Ce, Pr, Nd) and of Sm has been reported (Batsanov et al., 1976). X-ray diffraction data indicate that these dihalides are formed during shock pressurization (>2000 kbar) at high temperature (>1000°C). The structural chemistry and phase relationships of the intermediate ytterbium fluorides (cf. section 4.5) has recently been clarified (Greis, 1977). Analysis of powder X-ray diffraction data show the following YbF_x phases: a cubic solid solution in the range $2.00 < x < 2.20$, a tetragonal phase at $x = 2.333$, a rhombohedral phase at $x = 2.357$, a cubic phase at $x = 2.370$ and a rhombohedral phase of variable composition near $x = 2.41$. The 2.333 and 2.357 compositions are the $n = 15$ and $n = 14$ members of the Yb_nF_{2n+5} homologous series. The phase formulated as $YbF_{2.41-\delta}$ is assigned as the $n = 13$ member; the 2.370 composition ($n = 13.5$) is believed to result from the coherent intergrowth of the $n = 13$ and 14 phases. The relationship of the assigned cells to a fluorite substructure is described. Application of the substructure–superstructure relationships (Greis, 1977b) to the intermediate fluorides of Sm and Eu is expected. Cubic $TmF_{2.37}$ (cf. section 4.5.1) is apparently $Tm_{27}F_{64}$.

8.2. Thermodynamic data

A significant contribution to the evaluation and review of the thermodynamic properties of the trihalides has been prepared (Meyers and Graves, 1977a, b). A complete set of thermal functions has been derived for the gaseous molecules in the

range 298–1500 K. Although experimental data support pyramidal, C_{3v}, geometries, the calculated inversion barriers are approximately equal to kT at room temperature, and planar, D_{3h}, geometries have been assumed for all trihalides. The results are based on a consistent set of vibration frequencies and provide a uniquely valuable set of thermal functions for use in high temperature cycles. In a second report (Meyers and Graves 1977b) the vaporization thermodynamics of the trihalides are reviewed and evaluated using experimental pressures, estimated heat capacities and entropies, and the thermal functions for the gases. The third-law results appear to be the more reliable; several systems needing additional work are identified by marked disagreement between their second and third-law enthalpies.

Additional data on the melting points and enthalpies of fusion of $SmCl_2$ (Laptev et al., 1976) and $EuCl_2$ (Kulagin and Laptev, 1976) have appeared. Both dichlorides undergo polymorphic phase transitions approximately 90° below their melting points. The calibrated enthalpies of transition (4 ± 1 kcal/mol) are substantial and thermochemical cycles for these systems should be reexamined in light of these results.

Vaporization data have also been obtained for several reduced halide systems. An independent study of the Yb–F system (Petzel and Greis, 1976) confirm the results of a study cited previously (cf. section 4.4.3). The congruently vaporizing composition is $YbF_{2.37}(Yb_{27}F_{64})$. The vaporization thermodynamics of $EuBr_2$ (cf. section 4.4.3) have been remeasured (Haschke, 1977); the revised values ($\Delta H^\circ_{298} =$ 82.8 kcal/mole, $\Delta S^\circ_{298} = 47.8$ eu) are in good agreement with those of other europium dihalides. A study of the vaporization behavior of the Sm–Br system (Haschke, 1978) demonstrate that $SmBr_2$ is the congruently vaporizing phase. The dihalide pressures and thermodynamic results are identical with those of $EuBr_2$. In the range 800–900°C, the primary species from incongruently vaporizing $SmBr_3(\ell)$ is the gaseous tribromide; however, the Br/Sm ratio of the vaporizing liquid decreases with time because of the loss of bromine. Approximate equilibrium pressures for the hypothetical congruent reaction have been obtained by measuring the time dependence of $SmBr_3$ pressure and extrapolating to zero time. The second-law enthalpy of vaporization ($\Delta H^\circ_{298} = 65$ kcal/mol) obtained with recently derived ($\Delta H^\circ_T - \Delta H^\circ_{298}$) values (Meyers and Graves, 1977b) is in excellent agreement with those of isostructural tribromides.

New thermodynamic data have also been reported for the gaseous rare earth monohalides (Yokozeki and Menzinger, 1976). The dissociation energies of SmF, SmCl and YbF ($D^\circ_0 \geq 121, 100, 124$ kcal/mol, respectively) have been obtained from molecular beam chemiluminescence measurements.

8.3. Mixed metal halides

The mixed metal fluorides with the $Na_7Zr_6F_{31}$-type structures (cf. section 6.3) have been shown to be isostructural with the intermediate binary fluoride $Yb_{13}F_{32-\delta}$ (Greis, 1977a). Other mixed metal halides are isostructural with the intermediate binary chlorides and bromide phases (cf. section 4.5). The Sm_5YBr_{13} phase is isostructural with Yb_6Cl_{13} (Zzoli, 1977), and a particularly interesting series of

phases have been reported for rare earth-actinide-halide systems (Haire et al., 1978). Fluorite-related monoclinic chlorides and bromides of californium, Cf_4RX_{11}, have been identified for several rare earths by X-ray diffraction. The formation of such phases in which radiation damage is reduced by dilution with the rare earth may well be of importance in characterizing lower valence states of other short-lived transuranium elements.

Acknowledgement

The support of the Department of Chemistry at the University of Michigan during the preparation of this review is gratefully acknowledged.

References

Ardashnikova, E.I., M.P. Borzenkova and L.M. Kovba, 1974, Inorg. Material **10**, 1409.
Ashcroft, S.J. and C.T. Mortimer, 1968, J. Less-Common Metals **14**, 403.
Asker, W.J. and A.W. Wylie, 1964, Aust. J. Chem. **18**, 959.
Asprey, L.B. and F.H. Kruse, 1960, J. Inorg. Nucl. Chem. **13**, 32.
Asprey, L.B., T.K. Keenan and F.H. Kruse, 1964, Inorg. Chem. **3**, 1137.
Asprey, L.B., J.S. Colman and M.J. Reisfeld, 1967, Preparation, Structure and Spectra of some Tetravalent Praseodymium Compounds, in: Gould, R.F., ed., Advances in Chemistry Series No. 71 (American Chemical Society, Washington), pp. 122–126.
Austin, S.R., T. Matsushima and A. Schneider, 1970, Z. Anorg. Allg. Chem. **373**, 133.
Ayasse, C. and H.A. Eick, 1973, Inorg. Chem. **12**, 1140.
Baernighausen, H., 1973, Rev. Chim. Mineral. **10**, 77.
Baernighausen, H., 1975, private communication of unpublished manuscript, Baernighausen, H., University of Karlsruhe, Karlsruhe, Germany.
Baernighausen, H., 1976a, private communication of unpublished results, Baernighausen, H., A. Buerk, W. Kuhn and H. Warkentin, 1973–1975, University of Karlsruhe, Karlsruhe, Germany.
Baernighausen, H., 1976b, Mixed Valence Rare Earth Halides and Their Unusual Crystal Structures, in: Proceedings of the Twelfth Rare Earth Research Conference, Vail, Colorado, pp. 404–413.
Baernighausen, H. and J.M. Haschke, 1978, Inorg. Chem. 17, 18.
Baernighausen, H. and N. Schultz, 1969, Acta Crystallogr. **B25**, 1104.
Baernighausen, H. and E. Warkentin, 1973, Rev. Chim. Mineral. **10**, 141.
Baernighausen, H., H.P. Beck and H.-W. Grueninger, 1971, The Crystal Chemistry of the Salt-Like Rare Earth Dihalides and the Determination of the New Structure Type Ln_3O_4Br, in: Field, P.E., ed., Proceedings of the Ninth Rare Earth Research Conference, U.S. Atomic Energy Commission CONF-711001 (Vol. 1) (National Technical Information Service), pp. 74–83.
Baernighausen, H., H. Paetow and H.P. Beck, 1974, Z. Anorg. Allg. Chem. **403**, 45.
Baev, A.K. and G.I. Novikov, 1965, Russ. J. Inorg. Chem. **10**, 1337.
Bakakin, V.V., R.F. Klevstsova and L.P. Soloveva, 1974, Sov. Phys. Crystallogr. **15**, 723.
Banks, E. and M. Nimroff, 1974, Mater. Res. Bul. **9**, 965.
Beck, H.P. and H. Baernighausen, 1971, Z. Anorg. Allg. Chem. **386**, 221.
Beda, S., 1975, Senior Thesis, University of Michigan, Department of Chemistry, Ann Arbor, Michigan.
Bedford, R.G. and E. Catalano, 1970, Study of the Binary Systems, SmF_2–SmF_3, EuF_2–EuF_3 and YbF_2–YbF_3 and Their Equilibria with Corresponding Ln–Pt Systems, in: Henrie, T.A. and R.E. Linstrom, Proceedings of the Eighth Rare Earth Research Conference (Reno, Nevada), pp. 388–399.
Besenbruch, G., T.V. Charlu, K.F. Zmbov and J.L. Margrave, 1967, J. Less-Common Metals **12**, 375.
Bevan, D.J.M. and A.W. Mann, 1975, Acta Crystallogr. **B31**, 1406.
Biefeld, R.M., 1974, Ph.D. Thesis, Michigan State University, East Lansing, Michigan.
Biefeld, R.M. and H.A. Eick, 1975, J. Chem. Phys. **63**, 1190.
Biefeld, R.M. and H.A. Eick, 1976, J. Less-Common Metals **45**, 117.
Blacknik, R. and A. Schneider, 1971, Monatsh Chem. **102**, 1337.
Block, F.E. and T.T. Campbell, 1961, Rare Earth and Yttrium Halides for Metal Production-Chlorides Bromides Iodides, in: Spedding, F.H. and A.H. Daane, eds., The Rare Earths (John Wiley and Sons, New York), pp. 89–101.

Bode, H. and E. Voss, 1957, Z. Anorg. Allg. Chem. **290**, 1.
Bommer, H. and E. Hohmann, 1941a, Z. Anorg. Allg. Chem. **248**, 373.
Bommer, H. and E. Hohmann, 1941b, Z. Anorg. Allg. Chem. **248**, 383.
Borzenkova, M.P., G.N. Kuznetsova and A.V. Novoselova, 1971, Inorg. Mater. **7**, 214.
Bratsanova, L.R., 1971, Russ. Chem. Rev. **40**, 465.
Bratsanova, L.R. and L.V. Lukina, 1972, Russ. J. Inorg. Chem. **17**, 629.
Bratsanova, L.R., Y.V. Zakharev and A.A. Opalovskii, 1973, Russ. J. Inorg. Chem. **18**, 476.
Brewer, L., L.A. Bromley, P.W. Gilles and N.L. Lofgren, 1950, The Thermodynamic Properties of the Halides, in: Quill, L.L., ed., The Chemistry and Metallurgy of Miscellaneous Materials (McGraw-Hill, New York), pp. 76–192.
Britton, D., 1954, J. Chem. Educ. **31**, 667.
Brixner, L.H. and J.D. Bierlein, 1974, Mater. Res. Bull. **9**, 99.
Brixner, L.H., 1976, Mater. Res. Bull. **11**, 269.
Bronstein, H.R., 1969, J. Chem. Phys. **73**, 1320.
Bronstein, H.R., A.S. Dworkin and M.A. Bredig, 1962, J. Phys. Chem. **66**, 44.
Brouty, C. and P. Herpin, 1972, C.R. Acad. Sci., Paris, Ser. C. **272**, 2049.
Brown, D., 1968, Halides of the Lanthanides and Actinides, (John Wiley and Sons, New York).
Brown, D., S. Fletcher and D.G. Holah, 1968, J. Chem. Soc. **A1968**, 1889.
Brunton, G.D., 1969a, Acta Crystallogr. **B25**, 600.
Brunton, G.D., 1969b, Acta Crystallogr. **B25**, 2163.
Brunton, G.D., 1969c, Acta Crystallogr. **B25**, 1919.
Burns, J.H., 1965, Inorg. Chem. **4**, 881.
Burns, J.H., 1968, Acta Crystallogr. **B24**, 230.
Bush, G., E. Kaldis, J. Muheim and R. Bischof, 1971, J. Less-Common Metals **24**, 453.
Carlson, O.N. and F.A. Schmidt, 1961, Preparation of Rare Earth Fluorides, in: Spedding, F.H. and A.H. Daane, eds., The Rare Earths (John Wiley and Sons, New York), pp. 77–88.
Caro, P.E., 1972, Nat. Bur. Stand. (U.S.) Spec. Publ. **364**, 367.
Caro, P.E. and J.D. Corbett, 1969, J. Less-Common Metals **18**, 1.
Carter, F.L. and J.F. Murray, 1972, Mater. Res. Bull. **7**, 519.
Catalano, E., R.G. Bedford, V.G. Silveira and H.H. Wickman, 1969, J. Phys. Chem. Solids **30**, 1613.
Cho, K., K. Irisawa, J. Mochinago and T. Turoda, 1972, Electrochim. Acta **17**, 1821.
Ciach, S., A.J.C. Nicholson, D.L. Swingler and P.J. Thistlethwaite, 1973, Inorg. Chem. **12**, 2072.
Clink, B.L., 1974, M.S. Thesis, Michigan State University, East Lansing, Michigan.
Colwell, J.H., B.W. Mangum and D.B. Utton, 1969, Phys. Rev. **181**, 842.
Corbett, J.D., 1966, Metal Halides in Low Oxidation States, in: Jolly, W.L., ed., Preparative Inorganic Reactions (Interscience, New York), pp. 1–33.
Corbett, J.D., 1973, Rev. Chim. Mineral. **10**, 239.
Corbett, J.D., 1976, Reduced Halides of the Rare Earth Elements, in: Proceedings of the Twelfth Rare Earth Research Conference, Vail, Colorado, pp. 396–403.
Corbett, J.D. and B.C. McCollum, 1966, Inorg. Chem. **5**, 938.
Corbett, J.D., L.F. Druding, W.J. Burkhard and C.B. Lindahl, 1962, Disc. Faraday Soc. **32**, 79.
Corbett, J.D., D.L. Pollard and J.E. Mee, 1966, Inorg. Chem. **5**, 761.
Corbett, J.D., R.A. Sallach and D.A. Lokken, 1967, Physical Characterization of the Metallic LaI_2 and CeI_2 and of the Phase $LaI_{2.42}$, in: Gould, R.F., ed., Lanthanide-Acetinide Chemistry, Advances in Chemistry Series 71 (American Chemical Society, Washington), pp. 56–66.
Cox, D.E. and F.K. Fong, 1973, J. Crystal Growth **20**, 233.
Cunningham, B.B., D.C. Feay and M.A. Rollier, 1954, J. Am. Chem. Soc. **76**, 3361.
Daane, A.H. and F.H. Spedding, 1953, J. Electrochem. Soc. **100**, 442.
DaDilva, J.J.R.F. and M.M. Queimado, 1973, Rev. Port. Quim. **15**, 29; Chem. Abstr. 82:129929g.
DeKock, C.W. and D.D. Radtke, 1970, J. Inorg. Nucl. Chem. **32**, 3687.
DeKock, C.W., R.D. Wesley and D.D. Radtke, 1972, High Temp. Sci. **4**, 41.
Delaigue, A. and J.-C. Cousseins, 1972, Rev. Chim. Mineral. **9**, 789.
Deline, T.A., E.F. Westrum, Jr. and J.M. Haschke, 1975, J. Chem. Thermodynamics **7**, 671.
Dienstbach, F. and R. Blachnik, 1975, Z. Anorg. Allg. Chem. **412**, 97.
Doell, W. and W. Klemm, 1939, Z. Anorg. Allg. Chem. **241**, 239.
Drobot, D.V., B.G. Korshunov and G.P. Borodulenko, 1968, Russ. J. Inorg. Chem. **13**, 855.
Druding, L.F. and J.D. Corbett, 1961, J. Am. Chem. Soc. **83**, 2462.
Druding, L.F., J.D. Corbett and B.W. Ramsey, 1963, Inorg. Chem. **2**, 869.
Dudchik, G.P., A. Makhmadmurodov and O.G. Polyachenok, 1975, Zh. Fiz. Khim. **49**, 1856.
Dworkin, A.S. and M.A. Bredig, 1961, Disc. Faraday Soc. **32**, 188.
Dworkin, A.S. and M.A. Bredig, 1963a, J. Phys. Chem. **67**, 697.
Dworkin, A.S. and M.A. Bredig, 1963b, J. Phys. Chem. **67**, 2499.
Dworkin, A.S. and M.A. Bredig, 1971a, High Temp. Sci. **3**, 81.
Dworkin, A.S. and M.A. Bredig, 1971b, J. Phys. Chem. **75**, 2340.
Dworkin, A.S. and M.A. Bredig, 1973, J. Chem. Eng. Data **18**, 74.

Dworkin, A.S., H.R. Bronstein and M.A. Bredig, 1962, J. Phys. Chem. **66**, 1201.
Dworkin, A.S., R.A. Sallach, H.R. Bronstein, M.A. Bredig and J.D. Corbett, 1963, J. Phys. Chem. **67**, 1145.
Feber, R.C., 1965, U.S. Atomic Energy Comm. Report LA-3164, Los Alamos Scientific Laboratory, pp. 1–180.
Ferris, L.M., J.C. Mailen and F.J. Smith, 1972, J. Inorg. Nucl. Chem. **34**, 491.
Fishel, N.A. and H.A. Eick, 1971, J. Inorg. Nucl. Chem. **33**, 1198.
Foerthmann, R. and A. Schneider, 1969, Z. Anorg. Allg. Chem. **367**, 27.
Foerthmann, R., G. Vogel and A. Schneider, 1969, Z. Anorg. Allg. Chem. **367**, 19.
Forrester, J.D., A. Zalkin, D.H. Templeton and J.C. Wallmann, 1964, Inorg. Chem. **3**, 185.
Garashina, L.S. and B.P. Sobolev, 1971, Sov. Phys. Crystallogr. **16**, 254.
Gildseth, W.M., A. Habenschuss and F.H. Spedding, 1975, J. Chem. Eng. Data **20**, 292.
Giritcheva, N.I., G.V. Giritchev, K.S. Krasnov, E.Z. Zasorin and V.P. Spiridonov, 1974, Molecular Structure Determination of Some Rare Earth Trihalides by Gas Electron Diffraction, in: Haschke, J.M. and H.A. Eick, eds., Proceedings of the Eleventh Rare Earth Research Conference, U.S. Atomic Energy Commission CONF-741002-P2 (National Technical Information Service, Springfield), pp. 1087–1094.
Graeber, E.J., G.H. Conrad and S.F. Duliere, 1966, Acta Crystallogr. **21**, 1012.
Greiner, J.D., J.F. Smith, J.D. Corbett and F.J. Jelinek, 1966, J. Inorg. Nucl. Chem. **28**, 971.
Greis, O., 1976, Ph.D. Thesis, University of Freiburg, Freiburg/Br., Germany.
Greis, O. and T. Petzel, 1974, Z. Anorg. Allg. Chem. **403**, 1.
Gupta, S.K., 1976, J. Chem. Eng. Data **21**, 114.
Habenschuss, A. and F.H. Spedding, 1974, A Survey of Some Properties of Aqueous Rare Earth Salt Solutions. I. Volume, Thermal Expansion Raman Spectra and X-ray Diffraction, in: Haschke, J.M. and H.A. Eick, eds., Proceedings of the Eleventh Rare Earth Research Conference, U.S. Atomic Energy Commission CONF-741002-P2 (National Technical Information Service, Springfield), pp. 909–918.
Habenschuss, A. and F.H. Spedding, 1976, J. Chem. Eng. Data **21**, 95.
Haeseler, G. and F. Matthes, 1965, J. Less-Common Metals **9**, 113.
Hariharan, A.V., 1973, private communication of unpublished results, Iowa State University, Ames, Iowa, cited by H. Baernighausen (1976a).
Hariharan, A.V. and H.A. Eick, 1972a, High Temp. Sci. **4**, 91.
Hariharan, A.V. and H.A. Eick, 1972b, High Temp. Sci. **4**, 379.
Hariharan, A.V., N.A. Fishel and H.A. Eick, 1972, High Temp. Sci. **4**, 405.
Harris, A.L. and C.R. Veale, 1965, J. Inorg. Nucl. Chem. **27**, 1436.
Haschke, J.M., 1973, J. Chem. Thermodynamics **5**, 283.
Haschke, J.M., 1975a, J. Chem. Educ. **52**, 157.
Haschke, J.M., 1975b, J. Solid State Chem. **12**, 115.
Haschke, J.M., 1975c, J. Solid State Chem. **14**, 238.
Haschke, J.M., 1975d, High Temp. Sci. **7**, 152.
Haschke, J.M., 1976a, Inorg. Chem. **15**, 508.
Haschke, J.M., 1976b, J. Solid State Chem. **18**, 205(1976).
Haschke, J.M., 1976c, Structural Correlations of the Lanthanide Halides and Related Compounds, in: Proceedings of the Twelfth Rare Earth Research Conference, Vail Colorado, pp. 414–423.
Haschke, J.M., 1976d, Inorg. Chem. **15**, 298.
Haschke, J.M., 1976e, unpublished results.
Haschke, J.M. and H.A. Eick, 1970a, J. Inorg. Nucl. Chem. **32**, 2153.
Haschke, J.M. and H.A. Eick, 1970b, J. Am. Chem. Soc. **92**, 4550.
Haschke, J.M. and H.A. Eick, 1970c, J. Phys. Chem. **74**, 1806.
Hastie, J.W., P. Ficalora and J.L. Margrave, 1968, J. Less-Common Metals **14**, 83.
Hastie, J.W., R.H. Hauge and J.L. Margrave, 1971, High Temp. Sci. **3**, 56.
Hauge, R.H., J.W. Hastie and J.L. Margrave, 1971, J. Less-Common Metals **23**, 359.
Herrington, J.R., K.G. Sewell and W.B. Volz, 1975, Appl. Phys. Lett. **26**, 226.
Hessler, J.P. and E.H. Carlson, 1971, J. Appl. Phys. **42**, 1316.
Hinchley, R.J. and J.W. Cobble, 1970, Inorg. Chem. **9**, 917.
Hirayama, C. and F.E. Camp, 1972, J. Chem. Eng. Data **17**, 415.
Hirayama, C. and P.M. Castle, 1973, J. Phys. Chem. **77**, 3310.
Hirayama, C. and P.M. Castle, 1974, Vapors in Equilibrium Over Molten Mixtures of CeI_3 with CsI and NaI, in: Haschke, J.M. and H.A. Eick, Proceedings of the Eleventh Rare Earth Research Conference, J.S. Atomic Energy Commission CONF-741002-P2 (National Technical Information Service, Springfield), pp. 1048–1057.
Hirayama, H., P.M. Castle, R.W. Liebermann, R.J. Zollweg and F.E. Camp, 1974, Inorg. Chem. **13**, 2804.
Hirayama, C., J.F. Rome and F.E. Camp, 1975, J. Chem. Eng. Data **20**, 1.
Hirayama, C., G.L. Carlson, P.M. Castle, J.T. Rome and W.E. Snider, 1976, J. Less-Common Metals **45**, 293.
Holleck, L., 1938, Angew. Chem. **51**, 243.
Howell, K.J. and L.L. Pytlewski, 1969, J. Less-Common Metals **18**, 437.
Hund, F., 1950, Z. Anorg. Allg. Chem. **261**, 106.
Hyde, B.G., A.N. Bagshaw, S. Andersson and M. O'Keeffe, 1974, Ann. Rev. Mater. Sci. **4**, 43.
Ikrami, D.D., S. Dzhuraev and N.S. Nikolaev, 1972, Russ. J. Inorg. Chem. **17**, 539.

Illin, V.K., V.A. Krenev and V.I. Eudokinov, 1972, Russ. J. Inorg. Chem. **17**, 1497.
Jantsch, G. and N. Skalla, 1930, Z. Anorg. Allg. Chem. **193**, 391.
Jantsch, G., N. Skalla and H. Jawurek, 1931, Z. Anorg. Allg. Chem. **201**, 207.
Johnson, D.A., 1969, J. Chem. Soc. A 1969, 2578.
Johnson, D.A. and J.D. Corbett, 1969, Coll. Resch. Nat. Scient. **180**, 429.
Johnson, K.E. and J.R. Mackenzie, 1969, J. Electrochem. Soc. **116**, 1697.
Johnson, K.E. and J.R. Mackenzie, 1970, J. Inorg. Nucl. Chem. **32**, 43.
Jones, D.A. and W.A. Shand, 1968, J. Crystal Growth **2**, 361.
Kaiser, E.W., W.E. Falconer and W. Klemperer, 1972a, J. Chem. Phys. **56**, 5392.
Kaiser, E.W., W.A. Sunders and W.E. Falconer, 1972b, J. Less-Common Metals **27**, 383.
Kammermans, M.A., 1939, Z. Krist. **101**, 406.
Karraker, D.G., 1970, J. Chem. Educ. **47**, 424.
Keneshea, F.J. and D. Cubicciotti, 1961, J. Chem. Eng. Data **6**, 507.
Kent, R.A., K.F. Zmbov, A.S. Kamaan, G. Besenbruch, J.D. McDonald and J.L. Margrave, 1966, J. Inorg. Nucl. Chem. **28**, 1419.
Khanaev, E.I., Yu.A. Afanas'ev and T.P. Storozhenko, 1975, Zh. Fiz. Khim. **49**, 2454.
Kirshenbaum, A.D. and J.A. Cahill, 1960, J. Inorg. Nucl. Chem. **14**, 149.
Kiss, N.H., 1963, J. Res. Natl. Bur. Stands. **67A**, 343.
Klevtsova, R.F., P. Kozeeva and P.L. Klevtsov, 1967, Inorg. Mater. **3**, 1247.
Koch, C.W. and B. B. Cunningham, 1953, J. Am. Chem. Soc. **75**, 796.
Koch, C.W. and B. B. Cunningham, 1954, J. Am. Chem. Soc. **76**, 1471.
Koch, C.W., A. Broido and B.B. Cunningham, 1952, J. Am. Chem. Soc. **74**, 2349.
Krasnov, K.S. and T.G. Danilova, 1969, High Temp. **7**, 1131.
Krestkov, G.A., V.A. Kobenin and S.V. Semenovskii, 1972, Russ. J. Inorg. Chem. **17**, 421.
Krudryavtseva, O.V., L.S. Garashina, K.K. Rivkina and B.P. Sobolev, 1973, Sov. Phys. Crystallogr. **18**, 531.
Kummer, J. and M.E. Milberg, 1969, Chem. Eng. News **47**, 90.
Kutscher, J. and A. Schneider, 1971, Inorg. Nucl. Chem. Lett. **7**, 851.
Kutscher, J. and A. Schneider, 1974, Z. Anorg. Allg. Chem. **408**, 135.
Labeau, M., S. Aleonard, A. Vedrine, R. Boutonnet and J.-C. Cousseins, 1974, Mater. Res. Bull. **9**, 615.
Lambrecht, V.G., M. Robbins and R.C. Sherwood, 1974, J. Solid State Chem. **10**, 1.
Larson, A.C., R.B. Roof, Jr. and D.T. Cromer, 1964, Acta Crystallogr. **17**, 555.
Latimer, W.M., 1951, J. Am. Chem. Soc. **73**, 1480.
Lim, M. and A.W. Searcy, 1966, J. Phys. Chem. **70**, 1762.
Lishenko, G.L., T.S. Nazarova, Y. Polyakov and A.A. Rozen, 1973, Russ. J. Inorg. Chem. **18**, 484.
Liu, C.S. and R.J. Zollweg, 1974, J. Chem. Phys. **60**, 2384.
Loechner, U. and J.D. Corbett, 1975, Inorg. Chem. **14**, 426.
Loechner, U., H. Baernighausen and J.D. Corbett, 1976, to be published.
Lokken, D.A. and J.D. Corbett, 1973, Inorg. Chem. **12**, 556.
Lucas, J., M. Poulain, G. Fonteneau and P. Brun, 1974, Les Fluorozirconates de Terres Rares, in: Haschke, J.M. and H.A. Eick, Proceedings of the Eleventh Rare Earth Research Conference, U.S. Atomic Energy Commission CONF-741002-P2 (National Technical Information Service, Springfield), pp. 1030–1038.
Lueke, H. and H.A. Eick, 1976, The Structure of the M_6X_{13} Phase Yb_5ErCl_{13}, in: Proceedings of the Twelfth Rare Earth Research Conference, Vail, Colorado, pp. 424–432.
Machlan, G.R., C.T. Stubblefield and L. Eyring, 1955, J. Am. Chem. Soc. **77**, 2975.
Makhmadmurodov, A., G.P. Dudchik and O.G. Polyachenok, 1975, Zh. Fiz. Khim. **49**, 2159.
Mann, A.W. and D.J.M. Bevan, 1972, J. Solid State Chem. **5**, 410.
Mansmann, M., 1965, Z. Krist. **122**, 375.
Mar, R.W. and Searcy, A.W., 1967, J. Phys. Chem. **71**, 888.
Marezio, M., H.A. Plettinger and W.H. Zachariasen, 1961, Acta Crystallogr. **14**, 234.
Maroni, V.A., E.J. Hathaway and G.N. Papatheodorou, 1974, J. Phys. Chem. **78**, 1134.
Mayer, I. and S. Solotov, 1965, J. Inorg. Nucl. Chem. **27**, 1905.
McCollum, B.C. and J.D. Corbett, 1968, Chem. Commun. **1968**, 1666.
McCollum, B.C., M.J. Champ and J.D. Corbett, 1973, Inorg. Chem. **12**, 778.
McCreary, J.R. and R.J. Thorn, 1973a, High Temp. Sci. **5**, 97.
McCreary, J.R. and R.J. Thorn, 1973b, High Temp. Sci. **5**, 365.
McCreary, J.R. and R.J. Thorn, 1974a, Valence States in Lanthanide Solids, in: Haschke, J.M. and H.A. Eick, eds., Proceedings of the Eleventh Rare Earth Research Conference, U.S. Atomic Energy Commission CONF-741002-P2 (National Technical Information Service, Springfield), pp. 1068–1076.
McCreary, J.R. and R.J. Thorn, 1974b, High Temp. Sci. **6**, 205.
McCreary, J.R. and R.J. Thorn, 1974c, Entropy and Enthalpy of Sublimation of Dysprosium, Holmium and Erbium Trifluorides, in: Haschke, J.M. and H.A. Eick, eds., Proceedings of the Eleventh Rare Earth Research Conference, U.S. Atomic Energy Commission CONF-741002-P2 (National Technical Information Service, Springfield), pp. 1039–1047.

McKinley, J.D., 1965, J. Chem. Phys. **42**, 2245.
Mee, J.E. and J.D. Corbett, 1965, Inorg. Chem. **4**, 88.
Mellors, G.W. and S. Senderoff, 1959, J. Phys. Chem. **63**, 1110.
Meyers, C.E., 1975, Inorg. Chem. **14**, 199.
Mironov, K.E., R.V. Abdullin and E.N. Balyakina, 1974, Russ. J. Inorg. Chem. **19**, 768.
Moeller, T., 1973, The Lanthanides, in: Bailar, J.C., H.J. Emeleus, R. Nyholm and A.F. Trotman-Dickenson, eds., Comprehensive Inorganic Chemistry, Vol. 4 (Pergamon Press, Oxford), p. 67.
Moriarty, J.L.M., 1963, J. Chem. Eng. Data **8**, 422.
Morss, L.R. and J.A. Fahey, 1976, Enthalpies of Formation of the Lanthanide Dichlorides, in: Proceedings of the Twelfth Rare Earth Research Conference, Vail, Colorado, pp. 443–450.
Morss, L.R. and H.O. Haug, 1973, J. Chem. Thermodyn. **5**, 524.
Morss, L.R. and M.C. McCue, 1975, Inorg. Chem. **14**, 1624.
Mroczkowski, S., 1970, J. Crystal Growth **6**, 47.
Mundy, W.C. and F.H. Spedding, 1973, J. Chem. Phys. **59**, 2183.
Nafziger, R.H., R.L. Lincoln and N. Riazance, 1973, J. Inorg. Nucl. Chem. **35**, 421.
Novikov, G.I. and A.K. Baev, 1964, Russ. J. Inorg. Chem. **9**, 905.
Novikov, G.I. and F.G. Gavryucherkov, 1967, Russ. Chem. Rev. **36**, 156.
Novikov, G.I. and O.G. Polyachenok, 1963, Russ. J. Inorg. Chem. **8**, 545.
Novikov, G.I. and O.G. Polyachenok, 1964, Russ. Chem. Rev. **33**, 342.
Oftedal, I., 1929, Z. Phys. Chem. **5B**, 272.
Oye, H.A. and D.M. Gruen, 1969, J. Am. Chem. Soc. **91**, 2229.
Papatheodorou, G.N. and O.J. Kleppa, 1974, J. Phys. Chem. **78**, 178.
Papatheodorou, G.N. and T. Ostvold, 1974, J. Phys. Chem. **78**, 181.
Pastor, R.C. and M. Robinson, 1974, Mater. Res. Bull. **9**, 569.
Petzel, T. and O. Greis, 1972, Z. Anorg. Allg. Chem. **388**, 137.
Petzel, T. and O. Greis, 1973, Z. Anorg. Allg. Chem. **396**, 95.
Pierce, J.W. and H.Y.-P. Hong, 1973, Structural Studies in the System KF–YF_3, in: Kevane, C.J. and T. Moeller, eds., Proceedings of the Tenth Rare Earth Research Conference, U.S. Atomic Energy Commission CONF-730402-P1 (National Technical Information Service, Springfield), pp. 527–537.
Polyachenok, O.G., 1967, Russ. J. Inorg. Chem. **12**, 449.
Polyachenok, O.G. and G.I. Novikov, 1963a, Russ. J. Inorg. Chem. **8**, 793.
Polyachenok, O.G. and G.I. Novikov, 1963b, Russ. J. Inorg. Chem. **8**, 1478.
Polyachenok, O.G. and G.I. Novikov, 1963c, Russ. J. Gen. Chem. **33**, 2900.
Polyachenok, O.G. and G.I. Novikov, 1963d, Russ. J. Inorg. Chem. **8**, 1479.
Polyachenok, O.G. and G.I. Novikov, 1963e, Russ. J. Inorg. Chem. **8**, 816.
Polyachenok, O.G. and G.I. Novikov, 1964, Russ. J. Inorg. Chem. **9**, 429.
Poulain, M., M. Poulain and J. Lucas, 1972, Mater. Res. Bull. **7**, 319.
Poulain, M., M. Poulain and J. Lucas, 1973, J. Solid State Chem. **8**, 132.
Powell, J.E. and H.R. Burkholder, 1960, J. Inorg. Nucl. Chem. **14**, 65.
Rango, C.de, G. Touscaris and C. Zelwer, 1966, C.R. Acad. Sci., Paris, Ser. **C263**, 64.
Rard, J.A. and F.H. Spedding, 1974, A Survey of Some Properties of Aqueous Rare Earth Salt Solutions. II. Heats of Dilution, Heat Capacities, Activity Coefficients, Electrical Conductances and Relative Viscosities, in: Haschke, J.M. and H.A. Eick, eds., Proceedings of the Eleventh Rare Earth Research Conference, U.S. Atomic Energy Commission CONF-741002-P2 (National Technical Information Service, Springfield), pp. 919–928.
Reitschel, E.T. and H. Baernighausen, 1969, Z. Anorg. Allg. Chem. **368**, 62.
Rezuhkina, T.N., T.F. Sisoeva, L.I. Holokhonova and E.G. Ippolitov, 1974, J. Chem. Thermodyn. **6**, 883.
Roberts, J.A., Jr. and A.W. Searcy, 1972, High Temp. Sci. **4**, 411.
Rudzitis, E., H.M. Feder and W.N. Hubbard, 1965, J. Phys. Chem. **69**, 2305.
Sallach, R.A. and J.D. Corbett, 1963, Inorg. Chem. **2**, 457.
Sass, R.L., T. Brackett and E.B. Brackett, 1963, J. Phys. Chem. **67**, 2862.
Schaefer, H. and J. Karbinski, 1974, Z. Anorg. Allg. Chem. **403**, 116.
Schimazaki, E. and K. Niwa, 1962, Z. Anorg. Allg. Chem. **314**, 21.
Schlyter, K., 1953, Ark, Kemi **5**, 73.
Schumm, R.D., D.D. Wagman, S. Bailey, W.H. Evans and V.B. Parker, 1973, Selected Values of Chemical Thermodynamic Properties, National Bureau of Standards Technical Note 270-7 (U.S. Government Printing Office, Washington), pp. 1–75.
Seifert, K.-F., 1968, Fortschr. Mineral. **45**, 214.
Seiranian, K.B., P.P. Fedorov, L.S. Garashina, G.V. Molev, V.V. Karelin and B.P. Sobolev, 1974, J. Crystal Growth **26**, 61.
Selivanov, C.K., Y.N. Sekachev and A.A. Maltsev, 1973, Russ. J. Phys. Chem. **47**, 1239.
Shaimuradov, I.B., L.P. Reshetnikova and A.V. Novoselova, 1974, Inorg. Mater. **10**, 1264.
Skelton, W.H. and J.W. Patterson, 1973, J. Less-Common Metals **31**, 47.
Skinner, H.B. and A.W. Searcy, 1968, J. Phys. Chem. **72**, 3375.
Skinner, H.B. and A.W. Searcy, 1971, J. Phys. Chem. **75**, 108.
Smeggil, J.G. and H.A. Eick, 1971, Inorg. Chem. **10**, 1458.

Sobolev, B.P. and P.P. Fedorov, 1973, Soviet Phys. Crystallogr. **18**, 392.
Sommers, J.A., 1976, Ph.D. Thesis, University of Michigan, Ann Arbor, Michigan.
Soriano, J., M. Givon and J. Shamir, 1966, Inorg. Nucl. Chem. Lett. **2**, 13.
Spedding, F.H. and A.H. Daane, 1952, J. Am. Chem. Soc. **74**, 2783.
Spedding, F.H. and J.P. Flynn, 1954, J. Am. Chem. Soc. **76**, 1474.
Spedding, F.H. and J.C. Jones, 1966, J. Phys. Chem. **70**, 2450.
Spedding, F.H. and D.C. Henderson, 1971, J. Chem. Phys. **54**, 2476.
Spedding, F.H. and M.J. Pikal, 1966, J. Phys. Chem. **70**, 2430.
Spedding, F.H., D.A. Csejka and C.W. DeKock, 1966a, J. Phys. Chem. **70**, 2423.
Spedding, F.H., M.J. Pikal and B.O. Ayers, 1966b, J. Phys. Chem. **70**, 2440.
Spedding, F.H., D.C. Rulf and B.C. Gerstein, 1972, J. Chem. Phys. **56**, 1498.
Spedding, F.H., J.A. Rard and V.W. Saeger, 1974a, J. Chem. Eng. Data **19**, 373.
Spedding, F.H., B.J. Beaudry, D.C. Henderson and J. Moorman, 1974b, J. Chem. Phys. **60**, 1578.
Spedding, F.H., P.F. Cullen and A. Habenschuss, 1974c, J. Phys. Chem. **78**, 1106.
Spedding, F.H., D.L. Witte, L.E. Shiers and J.A. Rard, 1974d, J. Chem. Eng. Data **19**, 369.
Spedding, F.H., R.A. Nelson and J.A. Rard, 1974e, J. Chem. Eng. Data **19**, 379.
Spedding, F.H., J.P. Walters and J.L. Baker, 1975, J. Chem. Eng. Data **20**, 438.
Spitsyn, V.I., Y.M. Kiselev and M.I. Martynenko, 1973, Russ. J. Inorg. Chem. **18**, 593.
Spitsyn, V.I., Y.M. Kiselev and M.I. Martynenko, 1974, Russ. J. Inorg. Chem. **19**, 628.
Stezowski, J.J. and H.A. Eick, 1970, Inorg. Chem. **9**, 1102.
Strizhkov, B.V., E.D. Ruchkin, V.S. Krikorov, V.A. Pchelkin, L.S. Nikitenko and D.A. Khromov, 1972, Inorg. Mater. **8**, 1258.
Stubblefield, C.T., J.L. Rutledge and R. Phillips, 1965, J. Phys. Chem. **69**, 991.
Stuve, J.M., 1964, U.S. Bur. Mines Rept. Invest. No. 6640.
Stuve, J.M., 1965, U.S. Bur. Mines Rept. Invest. No. 6697.
Stuve, J.M., 1967a, U.S. Bur. Mines Rept. Invest. No. 6902.
Stuve, J.M., 1967b, U.S. Bur. Mines Rept. Invest. No. 7046.
Suvorev, A.V., E.V. Krzhizhanovskaya and G.I. Novikov, 1966, Russ. J. Inorg. Chem. **11**, 1441.
Tanguy, B., J. Portier, M. Vlasse and M. Pouchard, 1972, Bull. Soc. Chem. Fr. **1972**, 946.
Tanguy, B., P. Merle, M. Pezat and C. Fouassier, 1974, Mater. Res. Bull. **9**, 831.
Taylor, M.D., 1962, Chem. Rev. **62**, 503.
Taylor, M.D. and C.P. Carter, 1962, J. Inorg. Nucl. Chem. **24**, 387.
Thoma, R.E., 1962, Inorg. Chem. **1**, 220.
Thoma, R.E., 1966, The Rare Earth Halides, in: Eyring, L., ed., Progress in Science and Technology of the Rare Earths, Vol. 2 (Pergamon Press, New York), pp. 90–121.
Thoma, R.E., 1973, Rev. Chim. Mineral. **10**, 363.
Thoma, R.E. and G.D. Brunton, 1966, Inorg. Chem. **5**, 1937.
Thoma, R.E., C.F. Weaver, H.A. Friedman, H. Insley and L.A. Harris, 1961, J. Chem. Phys. **65**, 1096.
Thoma, R.E., H. Insley and G.M. Hebert, 1965, Inorg. Chem. **5**, 1222.
Thoma, R.E., G.D. Brunton, R.A. Penneman and T.K. Keenan, 1970, Inorg. Chem. **9**, 1096.
Tiller, C.O., A.C. Lilly and B.C. LaRoy, 1973, Phys. Rev. **B8**, 4787.
Topol, L., 1965, J. Phys. Chem. **69**, 11.
Vajnstejn, B.K. and Z.G. Pinsker, 1951, Zh. Fiz. Khim. **24**, 432.
Valon, P., J.-C. Cousseins, A. Vedrine, J.C. Gacon, G. Boulon and F.K. Fong, 1976, Mater. Res. Bull. **11**, 43.
Vedrine, A., R. Boutonnet, R. Sabatier and J.-C. Cousseins, 1975, Bull. Soc. Chem. Fr. **1975**, 445.
Vogel, G. and A. Schneider, 1972, Inorg. Nucl. Chem. Lett. **8**, 513.
Warkentin, E. and H. Baernighausen, 1976, The Structures of Dipraseodymium Pentaiodide and the Metallic Diiodides of Lanthanum Cerium and Praseodymium, in: Colloquium Abstracts of the Third European Crystallographic Meeting, Zurich, Switzerland, pp. 354–356.
Weigel, F., 1969, Fortschr. Chem. Forsch. **12**, 539.
Weigel, F. and H. Haug, 1961, Chem. Ber. **94**, 1548.
Weigel, F. and V. Schéurer, 1967, Radiochim. Acta **7**, 40.
Weigel, F. and G. Trinkl, 1970, Z. Anorg. Allg. Chem. **377**, 228.
Weigel, F. and V. Vishnevsky, 1969, Chem. Ber. **102**, 5.
Weigel, F. and V. Vishnevsky, 1970, Chem. Ber. **103**, 193.
Weigel, F. and V. Wishnevsky, 1972, Chem.
Weigel, F. and V. Wishnevsky, 1973, Chem. Ber. **106**, 1976.
Wendlandt, W.W., 1957, J. Inorg. Nucl. Chem. **5**, 118.
Wendlandt, W.W., 1959, J. Inorg. Nucl. Chem. **9**, 136.
Wendlandt, W.W. and J.L. Baer, 1959, Anal. Chim. Acta **21**, 439.
Wendlandt, W.W. and B. Love, 1959, Science **129**, 842.
Wesley, R.D. and C.W. DeKock, 1971, J. Chem. Phys. **55**, 3866.
Westrum, E.F., Jr., 1967, Developments in Chemical Thermodynamics of the Lanthanides, in: Gould, R.F., ed., Lanthanide-Actinide Chemistry, Advances in Chemistry Series 71 (American Chemical Society, Washington), pp. 25–50.

Westrum, E.F., Jr., 1968, Thermodynamic and Magnetic Properties of the Rare Earth Chalcogenides, Pnictides, Halides and Binary Semimetallic Compounds, in: Eyring, L., ed., Progress in Science and Technology of the Rare Earths, Vol. 3 (Pergamon Press, New York), pp. 459–514.
Westrum, E.F., Jr. and A.F. Beale, Jr., 1961, J. Phys. Chem. **65**, 353.
Wicks, C.E. and F.E. Block, 1963, Thermodynamic Properties of 65 Elements – Their Oxides, Halides, Carbides and Nitrides, U.S. Bureau of Mines Bulletin 605 (U.S. Government Printing Office, Washington), pp. 1–146.
Work, D.E. and H.A. Eick, 1973, High Temp. Sci. **5**, 313.
Wright, J.C., D.J. Zalucha, H.V. Lauer, D.E. Cox and F.K. Fong, 1973, J. Appl. Phys. **44**, 781.
Wyckoff, R.W.G., 1963, Crystal Structures, Vol. 1, 2nd. ed. (Interscience Publishers, New York), pp. 252–271.
Wyckoff, R.W.G., 1964, Crystal Structures, Vol. 2, 2nd. ed. (Interscience Publishers, New York), pp. 45–57.
Zachariasen, W.H., 1948, Acta Crystallogr. **1**, 256.
Zachariasen, W.H., 1949, Acta Crystallogr. **2**, 388.
Zalkin, A. and D.H. Templeton, 1953, J. Am. Chem. Soc. **75**, 2453.
Zalkin, A., D.H. Templeton and T.E. Hopkins, 1966, Inorg. Chem. **5**, 1466.
Zmbov, K.F. and J.L. Margrave, 1966, J. Chem. Phys. **45**, 3167.
Zmbov, K.F. and J.L. Margrave, 1967, J. Less-Common Metals **12**, 494.
Zmbov, K.F. and J.L. Margrave, 1968, Mass Spectrometric Studies of Scandium, Yttrium, Lanthanum and Rare Earth Fluorides, in: Gould, R.F., ed., Mass Spectrometry in Inorganic Chemistry, Advances in Chemistry Series 72 (American Chemical Society, Washington), pp. 267–290.
Zollweg, R.J., C.S. Liu, C. Hirayama and J.W. McNall, 1975, J. Illuminating Eng. Soc. **4**, 249.

References to section 8

Adolphson, D. G. and J. D. Corbett, 1976, Inorg. Chem. **15**, 1820.
Batsanov, S. S., V. A. Egorov and Yu. B. Khvostov, 1976, Dokl. Akad. Nauk SSSR **227**, 860.
Haire, R. G., J. P. Young, J. R. Peterson and R. L. Fellows, 1978, Adsorption Spectrophotometric and X-ray Diffraction Evidence for Mixed Valence Compounds in Anhydrous Halides of Lanthanide-Actinide Mixtures, in: McCarthy, G. J. and J. Rhyne, eds., The Rare Earths in Modern Science and Technology (Proceedings of the Thirteenth Rare Earth Research Conference) (Plenum Press) p. 501.
Haschke, J. M., 1977, High Temp. Sci. **9**, 77.
Haschke, J. M., 1978, unpublished results.
Greis, O., 1977a, Z. Anorg. Allgem. Chem. **430**, 175.
Greis, O., 1977b, Monatsh. Chem. **108**, 205.
Kulagin, N. M. and D. M. Laptev, 1976, Zh. Fiz. Khim **50**, 810.
Laptev, D. M., V. F. Goryushkin, N. M. Kulagin and E. S. Vorontsov, 1976, Zh. Neorg. Khim **21**, 2616.
Meyers, C. E. and D. T. Graves, 1977a, J. Chem. Eng. Data **22**, 436.
Meyers, C. E. and D. T. Graves, 1977b, J. Chem. Eng. Data **22**, 440.
Petzel, T. and O. Greis, 1976, J. Less-Common Met. **46**, 197.
Simon, A., H. Mattauch and N. Holzer, 1976, Angew. Chem. **88**, 685.
Yokozeki, A. and M. Menzinger, 1976, Chem. Phys. **14**, 427.
Zzoli, P. E., 1977, Masters Degree Thesis, Michigan State University.

Handbook on the Physics and Chemistry of Rare Earths, edited by K.A. Gschneidner, Jr. and L. Eyring

Chapter 33

RARE EARTH PNICTIDES

F. HULLIGER
Laboratorium für Festkörperphysik ETH, CH-8093 Zürich, Switzerland

Contents

Symbols

A_4, A_6 = geometrical coordination factors of the crystal-field potential
a = lattice constant
$B_\alpha^{[2]}$ = magnetoelastic coupling constant
C = Curie constant
c_{ij} = elastic constant
c_{mag} = specific-heat contribution of the 4f electrons
c_p = molar heat capacity measured at constant pressure
e = electron charge
E_i = energies of various crystal-field levels
F = free energy
g_J = Landé factor
g_i = magnetoelastic coupling constants
g_n = multiplicity of an energy level
H = magnetic field
H_m = molecular field
$\mathcal{H}$ = single-ion Hamiltonian
J = quantum number of total angular momentum $L \pm S$
$\mathcal{J}_i$ = exchange constant for ith neighbor interaction
K_4, K_6 = anisotropy constants
k = Boltzmann factor
L = Avogadro's number
Ln = symbol for a rare earth element
M = symbol for a cation or a metal atom
M = magnetization
M_J = magnetic quantum number
m^* = effective mass of the conduction electrons
N = number of rare earth ions per volume
n_e = concentration of conduction electrons per formula unit
O_n^m = Stevens operator equivalents

p = pressure
R = universal gas constant
$\langle r_i^n \rangle$ = nth moment of the distribution of the 4f electrons
S = entropy
T = absolute temperature
T_t = superconducting transition temperature
T_C = Curie temperature
T_N = Néel temperature
V_c = crystal-field potential
W = scale factor for the crystal-field splitting of the J ground-state energies
X = symbol for an anion, N, P, As, Sb or Bi
x = number defining the ratio of the 4th to the 6th order term in the crystal-field potential
Z = cation valence
Z = one-ion partition function
α = linear thermal-expansion coefficient
β = rhombohedral angle of the deformed NaCl cell $\beta = \frac{1}{2}\pi - \Delta\beta$
β = volume thermal-expansion coefficient
β_J = Stevens factor in the 4th order term of the crystal-field potential
Γ_i = crystal-field levels
γ = temperature coefficient of the specific-heat contribution of the conduction electrons
γ_i = Grüneisen parameter for the level E_i
γ_Γ = Stevens factor in the 6th order term of the crystal-field potential
Δ = overall crystal-field splitting of the ground-state J energy of the $4f^n$ electrons
ϵ_i = symmetry strains
θ_p = paramagnetic Curie temperature (Curie–Weiss constant)
κ = adiabatic compressibility
λ_p = molecular-field constant
λ_Q = quadrupolar parameter
μ_B = Bohr magneton
χ = magnetic susceptibility
$\psi_{n,m}$ = 4f eigenfunction belonging to the m-fold level Γ_n

1. Occurrence of phases

The rare earth elements are transitional in their chemical properties between the alkaline-earth elements, especially Ba, and the 5d transition elements Hf, Ta. With certain exceptions they behave like transition elements of the Sc group with additional f electrons in discrete levels. The exceptions are mainly due to the high stability of the empty, half- or completely-filled 4f shell. Certain compounds formed by Eu and Yb, in some cases also Sm and Tm, therefore show close similarities with the corresponding alkaline-earth compounds whereas Ce and Tb in fluorides and oxides resemble Hf^{4+} and Th^{4+} compounds. Because of the small radius of the 4f orbitals the crystal field plays a role only at low temperatures. The room-temperature crystal structures of the Ln compounds are therefore independent of the cation 4f configuration and are determined by the size of these cations only. As the radii of the Ln^{3+} ions vary by less than 20% we cannot expect to find a great variety of structures.

In order to get an idea about compound formation it is useful to compare the electronegativity values: Cs 0.7, Ba 0.9, La 1.1, . . ., Pr 1.2, . . ., Yb 1.1, Lu 1.2, Hf 1.3, . . ., N 3.0, P 2.1, As 2.0, Sb 1.9, Bi 1.85. Thus, bonding in the Ln nitrides is roughly 50% ionic while the bonds in the other pnictides are predominantly covalent. Quite a number of polyanionic compounds are known for the phosphides and arsenides as is seen in table 33.1. Several metallic phases are known for the arsenides, the antimonides and the bismuthides, whereas for the nitrides and the phosphides no phases are known with a cation concentration higher than

TABLE 33.1.

Phases and structure types observed in binary rare earth pnictides. For the Eu and Yb compounds see table 33.2. Phases marked with * contain (also) divalent cations.

	La	Ce	Pr	Nd	Sm	Eu^{3+}	Gd	Tb	Dy	Ho	Y	Er	Tm	Yb^{3+}	Lu
LnN	G	G	G	G	G	G	G	G	G	G	G	G	G	G	G
LnP	G	G	G	G	G	G	G	G	G	G	G	G	G	G	G
LnP_2	H	IH	I	I		*									
LnP_5	O	O	N	N	N		N	N	N	N			N	NP	N
LnP_7	Q	Q	Q			*									
Ln_3As				R											
Ln_5As_3						C*								C*	
Ln_4As_3	F	F	F	F	F	T*								FT*	
LnAs	G	G	G	G	G	GS	G	G	G	G	G	G	G	G	G
$LnAs_2$	IH	I	I	I		*									
Ln_3Sb									A		A				
Ln_2Sb	B	B	B	B	B										
Ln_5Sb_3	C	C	C	C	C	E*	C	C	C	C	C			C*E	
Ln_4Sb_3	F	F	F	F	F*		F	F	F	F	F			F*	
LnSb	G	G	G	G	G		G	G	G	G	G	G	G	G	G
$LnSb_2$	JR	J	J	J	J	*	JK	JK	K	K	K	K	K	L*	K
Ln_3Bi		R		R											
Ln_2Bi	B	B	B	B											
Ln_5Bi_3							D	D	D	D	D	D	D	D*	
$Ln_{5-\delta}Bi_3$	C	C	C	C		E*	C	C							
Ln_4Bi_3	F	F	F	F	F*	F*	F	F	F					F*	
LnBi	G	G	G	G	G		G	G	G	G	G	G	G		G
$LnBi_2$	M	M	M	M		*								*	

A Ti_3P structure
B Ti_2Bi structure
C Mn_5Si_3 structure
D Y_5Bi_3 structure
E anti-U_3S_5 structure
F anti-Th_3P_4 structure
G NaCl structure
H LaP_2 structure
I $NdAs_2$ structure
J $SmSb_2$ structure
K $HoSb_2$ structure
L $ZrSi_2$ structure
M $LaBi_2$ structure
N NdP_5 structure
O LaP_5 structure
P β-YbP_5 structure
Q LaP_7 structure
R unknown structure
S Possibly a high-pressure modification.
T Rhombohedrally distorted Th_3P_4 type.

TABLE 33.2.
The Eu and Yb pnictides in comparison with the alkaline-earth pnictides. Phases marked with * contain partly or exclusively (the NaCl-type phases) trivalent cations.

Ca pnictides	Yb pnictides	Sr pnictides	Eu pnictides	Ba pnictides
Ca_2P†		Sr_2P†	Eu_2P†	Ba_2P†
		Sr_4P_3	Eu_4P_3* (rhomb. anti-Th_3P_4)	Ba_4P_3
Ca_3P_2		Sr_3P_2 (Ce_2S_3 type)	Eu_3P_2 (Ce_2S_3 type)	Ba_3P_2 (Ce_2S_3 type)
		$Sr_{11}P_{10}$ ($Ba_{11}P_{10}$)	$EuP_{0.91}$*	$BaP_{0.9}$
CaP (Na_2O_2 type)	YbP* (NaCl type)	SrP (Na_2O_2 type)	EuP* (NaCl type)	
		Sr_4P_5 (Ba_4P_5 type)	Eu_4P_5*	Ba_4P_5
			$EuP_{1.82}$	$BaP_{1.82}$
		SrP_2	EuP_2	BaP_2 (SrP_2 type?)
CaP_3 (triclinic)		SrP_3 (mon., C2/m)	EuP_3 ($SrAs_3$ type)	BaP_3 (mon., ≠ SrP_3)
		Sr_3P_{14} (mon., $P2_1/c$)		Ba_3P_{14} (Sr_3P_{14} type)
CaP_5	α-YbP_5* (LaP_5 type)			
	β-YbP_5* (mon., $P2_1$)			
			EuP_7 (mon., $P2_1/m$)	BaP_{10} (~TlP_5)
Ca_2As (Ti_2Bi type)†		Sr_2As (Ti_2Bi type)†		Ba_2As (Ti_2Bi type)†
Ca_5As_3 (Mn_5Si_3 type)	Yb_5As_3* (Mn_5Si_3 type)	Sr_5As_3 (Mn_5Si_3 type)	Eu_5As_3 ($Mn_5Si_3 + Ca_5Pb_3$)	Ba_5As_3 (Mn_5Si_3 type)
Ca_3As_2		Sr_3As_2 (Ce_2S_3 type?)	Eu_3As_2 (Ce_2S_3 type)	
	Yb_4As_3 (anti-Th_3P_4 type)		$Eu_{3+x}As_2$ (tetrag.)	
	Yb_4As_3 (rhomboh. def.)		Eu_4As_3* (rhomb. anti-Th_3P_4)	
			Eu_5As_4 (orthorh.)	

			$Eu_{11}As_{10}$ (dist. $Ho_{11}Ge_{10}$)	
CaAs (Na_2O_2 type)	YbAs* (NaCl type)	SrAs (Na_2O_2 type)	EuAs (Na_2O_2 type)	
		Sr_3As_4 (Eu_3As_4 type)	Eu_3As_4 (orthorh.)	Ba_3As_4(Eu_3As_4 type)
Ca_2As_3 (monocl.)		Sr_2As_3 (Ca_2As_3 type)	Eu_2As_3 (Ca_2As_3 type)	
			$EuAs_2$ (orthorh.)	$BaAs_2$
$CaAs_3$ (CaP_3 type)		$SrAs_3$ (mon., C2/m)	$EuAs_3$ ($SrAs_3$ type)	$BaAs_3$
Ca_2Sb (Ti_2Bi type)†		Sr_2Sb (Ti_2Bi type)†	Eu_2Sb*(p) (Ti_2Bi?)	Ba_2Sb (Ti_2Bi type)†
	Yb_5Sb_3(r) (anti-U_3S_5 type) (h) (Mn_5Si_3 type)	Sr_5Sb_3 (Mn_5Si_3 type)	Eu_5Sb_3 (anti-U_3S_5)	Ba_5Sb_3 (Mn_5Si_3 type)
	Yb_4Sb_3* (anti-Th_3P_4 type)			
$Ca_{11}Sb_{10}$ ($Ho_{11}Ge_{10}$ type)	$Yb_{11}Sb_{10}$ ($Ho_{11}Ge_{10}$ type)	$Sr_{11}Sb_{10}$ ($Ho_{11}Ge_{10}$ type)	$Eu_{11}Sb_{10}$ ($Ho_{11}Ge_{10}$ type)	$Ba_{11}Sb_{10}$ ($Ho_{11}Ge_{10}$ type)
	YbSb* (NaCl type)			
		Sr_2Sb_3 (Eu_2Sb_3 type)	Eu_2Sb_3 (monocl.)	
$CaSb_2$ (monocl.)	$YbSb_2$* ($ZrSi_2$ type)	$SrSb_2$ ($CaSb_2$ type)	$EuSb_2$ ($CaSb_2$ type)	
		$SrSb_3$?		$BaSb_3$ ($SrAs_3$ type)
Ca_2Bi (Ti_2Bi type)†		Sr_2Bi (Ti_2Bi type)†		Ba_2Bi (Ti_2Bi type)†
Ca_5Bi_3 (anti-U_3S_5 type)	Yb_5Bi_3 (anti-U_3S_5 type)	Sr_5Bi_3 (anti-U_3S_5 type)	Eu_5Bi_3 (anti-U_3S_5 type)	Ba_5Bi_3 (Mn_5Si_3 type)
	Yb_4Bi_3* (anti-Th_3P_4 type)		Eu_4Bi_3 (anti-Th_3P_4 type)	
$Ca_{11}Bi_{10}$ ($Ho_{11}Ge_{10}$ type)	$Yb_{11}Bi_{10}$ ($Ho_{11}Ge_{10}$ type)	$Sr_{11}Bi_{10}$ ($Ho_{11}Ge_{10}$ type)	$Eu_{11}Bi_{10}$ ($Ho_{11}Ge_{10}$ type)	
	$YbBi_2$		$EuBi_2$ ($YbBi_2$ type)	
$CaBi_3$		$SrBi_3$ (Cu_3Au type)	$EuBi_3$ (Cu_3Au type)	$BaBi_3$ (Ti_3Cu type)

†The reported Ti_2Bi-type phases are in fact oxypnictides M_4X_2O. $Eu_2^{3+}Sb$ and $Eu_2^{3+}Bi$ may occur in the Ti_2Bi structure as pressure modifications. The oxypnictides M_4X_2O with M = Ca, Sr, Ba, Eu^{2+} and X = As, Sb, Bi crystallize in a filled-up Ti_2Bi structure with O in 2(b).

TABLE 33.3.
Enthalpies of formation of lanthanide monopnictides in kcal/mole.

YN	71.5[c]	YAs	77.4[h]	YSb	53.0[f]
LaN	72.0[a,e]	LaAs	73.0[h]		50.0[d]
CeN	78[a]	CeAs	68.9[h]	LaSb	70.8[a]
NdN	73[e]	PrAs	73.4[h]		52.0[d]
LuN	72.2*[e]	NdAs	72.7[h]	NdSb	58.8[d]
		SmAs	72.0[h]	GdSb	65.5[g,a]
YP	73.7*[e]	GdAs	74.4[h]	LuSb	44.7[e]
LaP	72.2*[e]	TbAs	75.0[h]		
LuP	73*[e]	DyAs	78.1[h]	YBi	44.0[f]
		HoAs	72.3[h]	LaBi	53.0[b]
		ErAs	75.6[h]	CeBi	53[d]
		TmAs	72.8[h]	PrBi	47.8[c]
		YbAs	61.8[h]	NdBi	53.2[b]
		LuAs	75.2[h]	DyBi	45[d]

*Calculated values.
[a]Bayanov (1975); [b]Borsese et al. (1974); [c]Borsese et al. (1975); [d]Borsese et al. (1976); [e]Chua and Pratt (1974); [f]Ferro et al. (1974); [g]Goryacheva et al. (1971); [h]Hanks and Faktor (1967).

corresponding to the 1:1 stoichiometry. Eu and Yb frequently occur in the divalent state. Since the effective radii of Eu^{2+} and Yb^{2+} are nearly as large as those of Sr^{2+} and Ca^{2+}, respectively, their pnictides are usually isostructural with their alkaline-earth analogs (table 33.2).

With certain exceptions, such as YbSb, the NaCl-type 1:1 compounds exhibit the highest melting points in the binary phase diagrams. For the Ln nitrides the melting points are between 2400 and 2600°C (LaN 2450°C, CeN 2560°C, PrN 2570°C, NdN 2560°C, GdN 2900°C (Vendl et al., 1976)), those for the phosphides lie in the range 2200–2600°C (2540°C for GdP (Beckenbaugh et al., 1974)), while the LnBi phases melt at temperatures around 1800°C. In table 33.3 we have listed some values for the enthalpies of formation. According to vapor-pressure measurements the thermal stability of the phosphides LnP decreases with increasing atomic number of Ln. The rare earth monophosphides begin to dissociate appreciably above 400°C (Torbov et al., 1971).

2. Preparation of the rare earth pnictides

2.1. *General remarks*

All lanthanide elements react in the solid state with pnigogen vapors. Except for nitrogen the chemical reaction takes place at temperatures below the melting point of the elementary pnigogen and can therefore be performed in fused-silica tubes. The reaction products are microcrystalline powders which usually serve only as starting materials for single-crystal growth. High-quality silica tubes can

be used up to about 1150–1200°C in favorable cases but for most purposes crucibles of glassy carbon, boron nitride, molybdenum, tantalum or tungsten are the only choice. Ln bismuthides can be synthesized by direct reaction and melting of the constituent elements in Ta, Mo and W crucibles whereas tungsten is appropriate for reactions with elementary antimony. Crucible problems can be avoided if the compounds are synthesized in an arc furnace with a cooled copper boat but then one has to take care of the stoichiometry because of evaporating constituents.

2.2. *Crystal growth by transport reactions*

A means of reducing crystal-growth temperatures considerably is the halogen-vapor transport method (Schäfer, 1964). For peritectically-forming compounds transport reactions are the usual way of growing single crystals. Preferentially, fused-silica tubes, either blank or carbonized, are used, but this tube material limits the operation temperatures to below ~1150°C. Typically, a quartz ampoule of 15–30 mm inner diameter and 20–25 cm length contains 1/100–5/100 mole of the prereacted pnictide or the constituent elements. Iodine, bromine or chlorine are added either in elemental form or as BiI_3, $BiBr_3$, SbI_3, etc. (or Pt dihalide locally separated from the charge (Murray and Taylor, 1970)). The ampoule is placed in a temperature gradient. At these low available temperatures the thermodynamic properties of the involved compounds are such that material transport invariably occurs from lower to higher temperatures. Crystal growth of Ln arsenides by iodide-vapor transport occurs as a result of reactions in which volatile ternary iodides are involved (Murray and Taylor, 1970). Temperatures in the range 800–1150°C (upper limit given by the tube material) are necessary for the growth of LnP and LnAs crystals (Hulliger, 1968; Torbov et al.; 1970, and 1974) whereas diarsenides and diantimonides form already when the hot zone is kept as low as 600–900°C (Murray and Taylor, 1970). Thus, on heating $NdAs_2 + I$ in the ratio 1:1 at 670°C NdAs needles up to 5 mm or octahedra formed in the hot zone kept at 800°C (Murray and Taylor, 1970). When excess arsenic was added to the charge ($NdAs_2 + 6As + I$) NdAs was again obtained but, in addition, crystals of the diarsenide grew in the vicinity of the charge at a temperature of only 590°C (Murray and Taylor, 1970). Both modifications of $LaSb_2$ were obtained on variation of the iodine concentration at temperatures around 700°C (Murray and Taylor, 1970). No transport was achieved with chlorine but well-crystallized metallic-looking compounds LaSbCl and La_2SbCl_2 were obtained instead. Similar phases formed with bromine (Murray and Taylor, 1970). Attempts to grow crystals of LaP, LaP_2, CeP and CeP_2 in silica tubes by an iodide transport led to ternary phases $LnSi_xP_y$ (Torbov et al., 1974). Ln polyphosphides, however, crystallize at 500–1100°C when iodine plus traces of sulfur or KI are added (v. Schnering et al., 1975; Wichelhaus and v. Schnering, 1975, 1976).

Usually the growth rates for the iodide-transport reactions performed in silica tubes are rather low. Thus in a favorable case growth of 3 mm octahedra of

DyAs in a 100 cm^3 quartz ampoule with 6 mg/cm^3 iodine in a gradient 900→980°C required three days. Under similar conditions a 10-days run with DyP yielded only octahedra with edge lengths up to 2 mm (Hulliger, 1976). Due to the lower stability of the heavier Ln phosphides (Torbov et al., 1971) halide transport works in fact best for the second half of the Ln elements (we obtained the largest phosphide crystals with Tm (Hulliger, 1976)).

In order to increase the growth speed by operating at higher temperatures the silica tubes have to be replaced by sealed Mo or W tubes (Beckenbaugh et al., 1974; Kaldis, 1974). In the case of the phosphides LnP it turned out that above 2300°C much better results are achieved by a phosphorus pressure transport (Kaldis, 1974). Phosphorus pressures up to 5–10 atm acting against the decomposition of the binary phosphides are generated at high temperatures by decomposing WP. Growth rates comparable to those of fast-growing crystals from the vapor phase, at relatively low apparent supercooling (ΔT = 50–60°C), enabled the growth of large single crystals of GdP, DyP and HoP with cm^3 dimensions (Beckenbaugh et al., 1974; Kaldis, 1974). It is not clear whether crystal growth is due to a transport reaction involving a complex Gd–W–P molecule or a polyphosphide analogous to the polysulfide transport in the case of EuS (Kaldis, 1974).

It is striking that iodide transport of the 1:1 Ln pnictides leads to crystals with octahedral habit whereas crystals grown from the melt or by sublimation or recrystallization invariably are bounded by {100} faces.

Low-temperature crystal growth appears to be feasible also in an appropriate flux material such as perhaps molten tin.

2.3. *Preparation of the nitrides*

Quite a number of processes are known for the preparation of the nitrides but none is fully satisfactory. The big problems are the stoichiometry and the high sensitivity against oxygen and humidity.

Direct reaction of N_2 with liquid Ln metal in an arc furnace, the so-called reactive arc melting, or the reaction with metal sponge at 800–1200°C, leads to dense products with low oxygen contents but poor homogeneity. In order to convert unreacted Ln metal inclusions the products have to be crushed and the procedure is repeated once or twice. This, however, increases the danger of oxygen contamination even if all handling is done under nitrogen. Working at high temperature and elevated N_2 pressure is a means to improve the homogeneity as well as the stoichiometry. Kieffer et al. (1972) were able to prepare stoichiometric nitrides and even N-rich phases LnN_{1+x} at N_2 pressures of either 30 or 1000 atm. The optimal reaction temperature was found to be near the melting point of the Ln metal.

An alternative to solve the diffusion problem is to use very fine Ln powders. The finest powders are prepared chemically by decomposing a relatively unstable Ln compound whose second component evaporates easily. Appropriate compounds are the amalgams and the hydrides. Rare earth amalgams are synthesized by heating metal turnings with mercury at 320°C in a sealed pyrex

tube (Busch et al., 1969; Magyar, 1968). Reactions start between room temperature (La) and 260°C (Sc). However, one drawback of this method is the extreme sensitivity of the amalgams against oxidation which increases the oxygen content of the products. The most reactive amalgams are those of Pr which are more sensitive than a blank surface of a liquid Na–K alloy (Busch et al., 1969).

Hydrides form almost as easily at 400–500°C and decompose at higher temperatures. Reaction of metal turnings in a molybdenum boat takes place with nitrogen at 600°C (Anselin, 1963) or at 900–1000°C (Schumacher and Wallace, 1966). An even faster nitridization is achieved with NH_3 (Kieffer et al., 1972; La Valle, 1962). Reaction temperatures of 600–800°C for La–Sm and 1000–1200°C for Gd–Lu were found necessary for obtaining single phase LnN products (Kieffer et al., 1972).

A related method working for divalent Ln only takes advantage of the solubility of these particular lanthanides in liquid ammonia. On dissolving Eu or Yb metal in liquid NH_3 the initially formed $M(NH_3)_6$ phase transforms slowly to the amide $M(NH_2)_2$ which can be retained on evaporating the ammonia (Hadenfeldt et al., 1970). Above 100°C the amides decompose on heating under vacuum to form the trivalent nitrides EuN and YbN. EuNH and Eu_3N_2 which we expect to be ferromagnetic insulators were never obtained as intermediate phases.

It is to be expected that mononitrides of the trivalent Ln metals form on decomposition of the corresponding amides $Ln(NH_2)_3$ (Juza et al., 1969; Hadenfeldt et al., 1974). The reaction of Eu or Yb ammonia solutions with phosphine, PH_3, leads to $Ln^{2+}(PH_2)_2\ 7NH_3$ and the subsequent thermal decomposition yields EuP and YbP (Howell and Pytlewski, 1970).

Single-crystalline layers of the Ln nitrides (Dismukes et al., 1970) and certainly also of the phosphides and arsenides can be prepared by vapor-phase epitaxial growth. Single-crystal plates of α-Al_2O_3 or $MgAl_2O_4$ and TiO_2, which have similar expansion coefficients, are used as substrates to grow adherent and crackfree ScN and LnN layers (Dismukes et al., 1970 and 1972). Ln metal contained in a carbon or boron nitride boat in zone I of an open carbon-coated silica tube is reacted with HCl in H_2 (or with Cl_2 in He) carrier gas to form a volatile Ln chloride which reacts further in zone II with NH_3 diluted with H_2 (or He) to form the mononitride. Reactions take place at temperatures of 850–950°C. A temperature gradient may (but needs not) be imposed between the source zone I and the decomposition zone II. HBr or HI may be used instead of HCl.

Single-crystal layers of ScP and ScAs were deposited by the same method. PH_3 and AsH_3 were used instead of NH_3 and the substrate was (100) silicon (Yim et al., 1972). For the epitaxial growth of LnP and LnAs layers a more appropriate substrate material has possibly to be chosen. Homogeneous mixed crystals can be grown by simply mixing different vapors (Yim et al., 1972). Reactive sputtering is a variation of the above method.

LnN (Kaldis and Zürcher, 1974) and Ln monopnictide layers can also be prepared by sublimation of powders or crystals. However, the stoichiometry remains a problem in all these vapor-phase methods (Kordis et al., 1972) although the views regarding the homogeneity ranges of the monopnictides are sometimes

contradictory. Finely dispersed metal inclusions may in fact simulate wider homogeneity ranges than would follow from X-ray analysis. A substoichiometric existence range LnN_{1-x} with $x < 0.05$ was found for PrN and $x \sim 0.10$ for HoN and ErN. The vaporization of LaN, CeN, PrN, GdN and TbN is incongruent at 1600°C whereas SmN, HoN, ErN and YbN vaporize congruently (Brown and Clark, 1974b).

3. The NaCl-type Ln pnictides

3.1. *Electronic properties*

The circumstance that the 4f electrons are well localized permits an unambiguous determination of the valence state of the Ln ions. The number of valence electrons engaged in bonding is thus known even in truly metallic phases. In all NaCl-type Ln monopnictides with the exception of CeN and CeP(p) the cation is trivalent. These monopnictides, therefore, are simple valence compounds which one might expect to be non-metallic. Nevertheless, the true conductivity character of the rare earth monopnictides is still the subject of speculation (Güntherodt et al., 1974; Honig, 1969). As an experimental fact all crystalline samples tested up to now exhibited very low resistivities with a metallic temperature dependence (Yaguchi, 1966; Goncharova et al., 1968a, b; Busch et al., 1970; Birgeneau et al., 1971; Wachter, 1972; Kaldis et al., 1975; Andersen et al., 1976; Hulliger, 1976). The Seebeck coefficient in LaSb (Goncharova et al., 1968a), for example, is low and linear in T from 400–1000 K; however, below room temperature one sample was p-type while the second was n-type. Generally, a low thermoelectric power was reported for the other pnictides but, surprisingly, positive and negative Seebeck coefficients were observed for the same compound (Hulliger, 1968). Resistivity measurements up to 500°C on polycrystalline samples of the system EuO-NdN revealed a linear decrease of the activation energy with increasing NdN contents. Samples with more than 22% NdN showed a metallic behavior. Semiconductor-like resistivity behavior was detected on pressed powders of EuN (Didchenko and Gortsema, 1963), GdN (Wachter, 1972) and YbN (Didchenko and Gortsema, 1963) and on films prepared either by evaporation (GdN (Kaldis and Zürcher, 1974), LnP and LnAs (Hulliger, 1976)) or by reactive sputtering (GdP (Hauger and Natterer, 1975)). The phosphide and arsenide films, however, were partly amorphous or rather badly crystallized. Queer enough, the activation energies derived from $\rho(T)$ curves of GdP films (Hauger and Natterer, 1975) match fairly well with the energy gap corresponding to the edge of the window in the optical absorption. These optical windows had been interpreted as a proof for the semiconductor character of these monopnictides, but they were all determined on similar films (Sclar, 1964; Hiscocks and Mullin, 1969; Goncharova et al; 1969). The increase of the absorption towards lower energies (towards 0.6 eV) was thought to be due to the plasma resonance of the free carriers brought in by deviations from

stoichiometry. This increase at energies < 0.7 eV was indeed less pronounced in a GdAs film that had a 100 times larger resistivity (Hulliger, 1976), but the measurements were cut off at 0.5 eV. However, the depth of the absorption windows was the same and this very depth appears to be roughly 10–100 times too weak to warrant a true energy gap. The observed energies, collected in table 33.4 may correspond to transitions from the valence band (originating from anion p-functions) to a conduction band based on cationic $d(e_g)$, s, p-functions since these energies are in line with gaps measured or predicted for the non-transition-element NaCl phases (Pantelides, 1975; Sclar, 1962). The $d(t_{2g})$ band which probably spoils the nonmetallic character of these Ln compounds is situated below the $d(e_g)$, s, p-conduction band so that an eventual gap is considerably smaller than the predicted values (Pantelides, 1975; Sclar, 1962). It seems therefore that most of the Ln monopnictides are semimetals in the crystalline state and semiconductors in the amorphous state. Bond considerations also support the view that these phases are not true metals. As mentioned above these compounds are normal valence compounds, as are the monochalcogenides of Sm, Eu and Yb. Their chemical bonding is in accordance with the Mooser-Pearson rule, so that their failure to be semiconductors can only be due to a weak energy overlap of valence and conduction bands. For PrP_{1-x} a homogeneity region with $x \leqq 0.15$ (Franceschi and Olcese, 1969) and $x \leqq 0.2$

TABLE 33.4.
Band gaps in eV derived from optical absorption of thin films.

YN	1.45*[a]	YP	1.35[c]	CeAs	~0.7[c]	YSb	~1.0[d]
	1.5[b]	CeP	1.1[c]	PrAs	~1.0[c]		0.9–1.0[c]
LaN	0.82*[a]	SmP	1.09[d]	NdAs	1.04[d]	LaSb	0.7–0.8[f]
PrN	1.03*[a]	GdP	1.2[c]	SmAs	1.03[d]	PrSb	0.66[d]
NdN	0.8*[a]		0.8[e]	GdAs	0.63[d]	SmSb	0.59[d]
SmN	0.7*[a]	DyP	1.25[c]		1.1[c]	GdSb	<0.5[c]
EuN	0.76*[a]	HoP	1.1–1.2[c]	TbAs	0.7[c]	TbSb	~0.35[c]
GdN	0.98*[a]	ErP	1.0–1.1[c]	DyAs	~1.0[d]	HoSb	~0.45[c]
	0.85[a]				~0.9[c]		
TbN	0.8[a]			HoAs	~0.8[c]		
DyN	0.91*[a]			TmAs	1.18[d]		
	0.95[b]			YbAs	1.02[d]		
HoN	1.05*[a]						
	0.73[a]						
ErN	1.2*[a]						
	1.3[b]						
TmN	1.1*[a]						
YbN	1.03*[a]						
	1.5[b]						
LuN	1.55*[a]						
	1.6[b]						

*Minimum of absorption power.

[a]Busch et al. (1970). [b]Dismukes et al. (1970). [c]Hulliger (1976). [d]Hiscocks and Mullin (1969). [e]Wachter (1972). [f]Goncharova et al. (1969).

(Torbov et al., 1972) was derived from X-ray measurements. Similarly for SmAs the homogeneity range at 700°C extends from $Sm_{0.98}As_{0.81}$ to $Sm_{0.98}As_{0.98}$; both anion and cation lattice sites are incompletely occupied (Taylor et al., 1974). The observed homogeneity ranges of these phases may be another indication for band overlap. Anion-deficient monopnictides must contain valence electrons in a partly occupied d-band. If there is no energy discontinuity with respect to the stoichiometric compound (i.e. overlapping bands) such anion deficiencies can establish easily.

The electronic contribution to the specific heat $C_{el} = \gamma T$ is proportional to the density of states at the Fermi energy. In order to check whether these NaCl-type phases are metallic we may use the free-electron model to estimate n_e, the number of free electrons per formula unit. The surprisingly high numbers are listed in table 33.5. For comparison we have added the data for the La monochalcogenides as well as for GeTe, SnTe and p-type Ge. The latter is a degenerate semiconductor with 5.4×10^{19} free carriers/cm^3 whereas the former are metals with one conduction electron per La atom. For the chalcogenides we estimate effective masses $m^* \approx 2.5 - 3m$, reflecting a narrow d-band. Needless to say that a high accuracy of the low-temperature specific-heat measurements is required in order to obtain meaningful figures. The experimental uncertainty of Bucher's results is 5–10% (Birgeneau et al., 1973; Bucher, 1976). These specific heat data appear to plead for a fairly metallic character of the tested NaCl-type pnictide samples. For the La, Y and Lu pnictides the specific-heat results could be checked by magnetic-susceptibility measurements. The presently available samples, however, may not yet be sufficiently free from other rare earth impurities to warrant meaningful results.

Energy-band schemes can be derived from optical and photoemission (UPS and above all XPS) measurements. The Kramers–Kronig analysis of the optical-reflectivity spectrum over a large energy range (0.03–12 eV) permitted the evaluation of the relative positions of the various empty and occupied states in the cases of GdN, GdP (Güntherodt and Wachter, 1974a, b) GdSb, GdBi, DyP and HoP (Kaldis et al., 1976). On comparing the dielectric functions of GdP with those of the isoelectronic insulator EuS (Güntherodt and Wachter, 1974a,b) one observes a certain difference due to the fact that in divalent Eu the $4f^7$ level is situated within the gap between valence band and crystal-field split d-bands whereas in GdP the $4f^7$ level lies roughly 6 eV below the Fermi energy and also well below the valence band. The f→d transitions therefore produce more structure in the EuS spectrum. A second difference between the GdP and the EuS spectrum is seen at very low energies. For EuS the imaginary part ϵ_2 becomes zero whereas in GdP it tends to infinity. Moreover, the real part levels off to a finite value in EuS whereas it tends to $-\infty$ in the case of GdP (Güntherodt and Wachter, 1974). This optical behavior of GdP is typical of a material with a high carrier concentration. Assuming that the minimum of ϵ_2 at 0.65 eV corresponds to the onset of interband transitions and that above this energy the contributions of free carriers to ϵ_2 are negligible, the dielectric

TABLE 33.5.

Comparison of the electronic specific heat of the Ln pnictides with those of the metallic (superconducting) La chalcogenides and those of the degenerate narrow-band (superconducting $T_c \leqq 0.4$ K) semiconductors GeTe (rhomboh.) and SnTe (NaCl type) as well as with that of degenerate p-type germanium, Ag and NiS. (n_e = number of conduction elections per formula unit.)

Compound	γ(mJ/K^2 mole)	n_e	m^*/m	Ref.	Compound	γ(mJ/K^2 mole)	n_e	Ref.
LaN	0	0		[a]	p-SnTe (8×10^{20} cm^{-3})	0.94	(−0.05)	[i]
	0.5	0.10	(1)	[b]	$Sn_{0.97}Te$ ($T_c \approx 0.20$ K)	1.1		[j]
	3.5			[c]	$Sn_{0.995}Te$ (2.7×10^{20} cm^{-3})	0.75		[k]
LaP	0.8	0.19	(1)	[d]	$Sn_{0.965}Te$ (1.4×10^{21} cm^{-3})	1.32		[k]
LaAs	~1.0	~0.3	(1)	[e]	p-GeTe (8×10^{19} cm^{-3})	0.554	(−0.004)	[i]
LaSb	0.8	0.12	(1)	[g]	$Ge_{1-x}Te$ ($x = 0.01 \cdots 0.03$)	$1.13 \cdots 1.34$		[m]
LaBi	0.95	0.16	(1)	[g]	$Ge_{0.95}Te$	1.32		[n]
CeN	8.3			[b]	p-Ge (5×10^{19} cm^{-3})	0.022	(−0.002)	[f]
PrN	2.4	(~13)	(1)	[a]	Ag	0.65		[f]
EuN	2.2	(~12)	(1)	[a]	NiS (semimetallic)	0.9		[o]
LuN	0.6	0.33	(1)	[a]	$Ni_{0.95}S$ (metallic)	6.2		[o]
LuP	0.83	0.35	(1)	[d]				
LuSb	0.9	0.26	(1)	[d]				
LuBi	0.9	0.24	(1)	[g]				
YSb	0.9	0.23	(1)	[f]				
LaS	3.28	(1)	2.5	[h]				
LaSe	3.77	(1)	2.7	[h]				
LaTe	4.65	(1)	2.9	[h]				

[a]Stutius (1969b). [b]Lallement and Veyssie (1968). [c]Veyssie et al. (1965). [d]Birgeneau et al. (1973). [e]Hulliger (1976). [f]Gambino et al. (1971). [g]Bucher (1976). [h]Bucher et al. (1975). [i]Bevolo et al. (1976). [j]Mathur et al. (1970). [k]Phillips et al. (1971). [m]Goodman and Marcucci (1966). [n]Finegold (1964). [o]Coey and Brusetti (1975).

functions can be decomposed into contributions from free and bound electrons. From the intersection of $\epsilon_1^{free} = 0$ at 1.53 eV the ratio of free-carrier concentration and optical effective mass is derived. Taking the value $m^* = 1.2\,m$ valid for SmAs, a carrier concentration of $2 \times 10^{21}\,cm^{-3}$ is calculated for a sample with claimed composition $GdP_{0.994}$ (Güntherodt et al., 1974). The lowest value observed in GdP is given as $1 \times 10^{21}\,cm^{-3}$ which is about the same as that reported for SmAs but about a factor of 20 (70?) smaller than in metallic GdS. However, this lowest value still corresponds to about 0.046 carriers per Gd atom. The authors (Güntherodt et al., 1974) propose an intrinsically semi-metallic character of GdP due to an overlap of the 5d conduction band at the X point of the Brillouin zone with the maximum of the valence band at point Γ. (If the $d(t_{2g})$ band would not overlap or just touch the valence band then the minimum concentration would correspond to $GdP_{0.985}$.)

High-resolution XPS measurements of Baer (1976) confirm the gross features of the above interpretation of the reflectivity data. The Fermi energy E_F is located ~0.6 eV above the edge of the valence band but energy states up to E_F appear to be occupied. Unfortunately the resolution is not sufficient to decide whether the valence band really overlaps with the $d(t_{2g})$ band or whether the valence band is simply smeared out by states due to defects. In the former case we deduce from the XPS curve that the GdP sample was anion deficient since in a stoichiometric semimetal the Fermi energy should lie closely below but not above the edge of the valence band.

A very similar photoemission spectrum was published for GdSb (Gambino et al., 1971). The reports of Campagna et al. (1974, 1975) show the XPS spectra of LaSb ... NdSb, SmSb, GdSb ... TmSb as well as a diagram with the photo-ionization energies of 4f electrons relative to E_F. Since these energies are of importance for the magnetic coupling we reproduce the diagram in fig. 33.1.

If in GdP the valence band overlaps only slightly with the $d(t_{2g})$ band one may hope to find other Ln monopnictides where no overlap takes place. On going from La to Lu the d-bands become slightly broader as a consequence of the decreasing lattice constants but the $t_{2g} - e_g$ splitting decreases as $\langle r_d^4 \rangle / a^5$. On

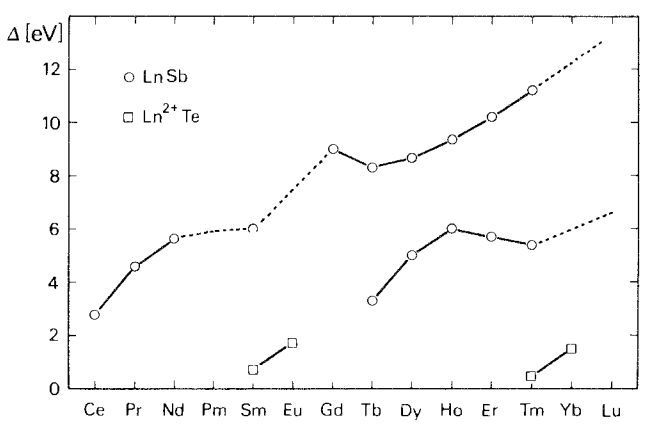

Fig. 33.1. Photo-ionization energies Δ of 4f electrons relative to the Fermi energy E_F.

varying only the anion from N to Bi the decrease of the d-band splitting is proportional to a^{-5}. At the same time the valence band based on anionic bonding p states becomes narrower (and the filled nonbonding anion s bands, being absent in the optical band picture but showing up in the XPS diagram, moves to lower energies) but the gap between valence band and conduction band based on cationic d(e_g),s,p antibonding states decreases as well. Possibly YbN is really such a pnictide with separated energy bands.

Based on optical measurements the NaCl-type Sc pnictides ScN (Dismukes et al., 1970), ScP and ScAs (Yim et al., 1972) were also reported to be semiconductors. Unfortunately it is impossible to derive meaningful values for the energy gaps of the Ln compounds by extrapolation from isoelectronic series:

KF(10.9 eV) → CaO(~7 eV) → ScN(2.0 or 0.1[a] eV?) → TiC(metal)

RbF(10.4 eV) → SrO(5.7 eV) → YN(?) → ZrC(metal)

CsF(10 eV) → BaO(4.9 eV) → LuN(?) → HfC(metal)

KCl(8.9 eV) → CaS(5.8 eV) → ScP(1.2 eV?)

BaS(3.9 eV) → LaP(?)

EuS(>2 eV) → GdP(semimetal?)

The Ti-group carbides are definitely metallic since there the carbon 2s electron is also engaged in bonding.

Although the energy gaps are not known for most members of the following group of nitrides and phosphides one is tempted to deduce nonmetallic properties at least for LuN:

Cs_3N(semicond.) → Ba_3N_2(semicond.?) → LuN(?) → Hf_3N_4(?) → Ta_3N_5(~2 eV)

Cs_3P(semicond.) → Ba_3P_2(semicond.) → LuP(?) → Hf_3P_4(nonexist.) → Ta_3P_5(nonexist.)

Cs_3Sb(1.6 eV) → Ba_3Sb_2(semicond.) → LuSb(?)

Cs_3Bi(0.55 eV).

Recently Hasegawa and Yanase (1977) presented energy-band calculations for the Gd pnictides. They used the APW method and found that the energy bands depend sensitively on the choice of the one-electron potential. The self-consistently calculated bands account qualitatively well for the semiconductivity suggested for GdN (Kaldis and Zürcher, 1974), the semimetallic behavior of GdP (Kaldis et al., 1975; Güntherodt et al., 1974) and the metallic properties of GdSb (Gambino et al., 1971). An energy gap of about 1 eV is suggested for GdN in the paramagnetic state, while a band overlap might occur in the ferromagnetic state. These band structure calculations thus give similar results as those of Switendick and Jones (1968) for ScN, ScP and ScAs.

[a]Weinberger et al. (1971).

3.2. *Uncommon valences*

As mentioned above CeN and CeP(p) are the only monopnictides in which the cation has a valence higher than +3. The 4f ionization energy increases so rapidly with the ionic charge that a +4 valence is possible only in certain favorable cases. For the pnictides cerium is the only rare earth cation in which the 4f energy lies close enough to the Fermi energy. In the brass-colored CeN cerium is nearly tetravalent already at normal pressure and room temperature. At high temperatures it converts back to the trivalent state as can be deduced from the temperature depence of the magnetic susceptibility (Danan et al., 1969) and of the lattice parameter (von Essen and Klemm, 1962). A similar transition was assumed to take place at low temperatures also in CeP and CeAs (Tsuchida and Wallace, 1965; Busch and Vogt, 1966; Tsuchida et al., 1970) but this opinion was disproved by Knight-shift measurements (Myers and Narath, 1973). In fact a pressure of ~100 kbar is required at room temperature to achieve the electronic transition in CeP (Jayaraman et al., 1976). Thereby its color changes from silvery grey to purple. In analogy to the Eu^{2+} chalcogenides it is expected that the pressure necessary to enforce the valence transition $Ce^{3+} \rightarrow Ce^{4+}$ in CeAs, CeSb and CeBi is distinctly higher and increases in this sequence. From their compressibility data Bartholin et al. (1977) estimate transition pressures of 180 and 300 kbar for CeAs and CeSb, resp. For CeBi we extrapolate to 325 kbar.

It is not surprising that pressures up to 220 kbar were insufficient to induce the transition in TbP (Jayaraman et al., 1976). In DyP and HoP the partially-filled 4f half shell is already 4 eV below the Fermi energy (Kaldis et al., 1976) and it will be still some eV below E_F even in TbN, the best case of the second half of the series of Ln compounds. We wonder whether PrN might undergo the valence transition at accessible pressures.

In fig. 33.2 we have plotted the lattice constants of the LnN phases versus the radii of the Ln^{3+} and Ln^{4+} ions, respectively. It is interesting to note the slight (ionicity-induced?) curvature in the plot which is even more pronounced in the case of the LnSb and LnBi phases. For CeN the contraction of the cell with regard to hypothetical $Ce^{3+}N$ is $\Delta a \sim -0.19$ Å and about the same for CeP, $\Delta a \approx -0.18$ Å. This contraction, however, appears to be slightly less than expected for truly tetravalent CeN (and CeP(p)). The difference is a consequence of valence fluctuations, i.e. the metallic CeN and CeP(p) are expected to be homogeneous mixed-valence compounds. The special position of the Fermi level within the narrow f-peak of the density-of-states curve (cf. recent XPS measurements of Baer and Zürcher, 1977) then accounts for the positive Seebeck coefficient.

In the fully-tetravalent state CeN and CeP(p) have the same valence-electron configuration as the NaCl-type superconductors ZrN, ZrP(h), HfN, ThN, ThP, YS, LaS, LuS, etc. By analogy we argued that CeN (Hulliger, 1968) and CeP(p) (Hulliger and Hull, 1970) might also show a transition to the superconductive state near 1 K. On our CeN samples, however, we were not able to detect a transition neither under a pressure of 25 kbar down to 1.2 K nor at normal

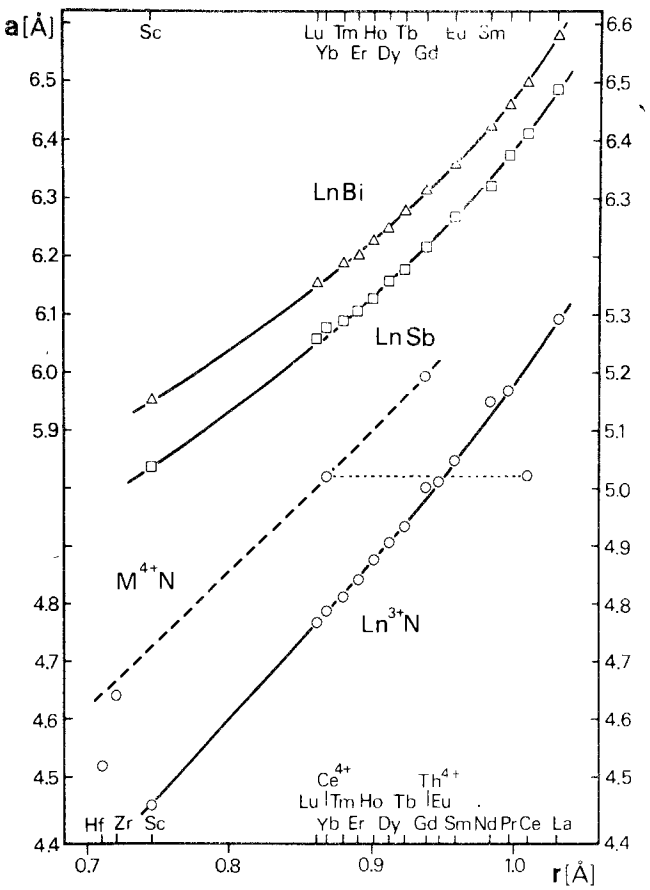

Fig. 33.2. Room-temperature lattice constants of NaCl-type pnictides versus cation radii (ionic radii given by Shannon, 1976).

pressure down to 0.03 K (Hulliger and Ott, 1976). The transition temperature might however strongly depend on stoichiometry ($\rightarrow Ce^{3+}$) and other rare earth impurities (von Essen and Klemm, 1962; Didchenko and Gortsema, 1963; Anselin et al., 1965). We would be curious about the concentration dependence of T_c of stoichiometric mixed nitrides (Zr, Ce)N, (Hf, Ce)N and (Th, Ce)N. The extremely high value reported for the electronic specific heat of CeN (table 33.5) seems to support our view of a homogeneous mixed-valence system or else it may be an indication for superconductivity rather than in the case of LaN. If the interpretation of the specific-heat and magnetic-susceptibility data of LaN is correct, then its superconductivity may be due to a considerable anion deficiency. LaN_{1-x} may behave like off-stoichiometric SnTe. A quite realistic value $x = 0.05$ corresponds already to 0.15 excess valence electrons per formula or 4×10^{21} free carriers per cm^3. Nominally stoichiometric LaP and LaBi were found to be normal down to 0.015 K (Bucher, 1976). We checked LaSb and LaBi samples down to 0.08 K without observing a transition to superconductivity (Hulliger and Ott, 1976).

3.3. *Low-temperature properties*

In this section we treat some physical properties of the NaCl-type compounds that reflect the influence of the crystal electric field on the energy of the J ground state of the cationic $4f^n$ levels. Due to the small radius of the 4f orbitals the crystal field of the anion neighbors acts as a small perturbation only. At room temperature no particular f orbitals are favored so that the crystal structure, for instance, is determined by the cation size only. Below say 100 K the influence of the crystal field on the physical properties becomes evident. In contrast to certain rare earth phosphates, arsenates and vanadates, however, crystal-structure distortions never occur due to the Jahn–Teller effect alone but are always coupled with a magnetic transition, that is, the structural changes are due to a magnetostrictive effect. However, the crystal field influences and may even inhibit magnetic transitions as in the case of certain Tm compounds.

3.3.1. *The crystal field*

The crystal field is something like a mystery and therefore it is commonly called the effective crystal field. Strictly speaking the crystal electric field acting on the open-shell electrons of a paramagnetic ion is basically due to the electrostatic field generated by the remaining ions of the crystal. Thus the 4f electrons possess an electrostatic potential energy that may be expanded in terms of spherical harmonics

$$V_c = \sum_{n,m} \beta_{n,m} \langle r_f^n \rangle \sum_i Y_{nm}(\theta_i, \varphi_i), \tag{33.1}$$

where $\boldsymbol{r} = (r_i, \theta_i, \varphi_i)$ are the positions of the 4f electrons, $\langle r_f^n \rangle = \langle R | r_f^n | R \rangle$ with R = radial part of the 4f wave functions, and the coefficients β_{nm} are determined by the charge distribution. The point symmetry of the Ln lattice sites and the orbital angular momentum of the individual open-shell electrons limit the number of terms in the expansion. For f electrons in cubic symmetry the electrostatic potential is fully described by a sum of polynomials of fourth and sixth degree. This simple electrostatic model has two attractive features. Assuming point charges on the neighboring anions the parameters and hence the J splitting can be exactly calculated (Hutchings, 1964). More generally, it provides a method of parametrizing the experimental data in terms of the quantities $\beta_{nm}\langle r_f^n \rangle$ (Newman, 1971). This procedure is a means to include all the unknown electronic effects such as overlap between the 4f wave functions of the Ln ion and the valence electrons of the anions, configuration mixing of the f^n states with states from excited configurations as well as covalency and other effects which apparently can dominate the observed crystal-field parameters (compare table 12 of Newman, 1971).

With Stevens' operator equivalents technique (where one replaces the terms in the expansion of the electrostatic potential by suitable angular-momentum operators) the potential energy of the 4f electrons with the polar axis J_z along

[100] of a cubic crystal is given by

$$V_c = A_4\langle r_f^4\rangle \beta_J (O_4^0 + 5\,O_4^4) + A_6\langle r_f^6\rangle \gamma_J (O_6^0 - 21\,O_6^4) \tag{33.2}$$

where the A_n are coefficients determining the energy scale of the J splitting, $\langle r_f^n\rangle$ is the nth moment of the distribution of the 4f electrons, β_J and γ_J are reduced matrix elements and O_n^m are the Stevens operator equivalents. It is customary also to use the terms introduced by Lea, Leask and Wolf (1962) who rewrote the potential as

$$V_c = W\left\{x\,\frac{O_4}{F(4)} + (1-|x|)\,\frac{O_6}{F(6)}\right\}, \tag{33.3}$$

with

$$Wx = A_4\langle r_f^4\rangle \beta_J F(4); \qquad W(1-|x|) = A_6\langle r_f^6\rangle \gamma_J F(6), \; |x| \leqq 1.$$

By diagonalizing the crystal-field Hamiltonian the eigenvalues and eigenfunctions are obtained with x as a parameter. Lea et al. (1962) have calculated them for $J = 2$ through $J = 8$. For the NaCl-type compounds, where each Ln ion is coordinated by an octahedron of six anions with charges Ze, the point-charge model leads to

$$A_4\langle r_f^4\rangle = 14\,e^2\,\frac{Z\langle r_f^4\rangle}{a^5}; \qquad A_6\langle r_f^6\rangle = 6\,e^2\,\frac{Z\langle r_f^6\rangle}{a^7} \tag{33.4}$$

if the more distant neighbors are neglected. (If the cation neighbors are included one has to replace $Z(X)$ by $Z(X) - (2\sqrt{2}-1)Z(\mathrm{Ln})/32$ for $A_4\langle r_f^4\rangle$ and by $Z(X) - (13\sqrt{2}-1)Z(\mathrm{Ln})/128$ for $A_6\langle r_f^6\rangle$. Assuming $Z(\mathrm{Ln}) \approx -Z(\mathrm{X})$ this means an increase of $A_4\langle r_f^4\rangle$ by 5.7% and of $A_6\langle r_f^6\rangle$ by 14% for TmSb (Birgeneau et al., 1971). If all neighbors are taken into account then the two crystal-field parameters are increased by a factor of about 1.05 and 1.3, respectively, as was exemplified by Erdös and Kang (1972) for PrSb and TmSb). Hartree–Fock values for $\langle r_f^4\rangle$ and $\langle r_f^6\rangle$ of all Ln ions have been calculated by Freeman and Watson (1965). These values are some 10–20% larger than those calculated by Wakim et al. (1972) using analytical self-consistent-field wave functions, but smaller than those obtained by Lewis (1971) using relativistic Dirac–Slater wave functions. For Gd^{3+}, for example, the three different methods give $\langle r_f^4\rangle = 1.515$, 1.254 and 2.48 a.u. while more recent relativistic Dirac–Fock calculations (Freeman and Desclaux, 1972) give $\langle r_f^4\rangle = 1.78$ a.u. The values for $\langle r^4\rangle$ and $\langle r^6\rangle$ as well as for β_J and γ_J are calculated for free ions, thus without taking into account the change of the charge distribution in the 4f shell due to the crystal field. This may lead to an incorrect ratio of the fourth- to sixth-order term.

Since most of the physical properties at low temperatures are modified by the crystal field, knowledge of the crystal-field parameters is rather important. Until recently these parameters have been derived from integral effects like specific heat and magnetic susceptibility. Direct information about the crystal-field-split energy levels can, however, be obtained by spectroscopic methods. For metallic compounds neutron spectroscopy plays a key role. We have made an attempt to collect the presently known data in table 33.6. We abstained from making a

TABLE 33.6.
Crystal-field data of the NaCl-type Ln pnictides. Data in *italics* are calculated according to the point-charge model while the experimental data are given in roman printing.

$J = \frac{5}{2}$	$a_{\sim 30\,K}$(Å)	$\Delta = E(\Gamma_7 \rightarrow \Gamma_8) = 6W$(K)
Ce^{3+} in LaN	5.29	*350Z*
CeP	5.90	*203Z*
		200[1,2], 160–170[3], 135[4], 146[5], 168[6], 161[7], 172[8], 157[20]
CeAs	6.06	*177Z*
		141[4], 140[9], 150[6], 158[10], 154[20] (12 K:159; 77 K:151; 160 K:140; 293 K:138[56])
Ce^{3+} in LaSb	6.48	ground state: Γ_7[11]
CeSb	6.40	*135Z*
		17(<25)[9], 20[3], 24[12], 34[20], ≦35[13], 38[8], 39[10], 37[64]
$Ce_{0.5}Y_{0.5}Sb$	6.28	20–29[14]
$Ce_{0.3}Y_{0.7}Sb$	6.23	30[58]
$Ce_{0.1}(Y, La)_{0.9}Sb$		~20[14]
$Ce_{0.2}La_{0.8}Sb$	6.46	35[58]
CeBi	6.49	*126Z*
		20.6[3], 4.0[5], ≦20[13], 9[10], 8[64]
(Ce, La)Bi		20[15]
SmN	5.035	*96.9Z*
		225[16]
SmP	5.75	*49.9Z*
		130[17,18,21], 200[19], 93[5], 92[20]
SmAs	5.91	*43.5Z*
		118[21], 89[20]
SmSb	6.26	*32.6Z*
		122[21], 65[65], 77[20]
SmBi	6.35	*30.4Z*
		121[21], 83[20]

$J=\frac{9}{2}$	$a_{30\,K}$(Å)	x	W(K)	$A_4\langle r_f^4\rangle$(K)	$A_6\langle r_f^6\rangle$(K)	$E(\Gamma_8^{(2)}\rightarrow\Gamma_6)$(K)	$E(\Gamma_8^{(2)}\rightarrow\Gamma_8^{(1)})$(K)	Z_4	Refs.
NdN	5.14	*0.886*	*−2.42Z*	*− 123Z*	*2.9Z*	*−17.0Z*	*132Z*		
		1					234		22
		0.9	−7.4	383	7.8	−64	406		23
		0.78	−8.4	373	19	56	467	3.1	24
NdP	5.826	*0.909*	*−1.26Z*	*65.7Z*	*1.2Z*	*−12.7Z*	*68.7Z*		
		0.75	−3.08	132	8.0	34	172	2.0	5
		0.765	−3.03	132	7.4	33	169	2.0	25
NdAs	5.958	*0.913*	*−1.12Z*	*58.7Z*	*1.0Z*	*−11.8Z*	*61.2Z*		
		0.766	−2.82	123	6.85	30	157	2.1	25
NdSb	6.31	*0.921*	*−0.84Z*	*44.1Z*	*0.7Z*	*−9.8Z*	*45.4Z*		
		0.783	−1.87	83.6	4.2	14	103	1.9	25
		0.76	−1.82	79.8	4.5	18	103	1.8	26
						18	117		20
NdBi	6.41	*0.942*	*−0.77Z*	*40.7Z*	*0.6Z*	*−9.2Z*	*41.8Z*		
		0.685	−1.87	73.5	6.2	37.1	105.5	1.8	5

$J=\frac{7}{2}$	$a_{30\,K}$(Å)	x	W(K)	$A_4\langle r_f^4\rangle$(K)	$A_6\langle r_f^6\rangle$(K)	$E(\Gamma_6-\Gamma_8)$K	$E(\Gamma_6-\Gamma_7)$K	Z_4	Refs.
YbN	4.775	*−0.970*	*7.58Z*	*70.9Z*	*1.2Z*	*96.4Z*	*237Z*		
		−1	37.5	361	~0	450	1200	4.9	16
		−0.8					875		19,27
YbP	5.543	*−0.978*	*3.58Z*	*33.7Z*	*0.43Z*	*44.8Z*	*112.5Z*		
		−0.804	13.31	103	14	222	363	3.06	5
		−0.8					400–500		19,27
						280			2
YbAs	5.69	*−0.979*	*3.13Z*	*29.5Z*	*0.35Z*	*39.2Z*	*98.7Z*		
		−0.8					400–500		19,27
YbSb	6.067	*−0.981*	*2.27Z*	*21.4Z*	*0.23Z*	*28.2Z*	*71.6Z*		
(La, Yb)Sb	6.48	Γ_6 ground state							

TABLE 33.6 (*Contd.*)

$J=4$	a_{30K}(Å)	x	W(K)	$A_4\langle r_f^4\rangle$ (K)	$A_6\langle r_f^6\rangle$ (K)	$E(\Gamma_1\rightarrow\Gamma_4)$ (K)	$E(\Gamma_1\rightarrow\Gamma_3)$ (K)	$E(\Gamma_1\rightarrow\Gamma_5)$ (K)	Z_4	Refs.
PrN	5.06	*−0.956*	*7.20Z*	*156Z*	*4.08Z*	*123Z*	*210Z*	*390Z*		
		−0.8	7.4			104	178	400		19,27
		−1	20.4	462	~0	285	489	1100	3.0	16
		−1						~240(?)		29
		−0.97	19.5	429	7.6	313	537	1055	2.75	30
						316				31,32
								1062		59
PrP	5.893	*−0.968*	*3.32Z*	*72.9Z*	*1.40Z*	*54Z*	*92.6Z*	*180Z*		
		−0.8	2.8			39	67	150		19
		−1	9.7	220	0	136	232	523		21
						136				2
		−0.955	7.38	160	4.3	126	217	400	2.2	5,33
		−0.944	7.43	159	5.45	133	229	404		31,34
		−1				128				11
		−0.8								54
		−1	9.45	214	0	132	226	509		57
PrAs	6.018	*−0.969*	*2.99Z*	*65.6Z*	*1.21Z*	*48.3Z*	*82.8Z*	*161.7Z*		
		−0.95	6.8	146	4.5	120	205	369		31,34

		−0.8	2.7					150	[19, 27]
		−0.955	6.59	142.7	4.1	133	194	433	2.2 [35]
		−1	9.1	206	0	127	218	491	[21]
		−1				115			[11]
PrSb	6.364	*−0.972*	*2.25Z*	*49.6Z*	*0.82Z*	*35.9Z*	*61.6Z*	*121.9Z*	
		−0.8	1.8					100	[19, 27]
								226	[36]
		−1	5.2			73	125	280	[37]
						74			[31]
		−0.966	4.40	96.3	2.0	72	124	238	1.9 [35]
				99.8	2.0				[34]
		−1				73			[11]
		−0.8				65			[54]
PrBi	6.448	*−0.973*	*2.11Z*	*46.5Z*	*0.75Z*	*33.5Z*	*57.4Z*	*114.0Z*	
						52		202	[36]
						73	125	280	[37]
						62			[31]
		−0.94	3.74	79.9	2.8	67	115	203	1.7 [38]
		−0.943	3.75	80	2.8	67.5	116	204	1.7 [35]
		−1				67			[11]
		−0.8				65			[54]
$La_{1-x}Pr_xBi$	~6.56							220	[37]

TABLE 33.6 (*Contd.*)

$J = 6$	a_{30K} (Å)	x	W(K)	$A_4\langle r_f^4\rangle$ (K)	$A_6\langle r_f^6\rangle$ (K)	$E(\Gamma_1 \to \Gamma_4)$ (K)	$E(\Gamma_1 \to \Gamma_5^{(2)})$ (K)	$E(\Gamma_1 \to \Gamma_2)$ (K)	$E(\Gamma_1 \to \Gamma_5^{(1)})$ (K)	$E(\Gamma_1 \to \Gamma_3)$ (K)	Z_4	Refs.
TbN	4.922	*−0.978*	*−0.68Z*	*90.2Z*	*1.79Z*	*20.0Z*	*42.8Z*	*124.7Z*	*151.7Z*	*159.9Z*		
		−1	−2.1							500	3.1	[16]
		−1	−1.5							350		[19]
TbP	5.675	*−0.983*	*−0.33Z*	*44.2Z*	*0.66Z*	*9.8Z*	*20.9Z*	*61.5Z*	*74.4Z*	*78.4Z*		
		−1	−0.55	74	0	16	35	105	124	131	1.7	[5]
TbAs	5.815	*−0.984*	*−0.29Z*	*39.2Z*	*0.57Z*	*8.7Z*	*18.5Z*	*54.5Z*	*65.8Z*	*69.4Z*		
						~16	~35					[39]
TbSb	6.17	*−0.986*	*−0.22Z*	*29.1Z*	*0.37Z*	*6.4Z*	*13.8Z*	*40.6Z*	*48.9Z*	*51.5Z*		
		−1	−0.48	65	0	14	31	92	109	115	2.2	[40]
		−1	−0.4			11.9						[41]
TbBi	6.27	*−0.986*	*−0.20Z*	*26.9Z*	*0.33Z*	*5.9Z*	*12.7Z*	*37.5Z*	*45.1Z*	*47.6Z*		
TmN	4.80	*−0.928*	*−0.81Z*	*76.8Z*	*1.37Z*	*23.1Z*	*49.9Z*	*135.5Z*	*174.5Z*	*184.8Z*		
		−1	−2.97	303	0	89	190	570	677	713		[42]
		−1	−3.13	319	0	94	200	600	713	750	4.2	[27]
		−1	−3.90	399	0	117	250	750	890	937		[29]
		−0.990	−3.47	351	0.82	103	222	654	785	827	4.6	[43]
		−1	−3.4	349	0	103	218	656	779	820	4.2	[16]
		−0.847	−3.48	300.6	12.5	93	204	480	694	741	3.9	[44]
						100						[32]
		−1	−4.0	408	0	120	256	768	912	960		[54]

TmP	5.56	*−0.946*	*−0.38Z*	*36.8Z*	*0.49Z*	*11.0Z*	*23.7Z*	*66.0Z*	*83.2Z*	*88.0Z*		
		−1	−1.25	128	0	38	80	240	285	300		19, 27
						28						2
		−0.80	−1.27	104	5.9	33	73	156	244	262	2.8	5
		−1	−1.02	104	0	31	65	195	232	244		21
		−1	−1.0	102	0	30	64	192	228	240		11, 54
TmAs	5.71	*−0.948*	*−0.33Z*	*32.3Z*	*0.41Z*	*9.6Z*	*20.7Z*	*57.9Z*	*72.8Z*	*76.9Z*		
										275		42
		−1	−1.04	106	0	31	67	200	238	250		19, 27
		−0.79	−1.23	99.2	6.2	31	70	145	233	250	3.1	45
		−1	−0.93	95.3	0	28	60	179	213	224		11, 54
										284		21
		−1	−1.141	116.5	0	34	73	219	260	274		61
TmSb	6.08	*−0.954*	*−0.24Z*	*23.6Z*	*0.26Z*	*7.0Z*	*15.1Z*	*42.6Z*	*53.1Z*	*56.1Z*		
		−1	−0.83	85	0	25	53	160	190	200		11, 19, 27, 54
		−1	−0.938	95.7	0	28	60	180	214	225		42, 61
		−1	−0.887	90.6	0	26.6	56.7	170	202	213	3.8	46, 47
		−0.785	−0.993	79.0	5.1	25	55.7	115	187	201	3.3	35, 48
		−0.80	−1.015	82.9	4.8	26.0	57.8	123	194	208	3.5(~2)*	49
						26.5						31
							55					55
TmBi	6.18	*−0.956*	*−0.22Z*	*21.7Z*	*0.23Z*	*6.5Z*	*13.9Z*	*39.3Z*	*48.9Z*	*51.7Z*		
		−0.81	−0.854	70.7	3.8	22	49	107	165	176	3.3	45
							45					55

*Using the experimental $\langle r_t^4 \rangle$ integral derived from polarized-neutron studies of the magnetic form factor of Tm metal.

TABLE 33.6 (*Contd.*)

$J=\frac{15}{2}$	$a_{30\,K}$(Å)	x	W(K)	$A_4\langle r_f^4\rangle$ (K)	$A_6\langle r_f^6\rangle$ (K)	$E(\Gamma_6\rightarrow\Gamma_8^{(1)})$ (K)	$E(\Gamma_6\rightarrow\Gamma_7)$ (K)	$E(\Gamma_6\rightarrow\Gamma_8^{(2)})$ (K)	$E(\Gamma_6\rightarrow\Gamma_8^{(3)})$ (K)	Z_4	Refs.
DyN	4.895	*−0.928*	*0.33Z*	*86.3Z*	*1.67Z*	*10.6Z*	*91.6Z*	*136.5Z*	*171.5Z*		
		−1 or −0.6							600		16
		−0.8	1.3	294	18	52	263	487	600	3.4	19,27
		−0.8	1.6	370	23	65	329	609	750	4.3	23
DyP	5.643	*−0.945*	*0.16Z*	*42.4Z*	*0.62Z*	*5.0Z*	*45.8Z*	*66.7Z*	*84.0Z*		
		−0.88	0.37	92	3	13.6	93	148	184	2.2	guess
DyAs	5.79	*−0.947*	*0.14Z*	*37.3Z*	*0.52Z*	*4.3Z*	*40.4Z*	*58.6Z*	*73.8Z*		
DySb	6.14	*−0.953*	*0.10Z*	*27.6Z*	*0.33Z*	*3.1Z*	*30.0Z*	*43.3Z*	*54.5Z*		
		−0.835	0.366	86	4.2	14.5	80.5	141	175	3.1	50
		~−1	0.27	76	~0				149		51
		−0.88	0.24	60	2	9	60.5	96	120	2.2	63
(La, Dy)Sb	6.48		Γ_6 ground state								28
DyBi	6.24	*−0.954*	*0.095Z*	*25.6Z*	*0.31Z*	*2.9Z*	*28.0Z*	*40.2Z*	*50.7Z*		

$J=\frac{15}{2}$	$a_{30\,K}$(Å)	x	W(K)	$A_4\langle r_f^4\rangle$ (K)	$A_6\langle r_f^6\rangle$ (K)	$E(\Gamma_8^{(1)}\rightarrow\Gamma_8^{(2)})$ (K)	$E(\Gamma_8^{(1)}\rightarrow\Gamma_7)$ (K)	$E(\Gamma_8^{(1)}\rightarrow\Gamma_8^{(3)})$ (K)	$E(\Gamma_8^{(1)}\rightarrow\Gamma_6)$ (K)	Z_4	Refs.
ErN	4.83	*0.836*	*0.25Z*	*78.6Z*	*1.43Z*	*23.8Z*	*34.5Z*	*112.4Z*	*112.6Z*		
		1							1500		16
		0.6							500		16
ErP	5.595	*0.873*	*0.12Z*	*37.7Z*	*0.51Z*	*11.5Z*	*18.2Z*	*53.5Z*	*54.3Z*		
		0.75	0.47	131	4.1	40	42	195	187	3.5	51
ErAs	5.734	*0.878*	*0.10Z*	*33.4Z*	*0.43Z*	*10.5Z*	*16.3Z*	*47.2Z*	*48.1Z*		
ErSb	6.095	*0.891*	*0.074Z*	*24.6Z*	*0.28Z*	*7.5Z*	*12.4Z*	*34.7Z*	*35.5Z*		
		0.78	0.366	106	2.9	34	38	155	151	4.3	52,60

(Lu, Er)Sb	6.05	0.77		$34A_6\langle r_f^6\rangle$									[28]
(Lu, Er)Bi	6.15	0.81		$46A_6\langle r_f^6\rangle$									[28]
(La, Er)Sb	6.48	0.783		$39A_6\langle r_f^6\rangle$									[28]
(La, Er)Bi	6.57	0.83		$54A_6\langle r_f^6\rangle$									[28]
ErBi	6.19	*0.894*	*0.068Z*	*22.7Z*	*0.25Z*	*6.9Z*	*11.6Z*	*32.1Z*	*32.9Z*				

$J = 8$	a_{30K}(Å)	x	W(K)	$A_4\langle r_f^4\rangle$ (K)	$A_6\langle r_f^6\rangle$ (K)	$E(\Gamma_1 \to \Gamma_4^{(2)})$ (K)	$E(\Gamma_1 \to \Gamma_3^{(2)})$ (K)	$E(\Gamma_1 \to \Gamma_5^{(2)})$ (K)	$E(\Gamma_1 \to \Gamma_4^{(1)})$ (K)	$E(\Gamma_1 \to \Gamma_3^{(1)})$ (K)	$E(\Gamma_1 \to \Gamma_5^{(1)})$ (K)	Z_4	Refs.
HoN	4.865	*0.856*	*−0.19Z*	*82.1Z*	*1.54Z*	*0.07Z*	*−0.004Z*	*78.2Z*	*86.4Z*	*110.9Z*	*115.3Z*		
		1									450		[19]
		1									550		[16]
		0.80	0.70	279	7.8				~300		380	3.4	[24]
HoP	5.615	*0.888*	*−0.09Z*	*40.1Z*	*0.56Z*	*0.60Z*	*0.85Z*	*37.1Z*	*42.9Z*	*54.4Z*	*56.8Z*		
		0.76	0.29	110	3.9	−6.5	−9.3	117	111	148	150	2.75	[5]
		0.75	0.29	108	4.0	−7.0	−10.0	115.4	108	145	147	2.7	[53]
HoAs	5.76	*0.893*	*−0.08Z*	*35.3Z*	*0.47Z*	*0.60Z*	*0.85Z*	*32.5Z*	*37.8Z*	*47.9Z*	*50.0Z*		
HoSb	6.12	*0.904*	*−0.06Z*	*26.1Z*	*0.31Z*	*0.55Z*	*0.80Z*	*23.8Z*	*28.1Z*	*35.4Z*	*37.0Z*		
				(81)	(4.6)								[65]
HoBi	6.215	*0.907*	*−0.05Z*	*24.1Z*	*0.28Z*	*0.53Z*	*0.78Z*	*22.0Z*	*26.0Z*	*32.8Z*	*34.3Z*		

[1]Jones (1966); [2]Myers and Narath (1974); [3]Wang and Cooper (1970); [4]Furrer et al. (1972); [5]Birgeneau et al. (1973); [6]Aeby et al. (1973); [7]Heer et al. (1973); [8]Heer et al. (1976); [9]Rainford et al. (1968); [10]Meier et al. (1976); [11]Sugawara et al. (1975); [12]Busch et al. (1971b); [13]Hulliger et al. (1975); [14]Cooper et al. (1972); [15]Tsuchida et al. (1974); [16]Stutius (1969b); [17]Jones and Hesse (1967); [18]Busch et al. (1965); [19]Junod et al. (1969); [20]Hulliger and Natterer (1976); [21]Jones (1969); [22]Schumacher and Wallace (1966); [23]Lallement and Veyssie (1968); [24]Furrer and Hälg (1976); [25]Furrer et al. (1972a); [26]Furrer et al. (1976); [27]Junod et al. (1966); [28]Davidov et al. (1974); [29]Schumacher and Wallace (1965); [30]Davis and Mook (1972); [31]Bucher et al. (1971); [32]Davidov et al. (1975); [33]Turberfield et al. (1971); [34]Turberfield et al. (1970); [35]Guertin et al. (1975); [36]Tsuchida and Wallace (1965); [37]Wallace et al. (1971); [38]Birgeneau et al. (1970); [39]Huang et al. (1975); [40]Stutius (1969a); [41]Cooper and Vogt (1970b); [42]Cooper (1966b); [43]Cooper et al. (1967); [44]Davis and Mook (1975); [45]Davis and Mook (1974); [46]Cooper and Vogt (1970a); [47]Foner et al. (1972); [48]Birgeneau et al. (1971); [49]Lander et al. (1973); [50]Bucher et al. (1972); [51]Stankevich et al. (1974); [52]Shapiro and Bak (1975); [53]Furrer and Kaldis (1975); [54]Sugawara et al. (1977); [55]Davidov and Baberschke (1975); [56]Heer et al. (1976b); [57]Paukov et al. (1976); [58]Sugawara and Huang (1976); [59]Weaver et al. (1977); [60]Ott and Lüthi (1977); [61]Cooper (1966a); [62]Landau and Rives (1974); [63]Kouvel et al. (1977); [64]Heer (1978); [65]Mullen et al. (1974).

choice. The scatter of the data may give an impression about the accuracy with which these parameters can be determined. Fig. 33.3 visualizes the J splitting observed in the LnP phases. Although the point-charge model supplies but one contribution to the crystal-field parameters it is all the more surprising that with few exceptions it represents a fairly useful approximation, apparently due to a systematic cancellation of contributions. Therefore we use it as a zeroth approximation, in those cases where no experimental data are available. A comparison of experimental data and point-charge calculations shows that the sixth-order terms, though still small, are in fact larger than estimated, because overlap and covalency effects are more important. From the experimental values of $A_4\langle r_f^4\rangle$ and $A_6\langle r_f^6\rangle$ we may formally derive effective charges Z_4 and Z_6. These figures may vary by a factor 2 depending upon the set of theoretical $\langle r_f^n\rangle$ values chosen. With our choice of the Freeman and Watson values (1965) Z_4 is around 2 for Pr ... Tb and near 3 for the following Ln^{3+} ions. If we took the effective-point-charge model literally then

$$A_4\langle r_f^4\rangle = \text{const.}\frac{\langle r_f^4\rangle Z_{\text{eff}}}{a^5} \tag{33.5}$$

where Z_{eff} should be related to the anion-cation electronegativity difference.

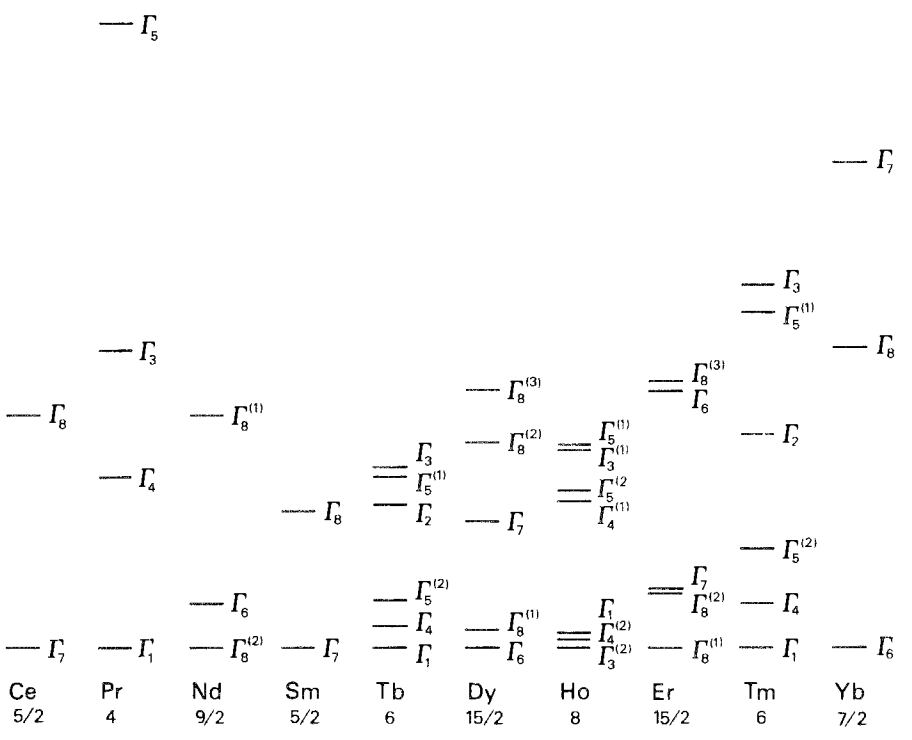

Fig. 33.3. Energy splitting of the J ground state in the LnP phases due to an effective crystal field. The J values are given below the cation symbols.

Bucher and Maita (1973) demonstrated that for the NaCl-type Pr pnictides and chalcogenides a linear relationship does indeed exist between the fourth-order crystal-field potentials $A_4\langle r_f^4\rangle$ and the electronegativity of the ligands. Thus, it looks as if the point-charge model – at least for the NaCl-type Ln compounds – yields quite reasonable results, in agreement with the experimental values obtained by the parametrization scheme. From the regularity of the presently known crystal-field parameters it is possible to deduce the splitting of the J ground state in any NaCl-type Ln pnictide. Birgeneau et al. (1973) have plotted an averaged curve for $A_4\langle r_f^4\rangle a^5$ and propose $A_6\langle r_f^6\rangle = 0.4 \pm 0.2$ meV for all compounds, which should ensure an accuracy of 10–20%. The thus gained energy-level sets allow a calculation of physical properties like the magnetic susceptibility, but the back ground still lies in the dark. The problem of the extremely weak splitting in CeSb and CeBi that persists also in diluted (La, Ce)Sb, etc., remains unsolved.

As can be seen from table 33.6 there is generally a rather marked difference between the effective Z_4 values derived for the nitrides compared with those for the remaining pnictides. As Yuan (1977) pointed out this difference is due to the extremely small Ln–Ln distances in the nitrides which are virtually the same as in the trivalent metals. In the nitrides, therefore, the 12 nearest Ln neighbors will have a nonnegligible influence on the crystal-field potential as they will alter the form of the f-electron cloud and hence the Stevens factors β and γ which were calculated for free rare earth ions.

3.3.2. *Specific-heat measurements*

In Ln^{3+} ions other than Sm or Eu the first excited state is sufficiently far from the ground state that only the crystal-field split ground state contributes to c_p. In the paramagnetic region the corresponding Schottky anomaly of c_p(mole) is given by the formula

$$c_{mag} = \frac{R}{T^2}\frac{d^2 \ln Z}{d(1/T)^2} = 2RT\frac{d \ln Z}{dT} + RT^2\frac{d^2 \ln Z}{dT^2} \tag{33.6}$$

where Z is the one-ion partition function, $Z = \sum_{n=0}^{N-1} g_n \exp((E_0 - E_n)/kT)$, with g_n = degeneracy of the nth of the N crystal-field-split levels. The entropy s of the f electrons is at high temperatures ($kT \gg E_{N-1} - E_0$)

$$s = k \ln \sum g_n$$

and the gain in entropy on heating from a very low temperature T_1 to a high temperature T_2 is (per mole)

$$\Delta S = S_2 - S_1 = \int_{T_1}^{T_2} \frac{1}{T} c_{mag}\, dT \approx S_\infty - R \ln g_0.$$

The entropy increase $\Delta S(T)$ is often a valuable criterion for the determination of the ground-state degeneracy (e.g. in Nd compounds).

Below the ordering temperature the contribution of the exchange energy to c_{mag} is usually dominating. This has been treated by Stutius (1969b) by means of a molecular-field approximation. Qualitatively we may assume that the exchange interaction can be described by an isotropic Heisenberg model, while the crystal field gives rise to a magnetic anisotropy. Both contributions can be included in an anisotropic Heisenberg model that yields quite similar results like a three-dimensional Ising model. Particularly it leads to a much more pronounced and asymmetric c_p peak at the ordering temperature compared with the isotropic Heisenberg model. Such a behavior (2nd order phase transition) was indeed observed for most of the NaCl-type compounds. Certain compounds, however, show a first-order transition (table 33.9), which reflects the influence of magnetostriction (section 3.3.4).

In order to obtain the specific heat of the 4f electrons, c_{mag}, the contributions of the lattice vibrations and the conduction electrons have to be subtracted from the experimental $c_p(T)$ curve. These contributions are usually approximated by the specific heat of an isostructural diamagnetic compound. However, any interpolation between the specific-heat data of the La and Lu compounds introduces a large uncertainty and therefore an unambiguous determination of the J splitting is possible only in the simplest cases such as the Ce and Sm compounds. For checking the interpolated lattice heats we compiled in table 33.7 some values for the Debye temperatures part of which were determined by other techniques. Those for the antimonides were obtained either from elastic or thermal-expansion measurements. We did not find θ_D values derived from X-ray intensity measurements. The Lindemann melting-point formula may be used to estimate the melting temperatures from the given θ_D values.

3.3.3. *Paramagnetic susceptibility*

The initial susceptibility χ_0 for the free Ln ion

$$\chi_0^{free} = \mu_B^2 g_J^2 J(J+1)/3\,kT \tag{33.7}$$

is modified by the effect of the crystal field on the orbital contributions to the magnetic moment. Under the perturbation of the crystal field the new eigenfunctions are linear combinations of the unperturbed wave functions with the same J but different M. In the magnetic field H the levels are further split and then have the energies

$$E_{nm} = E_n + E_{nm}^{(1)} H + E_{nm}^{(2)} H^2 + \ldots$$

where n is the crystal-field quantum number labelling the crystal-field split levels Γ_n of the J ground state, and m designates the additional splitting of these levels due to the magnetic field, and

$$E_{nm}^{(1)} = \langle n, m|\mu_z|n, m\rangle, \quad E_{nm}^{(2)} = \sum_{n', m' \neq n, m} \frac{|\langle n', m'|\mu_z|n, m\rangle|^2}{E_{n'm'} - E_{nm}}. \tag{33.8}$$

TABLE 33.7.

Debye temperatures θ_D in K. The values for the nitrides, phosphides and arsenides were derived from specific-heat measurements, those of ref. (g) from the elastic properties and those of ref. (e) from thermal expansion at 20–750°C according to the formula

$$\theta_D = \frac{19.37}{\bar{A}^{1/2} V^{1/3} \alpha^{1/2}},$$

where $\bar{A}$ is the root-mean-square atomic weight, V is the molecular volume and α is the thermal-expansion coefficient.

LaN	320[a]	LaSb	190[e]	DySb	175[e]
	~325[b]		211[g]		241[g]
PrN	355[a]		218[f]	HoSb	168[e]
NdN	360[b]		225[c]		247[g]
EuN	400[a]	CeSb	185[e]	ErSb	172[e]
TbN	440[a]	PrSb	185[e]		237[g]
LuN	440[a]		221[g]	TmSb	174[e]
		NdSb	174[e]		210–220[h]
LaP	299[c]		224[i]		237[g]
LuP	346[c]				
		SmSb	184[e]	YbSb	138[e]
LaAs	245[d]		232[g]	LuSb	177[e]
CeAs	260[k]				241[c]
LuAs	265[d]	GdSb	166[e]		
			233[g]		
YSb	217[e]	TbSb	197[e]	LuBi	179[j]
	228[f]		215[b]		

[a]Stutius (1969b); [b]Veyssie et al. (1964); [c]Birgeneau et al. (1973); [d]Hulliger (1976); [e]Samsonov et al. (1974); [f]Busch et al. (1971); [g]Mullen et al. (1974); [h]Stutius (1969a); [i]Wakabayashi and Furrer (1976); [j]Bucher (1976); [k]Heer et al. (1976).

The corresponding magnetic moment is

$$\mu_{nm} = -\partial E_{nm}/\partial H$$

and the initial susceptibility χ_0 per atom is given by

$$\chi_0 = \frac{\partial}{\partial H} \frac{\sum_{n,m} \mu_{nm} \exp(-E_{nm}/kT)}{Z} = \sum_{n,m} \left\{ \frac{(E^{(1)}_{nm})^2}{kT} - 2E^{(2)}_{nm} \right\} \frac{\exp(-E_n/kT)}{Z}. \tag{33.9}$$

The most instructive examples are the Ce^{3+} compounds where the $J = 5/2$ ground state splits in the crystal field into a doublet Γ_7 and a quartet Γ_8. The wave functions for [100] are (Lea et al., 1962)

$$\psi_{7,1} = \frac{1}{\sqrt{6}} \left| +\frac{5}{2} \right\rangle - \sqrt{\frac{5}{6}} \left| -\frac{3}{2} \right\rangle$$

$$\psi_{7,2} = \frac{1}{\sqrt{6}}\left|-\frac{5}{2}\right\rangle - \sqrt{\frac{5}{6}}\left|+\frac{3}{2}\right\rangle$$

$$\psi_{8,1} = 1\left|+\frac{1}{2}\right\rangle;\quad \psi_{8,3} = \sqrt{\frac{5}{6}}\left|+\frac{5}{2}\right\rangle + \frac{1}{\sqrt{6}}\left|-\frac{3}{2}\right\rangle$$

$$\psi_{8,2} = 1\left|-\frac{1}{2}\right\rangle;\quad \psi_{8,4} = \sqrt{\frac{5}{6}}\left|-\frac{5}{2}\right\rangle + \frac{1}{\sqrt{6}}\left|+\frac{3}{2}\right\rangle$$

and the Zeeman coefficients $E^{(1)}_{n,m}$ and $E^{(2)}_{n,m}$ are

$$E^{(1)}_{7,1} = \langle 7, 1|g_J\mu_B J_z|7, 1\rangle = \frac{5}{6}\, g_J\mu_B = -E^{(1)}_{7,2},$$

$$E^{(1)}_{8,1} = \langle 8, 1|g_J\mu_B J_z|8, 1\rangle = \frac{1}{2}\, g_J\mu_B = -E^{(1)}_{8,2},$$

$$E^{(1)}_{8,3} = \frac{11}{6}\, g_J\mu_B = -E^{(1)}_{8,4},$$

$$E^{(2)}_{7,1} = -\frac{1}{\Delta}\, g_J^2\mu_B^2\{\langle 8, 1|J_z|7, 1\rangle^2 + \langle 8, 2|J_z|7, 1\rangle^2 + \langle 8, 3|J_z|7, 1\rangle^2 + \langle 8, 4|J_z|7, 1\rangle^2\},$$

$$E^{(2)}_{7,2} = E^{(2)}_{7,1} = -\frac{20}{9}\frac{g_J^2\mu_B^2}{\Delta},$$

$$E^{(2)}_{8,1} = E^{(2)}_{8,2} = 0,\quad E^{(2)}_{8,3} = -E^{(2)}_{7,1},\quad E^{(2)}_{8,4} = -E^{(2)}_{7,2},$$

$$Z = 2 + 4\exp(-\Delta/kT) \text{ with } \Delta = E(\Gamma_8) - E(\Gamma_6).$$

Thus, the formula for the magnetic susceptibility of Ce^{3+} ions in a cubic crystal field becomes $\chi_0^{CF} = \chi_0^{free} f(\Delta/T)$ where

$$f\left(\frac{\Delta}{T}\right) = \frac{5 + 26\exp(-\Delta/kT) + 32(kT/\Delta)\{1 - \exp(-\Delta/kT)\}}{21\{1 + 2\exp(-\Delta/kT)\}}. \tag{33.10}$$

Schumacher and Hollingsworth (1966) have calculated the energy levels for all Ln^{3+} ions in cubic crystal fields as functions of a magnetic field applied along [100] and [111] and of a fourth-order crystal-field parameter, which is valid exactly only for Ce^{3+} and Sm^{3+} compounds.

If exchange interactions have to be taken into account the molecular-field approximation leads to (Murao and Matsubara, 1957; Wang and Cooper, 1970)

$$\chi = \frac{\chi_0^{CF}}{1 - \lambda_p\chi_0^{CF}} \tag{33.11}$$

χ_0^{CF} is given by eq. (33.9) whereas λ_p is the molecular-field parameter

$$\lambda_p = \frac{2(g_J - 1)^2}{g_J^2\mu_B^2}(12\mathcal{J}_1 + 6\mathcal{J}_2 + 24\mathcal{J}_3 + \ldots) \tag{33.12}$$

($\mathcal{J}_n$ is the exchange parameter for the nth neighbors) for NaCl-type compounds.

This is equivalent to

$$1/\chi = 1/\chi_0^{CF} - \lambda_p \tag{33.13}$$

which at high temperatures approximates the Curie–Weiss law

$$1/\chi = \frac{1}{C}(T - \theta_p) \text{ with } \theta_p = \lambda_p C. \tag{33.14}$$

Below T_N, where $H_m = \lambda_{af}\langle\mu_z\rangle$, $\lambda_{af} = 1/\chi_0^{CF}(T_N) = 2(g_J - 1)^2\mathcal{J}(Q)/g_J^2\mu_B^2$ with $\mathcal{J}(0, 0, 1) = -4\mathcal{J}_1 + 6\mathcal{J}_2 - 8\mathcal{J}_3 + \cdots$ and $\mathcal{J}(\frac{1}{2}, \frac{1}{2}, \frac{1}{2}) = -6\mathcal{J}_2 + \cdots$ for type I and type II antiferromagnetic order, respectively.

The derivation of the crystal-field parameters from magnetic-susceptibility data is not straightforward and the accuracy of the results is rather low as can be checked by inspection of table 33.6.

3.3.4. *Anisotropy and structural distortions*

Via spin-orbit coupling the magnetic moment of the 4f shell is strongly coupled to the charge distribution. The Γ_1 and Γ_2 singlet and the Γ_3 doublet states are non-magnetic. In a magnetic field the Γ_4 and Γ_5 triplets split isotropically like a spin $S = 1$ state. The Γ_6 and Γ_7 Kramers doublets are also isotropic but the splitting of the Γ_8 quartets is dependent upon the orientation of the magnetic field.

In a semiclassical treatment of the crystal field Trammell (1963) was able to predict the directions of easy magnetization for the rare earth nitrides. For this purpose J was assumed as a classical vector able to take any position relative to a quantization axis (which is more or less justified for high J values). The classical analog of the potential energy for J pointing in a certain direction is then the expected value of the potential energy for the state of maximum component of J along that direction. For $\boldsymbol{J}\|\boldsymbol{n}$ (where $\boldsymbol{n}$ is the unit vector of direction cosines x, y, z) the mean value of the potential on a sphere of radius 1 is

$$\langle V_c\rangle_n = K_4(x^4 + y^4 + z^4 - \tfrac{3}{5}) + K_6\{11(x^6 + y^6 + z^6) - 15(x^4 + y^4 + z^4) + \tfrac{30}{7}\} \tag{33.15}$$

with

$$K_4 = 20A_4\langle r_f^4\rangle\left\langle \sum P_4\left(\frac{z}{r}\right)\right\rangle_{M_J=J} = \frac{5}{2}\beta_J A_4\langle r_f^4\rangle\langle O_4^0\rangle_J$$

$$K_6 = 56A_6\langle r_f^6\rangle\left\langle \sum P_6\left(\frac{z}{r}\right)\right\rangle_{M_J=J} = \frac{7}{2}\gamma_J A_4\langle r_f^6\rangle\langle O_6^0\rangle_J$$

where $\langle r^l\rangle\langle\Sigma P_l(z/r)\rangle_{M_J=J}$ are 2^l-pole moments listed by Trammell (1963) and Junod et al. (1969). In the three crystallographic directions the potential has the values

$$\langle V_c\rangle_{100} = \frac{2}{5}K_4 + \frac{2}{7}K_6, \qquad \langle V_c\rangle_{111} = -\frac{4}{15}K_4 + \frac{32}{63}K_6,$$

$$\langle V_c\rangle_{110} = -\frac{1}{10}K_4 - \frac{13}{28}K_6. \tag{33.16}$$

Since the fourth-order term is dominant the effective potential for the magnetic moment either has six minima in [100] or eight minima in [111] direction depending on the sign of the 2^4-pole moment or, equivalently, of the Stevens multiplicative factor β. The minima of $\langle V_c \rangle$ are the easy directions of magnetization. If we extend the results to all Ln ions then Trammell's argument predicts the easy axis along [100] for f^2, f^3, f^9, f^{10} and f^{13} Ln ions, along [111] however for f^1, f^5, f^8, f^{11} and f^{12} ions. With the exception of a few Ce, Ho, Dy and Er compounds (Stevens and Pytte, 1973) the experiments confirmed Trammell's predictions.

Magnetocrystalline energies, $\langle V_c \rangle_{100} - \langle V_c \rangle_{111}$ and $\langle V_c \rangle_{100} - \langle V_c \rangle_{110}$, can be derived from magnetization measurements in the ferromagnetic state, and from these the crystal-field parameters can also be estimated.

All the Ln monopnictides that order magnetically at low temperatures suffer a structural distortion at the ordering temperature (Lévy, 1969; Jones and Morosin, 1967). It is reasonable to assume that these distortions affect the potential minima in such a way as to stabilize two of them at the expense of the others. Thus, compounds with [100] minima undergo tetragonal contractions while those with the easy axis along [111] suffer a rhombohedral compression. Exceptions are CeSb (Lévy, 1969) and CeBi (Hulliger et al., 1975)*. Stevens and Pytte (1973) attribute the anomalous distortion to the small J value of Ce^{3+} and to the special features of the tunnelling model which result when the number of crystal-field minima is larger than the number of states in the ground-state manifold. The lower-lying doublet of Ce^{3+} has Kramers degeneracy, thus cannot be split by a crystal field, and it is magnetically isotropic. Distortions therefore have to split the thermally populated quartet that corresponds to tunnelling states with large probabilities of being at maxima in the crystal-field potential. The Ce^{3+} ion therefore is particularly sensitive to strains of tetragonal symmetry which affect the maxima.

Further distortions result from the magnetic ordering if this has lower symmetry. In DySb a small monoclinic [111] distortion was observed (Bucher et al., 1972) in addition to the large tetragonal distortion predicted by the tunnelling model.

Appreciable lattice distortions appear to result only from a combination of crystal-field and magnetic interactions. Deformations are small and predominantly exchange induced in compounds with S-state cations or with rare earth ions that have a Kramers doublet as the ground state and a large energy gap to the next higher quartet level. In the first group we find the Gd pnictides, in the second group we have CeP and CeAs, already mentioned above, as well as SmP, SmAs, SmSb and probably YbP and YbAs.

Since the elastic constants are known for GdSb (Mullen et al., 1974) we can estimate the exchange-induced lattice distortion in this case. At the equilibrium distortions the gain in exchange energy is balanced by the deformation energy.

*In CeAs and particularly in CeP the expected tetragonal distortions at T_N are so small that we were not able to detect them röntgenographically.

In type II antiferromagnets we expect, at least in a first approximation, a rhombohedral deformation. The corresponding distortions are

$$\frac{\Delta a}{a} = \frac{4}{a^2(c_{11}+2c_{12})}\frac{\partial \mathcal{J}_2}{\partial a}\langle S\rangle^2, \qquad \Delta\beta = -\frac{4}{a^2 c_{44}}\frac{\partial \mathcal{J}_1}{\partial a}\langle S\rangle^2.$$

where $\Delta\beta = \beta - \frac{1}{2}\pi$ refers to the originally cubic NaCl cell. For GdSb $c_{11}+2c_{12} \approx 15\times 10^{11}$ dyn/cm^2, $c_{44} < 2.3\times 10^{11}$ dyn/cm^2 below the Néel point. From experimental T_N and θ_p data we derive $\partial \mathcal{J}_1/\partial a$ and $\partial \mathcal{J}_2/\partial a$ values of -0.9 and -0.5 K/Å, respectively, which lead to a maximum compression of the unit cell of $\Delta\beta \approx 0.70\times 10^{-3}$ rad. compared with an experimental value $\Delta\beta \approx 0.85\times 10^{-3}$ rad. (Hulliger and Stucki, 1977). In agreement with our estimation the distortions are most pronounced in GdBi, lower in GdAs and not detectable in GdP (Jones and Morosin, 1967). McGuire et al. (1969) found the spins in GdSb and GdBi to lie within the (111) planes which is consistent with a positive value of $\Delta\beta$. Therefore, we conclude that the true symmetry of the distorted structures of the Gd monopnictides is in fact monoclinic. The moment orientation corresponds to the minimum of the dipole energy.

3.3.5. *Thermal dilatation and elastic properties*

At low temperatures the thermal expansion of the Ln compounds exhibits anomalies due to the crystal field similar to the Schottky effect of the specific heat. The volume thermal-expansion coefficient β is a derivative of the free energy F:

$$\beta = -\kappa(\partial^2 F/\partial V\,\partial T)$$

where κ is the adiabatic compressibility. The crystal-field contribution to $\beta(=3\alpha)$ thus becomes (Ott and Lüthi, 1976)

$$\beta_{CF} = \frac{\kappa}{V_M kT^2}\{\langle E^2\gamma\rangle - \langle E\rangle\langle E\gamma\rangle\} \tag{33.17}$$

where V_M is the molar volume and $\langle X\rangle = (1/Z)\Sigma_i X_i \exp(E_i/kT)$ denote statistical averages over the crystal-field split energy levels E_i of the 4f electrons and $\gamma_i \equiv -\partial \ln E_i/\partial \ln V$ is the Grüneisen parameter for the level E_i. If we compare the expression for β_{CF} with that for the Schottky specific heat

$$c_{mag} = \frac{1}{RT^2}\{\langle E^2\rangle - \langle E\rangle^2\} \tag{33.18}$$

we see that β_{CF} is proportional to c_{mag} if either only two crystal-field levels are effective or if all the γ_i are equal (which however might be a crude approximation). Low-temperature thermal expansion has been analysed in detail for TmSb (Ott and Lüthi, 1977). Up to 9 K good agreement is obtained with a $\gamma_1 = \alpha V_M/\kappa c_p = -1.15$ arising from the volume dependence of the lowest energy splitting $\Gamma_1 - \Gamma_4 = 25$ K. The data above 10 K are influenced by the Grüneisen parameter γ_2 for the next higher level at 56 K, $\gamma_2 = +1.05$. In the frame work of the point-charge model a $\gamma_1 \approx +5/3$ would be expected (Ott and Lüthi, 1977).

The influence of the crystal field is evident also from the elastic properties. Similarly, as for the magnetic susceptibility, the isothermal elastic constants c_{ij} can be calculated (Mullen et al., 1974) as a strain susceptibility due to the crystal field

$$c_{ij} = -kT\partial^2 \ln Z/\partial\epsilon_i\partial\epsilon_j. \tag{33.19}$$

The dependence of the energy levels on the strains ϵ is determined from the secular equation

$$|E_0(\Gamma_j^i) - E + \langle\Gamma_{j'}^{i'}|\mathscr{H}'|\Gamma_j^i\rangle| = 0.$$

For the symmetry elastic constants $c_{11}-c_{12}$, c_{44} and $c_{11}+2c_{12}$ (corresponding to tetragonal, rhombohedral and volume strain) the magnetic ion–lattice interactions are given by Mullen et al., (1974):

$$\begin{aligned}
\mathscr{H}'(c_{11}-c_{12}) &= -g_2\left(\frac{c_{11}^0-c_{12}^0}{N}\right)^{1/2}\sum_i(\epsilon_2 O_{2,i}^2+\epsilon_3 O_{2,i}^0),\\
\mathscr{H}'(c_{44}) &= -g_3\left(\frac{c_{44}^0}{N}\right)^{1/2}\sum_i 2\epsilon_{xy}(J_xJ_y+J_yJ_x)_i+\cdots\\
\mathscr{H}'(c_{11}+2c_{12}) &= -g_1\left(\frac{c_{11}^0+2c_{12}^0}{N}\right)^{1/2}NJ^2(\epsilon_{xx}+\epsilon_{yy}+\epsilon_{zz})
\end{aligned} \tag{33.20}$$

where c_{ij}^0 are the background elastic constants, $\epsilon_2=(\epsilon_{xx}-\epsilon_{yy})/\sqrt{2}$ and $\epsilon_3=(2\epsilon_{zz}-\epsilon_{xx}-\epsilon_{yy})/\sqrt{6}$ are symmetry strains which transform under the two-dimensional representation Γ_3; c_{44} belongs to ϵ_{xy}, ϵ_{xz}, $\epsilon_{yz}(\Gamma_5)$ and $c_{11}+2c_{12}$ belongs to the volume strain $\epsilon_{xx}+\epsilon_{yy}+\epsilon_{zz}(\Gamma_1)$. The sum is performed over all N rare earth ions. The operator O_2^0 is defined as usual: $3J_z^2-J(J+1)$. The g_i are the magnetoelastic coupling constants. The point-charge model gives for the NaCl-type compounds

$$\begin{aligned}
g_2 &= \frac{9}{\sqrt{6}}\left(\frac{N}{c_0}\right)^{1/2}\alpha_J\langle r_f^2\rangle\frac{Ze^2}{a^3},\\
g_3 &= \frac{3}{2}\left(\frac{N}{c_0}\right)^{1/2}\alpha_J\langle r_f^2\rangle\frac{Ze^2}{a^3}.
\end{aligned} \tag{33.21}$$

Diagonalization of the secular equation leads to the energy eigenvalues $E(\Gamma_j,\epsilon)$. From these the elastic constants c can be evaluated as

$$\frac{c-c_0}{N} \approx \left\langle\frac{\partial^2 E}{\partial\epsilon^2}\right\rangle - \frac{1}{kT}\left\langle\left(\frac{\partial E}{\partial\epsilon}\right)^2\right\rangle.$$

Calculations and measurements have been carried out above all on antimonides (Lüthi et al., 1973; Mullen et al., 1974). The compounds can be divided into two classes, those for which $(c/c_0-1)/g_i^2$ remain finite for all temperatures and those which soften as $T\to 0$. The compounds in which the lowest crystal-field level Γ_l has a vanishing quadrupole matrix element, $\langle\Gamma_l^{i'}|\mathscr{H}'|\Gamma_l^i\rangle = 0$ (Pr and Tm with $\Gamma_l=\Gamma_1$, Sm(Γ_7), Dy(Γ_6)) show little variation of the elastic constants for all

temperatures. In this case crystal-field driven structural transitions could occur only for much larger g_i values. In the other class Γ_i is Γ_3(Ho) or Γ_8 (Nd and Er) and here the elastic constants soften as $T \to 0$. Thus, one expects a structural phase transition, triggered by the magnetic ion-lattice interaction.

In LaSb, PrSb and TmSb no evidence for a magnetic or structural transition was found down to ~1 K (Mullen et al., 1974). The elastic constants of LaSb show the normal stiffening at lower temperatures and a temperature independence at the lowest temperatures. The data of LaSb are used as a background estimate for the other samples. The elastic constants of PrSb and TmSb reveal a more complicated temperature dependence. Theoretical curves were fitted to the measured data by neglecting the effects of exchange and quadrupole–quadrupole interaction. The magnetoelastic coupling constants should be ~20 and 25 times larger to induce a structural transition in PrSb and TmSb, respectively. This is due to the absence of quadrupole matrix elements between the ground state Γ_1 and the next higher state Γ_4.

In SmSb the elastic constants begin to soften below 4 K and show strong softening in the ordered region. At T_N there is a kink in the elastic-mode curve, but the magnetoelastic coupling constant g_2 is 30 times too small to induce a crystal-field structural transition. The thermal-expansion data strongly suggest that the transition at the Néel point is purely magnetic.

In HoSb a strong softening of the $c_{11} - c_{12}$ mode is observed towards the Néel point. With the magneto-elastic constants derived from the elastic measurements a spontaneous strain $\epsilon_3 \approx 1.3 \times 10^{-3}$ is calculated as compared with the measured 2.4×10^{-3} (Lévy, 1969). The transition is believed to be close to second order. Thermal-expansion curves in a magnetic field of 12 and 15 kOe appear to have two broadened peaks. This could mean that either there are additional magnetic or structural transitions for $H > 0$ and $T < T_N$ or the structural and the magnetic transition separate.

In ErSb an almost steplike discontinuity in the elastic modes is observed at the Néel temperature. Application of a magnetic field has a similar effect as for GdSb: in both cases the anomaly is reduced. The thermal-expansion anomaly at T_N is about an order of magnitude larger than in SmSb. A magnetic field of 6.5 kOe increases the anomaly by another factor of 5. This large α-value is taken as evidence for a simultaneous magnetic and structural transition. With or without magnetic field only one anomaly is observed. With the possible exception of the case of HoSb, the magnetic (dipolar) and the structural (quadrupolar) transitions appear to coincide in all Ln monopnictides although there exist theoretical models which allow successive transitions (Chen and Levy, 1971, 1973; Levy and Chen, 1971; Sivardière and Blume, 1972). It is somewhat disappointing that the experimental values for the magnetoelastic coupling constants g_2 and g_3 deviate from the point-charge values by an order of magnitude (table 33.8). Since these coupling constants are the strain derivatives of the crystal-field parameters they provide a sensitive test for the latter, thus indicating that the agreement of the crystal-field parameters with the point-charge model was rather accidental.

TABLE 33.8.
The magnetoelastic coupling constants (in m K) of some LnSb phases (Mullen et al., 1974). Comparison of the experimental data with values calculated according to eq. (3.22) valid for the point-charge model with $Z = -2$ and $\langle r_f^2 \rangle$ values from Freeman and Watson (1965).

Compound	g_3^2 (expt.)	g_2^2 (expt.)	g_2^2 (calc.)
PrSb	5.4	4.9	168
SmSb	14	38	431
DySb		1.3	7
HoSb	1.1	0.11	0.75
ErSb		<0.2	1.1
TmSb	1.4	1.2	17

In Nd pnictides which have a Γ_8 ground state, quadrupole-quadrupole interactions appear to be dominant. For NdSb the tetragonal distortion below the Néel point (Lévy, 1969) due to the magnetoelastic effect has been interpreted with a Hamiltonian including crystal field, Weiss molecular field and a magnetoelastic term (Bak and Lindgård, 1973; Furrer et al., 1976; Wakabayashi and Furrer, 1976)

$$\mathcal{H}_{me} = -A\langle O_2^0 \rangle O_2^0$$

with

$$A = \frac{-3B_\alpha^{[2]}\bar{\epsilon}_{zz}}{\langle O_2^0 \rangle} = \frac{3\bar{\epsilon}_{zz}(c_{11} - c_{12})}{2\langle O_2^0 \rangle^2} = \frac{6(B_\alpha^{[2]})^2}{c_{11} - c_{12}} \tag{33.22}$$

where $B_\alpha^{(2)}$ is a magnetoelastic coupling constant defined by Callen and Callen (1963). The large value of the quadrupole parameter found from spin waves leads however to a weakly first-order transition instead of the observed second-order transition (Lévy, 1969). A second-order transition is indeed expected from the presence of fixed points in the renormalization group analysis of Bak et al. (1976) for type I antiferromagnets with the magnetic moments perpendicular to the layers as found in NdSb.

3.4. *Summary of the magnetic properties of the* NaCl-*type pnictides*

In table 33.9 we have collected the magnetic and structural data that refer to the magnetic ordering. The paramagnetic data such as the effective magneton numbers (which in the appropriate T interval agree with the free-ion values anyway), the paramagnetic Curie temperatures and the exchange constants derived therefrom can be found in recent reviews by Busch (1967), Lallement and Veyssie (1968), Westrum (1968), Jones (1969), Junod et al. (1969), Holtzberg et al. (1970), Nereson and Arnold (1971), Rhyne and McGuire (1972), Wachter

TABLE 33.9.

Magnetic ordering and accompanying lattice distortions in NaCl-type Ln pnictides. The entries give the ordering temperatures, the type of magnetic ordering, the direction of the magnetic moments (easy direction), the saturation moment, additional transitions as well as the symmetry of the structural distortion and the order of the phase transition.

	LnN	LnP	LnAs	LnSb	LnBi
Ce	no order down to 1.5 K[17] contains Ce^{4+}	T_N = 8.5 K[20] 6 ... 7 K[23] 9 K[43]	T_N = 7.5 K[35] 5 ... 7.5 K[23]	T_N = 18 K[34] 16 K[12]	T_N = 25 K[34] 26 K[33] 25.5 K[1]
		type I AFM[20] ↑ ∥[001], 0.83 μ_B[20]	type I AFM[35] ↑ ∥[001], 0.7 μ_B[35] 0.85 μ_B[20]	"mixed AFM[51] ↑ ∥[001], 1.9 μ_B[22,34] 2.05[55] complicated phase diagram[51]	type I AFM[34] ↑ ∥[001], 2.14 μ_B(2 K)[1]
				< 8 K: type IA AFM[51]	T_t = 12.5 K[22,33] type IA AFM[33,34]
		2nd order[20]	2nd order[20]	tetrag.[22,29] 1st order[31]	tetrag. 2nd order[22]
Nd	T_C = 29 K[18,49] 27.6 K[45] 32 K[27] 35 K[57]	T_N = 11 K[27,44] 7 K[54]	T_N = 13 K 12.5 K[44] 10.6 K[54]	T_N = 16 K[34] 15.5 K[44]	T_N = 25 K[33] 24 K[43]
	FM[17] ↑ ∥[001], 3.1 μ_B (4 K)[18,27] 2.5 μ_B[17] 1.8 μ_B (0 K)[49]	type I AFM[37] ↑ ∥[001], 1.83 μ_B (4 K)[37]	type I AFM[37] ↑ ∥[001], 2.18 μ_B (4 K)[37]	type I AFM[34] ↑ ∥[001], 2.98 μ_B (4 K)[37]	type I AFM[33] ↑ ∥[001], 3.14 μ_B[37]
	stoichiom. NdN AFM? tetrag. 2nd order[49]	metamag., H_c = 19 kOe[44] tetrag.	metamag., H_c = 42 kOe[44] tetrag. 2nd order[23]	metamag., H_c = 83 kOe[6] tetrag. 2nd order[29]	metamag., H_c = 160 kOe[24] tetrag. 2nd order[23]
Sm	T_N = 18 K(?)[40], < 2 K[27] 13 K[57]	T_N = 1.65 K[23] trigonal?	T_N = 1.8 K[23] trigonal?	T_N = 2.1 K[32] 2.8 K trigonal?	T_N = 8.6 K[23] trigonal?
Gd	T_C = 69 K[19,38] 72 K[28] 67 K[40] 90 K[53]	T_N = 15 K[5] 13 K[23]	T_N = 25 K[7]	T_N = 24 K[32] 25 K[42] 28 K[6]	T_N = 28 K[43] 28.7 K[23]
	FM[19] 6.6 μ_B[27] 6.96 μ_B[36] 6.9 μ_B[11] 7.2[47]	type II AFM[34] ↑ in (111), 7.1 μ_B[34]	type II AFM ↑ in (111)	type II AFM[30] ↑ in (111)[30]	type II AFM[30] ↑ in (111)[30]
	T_N = 35 ... 40 K[52]	M saturated at 95 kOe[5]	M saturated at 165 kOe[7]	M saturated at 340 kOe[10]	
	$H_c \approx$ 15 ... 20 kOe: FM[52]	~trigonal, compressed [111][25]	~trigonal, compressed [111][25]	~trig. compressed,[50] 2nd order[32]	~trig. compressed, 2nd order[50]
Tb	T_C = 42 K[13] 34 K[40] 39 K[47]	T_N = 9 K[13] 8 K[27]	T_N = 12 K[13] 10.5 K[27]	T_N = 14 K[13] 15 K[14] 16.5 K[27]	T_N = 18 K[33] 17 K[43]
	retarded spiral[13] ↑ ∥[111], 6.7, 7.0 μ_B[13]	type II AFM[13] ↑ ∥[111], 6.2 μ_B[13] > 8 μ_B[4] H_c ~ 4 kOe∥[111], 2 K: HoP-type FM[4]	type II AFM[13] ↑ ∥[111], 7.7 μ_B[13]	type II AFM[13] ↑ ∥[111], 8.2 μ_B[13]	type II AFM[33] ↑ ∥[111], 7.9 μ_B[33]
		trigonal 1st order[29]	trigonal 1st order[29]	trigonal 1st order[29]	trigonal 2nd order[23]

TABLE 33.9 (*Contd.*)

	LnN	LnP	LnAs	LnSb	LnBi
Dy	$T_C = 26$ K[13] 17.6 K[40] 17 K[47] retarded spiral[13] $\uparrow \parallel [100]$, 4.8, 7.4 μ_B[13] $T_N = 15$ K[11]	$T_C = 8$ K[27] 4.5 K[4,47] HoP-type FM[4] 7.8 μ_B[4] $H_c \approx 17$ kOe[4] tetrag. 1st order[29]	$T_C = 8.5$ K[27] HoP-type FM[27] tetrag. 1st order[29]	$T_N = 12$ K[34] 9.5 K[3,6] type II AFM[34] $\uparrow \parallel [001]$, 9.8 μ_B[34] $H_{[100]} > 22$ kOe $H_{[110]} > 17$ kOe } HoP-type FM[2] $H_{[100]} > 40$ kOe: FM[2,41] monocl. (tetrag.) 1st order[3,16]	$T_N = 13$ K[33] 12 K[43] type II AFM[33] 8.7 μ_B[33] $H_{[100]} > 37$ kOe: HoP type[23] $H_{[101]} > 52$ kOe: FM[23] ~tetrag. (monocl.?). 1st order[23]
Ho	$T_C = 18$ K[13] 13.3 $T_N = 11$ K[11] retarded spiral[13] $\uparrow \parallel [100]$, 6.0, 8.9 μ_B (4 K)[13] 6.1 μ_B[47] only ferromagnetic short-range order[17] $\Delta a/a < 2 \times 10^{-4}$ [13]	$T_C = 5.5$ K[13] flop-side FM[13] 8.8 μ_B[13] 9.2 μ_B[4] tetragonal[29]	$T_N = 4.8$ K[7] type II AFM[7] $\uparrow \parallel [001]$, 9.4 μ_B (1.7 K)[7] $H_c = 2$–3 kOe (2 K): HoP-type FM[7,9] tetragonal[29]	$T_N = 9$ K[13] 5 K[6,32,42] type II AFM[13] $\uparrow \parallel [001]$ 9.3 μ_B[13] $H_c = 10$–15 kOe (2 K): HoP-type FM[9] tetrag. 2nd order(?)[29]	$T_N = 6.7$ K[23] $H_c \approx 18$ kOe [001][24] tetragonal 2nd order[23]
Er	$T_C = 5$ K[13] 4.5 K[11] 6 K[47] 3.4 K[40] retarded spiral[13] 3.0, 6.0 μ_B[13] 5.5 μ_B[47]	$T_N = 3$ K[13] 2.3 K[21] type II AFM[13] $\uparrow \perp [111]$ 5.7 μ_B[13] > 8.5 μ_B[4] $H_c \approx 5$ kOe (2 K): HoP-type FM[4]	$T_N = 3.5$ K[27] 2.9 K[21] type II AFM $\uparrow \perp [111]$ monoclinic(?)	$T_N = 3.7$ K[13], 3.55 K[39] type II AFM[13] $\uparrow \perp [111]$, 7.0 μ_B[13] tetrag. 2nd order[39]	$T_N = 3.9$ K[43] 3.5 K[21] $H_s^{[100]} \sim 29$ kOe (1.4 K)[23] $H_s^{[111]} \sim 24$ kOe (1.4 K)[23]
Yb	$T_N < 1.7$ K[27] < 2 K[57] $\theta_p = -130$[5] -116[27] -90[15] -99 K[38] tetragonal?	$T_N < 1.4$ K[23] $\theta_p = -55$[27] -11 K[26]	$T_N < 1.6$ K[24] $\theta_p = -45$ K[27]	$\theta_p = -60$[27] -70 K[46]	

[1]Bartholin et al. (1974); [2]Brun et al. (1975); [3]Bucher et al. (1972); [4]Busch et al. (1964); [5]Busch et al. (1965a); [6]Busch et al. (1965b); [7]Busch et al. (1965c); [8]Busch and Vogt (1966b); [9]Busch et al. (1966); [10]Busch et al. (1967); [11]Busch et al. (1970); [12]Busch et al. (1971b); [13]Child et al. (1963); [14]Cooper and Vogt (1970b); [15]Didchenko and Gortsema (1963); [16]Felcher et al. (1973); [17]Fischer et al. (1976); [18]Furrer et al. (1976); [19]Gambino et al. (1970); [20]Heer et al. (1976a); [21]Hulliger and Natterer (1973); [22]Hulliger et al. (1975); [23]Hulliger (1976); [24]Hulliger and Landolt (1976); [25]Jones and Morosin (1967); [26]Jones (1969); [27]Junod et al. (1969); [28]Junod and Lévy (1966); [29]Lévy (1969); [30]McGuire et al. (1969); [31]Meier et al. (1976); [32]Mullen et al. (1974); [33]Nereson and Arnold (1971); [34]Nereson and Struebing (1971); [35]Rainford et al. (1968); [36]Rebouillat and Veyssié (1964); [37]Schobinger-Papamanteilos et al. (1973); [38]Schumacher and Wallace (1965); [39]Shapiro and Bak (1975); [40]Stutius (1969b); [41]Streit et al. (1974); [42]Taub et al. (1974); [43]Tsuchida and Wallace (1965b); [44]Tsuchida et al. (1969); [45]Veyssie et al. (1964); [46]Bodnar et al. (1968); [47]Busch et al. (1963); [48]Myers and Narath (1974); [49]Mourgout et al. (1977); [50]Hulliger and Stucki (1977); [51]Rossat-Mignod et al. (1977); [52]Zürcher (1977); [53]Cutler and Lawson (1975); [54]Aeby et al. (1973); [55]Bartholin et al. (1975); [56]Busch and Vogt (1966a); [57]Schumacher and Wallace (1966). Compare also Connolly and Copenhaver (1969).

(1972) and Guertin et al. (1975). Some of the data for non-S cations may be incorrect because the influence of the crystal field was often neglected.

Up to now ordering was observed in NaCl-type pnictides of Ce^{3+}, Nd, Sm, Gd, Tb, Dy, Ho and Er, but not with Pr, Eu^{3+}, Tm^{3+} and Yb^{3+}. For rocksalt phases with Ln^{3+} ions containing an odd number of f-electrons (J half integer as in Ce^{3+}, Nd^{3+}, Sm^{3+}, Dy^{3+}, Er^{3+} and Yb^{3+}) the crystal-field splitting will lead to a Kramers doublet or a fourfold degenerate Γ_8 ground state. Thus magnetic ordering will occur at low temperatures though possibly at very low temperatures as in the Yb monopnictides. If the f-shell contains an even number of electrons then the ground state may be a singlet Γ_1(Pr^{3+}, Tb^{3+}, Tm^{3+}, as well as Ho^{3+} for $x = 1$) or a nonmagnetic doublet Γ_3 (Ho^{3+} for $x < 0.75$). Trammell (1963) has shown that in such a case magnetic order will establish only when the magnetic exchange energy is of the order of the energy difference between the nonmagnetic ground state and the first excited Γ_4 state. The $\Gamma_1 - \Gamma_4$ energy difference is largest in Pr^{3+}, while in Ho^{3+} Γ_1, Γ_3 and Γ_4 almost coincide. In the Tb compounds the exchange forces are obviously large enough to induce magnetic ordering whereas this is not the case in the Tm pnictides (Birgeneau, 1972).

As was pointed out by Yuan (1977) there is a distinct difference between the rare earth nitrides and the other pnictides because of the smallness of the nitrogen anion. In the nitrides the Ln–Ln distances are practically the same as in the trivalent metals. Therefore, direct exchange ($\mathcal{J}_1$) will dominate here the superexchange ($\mathcal{J}_2$) via the anions. Many of the rare earth nitrides are indeed ferromagnetic at low temperatures.

3.4.1. Tm^{3+} *and* Pr^{3+} *compounds*

While in TmN an exchange energy $\mathcal{J}(0)(g_J - 1)^2 J(J+1)$ of 11 K is derived from paramagnetic-resonance studies (Cooper et al., 1967) the exchange in TmSb is virtually zero (~0.20 K, Cooper et al., 1967; Cooper and Vogt, 1970a; Birgeneau et al., 1971). The crystal-field-only behavior of TmSb is evident also from the fact that dilution with YSb does not change the magnetization per Tm^{3+} ion (Cooper and Vogt, 1971a). The behaviour of the Pr compounds is similar. In Tb compounds the same situation can be obtained by magnetic dilution. With $x > 0.6$ in $Tb_{1-x}Y_xSb$ the effective exchange field acting on a Tb ion is reduced below the critical value while the crystal field remains practically constant (Cooper and Vogt, 1970b, and 1971b).

TmSb was thoroughly studied both experimentally and theoretically. Cooper (1966) and Cooper and Vogt (1970a, 1971b) predicted large anisotropy effects in the high-field magnetization of the crystal-field-only paramagnets TmSb and TmBi. Neglecting exchange interactions the Hamiltonian for calculating the magnetization is

$$\mathcal{H} = \mathcal{H}_{CF} - g\mu_B \boldsymbol{H} J_z.$$

The crystal-field Hamiltonian $\mathcal{H}_{CF}$ given in eq. 33.2 and 33.3 is appropriate for $\boldsymbol{H} \| z$ in a [100] direction. For $\boldsymbol{H}$ along the other directions the corresponding

expressions are (Cooper and Vogt, 1970a or Bak and Lindgård, 1973):

$$[110]:\ \mathcal{H}_{CF} = -\frac{1}{4}A_4\langle r_t^4\rangle\beta_J[O_4^0 - 20O_4^2 - 15O_4^4] - \frac{13}{8}A_6\langle r_t^6\rangle\gamma_J \times \left[O_6^0 + \frac{105}{26}O_6^2 - \frac{105}{13}O_6^4 + \frac{231}{26}O_6^6\right]$$

$$[111]:\ \mathcal{H}_{CF} = -\frac{2}{3}A_4\langle r_t^4\rangle\beta_J[O_4^0 - 20\sqrt{2}O_4^3] + \frac{16}{9}A_6\langle r_t^6\rangle\gamma_J\left[O_6^0 + \frac{35}{4}\sqrt{2}O_6^3 + \frac{77}{8}O_6^6\right].$$

By choosing z parallel to the [100] axis the ground-state wave function for Tm^{3+} in zero field is

$$|\psi\rangle_{[100]}(H = 0) = 0.6614|4\rangle - 0.3536|0\rangle + 0.6614|-4\rangle$$

This corresponds to the Γ_1 singlet which has no magnetic moment. On applying a magnetic field a moment is induced since the ground state becomes a mixture of Γ_1 and Γ_4 states. As $E(\Gamma_1 - \Gamma_4) \approx 26$ K (table 33.6) the contribution from the Γ_4 state becomes important only at very high magnetic fields. In a field of 12.5 kOe parallel to the [100], [110] or [111] axis, as used in magnetic measurements, the corresponding ground-state wave functions become (Lander et al., 1973):

$$|\psi\rangle_{[100]}(12.5\text{ kOe}) = 0.7526|4\rangle - 0.3493|0\rangle + 0.5581|-4\rangle$$

$$|\psi\rangle_{[110]}(12.5\text{ kOe}) = 0.4114|6\rangle - 0.4718|4\rangle + 0.2392|2\rangle + 0.5637|0\rangle + 0.2059|-2\rangle - 0.3494|-4\rangle + 0.2621|-6\rangle$$

$$|\psi\rangle_{[111]}(12.5\text{ kOe}) = 0.4884|6\rangle + 0.4167|3\rangle + 0.6170|0\rangle - 0.3324|-3\rangle + 0.3110|-6\rangle.$$

The induced moment per Tm^{3+} then is 1.18, 1.19 and 1.20 μ_B, respectively, i.e. the magnetic moment is still nearly independent of the direction of the applied field. For very high magnetic fields the magnetization must approach the saturation value $gJ\mu_B = 7\mu_B$. For the hard direction [100] saturation is reached in steps (Cooper, 1966). First the Γ_1 level becomes almost completely polarized to give $J \approx 4$. At 400 kOe one of the Γ_4 excited states crosses the Γ_1 state to give $J \approx 5$ in the ground state ($T = 0$). At still higher fields one of the $\Gamma_5^{(2)}$ levels crosses the Γ_4 state giving another step ($J \approx 6$) in the magnetization. Since in TmBi the crystal-field splitting is somewhat smaller, the steps in the magnetization curve will occur at lower fields. To our knowledge no magnetization measurements have yet been carried out in sufficiently high fields to prove Cooper's theoretical predictions.

Non-ordering singlet-ground-state systems can be used for the generation of very low temperatures (Bucher et al., 1971). As one induces the electronic magnetization with an external field one also induces an effective magnetic field at the nuclei via the hyperfine interaction. This induced hyperfine field amplifies the effect of the external field H_a on the nucleus by up to two orders of

magnitude:

$$\frac{\Delta H_{hf}}{H_a} = \frac{a\chi_{CF}}{g_J\mu_B \cdot g_N\mu_N} \equiv K$$

with a = hyperfine constant. For nuclear cooling K should be as high as possible. Since $\chi_{CF} \sim 1/\Delta$, a small crystal-field splitting is desirable.

Experimental values are

PrBi:	$\chi(0) = 0.0602\ \mathrm{cm^3/mole}$,	K = 11
TmSb:	0.505	88
TmBi:	0.47	80

(Bucher et al., 1971). Empirically PrBi turned out to be one of the most efficient nuclear cooling materials, similar to $PrTl_3$ and $PrPt_5$.

The pressure dependence of the low-temperature susceptibility of the Pr and Tm pnictides is rather queer. Based on the point-charge model the crystal-field splitting is expected to increase under pressure and therefore the magnetic susceptibility χ_{CF} should decrease but the contrary is observed (Guertin et al., 1975). For TmSb the observed value for $\partial \ln \chi/\partial p = +3 \times 10^{-3}\,\mathrm{kbar^{-1}}$ is nearly accounted for the Grüneisen constant γ derived from dilatation (Ott and Lüthi, 1976):

$$\partial \ln \chi_{CF}/\partial p = -\partial \ln E(\Gamma_4 - \Gamma_1)/\partial p = -\kappa\gamma_1 = +2.3 \times 10^{-3}\,\mathrm{kbar^{-1}}.$$

In the Pr monopnictides the ratio of the magnetic exchange to the energy difference between the Γ_1 ground-state singlet and the next Γ_3 triplet, $\mathcal{J}/\Delta_1$, is not far from the critical value. From $\chi(p)$ a pressure of ~80 kbar was estimated to induce magnetic ordering in PrSb (Guertin et al., 1975). In PrP, on the other hand, a spontaneous magnetic moment is induced by anion deficiency: $PrP_{0.85}$ revealed a spontaneous moment of $0.35\ \mu_B$/Pr at 1.6 K (Westerholt and Methfessel, 1977). In the nonstoichiometric compound an additional ferromagnetic exchange interaction stems from the increased conduction-electron concentration. Moreover, the non-cubic symmetry around the anion defects splits the Γ_3 state so that for a part of the Pr ions the critical value for $\mathcal{J}/\Delta_1$ is exceeded. The statistical distribution of the anion defects leads to fluctuations of the crystal-field splitting and the exchange field and this gives rise to the observed spin-glass-like magnetic behavior. Compare also the magnetic measurements of Franceschi and Olcese (1969) on PrP_{1-x} ($x \leq 0.15$).

3.4.2. Ce *monopnictides*

The most interesting NaCl-type pnictides are those with Ce. Their anomalous behavior is largely due to the proximity of the 4f and 5d energies whose relative positions are influenced by the crystal field. CeN is a homogeneous-mixed-valence compound in which Ce is nearly tetravalent at low temperatures and nearly trivalent at high temperatures (Didchenko and Gortsema, 1963). The larger lattice constant of CeP is obviously sufficient to lift the $d(t_{2g})$ band but the

separation of $f - d(t_{2g})$ energies is rather small. CeP and CeAs still show some anomalous behavior. Thus the Knight shift fails to track the magnetic susceptibility χ below about 75 K (Myers and Narath, 1973), in contrast to normal Ln pnictides, where the Knight shift is proportional to χ. From the pressure-dependence of the Knight shift Weaver and Schirber (1976) conclude that these anomalies arise from a sharp feature in the conduction-electron density of states, located very near the Fermi energy. It might be very interesting if one could synthesize mixed crystals $CeN_{1-x}P_x$ in order to study the f- and d-band shift continuously. Could one perhaps reach magnetic ordering in $Ce_{1-x}La_xN$ before the Ce concentration is too low? Anyway, CeP and CeAs do order at low temperatures, but though their effective crystal field is not very much lower than expected according to the point-charge model, the structural distortions appear to disagree with Trammell's (1963) predictions. The magnetic order, too, is antiferromagnetic of type I (Meier et al., 1976) instead of the expected type II. The predominance of the crystal field is responsible for the low value of the ordered magnetic moment. High-field magnetization measurements identify Γ_7 as the ground state. In the antimonide and bismuthide type II ordering can be achieved with dilutions (Meier et al., 1976). In CeSb alloyed with YSb or LaSb the magnetization changes from being very anisotropic with a [100] easy direction to being very anisotropic with a [111] easy direction (Cooper and Vogt, 1971b; Cooper et al., 1973). CeSb and CeBi display a rather complicated behavior probably because exchange and crystal-field effects are of comparable strength. In CeBi the influence of the crystal field is weakest. CeBi undergoes a second-order transition at 25 K to type I antiferromagnetism accompanied by a tetragonal distortion of the unit cell. Near 13 K a first-order transition (Tsuchida et al., 1973; Hulliger et al., 1975) occurs to type IA antiferromagnetism with no detectable structural change (Hulliger et al., 1975). In the low-temperature phase fields $H_a \geq 16$ kOe induce a ferrimagnetic phase (+++−) (Tsuchida and Nakamura, 1967; Hulliger et al., 1975; Lander et al., 1975). Above 12.5 K the magnetic phase diagram appears to be complicated, as follows from both magnetization (Bartholin et al., 1974) and magnetostriction curves (Hulliger et al., 1975).

The behavior of CeSb is anomalous in various ways. The unit-cell volume exhibits a crystal-field induced anomalous expansion near $T_N = 16$ K. The structural transition appears to be of second order whereas from the intensities of the antiferromagnetic reflections (Meier et al., 1976) the transition is concluded to be of first order. At 8.5 K another phase transition takes place in zero magnetic field with a minor change of the unit cell (Hulliger et al., 1975). At this temperature the magnetic structure changes from "mixed" to type IA. In the vicinity of the Néel temperature the magnetic behavior of CeSb is rather peculiar. A total of five "mixed" structures have been derived from neutron-diffraction studies (Bartholin et al., 1977; Fischer et al., 1978). These "mixed" structures result from periodic combinations of ferromagnetic (001) layers with moments along ±[001], and completely disordered, paramagnetic (001) layers. In applied fields various ferrimagnetic arrangements become stable.

The energy-level variation with molecular field has been calculated by Wang and Cooper (1970) for a Ce^{3+} ion in a cubic field and was used to explain the anomalous $\chi(T)$ curves of CeSb near T_N.

3.4.3. Sm *monopnictides*

Very little is known about the magnetic properties of Sm^{3+} pnictides. Whereas Junod et al. (1969) measured on SmN a nearly temperature-independent susceptibility with a slight increase below 50 K, reminiscent of Sm compounds displaying valence fluctuations, Stutius interpreted a peak in the specific heat of SmN at 18 K as a Néel point. In the Sm^{3+} ion the energy separation to higher spin-orbit J states is ~1500 K and ~3400 K. At least the first excited state has to be taken into account on calculating $\chi(T)$ curves. This is a $^6H_{7/2}$ state which decomposes into $\Gamma_6+\Gamma_7+\Gamma_8$. Junod et al. (1969) have calculated the susceptibility of Sm^{3+} assuming a $^6H_{5/2}-{}^6H_{7/2}$ separation of 1580 K and an overall splitting of 200 K and 100 K for ground state and first excited state, respectively. Fair agreement is achieved with the experimental data for SmP, to a lesser degree for SmSb and SmAs.

Neglecting exchange as well as the weak splitting of the excited levels the susceptibility below room temperature is

$$\chi(T) \approx C_M\{f(\Delta/T)/T + 12k/E_1\} \tag{33.23}$$

where the first term is identical with eq. (33.10) and $C_M = 0.089$ for the Sm^{3+} $J = 5/2$ ground state. Jones (1969) obtained fair agreement for $\chi(T)$ of SmAs between 77 and 300 K with $\Delta/k = 118$ K and $E_1/k = 1405$ K (using a diamagnetic correction $\chi_{dia} \approx -60 \times 10^{-6}$ emu/mole for SmAs). Exchange interactions between Sm^{3+} spins are weak. Ordering temperatures are around 2 K in SmP, SmAs and SmSb, but 9 K in SmBi.

3.4.4. EuN *and* EuP

In EuN and EuP $J_0 = 0$, therefore only a weak Van Vleck-type paramagnetism corresponding to the second term in eq. (33.10) is to be expected. Traces of divalent Eu therefore will render any $\chi(T)$ measurement unreliable. Junod et al. (1969) indicate that the experimental susceptibility data are ~25% higher than calculated, without however presenting the χ curves.

The Eu^{2+} handicap can be overcome either by specific-heat measurements or by means of the NMR technique. Above the Curie point Eu^{2+} impurities of low concentration are harmless in the specific heat. Stutius (1969b) thus derived for EuN a splitting of 500 K between the ground state $J = 0$ and the first excited state $J = 1$ which remains triply degenerate in the octahedral crystal field. The presence of other phases generally does not affect the Knight-shift measure ments of the compound being studied. The interaction between the conduction electrons and the nuclear magnetic moment shifts the NMR frequency by an

amount $K = \Delta H/H$ (compare Taylor and Darby (1972) p. 248):

$$K = K_0 + K_f(T)$$

K_0 is the Knight shift in the absence of s – f exchange, while $K_f(T)$ accounts for the polarization of the conduction-electron spins s by the localized spins $\boldsymbol{S}$ of the 4f electrons via the s – f exchange $-\mathcal{J}_{sf}\boldsymbol{S}\boldsymbol{s}$. For most of the Ln^{3+} ions $K(T)$ can be represented as

$$K(T) = K_0\left\{1 + \mathcal{J}_{sf}\frac{(g_J - 1)\chi_{4f}(T)}{2Lg_J\mu_B^2}\right\}.$$

For Sm^{3+}, Sm^{2+} and Eu^{3+} compounds, where the time average $\langle \boldsymbol{S}\rangle \neq (g_J - 1)\langle J\rangle$ at room temperature, the original form of $K(T)$ should be used:

$$K(T) = K_0\left\{1 - \mathcal{J}_{sf}\frac{\langle S(T)\rangle}{2\mu_B H}\right\}.$$

Neglecting the cubic crystal-field interaction for the $J = 2$ state the average value of the Eu^{3+} spin $\langle S_z(T)\rangle$ is

$$\langle \boldsymbol{S}_z\rangle = \frac{-\mu_B H}{2ZE_1}\,\frac{16 + (3\epsilon - 1)\exp(-\epsilon) + (15\epsilon - 5/3)\exp(-3\epsilon)}{1 + (\lambda\mu_B/AZ)[16 + (\epsilon - 1)\exp(-\epsilon) + (5\epsilon - 5/3)\exp(-3\epsilon) + \ldots]}$$

where $\epsilon = E_1/kT$, $E_1 = E(^7F_1) - E(^7F_0) = A$, $Z = 1 + 3\exp(-\epsilon) + 5\exp(-3\epsilon) + \ldots$ neglecting the splitting, $\lambda = H_{exch}/\langle S\rangle$ is the molecular-field parameter for the exchange energy $E_{exch} = 2\mu_B H_{exch} S$, and the Landé interval rule $E_J - E_{J-1} = AJ$ is applied. The phosphorus Knight shift in EuP was measured by Jones between 100 and 600 K. The experimental data were best reproduced with $E_1/k = 470$ K, $\lambda\mu_B/k = +6.5$ K and $\mathcal{J}_{sf}/k = -4.6$ K (Jones, 1969) or with 525 K, 0 K and −4.3 K (Jones, 1968), respectively.

3.4.5. Gd *monopnictides*

The Gd pnictides are the isoelectronic analogs of the famous Eu^{2+} chalcogenides, of which EuO is a ferromagnetic insulator with a Curie temperature of 69 K while EuTe is antiferromagnetic. GdN was reported to be ferromagnetic with the same Curie point as EuO. In the insulating Eu compounds the exchange interactions have to be indirect whereas in the Gd compound an additional contribution may stem from 4f-conduction electron polarization. In the NaCl structure nearest-neighbor exchange ($\mathcal{J}_1$) has the same symmetry as the $d(t_{2g})$ wave functions, while in the next-nearest-neighbor exchange ($\mathcal{J}_2$) the $d(e_g)$ wave functions are involved. According to Goodenough (1963)

$$\mathcal{J}_1 = b^2\mathcal{J}_{fd}/2S^2E^2_{f\to dt_{2g}}$$

where b is the transfer integral, which depends on the overlap between the $5d(t_{2g})$ levels, and $\mathcal{J}_{fd}$ is the intra-atomic exchange energy.

A similar formula holds for the antiferromagnetic superexchange with $E[p\to d(\epsilon_g)]$, the energy difference between the valence band and the $5d(e_g)$ band. On

going from EuO to EuTe the f energy drops and in the Gd compounds the f^7 level is about 5eV below the Fermi level. Therefore one might expect antiferromagnetism in non-metallic GdN and indeed there are some indications that elimination of the excess charge carriers converts the ferromagnet into an antiferromagnet (Busch et al., 1970, Zürcher, 1977). Mixing with metals such as the Gd chalcogenides, however, also enforces the antiferromagnetic coupling due to the different d-band of the metallic chalcogenides. While in $GdN_{1-x}O_x$ (Busch et al., 1970; Gambino et al., 1970), the coupling 4f–coupling electrons appears to be dominant, it is strong enough to induce ferromagnetic order in $GdP_{1-x}S_x$ (Wachter et al., 1978), $GdAs_{1-x}Se_x$ (McGuire et al., 1969), $GdSb_{1-x}Te_x$ (McGuire et al., 1969), as was discussed for the Gd pnictides by Kuznietz (1971). It is quite impressive that in $Gd_4N_{3.5}C_{0.5}$ the Curie temperature is as high as 190 K (Rhyne and McGuire, 1972). In the system EuO–EuN the Curie point increases up to 77 K at the homogeneity limit $EuO_{0.7}N_{0.3}$ (Chevalier et al., 1973).

The difference in the exchange mechanism acting in EuO and GdN is reflected also by the pressure dependence of the Curie point (McWhan, 1966) which is +0.4 K/kbar in the former and +0.08 K/kbar in the latter. In GdN, however, the Curie temperature does not rise above 77 K even at 100 kbar, in contrast to EuO.

The Gd pnictides show virtually no magnetic anisotropy since the Gd^{3+} is in an S state which is not influenced by the crystal field. The magnetization of antiferromagnetic Gd pnictides exhibits a characteristic field dependence (Busch et al., 1966). In a minor external field the antiferromagnetic spin arrangement is oriented perpendicularly to the field. Thus, what is seen is the temperature- and field-independent $\chi_\perp$ of the cubic antiferromagnet. The magnetic moment increases linearly with the applied field until all spins are arranged parallel to the field. The magnetic field necessary to saturate the magnetization is ~90 kOe in GdP, 165 kOe in GdAs and probably about 340 kOe in GdSb.

3.4.6. Nd *monopnictides*

NdP, NdAs, NdSb and NdBi are metamagnets with a type I antiferromagnetic order below their threshold fields of 19, 42 (Tsuchida et al., 1969), 83 (Busch et al., 1965) and 160 kOe (Hulliger and Landolt, 1976), respectively. For a $\Gamma_8^{(2)}$ ground state ($x \approx 0.77$) a saturation magnetization of 2.13 μ_B is calculated in fair agreement with the magnetization data for NdP and NdAs (Tsuchida et al., 1969). In fact the tetragonal distortion of the NaCl cell splits the Γ_8 quartets into two doublets which are further split by the molecular field. Furrer et al. (1976) have described the magnetic behavior of NdSb by a Hamiltonian which contains crystal-field $\mathcal{H}_{CF}$, exchange $\mathcal{H}_{ex}$ and magnetoelastic interactions $\mathcal{H}_{me}$ equivalent to eq. (33.22)

$$\mathcal{H}_{me} = -\sum_i \lambda_Q \langle O_2^0 \rangle O_2^0(i)$$

where

$$\lambda_Q = \frac{3a^3}{N(c_{11} - c_{12})} (B_\alpha^{[2]})^2.$$

With Lévy's $\bar{\epsilon}_{zz} = -1.69 \times 10^{-3}$ (after removing the volume change $\delta V/V = -0.63 \times 10^{-3}$)

$$\lambda_Q = \frac{3a^3(c_{11} - c_{12})\bar{\epsilon}_{zz}^2}{2\langle O_2^0 \rangle^2}$$

and from the elastic constants $c_{11} = 1.7 \times 10^{12}$ dyne/cm^2 and $c_{12} = 0.22 \times 10^{12}$ dyne/cm^2 λ_Q is calculated as 0.2 meV (Furrer et al., 1976). Similar calculations by Bak and Lindgård (1973) were based on estimated values for the elastic constants.

Furrer and Heer (1973) have demonstrated that for NdSb the dynamical exchange-interaction term in the Hamiltonian

$$\mathcal{H}_{\text{dyn}} = -\sum_{i,j} \mathcal{J}_{ij}(\boldsymbol{J}_i - \langle \boldsymbol{J}_i \rangle)(\boldsymbol{J}_j - \langle \boldsymbol{J}_j \rangle)$$

should not be neglected in calculating the magnetic properties. Including this term and taking the "exact" crystal-field term

$$\mathcal{H}_{\text{CF}} = B_2 O_2^0 + B_4 \left\{ \left(1 - \frac{10}{7}\frac{\Delta a}{a}\right) O_4^0 + 5 O_4^4 \right\} + B_6 \left\{ \left(1 - \frac{28}{3}\frac{\Delta a}{a}\right) O_6^0 - 21 O_6^4 \right\}$$

for the tetragonally distorted phase, Furrer and Heer calculated the zero-field magnetization $M = g\mu_B \langle J_z \rangle$ and obtained excellent agreement with the experimental curve whereas otherwise a discrepancy of ~10% remained. On the same substance Furrer and Tellenbach (1975) have exemplified the importance of contributions from higher J states in compounds with large sixth-order contributions to the crystal-field potential. In Nd^{3+} the first and the second excited J states $^4I_{11/2}$ and $^4I_{13/2}$ are, respectively, 2700 K and 5570 K above the $^4I_{9/2}$ ground state. While $\Gamma_8^{(1)}$ is virtually unaltered, Γ_6 and to a higher extent the ground state $\Gamma_8^{(2)}$ are shifted to lower energies (1–2%). Including J-admixture in the calculations the magnetic moment can quantitatively be accounted for. Thus, the zero-field magnetization is reduced from 3.13 μ_B to 3.01 μ_B as compared with an observed value of 2.98 μ_B (Furrer and Tellenbach, 1975).

3.4.7. *The* HoP *flop-side magnetic structure*

In this unique magnetic structure the moments are parallel to two cube axes, say x and y. In consecutive ferromagnetic (111) planes the magnetic moments are mutually perpendicular. It is unclear whether the flopside spin structure is stabilized by dipole forces (Trammell, 1963), by quadrupole interactions (Lévy and Chen, 1971) or by potential-minima effects based on the tunnelling model (Stevens and Pytte, 1973). Furrer and Kaldis (1976) were able to explain the appearance of this magnetic structure from an analysis of magnetic excitations in HoP single crystals based upon the many-level spin-wave model of Buyers et al. (1971). The magnetic behavior of HoP is described by the same Hamiltonian as was used for NdSb. The bilinear exchange was assumed to be isotropic and only nearest and next-nearest neighbor exchange interactions have been taken into account. The exchange between a Ho^{3+} ion and its 12 first and 6 second neighbors reduces to the ferromagnetic exchange with its six nearest neighbors of

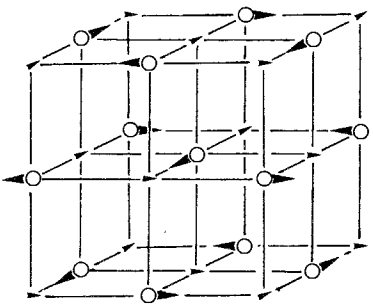

Fig. 33.4. The magnetic structure of HoP; $\frac{1}{8}$ of the magnetic cell. Small arrows correspond to moments on the Ho^{3+} ions, large arrows indicate the proposed anion displacements (Furrer and Kaldis, 1976).

the same sublattice, since the exchange energy with the perpendicular magnetic moments of the neighbors on adjacent sublattices vanishes in the Heisenberg-type exchange. The experimental data at 1.5 and 4.2 K yield (Furrer and Kaldis, 1976; Furrer et al., 1977):

$$\mathcal{J}_1 = 3.1 \times 10^{-3}\,\text{meV}, \quad \lambda_Q = -2.5 \times 10^{-5}\,\text{meV}.$$

This indicates that Trammell's calculations were based on a wrong estimate for the exchange energy between a Ho^{3+} ion and its neighbors on the same sublattice, namely 0.7 meV, while the present experiment predicts 3.6 meV. In the tunnelling model, where the magnetic moments are assumed to tunnel between equivalent potential minima, Stevens and Pytte (1973) suppose that the P ions are alternately displaced along the $+x$ and $-x$ direction. Half the Ho ions then would be in compressed anion octahedra and half in elongated octahedra, so that the resulting quadrupole interaction should average to zero, in contradiction to the experimental result. The anion displacement has to elongate the octahedra in the moment directions since $\lambda_Q < 0$ (fig. 33.4).

The flop-side magnetic structure is found also in the zero-field phase of DyP and DyAs, as well as in the first high-field phases of HoAs, HoSb and DySb.

For the magnetic structures of the nitrides of Tb $\cdots$ Er a complicated retarded-spiral arrangement was proposed (Child et al., 1963). In the case of HoN, however, no long-range order appears to exist at all, but only a short-range ferromagnetic order (Fischer et al., 1976).

4. Other binary pnictides

4.1. *Anti*-Th_3P_4-*type and related compounds*

The Th_3P_4 structure and its anti-type, the Gd_4Bi_3 structure, can be represented as an arrangement of $[ThP_8]$ or $[BiGd_8]$ octaverticons (fig. 33.5). Such an octaverticon contains triangular faces only and it may be derived from a cube by strong twisting. Each octaverticon is surrounded by eight similar polyhedra which have faces in common. The Th or Bi sublattice can be divided into three deformed diamond or ZnS sublattices.

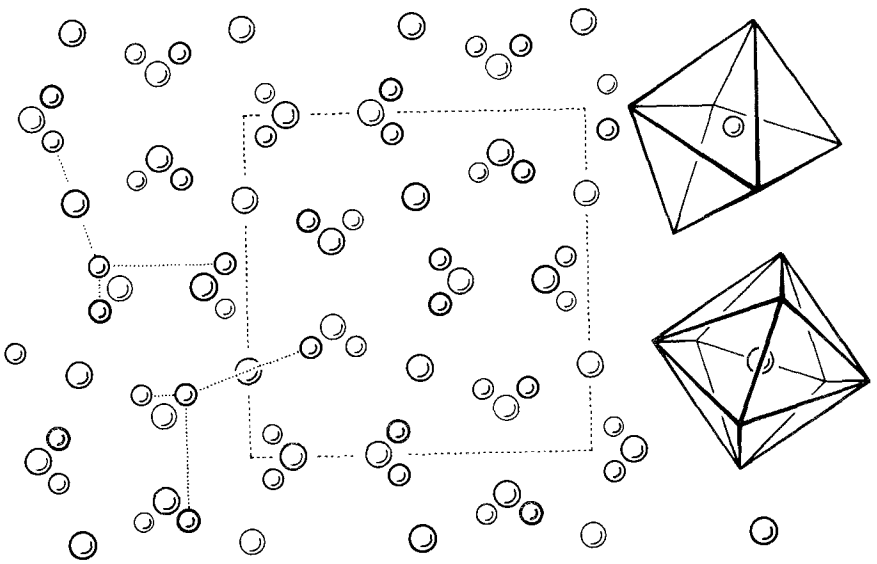

Fig. 33.5. The anti-Th_3P_4 or Gd_4Bi_3 structure. Large spheres: Bi, small spheres: Gd. The coordination polyhedra [$GdBi_6$] and [$BiGd_8$] are emphasized on the right part. On the left the additional Gd–3Gd contacts are indicated by dotted lines for each of the two distinguishable Gd sublattices.

Each P atom (or Gd atom in the anti-type) is surrounded by 3 + 3 Th (or Bi) atoms which define a distorted octahedron [PTh_6] or [$GdBi_6$]. As was pointed out by Kripyakevich (1963) and by Kharitonov et al. (1966) the 16 octahedra per bcc unit cell fill the space together with 12 vacant tetrahedra, i.e. with much fewer than in a close packing where we have twice as many tetrahedra as octahedra. Each octahedron shares 5 faces with neighboring octahedra and 3 with empty tetrahedra. The octahedra occur in two enantiomorphous forms and these are connected alternately by opposite faces into four non-intersecting columns. The three lateral faces make contact with the other columns. Within the columns (e.g. along $[1\bar{1}\bar{1}]$) Gd–Gd distances in Gd_4Bi_3 are $a\sqrt{3}/4 = 4.06$ Å, while towards the other columns Gd–Gd = $a(8x^2 - 2x + 1/4)^{1/2} = 3.50$ Å (for $x = 1/12$) only, which is ~2% shorter than the nearest-neighbor distance in Gd metal. The shortest Gd–Gd distance ($0.372a$ if $x = 1/12$) defines two nets of Gd atoms which are crystallographically identical but rotated and translated from each other (Holtzberg et al., 1964).

In the cubic Ln_4As_3 phases the site parameter x will be definitely lower than 1/12, the ideal value for the Th_3P_4 structure which leads to equal M – X distance. With $x = 1/12$ the three close Pr–Pr distances in Pr_4As_3 would be as low as 3.32 Å. With $x = 0.007$ M–3M = 3.44 Å while with $x = 0.06$ M–3M = 3.54 Å. The more reasonable M–3M distance, however, goes on account of the M–X bond distance. With decreasing value of x the two M–3X distances diverge more and more: 3.21 Å and 2.95 Å in the case $x = 0.07$ and 3.32 and 2.87 Å in the

TABLE 33.10.
Anti-Th_3P_4-type pnictides. The arsenides, the antimonides and the bismuthides are ordered according to decreasing values of r_M/r_X.

Compound	Melting behavior	Properties
La_4As_3[a]	incongruent[a]	supercond., $T_c = 0.5$ K[a]
Ce_4As_3[b,c]	incongruent	
Pr_4As_3[b,c]	incongruent	
Nd_4As_3[n]		
$Sm_4^{3+}As_3$[n]		
Yb_3GdAs_3[d]		
$Yb_3^{2+}Yb^{3+}As_3$[c,d]		
$Eu_3^{2+}GdSb_3$[d]	congruent[d]	antiferromagnetic[f]
Eu_3DySb_3[d]	congruent[d]	magnetic order below ~11 K[f]
La_4Sb_3[e]	congruent[d]	supercond., $T_c = 0.25$ K[a]
Ce_4Sb_3[e]	incongruent[d]	
Pr_4Sb_3[e]	incongruent[d]	ferromagnetic, $T_C = 38$ K[g]
Nd_4Sb_3[e]	incongruent[d]	
$Yb_3^{2+}GdSb_3$[d]	congruent[d]	
$Yb_3^{2+}DySb_3$[d]	congruent[d]	
$Sm_3^{3+}NdSb_3$[d]	congruent[d]	
$Sm_4^{3+}Sb_3$[d]	incongruent[d]	antiferromag.; $T_N = 140$ K[g]
$Yb_3^{2+}Yb^{3+}Sb_3$[d]	congruent[d,h]	[g]
$Sm_3^{3+}GdSb_3$[d]	incongruent[d]	
Gd_4Sb_3[i]	incongruent[d]	ferromagnetic, $T_C = 260$ K[i]
Tb_4Sb_3[e]	incongruent[d]	
Dy_4Sb_3[e]	incongruent[d]	ferromagnetic, $T_C = 17$ K[m]
Ho_4Sb_3[e]		
Y_4Sb_3[k]	stable 1660–2120°C[k]	
Tm_4Sb_3(?)[g]		ferromagnetic, $T_C = 17$ K[g]
Eu_4Bi_3[d]	congruent[d]	afm, $T_N = 12$ or 37 K[g]
$Eu_3^{2+}GdBi_3$[d]	congruent[d]	antiferromagnetic[f]
$Sm_{3-3}^{2+}Sm_{-1}^{3+}Bi_3$[d]	congruent[d]	mixed valence
La_4Bi_3[e]	congruent[d]	supercond., $T_c = 0.15$ K[a]
Ce_4Bi_3[e]	congruent[d]	mixed valence at low T
Pr_4Bi_3[e]	incongruent[d]	
Nd_4Bi_3[e]	incongruent[d]	
Yb_4Bi_3[d]	congruent[d]	mixed valence
Gd_4Bi_3[j]	incongruent[d]	ferromagnetic, $T_C = 340$ K[j]
Gd_3DyBi_3[d]	incongruent[d]	
Tb_4Bi_3[e]		

[a]Hulliger and Ott (1976); [b]Rieger and Parthé (1969); [c]Ono et al. (1970); [d]Gambino (1967); [e]Hohnke and Parthé (1966); [f]Hulliger (1976); [g]Bucher (1976); [h]Bodnar and Steinfink (1967); [i]Holtzberg et al. (1964); [j]Methfessel and Kneller (1963); [k]Schmidt and McMasters (1970); [m]Holtzberg et al. (1970); [n]Taylor et al. (1978).

case $x = 0.06$, which is to be compared with M–6X = 3.00 Å in PrAs. Thus the counteracting M–3X and M–3M distances will determine the domain of existence of these phases.

According to Gambino (1967) the anti-Th_3P_4 structure occurs within a rather

narrow range of radius ratios. In table 33.10 we have listed the known arsenides, antimonides and bismuthides in a sequence of decreasing r_M/r_X ratios.

Although many of these phases melt congruently this structure family is very badly characterized as regards the physical properties. Gd_4Bi_3, the representative found first (Methfessel and Kneller, 1963), is ferromagnetic with the highest Curie temperature of all rare earth compounds. The ordering temperature can be varied continuously between 340 K and 260 K in the system Gd_4Bi_3–Gd_4Sb_3 (Holtzberg et al., 1964). The variation of T_C with lattice constant is unexpectedly strong and opposite to that in the europium monochalcogenides. Ferromagnetic ordering was observed also in Pr_4Sb_3 and in Tm_4Sb_3 (the adherance to this structure type is uncertain for the latter) (Bucher, 1976). The lanthanum compounds are superconductors probably due to f-band enhancement of the density of states, since alloying with Y_4Sb_3 drastically lowers the critical temperature (Hulliger and Ott, 1976b). These La compounds contain 6 excess valence electrons per primitive cell. Reduction of this concentration by substituting Bi with Pb markedly lifted the transition temperature.

In the antimonides Sm is always trivalent (at least at room temperature) as can be deduced from the lattice constants. In Sm_4Bi_3, however, Sm is in a mixed-valence state. From the reported lattice constant we might conclude that Yb_4Sb_3 is $Yb_3^{2+}Yb^{3+}Sb_3$ which would be adequate for a semiconductor. The magnetic susceptibility and the metallic resistivity (Bodnar et al., 1968) prove however that Yb_4Sb_3 is a temperature-dependent mixed-valence compound. Yb_4Bi_3, on the other hand, is expected to display mixed valences already at room temperature. Eu is divalent in antiferromagnetic Eu_4Bi_3 as well as in the ternary phases. Sm_4Bi_3, Yb_4Sb_3 and Yb_4Bi_3 are of interest for Peltier cooling because mixed-valence compounds have a high figure of merit (Bucher, 1976). The unique rhombohedrally deformed Gd_4Bi_3 structure of Yb_4As_3 (Ono et al., 1970) may be induced by a deviating stoichiometry rather than an electronic rearrangement since the unit cells of the cubic and the trigonal modification differ only slightly.

It is well known that the normal Th_3P_4 structure is stable also with holes in the 8-coordinated sites. Thus Ln_3S_4–Ln_2S_3 mixtures exist with practically unchanged lattice constant. The equivalent to these subtraction series $Ln_{6-x}\square_xS_8(x \leqq 2/3)$ would be $Gd_8Bi_{6-x}\square_x$ if we refer the formula to the primitive unit cell. "Anion" deficiency is indeed possible in the anti-Th_3P_4 type and this is a means to increase the number of excess valence electrons or to counterbalance divalent Ln cations. The latter is met in Eu_3P_2 and Eu_3As_2, which, like Ba_3P_2 and Sr_3P_2, crystallize in the anti-Ce_2S_3 structure.

Eu_3P_2 is a ferromagnetic semiconductor with a Curie temperature of 25 K (Hulliger and Vogt, 1970; Busch et al., 1971). Eu_3As_2 appears to be metamagnetic below 17.5 K with a low threshold field, as was deduced from the photoconductivity as well as from the red-shift of the absorption edge (Wachter and Wullschleger, 1972). For Eu_3P_2 the magnetization-dependent red-shift of the absorption near the band gap amounts to 0.08 eV for thin films. The spectral sensitivity of the photoconductivity exhibits maxima near the absorption edge. With decreasing temperature the photoconductivity decreases to a pronounced

minimum at the ordering temperature. The absorption edge is at about 1.2–1.3 eV for Eu_3P_2 and Eu_3As_2. At higher photon energies the absorption spectrum shows similarities with that of the Eu^{2+} chalcogenides.

It is unclear whether pure Eu_3Sb_2 does exist or not. In an attempt to synthesize Eu_4Sb_2Te we obtained a Gd_4Bi_3-type phase with a much too low Te concentration. At present we ignore whether this was Te-stabilized Eu_3Sb_2 or Eu_4Sb_3. Eu_4P_2S and Eu_4As_2Se, on the other hand, are of the filled-up Gd_4Bi_3 type. Eu_4P_2S is the analog of $EuLa_2S_4$ and in this case also we wonder about an ordered distribution of P and S among the "diamond-type" sublattices (Hulliger, 1966; Carter, 1972). Eu_4P_2S is a red ferromagnetic insulator with $T_C = 23$ K whereas our Sb phase was antiferromagnetic. In analogy to Th_3P_4-type phases of the kind Ce_3AsS_3, we expect that the different size of the anions in compounds like Eu_4P_2Se, Eu_4As_2S or Eu_4As_2Te will not give rise to a change of the structure. The oxide phase Eu_4As_2O, however (and we assume the same for Eu_4P_2O, Eu_4Sb_2O and Eu_4Bi_2O) crystallizes no longer in the anti-Th_3P_4 structure but in a filled-up version of the Ti_2Bi type (Wang et al., 1977a).

While in binary Ln–pnigogen systems only the inverted Th_3P_4 structure is known, Dwight (1977) recently found a filled-up version of the normal Th_3P_4 structure in the $Y_3Au_3Sb_4$-type phases $Ln_3Au_3Sb_4$ with Ln = Nd, Sm, Gd, ..., Tm, Lu. Here the Au atoms are inserted in the 12(b) positions of the Th_3P_4 space group $I\bar{4}3d$ (Nr. 220) where they are in contact with four equidistant Sb atoms that form a strongly deformed tetrahedron. It is striking that these phases possess the same number of valence electrons as the semiconducting prototype of the unfilled structure, Th_3P_4. Therefore we speculate about the existence of possibly nonmetallic $Li_3Ln_3Sb_4$ phases. Since with actinide cations the Th_3P_4 structure occurs with P, As, Sb and Bi the $M_3^+Ln_3^{3+}X_4$-type phases are probably not restricted to Sb as the only possible anion. Furthermore we wonder whether this type might be stable also with divalent rare earth ions, Eu^{2+} and Yb^{2+}, and another divalent cation like Cd, e.g. $Cd_3Eu_3Sb_4$.

4.2. Ln_5X_3 *phases*

Among the pnictides with 5:3 stoichiometry we meet mainly two structure types, the hexagonal Mn_5Si_3 structure and the orthorhombic Y_5Bi_3 structure. A third type, the orthorhombic anti-U_3S_5 structure, occurs in the low-temperature modification of Yb_5Sb_3 as well as in Yb_5Bi_3, Eu_5Sb_3 and Eu_5Bi_3.

Most of the 1:1 rare earth pnictides crystallize in the rocksalt structure but no example is known with a NiAs structure. For the transition-element pnictides the NiAs structure and its distorted version, the MnP structure, are the rule whereas the NaCl structure is met only in some nitrides. The NiAs structure is based on a hexagonal close packing of the "anions" with the "cations" occupying all octahedral holes. The empty tetrahedral holes are arranged in pairs equivalent to a bipyramidal hole, that can take up a correspondingly larger cation. Both octahedral and bipyramidal sites are occupied in the Ni_2In structure. In the Mn_5Si_3 structure (= $Mn_5\square Si_3$) one third of the octahedrally coordinated cations is removed (small squares in fig. 33.6) which leads to a $\sqrt{3}\,a_0$ supercell. The empty

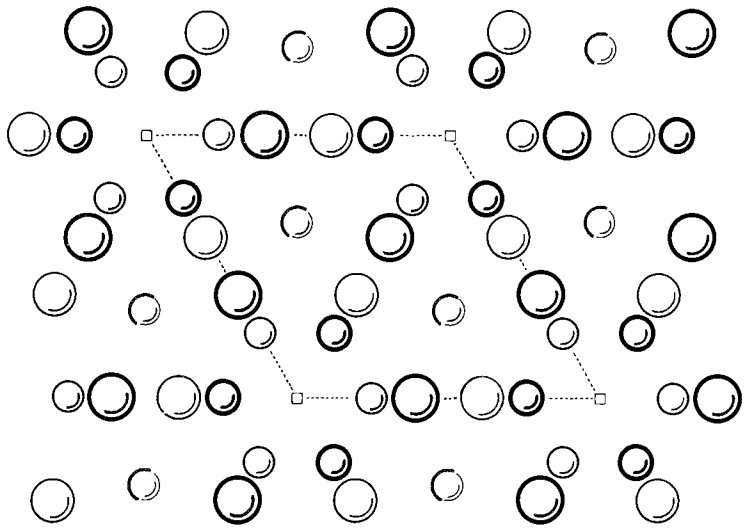

Fig. 33.6. Projection on (001) of the hexagonal Mn_5Si_3 structure. Small spheres: "cations"; large spheres: "anions". The squares indicate the empty octahedral sites of the Ni_2In structure.

octahedra are blown up and the bipyramidal cations are shifted towards the empty space. These displacements increase the coordination numbers. As compared with the NiAs structure the number of metal chains along the c-axis is reduced to 2/3 but the M – M distances ($=\frac{1}{2}c$) are still very short. In Ho_5Sb_3, $\frac{1}{2}c = 3.117$ Å, which corresponds to a metallic Ho – Ho bond.

The Mn_5Si_3 structure is stable within a broad range of electron concentrations: Ln_5Ga_3 (24 el.) – Sr_5Sb_3 (25 el.) – Ln_5Sn_3 (27 el.) – Zr_5Ga_3 (29 el.) – Ln_5Sb_3 (30 el.) – Zr_5Pb_3 (32 el.) – Ti_5P_3 (35 el.) – V_5Ge_3 (37 el.) – . . . . , which makes quasi-binary systems of these phases attractive for the study of superconductivity and magnetic s–f exchange interactions. Among the rare earth pnictides the Mn_5Si_3 structure has been observed in Yb_5As_3 (Ono et al., 1970), in most Ln_5Sb_3 phases (Rieger and Parthé, 1968), as well as in Ln_5Bi_3 with the larger Ln elements (Yoshihara et al., 1975). The Bi compounds appear to be slightly metal deficient ($Ln_{5-\delta}Bi_3$). Compare also table 33.2.

The Mn_5Si_3 structure is in some cases stabilized by small "impurity" atoms, such as carbon, nitrogen and oxygen, as well as by boron, as in $V_4As_3C_x$, $V_5P_3N_x$, $Hf_5Ge_3(O, C)_x$ and $Nd_5Si_3B_x$. For $x = 1$ the structure corresponds to an ordered Ni_2In superstructure. In the Ti_5Ga_4 type the octahedral hole within the deformed Ga close packing is taken by another Ga atom. The octahedral voids of the Mn_5Si_3 structure can, however, also be occupied by true metal atoms such as Ni, Cu, Zn, . . . (Ti_5Sb_3Cu, Zr_5Sb_3Ni, Hf_5Sb_3Zn, . . .) (Rieger and Parthé, 1968). Insertion of Cu into La_5Bi_3 . . . Tb_5Bi_3 increases slightly the a-axis but does not affect the c-axis (Hohnke and Parthé, 1969). We wonder whether insertion of such additional metal or non-metal atoms could stabilize the Mn_5Si_3 structure in the heavier Ln_5Bi_3 phases.

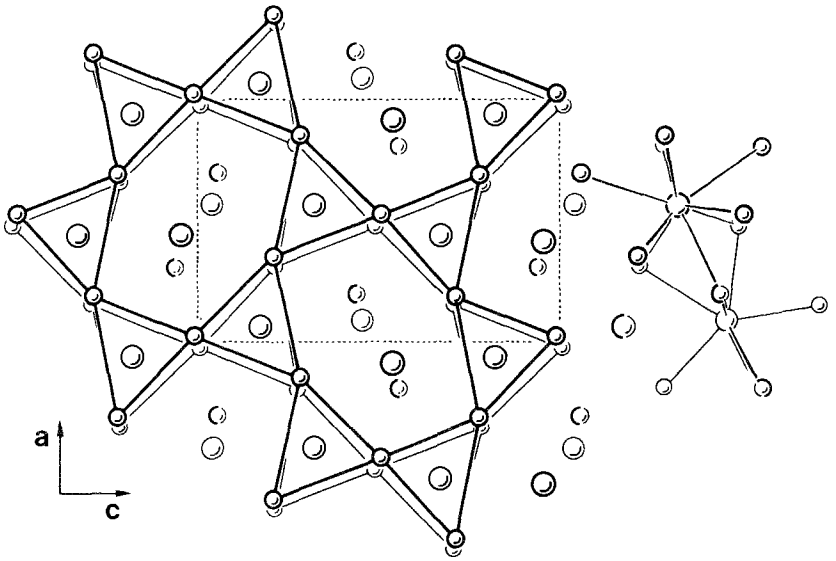

Fig. 33.7. (010) projection of the orthorhombic Y_5Bi_3 structure. The $[BiY_6]$ trigonal prism array is emphasized: Large spheres: Bi; small spheres: Y.

Whereas the magnetic properties of Ln_5Si_3 and Ln_5Ge_3 phases have been studied to some extent (e.g. Buschow and Fast, 1967) we are not aware of similar investigations on the corresponding pnictides. Tm_5Sb_3 is ferromagnetic below $T_C = 3.5$ K (Bucher, 1976); therefore we expect ferromagnetic properties also with Gd, Tb, etc. La_5Sb_3 is a superconductor with a critical temperature $T_c = 0.55$ K (Hulliger and Ott, 1977).

The other important 5:3 type, the Y_5Bi_3 structure (fig. 33.7), has recently been determined and described by Wang et al. (1976). This orthorhombic structure is built up of columns along [010] of $[BiY_{6/4}]$ trigonal prisms which share edges to form hexagonal channels. These channels are occupied by $[Y_2Bi_{2/2}]$ parallelograms which are connected via Bi corners to form a slightly twisted ribbon. The structure is very similar to the Rh_5Ge_3 structure. The two kinds of Bi atoms are coordinated to 9 and 8 metal atoms with distances Bi_I–Y = 3.174 · · · 3.466 Å and Bi_{II}–Y = 3.051 · · · 3.395 Å. The shortest metal–metal distances are relatively long: 3.363 Å, 3.487 Å and 3.509 Å in Y_5Bi_3. The Y_5Bi_3 structure and the Mn_5Si_3 structure can well be compared on Gd_5Bi_3 and Tb_5Bi_3 which crystallize in both types (table 33.1). There is a small increase of the volume on going from the Mn_5Si_3 type to the Y_5Bi_3 type but the average coordination number and the average Ln–Bi and Ln–Ln distances are not appreciably changed, except that in Gd_5Bi_3 the shortest Gd–Gd distance is increased from 3.21 Å to 3.39 Å. There is however a marked increase of the average Bi–Bi distance from 3.75 Å to 4.32 Å, which is roughly the Van der Waals distance.

In Lu_5Sb_3 the radius ratio is still larger than in Gd_5Bi_3 so that Lu_5Sb_3 will adopt

the Mn_5Si_3 structure. There is however one antimonide that crystallizes in a structure other than the Mn_5Si_3 type: Yb_5Sb_3. Orthorhombic "Yb_5Sb_2" turned out to be a low-temperature modification of Yb_5Sb_3, crystallizing in the anti-U_3S_5 structure (Brunton and Steinfink, 1971; Wang et al., 1976). A close similarity exists between the Y_5Bi_3 structure and the anti-U_3S_5 structure. Again $[SbYb_{6/4}]_\infty$ prism columns form hexagonal channels occupied by ribbons of $[Yb_2Sb_{2/2}]_\infty$ rhombs. The (010) projections of both structures are almost identical. The small difference between the two structure types arises mainly from the buckled layers at $y \approx 0, \frac{1}{2}$.

Yb_5Sb_3 is the only Ln_5Sb_3 phase of which two modifications are known. One might relate this fact with an $Yb^{3+} \rightarrow Yb^{2+}$ valence change. However, a comparison of the Ln_5Sb_3 volumes demonstrates that Yb is nearly divalent already in the hexagonal modification. The low-temperature modification has a slightly larger volume of 244.4 Å^3/formula unit compared with 240.7 Å/formula unit of the high-temperature modification. Susceptibility data (Bodnar et al., 1968) confirm that only a small part of the Yb atoms are trivalent in Yb_5Sb_3(h) and this percentage is indeed further decreased in the orthorhombic Yb_5Sb_3(r).

Bodnar et al. (1968) describe Yb_5Sb_3(r) as a p-type degenerate semiconductor. Their measurements yielded a room-temperature resistivity of $\sim 0.05\ \Omega$cm and a negative temperature coefficient between 80 and 370 K. The most striking property is the thermoelectric power: A Seebeck coefficient of $+323\ \mu V/K$ is reported, which is an order of magnitude larger than that of antimony that might have been present as a second phase. Judging from the crystal structure and the chemical formula we would exclude the possibility of semiconducting properties and ascribe the queer behavior to the mixed-valence state. Comparative electrical measurements on Ca_5Sb_3 may confirm this view.

Nonmetallic properties would require $\frac{1}{5}$ of the cations to be bonded in pairs according to the formula $M_8^{+2}(M_2)^{+2}Sb_3^{-3}$ in the simplest case.

In $Yb_5^{2+}Sb_3$ the radius ratio closely corresponds to that of La_5Sb_3 and Ca_5Sb_3. The fact that only Ca_5Sb_3 adopts the anti-U_3S_5 structure (table 33.2) may be an indication for the importance of the number of valence electrons engaged in bonding.

4.3. Ti_2Bi-*type compounds*

The tetragonal cell of the Ti_2Bi structure can be generated from the Cu_2Sb structure either by reflecting a Cu_2Sb cell at its basal plane or by superposing two Cu_2Sb cells displaced by $(\frac{1}{2}, \frac{1}{2}, 1)$. Thus, the basal $[MX_{4/4}]_\infty$ tetrahedron layer of the Cu_2Sb type transforms into a puckered layer of empty $[\square M_{4/2}X_2]$ octahedra sharing equatorial corners. The metal tetrahedron layers $[M_{4/4}]_\infty$ which connect the sandwiches to a three-dimensional network are of course the same in both structure types. It is noteworthy that a similar relation as between the Cu_2Sb and the PbFCl type exists also between the Ti_2Bi and the UGeTe type. A projection of the Ti_2Bi structure along the a-axis is shown in fig. 33.8. The eight nearest neighbors of M_I (the metal atoms in the mirror planes) lie at the corners

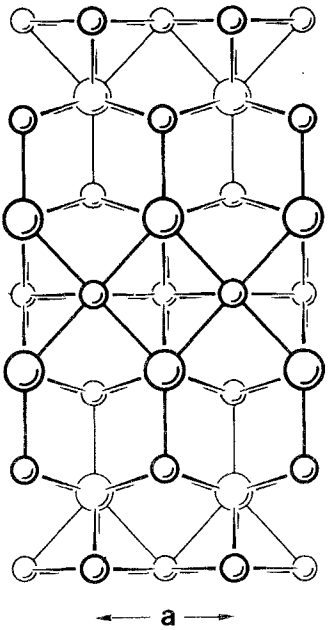

Fig. 33.8. (010) projection of the tetragonal Ti_2Bi structure met in the Ln_2Sb phases. Small spheres: metal atoms.

of a slightly distorted cube, while the 5X atoms around M_{II} form a square pyramid. The non-metal atoms have nine nearest M neighbors which form a monocapped square antiprism. The distances for La_2Sb are in detail (Stassen et al., 1970):

La_I – 4 La_I at 3.27 Å (square)

4 Sb at 3.40 Å (square)

(4 La_{II} at 3.98 Å (square))

La_{II} – 4 Sb at 3.30 Å ([$LaSb_4$] = flat square pyramid)

1 Sb at 3.36 Å (apex of the [Sb_5] pyramid)

(4 La_I at 3.98 Å (square pyramid))

Sb – 4 La_{II} at 3.30 Å ([$SbLa_4$] = flat square pyramid)

1 La_I at 3.36 Å (above the [4La_{II}] square)

4 La_I at 3.40 Å ([$SbLa_4$] square pyramid in the opposite direction)

The La_I–La_I distances within the planar metal sheets are extremely short compared with the distances in metallic lanthanum (3.73 and 3.77 Å). In the Cu_2Sb-type compounds the radius ratios r_M/r_X are generally ~0.8 · · · 0.9 so that the atoms in the planar layer are not close packed. In La_2Sb, however, r_M/r_X = 1.15 so that the La_I atoms have to be compressed by ~12% (Stassen et al., 1970).

Geometrically the Ti_2Bi structure thus might be stable for the remaining $Ln_2^{3+}Sb$ compounds as well as for $Ln_2^{3+}Bi$. It is however found only for Ln_2Sb with $Ln = La \cdots Sm$ (Hulliger, 1976), and Ln_2Bi with $La \cdots Nd$ (Yoshihara et al., 1975). On the other hand, the Ti_2Bi structure was reported also with Ca, Sr and Ba (Eisenmann and Deller, 1975), even for the arsenides (Better et al., 1976). The most striking property of these alkaline-earth phases is their non-metallic character (Eisenmann and Schäfer, 1974; Better et al., 1976). The puzzle was recently solved by Wang et al. (1977a) who demonstrated that Eu_2As is in fact Eu_4As_2O, an additional oxygen atom being inserted in the elongated M_I octahedral holes of the mirror planes of the Ti_2Bi-type structure. Other iso-electronic analogs of Eu_4As_2O might be $Na_2Ln_2Sb_2O$ and $Na_2Ln_2Bi_2O$ with trivalent Ln cations.

Deducing from the properties of Ca_4Sb_2O, La_2Sb thus appears to contain three excess valence electrons per formula and these metallic electrons induce a transition to the superconducting state at $T_c \approx 0.8$ K (Hulliger and Ott, 1976). Alloys like $(La, Ba)_2Sb$ or $(La, Zr)_2Sb$ may serve to vary T_c by varying the electron concentration.

Surprisingly the praseodymium compound is again ferromagnetic: In Pr_2Sb a Curie temperature $T_C = 62$ K was observed (Bucher, 1976).

4.4. $LnSb_2$ *and* $LnBi_2$ *phases*

As can be seen in table 33.1 at least five structure types occur in the $LnSb_2$ and $LnBi_2$ phases. The light rare earth diantimonides all crystallize in the orthorhombic $SmSb_2$ structure. For $LaSb_2$ a second modification was observed (Murray and Taylor, 1970). The occurrence of this second form in an iodine transport reaction may be coupled with a slightly different stoichiometry. Murray and Taylor remark that the formation of the bright, shiny flakes of $LaSb_2$(h) is favored by an excess of antimony in the charge. Moreover, both forms of $LaSb_2$ were obtained below 900°C while Wang and Steinfink (1967) detected no phase transition up to 1000°C. The latter authors synthesized their $LnSb_2$ samples by preheating the elements at 500°C and annealing the reaction products at 700–750°C. $LaSb_2$, $NdSb_2$ (and $YbSb_2$) were also prepared by a liquid–liquid reaction in tantalum tubes at about 1500°C. $NdSb_2$, $SmSb_2$ (and $YbSb_2$) also formed above 600°C at pressures from 15 to 70 kbar (Eatough and Hall, 1969).

In the $SmSb_2$ structure double sheets of a kind of square antiprisms $[SmSb_8]$ are held together by Sb–Sb bonds. These anion–anion bonds are inclined relative to the layer normal and the bond lengths are close to the single-bond distance: 2.88 Å in $LaSb_2$ and 2.79 Å in $SmSb_2$. Wang and Steinfink (1967) reasoned that the repulsion in the Sb–Sb bond becomes critical in $GdSb_2$ and causes the $SmSb_2$-type structure to become unstable. Eatough and Hall (1969), however, were able to synthesize $SmSb_2$-type $GdSb_2$ and $TbSb_2$ at pressures up to 70 kbar and temperatures up to 1800°C. Moreover, $NpSb_2$, $PuSb_2$ and $AmSb_2$ were found to adopt this structure, and in these phases too the shortest Sb–Sb distances are smaller than in $SmSb_2$ (Charvillat et al., 1977). According to Wang and Steinfink

(1967) the neighborhood in $SmSb_2$ is:

Sm–4 Sb_I at 3.134, 3.136 and 3.193 Å (2×) (slightly distorted square 0.82 Å below it)
4 Sb_I at 3.319 (2×) and 3.300 Å (2×) (in the rectangular layer 2.50 Å above it, rotated 45° with respect to the lower square)
1 Sb_I at 3.479 Å (below the Sb_I square layer in the adjacent double sandwich)
1 Sm at 4.198 Å

Sb_I–4 Sm at 3.134, 3.136 and 3.193 Å (2×) (slightly distorted square 0.82 Å above it)
1 Sm at 3.479 Å (of the adjacent double sandwich)
1 Sb_I at 2.720 Å (link to the adjacent sandwich)

Sb_{II}–4 Sm at 3.300 (2×) and 3.319 Å (2×) (distorted tetrahedron)
4 Sb_{II} at 3.026 (2×) and 3.086 Å (2×) (rectangle of the inner Sb sheets)

If the 4/4 Sb_{II}–Sb_{II} bonds were localized (they are omitted in fig. 33.9) the bonding scheme might be adequate for a nonmetallic $ThSb_2$ or $HfSb_2$. A

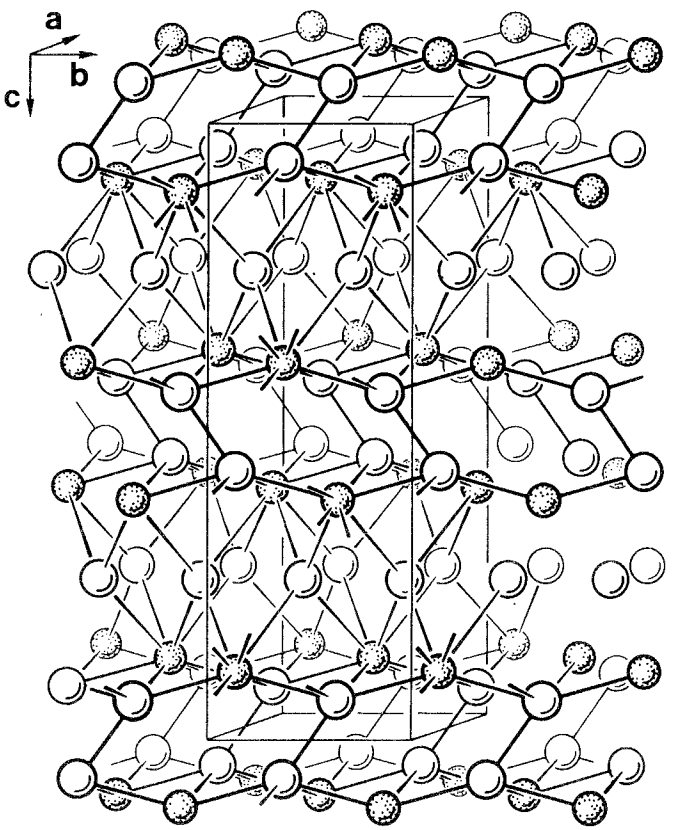

Fig. 33.9. The orthorhombic structure of $SmSb_2$. Stippled spheres: Sm.

distortive metal → semiconductor transition might be possible if the Sb_{II} square nets would separate into zigzag chains. Hall (1969) claimed the silver-grey, brittle diantimonides to be semiconductors but in the undistorted $SmSb_2$ structure the bonds are definitely not saturated, as is confirmed by the occurrence of superconductivity in $LaSb_2$ at $T_c \approx 0.4$ K (Hulliger and Ott, 1976).

$PrSb_2$ is antiferromagnetic below $T_N = 5.1$ K and undergoes a first-order transition to ferromagnetic ordering in a field of 6.5 kOe at 1 K (Bucher, 1976).

Obviously $TbSb_2$ represents the lower limit of stability of the $SmSb_2$ structure since with smaller metal atoms it was not possible to retain a metastable $SmSb_2$-type modification by quenching from high temperatures and pressures. The influence of the valence electron concentration becomes evident from the fact that $ThSb_2$ and USb_2 which according to their radius ratios correspond to $GdSb_2$ and $ErSb_2$, crystallize in the Cu_2Sb structure. The $LnSb_2$ phases with the heavier rare earth elements except $YbSb_2$ appear to exist only in a metastable form as they cannot be prepared by ordinary techniques but only by quenching from high temperatures and pressures. An almost too simple structure was derived for $HoSb_2$(p) from a powder pattern (Johnson, 1971). Sb zigzag chains are inserted into a hexagonal cell of the metal atoms. This arrangement leads to a rather open Ho–Sb coordination:

Ho–4 Sb at 3.15 Å	Sb–2 Sb at 3.02 Å
6 Ho at 3.34 Å	2 Ho at 3.15 Å

In fig. 33.10 only the Ln–Sb and the shortest Sb–Sb bonds are indicated. The single bonds of the Sb–Sb pairs in $SmSb_2$ are now replaced by roughly half bonds within the chains and the bonding is again metallic.

There is not much information available about the physical properties of these brittle compounds. $TmSb_2$ is a Van Vleck paramagnet, showing no magnetic order down to 0.5 K. Obviously the low symmetry of the crystal field acting on the Ln ions splits all low-lying levels into singlets (Bucher, 1976).

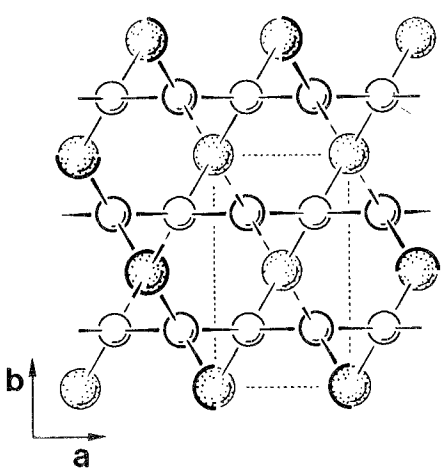

Fig. 33.10. (001) projection of the orthorhombic $HoSb_2$ structure. Stippled spheres: Ho.

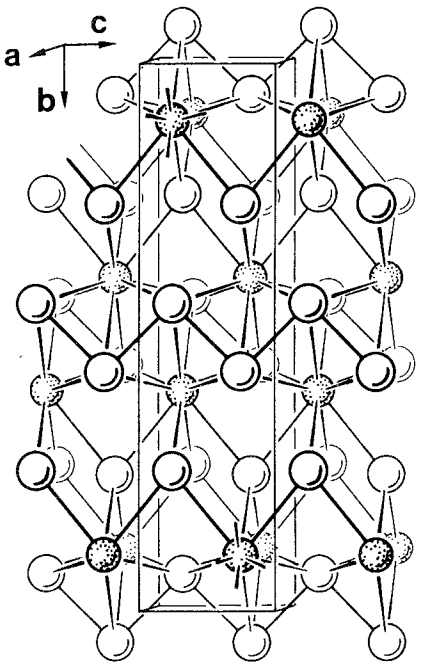

Fig. 33.11. The orthorhombic $ZrSi_2$ structure met in $YbSb_2$. Stippled spheres: metal atoms.

We wonder why the high-pressure experiments led to the normal-pressure $ZrSi_2$-type modification of $YbSb_2$ and not to a $HoSb_2$-type polymorph with trivalent Yb. Under normal pressure the $ZrSi_2$ structure is stable in $YbSb_2$ up to its melting point of 945°C (Bodnar and Steinfink, 1967). $YbSb_2$ contains only a small fraction of trivalent Yb as follows from a Curie–Weiss behavior between 100 and 300 K (Bodnar et al., 1968). Deviations due to the crystal field or an electronic rearrangement occur below 100 K. If the structure is a consequence of the cation valence then we might expect isostructural $CaSb_2$ to exist. The $ZrSi_2$ structure, however, is a very flexible structure. It is met also in phases such as $GdSn_2, \ldots, LuSn_2, UGe_2, \ldots$ According to the radius ratio $Yb^{2+}Sb_2$ would roughly correspond to $Ce^{3+}Sb_2$. The rare earth atoms display the same squeezed square-antiprism coordination as in the Cu_2Sb and the $SmSb_2$ type, but now with two additional Sb neighbors, as can be seen in fig. 33.11. We recognize similar double sandwiches Sb_I–Yb–$(Sb_{II})_2$–Yb–Sb_I as in $SmSb_2$ but interlinking of these units now gives rise to the occurrence of Sb_I zigzag chains instead of the Sb–Sb pairs met in $SmSb_2$. The coordination is as follows:

Yb–4 Sb_I at 3.193 Å (square 0.70 Å below it)
4 Sb_{II} at 3.264 (2×) and 3.296 Å (2×) (square 2.43 Å above it)
2 Sb_I at 3.570 Å (below the Sb_I square)
2 Yb at 4.062 Å

Sb_I–2 Sb_I at 2.966 Å (zigzag chain)
4 Yb at 3.193 Å ([$SbYb_4$] = flat square pyramid)
2 Yb at 3.570 Å

Sb_{II}–4 Yb at 3.264 (2×) and 3.296 Å (2×) (distorted tetrahedron)
4 Sb_{II} at 3.119 Å (within the puckered layer)

If the Sb_I–Sb_I bonds within the zigzag chains were single bonds then with a divalent cation we would have the same valence electron deficit as in $SmSb_2$. In fact the Sb_I–Sb_I distances correspond to half bonds only so that the cation/anion valence electron misfit is even more pronounced. This misfit is obviously necessary for the stability of the $ZrSi_2$ structure. Thus, the observed metallic conductivity (Bodnar et al., 1968) was to be expected.

Europium has a much higher tendency than Yb to behave as a divalent cation and to form nonmetallic compounds. Thus it is reasonable that $EuSb_2$ crystallizes in the $CaSb_2$ structure (Deller and Eisenmann, 1976b) found also in $SrSb_2$ (Deller and Eisenmann, 1976c). This monoclinic structure is in fact a distorted version of the $ZrSi_2$ structure as can be seen from fig. 33.12. The puckered Sb_{II} square nets met in the $ZrSi_2$-type structure of $YbSb_2$ are transformed into

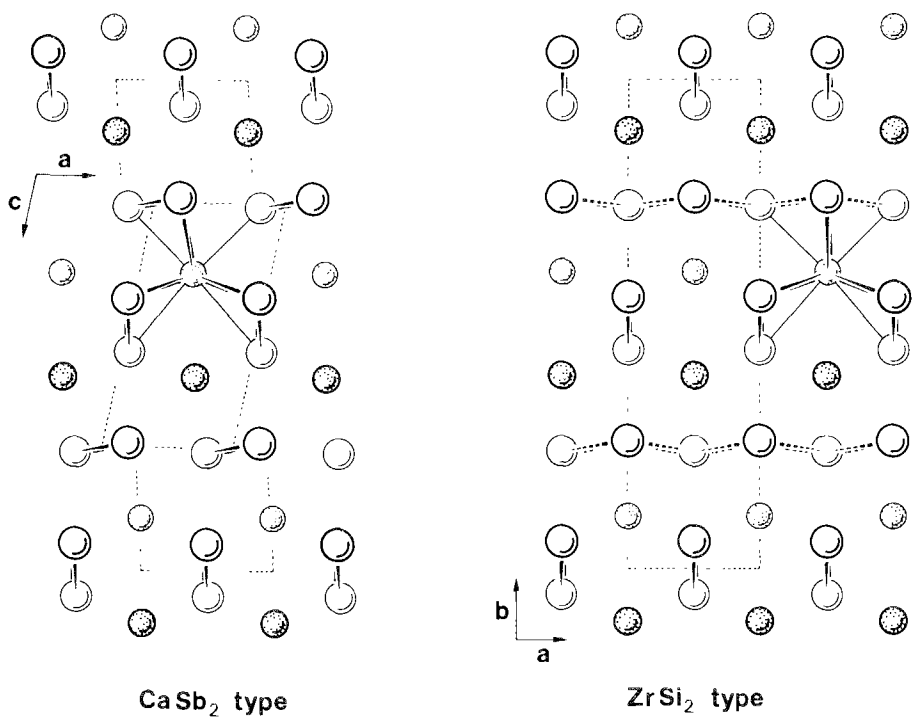

Fig. 33.12. The relation between the monoclinic $CaSb_2$-type structure of non-metallic $EuSb_2$ and the orthorhombic $ZrSi_2$-type structure of metallic $YbSb_2$. Stippled spheres: cations.

parallel zigzag chains in the $CaSb_2$ structure. Thus, the distortions are such that the four metallic fractional bonds of each Sb_{II} atom in the $ZrSi_2$ structure are replaced by two single bonds. The distortions lead to single bonds also within the zigzag chains formed by the Sb_I atoms. The bonding therefore is nonmetallic and the corresponding ionic formula $M^{2+}Sb_2^-$ demonstrates that $CaSb_2$, $SrSb_2$ and $EuSb_2$ are Mooser–Pearson phases.

The very soft, plate-like crystals of $LnBi_2$ appear to crystallize in a distorted version of the anti-Ti_2Bi structure (Yoshihara et al., 1975). Triclinic unit cells have been proposed for these air-sensitive phases that decompose at about 900°C. Nomura et al. (1977) deduced an orthorhombic cell from single-crystal X-ray studies.

4.5. LaP_2- *and* $NdAs_2$-*type compounds*

In contrast to the monophosphides the diphosphides are stable in air (Schmid and Hahn, 1970). The monoclinic polyphosphide LaP_2 crystallizes in brittle grey-black crystallites with a bright, metallic lustre. Its structure (fig. 33.13) (v. Schnering et al., 1975) consists of P_3 and P_5 fragments held together by the La^{3+} ions. Each La cation has 9 P neighbors at distances from 2.96 to 3.33 Å. The P_5 unit may be considered as part of a six-membered ring in saddle form as met in TlP_5. Bond angles within the P_3 and P_5 units vary between 103 and 114°. The P–P distances are ~2.22 Å obviously corresponding to single bonds. Formally the chemical bonding can be characterized by an ionic formula $LaP^{-1}P^{-2}$. LaP_2-type compounds are thus Mooser–Pearson phases and therefore expected to be semiconductors. According to table 33.1 the LaP_2 structure is found also in the high-temperature modification of CeP_2 (Hayakawa et al., 1975 and 1976) and

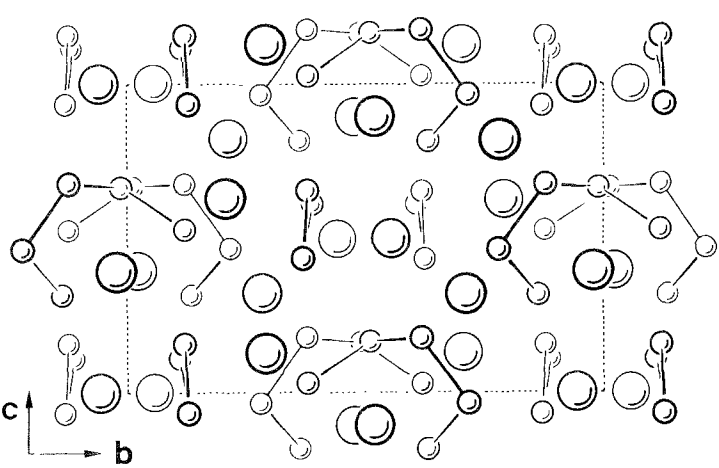

Fig. 33.13. The monoclinic LaP_2 structure projected on the (a, b) plane. Small spheres: P; large spheres: La.

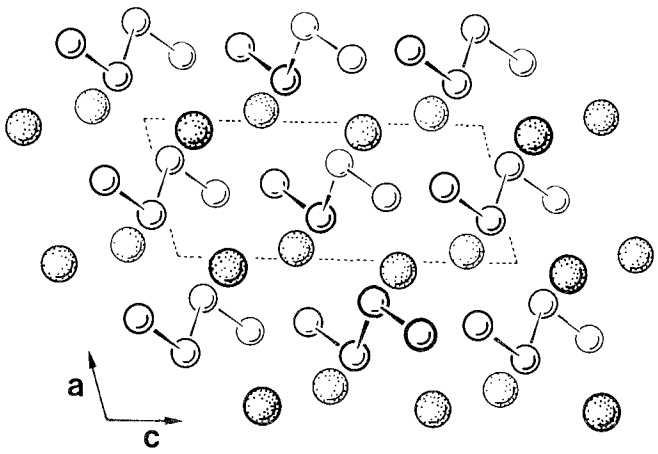

Fig. 33.14. The monoclinic $NdAs_2$-type structure of CeP_2. Large stippled spheres: Ce, small spheres: P. Only the covalent bonds within the P_4 chain fragments are indicated.

$LaAs_2$ (Ono et al., 1970). The remaining disphosphides (Hassler et al., 1974; Ono et al., 1974) and diarsenides crystallize in the monoclinic $NdAs_2$ structure, which contains P_4^{-6} groups. Since the high-temperature modifications of LaP_2 and $LaAs_2$ obviously are semiconductors a nonmetallic bonding in the low-temperature modifications was to be expected. The $NdAs_2$-type structure was recently solved for CeP_2 (Schnering and Wichelhaus, 1976). It is based on the same ionic formula $Nd^{+3}As^{-1}As^{-2}$ but in this case only one kind of As_4 zigzag fragments occur (fig. 33.14). A third modification might be derived from the formula $Ln^{+3}P^0P_3^{-2}$ with flat $[P^0P_3^{-3}]$ trigonal pyramids.

4.6. LnP_5 *compounds*

As the concentration of phosphorus is greatly increased these phases become more and more phosphorus-like. All LnP_5 compounds are resistent against nonoxidizing acids and dilute bases (v. Schnering et al., 1976). Black prismatic crystals up to 2 mm were grown in a temperature gradient by reacting red phosphorus and some iodine with Ln and alkali halide melt (Wichelhaus and v. Schnering, 1976). Three structure types have been reported up to now (v. Schnering et al., 1976), the LaP_5 type, the NdP_5 type and the β-YbP_5 type. The LaP_5 type is a superstructure of the NdP_5 type with $a = 2a_0$. The phosphorus framework of both structures may be described as a distorted black-phosphorus lattice from which $\frac{1}{6}$ of the atoms are removed. Therefore, three of the five anions have one valence electron available to bind a cation. The missing P atom, which would connect three 6-membered saddle-like P rings, leaves a 12-membered corrugated P ring (fig. 33.15). Adjacent P layers are only slightly displaced relative to each other so that large zig-zag channels are created,

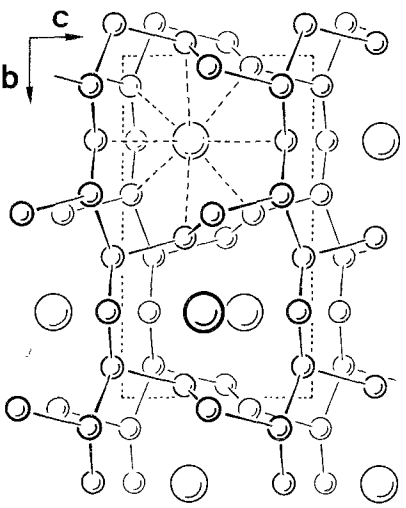

Fig. 33.15. The monoclinic NdP_5 structure projected on the (b, c) plane. Small spheres: P; large spheres: La.

appropriate to take up the large Ln^{3+} ions. In order to restore the charge balance we have to introduce 1 Ln^{+3} for each missing P atom. Each cation is coordinated to 8 P atoms. The non-metallic character of the bonding in these Mooser–Pearson phases $Ln^{+3}P_2^0P_3^{-1}$ is thus evident.

In α-YbP_5 the cation is trivalent. One might expect to find divalent Yb in the second modification, β-YbP_5. The P sublattice therein has indeed changed, as it contains partly 4-membered rings (v. Schnering, *et al.* 1976). However, the cation coordination is reduced to 7 and the volume is even smaller than that of α-YbP_5, so that the cation is certainly trivalent too. We may therefore expect the β-YbP_5 structure to be appropriate also for LuP_5 (and perhaps for $LaAs_5, \ldots$).

4.7. LnP_7 *compounds*

In the Mooser–Pearson phases $Ln^{+3}P_4^0P_3^{-1}$ pairs of 7-membered corrugated rings $P_5^0P_2^{-1}$ form P_{12} units by sharing a P^0 pair (Wichelhaus and v. Schnering, 1975). One P^0 atom of each $P_5^0P_2^{-1}$ ring links the $P_8^0P_4^{-1}$ units symmetrically into ribbons along [100] of the monoclinic cell (fig. 33.16). Four P^{-1} connect the P_{12} units via the remaining 4 P^0 atoms into a three-dimensional array $(P_8^0P_4^{-1} + \frac{4}{2}P^{-1})_\infty$. The Ln^{+3} ions which have to supply the bonding electron for the singly occupied p orbital of each P^{-1} are located in the holes of the phosphorus framework and each has 10 P neighbors (one of each P^0 and two of each kind of P^{-1}) at distances of 3.06–3.23 Å.

Strangely enough there is no marked difference between bond distances and other contacts, since $La–P^0 = 3.13–3.20$ Å and $La–P^{-1} = 3.06–3.23$ Å.

The P–P bond distances are between 2.17 and 2.25 Å and the bond angles vary from 88.5 to 114.4°. Up to now LnP_7 phases are known with the three largest elements only. We wonder whether $Eu^{2+}ThP_{14}$ might be stable in this structure

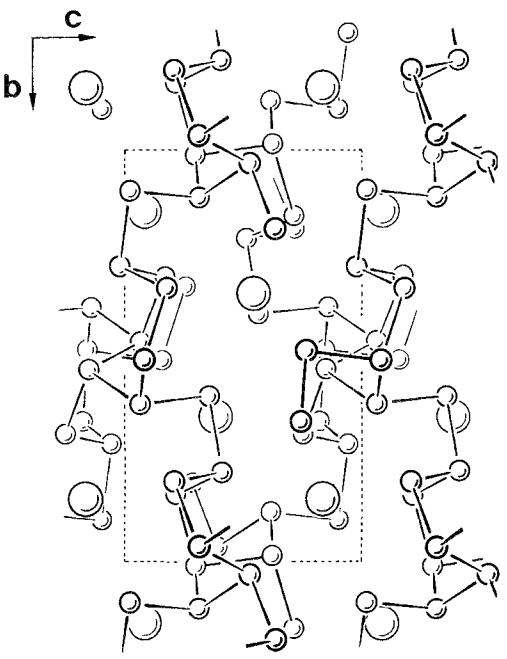

Fig. 33.16. The monoclinic LaP_7 structure projected on the (b, c) plane. Small spheres: P; large spheres: La.

too. The LnP_7 phases crystallize in the form of black flat rhombs (v. Schnering et al., 1976). The chemical stability of the polyphosphides LnP_n against acids and bases increases with higher phosphorus contents but, of course, the reverse holds for their thermal stability.

4.8. *Compounds with divalent cations* (EuAs, EuP_2, Eu_5As_4, Eu_2As_3, Eu_3As_4, EuP_3, EuP_7, $Yb_{11}Sb_{10}$)

Since the ionic radii of Eu^{2+} and Yb^{2+} match those of Sr^{2+} and Ca^{2+} almost exactly there is an extended analogy between their compounds, as can be checked in table 33.2. Unfortunately the crystal structures of many of these phases are yet unknown. In the equiatomic Eu and Yb pnictides decreasing electronegativity of the anion has a dramatic effect. In the case of europium the nitride and the phosphide are normal trivalent NaCl-type representatives. EuAs, however, contains divalent cations (Iandelli and Franceschi, 1973) and adopts a structure found also in the Mooser–Pearson phases CaP, SrP, CaAs and SrAs (Ono et al., 1971; Iandelli and Franceschi, 1973). The structures of EuSb and EuBi (if they exist at all under normal conditions) are not determined yet. The Yb pnictides are anomalous too, but in a different way. YbN, YbP and YbAs behave like other Ln^{3+} monopnictides, but YbSb, instead of melting at a maximum of the Yb–Sb phase diagram, decomposes peritectically near 900°C. YbBi, finally, cannot be prepared by common techniques. The closeness to a

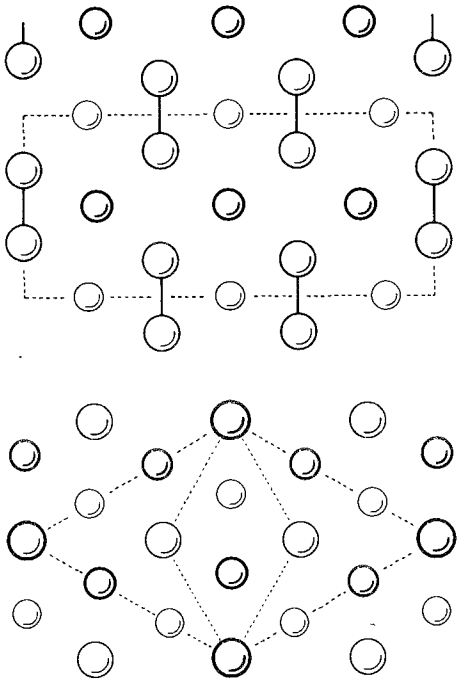

Fig. 33.17. The Na_2O_2-type structure of EuAs projected on (001) (below) and on (110) (above). Small spheres: cations; large spheres: anions.

valence instability renders these systems very attractive. Thus, it might be interesting to study the temperature and pressure diagram of the system EuP–EuAs. In contrast to the case of the Eu monochalcogenides the temperature- or pressure-induced transition that we expect for Na_2O_2-type $EuAs_{1-x}P_x$ compositions is not isostructural ($Na_2O_2 \rightarrow NaCl$) so that the conductivity character needs not to change. EuP may be converted to the divalent state and the Na_2O_2 structure also by adding SrP: $Eu_{1-x}Sr_xP$, whereas the trivalent state of Eu may be stabilized in mixed crystals $Lu_{1-x}Eu_xAs$. Similarly divalent Yb may establish in $Ca_{1-x}Yb_xP$ and $Ca_{1-x}Yb_xAs$, and a study of $Lu_{1-x}Yb_xBi$ might yield information about the possibility to synthesize NaCl-type YbBi at low temperatures.

The Na_2O_2-type structure of EuAs is an anti-NiAs-type $\sqrt{3}a_0$ superstructure distorted due to the formation of anion–anion pairs (fig. 33.17). Each Eu atom is thus surrounded by 6 As at the apices of a trigonal prism (Eu–As = 3.08–3.18 Å). The bonded –Ni–Ni–Ni–Ni– chains along the c-axis of the NiAs structure become

$$\cdots\cdots \underset{2.53\ \text{Å}}{\text{As}} \text{———} \underset{3.61\ \text{Å}}{\text{As}} \cdots\cdots \underset{2.53\ \text{Å}}{\text{As}} \text{———} \text{As} \cdots\cdots$$

in the distorted anti-type. Each cation has also six cation neighbors which form again a trigonal prism, Eu–Eu = 4.11 Å. A Curie–Weiss law was observed

between 80 and 470 K with a Bohr-magneton number of 7.46 and $\theta_p = 12$ K (Iandelli and Franceschi, 1973). Thus, EuAs is possibly another ferromagnetic semiconductor.

Nothing is known so far about (antiferromagnetic?) EuSb which might crystallize in the hexagonal Li_2O_2 structure met also in β-NaS.

Obviously, the structure of EuP_2 is different from that of SrP_2 and BaP_2 (Maass, 1970). Its powder diagram (Mironov and Brygalina, 1974; Mironov et al., 1974) contains much less lines. Since a structure according to a formula $M^{+2}P^0P^{-2}$ is geometrically impossible, a structure corresponding to a formula $M^{+2}P_2^{-1}$ will be realized with each anion being bonded to two other anions by forming zigzag chains or corrugated rings (Hulliger and Mooser, 1963 and 1965). The orthorhombic structure of $EuAs_2$ (Ono et al., 1971) will be related.

From its powder pattern we deduce that Eu_2As_3 crystallizes in the monoclinic Ca_2As_3 structure (Deller and Eisenmann, 1976a) shown in fig. 33.18. The correct dimensions of a related cell (a', b', c') were already reported by Ono et al. (1971): $\boldsymbol{a} = \boldsymbol{c}'$, $\boldsymbol{b} = -\boldsymbol{b}'$, $\boldsymbol{c} = \boldsymbol{a}' - \boldsymbol{c}'$. Based on the occurrence of isomorphous Ca_2As_3 we expect both compounds to be Mooser–Pearson phases, hence polyanionic compounds. The simplest structural arrangement in a nonmetallic $M_2^{2+}As_3$ compound might be based on As_6 zigzag chain or spiral fragments.

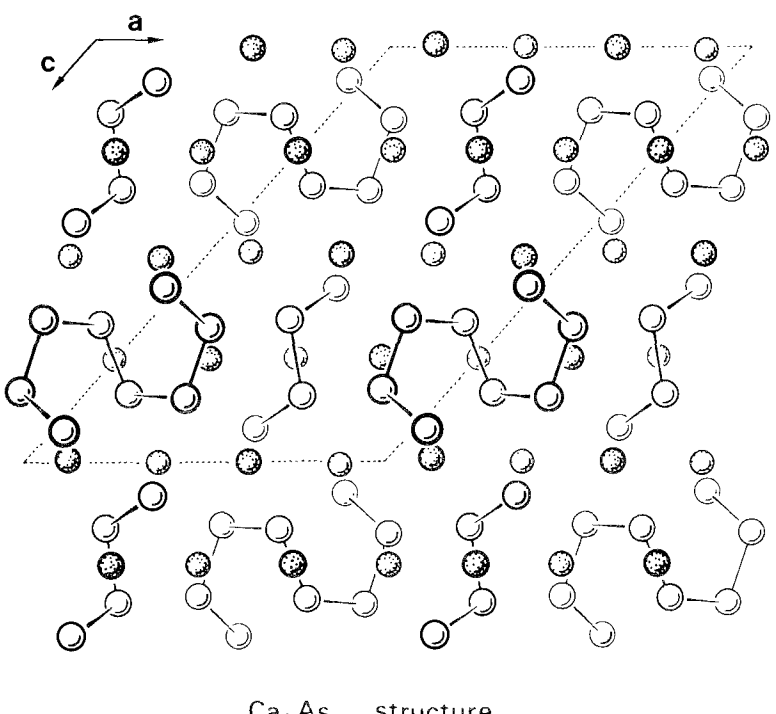

Fig. 33.18. The monoclinic Ca_2As_3 structure of Eu_2As_3. Stippled spheres: cations.

However, as in the case of LaP_2 a less regular arrangement is preferred: The anion array consists of As_4 and As_8 fragments which of course yield the same number of bonds and ionic formula $M_2^{+2}As^{-2}As_2^{-1}$.

According to Smart et al. (1977) the face-centered orthorhombic structure of Eu_3As_4 consists of a space-filling network of distorted triangular prisms of Eu atoms in which the prisms share rectangular faces so that the axes of adjacent prisms are either parallel or perpendicular. The arsenic atoms are distributed into $\frac{2}{3}$ of these prisms in such a way that three-dimensional chain fragments As^{-2}–As^{-}–As^{-}–As^{-2} with strict diad symmetry form (fig. 33.19). The As–As distances are 2.286, 2.551 and 2.286 Å and the angle is 120.4°. In the almost planar zigzag chains of $NdAs_2$ (Wang et al., 1977) the terminal and bridge As–As distance are 2.477 and 2.497 Å and the angle is 104.3°, and in Ca_2As_3 the corresponding values are 2.490 and 2.529 Å and 110.2° (Deller and Eisenmann, 1976a). The average Eu–As distance of 3.20 Å points to divalent europium. The terminal As–As distances are remarkably short whereas the bridge distance is

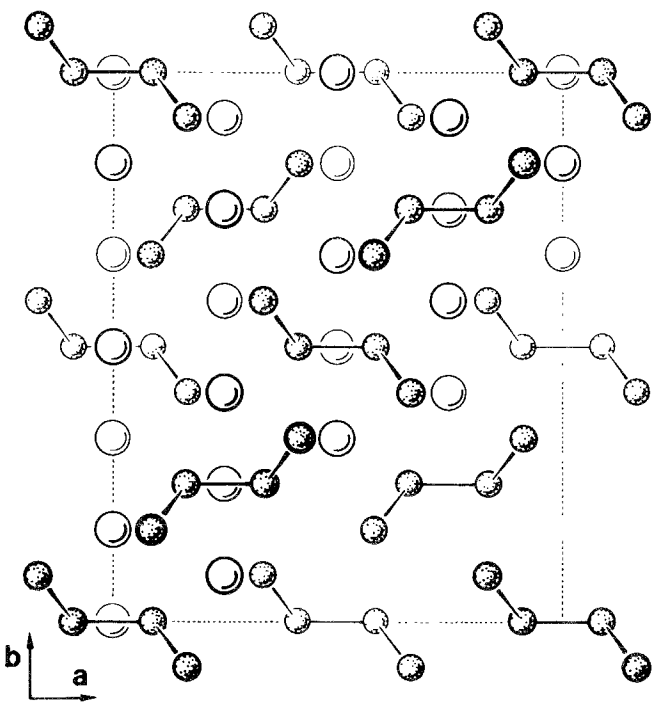

Eu_3As_4

Fig. 33.19. (001) projection of the fc orthorhombic Eu_3As_4 structure. Large spheres: Eu, small stippled spheres: As. Only the covalent bonds within the polyanion $(As_4)^{-6}$ are indicated. Certain cations (whose positions are defined by face centering) are omitted in order to emphasize the As chain fragments.

longer than in metallic arsenic (2.516 Å). If nevertheless we assume covalent single bonds, i.e. a formal charge as indicated above, then $Eu_3^{+2}(As_4)^{-6}$ obeys the valence rules and thus appears to be a true Mooser–Pearson phase. Semiconductivity is however questionable in the actual crystals which are described as deep violet, lustrous needles. We ignore whether this color is an intrinsic property of Eu_3As_4 or simply due to the excess valence electrons introduced by Ta atoms from the tantalum container. The authors reported that about 1 Ta atom per unit cell was inserted in the empty prisms ($Eu_{24}As_{32}Ta\square_{15}$, where $\square$ denotes an empty prism) although unreasonably short Ta–As distances result. Additional anions such as Si would in fact better fit into these holes. Occupation of all prism holes would lead to the formula MX_2 and the polyanion X sublattice then would resemble the "three-dimensional graphite"-type Si sublattice of α-$ThSi_2$. Meanwhile we have confirmed both color and semiconductivity of Eu_3As_4.

The orthorhombic structure of Eu_5As_4 was found by Wang et al. (1977c) to be a more symmetrical version of the Sm_5Ge_4 and the Gd_5Si_4 structures and possibly a stacking variant of the β-Yb_5Sb_4 structure (Bodnar and Steinfink, 1967). The structure can be built up from layers composed of pairs of trigonal Eu prisms which contain As pairs in the mirror plane (fig. 33.20). The square prisms within this array of Eu double prisms are centered by another Eu atom and capped by two As^{-3} ions. This latter Eu atom, which is located within the mirror plane $y = \frac{1}{4}$ perpendicular to the pseudo-tetragonal axis, thus acquires a fairly

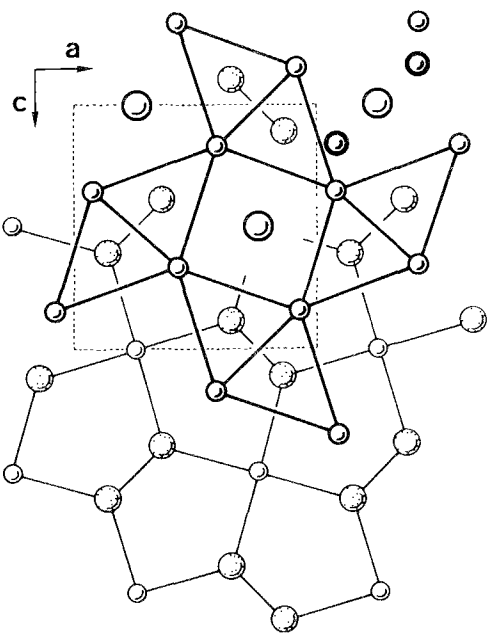

Eu_5As_4

Fig. 33.20. Projection on (010) of the structural unit of the Eu_5As_4 structure. The Eu prisms are shown in the upper part while chemical bonds are indicated in the mirror plane $y = \frac{1}{4}$. In the upper right corner two Eu atoms at $y = 0.6$ are added in order to visualize the coordination of the As^{-3} ions.

regular octahedral coordination (Eu–As distances are 3.14 (2×), 3.24 (2×) and 3.26 Å (2×)) while that of the other Eu atom is very irregular (3.08, 3.11, 3.14, 3.24, 3.26 and 3.42 Å). The average distances are Eu–As = 3.21 Å and Eu–Eu = 3.76 Å. The former distance pleads for divalent Eu while from the latter Wang et al. (1977) deduce the existence of Eu^{+3}. In fact Eu–Eu distances of 4.2 Å are observed in $Eu_3^{+2}As_4$ (Smart et al., 1977). Magnetic measurements will finally decide. The shortened Eu–Eu distance might as well indicate metallic properties although according to the formula $Eu_5^{+2}As_2^{-3}(As_2)^{-4}$ the compound could be non-metallic.

EuP_3 and $EuAs_3$ are Mooser–Pearson phases like CaP_3, SrP_3 and BaP_3 although they are not isotypic with any of the alkaline-earth polyphosphides. The monoclinic EuP_3 structure is however very similar to that of the triclinic CaP_3 and $CaAs_3$. The connection of the anions is in fact the same, only the package is slightly different (v. Schnering et al., 1976). In all the $M^{+2}P_3$ Mooser–Pearson phases $P_2^{-1}P^0$–$P^0P_2^{-1}$ units are connected to linear (as in BaP_3) or two-dimensional arrays. In CaP_3 and EuP_3 the phosphorus sheets may be interpreted as composed of corrugated $P_6^0P_8^{-1}$ rings interlinked at the three-coordinated P^0 atoms. Magnetic measurements confirmed the oxidation number 2 for the cation (v. Schnering et al., 1976).

Brice and Courtois (1976) reported that $EuAs_3$ has the same structure as $SrAs_3$, which is monoclinic (Deller and Eisenmann, 1976d).

While $EuSb_3$ is yet unknown, $EuBi_3$ is definitely no polycompound, despite its composition. $EuBi_3$ crystallizes in the same alloy structure as the superconducting $SrBi_3$ (Cu_3Au type) and orders antiferromagnetically below $T_N = 8$ K (Zinn, 1977).

The two-dimensional structure of monoclinic EuP_7 is characterized by 6-membered P rings in chair form with equatorial connection in one direction. The structure was said to be a derivative of the GeS (or black phosphorus) structure (v. Schnering et al., 1976).

In Yb the divalent state is obviously not stable enough in connection with P, and with Sb the tendency to form Mooser–Pearson phases is greatly reduced. Nevertheless, one queer polyanionic compound is known, $Yb_{11}Sb_{10}$. Judging from the chemical formula one might expect a metallic phase allthemore as it has the same structure as metallic $Ho_{11}Ge_{10}$. The occurrence of isostructural $Ca_{11}Sb_{10}$ and $Ca_{11}Bi_{10}$, on the other hand, increases the probability that the pnictides with the divalent cations might be non-metallic or semimetallic. The bc tetragonal unit cell of $Yb_{11}Sb_{10}$ (Clark et al., 1970) contains 5 kinds of anions. Sb_I, Sb_{II} and Sb_{IV} are surrounded by cations only. Sb_{III} has, in addition to 7 cations, 4 Sb neighbors arranged as a distorted tetrahedron with two short Sb–Sb distances of 3.00 Å and two longer distances of 3.28 Å. The shorter distance corresponds to a half bond, if we take 1.38 Å as the single-bond radius of Sb. The Sb–Sb pairs met with Sb_V are not close enough either (2.94 Å) to correspond to single bonds. This however would be needed in order to make these pnictides nonmetallic:

$$M_{11}^{+2}(Sb_I)_2^{-3}Sb_{II}^{-3}(Sb_{III})_2^{-1}Sb_{IV}^{-3}(Sb_V)_4^{-2}$$

As follows from the formula, Sb_{III} should bind two electrons either by forming 4 half bonds with its four Sb neighbors or by forming only two single bonds with the closer Sb neighbors. The resistivity curve and the low Seebeck coefficient of $Yb_{11}Sb_{10}$ (Bodnar et al., 1968) point in fact to a metallic character of this phase.

5. Ternary compounds

5.1. NaCl-*type related phases*

It is likely that the NaCl-type phosphides, arsenides, antimonides and bismuthides are thoroughly miscible with the corresponding chalcogenides. Nitride mixtures $LnN_{1-x}O_x$ are of particular interest since the monoxides $Ln^{3+}O$ do not exist. Incorporation of oxygen gives rise to a contraction of the lattice except in the case of CeN where oxygen appears to stabilize Ce^{3+} (Holleck et al., 1969). Thus, a lattice constant smaller than that corresponding to the ideal LnN (if ever known) may be an indication for oxygen contamination and not only for substoichiometric nitrogen content. The oxygen solubility decreases from La to Lu, as well as with higher preparation temperature. In $LnN_{1-x}O_x$ maximum values appear to be $x \leqq 0.5$/1500°C for La (Brown and Clark, 1974), $x \leqq 0.49$ for Ce (cited by Lorenzelli et al., 1970), $x \leqq 0.38$/1500°C for Pr (Brown and Clark, 1974), $x \leqq 0.28$ for Nd (Mourgout et al., 1977), $x \leqq 0.5$ for Sm (Felmlee and Eyring, 1968), $x \leqq 0.08$/1200°C for Eu (Chevalier et al., 1973), $x \leqq 0.35$/1200°C and $x \leqq 0.28$/1600°C for Gd (Lorenzelli et al., 1970), $x \leqq 0.30$/1500°C for Tb (Brown and Clark, 1974), $x \leqslant 0.05$ for Ho (Lorenzelli et al., 1970). The exceptional behavior of $EuN_{1-x}O_x$ is coupled with the divalence of Eu. The colors and lattice constants reported for the Sm phases demonstrate that Sm is trivalent. The increase of the excess-electron concentration in a series $SmN_{0.93-x}O_x$ is reminiscent of alloys like CeTe–CeSe–CeS: $x \approx 0.2$ greenish blue, $x \approx 0.25$ blue, $x \approx 0.33$ purple, $x \approx 0.4$ red, $x \approx 0.5$ orange, $x \approx 0.6$ yellow (Felmlee and Eyring, 1968). We wonder whether a $Sm^{3+} \rightarrow Sm^{2+}$ transition could not be induced by a temperature variation.

Nitrogen in the LnN phases can be replaced also by carbon, either methylic in $LnN_{1-x-y}C_x\square_y$ or acetylic ($C \equiv C$) with C_2 instead of C. The golden color of CeN thereby changes to purple and red (Anderson et al., 1969).

The rare earth monopnictides are not only mutually miscible but mix also with Th, U, Np and Pu monopnictides. Végard's law was verified in systems LnN–UN by Holleck et al. (1969).

The anion sublattice of the NaCl structure contains two empty tetrahedral holes per anion. Geometrically, it would therefore be possible to insert hydrogen up to a concentration $LnXH_2$ but this hydridization would create problems with the valence. It is however possible to fill half the tetrahedral voids of the NaCl structure with transition elements such as Ni and Pt (fig. 33.21). Dwight (1974a) synthesized quite a series of these filled-up NaCl-type phases: NiLnSb with Ln = Gd, . . . , Lu, Y; NiLnBi with Ln = Gd, Dy, Tm, Lu, Y; PtLnSb with Ln =

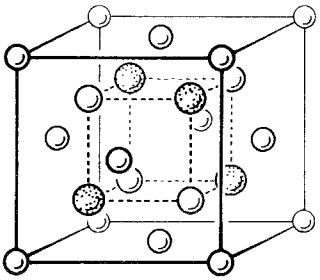

Fig. 33.21. The NiMgSb-type unit cell of NiDySb. Smallest spheres: Ni; stippled spheres: Sb.

Gd,..., Lu, Y; PtLnBi with Ln = Gd, Dy, Ho, Er. The occurrence of this structure type appears to be connected with the valence-electron concentration. Thus, the NiMgSb-type structure is met also in PtHfSn and PtThSn, as well as in RhHfSb and RhThSb (Dwight, 1974b), which all are isoelectronic with PtLnSb. RhThSn, which contains one electron less, adopts the hexagonal Fe_2P structure. If the analogy is perfect then hypothetical CoLnSb, RhLnSb and IrLnSb should also crystallize in the ordered Fe_2P structure.

5.2. Ce_2O_2S- *and* Nd_2O_2Te-*type compounds*

The hexagonal Ce_2O_2S structure, which represents a superstructure of the La_2O_3 type, may be derived from a distorted hexagonal close-packing of La^{3+} ions where the S anions occupy half the octahedral holes and the O anions half of each of the two sets of tetrahedral holes. Alternatively, the Ce_2O_2S structure may be based on a distorted cubic anion close-packing with the La cations occupying two of three layers of octahedral holes (as found less distorted in γ-In_2S_3). The former description is in fact appropriate for the pnictides which crystallize in the anti-Ce_2O_2S structure: $Li_2M^{4+}N_2$ with M^{4+} = Zr (Palisaar and Juza, 1971), Hf (Barker and Alexander, 1974). Ce (Halot and Flahaut, 1971) and Li_2LnP_2 with Ln = Ce, Pr (El Maslout et al., 1975). A $\sqrt{3}\,a_0$ superstructure due to slightly puckered M^{4+} layers is observed in Li_2ThN_2 and Li_2UN_2 (Palisaar and Juza, 1971). The occurrence of tetravalent Ce and above all tetravalent Pr in the phosphide appears to be quite extraordinary. It is however less surprising that Li_2TbP_2 did not form (El Maslout et al., 1975). High pressure may be required even for the synthesis of Li_2TbN_2. The existence of nonmetallic Li_2PrP_2 implies the existence of the nitride Li_2PrN_2 which was not obtained by Halot and Flahaut (1971). Admittedly we only assumed that the black phosphides are semiconductors as well as we deduced an insulator behavior from the reported red-orange color of Li_2CeN_2, although the transparency was not explicitly stated, and metallic $SmN_{0.55}O_{0.45}$ is red-orange too. Our assumption of tetravalent rare earth ions in Li_2LnP_2 thus should not yet be taken for granted, all the more as the Ce–P distance of 3.05 Å reported for Li_2CeP_2 is even larger than in CeP(2.96 Å) which contains Ce^{3+} (in Li_2CeN_2, however, Ce–N = 2.53 Å compared with 2.51 Å in CeN where Ce is indeed nearly tetravalent). If Li_2PrP_2 contains

normal Pr^{3+} then metallic phases Li_2LnP_2 with Ln = La, Nd, etc., should exist as well. Nonmetallic analogs of Li_2CeN_2, however, might be $LiBeLnN_2$ and $Be_2Eu^{2+}P_2$, etc.

From the existence of anti-Ce_2O_2S-type (or $CaAl_2Si_2$-type) $CaMn_2Sb_2$, $CaMn_2Bi_2$ and $SrMn_2Sb_2$ (Cordier and Schäfer, 1976) and the family AM_2X_2 with A = Sr, Ba, Yb, Eu; M = Zn, Cd and X = P, As (Klüfers and Mewis, 1977) as well as with A = Ca, Sr, Ba; M = Mg; X = As, Sb, Bi (Deller and Eisenmann, 1977) we conclude on the existence of isostructural and possibly semiconducting phases $EuMn_2P_2$, $EuMn_2As_2$, $EuMn_2Sb_2$, $EuMn_2Bi_2$, $EuMg_2P_2$, $EuMg_2As_2$, $EuMg_2Sb_2$, $EuMg_2Bi_2$, $EuZn_2P_2$, $EuZn_2As_2$, $EuCd_2P_2$, $EuCd_2As_2$, etc.

A certainly tetravalent cation is met in the sage green Ce_2N_2O which crystallizes in the normal Ce_2O_2S-type structure (Barker and Alexander, 1974) like Th_2N_2O (Benz and Zachariasen, 1966), Th_2N_2S, U_2N_2S, Th_2N_2Se, U_2N_2Se, Th_2ONP, Th_2ONAs and metallic U_2N_2P, U_2N_2As (Benz and Zachariasen, 1969). Attempts to prepare (metallic?) Ce_2O_2P and Ce_2O_2As were unsuccessful (Benz, 1971). Nonmetallic Pr_2N_2O and Ce_2N_2S might also have some chance to exist in this structure. The lattice constants reported for PrN_2 and NdN_2 (Kieffer et al., 1972) correspond in fact closely to what we expect for Pr_2N_2O and Nd_2N_2O. Nonmetallic Nd_2N_2O with tetravalent neodymium, however, would be rather exciting. We expect this structure to occur also in phases $LnCeO_2N$, $LnThO_2N$, ... and perhaps even in $LnCeN_2F$. The ordered arrangement of the two kinds of cations should give rise to the occurrence of a superstructure.

No ordered distribution of Ce^{3+} and Ce^{4+} can be detected in Ce_2O_2Sb and Ce_2O_2Bi which crystallize in the Nd_2O_2Te structure. This *bc* tetragonal structure is found also in Th_2N_2Te, U_2N_2Te, Th_2ONSb and metallic Th_2N_2Sb, U_2N_2Sb, Th_2N_2Bi and U_2N_2Bi (Benz and Zachariasen, 1970), as well as in $Na_{1/2}Bi_{3/2}O_2Cl$ and Bi_2O_2Se, etc. Geometrically the Nd_2O_2Te structure is the anti-$ThCr_2Si_2$ type, which however is chemically different due to the formation of Si–Si pairs. The structure of Ce_2O_2Sb is characterized by puckered $(CeO_2Ce)_n$ layers in which the anion is tetrahedrally surrounded by the cations (Ce–O = 2.38 Å compared with 2.37 Å in Ce_2O_2Te and 2.39 Å in Ce_2O_2Bi). These layers are held together by antimony atoms which bind 8Ce atoms situated at the corners of a cube (Ce–Sb = 3.55 Å). The Ce atoms themselves obtain a coordination of 4O + 4Sb forming some kind of square antiprism. We wonder whether Ce_2O_2Sb and Ce_2O_2Bi are metallic mixed-valence compounds and whether Ce_2O_2Sb is thoroughly miscible with nonmetallic Ce_2O_2Te.

Based on the existence of $ThCr_2Si_2$-type phases $M^{2+}T_2X_2$ with M = Ca, Sr; T = Fe, Co, Ni, Cu; X = P, As (Klüfers and Mewis, 1977) one might expect the existence of similar Eu^{2+} and Yb^{2+} compounds.

If we interchange the smaller metal atoms and the nonmetal atoms in every second square-pyramid layer of the $ThCr_2Si_2$-type structure we end up with the $CaBe_2Ge_2$-type structure found also in $SrCu_2Sb_2$ (Cordier et al., 1976). We are tempted to speculate on the existence of isostructural $EuCu_2Sb_2$ and eventually even $YbCu_2Sb_2$.

$SrZnBi_2$ crystallizes in a related tetragonal structure type (Cordier et al., 1976)

found also in $SrMnBi_2$, $BaMnSb_2$ and $BaMnBi_2$ (Cordier and Schäfer, 1977). $EuZnBi_2$, $EuCdBi_2$ and $EuMnBi_2$ may be further representatives.

5.3. PbFCl-*type derivatives*

With tetravalent actinides An^{4+} = Th and U metallic chalcogenides AnXY, such as ThPS, ThSbTe, etc., exist which crystallize in the PbFCl structure (Hulliger, 1968d). The dipnictides themselves ($ThAs_2$, $ThSb_2$, . . .) adopt the same structure. Isoelectronic rare earth analogs exist too, but only those with the heavy anions ($LnTe_2$, LnSbTe and possibly LnSbSe) show also analogous physical properties. The phases with the lighter anions, however, all appear to be nonmetallic and therefore their structure must be either distorted or different from the PbFCl type. The monoclinic structure of CeAsS is indeed a distorted version of the PbFCl type (Sfez and Adolphe, 1972). The As layer corresponding to the square array of F atoms in the $ClPbF_2PbCl$ sandwich of the PbFCl structure is distorted in such a way as to give rise to the formation of As zigzag chains. As–As = 2.52 and 2.60 Å within the chain and 3.09 and 3.11 Å towards the neighboring chain, compared with a 2.83 Å square in an undistorted PbFCl structure. Quite a number of LnPS phases exist with the closely related GdPS structure. The nonmetallic character of GdPS (Hulliger, 1968c) requires the occurrence of either P chains, P squares or P–S pairs, the latter being however excluded in a PbFCl-type derivative. Thus instead of the simple saw-tooth pnigogen chains of the CeAsS structure we find ⎍⎍⎍-type P chains in GdPS (Hulliger et al., 1977).

Obviously the occurrence of the metallic phases is not restricted to the LnXY stoichiometry. The system $LaTe_2$–$LaSb_{1.5}Te_{0.5}$ was found to be quasi continuous. The tetragonal unit cell of $LaTe_2$ becomes orthorhombically distorted already in $LaTe_{1.8}Sb_{0.2}$ (Wang et al., 1967). For the system $LaSb_{2-x}Sn_x$ no homogeneous mixtures were obtained but a phase $LaSnSb_2$ was detected. Its structure was reported by Wang et al. (1967) to be that of $NdTe_3$, and thus it is nevertheless closely related to the PbFCl structure.

5.4. *Miscellaneous oxynitrides*

In certain oxides part of the oxygen can isostructurally be replaced by nitrogen. Thus in the K_2NiF_4-type phases $M^{2+}Ln^{3+}AlO_4$ (M = Ca, Sr, Eu) MO can be replaced by LnN. In practice pressed mixtures Ln_2O_3 + AlN are sintered at 1350°C in sealed nickel tubes (Marchand, 1976). The K_2NiF_4 structure was verified on the yellow, air-stable powders Ln_2AlO_3N obtained with Ln = La, Nd and Sm. The tetragonal K_2NiF_4 structure is a layered combination of the rocksalt and the perovskite structure. Ni is six-coordinated as in $KNiF_3$, but the K^+ ions are only 9-coordinated (12-coordinated in perovskite-type $KNiF_3$). Other structures intermediate between rocksalt and perovskite type are known and might give rise to oxynitrides as well. Thus $Eu_3Ti_2O_7$, $Sr_3Zr_2O_7$ or $Na_3Y_3Ti_4O_{14}$ may be transformed into $LnEu_2^{II}Ti_2O_6N$, $La_2EuZr_2O_5N_2$ or $Eu_3Gd_3Ti_4O_{11}N_3$.

Oxygen can partially be replaced by nitrogen also in the orthorhombic olivine-type and β-K_2SO_4-type oxides $M_2^{2+}SiO_4$. Thus, oxynitrides $Ln^{3+}Eu^{2+}SiO_3N$ with Ln = La, Nd, Sm and Gd have been synthesized at 1350°C according to the reaction (Marchand et al., 1976):

$$3Ln_2O_3 + 3Eu_2O_3 + 2Si_3N_4 \rightarrow 6LnEuSiO_3N + N_2\uparrow.$$

The olivine $(Mg, Fe)_2SiO_4$ structure can be interpreted as a hexagonal anion close packing, pseudohexagonal along [010], with the Si atoms in both sets of tetrahedral holes τ_1 and τ_2 and the divalent cations at octahedral sites Ω: $\frac{1}{16}\tau_1 + \frac{1}{16}\tau_2 + \frac{1}{2}\Omega$. The cations are arranged in zigzag chains with a period $\sim a$, equivalent to two M–M distances, so that half the cations possess 2M and half possess 4M neighbors at a distance $\approx\frac{1}{2}a$. The olivine structure is found with the smaller cations, e.g. in Ca_2SiO_4, Ca_2GeO_4, Ca_2SiS_4, Ca_2GeS_4, Ca_2SnS_4, Ca_2GeSe_4; ordered versions in $LiLnSiO_4$, $NaLnSiO_4$, $LiLnGeO_4$, $NaLnGeO_4$, $CaMnSiO_4$, . . . , $CaMgSiO_4$. Substitutions of the types $Fe^{II}Ln^{III}SiO_3N$, $CaLnGeO_3N$, etc., might be feasible. With large cations the common A_2BX_4 structure is the orthorhombic β-K_2SO_4 type. In this structure isolated $[SO_4]$ tetrahedra are held together by the two kinds of crystallographically independent cations which are coordinated by 9 and 10 oxygen atoms. Representatives are Ca_2SiO_4(h), Sr_2SiO_4, Ba_2SiO_4, Sr_2GeO_4, Ba_2GeO_4, Ba_2FeO_4, Ba_2GeS_4. Starting from the oxide examples we may, by double substitution, create oxynitrides of the kind

$$Sr_2SiO_4 \rightarrow LnSrSiO_3N,\ Lu_2BO_3N,\ LnCe^{4+}BeO_3N$$

or $LnEu^{II}SiO_3N$, the examples realized by Marchand et al. (1976). Obviously the olivine and β-K_2SO_4-type compounds can easily be confused due to similarities in crystal symmetry and unit-cell dimensions, but the β-K_2SO_4 type is indeed more reasonable for $LaEuSiO_3N \cdots GdEuSiO_3N$ (Marchand, 1976). We wonder whether it might even be possible to substitute for two oxygen atoms: $Ln_2^{3+}SiO_2N_2$?

On studying the Si_3N_4–Ln_2O_3 system Wills et al. (1976) synthesized a number of oxynitrides which turned out to be isostructural with known oxide or oxyfluoride minerals. Thus åkermanite $Ca_2Mg[Si_2O_7]$ analogs exist with the formula $Ln_2Si_3O_3N_4$ (Ln = La, Nd, Sm, Gd, Dy, Ho, Er, Yb, Y (Marchand et al., 1976b)). The X-ray patterns observed for the phases with Dy and Er required a larger cell with $a = 2a_0$ and $c = 3c_0$. The tetragonal åkermanite structure contains $[Si_2O_7]$ double tetrahedra linked to layers parallel to (001) by the tetrahedrally coordinated Mg. The square-antiprismatically coordinated Ca ions connect the tetrahedron layers. Thus, a number of Ln containing åkermanite-type compounds with lower N contents appear to be feasible, such as $Ln_2AlSi_2O_4N_3$, $Ln_2MgSi_2O_5N_2$, $Ln_2Al[AlSiO_5N_2]$, $Ln_2Al[Al_2O_6N]$, etc.

The oxynitrides $Ln_4Si_2O_7N_2$ with Ln = La, Nd, Sm, Gd, Dy, Ho, Er, Yb, Y (Marchand et al., 1976b) are isostructural with monoclinic cuspidine $Ca_4Si_2O_7F_2$ which also contains $[Si_2O_7]$ groups. $La_4Si_2O_7N_2$ has lattice parameters $a = 2a_0$, $c = 2c_0$, so that its structure will be closely related to cuspidine (Wills et al., 1976).

Finally, $Y_5(SiO_4)_3N$ was found to be isomorphous with apatite $Ca_5(PO_4)_3F$. This was verified also for $Ln_5(SiO_4)_3N$ with Ln = La, Nd, Sm and Gd by Gaudé et al. (1975). In the ideal hexagonal structure of apatite the $[PO_4]$ tetrahedra are linked by two kinds of cations. Ca_I in 4(f) lies on a triad axis and is 9-coordinated (6 O forming a trigonal prism + 3 equatorial O atoms). Ca_{II} has 6O + 1F (or 2Cl in $Ca_5(PO_4)_3Cl$) neighbors. Cation- and anion-deficient apatites are known: $\square CaLa_8(SiO_4)_6F_2$, $Ca_{10}(PO_4)_6O\square$, $\square Sr_3Nd_6(SiO_4)_6\square_2$, $\square_2Ln_8(SiO_4)_6\square_2$, $\square_2ThSrNd_6(SiO_4)_6\square_2$, $\square_3Th_3Nd_4(SiO_4)_6\square_2$ as well as mixed-cation phases such as $Na_2La_2Sr_6(PO_4)_6Cl_2$, $Ca_8La_2(PO_4)_6O_2$, $Sr_4La_6(SiO_4)_6F_2$, etc (Grisafe and Hummel, 1970). Obviously, not only the isolated F ion can be replaced by nitrogen but also some of the tetrahedral oxygen atoms as in $La_9TiSi_6O_{23}N_3$, $Gd_8Ti_2Si_6O_{22}N_4$, $Ln_8Ge_2Si_6O_{22}N_4$ and $Sm_{8.65}V_{1.35}Si_6O_{21.3}N_{4.7}$ (Guyader et al., 1975). Ln can partially be replaced also by Cr^{3+}: $Gd_8Cr_2Si_6O_{24}N_2$ (Hamon et al., 1975; Marchand et al., 1976). The nitride analog of the third example given above for deficient apatites would be $\square Ln_9(Si_6O_{21}N_3)\square_2$. Certainly, many more substitutional nitride derivatives of apatite are feasible.

Oxynitrides may exist also with the $CaFe_2O_4$ structure. In this orthorhombic structure Fe^{3+} is octahedrally coordinated while the divalent cation has a coordination number 8. This structure is met also in $CaLn_2O_4$, $SrLn_2O_4$ and $EuLn_2O_4$, so that possibly $LaLu_2O_3N$ or $GdSc_2O_3N$, etc., may exist in this structure as well. We wonder whether it might even be possible to synthesize e.g. $LnMoO_3N$ with the scheelite structure or $LnTiO_2N$ with the perovskite structure. The garnet structure offers another variety of possible oxynitrides such as $Ln_3Al_2(SiO_3N)_3$, $Ln_3Zr_2(Al_2SiO_9N_3)$, $Ln_3Hf_2(Si_3O_7N_5)$, $Ln_3Ga_2(GeO_3N)_3$, $LnSr_2Ti_2(GeO_3N)_3$, etc.

The existence of $YSiO_2N$ and $LaSiO_2N$ with the α-$CaSiO_3$ pseudowollastonite structure (Morgan et al., 1977) reveals the feasability of quite a number of isostructural $LnSiO_2N$ compounds. In this structure type the rare-earth ion is coordinated by 6O + 2N, oxygen has 3Ln + 1Si neighbors, N is four-coordinate by 2Ln + 2Si and Si is tetrahedrally surrounded by 3Ln + 1Si. Stacking disorder along the c-axis makes a unique unit-cell determination in this hexagonal structure a serious problem.

5.5. *Ternary phases derived from binaries*

An interesting family of compounds can be derived from the Th_3P_4 structure. A large number of phases $Ln_3Z_xX_{4-x}$, $x \leq 1$, with Z = P, As, Sb; X = S, Se, Te, was synthesized and those with the lighter Ln were found to crystallize in the Th_3P_4 structure (Hulliger, 1976). The end member with $x = 1$, such as La_3PS_3, Nd_3AsSe_3, Pr_3AsS_3, etc., are semiconductors. The elimination of the excess valence electrons converts the metallic ferromagnet Nd_3S_4 into a nonmetallic antiferromagnet Nd_3PS_3.

While no rare earth polypnictide with the cubic skutterudite ($CoAs_3$) structure is known Jeitschko and Braun (1977) synthesized ternary phases of the type $LnFe_4P_{12}$ (Ln = La · · · Sm), $LnRu_4P_{12}$ (Ln = La · · · Nd, Eu) and $LnOs_4P_{12}$ (Ln =

La · · · Nd) which crystallize in a filled $CoAs_3$ structure. The polyanions form discrete X_4 units which are squares in skutterudite but rectangles in the filled type (in $LaFeP_{12}$ the P–P distances are 2.288 and 2.356 Å, the P–P–P angle is 90.0°). The transition-element cations are in distorted octahedral coordination ($LaFe_4P_{12}$: P–Fe–P = 97.9° and 82.1° instead of 90°) while the rare earth ions occupy the two nearly icosahedral voids at (0, 0, 0) and $(\frac{1}{2}, \frac{1}{2}, \frac{1}{2})$ of the body-centered cubic cell.

Obviously the appropriate composition of these phases is $M^{4+}Fe_4P_{12}$, and Ce in $CeFe_4P_{12}$ is indeed tetravalent. With low-spin Fe^{2+} this compound has the same number of valence electrons as CoP_3 and thus non-metallic properties are to be expected in agreement with the energy-level diagram proposed by Jeitschko and Braun. If the phases with the trivalent rare earth ions are non-metallic as well, then one quarter of the transition-element cations has to be trivalent too (d^5 configuration with $S = \frac{1}{2}$). In $EuFe_4P_{12}$, $EuRu_4P_{12}$ and probably in $SmFe_4P_{12}$ the rare earth ion is divalent so that half the Fe or Ru cations have to adapt a d^5 configuration. It should be possible to replace them by Co or Rh, respectively ($LaFe_3CoP_{12}$, $EuRu_2Rh_2P_{12}$, . . .). Unusual properties are to be expected from $CeRu_4P_{12}$ and $CeOs_4P_{12}$ which according to their lattice constants appear to contain cerium in a mixed-valence state.

Since normal skutterudites exist with As and Sb it might well be possible to synthesize the corresponding ternary arsenides and antimonides.

Of course, there may exist a lot of other ternary and quaternary pnictide phases. Little systematic research has been done so far. Certain new phases will be discovered accidentally, as the silicophosphides, which formed as a consequence of a tube attack during a transport reaction in a silica tube (Hayakawa et al., 1975). Thus, orthorhombic $CeSiP_3$, $LaSi_2P_6$ and $CeSi_2P_6$ crystals as well as crystals of another orthorhombic ternary La–Si–P and Ce–Si–P compound grew in addition to the desired polyphosphide crystals.

6. Recent developments

Anti-Nd_2O_2Te-type Eu^{2+} pnictides, anticipated in §5.2, have meanwhile been synthesized by Marchand and Jeitschko (1978): EuM_2P_2 and EuM_2As_2 (M^{2+} = Fe, Co, Ni) and $EuNi_2Sb_2$. The same structure was found also with Ln^{3+} cations: $LnCo_2As_2$ (Ln = La . . . Nd), $GdNi_2X_2$ (X = P, As, Sb), and $YbNi_2P_2$. We expect the phases with Ln^{3+} cations to show the anion pairs characteristic of the $ThCr_2Si_2$ structure. Nonmetallic properties, however, would require a 1 : 1 mixture of the anti-Nd_2O_2Te and the $ThCr_2Si_2$ structure.

A new "impure" polyphosphide type was discovered by Braun and Jeitschko (1978) in $Ln_6Ni_6P_{17}$ (Ln = La, Ce, Pr). The cubic cell contains $8P^0P_3^{2-}$ polyanions in the form of trigonal pyramids, and $2P^{3-}$ anions. Ni is in tetrahedrally distorted square-planar coordination. Metallic properties thus are expected.

The Mn_5Si_3-type Eu_5As_3 was identified as a low-temperature modification, while the high-temperature form is a disordered variant of the Ca_5Pb_3 structure (Wang et al., 1978). A rhombohedrally deformed Gd_4Bi_3 type, analogous to that reported for

Yb_4As_3 (Ono et al., 1970), was detected in ferromagnetic $Eu_4As_3 = Eu_3^{2+}Eu^{3+}As_3$ (Hulliger, 1974).

Acknowledgments

I am greatly indebted to Professor G. Busch, director of the Solid-State Physics Laboratory ETH, for his interest and support. Moreover, I would like to thank Bernhard Natterer and Dr. Si Yuan for their valuable help.

References

Aeby, A., F. Hulliger and B. Natterer, 1973, Solid State Commun. **13**, 1365.
Andersen, N.H., P.E. Lindelof, H. Smith, O. Splittorff and O. Vogt, 1976, Phys. Rev. Lett. **37**, 46.
Andersen, N.H., P.E. Gregers-Hansen, E. Holm, F.B. Rasmussen and O. Vogt, 1973, Proc. Int. Conf. Magn. (Publ. House Nauka, Moscow) p. 234.
Anderson, J.S., N.J. Clark and I.J. McColm, 1969, J. Inorg. Nucl. Chem. **31**, 1621.
Anselin, F., 1963, C.R. Acad. Sci. Paris **256**, 2616.
Anselin, F., N. Lorenzelli, R. Lallement and J.J. Veyssie, 1965, Phys. Lett. **19**, 174.
Baer, Y., 1976, private communication.
Baer, Y. and C. Zürcher, 1977, Phys. Rev. Lett. **39**, 956.
Bak, P. and P.A. Lindgård, 1973, J. Phys. C**6**, 3774.
Bak, P., S. Krinsky and D. Mukamel, 1976, Phys. Rev. Lett. **36**, 52.
Barker, M.G. and I.C. Alexander, 1974, J. Chem. Soc., Dalton Trans. 2166.
Bartholin, H., D. Florence, Wang Tscheng-si and O. Vogt, 1974, Phys. Stat. Sol. **A24**, 631.
Bartholin, H., D. Florence, Wang Tscheng-Si and O. Vogt, 1975, Phys. Stat. Sol. **A29**, 275.
Bartholin, H., D. Florence, G. Parisot, J. Paureau and O. Vogt, 1977, Phys. Lett. **60A**, 47.
Bartholin, H., D. Florence and O. Vogt, 1978, J. Phys. Chem. Solids **39**, 89.
Bayanov, A.P., 1975, Russ. Chem. Revs. **44**, 122.
Beckenbaugh, W., J. Evers, E. Kaldis and V. Hildebrandt, 1974, Helv. Phys. Acta **47**, 423.
Benz, R., 1971, Acta Cryst. **B27**, 853.
Benz, R. and W.H. Zachariasen, 1966, Acta Cryst. **21**, 838.
Benz, R. and W.H. Zachariasen, 1969, Acta Cryst. **B25**, 294.
Benz, R. and W.H. Zachariasen, 1970, Acta Cryst. **B26**, 823.
Better, B., A. Hütz and G. Nagorsen, 1976, Z. Metallkde. **67**, 118.
Bevolo, A.J., H.R. Shanks and D.E. Eckels, 1976, Phys. Rev. **B13**, 3523.
Birgeneau, R.J., E. Bucher, L. Passell, D.L. Price and K.C. Turberfield, 1970, J. Appl. Phys. **41**, 900.
Birgeneau, R.J., E. Bucher, L. Passell and K.C. Turberfield, 1971, Phys. Rev. **B4**, 718.
Birgeneau, R.J., 1972, AIP Conf. Proc. **10**, 1664.
Birgeneau, R.J., E. Bucher, J.P. Maita, L. Passell and K.C. Turberfield, 1973, Phys. Rev. **B8**, 5345.
Bleaney, B., 1972, in Magnetic Properties of Rare Earth Metals (ed. R.J. Elliott, Plenum).
Bodnar, R.E. and H. Steinfink, 1967, Inorg. Chem. **6**, 327.
Bodnar, R.E., H. Steinfink and K.S.V.L. Narasimhan, 1968, J. Appl. Phys. **39**, 1485.
Borsese, A., G. Borzone, A. Calabretta, R. Capelli and R. Ferro, 1976, Proc 12th Rare Earth Res. Conf., Vail (CO), p. 881.
Borsese, A., R. Capelli, S. Delfino and R. Ferro, 1974, Thermochim. Acta **9**, 313.
Borsese, A., R. Ferro, R. Capelli and S. Delfino, 1975, Thermochim. Acta **11**, 205.
Brice, J.F. and A. Courtois, 1976, C.R. Acad. Sci. Paris **283C**, 479.
Brown, R.C. and N.J. Clark, 1974a, J. Inorg. Nucl. Chem. **36**, 2287.
Brown, R.C. and N.J. Clark, 1974b, J. Inorg. Nucl. Chem. **36**, 2507.
Brun, T.O., G.H. Lander, F.W. Korty and J.S. Kouvel, 1975, AIP Conf. Proc. **24**, 244.
Brunton, G.D. and H. Steinfink, 1971, Inorg. Chem. **10**, 2301.
Bucher, E., 1976, private communication.
Bucher, E. and J.P. Maita, 1973, Solid State Commun. **13**, 215.
Bucher, E., K. Andres, J.P. Maita, A.S. Cooper and L.D. Longinotti, 1971, J. Phys. (Paris) **32**, Suppl. C1, 114.
Bucher, E., R.J. Birgeneau, J.P. Maita, G.P. Felcher and T.O. Brun, 1972, Phys. Rev. Lett. **28**, 746.
Bucher, E., K. Andres, F.J. Di Salvo, J.P. Maita, A.C. Gossard, A.S. Cooper and G.W. Hull, Jr., 1975, Phys. Rev. **B11**, 500.
Bucher, E., A.S. Cooper, D. Jaccard and J. Sierro, 1977, Valence Instabilities and Related Narrow-Band Phenomena (ed. R.D. Parks, Plenum, N.Y.) p. 529.

Busch, G., 1967, J. Appl. Phys. **38**, 1386.
Busch, G. and O. Vogt, 1966a, Phys. Lett. **20**, 152.
Busch, G. and O. Vogt, 1966b, Phys. Lett. **22**, 388.
Busch, G. and O. Vogt, 1967, Phys. Lett. **25A**, 449.
Busch, G. and F. Lévy, 1970, Coll. Int. CNRS No. 180, Paris–Grenoble 1969, Vol. II, p. 363.
Busch, G., P. Junod, O. Vogt and F. Hulliger, 1963, Phys. Lett. **6**, 79.
Busch, G., P. Junod, F. Lévy, A. Menth and O. Vogt, 1965a, Phys. Lett. **14**, 264.
Busch, G., O. Marinček, A. Menth and O. Vogt, 1965b, Phys. Lett. **14**, 262.
Busch, G., O. Vogt and F. Hulliger, 1965c, Phys. Lett. **15**, 301.
Busch, G., P. Schwob and O. Vogt, 1966, Phys. Lett. **23**, 636.
Busch, G., O. Vogt and P. Schwob, 1967, Coll. Int. CNRS No. 166 (Les Champs Magnétiques Intenses, Grenoble 1966), p. 401.
Busch, G., E. Kaldis, E. Schaufelberger-Teker and P. Wachter, 1970, Coll. Int. CNRS No. 180, Paris–Grenoble 1969, Vol. I, p. 359.
Busch, G., M. Campagna, F. Hulliger and H.C. Siegmann, 1971a, J. Phys. Chem. Solids **32**, 2173.
Busch, G., W. Stutius and O. Vogt, 1971b, J. Appl. Phys. **42**, 1493.
Buschow, K.H.J. and J.F. Fast, 1967, Phys. Stat. Sol. **21**, 593.
Buyers, W.J.L., T.M. Holden, E.C. Svensson, R.A. Cowley and M.T. Hutchings, 1971, J. Phys. **C4**, 2139.
Callen, E.R. and H.B. Callen, 1963, Phys. Rev. **129**, 578.
Campagna, M., E. Bucher, G.K. Wertheim, D.N.E. Buchanan and L.D. Longinotti, 1974, Proc. 11th Rare Earth Conf., Traverse City, MI, p. 81.
Campagna, M., G.K. Wertheim and E. Bucher, 1975, AIP Conf. Proc. **24**, 22.
Carter, F.L., 1972, J. Solid State Chem. **5**, 300.
Charvillat, J.P., D. Damien and A. Wojakowski, 1977, Rev. chim. minér. **14**, 178.
Chen, H.H. and P.M. Levy, 1971, Phys. Rev. Lett. **27**, 1383.
Chen, H.H. and P.M. Levy, 1973, Phys. Rev. **B7**, 4267.
Chevalier, B., J. Étourneau, B. Tanguy, J. Portier and P. Hagenmuller, 1973, C.R. Acad. Sci. Paris **277C**, 1029.
Chevalier, B., J. Étourneau and P. Hagenmuller, 1976, C.R. Acad. Sci. Paris **282C**, 375.
Child, H.R., M.K. Wilkinson, J.W. Cable, W.C. Koehler and E.O. Wollan, 1963, Phys. Rev. **131**, 922.
Chua, K.S. and J.N. Pratt, 1974, Thermochim. Acta **8**, 409.
Clark, H.L., H.D. Simpson and H. Steinfink, 1970, Inorg. Chem. **9**, 1962.
Coey, J.M.D. and R. Brusetti, 1975, Phys. Rev. **B11**, 671.
Connolly, T.F., and E.D. Copenhaver, 1969, Bibliography of magnetic materials and tabulation of magnetic transition temperatures, ORNL-RMIC-7.
Cooper, B.R., 1966, Phys. Lett. **22**, 24 and 244.
Cooper, B.R., I.S. Jacobs, R.C. Fedder, J.S. Kouvel and D.P. Schumacher, 1966, J. Appl. Phys. **37**, 1384.
Cooper, B.R., R.C. Fedder and D.P. Schumacher, 1967, Phys. Rev. **163**, 506.
Cooper, B.R. and O. Vogt, 1970a, Phys. Rev. **B1**, 1211.
Cooper, B.R. and O. Vogt, 1970b, Phys. Rev. **B1**, 1218.
Cooper, B.R. and O. Vogt, 1971a, J. Phys. Paris **32** Suppl., C1–958.
Cooper, B.R. and O. Vogt, 1971b, J. Phys. Paris **32** Suppl., C1–1026.
Cooper, B.R., 1972, in Magnetic Properties of Rare Earth Metals (ed. R.J. Elliott, Plenum N.Y.) p. 9.
Cooper, B.R., A. Furrer, W. Bührer and O. Vogt; 1972, Solid State Commun. **11**, 21.
Cooper, B.R., M. Landolt and O. Vogt, 1973, Int. Conf. Magnetism Moscow.
Cordier, G. and H. Schäfer, 1976, Z. Naturforsch, **31b**, 1459.
Cordier, G. and H. Schäfer, 1977, Z. Naturforsch, **32b**, 383.
Cordier, G., B. Eisenmann and H. Schäfer, 1976, Z. anorg. allg. Chem. **426**, 205.
Cox, D.E., 1972, IEEE Trans. Magnetics, MAG-8, 161.
Cutler, R.A. and A.W. Lawson, 1975, J. Appl. Phys. **46**, 2739.
Danan, J., C. de Novion and R. Lallement, 1969, Solid State Commun. **7**, 1103.
Davidov, D., and K. Baberschke, 1975, Phys. Lett. **51A**, 144.
Davidov, D., E. Bucher, L.W. Rapp, Jr., and L.D. Longinotti, 1974, Phys. Rev. **B9**, 2879.
Davidov, D., J.M. Bloch, R. Levin, C. Rettori and D. Shaltiel, 1975, Phys. Lett. **53A**, 290.
Davis, H.L. and H.A. Mook, 1972, AIP Conf. Proc. **10**, 1548.
Davis, H.L. and H.A. Mook, 1974, AIP Conf. Proc. **18**, 1068.
Davis, H.L. and H.A. Mook, 1975, AIP Conf. Proc. **24**, 229.
Deller, K. and B. Eisenmann, 1976a, Z. Naturforsch. **31b**, 1023.
Deller, K. and B. Eisenmann, 1976b, Z. anorg. allg. Chem. **425**, 104.
Deller, K. and B. Eisenmann, 1976c, Z. Naturforsch. **31b**, 1146.
Deller, K. and B. Eisenmann, 1976d, Z. Naturforsch. **31b**, 1550.
Deller, K. and B. Eisenmann, 1977, Z. Naturforsch. **32b**, 612.
Didchenko, R. and F.P. Gortsema, 1963, J. Phys. Chem. Solids **24**, 863.
Dismukes, J.P., W.M. Yim, J.J. Tietjen and R.E. Novak, 1970, RCA Rev. 31, 680.
Dismukes, J.P., W.M. Yim and V.S. Ban, 1972, J. Crystal Growth **13/14**, 365.
Dwight, A.E., 1974a, Proc. 11th Rare Earth Conf., Traverse City, Mi., p. 642.
Dwight, A.E., 1974b, J. Less-Common Met. **34**, 279.

Busch, G., P. Schwob, O. Vogt and F. Hulliger, 1964, Phys. Lett. 11, 100.

Dwight, A.E., 1977, Acta Cryst. **B33**, 1579.
Eatough, N.L. and H.T. Hall, 1969, Inorg. Chem. **8**, 1439.
Eatough, N.L. and H.T. Hall, 1970, Inorg. Chem. **9**, 416.
Eisenmann, B. and K. Deller, 1975, Z. Naturforsch. **30b**, 66.
Eisenmann, B. and H. Schäfer, 1974, Z. Naturforsch. **29b**, 13.
El Maslout, A., J.P. Motte, A. Courtois and C. Gleitzer, 1975, C.R. Acad. Sci. Paris **280C**, 21.
Erdös, P. and J.H. Kang, 1972, Phys. Rev. **B6**, 3393.
Essen, V.U. von and W. Klemm, 1962, Z. anorg. allg. Chem. **317**, 26.
Felcher, G.P., T.O. Brun, R.J. Gambino and M. Kuznietz, 1973, Phys. Rev. **B8**, 260.
Felmlee, T.L. and L. Eyring, 1968, Inorg. Chem. **7**, 660.
Ferro, R., A. Borsese, R. Capelli and S. Delfino, 1974, Thermochim. Acta **8**, 387.
Finegold, L., 1964, Phys. Rev. Lett. **13**, 233.
Fischer, P., W. Hälg, E. Kaldis and C. Zürcher, 1976, Spring Meeting Swiss Phys. Soc., Bern.
Fischer, P., B. Lebech, G. Meier, B.D. Rainford and O. Vogt, 1978, J. Phys. **C11**, 345.
Foner, S., B.R. Cooper and O. Vogt, 1972, Phys. Rev. **B6**, 2040.
Franceschi, E. and G.L. Olcese, 1969, J. Phys. Chem. Solids **30**, 903.
Freeman, A.J. and R.E. Watson, 1965, in Magnetism Vol. IIA (edited by G.T. Rado and H. Suhl, Acad. Press) p. 167.
Freeman, A.J. and J.P. Desclaux, 1972, Int. J. Magn. **3**, 311.
Furrer, A., J. Kjems and O. Vogt, 1972a, J. Phys. **C5**, 2246.
Furrer, A., W. Bührer, H. Heer, W. Hälg, J. Beneš and O. Vogt, 1972b, Neutron Inelastic Scattering, IAEA, Vienna, p. 563.
Furrer, A. and H. Heer, 1973, Phys. Rev. Lett. **31**, 1350.
Furrer, A. and E. Kaldis, 1976, AIP Conf. Proc. **29**, 264.
Furrer, A. and U. Tellenbach, 1975, Helv. Phys. Acta **48**, 451.
Furrer, A., G. Meier and O. Vogt, 1975, Report AF-SSP-84, Institut für Reaktortechnik ETH, Würenlingen, p. 10.
Furrer, A. and W. Hälg, 1976, Report AF-SSP-94, Institut für Reaktortechnik ETH, Würenlingen; J. Phys. **C9**, 3499.
Furrer, A., W.J.L. Buyers, R.M. Nicklow and O. Vogt, 1976, Phys. Rev. **B14**, 179.
Furrer, A., P.M. Levy and E. Kaldis, 1977, Crystal Field Effects in Metals and Alloys (ed. A. Furrer, Plenum, N.Y.) p. 24.
Gambino, R.J. and J.J. Cuomo, 1966, J. Electrochem. Soc. **113**, 401.
Gambino, R.J., 1967, J. Less-Common Met. **12**, 344.
Gambino, R.J., T.R. McGuire, H.A. Alperin and S.J. Pickart, 1970, J. Appl. Phys. **41**, 933.
Gambino, R.J., D.E. Eastman, T.R. McGuire, V.L. Moruzzi and W.D. Grobman, 1971, J. Appl. Phys. **42**, 1468.
Gaudé, J., J. Guyader and J. Lang, 1975, C.R. Acad. Sci. Paris **280C**, 883.
Goodenough, J.B., 1963, Magnetism and the Chemical Bond, Wiley New York, p. 149.
Goodman, B.B. and S.G. Marcucci, 1966, cited by Bevolo et al. (1976).
Goncharova, E.V., T.B. Zhukova and Z.I. Lopatina, 1968a, Inorg. Mater. **4**, 34.
Goncharova, E.V., V.P. Zhuze, V.V. Zhdanova, T.B. Zhukova, I.A. Smirnov and E.V. Shadrichev, 1968b, Sov. Phys.–Solid State **10**, 1052.
Goncharova, E.V., V.P. Zhuze and D.P. Lukirskii, 1969, Sov. Phys.–Solid State **10**, 1784.
Goryacheva, V.I., A.N. Nikol'skaya and Ya. I. Gerasimov, 1971, Doklady Phys. Chem. Sect. **197**, 258.
Grisafe, D.A. and F.A. Hummel, 1970, Amer. Mineral. **55**, 1131.
Guertin, R.P., J.E. Crow, L.D. Longinotti, E. Bucher, L. Kupferberg and S. Foner, 1975, Phys. Rev. **B12**, 1005.
Güntherodt, G. and P. Wachter, 1974a, Proc. 11th Rare Earth Conf., Traverse City, Mi., p. 820.
Güntherodt, G. and P. Wachter, 1974b, Proc. 12th Int. Conf. Phys. Semicond., Stuttgart, p. 899.
Güntherodt, G., E. Kaldis and P. Wachter, 1974, Solid State Commun. **15**, 1435.
Guyader, J., R. Marchand, J. Gaudé and J. Lang, 1975, C.R. Acad. Sci. Paris 281C, 307.
Hadenfeldt, C., H. Jacobs and R. Juza, 1970, Z. anorg. allg. Chem. **379**, 144.
Hadenfeldt, C., B. Gieger and H. Jacobs, 1974, Z. anorg. allg. Chem. **410**, 104.
Hall, H.T., 1969, Rev. Phys. Chem. Japan **39**, 110.
Halot, D. and J. Flahaut, 1971, C.R. Acad. Sci. Paris **272C**, 465.
Hamon, C., R. Marchand, M. Maunaye, J. Gaudé and J. Guyader, 1975, Rev. chim. minér. **12**, 259.
Hanks, R. and M.M. Faktor, 1967, Trans. Faraday Soc. **63**, 1130.
Hasegawa, A., and A. Yanase, 1977, J. Phys. Soc. Japan **42**, 492.
Hassler, E., T. Johnsson and S. Rundqvist, 1974, Acta Chem. Scand. **A28**, 123.
Hauger, R. and B. Natterer, 1975, unpublished.
Hayakawa, H., T. Sekine and S. Ono, 1975, J. Less-Common Met. **41**, 197.
Hayakawa, H., K. Nomura and S. Ono, 1976, J. Less-Common Met. **44**, 327.
Heer, H., A. Furrer and O. Vogt, 1973, Report AF-SSP-74, Institut für Reaktortechnik ETH, Würenlingen, p. 29.
Heer, H., A. Furrer and W. Hälg, 1976a, J. Magnetism Magn. Mater. **3**, 55.
Heer, H., A. Furrer, W. Hälg and O. Vogt, 1976b, Crystal Field Effects in Metals and Alloys, Plenum N.Y., p. 278.

Heer, H., 1978, Doctoral Thesis, ETH, Zürich.
Hiscocks, S.E.R. and J.B. Mullin, 1969, J. Mater. Sci. **4**, 962.
Hohnke, D. and E. Parthé, 1966, Acta Cryst. **21**, 435.
Hohnke, D. and E. Parthé, 1969, J. Less-Common Met. **17**, 291.
Holleck, H., E. Smailos and F. Thümmler, 1969, J. nucl. Mater. **32**, 281.
Holtzberg, F., T.R. McGuire, S. Methfessel and J.C. Suits, 1964, J. Appl. Phys. **35**, 1033.
Holtzberg, F., T.R. McGuire and S. Methfessel, 1970, Landolt–Börnstein, Numerical Data, New Series Group III, Vol. 4a, p. 41.
Honig, J.M., 1969, J. Solid State Chem. **1**, 19.
Howell, J.K. and L.L. Pytlewski, 1970, Inorg. Nucl. Chem. Lett. **6**, 681.
Huang, C.Y., K. Sugawara and B.R. Cooper, 1975, AIP Conf. Proc. **24**, 248.
Hulliger, F. and E. Mooser, 1963, J. Phys. Chem. Solids **24**, 283.
Hulliger, F. and E. Mooser, 1965, Progr. Solid State Chem. **2**, 330.
Hulliger, F., 1966, Helv. Phys. Acta **39**, 199.
Hulliger, F., 1968a, Helv. Phys. Acta **41**, 945.
Hulliger, F., 1968b, US Patent 3,403,002.
Hulliger, F., 1968c, Nature **219**, 373.
Hulliger, F., 1968d, J. Less-Common Met. **16**, 113.
Hulliger, F. and G.W. Hull, Jr., 1970, Solid State Commun. **8**, 1379.
Hulliger, F. and O. Vogt, 1970, Solid State Commun. **8**, 771.
Hulliger, F. and B. Natterer, 1973, Solid State Commun. **13**, 221.
Hulliger, F., M. Landolt, H.R. Ott and R. Schmelczer, 1975, J. Low-Temp. Phys. **20**, 269.
Hulliger, F., 1976, unpublished work 1968–1976.
Hulliger, F. and M. Landolt, 1976, unpublished.
Hulliger, F. and H.R. Ott, 1976a, unpublished.
Hulliger, F. and H.R. Ott, 1976b, AIP Conf. Proc. **34**, 70.
Hulliger, F. and B. Natterer, 1976, unpublished.
Hulliger, F., R. Schmelczer and D. Schwarzenbach, 1977, J. Solid State Chem. **21**, 371.
Hulliger, F. and F. Stucki, 1977, Conf. Rare Earths Actinides, Durham.
Hulliger, F. and H.R. Ott, 1977, J. Less-Common Met. **55**, 103.
Hutchings, M.T., 1964, Solid State Physics Vol. 16, 227.
Iandelli, A. and E. Franceschi, 1973, J. Less-Common Met. **30**, 211.
Jayaraman, A., W. Lowe, L.D. Longinotti and E. Bucher, 1976, Phys. Rev. Lett. **36**, 366.
Jeitschko, W. and D. Braun, 1977, Acta Cryst. **B33**, 3401.
Johnson, Q., 1971, Inorg. Chem. **10**, 2089.
Jones, E.D., 1966, Phys. Lett. **22**, 266.
Jones, E.D. and J.E. Hesse, 1967, J. Appl. Phys. **38**, 1159.
Jones, E.D. and B. Morosin, 1967, Phys. Rev. **160**, 451.
Jones, E.D., 1968, J. Appl. Phys. **39**, 1090.
Jones, E.D., 1969, Phys. Rev. **180**, 455.
Junod, P. and F. Lévy, 1966, Phys. Lett. **23**, 624.
Junod, P., A. Menth and O. Vogt, 1966, Phys. Lett. **23**, 626.
Junod, P., A. Menth and O. Vogt, 1969, Phys. kondens. Mat. **8**, 323.
Juza, R., H. Jacobs and H. Gerke, 1969, Ber. Bunsenges. phys. Chem. **370**, 254.
Kaldis, E., 1974, J. Crystal Growth **24/25**, 53.
Kaldis, E. and C. Zürcher, 1974, Helv. Phys. Acta **47**, 421.
Kaldis, E., G.v. Schulthess and P. Wachter, 1975, Solid State Commun. **17**, 1401.
Kaldis, E., A. Schlegel, P. Wachter and C. Zürcher, 1976, J. Magnetism Magn. Mater. **3**, 1.
Kharitonov, Yu. A., N.L. Smirnova and N.V. Belov, 1966, Russ. J. Struct. Chem. **7**, 825.
Kieffer, R., P. Ettmayer and Sw. Pajakoff, 1972, Monatsh. Chem. **103**, 1285.
Klüfers, P. and A. Mewis, 1977, Z. Naturforsch. **32b**, 353.
Kordis, J., K.A. Gingerich, R.J. Seyse, E. Kaldis and R. Bischof, 1972, J. Crystal Growth **17**, 53.
Kouvel, J.S., T.O. Brun and F.W. Korty, 1977, Physica **86–88B**, 1043.
Kripyakevich, P.I., 1963, Sov. Phys. – Cryst. **7**, 556.
Kuznietz, M., 1971, J. Appl. Phys. **42**, 1470.
Lallement, R. and J.J. Veyssie, 1968, Progr. Sci. Technol. Rare Earths Vol. III, p. 284.
Landau, D.P. and J.E. Rives, 1974, Solid State Commun. **15**, 665.
Lander, G.H., T.O. Brun and O. Vogt, 1973, Phys. Rev. **B7**, 1988.
Lander, G.H., M.H. Mueller and O. Vogt, 1975, AIP Conf. Proc. **24**, 430.
LaValle, D.E., 1962, J. Inorg. Nucl. Chem. **24**, 930.
Lea, K.R., M.J.M. Leask and W.P. Wolf, 1962, J. Phys. Chem. Solids **23**, 1381.
Lévy, F., 1969, Phys. kondens. Mat. **10**, 85.
Levy, P.M., 1970, Phys. Rev. **B2**, 1429.
Levy, P.M. and H.H. Chen, 1971, Phys. Rev. Lett. **27**, 1385.
Lewis, W.B., 1971, in Magnetic Resonance and Related Phenomena, Proc. 16th Congress AMPERE, Bucharest 1970 (ed. by I. Ursu, Publ. House Acad. Romania, Bucharest), p. 717.
Lorenzelli, N., J. Melamed and J.P. Marcon, 1970, Coll. Int. CNRS No. 180, Paris-Grenoble 1969, Vol. I, p. 375.
Lüthi, B., M.E. Mullen and E. Bucher, 1973, Phys. Rev. Lett. **31**, 95.
Maass, K.E., 1970, Z. anorg allg. Chem. **374**, 19.
Magyar, B., 1968, Inorg. Chem. **7**, 1457.
Marchand, R., 1976 , C.R. Acad. Sci. Paris **282C**, 329 and **283C**, 281.

Hulliger, F., 1979, Mater. Res. Bull. 14, 33.

Marchand, R., Y. Laurent and J. Lang, 1976a, 5th Int. Conf. Solid Compounds of Transition Elements Uppsala, Abstracts p. 51.
Marchand, R., A. Jayaweera, P. Verdier and J. Lang, 1976b, C.R. Acad. Sci. Paris **283C**, 675.
Mathur, M.P., D.W. Deis, C.K. Jones, A. Patterson, W.J. Carr, Jr. and R.C. Miller, 1970, J. Appl. Phys. **41**, 1005.
McGuire, T.R., R.J. Gambino, S.J. Pickart and H.A. Alperin, 1969, J. Appl. Phys. **40**, 1009.
McWhan, D.B., 1966, J. Chem. Phys. **44**, 3528.
Meier, G., W. Hälg and O. Vogt, 1976, Spring Meeting Swiss Phys. Soc., Bern.
Menge, G. and H.G.v. Schnering, 1976, Z. anorg. allg. Chem. **422**, 226.
Methfessel, S. and E. Kneller, 1963, Appl. Phys. Lett. **2**, 115.
Mewis, A., 1977, Z. Naturforsch. **32b**, 351.
Mironov, K.E., I.G. Vasil'eva and T.G. Pritchina, 1973, Rev. Chim. minér. **10**, 383.
Mironov, K.E. and G.P. Brygalina, 1974, Inorg. Mater. **10**, 787.
Mironov, K.E., G.P. Brygalina and V.N. Ikorskii, 1974, Proc. 11th Rare Earth Conf., Traverse City, Mi., p. 105.
Morgan, P.E.D., P.J. Carroll and F.F. Lange, 1977, Mat. Res. Bull. **12**, 251.
Mourgout, C., B. Chevalier, J. Étourneau, J. Portier, P. Hagenmuller and R. Georges, 1977, Rev. int. Htes. Temp. Réfract. **14**, 89.
Mullen, M.E., B. Lüthi, P.S. Wang, E. Bucher, L.D. Longinotti, J.P. Maita and H.R. Ott, 1974, Phys. Rev. **B10**, 186.
Murao, T. and T. Matsubara, 1957, Progr. Theor. Phys. **18**, 215.
Murray, J.J. and J.B. Taylor, 1970, J. Less-Common Met. **21**, 159.
Myers, S.M. and A. Narath, 1973, Solid State Commun. **12**, 83.
Myers, S.M. and A. Narath, 1974, Phys. Rev. **B9**, 227.
Nereson, N. and G. Arnold, 1971, J. Appl. Phys. **42**, 1625.
Nereson, N. and V. Struebing, 1971, AIP Conf. Proc. **5**, 1385.
Newman, D.J., 1971, Adv. Phys. **20**, 197.
Nomura, K., H. Hayakawa and S. Ono, 1977, J. Less-Common Met. **52**, 259.
Ono, S., J.G. Despault, L.D. Calvert and J.B. Taylor, 1970, J. Less-Common Met. **22**, 51.
Ono, S., F.L. Hui, J.G. Despault, L.D. Calvert and J.B. Taylor, 1971, J. Less-Common Met. **25**, 287.
Ott, H.R. and B. Lüthi, 1976, Phys. Rev. Lett. **36**, 600.
Ott, H.R. and B. Lüthi, 1977, Z. Phys. **B28**, 141.
Palisaar, A.P. and R. Juza, 1971, Z. anorg. allg. Chem. **384**, 1.
Pantelides, S.T., 1975, Phys. Rev. **B11**, 5082.
Paukov, I.E., F.S. Rakhmenkulov and G.I. Frolova, 1976, Sov. Phys. Solid State **18**, 662.
Phillips, N.E., B.B. Triplett, R.D. Clear, H.E. Simon, J.K. Hulm, C.K. Jones and R. Mazelsky, 1971, Physica **55**, 571.
Rainford, B., K.C. Turberfield, G. Busch and O. Vogt, 1968, J. Phys. **C1**, 679.
Rebouillat, J.P. and J.J. Veyssié, 1964, C.R. Acad. Sci. Paris **259**, 4239.
Rhyne, J.J. and T.R. McGuire, 1972, IEEE Trans. Magnetics, MAG-8, 105.
Rieger, W. and E. Parthé, 1968, Acta Cryst. **B24**, 456.
Rieger, W. and E. Parthé, 1969, Monatsh. Chem. **100**, 1370.
Rossat-Mignod, J., P. Burlet, J. Villain, H. Bartholin, Wang Tscheng Si, D. Florence and O. Vogt, 1977, Phys. Rev. **B16**, 440.
Samsonov, G.V., M.N. Abdusalyamova and Kh. Shokirov, 1974, Inorg. Mater. **10**, 790.
Schäfer, H., 1964, Chemical Transport Reactions, Academic Press, New York.
Schmid, R. and H. Hahn, 1970, Z. anorg. allg. Chem. **372**, 106.
Schmidt, F.A. and O.D. McMasters, 1970, J. Less-Common Met. **21**, 415.
Schnering, H.G.v. and W. Wichelhaus, 1976, private communication.
Schnering, H.G.v., W. Wichelhaus and M. Schulze Nahrup, 1975, Z. anorg. allg. Chem. **412**, 193.
Schnering, H.G.v., W. Wichelhaus and M. Wittmann, 1976, 5th Conf. Transition-Element Compounds Uppsala, PII 68.
Schobinger-Papamantellos, P., P. Fischer, O. Vogt and E. Kaldis, 1973, J. Phys. **C6**, 725.
Schumacher, D.P. and W.E. Wallace, 1965, J. Appl. Phys. **36**, 984.
Schumacher, D.P. and W.E. Wallace, 1966, Inorg. Chem. **5**, 1563.
Schumacher, D.P. and C.A. Hollingsworth, 1966, J. Phys. Chem. Solids **27**, 749.
Sclar, N., 1962, J. Appl. Phys. **33**, 2999.
Sclar, N., 1964, J. Appl. Phys. **35**, 1534.
Sfez, G. and C. Adolphe, 1972, Bull. Soc. Fr. Minéral. Crist. **95**, 553.
Shannon, R.D., 1976, Acta Cryst., **A32**, 751.
Shapiro, S.M. and P. Bak, 1975, J. Phys. Chem. Solids **36**, 579.
Shiles, E., G.B. Taggart and R.A. Tahir-Kheli, 1974, AIP Conf. Proc. **18**, 1317.
Sivardière, J. and M. Blume, 1972, Phys. Rev. **B5**, 1126.
Smart, M., L.D. Calvert and J.B. Taylor, 1977, private communication.
Stankevich, V.G., I.I. Lukashevich, N.I. Filippov and I.A. Gladkikh, 1974, Sov. Phys. – JETP **39**, 134.
Stassen, W.N., M. Sato and L.D. Calvert, 1970, Acta Cryst. **B26**, 1534.
Stevens, K.W.H. and E. Pytte, 1973, Solid State Commun. **13**, 101.
Streit, P., G.E. Everett and A.W. Lawson, 1974, Phys. Lett. **50A**, 199.
Stutius, W., 1969a, Phys. kondens. Mat. **9**, 341.
Stutius, W., 1969b, Phys. kondens. Mat. **10**, 152.
Sugawara, K., C.Y. Huang and B.R. Cooper, 1975, Phys. Rev. **B11**, 4455.
Sugawara, K. and C.Y. Huang, 1976, Phys. Stat. Sol. **78b**, K7.
Sugawara, K., C.Y. Huang, C.W. Chu and B.R. Cooper, 1977, Solid State Commun. **21**, 189.

Ono, S., K. Nomura and H. Hayakawa, 1974, J. Less-Common Met. 38, 119.

Switendick, A.C. and E.D. Jones, 1968, Bull. Am. Phys. Soc. **13**, 365.
Taub, H. and S.J. Williamson, 1973, Solid State Commun. **13**, 1021.
Taub, H., S.J. Williamson, W.A. Reed and F.S.L. Hsu, 1974, Solid State Commun. **15**, 185.
Taub, H. and C.B.R. Parente, 1975, Solid State Commun. **16**, 857.
Taylor, J.B., L.D. Calvert, J.G. Despault, E.J. Gabe and J.J. Murray, 1974, J. Less-Common Met. **37**, 217.
Taylor, J.B., L.D. Calvert, T. Utsunomiya, Yu Wang and J.G. Despault, 1978, J. Less-Common Met. **57**, 39.
Taylor, K.N.R. and M.I. Darby, 1972, Physics of Rare Earth Solids, Chapman and Hall.
Torbov, V.I., V.I. Chukalin and E.I. Yarembash, 1970, Inorg. Mater. **6**, 1559.
Torbov, V.I., L.A. Egorov, V.I. Chukalin and E.I. Yarembash, 1971, Inorg. Mater. **7**, 1434.
Torbov, V.I., L.A. Egorov, V.I. Chukalin and E.I. Yarembash, 1972, Inorg. Mater. **8**, 1152.
Torbov, V.I., V.I. Chukalin, V.N. Doronin, L.G. Nikolaeva and Z.S. Medvedeva, 1974, Russ. J. Inorg. Chem. **19**, 21.
Trammell, G.T., 1963, Phys. Rev. **131**, 932.
Tsuchida, T. and W.E. Wallace, 1965a, J. Chem. Phys. **43**, 2087.
Tsuchida, T. and W.E. Wallace, 1965b, J. Chem. Phys. **43**, 2885.
Tsuchida, T. and Y. Nakamura, 1967, J. Phys. Soc. Japan **22**, 942.
Tsuchida, T. and Y. Nakamura, 1968, J. Phys. Soc. Japan **25**, 284.
Tsuchida, T., Y. Nakamura and T. Kaneko, 1969, J. Phys. Soc. Japan **26**, 284.
Tsuchida, T., M. Kawai and Y. Nakamura, 1970, J. Phys. Soc. Japan **28**, 528.
Tsuchida, T., S. Onga, T. Kawai and S. Kawarazaki, 1973, J. Phys. Soc. Japan **35**, 1788.
Tsuchida, T., A. Hashimoto and Y. Nakamura, 1974, J. Phys. Soc. Japan **36**, 685.
Turberfield, K.C., L. Passell, R.J. Birgeneau and E. Bucher, 1970, Phys. Rev. Lett. **25**, 752.
Turberfield, K.C., L. Passell, R.J. Birgeneau and E. Bucher, 1971, J. Appl. Phys. **42**, 1746.
Vendl, A., P. Ettmayer and W. Prohaska, 1976, Proc. 5th Int. Conf. Transition Element Compounds, Uppsala, p. 38.
Vendl, A., P. Ettmayer and W. Prohaska, 1977, High Temp-High Press. **9**, 313.
Veyssié, J.J., J. Chaussy and A. Berton, 1964, Phys. Lett. **13**, 29.
Veyssié, J.J., D. Brochier, A. Nemoz and J. Blanc, 1965, Phys. Lett. **14**, 261.
Wachter, P., 1972, CRC Crit. Rev. Solid State Sci. **3/12**, 189.
Wachter, P. and J. Wullschleger, 1972, J. Phys. Chem. Solids **33**, 939.
Wachter, P., E. Kaldis and R. Hauger, 1978, Phys. Rev. Lett. **40**, 1404.
Wakabayashi, N. and A. Furrer, 1976, Phys. Rev. **B13**, 4343.
Wakim, F.G., M. Synek, P. Grossgut and A. Da Mommio, 1972, Phys. Rev. **A5**, 1121.
Wallace, W.E., C. Deenadas, A.W. Thompson and R.S. Craig, 1971, J. Phys. Chem. Solids **32**, 805.
Wang, R., R. Bodnar and H. Steinfink, 1966, Inorg. Chem. **5**, 1468.
Wang, R. and H. Steinfink, 1967, Inorg. Chem. **6**, 1685.
Wang, R., H. Steinfink and A. Raman, 1967, Inorg. Chem. **6**, 1298.
Wang, Y.L. and B.R. Cooper, 1970, Phys. Rev. **B2**, 2607.
Wang, Y., E.J. Gabe, L.D. Calvert and J.B. Taylor, 1976, Acta Cryst. **B32**, 1440.
Wang, Y., L.D. Calvert, E.J. Gabe and J.B. Taylor, 1977a, Acta Cryst. **B33**, 3122.
Wang, Y., R.D. Heyding, E.J. Gabe, L.D. Calvert and J.B. Taylor, 1977b, private communic. (to appear in Acta Cryst. **B34**).
Wang, Y., L.D. Calvert, E.J. Gabe and J.B. Taylor, 1977c, private communication.
Warming, E. and P. Bak, 1975, J. Phys. **C8**, 1054.
Weaver, H.T. and J.E. Schirber, 1976, Phys. Rev. **B13**, 1363.
Weaver, H.T., J.E. Schirber and B. Morosin, 1977, Solid State Commun. **23**, 785.
Westerholt, K. and S. Methfessel, 1977, Physica **86–88B**, 1160.
Westrum, E.F., 1968, Progr. Sci. Technol. Rare Earths, Vol. III, p. 459.
Wichelhaus, W. and H.G.v. Schnering, 1975, Naturwiss. **62**, 180.
Wichelhaus, W. and H.G.v. Schnering, 1976, Z. anorg. allg. Chem. **419**, 77.
Wills, R.R., R.W. Stewart, J.A. Cunningham and J.M. Wimmer, 1976, J. Mater. Sci. **11**, 749.
Yaguchi, K., 1966, J. Phys. Soc. Japan **21**, 1226.
Yim, W.M., E.J. Stofko and R.T. Smith, 1972, J. Appl. Phys. **43**, 254.
Yoshihara, K., J.B. Taylor, L.D. Calvert and J.G. Despault, 1975, J. Less-Common Met. **41**, 329.
Yuan, S., 1977, private communication.
Zinn, W., 1977, private communication.
Zürcher, C., 1977, Doctoral Thesis, ETH Zürich.

References to section 6

Braun, D.J., and W. Jeitschko, 1978, Acta Cryst. **B34**, 2069.
Marchand, R., and W. Jeitschko, 1978, J. Solid State Chem. **24**, 351.
Wang, Y., L.D. Calvert, E.J. Gabe and J.B. Taylor, 1978, Acta Cryst. **B34**, 2281.
Weinberger, P., K. Schwarz and A. Neckel, 1971, J. Phys. Chem. Solids, 32, 2063.

Handbook on the Physics and Chemistry of Rare Earths, edited by K.A. Gschneidner, Jr. and L. Eyring

Chapter 34

CHEMISTRY AND PHYSICS OF R-ACTIVATED PHOSPHORS

G. BLASSE
Solid State Chemistry Department, State University, Utrecht, The Netherlands

Contents

Symbols

A = activator
S = sensitizer
R = rare earth ion
P_s^r = probability of radiative return to ground state
P_s^{nr} = probability of non-radiative return to ground state
P_{sa} = probability of energy transfer from S to A
P_{ss} = probability of energy transfer from S to S
τ_s = life time of luminescent state of S
q = quantum efficiency
r_{sa} = distance between centres S and A
n = dielectric constant of the host lattice
$f_s(E)$ = normalized emission band
$f_a(E)$ = normalized absorption band
Q_a = integrated absorption of A
E = photon energy
Z = overlap integral
r_i = position coordinate of an electron
a = lattice spacing
t_h = average hopping time
c.t. = charge transfer
Δr = expansion of luminescent center

1. Introduction

Phosphors are materials capable of emitting radiation when subjected to ultraviolet radiation, X-rays, electron bombardment, friction or some other form of excitation. This emission is known as luminescence.* In a tubular fluorescent lamp, for example, the energy of the mercury line at 253.7 nm is converted into radiation covering the whole visible region. In a television tube the energy of fast electrons is converted into visible radiation. For a general introduction to luminescence see Curie (1963), Garlick (1958), Goldberg (1966) and Riehl (1971).

The present article gives a review of the fundamental research done on phosphors that show characteristic emission. In such phosphors the emission comes from luminescent centres as a result of an electron transition that, in principle, would also be possible if the centre were situated in free space instead of in a crystal lattice. Nevertheless, as will be seen, the crystal lattice does play an important part.

The physical processes involved in the phenomenon of characteristic luminescence are presented schematically in fig. 34.1. The figure shows part of a crystal M in which two kinds of foreign ions or ionic groups (centres) are incorporated. One centre of each type is shown, marked A and S. We assume that the host lattice absorbs no radiation. The centre in the right half is raised to an excited state as a result of radiation absorbed by that centre. The centre returns to the ground state by giving up the excitation energy as radiation or as heat. The former case is referred to as luminescence, and the centre involved is called an activator.

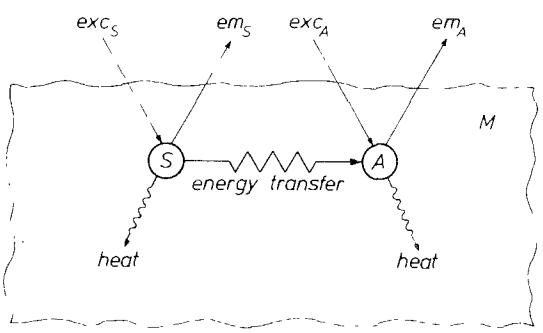

Fig. 34.1. Diagrammatic representation of luminescence. Incorporated in a host lattice M are an activator A and a sensitizer S. The host lattice does not absorb incident radiation. The activator A can absorb radiation (exc_A). This excitation is followed by emission (em_A) and/or by the dissipation of heat. The activator can also be excited via the sensitizer S. In that case S absorbs the radiation (exc_S) and then transfers excitation energy to A. Emission and/or heat dissipation from S are also possible (from Blasse and Bril, 1970).

*The terms fluorescence and phosphorescence have been in use much longer than luminescence, although with different meanings in different branches of science. We have therefore avoided their use here. Particulars of the terminology used in this field will be found in Garlick (1958).

It is also possible to excite the activator A by indirect means. If, for example, we want to excite a phosphor with the 253.7 nm radiation from a mercury lamp, and if A does not absorb this radiation, the excitation can nevertheless take place via the centre S which does absorb this radiation. In some cases the host lattice itself plays the part of S. The excited centre S can return to the ground state in three ways: by radiation, by the dissipation of the excitation energy in the form of heat, and by transfer of the excitation energy to A. In the latter case the excitation energy absorbed by S, or part of it, is emitted by A. S is then often referred to as a sensitizer of the luminescence from A, although it may itself also act as activator.

In what follows, the role of activator is played by one of the ions of the rare earth metals (R ions). Research on these phosphors in particular has considerably advanced the understanding of characteristic luminescence, since the properties of these phosphors can be studied on simple model compounds. This is possible because of the similarity between these ions. The host lattice may be, for instance, a compound of the ions La^{3+}, Y^{3+} or Lu^{3+}. The latter ions do not absorb ultraviolet radiation. Rare earth ions, for example Eu^{3+} or Tb^{3+}, are now substituted for a small proportion of the host lattice ions. These R ions occupy in the host lattice the crystallographic sites of La^{3+}, Y^{3+} or Lu^{3+} in a virtually random distribution. It is possible in this way to make phosphors whose chemical constitution is well defined.

In section 2 of this chapter we shall examine the possible excitation and emission transitions in phosphors. Further we will deal with radiationless losses and energy transfer. This section is called Physics of Phosphors. In section 3 (Chemistry of Phosphors) we will consider the influence of chemical composition and crystal structure on the physical properties mentioned in section 2. In section 4 we will illustrate how the ideas presented in sections 2 and 3 work in the case of luminescent rare earth (R) ions where those ions that find technical applications nowadays will be treated in more detail. In section 5, finally, we shall take a look at the application of R-activated phosphors.

Reviews on this subject have appeared during the last 10 years. We refer to Palilla (1968), Blasse and Bril (1968, 1970), Lange (1971) and Stevels (1976). We follow an outline given in the 1970 review.

2. Physics of R-activated phosphors

2.1. *The energy-level diagram of the R ions*

The characteristic properties of the R ions are attributable to the presence in the ion of a deep-lying 4f shell which is not entirely filled. The electrons of this shell are screened by the outer electron shells, and as a result they give rise to a number of discrete energy levels. Since the presence of the crystal lattice scarcely affects the positions of these levels, there is a close resemblance

between the energy-level diagram of the free ion and that of the incorporated ion (see also chapter 23).

The 4f shell may contain 14 electrons. Table 34.1 shows the most common valencies of the R ions and the number of 4f electrons in the ground state of the relevant ions. The energy-level diagrams for Ce^{3+}, Eu^{2+}, Eu^{3+}, Gd^{3+} and Tb^{3+} are given in fig. 34.2. These energy-level diagrams have been chosen here as examples because they are the simplest ones and are at the same time representative of all the types encountered. In most R ions and the number of levels is fairly large, except in Ce^{3+} and Eu^{2+} (and Yb^{3+}). The Ce^{3+} ion has only one 4f electron, and this gives rise to two energy levels: in the one state the orbital and spin moments of the electron are parallel ($^2F_{7/2}$), and in the other state antiparallel ($^2F_{5/2}$). As the number of electrons increases, there is in general a rapid increase in the number of possible states.

Figure 34.2 shows that in addition to the discrete 4f levels there are other levels present. These are represented schematically as broad, hatched bands. The energy levels of these bands depend to a great extent on the lattice.

The bands referred to fall into two groups. In the first group one of the 4f electrons is raised to the higher 5d level: $4f^n \rightarrow 4f^{n-1}5d$. This 5d level can be strongly influenced by the lattice. In the Eu^{2+} ion, the $4f^6 5d$ level lies so low that

TABLE 34.1
The ions of the rare earth metals and the number of 4f electrons in their respective ground states

Ion		Number of 4f electrons
La^{3+}		0
Ce^{3+}		1
	Ce^{4+}	0
Pr^{3+}		2
Nd^{3+}		3
Pm^{3+}		4
Sm^{2+}		6
Sm^{3+}		5
Eu^{2+}		7
Eu^{3+}		6
Gd^{3+}		7
Tb^{3+}		8
	Tb^{4+}	7
Dy^{3+}		9
Ho^{3+}		10
Er^{3+}		11
Tm^{3+}		12
Yb^{2+}		14
Yb^{3+}		13
Lu^{3+}		14

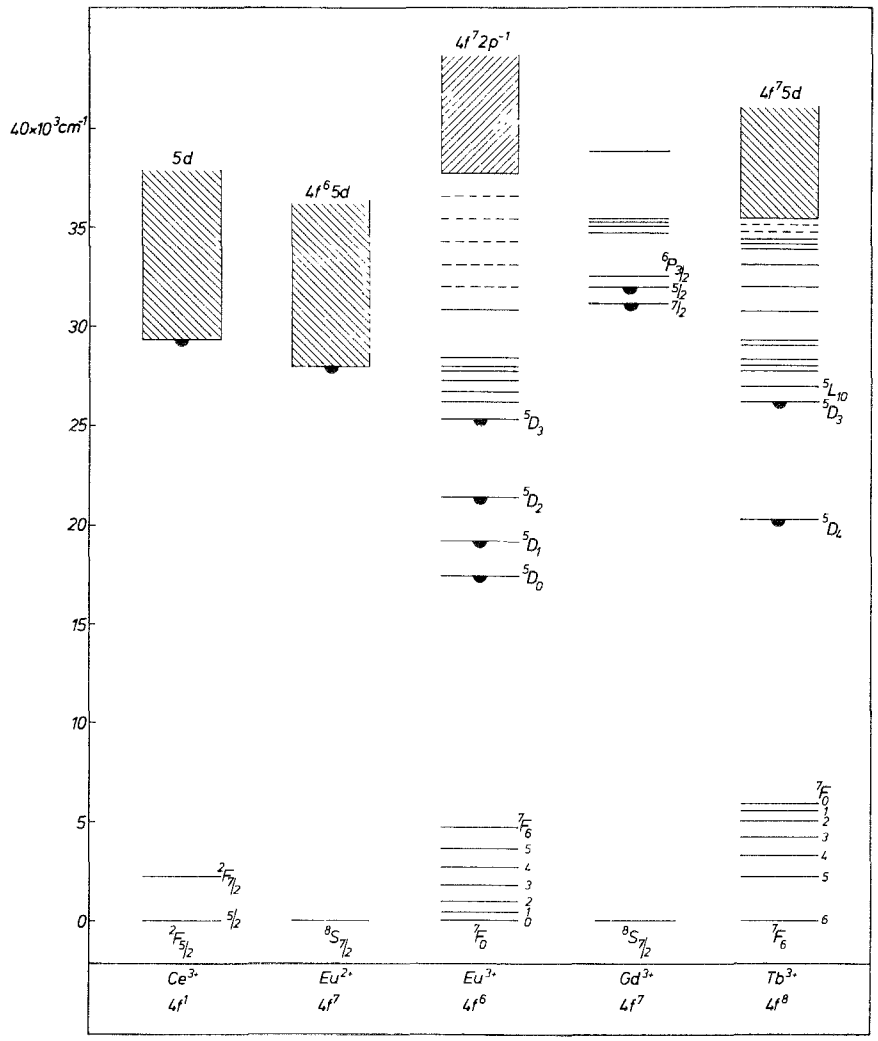

Fig. 34.2. Energy-level diagram of some ions of rare earth metals in oxide host lattices. Horizontal lines indicate the narrow 4f levels. Where the levels are not well known they are shown as dashed lines. The hatched broad bands indicate schematically charge-transfer (Eu^{3+}) or $4f^{n-1}5d$ states (Ce^{3+}, Eu^{2+}, Tb^{3+}). For Gd^{3+} these states have such a high energy that they cannot be shown in the figure. Levels labelled with black half-circles are levels from which luminescence is observed (from Blasse and Bril, 1970).

the $4f^7$ levels present (except for the ground level) are completely overlapped (fig. 34.2). In the second group one of the electrons of the surrounding anions is promoted to the 4f orbit of the central R ion (charge-transfer state). Obviously the position of this energy band depends on the nature of the surrounding ions.

What is it that determines whether the energetically lowest band corresponds to a $4f^{n-1}5d$ state or to a charge transfer state? The answer to this question is bound

up with the fact that a state with a completely or half-filled electron shell is very stable. If we compare, for example, the trivalent ions with one another, we get the following picture. The excited states of Gd^{3+} ($4f^7$, hence half-filled) lie at a high energy level (fig. 34.2). In the case of Tb^{3+} ($4f^8$, half-filled plus one) the 4f shell readily releases an electron, and the transition $4f^8 \rightarrow 4f^7 5d$ takes place at relatively low energy, while in the case of Eu^{3+} ($4f^6$, half-filled less one) the 4f shell readily accepts an electron and thus the charge-transfer state has a low energy.

Having seen which states play a part in the R ions and considered the basic structure of the energy-level diagrams of these ions, we shall deal in the following sections with the optical transitions between these levels (see also chapter 23).

Situations will be encountered where the electric-dipole transition between two levels is allowed, and others where such a transition is forbidden. It will be seen that in the latter case, apart from magnetic-dipole radiation, electric-dipole radiation is nevertheless frequently observed, albeit very much weaker. We shall look at the conditions in which a forbidden transition partly ceases to be forbidden.

2.2. Optical transitions involving a 5d *or a charge transfer state*

Let us look first at 4f–5d transitions. These transitions are allowed for the emission and absorption of electric-dipole radiation. It may be derived from fig. 34.2 that this absorption lies in the ultraviolet part of the spectrum for the ions mentioned in the figure (Ce^{3+}, Eu^{2+}, Tb^{3+}). For a vacuum-ultraviolet study see Heaps et al. (1976). Figure 34.3 gives reflection and excitation spectra for the garnets $Y_3Al_5O_{12}$ and $(Y, Ce)_3Al_5O_{12}$. Both the reflection spectrum and the excitation spectrum give a picture of the absorption, and we see that in the activated crystals there is indeed strong absorption in the UV. It is noticeable here, particularly in the excitation spectra, that this absorption takes place in a

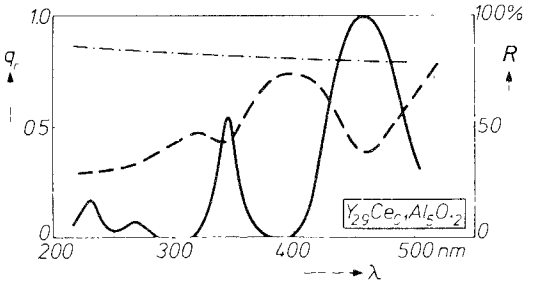

Fig. 34.3. The chain-dotted line gives the reflection spectrum of $Y_3Al_5O_{12}$. The dashed line indicates the reflection spectrum of $Y_{2.9}Ce_{0.1}Al_5O_{12}$. The solid line gives the excitation spectrum of the Ce^{3+} luminescence of $Y_{2.9}Ce_{0.1}Al_5O_{12}$: the relative quantum yield q_r of the luminescence is plotted as a function of the wavelength of the exciting radiation. The Ce^{3+} absorption bands correspond to the various 4f–5d transitions. The distance between them in the spectrum is equal to the crystal-field splitting of the 5d level (from Blasse and Bril, 1970).

number of discrete bands. This may be explained as follows. The excited 5d state is strongly influenced by the crystal field which splits the 5d level into a number of levels which are roughly 15 000 to 20 000 cm^{-1} apart. The number of these levels is determined by the crystallographic symmetry at the position of the rare-earth ion. Since the crystal-field splitting varies considerably from one lattice to another, so too does the spectral position of the absorption bands appertaining to a particular 4f–5d transition.

Now let us see what happens when an activator in which 4f–5d transitions take place is excited in the corresponding absorption bands in the UV.

In the case of Tb^{3+}, excitation in the 4f–5d absorption bands is followed by green emission. As a result of absorbing UV radiation, the ion is raised to a $4f^7 5d$ state; it then decays stepwise from this state to the $^5D_3$ or the $^5D_4$ state, or both (see fig. 34.2), thereby giving up phonons to the lattice. Because of the large distance between these states and the ^7F levels, the process stops here and the ion then returns to the ground state by emitting radiation (luminescence). Although the position of the 4f–5d absorption and excitation bands depends to a very great extent on the nature of the lattice, the (green) emission does not. This, of course, is because the emission is the consequence of a transition between 4f levels (in principle a strictly forbidden transition for electric-dipole radiation, as will be discussed below).

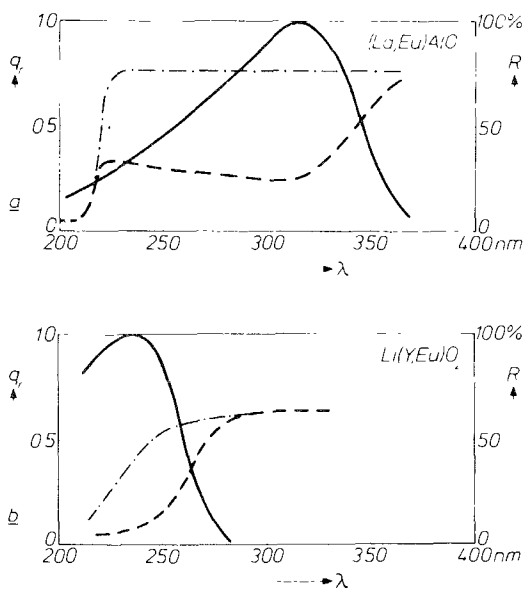

Fig. 34.4. (a) Reflection spectrum of the host lattice $LaAlO_3$ (chain-dotted line) and of (La, Eu)AlO_3 (dashed). The solid line is the excitation spectrum of the Eu^{3+} luminescence of (La, Eu)AlO_3. The absorption and excitation bands at about 310 nm correspond to the charge-transfer absorption. R is the reflectance, q_r is the relative quantum yield. (b) As (a), but now for Li(Y, Eu)O_2 (from Blasse and Bril, 1970).

The situation as far as the Ce^{3+} ion is concerned is entirely different. Excitation in the 4f–5d absorption bands is followed by emission from the 5d states themselves. Contrary to the case of Tb^{3+}, the emission here depends strongly on the lattice.

We shall now consider the optical absorption caused by a transition to a charge-transfer state. The Eu^{3+} ion shows absorption of this type. Some examples of reflection spectra are presented in fig. 34.4. These transitions, too, correspond to allowed optical transitions. Unlike the 4f–5d transitions, however, there is no distinct splitting in the absorption spectra (compare figs. 34.3 and 34.4).

In the emission process of the Eu^{3+} ion the charge-transfer level plays no part, since the ion decays from the charge-transfer level via a number of 4f levels to the ^5D levels, from which the ground state is reached by the emission of radiation (fig. 34.2). More will be said about this under the next heading.

2.3. *Optical transitions between* 4f *levels*

Electric-dipole transitions between 4f levels of rare earth ions are strictly forbidden, because the parity does not change (Laporte's selection rule). We shall now consider as an example the transitions between the ^5D and ^7F levels of the Eu^{3+} ion. The electric-dipole transition between these levels is forbidden not only because of the above-mentioned Laporte's selection rule, but also because the spin quantum number S of the total angular momentum changes (from 2 to 3).

How, then, can the relevant transitions nevertheless be observed? No more than a very brief summary of the underlying theory is given here. (For a full account see Wybourne (1965), Ofelt (1962), Peacock (1975).)

The *spin prohibition* is not strict because the description of the ^7F levels as states with six parallel spins is not entirely correct. Because of spin-orbit coupling it is necessary to consider what we call ^7F states as being composed of a pure ^7F state with a slight "admixture" of the pure ^5D state.

The *parity prohibition* can be lifted only by the influence of the crystal lattice. Just as the spin prohibition was cancelled by mixing of the ^7F state with the ^5D state as a result of spin-orbit coupling, so too can the parity prohibition be cancelled by mixing the $4f^6$ configuration with a state possessing a different parity. The interaction responsible for this is formed by the odd crystal-field terms, that is to say those terms that change sign on inversion with respect to the R ion. If the R ion is located at a site that is a centre of symmetry in the crystal lattice, the odd crystal field terms are absent and the parity prohibition cannot be lifted.

In that case only magnetic-dipole transitions are possible. The selection rule here is: $\Delta J = 0, \pm 1$ (except that $J = 0 \rightarrow J = 0$ is forbidden). If the Eu^{3+} ion is situated at a centre of symmetry and is brought into the $^5D_0$ state (fig. 34.2), the only possible transition accompanied by the emission of radiation is $^5D_0 \rightarrow {}^7F_1$. Figure 34.5 shows the emission spectrum of an Eu^3 ion situated at a centre of

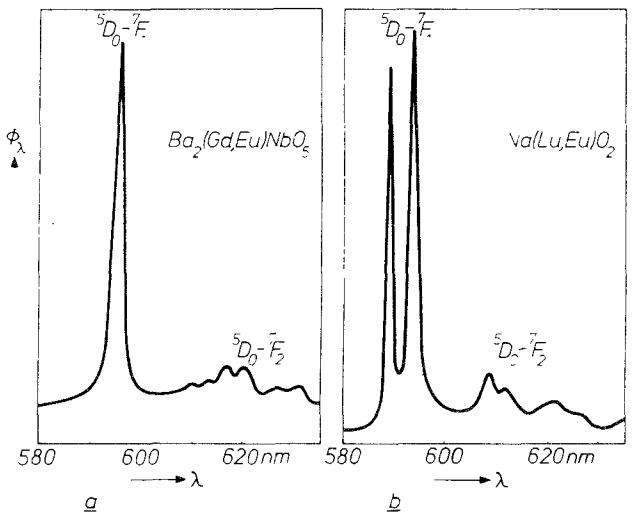

Fig. 34.5. Emission spectrum of the Eu^{3+} ion when it occupies a site with a centre of symmetry. Excitation with 254 nm radiation, (a) in Ba_2GdNbO_6, (b) in $NaLuO_2$ (from Blasse and Bril, 1970).

symmetry. As expected, this spectrum consists of emission lines that correspond to the $^5D_0$–$^7F_1$ transition. The colour of this emission is orange. The figure also shows that in the case of Eu^{3+} in Ba_2GdNbO_6 only one $^5D_0$–$^7F_1$ line is found. For Eu^{3+} in $NaLuO_2$ two $^5D_0$–$^7F_1$ emission lines are found. We have already mentioned above that energy levels can be split by the field of the surrounding ions (crystal-field splitting). For the 5d level the splitting is considerable. Crystal-field splitting is also found for 4f levels but, since the 4f electrons are well screened from the environment, the splitting is much smaller.

For d electrons the splitting may amount to a few 10 000 cm^{-1}, but for the 4f electrons it may be no more than a few 100 cm^{-1}. Now a level with $J = 0$ is a single, non-degenerate state and cannot be split. A level with $J = 1$ is triply degenerate and can be split. A field possessing cubic symmetry permits triple degeneration and does not cause splitting. Tetragonal and trigonal fields cause splitting into two levels; fields with lower symmetry cause splitting into three levels.

In Ba_2GdNbO_6 the Eu^{3+} ion occupies the position of Gd^{3+}. This is a crystallographic site with cubic symmetry. The $^7F_1$ level is therefore not split. The $^5D_0$ level ($J = 0$) can never be split. The emission transition $^5D_0$–$^7F_1$ therefore consists of one line. In $NaLuO_2$ the symmetry at the location of the Eu^{3+} ion is trigonal. The $^7F_1$ level is split into two sublevels, and the emission transition $^5D_0$–$^7F_1$ therefore consists of two lines.

Let us now consider the situation where the Eu^{3+} ion occupies a crystallographic site that does not coincide with a centre of symmetry. In this case not only magnetic-dipole transitions are possible but also electric-dipole transitions. The latter are known as forced electric-dipole transitions and are similarly

subject to selection rules, viz. $\Delta J \leqq 6$. If, however, $J = 0$ for the initial or final level, then $\Delta J = 2, 4$ or 6.

In the example we have chosen (emission starting from the $^5D_0$ level of the Eu^{3+} ion) we have $J = 0$ for the initial level. We may therefore expect the following electric-dipole transitions: $^5D_0$–$^7F_2$, $^7F_4$, $^7F_6$ with, in addition, $^5D_0$–$^7F_1$ (magnetic-dipole transition). The transitions $^5D_0$–$^7F_0$, $^7F_3$, $^7F_5$ will necessarily be of low intensity, and this is in fact observed (Ofelt, 1962).

Figure 34.6 gives an example of an emission spectrum of the Eu^{3+} ion in a host lattice where it occupies a site which is not a centre of symmetry. The colour of the emission from this phosphor is red. It is interesting to compare the emission spectra of Eu^{3+} in $NaLuO_2$ (fig. 34.5b) and in $NaGdO_2$ (fig. 34.6). Both host lattices crystallize in the rock-salt structure (fig. 34.7). In $NaLuO_2$ ($NaGdO_2$) the Mg^{2+} ions in MgO are replaced by Na^+ and Lu^{3+} (Gd^{3+}) ions. The monovalent and trivalent ions, however, are ordered over the cation sites. This differs for the combinations $Na^+ + Lu^{3+}$ and $Na^+ + Gd^{3+}$ (see fig. 34.7). Owing to the difference in superstructure, Eu^{3+} occupies a centre of symmetry in $NaLuO_2$, but not in $NaGdO_2$. This seemingly minor difference in structure has a considerable influence on the relative intensities of the Eu^{3+} emission lines. In $NaGdO_2$ the electric-dipole lines predominate and the colour of emission is red; in $NaLuO_2$ they are absent and the colour of emission is orange.

A comparison of the emission spectra also shows that the Eu^{3+} ion in $NaLuO_2$ does show some emission at the position of the $^5D_0$–$^7F_2$ lines. This emission consists of weak, fairly broad lines. The relevant transitions occur because the ions of the host lattice vibrate. These vibrations can cause a deviation from pure inversion symmetry, which means that the electric-dipole transitions are no longer forbidden.

It is worth noting that the lifetime of the luminescent $^5D_0$ level is about 10^{-3} s. This is approximately 10^5 times longer than the lifetime of a level that luminesces via an allowed electric-dipole transition, and roughly equal to the

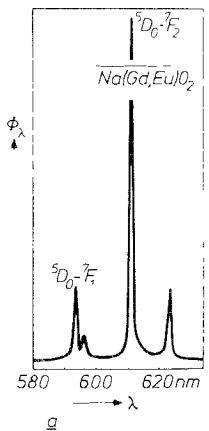

Fig. 34.6. Emission spectrum of the Eu^{3+} ion when not located at a centre of symmetry. Excitation with 254 nm radiation. The host lattice is $NaGdO_2$ (from Blasse and Bril, 1970).

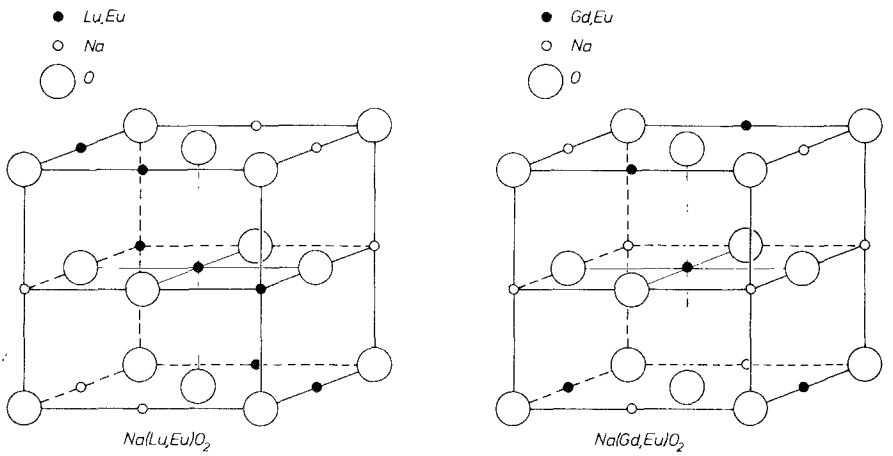

Fig. 34.7. Crystal structure of $NaLuO_2$ and $NaGdO_2$ (schematic). To make the relation between the two structures clear, the unit cube of the rock-salt structure is drawn rather than the unit cells. Deformations of the ideal structure are not represented (from Blasse and Bril, 1970).

values expected for a magnetic-dipole transition. This illustrates how strictly forbidden the 4f–4f transitions are.

The case of Eu^{3+} is fairly simple, because the $^5D_0$ level is not split and a simple selection rule applies to the electric-dipole transition. Usually the 4f–4f emission of R ions is more complicated, although not essentially different. This will be illustrated in section 4.

In this part of the chapter we have looked at the energy diagram and associated optical transitions of a number of rare-earth ions. These diagrams and transitions are nowadays well known. The influence of the crystal lattice on the situation and intensity of absorption and emission bands or lines can also be well understood. In the next part we consider the efficiency of the luminescence.

2.4. *The efficiency of phosphors excited in the activator*

The conversion efficiency of a phosphor can be numerically expressed in various ways. We shall refer only to the quantum efficiency (the ratio of the number of quanta emitted by the phosphor to the number of quanta it absorbs). Since the end of the thirties, various models have been proposed to explain the presence or absence of luminescence. These models are based on what is termed the configurational-coordinate diagram. For a full account see e.g. Di Bartolo (1968) or Curie (1963). We shall start by considering this type of diagram (figs. 34.8 and 34.9). The potential energy of the luminescent centre in the crystal lattice is plotted as a function of the configurational coordinate r. To see what r represents, we take a metal ion M^{n+} surrounded by four O^{2-} ions at the corners

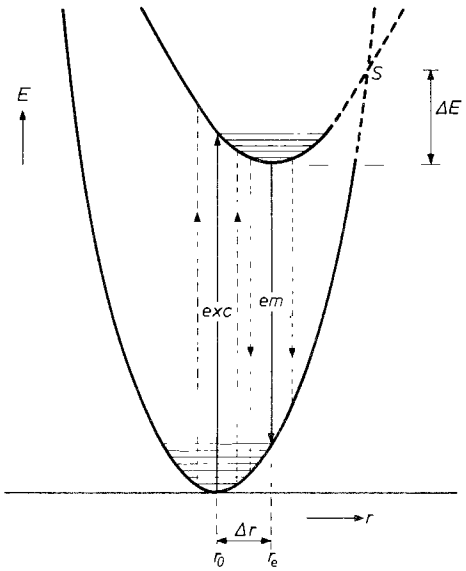

Fig. 34.8. Configurational-coordinate diagram of a luminescent centre. The potential energy E of the centre in the lattice is plotted as a function of the configurational coordinate r for the ground state and the first excited state. Vibrational states are represented schematically by horizontal lines in the parabolae. In the region where the two parabolae intersect, the curve is marked by dashes since the situation is actually more complicated than is indicated here (from Blasse and Bril, 1970).

of a tetrahedron. In the symmetric vibrational mode the M^{n+} ion remains stationary, while the O^{2-} ions vibrate in phase along the M–O bonding axis. When drawing the configurational-coordinate diagram it is assumed (on not unreasonable grounds) that we need only take this symmetric valence vibration into account. The quantity r then represents the distance M–O.

At absolute zero the luminescent centre will occupy the lowest vibrational

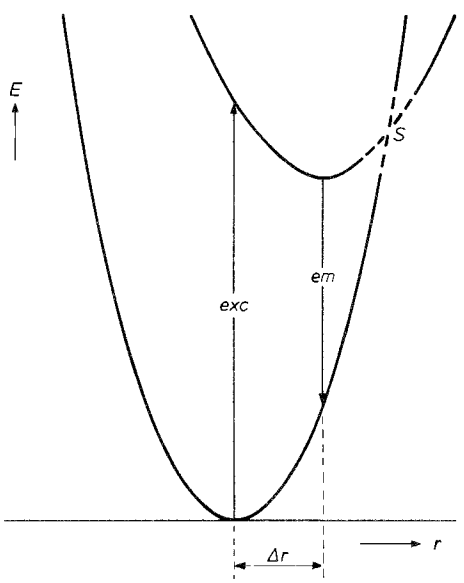

Fig. 34.9. The Dexter–Klick–Russell model for explaining a low luminescence efficiency or the absence of luminescence. The intersection point S of the two curves lies below the vibrational level reached after excitation. The non-radiative return to the ground state requires no activation energy (from Blasse and Bril, 1970).

level of the ground state. The ions surrounding the central ion vibrate about their equilibrium positions situated at a distance r_0 from the central ion. At higher temperature, higher vibrational levels may be occupied. In fig. 34.8 the horizontal lines represent vibrational states.

Due to the absorption of radiation of the appropriate wavelength the centre is raised to an excited state. Since the equilibrium distance r_e of the excited state will not in general be equal to that of the ground state, and since the centre may be at different vibrational levels, this transition will correspond to a fairly broad absorption band. The fact that the optical absorption corresponds to a vertical transition in fig. 34.8 is attributable to the rapid nature of electronic transitions as compared to vibrational movements, which involve the (heavier) nuclei.

Once in an excited state, the system will relax towards the equilibrium state (of the excited level) by dissipating heat. From this state or nearby levels the system returns to the ground state, thereby emitting radiation. The emission too, therefore, consists of a broad band. Line emission is found in the case of small Δr as for example in the case of rare earth ions. The emission generally lies at a lower energy than the absorption. This displacement of emission with respect to absorption is known as the Stokes shift.

From the configurational-coordinate diagram in fig. 34.8 we can now understand also why the emission will be quenched at higher temperature. If the luminescent centre is in the equilibrium configuration of the excited state, it may also, as a result of thermal activation, occupy a vibrational level situated at the point of intersection S of the curves representing the excited and ground states (activation energy ΔE). Having arrived here, the centre will return non-radiatively to the equilibrium configuration of the ground state, dissipating heat in the process. Figure 34.10 shows the way in which the luminescence of some phosphors depends on temperature. It can be seen that the luminescence decreases with rising temperature.

With the aid of the simple model in fig. 34.8 (the Mott–Seitz model) we can therefore explain

(a) the broad-band character of the emission and absorption of many centres;
(b) the Stokes shift of the emission;
(c) the temperature dependence of the emission.

If now the equilibrium configuration of the excited state lies outside the curve of the ground state, then after excitation the intersection point of both curves is reached before the above-mentioned equilibrium configuration, and the system relaxes non-radiatively to the ground state. No emission is then possible. This is the model which Seitz (1939) proposed to explain the absence of luminescence in certain cases.

Dexter et al. (1955) proposed a different model. This shows that under less rigorous circumstances non-radiative transitions to the ground state may occur (fig. 34.9). The characteristic feature of the situation in fig. 34.9 is that the intersection point S of the two curves is lower than the level reached after excitation. When, after excitation, the system relaxes to the equilibrium position of the excited state, the intersection point of the two curves is passed. Here too,

a temperature-independent, radiationless return to the ground state can take place.

We learn from these models that the difference Δr between the equilibrium configuration of the excited state and that of the ground state must be small if luminescence is to occur.

Recently Struck and Fonger (1975) have indicated ways to calculate quantitatively the temperature dependence of radiationless transitions in the configurational-coordinate diagram.

2.5. *Energy transfer*

In the preceding parts of this chapter we have looked at the electron transitions inside a centre and at the quantum efficiency when the activator is excited directly. In this part we shall discuss the case where the excitation energy is not absorbed in the activator itself but in another centre, which then transfers the energy to the activator.

As already mentioned the centre (ion or group of ions) which absorbs the radiation is called the sensitizer, and the centre to which the energy is transferred is the activator. We also pointed out that there is in fact no fundamental difference between these two kinds of centre.

If a centre S has absorbed a quantum of the exciting radiation, four things can happen:

(1) S luminesces itself (thus acting as an activator). The probability of this process will be called P_s^r.

(2) S returns non-radiatively to the ground state, while dissipating heat to the lattice. The probability of this process will be called P_s^{nr}. Unless otherwise stated, we shall disregard this process (see chapter 36).

(3) S transfers its excitation energy to A. The probability of this energy transfer will be called P_{sa}. This process can be followed by emission from A, or by radiationless return to the ground state.

(4) S transfers its energy to another centre S. The probability of this process will be called P_{ss}.

There are various methods that can be used to demonstrate the occurrence of energy transfer. One can, for example, measure the excitation spectrum of the emission from A. This is done by measuring the quantum yield of the emission from A as a function of the wavelength of the incident radiation. A band in the excitation spectrum corresponds, of course, to an absorption band.

If the excitation spectrum of the A emission shows the excitation bands of S in addition to those of A, this indicates energy transfer from S to A, since the excitation energy is absorbed by S and emitted by A. This is illustrated in fig. 34.11 for energy transfer by the Ce^{3+} to the Tb^{3+} ion in $(Y, Ce, Tb)Al_3B_4O_{12}$. The excitation spectrum of the Tb^{3+} emission contains not only a band corresponding to excitation of the Tb^{3+} ion itself but also bands that correspond to excitation of the Ce^{3+} ion.

Another method of demonstrating energy transfer is to measure the decay

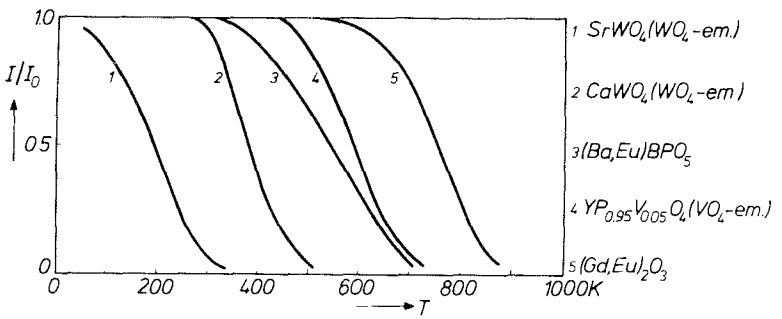

Fig. 34.10. Thermal quenching of the luminescence. The relative intensity of the luminescence from a number of phosphors, obtained by excitation with 254 nm radiation, plotted as a function of absolute temperature (after Blasse and Bril, 1970).

time of the luminescence from S as a function of the concentration of A. If S is situated in the host lattice in an isolated position, the average lifetime τ_s of the excited state of S (i.e. the decay time of the luminescence) is equal to the reciprocal of P_s^r. If we now add A ions we make an extra process possible in which S can lose its excitation energy. As a result τ_s will become shorter and so will the decay time of the luminescence from S. By measuring τ_s as a function of the concentration of A we can thus obtain information about P_{sa}.

The quantum efficiency q of the emission from A is defined in the case of

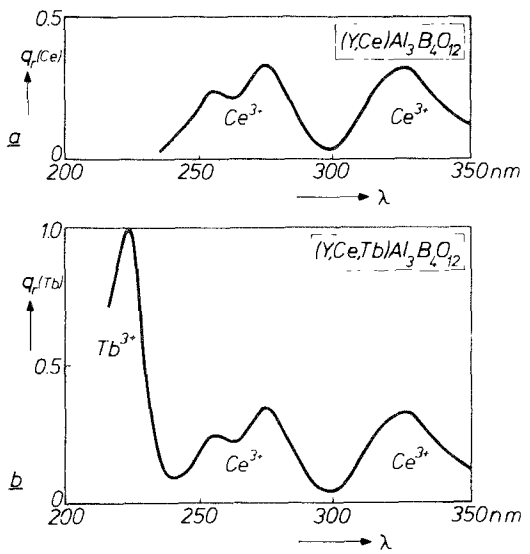

Fig. 34.11. (a) Excitation spectrum of the Ce^{3+} emission of $(Y, Ce)Al_3B_4O_{12}$. The excitation bands correspond to Ce^{3+} absorption bands. (b) Excitation spectrum of the Tb^{3+} emission of $(Y, Ce, Tb)Al_3B_4O_{12}$. This spectrum shows the same bands as the excitation spectrum of the Ce^{3+} emission, with in addition a band which is characteristic of Tb^{3+} itself (at about 225 nm) (from Blasse and Bril, 1970).

excitation in S as the ratio of the number of quanta emitted by A to the number absorbed by S. If we want a high q we must ensure that $P_{sa} \gg P_s^r$. Now of course P_{sa} is a function of the distance r_{sa} between S and A. At low A concentrations, that is to say large r_{sa}, it is often difficult to make P_{sa} sufficiently large. As will later be shown, it is essential in many cases to keep the A concentration low. One can then still cause the energy of S ions to be transferred to A ions by increasing the S concentration. The energy then goes through the lattice from one S ion to the other (at least where $P_{ss} \gg P_s^r$) until an A ion is reached.

Up to now it has been assumed that the symbols S and A represent ions or ionic groups incorporated in a non-absorbing host lattice. In many cases, however, S is an ion or ion group of the host lattice itself. In $(Y, Eu)VO_4$, for example, short-wavelength uv radiation is absorbed by the vanadate group. The emission, however, takes place in the Eu^{3+} ion, and a transfer of energy takes place from the vanadate group to the Eu^{3+} ion.

We shall consider here only those forms of energy transfer that involve no displacement of electric-charge carriers. We shall also disregard energy transfer by radiation (S radiates its energy and this is then absorbed by A). This case is seldom of importance in the phosphors of interest to us. The process most frequently observed is the non-radiative transfer of energy. The underlying theory was given by Förster (1948) and later worked out in more detail by Dexter (1953).

If the excited S centre is to transfer its excitation energy to another centre A, this is only possible if one of the energy levels of A lies at the same height as the excited level of S (resonance). Further we need an interaction that can be of two essentially different types.

In the first place the transfer can be brought about by the Coulomb interaction between S and A. If S and A are so far apart that their charge clouds do not overlap, this form of energy transfer is the only one possible.

If the charge clouds of S and A do overlap, however, another transfer process is possible by exchange interaction between the electrons of S and A. The essential difference between the previous process and this one is that here electrons are exchanged between S and A, whereas in the Coulomb interaction process the electrons remain with their respective ions or ionic groups.

A mathematical treatment of these mechanisms is outside the scope of this chapter [see Dexter (1953)]. We will, however, discuss the result, because it gives some idea of what takes place in the process of energy transfer. We begin with energy transfer by Coulomb interaction, and consider the case where the dipole–dipole interaction is much stronger than that of multipoles of higher order, so that we can disregard the contributions of the latter. In that case the probability $P_{sa}(dd)$ of energy transfer from S to A is given by the expression:

$$P_{sa}(dd) = \frac{3h^4c^4Q_a}{4\pi n^2 \tau_s r_{sa}^6} \int f_s f_a \frac{dE}{E^4},$$

where n is the dielectric constant of the host lattice, τ_s is the decay time of the

emission from S in the absence of A (this quantity is equal to the reciprocal of P_s^r).

The integral represents the overlapping of the normalized emission band $f_s(E)$ of S and the normalized absorption band $f_a(E)$ of A, both given as functions of photon energy E. Q_a is the integrated absorption of A.

It is possible to determine experimentally whether the levels involved are in resonance with one another by comparing the emission band of S with that of the relevant absorption band of A. The more these bands overlap, the better the resonance condition is fulfilled.

Let us now examine more closely the part $Q_a/\tau_s r_{sa}^6$. We see that the transfer probability for electric dipole–dipole interaction depends on the absorption area of the relevant transition in A. The transfer probability is greatest if the relevant transition is an allowed electric-dipole transition in A. The transfer probability also depends to a great extent on the distance between S and A.

If $Q_a = 0$ (forbidden electric-dipole transition in A) there can still be a certain transfer probability by interaction due to terms of higher order. The mathematical expressions for these are not fundamentally different. For electric-dipole-quadrupole interaction the distance term now appears as the eighth power and Q_a represents the absorption area resulting from a quadrupole transition, etc. The resultant transfer probabilities are in some cases, surprisingly, scarcely less than those for electric dipole–dipole interaction (Dexter, 1953).

We now want to know over what distances energy can be transferred by Coulomb interaction. Taking for Q_a the value for an allowed electric-dipole transition and for the overlapping integral a value which corresponds to a fairly high overlap, find:

$$P_{sa}(\mathrm{dd}) = (27/r_{sa})^6 \tau_s^{-1}$$

In this equation the distance r_{sa} must be expressed in Å. When A centres also are present the probability of emission from S and the probability of transfer from S to A are equal to one another if $r_{sa} = 27$ Å, an appreciable distance. This distance, called the critical distance for energy transfer is denoted by the symbol r_{sa}^0. For $r_{sa} > r_{sa}^0$ the emission is almost exclusively in S. For $r_{sa} < r_{sa}^0$ energy transfer dominates, and is more important the smaller the value of r_{sa}.

We shall now discuss the equation for the probability of transfer by exchange interaction:

$$P_{sa}(\mathrm{ex}) = \frac{2\pi}{\hbar} Z^2 \int f_s f_a \, \mathrm{d}E.$$

This equation, of course, again contains the spectral overlap integral. The quantity Z cannot be obtained directly from optical experiments; it is proportional to the exchange integral

$$\int \{\Psi_a^e(r_1)\Psi_s^0(r_2)\}^* \frac{e^2}{r_1 - r_2} \{\Psi_a^0(r_2)\Psi_s^e(r_1)\} \, \mathrm{d}r_1 \, \mathrm{d}r_2.$$

This expression contains the position coordinates r_1 and r_2 of the two electrons, and also the quantum-mechanical wave functions Ψ of the two centres.

The product between the first set of curly brackets gives the final state: S is then in the ground state (Ψ_s^0), A in the excited state (Ψ_a^e). The product between the second pair of curly brackets gives the initial state: S is in the excited state (Ψ_s^e), A in the ground state (Ψ_a^0). The complex character of the exchange integral is a consequence of the fact that electron 1 is in the initial state at S but in the final state at A. The converse applies to electron 2 (exchange). Since the density of charge clouds decreases exponentially with the distance of the electron to the nucleus, the dependence of Z upon distance will also be exponential and so too will that of $P_{sa}(ex)$. Significant overlapping of the charge clouds of two cations in a crystal lattice is found only between cations that are nearest neighbours (separation 3 to 4 Å). Exchange interaction is therefore limited to neighbouring cations in the lattice. The critical distance for this transfer will never be much greater than 4 Å.

We note that $P_{sa}(ex)$ does not comprise the optical properties of S and A (apart from the overlap integral). Exchange transfer, then, unlike transfer by Coulomb interaction, is not dependent on the oscillator strength or transition probability of the relevant transitions, and may even take place to a level from which a return to the ground state is strictly forbidden.

Following models originating from the field of organic luminescence (see e.g. Wolf, 1967; Powell and Soos, 1975) it has also been proposed to consider the migration of excitation energy through the lattice from one host ion to another as exciton diffusion (Treadaway and Powell, 1975). In many cases it is possible to describe the migration as a nearest neighbour random walk with diffusion constant $D = a^2/6t_h$, where a is the lattice spacing and t_h the average hopping time for the exciton. Each hop in the random walk can be considered as a single-step energy transfer process described above. The hopping time is the reciprocal of the transfer rate P mentioned above.

2.6. *Concentration quenching*

In order to obtain a high emission intensity it would seem obvious to make the activator concentration as high as possible. In many cases, however, it is found that the emission efficiency decreases if the activator concentration exceeds a specific value known as the critical concentration. An example is to be seen in fig. 34.12. This effect, called concentration quenching, may be explained in a number of cases as follows. If the concentration of the activator becomes so high that the probability of energy transfer exceeds that from emission, the excitation energy starts migrating through the lattice. Now the host lattice is not perfect: it contains all kinds of sites where the excitation energy may, in some obscure way, be lost, such as at the surface, at dislocations, impurities, etc. The efficiency then decreases, in spite of the increase of the activator concentration (Dexter and Schulman, 1954).

In a similar way, concentration quenching for S centres can also take place.

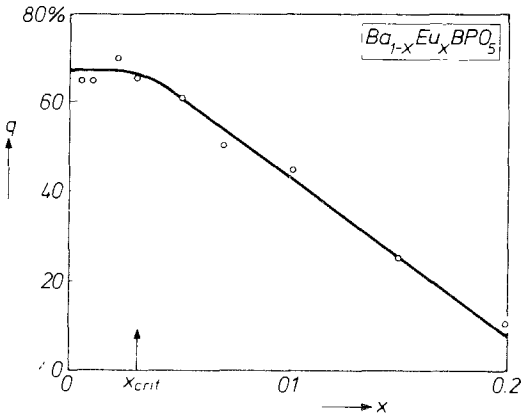

Fig. 34.12. Concentration quenching of the Eu^{2+} emission of $Ba_{1-x}Eu_xBPO_5$. For Eu^{2+} concentrations x which are greater than the critical concentration x_{crit} the quantum efficiency q decreases with increasing x (after Blasse and Bril, 1970).

The value of the critical concentration of S centres provides information about P_{ss}: if the critical concentration is high, then P_{ss} is low and *vice versa*.

This model describes concentration quenching of host lattice emission. At room temperature the luminescence of the VO_4 group in YVO_4, for example, is concentration quenched. The vanadate emission can be observed by either lowering the temperature, so that the energy migration through the lattice is stopped (Palilla et al., 1965) or by diluting the vanadate groups with phosphate groups (system $YP_{1-x}V_xO_4$) so that the energy migration is stopped because of the increasing V–V distance (Blasse, 1968c).

The model also explains why in other host lattices that are often applied to introduce rare earth ions, e.g. $CaWO_4$ and $YNbO_4$, no concentration quenching of host lattice emission occurs (Blasse, 1968c; Treadaway and Powell, 1974). Here the emission is so strongly Stokes shifted from the absorption of the relevant host lattice group that the spectral overlap integral $\int f_s f_a \, dE$, and therefore the transfer rate, becomes very small.

Concentration quenching of broad-band emitting R ions, like Ce^{3+} and Eu^{2+}, can also be described in this way. To explain concentration quenching of Eu^{3+} and Tb^{3+} luminescence originally a model has been proposed in which clusters of 3 or 4 R ions played the role of a centre where radiationless losses occurred (Van Uitert and Johnson, 1966). Later, however, it has been realized that concentration quenching is also for these ions due to energy migration through the lattice (Van der Ziel et al., 1972).

Recently Danielmeyer (1976) has made an interesting proposal for the transfer mechanism in concentrated rare earth systems. It is assumed that two degenerate 4f states φ_1, and φ_2 of two R ions 1 and 2 interact by mixing of the $4f_1$ wave function with the $5d_2$ wave function through the local crystal field (in classical theories $4f_1$ is only mixed with $5d_1$). Since 4f wave functions drop to 1% of their maximum amplitude at 2.5 Å, but 5d wave functions at 8 Å, this so called crystal field overlap mixing increases the distance over which interaction may occur considerably (up to 10 Å).

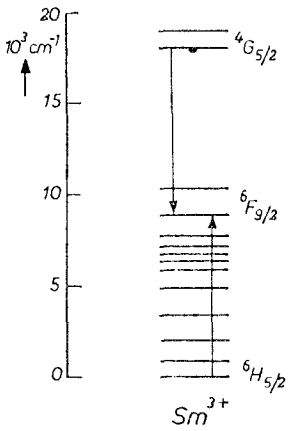

Fig. 34.13. Energy level scheme of Sm^{3+} showing concentration quenching of the $^4G_{5/2}$ emission by cross-relaxation between two Sm^{3+} ions.

The explanation of concentration quenching by cross relaxation (see chapter 36) where radiationless losses occur due to interaction between two R ions should finally be mentioned. The concentration quenching of Sm^{3+} and Dy^{3+} luminescence has been explained in this way (Van Uitert and Johnson, 1966; Van Uitert, 1968). This is shown in fig. 34.13 for Sm^{3+}. This ion luminesces from the $^4G_{5/2}$ level. For high Sm^{3+} concentration the following transfer occurs: $Sm(^4G_{5/2}) + Sm(^6H_{5/2}) \rightarrow 2\,Sm(^6F_{9/2})$, so that the orange $^4G_{5/2}$ emission is quenched. As a matter of fact it is necessary that the transitions $^4G_{5/2} \rightarrow {}^6F_{9/2}$ and $^6H_{5/2} \rightarrow {}^6F_{9/2}$ match each other. The critical distance for this process is some 20 Å.

3. Chemistry of R-activated phosphors

In this section we will indicate how luminescence properties like those mentioned in section 2 are influenced by the chemical nature of the surroundings of the luminescent centre. This is a very difficult topic and at present our knowledge of this field is only qualitative and fragmentary. Nevertheless the field is not only interesting, but also of importance for those who want to develop useful luminescent materials.

3.1. *The influence of composition on energy levels and transition probabilities*

The influence of the surroundings of an R ion on its 4f levels is very weak as is to be expected. This results in a very weak crystal-field splitting of these levels (see section 2.3). Different surroundings cause different splittings and, therefore, slightly different emissions occur (see fig. 34.5a,b). Applying this phenomenon the luminescence of the Eu^{3+} ion has often been used as a probe for site symmetry (see for illustrative examples Nieboer, 1975; Blasse and Bril, 1967a; Brecher and Riseberg, 1976). The transition probabilities for 4f–4f transitions can be strongly influenced by the surroundings as was illustrated in section 2.3. The absence or presence of inversion symmetry at the crystallographic site of the R

ion determines whether forced electric dipole transitions will occur or not, respectively.

Energy levels and transitions involving a charge-transfer or a 5d state are more strongly influenced by the R-ion surroundings in the lattice. The reader will not be surprised too much by this.

We note that as a general rule the c.t. bands shift to lower energies with increasing oxidation state, whereas 4f–5d transitions shift to higher energies. It may, therefore, be expected that the lowest absorption bands of the tetravalent R ions will be due to c.t. transitions and those of the divalent R ions to 4f–5d transitions. This is in fact the case. The c.t. bands of the R^{4+} ions have been studied in more detail by Hoefdraad (1975a). He introduced Ce^{4+}, Pr^{4+} and Tb^{4+} in a number of oxidic host lattices where the coordination of the R^{4+} ions would be fixed, viz. either six- or eight-coordination. His results are as follows:

(a) In six-coordination the position of these c.t. bands does not depend on the host lattice.

(b) In eight-coordination, however, this position depends on the host lattice in such a way that the R^{4+}–O^{2-} distance influences the spectral position of the c.t. band. The longer the distance, the lower the energy of the band.

Hoefdraad was able to explain his results with a relatively simple model for which we refer to the original paper.

After this discussion of c.t. transitions on Ln^{4+} ions we now turn to the divalent lanthanide ions. Here the first allowed transitions in the spectra are 4f–5d transitions as expected. They have been studied in detail. We will here mention some relevant results.

The 4f–5d transitions of nearly all Ln^{2+} ions have been observed in CaF_2 (McClure and Kiss, 1963). In good approximation these spectra can be ascribed as transitions between the $4f^n$ ground state and the d crystal-field components of the $4f^{n-1}5d$ state. The influence of the surroundings on these transitions is twofold: the position of the centre of gravity of the 5d level is influenced by the nature of the surrounding ions or ligands (nephelauxetic effect, Jørgensen, 1971), but the crystal-field splitting of this 5d level depends also on the nature and arrangement of these ions. In table 34.2 we have given some examples for the case of Eu^{2+}.

We now turn to the common valency of the rare earths, viz. three. There is no essential difference with the observations made above:

(a) c.t. transitions. There is ample evidence that for a given R^{3+} ion the position of the c.t. transition is at lower energy if the surrounding ligands are more reducing (or less electronegative). This well-known fact will here not be discussed further. We note that there is a tendency to have the c.t. transition at lower energy, if the number of surrounding ligands is larger (see e.g. Barnes and Pincott, 1966; Day et al., 1974; Blasse, 1972). Finally the dependence on the host lattice for a given coordination with the same kind of ligands follows from the work of Hoefdraad (1975b). The latter is especially of importance in oxides. In table 34.3 we have illustrated these rules for the case of Eu^{3+}.

(b) 4f–5d transitions. As mentioned above the spectral position of these tran-

TABLE 34.2
Absorption bands, crystal-field splitting and centre of gravity of the 5d level of Eu^{2+} in several host lattices (all values in kK)

Host lattice	Coordination Eu^{2+} ion	Absorption bands	Crystal-field splitting	Centre 5d level	Ref.
CaF_2	cube	27.1 45.0	17.9	37.9	[a]
SrF_2	cube	27.9 43.5	15.6	37.3	[a]
BaF_2	cube	28.5 42.7	14.2	37.0	[a]
NaCl	octahedron	29.4 41.5	12.1	34.2	[b]
KCl	octahedron	29.1 40.1	11.0	33.5	[c]
		29.7 41.4	10.7	34.4	[b]
KBr	octahedron	29.0 40.2	11.2	33.5	[c]
		29.7 38.1	8.4	33.1	[b]
$BaZrO_3$	regular 12 coordination	25.2 38.2	13.0	33.0	[d]

[a]Kaplyanski and Feofilov (1962); [b]Kirs and Niilks (1962); [c]Reisfeld and Grabner (1964); [d]Blasse et al. (1968).

sitions is determined mainly by the nephelauxetic effect and the crystal field effecting the 5d level.

Finally we note some other properties of these allowed transitions of the lanthanide ions. In general the 4f–5d bands have a smaller band width than the c.t. transitions, typical values being 1000 and 2000 cm^{-1}, respectively. In this connection it is interesting to find that at low temperatures the 4f–5d absorption and emission bands often show a distinct and extended vibrational fine structure

TABLE 34.3
Position of the first c.t. band of Eu^{3+} in some oxides (after Blasse, 1972; Hoefdraad, 1975b; Krol, 1976)

Compound	Coordination	Position c.t. band (kK)
$ScBO_3$–Eu^{3+}	6	43
$LiLuO_2$–Eu^{3+}	6	43.0
$NaYGeO_4$–Eu^{3+}	6	43.1
YBO_3–Eu^{3+}	6	42.7
Y_2O_3–Eu^{3+}	6	41.7
$NaGdO_2$–Eu^{3+}	6	41.1
$CaLaGaO_4$–Eu^{3+}	6	42
$ScPO_4$–Eu^{3+}	8	~48
YPO_4–Eu^{3+}	8	~45
$Y_3Ga_5O_{12}$–Eu^{3+}	8	42.5
$LaPO_4$–Eu^{3+}	8	37
$LaTaO_4$–Eu^{3+}	8	36
$GdGaO_3$–Eu^{3+}	12	40.5
$LaAlO_3$–Eu^{3+}	12	32.3
$SrLaLiWO_6$–Eu^{3+}	12	30.5

(Ce^{3+} (Hoshina and Kuboniwa, 1971), Tb^{3+} (Nakazawa and Shionoya, 1974), Eu^{2+} (Kaplyanski and Feofilov, 1962; Ryan et al., 1974), Yb^{2+} (Witzke et al., 1973)), whereas c.t. transitions do not. From this it seems probable that in the excited c.t. state the interaction between the R ion and its surroundings is stronger than in the excited $4f^{n-1}5d$ state. This is not unexpected. As far as we are aware nobody has ever reported vibrational fine structure for the c.t. transitions. Note also that luminescence from c.t. states has not been observed for the rare earths, whereas luminescence from $4f^{n-1}5d$ states is quite common (Ce^{3+}, Eu^{2+}).

3.2. *The influence of composition on luminescence efficiency and thermal quenching*

Whereas section 3.1 deals essentially with the emission colour of R-phosphors, this section treats the efficiency of R-luminescence.

In the present state of knowledge it is not possible to state in *quantitative* terms how the efficiency of the luminescence depends on the host lattice. Proceeding from the idea given at the end of section 2.4 that it is the magnitude of Δr that determines the *quenching temperature* of the luminescence, and hence also the efficiency at room temperature, we were able to indicate a rough relationship between the quenching temperature of the luminescence and the radius and charge of the cations of the host lattice (Blasse, 1969). In this treatment the sign of Δr plays a significant part.

In figs. 34.8 and 34.9 it is assumed that Δr is positive, in other words that the luminescent centre expands after excitation. However, Δr may be negative as well as positive. This was shown long ago by Williams (1951) in his pioneering work on (K, Tl)Cl. In the ground state the Tl^+ ion has $(6s)^2$ configuration. Upon excitation the electron-charge distribution of the ion moves somewhat farther away from the nucleus (due to the transition of one of the electrons from $6s \rightarrow 6p$). The negative charge cloud becomes more diffuse and as a result the cation effectively assumes a greater positive charge. It therefore attracts the negative ions more strongly, so that the equilibrium distance of the luminescent centre in the excited state is smaller than that of the ground state (see also Dexter, 1958). Williams's calculations showed that in the case of Tl^+ in KCl, Δr has a negative value and is 0.2 Å. The reasoning adopted applies to all cases where the luminescent cation itself is excited. These include, for example, the 4f–5d transitions of the ions of the rare earth metals.

A positive value of Δr is to be expected when the anion is excited. The electron cloud becomes more diffuse and the anion thus effectively assumes a greater positive charge (that is to say becomes less negative) and therefore attracts the cations less strongly, so that the equilibrium distance becomes greater. The only case of excitation of anion electrons of interest to use is that of the charge-transfer transitions already dealt with.

In the considerations that follow, we shall divide the luminescent centres into two groups, those with $\Delta r > 0$ (excitation of anion electrons) and those with $\Delta r < 0$ (excitation of cation electrons). We shall now see how Δr depends on the

TABLE 34.4
The relation between the quenching temperature T_q of the emission and the radius and charge of the host lattice cations, in accordance with the thermal-quenching model proposed in this article

Radius and charge of cations	$\Delta r < 0$ (e.g. Tl^+, Eu^{2+}, Ce^{3+})	$\Delta r > 0$ (e.g. Eu^{3+}, VO_4^{3-})
Activator ion larger than host-lattice ion	T_q low	T_q high
Activator ion smaller than host-lattice ion	T_q high	T_q low
Host lattice with small, highly charged cations	T_q high	T_q high
Host lattice with large cations of low charge	T_q low	T_q low

size of the host lattice ion for which the activator ion has been substituted and on the magnitude of the charge and size of the host-lattice ions surrounding the activator.

If the activator ion is larger than the host-lattice ion which it replaces, e.g. Eu^{3+} (ionic radius 0.98 Å) or Ce^{3+} (1.07 Å) in a Lu^{3+} host lattice (0.85 Å), the environment of the activator will be compelled to expand in order to make room for the activator. If the activator is raised to the excited state, and if this is accompanied by an increase of the equilibrium distance (anion excitation, $\Delta r > 0$), then the environment of the activator will have to expand yet further. Since this expansion costs energy, the lattice will tend to oppose the expansion of the luminescent centre, in other words Δr will be relatively small.

The opposite is the case if the activator is located at a site which is occupied in the host lattice by a larger ion, for example Eu^{3+} (0.98 Å) in a La^{3+} compound (1.14 Å). Upon excitation in the charge-transfer absorption band of the Eu^{3+} ion ($\Delta r > 0$) we shall then find Δr to be relatively large.

If the excitation of the activator ion occurs by an electronic transition at the ion itself ($\Delta r < 0$), the situation is reserved as compared with that involving an activator with $\Delta r > 0$ (charge transfer). If, for example, the site in the lattice occupied by an activator with $\Delta r < 0$ is too small, then the environment expansion that occurs for the activator in the ground state is partly reversed by excitation. In that case Δr is not constrained to remain small.

The second of the factors just mentioned that determine Δr, the influence of the cations surrounding the luminescent centre, may be sketched as follows. Small, highly charged cations will give the host lattice great bonding strength. In such a rigid lattice it is evident that Δr will be relatively small (irrespective of whether Δr is positive or negative). If the lattice contains large cations of low

charge, the bonding in the lattice will be weak. Such a lattice can thus comply with the tendency of the activator to expand or shrink upon excitation. The absolute value of Δr in this case will therefore be relatively large.

Table 34.4 summarizes these conclusions. The experimental results agree with these predictions (Blasse and Bril, 1970). They will be partly mentioned in the next section.

It is interesting to note that Paulusz (1974) has shown this influence of site dimension on luminescence efficiency to exist in a complete different way, viz. from the vibrational fine structure of certain emission bands.

4. Examples

The models evaluated above for R-activated materials will now be applied to a number of examples. These are only meant to be illustrative and not to be exhaustive.

4.1. *The* Ce^{3+} *ion* ($4f^1$)

The emission of the Ce^{3+} ion corresponds to a $5d \rightarrow 4f$ transition (see section 2.1). Since the configurational-coordinate curves of these two levels are different, the emission has broad-band character. The vibrational fine structure can often be resolved at low temperatures (see e.g. Nakazawa and Shionoya, 1974). This band has a doublet character due to the ground-state splitting ($^2F_{5/2}$ and $^2F_{7/2}$, see figs. 34.2 and 34.14). The excitation spectrum in the ultraviolet consists usually of a number of broad bands corresponding to the crystal field components of the 5d level (see fig. 34.3). These 4f–5d transitions are electric-dipole allowed. As a consequence the emitting level has a short lifetime, a property which is applied in certain phosphors (see section 5.2). A very short lifetime has been reported for CeP_5O_{14} (12 and 36 nsec, Bimberg et al., 1975).

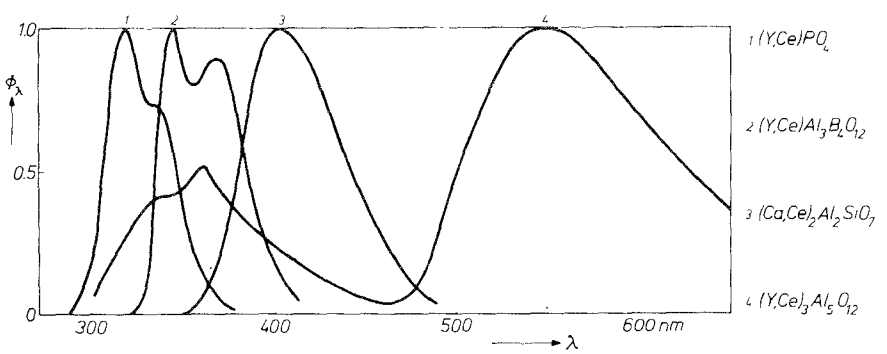

Fig. 34.14. Emission spectrum of some Ce^{3+} phosphors for excitation with 254 nm radiation. The quantity ϕ_λ is the relative spectral radiance. The maxima are put equal to 1 (from Blasse and Bril, 1970).

Concentration quenching occurs generally at a few percent of cerium due to Ce^{3+}–Ce^{3+} transfer followed by transport to killer sites.

The emission of the Ce^{3+} ion is usually situated in the u.v. or blue spectral region (Blasse and Bril, 1967b). In recent years, as a result of a search for fast-emitting phosphors in the green and red, the Ce^{3+} ion has also been found to emit at longer wavelengths. From section 4.1 it will be clear that conditions for such an emission are: the centre of the 5d level at relatively low energy (strong nephelauxetic effect) and the crystal field very strong. Long-wavelength emission was first observed for $(Y, Ce)_3Al_5O_{12}$ (Blasse and Bril, 1967c) and later, for example, in sulfides (Lehmann and Ryan, 1971).

The Ce^{3+} ion is an example of an activator whose emission shows a high quenching temperature in silicates, borates, phosphates, etc. This sustains the rules given in table 34.4. The small highly-charged ions clearly exert a masked effect on the quenching temperature of the emission.

4.2. *The* Pr^{3+} *ion* ($4f^2$)

The Pr^{3+} ion shows a number of different emissions depending on the host lattice in which it is incorporated, viz. red (from the $^1D_2$ level), green (from the $^3P_0$ level), blue (from the $^1S_0$ level) and ultra-violet (from the 4f5d state). The energy level scheme of Pr^{3+} is shown in fig. 34.15. The excited state is one of the important factors that determine which of the emissions is to be expected.

In some fluorides (e.g. YF_3, LaF_3, $NaYF_4$) the lowest crystal-field component of the 4f5d state of Pr^{3+} is situated above the $^1S_0$ level. Excitation with short-wavelength ultraviolet radiation (e.g. 185 nm) or cathode-rays excites the Pr^{3+} ion from the $^3H_4$ ground state into the 4f5d level, from where it decays radiationless to the $^1S_0$ level. From here the Pr^{3+} ion returns to the ground state by two-photon luminescence (Piper et al., 1974, Sommerdijk et al., 1974a): the

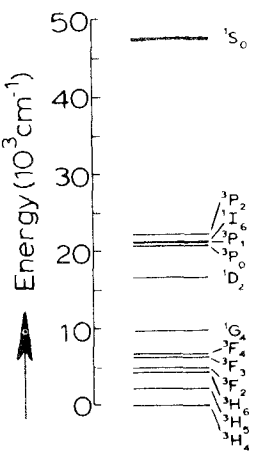

Fig. 34.15. Energy level diagram of the Pr^{3+} ion.

emission spectrum contains a group of transitions in the blue and another group in the green and in the red. The latter is ascribed to emission from the $^3P_0$ level. The former is ascribed to the $^1S_0$–$^3P_2$ transition by Sommerdijk et al. (1974a) and to the $^1S_0$–$^1I_6$ transition by Piper et al. (1974).

If, however, the lowest 4f5d state is below the $^1S_0$ level, two-photon luminescence is no longer observed. In a number of host lattices luminescence from this 4f5d state has been observed, e.g. $LiYF_4$, KYF_4, $BaYF_5$, YPO_4, $Y_2(SO_4)_3$ (Piper et al., 1974) and $Y_3Al_5O_{12}$ (Weber, 1973).

If the 4f5d levels are situated at still lower energy, no $5d \rightarrow 4f$ emission is observable. Instead emission from the $^3P_0$ level occurs. Weber (1973) has studied in $Y_3Al_5O_{12}$–Pr^{3+} the nonradiative decay from the luminescent 4f5d level of Pr^{3+} to the $^3P_{0,1,2}$ and $^1I_6$ level. For temperatures below 250 K the decay time of the $5d \rightarrow 4f$ luminescence is constant and amounts to about 2×10^{-8} sec (as is to be expected for an allowed electric-dipole transition). Above 250 K the life-time of this 4f5d level decreases rapidly due to nonradiative decay to the $4f^2$ levels.

This is the situation in oxides where excitation into the 4f5d levels of Pr^{3+} is followed by emission from the $^3P_0$ level. In many cases, however, emission from $^1D_2$ occurs too. In tungstates, vanadates, niobates and related compounds the $^1D_2$ emission even dominates. Two models that are closely related have been proposed to explain effective $^3P_0 \rightarrow {}^1D_2$ relaxation:

(a) Reut and Ryskin (1973) have proposed a virtual recharge mechanism. It is assumed that the charge-transfer state $Pr^{4+} + V^{4+}$ (if we take a vanadate lattice like YVO_4 as example) has a considerably larger (or smaller) equilibrium distance than the $Pr^{3+}(4f^2)$–V^{5+} states. Although this c.t. state is found above the $^3P_0$ level in absorption spectra, it facilitates radiationless decay from $^3P_0$ to $^1D_2$.

(b) Hoefdraad and Blasse (1975) have argued that the state with larger or smaller equilibrium distance may be a 4f5d level of Pr^{3+} itself. This can be the case, if it is at low enough energy. This model was illustrated by the Pr^{3+} emission in two calcium zirconates ($CaZrO_3$ and calcium-modified ZrO_2). In the fluorite phase the lowest 4f5d level is at about 34 kK and the emission occurs in equal amounts from $^3P_0$ and $^1D_2$. In the perovskite the lowest 4f5d level is at 41 kK and the emission contains practically only $^3P_0$ transitions.

It will be obvious that Δr, the difference between the equilibrium positions of the ground state and the excited 4f5d state will determine to a great extent which emission will be observed.

This shows the enormous influence of the 4f5d state of the Pr^{3+} ion on its emission characteristics. Two properties of the lowest 4f5d level are of importance, viz. its energetic position and the value of Δr. This statement is valid for more cases.

4.3. *The* Nd^{3+} *ion* ($4f^3$)

The emission of the Nd^{3+} ion is situated in the infrared region (1.06 μm). It has found wide application in laser materials (see chapter 35).

4.4. *The* Eu^{3+} *ion* ($4f^6$)

The Eu^{3+}-activated phosphors emit in the orange ($^5D_0$–$^7F_1$) if the Eu^{3+} ion occupies a centre of symmetry and in the red ($^5D_0$–$^7F_2$) and infrared ($^5D_0$–$^7F_4$) if not so (see fig. 34.2 and section 2.3). Schwarz and Schatz (1973) have mentioned a very fine host lattice, viz. Cs_2NaYCl_6, for the study of Eu^{3+} on a site with inversion symmetry and also given results for the vibrational fine structure in that case (Schwarz, 1975).

Forced electric dipole emission occurs if it is possible to mix even functions into the uneven 4f functions, so that the parity selection rule is relaxed. It is usually assumed that this occurs by 4f–5d mixing. For Eu^{3+}, however, the $4f^55d$ state is at very high energy. Since the electric-dipole emission dominates for Eu^{3+} on sites without inversion symmetry, it seems obvious to assume that another state is used to relax the parity selection rule. This must occur by mixing the $4f^6$ configuration with the levels of opposite parity of the c.t. state.

This is nicely confirmed by a study of some Eu^{3+}-activated phosphates and vanadates with zircon structure (Blasse and Bril, 1969). The observed ratio of electric to magnetic dipole emission of the Eu^{3+} luminescence in these hosts is correlated with the position of the lowest excitation (and absorption) band of these materials and the intensity ratio. This absorption band is a c.t. transition in which either europium or vanadium or both are involved. It has, therefore, been proposed that the parity-forbidden 4f–4f transitions of the Eu^{3+} ion borrow intensity from the lowest strong absorption band (either host lattice absorption or charge-transfer absorption within the Eu^{3+} centre) and not from the 4f–5d absorption band. In conclusion we find that for intense forced electric-dipole emission from Eu^{3+} two conditions must be fulfilled, viz. absence of inversion symmetry at the Eu^{3+} crystallographic site and c.t. transitions at low energies.

Similar results have been reported for Eu^{3+} in glasses (Reisfeld and Lieblich, 1973): germanate glasses where the Eu^{3+} c.t. band is situated at 38462 cm^{-1} show a more intense forced electric-dipole emission than phosphate glasses, where the c.t. band lies at 49 020 cm^{-1}. These examples illustrate the influence of the c.t. state upon the Eu^{3+} 4f–4f emission.

The processes responsible for radiationless losses in the Eu^{3+} ion upon excitation into the charge-transfer state have been elucidated mainly by Struck and Fonger (1970a).

The first indication that the c.t. state of Eu^{3+} plays a role in the luminescence quenching process was the fact that there is a relation between the spectral position of the first c.t. band of Eu^{3+} and the quenching temperature and room-temperature quantum-efficiency of the luminescence under excitation into the c.t. band (Blasse, 1966). A similar relation exists also for some other luminescent groups, e.g. the niobate octahedron $[NbO_6]^{7-}$ (Blasse, 1968a) and the uranate octahedron $[UO_6]^{6-}$ (Blasse, 1968b). Bril and coworkers (1968) showed that at room temperature the luminescence quantum efficiency for Eu^{3+} in $YAl_3B_4O_{12}$ amounts to 35% for excitation into the c.t. band and to 100% for excitation into the narrow 4f levels. It is a simple task to show that in a simple

configurational coordinate model the quenching temperature of the luminescence and the room-temperature quantum efficiency decreases, if the position of the c.t. band is at increasingly lower energy (Blasse, 1968a).

The picture became more clear by the work of Struck and Fonger on temperature quenching of trivalent lanthanides in the oxysulfides (Struck and Fonger, 1970a, 1976). In host lattices like Y_2O_2S and La_2O_2S the c.t. band of the Eu^{3+} ion is situated at about 30 000 cm^{-1}. This is lower than in the greater part of the oxides due to the lower electronegativity of sulfur. Struck and Fonger observed direct feeding of the excited $^5D(4f^6)$ levels of Eu^{3+} by the c.t. state, but also ^5D quenching via the c.t. state. They used a configuration coordinate diagram as given in fig. 34.16. The important effect is that, although the c.t. state lies well above the emitting ^5D states in the absorption and excitation spectra, its Franck–Condon shifted minimum lies relatively low (somewhere near $^5D_3$). As a consequence crossovers from ^5D levels to the c.t. state are possible.

The direct contact between the c.t. state and the ^5D levels is shown by direct feeding of the ^5D levels by the c.t. state. If the Eu^{3+} ion in Y_2O_2S is excited into the $^5L_7$ level, emission is observed from $^5D_3$, $^5D_2$, $^5D_1$ and $^5D_0$. The same emission spectrum is observed for excitation into the $^5D_3$ level. If excitation is into the c.t. state, i.e. at higher energies, emission occurs only from $^5D_2$, $^5D_1$ and $^5D_0$ in the

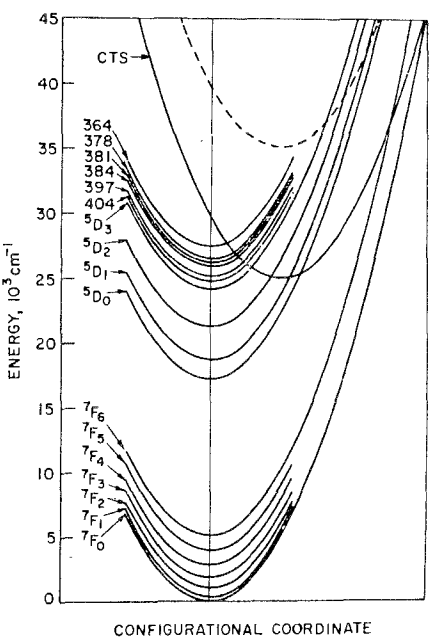

Fig. 34.16. Configuration coordinate model for the $4f^7$ and c.t. states (CTS) of Eu^{3+} in Y_2O_2S. The dotted curve shows qualitatively the higher position of the CTS in many oxidic hosts. The 4f states above $^5D_3$ are indexed by their absorption wavelengths (nm) from $^7F_0$. After Struck and Fonger (1970a).

same ratio as if the excitation had occurred into the $^5D_2$ level. This means that c.t. excitation skips the $^5L_7$ and $^5D_3$ levels and feeds directly the $^5D_2$ level. In La_2O_2S–Eu, where the c.t. band is at still lower energy, the excited c.t. state feeds directly the $^5D_1$ level for about two-thirds and the $^5D_2$ level for about one-third.

The temperature dependence of the several ^5D emissions in Y_2O_2S–Eu^{3+} for excitation into the c.t. state has also been studied. Although the total emission intensity is practically temperature-independant below 500 K the separate ^5D emissions quench sequentially in the order $^5D_3$, $^5D_2$, $^5D_1$ with increasing temperature. For La_2O_2S–Eu^{3+} the same sequence has been found, but the corresponding quenchings occur at lower temperatures. These quenchings are due to thermally promoted transitions from the ^5D levels to the c.t. state followed by return crossovers to lower ^5D states. In the oxysulfides the c.t. state is low enough to allow such transitions. The crossover rates for c.t. state $\rightarrow$ ^5D levels are estimated to be 10^{11}–10^{12} sec^{-1}, so that the absence of luminescence from the c.t. state is understandable.

It will be clear that, if the c.t. state is at higher energy, these phenomena will no longer be observable.

The example of the Eu^{3+} ion is, finally, suitable to illustrate energy transfer from host lattices to R ions.

In table 34.5 we have listed a number of phosphors and subdivided them as follows. The transfer from a centre S to a centre A takes place either over distances greater than the distance between the nearest cation neighbours (SA+), or over distances equal to or smaller than the distance between nearest neighbours (SA−). We make the same division for the transfer from one S centre to another. The phosphors then fall into four groups (SS+ and SA+, SS+ and SA−, SS− and SA+, and SS− and SA−). The probability of a high emission yield is of course greatest with a transfer of the type SA+ or of the type SS+, and certainly if both of them are possible at the same time.

Consider, for example, (Y, Eu)VO_4. The critical distance for VO_4^{3-}–VO_4^{3-} transfer amounts to about 8 Å (Blasse, 1968c; Hsu and Powell, 1975). This relatively long distance must be related to the sizeable spectral overlap of the vanadate emission and excitation band and is also responsible for concentration quenching of the vanadate group (see section 2.6). Transfer from vanadate to rare earths is assumed to occur by exchange interaction and is, therefore, restricted to short distances.

In (Y, Eu)NbO_4 migration through the host lattice is practically absent due to the strong relaxation of the excited niobate state resulting in negligible spectral overlap. The same is true for (Y, Eu)TaO_4 but in this phosphor the $TaO_4^{3-} \rightarrow Eu^{3+}$ transfer occurs over large distances, probably by dipole–dipole interaction (the TaO_4^{3-} emission band overlaps the Eu^{3+} charge-transfer band).

4.5. *The* Eu^{2+} *ion* ($4f^7$)

Up till some years ago the Eu^{2+} ion was known as a broad band $4f^65d \rightarrow 4f^7$ emitter (Blasse et al., 1968). The ground state is $^8S(4f^7)$ and the lowest excited

TABLE 34.5
Some Eu^{3+}-phosphors classified according to transfer probabilities

	SA+	SA−
SS+	$(Y, Bi, Eu)Al_3B_4O_{12}$ $S = Bi^{3+}$, $A = Eu^{3+}$	$(Y, Eu)VO_4$ $S = VO_4^{3-}$, $A = Eu^{3+}$
SS−	$(Y, Eu)TaO_4$ $S = TaO_4^{3-}$, $A = Eu^{3+}$	$(Y, Eu)NbO_4$ $S = NbO_4^{3-}$, $A = Eu^{3+}$

state $4f^65d$ (see fig. 34.2). Some years ago, however, sharp line emission for Eu^{2+} has been reported (Hewes and Hoffmann, 1971; Hoffmann, 1971; 1972). This means that the ^6P_J states of the $4f^7$ configuration are situated below the lowest $4f^65d$ level, so that the emission occurs within the $4f^7$ configuration (compare the Gd^{3+}, $4f^7$, level scheme in fig. 34.2). The position of the lowest $4f^65d$ level relative to the ^6P_J states determines, whether the Eu^{2+} ion will show narrow-line or broad-band emission. Narrow-line emission for Eu^{2+} is expected in lattices where the centre of gravity of the $4f^65d$ level is at high energy, the crystal-field is weak, and the cohesion energy is high (so that Δr, and consequently the Stokes shift of the broad-band emission, is small) (Blasse, 1973). This is in qualitative agreement with the experimental results: narrow-line emission in many fluorides and also in strongly-bound oxides: $BaAlF_5$ and $SrAlF_5$ (Hewes and Hoffmann 1971; Hoffmann 1971, 1972), $BaMg(SO_4)_2$ (Ryan et al., 1974), and $SrBe_2Si_2O_7$ (Verstegen and Sommerdijk, 1974). The occurrence of line emission in compounds MeFX (Me = Sr, Ba and X = Cl, Br) (Tanguy et al., 1973; Sommerdijk et al., 1974b) is rather unexpected in view of the conditions mentioned above. These compounds have highly anisotropic crystal lattices. This is also the case for $SrAl_{12}O_{19}$–Eu^{2+} with line emission, whereas the analogous Ca and Ba compounds show band emission (Verstegen et al., 1974a). The more intense line emission is in fact observed for the compounds with a relatively small Stokes shift of the band emission.

An interesting study in this connection is the work by Ryan et al. (1974). They studied emission and excitation spectra of Eu^{2+} in $CaSO_4$ and $BaMg(SO_4)_2$ at 1.8°K. For $CaSO_4$–Eu^{2+} the emission (with decay time 0.4 μsec) is of the $5d \rightarrow 4f$ type and consists of a zero-phonon line followed by a large number of phonon replicas (due to density of states peaks in the normal lattice modes of $CaSO_4$). The excitation spectrum of this Eu^{2+} emission consists of 56 lines which are ascribed to purely electronic transitions to the levels of the $4f^6(^7F_J)5d(e_g)$ system, split by strong exchange interaction between the 4f and 5d electrons.

In $BaMg(SO_4)_2$–Eu^{2+}, however, the emission is of the 4f–4f type (decay time 3.5 msec) and consists of a zero-phonon line (the $^6P_{7/2} \rightarrow {}^8S_{7/2}$ transition) with a large number of phonon replicas at lower energy. The excitation band contains seven narrow bands ascribed to the seven ^7F_J levels of the Eu^{3+} core of the excited $4f^65d$ state. Obviously the exchange interaction between the 4f and 5d electrons is much smaller in $BaMg(SO_4)_2$ than in $CaSO_4$, which means that the 5d

electron of the Eu^{2+} ion is stronger localized in $CaSO_4$ than in $BaMg(SO_4)_2$. Strong exchange interaction depresses the $4f^65d$ levels and suppresses, therefore, the sharp line emission.

4.6. *The* Gd^{3+} *ion* ($4f^7$)

The Gd^{3+} ion is isoelectronic with the Eu^{2+} ion, but its $4f^65d$ state lies at much higher energies. As a consequence the luminescence of the Gd^{3+} ion consists of sharp line $^6P \rightarrow {}^8S$ transitions (see fig. 34.2) mainly at 313 nm. Due to its high energetic position this emission can only be observed in lattices with optical absorption at high energy. Often energy transfer from the ^6P manifold of Gd^{3+} to other R ions or host lattice groups occurs.

4.7. *The* Tb^{3+} *ion* ($4f^8$)

The Tb^{3+} ion is well known for its green emission originating from transitions from the $^5D_4$ level to the ground state ^7F manifold (see fig. 34.2). Blue and ultraviolet emission has also been observed from the $^5D_3$ level but is easily concentration-quenched, probably via the transfer process $Tb(^5D_3) + Tb(^7F_6) \rightarrow Tb(^5D_4) + Tb(^7F_0)$ (Van Uitert and Johnson, 1966). Concentration quenching of the green $^5D_4$ emission occurs by migration of excitation energy as nicely shown by Van der Ziel et al. (1972). The absorption (and excitation) spectrum of Tb^{3+}-activated materials show in the ultraviolet spectral region a number of strong bands corresponding to the crystal field components of the excited $4f^75d$ state. If Ce^{3+} and Tb^{3+} are studied in the same host lattice one finds similar allowed 4f–5d bands in the ultraviolet. The fact that the luminescence of Ce^{3+} and Tb^{3+} show identical temperature quenching upon 4f–5d excitation if the ions are introduced separately in the same host lattice sustains the theory on the influence of host lattice on temperature quenching (section 3.2).

Energy transfer from host lattice groups to Tb^{3+} does often not occur; in many cases the Tb^{3+} as well as the host lattice emission is quenched. A well-known example is YVO_4–Tb^{3+}. Usually the vanadate group transfers easily to R ions, but not so to Tb^{3+}. This has been ascribed to charge-transfer states V^{4+}–Tb^{4+}, from which radiationless return to the ground state occurs (see Delosh et al., 1970). If the charge-transfer state is at high energy, as, for example, in $CaSO_4$–V, Tb^{3+}, efficient transfer from the VO_4 group to the Tb^{3+} does occur (Draai and Blasse, 1974).

4.8. *The* Dy^{3+} *ion* ($4f^9$)

The Dy^{3+} ion shows in the visible region two emissions, viz. in the region 470–500 nm ($^4F_{9/2} \rightarrow {}^6H_{15/2}$) and 570–600 nm ($^4F_{9/2} \rightarrow {}^6H_{13/2}$). As a consequence the total emission is often near-white which has attracted some interest. It is not possible to excite Dy^{3+}-activated phosphors successfully with ultraviolet radiation, because the charge-transfer state as well as the 5d level are situated above

50.000 cm^{-1}. Energy transfer from host lattice groups to Dy^{3+} occurs, but leads only to a highly efficient phosphor in the case of YVO_4–Dy. For more details the reader is referred to the literature (Sommerdijk and Bril, 1975).

5. Applications

Before mentioning phosphors for specific applications we would like to mention the fact that the only R activator that has brought about a real break-through is the Eu^{3+} ion as will be explained now. The light output of colour television tubes was limited up till the sixties by the red primary phosphor (silver-activated zinc- and zinc-cadmium sulfides). This is not caused by the low conversion efficiency of these phosphors but by the combination of the very broad emission band of the red luminescence and the rapidly decreasing eye sensitivity in the red towards longer wavelengths (see fig. 34.17). From this figure it is evident that a lot of energy is wasted, because the emission is in a region where the eye is not sensitive. Already in 1955 Bril and Klasens predicted that a good red primary should have a narrow emission band near 610 nm. Eu^{3+}-activated phosphors satisfy this condition (see fig. 34.17) and this, together with a reasonable radiant efficiency, forms the basis of their successful application. Whereas the lumen equivalent of the red sulfide is only 75, it amounts to 245 for YVO_4–Eu^{3+} and even 300 for Y_2O_3–Eu^{3+} (Bril and De Laat, 1966).

We will now illustrate the broad application and possibilities for application of R-activated phosphors without aiming at completeness or detail.

5.1. *Phosphors for uv excitation*

Eu^{3+}-activated phosphors, especially YVO_4–Eu^{3+}, have found application in high pressure mercury vapour lamps for improving the appearance and the colour rendering (Wanmaker and Ter Vrugt, 1971).

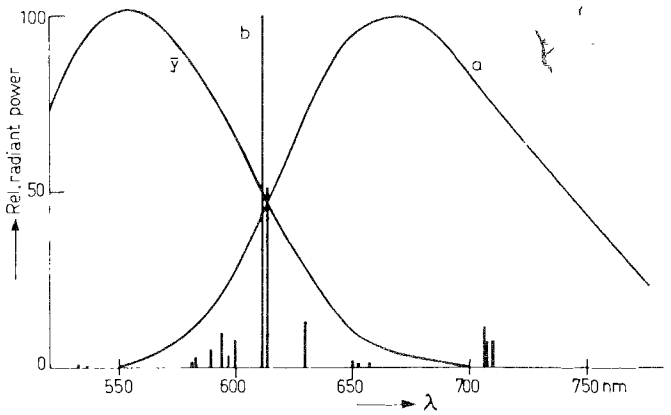

Fig. 34.17. Comparison of the relative spectral energy distribution of $Zn_{0.2}Cd_{0.8}S$–Ag (curve a) and Gd_2O_3–Eu (curve b). The curve denoted by y represents the eye-sensitivity curve (from Bril and De Laat, 1966).

Eu^{2+}-activated phosphors have found many applications in fluorescent lamps. The Eu^{2+} ion has not only a high luminescence output in many host lattices, but also its emission colour can be varied over a wide range (Blasse et al., 1968). We mention some examples: $Sr_2P_2O_7$–Eu^{2+} has been applied in lamps for photo-copying (Wanmaker and Ter Vrugt, 1971); several blue-green emitting Eu^{2+}-phosphors have been proposed for lamps with improved colour-rendering properties. By far the most impressing application is a new generation of "Deluxe" fluorescent lamps described by Verstegen et al. (1974b). These lamps combine a high efficacy with a very good colour rendering. Three different R-activated phosphors are applied simultaneously, viz. blue-emitting $(Ba, Eu^{2+})Mg_2Al_{16}O_{27}$, green-emitting $(Ce, Tb^{3+})MgAl_{11}O_{19}$ and red-emitting $(Y, Eu^{3+})_2O_3$. Other R-activated phosphors, however, may also be used. The near future will teach us whether this combination of three R-activated phosphors will make the well-known halophosphates obsolete.

Co-doped materials, like Eu^{2+}, Mn^{2+}- and Ce^{3+}, Mn^{2+}-activated aluminates seem to be promising for photo-copying lamps (Stevels, 1976).

Ultraviolet-emitting Eu^{2+}-phosphors have been proposed for certain professional applications (Stevels, 1976).

5.2. *Phosphors for cathode-ray excitation*

The application of Eu^{3+}-activated phosphors as a red primary in colour television tubes was mentioned above. Originally the more efficient, but less red Gd_2O_3–Eu^{3+} and Y_2O_3–Eu^{3+} and the less efficient, but more red YVO_4–Eu^{3+} have been applied (for a summary see Bril and De Laat, 1966 and Levine and Palilla, 1964). Nowadays the Eu^{3+}-activated Y_2O_2S has found general application for this purpose (Royce and Smith, 1968, Yocom and Shrader, 1968). The problems inherent in the fabrication of luminescent screens and the influence of impurities on the phosphor properties have been reviewed by Mathers (1973).

Anti-pollution programs have led to the reduction of the cadmium content in sulphides phosphors. This may have consequences for the green-emitting sulphide phosphor. Tb^{3+}-activated phosphors have the potentiality to replace these green-emitting sulphides, so that much effort has been devoted into this direction (Stevels, 1976, Tecotzky, 1973).

Ce^{3+}-activated phosphors have found application as fast phosphors in the cathode-ray tube for the flying-spot scanner and the beam-indexing tube due to their short decay time (Bril et al., 1971). The garnet Ce^{3+}-activated $Y_3Al_5O_{12}$ has been applied in the flying-spot scanner for colour television signals. A number of ultraviolet-emitting Ce^{3+}-phosphors have been proposed for the beam-indexing tube, e.g. $Y_2Si_2O_7$–Ce^{3+} and YPO_4–Ce^{3+}.

For other display screens using R-phosphors see Tecotzky (1973).

5.3. *Phosphors for X-ray excitation*

Several R-activated phosphors have been proposed for application in X-ray intensifying screens to replace the well-known $CaWO_4$. Here we mention BaFCl–Eu^{2+} and Gd_2O_2S–Tb^{3+} (Stevels, 1976; Tecotzky, 1973).

6. Latest developments

After the submission of this manuscript a number of papers have appeared in this field which are worth mentioning as additions to the text.

2.2. Research in the vacuum ultraviolet region is continuing. As examples we may mention the reported far-uv emission from Nd^{3+}, Er^{3+} and Tm^{3+} (Yang and DeLuca, 1976), but also work to elucidate the efficiency of R-activated phosphors under high-energy excitation (see e.g. Robbins et al., 1977).

2.4. The study of non-radiative transitions is going on and extends our understanding of the factors determining the quantum efficiency of R-activated phosphors. A very recent review has been given by Auzel (1978). Fong (1975) has given a rigorous treatment especially applied to R-activated materials. This summary covers a good deal of the work performed by Fong and his coworkers. The theory can explain experimental observations satisfactorily. The intraconfiguration $4f^n \rightarrow 4f^n$ transitions are treated in the weak-coupling limit, whereas the interconfiguration $f \rightarrow d$ transitions are examples of the intermediate-coupling case. It is interesting to note that the effective mediating phonon frequency in the latter case is less than half that of the maximum-frequency; in the weak-coupling case the mediating phonon frequency does not differ greatly from the maximum phonon frequency.

Fong has also treated the case of Sm^{2+} ($4f^6$). There is a strong analogy with Eu^{3+} ($4f^6$). In the case of Eu^{3+} there is in addition to the $4f^6$ levels a charge-transfer state which plays an important role in thermal quenching processes, in the case of Sm^{2+} there is a $4f^5 5d$ state. In contradiction to the Eu^{3+} charge-transfer state, the 5d state can also be the origin of luminescence. Since the position of this 5d state depends on the crystal lattice and composition, the intensity ratio of the $^5D_0$, $^5D_1$ and 5d emission does also. It appears that direct multiphonon decay from $^5D_1$ to $^5D_0$ does not occur; this nonradiative transition occurs by intermediate coupling via the 5d state.

The simple calculations by Struck and Fonger (applying the Manneback recursion formulae on the harmonic oscillator) have been applied on Eu^{3+} in the oxysulfides (1976). A quantitative interpretation of the phenomena mentioned in section 4.4 appeared to be possible.

2.5. Recent work by Venikouas and Powell (1977) has provided a more quantitative insight in the energy transfer processes in YVO_4–Eu^{3+}. At low temperatures there is only acting an (inefficient) one-step transfer process from vanadate to Eu^{3+}. Transfer within the vanadate host lattice is unimportant. At higher temperatures, however, thermally activated exciton hopping occurs yielding an efficient Eu^{3+} phosphor at room temperature. Activator-induced host traps play an important role in the transfer process to the Eu^{3+} ion.

A recent review on energy transfer in which the microscopic transfer rates are related to observable quantities has been given by Watts (1975) and also by Reisfeld (1976).

2.6. Interest in concentration quenching has been stimulated by the so-called

"stoichiometric laser materials", where a luminescent ion shows high luminescence efficiency in spite of the fact that it occupies all of the lattice sites of a certain type in the crystal structure. Examples are NdP_5O_{14}, EuP_5O_{14} and $NdAl_3B_4O_{12}$. These materials are at present studied intensively.

3.2. In section 3.2 luminescent centres were divided in two groups depending on the sign of Δr (expansion or shrinkage after excitation). Recent high pressure work by Drickamer et al. (1976, 1977) seems to justify this distinction.

Bieg and Drickamer (1977) showed in an elegant way that the energy transfer probability increases strongly if the spectral energy overlap increases (see section 2.5). They studied the system KCl:Ag,Tl under pressure. Due to a different pressure dependence of the relevant excitation and emission band the spectral overlap increases with pressure.

4.4. By studying the Eu^{3+} luminescence in the two modifications of $CaLaGaO_4$ with strongly different crystal structures, Ronde et al. (1977) were able to show directly the strong influence of crystal structure on the position of the Eu^{3+} charge-transfer band. This influence could be explained according to the model in section 3.1 and is also of importance for the value of the quantum efficiency of the luminescence.

4.7. Concentration quenching of the $^5D_3$ emission of Tb^{3+} has been shown to occur via electric dipole–dipole interaction, with a critical distance of 13 Å in the case of $Y_3Al_5O_{12}$–Tb^{3+} (Robbins et al., 1976).

5.1. Relating to the new "three-bands" fluorescent lamps it is interesting to note that lamps with efficacies of 100 lm/W have been reported (Peters and Tak, 1977).

5.3. Interest in X-ray phosphors is still increasing during recent years (see e.g. the Proceedings of the Electrochemical Society Spring Meeting 1977 in Philadelphia). It is still uncertain which materials will prove the most feasible ones for certain applications, but the rare earth ions will certainly be used in it.

7. Note added in proof

An extended report on nonradiative transitions in R ions in glasses has been given recently by Layne et al. (1977). Hoshina et al. (1977) have given an original approach to the influence of the charge-transfer state on the $4f^6$ levels considering spin-restricted covalency. In this way they could explain a large number of experimental details in the emission and excitation spectra of Eu^{3+}-activated oxysulfides. Energy transfer between several types of Pr^{3+} ions in PrF_3 has recently been measured using selective laser excitation and its mechanism discussed by Hamilton et al. (1977). An application of R luminescence in the field of catalysis ("cataluminescence") has been given by Breysse et al. (1977) and Aras et al. (1977).

References

Auzel, F., 1978, Proc. Summer School, Luminescence of inorganic solids, Erice, ed. B. Di Bartolo (Plenum Press, New York).

Barnes, J.C. and H. Pincott, 1966, J. Chem. Soc. 842.

Bleg, K.W. and H.G. Drickamer, 1977, J. Chem. Phys. **66**, 1437.

Bimberg, D., D.J. Robbins, D.R. Wight and J.P. Jeser, 1975, Appl. Phys. Letters **27**, 67.

Blasse, G., 1966, J. Chem. Phys. **45**, 2356.

Blasse, G. and A. Bril, 1967a, J. Inorg. Nucl. Chem. **29**, 2231.

Blasse, G. and A. Bril, 1967b, J. Chem. Phys. **47**, 5139.

Blasse, G. and A. Bril, 1967c, Appl. Phys. Letters **11**, 53.

Blasse, G., 1968a, J. Chem. Phys. **48**, 3108.

Blasse, G., 1968b, J. Electrochem. Soc. **115**, 738.

Blasse, G., 1968c, Philips Res. Repts **23**, 344.

Blasse, G. and A. Bril, 1968, J. Electrochem. Soc. **115**, 1067.

Blasse, G., W.L. Wanmaker, J.W. ter Vrugt and A. Bril, 1968, Philips Res. Repts **23**, 189.

Blasse, G., 1969, J. Chem. Phys. **51**, 3529.

Blasse, G. and A. Bril, 1969, J. Chem. Phys. **50**, 2974.

Blasse, G. and A. Bril, 1970, Philips Techn. Rev. **31**, 304.

Blasse, G., 1972, J. Solid State Chem. **4**, 52.

Blasse, G., 1973, Phys. Stat. Sol. (b) **55**, K 131.

Brecher, C. and L.A. Riseberg, 1976, Phys. Rev. B, **13**, 81.

Bril, A. and H.A. Klasens, 1955, Philips Res. Repts **10**, 305.

Bril, A. and C.D.J.C. de Laat, 1966, Electrochem. Techn. **4**, 21.

Bril, A., G. Blasse and J.A.A. Bertens, 1968, J. Electrochem. Soc. **115**, 395.

Bril, A., G. Blasse, A.H. Gomes de Mesquita and J.A. de Poorter, 1971, Philips Techn. Rev. **32**, 125.

Curie, D., 1963, Luminescence in crystals (Methuen, London).

Danielmeyer, H.G., 1976, J. Luminescence **12/13**, 179.

Day, P., P.J. Diggle and G.A. Griffiths, 1974, J. Chem. Soc., Dalton Transactions, 1446.

De Losh, R.G., T.Y. Tien, E.F. Gibbins, P.J. Zacmanides and H.L. Stadler, 1970, J. Chem. Phys. **53**, 681.

Dexter, D.L., 1953, J. Chem. Phys. **21**, 836.

Dexter, D.L. and J.H. Schulman, 1954, J. Chem. Phys. **22**, 1063.

Dexter, D.L., C.C. Klick and G.A. Russell, 1955, Phys. Rev. **100**, 603.

Dexter, D.L., 1958, Solid State Physics **6**, 353.

DiBartolo, B., 1968, Optical interactions in solids (Wiley, New York).

Draai, W.T. and G. Blasse, 1974, Phys. Stat. Sol. (a), **21**, 569.

Drickamer, H.G., et al., 1976, Phys. Rev. **13**, 4568.

Drickamer, H.G., et al., 1977, J. Chem. Phys. **67**, 4103, 4116.

Fong, F.K., 1975, Theory of Molecular Relaxation, Wiley, New York.

Förster, Th., 1948, Ann. Physik (6) **2**, 55.

Garlick, G.F.J., 1958, Handbuch der Physik, ed. S. Flügge, Vol. XXVI, Springer, Berlin, p. 1.

Goldberg, P., 1966, Luminescence of inorganic solids (Academic Press, New York).

Heaps, Wm.S., L.R. Elias and W.M. Yen, 1976, Phys. Rev. B, **13**, 94.

Hewes, R.A. and M.V. Hoffmann, 1971, J. Luminescence **3**, 261.

Hoefdraad, H.E., 1975a, J. Inorg. Nucl. Chem. **37**, 1917.

Hoefdraad, H.E., 1975b, J. Solid State Chem. **15**, 175.

Hoefdraad, H.E. and G. Blasse, 1975, Phys. Stat. Sol. (a) **29**, K95.

Hoffmann, M.V., 1971, J. Electrochem. Soc. **118**, 933.

Hoffmann, M.V., 1972, J. Electrochem. Soc. **119**, 905.

Hoshina, T. and S. Kuboniwa, 1971, J. Phys. Soc. Japan **31**, 828.

Hsu, C. and R.C. Powell, 1975, J. Luminescence **10**, 273.

Jørgensen, C.K., 1971, Modern aspects of ligand field theory (North-Holland, Amsterdam).

Kaplyanski, A.A. and P.P. Feofilov, 1962, Opt. Spectry. **13**, 129.

Kirs, J. and A. Niilks, 1962, Tr. Inst. Fiz. i Astron. Akad. Nauk Est. SSR **18**, 36.

Krol, D., 1976, unpublished result.

Lange, H., 1971, Einführung in die Lumineszenz, Ed. N. Riehl (Karl Thiemig, München) p. 110.

Lehmann, W. and F.M. Ryan, 1971, J. Electrochem. Soc. **118**, 477.

Levine, A.K. and F.C. Palilla, 1964, Appl. Phys. Letters **5**, 118.

Mathers, J.E., 1973, Analysis and application of rare earth materials, Ed. O.B. Michelson, Universitets forlaget, Oslo, p. 241.

McClure, D.S. and Z.J. Kiss, 1963, J. Chem. Phys. **39**, 3251.

Nakazawa, E. and S. Shionoya, 1974, J. Phys. Soc. Japan **36**, 504.

Nieboer, E., 1975, Structure and Bonding, **22**, 1.

Ofelt, G.S., 1962, J. Chem. Phys. **37**, 511.

Palilla, F.C., A.K. Levine and M. Rinkevics, 1965, J. Electrochem. Soc. **112**, 776.

Palilla, F.C., 1968, Electrochem. Techn. **6**, 39.

Paulusz, A.G., 1974, private communication; recent news paper at the Electrochem. Soc. Spring Meeting, San Francisco.

Peacock, R.D., 1975, Structure and Bonding **22**, 83.

Peters, R.C. and M.G.A. Tak, 1977, Extended Abstracts 77-1, Electrochemical Society, Philadelphia, nr. 129.

Piper, W.W., J.A. Deluca and F.S. Ham, 1974, J. Luminescence **8**, 344.

Powell, R.C. and Z.G. Soos, 1975, J. Luminescence **11**, 1.

Reisfeld, R. and A. Grabner, 1964, J. Opt. Soc. Am. **54**, 331.
Reisfeld, R. and N. Lieblich, 1973, J. Phys. Chem. Solids **34**, 1467.
Reisfeld, R., 1976, Structure and Bonding **30**, 65.
Reut, E.G. and A.I. Ryskin, 1973, Phys. Stat. Sol. (a) **17**, 47.
Riehl, N., 1971, Einführung in die Lumineszenz, Thiemig-Taschenbücher 35 (Karl Thiemig, München).
Robbins, D.J., B. Cockayne, B. Lent and J.L. Glasper, 1976, Solid State Commun. **20**, 673.
Robbins, D.J., B. Cockayne, B. Lent and J.L. Glasper, 1977, Extended Abstracts 77-1, Electrochemical Society, Philadelphia, nr. 140.
Ronde, H., D.M. Krol and G. Blasse, 1977, J. Electrochem. Soc. **124**, 1276.
Royce, M.R. and A.L. Smith, 1968, Electrochem. Soc. Spring Meeting, Extended Abstracts, 17, nr. 34, The Electrochem. Soc., New York.
Ryan, F.M., W. Lehmann, D.W. Feldman and J. Murphy, 1974, J. Electrochem. Soc. **121**, 1475.
Schwartz, R.W. and P.N. Schatz, 1973, Phys. Rev. B., **8**, 3229.
Schwartz, R.W., 1975, Mol. Phys. **30**, 81.
Seitz, F., 1939, Trans. Faraday Soc. **35**, 74.
Sommerdijk, J.L., A. Bril and A.W. de Jager, 1974a, J. Luminescence **8**, 341; **9**, 288.
Sommerdijk, J.L., J.M.P.J. Verstegen and A. Bril, 1974b, J. Luminescence **8**, 502.
Sommerdijk, J.L. and A. Bril, 1975, J. Electrochem. Soc. **122**, 952.
Stevels, A.L.N., 1976, J. Luminescence **12/13**, 97.
Struck, C.W. and W.H. Fonger, 1970a, J. Luminescence **1, 2**, 456.
Struck, C.W. and W.H. Fonger, 1970b, J. Chem. Phys. **52**, 6364.
Struck, C.W. and W.H. Fonger, 1975, J. Luminescence **10**, 1.
Struck, C.W. and W.H. Fonger, 1976, J. Chem. Phys. **64**, 1784.
Tanguy, B., M. Pezat, C. Fontenit and C. Fouassier, 1973, C.R. Ac. Sci. Paris, **277**, 25.
Tecotzky, M., 1973, Analysis and application of rare earth materials, Ed. O.B. Michelson, Universitetsforlaget, Oslo, p. 359.
Treadaway, M.J. and R.C. Powell, 1974, J. Chem. Phys. **61**, 4003.
Treadaway, M.J. and R.C. Powell, 1975, Phys. Rev. B. **11**, 862.
Van der Ziel, J.P., L. Kopf and L.G. Van Uitert, 1972, Phys. Rev. B **6**, 615.
Van Uitert, L.G. and L.F. Johnson, 1966, J. Chem. Phys. **44**, 3514.
Van Uitert, L.G., 1968, Int. Conf. Luminescence, Budapest, Ed. G. Szigeti (Akad. Kiadó), p. 1588.
Venikouas, G.E. and R.C. Powell, 1978, J. Luminescence **16**, 29.
Verstegen, J.M.P.J., J.L. Sommerdijk and A. Bril, 1974a, J. Luminescence **9**, 420.
Verstegen, J.M.P.J., D. Radielović and L.E. Vrenken, 1974b, J. Electrochem. Soc. **121**, 1627.
Verstegen, J.M.P.J. and J.L. Sommerdijk, 1974, J. Luminescence **9**, 297.
Wanmaker, W.L. and J.W. ter Vrugt, 1971, Lighting Res. and Techn. **3**, 147.
Watts, R.K., 1975, Optical properties of ions in solids, ed. B. Di Bartolo, Plenum Press, New York, p. 307.
Weber, M.J., 1973, Solid State Commun. **12**, 741.
Williams, F., 1951, J. Chem. Phys. **19**, 457.
Witzke, H., D.S. McClure and B. Mitchell, 1973, Luminescence of crystals, molecules and solutions (Proc. Int. Conf. Leningrad, Ed. F. Williams, Plenum, New York).
Wolf, H.C., 1967, Advances in Atomic and molecular physics, eds. D.R. Bates and I. Estermann, **3**, 119, Academic Press.
Wybourne, B.G., 1965, Spectroscopic properties of rare earths (Interscience, New York).
Yang, K.H. and J.A. DeLuca, 1976, Appl. Phys. Letters **29**, 499.
Yocom, P.N. and R.E. Shrader, 1968, Proc. Int. Conf. Rare Earth Research, **7**, 601.

References to section 7

Aras, V.M., M. Breysse, B. Claudel, L. Faure and M. Guenin, 1977, J. Chem. Soc. Faraday Trans. I **73**. 1039.
Breysse, M., B. Claudel, L. Faure and M. Guenin, Proc. 13th Rare Earth Conference, in press.
Hoshina, T., S. Imanaga and S. Yokono, 1977, J. Luminescence **15**, 455.
Hamilton, D.S., P.M. Selzer and W.M. Yen, 1977, Phys. Rev. B **16**, 1858.
Layne, C.B., W.H. Lowdermilk and M.J. Weber, 1977, Phys. Rev. B **16**, 10.

Handbook on the Physics and Chemistry of Rare Earths, edited by K.A. Gschneidner, Jr. and L. Eyring

Chapter 35

RARE EARTH LASERS

Marvin J. WEBER
Lawrence Livermore Laboratory, University of California, Livermore, California 94550 USA

Contents

Symbols

a = parameter for exponential energy gap dependence of multiphonon emission on energy gap
E = energy
ΔE = energy gap between two levels
G = gain per unit length
l = length of lasing medium
M = alkali ion
N = ion population density
n = refractive index
n_2 = nonlinear refractive index
Q^+ = cation
R = reflectivity
S = line strength
T = temperature
U = tensor operator
$W(0)$ = spontaneous multiphonon emission rate
W_{mp} = multiphonon emission rate
α = gain coefficient
α_s = scattering loss coefficient
α_i = impurity absorption coefficient
ϵ = optical electric-field amplitude
λ_p = wavelength of fluorescence peak
$\Delta\lambda_{eff}$ = effective fluorescence linewidth
σ_{23} = absorption cross section
σ_{32} = stimulated emission cross section
σ_{esa} = excited-state absorption cross section
τ_R = radiative lifetime
$\Omega_{2,4,6}$ = Judd–Ofelt intensity parameters

1. Introduction

Rare earths have been employed extensively for lasers. To date, stimulated emission has been observed from three divalent and nine trivalent lanthanide

ions; in hosts including crystalline and amorphous solids, metallo-organic and inorganic aprotic liquids, and neutral and ionized vapors; at wavelengths in the visible and infrared; from lasers operating pulsed and continuously; and from lasers ranging in size from thin films and small fibers for integrated optics applications to large, high-power glass lasers for controlled fusion experiments.

The first lasers – ruby and helium–neon – appeared in 1960. In the following year the use of rare earths for lasers began with divalent samarium in CaF_2 (Sorokin and Stevenson, 1961), and trivalent neodymium in $CaWO_4$ (Johnson and Nassau, 1961) and in glass (Snitzer, 1961). The first liquid material to exhibit laser action was a rare earth chelate (Lempicki and Samelson, 1963). Investigations of rare earth laser action in various hosts proliferated in the 1960's. Additional laser transitions and material developments have continued to emerge in the 1970's. This research has resulted in the diversity of rare earth lasers cited above.

Rare earths have found their widest application in optically-pumped solid-state lasers. Of the different transition metal ion groups which fluoresce in solids and which are thereby candidates for stimulated emission, the rare earths predominate. Ions used for crystalline lasers are listed in fig. 35.1 together with the number of crystal hosts which have been employed for each ion through 1975. Of the approximately 200 crystalline lasers reported, all are based upon rare earths except for a few iron group ions and one actinide ion.

The wide applicability and versatility of rare earths for lasers arise from several attractive spectroscopic properties. The electronic states of the ground $4f^n$ configuration of rare-earth ions provide complex and varied optical energy level structures. Thus, there are many possible three- and four-level lasing

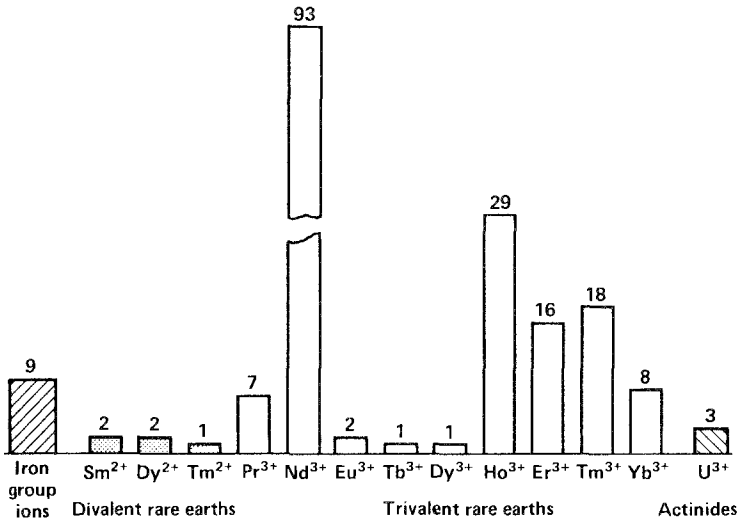

Fig. 35.1. Number of different ion-crystal laser combinations reported through 1975 grouped by lasing ion.

schemes. The large number of excited states suitable for optical pumping and subsequent decay to metastable states having high quantum efficiencies and narrow f→f emission lines are also favorable for achieving laser action. Because the locations of the energy levels do not change greatly with host, a given ion can be lased in many different hosts. The host can, therefore, be selected to optimize performance for a specific application. Trivalent neodymium, with its numerous, well-located energy levels for optical pumping and a four-level lasing scheme at ambient temperatures provided by the $^4F_{3/2} \rightarrow {}^4I_{11/2}$ transition, has been the prime rare earth laser ion, having been lased in nearly 100 different crystals, numerous glasses and liquids, and at wavelengths ranging from 0.9 to 1.8 μm.

The spectral range covered by rare earth lasers is shown in fig. 35.2. It extends from approximately 0.5 to 3.0 μm, a wavelength factor of six. While this is small compared to that for gas or semiconductor lasers, it is larger than that for organic dye and many other specific types of lasers. The operating wavelengths of some selected rare earth lasers are included in fig. 35.2. Rare earth lasers have been reported which operate at intervals of about every 0.1 μm throughout the range shown.

Rare-earth lasers provide pulsed or continuous monochromatic radiation of high intensity, coherence, and directionality. Their many and varied applications include laboratory use and research (optical spectroscopy, holography, laser fusion, medical), materials processing (cutting, scribing, drilling, welding), communications (integrated optics, high-data-rate transmission, satellite communications systems), and military (range finders, target designators).

This chapter begins with a brief review (in section 2) of the fundamental physics of lasers, the energy levels, radiative and nonradiative transitions, and sensitization of rare earth ions, and the relationship of these properties to achieving stimulated emission. Laser action in various media – crystals, glasses, liquids, and gases – is surveyed in sections 3 through 6. Differences in the rare earth host media and their effect on laser properties are discussed. Representative laser parameters and characteristics are given. Throughout, the emphasis is on rare earth ions and the extent to which they have been utilized

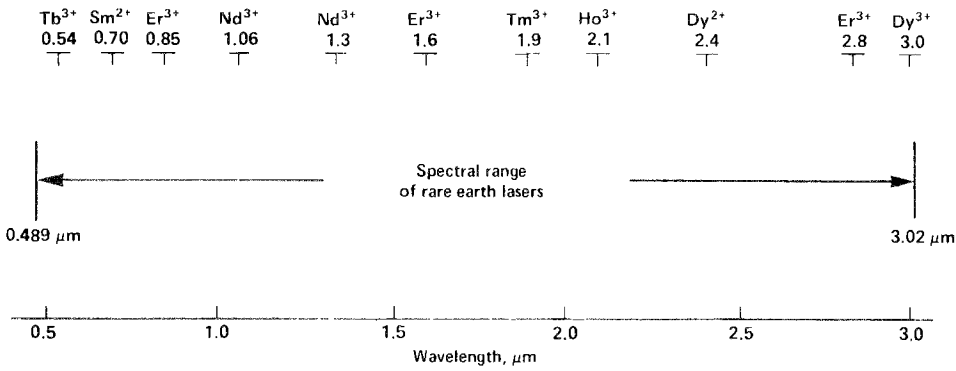

Fig. 35.2. Spectral range and wavelengths of selected rare earth lasers.

for lasers. Detailed descriptions of laser physics, device performance, and applications are beyond the scope of this article. In many instances, these topics are adequately covered in books on lasers, such as Lengyel (1971) and Smith and Sorokin (1966), and various review articles; references to appropriate reviews are given, when available. In the concluding section, some possible further developments of rare earth lasers are mentioned.

2. Background

2.1. *Laser fundamentals*

To obtain stimulated emission between two energy levels, a population inversion is necessary. This is usually achieved by excitation into a third level (or levels) which rapidly and efficiently transfers its energy to a metastable upper laser level. A generalized energy level scheme for laser action is shown in fig. 35.3. If the terminal laser level is the ground state, then more than one-half of the ions must be excited to obtain an inverted population. If, instead, the terminal level 2 is above the ground state, then only an excited-state population sufficient to overcome the Boltzmann thermal equilibrium population in the terminal level is needed. This reduces the pumping requirements. In phonon-terminated lasers, level 2 is a vibrational-electronic state. The four-level laser scheme depicted in fig. 35.3 is representative of that employed for most rare earth lasers.

Almost all rare earth lasers are optically pumped. The lasing material is placed in an optical resonator cavity formed by two mirrors and excited with a flashlamp or continuous light source. The most commonly used pumping

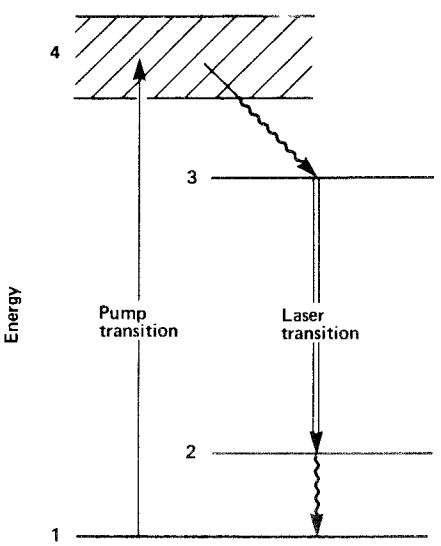

Fig. 35.3. Energy level diagram for a four-level laser scheme.

geometry is an elliptical cylinder reflector with the laser rod or liquid container at one foci and the pump source at the other. By enclosing the rod in a cylindrical dewar, laser action has been obtained from materials at temperatures ranging from that of liquid helium to ~1000 K.

The threshold condition for laser oscillation is given by

$$R_1R_2 \exp(2Gl) = 1, \tag{35.1}$$

where R_1 and R_2 are the reflectivities of the mirrors in the optical resonator cavity, G is the gain per unit length, and l is the length of the active lasing medium. The gain is determined by

$$G = \alpha - \alpha_s - \alpha_i, \tag{35.2}$$

where α is the gain coefficient of the laser medium, and α_s and α_i are loss coefficients due to scattering and impurity absorption. If N_3 and N_2 are the populations in the upper and lower laser levels in fig. 35.3, the net gain of the laser medium is

$$\alpha = N_3\sigma_{32} - N_2\sigma_{23} - N_3\sigma_{esa}. \tag{35.3}$$

In eq. (35.3), σ_{32} and σ_{23} are the cross sections for stimulated emission and absorption. For narrow-line absorption and emission spectra, these two cross sections are equal. For broadband spectra with emission bandwidth greater than kT, the cross sections are connected by a generalized Einstein relation (McCumber, 1964). The final term in eq. (35.3) accounts for possible excited-state absorption from the upper laser level to higher excited states (not shown in fig. 35.3). If $\sigma_{esa} > \sigma_{32}$, absorption from level 3 dominates stimulated emission and laser action is not possible.

The gain, from eq. 35.3, is governed by a product of the stimulated emission cross section σ and the population inversion (N_3–N_2). The latter is dependent upon the absorption spectrum and its spectral match with the pump source, the lifetime of the metastable level 3 which determines the pumping rate required, and the quantum efficiency. For lasers, the last quantity includes (1) the fluorescence conversion efficiency (the number of ions excited to the fluorescing level per incident pump photon), (2) the quantum efficiency of the fluorescing state (the fractional number of photons emitted per excited ion in the upper laser level), and (3) the energy efficiency (the laser photon energy out per pump photon energy in). In general, for low-threshold laser operation it is desirable to have:

- Large stimulated emission cross section (narrow fluorescence linewidth)
- Broad (numerous) absorption bands for optical pumping
- High fluorescence conversion efficiency
- High fluorescence quantum efficiency
- Terminal laser level at energy $E \gg kT$
- No excited-state absorption.

In the following sections, the spectroscopic properties of rare earth ions are examined with respect to satisfying these criteria. For detailed reviews of

rare earth energy levels, see Dieke (1968) (experimental) and Wybourne (1965) (theoretical treatment). Radiative and nonradiative relaxation phenomena of rare earths are reviewed by Riseberg and Weber (1976). Radiative and nonradiative transitions of divalent rare earths are discussed by Sorokin (1964).

2.2. *Energy levels*

Energy levels associated with the $4f^n$ ground electronic configuration of rare-earth ions fulfill the requirements of fig. 35.3 for optically-pumped laser action. The energy level schemes for states up to $\approx 30\,000$–$40\,000\ cm^{-1}$ are well established for trivalent rare earths (Dieke, 1968). The ligand or crystal field of the host reduces the $(2J + 1)$-fold degeneracy of the free-ion states. Because the 4f electrons are shielded by the outer $5s^2$ and $5p^6$ shells, the shift in the center of gravity of the free-ion energy levels and the extent of the crystalline Stark splitting are small, on the order of a few hundred cm^{-1}. Levels of $4f^{n-1}5d$ and other configurations occur at higher energies [5d bands for rare earths are reported for CaF_2 by Loh (1966, 1968) and for LaF_3 by Heaps et al. (1976)]. In many materials these levels are near or above the fundamental absorption edge and, therefore, are only of limited usefulness for optical pumping.

The $4f^n$ and $4f^{n-1}5d$ energy levels of divalent rare earths in CaF_2 are published by McClure and Kiss (1963). For this valence state, the 5d levels occur at lower energies; in most cases the absorption bands extend into the visible. Since the $4f \rightarrow 5d$ transitions are broad and parity-allowed, they provide strong absorption bands for optically pumping divalent rare earth lasers. A summary and comparison of the spectral properties of f–f and f–d transitions in crystals are given in table 35.1.

To illustrate the spectroscopic features of rare earth ions, in the following and throughout this section we shall use trivalent neodymium as a paradigm. This is appropriate since (a) most of the physical phenomena relevant to rare-earth lasers are present in Nd^{3+} and (b) Nd^{3+} is the most extensively used rare earth for lasers and has been lased in all forms of condensed matter – crystals, glasses,

TABLE 35.1.
Comparison of spectral properties of f–f and f–d transitions of rare earths in crystals.

	$4f \rightarrow 4f$	$5d \rightarrow 4f$
Electric-dipole oscillator strength	$\sim 10^{-6}$	$\sim 10^{-1} - 10^{-2}$
Ion–lattice coupling	weak	intermediate–strong
Fluorescence wavelength	~200–5000 nm	~150–1000 nm
Fluorescence linewidth	$\sim 10\ cm^{-1}$	$\lesssim 1000\ cm^{-1}$
Fluorescence lifetime	$10^{-5} - 10^{-2}$ sec	$10^{-8} - 10^{-6}$ sec
Excited-state absorption	$f \rightarrow f$	$d \rightarrow d$
	$f \rightarrow d$	$d \rightarrow$ higher configurations

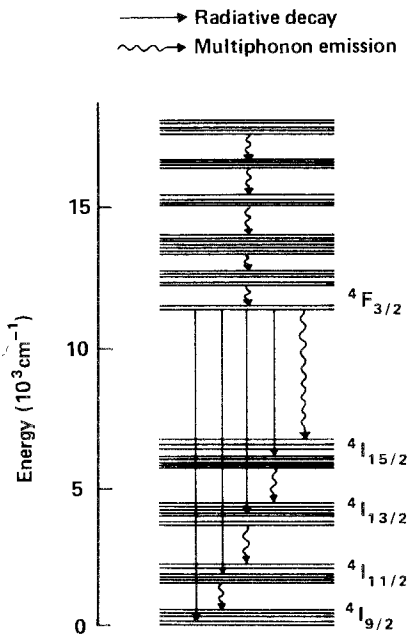

Fig. 35.4. Energy levels and radiative (solid line) and nonradiative (wavy line) transitions of Nd^{3+}. All transitions between individual Stark levels are not shown.

and liquids. The lower energy levels of Nd^{3+} are shown in fig. 35.4 (the exact barycenters and Stark structure of the J states vary with host). Fluorescence is observed from the $^4F_{3/2}$ levels to levels of the ^4I ground multiplet*. Fluorescence is excited by absorption into the levels above $^4F_{3/2}$, followed by a nonradiative (and possibly radiative) cascade to $^4F_{3/2}$. The absorption spectra of Nd^{3+} in a crystal and in a glass are compared in fig. 35.5. In the latter, because of the distribution of local sites, the lines are inhomogeneously broadened and the Stark structure is poorly resolved. The large number of lines in the visible and near-infrared contribute to the high pumping efficiency of Nd lasers.

The most intense Nd^{3+} fluorescence is from $^4F_{3/2}$ to $^4I_{11/2}$. Examples of this spectrum for a crystal and a glass are shown in fig. 35.6. Since the $^4I_{11/2}$ terminal state is $\approx 2000\ cm^{-1}$ above the ground, the fractional ion population is very small at ambient temperatures ($\sim 10^{-4}$). In most materials the $^4I_{11/2}$ population rapidly relaxes to the ground state by nonradiative processes. Therefore, the $^4F_{3/2} \rightarrow {}^4I_{11/2}$ transition of Nd^{3+} represents a near-ideal embodiment of the four-level laser scheme in fig. 35.3. If the rate of $^4I_{11/2} \rightarrow {}^4I_{9/2}$ relaxation is slow compared with the rate of stimulated emission, as may occur in short-pulse Q-switched operation, the laser action will become self-terminating when $N_3 = N_2$. High-lying Stark levels of the $^4I_{9/2}$ ground manifold can also be used for terminal laser levels. To obtain low pumping thresholds, cooling of the host is required to depopulate the terminal level.

* In some materials fluorescence is also readily observed from higher excited states.

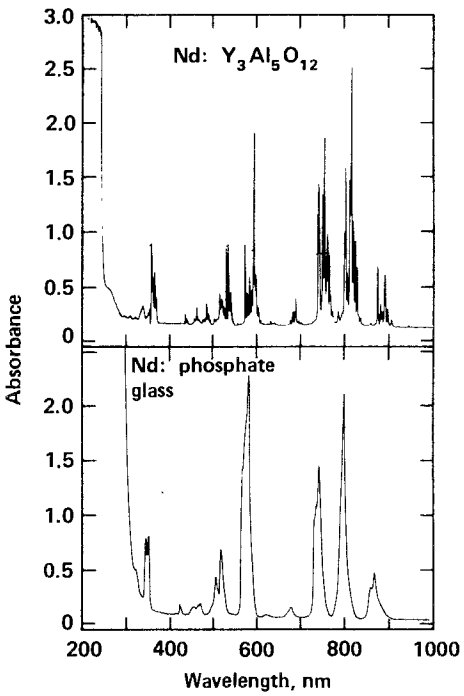

Fig. 35.5. Absorption spectra of Nd^{3+} in a $Y_3Al_5O_{12}$ crystal (top) and in a phosphate glass (bottom) at 295 K.

2.3. *Radiative transitions*

Optical transitions between $4f^n$ levels used for optical pumping and stimulated emission are predominantly of electric-dipole nature. Although f–f transitions are forbidden by Laporte's rule, if the rare earth is located in a non-centrosymmetric site, odd-order terms in the expansion of the static (or dynamic) crystal-field admix states of higher, opposite-parity configurations, such as $4f^{n-1}5d$, into $4f^n$ and transitions become allowed. The oscillator strengths of transitions between J states are small, $\sim 10^{-6}$. While *ab initio* calculations of the probabilities for electric-dipole transitions are not possible, spectral intensities can be treated using the Judd–Ofelt approach discussed below.

Electric-dipole transitions between states of 4f and 5d configurations are parity-allowed. The oscillator strengths for f–d transitions are therefore much larger than for f–f transitions and have magnitudes of 10^{-1} to 10^{-2}. Emission from 5d states, while not common, has been observed for several rare earths where there is a large energy gap to lower-lying 4f states (Weber, 1973); Ce^{3+} and Eu^{2+} are notable examples. To calculate the probability for $5d \rightarrow 4f$ radiative decay by electric-dipole transitions, eigenstates and interconfigurational radial integrals are required. For an example of such calculations, see Manthey (1973).

Magnetic-dipole and electric-quadrupole transitions are allowed between states of $4f^n$ configurations and can be calculated straightforwardly, given appropriate eigenstates. Since magnetic-dipole transitions are subject to $|\Delta J| \leq 1$

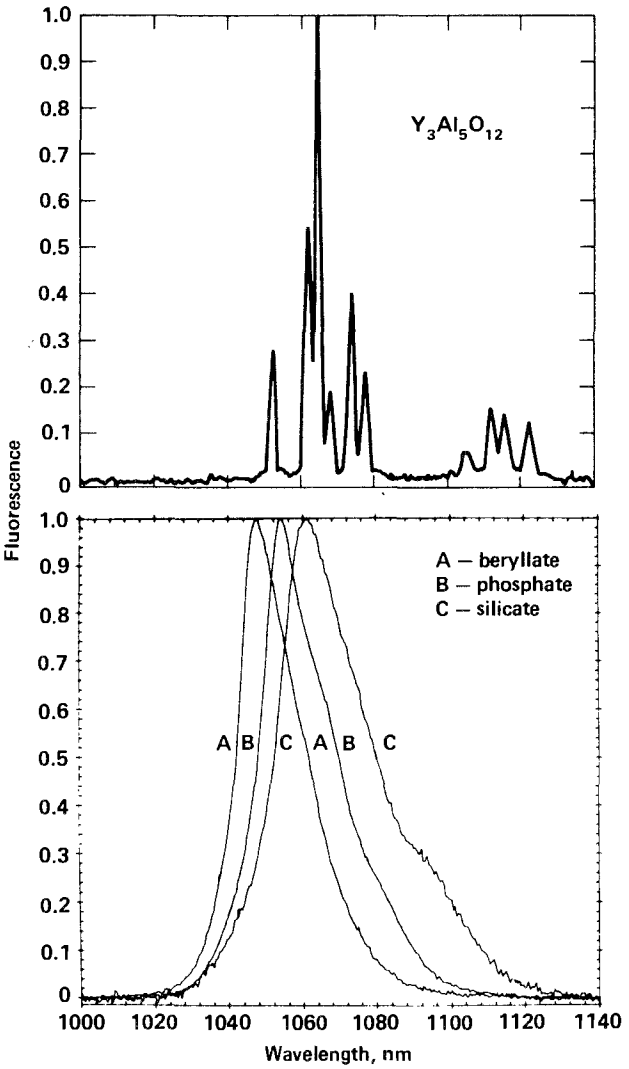

Fig. 35.6. Comparison of the $^4F_{3/2} \rightarrow {}^4I_{11/2}$ fluorescence of Nd^{3+} in a $Y_3Al_5O_{12}$ crystal (top) and in different glasses (bottom) at 295 K.

and $\Delta S = \Delta L = 0$ selection rules, they are usually only significant for intramultiplet transitions. Electric-quadrupole transitions are much less probable than dipolar processes and have not been observed for rare earth ions.

2.3.1. *Judd–Ofelt treatment*

Judd (1962) and Ofelt (1962) have shown that calculations of f–f intensities in rare-earth spectra can be made tractable by treating the excited configuration as completely degenerate. The electric-dipole line strength can then be expressed as a sum of products of phenomenological intensity parameters Ω and matrix

elements of tensor operators $U^{(t)}$ connecting states of $4f^n$. The Judd–Ofelt approach is applicable to transitions between Stark levels, however crystal-field eigenstates are frequently not available. For transitions between J manifolds, the line strength has the simple form

$$S(aJ, bJ') = e^2 \sum_{t=2,4,6} \Omega_t \langle f^n \alpha SLJ \| U^{(t)} \| f^n \alpha' S'L'J' \rangle^2. \tag{35.4}$$

The Ω parameters for a given ion-host combination are derived from a least squares fit of calculated and observed intensities. The validity of the Judd–Ofelt treatment has been tested for most trivalent rare earths in both crystals and solutions and has been applied to rare earth molecular vapors. Peacock (1975) has presented a thorough review of the Judd–Ofelt theory and experimental results.

An attractive feature of the Judd–Ofelt approach is that once the intensity parameters are determined, they can be used to calculate the probability of transitions between any $4f^n$ levels of interest for laser action. This includes absorption and fluorescence intensities, excited-state absorption, radiative lifetimes and branching ratios, and, combined with fluorescence spectra, stimulated emission cross sections (Krupke, 1974a). Best results are obtained for the lower-lying levels of $4f^n$ which are well separated from the opposite-parity configurations and thus in keeping with the approximations made by Judd and Ofelt. Since the Judd–Ofelt parameters are not expected to differ greatly for adjacent ions in the lanthanide series, estimates can be made using extrapolated Ω values.

2.4. *Nonradiative transitions*

Nonradiative transitions due to ion-phonon and ion–ion interactions affect the efficiency and performance of rare earth lasers. Relaxation by phonon processes arises from the interaction of the rare earth ion with the fluctuating crystalline or ligand field. In these processes the electronic energy of the excited rare earth is transferred to vibrational energy of the host lattice or molecule. Nonradiative relaxation between crystalline Stark levels, which are separated by tens to hundreds of cm^{-1}, occurs by one- and two-phonon processes and can be very fast, $\lesssim 10^{-12}$s. Nonradiative relaxation between J states, which may be separated by several hundreds to thousands of cm^{-1}, requires the simultaneous emission of many phonons to conserve energy and hence proceeds at much slower rates. Orbach (1975) has given a general discussion of nonradiative relaxation by one-phonon and multiphonon processes and of energy transfer by ion–ion interactions.

2.4.1. *Multiphonon processes*

Multiphonon decay rates from excited states of rare earth ions determine three important properties of rare-earth lasers: pump conversion efficiency,

radiative quantum efficiency, and the lifetime of the terminal laser level. These transitions are indicated by wavy lines in figs. 35.3 and 35.4. For transitions between 4f levels, the ion–phonon interaction is characteristic of weak coupling. Although several treatments of multiphonon relaxation processes for rare earth ions have been developed (Riseberg and Moos, 1968; Miyakawa and Dexter, 1970; Fong et al., 1972), calculations of rates are formidable and require information about crystal-field interactions and phonon dynamics which is generally not available. Studies of multiphonon emission from rare earths in several different hosts have shown, however, that the most important factor influencing the multiphonon emission rate is the energy gap to the next-lower level (see, for example, Moos, 1970). In these high-order processes, the detailed properties of the individual electronic states and phonon modes involved are averaged out.

The rate of multiphonon emission for rare earths in solids is found to exhibit an approximate exponential dependence on energy gap ΔE to the next-lower level of the form

$$W_{mp} = W(0)\exp(-a\Delta E). \tag{35.5}$$

The constants $W(0)$ and a are dependent on the host and strength of the ion-lattice coupling but not on the specific rare earth ion or electronic state. Data for multiphonon relaxation in several different crystals and in a glass are summarized in fig. 35.7. Experimental points correspond to different electronic states and ions. The numbers in parentheses are the phonon energies which, based upon the temperature dependence of multiphonon rates and vibronic spectra, appear to be most important for relaxation. In general, the major contribution to multiphonon processes involves the highest energy vibrations

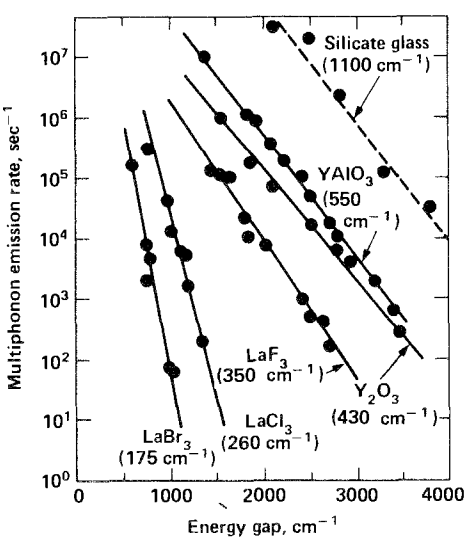

Fig. 35.7. Spontaneous multiphonon emission rates from excited states of trivalent rare earths as a function of energy gap to the next-lower level. Dominant phonon energies are shown in parentheses.

since they can conserve energy in the lowest-order process. For a given ΔE in fig. 35.7, the rates are larger as the effective phonon energy increases. The rates shown are for spontaneous phonon emission; at higher temperatures, stimulated emission becomes important and rates $W(T)$ become faster.

Once multiphonon rate data sufficient to define parameters in eq. (35.5) is obtained, the results can be used to predict nonradiative decay rates from other rare earth excited states in the same host. The only exceptions are for states where strong selection rules are operative or matrix elements are small (German and Kiel, 1973), or for the regime of small energy gaps where the statistical averaging that occurs for high-order processes no longer predominates.

The multiphonon emission rates for the silicate glass in fig. 35.7 are much faster than for the crystals. Studies of rare earths in glass demonstrate that multiphonon relaxation is due predominantly to the highest frequency vibrational modes which are associated with the glass network former (Reisfeld, 1975). In both crystalline and amorphous rare earth hosts, materials having low vibrational frequencies generally have more fluorescing levels and hence more possibilities for laser action.

For liquids and rare earth molecular vapors, high-frequency molecular vibrations are present. These lead to strong nonradiative deactivation of excited states and, as discussed in the sections on liquid and gas lasers, are a determining factor for achieving stimulated emission.

For most divalent and trivalent lanthanide ions, levels of the $4f^{n-1}5d$ configuration overlap those of the $4f^n$ configuration. Ions excited into 5d levels therefore rapidly decay nonradiatively to nearby 4f levels. Thus, 5d bands can be used for optical pumping, but because of their large absorption coefficients, pumping may be nonuniform. For other ions such as Ce^{3+}, Pr^{3+}, and Eu^{2+}, there are large energy separations from the lowest 5d level to levels of 4f and $5d \rightarrow 4f$ fluorescence is observed. These are potential laser transitions (see section 7). Investigations of nonradiative decay from 5d states of trivalent rare earths (Weber, 1973; Lauer and Fong, 1974) confirm that an intermediate-strength coupling rather than weak coupling approximation is valid for 5d relaxation.

2.4.2. *Ion–ion interactions*

Nonradiative energy transfer between like and unlike paramagnetic ions occurs at concentrations where the ion separations become small ($\lesssim$1–2 nm) and interaction via electric multipolar or exchange forces are possible. Depending upon the ions and transitions involved, this may lead to energy migration, fluorescence quenching, and fluorescence sensitization. All of these processes are observed for rare earths in solids. The relative importance of the different multipolar terms – dipole–dipole, dipole–quadrupole, quadrupole–quadrupole – varies with concentration due to their different range dependences. These processes are treated by Dexter (1953). Exchange coupling and the analysis of the time-dependence of ion–ion energy transfer are treated by Inokuti and

Hirayama (1965). Energy transfer phenomena relevant to rare earths have been reviewed recently by Kushida (1973) and Watts (1975).

To illustrate the effects of ion–ion energy transfer on rare earth laser action, again consider Nd^{3+}. Energy levels and pairs of energy-conserving transitions for two nearby ions are shown in fig. 35.8. The process at the left leads to spatial energy migration but no net relaxation. Migration has two effects: (1) Rapid energy diffusion leads to a spatial equilibrium of excitation. Since standing waves in an optical resonator can cause spatial hole-burning in the laser gain, this is ameliorated by energy migration. (2) If other ions or imperfections are present which can act as quenching centers, then relaxation may occur either via a one-step direct process or a multistep process involving energy migration and transfer. The theory for the latter process was developed by Dexter and Schulman (1954). The rate and time-dependence of the donor ion decay are dependent upon whether the process is characteristic of fast-diffusion or diffusion-limited relaxation (Weber, 1971a). Energy migration in inhomogeneously broadened glass systems is treated by Motegi and Shionoya (1973).

An important consideration for rare earth lasers and Nd^{3+} in particular is the existence of pairs of transitions which give rise to self-quenching. These are shown in fig. 35.8 and can cause serious reduction in fluorescence lifetime and quantum efficiency at rare earth concentrations $\gtrsim 1\%$. An example of this behavior is given in fig. 35.9. Similar concentration quenching curves are obtained for Nd^{3+} in other crystals and glasses. When self-quenching is present, it limits the improvement in optical pumping efficiency possible by increasing the laser ion concentration.

The rate of self-quenching for a given rare earth ion density is dependent upon the oscillator strengths and the spectral match of the two transitions. If transitions are sufficiently nonresonant, self-quenching is reduced and materials with

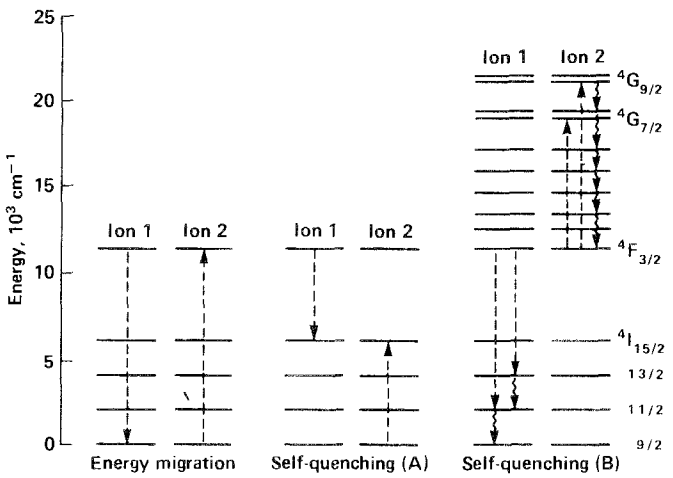

Fig. 35.8. Pairs of energy-conserving transitions for Nd^{3+} arising from ion–ion interactions.

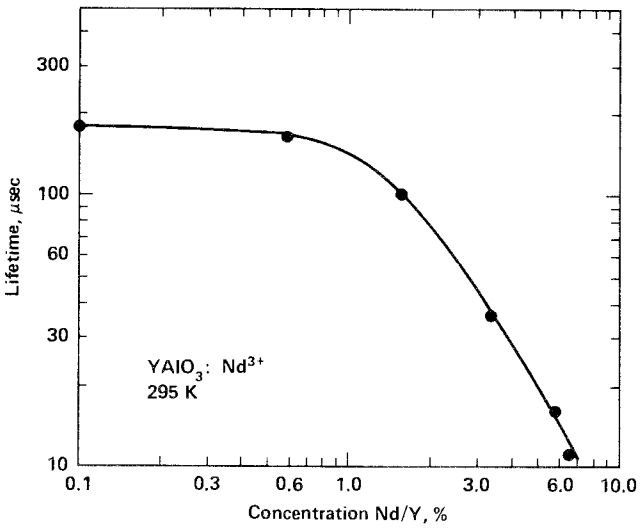

Fig. 35.9. Concentration dependence of the $^4F_{3/2}$ fluorescence lifetime of Nd^{3+} in $YAlO_3$ (from Weber et al., 1969).

Nd^{3+} concentrations up to 100% can be used for lasers; these are discussed in Section 3.3. Energy transfer is possible even when the energy differences between pairs of transitions become large. Miyakawa and Dexter (1970) predicted that the rate of phonon-assisted energy transfer should exhibit an approximately exponential dependence on energy mismatch similar to that found for multiphonon emission. This was experimentally verified by Yamada et al. (1972) for transfer between like and unlike rare earths.

Another case of self-quenching involving excited states of two ions is shown at the right in fig. 35.8. This process becomes significant only when the excited ion density is large.

Energy transfer transitions of the type illustrated in fig. 35.8 can also occur radiatively wherein a photon emitted by one ion is absorbed by a second ion. This leads to radiation trapping but not to lifetime shortening.

2.5. *Sensitized fluorescence*

The optical pumping efficiency and output power of many rare earth lasers can be increased by codoping the medium with other ions which absorb pump radiation and effectively transfer the excitation to the upper laser level. This transfer may be either radiative or nonradiative. In general, sensitization schemes used for phosphors and other luminescence phenomena are also applicable to lasers (Van Uitert, 1966). Requirements for the sensitizer ion include (a) no ground- or excited-state absorption at the laser wavelength, (b) absorption bands which complement rather than compete with absorption bands of the laser ion, since the fluorescence conversion efficiency usually is less for the former, (c) one or more metastable energy levels above the upper laser level,

and (d) no other pairs of levels which can quench the activator fluorescence*. In addition, for efficient transfer the concentration of sensitizer ions must be sufficiently high to provide significant transfer within the fluorescence lifetime of the activator.

Of possible sensitizer ions for rare earth lasers, rare earth ions have found the widest and most varied use. They have been present both as impurities and as a component of the host crystal, such as in $Ho^{3+}:Er_2O_3$ and $Nd^{3+}:CeF_3$ lasers. Ions from other transition metal groups, e.g., Cr^{3+}, Mn^{2+}, and UO_2^{2+}, have also been employed. The latter ions have broad absorption bands and, therefore, are attractive when broadband pumping sources are used. Of the many sensitization schemes reported, some offer dramatic improvement in pumping efficiency and reduced threshold while others offer only marginal improvement. The most efficient optically-pumped insulating crystal laser is the "alphabet" holmium laser: Ho^{3+} sensitized by Er^{3+}, Tm^{3+}, and Yb^{3+} (Johnson et al., 1966). The absorption bands of these ions combine to form a quasi-continuous spectrum. Via a complex cascade, energy absorbed by the various ions is eventually transferred to the $^5I_7$ lasing level of Ho^{3+}.

A list of sensitized rare earth lasers is given in table 35.2. Other rare earth sensitization schemes are known, but only those actually used for lasers are included. The laser transitions are shown later in section 3.1. For figures of the energy levels and transitions of the sensitizer and activator ions, and original references, see Weber (1971b) and Kaminskii (1975).

The concept of upconversion, which is well established in phosphors (Auzel, 1973), is one in which higher-lying states of an activator are excited by successive energy transfers from a less energetic sensitizer. This process has been

TABLE 35.2.
Ions used as sensitizers for optically-pumped rare earth lasers.

Laser ion	Laser transition	Sensitizer ion(s)
Nd^{3+}	$^4F_{3/2} \rightarrow {}^4I_{11/2}$	Ce^{3+}, Cr^{3+}, Mn^{2+}, UO_2^{2+}
Tb^{3+}	$^5D_4 \rightarrow {}^7F_5$	Gd^{3+}
Dy^{3+}	$^6H_{13/2} \rightarrow {}^6H_{15/2}$	Er^{3+}
Ho^{3+}	$^5I_7 \rightarrow {}^5I_8$	Er^{3+}, Tm^{3+}, Yb^{3+}, Cr^{3+}, Fe^{3+}, Ni^{2+}
	$^5S_2 \rightarrow {}^5I_8$	Yb^{3+} [a]
Er^{3+}	$^4I_{13/2} \rightarrow {}^4I_{15/2}$	Yb^{3+}
	$^4F_{9/2} \rightarrow {}^4I_{15/2}$	Yb^{3+} [a]
Tm^{3+}	$^3H_4 \rightarrow {}^3H_6$	Er^{3+}, Yb^{3+}, Cr^{3+}
	$^3F_4 \rightarrow {}^3H_5$	Cr^{3+}
Yb^{3+}	$^2F_{5/2} \rightarrow {}^2F_{7/2}$	Nd^{3+}

[a] Multistep upconversion process.

*As an example, the $^4F_{3/2}$ fluorescence of Nd^{3+} is sensitized by transfer via the ^5D states of Eu^{3+} but is also quenched by $^7F_0 \rightarrow {}^7F_J$ transitions of Eu^{3+} (Sharp et al., 1970).

applied to rare earth lasers by Johnson and Guggenheim (1971). The basic sensitization and lasing schemes are illustrated in fig. 35.10. The materials were codoped crystals of $BaY_{1.2}Yb_{0.75}Er_{0.05}F_8$ and $BaY_{1.4}Yb_{0.59}Ho_{0.01}F_8$. Pumping in the first case involves absorption by Yb^{3+} followed by two or more successive transfers to Er^{3+}. In the case of Ho^{3+}, comparative measurements using light of wavelengths (a) >400 nm and (b) >610 nm demonstrated that 56% of the inversion was obtained by upconversion and 44% by direct pumping of $^5S_2$ and higher states of Ho^{3+}. The upconversion sensitization technique has the potential of providing excitation for short wavelength laser action.

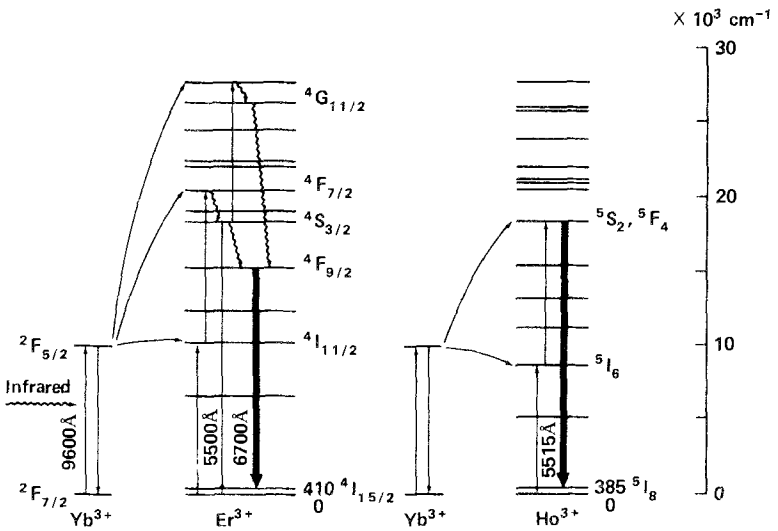

Fig. 35.10. Sensitized laser action in BaY_2F_8 using multistep infrared-to-visible upconversion (from Johnson and Guggenheim, 1971).

3. Crystal lasers

Rare earths have enjoyed their greatest utilization for lasers in optically-pumped insulating crystal environments. As shown in fig. 35.1, rare earths have already been reported to lase in 180 different ion-crystal combinations. The extremes of the laser wavelength range in fig. 35.2 were obtained from rare earths in crystals. General surveys of solid-state lasers are given by Johnson (1966), Kiss and Pressley (1966), Van Uitert (1966), and Chesler and Geusic (1972). The rare earths are generally introduced into the host crystal as a substitutional impurity in concentrations in the order of 1%. Oscillation has also been obtained with the rare earth as a stoichiometric component of the host. Among the desired properties of a host laser crystal, in addition to ability to incorporate the rare-earth ion with a homogeneous doping distribution, are high optical quality, transparency to the excitation and laser wavelengths, hardness sufficient for good optical finishing, and, in the case of high repetition rate or continuous

TABLE 35.3.
Representative types of host crystals used for rare earth lasers. See also table 35.4.

Material	Examples	Symmetry (structure)	R substitution site (symmetry)
Oxides			
Simple	Y_2O_3, Er_2O_3	cubic (bixbyite)	$Y^{3+}(C_2, C_{3i})$
	La_2O_3	hexagonal	$La^{3+}(C_{3v})$
	Gd_2O_3	monoclinic	$Gd^{3+}(C_s)$
Complex	$YAlO_3$	orthorhombic (distorted perovskite)	$Y^{3+}(C_{1h})$
	$Y_3Al_5O_{12}$	cubic (garnet)	$Y^{3+}(D_2)$
	$La_2Be_2O_5$	monoclinic	$La^{3+}(C_1)$
Molybdate	$CaMoO_4$	tetragonal (scheelite)	$Ca^{2+}(S_4)$
	$NaLa(MoO_4)_2$	tetragonal (scheelite)	$Ca^{2+}(S_4)$
	$Gd_2(MoO_4)_3$	orthorhombic	Gd^{3+}
Niobate	$LiNbO_3$	rhombohedral (illmenite)	Li^+ or Nb^{5+}
	$LaNbO_4$	monoclinic	La^{3+}
	$Ca(NbO_3)_2$	orthorhombic	Ca^{2+} [a]
Tungstate	$CaWO_4$	tetragonal (scheelite)	$Ca^{2+}(S_4)$ [a]
	$NaLa(WO_4)_2$	tetragonal (scheelite)	$La^{3+}(S_4)$
Vanadate	YVO_4	tetragonal (zircon)	$Y^{3+}(D_{2d})$
	$Ca_3(VO_4)_2$	monoclinic	Ca^{2+}
Fluorides			
Simple	CaF_2, SrF_2	cubic (fluorite)	$Ca^{2+}(O_h)$ [b]
	LaF_3, CeF_3	hexagonal (tysonite)	$La^{3+}(C_2)$
Complex	$LiYF_4$	tetragonal (scheelite)	$Y^{3+}(S_4)$
	BaY_2F_8	monoclinic	$Y^{3+}(C_{2h})$
Solid solutions	$CaF_2 + YF_3$	(yttrofluorite)	Ca^{2+}, Y^{3+}
	$5NaF \cdot 9YF_3$	(yttrofluorite)	Y^{3+}
Others			
Oxysulfide	La_2O_2S	hexagonal	$La^{3+}(C_{3v})$
Fluorapatite	$Ca_5(PO_4)_3F$	hexagonal (apatite)	$Ca^{2+}(C_{1h}, C_3)$
Oxyapatite	$CaY_4(SiO_4)_3O$	hexagonal (apatite)	Ca^{2+}, Y^{3+}
Germanate	$Ba_2MgGe_2O_7$	tetragonal (akermanite)	Ba^{2+} [a]

[a] When used as a host for trivalent rare earths, Na^+ or other ions are used for charge compensation.

[b] Charge compensation occurs in many different ways resulting in different site symmetries. For example, $Ca^{2+} \rightarrow R^{3+}$ + interstitial $F^-(C_{4v})$; $Ca^{2+} + F^- \rightarrow R^{3+} + O^{2-}(C_{3v})$.

operation, good thermal conductivity and small stress-optic coefficients. Crystals and other transparent optical materials are susceptible to damage by laser-induced electric breakdown. This phenomenon is reviewed by Bloembergen (1974).

The number of different crystalline hosts used for rare earth lasers, eliminating duplications in fig. 35.1, presently totals approximately 120. These include simple and mixed oxides, simple and mixed fluorides, and more complex compositions and structures. Examples of these crystalline hosts, together with ion site and symmetry for rare earth substitution, are given in table 35.3. Of these, the garnet $Y_3Al_5O_{12}$ (YAG) has a particularly favorable combination of being a very hard, optically isotropic crystal with sites suitable for trivalent rare earth ion substitution without charge compensation. When the substitutional sites for R^{3+} ions are divalent, such as in alkaline earth fluorides, excessive fluorine or other charge-compensating ions are added to maintain charge neutrality. The chemistry of laser crystals is discussed in detail by Nassau (1971).

In view of the high optical quality and size of lasing media required to achieve net gain, the large number of different laser crystals produced is testimony to the ability and diligence of the crystal growers. Several crystal growth techniques have been employed to prepare laser size and quality crystals. These include Czochralski (pulling from a melt), Verneuil (flame fusion), Bridgman-Stockbarger, flux growth, and zone growth. Nassau (1971) also surveys and compares the equipment, crucibles, and attendent difficulties associated with these various growth techniques.

In the subsections to follow, trivalent and divalent rare earth ions and transitions used for crystal lasers are reviewed. The literature on rare earth crystal lasers is too voluminous to attempt a comprehensive listing of all ion-crystal combinations. Instead, the following references and tables therein should be consulted: Kaminskii and Osiko (1970), Weber (1971b), and Kaminskii (1975). These articles contain references to the original work.

3.1. *Trivalent laser ions*

Trivalent lanthanide ions are used extensively for optically-pumped solid-state lasers because they possess suitable absorption bands and numerous fluorescence lines of high quantum efficiency in the visible and near-infrared. Figure 35.11 summarizes the energy levels, transitions, and approximate wavelengths of trivalent lanthanide ion lasers. In cases where the transitions are to Stark levels of the ground J-state manifold, operation at low temperatures is usually required. The number of different crystalline hosts in which each ion has lased is indicated in fig. 35.1. For several ions, stimulated emission has been observed between more than one pair of J states. A frequency-selective element (e.g., prism, grating, filter) is usually added to the resonator cavity to accomplish this.

Most trivalent rare earth crystalline lasers are operated in a pulsed mode. Continuous oscillation has been reported at room temperature for Nd^{3+} in

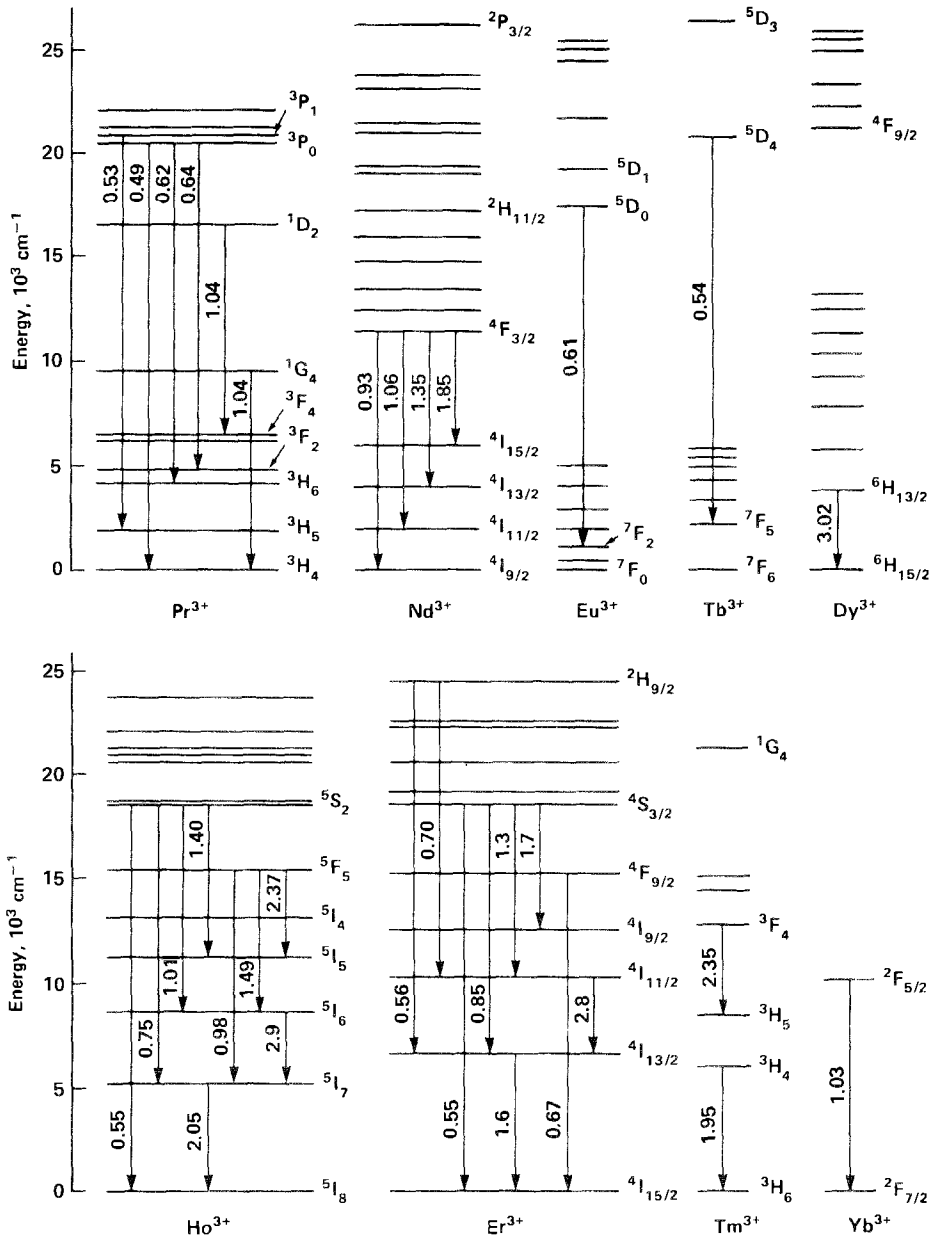

Fig. 35.11. Energy levels and laser transitions of trivalent rare earth ions. Wavelengths of transitions are in μm.

$CaWO_4$, $Y_3Al_5O_{12}$, $YAlO_3$, $Ca_5(PO_4)_3F$, La_2O_2S, $La_2Be_2O_5$, $CeCl_3$, and in stoichiometric materials discussed in Section 3.3, and at temperatures of ≤ 77 K for Ho^{3+} in $Y_3Al_5O_{12}$, Er_2O_3, CaF_2, and for Tm^{3+} in $Y_3Al_5O_{12}$, Er_2O_3, and $Er_3Al_5O_{12}$.

Comments about laser action for individual lanthanide ions are given below.

Cerium

Trivalent Ce has only two J manifolds in the $4f^1$ ground configuration, $^2F_{5/2}$ and $^2F_{7/2}$. Since the energy separation of these states is $\sim 2000\ cm^{-1}$, multiphonon emission is the dominant decay. Lasing would be possible only with special pumping conditions or materials. Intense, Stokes-shifted $5d \rightarrow 4f$ emission from Ce^{3+} is present in the near-ultraviolet and has been considered for laser action (see Section 7). Transitions to levels of $^2F_{7/2}$ provide a possible four-level laser scheme. Because of the short radiative lifetime of the lowest 5d state, an intense ultraviolet pump source or electron beam pumping may be required to achieve inversion. In addition, excited state absorption may prevent losing in some materials.

Praseodymium

Pulsed laser action is observed from several fluorescing levels at 300 K and lower temperatures. Absorption bands are intense but few in number for broadband pump sources, hence the thresholds are high. The shortest wavelength rare earth laser demonstrated is the $^3P_0 \rightarrow {}^4H_4$ transition of Pr^{3+} in $PrCl_3$ (German et al., 1973).

Neodymium

As evident from fig. 35.1, Nd^{3+} is the most extensively studied laser ion. The many absorption bands of Nd^{3+} distributed throughout the visible and rapid energy cascade to $^4F_{3/2}$ provide good optical pumping efficiency. Stimulated emission has been observed from Nd^{3+} in approximately 100 different crystals, with cross sections for the $^4F_{3/2} \rightarrow {}^4I_{11/2}$ transition ranging from $<10^{-19}$ to $16 \times 10^{-19}\ cm^2$. This provides variability with respect to gain and saturation properties.

The most widely used solid-state laser is Nd:YAG. A recent review article by Danielmeyer (1976) is devoted to the status of Nd:YAG lasers. All fluorescence transitions from $^4F_{3/2}$ to the ^4I_J states have lased in YAG. Cooling is required for $^4F_{3/2} \rightarrow {}^4I_{9/2}$ transitions; all others operate at ambient temperatures. Laser action was also observed from epitaxially-grown thin films (van der Ziel et al., 1973) and single-crystal fibers (Burrus and Stone, 1975) of Nd:YAG. While Nd:YAG is a low-threshold material, CW Nd^{3+} laser action in anhydrous $CeCl_3$ (Singh et al., 1975b) has a threshold 0.6 times that in YAG.

Various broadband lamp sources have been employed to optically pump Nd^{3+}: tungsten, mercury, xenon, and krypton. The last source provides an especially good spectral match to the near-infrared absorption bands of Nd^{3+} in YAG. To reduce lattice heating resulting from the multiphonon emission cascade to $^4F_{3/2}$, semiconductor diodes and laser sources at $\sim 0.8\ \mu m$ have been used for pumping Nd lasers. Sun-pumped Nd and chromium-sensitized Nd lasers have been

demonstrated and considered for space applications (Falk et al., 1975). Lasing of Nd^{3+} has also been reported for electron beam excitation (Voronko et al., 1971).

Promethium

This ion has no stable isotopes. The isotope Pm^{147} is a β emitter (0.22 MeV) with a half-life of 2.6 a. This radioactivity poses problems for the growth, fabrication, operation, and lifetime of a solid-state laser, and stimulated emission has not been reported.

The energy level scheme of Pm^{3+} is very similar to that of Nd^{3+} and hence is attractive for laser action. There are numerous absorption bands for optical pumping and fluorescence from the $^5F_1$ state to levels of $^5I_4$ to $^5I_8$ occurs at wavelengths ranging from ≈ 0.81 to $1.72\,\mu$m. Krupke (1972), using Judd–Ofelt intensity parameters extrapolated from Nd^{3+}, calculated fluorescence intensities and the $^5F_1$ lifetime for Pm:YAG. The most promising transitions for lasing are $^5F_1 \rightarrow {}^5I_5$ at $0.92\,\mu$m and $^5F_1 \rightarrow {}^5I_6$ at $1.09\,\mu$m, both of which have predicted oscillator strengths within 70% of the value for the $^4F_{3/2} \rightarrow {}^4I_{11/2}$ transition of Nd^{3+}.

Samarium

Stimulated emission has not been reported for trivalent samarium in any medium. There are numerous absorption bands at wavelengths $\lesssim 500$ nm, and efficient fluorescence occurs from the $^4F_{5/2}$ level. However, the emission is divided among many terminal levels and several self-quenching transitions are possible. The probability for excited-state absorption from $^4F_{5/2}$ may, in many cases, be stronger than for stimulated emission.

Europium

Only pulsed laser action at reduced temperatures has been observed from Eu^{3+}. There are no intense absorption bands in the visible. For efficient utilization of the higher-lying pump bands, a rapid nonradiative cascade through the ^5D levels is necessary to minimize fluorescence losses. Emission cross sections are small.

Gadolinium

No well-verified Gd^{3+} laser action has been reported. Fluorescence from the lowest excited level, $^6P_{7/2}$, occurs at $\sim 0.31\,\mu$m and terminates on the $^8S_{7/2}$ ground state to form a three-level lasing scheme. The high threshold for three-level operation and the requirements of good host transparency and an ultraviolet source ($\lambda \leq 0.31\,\mu$m) for optical pumping are obstacles to obtaining stimulated emission.

Terbium

The $^5D_4 \rightarrow {}^7F_5$ fluoresence has the largest branching ratio from $^5D_4$, and the transition forms a four-level laser scheme at ambient temperatures. Stimulated emission has been observed in only one crystal, $LiYF_4$ (Jenssen et al., 1973). As in the case of Eu^{3+}, the principal absorption bands for optical pumping lie in the near-ultraviolet. If these are used to excite the $^5D_4$ level, the $\approx 6000\,cm^{-1}$

$^5D_3 \rightarrow {}^5D_4$ energy gap must be efficiently bridged. In $LiYF_4$ this was done by using a high Tb concentration ($\gtrsim$20%) so that there was rapid $^5D_3 \rightarrow {}^5D_4$ decay by ion–ion interactions. The 5d bands of Tb^{3+} are the lowest-lying of the trivalent lanthanides and, if too low, they can prevent lasing due to strong, electric-dipole allowed $^5D_4 \rightarrow$ 5d excited-state absorption. In $LiYF_4$, the 5d bands are sufficiently high to avoid this difficulty; this is not the case in many other crystals. Tb:$LiYF_4$ is the shortest wavelength (544.5 nm) rare earth laser operating at room temperature.

Dysprosium

Stimulated emission from Dy^{3+} in Er^{3+}-sensitized BaY_2F_8 at 3.02 μm is the longest wavelength rare earth laser (Johnson and Guggenheim, 1973). Laser action was obtained at 77 K and involved a $^6H_{13/2} \rightarrow {}^6H_{15/2}$ transition. Fluorescence also occurs from the $^4F_{9/2}$ level located at $\sim$21 000 cm^{-1} with intense emission to $^6H_{15/2}$ and $^6H_{13/2}$, but no laser action has been reported. The comments made earlier about the absence of stimulated emission from Sm^{3+} are again apropos.

Holmium

This is the second most extensively exploited lanthanide laser ion. Stimulated emission is observed for pulsed and CW operation, for nine different transitions ranging from 0.55 to 2.9 μm, and in many crystalline hosts including the first stoichiometric laser material (HoF_3 – Devor et al., 1971) and thin films (van der Ziel et al., 1973). The most common laser transition is $^5I_7 \rightarrow {}^5I_8$, however low temperatures are required for low-threshold operation. Phonon-terminated laser action has also been reported for Ho^{3+} in BaY_2F_8 (Johnson and Guggenheim, 1974). As indicated in table 35.2, many sensitizer ions can be used to improve optical pumping efficiency of Ho^{3+}, the most successful being the combination of sensitizers cited in Section 2.5.

Erbium

The energy level scheme of Er^{3+} is similar to that of Ho^{3+}, and stimulated emission involving a like number of transitions, wavelength range, and diversity of materials is possible. Among particularly useful laser transitions are (a) $^4I_{13/2} \rightarrow {}^4I_{15/2}$, which at $\approx$1.6 μm is at a wavelength that is absorbed by the ocular media of the eye, thereby offering protection for the retina, and (b) $^4S_{3/2} \rightarrow {}^4I_{13/2}$ at $\approx$0.85 μm, which is near the peak sensitivity for S-1 photo-emissive surfaces.

Thulium

Stimulated emission has been obtained from two levels of Tm^{3+} – $^3H_4$ and $^3F_4$ – and should be obtainable from other higher-lying fluorescing levels using selective excitation into the upper laser level. Both pulsed and CW laser action were observed for the $^3H_4 \rightarrow {}^3H_6$ transition at wavelengths of $\sim$1.9 to 2.0 μm. Tm^{3+} has only a few absorption bands in the visible and energy cascade is inefficient due to the large energy gaps between J states. Er^{3+} is an effective sensitizer for $^3H_4$ laser action. Cr^{3+} has been used as a sensitizer for $^3F_4 \rightarrow {}^3H_5$ laser action.

Ytterbium

There is only one absorption band, $^2F_{5/2}$, for optically pumping $^2F_{5/2} \rightarrow {}^2F_{7/2}$ laser action. Therefore, unless a narrowband resonant source such as a light-emitting semiconductor diode is used, the thresholds for oscillation are high. Also, since stimulated emission terminates on a Stark level of the ground state manifold, low temperatures are required for low-threshold operation. Neodymium has been used as a sensitizer for Yb^{3+} with energy transfer from the $^4F_{3/2}$ state of Nd^{3+} to the $^2F_{5/2}$ state of Yb^{3+}. Because of the longer radiative lifetime of the $^2F_{5/2}$ state, Yb^{3+} provides good energy storage.

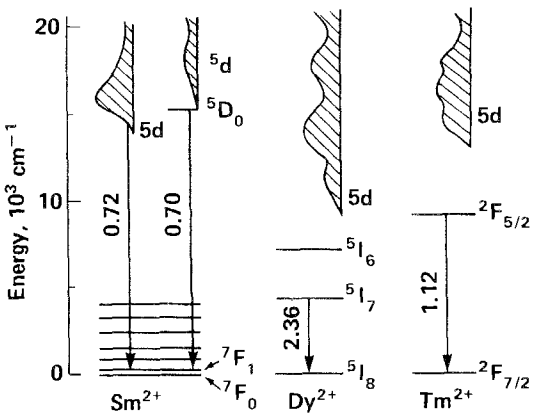

Fig. 35.12. Energy levels and laser transitions of divalent rare earth ions. Wavelengths of transitions are in μm.

3.2. *Divalent laser ions*

Figure 35.12 summarizes the energy levels, transitions, and approximate wavelengths of divalent lanthanide ion lasers. The $4f^n \rightarrow 4f^{n-1}5d$ transitions provide intense, broad absorption bands for optical pumping. Stimulated emission has involved purely electronic $4f \rightarrow 4f$ transitions for Sm^{2+}, Dy^{2+}, and Tm^{2+}; phonon-terminated transitions for Sm^{2+} in CaF_2; and $5d \rightarrow 4f$ transitions for Sm^{2+} in SrF_2 at or below liquid nitrogen temperatures. Dy^{2+} lasers have been operated CW using tungsten filament lamps, high-pressure xenon arc lamps, and sunlight as the optical excitation sources. The $Tm^{2+}:CaF_2$ laser involves a magnetic-dipole transition and has been operated in both pulsed and CW modes.

Alkaline-earth fluoride crystals have been the principal hosts for divalent lanthanide laser ions. These are relatively soft, optically isotropic materials. Rare earths occupy cubic Ca^{2+} sites. The allowed radiative transitions between 4f states are magnetic-dipole or vibronic. Since these are relatively weak, the fluorescence lifetimes are long, ~10 ms. In comparison, the fluorescence lifetime of the $5d \rightarrow 4f$ transition of $SrF_2:Sm^{2+}$, which is electric-dipole allowed, is short, $\approx 2\ \mu$s.

Of the lanthanide ions, Eu and Yb can be readily reduced to the divalent state

and remain stable in many materials. This is true to a lesser degree for Sm and Tm. For the remaining ions, special methods must be employed to reduce trivalent lanthanides to the divalent state. These include irradiation with x-rays, β and γ rays, and metal diffusion, electrolysis, and photochemical reaction. Frequently, the resulting materials are not stable with respect to thermal and photochemical effects and the ions revert back to the trivalent state.

3.3. *Stoichiometric materials*

In contrast to other lasers where the active ion is dispersed in a crystalline or glassy host, stoichiometric materials are pure chemical compounds of rare earths. Therefore, there is no question of rare earth ion size, charge, or coordination to be considered as in other laser materials. Also, since the rare earth is not a dilute substitutional impurity, the inhomogeneous broadening is very small and there is no statistical distribution of ion–ion separations. Other spectroscopic properties, including intensities and cross sections, are similar to those in other crystalline hosts.

At the high rare earth concentration present in stoichiometric materials the major question is to identify ions and compounds where the desired fluorescence is not severely quenched by the types of ion–ion interactions and processes described in section 2.4.2. The concentration quenching behavior observed for

TABLE 35.4.
Rare earth crystals used for stoichiometric lasers.

Crystal	Laser transition(s)	Wavelength (nm)	Operation*	Ref.
Pr^{3+}				
$PrCl_3$	$^3P_0 \rightarrow {}^3H_4$, $^3H_6$, $^3F_2$	489.2, 616.4, 645.2	P, ≤65 K–300 K	a
	$^3P_1 \rightarrow {}^3H_5$	529.8	P, 35 K	a
$PrBr_3$	$^3P_0 \rightarrow {}^3F_2$	640	P, 300 K	b
Nd^{3+}				
NdP_5O_{14}†	$^4F_{3/2} \rightarrow {}^4I_{11/2}$	1051	CW, 300 K	c
$LiNdP_4O_{12}$	$^4F_{3/2} \rightarrow {}^4I_{11/2}$	1048	CW, 300 K	d
$NaNdP_4O_{12}$	$^4F_{3/2} \rightarrow {}^4I_{11/2}$	1051	CW, 300 K	e
$KNdP_4O_{12}$	$^4F_{3/2} \rightarrow {}^4I_{11/2}$	1051	CW, 300 K	f
$NdAl_3(BO_3)_4$	$^4F_{3/2} \rightarrow {}^4I_{11/2}$	1065	CW, 300 K	f
Ho^{3+}				
HoF_3	$^5I_7 \rightarrow {}^5I_8$	2090	P, 77 K	g
$LiHoF_4$	$^5F_5 \rightarrow {}^5I_5$, $^5I_6$, $^5I_7$	2352, 1486, 979	P, ≈90 K	h
$Ho_3Al_5O_{12}$	$^5I_7 \rightarrow {}^5I_8$	2122, 2129	P, 90 K	i
Er^{3+}				
$LiErF_4$	$^4S_{3/2} \rightarrow {}^4I_{9/2}$	1732	P, ≈90 K	h

* P – pulsed, CW – continuous; temperature.

† Also $La_{0.5}Nd_{0.5}P_5O_{14}$ (Damen et al., 1973).

References: a. German et al. (1973); b. Varsanyi (1971); c. H.P. Weber, et al. (1973); d. Otsuka and Yamada (1975); e. Nakano et al. (1976); f. Chinn and Hong (1975); g. Devor et al. (1971); h. Morozov et al. (1975); i. Ivanov et al. (1975).

concentrated Nd materials in which Nd^{3+} ions are separated by complexes such as PO_4, BO_3, or WO_4 is similar to and not as serious as shown in fig. 35.9 for other crystals. In $La_{1-x}Nd_xP_5O_{14}$, the fluorescence lifetime was only reduced from 310 μs to 120 μs as x increased to unity. In general, for high fluorescence quantum efficiency there should be (a) sufficient spectral mismatch of transitions to reduce cross-relaxation, and (b) the absence of imperfections which can serve as quenching centers via energy migration. Suggested increases in transition probabilities through rare earth ion pairing have not been confirmed experimentally (Auzel, 1976).

Several stoichiometric hosts, laser ions, and transitions are given in table 35.4. Of the laser ions listed, Nd^{3+} has again received the most attention. Reported cross sections range from $1.8\times10^{-19}\,cm^2$ for NdP_5O_{14} to $9\times10^{-19}\,cm^2$ for $LiNdP_4O_{12}$. Continuous oscillation at room temperature has been demonstrated for several different materials. Because of the high density of active ions ($>10^{21}\,cm^{-3}$), stoichiometric laser materials are of interest for miniature solid-state oscillators and amplifiers. Thin-film lasers appropriate for integrated optics technology have also been made. Since the absorption coefficients are high, efficient optical pumping with semiconductor lasers or light-emitting diodes is possible (Chinn et al., 1976; Saruwatari et al., 1976). Resonant absorption losses in high rare earth-concentration materials can affect the threshold and slope efficiency for laser oscillation; this has been studied in $LiNdP_4O_{12}$ by Otsuka and Yamada (1976). For a review of the physics of stoichiometric materials and the applications of stoichiometric lasers, see Danielmeyer (1975).

3.4. *Polycrystalline materials, mixed crystals, and solid solutions*

In addition to single crystals, rare earth laser hosts have also included polycrystalline materials, mixed crystals, and solid solutions. For crystals which are optically isotropic, a polycrystalline form is attractive since conventional ceramic processing techniques rather than single-crystal growth can be used. Materials used to date, however, have been plagued by large optical scattering losses which reduce laser performance.

Stimulated emission from a polycrystalline host was first reported for divalent dysprosium in hot-pressed CaF_2 (Hatch et al., 1964). $CaF_2:Dy^{2+}$ material of essentially theoretical density was achieved. More recently, Greskovich and Chernock (1973) investigated a cubic solid solution of 89% Y_2O_3, 10% ThO_2, and 1% Nd_2O_3. At room temperature, the absorption and emission linewidths observed were intermediate to those measured in crystals and glasses. Residual porosity and undetermined submicroscopic scattering centers cause significant optical losses.

A mixed-crystal approach has been used by Riseberg et al. (1973) and Watts and Holton (1974) to obtain garnet materials with lower stimulated emission cross sections and gain coefficients. The authors noted that the positions of the Nd^{3+} fluorescence lines in $Y_3Al_5O_{12}$ and $Y_3Ga_5O_{12}$ are slightly different and that mixed crystals of $Y_3(Al_{1-x}Ga_x)_5O_{12}$ can be prepared which are isotropic and which maintain the garnet structure over the entire range of compositions

$0 \leq x \leq 1$. Therefore, because of the different possible distributions of Ga^{3+} ions on Al^{3+} sites, the crystal field at the Nd^{3+} sites in the mixed crystal varies between the two extremes. Spectrally, this appears as inhomogeneous line broadening and results in lower cross sections.

Another large class of crystalline materials that has been utilized for rare earth lasers is solid solutions of fluorides such as the yttrofluorite $CaF_2 + YF_3$ and ternary systems such as $CaF_2 + NaYF_4 + YF_3$. These are not definite compositions but form solid solutions with no apparent ordering of the cations. Many of these materials are characterized by large optical linewidths and spectral properties approaching those in glasses. More extensive listings of these laser materials are given by Kaminskii and Osiko (1970) and Nassau (1971).

4. Glass lasers

Most of the conditions required for obtaining stimulated emission from rare earths in crystals also apply to glasses. Glasses possess excellent optical quality, are optically isotropic, have sufficient hardness and environmental durability to retain good optical surfaces, and can be doped homogeneously with rare earths to high concentrations. In addition, glass can be cast into various sizes and shapes and clad with specially doped or index-matching glass layers. Compared to crystals, the thermal conductivity is low and temperature gradients lead to thermally-induced birefringence and optical distortion. The increased optical linewidths in glass (see figs. 35.5 and 35.6) are favorable for good pumping efficiency. The stimulated emission cross sections are smaller, however, and range between $\approx(1\text{–}5) \times 10^{-20}\,\mathrm{cm}^2$. This reduces losses by amplified spontaneous emission but increases the thresholds for laser action. Energy storage in Nd glass lasers can be high, $\sim 1\,\mathrm{J/cm}^3$. In general, crystal hosts are better for CW and high-repetition-rate operation; glasses are better for low-repetition rate, Q-switched, and large energy storage operation.

Reviews of the properties and applications of glass lasers have appeared over the years and include Snitzer and Young (1966), Patek (1968), Young (1969), and Snitzer (1973). Properties of some commercial laser glasses are tabulated by Woodcock (1971). Fluorescence from rare earths in glass is surveyed by Rindone (1966) and Reisfeld (1973). Reisfeld (1975) discusses radiative and nonradiative processes for rare earths in glass.

4.1. *Glass properties*

Inorganic glass formers include elements (S, Se, ...), simple (SiO_2, B_2O_3, P_2O_5, ...) and conditional (Al_2O_3, WO_3, ...) glass forming oxides, halides (BeF_2, AlF_3, $ZnCl_2$, ...), chalcogenides (As_2S_3, As_2Se_3, ...) and hydrogen-bonded compounds (H_2O, HCl, ...) (Rawson, 1967). Of these, only a few have been used as laser hosts – principally oxide glasses and one fluoride glass. Many glasses are ruled out because of poor physical properties and inadequate optical transmission in the wavelength region of interest. The above ion groups form the

random glass network; other compounds play the role of network modifier ions. Examples of the latter are alkali, alkaline earth, and other higher valence state cations. These ions are added to enhance glass forming and other physical/chemical properties.

Both the glass network former and network modifier ions affect the spectroscopic and laser properties of rare earths. Changes in the fluorescence width and peak wavelength with glass type are shown in fig. 35.6. Another striking illustration is given in table 35.5. Here, the alkali ion in a simple alkali disilicate glass ($M_2O:2SiO_2$, where M = Li, Na, K, Rb) was varied and the spectroscopic parameters associated with the $^4F_{3/2} \rightarrow {}^4I_{11/2}$ transition of Nd^{3+} measured. The probability for this transition is determined by the Judd–Ofelt parameters Ω_4 and Ω_6. These parameters exhibit large systematic changes through the series. This produces a decrease in the stimulated emission cross section σ and an increase in the radiative lifetime τ_R with increasing alkali ion size. There is also a small change in linewidth $\Delta\lambda$ and a small shift in the wavelength λ_p of the fluorescence peak. Systematic changes are also observed for ternary glasses – alkali alkaline-

TABLE 35.5.
Variation of spectroscopic properties of Nd^{3+} with alkali ion in alkali disilicate glass ($M_2O:2SiO_2$) (From Jacobs and Weber, 1976).

Alkali (M)	Li^+	Na^+	K^+	Rb^+
Nd^{3+} intensity parameters (10^{-20} cm^2)				
Ω_2	3.4	4.3	5.1	5.6
Ω_4	4.5	3.2	2.4	2.2
Ω_6	4.6	3.2	2.0	1.9
$^4F_{3/2} \rightarrow {}^4I_{11/2}$ fluorescence				
$\sigma(10^{-20}$ cm$^2)$	2.6	1.8	1.1	0.97
$\Delta\lambda_{eff}$ (nm)	33.8	33.4	35.6	37.7
τ_R (μs)	395	600	910	945
λ_p (nm)	1061	1060	1059	1058

with glass network and modifier ions are recorded by Jacobs and Weber (1976) and references cited therein. By such changes, laser glass compositions can be tailored to achieve, for example, high stimulated emission cross sections or high energy storage.

Rare earth ions are distributed randomly in most laser glasses. Ions which exhibit self-quenching in crystals exhibit similar behavior in glasses. Because of the random nature of the bonding strengths and angles and the complex compositions of most practical glasses, the local fields at individual rare earth sites vary considerably. This is the origin of the inhomogeneous broadening. Variations in the crystal fields in glasses have been vividly demonstrated in laser-induced fluorescence line narrowing studies of rare earths by Motegi and Shionoya (1973) and by Brecher and Riseberg (1976). In addition to site-to-site variations in the Stark splitting of rare earths in glass, the transition probabilities

for both radiative and nonradiative transitions and for energy transfer also vary (Weber et al., 1976). These give rise to non-single-exponential fluorescence decay dependences following broadband excitation.

Nonradiative decay by multiphonon emission is particularly important in glass hosts due to the existence of high-frequency vibrational modes associated with the network former molecules. The vibrational frequencies vary with glass former, being large for light ions such as boron and low for heavy ions such as tellurium. The dependence of multiphonon emission rates on glass composition has been examined by Reisfeld et al. (1975) and Layne et al. (1977). Borate glasses, with their high vibrational frequencies, are unfavorable hosts for many ions, such as Nd^{3+}, because strong multiphonon emission from the $^4F_{3/2}$ state reduces the quantum efficiency.

The index of refraction of glasses changes with composition and ranges from ≈ 1.3 for beryllium fluoride based glasses to >2 for tellurite glasses and glasses containing large polarizable ions of high atomic number such as lead and tantalum. For high-power fusion lasers, the nonlinear index coefficient n_2^* is of paramount importance (Weber, 1976). Measurements have shown the glasses with small linear indices and dispersion also have small nonlinear indices (Milam and Weber, 1976). Because (1) a major contribution to the refractive index of most glasses is due to the oxygen ions and (2) fluorine is less polarizable than oxygen, fluoride glasses are preferable for laser applications where low n_2 is important to avoid the effects of self-focusing.

Undesirable absorption bands due to transient and stable color centers are frequently induced in glasses by exposure to ultraviolet radiation from the flashlamps (Landry et al., 1971). For laser glasses in which this occurs, either the deleterious wavelengths must be removed by spectral filtering or antisolarizing agents such as cerium, antimony, or molybdenum ions added to the glass to inhibit the formation of color centers. In addition, the presence of platinum particles or other absorbing impurities in a glass can lead to damage in the intense optical fields present in lasers.

4.2. *Laser ions*

Laser action in glass has been observed only from trivalent rare earths. Because of the smaller number of metastable fluorescing states, the number of rare-earth ions lased and the spectral range covered are substantially less for glasses than for crystals. Laser ions and transitions are listed in table 35.6. Where a range of laser wavelengths is given, it arises from the use of different host glasses or temperatures. All glass laser transitions are the same as in crystalline lasers and therefore are included in fig. 35.11. For references to the original reports of glass laser action, the reader should consult the review articles cited at the beginning of this section.

* The refractive index is given by $n = n_0 + \Delta n$, where n_0 is the index normally measured with low-intensity light and Δn is the change in index induced by an intense optical beam. Δn is expressed in terms of the time-averaged optical electric-field amplitude ϵ as $n_2\langle\epsilon^2\rangle$.

The addition of sensitizer ions improves optical pumping efficiency; those actually used for glass lasers are noted in table 35.6. Many additional ions have been used to sensitize rare earth fluorescence, such as $Cr^{3+} \rightarrow Nd^{3+}$, $Cr^{3+} \rightarrow Yb^{3+}$, and $Mo^{3+} \rightarrow Er^{3+}$ (see Young, 1969, for references). Energy transfer and sensitization schemes for rare earths in glasses are discussed by Reisfeld (1973).

TABLE 35.6.
Rare earth glass lasers.

Ion	Transition	Wavelength (μm)	Sensitizer	Glasses
Nd^{3+}	$^4F_{3/2} \rightarrow {}^4I_{9/2}$	0.921		borate, silicate (77 K)
	$^4F_{3/2} \rightarrow {}^4I_{11/2}$	1.047–1.08	Mn^{2+}, UO_2^{2+}	borate, silicate, phosphate, germanate, tellurite, aluminate, fluoroberyllate
	$^4F_{3/2} \rightarrow {}^4I_{13/2}$	1.32–1.37		borate, silicate, phosphate
Ho^{3+}	$^5I_7 \rightarrow {}^5I_8$	1.95–2.08	Yb^{3+}, Er^{3+}	silicate
Er^{3+}	$^4I_{13/2} \rightarrow {}^4I_{15/2}$	1.54–1.55	Yb^{3+}	silicate, phosphate
Tm^{3+}	$^3H_4 \rightarrow {}^3H_6$	1.85–2.02	Yb^3, Er^{3+}	silicate
Yb^{3+}	$^2F_{5/2} \rightarrow {}^2F_{7/2}$	1.01–1.06	Nd^{3+}	borate, silicate

The types of host glass (network former) employed are given in the final column of table 35.6. Mixed glasses such as borosilicates and fluorophosphates have also been used for Nd^{3+} lasers. A stoichiometric material, NdP_5O_{14}, has been prepared in a glassy phase and lased (H. P. Weber et al., 1973). Because of the smaller cross sections in the glass, the laser threshold was more than five times higher than in the crystal. Neodymium lasers have been reported for glass ceramics (Müller and Neuroth, 1973; Rapp and Chrysochoos, 1973). The large fluorescence linewidths and short lifetimes of Nd^{3+} are evidence that trivalent rare earths are segregated in the residual glassy phase rather than the crystalline phases in these materials.

Of the rare earth glass lasers, Nd^{3+} has received the most effort. It is the only ion for which more than one $J \rightarrow J'$ transition has lased. The longest wavelength (1.08 μm) for $^4F_{3/2} \rightarrow {}^4I_{11/2}$ laser action is observed for Nd^{3+} in fused silica (Stone and Burrus, 1973). This material can be fabricated into fibers of micron-size diameters, can be clad, and has superior thermal properties. The solubility of Nd in pure SiO_2 is low, however. The introduction of other oxides, such as Al_2O_3, into SiO_2 improves the solubility, but the spectral and other properties become more characteristic of those in silicate glasses.

Recently thin-film waveguides of Nd silicate glass have been fabricated using an rf-sputtering technique (Chen and Tang, 1976). The spectral properties of the 1.06-μm fluorescence band for the bulk and thin-film waveguide glasses were the same. By optically pumping with a CW rhodamine 6G dye laser, large optical gains of $\sim 1\,cm^{-1}$ were obtained at 1.058 μm. This should be attractive for thin-film optical communications systems.

At the other extreme in size, lasers for fusion experiments employ long chains of Nd:glass amplifiers with rod diameters to ≈ 10 cm and elliptical disks to

30×60 cm. The total volume of Nd laser glass for multiple beam lasers can be $\gtrsim 10^6$ cm^3. Important materials properties for these high-power lasers are the nonlinear refractive index which governs the deliverable focusable power to a fusion target, the gain coefficient with affects the overall efficiency, and the stimulated emission cross section which determines the gain saturation behavior (Weber, 1976).

Ytterbium silicate glass lasers have been operated at 1.015 μm at 77 K and at 1.06 μm at 300 K, the transitions terminating on a low-lying level and the highest Stark level of the $^2F_{7/2}$ manifold, respectively. The latter wavelength is compatible with Nd^{3+} lasers. The stimulated emission cross section and gain coefficient for Yb^{3+} are smaller, however. Because the fluorescence lifetime for Yb^{3+} is longer than for Nd^{3+} (~2.2 ms versus ~0.6 ms), more energy can be stored. Yb^{3+} has only one 4f level for optical pumping. Because of the high probability for $Nd^{3+}(^4F_{3/2}) \rightarrow Yb^{3+}(^2F_{5/2})$ transfer, the good pumping efficiency of Nd^{3+} can be utilized for Yb^{3+} lasing by codoping with this ion.

Erbium glass lasers operating at ≈ 1.55 μm have been developed for applications where eye safety is an important consideration. Radiation at this wavelength is attenuated in the eye by many orders of magnitude before reaching the retina. Yb^{3+} is added as a sensitizer for Er^{3+} lasers. Further improvement in optical pumping efficiency is possible by codoping with Nd^{3+}, however Nd^{3+} also quenches the Er^{3+} $^4I_{13/2} \rightarrow {}^4I_{15/2}$ fluorescence via an energy-conserving $^4I_{9/2} \rightarrow {}^4I_{15/2}$ transition. To avoid this, laser rods were made in which the Yb^{3+}-sensitized Er^{3+} core is clad with a Nd^{3+}–Yb^{3+} codoped glass. Pump light absorbed by Nd^{3+} is transferred to Yb^{3+}, then by radiative transfer from Yb^{3+} in the cladding to Yb^{3+} in the core, and subsequently to Er^{3+}. Further descriptions of Yb^{3+} and Er^{3+} glass lasers are given by Young (1969).

5. Liquid lasers

Rare earth laser action has been obtained for two groups of liquids: metallo-organic and inorganic aprotic liquids. The first group are chelate lasers and are reviewed by Lempicki and Samelson (1966); research on aprotic materials and systems for high-power, pulsed liquid lasers are reviewed by Samelson and Kocher (1974). Stimulated emission in both liquids occurs between 4f states of trivalent rare earths. Optical pumping is via xenon-filled flashlamps in optical cavities and resonators similar to those used in solid-state lasers. Rare earth liquid lasers have only been operated pulsed.

The spectroscopic properties of rare earths in liquids are characterized by broad absorption and emission bands with linewidths which can approach those in glasses (figs. 35.5 and 35.6). Fluorescence is less prevalent than in solids because high frequency vibrations associated with the solvent cause nonradiative relaxation of excited electronic states. The thrust of liquid laser research has been directed toward finding solutions in which rare earth fluorescence is not quenched and the quantum efficiency is sufficiently high to achieve laser action.

Liquids have the additional characteristic of large changes in refractive index with temperature. Thus, thermal gradients in liquid lasers can cause optical distortions and reduction of beam quality. However, unlike solid-state lasers, the active lasing medium can be circulated to dissipate heat generated by pump excitation. In addition, laser liquids are available in large, homogeneous volumes and are free of damage problems.

5.1. *Chelates*

In chelates, the rare earth ion is complexed to several organic groups or ligands. There are two general types of compounds:

$R^{3+}[\text{ligand}]_3$ tris chelates

and

$R^{3+}[\text{ligand}]_4\text{-}Q^+$ tetrakis chelates

where Q^+ represents a cation. Chelates are soluble in many organic solvents. In the first chelate laser, Eu^{3+} had benzoylacetone ligands and piperidinium as the counter ion in an alcohol solution (Lempicki and Samelson, 1963). Lempicki (1971) lists several ligands, cations, and solvents commonly used for rare earth chelate lasers. As in the case of glasses, the wavelengths of bands in the optical spectra of rare earths exhibit small shifts with changing ligand or cation (Schimitschek et al., 1967).

TABLE 35.7.
Rare earth chelate lasers. See Lempicki (1971) for details of ligands and solvents used.

Ion	Transition	Wavelength (nm)	Temperature (°C)	Threshold (J)	Ref.
Nd^{3+}	$^4F_{3/2} \rightarrow {}^4I_{11/2}$	1057	30	300	a
Eu^{3+}	$^5D_0 \rightarrow {}^7F_2$	611–613	−150 to +30*	≳300	b, c
Tb^{3+}	$^5D_4 \rightarrow {}^7F_5$	547	30	1500	d

* Room-temperature operation was achieved using benzoyltrifluoroacetone as the ligand and acetonitrite as the solvent.

References: a. Heller (1967); b. Lempicki and Samelson (1963); c. Samelson et al. (1964); d. Bjorklund, et al. (1967).

Laser action has been reported for three rare earths – Nd^{3+}, Eu^{3+}, and Tb^{3+}. Laser transitions, wavelengths, and operating conditions are tabulated in table 35.7. The principal optical pumping for Eu^{3+} and Tb^{3+} is ascribed to absorption into the singlet state of the ligand followed by intersystem crossing to the triplet state and subsequent intermolecular transfer to an excited state of the rare earth (Lempicki and Samelson, 1966). For the Eu^{3+} and Tb^{3+} chelate lasers, rare earth concentrations were $\sim 10^{18}$ to $10^{19}\,cm^{-3}$. Since the singlet absorption is very strong at the concentration necessary for lasing, only small volumes of active

material can be pumped effectively. For the Nd chelate laser, many absorption bands of Nd^{3+} are below the ligand bands and are utilized for optical excitation.

The $^5D_0$ and $^5D_4$ emitting states of Eu^{3+} and Tb^{3+} have large energy gaps to the next-lower level; thus, nonradiative deactivation and lifetime shortening in chelate solutions is not severe. This is not the case for Nd^{3+}, however. To reduce the nonradiative decay and obtain lasing, a pentafluoropropionate *o*-phenanthroline ligand, in which the second-nearest hydrogen was replaced by fluorine, was used in a dimethylsulfoxide solvent (Heller, 1967). The lifetime of the $^4F_{3/2}$ fluorescence was still very short, only 5 μs.

The thresholds for laser action in the chelate lasers are high – several hundred joules – and the overall efficiencies are low. Searches for different ligands and cation combination have not yielded materials of good chemical stability and significantly higher efficiencies and, accordingly, research interest in rare earth chelate lasers was waned. Among the difficulties and restrictions to obtaining efficient laser action are:

(1) If the principal excitation is via the ligands, then since the triplet must be above the upper laser level of the rare earth, the singlet state must be at even higher energy which limits the usable spectrum of the pump radiation.

(2) Potential upper laser levels are limited to those having a large energy gap to the next-lower level because of the large probability for non-radiative quenching in chelate laser solutions.

5.2. *Aprotic liquids*

The fluorescence quantum efficiency of excited rare earths in most liquids is very low. To reduce fluorescence quenching due to interactions with high-frequency vibrations in liquids, solvent molecules should have no tightly bonded atoms of low atomic mass (Heller, 1966). Solvents containing hydrogen or other light atoms are, therefore, undesirable. Aprotic liquid laser materials consist of solutions of a rare-earth salt and an inorganic aprotic solvent.

The first example of this type of laser was Nd^{3+} in selenium oxychloride. Later, a less toxic and less corrosive solvent, phosphorus oxychloride, was employed. These solutions are acidified by a Lewis acid such as $SnCl_4$. Recently, laser action in phosphorus tribromide, which also has low toxicity, has been reported. $AlBr_3$ and $SbBr_3$ were added to improve the solubility of Nd.

The spectroscopic properties and chemistry of aprotic Nd^{3+} laser liquids plus references to earlier studies are discussed by Brecher and French (1973). The oscillator strengths and fluorescence lifetimes are comparable to those in solids with quantum efficiencies near unity. Since fluorescence linewidths are less than in glasses, the stimulated emission cross sections are greater (Samelson et al., 1968), although still smaller than in crystals. As an example, for Nd^{3+} in PBr_3, the $^4F_{3/2} \rightarrow {}^4I_{11/2}$ linewidth and cross section are 11.3 nm and $\sim 8 \times 10^{-20}$ cm^2, respectively; the $^4F_{3/2}$ fluorescence lifetime and quantum efficiency are 230 μs and 83% (Bondarev et al., 1976).

Aprotic liquid laser materials and references are listed in table 35.8. Thus

TABLE 35.8.
Neodymium aprotic liquid lasers.

Solvent	Transition	Wavelength (nm)	Ref.
$SeOCl_2:SnCl_4$	$^4F_{3/2} \rightarrow {}^4I_{11/2}$	1055	a
	$^4F_{3/2} \rightarrow {}^4I_{13/2}$	1330	b
$POCl_3:SnCl_4$	$^4F_{3/2} \rightarrow {}^4I_{11/2}$	1051	c
$POCl_3:ZnCl_4$	$^4F_{3/2} \rightarrow {}^4I_{11/2}$	1051	d
$POCl_2:TiCl_4$	$^4F_{3/2} \rightarrow {}^4I_{11/2}$	1053	d
$PBr_3:AlBr_3$, $SbBr_3$	$^4F_{3/2} \rightarrow {}^4I_{11/2}$	1066	e

a. Lempicki and Heller (1966); b. Heller and Brophy (1968); c. Blumenthal et al. (1968); d. Schimitschek (1968); e. Bondarev et al. (1976).

far, only Nd^{3+} has been used as the laser ion; typical Nd concentrations are $\sim 10^{20}\,cm^{-3}$. Optical pumping thresholds of <10 J are possible. Laser pulses of 40 J total energy, peak power of 200 kW, and average powers in excess of 400 W with overall efficiency of more than 2% have been reported by Samelson and Kocher (1974). Using a large $POCl_3:ZnCl_4$ liquid amplifier, giant pulses of 10 ns duration and 0.5 J energy have been amplified to a peak power of ~3 GW at an extraction efficiency of ~50% (Green et al., 1976). Thermal distortions induced in the medium by optical pumping and relatively large beam divergence (~20 mrad) are problems.

Self-focusing has not been a problem in aprotic lasers, but stimulated Brillouin and Raman scattering have been observed (Alfano et al., 1971). The thresholds for these scatterings are 35 and 100 MW/cm^2, respectively, which limits the usable flux densities in these lasers. In multimode operation, the energy converted to Raman-shifted wavelengths was reported to be <10% (Green et al., 1975).

6. Gas lasers

Gas lasers are attractive for high-power, high-efficiency systems and offer advantages of low materials cost, ability to flow the lasing medium to remove heat, and low susceptibility to damage and distortion due to high intensity optical fields. Two approaches to obtaining rare earth laser action in a gaseous media are (1) rare earth metal vapors in a gas discharge tube, and (2) rare earth molecular vapors excited optically or with an electron beam. To date, stimulated emission has been demonstrated using only the first approach.

6.1. *Metal vapors*

Stimulated emission in the infrared wavelength region has been observed from neutral and/or single-ionized atoms of four rare earths: samarium, europium,

TABLE 35.9.
Rare earth metal vapor lasers

Rare earth	Laser wavelengths (nm)	Ref.
Sm I	1912.0–4865.6 (8 lines)	a
Eu I	1759.6–6057.9 (11 lines)	a
Eu II	1002, 1016.6, 1361	b
Tm I	1304.0–2385.0 (14 lines)	a
Yb I	1032.2–4801.1 (8 lines)	a
	1478.7, 1797.7	c
Yb II	1649.8, 2437.7	a
	1271.4, 1345.3, 1805.7	c
Yb(?)	2148.0	c

a. Cahuzak (1971); b. Bokhan et al. (1973); c. Klimkin (1975).

thulium, and ytterbium. A list of rare earth vapor lasers, wavelengths, and references is given in table 35.9. Since the energy level structures for rare earth vapors are complex and comprehensive spectroscopic data is not always available, identification of some of the laser transitions and details of the mechanisms for population inversion are uncertain. Partial energy level diagrams and laser transitions for YbI and YbII, which illustrate the types of levels and optical transitions used for laser action in metal vapors, are shown in fig. 35.13. For atomic YbI, the upper laser levels are not connected to the ground state by optical transitions (dashed lines in fig. 35.13); therefore, they have small cross sections for excitation by electrons. Inelastic collisions between atoms have been proposed as playing an important role in the population inversion process (Klimkin, 1975).

Experimentally, the rare earth metal vapor is excited in a standard gas discharge tube equipped with windows and placed within an optical resonator cavity. Population inversion is obtained using current pulses up to several hundred amperes and durations of a few microseconds or longer. Buffer gases such as Ne, Ar, and He are added. Investigations of Eu and Yb vapors have shown that stimulated emission is possible over a range of buffer gas pressures as high as several hundred Torr. For atomic emission, the optimal Yb vapor pressures were 0.2 to 0.4 Torr with He buffer gas pressures of ≈ 50 Torr. For ionic emission, the optimal pressures were both lower: $(6–8) \times 10^{-2}$ Torr for Yb and 2–3 Torr for He. Rare earth vapor pressures in the other lasers were generally $< 10^{-2}$ Torr. The quantum efficiency of transitions used for stimulated emission do not exceed 40 percent. The overall electrical efficiency of the rare earth vapor laser is considerably less.

6.2. *Molecular vapors*

While laser action in rare earth molecular vapors has not been achieved, Krupke (1976) has examined cases where fluorescence of high quantum

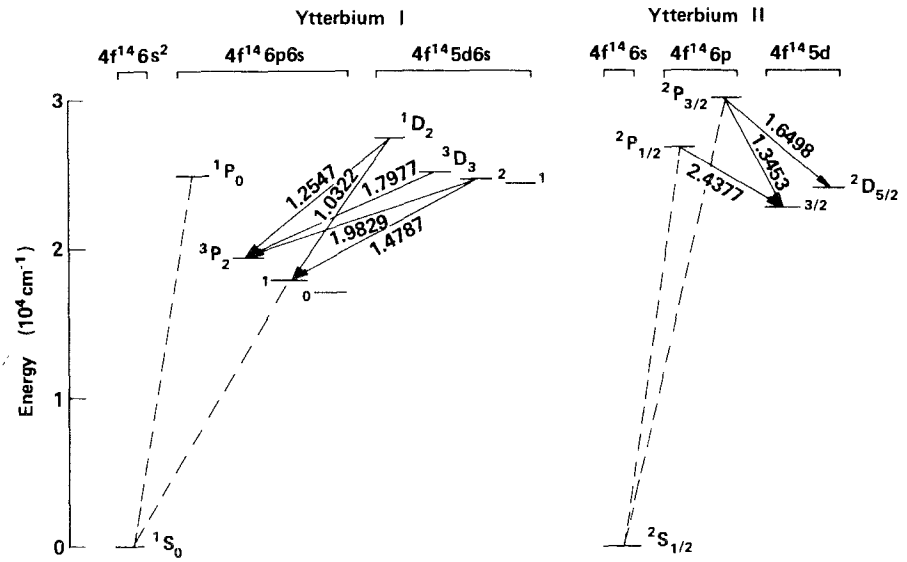

Fig. 35.13. Energy level diagrams and laser transitions for YbI and YbII vapor lasers. Wavelengths of transitions are in μm.

efficiency and suitable for stimulated emission might be achieved. Unlike metal vapors, in molecular vapors lasing would involve f–f transitions of rare earth ions. The volatility of the material should be reasonably high (~10 Torr) at operating temperatures of $\gtrsim$1000 K, yet the molecule must be stable. The molecule should not possess high-frequency vibrational modes to quench the fluorescence. Therefore again, as in aprotic liquids, light, tightly-bound atoms are to be avoided. Relaxation by bimolecular collisional processes is also a consideration in gases.

One group of candidates for molecular vapor lasers considered by Krupke is the rare earth trihalogens. The volatility of these molecules can be increased by several orders of magnitude when the rare earth trihalogens are complexed with transition metal trihalogens (Øye and Gruen, 1969). The absorption bands of rare earth trihalide, aluminum-chloride complexes are broad (Gruen, 1971). The oscillator strengths and radiative transition probabilities calculated using the Judd–Ofelt model (Krupke, 1976) are comparable to those found in liquids and solids. Quantitative experimental information about fluorescence properties is presently lacking. Knowledge of excited-state lifetimes, radiative quantum efficiencies, and linewidths and their dependence on temperature and pressure is needed to estimate attainable excited-ion densities and the potential for achieving laser action.*

A second group of candidates are vapors of rare earth chelates. Lanthanum

*Investigation of these properties is under way (R.R. Jacobs and W.F. Krupke, private communication).

chelates, such as $R(thd)_3$, have high volatility. Excitation is possible via singlet absorption in the ligands and subsequent intersystem crossing and transfer to high-lying 4f states of the rare earth. These complex hydrogen-containing molecules, however, have high-frequency vibrational modes which can promote nonradiative decay. Fluorescence quenching of Tb^{3+} in chelate vapor has been reported at temperatures of only a few hundred °C (Jacobs et al., 1975). This is attributed to relaxation via excited states of the chelate. As in liquid chelate lasers, the positions of the bands of the ligands can be critical for achieving efficient, optically-pumped laser action.

7. Concluding remarks

The energy levels and the rates and relative importance of most radiative and nonradiative processes for rare earths are now well established. With this experimental data base acquired over the past two decades, new lasing schemes can be predicted using a calculational approach. Although *ab initio* calculations are not possible, phenomenological parameters can be derived from which excitation and decay modes can be predicted and their rates estimated. This approach provides a method for prescreening promising new ion-host combinations. An example of the use of Judd–Ofelt theory and the phenomenological treatment of multiphonon relaxation to predict rare earth quantum electronic devices in solids has been given by Krupke (1974b).

To extend the wavelength coverage of rare earth lasers, several considerations are in order. At longer wavelengths there is an increasing competition between the probability for radiative transitions, which decreases as the third power of the frequency, and the probability for nonradiative transitions by multiphonon emission, which increases approximately exponentially with decreasing frequency. Thus, hosts are required which have only low-frequency vibrations, thereby limiting nonradiative decay to higher-order, less probable multiphonon processes. This reasoning was applied to obtain $^6H_{13/2} \rightarrow {}^6H_{15/2}$ laser action from Dy^{3+}, the longest wavelength solid-state rare earth laser reported to date (Johnson and Guggenheim, 1973).

To obtain laser action at shorter wavelengths, in the blue and near-ultraviolet, the availability of optical sources (incoherent or lasers) or other excitation sources (such as electron beams) with pumping rates competitive with the faster decay rates typical of higher-lying excited states will be important. One method which might be used to circumvent the need for intense, short-wavelength pump sources is multistep excitation such as shown in fig. 35.10. For higher-lying 4f levels, there are frequently more excited-state absorption possibilities to prevent oscillation. This is particularly important if $4f^{n-1}5d$ bands are nearby, since the probabilities for $f \rightarrow d$ transitions are large.

In addition to the above considerations and potential difficulties, the motivation for and value of achieving rare earth laser action at new wavelengths may, in many instances, be reduced by competition from two sources: (1) advances in

harmonic generation techniques and laser-pumped optical parametric oscillators using nonlinear crystals, and (2) the development of tunable organic dye and other lasers having more favorable properties.

Optical pumping and laser action of rare earths in condensed media have utilized f–f transitions. The only exception is the $5d \rightarrow 4f$ lasing transition of Sm^{2+}. As noted in section 2, $4f^n \rightarrow 4f^{n-1}5d$ transitions are electric-dipole allowed and thus strong absorption and optical pumping are possible. Broad, intense, Stokes-shifted $5d \rightarrow 4f$ fluorescence bands of high quantum efficiency have been observed for several divalent and trivalent rare earths. With either optical or electron-beam pumping rates sufficient to compensate for the faster decay rates and in the absence of deleterious excited-state absorption, it should be possible to obtain laser action using these emissions. Candidate ions for $5d \rightarrow 4f$ lasing include Ce^{3+}, Pr^{3+}, Sm^{2+}, Eu^{2+}, and Yb^{2+}. Recently Yang and DeLuca (1976) observed efficient vacuum-ultraviolet fluorescence from high-lying states of Nd^{3+}, Er^{3+}, and Tm^{3+} in fluoride crystals. They suggested that these $5d \rightarrow 4f$ transitions may also be utilized for tunable coherent laser sources.

Qualitatively, there are many similarities between the energy levels and spectral features of the $4f^n$ configuration of lanthanide ions and the $5f^n$ configuration of actinide ions. Hence, many of the comments and discussion of rare earth lasers in this chapter are also apropos to possible actinide lasers. Thus far, only one actinide ion – uranium – has lased, although oscillation of other actinide ions has been attempted (see, for example, Friedman and Ball, 1972). The radioactivity of most of the actinides limits the selection of ions. In comparison to the lanthanides, there is a paucity of spectroscopic and intensity data for many actinide ions. Since 5f electrons of the latter are less well shielded, the oscillator strengths of electric-dipole transitions are more intense due to greater admixing of opposite-parity states into $5f^n$. The ion-host interaction should also be stronger. Therefore, the homogeneous linewidths arising from transitions between nearby Stark levels will be larger and there will be fewer emitting states with high radiative quantum efficiencies. These properties are considerations when surveying potential candidates for actinide laser action.

In conclusion, the field of rare earth lasers is mature, but it is not exhausted. Additional laser schemes and materials will undoubtedly be exploited. For example, there are 1639 free-ion energy levels associated with the $4f^n$ configurations of the thirteen trivalent lanthanide ions. Yet, of the 192 177 possible transitions between pairs of levels, only 34 have been used for lasers. It is certain that, given suitable pump sources and materials, stimulated emission involving many more transitions can be obtained. This is particularly true with the increasing availability of lasers at new wavelengths for pump sources and of tunable lasers for selective excitation of levels.

8. Recent developments

The first observation of optical gain from a rare-earth molecular vapor has been reported by Jacobs and Krupke (1977) for the $^4F_{3/2} \rightarrow {}^4I_{11/2}$ transition of Nd^{3+} in a

neodymium chloride–aluminum chloride vapor complex. The lasing medium was excited at 587 nm by a flashlamp–pumped dye laser; the gain was probed at 1064 nm with a Nd:YAG laser. Gain coefficients $\geq 0.25\%$/cm were measured for excited-state population densities of $\approx 2 \times 10^{17}$ cm^{-3} sustained for times $\geq 10\ \mu$s. The corresponding stored energy is ≈ 35 J/l.

The $^4F_{3/2}$ fluorescence lifetimes of Nd^{3+} in the gaseous media investigated thus far are much shorter than in solids. Kinetic studies of the above Nd–Al–Cl complex (Jacobs et al., 1977, and Jacobs and Krupke, 1977) demonstrate that both of the self-quenching processes illustrated in fig. 35.8 are active. The first involves a near-resonant binary collisonal deactivation of a Nd molecule in the $^4F_{3/2}$ state by a second Nd molecule in the $^4I_{9/2}$ ground state. Under conditions of high excited-state densities in the $^4F_{3/2}$ level, $\gtrsim 10^{17}$ cm^{-3}, an even faster binary deactivation occurs which is tentatively identified as a near-resonant process involving two Nd^{3+} molecules in the $^4F_{3/2}$ level. The fluorescence decay for similar conditions of large $^4F_{3/2}$ excited-state densities in $Nd(thd)_3$ chelate vapors revealed a near-constant lifetime of $\approx 0.5\ \mu$s for varied conditions of ground and excited-state densities and temperature. A strong coupling to multiple vibrational excitation of the carrier chelate was considered responsible for this behavior (Krupke and Jacobs, 1978).

Spectral and kinetic studies of the Tb–Al–Cl complex by Hessler et al. (1977) and Krupke and Jacobs (1977) indicate that the fluorescence properties of the $^5D_4$ state of Tb^{3+} in this molecular vapor also satisfy the dynamical requirements for achieving optical gain. Rare-earth vapors are presently being considered as the amplifying medium in large lasers for inertial confinement fusion experiments.

As mentioned in the introduction, the emphasis of this article is on the spectroscopic features of rare earths in various lasing media. The most extensive application of rare earths has been in solid-state lasers. For those interested in the design and use of these lasers. a recent book by Koechner (1976) on solid-state laser engineering is recommended.

References

Alfano, R.R., A. Lempicki, and S.L. Shapiro, 1971, IEEE J. Quant. Electron. **QE-7**, 416.

Auzel, F., 1966, Compt. Rend. **262**, 1016.

Auzel, F., 1973, Proc. IEEE **61**, 758.

Auzel, F., 1976, IEEE J. Quant. Electron. **QE-10**, 258.

Bjorklund, S., G. Kellermeyer, C.R. Hunt, and N. Filipescu, 1967, Appl. Phys. Lett. **10**, 160.

Bloembergen, N., 1974, IEEE J. Quant. Electron. **QE-10**, 375.

Blumenthal, N., C.B. Ellis, and D. Grafstein, 1968, J. Chem. Phys. **48**, 5726.

Bokhan, P.A., V.M. Klimkin, and V.E. Prokop'ev, 1973, JETP Letters **18**, 44.

Bondarev, A.S., V.A. Buchenkov, V.M. Volynkin, A.A. Mak, A.A. Pogodaev, A.E. Przhevuskii, Yu. K. Sidorenko, L.N. Soms, and A.I. Stepanov, 1976, Sov. J. Quant. Electron. **6**, 202.

Brecher, C. and K.W. French, 1973, J. Phys. Chem. **77**, 1370.

Brecher, C. and L.A. Riseberg, 1976, Phys. Rev. **B13**, 81.

Burrus, C.A. and J. Stone, 1975, Appl. Phys. Lett. **26**, 318.

Cahuzac, Ph., 1971, J. Phys. **32**, 499.

Chen, Bor-Ue and C.L. Tang, 1976, Appl. Phys. Lett. **28**, 435.

Chesler, R.B. and J.E. Geusic, 1972, Solid-state ionic lasers, in: Arecchi, F.T. and E.O. Schulz-DuBois, eds., Laser Handbook, vol. 1 (North-Holland Publishing Co., Amsterdam), pp. 325–368.

Chinn, S.R. and H.Y-P. Hong, 1975, Opt. Commun. **15**, 345.

Chinn, S.R., J.W. Pierce, and H. Heckscher, 1976, Appl. Opt. **15**, 1444.

Damen, T.C., H.P. Weber, and B.C. Tofield, 1973, Appl. Phys. Lett. **23**, 519.

Danielmeyer, H.G., 1975, Stoichiometric laser materials, in: Queisser, H.J., ed., Festkörperprobleme (Advances in Solid State Physics), vol. XV (Pergamon/Vieweg, Braunschweig), pp. 253–277.
Danielmeyer, H.G., 1976, Progress in Nd: YAG lasers, in: Levine, A.K. and A.J. DeMaria, eds., Lasers, vol. 4 (Marcel Dekker, Inc., New York and Basel), pp. 1–71.
Devor, D.P., B.H. Soffer, and M. Robinson, 1971, Appl. Phys. Lett. **18**, 122.
Dexter, D.L., 1953, J. Chem. Phys. **21**, 836.
Dexter, D.L. and J.H. Schulman, 1954, J. Chem. Phys. **22**, 1063.
Dieke, G.H., 1968, Spectra and Energy Levels of Rare Earth Ions in Crystals (John Wiley and Sons, Inc., New York).
Falk, J., L. Huff, and J.D. Taynai, 1975, IEEE J. Quant. Electron. **QE-11**, 14D.
Fong, F.K., S.L. Naberhuis, and M.M. Miller, 1972, J. Chem. Phys. **56**, 4020.
Friedman, H.A. and J.T. Ball, 1972, J. Inorg. Nucl. Chem. **34**, 3928.
German, K.R. and A. Kiel, 1973, Phys. Rev. **B8**, 1846.
German, K.R., A. Kiel, and H. Guggenheim, 1973, Appl. Phys. Lett. **22**, 87.
Green, M., D. Andreou, V.I. Little, and A.C. Selden, 1975, J. Appl. Phys. **46**, 4854.
Green, M., D. Andreou, V.I. Little, and A.C. Selden, 1976, J. Phys. D: Appl. Phys. **9**, 701.
Greskovich, C. and J.P. Chernock, 1973, J. Appl. Phys. **44**, 4599.
Gruen, D.M., 1971, Prog. in Inorganic Chem **14**, 119, and references cited therein.
Hatch, S.E., W.F. Parsons, and R.J. Weagley, 1964, Appl. Phys. Lett. **5**, 153.
Heaps, W.S., L.R. Elias, and W.M. Yen, 1976, Phys. Rev. **B13**, 94.
Heller, A., 1966, Appl. Phys. Lett. **9**, 106.
Heller, A., 1967, J. Amer. Chem. Soc. **89**, 167.
Heller, A. and V. Brophy, 1968, J. Appl. Phys. **39**, 4086.
Inokuti, M. and F. Hirayama, 1965, J. Chem. Phys. **43**, 1978.
Ivanov, A.O., I.V. Mochalov, A.M. Tkachuk, V.A. Fedorov, and P.P. Feofilov, 1975, Sov. J. Quant. Electron. **5**, 115.
Jacobs, R.R., M.J. Weber, and R.K. Pearson, 1975. Chem. Phys. Lett. **34**, 80.
Jacobs, R.R. and M.J. Weber, 1976, J. Quant. Electron. **QE-12**, 102.
Jenssen, H.P., D. Castleberry, D. Gabbe, and A. Linz, 1973, IEEE J. Quant. Electron. **QE-9**, 665.
Johnson, L.F., 1966, Optically pumped pulsed crystal lasers other than ruby, in: Levine, A.K., ed., Lasers, vol. 1 (Marcel Dekker, Inc., New York).
Johnson, L.F. and K. Nassau, 1961, Proc. IRE **49**, 1704.
Johnson, L.F., J.E. Geusic, and L.G. Van Uitert, 1966, Appl. Phys. Lett. **8**, 200.
Johnson, L.F. and H.J. Guggenheim, 1971, Appl. Phys. Lett. **19**, 44.
Johnson, L.F. and H.J. Guggenheim, 1973, Appl. Phys. Lett. **23**, 96.
Johnson, L.F. and H.J. Guggenheim, 1974, IEEE J. Quant. Electron. **QE-10**, 442.
Judd, B.R., 1962, Phys. Rev. **127**, 750.
Kaminskii, A. and V. Osiko, 1970, Izv. Akad. Nauk. SSSR Neorg. Mat. **6**, 629.
Kaminskii, A.A., 1975, Laser Crystals [in Russian] (Nauka, Moscow).
Kiss, Z. and R. Pressley, 1966, IEEE Proc. **54**, 1236.
Klimkin, V.M., 1975, Sov. J. Quant. Electron. **5**, 326.
Krupke, W.F., 1972, IEEE J. Quant. Electron. **QE-8**, 725.
Krupke, W.F., 1974a, IEEE J. Quant. Electron. **QE-10**, 450.
Krupke, W.F., 1974b, New Rare Earth Quantum Electronic Devices: A Calculational Approach, IEEE Region VI Conference, Albuquerque, N.M.
Krupke, W.F., 1976, Opt. Commun. **18**, 182 and Proc. 12th Rare Earth Research Conference.
Kushida, T., 1973, J. Phys. Soc. Japan **34**, 1318, 1327, 1334.
Landry, R.J., E. Snitzer, and R.H. Bartram, 1971, J. Appl. Phys. **42**, 3827.
Lauer, H.V. and F.K. Fong, 1974, J. Chem. Phys. **60**, 274.
Layne, C.B., W.H. Lowdermilk, and M.J. Weber, 1977, Phys. Rev. **B16**, 10.
Lempicki, A. and H. Samelson, 1963, Appl. Phys. Lett. **4**, 133.
Lempicki, A. and A. Heller, 1966, Appl. Phys. Lett. **9**, 108.
Lempicki, A. and H. Samelson, 1966, Organic laser systems, in: Levine, A.K., ed., Lasers, vol. 1 (Marcel Dekker, Inc., New York), p. 181.
Lempicki, A., 1971, Rare earth liquid lasers, in: Pressley, R.J., ed., Handbook of Lasers (The Chemical Rubber Co., Cleveland), pp. 355–359.
Lengyel, B.A., 1971, Lasers, 2nd ed. (Wiley-Interscience, New York).
Loh, E., 1966, Phys. Rev. **147**, 332.
Loh, E., 1968, Phys. Rev. **175**, 533.
Manthey, W.J., 1973, Phys. Rev. **B8**, 4086.
McClure, D.S. and Z. Kiss, 1963, J. Chem. Phys. **39**, 3251.
McCumber, D.E., 1964, Phys. Rev. **136**, A954.
Milam, D. and M.J. Weber, 1976, J. Appl. Phys. **47**, 2497, and IEEE J. Quant. Electron. **QE-12**, 512.
Miyakawa, T. and D.L. Dexter, 1970, Phys. Rev. **B1**, 2961.
Moos, H.W., 1970, J. Luminescence **1**, 106.
Morozov, A.M., I.G. Podkolzina, A.M. Tkachuk, V.A. Fedorov, and P.P. Feofilov, 1975, Opt. Spectrosc. **39**, 338.
Motegi, N. and S. Shionoya, 1973, J. Luminescence **8**, 1.
Müller, G. and N. Neuroth, 1973. J. Appl. Phys. **44**, 2315.
Nakano, J.K. Otsuka, and T. Yamada, 1976, J. Appl. Phys. **47**, 2749.
Nassau, K., 1971, The chemistry of laser crystals, in: Wolfe, R., ed., Applied Solid

State Science, vol. 2 (Academic Press, New York), pp. 173–299.
Ofelt, G.S., 1962, J. Chem. Phys. **37**, 511.
Orbach, R., 1975, Relaxation and energy transfer, in: DiBartolo, B., ed., Optical Properties of Ions in Solids (Plenum Press, New York and London), pp. 355–400.
Otsuka, K. and T. Yamada, 1975, Appl. Phys. Lett. **26**, 311.
Otsuka, K. and T. Yamada, 1976, Opt. Commun. **17**, 24.
Øye, H.A. and D.M. Gruen, 1969, J. Amer. Chem. Soc. **91**, 2229.
Patek, K., 1968, Glass Lasers (Butterworth and Co., Ltd., London).
Peacock, R.D., 1975, Structure and Bonding **22**, 83.
Rapp, C.F. and J. Chrysochoos, 1973, J. Luminescence **8**, 149.
Rawson, H., 1967, Inorganic Glass-Forming Systems (Academic Press, London and New York).
Reisfeld, R., 1973, Struct. Bonding **13**, 53.
Reisfeld, R., 1975, Struct. Bonding **22**, 123.
Reisfeld, R., L. Boehm, Y. Eckstein, and N. Lieblich, 1975, J. Luminescence **10**, 193.
Rindone, G.E., 1966, Luminescence in the glassy state, in: Goldberg, P., ed., Luminescence of Inorganic Solids (Academic Press, New York), pp. 419–464.
Riseberg, L.A. and H.W. Moos, 1968, Phys. Rev. **174**, 429.
Riseberg, L.A., R.M. Brown, and W.C. Holton, 1973, Appl. Phys. Lett. **23**, 127.
Riseberg, L.A. and M.J. Weber, 1976, Relaxation phenomena in rare-earth luminescence, in: Wolf, E., ed., Progress in Optics, vol. XIV (North-Holland Publishing Co., Amsterdam).
Samelson, H., A. Lempicki, C. Brecher, and V. Brophy, 1964, Appl. Phys. Lett. **5**, 113.
Samelson, H., A. Heller, and C. Brecher, 1968, J. Opt. Soc. Am. **58**, 1054.
Samelson, H. and R. Kocher, 1974, High Energy Pulsed Liquid Laser—Final Technical Report, Contract N0014-68-C-0110 (U.S. Office of Naval Research, Washington, D.C.).
Saruwatari, M., T. Kiumira, and K. Otsuka, 1976, Appl. Phys. Lett. **29**, 291.
Schimitschek, E.J., R.B. Nerich, and J.A. Trias, 1967, J. Chem. Phys. **64**, 173.
Schimitschek, E.J., 1968, J. Appl. Phys. **39**, 6120.
Sharp, E.J., M.J. Weber, and G. Cleek, 1970, J. Appl. Phys. **41**, 364.
Singh, S., R.B. Chesler, W.H. Grodkiewicz, J.R. Potopowicz, and L.G. Van Uitert, 1975a, J. Appl. Phys. **46**, 436.
Singh, S., D.C. Miller, J.P. Potopowicz, and L.K. Shick, 1975b, J. Appl. Phys. **46**, 1191.
Smith, W.V. and P.P. Sorokin, 1966, The Laser (McGraw-Hill, New York).
Snitzer, E., 1961, Phys. Rev. Lett. **7**, 444.
Snitzer, E. and G. Young, 1966, Glass lasers, in: Levine, A.K., ed., Lasers, vol. 2 (Marcel Dekker, Inc., New York), pp. 191–256.
Snitzer, E., 1973, Amer. Ceram. Soc. Bull. **52**, 516.
Sorokin, P.P., 1964, Transitions of RE^{+2} ions in alkaline earth halide lattices, in: Grivet, P. and N. Bloembergen, eds., Quantum Electronics (Columbia University Press, New York), pp. 985–997.
Sorokin, P.P. and M.J. Stevenson, 1961, IBM J. Res. Dev. **5**, 56.
Stone, J. and C.A. Burrus, 1973, Appl. Phys. Lett. **23**, 388.
van der Ziel, J.P., W.A. Bonner, L. Kopf, S. Singh, and L.G. Van Uitert, 1973, Appl. Phys. Lett. **22**, 656.
Van Uitert, L.G., 1966, Luminescence of insulating solids for optical masers, in: Goldberg, P., ed., Luminescence of Inorganic Solids (Academic Press New York), pp. 465–539.
Varsanyi, F., 1971, Appl. Phys. Lett. **19**, 169.
Voron'ko, Yu. K., E.L. Nolle, V.V. Osiko, and M.I. Timoshechkin, 1971, JETP Letters **13**, 86.
Watts, R.K. and W.C. Holton, 1974, J. Appl. Phys. **45**, 873.
Watts, R.K., 1975, Energy transfer phenomena, in: DiBartolo, B., ed., Optical Properties of Ions in Solids (Plenum Press, New York and London), pp. 307–336.
Weber, H.P., T.C. Damen, H.G. Danielmeyer, and B.C. Tofield, 1973, Appl. Phys. Lett. **22**, 534.
Weber, M.J., M. Bass, K. Andringa, R.R. Monchamp, and E. Comperchio, 1969, Appl. Phys. Lett. **15**, 342.
Weber, M.J., 1971a, Phys. Rev. **B4**, 2932.
Weber, M.J., 1971b, Insulating crystal lasers, in: Pressley, R.J., ed., Handbook of Lasers (The Chemical Rubber Co., Cleveland), pp. 371–417.
Weber, M.J., 1973, Solid State Commun. **12**, 741.
Weber, M.J., 1976, Optical materials for neodymium fusion lasers, in: Stein, C., ed., Critical Materials Problems in Energy Production (Academic Press, New York).
Weber, M.J., J.A. Paisner, S.S. Sussman, W.M. Yen, L.A. Riseberg, and C. Brecher, 1976, J. Luminescence **12**, 729.
Woodcock, R.F., 1971, Commercial laser glasses, in: Pressley, R.J., ed., Handbook of Lasers (The Chemical Rubber Co., Cleveland), pp. 360–364.
Wybourne, B.G., 1965, Spectroscopic Properties of Rare Earths (Wiley Interscience, New York).
Yamada, N.S., S. Shionoya, and T. Kushida, 1972, J. Phys. Soc. Japan **32**, 1577.
Yang, K.H. and J.A. DeLuca, 1976, Appl. Phys. Lett. **29**, 499.
Young, C.G., 1969, Proc. IEEE **57**, 1267.

References to section 8

Hessler, J.P., F.Wagner, Jr., C.W. Williams and W.T. Carnall, 1977, J. Appl. Phys. **48**, 3260.
Jacobs, R.R. and W.F. Krupke, 1977, Appl. Phys. Lett. **32**, 31.
Jacobs, R.R., W.F. Krupke, J.P. Hessler and W.T. Carnall, 1977, Opt. Commun. **21**, 395.
Koechner, W., 1976, Solid-State Laser Engineering (Springer-Verlag, New York, Heidelberg, Berlin).
Krupke, W.F. and R.R. Jacobs, 1978, in Proc. 13th Rare Earth Research Conference (Plenum Press, New York and London).

Handbook on the Physics and Chemistry of Rare Earths, edited by K.A. Gschneidner, Jr. and L. Eyring

Chapter 36

NONRADIATIVE PROCESSES OF RARE EARTH IONS IN CRYSTALS

Francis K. FONG
Department of Chemistry, Purdue University, West Lafayette, Indiana 47907, USA

Contents

1. Introduction

The optical properties of rare earth ions in crystalline hosts have been the subject of intensive investigation over several decades. The longstanding interest may be attributed to the attractive model systems afforded by the rare earth compounds in exemplifying physical phenomena of fundamental interest. For example, the $4f^n$ configurations of the lanthanide series may be described in terms of the Russell–Saunders coupling scheme; optical spectra of rare earth systems have been subjected to many in-depth analyses, and these analyses have provided elegant case studies in atomic spectroscopy (Dieke, 1968; Judd, 1966; Wybourne, 1970). As another example, the inner 4f electrons of the lanthanides, being shielded from the host environment, can be treated in terms of the weak field case in crystal field theory. Stark splittings of electronic levels in the $4f^n$ configurations can thus be considered, in the lowest order of approximation, within the individual J manifolds. Extensions of the weak field analyses of rare earth spectra have made available a number of spectroscopic tools making use of externally applied electric and magnetic fields in the study of site symmetries in solid state problems (Fong and Wong, 1967a; Kiss and Weakliem, 1965; Rector et al., 1966).

During the last decade the study of the photophysical properties of rare earth ions in crystals has taken on a shift in emphasis, partly because of an upsurge in interest in the use of rare earth ions in optical device applications. The feasibility

considerations of laser and infrared quantum counter applications led to the question of nonradiative losses (Fong, 1975a; Fong and Miller, 1971; Fong et al., 1972; Fong and Wassam, 1973; Fong et al., 1975; Kiel, 1964; Lauer and Fong, 1974; Riseberg and Weber, 1976). The focus of the basic research has accordingly been directed away from the spectroscopic analysis of rare earth energy levels to dynamical interactions that bring about the radiationless transitions.

The present chapter is concerned with the recent developments in the treatment of two broad classes of nonradiative phenomena: (i) electron–lattice relaxation processes in which the electronic excitation within a single ion is dissipated into the vibrational modes of the host lattice; and (ii) energy transfer processes that result in the transmittance of the excitation energy from one rare earth ion to another. In (i) the relaxation phenomenon may be likened to the radiative process except that the coupling of the initial and final states in a given transition results in the emission of lattice phonons. In (ii) the transfer of excitation energy may occur via resonance or nonresonance processes. Resonance energy transfer phenomena have been extensively discussed in a recent review (Wright, 1976). Nonresonant energy transfer processes are made possible through the participation of lattice phonons in type (i) relaxation processes. The following sections provide a review of the molecular mechanisms responsible for f $\leftrightarrow$ f and f $\leftrightarrow$ d radiationless transition and energy transfer processes in rare earth doped crystals. The adiabatic theory of multiphonon transitions is outlined and its various applications in the analysis of experimental observations are described.

2. f $\leftrightarrow$ f transitions

In this section we consider the interaction of the rare earth 4f electrons with the ions of the host lattice in the adiabatic approximation. The electron-lattice Hamiltonian can be written in the form

$$\boldsymbol{H} = -(\hbar^2/2m)\sum_i (\partial^2/\partial r_i^2) + V(\boldsymbol{r}, \boldsymbol{R}) - \tfrac{1}{2}\hbar^2 \sum_j (\partial^2/M_j \partial R_j^2), \tag{36.1}$$

where $\boldsymbol{r}, \boldsymbol{R}$ are collective coordinates for the electrons and lattice ions, respectively, and $V(\boldsymbol{r}, \boldsymbol{R})$ includes all the ion–ion as well as the electron–ion interactions. The adiabatic approximation is based on the assumption that the operator for the kinetic energy of the ions can be regarded as a small perturbation. To zeroth order, the problem of finding the eigenstates of $\boldsymbol{H}$ reduces to the solution of the Schrödinger equation,

$$[-(\hbar^2/2m)\sum_i (\partial^2/\partial r_i^2) + V(\boldsymbol{r}, \boldsymbol{R})]|\alpha(\boldsymbol{r}, \boldsymbol{R})\rangle = \epsilon_\alpha(\boldsymbol{R})|\alpha(\boldsymbol{r}, \boldsymbol{R})\rangle \tag{36.2}$$

for fixed values of the ionic coordinates $\boldsymbol{R}$. The Born–Oppenheimer eigenstates $|\alpha(\boldsymbol{r}, \boldsymbol{R})\rangle$ and eigenvalues $\epsilon_\alpha(\boldsymbol{R})$ depend parametrically on $\boldsymbol{R}$. We use $\epsilon_\alpha(\boldsymbol{R})$ as the effective adiabatic potential for the ionic motion. In the harmonic approximation

the expansion of $\epsilon_\alpha(\boldsymbol{R})$, in powers of the displacements ΔR_α^j from the equilibrium positions R_0 corresponding to the electronic ground state, contains terms linear in ΔR_α^j,

$$\epsilon_\alpha(\boldsymbol{R}) = \epsilon_0^0(\boldsymbol{R}_0) + \sum_i [\partial\epsilon_\alpha(\boldsymbol{R})/\partial R_i]_{R_j=R_0^j}\Delta R_\alpha^j + \tfrac{1}{2}\sum_j [\partial^2\epsilon_\alpha(\boldsymbol{R})/\partial R_j^2]_{R_j=R_0^j}(\Delta R_\alpha^j)^2. \tag{36.3}$$

Introducing the electron and phonon annihilation and creation operators, a_α, $a_\alpha^\dagger$; b_j, $b_j^\dagger$, we can rewrite the Hamiltonian in the notation of second quantization after a canonical transformation

$$\tilde{H} = \sum_\alpha \epsilon_\alpha a_\alpha^\dagger a_\alpha + \sum_{\alpha,j} \hbar\omega_\alpha^j a_\alpha^\dagger a_\alpha b_j^\dagger b_j - \sum_{\alpha\neq\alpha',j} \hbar^2\left(\frac{\omega_j}{2M_j\hbar}\right)^{1/2} \frac{\langle\alpha|(\partial V/\partial R_j)_{R_j=R_0^j}|\alpha'\rangle}{[\epsilon_\alpha(R_j)-\epsilon_{\alpha'}(R_j)]} a_\alpha^\dagger a_{\alpha'} B_\alpha^\dagger B_{\alpha'}(b_j - b_j^\dagger) \tag{36.4}$$

where ω_α^j is the frequency of the jth normal mode of effective mass M_j when the electron is in the Born–Oppenheimer state $|\alpha\rangle$. The last term in eq. (36.4) is the nonadiabatic part of the electron–phonon coupling, arising from the kinetic energy of the ions, which gives rise to radiationless transitions between different Born–Oppenheimer states. It should be distinguished from the spin–orbit perturbation that causes transitions between states of different multiplicity. The Born–Oppenheimer states $|\alpha(\boldsymbol{r}, \boldsymbol{R}_0)\rangle$ correspond to the crystal symmetrized states formed from the appropriate $|LSJM_J\rangle$ free ion states. In eq. (36.4), the symbols $B_\alpha^\dagger$ and ϵ_α are given by

$$B_\alpha^\dagger = \exp\sum_j g_\alpha^j(b_j^\dagger - b_j), \tag{36.5}$$

$$\epsilon_\alpha = \epsilon_\alpha^0 - \sum_j g_\alpha^{j2}\hbar\omega_\alpha^j, \tag{36.6}$$

where g_α^j is a dimensionless parameter

$$g_\alpha^j = (M_j\omega_\alpha^j/2\hbar)^{1/2}\Delta R_\alpha^j. \tag{36.7}$$

It is convenient to use the Kubo time correlation function representation (Kubo et al., 1957) to evaluate the rate constant $W_{\alpha\alpha'}$ for radiationless transitions between two electronic states $|\alpha\rangle$ and $|\alpha'\rangle$. The variable in the time correlation function is the time derivative of the number operator which specifies the electron occupancy of the state $|\alpha\rangle$. In the canonically transformed representation,

$$W_{\alpha\alpha'} = (\beta\langle N_\alpha\rangle)^{-1}\int_0^\infty \mathrm{d}t \int_0^\beta \mathrm{d}\lambda\langle(\mathrm{d}\tilde{N}_\alpha/\mathrm{d}t)(-t - i\hbar\lambda)(\mathrm{d}\tilde{N}_\alpha/\mathrm{d}t)(0)\rangle_{\tilde{H}}, \tag{36.8}$$

where

$$d\tilde{N}_\alpha/dt = (i/\hbar)[\tilde{H}, \tilde{N}_\alpha]$$

$$= (-i/\hbar) \sum_{\alpha'} C^j_{\alpha\alpha'} a^\dagger_\alpha a_{\alpha'} B^\dagger_\alpha B_{\alpha'} (b_j - b^\dagger_j) + \text{h.c.}, \tag{36.9}$$

$$C^j_{\alpha\alpha'} = -\left(\frac{\hbar^3 \omega_j}{2M_j}\right)^{1/2} \frac{\langle\alpha|(\partial V/\partial R_j)_{R_j=R_j}|\alpha'\rangle}{[\epsilon_\alpha(R_j) - \epsilon_{\alpha'}(R_j)]}\bigg|_{R_j = R^j_0} \tag{36.10}$$

and the brackets indicate an average over the density operator,

$$\rho = \exp(-\beta\tilde{H})/\text{Tr}\exp(-\beta\tilde{H}). \tag{36.11}$$

Equation (36.8) is valid to arbitrary order in the nonadiabatic perturbation. For the application considered here, the interaction is small, and we evaluate $W_{\alpha\alpha'}$ to lowest order in the perturbation. For the decay rate $W_{\alpha\alpha'}$ of an ion relaxing from the initial state $|\alpha\rangle$ to the final state $|\alpha'\rangle$, after making use of the technique of parameter differentiation and operator identities, (Fong, 1975a), eq. (36.8) becomes

$$W_{\alpha\alpha'} = (\hbar^2\beta)^{-1} \int_0^\infty dt \int_0^\beta d\lambda\, Z^{\text{vib}}_{\alpha\alpha'}(t + i\hbar\lambda)(Z^{\text{vib}}_\alpha)^{-1} \exp\left[-\frac{i}{\hbar}(\epsilon_\alpha - \epsilon_{\alpha'})(t + i\hbar\lambda)\right]$$

$$\times \sum_{jk}\sum C^j_{\alpha\alpha'} C^k_{\alpha\alpha'} (\tfrac{1}{2}g_j)(\partial/\partial\lambda_j)(2/g_k)(\partial/\partial_{\lambda_k}) \Big\langle \exp 2\left[\sum_{j,k} (g_j\lambda_j$$

$$\times \exp(-x^j_{\alpha'})b^\dagger_j - g_k\lambda_k b^\dagger_k) - \sum_{j,k} 4(g_j\lambda_j \exp(x^j_{\alpha'})b_j - g_k\lambda_k b_k)\right]$$

$$\times \exp \tfrac{1}{2}\left\{\sum_{j=k} g_j g_k \lambda_j \gamma_k [\exp(x^j_{\alpha'}) - \exp(-x^j_{\alpha'})]\right\}\Big\rangle \tilde{H}^{\text{vib}}_{\alpha\alpha'}\Big|_{\lambda_j=1,\,\gamma_k=1}. \tag{36.12}$$

In eq. (36.12), $g_j = g^j_\alpha - g^j_{\alpha'}$ and $x^j_{\alpha'} = i\omega_{\alpha'}(t + i\hbar\lambda)$, with

$$\tilde{H}^{\text{vib}}_{\alpha\alpha'}(t) = \sum \hbar\omega_{\alpha\alpha'}(t) b^\dagger_j b_j, \tag{36.13}$$

$$\omega_{\alpha\alpha'}(t) = \omega^j_\alpha + \left(\frac{it}{\hbar\beta}\right)(\omega^j_\alpha - \omega^j_{\alpha'}), \tag{36.14}$$

and

$$Z^{\text{vib}}_{\alpha\alpha'}(t) = \text{Tr}\exp[-\beta\tilde{H}^{\text{vib}}_{\alpha\alpha'}(t)] = \prod_j \{1 - \exp[-\beta\hbar\omega^j_{\alpha\alpha'}(t)]\}^{-1}. \tag{36.15}$$

Using the theorem

$$\langle \exp \mathbf{0}\rangle = \exp(-\tfrac{1}{2}\langle \mathbf{0}^2\rangle), \tag{36.16}$$

where $\mathbf{0}$ is a linear form in $b^\dagger$ and b, we obtain

$$W_{\alpha\alpha'} = \hbar^{-2}\exp(-\sigma)\int_{-\infty}^{+\infty} dt \exp[h(t + i\hbar\beta)], \tag{36.17}$$

where

$$\sigma = \sum_j g_j^2(2n_\alpha^j + 1), \tag{36.18}$$

and

$$\begin{aligned} h(t + i\hbar\beta) = &- (i/\hbar)(\epsilon_\alpha - \epsilon_{\alpha'})(t + i\hbar\beta) - \ln Z_{\alpha\alpha'}^{\text{vib}}(t + i\hbar\beta) - \ln Z_\alpha^{\text{vib}} \\ &+ \sum_j g_j^2[(n_{\alpha\alpha'}^j(t + i\hbar\beta) + 1)\exp(x_{\alpha'}^j) + n_{\alpha\alpha'}^j(t + i\hbar\beta)\exp(-x_{\alpha'}^j)] \\ &- \tfrac{1}{2}\sum_j g_j^2[n_{\alpha\alpha'}^j(t + i\hbar\beta) - n_\alpha^j] \\ &+ \ln\Big[2\sum_j C_{\alpha\alpha'}^j g_j(2n_{\alpha\alpha'}^j(t + i\hbar\beta) + 1) - (n_{\alpha\alpha'}^j(t + i\hbar\beta) + 1)\exp(x_{\alpha'}^j) \\ &- n_{\alpha\alpha'}^j(t + i\hbar\beta)\exp(-x_{\alpha'}^j)\Big]^2 \\ &+ \sum_j C_{\alpha\alpha'}^{j2}[(n_{\alpha\alpha'}^j(t + i\hbar\beta) + 1)\exp(x_{\alpha'}^j) \\ &+ n_{\alpha\alpha'}^j(t + i\hbar\beta)\exp(-x_{\alpha'}^j)] \end{aligned} \tag{36.19}$$

with

$$n_{\alpha\alpha'}^j(t + i\hbar\beta) = \{\exp[\beta\hbar\omega_{\alpha\alpha'}(t + i\hbar\beta)] - 1\}^{-1}. \tag{36.20}$$

Since the number of phonon modes is very large in a macroscopic crystal, the sums in eq. (36.19) are in reality integrals over a continuum of vibronic states. The integral in eq. (36.17) can therefore be evaluated by the method of steepest descent.

In rare earth ions, the adiabatic potentials of electronic levels are minimally distorted since that we can assume $\omega_\alpha = \omega_{\alpha'}$. In this case, the imaginary part of eq. (36.14) vanishes, and we have simply

$$\omega_{\alpha\alpha'}^j(t) = \omega_\alpha^j. \tag{36.21}$$

If we further assume that there is only one dominant mode of coupling, the symbol $\Sigma_j g_j^2$ can be replaced by $L_m g_m^2$, where L_m is an effective degeneracy factor, and the subscript m denotes the effective phonon mode responsible for the radiationless process. Of the modes responsible for the decay, the highest energy optical phonon modes can be expected to make the greatest contribution. We further note that, for radiationless transitions in rare earth ions in crystals, the inequality

$$\epsilon_\alpha - \epsilon_{\alpha'} \gg L_m g_m^2 \hbar\omega_\alpha^m \tag{36.22}$$

is valid for most cases where the transitions involve electronic states within the $4f^n$ configuration. With these assumptions, we can rewrite eq. (36.17) to first order in $n_\alpha^m = [\exp(\beta\hbar\omega_\alpha^m) - 1]^{-1} < 1$,

$$W_{\alpha\alpha'} = \frac{L_m C_{\alpha\alpha'}^{m^2}}{\hbar^2} \exp(-\sigma) \int_{-\infty}^{+\infty} dt \exp[f(t + i\hbar\beta)], \tag{36.23}$$

with

$$\begin{aligned} f(t) = &-(i/\hbar)(\epsilon_\alpha - \epsilon_{\alpha'})t + L_m g_m^2[(n_\alpha^m + 1)\exp(i\omega_\alpha^m t) + n^m \exp(-i\omega_\alpha^m t)] \\ &+ \ln\{L_m g_m^2[1 + 6n_\alpha^m + (2n_\alpha^m + 1)\exp(2i\omega_\alpha^m t) - 2(3n_\alpha^m + 1) \\ &\times \exp(i\omega_\alpha^m t)] + (n_\alpha^m + 1)\exp(i\omega_\alpha^m t) + n_\alpha^m \exp(-i\omega_\alpha^m t)\}. \end{aligned} \tag{36.24}$$

The saddle point is determined by the equation for $n_\alpha^m < 1$:

$$\begin{aligned} f'(t^s) = 0 = &-(i/\hbar)(\epsilon_\alpha - \epsilon_{\alpha'}) + L_m g_m^2 i\omega_\alpha^m \exp(i\omega_\alpha^m t^s)(1 + n_\alpha^m) \\ &+ \frac{i\omega_\alpha^m + i\omega_\alpha^m (1 + n_\alpha^m) L_m g_m^2 \exp(i\omega_\alpha^m t^s)}{1 + L_m g_m^2 (1 + n_\alpha^m)\exp(i\omega_\alpha^m t^s)} \end{aligned} \tag{36.25}$$

Solving eq. (36.25) to first order in n_α^m, we obtain

$$t^s = (i\omega)^{-1} \ln[\tfrac{1}{2}(L_m g_m^2)^{-1} f (1 + n_\alpha^m)^{-1}], \tag{36.26}$$

where

$$f = (p - 3) + [(p - 1)^2 + 4]^{1/2}, \tag{36.27}$$

$$p = (\epsilon_\alpha - \epsilon_{\alpha'})/\hbar\omega_\alpha^m. \tag{36.28}$$

Differentiating eq. (36.25) with respect to t^s, evaluating eq. (36.24) at t^s, and substituting these expressions into the usual formula for the saddle-point approximation (Freed and Jortner, 1970), we obtain the final expression for the rate constant

$$W_{\alpha\alpha'} = \frac{(2\pi)^{1/2}}{\hbar^2 \omega_\alpha^m} A(L_m g_m^2, f) \exp[-pB(L_m g_m^2, f)](1 + n_\alpha^m)^p \exp(-2L_m g_m^2 n_\alpha^m), \tag{36.29}$$

where

$$A(L_m g_m^2, f) = L_m C_{\alpha\alpha}^{m^2} \{\tfrac{1}{2} f[1 + (1 + \tfrac{1}{2}f)^{-2}]\}^{-1/2} \exp(-L_m g_m^2), \tag{36.30}$$

$$B(L_m g_m^2, f) = \ln(f/2\, L_m g_m^2) - p^{-1}[\tfrac{1}{2}f + \ln(f/4\, L_m g_m^2)(2 + f)]. \tag{36.31}$$

Equation (36.29) gives explicit dependences of the many-phonon radiationless transition on the transition energy gap and temperature.

The multiphonon decay rate from a single excited level to a lower level is given in eq. (36.29). More realistically, it is necessary to consider the total radiationless relaxation rate of a lower Stark multiplet of a rare earth ion in the crystalline lattice. This total thermal average of the individual rates is

$$\bar{W} = \sum_i W_i \exp(-\Delta_i/kT) \Big/ \sum_i \exp(-\Delta_i/kT) \tag{36.32}$$

where the summation is carried over all thermally accessible states, W_i is given by eq. (36.29), and Δ_i is the energy difference between the ith level and the lowest level of the decaying multiplet. A number of measurements have been

made by Partlow and Moos (1967) and Riseberg and Moos (1968) on the temperature dependence and the energy gap dependence of multiphonon transition rates of several rare earth ions in different crystals. Specifically these measurements have been made on the F→E, A→W, E→D, K→I, and S→R, in $LaF_3:Ho^{3+}$, $LaCl^3:Dy^{3+}$, $LaBr_3:Dy^{3+}$, $LaF_3:Er^{3+}$, and $LaCl_3:Nd^{3+}$, respectively, where the notations for the transitions are taken after Carlson and Dieke (1961). Except for the $LaF_3:Ho^{3+}$ system, the Stark splittings of the energy levels involved in the radiationless transition can be readily obtained from the literature (Carlson and Dieke, 1961). In the numerical fit (Fong et al., 1972) of the experimental data, $LaF_3:Ho^{3+}$ has been accordingly omitted from consideration. In eq. (36.29) the quantities $L_m g_m^2$, $L_m C_{\alpha\alpha'}^{m^2}$, and $\hbar\omega_\alpha^m$ are effective averages, since an attempt at ab initio calculations of these quantities is not possible at present. In the numerical comparison between theory and experiment, a grid search employing the least squares criterion was carried out in the $L_m g_m^2 - L_m C_{\alpha\alpha'}^{m^2}$ parameter space using a guessed value of the effective phonon energy, $\hbar\omega_\alpha^m$, which was varied until the best fit was obtained.

The results of the numerical fit of the temperature dependence of multiphonon transition rates are displayed in figs. 36.1–36.4. The theoretical fit of the energy gap dependence of multiphonon rates in $LaCl_3$ is shown in fig. 36.5. The values of the effective parameters for the best fits are given in table 36.1.

For the temperature dependence of the rate of a given multiphonon transition, the least squares fits to the experimental data employing eq. (36.32) are excellent. (See, for example, the sums of squares given in table 36.1.) The comparison of theory and experiment, however, is not clearly satisfactory when the numerical fit involves the multiphonon rates of several rare earth ions in a given crystal, as in the fit of the energy gap dependence. The reason for this difficulty most probably arises from the fact that multiphonon transitions between different electronic levels are coupled to different phonon modes of the crystals, and the concept of a unique fit of effective parameters is, therefore, questionable. Of the effective parameters, $L_m C_{\alpha\alpha'}^{m^2}$ deserves further examination. There are rigorous

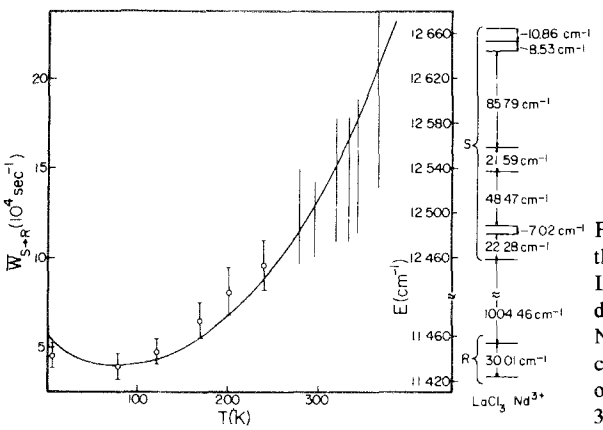

Fig. 36.1. Temperature dependence of the multiphonon rate $\bar{W}_{S\to R}$ in $LaCl_3:Nd^{3+}$ and the energy level diagram of the S and R multiplets of Nd^{3+} in $LaCl_3$. The solid curve is calculated from eq. (36.32) using the values of $L_m g_m^2$, $L_m C_{\alpha\alpha'}^{m^2}$, and $\hbar\omega_\alpha^m$ given in table 36.1.

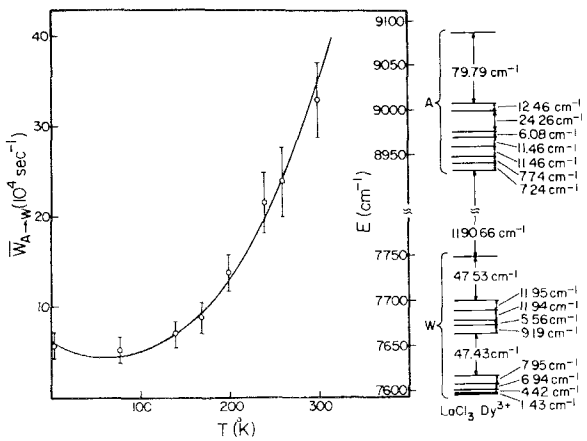

Fig. 36.2. Temperature dependence of the multiphonon rate $\bar{W}_{A\to W}$ in $LaCl_3:Dy^{3+}$ and the energy level diagram of the A and W multiplets of Dy^{3+} in $LaCl_3$. The solid curve is calculated from eq. (38.32) using the values of $L_m g_m^2$, $L_m C_{\alpha\alpha'}^{m^2}$, and $\hbar\omega_\alpha^m$ given in table 36.1.

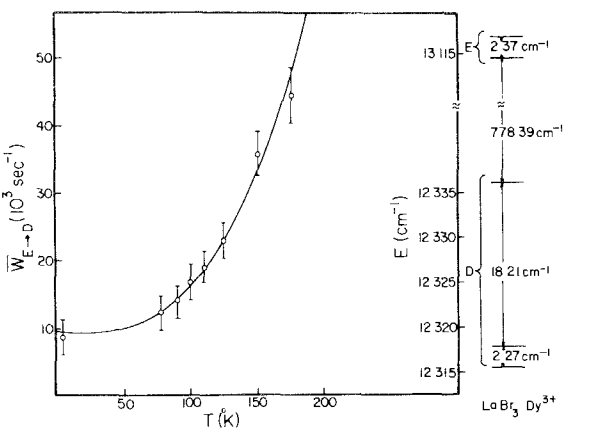

Fig. 36.3. Temperature dependence of the multiphonon rate $\bar{W}_{E\to D}$ in $LaBr_3:Dy^{3+}$ and the energy level diagram of the E and D multiplets of Dy^{3+} in $LaCl_3$. The solid curve is calculated from eq. (38.32) using the values of $L_m g_m^2$, $L_m C_{\alpha\alpha'}^{m^2}$, and $\hbar\omega_\alpha^m$ given in table 36.1.

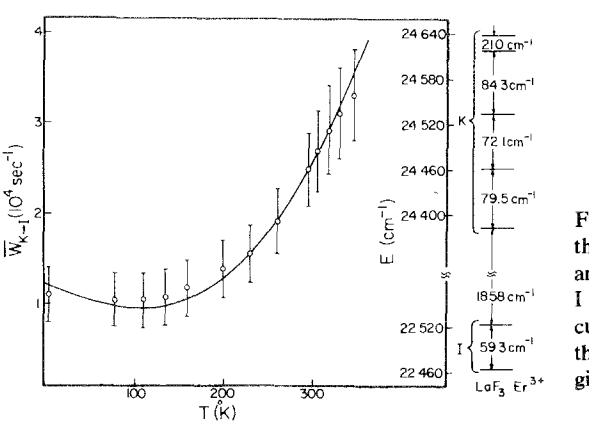

Fig. 36.4. Temperature dependence of the multiphonon rate $\bar{W}_{K\to I}$ in $LaF_3:Er^{3+}$ and the energy level diagram of the K and I multiplets of Er^{3+} in LaF_3. The solid curve is calculated from eq. (36.32) using the values of $L_m g_m^2$, $L_m C_{\alpha\alpha'}^{m^2}$, and $\hbar\omega_\alpha^m$ given in table 36.1.

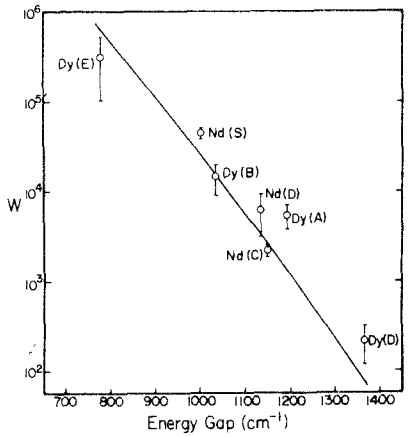

Fig. 36.5. Transition energy gap dependence of 4.2 K multiphonon rates of rare-earth ions in $LaCl_3$. The solid curve is calculated from eq. (36.29) using the values of $L_m g_m^2$, $L_m C_{\alpha\alpha'}^{m2}$, and $\hbar\omega_\alpha^m$ given in table 36.1.

selection rules which govern the coupling of the electronic levels by the phonon modes. It is well known, for example, that radiationless transitions between $|J = 1\rangle$ and $|J = 0\rangle$ crystal states are suppressed in certain symmetries. This is probably the cause for the difficulty encountered in arriving at theoretical fits of energy gap data where different electronic levels in different rare earth ions are involved. A study of the selection rules for the coupling of electronic states through lattice phonon modes in individual cases should be of interest in future investigations.

It is interesting to compare the effective phonon energy $\hbar\omega_\alpha^m$ with the maximum cutoff phonon energy (table 36.1). In all cases where convergence is attained in the least squares fit, the effective phonon energy is invariably somewhat lower than the maximum cutoff energy.

TABLE 36.1.

Numerical values of the effective parameters and sums of squares for the best curve fits. The first four rows correspond to temperature dependence calculations; the fifth row corresponds to an energy gap calculation.

	$L_m g_m^2$	$L_m C_{\alpha\alpha'}^{m2}$	$\hbar\omega_\alpha^m(\mathrm{cm}^{-1})$	Phonon energy cut off (cm^{-1})	Sum of squares
$LaCl_3:Nd^{3+}$	0.036	2.0×10^{-32}	238	260	6.98
$LaCl_3:Dy^{3+}$	0.037	3.2×10^{-31}	220	260	1.23
$LaBr_3:Dy^{3+}$	0.045	3.2×10^{-32}	155	175	1.20
$LaF_3:Er^{3+}$	0.036	2.9×10^{-28}	310	360	.93
$LaCl_3$	0.051	1.5×10^{-33}	260	260	24.4

3. d ↔ f transitions

Due to the fact that the inner $4f^n$ configurations of the lanthanide ions are well shielded from the environment, it is reasonable to envisage the f→f decay in the

weak coupling limit. The numerical fit of the theory to experiment given in figs. 36.1–36.5 appears to support the validity of this asymptotic behavior. States belonging to the $4f^{n-1}5d$ configuration, being sensitive to the crystalline field effects of the surrounding lattice, are expected to be prescribed by adiabatic potential surfaces whose equilibrium positions undergo larger displacements relative to those corresponding to the states of the $4f^n$ configuration. It is well known that while the crystal field splittings of the $4f^n$ states are typically on the order of $10^2\,cm^{-1}$, the corresponding splittings characteristic of the 5d states are usually on the order of $10^5\,cm^{-1}$. The larger displacements in the adiabatic potential minima of the 5d states are readily evidenced in the Franck-Condon progression often observed in the f→d absorption bands (Fong and Wong, 1967b). The derivation of the rate constant must therefore be generalized in order to obtain a reasonable description of d ↔ f transitions.

Upon rearrangement, eq. (36.17) can be rewritten

$$W = \hbar^{-2}L|C|^2 \exp\left[-\tfrac{1}{4}Lg^2(2n+1)\right] \sum_{\nu=-2}^{+2} \lambda_\nu \int_{-\infty}^{\infty} dt \exp f_\nu(t + i\hbar\beta), \tag{36.33}$$

where

$$f_\nu(t) = f_\nu(t' + i\hbar\beta) = (-i/\hbar)\Delta(t' + i\hbar\beta) + Lg^2 \cosh(i\omega t' - \tfrac{1}{2}\beta\hbar\omega)/\sinh(\tfrac{1}{2}\beta\hbar\omega), \tag{36.34}$$

with

$$\Delta_\nu = \epsilon_\alpha - \epsilon_{\alpha'} - \nu\hbar\omega, \tag{36.35}$$

$$\lambda_0 = Lg^2[6n(n+1)+1], \tag{36.36}$$

$$\lambda_1 = -2Lg^2(2n+1)(n+1) + n + 1, \tag{36.37}$$

$$\lambda_{-1} = -2Lg^2(2n+1)n + n, \tag{36.38}$$

$$\lambda_2 = Lg^2(n+1)^2, \tag{36.39}$$

$$\lambda_{-2} = Lg^2n^2. \tag{36.40}$$

In eqs. (36.33)–(36.40), the indices m, α, and α' have been suppressed in most cases for the sake of simplicity of notation.

The time integration in eq. (36.33) can be performed using the saddle point approximation. At the saddle point t_ν^s

$$df_\nu(t_\nu^s)/dt = 0 = (-i/\hbar)\Delta_\nu + i\omega Lg^2 \sinh(i\omega t_\nu^s - \tfrac{1}{2}\beta\hbar\omega)/\sinh(\tfrac{1}{2}\beta\hbar\omega), \tag{36.41}$$

from which we obtain

$$t_\nu^s = -\tfrac{1}{2}i\beta\hbar + \frac{1}{\omega}\ln[x + (x^2+1)^{1/2}], \tag{36.42}$$

where

$$x = 4\Delta_\nu \sinh(\tfrac{1}{2}\beta\hbar\omega)/Lg^2\hbar\omega. \tag{36.43}$$

Evaluation of $f_\nu''(t_\nu^s)$ at the saddle point gives

$$f_\nu''(t_\nu^s) = -\tfrac{1}{4}Lg^2\omega^2 \cosh(i\omega t_\nu^s - \tfrac{1}{2}\beta\hbar\omega)/\sinh(\tfrac{1}{2}\beta\hbar\omega). \tag{36.44}$$

The final result for the radiationless relaxation rate can now be cast in the form

$$W = [(2\pi)^{1/2}\hbar^{-2}L|C_{\alpha\alpha'}|^2] \sum_{\nu=-2}^{2} \lambda_\nu [-f''_\nu(t^s_\nu)]^{-1/2} \exp[-Lg^2(2n+1) + f_\nu(t^s_\nu)]. \quad (36.45)$$

Combining eqs. (36.34), (36.44), and (36.45), we obtain (Lauer and Fong, 1974)

$$\begin{aligned} W = {} & [(2\pi)^{1/2}\hbar^{-2}L|C|^2] \sum_{\nu=-2}^{2} \lambda_\nu [\sinh(\tfrac{1}{2}\beta\hbar\omega)/Lg^2\omega^2(x^2+1)^{1/2}]^{1/2} \\ & \times \exp[-L_m g_m^2(2n_m+1) + (\Delta_\nu/\hbar\omega)\tfrac{1}{2}\beta\hbar\omega - \ln[x + (x^2+1)^{1/2}] \\ & + Lg^2(x^2+1)^{1/2}/\sinh(\tfrac{1}{2}\beta\hbar\omega)], \end{aligned} \quad (36.46)$$

where Δ_ν and x are respectively defined in eqs. (36.35) and (36.43), and the coefficients λ_ν are given in eqs. (36.36)–(36.40). Under the conditions of the low-temperature strong coupling limit

$$\beta\hbar\omega \gg 1 \qquad \text{and} \qquad S = \Delta_{\nu=0}/Lg^2\hbar\omega \gg 1,$$

eq. (36.46) reduces identically to eq. (36.29).

In the present section, eq. (36.46) is applied (Lauer and Fong, 1974) to the numerical analysis of the experimental measurements of the 4f→4f radiationless decay rates of $Eu^{3+}(^5D_3 \rightarrow {}^5D_2)$, $Ho^{3+}(^5I_6 \rightarrow {}^5I_7)$, and $Er^{3+}(^4I_{11/2} \rightarrow {}^4I_{13/2})$ in $YAlO_3$ (Weber, 1973a) and the 5d→4f radiationless relaxation rate of Pr^{3+} in $Y_3Al_5O_{12}$ (Weber, 1973b). The analysis is carried out in a manner similar to that described in the preceding section, except that a thermal average over the initial and final states has not been performed due to the lack of detailed information of the Stark splittings. The energy gap $\Delta_{\nu=0}$ is thus an effective average. The parameters for the numerical fits are given in table 36.2.

The fit of eq. (36.46) to the relaxation data of $Er^{3+}(^4I_{11/2} \rightarrow {}^4I_{13/2})$ in $YAlO_3$ is shown in fig. 36.6. The temperature dependence of the relaxation rate is seen to be a sensitive function of $\hbar\omega$. The fit for $\hbar = 570\ cm^{-1}$ (solid curve) is in excellent agreement with experiment, while the fits using $\hbar\omega = 480$ and $700\ cm^{-1}$ (two possible phonon energies indicated by vibronic spectra (Weber, 1973a) while maintaining the same values for the other parameters ($\Delta_{\nu=0}$, Lb^2, and $L|C|^2$) result in temperature dependences that are clearly in disagreement with the experiment. Excellent fit between theory and experiment is also obtained for the

TABLE 36.2.
Numerical values of the effective parameters for several rare-earth f→f and d→f radiationless transitions in $YAlO_3$ and $Y_3Al_5O_{12}$.

Transition	$\Delta_{\nu=0}$ (cm^{-1})	Lg^2	$L\|C\|^2$($ergs^2$)	$\hbar\omega$(cm^{-1})	S
$YAlO_3:Er^{3+}$ ($^4I_{11/2} \rightarrow {}^4I_{13/2}$)	3400	0.025	9.3×10^{-29}	570	59.65
$YAlO_3:Ho^{3+}$ ($^5I_6 \rightarrow {}^5I_7$)	3200	0.025	1.1×10^{-31}	585	54.70
$YAlO_3:Eu^{3+}$ ($^5D_3 \rightarrow {}^5D_2$)	2700	0.025	1.4×10^{-32}	585	46.15
$Y_3Al_5O_{12}:Pr^{3+}$ (5d→4f)	10000	3.1	8.5×10^{-23}	350	2.29

$Y_3Al_5O_{12}:Pr^{3+}$

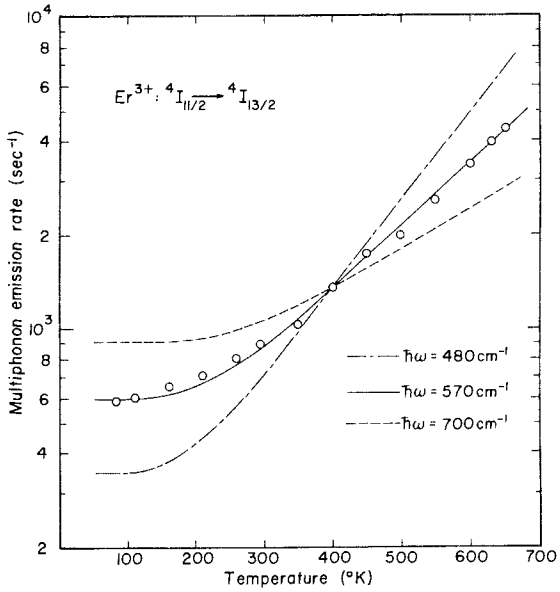

Fig. 36.6. Numerical comparison of eq. (36.46) to the experimentally observed rates of the radiationless Er^{3+} $^4I_{11/2} \rightarrow {}^4I_{13/2}$ transition in $YAlO_3$. The relevant parameters are given in table 36.2.

$Eu^{3+}(^5D_3 \rightarrow {}^5D_2)$ and $Ho^{3+}(^5I_6 \rightarrow {}^5I_7)$ relaxation processes in $YAlO_3$ (see fig. 36.7).

In all the three cases where $f \rightarrow f$ radiationless couplings are involved, the best-fit parameters are in close agreement with those listed in table 36.1 for the weak coupling limit treatment of rare earth relaxation in lanthanum halides. The electronic coupling parameters $L|C|^2$ (table 36.2) are seen to fall approximately in the range $5.3 \times 10^{-29} - 2.1 \times 10^{-33}$ erg^2 found in the weak coupling study detailed in ch. 36 section 2. The $Lg^2 = 0.025$ value is indistinguishable from the average value $Lg^2 = 0.04$ given in table 36.1. (Increasing the value of Lg^2 from 0.1 to

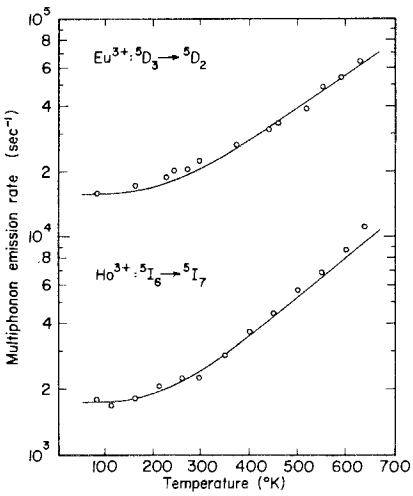

Fig. 36.7. Numerical comparison of eq. (36.46) to the experimentally observed rates of the radiationless Eu^{3+} $^5D_3 \rightarrow {}^5D_2$ and Ho^{3+} $^5I_6 \rightarrow {}^5I_7$ transitions in $YAlO_3$.

0.2 in our present analysis decreases the ratio of the decay rate at 650 K to that at 100 K by approximately 2%). The effective mediating phonon energy $\hbar\omega = 570$–$585\ \mathrm{cm}^{-1}$ falls somewhat below the $\sim 625\ \mathrm{cm}^{-1}$ peak of the observed (Weber, 1973a) maximum energy phonon band.

Reasonably good agreement between theory and experiment is also observed for the Pr^{3+} 5d→4f relaxation in $Y_3Al_5O_{12}$ (see fig. 36.8). In this case, a good fit is possible only for parameters (table 36.2) which offer features in sharp contrast with those typically observed for the f→f transitions:

(a) For the three f→f transitions analyzed, we obtain the average coupling strength $S = 53.5$ (weak coupling) and $Lg^2 = 0.025$. The values $S = 2.3$ and $Lg^2 = 3.1$ obtained for the d→f transition in $Y_3Al_5O_{12}:Pr^{3+}$ indicates an intermediate coupling strength corresponding to the expectedly larger equilibrium displacement between the adiabatic surfaces of the 5d and 4f states.

(b) The value $L|C|^2 = 8.5 \times 10^{-23}\ \mathrm{erg}^2$ is 10^8–10^{10} larger than the corresponding values typical of f→f transitions in spite of the much larger energy gap of the f→d transition (see table 36.2). This difference is no doubt a reflection of the involvement of opposite-parity states in the electronic coupling matrix element $\langle \mathrm{d}|\partial V/\partial R|\mathrm{f}'\rangle$.

(c) The effective mediating phonon energy $\hbar\omega = 350\ \mathrm{cm}^{-1}$ is less than half that of the maximum energy phonon peak at $830\ \mathrm{cm}^{-1}$ (Slack et al., 1969). This result can be qualitatively understood in terms of the fact that in intermediate coupling the radiationless relaxation rate is relatively insensitive of the energies of the accepting modes. In this case, it appears reasonable to expect the effective mediating phonon energy $\hbar\omega$ to be an approximate average of the phonon spectrum.

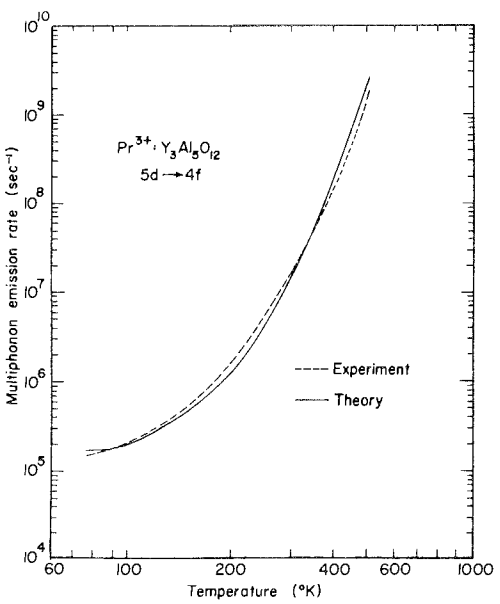

Fig. 36.8. Numerical comparison of eq. (36.46) to the experimentally observed 5d→4f radiationless relaxation in $Y_3Al_5O_{12}:Pr^{3+}$.

4. Energy transfer processes

Since the early work of Cario and Franck (1923), who observed the emission spectra of both mercury and thallium in gaseous mixtures when only the mercury was excited, there have been a large number of studies on sensitized luminescence and fluorescence (Franck and Livingston, 1949; Kellog, 1970; Knox, 1975a). A number of classical and quantum studies on energy transfer by several authors (Kallman and London, 1928; F. Perrin, 1932; J. Perrin, 1925; J. Perrin, 1927) led to the investigations of Förster (1948 and 1959), who related the rate of energy transfer to the overlap of the donor emission and the acceptor absorption spectra and to R^{-6}, where R is the distance between the donor and the acceptor. The Förster treatment, originally addressed to energy transfer between molecules, was also found (Dexter, 1953) to be applicable to ions in crystals, as much of the later work (Inokuti and Hirayama, 1965; Krasutsky and Moos, 1973; Van der Ziel et al., 1972; Watts and Richter, 1972) established Förster's original formulation of firm experimental and theoretical grounds.

The widespread interest in energy transfer processes has resulted from the breadth of phenomena encompassed by these processes. Current topics under investigation include: (1) energy diffusion and migration in liquids (Cheshnovsky et al., 1973), rare earth crystals (Bourcet and Fong, 1974; Weber, 1971), glasses (Reisfeld et al., 1972), and mixed molecular crystals (Kopelman, 1976); (2) annihilation interactions between excited singlets and triplets in polyatomic molecules (Johnson et al., 1967; Kawada and Jarnagin, 1966; Merrifield, 1968; Silver et al., 1963); (3) energy upconversion phenomena in rare earth materials (Auzel, 1973; Zalucha et al., 1973 and 1974); and (4) energy upconversion processes in in vitro (Knox, 1975b; Rahman and Knox, 1973) and in vivo (Fong, 1974a, 1974b, and 1975) biological systems.

Nearly all of the above-cited literature is specialized to resonance energy transfer corresponding to the overlap of donor emission and the acceptor absorption spectra in the Förster theory. In recent years there has been some interest in the question of non-resonant energy transfer phenomena arising from mismatches in the donor emission and acceptor absorption. Two different processes that may result from such energy mismatches are: (a) the donor excitation is transferred to two or more acceptors, and (b) the discrepant energy is dissipitated through the excitation of the bath vibrational modes. It has been shown (Fong and Diestler, 1972) that process (a) appears to play an important role in the question of concentration quenching. Process (b) appears to bear (Miyakawa and Dexter, 1970) a strong kinship to the problem of multiphonon relaxation discussed in the preceding sections. As the problem of resonance energy transfer in rare earth systems has been fully discussed elsewhere (Wright, 1976), we shall address ourselves in the following to the phenomenon of nonresonance transfer (Wassam and Fong, 1976).

The electronic eigenstates and eigenvalues of a system consisting of N noninteracting rare-earth ions randomly distributed in a host lattice have been described in preceding sections. Energy transfer processes involve transitions

between product states characterized by different localized electronic states on two or more molecules. These transitions formally arise from the off-diagonal terms involving the Coulomb interaction between guest molecules. For the sake of simplicity, we confine our considerations here to processes involving no more than three molecules, and write to second order in perturbation theory and coupling terms as (Fong and Diestler, 1972; Wassam and Fong, 1976):

$$\boldsymbol{H}'_{\alpha\alpha'} = \langle \Phi_\alpha | V | \Phi_{\alpha'} \rangle + \sum_{\beta \neq \alpha} \langle \Phi_\alpha | V | \Phi_\beta \rangle \langle \Phi_\beta | V | \Phi_{\alpha'} \rangle (E_\alpha - E_\beta)^{-1}, \tag{36.47}$$

where the zeroth order states are given as products of the donor and acceptor molecules

$$|\Phi_\alpha\rangle = |\phi_{\alpha 1}\rangle |\phi_{\alpha 2}\rangle |\phi_{\alpha 3}\rangle \tag{36.48}$$

with the zeroth order energies expressed as sums of the corresponding molecular energies (that are parametrically dependent on the collective nuclear coordinates $\boldsymbol{Q}$).

$$E_\alpha = \epsilon_{\alpha 1}(\boldsymbol{Q}) + \epsilon_{\alpha 2}(\boldsymbol{Q}) + \epsilon_{\alpha 3}(\boldsymbol{Q}) \tag{36.49}$$

and the Coulomb interaction energy operator

$$V = \tfrac{1}{2} \sum_{i,j=1}^{3} V(\boldsymbol{q}_i, \boldsymbol{q}_j) \tag{36.50}$$

is given in terms of the collective electronic coordinates $\boldsymbol{q}$ of the ith and jth molecules.

The first order contribution to eq. (36.47) is of the form:

$$\langle \phi_{\alpha 1} \phi_{\alpha 2} \phi_{\alpha 3} | V(\boldsymbol{q}_1, \boldsymbol{q}_2) | \phi_{\alpha' 1} \phi_{\alpha' 2} \phi_{\alpha' 3} \rangle = \langle \phi_{\alpha 1} \phi_{\alpha 2} | V(\boldsymbol{q}_1, \boldsymbol{q}_2) | \phi_{\alpha' 1} \phi_{\alpha' 2} \rangle \langle \phi_{\alpha 3} | \phi_{\alpha' 3} \rangle. \tag{36.51}$$

For an orthonormal basis, eq. (36.51) becomes simply

$$\langle \phi_{\alpha 1} \phi_{\alpha 2} | V(\boldsymbol{q}_1, \boldsymbol{q}_2) | \phi_{\alpha' 1} \phi_{\alpha' 2} \rangle. \tag{36.52}$$

The matrix element (36.52) gives rise to two-body energy transfer between ions 1 and 2.

The second-order contribution to eq. (36.47) is a sum of two types of terms:

$$\sum_{\substack{\beta 1 \\ (\beta 1, \beta 2, \beta 3 \neq \alpha 1, \alpha 2, \alpha 3)}} \sum_{\beta 2} \sum_{\beta 3} \langle \phi_{\alpha 1} \phi_{\alpha 2} \phi_{\alpha 3} | V(\boldsymbol{q}_1, \boldsymbol{q}_2) | \phi_{\beta 1} \phi \beta_2 \phi_{\beta 3} \rangle \times \langle \phi_{\beta 1} \phi_{\beta 2} \phi_{\beta 3} | V(\boldsymbol{q}_1, \boldsymbol{q}_2) | \phi_{\alpha' 1} \phi_{\alpha' 2} \phi_{\alpha' 3} \rangle \Delta E_{\alpha\beta}^{-1} \tag{36.53}$$

and

$$\sum_{\substack{\beta 1 \\ (\beta 1, \beta 2, \beta 3 \neq \alpha 1, \alpha 2, \alpha 3)}} \sum_{\beta 2} \sum_{\beta 3} \langle \phi_{\alpha 1} \phi_{\alpha 2} \phi_{\alpha 3} | V(\boldsymbol{q}_1, \boldsymbol{q}_2) | \phi_{\beta 1} \phi_{\beta 2} \phi_{\beta 3} \rangle \times \phi_{\beta 1} \phi_{\beta 2} \phi_{\beta 3} | V(\boldsymbol{q}_2, \boldsymbol{q}_3) | \phi_{\alpha' 1} \phi_{\alpha' 2} \phi_{\alpha' 3} \rangle \Delta E_{\alpha\beta}^{-1} \tag{36.54}$$

where

$$\Delta E_{\alpha\beta} = (\epsilon_{\alpha 1} + \epsilon_{\alpha 2} + \epsilon_{\alpha 3}) - (\epsilon_{\beta 1} + \epsilon_{\beta 2} + \epsilon_{\beta 3}). \tag{36.55}$$

We rewrite eq. (36.53)

$$\sum_{\substack{\beta 1\,\beta 2\,\beta 3 \\ (\beta 1,\,\beta 2,\,\beta 3\neq\alpha 1,\,\alpha 2,\,\alpha 3)}}\sum\sum \langle\phi_{\alpha 1}\phi_{\alpha 2}|V(\boldsymbol{q}_1,\boldsymbol{q}_2)|\phi_{\beta 1}\phi_{\beta 2}\rangle \times\langle\phi_{\alpha 3}|\phi_{\beta 3}\rangle\langle\phi_{\beta 1}\phi_{\beta 2}|V(\boldsymbol{q}_1,\boldsymbol{q}_2)|\phi_{\alpha' 1}\phi_{\alpha' 2}\rangle\langle\phi_{\beta 3}|\phi_{\alpha' 3}\rangle\Delta E_{\alpha\beta}^{-1} \tag{36.56}$$

and note that eq. (36.56) vanishes unless $(\alpha 3)=(\beta 3)=(\alpha' 3)$. We thus eliminate the summation over $(\beta 3)$ and simplify eq. (36.56) to read

$$\sum_{\substack{\beta 1\,\beta 2 \\ (\beta 1,\,\beta 2\neq\alpha 1,\,\alpha 2)}}\sum \langle\phi_{\alpha 1}\phi_{\alpha 2}|V(\boldsymbol{q}_1,\boldsymbol{q}_2)|\phi_{\beta 1}\phi_{\beta 2}\rangle \times\langle\phi_{\beta 1}\phi_{\beta 2}|V(\boldsymbol{q}_1,\boldsymbol{q}_2)|\phi_{\alpha' 1}\phi_{\alpha' 2}\rangle[(\epsilon_{\alpha 1}+\epsilon_{\alpha 2})-(\epsilon_{\beta 1}+\epsilon_{\beta 2})]^{-1} \tag{36.57}$$

Similarly, three-body interaction terms given by eq. (36.54) may be rewritten, for example:

$$\sum_{(\beta 1)\neq(\alpha 1)}\langle\phi_{\alpha 1}\phi_{\alpha 2}|V(\boldsymbol{q}_1,\boldsymbol{q}_2)|\phi_{\beta 1}\phi_{\alpha' 2}\rangle\langle\phi_{\beta 1}\phi_{\alpha 3}|V(\boldsymbol{q}_1,\boldsymbol{q}_2)|\phi_{\alpha' 1}\phi_{\alpha' 3}\rangle[(\epsilon_{\alpha 1}+\epsilon_{\alpha 2})-(\epsilon_{\beta 1}+\epsilon_{\alpha' 2})]^{-1} \tag{36.58}$$

We observe from eqs. (36.52), (36.57) and (36.58) that whereas three-body interactions can only arise from second-order terms, pairwise interactions are obtained both in first-order and second-order perturbation theory.

If molecules i and j are well separated, the pairwise Coulomb interaction Hamiltonian operator $V(\boldsymbol{q}_i,\boldsymbol{q}_j)$ can be expanded as (Dexter, 1953; Fong and Diestler, 1972; Kihara, 1958)

$$V(\boldsymbol{q}_i,\boldsymbol{q}_j)=(e^2/kR_{ij}^3)\boldsymbol{r}_i\cdot\boldsymbol{T}(ij)\cdot\boldsymbol{r}_j+\text{higher order terms} \tag{36.59}$$

where $\boldsymbol{T}(\boldsymbol{q}_i,\boldsymbol{q}_j)=\mathbf{1}-3(\boldsymbol{R}_{ij}\boldsymbol{R}_{ij})$; $e\boldsymbol{r}_i$, $e\boldsymbol{r}_j$ are the electric dipole moment operators for molecules i and j; $\boldsymbol{R}_{ij}$ is the vector separation of i and j, $\bar{\boldsymbol{R}}_{ij}$ is a unit vector in the direction $\boldsymbol{R}_{ij}$; and k is the dielectric constant for the host medium. For our present purpose, only the first term on the r.h.s. of eq. (36.59), i.e., the electric dipole–dipole interaction terms will be considered. Using eq. (36.59), we rewrite eqs. (36.52) and (36.58) respectively

$$C_{\alpha\alpha'}^{12}(\boldsymbol{Q})=(e^2/kR_{12}^3)\boldsymbol{D}_{\alpha 1,\alpha' 1}\cdot\boldsymbol{T}(12)\cdot\boldsymbol{D}_{\alpha 2,\alpha' 2} \tag{36.60}$$

and

$$C_{\alpha\alpha'}^{123}(\boldsymbol{Q})=(e^4/kR_{12}^3R_{13}^3)\sum_{\beta 1\neq\alpha 1}\boldsymbol{D}_{\alpha 1,\beta 1}\cdot\boldsymbol{T}(12)\boldsymbol{D}_{\alpha 2,\alpha' 2}\cdot\boldsymbol{D}_{\beta 1,\alpha 1}\cdot\boldsymbol{T}(13) \cdot\boldsymbol{D}_{\alpha 3,\alpha' 3}[\Delta\epsilon_{\alpha 1,\beta 1}+\Delta\epsilon_{\alpha 2,\alpha' 2}]^{-1}, \tag{36.61}$$

where

$$\boldsymbol{D}_{\alpha i,\alpha' i}=\langle\phi_{\alpha i}(\boldsymbol{q}_i,\boldsymbol{Q})|\boldsymbol{r}_i|\phi_{\alpha' i}(\boldsymbol{q}_i,\boldsymbol{Q})\rangle \tag{36.62}$$

and

$$\Delta\epsilon_{\alpha i,\alpha' i}=\epsilon_{\alpha i}(\boldsymbol{Q})-\epsilon_{\alpha' i}(\boldsymbol{Q}). \tag{36.63}$$

The coupling parameters $C_{\alpha\alpha'}$ in eqs. (36.60) and (36.61) are $\boldsymbol{Q}$ dependent on account of the $\boldsymbol{Q}$ dependence of the kets $|\phi_{\alpha i}\rangle$. For small nuclear displacements, it is convenient to expand $C_{\alpha\alpha'}(\boldsymbol{Q})$ in powers of the displacements ΔQ_α^l from the equilibrium positions $\boldsymbol{Q}_0$ ground state:

$$C_{\alpha\alpha'}(\boldsymbol{Q}) = C_{\alpha\alpha'}(\boldsymbol{Q}_0) + \sum_l [\partial C_{\alpha\alpha'}(\boldsymbol{Q})/\partial \boldsymbol{Q}_l]|_{\boldsymbol{Q}_0} \Delta Q_\alpha^l. \tag{36.64}$$

Assuming harmonic behavior for the potential surfaces of the adiabatic states $|\Phi_\alpha\rangle$, the total Hamiltonian operator can be written in the usual manner:

$$\boldsymbol{H} = \sum_\alpha |\Phi_\alpha\rangle \left[E_\alpha + \sum_k \hbar\omega_k(\alpha) b_k^\dagger b_k \right] \langle\Phi_\alpha| + \sum_\alpha \sum_{\alpha' \neq \alpha} |\Phi_\alpha\rangle B_\alpha^\dagger C_{\alpha\alpha'}(\boldsymbol{Q}) B_{\alpha'} \langle\Phi_{\alpha'}| \tag{36.65}$$

where $b_k^\dagger$ and b_k are respectively the phonon creation and annihilation operators,

$$B_\alpha^\dagger = \exp\left[\sum_k g_\alpha^k (b_k - b_k^\dagger) \right], \tag{36.66}$$

$$B_{\alpha'} = \exp\left[\sum_k g_{\alpha'}^k (b_k^\dagger - b_k) \right], \tag{36.67}$$

and

$$E_\alpha = E_\alpha^0 - \sum_k g_\alpha^{k2} \hbar\omega_k(\alpha) \tag{36.68}$$

with

$$g_\alpha^k = (M_k \omega_\alpha^k / 2\hbar)^{1/2} \Delta Q_{\alpha 0}^k. \tag{36.69}$$

The summation over k in eqs. (36.65)–(36.68) enumerates all normal modes of the host–guest system. In eq. (36.65), the first term is diagonal in the adiabatic basis $\{|\Phi_\alpha\rangle\}$ wheas the second term gives rise to the non-Born-Oppenheimer coupling that results in energy transfer. The dimensionless parameter g_α^k is given in terms of $\Delta Q_{\alpha 0}^k$, the displacement between the equilibrium positions corresponding to the αth and ground adiabatic states.

Making use of the formalism detailed in ch. 36 section 2, we write for the rate constant expression to lowest order in $\boldsymbol{H}$:

$$\begin{aligned} W_{\alpha\alpha'} = (\hbar^2 \beta \langle \boldsymbol{N}_\alpha \rangle)^{-1} \int_0^\infty \mathrm{d}t \int_0^\beta \mathrm{d}\alpha \, \mathrm{Tr}\{ & \exp(-\beta \boldsymbol{H}_0) \exp[-(\mathrm{i}/\hbar)\boldsymbol{H}_0(t + \mathrm{i}\hbar\lambda)] \Phi_\alpha\rangle \\ & \times C_{\alpha\alpha'}(\boldsymbol{Q}_0) B_\alpha^\dagger B_{\alpha'} \langle\Phi_{\alpha'}| \exp[+(\mathrm{i}/\hbar)\boldsymbol{H}_0(t + \mathrm{i}\hbar\lambda)] |\Phi_{\alpha'}\rangle \\ & \times C_{\alpha'\alpha}(\boldsymbol{Q})_0 B_{\alpha'}^\dagger B_\alpha \langle\Phi_\alpha|\}/\mathrm{Tr} \exp(-\beta \boldsymbol{H}_0) \end{aligned} \tag{36.70}$$

where H_0 contains the first two terms in eq. (36.65). Equation (36.70) is of a standard form, and the integration over λ and t can be readily carried out. For the case of zero distortion, i.e., $\omega_\alpha^l = \omega_{\alpha'}^l = \omega_l$, we obtain the corresponding weak coupling limit result

$$W_{\alpha\alpha'} = \frac{(2\pi)^{1/2}}{\hbar^2} \langle |C_{\alpha\alpha'}(\boldsymbol{Q}_0)|^2 \rangle \exp\left[-L_m g_m^2 (2n_m + 1)\right]$$

$$\times [\Delta\omega_m/\hbar]^{-1/2} \exp\left\{-\frac{\Delta}{\hbar\omega_m}\left[\ln \frac{\Delta}{L_m g_m^2 \hbar\omega_m (n_m + 1)} - 1\right]\right\} \tag{36.71}$$

where the "energy gap" $\Delta = E_\alpha - E_{\alpha'}$ is the amount of energy that must be partitioned into vibrational degrees of freedom. In writing eq. (36.71), we have assumed that only a narrow range of normal modes with an effective frequency about ω_m and an effective degeneracy L_m accept the electronic energy mismatch. Here the Franck-Condon approximation has been used, and the angular brackets about $|C_{\alpha\alpha'}|^2$ in eq. (36.71) denote an average value reminding us that we are dealing with a random distribution of guest molecules such that it is necessary to consider statistically weighted values for the separation distances R_{ij} in eqs. (36.60) and (36.61).

The weak-coupling result (36.71) has been applied (Wassam and Fong, 1976) to a numerical analysis of experimentally observed (Okamoto et al., 1972; Yamada et al., 1972) pairwise energy transfer rates in phosphors activated with trivalent rare earth ions. In the cases of interest, the observed energy transfer rates are Boltzmann averages over the relevant Stark multiplets of the donor and acceptor ions according to the expression

$$\langle W \rangle = \sum_{\alpha'} \sum_{\alpha} W_{\alpha\alpha'} \exp(-\Delta_\alpha/kT) \Big/ \sum_{\alpha} \exp(-\Delta_\alpha/kT) \tag{36.72}$$

where the indices α and α' respectively label the initial and final product states:

$$|\Phi_\alpha\rangle = |\phi_{\alpha D}\rangle|\phi_{\alpha A}\rangle \qquad |\Phi_{\alpha'}\rangle = |\phi_{\alpha' D}\rangle|\phi_{\alpha' A}\rangle. \tag{36.73, 74}$$

In eqs. (36.73) and (36.74), αD and αA label the components of the initial Stark manifolds for the donor and acceptor ions, respectively. Similarly, α'D and α'A respectively label the levels of the corresponding final Stark manifolds. In eq. (36.72), Δ_α is given by

$$\Delta_\alpha = \Delta_{\alpha D} + \Delta_{\alpha A} \tag{36.75}$$

where $\Delta_{\alpha D}$ is the separation between the level αD and the lowest lying level of the initial Stark manifold for the donor, and $\Delta_{\alpha A}$ is the separation between the level αA and the lowest lying level of the initial Stark manifold for the acceptor.

Figs. 36.9–36.11 display the results (Wassam and Fong, 1976) of the numerical comparison between theory and the observed (Okamoto et al., 1972; Yamada et al., 1972) transfer rates in $LaF_3:Er^{3+}$, Yb^{3+}, $Y_2O_3:Eu^{3+}$, Yb^{3+} and $Y_2O_3:Tb^{3+}$, Yb^{3+}. In all three systems, the Yb^{3+} ion acts as the acceptor. In the analysis for $LaF_3:Er^{3+}$, Yb^{3+}, it is assumed that the levels corresponding to the initial product states are characterized by identical potential surfaces. This assumption has also been made for the final product states. It is further assumed a constant coupling parameter $\langle |C_{\alpha\alpha'}(\boldsymbol{Q})_0|^2 \rangle$ in the statistical weighting procedure given by eq. (36.72). The numerical comparison between theory and experiment has been accomplished through a grid search in the $L_m g_m^2 - \hbar\omega_m - \langle |C|^2 \rangle$ parameter space

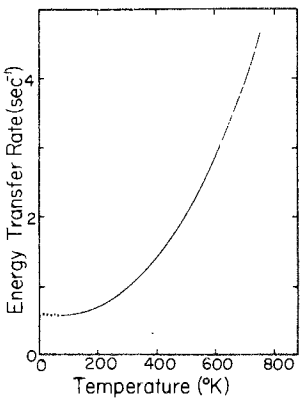

Fig. 36.9. The temperature dependence of the energy transfer rate transition $Er^{3+}\ {}^4S_{3/2}\ Yb^{3+}\ {}^2F_{7/2} \rightarrow Er^{3+}\ {}^4I_{13/2}\ Yb^{3+}\ {}^2F_{5/2}$ in LaF_3. The dashed line has been calculated from eq. (36.71) using the values of $L_m g_m^2$, $\langle |C|^2 \rangle$, and $\hbar\omega_m$ given in table 36.3. The solid line corresponds to the experimentally determined energy transfer rate.

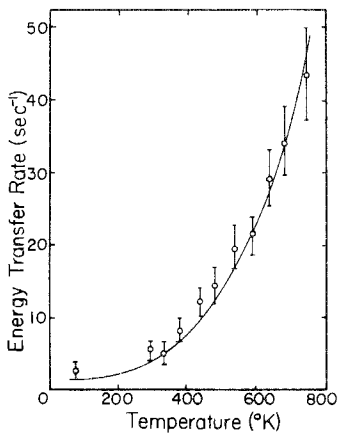

Fig. 36.10. The temperature dependence of the energy transfer rate for the transition $Eu^{3+}\ {}^5D_0\ Yb^{3+}\ {}^2F_{7/2} \rightarrow Eu^{3+}\ {}^7F_6\ Yb^{3+}\ {}^2F_{5/2}$ in Y_2O_3. The theoretical curve is calculated from eq. (36.71) using the values of $L_m g_m^2$, $\langle |C|^2 \rangle$, and $\hbar\omega_m$ given in table 36.3.

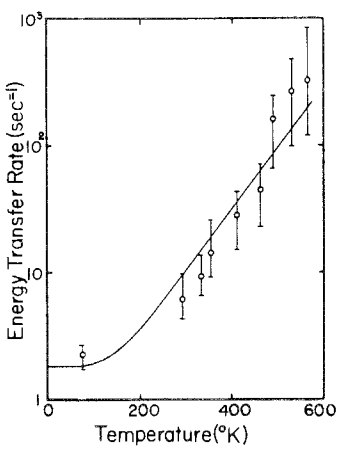

Fig. 36.11. The temperature dependence of the energy transfer rate for the transition $Tb^{3+}\ {}^5D_4\ Yb^{3+}\ {}^7F_{7/2} \rightarrow Tb^{3+}\ {}^7F_0\ Yb^{3+}\ {}^2F_{5/2}$ in Y_2O_3. The theoretical curve is calculated from eq. (36.71) using the values of $L_m g_m^2$, $\langle |C|^2 \rangle$, and $\hbar\omega_m$ given in table 36.3.

employing guessed initial values for these parameters until convergence was obtained in the least-squares criterion. The analysis for $Y_2O_3:Eu^{3+}$, Yb^{3+} and $Y_2O_3:Tb^{3+}$, Yb^{3+} has been carried out in a manner similar to that for the $LaF_3:Er^{3+}$, Yb^{3+}, except that a thermal average over the initial and final states was not performed because detailed information concerning the Stark splittings of Yb^{3+}, Tb^{3+}, and Eu^{3+} in Y_2O_3 was unavailable at the time of the analysis. The energy mismatch in these systems was taken to be an effective average. The parameters for the best theoretical fits are listed in table 36.3.

A major problem encountered in the comparison of theory and experiment is the lack of a detailed analysis of the vibronic spectra associated with the relevant electronic transitions. Of some interest is the value of the $L_m g_m^2$ parameter. In this treatment, as in the related discussions in the preceding sections, we have introduced the ad hoc assumption that only one effective mode is responsible for accepting the mismatch energy. This assumption seems to be tolerable in view of the excellent agreement between theory and experiment obtained, particularly in the case of the $LaF_3:Er^{3+}$, Yb^{3+} system. The values for Lg_m^2 listed in table 36.3 fall in the expected range for the weak-coupling limit in which eq. (36.71) was derived.

The coupling parameter $\langle|C_{\alpha\alpha'}(\boldsymbol{Q}_0)|^2\rangle$ in eq. (38.71) cannot be calculated by ab initio methods. Accordingly we are not in a position to interpret in quantitative terms the values for $\langle|C|^2\rangle$ listed in table 36.3. However, the magnitude of $\langle|C|^2\rangle$ may be expected to depend on (i) the host matrix and (ii) the specific rare earth transitions involved in the energy transfer process. Condition (i) results from the fact that electric dipole transitions in rare earth ions occur through admixtures of odd-parity states. It is known, for example, forced electric dipole $f \rightarrow f$ transitions in rare earth ions are much more probable in Y_2O_3 (C_2 site symmetry) than in LaF_3 (D_{3h} site symmetry). The observed radiative lifetime of the Eu^{3+} $^5D_0$ level (reflecting the overall decay of $^5D_0$ to the seven ^7F_J manifolds) is 0.89(5) msec (Riedel, 1970) and 6.7 msec (Weber, 1967) in Y_2O_3 and LaF_3 respectively. In a given host, the dipole transition probabilities in rare earth ions can vary over several orders of magnitudes. For example, the electric-dipole transition probabilities for Eu^{3+} $^5D_1 \rightarrow {}^7F_3$ and $^5D_1 \rightarrow {}^7F_6$ are 33.9 and 0.06 sec^{-1} respectively (Weber, 1967). The variation over four orders of magnitude for the $\langle|C|^2\rangle$ parameters given in table 36.3 may thus be rationalized.

The values for the effective phonon frequency $\hbar\omega_m$ listed in table 36.3 are in

TABLE 36.3.
Numerical values of the effective parameters for the comparison of theory and experiment.

			Transitions				
Donor	Acceptor	Host	Donor	Acceptor	$L_m g_m^2$	$\langle\|C\|^2\rangle$(Erg^2)	$\hbar\omega_m$(cm^{-1})
Er^{3+}	Yb^{3+}	LaF_3	$^4S_{3/2} \rightarrow {}^4I_{13/2}$	$^2F_{7/2} \rightarrow {}^2F_{5/2}$	0.0482	9.065×10^{-26}	300
Eu^{3+}	Yb^{3+}	Y_2O_3	$^5D_0 \rightarrow {}^7F_6$	$^2F_{7/2} \rightarrow {}^2F_{5/2}$	0.0193	4.168×10^{-23}	340
Tb^{3+}	Yb^{3+}	Y_2O_3	$^5D_4 \rightarrow {}^7F_0$	$^2F_{7/2} \rightarrow {}^2F_{5/2}$	0.5000	5.616×10^{-22}	380

general agreement with the analyses of multiphonon relaxation (not involving energy transfer) of electronically excited rare earth ions in various hosts given in the preceding sections. An inspection of eq. (36.71) reveals that the transfer rate constant $W_{\alpha\alpha'}$ follows an approximate exponential dependence on the energy gap Δ and the phonon frequency $\hbar\omega_m$ in agreement with the apparent exponential energy gap law experimentally observed for non-resonant energy transfer and nonradiative multiphonon relaxation processes (see fig. 36.5).

The form of eq. (36.71) is approximately similar to, though somewhat simpler than, the form of the rate constant expression in eq. (38.29) derived for nonadiabatic coupling operators that bear an explicit dependence on the nuclear coordinate as in the case of the nuclear kinetic energy operator. In the latter case, the phonon modes are not only responsible for the partitioning of the energy mismatch but also play a crucial role in promoting the radiationless transition. In the present description, the energy transfer transitions are induced by the Coulomb interactions between the valence electrons of the donor and acceptor molecules, and the phonon modes primarily function as energy-accepting bath modes. The functional form chosen for the interaction $V(\boldsymbol{q}_i, \boldsymbol{q}_j)$ in eq. (36.59) focuses our attention on multipolar coupling mechanisms. It should be emphasized, however, that this choice for $V(\boldsymbol{q}_i, \boldsymbol{q}_j)$ does not limit the usefulness of the present theory in the discussion of triplet–triplet transfer processes. It is only necessary to begin with a proper admixture of singlet character in the stationary triplet states.

The extension of the adiabatic theory of radiationless relaxation to a quantitative assessment of the non-resonant energy transfer problem helps illustrate the variety of ways in which the adiabatic separation of molecular degrees of freedom can be made in setting up the formal treatment of a multiplicity of physically different phenomena. As the mathematical apparatus for the basic theory becomes more or less standardized, the theoretical interpretation of most nonradiative relaxation phenomena appears to be a matter of physical modeling and of a proper choice for the nonadiabatic perturbation operator (Fong, 1976).

5. Discussion

The theory presented in the present chapter has been based on the following assumptions:

(a) The stationary states of the system can be described by the adiabatic approximation.

(b) The transition takes place between two electronic states.

(c) The transition always originates from a Boltzmann distribution of vibrational levels.

(d) The integral for the rate constant can be approximated by using the method of saddle-point integration.

(e) One effective lattice mode of coupling accounts for the relaxation process.

(f) The inequality $\epsilon_\alpha - \epsilon_{\alpha'} \gg L_m g_m^2 \hbar\omega_\alpha$ is valid in the weak coupling limit.

Assumptions (a), (c), and (d) are standard in the literature on multiphonon processes (Englman and Jortner, 1970; Kubo and Toyozawa, 1955; Lin, 1966). The usual criterion for the validity of the adiabatic approximation is that the electronic energy difference is large compared with the energy of the phonons which mediate the transition, i.e., $(\epsilon_\alpha - \epsilon_{\alpha'}) \gg \hbar\omega_\alpha^m$, and this same criterion also ensures that the saddle-point approximation is valid. We remark that due to the smallness of the relative displacements of the origins of the normal coordinates in the two electronic states in rare earth ions, the adiabatic approximation may be valid even if the inequality is violated (Davydov, 1963). It should also be noted that the error involved in using the saddle-point method is rather small even in the case of transitions involving small numbers of phonons: For example, for a two-phonon process, the error involved in approximating 2! using Stirling's formula in ≈7%.

The statement that nonradiative transitions always originate from a Boltzmann distribution of vibrational levels is equivalent to the assumption that the vibrational lifetime due to phonon–phonon interactions is much smaller than the nonradiative relaxation time.

Assumption (e), in light of the good fits obtained, in figs. 36.1–36.11, seems to be valid. If we set $\omega_\alpha^m \simeq \omega_{\max}$ in the evaluation of eq. (36.29), it is possible to estimate the error involved in the omission of the role of some lower energy phonon modes in the manner discussed by Freed and Jortner (1970). In particular, these authors have shown that the contribution of the mode with the next highest frequency ω_n, i.e., $\omega_n < \omega_\alpha^m = \omega_{\max}$ to the relaxation process can be neglected if the inequality,

$$(\epsilon_\alpha - \epsilon_{\alpha'})/\hbar\omega_\alpha^m \gg L_m g_m^2 (L_n g_n^2 / L_m g_m^2)\omega_\alpha^m/(\omega_\alpha^m - \omega_n),$$

is satisfied.

If $L_n g_n^2 / L_m g_m^2 \sim 1$, $L_m g_m^2 \gg 1$ ($L_m g_m^2 \simeq 0.15$ from table 36.1), and $(\epsilon_\alpha - \epsilon_{\alpha'})/\hbar\omega_\alpha^m > 1$ for multiphonon transitions, the above inequality is valid, and our assumption of one effective phonon mode with energy close to $\hbar\omega_{\max}$ therefore appears to be realistic. We note that the above argument also provides the justification for assumption (f).

References

Auzel, F.E., 1973, Proc. IEEE **61**, 758.
Bourcet, J.-C. and F.K. Fong, 1974, J. Chem. Phys. **60**, 34.
Cario, G. and J. Franck, 1923, Z. Physik **17**, 202.
Carlson, E.H. and G.H. Dieke, 1961, J. Chem. Phys. 34, 1602.
Cheshnovsky, O., B. Raz and J. Jortner, 1973, J. Chem. Phys. 59, 5554.
Davydov, A., 1963, Quantum Mechanics, in: Ter Haar, D., ed. (Addison-Wesley, Reading, Mass.) p. 470.
Dexter, D.L., 1953, J. Chem. Phys. **21**, 836.
Dieke, G.H., 1968, Spectra and Energy Levels of Rare Earth Ions in Crystals (Interscience, New York).
Englman, R. and J. Jortner, 1970, Mol. Phys. **18**, 145.
Fong, F.K., 1974(a), J. Theoret. Biol. **46**, 407.
Fong, F.K., 1974(b), Proc. Nat. Acad. Sci. USA **71**, 3692.
Fong, F.K., 1975(a), Theory of Molecular Relaxation: Applications in Chemistry and Biology, (Wiley-Interscience, New York).
Fong, F.K., 1975(b), Appl. Phys. **6(2)**, 151.
Fong, F.K., 1976, Introduction, in: Fong, F.K., ed., Radiationless Processes in Molecules and

Crystals, Vol. 15 (Springer-Verlag, Heidelberg, Germany).
Fong, F.K., and D.J. Diestler, 1972, J. Chem. Phys. **56**, 2875.
Fong, F.K., H.V. Lauer, C.R. Chilver and M.M. Miller, 1975, J. Chem. Phys. **63**, 366.
Fong, F.K. and M.M. Miller, 1971, Chem. Phys. Letters **10**, 408.
Fong, F.K., S.L. Naberhuis and M.M. Miller, 1972, J. Chem. Phys. **56**, 4020.
Fong, F.K. and W.A. Wassam, 1973, J. Chem. Phys. **58**, 957.
Fong, F.K. and E.Y. Wong, 1967(a), Phys. Rev. **162**, 348.
Fong, F.K. and E.Y. Wong, 1967(b), in Proceedings of the Conference on Optical Properties of Crystals (Wiley, New York) p. 137.
Förster, Th., 1948, Ann. Physik **2**, 55.
Förster, Th., 1959, Discussions Faraday Soc. **27**, 7.
Franck, J. and R. Livingston, 1949, Rev. Modern Phys. **21**, 505.
Freed, K.F. and J. Jortner, 1970, J. Chem. Phys. **52**, 6272.
Inokuti, M. and F. Hirayama, 1965, J. Chem. Phys. **43**, 1978.
Johnson, R.C., R.E. Merrifield, P. Avakian, and R.B. Flippen, 1967, Phys Rev. Lett. **19**, 285.
Judd, B., 1966, Operator Techniques in Atomic Spectroscopy (McGraw Hill & Co., New York).
Kallman, H. and F. London, 1928, Z. Physik. Chem. **B2**, 207.
Kawada, A. and R.C. Jarnagin, 1966, J. Chem. Phys. **44**, 1919.
Kellog, R.E., 1970, J. Luminescence **2**, 435.
Kiel, A., 1964, in: Goivel, P. and N. Bloembergen, eds., Quantum Electronics (Columbia University, New York) pp. 765–777.
Kihara, T., 1958, Advan. Chem. Phys. **1**, 267.
Kiss, Z.J. and W.A. Weakliem, 1965, Phys. Rev. Letts **15**, 457.
Knox, R.S., 1975(a), in: Govindjee, ed., Bioenergetics of Photosynthesis (Academic Press, New York).
Knox, R.S., 1975(b), Photochem. Photobiol. **22**, 149.
Kopelman, R., 1976, Exciton Percolation in Molecular Alloys and Aggregates, in: Fong, F.K. ed., Radiationless Processes in Molecules and Crystals, Vol. 15 (Springer-Verlag, Heidelberg, Germany).
Krasutsky, N. and H.W. Moos, 1973, Phys. Rev. **B8**, 1010.
Kubo, R. and V. Toyozawa, 1955, Progr. Theoret. Phys. (Kyoto) **13**, 162.
Kubo, R., N. Yokota, and S. Nakajima, 1957, J. Phys. Soc. Japan **12**, 1203.
Lauer, H.V. and F.K. Fong, 1974, J. Chem. Phys. **60**, 274.
Lin, S.H., 1966, J. Chem. Phys. **44**, 3759.
Merrifield, R.E., 1968, J. Chem. Phys. **48**, 4318.
Miyakawa, T. and D.L. Dexter, 1970, Phys. Rev. **B1**, 2961.
Okamoto, E., H. Masui, K. Muto and K. Amazu, 1972, J. Appl. Phys. **43**, 2122.
Partlow, W.D. and H.W. Moos, 1967, Phys. Rev. **157**, 252.
Perrin, F., 1932, Ann. Chim. Phys. **17**, 283.
Perrin, J., 1925, 2me conseil de Chime Solvay (Gautier and Villar, Paris) p. 322.
Perrin, J., 1927, Compt. Rend. **184**, 1097.
Rahman, T.S. and R.S. Knox, 1973, Phys. Stat. Sol. **58**, 715.
Rector, C.W., B.C. Pandey, and H.W. Moos, 1966, J. Chem. Phys. **45**, 171.
Reisfeld, R., E. Greenberg, R. Velapoldi, and B. Barnett, 1972, J. Chem. Phys. **56**, 1698.
Riedel, E.P., 1970, J. Luminescence **1, 2**, 176.
Riseberg, L.A., 1968, Ph.D. dissertation, The Johns Hopkins University, Baltimore, Maryland, unpublished.
Riseberg, L.A. and H.W. Moos, 1968, Phys. Rev. **174**, 429.
Riseberg, L.A. and M.J. Weber, 1976, in Progress in Optics, vol. XIV, ed. E. Wolf (North-Holland, Amsterdam) p. 89.
Silver, M., D. Olness, M. Sincord, and R.C. Jarnagin, 1963, Phys. Rev. Lett. **10**, 12.
Slack, G.A., D.W. Oliver, R.M. Chrenko, and S. Roberts, 1969, Phys. Rev. **177**, 1308.
Van der Ziel, J.P., L. Kopf, and L.G. Van Uitert, 1972, Phys. Rev. **B6**, 615.
Wassam, W.A. and F.K. Fong, 1976, J. Chem. Phys., **65**, 3402.
Watts, R.K. and H.J. Richter, 1972, Phys. Rev. **B6**, 1584.
Weber, M.J., 1967, in: Crosswhite, H.M., ed., Optical Properties of Ions in Crystals (Wiley-Interscience, New York) pp. 467–484.
Weber, M.J., 1971, Phys. Rev. **B4**, 2932.
Weber, M.J., 1973(a), Phys. Rev. **B8**, 54.
Weber, M.J., 1973(b), Solid State Commun. **12**, 741.
Wright, J.C., 1976, Upconversion and Excited State Energy Transfer in Rare-Earth Doped Materials, in: Fong, F.K., ed., Radiationless Processes in Molecules and Crystals, Vol. 15 (Springer-Verlag, Heidelberg, Germany).
Wybourne, B.G., 1970, Symmetry Principles and Atomic Spectroscopy (Wiley, New York).
Yamada, N., S. Shionoya, and T. Kashida, 1972, J. Phys. Soc. Japan **32**, 1577.
Zalucha, D.J., J.C. Wright, and F.K. Fong, 1973, J. Chem. Phys. **59**, 997.
Zalucha, D.J., J.A. Sell, and F.K. Fong, 1974, J. Chem. Phys. **60**, 1660.

Handbook on the Physics and Chemistry of Rare Earths, edited by K.A. Gschneidner, Jr. and L. Eyring

Chapter 37A

CHEMICAL SPECTROPHOTOMETRIC AND POLAROGRAPHIC METHODS

Jerome W. O'LAUGHLIN
Department of Chemistry, University of Missouri-Columbia, Columbia, Missouri 65201, USA

Contents

1. Introduction

The unique chemical similarity of the rare earth group of elements makes the determination of individual members of this group by chemical methods of analysis exceedingly difficult with but only a few exceptions. Ce and Eu can readily be determined by various electrochemical methods with good sensitivity. With the exception of La and Lu, the other lanthanide elements can be determined based on their characteristic sharp line absorption spectra in aqueous solution although the molar absorptivities are low, with a maximum value of approximately 12 ℓ/mole·cm (based on the spectrophotometer used) for Nd. Considerably larger values are observed in the case of Ce for a rather intense broad charge-transfer band below 340 nm, but the shape and intensity of this band varies so greatly with temperature and the various anions in solution that it has not proven to be a useful method for the determination of cerium and furthermore is not characteristic for cerium.

Eu and Tb can be determined by their unique fluorescence spectra in aqueous solution. The individual rare earths can also be determined by separation on an ion-exchange column or by other chromatographic methods. These are generally quite tedious and lengthy procedures and not of great analytical value at present.

Probably the most important chemical procedure in the determination of the rare earths is the determination of total rare earths in some matrix which usually involves the precipitation of the rare earth oxalates and ignition to the oxides, R_2O_3. This procedure also serves to separate the rare earth group from other elements present in solution prior to the determination of the individual rare earths by other methods such as flame emission spectrometry. Chemical methods can also be employed to separate the light rare earth fraction from the heavy rare earth fraction with minimum difficulty. Chemical methods such as solvent extraction are also quite useful in the preconcentration of the rare earths where they are present at extremely low concentrations prior to their determination by other methods.

Although various analytical procedures for the rare earths have appeared in many monographs on the chemistry and metallurgy of these elements, only two texts devoted exclusively to the analytical chemistry of the rare earths have been published. The earliest was by Vickery (1953) and the latest by Ryabchikov and Ryabukhin (1966). The latter has been translated into English by Aladjem (1970) and very thoroughly covers the analytical chemistry of the rare earths. This text has an extremely complete bibliography with 2084 references (the latest for 1966) which are divided on the basis that the first 594 refer to Russian literature and the remaining references with papers from other countries. Each section is arranged in alphabetical order in terms of the authors last names. A chapter on the analytical chemistry of the rare earths by Woyski and Harris (1963) is included in the treatise on Analytical Chemistry by Kolthoff and Elving (1963). Another chapter on the "Analytical Chemistry of the Rare Earths," by Banks and Klingman (1961) contains much useful information on practical chemical methods for the determination of the rare earths.

1.1. *Overview of methods used for the separation and determination of the rare earths*

The most selective precipitating reagent for the rare earths is oxalic acid. In the presence of an excess of the oxalate ion, however, Sc forms a soluble oxalate complex and the heavy lanthanides are not completely precipitated.

Classical chemical methods for the qualitative determination of the rare earths have been described by Noyes and Bray (1927) but these methods are of no practical use at present because the presence of these elements is much more readily confirmed by spectroscopic methods. Ce and Eu might again be considered as exceptions to the above statement. A large number of qualitative reactions fairly selective for these two elements have been described. In the case of Ce these are generally based on the strong oxidizing power of Ce(IV). Ce(IV) together with Th can be isolated from the other rare earths by precipitation as the iodate or

periodate. Many of the qualitative reactions fairly specific for Ce(IV) and several other rare earths including La, Pr, Sm, Eu, and Tb are summarized by Aladjem (1970), pp. 40–49. Europium(III) complexes with various β-diketones in the presence of neutral donors such as tri-n-octylphosphine oxide exhibit a strong red fluorescent band centered near 617 nm when irradiated with ultraviolet light. A quantitative study of the effect of the neutral donor concentration on this fluorescence band has been reported by Carey and Banks (1969). Arsenazo III has been shown by Savvin (1964) to be an extremely useful and sensitive reagent for the rare earths, thorium, uranium, and other actinides.

Although not specific for any individual rare earth, Arsenazo III has been shown by O'Laughlin and Banks (1964) to be very useful for the detection of the location of individual rare earths after separation of the rare earths by paper chromatography. Chlorophosphonazo III reported by Nemodruk et al., 1961, is also an extremely sensitive reagent for rare earths and, although it reacts with a large number of elements, can be used to detect very small amounts of the individual rare earths after separation by paper or thin layer chromatography.

More recently methods for the determination of subgroups of the rare earths by methods involving the use of competing ligands have been described, such as the method for the yttrium-subgroup described by Polyektov et al., 1973, based on the color reaction of this subgroup with quinalizarin and using benzoic acid as the competing ligand. The reagent 1,5-di-(2′-hydroxy-5′-sulfophenyl)-3-cyanoformazan has been shown by Dziomkov et al. (1970) to be highly selective for scandium and these authors were able to determine scandium in the presence of the other rare earths and thorium where the ratio of the rare earths to scandium did not exceed 1000 to 1. Elements such as Cu(II), Co(III), Fe(III), Ga, Zn, Pb, and Hg which also react with the reagent can be separated from scandium fairly easily.

1.2. *Gravimetric methods*

The initial step in the chemical analysis of the rare earths is the dissolution of the sample. Rare earths in phosphate minerals such as the monazite or xenotime ores can be put into solution almost completely by heating the sample with concentrated sulfuric acid. The sample is then leached with water and the solid residue again treated with sulfuric acid to extract any rare earths remaining after the first step. The rare earths can then be precipitated as the oxalates. Various fusion procedures can also be employed. Fusion of monazite sands with KHF_2 results in the complete dissolution of this mineral. All the rare earths and thorium remain as insoluble fluorides. The residue may then be digested in dilute sulfuric acid and the insoluble rare earth and thorium fluorides separated by centrifugation. The thorium can be separated from the rare earths after dissolution of the insoluble fluorides by solvent extraction as shown by Banks and Byrd (1953). Numerous other fusion and acid digestion-fusion procedures have been proposed. These include fusion with Na_2CO_3, Na_2O_2, Na_2F_2 and $NaHF_2$ and leaching of the rare earths from various ores by digestion with nitric or

perchloric acids. Silicate minerals containing the rare earths are most conveniently decomposed by treatment with hydrofluoric acid or fusion with $NaHF_2$ or KHF_2. A detailed discussion of decomposition methods most suitable for particular minerals and other materials with references to the original papers is given by Aladjem (1970), pp. 197–205.

The most common gravimetric method for the determination of the lanthanides and yttrium is the precipitation of the oxalates followed by ignition at 800°C or higher to the oxides, R_2O_3. Pr and Tb form the oxides Pr_6O_{11} and Tb_4O_7 under these conditions and Ce is oxidized to CeO_2 at temperatures over 350°C.

The composition and thermal properties of the normal rare earth oxalates as well as the solubility of the rare earth oxalates in the common mineral acids as a function of both the mineral acid concentration and oxalic acid concentration is summarized by Aladjem (1970), p. 270–271.

Although the precipitation of the rare earth oxalates is probably the single most effective method for the separation of the rare earth group from other elements, careful attention must be given to the conditions under which the precipitation is made. The solubility products are not as small as might be desired, approximately 10^{-26} for cerium(III) as reported by Aladjem (1970), p. 52, and the heavier rare earths tend to form complex ions in the presence of excess oxalate. The solubility appears to be a function of the activity of the oxalate ion alone. Thus careful attention to the pH of the solution is critical. Furthermore, a number of other elements which form insoluble oxalates tend to coprecipitate with the rare earths. The dissolution of the initial oxalate precipitate and reprecipitation of the rare earth oxalates essentially eliminates interferences from other ions, except thorium and the trivalent transuranium elements, but will result in the loss of some of the rare earths. The minimum solubility for all the rare earth oxalates occurs when the activity of the oxalate ion lies between 10^{-4} and 10^{-5} as reported by Woyski and Harris (1963), p. 30. This corresponds to molar solubilities ranging from 1.5×10^{-6} for Ce(III) to 3.2×10^{-5} for Yb. Several specific procedures for the precipitation of the rare earth oxalates are given by Woyski and Harris (1963), p. 34–35. A procedure recommended by Broadhead and Heady (1960) should be considered for the precipitation of small amounts of the rare earths (where the initial concentration is less than 0.01M).

The rare earths can be precipitated as the hydroxides, but because of the relatively large difference in the basicity in the rare earths this is not an effective method for the separation of the rare earths from any elements except the alkali and the alkaline earth cations. The precipitate is bulky, amorphous and difficult to filter. The light lanthanides are quite basic and lanthanum is not completely precipitated at a pH less than 10. Precipitation of the rare earth hydroxides is sometimes a useful procedure for the preliminary separation of small amounts of the rare earths from solutions in which the concentration of a number of other elements is high. The hydroxide precipitate is most conveniently separated by centrifugation, redissolved and the rare earths precipitated as the oxalates.

The rare earths can also be precipitated as the fluorides and separated from

essentially the same elements as in the case of the oxalate precipitation. The precipitate, as in the case of the hydroxides, is difficult to filter and is best separated from the solution by centrifugation. The precipitate is then redissolved and the rare earths precipitated as the oxalates then ignited to the oxides. Plastic and platinum vessels must be employed.

Ce(IV) can be precipitated as the iodate or periodate and separated from the other rare earths although any thorium present will also be precipitated.

A large number of organic precipitants have been proposed for the rare earths. In general, all the rare earths with the exception of Ce(IV) react in a similar manner with these reagents. Among those widely used are 8-hydroxyquinoline, 8-hydroxyquinaldine, benzoic acid, cupferron, phenylarsonic acid, and 1- and 2-naphthylarsonic acids. These reagents are not particularly selective for the rare earths and precipitate many other cations. The reagent 8-hydroxyquinaldine has been used to separate the rare earths from aluminum and by careful control of the pH and the use of masking agents procedures have been developed with several of the above reagents which are somewhat selective for the rare earth group. These methods are described by Woyski and Harris (1963) and by Aladjem (1970).

1.3. *Titrimetric methods*

The two most useful titrimetric methods for the determination of the rare earths are the determination of Ce by the titration of Ce(IV) with a standard solution of some reducing reagent, commonly Fe(II), and the titration of the rare earths as a group with a complexing reagent such as ethylenediamine tetracetic acid, EDTA.

The determination of Ce after oxidation of Ce(III) to Ce(IV) is undoubtedly the most widely used titrimetric method for any individual rare earth. The only major problem with this method is the high oxidation potential of Ce(IV). The formal single electrode potentials for Ce(IV) in 1 N perchloric, nitric, sulfuric and hydrochloric acids are 1.70, 1.61, 1.44 and 1.28 volt respectively as reported by Smith and Getz (1938). Thus the oxidation of Ce(III) to Ce(IV) is difficult and requires an extremely strong oxidizing reagent. The two most useful are potassium peroxydisulfate, $K_2S_2O_8$ and sodium bismuthate, $NaBiO_3$. The original procedure by Von Knorre (1897) for the oxidation of cerium with peroxydisulfate was not completely satisfactory, but since the discovery of the catalytic effect of Ag(I) by Barbieri (1916) it has given excellent results as shown by Willard and Young (1928). More recently Banks et al. (1956) showed that Ce in Ce–Cr–U alloys could be determined very accurately even by an indirect method by the peroxydisulfate procedure. Both Ce and Cr were oxidized with $K_2S_2O_8$ with Ag(I) as the catalyst. On a separate portion of the solution the chromium was oxidized by fuming with perchloric acid which, in the absence of sulfuric or phosphoric acids, does not oxidize cerium. The cerium was determined by difference with a relative standard deviation of 0.159%.

Standard solutions of Ce(IV) are also widely used for the oxidation of many

inorganic and organic compounds and this technique is now referred to as cerimetry. Many specific procedures concerning the preparation of standard cerium solutions and a number of applications of cerimetry are described in a monograph by Smith (1942).

Eu(III) can be reduced to Eu(II) by passing a solution of Eu(III) in hydrochloric acid through a column packed with amalgamated zinc (Jones reductor). Foster and Kern (1953) describe one method in which the column effluent is passed directly into a flask containing an aqueous solution of $FeCl_3$. A CO_2 atmosphere is maintained over the $FeCl_3$ solution to prevent air oxidation of the Eu(II). An amount of Fe(III) equivalent to the Eu(II) is reduced to Fe(II) which is then titrated with a standard solution of $K_2Cr_2O_7$. Diphenylamine sulfonate was used as the indicator. The Fe(II) may also be conveniently titrated with a standard solution of Ce(IV) with Ferroin as the indicator. The Eu(II) can also be collected in a solution containing a small excess of I_2 and any I_2 remaining back titrated with thiosulfate.

Titrimetric methods for the determination of Tb, Yb, and Sm, based on their reduction to the divalent state, have been proposed as reported by Aladjem (1970), but have seldom been used. None of these elements are reduced by a Jones reductor.

The formation constants for all the rare earths with various polydentate chelating reagents are very large. The formation constants for the rare earths with EDTA, for example, range from approximately 10^{15} for La to 10^{20} for Lu. The formation constants with diethylenetriaminepentaacetic acid, DTPA, are even larger, ranging from approximately 10^{20} to 10^{23} for La and Lu, respectively. Other chelating reagents have been used for the titration of the rare earths such as nitrilotriacetic acid, NTA, and even citric acid, but EDTA is by far the most widely used reagent by analytical chemists for the titration of the rare earth group. Although there is a significant difference in the formation constants for lanthanum and lutetium, the increase in the formation constants is not a monotonic function of the atomic number with EDTA or other chelating reagents and the titration of individual rare earths is not practical. The rare earths are generally titrated as a group.

A large number of metallochromic indicators have been proposed for the detection of the equivalence point for the titration of the rare earths with EDTA and other polydentate ligands. These include Alizarin Red, Arsenazo I, Xylenol Orange, Eriochrome Black T, and Murexide to name only a few. The structure, conditions under which these indicators can be used, possible interferences, and references to the original papers are summarized by Aladjem (1970), p. 287.

The endpoint in the titration of the rare earths can also be determined potentiometrically using a mercury indicator electrode as reported by Reilley et al. (1958). The determination of the hydrogen ions liberated as a result of complex formation has also been employed to determine the amount of rare earths present, but, as reported by Woyski and Harris (1963), is now only of historical interest. The rare earths can also be determined by precipitation titrations with oxalic acid where the excess oxalic acid is determined after separation of the

insoluble rare earth oxalates. This method is seldom used in view of the much better results obtained by the EDTA method.

1.4. *Liquid–liquid extraction procedures*

The separation of the rare earths as a group and the separation of individual rare earths from each other by solvent extraction procedures is possible and is the subject of another chapter. Only those extraction methods of particular importance in the determination of the rare earths are discussed in this section. The separation of the individual rare earths by solvent extraction involves a multistage process and is too cumbersome to be of practical importance for the determination of the rare earths. Solvent extraction procedures are extremely useful, however, in the separation of Th, Zr, Hf, U and other elements which are difficult to separate from the rare earths by other procedures. Ce(IV) can also be readily separated from the trivalent rare earths by solvent extraction.

Several of the most widely used extractants for Th, U(IV) and other tetravalent metals as reported by Woyski and Harris (1963) are tri-n-butylphosphate, TBP, di-2-ethylhexyphosphoric acid, and tri-n-octylphosphine oxide, TOPO. Methylene-bis-(di-n-hexylphosphine oxide), MHDPO, first synthesized by Richard et al. (1961) is also a powerful extractant. This compound and analogous diphosphonates are extremely powerful extractants for many metals as reported by O'Laughlin (1966) in the case of the diphosphine oxides and by Meider-Gorican (1967) for the diphosphonates. All the above compounds can be used to extract the rare earths as well as other elements, but by proper control of the acidity and ionic strength of the solution it is possible to separate thorium and other tetravalent metals from the rare earth group. Other extractants commonly used are various ethers, ketones and esters. Diethyl ether is among the weakest of the extractants, but is useful because the uranyl ion, UO_2^{+2}, can be extracted from nitric acid media even in the absence of free acid or salting out reagents. Other tetravalent metals such as Th(IV) and Pu(IV) and Au(III) can be extracted in the presence of excess nitric acid or salting-out reagents and single stage separations of these elements from the rare earths are possible. Extraction data for these and other elements into diethyl ether are summarized by Aladjem (1970), pp. 117–119.

Mesityl oxide is an effective extractant for thorium and a single stage separation from the rare earths was reported by Banks and Byrd (1953). Various β-diketones are effective extractants for the rare earths. One of the more widely used is 2-thenoyltrifluoroacetone, TTA. Th, U, Zr and Sc can be extracted at a pH of less than 1.5. The remaining rare earths can be extracted at a pH of 4.5 which serves to separate the rare earths, with the exception of Sc, from most of the other elements. Healy (1963) and De (1965) reported on the strong synergistic enhancement in the extraction of metallic species by TTA in the presence of a neutral donor such as TBP or TOPO. The extraction constants for many metallic species, including the rare earths, with TTA in the presence of a neutral donor are greater by up to 10^8 times their values in the absence of the neutral donor.

Although this makes the quantitative extraction of the rare earths possible in a single extraction it does not necessarily improve the selectivity of the extraction method because many other elements are also quantitatively extracted. Sieck and Banks (1971) reported that the rare earths were quantitatively extracted in a single stage operation by various fluorinated β-diketones and dibutylsulfoxide (the neutral donor). These ternary complexes were sufficiently volatile that several individual rare earths could be separated by gas–liquid chromatography.

1.5. *Chromatographic methods*

The separation of the individual rare earths from each other by chromatographic methods is covered in ch. 23. The only technique of importance for the analytical separation and determination of individual members of the rare earth group is elution chromatography (gas–liquid or liquid–liquid), paper, or thin layer chromatography. Although the separation of the individual rare earths on ion exchange columns, as discussed in ch. 23, is the method of choice for the preparation of pure individual rare earths, it is not widely used for the analytical determination of the individual rare earths. Although the rare earths can be separated by elution methods from ion exchange columns, this method is too tedious to be of great importance. It has been used, however, as reported in Aladjem (1970), pp. 19–194, for separation of trace amounts of the rare earths in radioactive mixtures and in neutron activation methods. A strong acid cation exchange resin, such as Dowex-50, which is 6–12% in divinylbenzene, DVB, and with a mesh size of 200–500 is ordinarily employed in these separations. The separation factors of the rare earths on these resins are too small in the absence of a complexing reagent to give any useful separations. Use is made of the relatively large differences in the formation constants of the rare earths with reagents such as lactic acid, α-hydroxyisobutyric acid, EDTA, and similar chelating reagents. The separation factors for the different rare earths from each other is a relatively complicated function of the pH, temperature, flow rate and reagent used. This is discussed in chapter 23.

Mitchell and Banks (1971 and 1972) studied the thermal properties of various fluorinated β-diketonates of the rare earths, uranium, and thorium and found the volatility and thermal stability of the chelates were improved when an adduct was formed with some neutral donor. Butts and Banks (1970) and later Sieck and Banks (1972) demonstrated that the separation of the lanthanides as ternary complexes with a fluorinated β-diketone and TBP or di-n-butylsulfoxide by gas-liquid chromatography was possible. Although this method is reasonably sensitive it has not been demonstrated to be reliable at trace levels of the rare earths.

O'Laughlin et al. (1966a,b), reported the rare earths and a number of other elements could be separated by extraction (also referred to as reversed-phase partition) chromatography. The rare earths were spotted on chromatographic paper treated with various neutral organophosphorus reagents including TBP, TPOP, and MHDPO and the papers developed with hydrochloric, nitric, or perchloric acids of various concentrations.

The largest difference in R_f values for various rare earth pairs was observed when relatively concentrated nitric acid was used to elute the rare earths. The individual rare earths were detected by spraying the papers (after drying) with 8-hydroxyquinoline or Arsenazo I. Sub-microgram amounts of the individual rare earths could be detected and the separation of up to five rare earths was accomplished in less than an hour by radial chromatography.

O'Laughlin and Jensen (1968) also studied column separations of the rare earths on glass columns packed with a fluorinated polymer (Kel-F) and impregnated with MHDPO. The rare earths could be eluted separately but the method was slow and the capacity of the columns quite low. This method, like ion exchange chromatography, is quite useful for the rapid separation of the rare earth group from Th and U.

An extensive summary of methods for the chromatographic isolation and separation of the rare earth group is given by Aladjem (1970), pp. 77–108, including many paper chromatographic separations using various ethers, ketones, and alcohols and mixtures of these to elute the rare earths.

1.6. *Chemical methods for the determination of individual rare earths*

The only practical chemical methods for the determination of any of the individual rare earths from each other and, especially, adjacent lanthanides are based on the oxidation of cerium(III) to cerium(IV) and the determination of Ce(IV) by gravimetric or volumetric methods as discussed in previous sections. Fractional crystallization methods can be used to separate the rare earths into subgroups, but clean separations of adjacent rare earths are not feasible. As mentioned previously, Eu, Sm, and Yb can be reduced to the plus two oxidation state, but only Eu(II) can really be satisfactorily determined by chemical methods.

A number of photometric-extraction methods have recently been described for the determination of individual rare earths which will be described in a subsequent section on spectrophotometric methods.

1.7. *Miscellaneous methods*

The rare earth group can be effectively separated from many other elements which form volatile chlorides by thermal methods because the rare earth chlorides are not volatile. Fusion of the rare earth nitrates with $NaNO_3$ at temperatures under 300°C results in the selective formation of CeO_2. The melt is simply dissolved in water and the CeO_2 separated by filtration. These and other thermal methods are summarized by Aladjem (1970), pp. 138–139.

Several other rather novel methods for the separation of the lanthanides are discussed in the above text. Eu, Yb, and Sm can be reduced by amalgams of the alkali or alkaline earth metals to either the metal or the divalent ions which can be precipitated as sparingly soluble sulfates, RSO_4. Electrolytic reduction at a mercury cathode can be used to separate the above three elements. A number of

the rare earths can also be isolated by electrolysis from nonaqueous media. Electrophoresis has also been employed to separate the rare earths.

2. Molecular spectrometric methods

2.1. *Spectrophotometric methods based on the absorption spectra of the lanthanide ions*

The absorption spectra of the lanthanide ions are quite characteristic of the individual lanthanides. Scandium, yttrium, lanthanum, and lutetium do not absorb in the spectral region from 200–1000 nm. The remaining lanthanides all absorb in this region, although the molar absorptivities of even the most intense bands are less than 12 ℓ/mole·cm as is shown in table 37A.1.

The absorption bands for the lanthanides are extremely narrow even in solution because they reflect electronic transitions in the 4f sub-shell. The spectra are quite characteristic for the individual lanthanides and, although the molar absorbtivities are quite low (less than 12 ℓ/mole·cm), these bands can be employed to determine the individual lanthanides in mixtures with the aid of a good spectrophotometer. The most intense and analytically useful absorption bands for the various lanthanides occur at the wavelengths indicated in table 37A.1 with the major absorptivities for the particular spectrophotometer indicated (Cary 14) given in bold-faced type. Because the absorption bands are so narrow, it is quite important to specify the exact conditions under which the molar absorptivities are obtained and to carefully calibrate the wavelength scale of the spectrophotometer. The lanthanides are preferably determined as solutions of the chlorides or perchlorates in moderately acidic solutions as reported by Banks and Ryan (1956). Considerable care must be taken to insure that the molar absorptivities, or Beers law plots, are taken, so far as possible, under exactly the same conditions for the unknown and standard samples. Very slight errors in adjusting the wavelength could result in large errors in the determination of an unknown if published values for the molar absorptivity are used. For reasonably accurate results (in the ±2% range) it is imperative that calibration plots be prepared at the same time the unknown is determined, on the same instrument, and with no change in the wavelength. The wavelengths for the absorption maximum for several of the bands for some of the rare earths are shifted slightly by changes in the nature of the anion present or the concentration of other salts in the solution. Complexing reagents present in the solution also result in wavelength shifts for some rare earth absorption bands. Banks et al. (1956, 1958) showed that several lanthanides and several simple mixtures of lanthanides in the presence of Y could be determined very precisely by differential spectrophotometric methods with relative standard deviations less than 0.1%. This method has been discussed in detail by O'Laughlin and Banks (1960) and involves the measurement of the difference in absorbance of the unknown solution and a standard solution of known composition which matches the composition of the

TABLE 37A.1
Molar absorptivity of rare earth ions at analytical wavelengths*

	Molar absorptivity, ϵ (ℓ/mole·cm)									
λ(Å)	Pr	Nd	Sm	Eu	Gd	Dy	Ho	Er	Tm	Yb
272.8	1.13	0.210	0.166	0.335	4.20*	0.215	0.227	0.698	0.685	0.365
287.9	0.511	1.185	–	0.132	–	0.140	3.59	0.316	0.521	0.266
350.4	–	2.60	0.052	–	–	2.54*	0.057	0.096	0.145	–
354.0	–	5.20	0.087	–	–	0.737	0.047	0.382	0.454	–
361.1	–	0.042	0.453	0.053	–	0.271	2.34*	0.296	0.801	–
365.0	–	0.025	0.244	0.062	–	2.10	0.331	1.94	0.154	–
379.6	–	0.067	0.052	0.299	–	0.252	0.047	7.18*	–	–
394.2	–	0.025	0.148	3.06*	–	0.233	0.123	0.096	–	–
401.5	–	–	3.31*	0.097	–	0.187	0.038	0.086	–	–
444.2	10.49*	–	0.044	–	–	0.047	0.454	0.306	–	–
450.8	1.29	0.025	–	–	–	0.261	4.16	0.497	–	–
521.6	–	4.41*	–	–	–	–	0.047	2.10	–	–
523.5	–	1.68	–	–	–	–	0.076	3.20*	–	–
537.9	–	–	–	–	–	–	5.16*	0.076	–	–
575.5	0.102	6.93	–	–	–	–	–	–	–	–
640.4	–	–	–	–	–	–	3.53*	0.153	–	–
683.0	–	0.336	–	–	–	–	–	–	2.56*	–
739.5	–	7.20	–	–	–	–	–	–	0.058	–
794.0	–	11.78*	–	–	–	0.084	–	0.143	0.579	–
908.0	–	–	–	–	–	2.46*	0.113	–	–	0.089
974.0	–	–	0.052	–	–	0.047	–	1.29	–	2.12*

*The spectra were recorded by a Cary-14 recording spectrophotometer with a wavelength scale calibrated with reference to mercury lines. Cells with $\ell = 10$ mm were used (20 mm cell for Yb, and 50 mm cell for Tb). All solutions contained 20 mg of oxide in 1 ml of 1 M $HClO_4$ (except in the case of Er, 10 mg/ml). The figures with asterisks refer to the coefficients at the wavelengths used (or recommended) for determining the respective element [from Banks et al. (1956)].

unknown as closely as possible, but where the concentration of the species being determined in the standard solution is slightly less than in the unknown.

Although applications of this method to the determination of the lanthanides are limited in scope, it has proved useful in the precise determination of selected rare earths in alloys where the approximate composition was known, and in the direct determination of purity of rare earth oxides. One of the major advantages of the method is the compensation for any errors introduced in the spectrophotometric measurement itself since the standard and unknown solutions are affected to nearly the same extent.

The absorption spectra of Ce(III), Gd, and Tb lie entirely in the ultraviolet region of the spectrum as can be seen in fig. 37A.1. The broad charge transfer band due to Ce(III) is so much more intense ($\epsilon \cong 700$ ℓ/mole·cm) than the most intense bands for Gd and Tb ($\epsilon \cong 4.2$ for Gd and $\epsilon < 2$ for Tb) that neither of the latter elements can be determined in the presence of even a small amount of Ce(III). The spectrum of Ce(III) is strongly affected by the presence of various

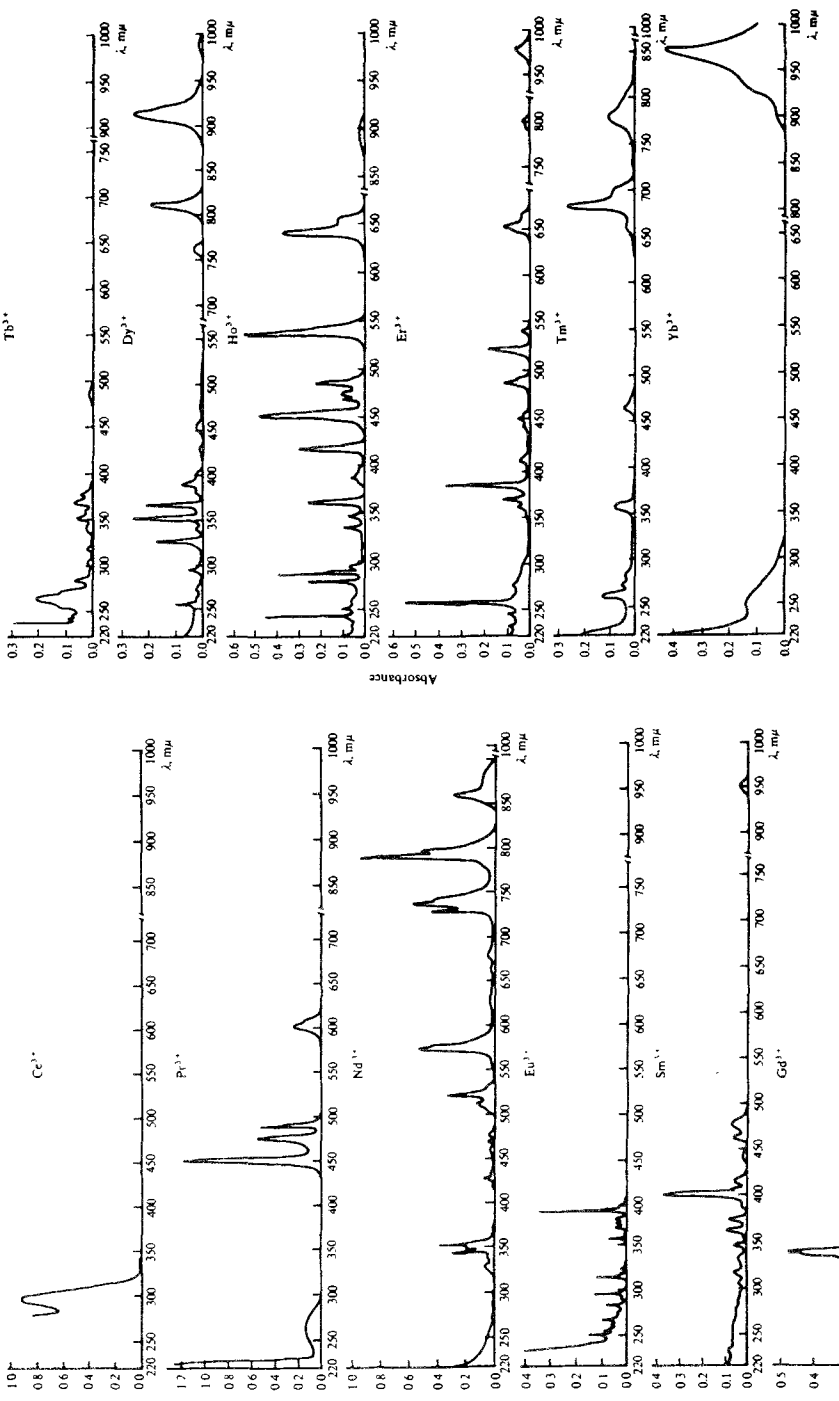

Fig. 37A.1. Absorption spectra of rare earth elements in 1 M $HClO_4$ [From Banks, et al. (1956)].

anions and, of course, any other species which absorb in the ultraviolet region would constitute a serious interference. Although it has been used to determine Ce(III) in binary alloys by Greenhaus et al. (1957) based on the absorption of Ce(III) in 1 N sulfuric acid at 253.6 nm, there are many interferences. The above authors claimed the method was superior to methods involving the oxidation of Ce(III) with peroxide in basic solution or methods involving the determination of Ce(IV) in acidic solution. The major difficulty in the latter case is the complete removal of excess oxidizing reagent and the instability of very dilute Ce(IV) solutions in acidic medium.

2.2. *Methods based on reactions of the rare earths with chromogenic reagents*

A great many chromogenic reagents have been reported for the rare earths. Except in the case of cerium, these methods are not specific for the rare earths, although in some cases they are resonably selective toward a particular subgroup. These methods are very sensitive with molar absorptivities for the rare earth complexes with some reagents on the order of 7×10^4 ℓ/mole·cm. Aladjem (1970), pp. 168–177, has summarized much of the information prior to 1966 on the colorimetric or spectrophotometric determination of the rare earths based on reactions with chromogenic reagents.

Ce is the only rare earth that can be determined selectively in the presence of the other rare earths and even other quadrivalent metals based on the powerful oxidizing power of Ce(IV). These methods involve the oxidation of cerium to Ce(IV) which quantitatively reacts with many colored reagents and organic dyes. Ce(IV) can also be determined based on the quantitative oxidation of Ferroin, tris-(1,10 phenanthroline) iron II, in dilute sulfuric acid. The Ce(IV) is added to an excess amount of Ferroin and the decrease in absorbance at 505 nm is observed. The useful working range is in the order of 0.2–10 mg/ml. Similar methods for the determination of Ce(IV) based on the oxidation of reagents such as strychnidine to give colored oxidation products have been reported by Aldajem (1970) p. 176.

Several chromogenic reagents used for the determination of the trivalent rare earths include: 8-hydroxyquinoline ($\epsilon \cong 5230$), Alizarin S ($\epsilon \cong 10^4$), Arsenazo I ($\epsilon \cong 10^4$), Arsenazo III ($\epsilon \cong 5 \times 10^4$). Arsenazo III has been reported by Savvin (1964, 1964a) to form 1:1 complexes with the rare earths and to be more selective than Arsenazo I and II. Cations which have a radius of less than 0.7–0.8 Å show no color reaction with Arsenazo III. These include Be, Zn, Al, Ga, In, Ge, Ti, and Sn. Sc, however, with an ionic radius of 0.81 (compared to 0.95 for In) does form a colored complex at pH of 1 to 2 as do the other rare earths, which suggests the ionic radius is not the only criterion to be considered. Arsenazo III also is an extremely sensitive reagent for tetravalent cations and the reaction with these cations can be carried out in strongly acidic media. Molar absorptivities as high as 1.5×10^5 ℓ/mole·cm have been reported.

Nemodruck et al. (1961) reported that the reagent Chlorophosphonazo III formed intensely colored complexes with many cations. O'Laughlin (1970) and Jensen

reported on the spectrophotometric determination of the lanthanides with this reagent. The reagent is intensely colored with a broad absorption maximum in the 550–580 nm region and a molar absorptivity of 3.7×10^4 ℓ/mole·cm. A less intense absorption band at 404 nm with a shoulder near 645 nm was also reported. The rare earth complexes had maxima near 675 nm with molar absorptivities ranging from 4×10^4 for La which increased up to 7×10^4 for Er. The maximum values for the remaining lanthanides fell between these extremes. The molar absorptivities were reasonably constant from pH 4 to pH 2 with maximum values near pH 2.3. A decrease in the molar absorptivity was noted below pH 1 which was most noticeable for the heavy lanthanides.

Although recent developments, especially in the areas of atomic absorption and emission spectroscopy, make these methods superior for the determination of trace amounts of individual rare earths, chemical methods, especially for elements such as Ce continue to be of interest. New more sensitive and selective reagents have been synthesized and techniques such as extraction-photometric methods and the use of competing ligands to improve the selectivity of chemical methods have made spectrophotometric methods more attractive in view of the rapidly rising cost of the sophisticated instruments necessary to determine the rare earths.

Poluektov et al. (1972) have described a photometric-extraction method for the selective determination of Sm and Eu in binary alloys with La. The rare earths are extracted into isobutanol as a ternary complex with Bromopyrogallol Red and N-benzoyl-N-phenylhydroxylamine (BHPA). The alcohol phase was equilibrated with nitrilotriacetic acid (NTA) which back extracted lanthanum but did not affect the Sm or Eu complexes. Similar methods were employed by Poluektov et al. (1973) to separate the yttrium subgroup from the cerium subgroup. Complexes of the lanthanides with quinalizarin (QA) and benzoic acid (BA) were extracted into n-butanol at pH 9.7–10.4 as the ternary complex $R(QA)(BA)_2$. The benzoic acid was reported to suppress the color reaction with the cerium subgroup but did not affect the color reaction with the yttrium subgroup. Savvin et al. (1974) described a spectrophotometric method for the spectrophotometric determination of La, Ce, Pr, and Nd in the presence of a 650-fold excess of Fe(III) based on the color reaction of the rare earths with carboxynitrazo. Interference by Fe(III) and the heavy rare earths was masked by the addition of EDTA. It was reported that as little as 0.089% La in steel could be determined. Poluektov et al. (1971) reported the determination of the rare earths in natural waters based on the extraction of the ternary complexes of the rare earths with Arsenazo III and diphenylquanidine into butyl alcohol. Nemodruck et al. (1973) investigated the photochemical oxidation of Ce(III) to Ce(IV) in carbonate solutions and reported this technique could be employed to determine micro-amounts of Ce in the presence of other rare earths. Elbeih et al. (1975) recently reported a sensitive method for the determination of Ce(IV) based on the bleaching of the dye 4-dimethyl-amino-azobenzene-4'-arsonic acid which has an absorption maximum at 490 nm.

Sensitive chemical methods for the determination of Ce are of particular

importance because it is difficult to determine Ce spectroscopically due to its complex spectrum and the absence of any intense spectral lines. Methods for the chemical determination of Ce have been recently reviewed by Kharlamova et al. (1974).

2.3. *Spectrophotofluorimetric methods*

Solutions of salts of Pr, Sm, Eu, Gd, Tb and Dy exhibit characteristic fluorescence spectra when irradiated by ultraviolet light but the fluorescence is low in intensity and often quenched by other ions or compounds present in solution as noted by Aladjem (1970), p. 182. Consequently the direct determination of the rare earth ions in solutions based on their fluorescence spectra is not generally attempted. Very sensitive methods for the determination of several rare earths based on the fluorescence of these elements in solid matrices have been developed and are described in another section.

Carey and Banks (1969) utilized the fluorescence of ternary complexes of Eu(III) with various β-diketones such as thenoyltrifluoroacetic acid, TTA, and various neutral donors such as TBP, TOPO and MHDPO to study the stoichiometry of these species. The intensity of the red fluorescence band by these ternary complexes is much greater than that exhibited by the simple chelates of Eu(III) with β-diketonates and can be used for the determination of Eu(III) at the ultra trace levels. The ternary complexes can be conveniently prepared by the synergic extraction of the Eu(III) chelate into an organic solvent containing a neutral donor such as TBP, TOPO or MHDPO.

Several rare earths, including La, Gd, Lu, Y and Sc form intensely fluorescent chelates with reagents such as 8-hydroxyquinolines and various other chelating reagents. The analytical usefulness of methods based on the fluorescence of these chelates is limited, however, because other elements, notably the alkaline earths, also form fluorescent chelates and the presence of other rare earths, various anions, and other compounds tend to quench the fluorescence.

3. Polarographic methods

The rare earth earths, with the exception of Sm, Eu and Yb which can be reduced to an intermediate divalent state and Ce which shows an anodic wave due to oxidation to the quadrivalent state, do not have desirable electrochemical properties and are not usually determined by electrochemical methods. The reduction of the rare earth elements at a mercury cathode as evidenced by a single polarographic wave with an $E_{1/2}$ of from approximately -1.8 to -2.0 volts relative to the saturated calomel electrode is obscured by the wave due to the reduction of the hydrogen ion in acidic media and other parallel electrochemical reactions. Aladjem (1970) summarizes reported values for $E_{1/2}$ for the rare earths for the reaction,

$$R^{+3} + 3e^- \rightarrow R$$

TABLE 37A.2
$E_{1/2}$ values for the reduction of the rare earths at a mercury cathode relative to a saturated calomel electrode at 25°C [from Aladjim (1970)].

Element	$E_{1/2}$(V) vs. SCE at 25°C	Element	$E_{1/2}$(V) vs. SCE at 25°C
La	−1.79 to −2.04	Dy	−1.90 to −1.94
Ce	−1.74 to −2.01	Ho	−1.88
Pr	−1.82 to −2.00	Er	−1.88
Nd	−1.79 to −2.01	Tm	−1.85 to −2.02
Sm	−1.96 to −2.01	Yb	−2.00 to −2.03
Eu	−2.51	Lu	−1.82
Gd	−1.77 to −1.99	Y	−1.88 to −1.98
Tb	−1.92		

and reports a range of values (under different polarographic conditions) as shown in table 37A.2.

The reduction potentials for the reaction,

$$R^{+3} + 1e \rightleftharpoons R^{+2}$$

are considerably more positive as shown in table 37A.3 and permits the polarographic determination of these elements. Europium can be readily determined polarographically and Eu and Yb by differential polarography as shown by Pomeroy et al. (1952). The pH is more critical in the case of Yb because the reduction potential for Yb^{+3} is close to that of the hydrogen ion.

The presence of either the nitrate or nitrite ions has been found to markedly enhance the height of the polarographic wave for Yb and a differential pulse polarographic method for the determination of these anions based on this phenomenon has been proposed by Boese et al. (1977).

Scandium (1–10 mg) can be determined by an indirect polarographic method in the presence of up to 100 times its amount of the other rare earths as shown by Sevryukov and Berofeeva (1973) based on the displacement of In^{+3} from the complex $In(EDTA)^{-}$. Thorium interfers. The total amount of thorium and the rare earths can be determined by the displacement of Mn^{+2} from the complex $Mn(EDTA)^{-2}$.

TABLE 37A.3
$E_{1/2}$ values for Sm, Eu, and Yb at a mercury cathode for the system R^{+3}/R^{+2} at 25°C [from Aladjem (1970)].

Element	$E_{1/2}$
Sm	−1.72 to −1.82
Eu	−0.671 to −0.73
Yb	−1.41 to −1.46

Polarographic methods are not as sensitive nor as accurate as spectrometric methods and are seldom employed at this present time.

References

Aladjem, A., 1970, Analytical Chemistry of Yttrium and the Lanthanide Elements (Ann Arbor-Humphrey Science Pub., Inc., Ann Arbor, Mich.).

Banks, C.V. and C.H. Byrd, 1953, Anal. Chem. **25**, 416.

Banks, C.V. and D.W. Klingman, 1956, Anal. Chem. Acta. **15**, 356.

Banks, C.V. and D.W. Klingman, 1961, Analytical Chemistry of the Rare Earths, in: Spedding, F.H. and A.H. Daane, eds., The Rare Earths, 1961, (John Wiley and Sons, Inc., New York) Chap. 23.

Banks, C.V. and J.W. O'Laughlin, 1956, Anal. Chem. **28**, 1338.

Banks, C.V., J.L. Spooner and J.W. O'Laughlin, 1956, Anal. Chem. **28**, 1848.

Banks, C.V., J.L. Spooner and J.W. O'Laughlin, 1958, Anal. Chem. **30**, 458.

Barbieri, G.A., 1916, Atti accad. Lincei **25**, No. 1, 37.

Boese, S.W. and V.S. Archer and J.W. O'Laughlin, 1977, Anal. Chem. **49**, 479.

Broadhead, K.G. and H.H. Heady, 1960, Anal. Chem. **32**, 1603.

Burgett, C.A. and J.S. Fritz, Anal. Chem. **44**, 1738 (1972).

Butts, W.C. and C.V. Banks, 1970, Anal. Chem. **42**, 133.

Carey, M.A. and C.V. Banks, 1969, J. Inorg. Nucl. Chem. **31**, 533.

De, A.K., 1965, J. Sci. Ind. Res., 1965, **24**, No. 2, 82.

Dziomko, V.M., V.M. Ostrovskaya and O.V. Kon'kova, 1970, Russ. J. Anal. Chem. **25**, No. 2, 222.

Elbeih, I.M., A.S. Shawali and M.A. Aboutabl, 1975, Z. Anal. Chem. **274**, No. N1, 31.

Foster, D.C. and H.E. Kremers, 1953, Anal. Chem. **25**, 1921.

Greenhaus, H.L., A.M. Feibush and L. Gordon, 1957, Anal. Chem. **29**, 1531.

Healy, T.V., Nucl. Sci. Eng. **16**, N.4, 413.

Kharlamova, L.T., T.A. Borch and V.T. Solomatin, 1974, Russ. J. Anal. Chem. **40**, No. 10, 1393.

Meider-Gorican, H., 1967, Some Novel Phosphoryl Compounds as Extractants for Zirconium, Niobium and Tantalum, in: Dyrssen, D., Liljenzin, J.O., and Rydberg, J., eds., Solvent Extraction Chemistry, 1967, (North Holland Pub. Co., Amsterdam), pp. 278–282.

Mitchell, J.W. and C.V. Banks, 1972, Talanta **19**, 1157.

Mitchell, J.W. and C.V. Banks, 1971, Anal. Chem. Acta. **57**, 415.

Nemodruk, A.A., Y.P. Novikov, A.Am. Lukin and I.D. Kalinina, 1961, Russ. J. Anal. Chem. **16**, No. 2, 187.

Noyes, A. and B. Bray, 1927, A System of Qualitative Analysis for the Rare Earth Elements (Macmillan, London).

O'Laughlin, J.W., 1966, Chap. 2 in: Progress in Nuclear Energy, Stewart, D.C. and H.A. Elion, eds., (Pergamon Press, London).

O'Laughlin, J.W. and C.V. Banks, 1964, Anal. Chem. **36**, 1222.

O'Laughlin, J.W. and C.V. Banks, 1960, Differential Spectrophotometry in: Clark, G.L., ed., Encyclopedia of Spectroscopy, 1960 (Reinhold Pub. Corp., New York).

O'Laughlin, J.W., J.W. Ferguson, J.J. Richard and C.V. Banks, 1966b, J. Chromatog. **24**, 376.

O'Laughlin, J.W. and D.F. Jensen, 1968, J. Chromatog. **32**, 567.

O'Laughlin, J.W. and D.F. Jensen, 1970, Talanta **17**, 329.

O'Laughlin, J.W., G.J. Kamin and C.V. Banks, 1966a, J. Chromatog. **21**, 460(a).

Poluektov, N.S., T.N. Kamnera, R.S. Lauer and S.F. Ognichenko, 1972, Russ. J. Anal. Chem. **27**, No. 6, 981.

Poluektov, N.S., A.I. Kirillov and O.P. Makarenko, 1971, Industrial Laboratory, **37** No. 5, 680.

Poluektov, N.S., O.P. Makarenko, A.I. Kirillov and R.S. Lauer, 1973, Russ. J. Anal. Chem. **28**, No. 2, 242.

Pomeroy, P.R., R.A. White and G.H.R. Gwatkins, 1952, Metallurgico **46**, 157.

Reilley, C.N., R.W. Schmid and D.W. Lamson, 1958, Anal. Chem. **30**, 953.

Richard, J.J., K.E. Burke, J.W. O'Laughlin and C.V. Banks, 1961, J. Amer. Chem. Soc. **83**, 1722.

Ryabchikov, D.I. and V.A. Ryabukhin, 1966, Analiticheskaya Khimiya Redkozemel'nykh Elementov I Iffriya (Instut Geokhimii i Analiticheskoi Khimii im. Vernadskogo, Moskva).

Savin, S.B., 1964, Talanta **11**, 1.

Savin, S.B., 1964a, Talanta **11**, 7.

Savin, S.E., T.V. Petrova and P.N. Romanova, 1974, Russ. J. Anal. Chem. **24**, No. 10, 1663.

Sevryukov, N.N. and G I. Dorofeeva, 1973, Russ. J. Anal. Chem. **28**, No. 1, 62.

Sieck, R.F. and C.V. Banks, 1972, Anal. Chem. **44**, 2307.

Smith, G.F., 1942, Cerate Oxidimetry, G. Frederick Smith Chemical Co., Columbus, Ohio.

Kolthoff, I.M. and P.J. Elving, Eds., Treatise on Analytical Chemistry, 1963, (Interscience Pub., New York).

Nemodruck, A.A., E.V. Bezrogova, B.F. Myasoedov, 1973, Zh. Anal. Khim. 28, 1947.

Smith, G.F. and C.A. Getz, 1938, Ind. Eng. Chem., Anal. Ed., **10**, 191.
Vickery, R.C., 1953, Chemistry of the Lanthanons (Academic Press, Inc., N.Y.).
Von Knorre, G.Z., 1897, Z. Angew. Chem. **11**, 717.
Willard, H.H. and P. Young, 1928, J. Am. Chem. Soc. **50**, 1379.
Woyski, M.M. and R.E. Harris, 1963, The Rare Earths and Rare Earth Compounds, in: Kolthoff, I.M. and P.J. Elving, eds., Treatise on Analytical Chemistry, 1963, Vol. 8, Part II (Interscience Pub., N.Y.) pp. 1–146.

Handbook on the Physics and Chemistry of Rare Earths, edited by K.A. Gschneidner, Jr. and L. Eyring

Chapter 37B

TRACE ELEMENT ANALYSIS OF RARE EARTH ELEMENTS BY SPARK SOURCE MASS SPECTROMETRY

S.R. TAYLOR
Research School of Earth Sciences, Australian National University, Canberra, Australia

"I feel sure that there are many problems in Chemistry which could be solved with far greater ease by this than by any other method. The method is surprisingly sensitive – more so even that of Spectrum Analysis, requires an infinitesimal amount of material and does not require this to be specially purified: The technique is not difficult if appliances for producing high vacua are available."

Thompson, J.J., 1913, *Rays of Positive Elasticity and their Application to Chemical Analyses* (Longmans, Green, London).

Contents

Symbols

d = photographic density
I_x = intensity value for isotope x
I_{Lu} = intensity for lutetium internal standard
$\tan\theta$ = photoplate gamma

1. Introduction

Following the development of the spark source mass spectrometer in the 1950's as an analytical tool for the detection of ppm levels of impurities in materials of interest to solid state physicists (Craig et al., 1959; Brown et al., 1962), the instrument was adapted to the trace element analysis of REE in geological samples by Taylor (1965a,b) and Nicholls et al., (1967), and for biological materials by Evans and Morrison (1968).

This early work demonstrated the potential of the method for the determination of chemical elements in geological materials down to about levels of 0.01 ppm. Early problems in precision and accuracy were resolved by Taylor (1971) and the technique is now well established and competitive with neutron activation methods.

There are several inherent advantages, in the technique:

(1) All REE are detectable, and measurable.

(2) Only small samples (typically 50 mg) are required, and samples down to one milligram have been analysed.

(3) The method is rapid. Typically one or two samples can be handled per working day, using the techniques described here.

(4) The method is comprehensive. Under the conditions described, data for U, Ba, Cs, Hf, Nb, Pb, Sn, Th, U, Y and Zr are typically obtained, with values for Bi, Tl and W often being obtained in addition.

(5) The method is sensitive to 0.01 ppm. Under the conditions described, the optimum concentration range lies between 0.1 ppm and about 200 ppm.

The REE are typically present in geological materials at levels of a few parts per million. Abundance levels are given in table 37B.1 for chondritic meteorites, where the range in concentration is from 0.031 ppm for Lu up to 0.84 ppm for Ce. The data in table 37B.1 illustrate the well-known alternation in absolute

TABLE 37B.1
REE abundances in chondrites and sedimentary rocks used for normalising.

Atomic No.		NASC 1	PAAS 2	3
57	La	0.30	32	38
58	Ce	0.84	70	80
59	Pr	0.12	7.9	8.9
60	Nd	0.58	31	32
62	Sm	0.21	5.7	5.60
63	Eu	0.074	1.24	1.10
64	Gd	0.30	5.2	4.7
65	Tb	0.049	0.85	0.77
66	Dy	0.31	5.0	4.4
67	Ho	0.073	1.04	1.0
68	Er	0.21	3.4	2.9
69	Tm	0.033	–	0.50
70	Yb	0.20	3.1	2.8
71	Lu	0.031	–	0.50
39	Y	2.00	–	28.0

1. Average chondrite values from Haskin et al. (1966, 1968). 2. Average North American Shale composite Haskin et al. 1966 (NASC). 3. Post-Archean average Australian Sedimentary rock (PAAS) (Nance and Taylor, 1976).

abundances between the REE of even and odd atomic number. This zig-zag effect in the abundance pattern, well known as the Oddo–Harkins Rule, is a consequence of the relative stability of nuclei with even and odd numbers of protons and neutrons (see appropriate section).

The abundances in different chondritic meteorites show close relative and absolute similarities, and this uniformity is commonly interpreted to indicate that the chondrites are displaying the relative REE abundance patterns of the primordial solar nebula.

The second abundance pattern which is also very uniform is that displayed by sedimentary rocks (table 37B.1). The range in abundance is from 0.50 ppm Lu up to 80 ppm Ce. In table 37B.1, the abundances of a composite sample of North American Shales (NASC) is compared with an average of Post-Archean Australian sedimentary rocks (PAAS). Note again the even-odd abundance variations. The general uniformity of these patterns is commonly interpreted as resulting from very thorough mixing during weathering, erosion and deposition of sediments, and hence this pattern is often taken as representing an average for the upper crustal rocks of the earth, exposed to such geological processes.

The abundance levels in table 37B.1 are typical of those encountered during analysis of geological materials, and the techniques have been designed for such levels.

The inherent usefulness of the REE for geochemical investigations is mainly due to the smooth variation in ionic radii of the trivalent ions. Ce^{4+} and Eu^{2+} are the only notable variations in valency under geochemical conditions. These properties provide a powerful tool for studying crystal-liquid fractionation. Under the more extreme conditions in the solar nebula, the relative volatility of Eu and Yb relative to the other REE provide a powerful method for studying gas-solid equilibria, through phases preserved in meteorites.

2. Presentation of REE data

In order to avoid the zig-zag effect, and to provide a ready method to compare and contrast REE abundances, it is customary to normalise the trace REE data, element by element, to the uniform chondritic abundances. This procedure was suggested by Coryell et al. (1963). The effect of normalising element by element removes some of the analytical uncertainty caused by normalising to one element. It also allows for ready comparison of both relative patterns and absolute abundances between different samples.

3. Principles of spark source mass spectrometry

In this method, a pulsed RF spark is used to produce an ion beam, which is resolved into the individual masses (e/m) in a double focussing mass spectrometer, with the masses being recorded either photographically or electrically.

The high energy of the RF spark source means that the relative sensitivity of all elements is within an order of magnitude, and that mass spectra of all elements present are produced. The method is very sensitive, and interferences are not extensive. For these reasons the technique is suited to the analysis of geological materials in which most of the elements in the Periodic Table are present. The advantages of the RF source thus lie in the high sensitivity, roughly equal efficiency for all elements, and in the small amount of sample consumed. However, the ion beams so produced show a very wide spread in energy, and random fluctuations of intensity with time. These limitations are overcome by using a double focussing mass spectrograph design which focusses ions of one mass (e/m) at a point irrespective of their initial energy and direction. Due to the great intensity fluctuations, an integrating detector is required. For this reason, a photoplate is commonly employed. The double-focussing design of Mattauch and Herzog (1934) brings the differing masses into focus in one plane, making possible the use of a photoplate as a detector.

4. The mass spectrograph

The instrument used in this laboratory is manufactured by Associated Electrical Industries in Manchester, as their type M.S.7 (Brown et al., 1962; Craig et al., 1959). It is a double focussing mass spectrograph based on the design by Mattauch and Herzog (1934). This design compensates for the wide spread of ion energies produced in the spark source and ions are brought to focus in a single plane depending on their mass and not on their initial energies. This focussing arrangement allows a photographic plate to be used as detector. The photographic plate is also able to integrate the variable ion beam due to wide fluctuations in the output from the spark source. Electrical detection systems are also available (e.g. Conzemius and Svec, 1968).

The basic layout of the instrument is shown in fig. 37B.1. The source parts which are exposed to the spark are made of tantalum, which has one major isotope at mass 181. The electrode holders may be moved from the outside, through bellows, during operation. The source area can be isolated from the main vacuum by hydraulic valves to allow the sample to be changed.

The beam from the spark source is accelerated by a 20 kV differential potential, and passes through 3 slit plates to define the beam. About 50 per cent of the beam is intercepted by the monitor collector plate and the output from the monitor amplifier is displayed on a meter. The output from the monitor is integrated to provide a rough measure of exposure, and this is displayed on a second, or integrator meter.

Two rotary pumps and four oil diffusion pumps with associated cold traps are used to evacuate the instrument. The pumping outlets are indicated on fig. 37B.1 and show that the system comprises four main regions, the source, the source-analyser interspace, the analyser, and the photoplate magazine. When an analysis is being carried out, the only connections between source and analyser

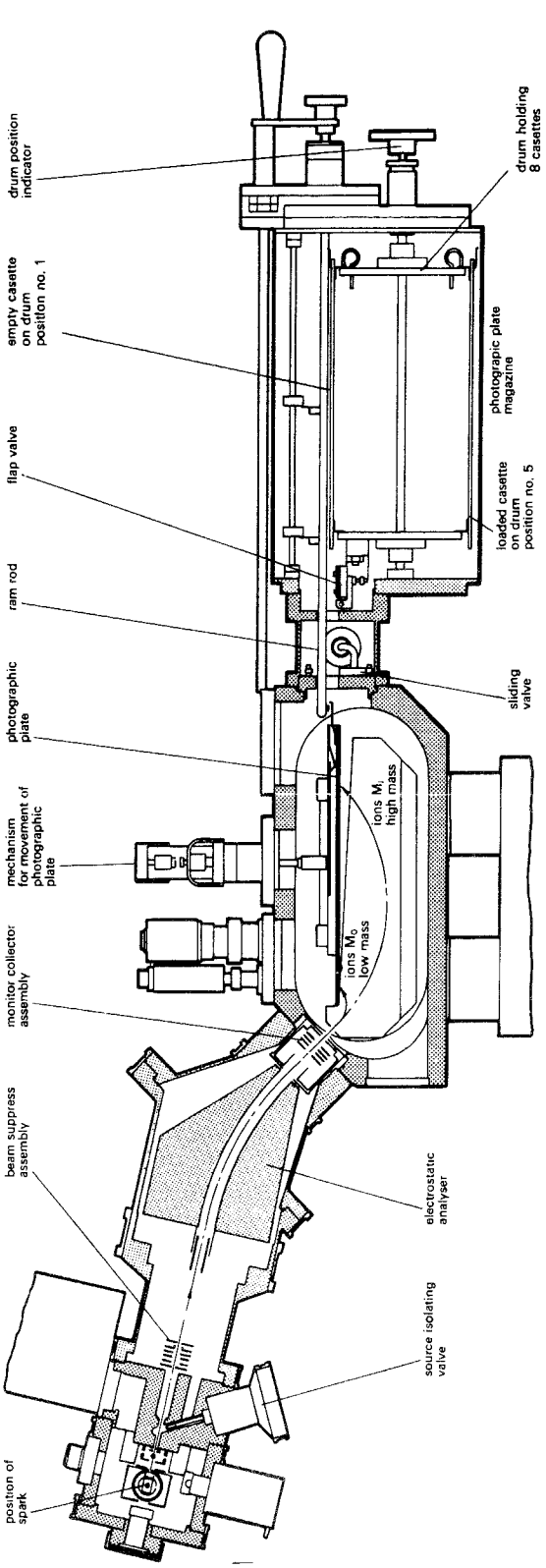

Fig. 37B.1. Double focussing spark source mass spectrometer (A.E.I. MS7).

regions are through narrow slits, allowing differential pumping factors of several thousand between the source and analyser region. The sliding valve (fig. 37B.1) likewise ensures a differential pumping factor of several hundred between the analyser and photoplate magazine.

Pressures of $<1 \times 10^{-8}$ mm mercury (torr) are obtained in the analyser region with photoplate inserted, and 1×10^{-7} torr in the source region, with sample inserted. Provision for baking the instrument is built in.

5. Sample preparation

The usual problems associated with preparation of geological samples for analysis are intensified because of the small amount of sample consumed. This calls for a high degree of homogeneity, and there is the possibility of contamination because of the low concentration levels sought. Extreme care is taken to avoid introducing impurities.

The procedure adopted in its entirety is as follows:

(1) The large rock samples are split down to 1 in size in a jaw splitter and passed through large and small jaw crushers to produce fragments about $\frac{1}{4}$ inch in size. These are then reduced to a fine powder (<200 mesh) in a TEMA mill using either tungsten carbide or agate grinding vessels. The use of tungsten carbide introduces up to 50 ppm W contamination. From 1–5 ppm interference on $^{93}Nb^{+}$ results from superposition of $^{186}W^{2+}$ at the same mass number, at these levels.

(2) The homogenised rock powder is mixed 1/1 with briquetting graphite [National Carbon Co. SP-1 grade, to which internal standard, Lu has been added (see section on internal standards). Mixing is carried out for 2 minutes in an agate vial in a Spex 5000 mixer mill. The agate vials must be cleaned before use to remove REE contamination from polishing compounds used during manufacture.

(3) About 100 mg of the mixture is placed in a 15×2 mm hole drilled in a polyethylene slug. This is placed in an AEI die and a pressure of 20 tons applied for about 30 seconds. Several electrodes are prepared for each sample.

6. Instrument operation

The electrodes are placed in position, the source is sealed and, after preliminary pumping, is opened to the main vacuum and the analyser region by means of hydraulic valves. The pressure is allowed to reach 10^{-6} torr before sparking. A few minutes pumping suffices to reach this figure and 10^{-7} torr is obtained in about an hour.

The photographic plate which has been stored and prepumped overnight in the magazine, is inserted into the analyser region, which is re-isolated by closing the sliding valve. The analyser pressure is then allowed to reach 1×10^{-8} torr before exposure commences. When the requisite pressures have been reached, the high

voltage and spark are switched on. The amplifier, magnet and deflector plate amplifiers are zeroed and sparking is commenced. The normal spark voltage is 25 kV. After waiting a few minutes to ensure a steady spark the plate is moved into position and the ion beam is allowed to pass into the analyser region. The electrode alignment is critical for producing a beam of suitable intensity and continuous monitoring of the beam is necessary. For the longer exposures, a beam intensity of about half the full scale deflection of the monitor amplifier meter is desirable. For the shorter exposures, a deflection of about 10% F.S.D. is suitable. The instantaneous beam currents vary from about 10^{-12} A for the shortest exposure conditions rising to about 10^{-9} A for the longer exposures.

The electrode alignment controls enable the electrode positions to be changed as the electrode is burnt away. It is desirable to maintain the pulse length and pulse repetition rates of the spark constant during exposure. For all exposures a pulse repetition rate of 300 c/s and a pulse length of 100 μsec is employed. The great majority of the elements of interest are determined using these conditions. If these parameters are changed, variations in the production of interfering species and in the ratio of singly to doubly charged ions occur.

To determine elements whose abundances are greater than about 100 ppm, the ion beam is attenuated. This is necessary to provide for a long sample burn to avoid sampling problems due to heterogeneity. Due to the sensitivity of the method and of the photoplate employed, abundant elements (> 100 ppm) produce a readable mass spectrum in very short time (< 10–30 seconds). A "beam chop" which deflects the ion beam by using an applied voltage of 500 volts is used to attenuate the beam. Only a few percent of the beam reaches the plate under these operating conditions.

The plates used are Ilford Q-2 2 × 10 in plates. These Schumann-type plates are very sensitive to abrasion and require careful handling and storage. They are developed for 3 min in Kodak D-19 developer at 20°C, washed, and fixed for 1 min in Kodak rapid liquid fixer followed by 5 min washing and 1 min rinse in distilled water containing Kodak Photo-flo.

The undeveloped plates are stored in a refrigerator at 4°C and are thawed, four or eight at a time, for 4 hours before placing in the photoplate magazine. This is left to pump down overnight before plates are inserted into the analyser.

7. Mass numbers and interferences

The mass numbers used for REE determinations are listed in table 37B.2 together with a list of possible interferences, which may arise as follows:

(1) Formation of multiply charged ions. The production of doubly charged ions results in the appearance of a line at half the mass number; a trebly charged ion produces a line at one third the nominal mass of the parent species. The production rate of these species falls off sharply.

(2) Polyatomic ion formation. The most notable example with the present technique is the appearance of lines at most multiples of twelve due to carbon.

TABLE 37B.2
List of REE nuclides used in SSMS technique

Element	Mass No.	Potential Interferences
Lu	176	^{176}Hf, ^{176}Yb
	175	–
Yb	174	^{150}[Sm, Nd] C_2, $^{138}BaC_3$
	173	$^{149}Sm\ C_2$, $^{137}BaC_3$
	172	^{148}[Sm, Nd]C_2, $^{136}BaC_3$
	171	$^{147}Sm\ C_2$, Ca_2AlO_4 in anorthite, $^{135}BaC_3$
Tm	169	$^{12}C_{14}H$
Er	167	$^{143}NdC_2$
	166	^{142}(Ce Nd)C_2
Ho	165	$^{141}Pr\ C_2$
Dy	163	$^{139}La\ C_2$
	161	$^{137}Ba\ C_2$
Tb	159	$^{135}Ba\ C_2$
Gd	158	$^{134}Ba\ C_2$
Eu	153	$^{137}Ba\ O$
	151	$^{135}Ba\ O$
Sm	149	
	147	$^{49}Ti_3$ in rutile
Nd	146	$^{26}Mg\ C_{10}$ in olivine
	143	
Pr	141	$^{47}Ti_3$ in rutile
		$Na_3\ ^{37}Cl_2$ in chlorides
Ce	140	$^{28}Si_5^+$, Mg_2SiO_4
		$Na^{35}Cl_2$ in chlorides
La	139	$^{40}Ca_2AlO_2$ in plagioclase
		$^{40}CaAl\ ^{48}TiC_2$ in Ti rich samples.
Y	89	$^{25}MgO_4$

Carbon interference appears at mass 144 due to $^{12}C_{12}^+$, at 156 due to $^{12}C_{13}^+$ and at 168, due to $^{12}C_{14}^+$.

The process is less efficient than the production of multiply charged ions, and is a problem only with the common elements.

The overall abundance pattern of the elements tend to minimise the effects of these two interferences. The formation of multiply charged ions is common, but the elements of lower mass, which are subject to this interference, are generally very much more abundant than the interfering species of higher mass. The interferences are not serious except in a few cases. Thus $^{45}Sc^+$, which commonly has a concentration of 20–50 ppm suffers from interference due to $^{90}Zr^{2+}$ which is generally much more abundant. Likewise $^{69}Ga^+$ with an average abundance of 20 ppm suffers interference from $^{138}Ba^{2+}$.

(3) Oxide or carbide formation. The principal interference for REE analyses using this technique arise from carbide formation. This is not a very efficient

process, but contributes notably when Ba and the light REE (La–Sm) are enriched relative to the heavy REE [Gd–Lu]. Interference levels are commonly less than 0.5 ppm due to this cause and are removed during computer processing of the data.

(4) Introduction of impurities. These can arise from many sources. Very careful handling procedures are required to avoid the introduction of hydrocarbons and the source parts, electrodes, photographic plates are always handled with tweezers or gloves. The laboratory is maintained in an ultra-clean condition. Air conditioning is provided as an aid to instrument stability.

8. Internal standards

If each sample contains the same, or a known concentration of an element the variations in source conditions and in plate sensitivity may be measured. This is the principle of the internal standard, introduced into emission spectroscopy by Gerlach (1925).

The requirements for an ideal internal standard are quite stringent. If a single element is sought, then an enriched isotope can be used as in the isotope dilution technique. However, the chief usefulness of the spark source technique lies in its ability to determine many elements and the considerations which are listed below are based on that premise:

(1) It should possess similar behaviour to the elements sought under the sparking conditions.

(2) It should preferably be added as an oxide since the elements sought are in general bonded to oxygen.

(3) It should possess a similar volatility and ionisation potential to the elements sought.

(4) It should possess at least two isotopes with a ratio of at least 50, enabling lines of readable density to be recorded on widely varying exposures.

(5) The isotopes should be odd-numbered to minimise interferences. Thus lines due to M^{2+} will occur at fractional masses.

(6) The isotopes should have masses greater than 120 to enable use on long exposures and to avoid interferences from multiple ion formation from $2M^{+}$ etc.

(7) It should not be an element of interest.

(8) It should be a rare element so that low concentrations (~ 10 ppm) are sufficient to swamp any natural concentration.

(9) The concentration to be added must be sufficiently high (> 1 ppm) to ensure adequate mixing.

(10) The material added must not contain other elements. This condition is aided by adding a low concentration.

(11) The concentration added must be such that an internal standard line be readable on each exposure of the photoplate.

The ultimate solution to these problems will probably be found in the use of enriched isotopes of the rarer elements and work was begun in this laboratory

using ^{113}Cd, ^{186}W, ^{176}Yb and ^{151}Eu, obtained from the Oak Ridge National Laboratory. However, these all contained impurities at the levels sought and attention was directed towards the use of pure compounds of elements which might meet the criteria listed above. Tests using the monoisotopic elements Ho and Tm showed that they showed sympathetic variation with elements of such diverse character as Cs, Ba, Zr and the rare earths. This work indicated that selective distillation effects are not serious, although wide variations in element sensitivity are encountered.

Lutetium is unique in having only two isotopes with an abundance ratio of 37–61, with the odd mass numbered isotope 175 being the most abundant. Thus all interferences due to multiply charged ions are insignificant. When 50 ppm Lu_2O is added, densities of the two Lu isotope lines 175 and 176 lie on the linear portion of the photoplate calibration curve for a wide range of exposures. Thus ^{175}Lu is usable for short exposures ($1–50 \times 10^{-9}$ C) while ^{176}Lu is at appropriate density levels for the longer exposures of $50–2000 \times 10^{-9}$ C. On the short exposures, there are no interferences on the ^{175}Lu line. Interferences due to ^{176}Hf, ^{176}Yb and natural ^{176}Lu are present on the ^{176}Lu line. These are corrected for as follows:

$$^{176}Lu = {}^{176}Lu\ (\text{measured}) - (0.19\,{}^{178}Hf + 0.89\,{}^{171}Yb)$$

The amount of natural ^{175}Lu and ^{176}Lu is calculated and corrected for in the computer processing of the data.

The preparation of the internal standard mixture is carried out as follows: 20 mg Johnson-Matthey Cat. No. 320 Specpure Lu_2O_3 is mixed with 100 mg of National Carbon Co. SP-1 graphite in a hand agate mortar, and then for 8 min in an agate vial (and ball) in a Spex 5000 mixer mill. The process is repeated during addition of another 400 mg of graphite. The mixture is then transferred to an alumina ceramic vial and mixed using a Spex 8000 mixer mill for 3 h, during addition to a total of 4.00 g. Two 1 in lengths of $\frac{1}{8}$ in. National Carbon Co. special spectrographic grade carbon are used to facilitate mixing, since the use of balls introduces contamination and packing of the powder. This master mix containing 5000 ppm Lu_2O_3, is used to prepare subsequent batches containing 50 ppm Lu_2O_3. These were prepared by taking 100 mg of the master mix and diluting to 10 g following the mixing procedure outlined above, with successive additions of graphite. It is not desirable to use plastic mixing vials in order to avoid possible introduction of hydrocarbons. Most other materials will introduce contamination. Minor contamination by Al is acceptable, since Al is not determined by this method.

9. Crystal lattice site internal standards (CLIS)

When the concentration of an element is already known, it may be used as a variable internal standard. This enables the use of elements which occupy the same crystal lattice sites as those whose concentration is sought (e.g. one rare

earth as internal standard for the other REE). This procedure has the following advantages (1) mixing problems caused by adding internal standards are removed; (2) since elements occupying the same lattice sites in crystals do so because of similar geochemical parameters, minimal chemical differences exist between internal standard and unknown elements. For example, ionization potentials and other factors important in ion beam production will generally be similar, and (3) release rates of elements from the lattice site during sparking will be similar, thus minimising effects due to varying volatility. The requirement that the internal standard isotope line be measured on the same exposure on the photoplate as that of the unknown, imposes a considerable limitation in practice, since the internal standard element needs to be in the same order of magnitude concentration range as the isotope to be measured.

10. Method of measurement of ion beam

The instantaneous ion beam current produced by sparking varies from 10^{-12} to 10^{-14} A depending on sparking parameters and may vary by factors up to 5 over periods of 1 sec. This instantaneous current measurement is integrated and this integrated beam current is used as a measure of exposure. The longest exposures record a total charge of 1000×10^{-9} C and take about an hour to record on the Ilford Q-2 photoplate detector with ion beam monitor readings of 40% of fullscale deflection. Continuous monitoring of the ion beam and frequent adjustment of the electrode positions are required to maintain the ion beam, causing variations in source geometry relative to the primary slit. Automated controls are available as an aid in this (e.g. Conzemius and Svec, 1973b). The distance between the electrodes and the primary slit is 1–2 mm.

The net effect of fluctuating ion beam and varying electrode geometry is that the instrument is not capable of measuring relative exposures accurately. In our experience, variations of $\pm 10\%$ of the apparent exposures are common and difference of ± 50–100% from the apparent measured exposure are not uncommon. Whether these differences are due to failure of the amplifiers to monitor the fluctuating ion beam adequately, or to varying electrode geometry is not clear. The ion beam is measured just before it enters the magnetic analyser. Fifty per cent of the ion beam is intercepted at this point, and the changes in electrode geometry may alter this parameter. Certainly relatively precision of measurement of shorter exposures, when electrodes are not moved, is better than for longer exposures. In any event, the relative exposures (measured in units of 10^{-9} C), are only a rough guide to the actual exposures recorded on each photoplate.

It has been common to use the relative exposures on the photoplate as an intensity scale, and so obtain the density vs. intensity relationship for the photoplate by this means. The method discussed here does not make use of the relative exposures to obtain the photoplate calibration curve, and so avoids the errors introduced by the poor precision of measurement of this parameter.

11. Photoplate recording

Photoplates constitute an excellent method of integrating exposures from a fluctuating source such as the ion beam produced in spark source mass spectrography, but they possess a limited response to incident intensity. Figure 37B.2 shows the response of Ilford Q-2 emulsion to ions. This calibration curve was constructed by the two-line method of Churchill (1944) using lines due to ^{171}Yb and ^{172}Yb. The linear portion of the photoplate density versus intensity curve is extended by the use of the empirical Seidel function, $\log(d_0/d - 1)$, where d_0 is the galvonometer deflection for clear plate (set at 100) and d is the galvonometer deflection for an exposed line, with the scale set at zero for no light reaching the photocell (Ahrens and Taylor, 1961, ch. 11).

On a single exposure, an intensity range of about 50 can be covered. In order to accommodate the range of about 1500 in intensity ratios produced under normal analytical conditions, it is necessary to record a graded series of exposures. It is clear from fig. 37B.2 that Ilford Q-2 plates show a regular and precise relationship between density and intensity.

Since the spark source mass spectrograph does not provide a consistent precise relative exposure measurement, it is necessary to treat each exposure as a separate entity. Thus the data available to establish the density versus intensity relationship (calibration curve) are restricted to density readings on individual exposures. The only independent and absolute intensity scale available is that provided by the isotopic ratios of individual elements. Varying sensitivities do not allow use of lines due to different elements, even though their concentrations might be known from other analytical techniques.

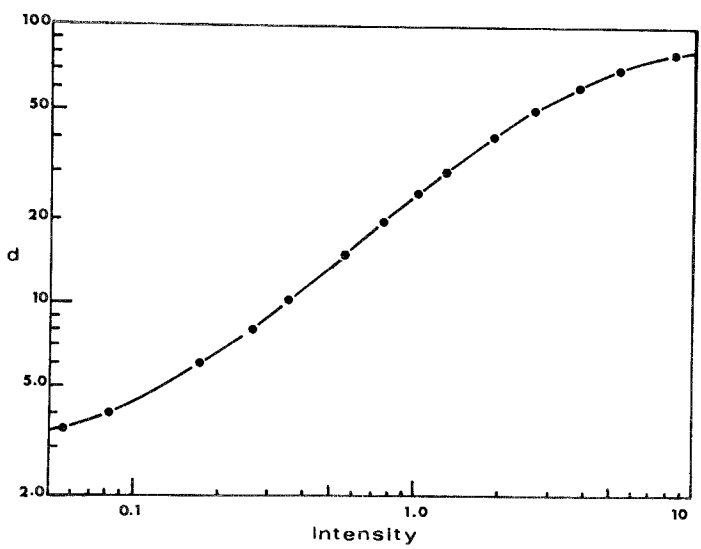

fig. 37B.2. Density versus intensity relationship for Ilford Q-2 photoplates for incident mass
Reproduced, with permission, from Geochim. Cosmochim. Acta, 35 (1971) 1190, Pergamon Press.)

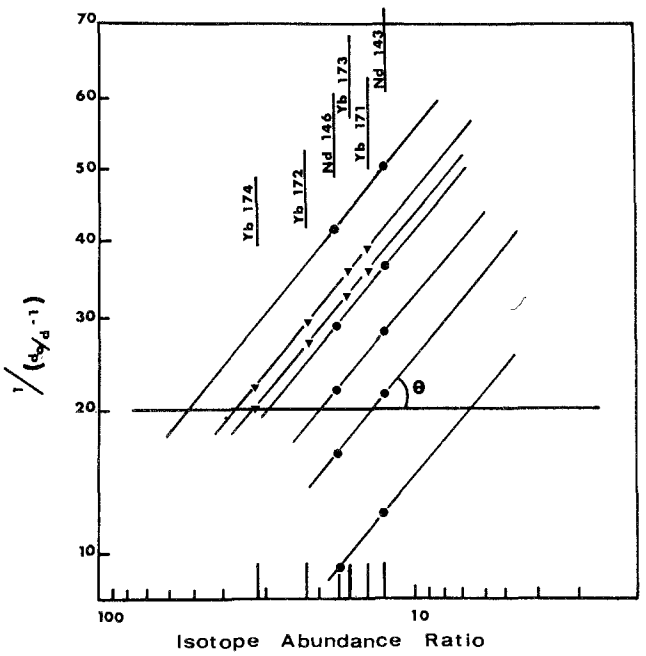

Fig. 37B.3. Ilford Q-2 photoplate calibration curves established using intensity ratios for isotopes recorded on the same exposure. Several curves are depicted, utilising data from several exposures. From this information an average value of tan θ ("gamma") is computed. Note that the reciprocal of the Seidel function is plotted on the vertical axis. (Reproduced, with permission, from Geochim Cosmochim. Acta, **35** (1971) 1190, Pergamon Press.)

To establish the calibration curve, the density values of a selected series of isotope lines are plotted against their relative abundance. Figure 37B.3 shows a plot of photoplate density values for a number of different exposures on the same photoplate. From these curves, the average value of tan θ or "gamma" of the individual photoplate is obtained. The value is calculated for several isotope ratios. This procedure can be adapted to allow for variations in tan θ for differing exposures.

12. Method of obtaining relative intensity data

The establishment of the slope of the photoplate density-intensity relationship enables relative intensities to be obtained from single density values. Figure 37B.4 shows the graphical procedure employed. The density value (d) is obtained using a microphotometer-densitometer. Transmission is set at 100% for clear plate and the per cent transmission values obtained for individual lines, with zero transmission corresponding to no light reaching the photocell (Ahrens and Taylor, 1961, ch. 11).

The density value is plotted on the appropriate exposure (E) value, and a line is drawn through this point, using the appropriate angle established from the plate calibration curve. This line then establishes the intensity versus density relationship for the particular d value. The intercept of this line with the relative intensity scale is read at a value of $d = 25$ (selected as the mid-point of the most

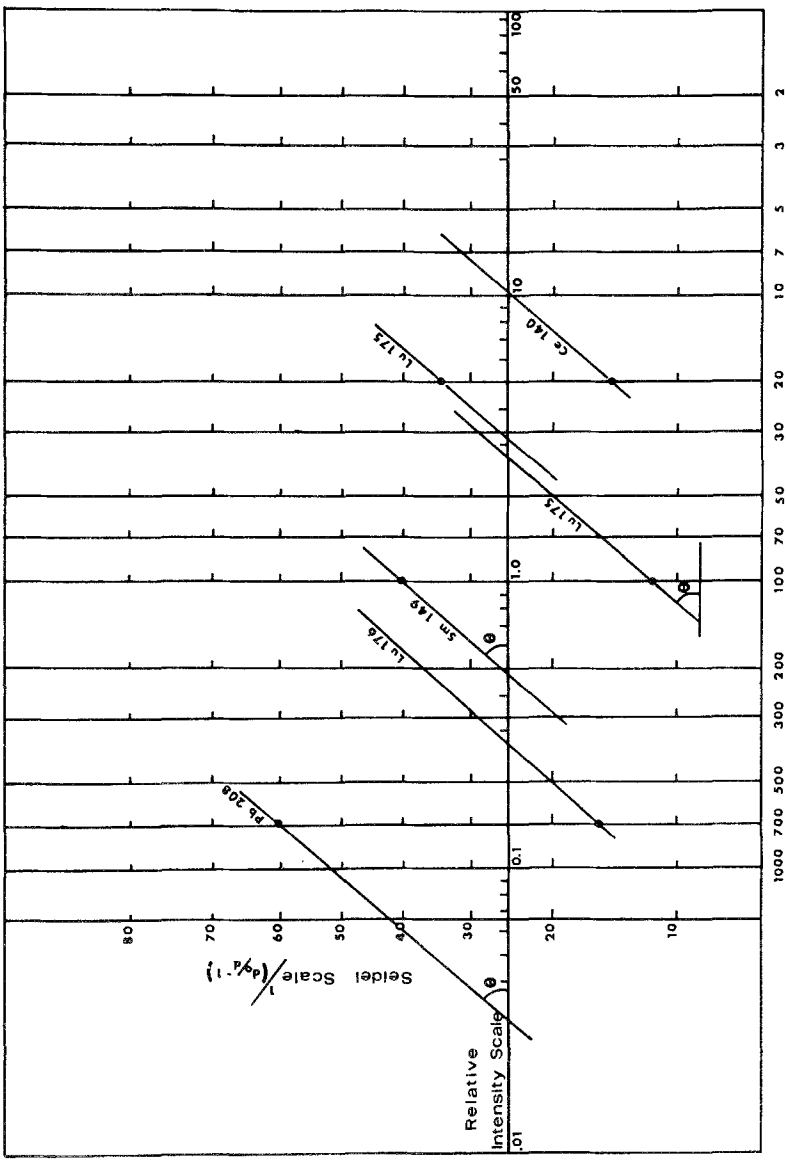

Fig. 37B.4. Graphical method of obtaining relative intensities, using densities from single exposures. The gamma value derived from the isotope ratios is used to produce a calibration curve from a single density reading. The intercept of this line at a d value of 25 (selected as the median value of the linear portion of the curve) gives the relative intensity. This value is ratioed to an internal standard intensity (^{175}Lu or ^{176}Lu) *recorded on the same exposure*. Note that the reciprocal of the Seidel function is plotted on the vertical axis. (Reproduced, with permission, from Geochim. Cosmochim. Acta, **35** (1971) 1191, Pergamon Press.)

reliable set of densitometer readings). All isotope lines for the same exposure are treated similarly, as is the internal standard line, and the intensity value (I_x) obtained for isotope x is rationed to the intensity value (I_{Lu}) obtained for the internal standard line. Since both values are obtained on the same exposure, they are directly comparable.

A computer program, written in FORTRAN IV has been developed to make the calculations, and operates as follows

(1) d values for each exposure are read in.

(2) d values are converted to Seidel values.

(3) The slope of the density vs. intensity relationship (fig. 37B.2) is calculated, using specifically selected isotope pairs. Values of tan θ lying between 0.84 and 1.6 are accepted. The average value of tan θ is calculated. If desired, the program may operate on a preset value for tan θ.

(4) Using the slope the calibration curve derived from Step 3, the intensities are calculated for each d value, as shown in fig. 37B.3.

(5) The intensity value of ^{176}Lu is corrected for interference by Hf, Yb and natural ^{176}Lu. ^{175}Lu intensities are converted to $I(^{176}Lu)$ values. Correction is made for natural Lu.

(6) All intensity values are normalised to the appropriate intensity value for ^{176}Lu on the same exposure.

(7) The program prints out (a) the densitometer reading input; (b) the intensity values, and (c) I_x/I_{Lu} values, concentrations in ppm and selected element ratios (La/Yb) (Eu/Eu*) etc.

13. Determination of element abundances

The intensity values I_x/I_{Lu} are plotted against element concentrations of standard samples, such as the USGS standard rocks. Figure 37B.5 shows a typical intensity versus concentration ("Working curve") relationship for the rare earth element, lanthanum. The slope of these plots lies at 45° over several orders of magnitude. A considerable body of analytical data of high quality has been incorporated over a period of years. Most terrestrial standards samples have been analysed and a cross check has been provided by analyses of lunar samples determined in this laboratory with analyses of the same samples by differing methods elsewhere. This information is incorporated into the computer program to allow the actual abundance values to be calculated. The program also eliminates abberant data through statistical tests. Other workers, e.g. Conzemius and Svec (1973b), use relative sensitivity coefficients.

14. Accuracy and precision

Accuracy and precision of the method are dependent upon the total number of exposures used to calculate the abundance of each element, as well as other

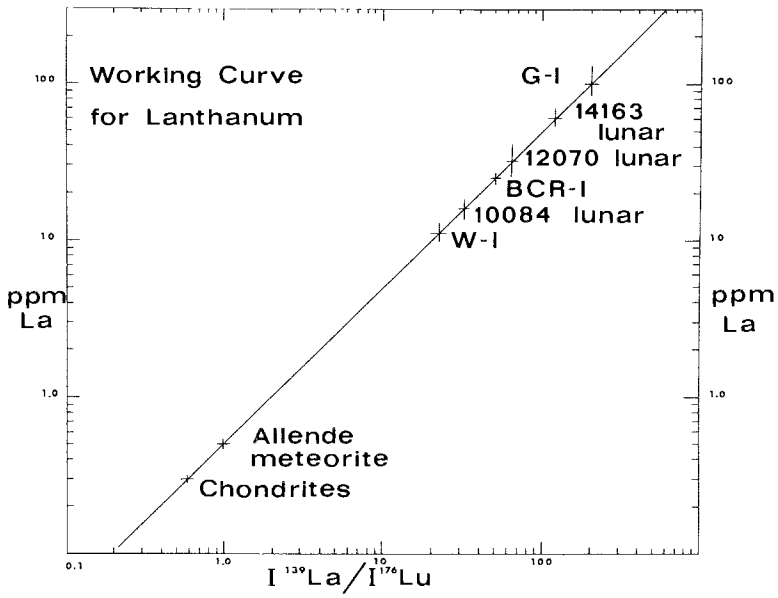

Fig. 37B.5. Intensity versus element concentration relationship for lanthanum.

TABLE 37B.3
REE abundances in USGS Standard BCR-1.

	1	2	3	4	5	6	7	8	9	10
La	24.5	–	24.2	24.0	–	24.4	25.5	–	25.2	26.1
Ce	52.8	54.3	53.5	51.3	53.7	54.4	53	53.6	54.12	54.9
Pr	(	–	–	–	–	–	–	–	–	–
Nd	29.2	27.8	29.3	28.5	29.0	28.9	–	28.2	30.5	28.8
Sm	6.21	6.41	6.67	6.60	6.74	6.73	7.0	6.60	7.23	6.74
Eu	1.92	1.92	1.94	1.87	2.02	1.98	1.95	1.94	1.97	1.97
Gd	6.56	6.43	6.76	–	6.55	6.67	–	6.64	8.02	–
Tb	1.01	–	–	1.1	–	–	0.96	–	1.15	–
Dy	6.47	6.26	6.33	–	6.47	6.36	6.9	6.36	6.55	6.20
Ho	1.31	–	–	1.46	–	–	–	–	1.34	–
Er	3.62	3.52	3.67	–	3.57	3.69	–	3.55	3.51	3.71
Tm	0.58	–	–	–	–	–	–	–	–	–
Yb	3.63	3.42	3.49	3.43	3.49	3.39	3.55	3.40	3.48	3.68
Lu	0.55	0.59	–	0.56	–	0.50	0.55	0.54	0.53	0.59
Y	36	–	–	25	–	–	–	–	–	–

1. This laboratory; 2. Arth and Hanson (1975); 3. Hooker et al. (1975); 4. Frey et al. (1974); 5. Shimizu (1974); 6. Nakamura et al. (1973); 7. Laul and Schmitt (1973); 8. Philpotts et al. (1972); 9. Haskin (1970); 10. Gast et al. (1970).

TABLE 37B.4
Data for Smithsonian Institution Allende Meteorite Standard Sample obtained by spark source mass spectrometry.

	Split 13 No. 23	Split I No. 27		Split 13 No. 23	Split I No. 27		
	1	2	3	4	5	6	7
Cs	0.11	–	–	0.14	0.09	0.09	–
Ba	4.5	4.4	4.42	5.2	4.6	4	–
Pb	1.30	1.26	–	1.35	1.46	1.3	–
Th	–	–	–	0.057	0.057	0.06	–
U	–	–	–	–	–	0.016	–
Zr	6.5	5.8	6.4	5.8	5.8	10	–
Hf	0.13	–	–	0.20	0.18	0.2	–
Nb	0.56	0.55	0.51	0.48	0.44	0.7	–
La	0.50	0.49	0.48	0.47	0.48	0.51	0.44
Ce	1.3	1.34	1.34	1.32	1.30	1.3	1.25
Pr	0.20	0.18	0.18	0.18	0.17	0.21	0.20
Nd	0.92	0.84	0.84	0.90	0.91	0.97	0.91
Sm	0.30	0.31	0.28	0.29	0.27	0.34	0.29
Eu	0.10	0.10	0.09	0.10	0.09	0.11	0.107
Gd	0.35	0.40	0.35	0.35	0.33	0.42	0.43
Tb	0.06	0.07	0.06	0.06	0.06	0.08	0.074
Dy	0.37	0.41	0.36	0.43	0.40	0.42	0.42
Ho	0.09	0.11	0.09	0.08	0.09	0.11	0.12
Er	0.27	0.28	0.25	0.25	0.25	0.29	0.31
Tm	0.050	0.069	–	0.058	0.048	0.06	0.049
Yb	0.28	0.33	0.25	0.28	0.26	0.31	0.32
Lu	0.047	0.065	–	0.055	0.045	0.05	0.058
Y	2.0	2.2	2.0	2.7	2.10	3.1	3.0

Analysts: 1 and 2, B.H. Mason (1973); 3. P.M. Martin (1973); 4 and 5, P.E. Muir and S.R. Taylor (1976); 1–5, A.N.U. SSMS; 6. E. Jarosewich (1987); 7. Wakita and Schmitt (1970).

factors. Two to six photoplates are exposed for each sample, each with about 15 exposures, and determinations for many elements are based on more than one isotope. This results in the measured abundance of each element being based on 8–10 determinations. The precision obtained for all elements was about ±5% expressed as standard error. Results obtained by this technique on standard rocks and lunar samples have been compared with results obtained on the same samples by other well recognized methods. The ultimate tests of accuracy of the method comes from interlaboratory comparisons of results on standard samples. Table 37B.3 provides data for this laboratory compared with that from nine others, using a variety of analytical techniques for the USGS standard rock BCR-1. The levels in this sample are typical of many common geological samples. Table 37B.4 provides data, at a lower level of REE abundances, for the Allende meteorite standard. Although less comparative data are available, the accuracy of the method at these levels seems well established.

References

Ahrens, L.H. and S.R. Taylor, 1961, Spectrochemical Analysis (Addison-Wesley, New York).

Arth, J.G. and G.N. Hanson, 1975, Geochemistry and origin of the early Precambrian Crust of Northeastern Minnesota. Geochim. Cosmochim. Acta **39**, 325.

Brown, R.W., R.D. Craig and R.M. Elliott, 1962, Spark source mass spectrometry as an analytical technique. Advanc. Mass Spectr. **2**, 141.

Churchill, J.R., 1944, Techniques of quantitative spectrographic analysis. Ind. Eng. Chem. Anal. Ed. **16**, 653.

Conzemius, R.J. and H.J. Svec, 1968, An electrical detection system for a spark source mass spectrometer. Talanta **16**, 365.

Conzemius, R.J. and H.J. Svec, 1973a, Relative sensitivity coefficients for rare earths in spark source mass spectrometry. Talanta **20**, 575.

Conzemius, R.J. and H.J. Svec, 1973b, Automatic control of the ion-illumination angle in a spark-source mass spectrometer. Talanta **20**, 477.

Craig, R.D., G.A. Errock and J.D. Waldron, 1959, Determination of impurities in solids by spark source mass spectrometry. Advanc. Mass Spectr. **1**, 136.

Evans, C.A. and G.H. Morrison, 1968, Trace element survey analysis of biological materials by spark source mass spectrometry. Anal. Chem. **40**, 869.

Frey, F.A., W.B. Bryan and G. Thompson, 1974, Atlantic ocean floor: Geochemistry and petrology of basalts from Legs 2 and 3, DSDP, J. Geophys. Res. **79**, 5507.

Gast, P.W., N.J. Hubbard and H. Wiesmann, 1970, Chemical composition and petrogenesis of basalts from Tranquility Base. Proc. Apollo II Lunar Sci. Conf. **2**, 1143.

Gerlach, W., 1925, Zur Frage der richtigen Ausfuhrung und Deutung der "quantitativen Spektral-analyse". Z. anorg. chem. **142**, 383.

Haskin, L.A., 1970, Rare Earths and other trace elements in Apollo II lunar samples. Proc. Apollo II Lunar Sci. Conf. **2**, 1213.

Haskin, L.A., F.A. Frey, R.A. Schmitt and R.H. Smith, 1966, Meteoritic, solar and terrestrial rare earth distributions. Phys. Chem. Earth **7**, 169. Pergamon.

Haskin, L.A., M.A. Haskin, F.A. Frey and T.R. Wildeman, 1968, Relative and absolute terrestrial abundances of the rare earths. In Origin and Distribution of the Elements, (editor L.H. Ahrens), pp. 889–912. Pergamon Press.

Hooker, P.J., R.K. O'Nions and R.J. Pankhurst, 1975, Determination of REE in USGS standard rocks by mixed-solvent ion exchange and mass spectrometric isotope dilution. Chem. Geol. **16**, 189.

Laul, J.C. and R.A. Schmitt, 1973, Chemical composition of Apollo 15, 16 and 17 samples Proc. Fourth Lunar Sci. Conf. **2**, 1349.

Mattauch, J. and R. Herzog, 1934, Uber einen neuen Massenspektrographen Z. Phys. **89**, 786.

Nakamura, N., A. Masuda, T. Tanaka and H. Kurasawa, 1973, Chemical compositions and rare earth features of four Apollo 16 samples. Proc. Fourth Lunar Sci. Conf. **2**, 1407.

Nance, W.B. and S.R. Taylor, 1976, Rare earth element patterns in Australian sedimentary rocks Geochim. Cosmochim. Acta **40**, 1539.

Nicholls, G.D., A.L. Graham, E. Williams and M. Wood, 1967, Precision and accuracy in trace element analysis of geological materials using solid source spark mass spectrography. Anal. Chem. **39**, 584.

Philpotts, J.A., C.C. Schnetzler, M.L. Bottino, S. Schuhmann and H.H. Thomas, 1972, Luna 16: Some Li, K, Rb, Sr, Ba, REE, Zr and Hf concentrations EPSL **13**, 429.

Shimizu, N., 1974, An isotope dilution technique for analysis of the rare earths. Carnegie Inst. Yearbook **73**, 941.

Taylor, S.R., 1965a, Geochemical application of spark source mass spectrography. Nature **205**, 34.

Taylor, S.R., 1965b, Geochemical analysis by spark source mass spectrography. Geochim. Cosmochim. Act. **29**, 1243.

Taylor, S.R., 1971, Geochemical application of spark source mass spectrography II Photoplate data processing. Geochim. Cosmochim. Acta. **35**, 1187.

Coryell, C.D., J.W. Chase and J. W. Winchester, 1963, J. Geophysical Research, **68**, 599.

Jarosewich, E., 1987, Smithsonian Contributions to Earth Science, **27**, 49 pp.

Martin, P.M., 1973, personal communication.

Mason, B.H., 1973, personal communication.

Muir, P.E. and S.R. Taylor, 1976, personal communication.

Wakita, H. and R.A. Schmitt, 1970, Proc. Apollo II Lunar Science Conference, 1685, Pergamon Press.

Handbook on the Physics and Chemistry of Rare Earths, edited by K.A. Gschneidner, Jr. and L. Eyring

Chapter 37C

ANALYSIS OF RARE EARTH MATRICES BY SPARK SOURCE MASS SPECTROMETRY

R.J. CONZEMIUS
Ames Laboratory, US DOE, Iowa State University, Ames, Iowa 50011, *USA*

Contents

1. Introduction

Spark source mass spectrometry (SSMS) is characterized by several distinguishing features. Perhaps the foremost is the ability to provide wide elemental coverage with attendant high sensitivity without requiring chemical separation of the sample. However the technique is highly susceptible to errors due to sampling of small volumes when impurities are not homogeneously distributed. Semiquantitative estimates of impurity levels are obtained easily without requiring preparation of standards. However quantitative results are quite difficult to attain routinely.

The application of SSMS to analysis of rare earth matrices began slowly. Initial work was reported by Guthrie (1963, 1964a,b,c) who showed that in spite of difficulties due to inhomogeneities SSMS was applicable to the analysis of these elements. Now rare earth matrices are considered to be ideal for SSMS analytical techniques (Griffith et al., 1971). A pragmatic reason for the limited application of SSMS to analysis of these elements is the costliness of the instrument (approximately $150 000). This cost restriction is magnified by a limited rate of sample through-put for the instrument.

The author has been active in developing techniques for analysis of solids,

including rare earth matrices, by mass spectrometry for the past fifteen years. In this period of time the analytical group with which the author is associated has used SSMS for analysis of approximately 1600 rare earth samples, about one half the analytical work load for the instrument. These samples were mainly rare earth metals (580), oxides (830), and fluorides (150). Other types were selenides, carbonates, chlorides, hexaborides, alloys, etc. It is mainly through this experience and through the use of the limited number of literature references on this highly specialized subject that the author hopes to aid the experimentalist interested in analyzing rare earths by SSMS or the scientific group considering the addition of SSMS to their analytical capability.

The question may be posed: "Is there any difference between analysis of rare earth matrices and other types of matrices by SSMS?" The answer is: "Generally, no". However, analysis of rare earth matrices may be handled as a group within which reliable techniques can be applied to improve confidence levels in determinations. In describing how these matrices may be handled, the author assumes that the reader is knowledgeable of current techniques in SSMS, instrumentation, detection limits, etc. either by having read the previous chapter or from other more general descriptions such as Ahearn (1972).

It should be noted that only information, techniques, or trends are presented here which have been judged to be pertinent to the analysis of rare earth matrices by SSMS. Some of the contents may be considered typical of other elements or groups of elements and some contents are peculiar to rare earths. For any applicability of the contents described in this chapter to other matrices the reader is referred to more general references (Ahearn, 1966, 1972).

2. Sample preparation

2.1. *Metals*

Very little information can be found in the formal literature concerning the preparation of rare earth metals for analysis by SSMS. Samples have been "broken" to expose an uncontaminated area for analysis. Usually an organic rinse has also been used prior to loading the sample into the spectrograph and the site chosen for analysis has been presparked for about 30 minutes prior to actual analysis. Within 30 minutes several mg of sample will be consumed and a fresh sampling of the interior is assumed. Although the above procedures allow for minimum handling of the sample, they are frequently unsatisfactory. Fracturing or breaking the metal may not be easy or the exposed interior metal may be irregularly shaped and not amenable to spark electrode control or to good ion illumination of the ion optical system. Simple presparking of a metal "as received" may be insufficient to remove completely gross contaminants such as oils or metals imbedded from tooling procedures. Certain sample forms such as metal sponges contain surface areas too large and complex to clean adequately by rinsing and presparking. The metal sample may require special handling such

as described by Busch et al. (1971) for the analysis of Eu by attaching the metal to a high purity gold foil.

Techniques developed at the Ames Laboratory for preparation of rare earth metals have been found to be generally satisfactory and will be discussed briefly. The entire bulk metal to be sampled is homogenized if possible. The type of homogenization depends upon the rare earth. The metals Sc, Y, and lanthanides Sm thru Lu are generally prepared in a final step involving sublimation and the distillate metal is considered to be inhomogeneous. The elements Sc, Y, Gd, Tb, Dy, Ho, Er, and Lu are homogenized by arc melting in a single step process. The elements Yb, Eu, and Sm are simply melted in a tantalum crucible. Thulium is sampled directly from the distillate since its vapor pressure is too high for arc melting and melting would dissolve excessive amounts of crucible material. The metals La, Ce, Pr, and Nd are formed normally in a tantalum reaction vessel and are cut directly from their container. The billet is considered to be homogeneous except for tantalum precipitates which are cut away.

Sampling is performed by sectioning the homogenized metal into a specified and recorded pattern from which the sample is selected. Samples specifically sectioned for analysis by SSMS are shaped as rods, approximately one cm long and one square mm cross section with slightly rounded edges. Cutting, sectioning, or shaping is performed with new saw blades or files which have been precleaned in an organic rinse.

The metal rods are electropolished at −78°C in a freshly prepared 6 percent perchloric acid-methanol bath in a glass beaker (a stainless steel beaker was found to contribute nickel and iron to the sample even though the crucible was connected to the cathode). The platinum cathode and the platinum tipped anode sample holders are cleaned by pre-etching. Immediately after etching, the samples are rinsed in a −75°C acetone bath followed by rinsing in methanol until the sample has warmed to room temperature.

All of the above steps are performed in the metallurgist's laboratory. The samples are transferred in glass vials to the mass spectrometer laboratory where they are handled in a dust free atmosphere with teflon coated tweezers which are used only for specific rare earths. The samples are set into niobium clamps and mounted into the ion source vacuum chamber. Following evacuation to the low 10^{-7} torr region, the samples are presparked for ~20 minutes to an exposure of 3×10^{-7} coulombs. The ion source chamber is pumped with a liquid nitrogen trapped, 100 liter-per-second mercury diffusion pump and with a liquid nitrogen cooled trap within the chamber. Pressure during sparking is highly dependent upon both the sample and selected sparking conditions but is typically 5×10^{-6} torr.

The pulse repetition rate is normally 100 pulses per sec. with pulse durations of either 10 or 32 μs. After presparking, spark gap and ion illumination angle control is performed automatically (Conzemius and Svec, 1973b) and the analytical measurements are recorded by either electrical or photographic ion detection techniques.

2.2. *Non-metals*

Non-metallic compounds. Techniques generally established (Morrison and Roth, 1972) for handling non-conductive compounds are also applicable to rare earths. A few brief remarks may be appropriate.

2.2.1. *Oxides*

Oxides of La, Pr, Nd, Sm, and Eu require drying (800°C for 1 h) prior to pelleting and entry into the spectrograph. This not only permits more reliable consistency of the pellet but also simplifies the mass spectrum by lowering the intensity of molecular ions containing hydrogen. As with other powder samples, graphite provides a reliably pure pelleting medium (Oblas et al., 1966; Griffith et al., 1971; Haaland and Stijfhoorn, 1973). However the choice of certain weight ratios of rare earth oxide to graphite used in preparing the pellet have been quite different and the reasons for these choices have not been well documented. Figure 37C.1 is a plot of the response of the mass spectrograph to the Dy^{+1} ion signal for a pelleted Dy_2O_3-graphite sample containing different mole ratios of Dy (Peterson, 1976). As expected, the response increases along with Dy content although the rate of increase diminishes at higher mole ratios. As the mole ratio approaches 0.3 the pellet gradually becomes semi-conductive, the initiation of spark breakdown becomes more difficult and some localized heating is observed in the immediate area of the spark. When these conditions occur the response of the instrument to Dy becomes erratic and has been observed to be lower than

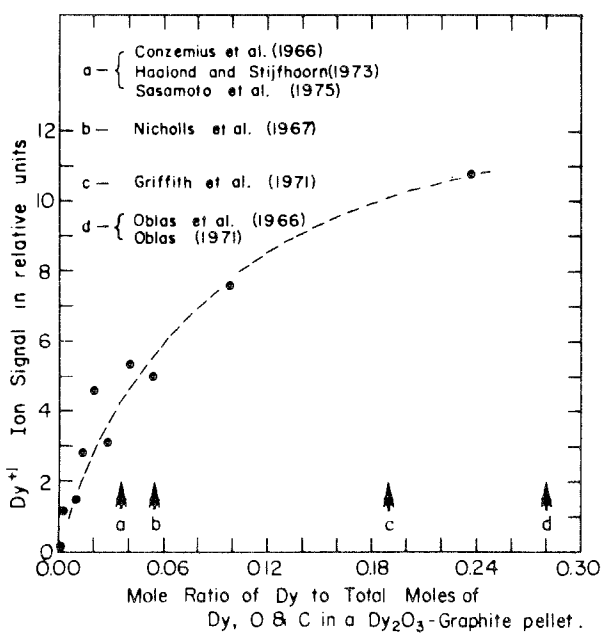

Fig. 37C.1. Spark source mass spectrometric response to rare earth content in an oxide-graphite pelleted sample.

that obtained with lower mole ratios of rare earth in the pellet. This may be due to preferential sparking to areas of high graphite content. Other changes in the spectra are observed as the mole ratio is changed. The relative intensity of multiply charged ion signals is greater for mole ratios below 0.1 and above 0.2 indicating some altered mechanisms or rates of different ion production. Molecular ion intensities vary systematically with graphite content and will be discussed later in more detail.

The arrows at the bottom of fig. 37C.1 indicate the ratios chosen for the reference work noted on the figure. The pellets containing lower mole ratios of rare earth offer much higher structural stability, better thermal properties, and perhaps less susceptibility to matrix effects. Another criterion for choice of an optimum mole ratio would be the confidence placed in reproducing the conditions chosen for forming the pellet.

2.2.2. *Other compounds*

Muheim (1973) has reported on the nature of spectra derived from chalcogenides and pnictides by SSMS. However references to analysis of rare earth compounds other than oxides were not found in the literature. At the Ames Laboratory no particular difficulty has been experienced in characterizing the general purity of rare earth fluorides by SSMS. These samples were first fractured into small crystals, then ground in a boron carbide mortar and pestle, mixed in a weight ratio of three parts rare earth fluoride to one part graphite and pelleted into sample rods (Brown et al., 1967) for analysis. Selenides of Gd have also been analyzed and were treated similarly. Adequate venting of these samples is prescribed as a precaution against the buildup of any toxic fumes due to chemical alteration of the pellet. Lanthanum hexaboride is an example of a rare earth compound which provides excellent self electrodes. Concentration profiles along a LaB_6 rod have also been measured by Conzemius (1976) by SSMS in which a gold counter electrode was used in a manner similar to that described by Schmidt et al. (1974) for measuring trace levels of solutes in vanadium. However, for the LaB_6, photographic ion detection was used since a general survey of all elements was desired.

3. Rare earth spectra

No unusual characteristics in the spectra of rare earth matrices have been reported. General comparisons of major ion intensities in spectra obtained by SSMS have not been studied so quantitative comparisons with non-rare earth spectra cannot be made. However, general characteristics will be described briefly. Figure 37C.2 is a reproduction of a photographic plate which contains typical spectra. The top part of the plate was obtained from a Gd metal sample and the lower part from a Gd oxide/graphite pelleted sample. The exposure levels and major ion species are identified on the figure. The background (fog)

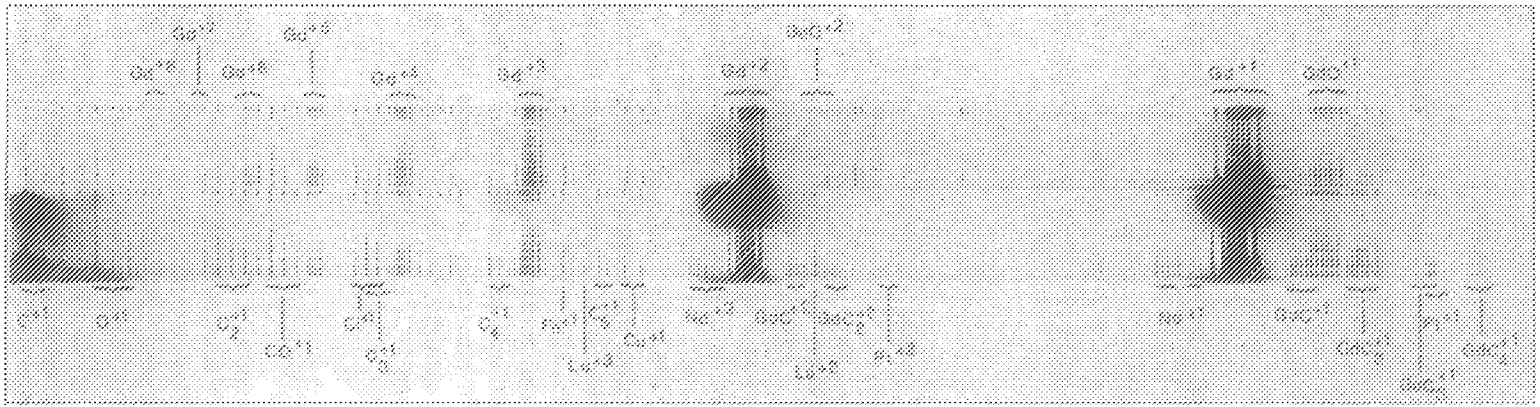

Upper 11 exposures (Gd metal)

No.	1	2	3	4	5	6	7	8	9	10	11	12
nC	200.	9.3	0.04	0.11	0.31	0.90	2.7	9.4	96.	280.	560.	

Lower 12 exposures (Gd_2O_3–graphite pellet)

nC	150.	2.6	0.031	0.12	0.25	0.90	2.7	9.6	28.	95.	280.	570.

Fig. 37C.2. Typical spark source mass spectrographic spectra.

level varies with instrument type as well as with the type of photo-emulsion developing procedure (Cavard, 1968) especially in regions near intense signals.

3.1. *Multiply charged ions*

Figure 37C.3 is a plot of the relative intensities of multiply charged ions for spectra from rare earth metals and from rare earth oxide/graphite pellets as identified on the figure. All intensities have been normalized to the +4 ion and are plotted on a logarithmic scale. The oxide/graphite pellets contained a mole ratio of 0.14 of rare earth. A significant difference between the metal and oxide spectra is the greater intensity of singly and doubly charged ions relative to the higher charged ions for the oxide. There is also a slight indication of lower intensities for the +6, +7, and +8 ion signals and an enhancement of the +9 signal relative to the metal. The higher charged ions for the oxide are not as easily detected due to higher fog levels from intense singly charged carbon and oxygen ions. Table 37C.1 lists data from fig. 37C.3 along with relative standard deviations. The data for the metal samples were tabulated from 30 spectra including 10 different rare earth metals. For the oxide samples 17 spectra were tabulated including 5 different rare earth matrices. Within the indicated error limit, the only discernable differences among the rare earths were the observations of more intense doubly charged ions for the more volatile rare earths (Sm, Eu, and Yb). More detailed considerations of variations in multiply charged ion signals have been made by Muheim (1973).

3.2. *Molecular ions*

3.2.1. *Metals*

Molecular ions are observed in spectra from rare earth metals with ion intensities similar to non-rare earth samples. Table 37C.2 lists typical intensity relationships observed in rare earth metal spectra for oxygen, fluorine, and carbon impurities and their associated matrix cluster ion intensities. Although the source of these ions relative to the solid sample has been studied by Muheim (1972, 1973), certain facets of their character remain clouded. Their intensities tend to be erratic and depend upon many parameters such as non-metallic impurity content, residual gas level in the spectrometer ion source chamber, contaminants on the surface of the metal sample, chemical environment, etc. The analytical usefulness of these cluster ion signals has not been established.

3.2.2. *Compounds–oxides*

Radio-frequency spark spectra from pelleted samples of oxides and other compounds contain high molecular ion intensities due to fragments of the inorganic compound. There are also high intensity molecular ions due to formation of almost any imaginable combination of individual atoms with atoms of the

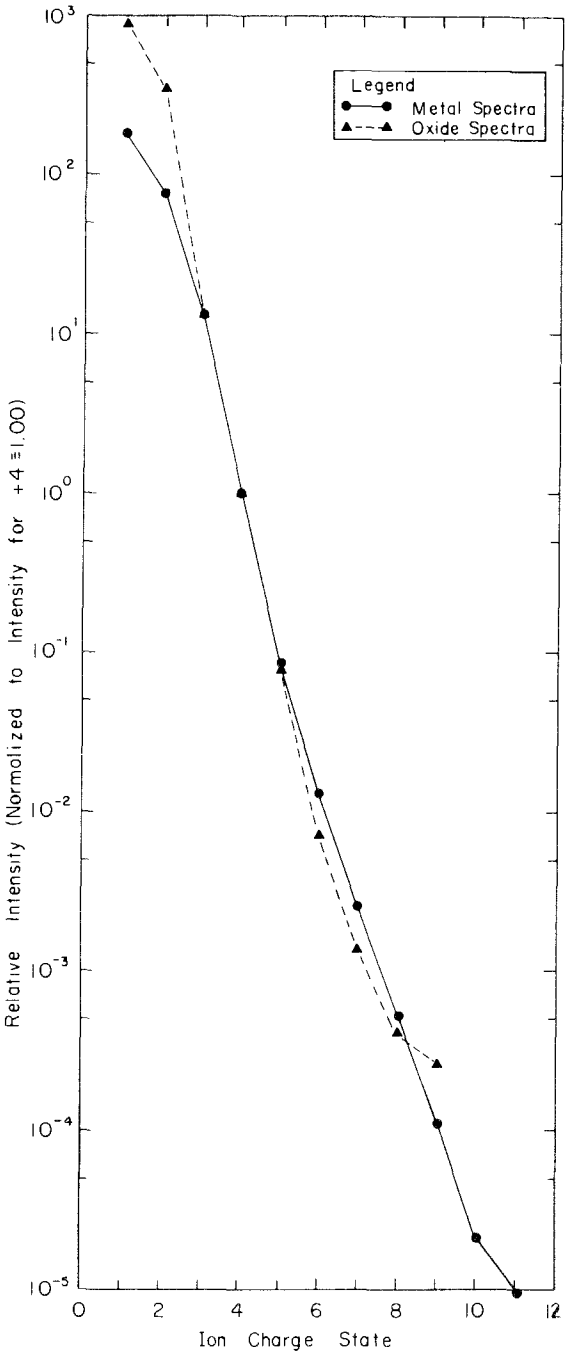

Fig. 37C.3. Decrease in ion intensity with increased ion charge.

TABLE 37C.1.
Relative intensities of multiply charged rare earth signals.

Ion charge	Metal sample		Oxide sample	
	Intensity[a]	Rel. S.D.[b] %	Intensity[a]	Rel. S.D.[b] %
1	180	24	880	28
2	76	45	350	28
3	13	34	13	57
4	≡1.	–	≡1.	–
5	0.087	29	0.077	30
6	0.013	33	0.0071	58
7	0.0026	22	0.0014	28
8	0.00052	15	0.00042	38
9	0.00011	25	0.00026	28
10	0.000021	30		
11	0.0000095	47		

[a]Intensity relative to +4 signal ≡1.00. [b]Relative standard deviation.

pelleting medium. A few brief comments will help characterize these ions by examining some reproducible spectral patterns that have been observed for rare earth oxide/graphite pelleted samples. With graphite pelleted samples a regular pattern of C_n^+ signals is observed (Dornenburg and Hintenberger, 1959) as well as a large number of molecular ions due to combinations of carbon atoms with the rare earth (R) matrix element. Molecular ions which include the matrix rare earth as a component are of the greatest concern since interferences due to these ions require higher resolution than is available with most SSMS instrumentation to separate them from M/z signals due to elemental impurities. Figure 37C.4 shows an intensity pattern from a Y_2O_3/graphite pelleted sample described by Cook (1966) which is typical of patterns for RC_n^{+1} ions. These patterns do not correspond to C_n^{+1} ions and are quite independent of sparking conditions except for a dependency upon the thickness of the pellet, i.e. a large sparking area along the ion axis. Intensity patterns for multiply charged ions due to RC_n ions usually show much greater reduction in intensity with additional ion charge than the

TABLE 37C.2.
Typical intensity ratios for molecular ions in rare earth metal spectra.

Non-metal specie (X)	O	F	C	C_2
$RX^{+1}/X^{+1} \pm SD$[a]	0.3 ± 0.2	0.6 ± 0.7	0.009 ± 0.006	–
$RX^{+1}/RX^{+2} \pm SD$	340 ± 230	300	50 ± 40	200 ± 200
$RX^{+1}/RX_2^{+1} \pm SD$	700 ± 300	20	0.5 ± 0.2	10

Note: $RC_3^{+1}/RC^{+1} = 0.5 \pm 0.2$.
[a]±SD = standard deviation given when sufficient data was available.

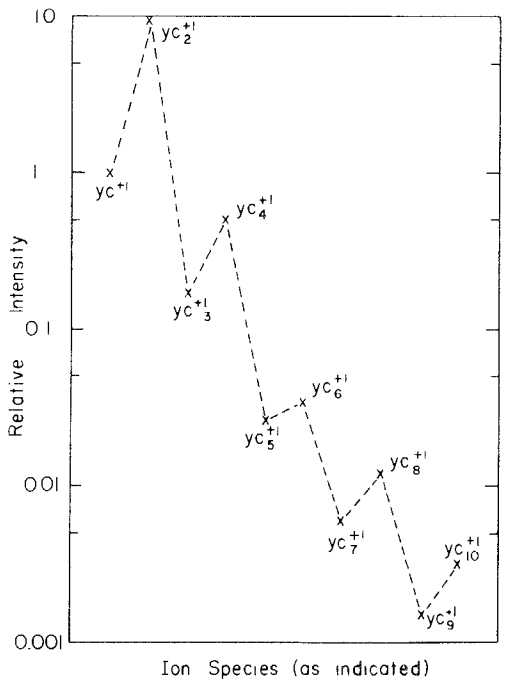

Fig. 37C.4. Intensity pattern of carbide molecular ions from a Y_2O_3-graphite pellet spectra (from Cook, 1966).

reductions shown in fig. 37C.3 for elemental ions. However the patterns vary for different values of n. For example Cook (1966) observed that the +1/+2 ion intensity ratio for RC and RC_3 was approximately four whereas the same ratio for RC_2 and RC_4 was 50. The intensity of the RC_n^{+1} as well as the RO_n^{+1} ion signals depend upon the ratio of the oxide/graphite content of the pellet and the general trend in this dependency is shown in fig. 37C.5 for the C_n^{+1}, RC_n^{+1}, and RO^{+1} ion signals. The increase in the carbon lines at higher mole ratios of rare earth is indicative of preferential sparking to carbon-rich areas of the pellet. The di-, tri-, and tetracarbide signals increase at faster rates than the monocarbide at increased graphite content for the pellet and the change in the ratios of these ion signals is shown in fig. 37C.6. Typically the monocarbide will have an intensity of about 400 ppma (relative to the $R \equiv 10^6$ ppma) for oxide/graphite pellets containing a mole ratio of 0.055 for the rare earth.

A dependence of the intensity of the RC^{+1} signals upon the particular rare earth has not been established but Oblas (1971) has reported one for the RO^{+1} ion signals and the data showing this dependence is listed in table 37C.3. These data represent unusually intense oxide signals and are at least in part due to the high oxide content of the pellets used in the study. Muheim (1972, 1973) showed that intensity relationships of molecular ions reveal the electronic milieu of the cation in the crystal. Unless such information as bond energies, chemical environment within the solid, or some diagnostic information concerning mechanisms for ion production can be gleaned from these molecular ion in-

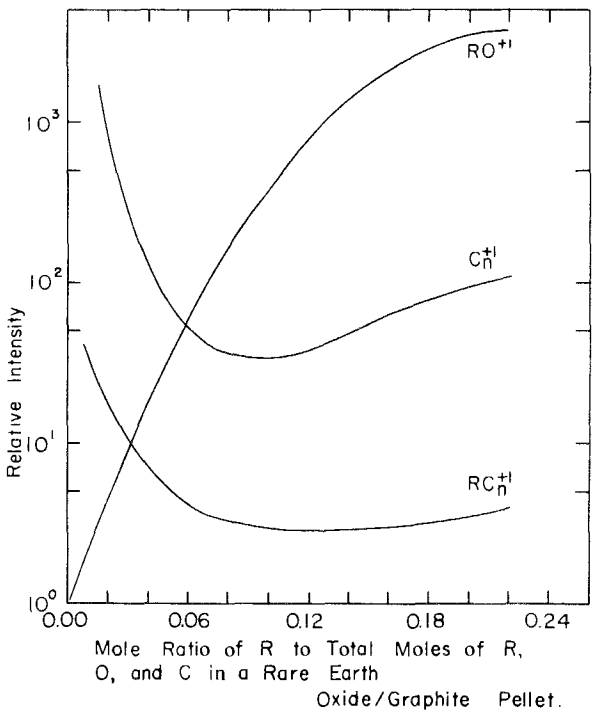

Fig. 37C.5. Trends in intensity response for molecular ions with changing rare earth content of pelleted sample.

tensities, they serve only to interfere with the analytical usefulness of the spectra. Such interferences can be difficult to interpret as additional atom combinations appear such as ROH^+, RCH^+, RCO^+, etc.

3.3. *Interferences*

The paragraphs above indicate levels of major spectral ion signals. Many of these cause slight or occasionally severe interferences with M/z ion signals commonly chosen for measurement in the determination of impurity levels.

TABLE 37C.3.
Intensities of rare-earth monoxide ion signals relative to the rare earth ion signal [from Oblas (1971)].

Rare earth oxide	RO^{+1}/R^{+1}	Rare earth oxide	RO^{+1}/R^{+1}
Y_2O_3	0.2	Tm_2O_3	0.0005
Sm_2O_3	0.015	Yb_2O_3	0.0008
Eu_2O_3	0.0005	Lu_2O_3	0.0019
Dy_2O_3	0.004	Gd_2O_3	0.083
Ho_2O_3	0.0008	La_2O_3	0.2
Er_2O_3	0.0026	Nd_2O_3	0.14

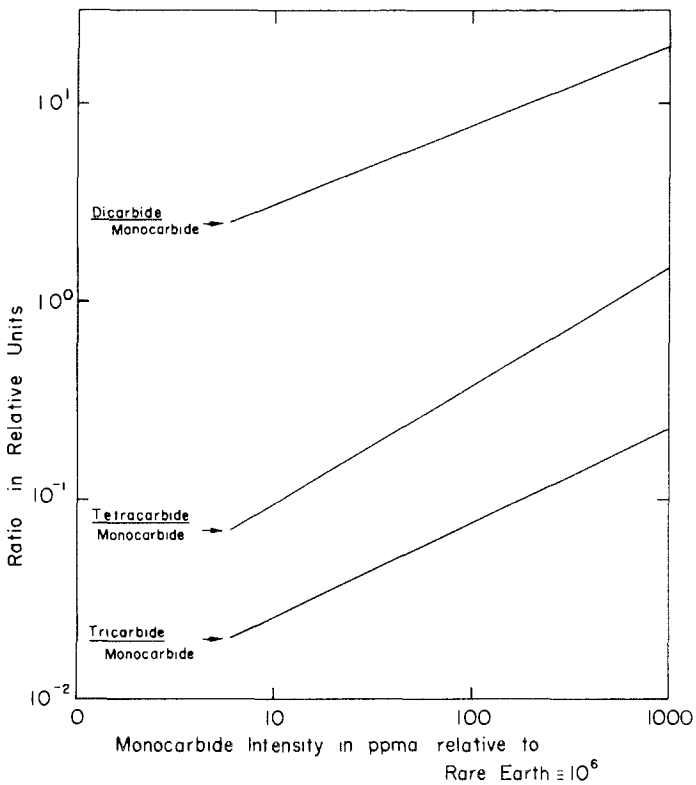

37C.6. Typical changes in RC_2^{+1}, RC_3^{+1}, and RC_4^{+1} relative to the RC^{+1} ion signal.

Figure 37C.7 gives an illustration of the types of interferences encountered and the best probable choices for M/z signals for determining rare earth impurities in a cerium matrix. Such tables, constructed similarly for the other rare earths and incorporating their unique isotopic patterns, are useful in characterizing spectra manually. Such interferences are sufficiently complex to warrant computer aids (Conzemius et al., 1967; Woolston, 1972) in identifying and substracting the interfering signals from signals caused by elemental impurities. Some interferences are sufficiently severe to limit sensitivity to unusually high levels. Table 37C.4 lists some examples for each of the rare earth matrices. Among the reasons given in the table for the listed severe interferences is increased background near the major isotopes of the matrix. This type of interference is due to space charge broadening of very intense ion signals as well as very high fog levels and perturbed photographic images near these signals. However the effect is not as serious when special photo emulsion developing procedures are used to enhance the internal image (Cavard, 1968; Kennicott, 1972) or when electrical ion detection is employed (Hull, 1969).

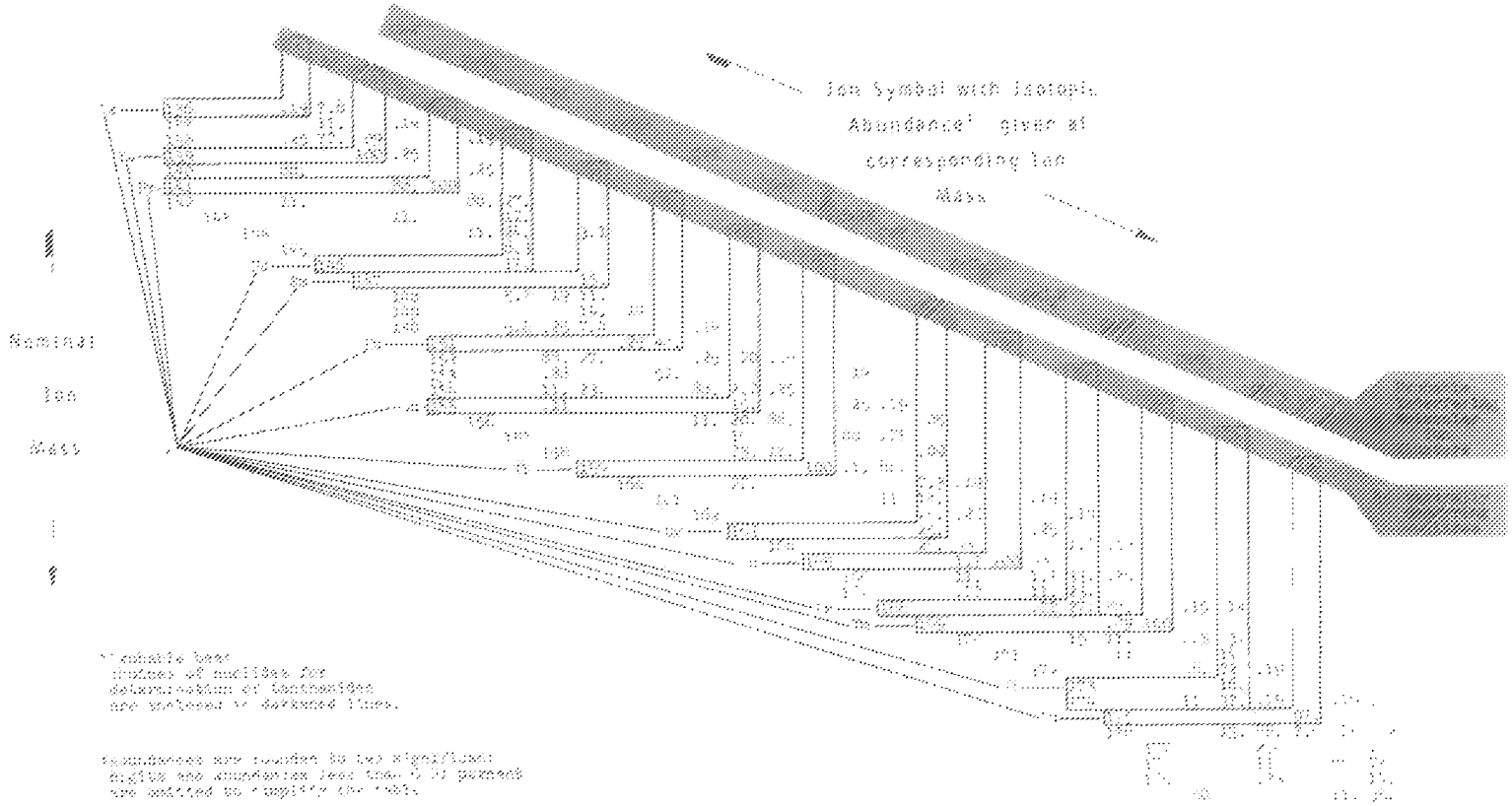

Fig. 37C.7. Nuclidic table representation of rare earths and interfering molecular ions for a cerium matrix.

TABLE 37C.4.
Typical interferences for the different rare earths as matrices.

Matrix	Interfered element Molecular ion(s) causing interference[a] Rare earths	Common elements	Others
Sc		$\frac{Co}{N, CH_2}, \frac{Ni}{CH_n}, \frac{Nb}{C_4}$	$\frac{Ga, Ge}{C_2H_n}$
Y	Sc^b	$\frac{Rh}{N, CH_2}, \frac{Au}{Y_2OH_2}$	$\frac{Sb}{O_2H_n}, \frac{I}{F_2}$
La	$Ce^b, \frac{Pr^b}{H_2}, \frac{Eu}{CH_n, N}, \frac{Lu}{C_3}$		Ga^b
Ce	$La^b, \frac{Pr^b}{H}, \frac{Tb}{F}$		Ga^b
Pr	$La^b, Ce^b, \frac{Tb}{OH_2}, \frac{Ho}{C_2}, \frac{Tm}{C_2H_4}, \frac{Lu}{O_2H_2}$		Ga^b
Nd	$Ce^b, Pr^b, \frac{Gd, Tb, Dy, Ho}{C \quad O \quad F}, \frac{Yb, Lu}{OC \; O_2}$	$\frac{Ta}{F_2}, \frac{W}{F_2},$	$As^c, Ge^{c,b}, \frac{Ir}{C_4}, \frac{Tl}{C_5}$
Sm	$\frac{Eu^b}{H}, \frac{Tb}{C}, \frac{Ho}{O}, \frac{Dy}{C, N}, \frac{Tm}{F}, \frac{Yb}{C_2}, \frac{Lu}{OC}$	$\frac{Ta}{O_2}, \frac{Au}{C_4}$	$As^c, \frac{Re}{F_2}$
Eu	$\frac{Ho}{C, N}, \frac{Tm}{O}, \frac{Lu}{C_2}$	$V^c, \frac{Ta}{OC}$	As^b

Gd	$\frac{Tb^b}{H}, \frac{Er}{C}, \frac{Tm}{C,N}, \frac{Yb}{O}, \frac{Lu}{F,OH}$	$\frac{Pt}{F_2}, Cr^{c,b}, Ca^c, \frac{W}{OC}, \frac{Sr}{O}$	$Br^{c,b}, \frac{Se^c}{C}, \frac{Rb}{O}$
Tb	$\frac{Lu}{O}, \frac{Ho}{Tb_2C^{+2}}$	$\frac{Au}{F_2}$	
Dy	$\frac{Ho^b}{H}, \frac{Lu}{C,N}$	$Ca^c, Cr^{c,b}, \frac{Au}{C_3}, \frac{Pt}{O_2}, \frac{Ta}{F}, \frac{Sr}{C}$	$Br^c, Se^{c,b}, \frac{Os}{OC}, \frac{Re}{C_2}, \frac{HF,Rb}{O,C}$
Ho		$Mn^c, \frac{Ta}{O}, \frac{Au}{O_2}$	
Er	$\frac{Tm^b}{H}$	$\frac{W}{O}, \frac{Pt}{OC}, \frac{Ta}{N}, Fe^{c,b}, Al^c$	$Br^{c,b}$
Tm	$\frac{Lu}{Tm_2C^{+2}}$	$\frac{Ta}{C}, \frac{Au}{OC}$	
Yb	$\frac{Lu^b}{H,H_2}, Y^b$	$Fe^c, Sr^{c,b}, \frac{Pb}{O_2,C_3}, \frac{Au,Pt}{C_2}, \frac{Hg}{OC}, \frac{W}{C}$	$Rb^c, \frac{Ir}{F}, \frac{Os}{O}, \frac{Nb}{C}, \frac{Th}{C_5}$
Lu	Y^b	Co^b	$\frac{Ir}{OH_n}$

[a]Molecular ion formed when matrix is combined with indicated specie(s). (eg. ScC_4 interferes with the determination of Nb.) [b]Fog level from matrix interferes with determination of this element. [c]Multiply charged ion from matrix interfere with determination of this element.

4. Quantification

In SSMS two primary measurements, made simultaneously, are frequently required for a determination. One is the total ion current in the spectrograph and the other is a specific spectral ion signal level. The total ion current, measured at the beam monitor in the field-free region between the electrostatic and magnetic analyzers, is affected only by the major ion signals. For metal samples, these signals consist of the singly, doubly, and triply charged ions of the rare earth matrix (see fig. 37C.3). For oxides or other powdered samples, these signals consist of the same rare earth ions plus intense ion signals due to oxygen (or other compound constituent) ions and to ions from the pelleting medium, carbon. The total ion current provides a common denominator for comparing photographic measurements from different exposures or electrical measurements of spectral ion signals. Certain techniques permit nullification of errors which may enter into the measurement through this common denominator. Impurity levels are determined by comparing the spectral ion signal with a reference signal. The reference signal may be any one of several possibilities: (1) instrument response of a previously analyzed standard (Total Beam Referencing); (2) a matrix spectral signal (Matrix Referencing); (3) an externally supplied spectral signal (External Referencing); or (4) an internally supplied spectral signal (Internal Referencing). These techniques are described in section 4.3. Standards are required for all of the referencing techniques except in the case where the internal reference is a separated isotope and isotope dilution techniques are used.

4.1. *Preparation of standards*

Preparation of rare earth standards as *metals* is not feasible due to the cost and complexity of preparing accurate and homogeneous samples doped at trace levels. However, rare earth *oxides* present a favorable chemical system for quantification. Three different methods of preparing oxide standards were reported by Griffith et al. (1971) which will be reviewed briefly.

The first method described was a dry blending technique which followed closely the procedures outlined by Taylor (1965). The homogeneity of such a blend pelleted with graphite was tested with an electron microprobe. The results are reproduced in fig. 37C.8 which shows variations in concentrations of trace level constituents, Gd_2O_3 and In_2O_3, which have been dry blended with the matrix rare earth, Tm_2O_3, and with graphite prior to pelleting. The large variations are due to changes in the relative amounts of oxide and graphite in scanning across the pellet. The data indicate that intimate mixing of In_2O_3 and Gd_2O_3 with the matrix oxide was attained. An advantage of dry blending is that chemically dissimilar compounds can be mixed to produce standards which otherwise may be very difficult to prepare quantitatively, i.e. addition of some non-rare earth elements into a rare earth matrix. The success of the dry blending technique was only partially satisfactory since relative reproducibilities of about

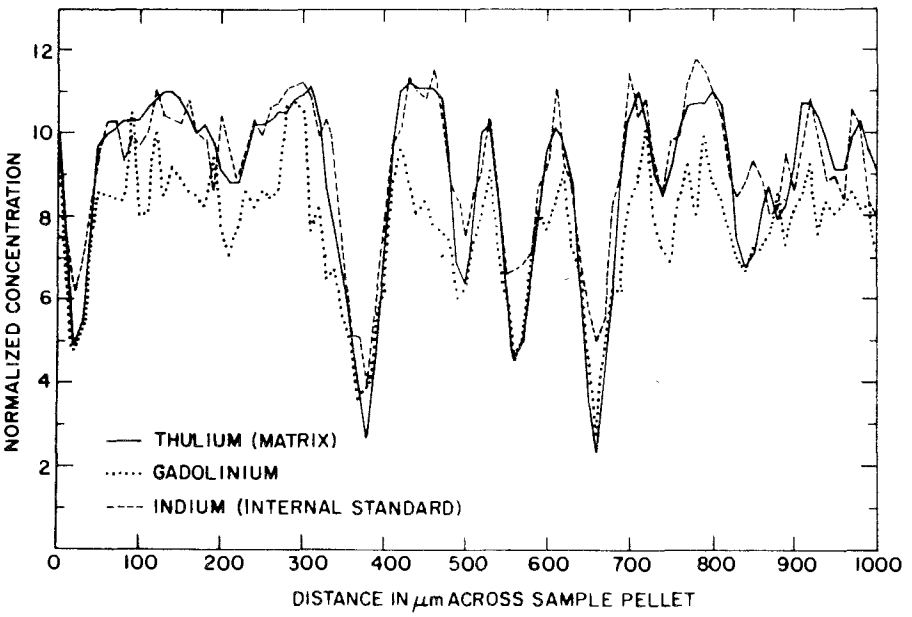

Fig. 37C.8. Spacial distribution of Gd, In, and Tm in a Tm_2O_3-graphite pellet. Adapted from Griffith et al. (1971).

±21 percent were obtained. The uncertainty remains in the application of this type of standard preparation whether elemental compounds dry blended at trace levels will adequately predict the response of the same element chemically bonded to the rare earth matrix.

The second method, oxalate precipitation of rare earth standards, provides chemically bonded constituents. However, relative reproducibilities of 17 percent were obtained with this type of preparation, only slightly better than with dry blended standards. A source of error in attempting broad range quantification of different intensity levels is the fluctuation in the total ion beam composition at the beam monitor. Any determinations dependent upon relative exposure levels will include this error.

The third method was based upon dissolution of the rare earth in nitric acid followed by conversion to the oxide by calcination of the nitrate. Carefully controlled aliquots of standard preparations may be added to the dissolved rare earth samples to adjust spectral intensities to optimum levels. Comparisons of similar rare earths by this means of standard preparation provided relative reproducibilities of 7 percent.

4.2. *Relative sensitivity coefficients*

The quantification of measurements in SSMS involves the comparison of spectral signal intensities corrected for known instrumental effects due to mass,

TABLE 37C.5.

Average relative sensitivity coefficients for rare earths from standards prepared by three different techniques in selected rare earth matrices [from Griffith et al., (1971)].

Matrix	Y_2O_3			Tm_2O_3			Er_2O_3		Sc_2O_3		Ho_2O_3			Average deviation, %
Element	I[a]	II[a]	III[a]	I	II	III	I	II	II	III	II	III	Overall average[b]	
Y	–	–	–	–	.83	–	1.20	1.38	1.06	–	–	–	1.12	15
La	1.00	1.00	1.00	1.00	1.00	1.00	1.00	1.00	1.00	1.00	1.00	1.00	–	
Ce	–	0.68	–	–	0.71	–	–	0.66	0.81	–	0.69	–	0.71	5.6
Pr	1.36	1.31	–	(1.00)[c]	1.42	–	1.29	1.41	1.42	–	1.32	–	1.32	6.6
													(1.36)	(3.5)
Nd	1.40	1.43	1.43	(0.84)	1.37	1.26	1.36	1.08	1.25	1.10	1.34	1.31	1.26	10
													(1.30)	(7.3)
Sm	1.78	1.99	–	1.73	1.94	–	1.48	1.65	1.63	–	2.18	–	1.80	10
Eu	2.16	2.05	2.20	–	2.88	2.24	1.74	2.30	1.81	1.92	2.38	2.66	2.21	12
Gd	1.05	1.18	–	0.82	1.31	–	1.14	0.97	1.49	–	1.43	–	1.17	15
Tb	–	1.09	–	–	1.17	–	–	0.92	0.98	–	1.17	–	1.07	8.7
Dy	1.36	1.70	1.30	1.30	1.12	0.83	0.93	1.00	1.19	1.06	(1.81)	–	1.24	19
													(1.18)	(16)
Ho	1.11	1.34	–	(0.82)	(0.97)	–	(0.46)	(0.66)	1.33	–	–	–	0.96	28
													(1.26)	(7.9)
Er	1.20	1.43	–	(0.91)	(0.84)	–	–	–	1.09	–	–	–	1.09	16
													(1.24)	(10)
Tm	1.36	1.48	–	–	–	–	(0.43)	(0.93)	1.47	–	(2.13)	–	1.30	32
													(1.44)	(3.6)
Yb	2.13	2.58	–	(3.00)	(2.95)	–	(1.12)	–	1.78	–	–	–	2.26	26
													(2.16)	(13)
Lu	–	1.05	–	–	0.87	–	–	0.65	0.75	–	1.15	–	0.89	18

[a]Type of method used for standard preparation: I–dry blending, II–oxalate co-precipitation, III–nitrate calcining. [b]Values in parenthesis obtained by recalculation after deleting values enclosed in parenthesis in the body of the table. [c]Values deleted because they fall outside Student's test at 95% confidence level.

emulsion response, exposure level, isotopic abundance, etc. and also corrected for instrument response due to elemental chemical differences. This latter correction is called the relative sensitivity coefficient (RSC) (Farrar, 1972). Relative sensitivity coefficients are established using standards such as the ones described above and examples of their magnitude are shown in table 37C.5 for the three types of standard preparation. Within the limit of error, matrix effects are not evident. The degree of confidence in applying RSC's in different matrices (e.g. using RSC's determined in oxide preparations for metal samples) will affect the analyst's choice for type of referencing.

4.3. *Referencing*

4.3.1. *Total beam referencing*

A standard sample of the same matrix is analyzed just prior to an analytical sample and the intensity of the analyte spectral signal relative to the total beam monitor signal is established. Then the analytical sample is analyzed under the same conditions and the same instrument response relationship is assumed. An advantage in this type of beam referencing is that spectral signals due to the matrix (frequently difficult to measure accurately due to space charge aberrations) need not be measured for the standard nor for the analytical sample. A disadvantage is the difficulty in obtaining a standard sample in the same form as the analytical sample and maintaining identical conditions during their analysis. The error incurred due to the lack of identical conditions is likely to be due to altered relative intensities of the singly, doubly, or triply charged lines for the matrix rare earth or a shift in the ion illumination angle from the optic axis of the spectrograph due to altered electrode geometry. Both of these altered conditions can cause the total beam monitor to yield a different instrument response relationship between the standard and the analytical sample. Experiments by Conzemius and Svec (1973b) have shown that altered instrument response due to the ion illumination angle can produce a 30% change in the relationship. Total beam referencing is also susceptible to errors caused when the magnitude of carbon or oxygen ion signals (for an oxide/graphite pellet sample) vary thus changing the total ion beam monitor signal relative to spectral rare earth signals.

4.3.2. *Matrix referencing*

Matrix referencing requires accurate measurement of the matrix spectral signal with which to compare directly the analyte spectral signal level with appropriate corrections for abundance, line width, mass effects, multiple charge ratios and RSC. The advantages of this technique are the speed and simplicity in obtaining analytical data. However space charge aberrations can cause large errors in measuring the matrix spectral signal, especially for anisotopic rare earths. A source of uncertainty in metal analyses is the questionable validity of using RSC's which have been determined in oxide samples. Another uncertainty

is the assumption that the full dynamic range of the instrument can be used by simply measuring the matrix and analyte spectral signals. The intensities of these signals may differ by seven orders of magnitude or more and errors may enter due to alteration in such parameters as ion illumination angle or ion transmission efficiencies. The combined magnitude of errors in matrix referencing is estimated to be a factor of two and in unfavorable cases could easily be higher.

4.3.3. *External reference*

External signal referencing has frequently been used in analyses by SSMS such as those described by Taylor (1965). It is not practical for metal samples but with pelleted samples some excellent reproducibilities are possible (Nicholls et al., 1967). The normal means of including an external reference with a pelleted sample is to dry blend, freeze dry, or slurry-mix a known quantity of a selected reference element into graphite which is subsequently blended with the powdered sample prior to pelleting. Spectral signal levels are compared with the external reference level and appropriate corrections are applied including the RSC based upon previously analyzed standards. The principle advantage is that the analyte spectral signal is compared to the external reference signal which is of similar intensity and the matrix spectral signals need not be measured. Confidence in performing accurate analyses routinely is limited by the stringent requirement for intimate mixing of the sample with the external reference. There also remains an uncertainty in whether the behavior of the impurities and the external reference will be sufficiently similar for slightly altered sample geometry or chemical environment.

4.3.4. *Internal referencing*

The best results by SSMS are obtained by comparison of very similar intensities of closely spaced spectral lines of very similar elements that are homogeneously distributed throughout the sample. The optimum case would be the utilization of isotope dilution. When practical, isotope dilution is a more reliable technique (Haaland and Stijfhoorn, 1973) for determination of specific elements than any of the procedures described in this chapter. Of course for many elements it is impossible due to anisotopic abundances; it is impractical due to difficulty in achieving chemical equilibration; or it is very difficult since required sample manipulations may introduce contaminants. Internal referencing described by Griffith et al. (1971) utilized procedures in which a trace level element is chemically homogenized with the matrix rare earth in a nitric acid solution followed by calcination of the nitrate to the oxide. Analyte signals are then compared to the added element and appropriate corrections are applied. Accuracies using this technique *approach* that possible with isotope dilution using SSMS. However some guidelines must be followed: (1) The added level of the internal reference should allow measurement of the analyte signal and the reference on the same exposure with intensity ratios not greater than 1.5, (2) Multiple exposures allowing many measurements are desirable to permit statis-

tical smoothing of fluctuations due to variation in the spark or the photo emulsion, (3) Ideally, although perhaps not practical, the standard sample from which the RSC's are to be computed should be analyzed immediately before or after the analytical sample and should be exposed on the same photographic plate, and (4) The mass difference and the chemical difference between analyte element and reference should be small.

An example of results using internal standardization for the determination of rare earths is shown in table 37C.6 in which lanthanum was the internal reference for the determination of Nd, Eu, and Dy in the four indicated matrices. Two principle advantages of internal referencing are: the higher reliability of relative sensitivity factors and the lessened requirement for intimate blending of the powder with graphite prior to pelleting. Among the disadvantages are the necessary chemical steps and the possible different responses of the reference and analyte signals to variations in spark electrode geometry or spark ion production processes. A form of internal referencing is utilized when an impurity level, established by an independent technique, is available for comparison with other impurity levels as described by Oblas et al. (1966). In this case there is usually very little choice in optimizing parameters such as intensities, chemical similarity with impurity, etc.

4.4. *Combined referencing*

Guidelines with regard to referencing procedures, standard preparations, etc. in the application of SSMS to analysis of rare earths have evolved at the Ames Laboratory and will be discussed briefly. The principal advantage of SSMS, to provide semiquantitative surveys with broad elemental coverage and high sensitivity, is utilized first. Samples are analyzed "as received" with only the preparative steps performed as described earlier. Determinations are made by the matrix referencing technique. However, close attention is given to the reliability of the measurement of the available matrix spectral lines. Absolute instrument response to the matrix ion signals is compared with previous analyses (i.e. a log of absolute instrument response is maintained). Experience has shown that the absolute instrument response is constant to within the confidence level with which it can be measured, approximately 30 percent. If a matrix is being analyzed for which a reliable spectral line is not available, the absolute sensitivity is adjusted to that predicted by the log. The analytical results are thus determined and communicated to the scientist(s) as semiquantitative determinations (i.e. errors in the reported values may be a factor of three from the absolute values and relative differences may be in error by 30 percent). The scientist and the analyst then mutually decide if further analytical work by SSMS on the sample is necessary. Generally, further work will not be warranted if:

(1) All impurities are observed at or near the detection limit.

(2) Determined levels and associated uncertainties will not affect the intended use of the rare earth.

TABLE 37C.6.
Relative standard deviations[a] of rare earth sensitivities using lanthanum as an internal reference

Matrix	Sc_2O_3 plates			Tm_2O_3 plates			Ho_2O_3 plates			Y_2O_3 plates		
Element	844	845	Combined[b]	846	847	Combined[b]	848	849	Combined[b]	851	852	Combined[b]
Nd	5.6	3.7	4.9	5.4	4.5	5.2	4.4	5.3	5.3	7.8	7.4	7.5
Eu	7.1	9.6	10.8	13.0	9.2	12.6	7.9	12.0	11.5	9.1	8.9	8.9
Dy	6.6	5.3	7.2	5.2	12.0	9.3	–	–	–	4.8	6.5	6.0

[a]Each S_{rel} value computed from between 18 to 25 determination on each plate. [b]Data from both photoplates treated as a single population.

(3) Elements that require higher accuracies are not rare earth impurities and can be determined much more accurately by other techniques (e.g. iron by wet chemical methods).

Further analytical work by SSMS on the sample is considered if certain rare earth impurities require lower error limits. Internal referencing is employed in which the reference is an appropriately selected rare earth. The rare earth levels, determined with internal referencing, are then compared to the determinations for these same elements in the original sample. The ratios of these determinations should be constant and this constant can be used as a correction factor for all of the determinations in the original sample. The Laboratory is presently changing the internal standardization step to incorporate the use of isotope dilution when it is practical.

5. Miscellaneous

5.1. *Inhomogeneities*

Inhomogeneity of impurities in rare earth metals has been noted from the earliest application of SSMS (Guthrie, 1964a,b,c). This type of information is frequently quite valuable when analyses are used for diagnostic purposes in guiding metallurgical processes (Parsons, 1971). Some of the inhomogeneities are expected. For example, tantalum is frequently used as a container for molten metals. Dissolution of some of the tantalum in the molten rare earth results in precipitation of tantalum dendrites during solidification. In addition, the solidified metal must be cut or peeled from the container. Some tantalum may be retained if the process is not performed carefully.

Conversion of a fluoride to the metal can leave areas of the metal with fluorine content much higher than the average composition. It is not uncommon in these cases for the determination of fluorine to be in error by two to three orders of magnitude. Rare earths prepared or purified in a vaporization step produce a condensed metal which, if sampled directly for analysis by SSMS, can yield erroneous data due to heterogeneous impurity content since only a few mg of sample are consumed in the analysis by SSMS (Svec and Conzemius, 1968).

5.2. *Contamination*

Standard procedures commonly in use for handling samples are generally considered adequate. Some techniques in use at the Ames Laboratory to minimize contamination in handling many diverse rare earth samples may be of interest. Automatic blending of powdered rare earth compounds with graphite in ultrapure graphite crucibles eliminates possible contamination from blending in a mortar and pestle. The crucibles are charged with a pure graphite rod $2\frac{1}{2}$ mm dia., 3 mm long and with measured weights of graphite and are then stored in a clean area. When a powder is to be blended, it is weighed and dropped into a graphite

crucible selected to contain the desired amount of previously charged graphite. Mixing is performed in a shaker for about five min. with the crucible being protected from shattering by a polyurethane cushioned plastic vial. The resulting blend is then pelleted with a polyethylene plug (Brown, et al., 1967). The graphite crucible, rod, plastic vial, and plug are not re-used.

The determination of gaseous impurities in metals by SSMS has been only partially successful (Roboz, 1972). Special surface preparation, high speed pumping, and high temperature baking of the ion source have all been used to reduce sources of contamination of oxygen, carbon, and nitrogen. The high reactivity of the rare earth metals complicates the determination of these impurities by SSMS and other more reliable techniques such as vacuum fusion, etc. are normally used (Beaudry and Palmer, 1974). Comparison of results determined by these techniques with SSMS results indicates that without any special standardizing procedures, an error factor of about X10 should be assumed for C, O, and N determinations by SSMS in rare earth metals. However, comparison of levels in diagnostic work has been shown to be useful even for hydrogen as described by Busch et al. (1971), Evers et al. (1975), and Parsons (1971).

5.3. *Instrument memory*

The anode source parts, the spark electrode sample holders, and the object slit are all known to contribute to the spectrum through various ion formation processes. At the Ames Laboratory these ion source parts have been fabricated from pure niobium. Thus niobium must be reported as an upper limit. More importantly however, any deposits from previous samples in the instrument will also contribute to the spectrum as instrument "memory". All of the anode source parts including the sample holders are cleaned mechanically with a wire brush and then chemically in boiling aqua regia. The parts are then rinsed in deionized water and dried in a clean atmosphere. The object slit cannot be changed conveniently between samples and contributes to instrument memory at about the 20 ppm level for subsequently analyzed samples. Spectral lines due to instrument memory for the spectrograph at the Ames Laboratory have unique features due apparently to the location of ion formation. The singly charged lines are unusually broad and slightly offset from the normal spectrum. Doubly charged lines from signals due to memory are unusually low in intensity. Instrument memory due to previous samples is kept under surveillance by monitoring the decrease in levels and is minimized by careful selection of the sequence of samples analyzed with the spectrograph and by cleaning the object slit at convenient intervals. The effects of instrument memory vary for different commercial instruments.

5.4. *Magnitude of relative sensitivity coefficient*

Attempts by Oblas (1971), Conzemius and Svec (1973a), and Sasamoto et al. (1975) to correlate the magnitude of the individual rare earth RSC's as measured

TABLE 37C.7.
Relative sensitivity coefficients of rare earths in Y_2O_3 by three different laboratories.

	Sasamoto et al. (1975)	Oblas (1971)	Griffith et al. (1971)
La	0.76	0.67	0.69
Ce	0.60	0.4	0.47
Pr	0.92	0.83	0.92
Nd	1.4	1.00	0.98
Sm	1.5	1.43	1.30
Eu	1.8	2.5	1.48
Gd	0.95	0.83	0.77
Tb	0.75	0.59	0.75
Dy	1.00	1.00	1.00
Ho	0.71	0.62	0.84
Er	0.86	0.71	0.91
Tm	0.82	0.71	0.98
Yb	1.2	1.25	1.62
Lu	0.71	0.4	0.72

in rare earth matrices have been reasonably successful. Table 37C.7 lists RSC's, normalized to Dy ≡ 1.00, reported for a Y_2O_3 matrix from three different laboratories, each using different commercial instruments and different oxide/graphite ratios in the sample. Differences in the values among the laboratories appear to be random but there is sufficient agreement of trends to motivate comparisons of RSC's with elemental properties. Figure 37C.9 is a plot of the data in table 37C.7 along with RSC's computed from physical constants according to the studies noted in the figure. Such comparisons permit closer scrutiny of the experimental values. For example, the experimentally determined RSC's in the Oblas data for Eu and Dy appear to be high compared to adjacent rare earths. There may be good reason for these higher values. The range of values (highest/lowest RSD) is greatest for the Oblas data at a factor of 6.2. For the Griffith et al. data the range is 3.4 and for Sasamoto et al., 3.1. This trend may be expected since Oblas used the highest oxide content, Sasamoto et al. used the highest graphite content (See fig. 1), and Conzemius (1976) has observed that the range of elemental RSC's tend to be greater as the amount of graphite in the pellet is reduced.

5.5. *Electrical ion detection*

The advantages of electrical ion detection (Conzemius and Svec, 1972) are especially applicable to the analysis of very low concentrations of rare earths adjacent in mass to the matrix, e.g. the determination of Ce in Pr. Electrostatic peak switching techniques described by Conzemius and Svec (1969) may also be utilized conveniently when only rare earths and common elements are to be determined. A single magnetic field setting allows a M/z range from 51 to 92 to

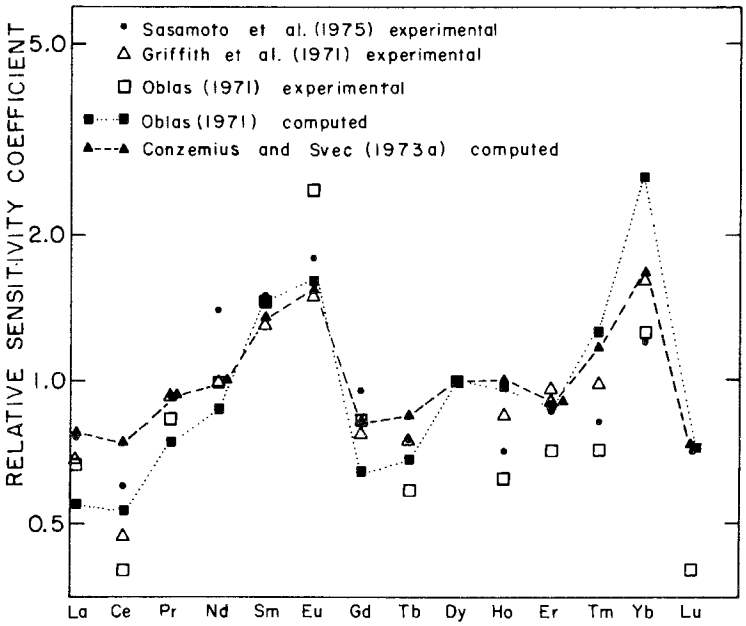

Fig. 37C.9. Plot of experimentally determined and of computed relative sensitivity coefficients for rare earths in Y_2O_3.

be measured. This permits measurement of the singly charged ions of vanadium thru zirconium and the doubly charged ions of barium, the rare earths, hafnium, tantalum and tungsten. A special ion collector has been shown by Conzemius and Svec (1974) to be useful when rare earth oxide-graphite pellets are being analyzed for rare earths whose masses are close to the mass of the matrix rare earth. This collector permits direct measurement of the rare earth-impurity/rare earth-matrix ion current ratio and avoids errors due to variable carbon and oxygen ion signals.

6. General evaluation of the technique

The application of SSMS to the semiquantitative survey of all impurities in rare earth matrices is very useful. All of the recent innovations for improvement of performance (Ahearn, 1972) are applicable to the analysis of rare earth matrices. The determination of rare earth impurities in rare earth matrices presents no unusual difficulties and the quantification of these impurity levels can be performed with relative ease if standards are prepared. Quantification of non-rare earth impurities in rare earth matrices by comparison with specially prepared standards has not been reported. These determinations are based frequently upon RSC's determined from non-rare earth metal standards or upon RSC's determined from dry blended preparations of rare earth oxide samples.

The principal disadvantages are the cost of acquisition of the instrument, the low rate of sample through-put, the susceptibility to errors due to surface contamination or inhomogeneity, and the difficulty in assigning appropriate confidence levels to determinations. Customers inquiring about the reliability of determinations frequently want a *generalized statement* of analytical accuracy. In SSMS there are many levels of reliability since estimates of concentration levels for all elements are desired. Each element has unique factors affecting reliability such as interferences, photoplate fog level, isotopic verification, inhomogeneity, surface contamination, instrument memory, and unreliable or undetermined elemental sensitivities. Thus good communication between the analyst and the customer is necessary in order to ensure that confidence limits are set within reasonable bounds.

Acknowledgement

This work was supported by the U.S. Department of Energy, Division of Basic Energy Sciences.

References

Ahearn, A.J., 1966, Mass Spectrometric Analysis of Solids, (Elsevier, Amsterdam).
Ahearn, A.J., 1972, Trace Analysis by Mass Spectrometry, (Academic Press, New York).
Beaudry, B.J. and P.E. Palmer, 1974, J. Less-Common Metals **34**, 225.
Brown, R., W.J. Richardson and H.W. Somerfield, 1967, Ann. Conf. Mass Spectrom., 15th, Denver, Colorado. ASTM E-14.
Busch, G., E. Kaldis, J. Muheim, R. Bischof, 1971, J. Less-Common Metals **24**, 453.
Cavard, A., 1968, In Advances in Mass Spectrometry. Volume 4. (Inst. of Petroleum. London.) pp. 419–429.
Conzemius, R.J., J. Capellen, H.J. Svec, 1966, Ann. Conf. Mass Spectrom, 14th Dallas, Texas. ASTM E-14.
Conzemius, R.J., R.D. Erbeck, S. Elbert, 1967, IS-1693. Computer Program for Interpretation of Mass Spectrograph Photoplates.
Conzemius, R.J., H.J. Svec, 1969, Talanta **16**, 365.
Conzemius, R.J., H.J. Svec, 1972, In Trace Analysis by Mass Spectrometry. A.J. Ahearn, Ed., (Academic Press, New York) pp. 135.
Conzemius, R.J., H.J. Svec, 1973a, Talanta **20**, 575.
Conzemius, R.J., H.J. Svec, 1973b, Talanta **20**, 477.
Conzemius, R.J., H.J. Svec, 1974, Talanta **21**, 171.
Conzemius, R.J., 1976, Unpublished Data. Ames Laboratory.
Cook, H.D., 1966, Ann. Conf. Mass Spectrom., 14th, Dallas, Texas. ASTM E-14.
Dornenburg, V.E., H. Hintenberger, 1959, Z. Naturforsch. (14a) 765.
Evers, J., E. Kaldis, J. Muheim, C. Zürcher, 1975, Helv. Phys. Acta (48) 462.
Farrar IV, H., 1972, In Trace Analysis by Mass Spectrometry. A.J. Ahearns, Ed., (Academic Press, New York) pp. 240–295.
Griffith, D.A., R.J. Conzemius, H.J. Svec, 1971, Talanta **18**, 665.
Guthrie, J.W., 1963, SC-TM 343-63, **14**. Mass Spectrographic Analysis of Erbium and Cerium Metal.
Guthrie, J.W., 1964a, Ann. Conf. Mass Spectrom., 12th. Montreal, Canada ASTM E-14.
Guthrie, J.W., 1964b, SC-TM-64-938. Analysis of Lutetium Metal by Spark Source Mass Spectroscopy.
Guthrie, J.W., 1964c, J. Less-Common Metals **7**, 420.
Haaland, J., D.E. Stijfhoorn, 1973, Analysis and Application of Rare Earth Materials. (Universitetsforlaget, Oslo) pp. 153–164.
Hull, C.W., 1969, Int. J. Mass Spectrom. and Ion Phys. **3**, 293.
Kennicott, P., 1972, In Trace Analysis by Mass Spectrometry. A.J. Ahearn, Ed., (Academic Press, New York) pp. 179–210.
Morrison, G.H., J.R. Roth, 1972, In Trace Analysis by Mass Spectrometry. A.J. Ahearn, Ed., (Academic Press, New York) pp. 297–322.
Muheim, J., 1972, Mat. Res. Bull. **7**, 1417.

Muheim, J., 1973, CONF-730402-P1. Proc. Tenth Rare Earth Conf., Carefree, Arizona.
Nicholls, G.D., A.L. Graham, E. Williams, M. Wood, 1967, Anal. Chem. **39**, 584.
Oblas, D.W., D.J. Bracco, D.Y. Yee, 1966, Trace Analysis in Oxidic Matrices by Solids Mass Spectroscopy. Symposium on Trace Characterization – Chemical and Physical (National Bureau of Standards, Gaithersburg, Maryland.) Oct. 3–7, 1966.
Oblas, D.W., 1971, Appl. Spec. **25**, 325.
Parsons, N.H., 1971, GEPP-85. Production of Bulk Quantities of Ultrapure Erbium.
Peterson, V., 1976, Private Communication, Ames Laboratory.
Roboz, J., 1972, In Trace Analysis by Mass Spectrometry. A.J. Ahearns, Ed., (Academic Press, New York) pp. 369–398.
Sasamoto, T., Y. Itoh, H. Hara, T. Sata, 1975, Bull. Tokyo Inst. Tech. **126**, 91.
Schmidt, F.A., R.J. Conzemius, O.N. Carlson, H.J. Svec, 1974, Anal. Chem. **46**, 810.
Svec, H.J., R.J. Conzemius, 1968, Advances in Mass Spectrometry, Volume 4, (Inst. of Petroleum. London.) pp. 457–464.
Taylor, S.R., 1965, Geochim. et Cosmochim. Acta **29**, 1243.
Woolston, J.R., 1972, In Trace Analysis by Mass Spectrometry. A.J. Ahearn, Ed. (Academic Press, New York) pp. 213–238.

Handbook on the Physics and Chemistry of Rare Earths, edited by K.A. Gschneidner, Jr. and L. Eyring

Chapter 37D

OPTICAL ATOMIC EMISSION AND ABSORPTION METHODS*

E.L. DeKALB and V.A. FASSEL
Ames Laboratory, US DOE and Department of Chemistry, Iowa State University, Ames, Iowa 50011, USA

Contents

1. Introduction

Atomic spectroscopic techniques provide several of the most useful and specific means for the determination of the rare earth elements at the trace, minor, and major constituent levels. Even though the chemical properties of the elements may be remarkably similar, the energy states within each atomic system are just as uniquely different for the individual rare earth elements as they are for other elements. As a consequence, the spectra produced by energy transitions between these states are also highly specific.

*Work performed for the US Energy Research and Development Administration under Contract No. W-7405-eng-82.

Two general groups of atomic spectroscopic analytical techniques will be described in this chapter. Sections 1–5 will be devoted to techniques utilizing atomic spectra within or near the optical range of wavelengths. Section 6 will describe techniques which depend upon the X-ray spectra of the rare earth elements. The sharp line absorption and fluorescence spectra of rare earth ions in solution are not considered here, but are discussed in ch. 37A.

1.1. *Optical spectra characteristics*

The arc and spark spectra of many of the rare earth elements are very complex, possessing thousands of lines of rather uniform intensity and lacking the characteristically intense lines found in the emission spectra of other elements. Figure 37D.1 shows a small segment of these spectra, photographed in the second order of a large grating spectrograph. It can be seen that the spectra of all the rare earths except lanthanum, europium, thulium, ytterbium, and lutetium fall into the complex category. The probability of line interferences is therefore high and difficulties are frequently encountered in locating interference-free lines. This is especially true for the determination of trace rare earth impurities in purified rare earths.

Combustion flames have the potential for producing simpler spectra because these atomization sources are less energetic. However, the flames used by early investigators provided rather disappointing detection limits because the spectra consisted almost entirely of monoxide band systems. These monoxide bands have been used for analytical determinations, but with limited success because extensive spectral overlap occurs for bands of many of the lanthanide elements. The absence of atomic line spectra resulted from the tendency of the rare earth elements to form stable monoxide molecules, and even the relatively high temperatures prevalent in stoichiometric oxyacetylene flames (~ 3200 K) are insufficient to effectively dissociate these molecules. Collaborative thermodynamic data can be found in the relatively high dissociation energies of these molecules. The high stability of these monoxide molecules greatly reduces the free-atom concentration in the flame and thus the atomic line emission will be weak or non-existent.

Fassel et al. (1962) found that flame chemistry, rather than flame temperature, was an important consideration in the production of free-atoms of the rare earth elements. Their studies have shown that the increase in the free-atom population is a direct result of the high concentration of carbon-containing species that are prevalent in fuel-rich, high-temperature hydrocarbon flames (see Broida and Shuler, 1957; Gaydon and Wolfhard, 1960). The reaction between atomic oxygen and the carbonaceous species is highly exothermic and thus the concentration of atomic oxygen in these flames should be very low (Finimore and Jones, 1958; Rasmuson, 1970; Chester et al., 1970; Fassel et al., 1970). This low concentration of atomic oxygen tends to shift the rare earth monoxide dissociation equilibrium in favor of the existence of a relatively high concentration of free atoms in the flame gases. The improvement in free atom production in the fuel-rich hydro-

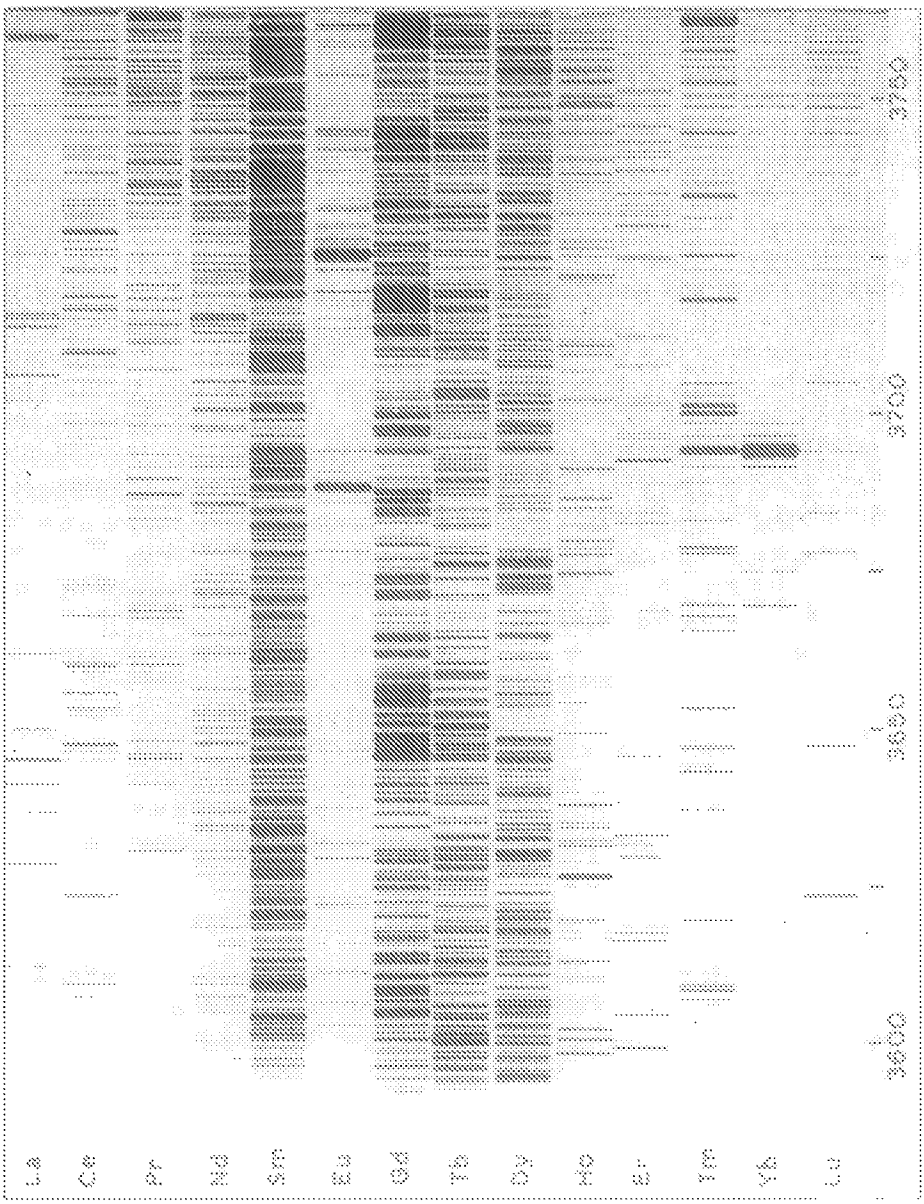

Fig. 37D.1. DC arc spectra of the lanthanides photographed on a large grating spectrograph.

carbon flame is illustrated for Sc in fig. 37D.2. The emission and absorption enhancement factors observed in the fuel-rich flame vary considerably, with the greatest enhancements observed for those rare earth elements which have the most stable monoxides (Fassel et al., 1970). Thus for both the flame atomic absorption and emission determination of the rare earths, flame stoichiometry is a critical variable. Very fuel-rich flames are necessary for the efficient formation of free atoms of those elements that form stable monoxides (e.g., La and Ce), whereas near stoichiometric flames produce maximal absorption or emission for Eu and Yb, whose monoxide dissociation energies are relatively low.

The spectra thus produced are relatively simple, so that a spectrometer of 0.5 m focal length is adequate for the analysis of rare earth mixtures (D'Silva, et al., 1964a). Preliminary studies indicate that the induction-coupled plasma (ICP) described by Fassel and Kniseley (1974) provides spectra which are similar to those obtained with dc arc excitation. Consequently, a spectrometer with greater dispersion capabilities than can be obtained with a 0.5 m focal length instrument will probably be necessary. Superior powers of detection have been reported for several of the rare earth elements by Fassel et al. (1973) and by Souilliart and Robin (1972) when aerosols of rare earth containing solutions are injected into inductively coupled plasmas. This excitation source possesses additional advantages, which will be discussed in section 2.2.4.

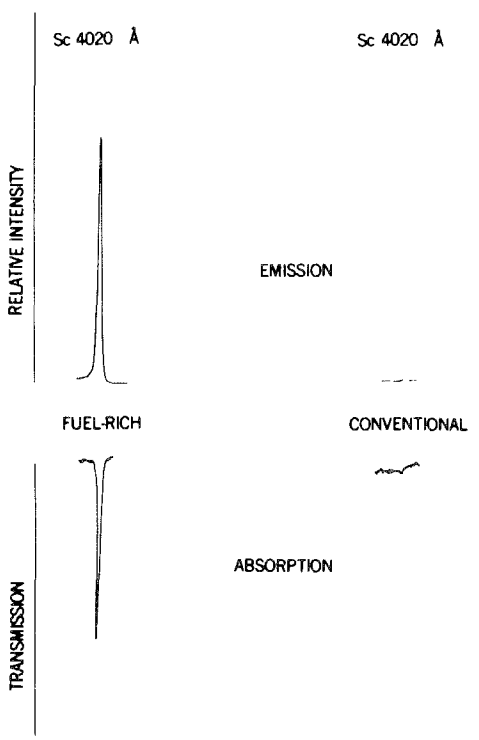

Fig. 37D.2. Emission and absorption by scandium in a stoichiometric and a fuel-rich nitrous oxide-acetylene flame.

1.2. *Spectral line identifications*

Because the optical spectra of many of the lanthanide elements are complex, line identification can be a difficult task. One of the most useful resources for rare earth line identification is the atlas "Spektren der Seltenen Erden" (Gatterer and Junkes, 1945). The NBS (Meggers et al., 1975) and MIT (Harrison, 1969) wavelength tables are also necessary references if any extensive work with these spectra is anticipated.

Accurate analyses also require that the selected analytical line be free of interfering spectral lines originating from other elements in the sample. Unless rare earth matrices free of the suspected impurities are available, it is difficult to establish whether the presence of spectral lines at the characteristic wavelength of persistent lines of the impurity are really caused by the rare-earth impurity, or by very weak lines of the matrix rare earth, or both. In the past, it has not been possible to place full reliance on the term "spectroscopically pure" because these tests may have been based on the absence of weaker impurity lines, whereas stronger impurity lines may still be detected but are assumed to be weak lines of the matrix rare earth.

These erroneous assumptions are fostered somewhat by line misidentifications in the published wavelength tables of the rare earths. Because of the complexity of some spectra and the difficulties in obtaining pure matrices, many lines in the tables are attributed to the matrix rare earth when in reality they are persistent lines of another rare earth present in trace amounts. In the MIT Wavelength Tables, for example, erbium lines are listed coincident with almost every sensitive dysprosium line. In reality, most of these lines originate from a dysprosium impurity in the erbium used in obtaining the spectra.

A tabulation of these misidentifications has been reported by Kniseley et al. (1959a). A few of the errors were corrected in a recent revised edition of the MIT Wavelength Tables (Harrison, 1969). Unfortunately, 18 rare earth lines which had been questioned by Smith and Wiggins (1949) were also eliminated, although Kniseley had verified the MIT identifications.

1.3. *Analytically useful spectral wavelengths*

Hundreds of papers describing atomic emission, absorption or fluorescence methods for the determination of individual rare earth elements have appeared in the scientific literature during the past 35 years. The spectral lines selected by various authors for specific analytical problems and for use with available spectral instruments are quite diverse. Still, certain wavelengths are seen to be selected again and again; a summary of these lines is shown in table 37D.1.

1.4. *Classification of analytical problems*

It is convenient to classify rare earth analyses into four broad categories: (1) the determination of rare earth in a "pure" rare earth; (2) the determination of

TABLE 37D.1
Analytically useful spectral wavelengths (Å)

Sc	Y	La	Ce	Pr	Nd	Sm	Eu
3353.7	3195.6	3245.1	3063.0	3908.4	3836.5	3568.3	2813.9
3613.8	3242.3	3337.5	3801.5	4008.7	3921.0	3609.5	3819.7
3907.5	3327.9	3380.9	3942.1[f]	4056.5	3941.5	3634.3	3907.1
3911.8[a,f]	3448.8	3927.6[a]	4012.4	4100.7	4012.2	3661.4	3930.5[f]
4020.4	3600.7	3929.2	4137.6	4179.4	4061.1	3670.8	3972.0
4246.8	3611.0	3949.1	4186.6	4206.7	4247.4[f]	3739.1[f]	4129.7
	3620.9	3988.5	4222.6	4223.0	4303.6	3885.3	4594.0[a]
	3633.2	3995.7	4460.2	4225.3	4451.6	4256.4	4627.2
	3210.3	4031.7	4562.4	4305.8[f]	4634.2[a]	4279.7	4661.9
	3282.6	4086.7	5699.2[a]	4408.8	4896.9[f]	4280.8	
	4077.4[a]	4333.7		4468.7	4924.5[a]	4296.7[a,f]	
	4102.4	4526.1		4496.5	4954.8	4420.5	
	4374.9	5501.3[a,f]		4939.7[a]		4424.3	
				4951.4[a,f]		4433.9	
						4434.3	
						4467.3	
						4760.3	
						4783.1	
						4884.0	

Gd	Tb	Dy	Ho	Er	Tm	Yb	Lu
3100.5	3293.1	3308.9	3399.0	3230.6	3131.3	2891.4	2615.4
3350.5	3324.4	3407.8	3453.1	3264.8	3133.9	2970.6	2911.4
3358.6	3509.2[f]	3531.7	3456.0	3312.4	3258.0	3031.1	3077.6
3362.2[f]	3561.7	3536.0[f]	3474.3	3372.7[f]	3291.0	3289.4[f]	3279.0
3422.5	3676.3	3645.4	3891.0	3499.1	3362.6	3464.4[f]	3281.7
3440.0	3703.9	3898.5	4053.9	3692.6	3425.1	3478.8	3312.1[a]
3654.6	3848.7	4000.5	4103.8[a,f]	3906.3	3441.5	3694.2	3472.5
3671.2	4318.8	4046.0	4163.0[a]	4008.0[a,f]	3462.2	3988.0[a]	4518.6
3684.1[a,f]	4326.4[a]	4103.9[a]			3717.9[a]		5135.1[f]
3712.7	4338.4[f]	4186.8[a,f]			3795.7[f]		
3768.4		4211.7[a]			3883.1		
3966.3					4094.2[a,f]		
4225.8[a]							
4401.9							

[a]Wavelength has been used for atomic absorption analyses. [f]Wavelength has been used for atomic fluorescence analyses.

other impurities in a rare earth; (3) the determination of rare earths in a mixture of various rare earths; and (4) the determination of rare earths in other materials. Each category will be discussed separately in the following sections (2 through 5) of this chapter.

2. Determination of rare earth impurities in a rare earth

2.1. *Oxide samples*

A problem posed by the atomic emission techniques is common to all spectrographic methods for analysis of nonmetallic samples. This problem is concerned with finding excitation conditions which will produce spectra of sufficient precision to allow determinations to be made with adequate accuracy, especially for major constituent determinations. A widely used technique for the excitation of nonmetallic samples involves vaporization of the powdered oxide in a high current d.c. arc discharge. Electrode temperatures attained in this manner, especially if the supporting electrode is used as the anode, provide adequate thermal energy to vaporize the refractory rare earth oxides. The volatilization process can be facilitated by admixing powdered graphite with the oxides. Apparently, at the prevailing electrode temperatures, chemical reduction to form the more volatile metals is at least partially achieved.

Unfortunately, the d.c. arc discharge is an uncontrolled source in which excitation temperatures vary continuously in a non-random manner. Analytical spectroscopists have demonstrated that internal compensation for these intensity fluctuations can be provided by measuring the intensity ratio of the analytical line with respect to the line of another element present in the arc column. However, internal compensation is successful only if both species are simultaneously present in the discharge column. This requirement is more easily satisfied for some members of the rare earth group of elements than for other groups of elements. The relative vapor pressures of the constituents in the sample – or their reaction or decomposition products – determine their order of introduction into the discharge zone. Because of the similarity in the physical and chemical properties of many of the rare earth oxides, there is a unique similarity in the vaporization behavior among some of the elements in this group (Fassel and Wilhelm, 1948; Fassel, 1949; Fassel et al., 1952; Fassel et al., 1955; Kniseley et al., 1958; Kniseley et al., 1959b). For the determination of trace rare earth impurities in purified rare earths, it is thus convenient to select a line of the matrix for internal reference purposes.

Detection limits as low as a few tenths of a ppm can be obtained if both the impurity and matrix rare earth element have relatively simple spectra. More often, the detection limits are in the range of 10 to 1000 ppm. Precision is unusually good for dc arc excitation, with $\pm 5\%$ often reported. This analytical technique is described in greater detail in the appendix to this chapter.

Modification to Fassel's basic method include (1) the use of controlled atmospheres to eliminate interfering cyanogen bands (Grampurohit and Bellary, 1970; Grampurohit and Kaimal, 1973 and 1975; Hammaker et al., 1958; Karpenko and Grechanovskii, 1972; Nash, 1968; Osumi et al., 1971b; Sato et al., 1971); (2) variation in the arcing current, sample electrode dimensions, and the sample weight; (3) the addition of a buffer such as CsCl (Osumi et al., 1971c; Osumi and Miyake, 1972 and 1973) or BaF_2 (Zmbova, 1972); and (4) the use of an

ac arc instead of the dc arc, which is claimed to improve both the detection limits and the precision (Zeeb et al., 1958; Rozsa and Stone, 1962).

The best detection limits via either arc or spark excitation without pre-concentration of which we are aware are listed in table 37D.2. Most of these values were taken from Nash (1968) and Sato et al. (1971).

2.2. *Dissolved samples*

Spark, flame and plasma excitation are applicable to the direct excitation of solution samples. Osumi et al. (1970) used spark excitation to a rotating disc electrode to obtain rare earth detection limits of 2 to 40 ppm in complex-spectra rare earth elements. They used a controlled atmosphere and the rare earth solution contained 60% methanol. The introduction of solutions into spark discharges via porous graphite electrode (Fadeeva and Karpenko, 1972) or as aerosols (Karpenko et al., 1974) has also provided satisfactory analyses.

2.2.1. *Flame emission spectroscopy (FES)*

Flame emission methods for the determination of rare earth elements in an essentially pure rare earth have been reported by several analysts.

The original work on the flame excitation of the line spectra of the rare earth elements was done with a total consumption burner (Beckman-type) that produced a highly turbulent flame. For most of the subsequent investigations in both emission and absorption, premixed O_2–N_2–C_2H_2, (Kniseley et al., 1963; D'Silva et al., 1964b), N_2O–C_2H_2 (Amos and Willis, 1966; Amos, 1967; Christian, 1968; Pickett and Koirtyohann, 1968; Hingle et al., 1969; Kniseley et al., 1969; Shifrin and Ramirez-Munoz, 1969) or O_2–C_2H_2 were employed (Fiorino et al., 1968). For N_2O–C_2H_2 and O_2–C_2H_2, slot burners of the type normally used in atomic absorption instruments were found particularly useful for emission observations as well.

The compressed wavelength scales usually employed in published flame

TABLE 37D.2
Detection limits for rare earth in rare earth determinations

Rare earth impurity	Detection limit (ppm)	Matrix	Rare earth impurity	Detection limit (ppm)	Matrix
Sc	0.5	Y_2O_3	Gd	0.5	Y_2O_3
Y	2	Sm_2O_3	Tb	5	Y_2O_3
La	3	Y_2O_3	Dy	1	Y_2O_3, Eu_2O_3
Ce	10	Y_2O_3, Sm_2O_3	Ho	5	Y_2O_3
Pr	5	Y_2O_3	Er	0.5	Y_2O_3
Nd	6	Sm_2O_3	Tm	0.5	Y_2O_3
Sm	3	Y_2O_3	Yb	0.01	Y_2O_3
Eu	0.5	Y_2O_3	Lu	0.1	Y_2O_3

emission spectra convey the impression that the spectra of these elements are very complex. In reality the spectra are relatively simple, as shown in fig. 37D.3. In this figure, the spectrum of samarium, one of the most complex in the group, is shown in both compressed and expanded form. Even though the spectra were recorded with a low dispersion 0.5 m grating spectrometer, the simplicity is readily apparent in the lower spectrum.

2.2.2. *Flame atomic absorption spectroscopy (AAS)*

In a systematic study on the absorption spectra of the rare earth elements in a fuel-rich, oxyacetylene flame fed with ethanolic solutions of these elements, Fassel and Mossotti (1963), and Mossotti and Fassel (1964) identified over 1000 absorption lines in the 2500 to 6500 Å region. Many of these lines were of sufficient intensity to be useful for analytical purposes. Skogerboe and Woodriff (1963) observed europium, thulium, and ytterbium in absorption in a turbulent, fuel-rich oxyacetylene flame. These investigators employed an oxyhydrogen flame fed with solutions of the respective rare earth salts as primary sources. Because of the low intensity and relative instability of these sources, the observed detection limits were not good. Later work by Fassel et al. (1966) provided detection limits for all of the rare earth elements except cerium. A continuum primary source combined with a small 0.5 meter spectrometer were used for these observations. The development of a long-path slot burner designed specifically for the observation of atomic absorption spectra of high burning velocity flames, such as oxygen-acetylene, led to an order of magnitude improvement in the detection limits (Fiorino et al., 1968). The detection limits reported later by Amos and Willis (1966) for fuel-rich nitrous oxide-acetylene flames compared favorably with those observed for fuel-rich oxyacetylene flames.

When higher temperature flames are employed as absorption cells, the degree of ionization of the rare earths may be significant (Manning, 1966). Since the degree of ionization in flames is suppressed by the presence of other easily ionizable elements, enhanced absorbances may be observed when other elements are introduced into the flame with the rare earths (Amos and Willis, 1966; Jaworowski et al., 1967).

A comparison of the detection limits for the rare earth elements in flame atomic emission and absorption spectrometry (table 37D.3 in section 2.2.5) allows certain conclusions to be made. The fuel-rich oxyacetylene and nitrous oxide-acetylene flames are very effective in producing free atoms of these elements and are the flames of choice for both atomic emission and absorption analysis. The emission detection limits are equal to or better than those obtained by absorption techniques, and thus flame atomic emission methods are generally superior. Future improvements in hollow cathode discharge tubes (or development of other primary sources) may lower the atomic absorption detection limits and thereby make the two techniques more complementary. However, Kinnunen and Lindsjo (1967) have emphasized that locating the proper rare earth ab-

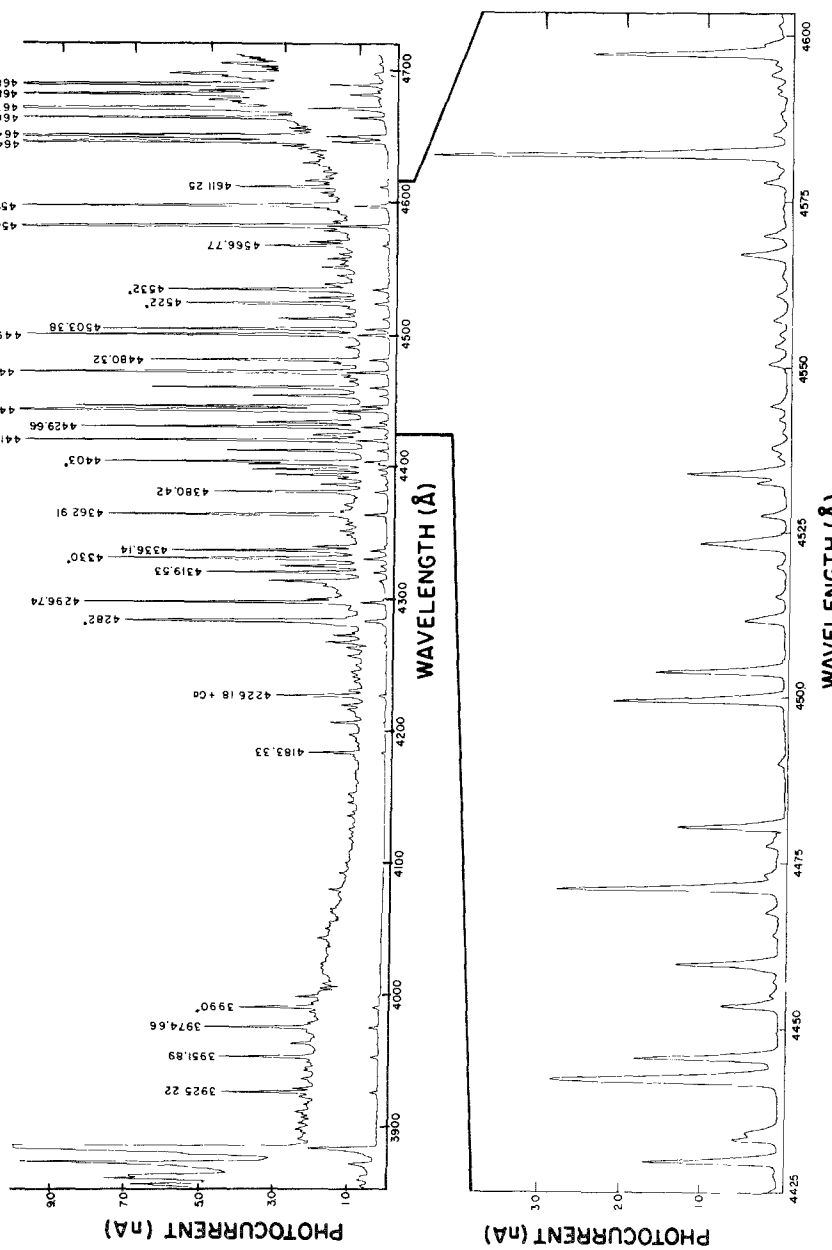

Fig. 37D.3. Recording of a portion of the flame emission spectrum of Sm using both a compressed and expanded wavelength scale.

sorption line is sometimes difficult because of the complexity of the spectra emitted by the hollow cathode lamps. This could cause difficulties in routine analytical application. The spectral lines used in some of these reports are included in table 37D.1, and are noted by a "a" after the respective wavelengths to indicate usefulness in AAS.

2.2.3. *Atomic fluorescence spectroscopy (AFS)*

There has been only one reasonably complete report on the application of AFS to the determination of rare earth elements. Omenetto et al. (1973) reported detection limits for both atomic and ionic fluorescence; the values reported were generally inferior to those obtained with other flame and plasma techniques. In table 37D.1, spectral lines found useful in AFS are identified with an "f" following the wavelength.

2.2.4. *Induction coupled plasma spectroscopy (ICP)*

"Electrical flames" or electrically generated "flame-like" plasmas possess physical and spectroscopic properties that make them potentially very useful as free atom generators and excitation sources for the determination of the rare earths. The ultimate potential of these plasmas for the analysis of rare earth mixtures has not been evaluated, but the preliminary result so far obtained in our laboratories are indeed encouraging. For example, the detection limits that have been measured in an electrodeless induction coupled plasma (ICP) (see table 37D.3 in section 2.2.5) are at least two to three orders of magnitude lower than the lowest values so far reported by flame emission.

A schematic diagram of the complete plasma configuration, including the assembly of concentric quartz tubes (a), argon flow patterns (b and c), and load coil (d) is shown in fig. 37D.4. The torodial shaped plasma (e) is initiated in the following manner. The tangential argon plasma support flow (b) is partially ionized with a tesla coil as it enters the concentric quartz tube configuration. The electrons liberated when the argon ionizes couple with the high frequency oscillating magnetic fields induced by the radio frequency current flowing in the load coil. The accelerated electrons cause additional ionization and the ions and electrons formed flow in closed annular paths (eddy currents) inside the quartz tube. Because the induced magnetic fields are time-varying in their strength and direction, the electrons and ions are accelerated on each half cycle. Joule heating results from the resistance to the flow of the electrons and ions. The foregoing step by step process occurs almost instantaneously and the plasma, once formed, is sustained and thermally isolated from the quartz tube walls by the tangentially introduced argon plasma support flow (b). In addition to this tangential stabilization flow of argon, a lower velocity laminar flow (c) of 1 ℓ/min transports the sample aerosol through the central tube for effective injection into the axial channel of the plasma where the aerosol experiences a high temperature.

Recognition that the ICP would be a nearly ideal excitation source for the

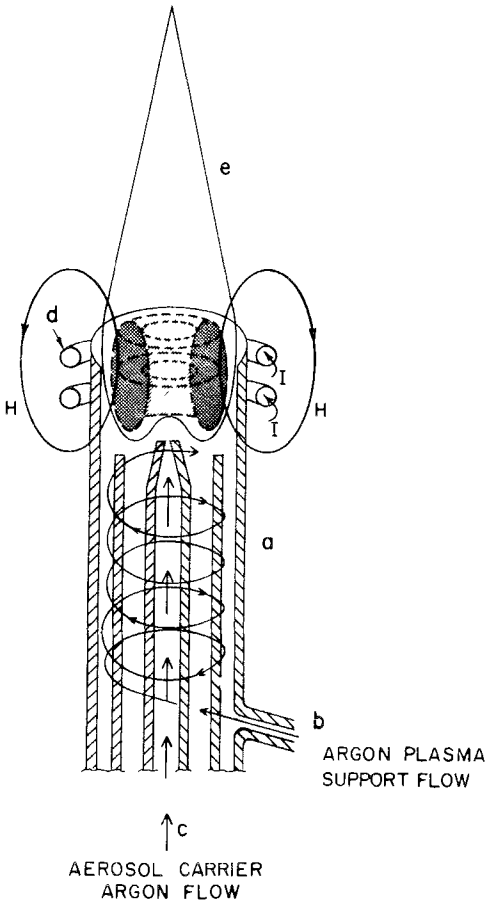

Fig. 37D.4. Complete plasma configuration: (a) concentric quartz tubes; (b) argon plasma support gas; (c) aerosol carrier argon flow; (d) load coil; (e) torodial shaped plasma.

spectroscopic determination of elements is based on the following experimentally observed characteristics of the plasma reported by Fassel (1977).

(1) The analyte emission is confined to a narrow axial channel surrounded by argon having a high gas temperature.

(2) Emission from analytes is usually observed above the atomization zone in a relatively constant temperature region (Kalnicky et al., 1975).

(3) The observation of the free atoms or ions confined to the narrow axial channel results in linear analytical curves over 4 to 5 orders of magnitude in concentration.

(4) The emission from a large number of analytes can be observed and recorded simultaneously at high powers of detection under one set of experimental parameters.

The conclusion can thus be drawn that the determination of rare earths occurring at trace and ultratrace concentrations in a wide variety of samples should be possible in conjunction with a conventional medium resolution spec-

trometer. Furthermore, the same determinations should be possible on a simultaneous multielement basis by employing a direct reading polychromator.

The application of an inductively coupled plasma system to the determination of rare earth impurities in a "pure" rare earth has not to our knowledge been reported. However, preliminary experiments in our laboratories indicate that trace rare earth spectral line intensities are essentially independent of the major constituent. Thus, a calibration curve for the determination of one rare earth in a matrix may well be valid for other rare earth matrices so long as spectral line interferences do not occur. Additional comments on these observations may be found in section 4.

2.2.5. *Dissolved sample detection limits*

Experimentally determined detection limits provide the analyst with realistic numerical data for comparing capabilities of several techniques for determining trace elements and for estimating the lowest concentrations determinable under specific circumstances. The analyst may draw these data from a variety of compilations (Fassel and Golightly, 1967; Slavin, 1968; Kniseley et al., 1970; Christian and Feldman, 1970 and 1971; and others cited earlier). Published comparisons may be viewed as reflecting the present "state of the art". A side-by-side comparison of flame emission spectroscopy (FES), atomic absorp-

TABLE 37D.3
Comparison of experimentally measured detection limits*

Element	FES	AAS	AFS	ICP
Ce	10	–	0.5	0.007
Dy	0.05	0.2	0.3	0.004
Er	0.04	0.1	0.5	0.001
Eu	0.0005	0.04	0.02	0.001
Gd	2	–	0.8	0.007
Ho	0.02	0.1	0.15	0.01
La	0.01[a]	2	–	0.003
Lu	1	3	3	0.008
Nd	0.7	2	2	0.05
Pr	0.07	4	1	0.06
Sc	0.03	0.1	–	0.003
Sm	0.2	0.6	0.15	0.02
Tb	0.03[a]	2	0.5	0.2
Tm	0.02	0.08	0.1	0.007
Y	0.03[a]	0.3	–	0.0002
Yb	0.002	0.02	0.01	0.0009

*Detection limits are defined as the concentrations (μg/ml) required to produce a signal level at least twice as great as the standard deviation of the total background noise fluctuations. [a]Band emission observed.

tion spectroscopy (AAS), atomic fluorescence spectroscopy (AFS) and the induction coupled plasma technique (ICP) is shown in table 37D.3. It is seen that FES detection limits are generally superior to those observed in AAS and AFS and that the ICP approach appears to be the excitation method of choice.

2.3. *Separation and preconcentration*

Separation and preconcentration procedures may be used to improve detection limits for the determination of rare elements in another rare earth. Ion exchange and chromatography separations have been used most often (Melamed et al., 1964; Zemskova et al., 1967; Shmanenkova et al., 1972; Herman, 1973). Extraction separations have also been employed by several authors (Zemskova et al., 1968; Eremin and Bondarenko, 1972; Vakulenko et al., 1973; Poluektov et al., 1975). In one paper, concentration factors of 15 were obtained for La, Pr and Nd in Ce by extracting the major constituent and analyzing the evaporated residues (Antonov et al., 1967).

3. Determination of other impurities in rare earths

3.1. *Arc and spark excitation*

The determination of non-rare earth impurities in rare earth matrices is complicated not only by the complex spectra of many of the rare earth elements but also by the very different volatilization rates of the impurities to be determined. Simple dc arc excitation methods are usually found to suffer from poor precision if a matrix element spectral line is used for internal standardization, because the impurity and matrix elements will likely be present in the arc column at different times, and will therefore experience different arc fluctuations. Four approaches have been used to improve precision. The first is to add reference elements to the sample with vaporization rates similar to the rates of the impurity elements to be determined.

Another method often employed is to minimize vaporization differences by using a spark-type of excitation which introduces the sample into the excitation zone by a sputtering process. At the Ames Laboratory, this second approach has been emphasized. Uniarc excitation, which is a combination of a spark and a unidirectional ac arc, has provided reliable analyses with adequate sensitivity for many impurities in most of the rare earth elements, and with a precision of better than $\pm 10\%$. A briquetted sample of one part rare earth oxide mixed with nine parts of pelleting graphite is used. The complex rare earth matrix spectra often causes spectral interference with the more sensitive spectral lines of impurity elements. For Pr and Nd, which have the most complex spectra, this problem is particularly serious, and alternate analytical approaches must be used if determinations at lower concentration levels are required.

Osumi, Kato and Miyake (1970) found the rotating disc electrode-spark

excitation-controlled atmosphere-methanol solution technique to be effective with both non-rare earth and rare earth impurities in neodymium. Apparently the complex neodymium spectrum was suppressed.

The two preceding techniques sought to avoid vaporization differences. The third approach to vaporization differences, the carrier distillation technique, makes use of these differences to improve detection limits and to suppress the complex matrix spectrum. Approximately 50 to 100 mg of sample oxide is blended with a "carrier" and loaded into a deeply cratered graphite electrode, which is then subjected to dc arc heating and excitation. The volatile impurities distill from the more refractory matrix, and are swept into the analytical gap by the carrier. Carriers which have been used with rare earth samples include Ga_2O_3 (Rozsa and Stone, 1962; Slyusareva et al., 1965; Pavlenko et al., 1967), Ga_2O_3 + AgF (Osumi et al., 1971a), Ga_2O_3 + LiF (Muntz, 1969), AgCl (Whitehead et al., 1966), AgCl + LiF (Joshi et al., 1971) and NaCl (Laktionova et al., 1975). Enhancement factors of 100 or more are obtained for those impurities which are more volatile then the matrix under the selected arcing conditions.

The separation of most non-rare earth impurities from a rare earth matrix is not particularly difficult, and this fourth method has been used to improve detection limits or to eliminate the complex rare earth spectrum (Slyusareva et al., 1965; Osumi et al., 1971d; Sato et al., 1971).

3.1.1. *Arc and spark detection limits*

Without prior separation of preconcentration steps, the detection limits shows in Table 37D.4 have been reported for non-rare earth impurities in various rare earth oxides when arc or spark excitation is used.

3.2. *Combustion flame and plasma atomization*

There are numerous reports of the determination of assorted non-rare earth elements in various materials using FES and AAS, and the general approaches do not differ from those commonly employed when the matrix material is a rare earth. The principal problems are to select an appropriate nebulization and excitation system and to find sensitive, interference-free analytical spectral lines.

TABLE 37D.4
Detection limits for determination of non-rare earths in rare earths

Detection limits	
1 ppm or less	Ag, Al, As, B, Ba, Bi, Ca, Cd, Co, Cr, Cu, Fe, K, Li, Mg, Mn, Na, Ni, Pb, Si, Sn, Ti, V, Zn
2 to 10 ppm	Be, Ge, Mo, Sb, Zr
11 to 100 ppm	Hf, Nb, Sr, Ta, Th, W

When detectabilities are inadequate, separation procedures become necessary. Because each situation is likely to be unique, the analyst must develop an approach to solve the particular analytical problem at hand.

4. Analysis of rare earth mixtures

4.1. *Arc and spark excitation*

This type of analysis is similar to the determination of impurities in a "pure" rare earth, except that no single rare earth element of known concentration is present in the sample to serve as the reference element for internal standardization. The most common approach to this problem is to add to the sample an excess of some element which can be independently determined and is chemically similar to the rare earths to be determined. Fassel (1949) used CeO_2, because its concentration in the sample can be measured through oxidation–reduction reactions. The problem of analyzing a mixture of rare earths thus becomes one of determining rare earths in a CeO_2 matrix. The primary disadvantage of this approach is that detection limits are raised by the dilution factor. Determinations in the range from about 1 to 90% can be readily accomplished. Other rare earth elements can also be used as the diluent. White et al. (1959) and Fadeeva et al. (1969) used La, and both Butler (1957) and Melamed et al. (1960) recommended Y as the diluent for their particular analytical problems.

4.2. *Flame excitation*

The discussions of various flame analysis techniques in section 2.2 are equally applicable to the determination of rare earth elements in a complex mixture of these elements. Net intensity or absorbance measurements usually provide adequate precision, so that an added reference element is not needed. In addition, there is no evidence of inter-element effects, and line interferences, even in small monochromators, are rarely a serious problem. This contrasts sharply with the selective enhancement and absorption effects observed in X-ray fluorescent spectrometric measurements. Analyses of rare earth mixtures by AAS have been described by Jaworowsk et al. (1967), Kriege and Welcher (1968) and many others.

D'Silva et al. (1964a) have reported a method for the analysis of complex mixtures using a fuel-rich, oxyacetylene flame from a Beckman-type burner. They obtained relative standard deviations which ranged from ± 1.3 to 3.7% of the amount present. This method was later adapted to use with the premixed, oxyacetylene flame. The lines which were most satisfactory with the premixed burner together with their useful analytical range are shown in table 37D.5. These lines were selected for minimal spectral interference, especially from neighboring atomic number rare earths, and thus are not necessarily the most sensitive. For the analysis of some mixtures, where fewer spectral interferences

TABLE 37D.5.
Analytical lines for flame emission analysis of complex rare earth mixtures.

Element	Wavelength (Å)	Range of analytical curve (wt. %)
Ce	5223.49	3–100
Dy	4589.37	0.2–100
Er	4007.97	0.1–100
Eu	4594.03	0.1–100
Gd	4346.46	0.5–100
	4346.62	
Ho	4163.03	0.1–100
La	5930.68	0.5–100
	5930.62	
Lu	3312.11	0.2–100
	4518.57	0.2–100
Nd	4866.74	0.5–100
Pr	5018.58	2–100
Sc	3269.91	1–100
Sm	4470.89	0.5–100
Tb	4493.08	2–100
Tm	3887.35	0.2–100
Y	4643.70	2–100
Yb	3987.98	0.01–100
	5556.48	1–100

exist, more sensitive lines may be used with a corresponding improvement in powers of detection.

A typical analytical curve is shown in fig. 37D.5. The concentration axis on the curve is expressed in terms of the percentage of the element in the original sample. Often the analytical curves can be extended to lower concentration levels. A typical example is shown in fig. 37D.6. The matrix composition in each of the standards used to prepare this analytical curve was changed. All of the experimental points cluster rather uniformly along a single congruent curve, with no apparent systematic deviations for any of the matrices. This behavior documents the high degree of freedom of this technique from both spectral and interelement interferences.

4.3. *Induction coupled plasma excitation*

Freedom from interelement effects is also a characteristic of ICP excitation, so that an analytical calibration for the determination of a rare earth will usually be valid for any complex mixture of rare earths if there is no spectral line interference. Two examples of this freedom can be seen in figs. 37D.7 and 37D.8, which show analytical calibration curves for the determination of Y in complex

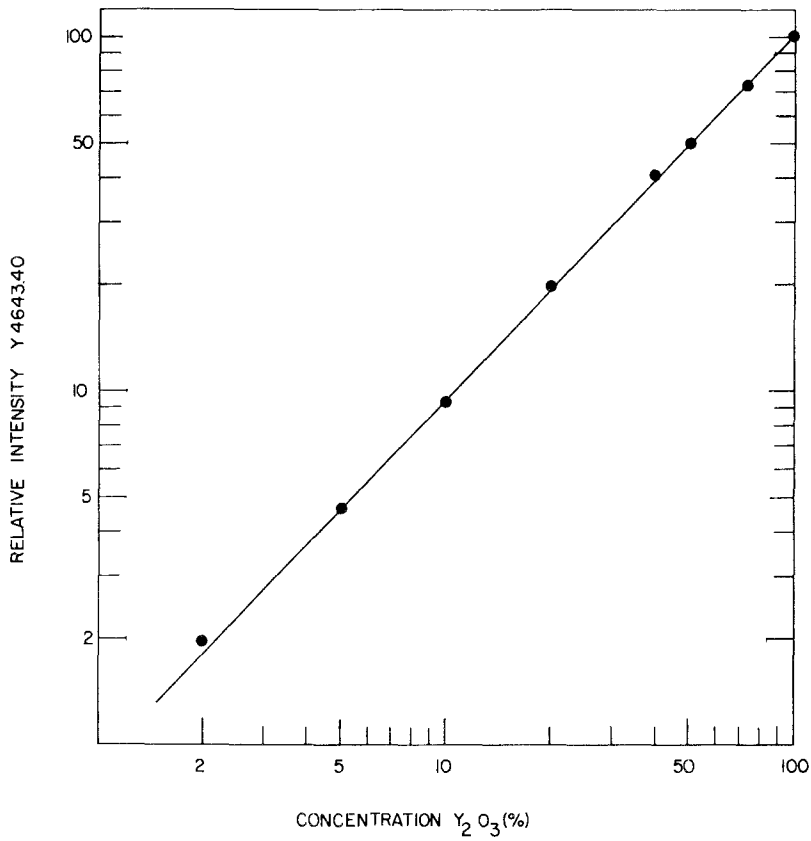

Fig. 37D.5. Analytical curve for the FES determination of yttrium in rare earth mixtures.

mixtures of Y, Gd, Tb, and Dy, and for La in mixtures of La, Pr, Nd, and Sm.

Induction coupled plasma excitation sources have the additional important advantage of linear analytical calibration curves that cover 4 and 5 orders of magnitude change in concentration. Self-absorption, which is one of the common causes of non-linear response to concentration in arc, spark and combustion flame sources, is rarely manifested. Figure 37D.9 illustrates both the extended concentration ranges that can be covered and freedom from interelement effects of analytical calibration curves for the determination of Tm and Yb in mixtures of Tm, Yb, and Lu. The Yb curve is found to be linear from the trace concentration of 50 ppm, through the minor and major concentration ranges, to the full 100% value. In these studies by C.C. Butler at our laboratory, the sample concentration in the nebulized solution was 0.1% in very dilute HNO_3. A spectrometer of 1.0 m focal length provided a reciprocal linear dispersion of 8.4 A/mm.

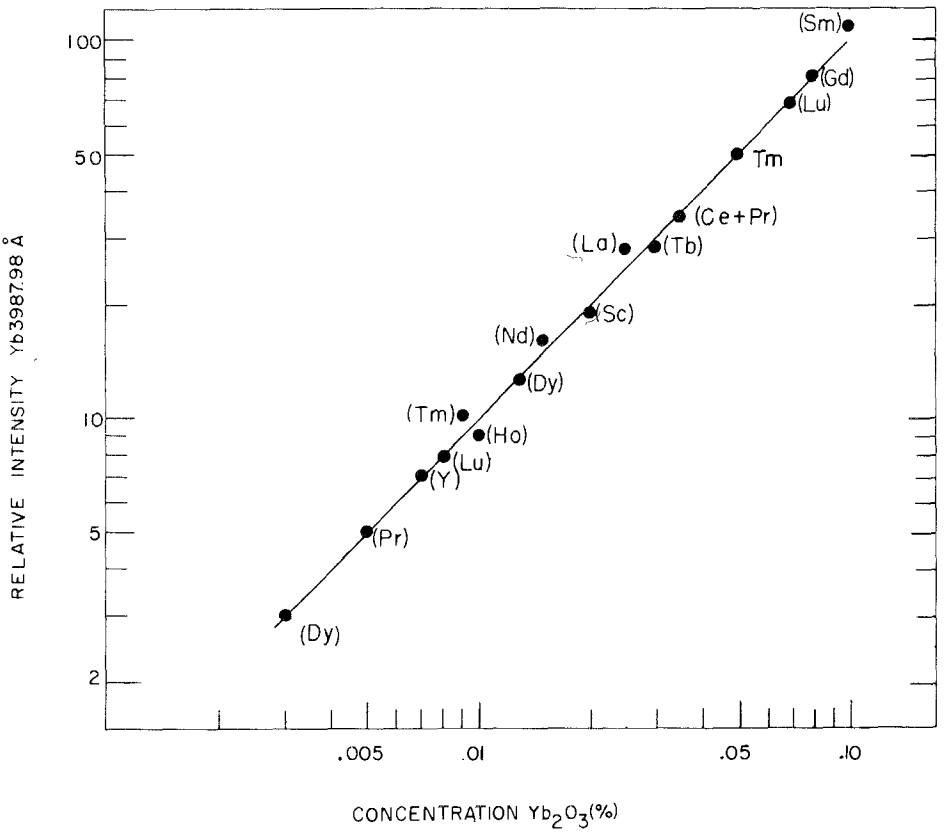

Fig. 37D.6. Analytical curve for the FES determination of low concentrations of ytterbium in rare earth mixtures.

5. Determination of rare earth elements in other materials

A thorough review of the various approaches to such analyses by emission spectroscopy is beyond the scope of this chapter, but some of the basic procedures can be mentioned. Although direct excitation of the sample will provide sufficient detectability, precision and accuracy for some samples, separation of the rare earths as a group ordinarily precedes the analysis. Separation not only allows for preconcentration of the rare earths so that lower detection limits are possible, but also simplifies the analytical problem when geological samples of widely varying composition are encountered. Nearly every type of separation of rare earths from a matrix can be found in the literature. Ion exchange and extraction procedures seem to be most popular, with precipitation steps suggested almost as often (Ooghe and Verbeek, 1974; Kalmykova et al., 1974; Folsom et al., 1974; Dolgorev and Lysak, 1975; Agrawal and Kapoor, 1976; Sen Gupta, 1976).

Regardless of the type of separation, one of the most fruitful refinements is to

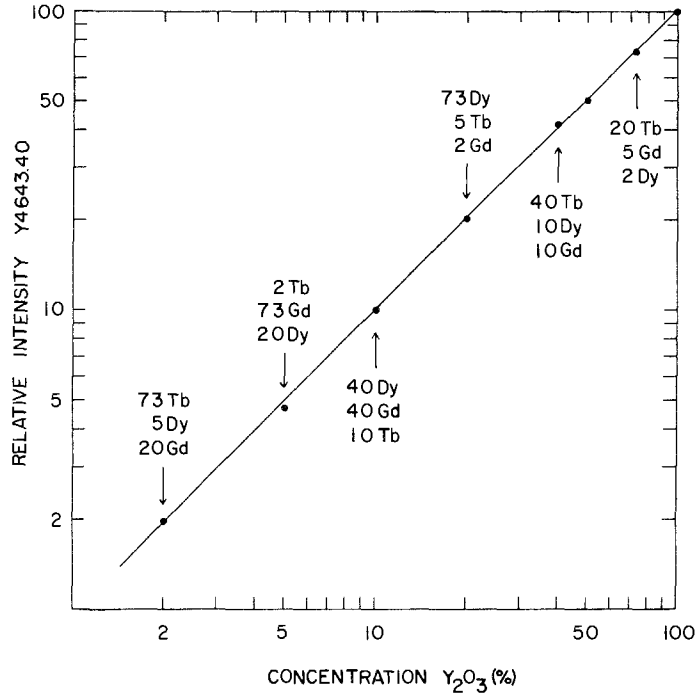

Fig. 37D.7. Analytical curve for the ICP determination of yttrium in rare earth mixtures.

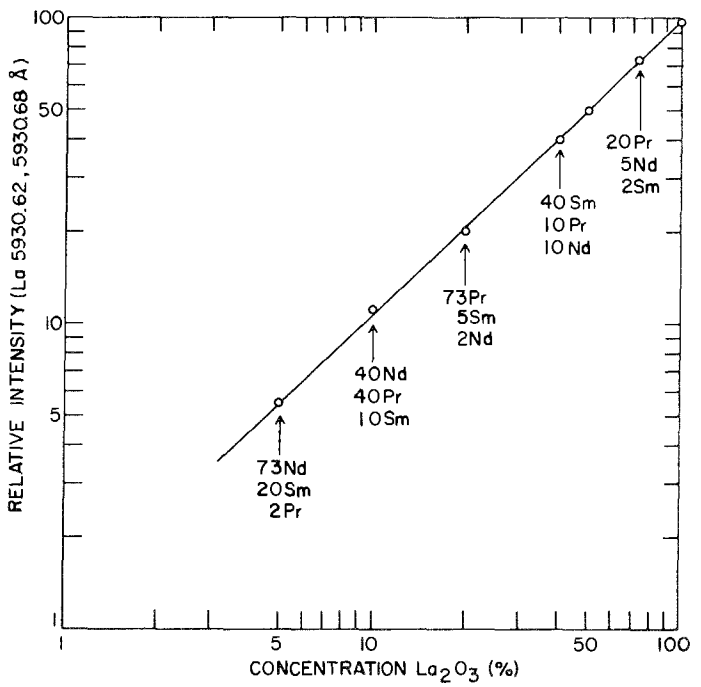

Fig. 37D.8. Analytical curve for the ICP determination of lanthanium in rare earth mixtures.

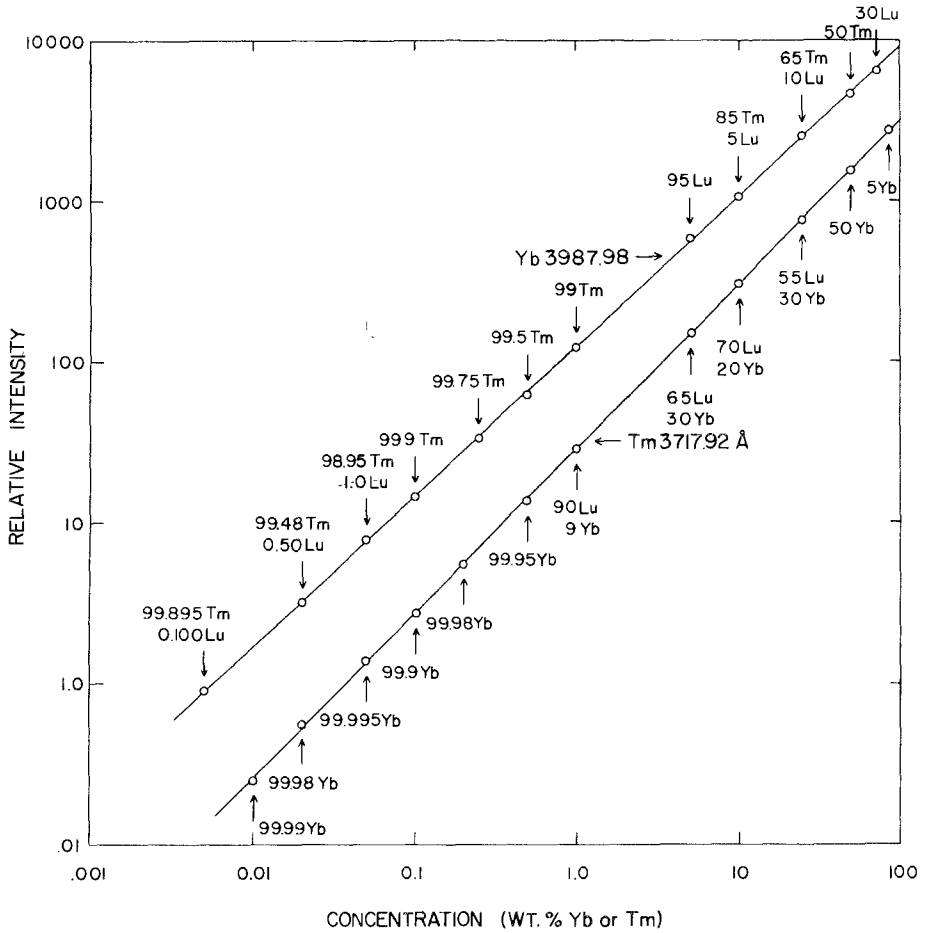

Fig. 37D.9. Analytical curves for the ICP determination of ytterbium and thulium in rare earth mixtures.

concentrate the rare earth elements with the aid of a carrier. Yttrium is frequently used as the carrier for a number of reasons (Hettel and Fassel, 1955). The ionic radius of Y^{3+} is about the same as for Tb^{3+} and Dy^{3+}, so that its chemical properties closely resemble those of the lanthanides. The emission spectrum of Y is relatively simple, hence line interferences rarely arise from the carrier.

In addition, any separation scheme devised can be monitored by a radioactive tracer, ^{90}Y, which is a β emitter and is easily obtained from ^{90}Sr.

Other carriers have also been suggested. Laktionova et al. (1974) used a combination of Y_2O_3 and CaO. Lanthanum was suggested by Zaidel et al. (1958), but is somewhat less desirable than yttria because La_2O_3 is hygroscopic. Non-rare earths such as Ca and Al (Waring and Mela, 1953) have also been used as carriers, particularly with precipitation separations.

After separation of the rare earths as a group, the spectral analysis can be accomplished with the techniques described in sections 2 and 4.

6. X-ray fluorescence spectrometry

One of the more rapidly developing rare earth analytical techniques is based on intensity measurement of the fluorescent X-rays emitted when a sample is irradiated with sufficiently energetic X-rays. This technique has been used for the determination of rare earths in rocks, minerals, rare earth concentrates, complex rare earth mixtures, essentially pure rare earths, and in other diverse materials such as steels and nuclear reactor fuel. Some advantages of X-ray spectrometry include minimal sample preparation and spectra that are much less complex than their optical counterparts.

6.1. *Spectral characteristics*

The X-ray spectra of the rare earths are similar to those of all other elements. The spectra consist of only a few lines and absorption edges that result from electronic transitions among the inner-most shells of the atom. Increases in atomic number cause a simple shift of the X-ray spectrum to higher energies or to lower wavelengths. Consequently, the X-ray spectrum is unique and characteristic for each element. With exciting radiation obtainable from commercially available 50- or 60-kilovolt X-ray tubes, the L series spectra of the lanthanides are readily excited. To excite the K spectra with adequate intensity, 100-kilovolt power supplies are required. Lines from the K series are used for the determination of Sc and Y. For lanthanide analyses, nearly all analysts recommend lines in the L series.

Despite the relatively simple X-ray spectrum, line interferences still occur, especially for elements which differ in atomic number by only a few units, as is the case for a sequence of lanthanides. These interferences can be overcome by either of two methods. For specific pure rare earths or for simple mixtures, it is likely that lines free of interference can be selected. The choice of analytical wavelengths thus depends somewhat on the composition of the matrix (Bonnevie-Svendsen and Follo, 1973; Lytle and Heady, 1959; Chandola et al., 1975).

Alternately, a single analysis line can be chosen for each of the rare earths, and experimentally determined correction factors applied where appropriate to compensate for the interferences (Rose and Cuttitta, 1968). Eby (1972) used a computer to calculate the corrected X-ray intensities.

6.2. *Absorption and enhancement effects*

Accurate analyses of rare earth mixtures are possible only if other experimental difficulties are overcome. These difficulties have their origin in the overlap of absorption edges with the fluorescent spectral lines.

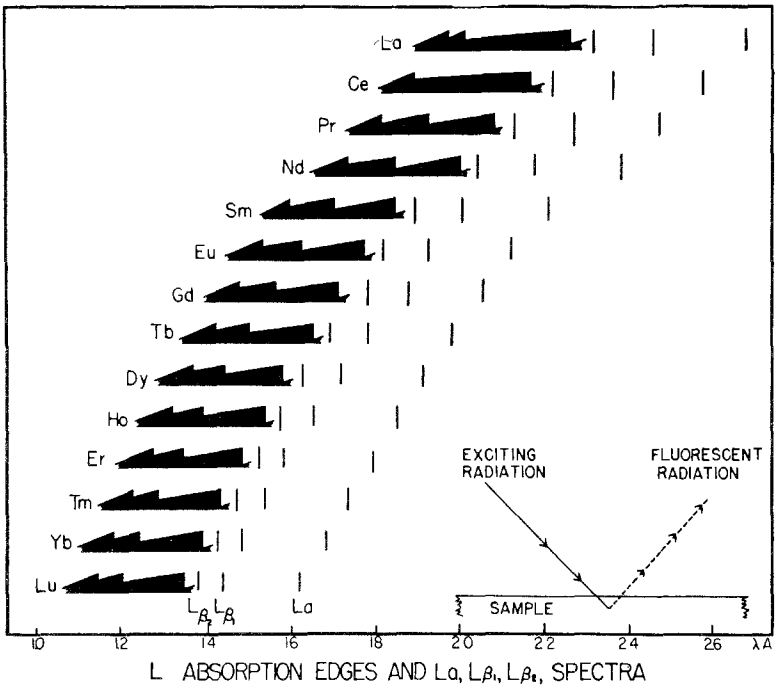

Fig. 37D.10. L absorption edges and $L_{\alpha 1}$, $L_{\beta 1}$, $L_{\beta 2}$ spectra of the lanthanides.

The very simplified diagram shown in fig. 37D.10 can serve to illustrate the nature of these problems. The sawtooth edges on the left-hand side of the figure represent absorption spectra of the individual lanthanides in the L region. Each edge represents the wavelength of exciting radiation required to eject an L electron from one of the 3L subshells to give rise to the L fluorescent lines. The strongest three lines of the L series are shown to the right (at higher wavelengths) of the absorption edges. Each rare earth also absorbs radiation at wavelengths higher and lower than the region of the absorption edges, corresponding to ejection of electrons from M and K shells, respectively.

Referring to the simplified model of fluorescent excitation and emission in the lower right hand corner of fig. 37D.10, it is seen that the incident exciting radiation will, of course, excite fluorescent emission of atoms at the surface of the specimen. But there is also a finite penetration of exciting radiation into the specimen. That part of the incident radiation which penetrates into the deeper layers may have its intensity distribution altered by absorption edge attentuation, particularly in the wavelength region most effective in exciting fluorescent radiation. Thus, the effectiveness of the incident radiation in exciting the fluorescent radiation of the subsurface layers of atoms may be impaired.

Aside from the selective absorption of incident radiation, there is a second type of interelement effect. This arises from the absorption of fluorescent radiation excited beneath the surface layer of the atoms. Thus, the L_{β_2} line of

thulium (1.463 Å) is selectively adsorbed by the L_{III} erbium absorption edge (1.482 Å) if erbium is present in the sample, and the L_{β_1} line of thulium (1.530 Å) is selectively absorbed by the $Ho_{L_{III}}$ edge at 1.535 Å.

A third type of interaction is extant but this differs from those discussed above in the sense that line intensities can be selectively enhanced by the presence of certain other elements in the sample. Thus, if holmium is present in a sample in which terbium is being determined, the $Ho_{L_{\beta_2}}$ line (1.619 Å) emitted in the deeper layer of atoms is readily absorbed by the $Tb_{L_{III}}$ edge (1.648 Å) causing enhancement of the Tb_L line intensity.

Several methods of dealing with absorption and enhancement effects are commonly employed in X-ray spectrometry. One approach is the preparation of standard samples with major constituent concentrations similar to those of the samples to be analyzed (Lytle et al., 1957). When mixtures consisting of a wide range of concentrations are encountered, it is necessary to prepare a large number of standard mixtures of known concentration. The closer these standard mixtures approximate the actual constitution of the sample, the better the analysis will be. Although the preparation of these standard mixtures is often tedious, time consuming, and expensive, this technique may in certain instances still be the most advantageous for analysis of some types of rare earth mixtures.

A second technique described by Bonnevie-Svendsen and Follo (1973) is the method of additions, in which known amounts of those elements to be measured are added to portions of the sample prior to the analysis. A graphic method is used to determine the residual concentrations in the original sample. This technique is useful only for the analysis of minor and trace constituents of a sample.

Absorption-enhancement effects can be minimized by preparing the samples as thin specimens. For instance, Bonnevie-Svendsen and Follo (1973) and Rose and Cuttitta (1968) deposited dissolved samples on filter paper discs or on cellulose fibers. Eby (1972) and Walton (1971) used an ion exchange paper to absorb the rare earths from solution. Each of these procedures produced a thin specimen for which absorption-enhancement effects were negligible.

A fourth method involves the dilution of the sample into a matrix so that the major constituents are the same for both standards and samples. Fusion fluxes often used for this purpose include borax, boric acid, lithium tetraborate and sodium tetraborate (Plowman, 1971; Matsumura et al., 1973; Chandola and Mohile, 1976). Dilution into a dry powder mixture is also effective. Lytle and Heady (1959) recommended $LiCO_3$ as a suitable diluent. For both the thin sample and the dilution techniques, detectability is sacrificed for improved accuracy. Consequently, these methods are mainly applied to rare earth determinations at the major and minor constituent levels.

Finally, compensation for absorption and enhancement effects can be achieved through the use of correction coefficients. The coefficients may be obtained experimentally from an extensive series of standard samples, or they may be derived from fundamental constants (Bertin, 1975). Tertian (1969) has developed a novel correction procedure which requires the analysis of each

sample at two different dilutions, followed by a relatively simple mathematical treatment to arrive at accurate concentration values. A small computer is almost a necessity when correction factors are used to compensate for absorption and enhancement effects.

Analysis of binary mixtures is not encumbered with the difficulties outlined above and it is a simple task to relate the intensity ratios of the selected lines to concentration ratios. A typical example is illustrated in fig. 37D.11.

When rare earths are determined as impurities in other highly purified rare earths, the interelement effects discussed above are generally not significant. For these determinations, the primary limitation encountered is spectral intensity. Since it is generally necessary to determine the neighboring atomic number elements in the pure matrix, adequate resolution must be achieved to resolve adjacent lines, at some loss in spectral intensity.

6.3. *X-ray fluorescence detectabilities*

In X-ray spectroscopy, detectabilities are a direct square-root function of analysis time. Some indication of lower analysis limits can be mentioned,

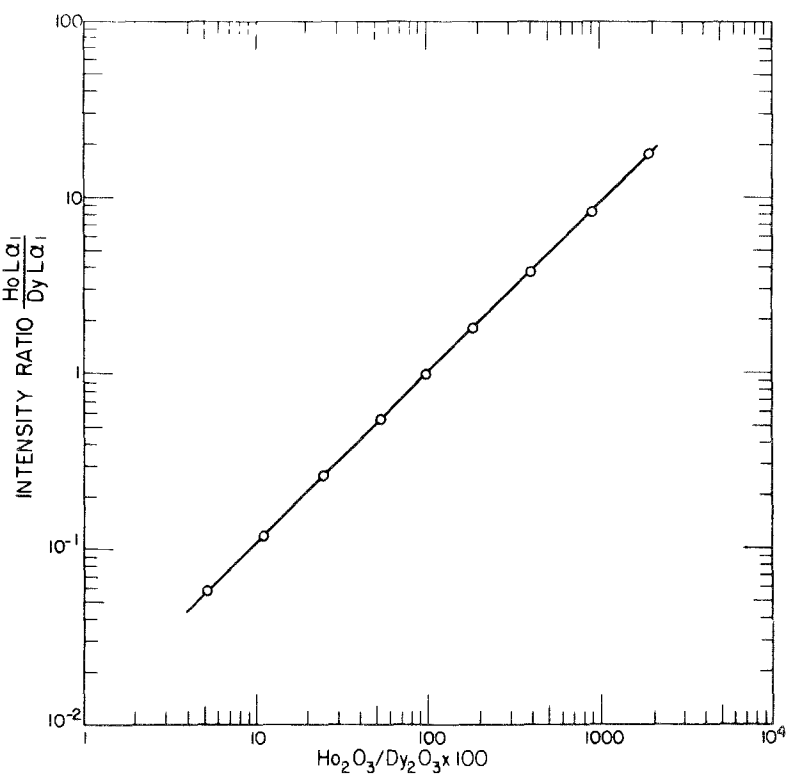

Fig. 37D.11. Analytical curve for the X-ray fluorescence determination of holmium in a holmium-dysprosium mixture.

however. Chandola et al. (1975) reported detection limits of 50 ppm for Y and 100 ppm for Sm, Eu, Gd, Dy and Ho in a Tb_4O_7 matrix at counting times of 100 seconds or less. Dixit and Deshpande (1975) found detection limits of 100 ppm for Yb and 50 ppm for Eu, Gd, Tb, Dy, Ho and Er in an Y_2O_3 matrix for a counting time of 100 sec.

Appendix

A general procedure for the DC carbon arc determination of trace rare earth impurities in highly purified rare earth materials

The following analytical procedures have been used in the Ames Laboratory during the past 30 years (Fassel and Wilhelm, 1948; Fassel et al., 1952 and 1955; Kniseley et al., 1958 and 1959b). The procedures and analytical calibrations were designed for the analysis of rare earth oxides, or for metals or compounds that can be converted to the oxide. The calibrations apply particularly to rare earths that are at least 98% pure, with none of the individual impurities exceeding one percent.

The choice of analytical lines and calibrations was dictated primarily by the requirements for quality control of purified rare earth elements. The line pairs selected covered the determination of the two rare earths of lesser and of greater atomic number than the matrix element. Because yttrium normally falls between different pairs of rare earths depending upon specific separation procedures used, calibrations were also established for the determination of yttrium in each of the lanthanide elements. In addition, line pairs were also selected for the determination of all other naturally occurring rare earths in yttrium because this element is often used as a carrier for other rare earths.

The selected line pairs are summarized in table 37D.7. The analyte lines differ from many of those previously suggested. This is not surprising because many of the earlier selected analysis lines represented a compromise between maximal power of detection and minimal spectral interference from other impurities in less pure samples. As purer base materials and better spectral data became available during the intervening years, continuing critical re-examinations of the earlier suggestions frequently led to a different choice of analysis line.

Summary of the methods

Samples and standards, in the form of the ignited oxide powder, are mixed with graphite powder which acts as a spectroscopic buffer, and prevents the formation of molten globules which tend to be ejected from the electrode cup. This mixture is loaded into an undercut graphite cup electrode. Direct-current arc excitation is employed, and the spectra of samples and standards are recorded on suitable photographic plates. Intensity ratios of selected line pairs are determined photometrically. The concentration of the element sought is read from an analytical curve that relates the logarithm of the concentration to the

TABLE 37D.6.
Exposure conditions.

Sample: A blend of equal amounts of dried oxide and graphite powder.
Lower electrode: The anode, a cupped, undercut graphite electrode [ASTM (1968) shape S-4] which is loaded with a suitable amount of the sample so that the exposure index is obtained.
Upper electrode: The cathode, a 3 mm graphite rod [ASTM (1968) shape C-6].
Analytical gap: Maintained at 4 mm throughout the exposure. The entire arc column is focused onto the spectrograph slit, except that the electrode tips are screened out.
Excitation: 15 ampere dc arc.
Spectral region: 2900 to 4700 Å.
Slit width: 0.040 mm.
Slit length: 12 mm.
Preburn period: None.
Exposure period: Complete consumption of charge.
Filter: Corning 0-53, 0-54, or equivalents.
Intensity attenuation: Rotating step sector with step factors of 1.58, dividing the slit length into 8 portions.
Photographic emulsions: Eastman "SA 1" plates for the spectral region below 3800 Å, and Eastman "Kodak M" plates for the spectral region above 3800 Å, or their equivalents.
Exposure index: Maintain transmittance of the following matrix spectral lines, in the unattenuated portion of the exposure, at approximately the listed percentages.

Y	3272.16	20%	Tb	4278.00	10%
La	4229.32	35%	Dy	3351.75	10%
Ce	4302.14	25%	Ho	3367.20	5%
Pr	3338.38	35%	Er	3907.84	10%
Nd	4419.52	15%	Tm	3265.30	40%
Sm	4300.19	10%	Yb	3442.36	30%
Eu	3664.96	30%	Lu	3264.94	20%
Gd	4108.91	20%			

Photometry: The relative transmittance of the various analytical and standard line pairs as shown in table B are measured with a microphotometer. Background corrections are made where necessary.

logarithm of the intensity ratio.

The spectrograph must have sufficient resolving power and linear dispersion to resolve the analytical lines from adjacent lines in the spectrum. A large grating instrument having a reciprocal linear dispersion of about 2.5 Å per mm was found to be satisfactory. The exposure conditions are outlined in table 37D.6. Table 37D.7 lists the selected line pairs, their concentration ranges, and other photometric parameters.

A controlled atmosphere device is necessary for the determination of Ce in Nd, and may be helpful in lowering detection limits for other determinations restricted by CN interferences. A modified sheathed arc discharge device (Stallwood, 1954) was used to provide an annular curtain of 70% Ar–30% O_2 mixture which was blown upwards around the arc column at a rate of 9 liters per minute.

TABLE 37D.7
Spectral line pairs

Matrix	Analysis line (Å)†	Matrix line (Å)†	Estimated visual detection limit (ppm)*	Concentration range (ppm)	Concentration index (ppm)	Background correction	Remarks
Y_2O_3	Sc 3353.73	Y 3337.84	2	2–1 000	850	Yes	CN interference may limit detection
	La 3949.10	Y 3918.25	20	20–2 000	800	Yes	CN group on lower edge of La limits detection
	Ce 4012.39	Y 3997.43	200	200–10 000	5600	Yes	CN interference limits detection
	Pr 4225.33	Y 4223.64[a]	100	100– 5 000	1000	Yes	CN interference limits detection
	Nd 4303.57	Y 4322.28	100	100–10 000	1700	No	A Pr line may interfere
	Sm 3670.82	Y 3675.47[a]	200	200–10 000	2500	No	CN interference may make determinations difficult at low concentration
	Eu 3971.99	Y 3997.43[b]	10	10– 5 000	250	Yes	
	Gd 3422.47	Y 3409.77[a]	30	100–10 000	800	No	
	Tb 3293.07	Y 3272.16[b]	200	500–10 000	1100	No	
	Dy 3407.80	Y 3409.77[a]	100	100–10 000	1000	No	CN interference limits detection
	Ho 3398.98	Y 3409.77[a]	60	100–10 000	1100	No	CN interference limits detection
	Er 3372.75	Y 3380.11[b]	50	100–10 000	800	No	CN interference limits detection
	Tm 3258.04	Y 3272.16[b]	10	10– 5 000	650	Yes	
	Yb 3289.37	Y 3280.91[b]	10	100–10 000	1300	No	
	Lu 3281.74	Y 3272.16[b]	20	20– 5 000	500	Yes	
La_2O_3	Y 3242.28	La 3267.31	20	20– 1 000	150	No	
	Ce 4222.60	La 4229.32[a]	350	350– 5 000	1200	Yes, Below 1200 ppm	
	Pr 4225.33	La 4229.32[a]	150	180– 5 000	600	Yes, Below 600 ppm	
	Nd 4303.57	La 4304.12	100	100– 5 000	550	No	Pr interference if Pr is > 1000 ppm
	Nd 4247.37	La 4229.32[a]	200	200– 5 000	1000		
CeO_2	Y 4374.94	Ce 4376.88	10	10– 1 000	360	Yes	Dy, Nd and Sm may interfere with Y

	Y	3242.28	Ce	3243.95	25	25– 1 000	90	No	Strong Ce line interferes with Y at low concentrations
	La	4333.73	Ce	4330.94	20	20– 5 000	650	Yes	
	Pr	4225.33	Ce	4223.15	100	100– 5 000	1700	Yes	Ce interferes making detection of low concentrations difficult
	Nd	4303.57	Ce	4302.14[a]	100	100–10 000	900	Yes	A Pr line may interfere
	Sm	3634.27	Ce	3634.43	70	100–10 000	1000	Yes	
Pr_6O_{11}	Y	4374.94	Pr	4376.26[a]	20	10– 200	60	Yes	Dy, Nd and Sm may interfere with Y
	Y	4374.94	Pr	4388.73	20	100– 1 000	200	No	Dy, Nd and Sm may interfere with Y
	La	3337.49	Pr	3338.38[a]	20	20– 5 000	200	Yes	There is a slight Pr interference
	Ce	4460.21	Pr	4462.63	100	200–10 000	4000	Yes	A Pr line at lower λ interferes with Ce
	Nd	3920.96	Pr	3921.20[a]	1200	1200–10 000	3500	Yes	There is a CN interference which limits detection
	Sm	4467.34	Pr	4462.63	70	100–10 000	1500	Yes, Below 2000 ppm	Slight Pr interference limits detection
Nd_2O_3	Y	3633.12	Nd	3632.70[a]	100	100– 2 000	400	Yes	
	Ce	4562.36	Nd	4562.59[a]	200	500–10 000	660	Yes	Controlled atmosphere used. Weak Nd interference restricts detection limit
	Pr	4408.84	Nd	4419.52[a]	500	500–10 000	4500	Yes	
	Sm	4433.88	Nd	4436.67[a]	100	100–10 000	4500	Yes	
	Eu	4661.88	Nd	4664.01	50	50– 5 000	200	Yes	
Sm_2O_3	Y	3242.28	Sm	3242.48	50	50– 5 000	1000	Yes, Below 1000 ppm	Sm interference restricts detection limit
	Pr	3908.43	Sm	3914.08	100	100–10 000	4000	Yes	Sm interference restricts detection limit
	Nd	4303.57	Sm	4300.19[a]	100	100–10 000	2000	No	Sm and Pr interference
	Eu	4129.74	Sm	4139.65	150	150– 5 000	450	No	CN band restricts detection limit
	Gd	3439.99	Sm	3450.01[a]	200	200– 5 000	1600	Yes	
Eu_2O_3	Y	4102.38	Eu	4111.07	10	50– 5 000	400	Yes, Below 250 ppm	
	Nd	4012.25	Eu	4010.18	40	80– 1 000	750	Yes	
	Sm	3661.35	Eu	3657.61	30	30– 1 000	400	Yes	

TABLE 37D.7. Contd.

Matrix	Analysis line (Å)†	Matrix line (Å)†	Estimated visual detection limit (ppm)*	Concentration range (ppm)	Concentration index (ppm)	Background correction	Remarks
	Sm 4424.34	Eu 4426.42	200	200– 5 000	1000	No	
	Gd 3422.47	Eu 3417.42	100	100– 500	500	Yes	Weak Eu interference under Gd line
	Gd 3422.47	Eu 3421.20[a]	100	200– 5 000	750	No	
	Tb 3676.35	Eu 3664.96[a]	50	100– 1 000	450	Yes	
	Tb 3324.40	Eu 3324.20[a]	50	150– 5 000	900	Yes	
	Yb 3694.20	Eu 3697.38[a]	1	3– 13	10	Yes	
	Yb 3694.20	Eu 3696.90[a]	1	10– 100	25	No	
	Yb 3031.11	Eu 3030.83[a]	–	70– 300	120	Yes	
	Yb 3031.11	Eu 3018.01[a]	–	150– 5 000	800	No	
Gd_2O_3	Y 4102.38	Gd 4108.91[a]	100	100– 5 000	400	Yes	
	Nd 4012.25	Gd 3991.70	100	100–10 000	5000	No	
	Sm 3634.27	Gd 3643.53[a]	100	100– 5 000	900	Yes	
	Eu 4129.74	Gd 4113.89[a]	200	200– 5 000	500	No	CN band restricts detection limit
	Tb 3676.35	Gd 3679.49	100	100–10 000	1700	Yes, Below 1700 ppm	CN band restricts detection limit
	Dy 4000.45	Gd 3979.74	50	50– 5 000	750	Yes	
	Ho 3453.13	Gd 3404.15[a]	50	50– 5 000	300	Yes	Dy interference restricts Ho detection limit. Pr and Tb may also interfere
Tb_4O_7	Y 3242.28	Tb 3241.33[b]	100	100– 5 000	750	No	Tb interference restricts Y detection limit
	Sm 4279.68	Tb 4278.00[a]	200	500–10 000	3000	No	
	Eu 3930.48	Tb 3937.15	20	20–10 000	500	Yes	Slight CN interference restricts Eu detection limit
	Gd 3358.62	Tb 3355.45[a]	200	200–10 000	1000	No	Tb interference restricts Gd detection limit
	Dy 4000.48	Tb 3985.45	100	100–10 000	3000	No	Tb and CN interference restricts Dy detection limit
	Ho 3474.26	Tb 3464.15[a]	100	200–10 000	2500	No	CN interference. Visual estimation of concentration only

Dy_2O_3	Y	3600.73	Dy	3611.90	10	50– 5 000	550	No	High concentration of Pr may interfere with the Y line
	Gd	3350.47	Dy	3351.75[b]	200	200–10 000	1000	No	Dy interference restricts Gd detection limit. Ho concentration >.1% will interfere with the Gd line
	Tb	3324.40	Dy	3351.75[b]	500	1000–10 000	2500	No	Dy interference restricts Tb detection limit
	Ho	3456.00	Dy	3443.46	100	200–10 000	2000	No	A Dy line interferes, but can be distinguished from the broadened Ho line
	Er	3692.64	Dy	3680.54[b]	50	100–10 000	1200	No	Dy interference restricts Er detection limit
Ho_2O_3	Y	4374.94	Ho	4379.15	10	200–10 000	2000	No	Dy, Nd and Sm may interfere with Y
	Y	3982.60	Ho	3975.88	100	200–10 000	2000	No	
	Tb	3703.92	Ho	3703.42[a]	60	60– 5 000	900	Yes	
	Dy	3645.42	Ho	3647.39[b]	50	150–10 000	1000	Yes, Below 1000 ppm	La and Sc may interfere if present
	Er	4007.97	Ho	3975.88	500	500–10 000	9000	No	
	Tm	3362.61	Ho	3367.20[a]	200	200–10 000	400	No	
	Yb	3694.20	Ho	3681.53[a]	60	60– 2 000	300	No	Er may interfere at concentration of 1% or more
Er_2O_3	Y	4374.94	Er	4378.34	10	100–10 000	1000	No	Dy, Nd and Sm may interfere with Y
	Y	3242.28	Er	3222.33[b]	10	50–10 000	300	No	
	Dy	3898.54	Er	3907.84[a]	100	100–10 000	3000	Yes	
	Ho	3456.00	Er	3436.95[b]	50	100– 5 000	1500	No	Er interference restricts Ho detection limit
	Tm	3362.62	Er	3328.30[b]	10	100–10 000	1500	No	
	Yb	3987.98	Er	3989.40[b]	50	50– 5 000	800	No	Eu, Gd, Pr, Th may interfere with the Yb line; CN interference restricts Yb detection limit
	Yb	2970.56	Er	2986.73[b]	100	200– 5 000	2000	No	Fe, Sm, Ti may interfere with the Yb line
Tm_2O_3	Y	4374.94	Tm	4367.91[b]	10	200–10 000	1300	No	Dy, Nd and Sm may interfere with Y

TABLE 37D.7. Contd.

Matrix	Analysis line (Å)†	Matrix line (Å)†	Estimated visual detection limit (ppm)*	Concentration range (ppm)	Concentration index (ppm)	Background correction	Remarks
	Ho 3456.00	Tm 3454.30[a]	200	200–10 000	3000	No	A strong Dy line is close to Tm which may interfere with analysis – use Ho 4053 as alternate
	Er 3264.78	Tm 3265.30[a]	35	50– 1 000	200	No	
	Er 3264.78	Tm 3264.48[a]	35	200–10 000	1000	No	
	Yb 3289.37	Tm 3289.66[a]	5	10– 500	90	No	
	Yb 3289.37	Tm 3284.62[a]	5	200– 5 000	600	No	
	Lu 3472.48	Tm 3459.06[b]	200	200–10 000	2500	No	A Tm line interferes with Lu preventing determinations below 200 ppm
Yb_2O_3	Sc 4246.83	Yb 4247.89	2	2– 500	45	No	
	Sc 4246.83	Yb 4277.73	2	100–10 000	550	No	
	Y 3242.28	Yb 3242.98[a]	2	5– 1 000	70	No	
	Y 3242.28	Yb 3246.06	2	100–10 000	1000	No	Fe at concentration >0.5% may interfere with the Yb line

	Er 3312.42	Yb 3328.51[b]	See Remarks	100–10 000	1000	No	An Yb line interferes at < 100 ppm. Er 3616.57 has a detection limit of ≈ 50 ppm
	Tm 3441.50	Yb 3442.36[b]	20	20– 1 000	120	Yes, Below 200 ppm	Dy interferes with the Tm line
	Tm 3441.50	Yb 3436.46	20	100–10 000	1800	No	Dy interferes with the Tm line
	Tm 3258.05	Yb 3267.89	50	100–10 000	1500	No	
	Lu 3312.11	Yb 3328.51[b]	10	30–10 000	700	No	Th may interfere with Lu line at concentrations > 1%
	Lu 3278.97	Yb 3267.89	50	200–10 000	2500	No	Th may interfere with Lu line at concentrations > 5%
	Th 3188.23	Yb 3190.81[b]	200	500–20 000	5000	No	
Lu_2O_3	Sc 3353.73	Lu 3280.50	5	100–10 000	1300	No	CN interference restricts Sc detection limit
	Y 3242.28	Lu 3280.50	10	100–10 000	1000	No	
	Er 3230.59	Lu 3222.57	10	100–10 000	500	No	
	Tm 3131.26	Lu 3167.33	10	100–10 000	400	No	
	Yb 3289.37	Lu 3264.94[a]	2	5– 200	20	No	Sm could interfere with Lu line
	Yb 3289.37	Lu 3280.50	2	100– 2 000	300	No	

†All wavelengths were taken from the MIT wavelength tables (Harrison, 1969) except as indicated by the following notations: [a]Wavelength was measured in the authors' laboratory. [b]Wavelength was taken from Gatterer and Junkes (1945).

*For analysis lines subject to spectral interference as the detection limit is approached, the value given represents the lowest concentrations determinable when intensity ratios are measured.

Acknowledgement

This work was supported by the U.S. Department of Energy, Division of Basic Energy Sciences.

References

Agrawal, Y.K. and H.L. Kapoor, 1976, Talanta **23**, 235.
Amos, M.D. and J.B. Willis, 1966, Spectrochim. Acta **22**, 1325.
Amos, M.D., 1967, The Element, No. 17 (Aztec Instruments, Westport, CT. USA).
Antonov, A.V., A.I. Drygin and Yu.A. Kalmykov, 1967, Zavod. Lab. **33**, 967.
ASTM, 1968, Designation of Shapes and Sizes of Graphite Electrodes, in: Methods for Emission Spectrochemical Analyses, 5th ed. (American Society for Testing and Materials, Philadelphia) pp. 105–110.
Bertin, E.P., 1975, Principles and Practice of X-ray Spectrometric Analysis, 2nd ed. (Plenum Press, New York) pp. 631–697.
Bonnevie-Svendsen, M. and A. Follo, 1973, X-ray Fluorescence Analysis of Rare Earth Elements, in Michelsen, O.B. ed., Analysis and Application of Rare Earth Materials (Universitetsforlaget, Oslo) pp. 87–107.
Broida, H.A. and K.E. Shuler, 1957, J. Chem. Phys. **37**, 933.
Butler, J.R., 1957, Spectrochim. Acta **9**, 332.
Chandola, L.C., I.J. Machado and A.N. Mohile, 1975, India At. Energy Comm., Report B.A.R.C.-807, Bhabha Atomic Research Centre, Bombay, India.
Chandola, L.C. and A.N. Mohile, 1976, India At. Energy Comm. Report B.A.R.C.-845, Bhabha Atomic Research Centre, Bombay India.
Chester, J.E., R.M. Dagnall and M.R.G. Taylor, 1970, Anal. Chim. Acta **51**, 95.
Christian, G.D., 1968, Anal. Lett. **1**, 845.
Christian, G.D. and F.J. Feldman, 1970, Atomic Absorption Spectroscopy (Wiley-Interscience, New York).
Christian, G.D. and F.J. Feldman, 1971, Appl. Spectrosc. **25**, 660.
Dixit, R.M. and S.S. Deshpande, 1975, India At. Energy Comm. Report B.A.R.C.-806, Bhabha Atomic Research Centre, Bombay, India.
Dolgorev, A.V. and Y.G. Lysak, 1975, J. Anal. Chem. USSR **30**, 1644.
D'Silva, A.P., R.N. Kniseley, V.A. Fassel, R.H. Curry and R.B. Myers, 1964a, Anal. Chem. **36**, 532.
D'Silva, A.P., R.N. Kniseley and V.A. Fassel, 1964b, Anal. Chem. **36**, 1287.
Eby, G.N., 1972, Anal. Chem. **22**, 426.
Eremin, Yu.G. and G.I. Bondarenko, 1972, Ind. Lab. **38**, 1010.
Fadeeva, L.A., L.I. Karpenko and S.V. Belty-ukova, 1969, J. Anal. Chem. USSR **24**, 815.
Fadeeva, L.A. and L.I. Karpenko, 1972, J. Appl. Spectrosc. **16**, 673.
Fassel, V.A. and H.A. Wilhelm, 1948, J. Opt. Soc. Am. **38**, 518.
Fassel, V.A., 1949, J. Opt. Soc. Am. **39**, 187.
Fassel, V.A., H.D. Cook, L.C. Krotz and P.W. Kehres, 1952, Spectrochim. Acta **5**, 201.
Fassel, V.A., B.B. Quinney, L.C. Krotz and C.F. Lentz, 1955, Anal. Chem. **27**, 1010.
Fassel, V.A., R.H. Curry and R.N. Kniseley, 1962, Spectrochim. Acta **18**, 1127.
Fassel, V.A. and V.G. Mossotti, 1963, Anal. Chem. **35**, 252.
Fassel, V.A., V.G. Mossotti, W.F.L. Grossman and R.N. Kniseley, 1966, Spectrochim. Acta **22**, 347.
Fassel, V.A. and D.W. Golightly, 1967, Anal. Chem. **39**, 466.
Fassel, V.A., J.O. Rasmuson, R.N. Kniseley and R.G. Cowley, 1970, Spectrochim. Acta **25B**, 559.
Fassel, V.A., R.N. Kniseley and C.C. Butler, 1973, Flame and Plasma Atomic Absorption, Emission and Fluorescence Spectroscopy of the Rare Earth Elements, in: Michelson, O.B. ed., Analysis and Application of Rare Earth Materials (Universitsforlaget, Oslo) pp. 71–86.
Fassel, V.A. and R.N. Kniseley, 1974, Anal. Chem. **46**, 1110A and 1155A.
Fassel, V.A., 1977. ASTM Spec. Tech. Pub. 618, (American Society for Testing and Materials, Philadelphia) pp. 22–42.
Finimore, C.P. and G.W. Jones, 1958, J. Phys. Chem. **62**, 178.
Fiorino, J.A., R.N. Kniseley and V.A. Fassel, 1968, Spectrochim. Acta **23B**, 413.
Folsom, T.R., N. Hansen, G.J. Parks, Jr. and W.E. Wrinz, Jr., 1974, Appl. Spectrosc. **28**, 345.
Gatterer, A. and J. Junkes, 1945, Spectren der Seltenen Erden, Specola Vaticana, Citta del Vaticano.
Gaydon, A.G. and J.G. Wolfhard, 1960, Flames, Their Structure, Radiations and Temperature, 2nd ed., (Chapman and Hall, London).
Grampurohit, S.V. and V.P. Bellary, 1970, India At. Energy Comm. Report B.A.R.C.-472, Bhabha Atomic Research Centre, Bombay, India.
Grampurohit, S.V. and V.N.P. Kaimal, 1973, India At. Energy Comm. Report B.A.R.C.-710, Bhabha Atomic Research Centre, Bombay, India.
Grampurohit, S.V. and V.N.P. Kaimal, 1975, Fresenuis' Z. Anal. Chem. **274**, 181.

Hammaker, E.M., G.W. Pope, Y.G. Ishida and W.F. Wagner, 1958, Appl. Spectrosc. **12**, 161.
Harrison, G.R., 1969, Massachusetts Institute of Technology Wavelength Tables (M.I.T. Press, Cambridge, MA).
Herman, E., 1973, Determination of Rare Earth Impurities in Pure Rare Earths by Means of Extraction Chromatography, in: Michelsen, O.B. ed., Analysis and Application of Rare Earth Materials (Universitetsforlaget, Oslo) pp. 39–53.
Hettel, H.J. and V.A. Fassel, 1955, Anal. Chem. **27**, 1311.
Hingle, D.N., G.F. Kirkbright and T.S. West, 1969, Analyst **94**, 864.
Jaworowski, R.J., R.P. Weberling and D.J. Bracco, 1967, Anal. Chim. Acta **37**, 284.
Joshi, B.D., B.M. Patel and A.G. Page, 1971, Anal. Chim. Acta **57**, 379.
Kalmykova, I.S., V.F. Mezentseva and E.V. Ponosova, 1974, J. Appl. Spectrosc. **21**, 1095.
Kalnicky, D.J., R.N. Kniseley and V.A. Fassel, 1975, Spectrochim. Acta **30B**, 511.
Karpenko, L.I. and V.P. Grechanovskii, 1972, J. Appl. Spectrosc. **17**, 766.
Karpenko, L.I., L.A. Fadeeva, L.D. Shevchenko, A.Ya. Vidisheva, 1974, J. Anal. Chem., USSR **29**, 1627.
Kinnunen, J. and O. Lindsjo, 1967, Chem. Analyst **56**, 25 and 26.
Kniseley, R.N., V.A. Fassel, B.B. Quinney, C. Tremmel, W.A. Gordon and W.J. Hayles, 1958, Spectrochim. Acta **12**, 332.
Kniseley, R.N., V.A. Fassel and C.F. Lentz, 1959a, Misidentifications in the Arc Spectra of the Rare Earths, Report IS-50, Ames Laboratory, Iowa State University, Ames, Iowa 50011.
Kniseley, R.N., V.A. Fassel, R.W. Tabling, B.G. Hurd and B.B. Quinney, 1959b, Spectrochim. Acta **13**, 330.
Kniseley, R.N., A.P. D'Silva and V.A. Fassel, 1963, Anal. Chem. **35**, 910.
Kniseley, R.N., C.C. Butler and V.A. Fassel, 1969, Anal. Chem. **41**, 1494.
Kniseley, R.N., V.A. Fassel and C.C. Butler, 1970, Atomic Emission and Absorption Spectrometry of the Rare Earth Elements, in: Mavrodineanu, R. ed., Analytical Flame Spectroscopy (Philips' Gleoilampenfabrieken, Eindhoven, Netherlands) pp. 379–410.
Kriege, O.H. and G.G. Welcher, 1968, Talanta **15**, 781.
Laktionova, N.V., A.V. Karyakin, V.A. Ryabukhin, N.S. Stroganova and L.V. Ageeva, 1974, J. Anal. Chem. USSR **29**, 1339.
Laktionova, N.V., A.V. Karyakin and L.V. Ageeva, 1975, J. Anal. Chem. USSR **30**, 590.
Lytle, F.W., T.I. Botsford and H.A. Heller, 1957, U.S. Bureau of Mines, Report of Investigation 5378.
Lytle, F.W. and H.H. Heady, 1959, Anal. Chem. **31**, 809.
Manning, D.C., 1966, At. Absorption Newsletter, **5**, 127.
Matsumura, T., R. Morooka, N. Kotani and T. Goto, 1973, Tetsu to Hagane **59**, 1159.
Meggers, W.F., C.H. Corliss and B.F. Scribner, 1975, Tables of Spectral Line Intensities: Pt. I-Arranged by Elements, Pt.II-Arranged by Wavelength (U.S. Govt. Printing Office, Washington).
Melamed, Sh.G., S.M. Polyakov and M.G. Zemskova, 1960, Indust. Lab **26**, 591.
Melamed, Sh.G., A.S. Kostygov and T.V. Lishchenko, 1964, Indust. Lab. **30**, 1665.
Mossotti, V.G. and V.A. Fassel, 1964, Spectrochim. Acta **20**, 1117.
Muntz, J.H., 1969, Spectrochim. Acta **24B**, 207.
Nash, D.L., 1968, Appl. Spectrosc. **22**, 101.
Omenetto, N., N.N. Hatch, L.M. Fraser and J.D. Winefordner, 1973, Anal. Chem. **45**, 195.
Ooghe, W. and F. Verbeek, 1974, Anal. Chim. Acta **73**, 87.
Osumi, Y., A. Kato and Y. Miyake, 1970, Z. Anal. Chem. **251**, 7.
Osumi, Y., A. Kato and Y. Miyake, 1971a, Z. Anal. Chem. **255**, 103.
Osumi, Y., A. Kato and Y. Miyake, 1971b, Z. Anal. Chem. **255**, 264.
Osumi, Y., Y. Miyake and K. Imahara, 1971c, Fresenius' Z. Anal. Chem. **256**, 182.
Osumi, Y., A. Kato and Y. Miyake, 1971d, Jap. Anal. **20**, 1393.
Osumi, Y. and Y. Miyake, 1972, Fresenius' Z. Anal. Chem. **260**, 97.
Osumi, Y. and Y. Miyaki, 1973, Fresenius' Z. Anal. Chem. **264**, 8.
Pavlenko, L.I., N.V. Laktionova and Yu.S. Sklyarenko, 1967, J. Anal. Chem. USSR **22**, 86.
Pickett, E.E. and S.R. Koirtyohann, 1968, Spectrochim. Acta **23B**, 235.
Plowman, C., 1971, Analyst **96**, Nr 1148, 776.
Poluektov, N.S., R.S. Lauer, L.A. Ovchar and S.F. Potapova, 1975, J. Anal. Chem. USSR **30**, 1275.
Rasmuson, J.O., 1970, An Experimental and Theoretical Evaluation of the Nitrous Oxide-Acetylene Flame as an Atomization Cell for Flame Spectroscopy, Ph.D. Thesis, Iowa State University, Ames, Iowa.
Rose, H.J., Jr. and F. Cuttitta, 1968, Appl. Spectrosc. **22**, 426.
Rozsa, J.T. and J. Stone, 1962, Develop. Appl. Spectry. **1**, 187.
Sato, M., H. Matsui and Matsubara, 1971, Jap. Anal. **20**, 215.
Sen Gupta, J.G., 1976, Talanta **23**, 343.
Shifrin, N. and J. Ramirez-Munoz, 1969, Appl. Spectrosc. **23**, 358 and 365.
Shmanenkova, G.I., M.G. Zemskova, Sh. G. Melamed and G.P. Pleshakova, 1972, Indust. Lab **38**, 1370.
Skogerboe, R.K. and R.A. Woodriff, 1963, Anal. Chem. **35**, 1977.
Slavin, W., 1968, Atomic Absorption Spectroscopy (Interscience, New York).
Slyusareva, R.L., L.I. Kondrat'eva and Sh.I. Peizulaev, 1965, Indust. Lab. **31**, 685.
Souilliart, J.C. and J.P. Robin, Analusia, **1**, 427 (1972).

Smith, D.M. and G.M. Wiggins, 1949, Analyst **74**, Nr 875, 95.
Stallwood, B.J., 1954, J. Opt. Soc. Am. **44**, 171.
Tertian, R., 1969, A Rapid and Accurate X-ray Determination of the Rare Earth Elements in Solid or Liquid Materials Using the Double Dilution Method, in: Barrett, C.S. et al., eds., Advances in X-ray Analysis, Vol. 12 (Plenum Press, New York) pp. 546–562.
Vakulenko, L.I., B.Ya. Kaplan, Yu.I. Merisov, A.I. Mikhailichenko and G.S. Skripkin, 1973, Indust. Lab. **39**, 1774.
Walton, R.D., 1971, High Precision Determination of Microgram Quantities of Rare Earth Metals by X-ray Emission Spectrography of Ion Exchange Paper Disc, in: Grove, E.L. and A.J. Perkins, eds., Developments in Applied Spectroscopy, Vol. 9 (Plenum Press, New York) pp. 287–305.
Waring, C.L. and H. Mela, Jr., 1953, Anal. Chem. **25**, 432.
White, A.L., M. Gerring and D.S. DeLa Haba, 1959, U.S. Bureau Mines Report of Investigation No. 5454.
Whitehead, A.B., B.C. Piper and H.H. Heady, 1966, Appl. Spectrosc. **20**, 107.
Zaidel, A.N., N.I. Kaliteevskii, A.A. Lipovskii, A.N. Razumovskii and P.P. Yakimova, 1958, Fiz. Sbornik L'vov Univ. **4**, 37.
Zeeb, L.E., J.T. Rozsa, D.C. Manning and T. Stone, 1958, Report No. APEX-431 (National Technical Information Services, U.S. Dept. of Commerce, Springfield, VA).
Zemskova M.G., N.A. Lebedev, Sh.G. Melamed, O.F. Saunkin, G.V. Sukhov, V.A. Khalkin, E. Kherrmann and G.I. Shmanenkova, 1967, Indust. Lab. **33**, 789.
Zemskova, M.G., N.A. Lebedev and Sh.G. Melamed, 1968, Nauch, Tr., Gos. Nauch. – Issled. Proekt. Inst. Redkometal. Prom. **22**, 116.
Zmbova, B., 1972, Teknika (Belgrade) **27**, 552.

Handbook on the Physics and Chemistry of Rare Earths, edited by K.A. Gschneidner, Jr. and L. Eyring

Chapter 37E

X-RAY EXCITED OPTICAL LUMINESCENCE OF THE RARE EARTHS*

A.P. D'SILVA and V.A. FASSEL
Ames Laboratory, US DOE and Department of Chemistry, Iowa State University, Ames, Iowa 50011, USA

Contents

1. Introduction

The optical luminescence exhibited by some of the rare earth complexes and ions in solids has been utilized for the detection and determination of the rare earths at the trace and ultratrace levels for many years (El'Yashevich, 1953; Dieke, 1968; Sinha, 1966). To date, optical luminescence of the rare earth ions in solids has been excited by flames (candoluminescence) (Neunhoeffer, 1951; Sweet et al., 1970); by ultraviolet or visible radiation (photoluminescence or UVEOL) (Ankina and Karyakin 1964; Ozawa and Terai 1968; Poluektov et al., 1971); by electron beams (cathodoluminescence) (Wickersheim et al., 1968; Larach, 1968; Kniseley et al., 1969); by accelerated protons (Antonov and Melamed 1970); by γ radiation (Derr and Gallagher 1964; Vakhidov et al., 1970); and by X-rays (Makovsky et al., 1962; Derr and Gallagher 1964; Low et al., 1964). Of all the luminescent techniques, X-ray excited optical luminescence (XEOL) of the rare earth ions has been used

*Work performed for the U.S. Department of Energy under Contract No. W-7405-eng-82.

more extensively than the others for the quantification of ultratrace level rare earths in a wide variety of matrices (Linares et al., 1965; Jaworowski et al., 1968; Burke and Wood, 1968; DeKalb et al., 1968; Shand, 1968; Sasaki, 1968; Fassel et al., 1974; DeKalb and Fassel, 1975). In contrast to UVEOL no optical crosstalk is encountered in XEOL, cathodoluminescence or excitation by γ rays or protons and in addition superior powers of detection for the rare earths can be obtained as demonstrated for Y_2O_3 (Ozawa and Toryu, 1968; Jaworowski et al., 1968). Though similar limits of detection can be achieved by both cathodoluminescence and XEOL techniques, the former suffers from the significant disadvantage in that the samples have to be in a vacuum during analysis. Thus of all the luminescent techniques the XEOL of the rare earth ions has been used more extensively than the others for the quantification of ultratrace level rare earths in a wide variety of matrices.

2. Origin of X-ray excited optical luminescence

A wide variety of inorganic and organic compounds luminesce when they are irradiated with X-rays (Leverenz, 1950; Curie, 1960; DeKalb et al., 1968). The following simplified treatment offers generalizations and suggests mechanisms that result in the observation of XEOL of trace level rare earth ions (activators) present as substitutional impurities in high purity phosphor hosts (crystalline insulators) (DeKalb et al., 1968; Fassel et al., 1973).

The high efficiency with which XEOL of ultratrace level rare earth activators in phosphors is observed cannot be attributed to processes involving the direct absorption of primary X-ray photons by the impurities followed by luminescence. Thus it is reasonable to assume that the interaction of primary incident X-ray photons with host atoms produces a large number density of secondary excitants which have a greater probability of eventually exciting the luminescence of the impurity ions. The direct absorption of the primary incident X-rays by the host and impurity atoms result in the ejection of inner shell photoelectrons (K, L, M) from the atoms and concurrent emission of fluorescent X-rays. Alternatively the absorbed energy may be internally converted with the ejection of Auger electrons which interact with extranuclear electrons resulting in the production of secondary excitants with energies of several electron volts. The secondary phenomenon that result in energy transfer from host ions to activator ions can be interpreted with the aid of the energy level diagram shown in fig. 37E.1, which is a simplified schematic one dimensional presentation of energy states in a crystalline insulator, e.g. YPO_4 containing traces of either rare earth (Tb^{3+}) or non-rare earth (Sr^{2+}) activators. The phosphor, i.e. YPO_4, is a crystalline insulator in which the valence band represents the range of energy states of the valence electrons that bind the atoms in the solid state, all energy levels being filled. The energy gap separates the valence band from the conduction band of energies which is initially empty. The absorption of discrete amounts of energy from the photo and Auger electrons formed by the primary absorption of

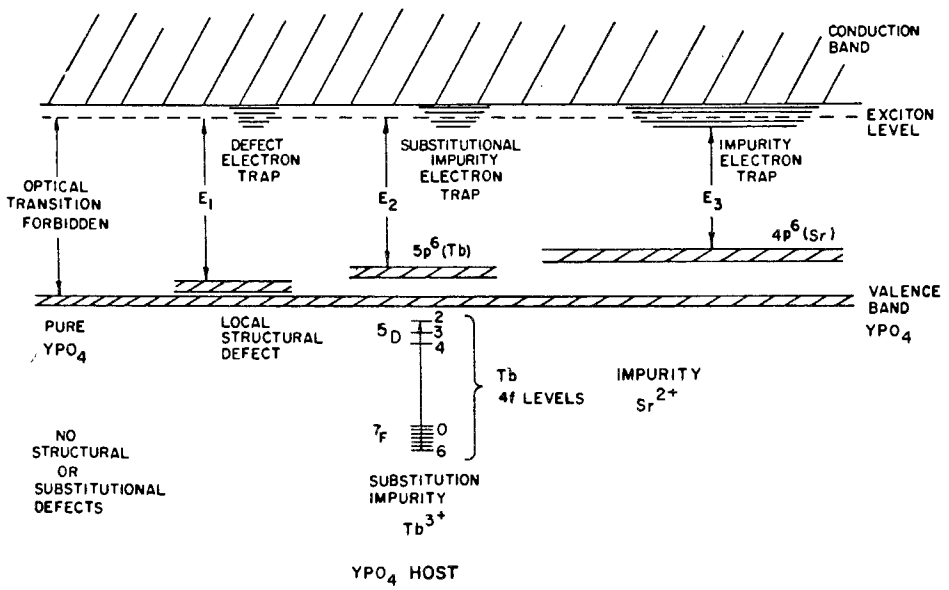

Fig. 37E.1. Schematic one-dimensional presentation of energy states in a crystalline insulator or semiconductor.

X-rays by the host may result in the excitation of an electron from the valence band into the conduction band leaving a positive hole (electron deficiency) in the normally filled valence band. The "free" electron in the conduction band and the hole in the valence band form a new mobile entity termed "exciton". which is free to wander in the crystal. If such a host is free from structural and compositional defects, the recombination of an electron and a hole is not an allowed process. Substitutional impurities or structural imperfections behave as if they were defects in an otherwise near perfect crystal. In contrast to a pure crystalline host, the recombination of an electron and a hole at a defect is an allowed process and results in release of energy at the defect site. If the recombination occurs at a compositional defect, e.g., Tb^{3+} substituting for Y^{3+}, the energy released may result in the excitation of $f \rightarrow f$ transitions, resulting in the observation of sharp line luminescent spectra. The combination of mobility of the exciton, the relatively short lifetime of the 4f excited states, and the repeated reexcitation of the same impurity ion may therefore lead to a highly efficient energy transfer process.

3. Instrumentation

An experimental facility specifically designed for the observation of XEOL spectra in the 180 nm–1200 nm region is shown in fig. 37E.2. The X-ray source consists of a tungsten target X-ray tube (OEG-50-T, Machlett Laboratories,

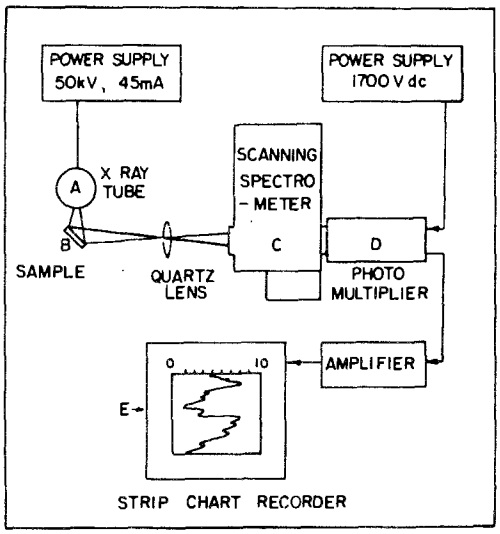

Fig. 37E.2. A schematic diagram of the experimental facility for observing XEOL spectra.

Springdale, CT or equivalent) powered by an appropriate power supply (Norelco XRG 5000, Philips Electronic Instruments, Mount Vernon, NY or equivalent). The X-ray tube is operated generally at 50 KV dc and 45 mA. Sample irradiation is performed in a chamber which permits sample exchange with the X-ray tube on at full power (DeKalb et al., 1968). An exploded view of the irradiation chamber designed in our laboratory is shown in fig. 37E.3. The powdered samples are usually pressed into 1 cm diameter by 2 mm deep Al planchets with a simple hand press. The sample planchets are positioned at an angle of 45° to the X-ray and optical beams. To facilitate the observation of XEOL at temperatures higher than ambient, a temperature controlled miniature heater assembly

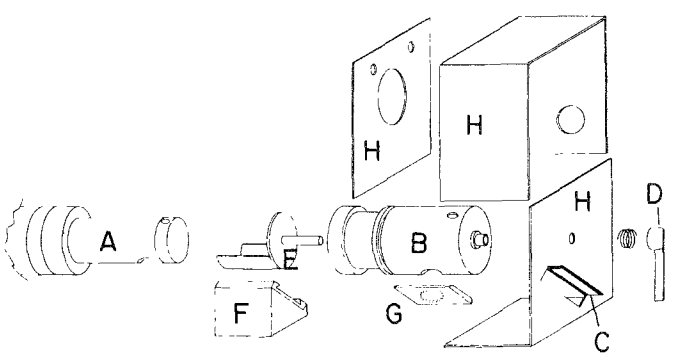

Fig. 37E.3. An exploded view of the irradiation chamber: (A) X-ray tube, (B) X-ray tube shield, (C) access door, (D) shutter lever, (E) shutter, (F) vee-way mounting block, (G) sample holder, (H) brass chamber.

mounted in the sample holder block is capable of heating the phosphor samples up to 200°C (D'Silva and Fassel, 1974a). The optical radiation from the sample is focused by an appropriately positioned fused silica lens on the entrance slit of the 0.25 meter focal length spectrometer (Jarrell-Ash, Waltham, MA, catalogue no. 82-410, or equivalent). The spectrometer is equipped with a dual grating assembly to facilitate the observation of XEOL in the 180 nm–800 nm region. To observe the most sensitive lines of Yb and Nd, which occur in the near infrared region, the dual grating assembly is replaced when needed by an alternate 600 grooves mm grating blazed for 1000 nm. The detection system consists of two photomultiplier tubes. An S-1 type spectral response tube (Amperex 150 cvp) is positioned normal to the exit slit and is mounted in a dry-ice cooled enclosure (Pacific Photometric Instruments, Berkley, CA, Model No. 77). The S-20 type spectral response tube (RCA C7268) is mounted at right angles to the exit slit and is illuminated when necessary by a front surface mirror positioned at 45° to the exit slit. Either of the two photomultipliers can be used by moving the mirror in and out of the optical path. The DC electronic detection system consists of a Keithley 417 Picoammeter and a two-pen, strip chart recorder. One of the pens records the spectrum at $\frac{1}{10}$ the gain as the other and thus permits a greater range of spectral intensities to be recorded during a single spectrum scan. The entrance and exit slits of the spectrometer are generally set at 250 μm and the spectrum is scanned usually at 20 nm per minute.

4. Phosphors for the observation of XEOL of rare earths

4.1. *Rare earth impurities in high-purity rare earths*

Of the rare earths, Y_2O_3, La_2O_3 and Gd_2O_3 have been utilized extensively in the preparation of efficient phosphors, laser hosts and in quality optical components. The efficiency or optical quality of several of these materials are known to be effected by rare earth impurities present at trace levels. Thus several of the early analytical studies on the XEOL of the rare earths have been directed to the quantification of the rare earth impurities in Y_2O_3, La_2O_3 and Gd_2O_3, as reported by Linares et al. (1965), Jaworowski et al. (1968), Burke and Wood (1968), DeKalb et al. (1968), Sasaki (1968), Nakajima et al. (1970) and Sato et al. (1971). To overcome some of the analytical limitations of the above hosts, Y_2O_2S, La_2O_2S and Gd_2O_2S phosphors have been examined by Ratinen (1972), and YPO_4–YVO_4 by D'Silva and Fassel (1973). Studies performed by D'Silva et al. (1974b) on XEOL of rare earth phosphates revealed several advantages of these host systems for analytical purposes. In La_2O_3 or La_2O_2S no Ce luminescence is observed, hence these hosts are not acceptable for the determination of Ce, which is usually present as an impurity in La_2O_3. In addition, La_2O_3 is highly hygroscopic and special care has to be exercised in obtaining the XEOL spectra of rare earth impurities in this compound. The XEOL spectrum of $LaPO_4$, which is not hygroscopic, as shown in fig. 37E.4, reveals the ultraviolet bands of Ce in

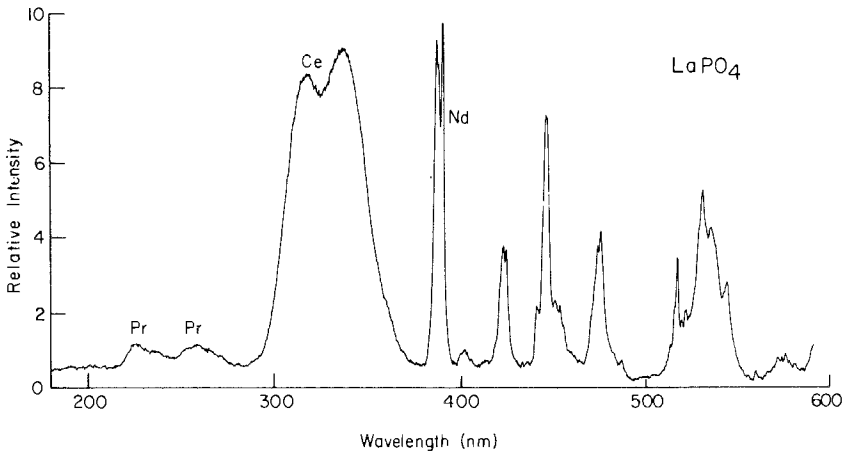

Fig. 37E.4. XEOL spectra of rare earths in $LaPO_4$.

the 300–380 nm region. These bands can be utilized for the determination of Ce at trace levels in $LaPO_4$ matrices. The spectral lines of Nd, which occur in the near infrared in La_2O_3 or La_2O_2S, are observed near 400 nm in $LaPO_4$. Thus $LaPO_4$ can be utilized as a host for the quantitation of Ce, Pr, Nd and Sm in La_2O_3. The advantages of utilizing either a YPO_4 or YVO_4 host rather than Y_2O_3 for the determination of part per giga level rare earth impurities in Y_2O_3 is illustrated in fig. 37E.5. An analytical procedure utilizing these observations has been published by D'Silva and Fassel (1973). $GdPO_4$ can be used to advantage to detect Ce as well as Eu and Tb with higher powers of detection than in Gd_2O_3. Preliminary observations on the advantages of using $CePO_4$ for the determination of certain rare earth impurities in CeO_2 and of $LuVO_4$ for the determination of Ho, Er, Tm and Yb in Lu_2O_3 were reported by Fassel et al. (1974). Analytical observations on $LuVO_4$ have been reported by Tritten (1974). The determination of Dy, Gd and Eu in Ho_2O_3 by XEOL was reported by Kawaguchi et al. (1969). Because Ho_2O_3 does not normally support the luminescence of other lanthanides, the determination of Dy, Gd and Eu was accomplished by diluting Ho_2O_3 with high purity Y_2O_3 in the ratio of 1 : 100 by weight. When such dilutions are made, caution must be exercised because corrections must usually be applied for the residual rare earths present in the Y_2O_3 diluent.

4.2. *Genesis of ultrasensitive non-rare earth phosphor hosts*

The XEOL of rare earths (usually Sm, Eu, Gd, Tb and Dy) present at the 100–1000 ppm level in a wide variety of simple, binary, ternary and quaternary oxide host systems have been reported by Jaworowski et al. (1968), Takashima et al. (1969), Kawaguchi et al. (1969), Saranathan et al. (1970), DeKalb et al. (1970) and D'Silva et al. (1970). In addition a limited number of halides, oxyhalides, sellenides and tellurides have been shown by Low et al. (1974),

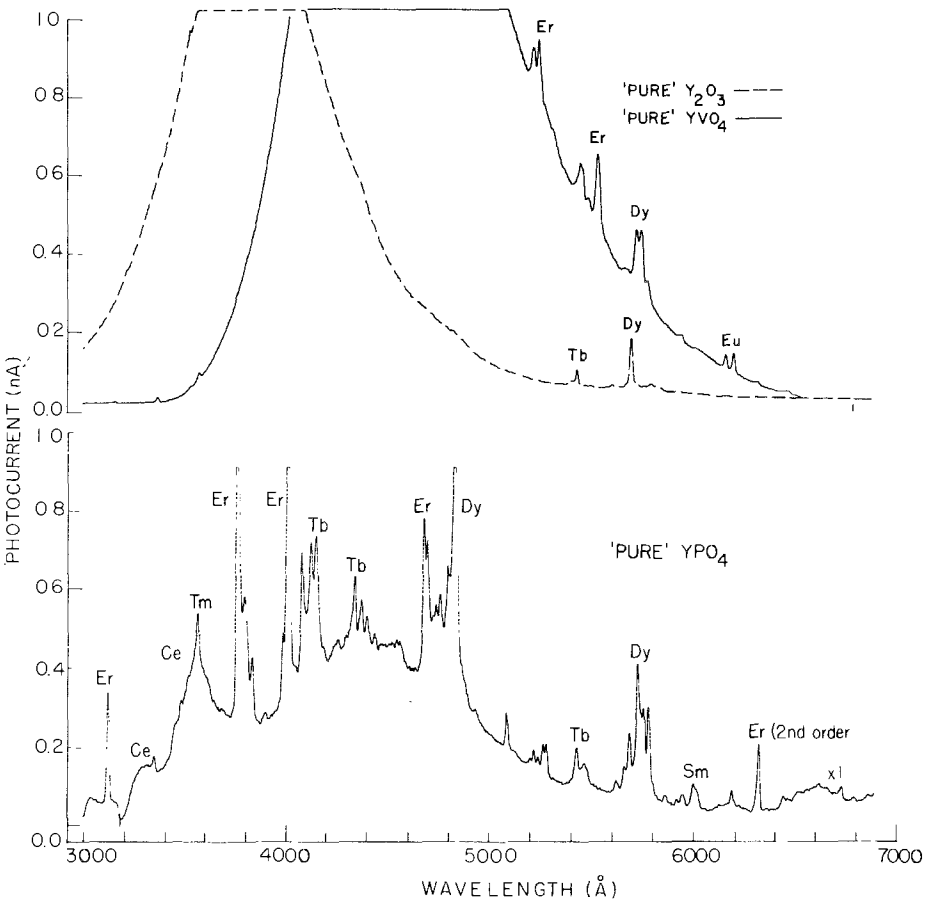

Fig. 37E.5. XEOL spectra of rare earths in Y_2O_3, YPO_4 and YVO_4 hosts.

DeKalb et al. (1970) and Ratinen (1972b), to be good hosts for the observation of XEOL of low concentrations of rare earths. Unfortunately the complex and lengthy procedures required to prepare many of the above hosts make them generally unsuitable for analytical purposes.

A generalized table of oxygen dominated hosts, which is an extension of the classification proposed by Johnson (1966) and DeKalb et al. (1970), is shown in table 37E.1. The emphasis in our studies has been to evolve analytically useful phosphors with a high degree of reproducibility in their preparation, freedom from interelement effects (see 5.1) and with the best possible limits of detection. In the periodic table shown in fig. 37E.6 the 57 elements enclosed by boxes when converted to an appropriate phosphor host support the luminescence of one or more of the lanthanides down to at least the 100 ppm level.

For most analytical purposes the determination of lanthanides at the 10–100 ppm level is generally adequate. In contrast, for the determination of the

TABLE 37E.1
Generalized composition of oxidic phosphor hosts in which XEOL of rare earths has been observed.

Simple oxides: A_2O_x	Binary oxides: $A_2O_x \cdot B_2O_y$
A^{2+} – Mg, Ca, Sr, Ba	A^{1+} – Li, Na, K
A^{3+} – Sc, Y, La, Gd, Lu, Al, Ga, In	A^{2+} – Be, Ca, Sr, Ba, Zn, Cd, Pb
A^{4+} – Cr, Zr, Hf, Th	A^{3+} – Y, Sc, La, Gd, Lu, Al
	A^{4+} – Ti, Zr, Hf, Ce, Th
	B^{3+} – B, Al, Ga, Y, La, Gd, Lu
	B^{4+} – Ge, Sn
	B^{5+} – V, Nb, Ta, P, As, Sb
	B^{6+} – Mo, W
Ternary oxides: $A_2O_x \cdot B_2O_y \cdot nC_2O_z$	
A^{1+} – Li, Na, K, Rb, Cs	
A^{2+} – Ca, Sr, Ba, Cu, Ni	
A^{3+} – Y, Sc, La, Gd, Lu	
B^{3+} – Cr, Fe	
B^{4+} – Ti, Zr, Hf, Mn, U	
C^{5+} – Nb, Ta, P, As	
C^{6+} – Mo, W	

"neutron poisons" (Gd, Sm, Dy, Eu) in high purity nuclear materials, such as UO_2, ThO_2, ZrO_2 and PuO_2, quantitative determinations at the fractional ppm level are required. These determinations are difficult analytical tasks (Goldbeck, 1964). Of the four matrix oxides mentioned above, analytically useful XEOL of the lanthanides has been observed at the fractional ppm level only in ThO_2 (Saranathan et al., 1970). In ZrO_2 (Kawaguchi et al., 1969) reported the detection of Dy, Gd and Tb at levels of 3 to 50 ppm, which are inadequate for evaluating nuclear grade ZrO_2. The XEOL determination of fractional ppm levels of the rare earths present in UO_2, ZrO_2 and TiO_2 was found possible by D'Silva et al. (1970) by incorporating the above oxides into a quaternary oxide host system the genesis of which is illustrated with reference to ZrO_2 in fig. 37E.7. The remark-

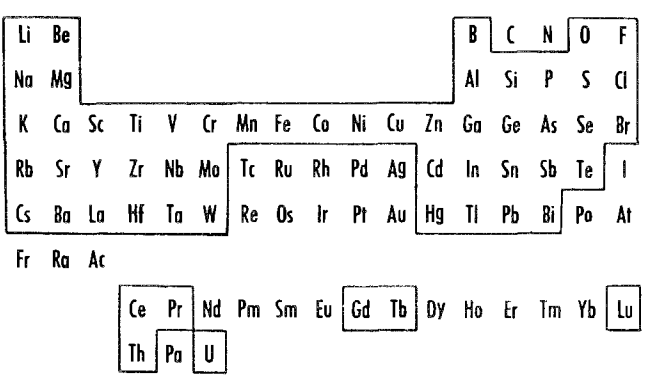

Fig. 37E.6. Elements within boxes have been found to form compounds which will support analytically useful XEOL of trace rare earth impurities.

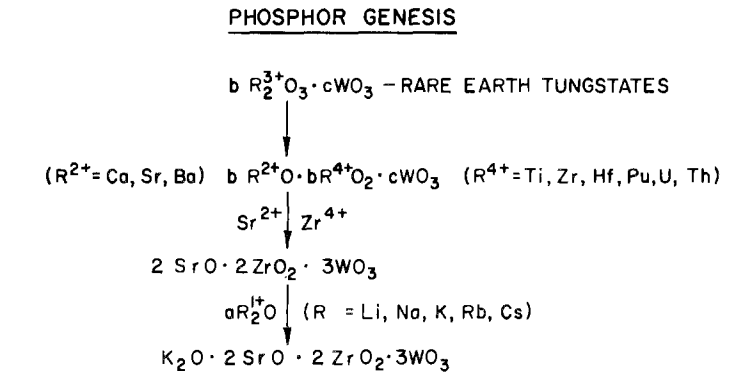

Fig. 37E.7. Phosphor genesis of a quaternary oxide host containing ZrO_2.

able enhancement in the XEOL of Sm in ZrO_2 as one sequentially proceeds from the simple oxide ZrO_2 to the final quaternary oxide host $K_2O \cdot 2SrO \cdot 2ZrO_2 \cdot 3WO_3$ is illustrated in the spectral recordings reproduced in fig. 37E.8. For trace level rare earth determinations in uranium, the exceptionally high powers of detection observed in quaternary oxide phosphor hosts that incorporate UO_2 or U_3O_8 is illustrated in fig. 37E.9. Although studies on rare earth luminescence in PuO_2 have not been reported, the observations summarized above suggest that similar quaternary oxide hosts should be useful for the determination of trace lanthanides in PuO_2.

4.3. *Rare earths in iron transition group oxides*

In oxygen dominated hosts the transition group elements Fe, Co and Ni have been often observed to act as quenchers of luminescence (DeKalb et al., 1968;

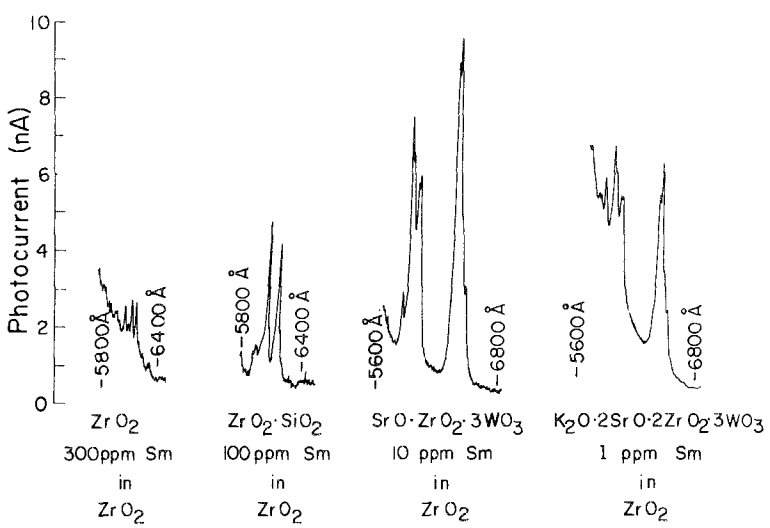

Fig. 37E.8. XEOL of Sm in ZrO_2 hosts.

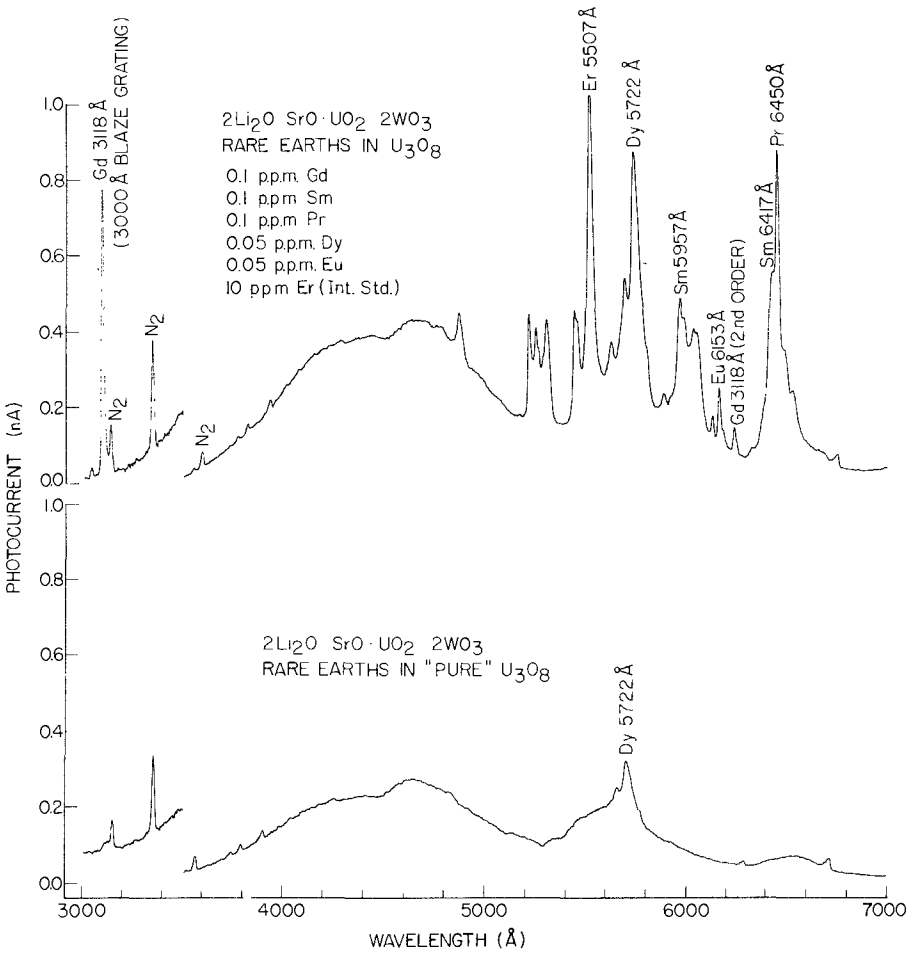

Fig. 37E.9. XEOL of trace level rare earths in the UO_2 phosphor: $2Li_2O{\cdot}SrO{\cdot}UO_2{\cdot}2WO_3$.

Jaworowski et al., 1968; Pringsheim, 1949). However, DeKalb and Fassel (1975) observed that when the above elements are incorporated as major constituents into a YPO_4 host, the rare earth activator luminescence could be observed at part per million levels. A typical application of the above observation was the determination of lanthanides in steel. The XEOL spectrum shown in fig. 37E.10 was obtained from a stainless steel sample to which several rare earths were added at the 100 ppm level. The direct procedure contrasts with the one reported by Kato et al. (1972) who separated the trace earth from the stainless steel matrix prior to incorporating the separated rare earths in a ThO_2 host.

5. Analytical calibrations

5.1. *The internal reference principle*

The intensities of the XEOL spectra of the rare earths, regardless of the chemical and physical nature of the phosphor host, are often markedly influenced by the presence in relatively large amounts of compositional impurities in the host material and by variations in preparative procedures. In many hosts the behavioral pattern of enhancement of suppression of the rare earth line intensities appears to be nearly identical for all the rare earths (DeKalb et al., 1968; Jaworowski et al., 1968). This observation suggests the use of one of the rare earths as an internal reference element, a principal effectively used in conventional optical emission spectroscopic analysis. When the internal reference principle is used, intensity ratio measurements are employed to compensate for enhancement or suppression effects. A typical example of the effective use of the internal reference element principle is illustrated in fig. 37E.11 The top half of the figure shows that increasing additions of Fe to Y_2O_3 results in the relative intensities of the luminescence of the lanthanide impurities in Y_2O_3 to undergo wide excursions, but in consort. The bottom half of the figure illustrates the effective use of Sm as the internal reference element. The

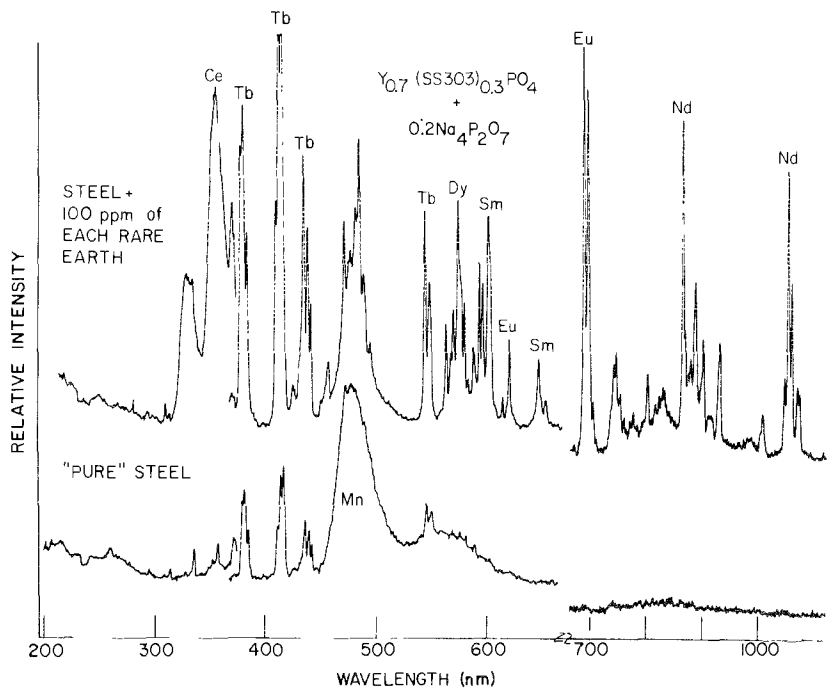

Fig. 37E.10. XEOL of rare earths in stainless steel containing phosphor: $Y_{0.8}(SS)_{0.2}PO_4$.

intensity ratios of Dy/Sm, Eu/Sm and Tb/Sm are practically unaffected in the presence of increasing amount of Fe in Y_2O_3. The internal reference element principle has been widely used in various analytical studies (Saranathan, 1970; Sato et al., 1971; Nakajima et al., 1970; D'Silva and A. Fassel 1971, 1973, 1974 Kato et al., 1972).

5.2. *Preparation of phosphor hosts*

In our analytical studies phosphor hosts varying widely in composition have been utilized, ranging from simple oxides, such as Y_2O_3 and ThO_2, to quaternary oxides, such as $2Li_2O{\cdot}SrO{\cdot}UO_2{\cdot}2WO_3$. Simple solid state reactions in the 800–1200 C range have generally been used to prepare the phosphor hosts. The reference element has often been incorporated into one of the components of the multicomponent phosphor base blends which were subsequently used to synthesize the hosts (D'Silva et al., 1971). Thus dissolution of the samples prior to analysis has not been necessary. Two typical preparative procedures that have provided high luminescence line intensities are described below. For the preparation of YPO_4, a blend of 0.226 g Y_2O_3, 0.264 g $(NH_4)_2HPO_4$ and 0.086 g $Na_4P_2O_7{\cdot}10\,H_2O$ was initially heated at 600°C for a few minutes, reground and heated at 1200°C for one hour. The quaternary oxide phosphor host

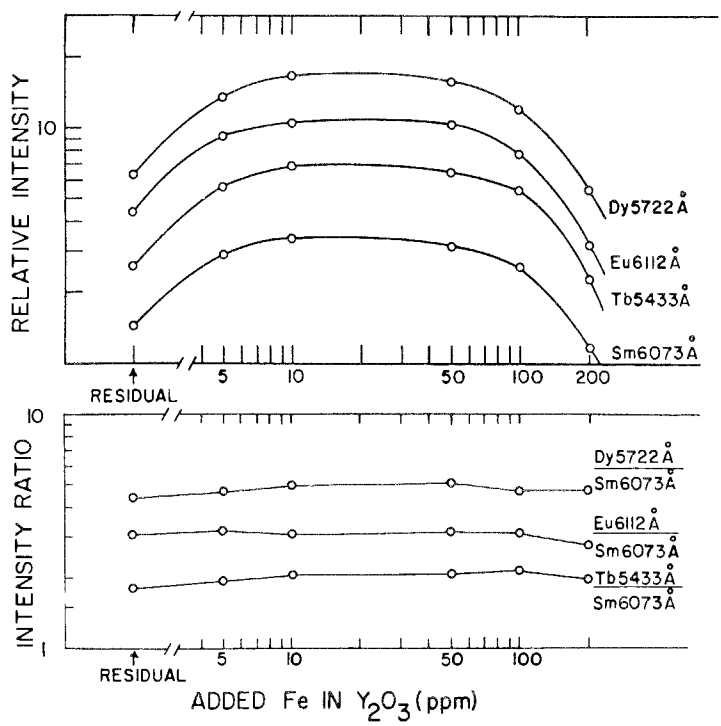

Fig. 37E.11. Effect of Fe on luminescence and intensity ratios of rare earths in ThO_2.

TABLE 37E.2

Limits of detection for trace level rare earth impurities in high-purity rare earth and non-rare earth phosphor hosts

	Y_2O_3[a,b]		YPO_4[c] YVO_4[d]		La_2O_3[e]/LaOCl[f]		$LuVO_4$[g]		Gd_2O_3[b]	
	λ	LD	λ	LD	λ	LD	λ	LD	λ	LD
Ce			356	0.005						
Pr	648	0.1[a]	244	0.005	510	0.2			643	0.1
	655	0.1[b]			502	0.005[f]				
Nd	898	0.001[a]	890	0.01[d]	425	20.0			891	0.14
	891	0.06[b]								
Sm	609	0.01	599	0.005	567	3.0			564	0.9
	565	0.06			565	0.02[f]				
Eu	614	0.01	619	0.05[d]	539	1.0			611	0.02
	611	0.03								
Gd	316	0.1	312	0.05	312	0.2			–	–
	318	0.03								
Tb	545	0.001	380	0.001					543	0.01
	544	0.003								
Dy	573	0.001	487	0.001	575	3.0			573	0.02
	573	0.003			571	0.1[f]				
Ho	540	0.1	754	0.5[d]	542	2.0	761	2.0	537	50.0
	536	0.5								
Er	526	0.1	318	0.05	545	1.0	866	0.4	562	30.0
	563	0.2								
Tm	456	0.01	286	0.05	458	1.0	806	0.05	453	6.0
	452	0.04			461	0.01[f]				
Yb	980	0.1	980	0.5[d]			991	1.0	974	10.0
	975	5.0								

	U_3O_8[h]		ZrO_2[i,j]		CaF_2[k]		Al_2O_3[l]		ThO_2[m]	
	λ	Ld	λ	LD	λ	LD	λ	LD	λ	LD
Ce										
Pr	645	0.005	485	0.05		1.0			460	0.08
			500	1.0[j]					503	0.04
Nd						1.0	395	0.1		
Sm	596	0.0025	596	0.05		5.0	572	1.0	571	0.05
			570	30						
Eu	615	0.01	615	0.10		5.0	591	1.0	590	0.02
			589	0.10						
Gd	312	0.0025	312	0.05		0.1	316	0.05	313	0.04
			313	0.5[j]						
Tb			542	0.1		0.1	382	0.1		
Dy	572	0.0025	572	0.02		1.0	493	0.1	577	0.1
			578	3.0[j]					584	0.1
Ho			541	50		0.1				
Er			545	10		0.1	408	1.0		
Tm						1.0				
Yb						10–100	355	0.1		

λ – wavelength in nm. LD – Limit of detection in ppm.

[a]Burke and Wood (1968); [b]Jaworowski et al. (1968); [c,d]D'Silva and Fassel (1973); [e]Nakajima et al. (1969); [f]Efrynshina et al. (1975); [g]Tritten (1974); [h]D'Silva and Fassel (1971); [i]D'Silva and Fassel (1974a); [j]Kawaguchi et al. (1969); [k]Shand (1968); [l]Takashima et al. (1969); [m]Saranthan et al. (1970).

$2Li_2O{\cdot}SrO{\cdot}UO_2{\cdot}2WO_3$ utilized for the determination of rare earth neutron poisons in UO_2 or U_3O_8 was prepared as follows. Initially the $Sr(NO_3)_2$ containing the reference element Er was prepared by the addition of 30 μg of Er in solution to a solution containing 2.11 g of $Sr(NO_3)_2$. The resulting solution was evaporated to dryness and the residue dehydrated at 110°C. The phosphor base mixture consisted of a blend of 1.47 g Li_2CO_3, and 2.11 g of the $Sr(NO_3)_2$ containing Er and 4.64 g WO_3. For the determination of rare earths in a sample of uranium, 0.270 g of UO_2 or U_3O_8 prepared from the metal was blended with 0.822 g of the phosphor base mixture and heated in a platinum crucible at 825°C initially for an hour. The phosphor was reground and heated at the same temperature for a further period of 2 hours.

5.3. *Analytical data*

The wavelengths of the analytical lines and the estimated limits of detection for different phosphor hosts are summarized in table 37E.2. The table is not exhaustive as several investigators who have utilized the XEOL technique for the determination of trace level rare earths have not tabulated the limits of detection. Typical analytical curves that have been obtained in our studies utilizing the internal reference element principle are shown in fig. 37E.12.

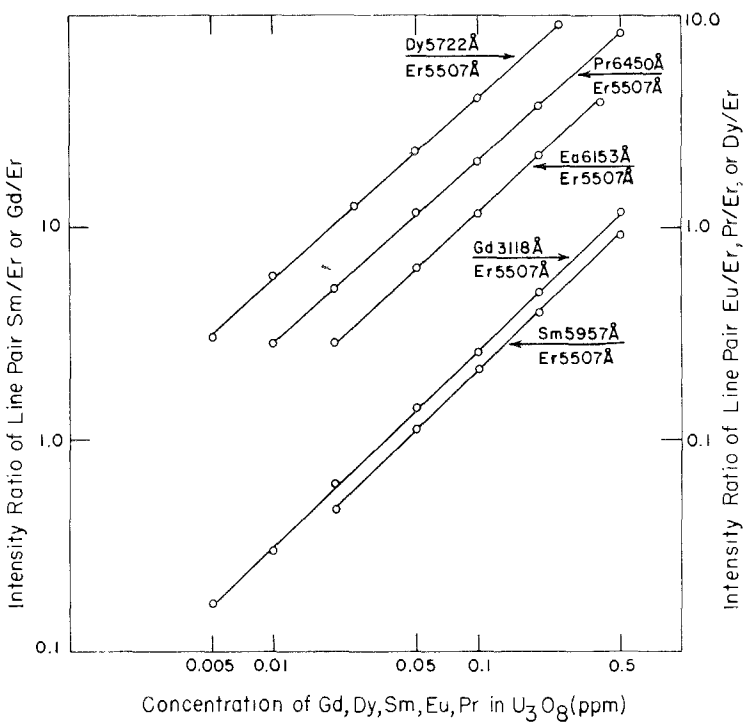

Fig. 37E.12. Analytical curves for the direct determination of rare earths in uranium.

6. Conclusion

This brief report summarizes the analytical potential of the XEOL technique for the determination of trace level rare earths in a variety of phosphor hosts. It has not been designed as an exhaustive review but should serve as a guide to those who wish to evaluate the XEOL technique for the determination of trace level rare earths in a wide variety of matrices.

Acknowledgement

This work was supported by the U.S. Department of Energy, Division of Basic Energy Sciences.

References

Ankina, L.I. and A.V. Karyakin, 1964, Russ. Chem. Rev. **33**, 571.

Antonov, A.V. and Sh.G. Melamed, 1970, Anal. Khim. Redk. Metal. Poluprov. Mater 149.

Burke, W.E. and D.L. Wood, 1968, Rare Earth Analyses by X-Ray Excited Optical Fluorescence, in: Newkirk, J.B., G.R. Mallett and H.G. Pfeiffer, eds., Advances in X-Ray Analysis, Vol. 11 (Plenum Press, New York) p. 204.

Curie, D., 1960, Luminescence in Crystals (Wiley, New York) p. 298.

DeKalb, E.L., V.A. Fassel, T. Taniguchi and T.R. Saranathan, 1968, Anal. Chem. **40**, 2082.

DeKalb, E.L., A.P. D'Silva and V.A. Fassel, 1970, Anal. Chem. **42**, 1246.

DeKalb, E.L., A.P. D'Silva and V.A. Fassel, 1972, Analytical Applications of X-Ray Excited Optical Luminescence, in: Williams, F. ed., Luminescence of Crystals, Molecules and Solutions (Plenium Publishing Corporation, New York) p. 675.

DeKalb, E.L. and V.A. Fassel, 1975, Anal. Chem. **47**, 2354.

Derr, V.E. and J.J. Gallagher, 1964, X-Ray Excited Fluorescence In Crystalline Solids, in: Quantum Electronics-Paris 1963 Conference (Columbia University Press, New York, New York) p. 817.

Dieke, G.H., 1968, Spectra and Energy Levels in Crystals (Wiley, New York).

D'Silva, A.P., E.L. DeKalb and V.A. Fassel, 1970, Anal. Chem. **42**, 1846.

D'Silva, A.P. and V.A. Fassel, 1971, Anal. Chem. **43**, 1406.

D'Silva, A.P. and V.A. Fassel, 1973, Anal. Chem. **45**, 542.

D'Silva, A.P. and V.A. Fassel, 1974a, Anal. Chem. **46**, 996.

D'Silva, A.P. and V.A. Fassel, 1974b, X-Ray Excited Optical Luminescence in Rare Earth Phosphates, 145th Meeting of the Electrochemical Society, San Francisco, Calif., paper #101.

Efryushina, N.P., N.S. Poluektov and N.I. Smirdova, 1975, Ukr. Khim. Zh. **41**, 81.

El'yashevich, M.A., 1953, Spectra of the Rare Earths (State Publishing House of Technical – Theoretical Literature, Moscow).

Fassel, V.A., E.L. DeKalb and A.P. D'Silva, 1973, Trace Level Rare Earth Determinations by X-Ray Excited Optical Fluorescence (XEOF) Spectroscopy, in: Michelsen, O.B., ed., Analysis and Application of Rare Earth Materials, NATO Advanced Study Institute, Kjeller, Norway (Universitets forlaget, Oslo).

Fassel, V.A., A.P. D'Silva, J.S. Tritten, and G.J. Oestreich, 1974, X-Ray Excited Optical Luminescence Methods for the Determination of Trace Level Rare Earth Impurities in Cerium and Lutetium, in: Harchke, J.M. and H.A. Eick, eds., Proceedings of the 11th Rare Earth Research Conference, Traverse City, Michigan, CONF-741002-P1 (United States Atomic Energy Commission Technical Information Center, Oak Ridge, Tenn.) p. 1105.

Goldbeck, G.C., 1964, Spectrochemical Methods – Chemical Separations, in: Rodden, C.J., ed., Analysis of Essential Nuclear Reactor Materials, Ch. 12.2 (U.S. Government Printing Office, Washington, D.C.) p. 959.

Johnson, P.D., 1966, Oxygen-Dominated Lattices, in: Goldberg, P., ed., Luminescence of Inorganic Solids, Ch. 5 (Academic Press, New York) p. 287.

Jaworowski, R.J., J.F. Cosgrove, D.J. Bracco

and R.M. Walters, 1968, Spectrochim. Acta **23B**, 751.
Karyakin, A.V., L.I. Ankina, L.I. Bin, LeViet and Yu.I. Belyaev, 1970, Zh. Anal. Khim. **25**, 1898.
Kato, K., K. Takashima and T. Nakajima, 1972, Jap. Anal. **21**, 1154.
Kawaguchi, H., T. Nakajima, K.T. Takashima and Y. Ouchi, 1969, Bunko Kenkyu **18**, 299.
Kniseley, R.N., F.C. Laabs and V.A. Fassel, 1969, Anal. Chem. **41**, 50.
Larach, S., 1968, Anal. Chim. Acta **41**, 189.
Leverentz, H.W., 1950, An Introduction to Luminescence of Solids (Wiley, New York) p. 421.
Linares, R.C., J.B. Schroeder and L.A. Hurlbert, 1965, Spectrochim. Acta **21**, 1915.
Low, W., J. Makovsky and S. Yatsiv, 1964, Fluorescence of Rare Earth Ions Upon X-Ray Excitation, in: Quantum Electronics-Paris 1963 Conference (Columbia University Press, New York) p. 655.
Makovsky, J., W. Low and S. Yatsiv, 1962, Phys. Letters **2**, 186.
Nakajima, T., H. Kawaguchi, K. Takashima and Y. Ouchi, 1969, Bunko Kenkyu **18**, 210.
Nakajima, T., Y. Ouchi, J. Kawaguchi and K. Takashima, 1970, Bunseki Kagaku **19**, 1183.
Neunhoeffer, O.N., 1951, Z. Analyt. Chem. **132**, 91.
Ozawa, R., 1968, Bunseki Kiki **6**, 108.
Ozawa, L. and T. Toryu, 1968, Anal. Chem. **40**, 187.
Poluektov, N.S., R.A. Vikun and S.A. Gava, 1969a, Zh. Anal. Khim. **24**, 693.
Poluektov, N.S. and S.A. Gava, 1969b, Zavod. Lab. **35**, 1458.
Poluektov, N.S., N.I. Smirdova, N.P. Efryushina, 1971, Ind. Lab. (USSR) (Engl. Transl.) **37**, 338.
Pringsheim, P., 1949, Fluorescence and Phospherescence (Interscience, New York), p. 322.
Ratinen, H., 1971, Acta Polytech. Scand., Ser. Chem. **107**, 19.
Ratinen, H., 1972a, Phys. Stat. Sol. **12**, 175.
Ratinen, H., 1972b, Phys. Stat. Sol. **12**, 447.
Saranathan, T.R., V.A. Fassel and E.L. DeKalb, 1970, Anal. Chem. **42**, 325.
Sasaki, N., 1968, Bunseki Kagaku **17**, 1387.
Sato, M., H. Matsui and M. Tadao, 1971, Jap. Anal. **20**, 70.
Shand, W.A., 1968, J. Mater. Sci. **3**, 344.
Sinha, S.P., 1966, Complexes of the Rare Earths (Pergamon Press, London).
Smirdova, N.I., N.P. Efryushina, 1970, Ind. Lab. (USSR) (Engl. Transl.) **36**, 1501.
Smirdova, N.I., N.P. Efryushina and N.S. Poluektov, 1974, Zh. Anal. Khim. **29**, 1483.
Sweet, J.R., W.B. White, H.K. Henisch and R. Roy, 1970, Phys. Lett. **33A**, 195.
Takashima, K., T. Nakajima, H. Kawaguchi and Y. Ouchi, 1969, Bunko Kenkyu **18**, 262.
Tritten, J., 1974, Rpt. No. IS-5-644, Ames Laboratory, Iowa State University, Ames, Iowa 50011, U.S.A.
Trofimov, A.K., 1957, Bull. Acad. Sci, USSR. Phys. Ser. **21**, 754.
Vakhidov, Sh.A., B. Kaipov and G.A. Tavshunskii, 1970, Opt. Spectrosc. (USSR) (Engl. Transl.) **28**, 515.
Wichersheim, K.A., R.A. Buchanan and L.E. Sobon, 1968, Anal. Chem. **40**, 807.
Zaidel, A.N., 1952, Dokl. Akad. Nauk SSSR **85**, 591.

Handbook on the Physics and Chemistry of Rare Earths, edited by K.A. Gschneidner, Jr. and L. Eyring

Chapter 37F

NEUTRON ACTIVATION ANALYSIS

William V. BOYNTON*
Institute of Geophysics and Planetary Physics, University of California, Los Angeles, CA 90024, *USA*

Contents

Symbols

t = duration of radiation
$t_{1/2}$ = half life
β = mode of nuclear decay emitting electrons
β^- = electrons emitted by β decay
γ = mode of nuclear decay emitting photons
λ = decay constant = $ln\ 2/t_{1/2}$
Φ = particle flux
θ = fractional isotope abundance
σ = nuclear cross section

1. Introduction

Neutron activation analysis offers a highly sensitive technique for the quantitative determination of the rare earths. In some applications, it may also be one of the quickest and most convenient techniques. De Soete et al. (1972) have provided a detailed discussion of all aspects of neutron activation. A brief discussion will be provided here to enable the reader to assess the strengths and weaknesses of neutron activation analysis of rare earths. The principles of neutron activation analysis are quite simple. A sample is irradiated in a flux of neutrons, generally in a nuclear reactor, in which isotopes of the various elements absorb neutrons. Many of these reactions form radioactive products, the activity of which is measured and related to the amount of element present.

Once the sample is removed from the reactor, laboratory contamination will have no effect on the results. Only contamination by the indicating radionuclide will yield errors, but it is quite easy to monitor the laboratory and to remove any

*Present address: Department of Planetary Sciences University of Arizona, Tucson, AZ 85721, USA

Table 37F. 1.
Important interferences in neutron activation of rare earth elements

Element sought	Interfering element	Reaction			Interference[a] (%)	Note
First-order interference						
Sc	Ti	$^{46}Ti(n, p)^{46}Sc$			0.007	b
Y	Zr	$^{90}Zr(n, p)^{90}Y$			0.040	b
Y	Nb	$^{93}Nb(n, \alpha)^{90}Y$			0.003	b
La	U	$^{235}U(n, f)^{140}La$			0.22	c
Ce	U	$^{235}U(n, f)^{141}Ce$			15.	c
Ce	Pr	$^{141}Pr(n, p)^{141}Ce$			0.004	b
Nd	U	$^{235}U(n, f)^{147}Nd$			21.	c
Sm	U	$^{235}U(n, f)^{153}Sm$			0.05	c
Lu	Yb	$^{176}Yb(n, \gamma)^{177}Yb$	(β^-)	^{177}Lu	0.39	d
Second-order interference						
Ce	La	$^{139}La(n, \gamma)^{140}La$	(β^-)	$^{140}Ce(n, \gamma)^{141}Ce$	0.0006	e
Eu	Sm	$^{152}Sm(n, \gamma)^{153}Sm$	(β^-)	$^{153}Eu(n, \gamma)^{154}Eu$	0.0058	e
Sm	Eu	$^{151}Eu(n, \gamma)^{152m}Eu$	(EC)	$^{152}Sm(n, \gamma)^{153}Sm$	0.22	e
Gd	Eu	$^{151}Eu(n, \gamma)^{152m}Eu$	(β^-)	$^{152}Gd(n, \gamma)^{153}Gd$	94.	e
Ho	Dy	$^{164}Dy(n, \gamma)^{165}Dy$	(β^-)	$^{165}Ho(n, \gamma)^{166}Ho$	0.28	e
Lu	Yb	$^{174}Yb(n, \gamma)^{175}Yb$	(β^-)	$^{175}Lu(n, \gamma)^{176m}Lu$	0.0008	e

[a]Apparent concentration of element sought in pure interfering element. See Bereznai (1971) for other, less important, interferences. [b]From Lukens (1964) assuming equal thermal and fission spectrum flux. [c]From Allen et al. (1970). [d]Measured by the author. [e]Calculated for flux = 1×10^{14} n · cm^{-2} · s^{-1} and duration = 24 h using the method of Maenhaut and Op de Beeck (1970). Interferences decreases with decreasing flux and/or duration. See Op de Beeck (1969, 1970) for other, less important, interferences.

source of radioactivity. This is a distinct advantage of neutron activation analysis since it allows operations such as contamination-free mineral separations to be performed. The operations are, of course, constrained by the half-lives of the nuclides under study and the radiation dose to the investigator.

2. Relation of induced activity to the amount of element present

If, for example, a sample containing Dy is irradiated in a flux of neutrons, the following reaction will occur

$$^{164}\mathrm{Dy}(\mathrm{n},\gamma)\,^{165}\mathrm{Dy}\xrightarrow[t_{1/2}=141\ \mathrm{min}]{\beta^-,\gamma}{}^{165}\mathrm{Ho} \tag{37F.1}$$

in which ^{164}Dy absorbs a neutron and emits a prompt γ-ray to form ^{165}Dy, which decays by emission of a β^- particle and associated γ-rays with a half-life of 141 m. The disintegration rate or activity of ^{165}Dy is proportional to the amount of Dy in the sample.

The activity, A, is given by

$$A = N\varphi\sigma\theta(1 - \mathrm{e}^{-\lambda t}) \tag{37F.2}$$

where: N is the number of atoms of the element in the sample, Φ is the neutron flux, σ is the cross section of the target nuclide, θ is the fractional isotopic abundance of the target nuclide, λ is the decay constant of the product nuclide $= \ln 2/t_{1/2}$, and t is the duration of irradiation. Thus the activity can be measured, and with knowledge of the parameters in eq. (37F. 2), the amount of the element can be determined. In practice, however, this equation is not used for precise determinations since the cross section and the neutron flux are both functions of neutron energy and the activity measurement requires that the efficiency of the detector and decay scheme of the nuclide be known. The above equation will only yield results accurate to 10–20% under the best of circumstances; nuclides which have large peaks (resonances) in their cross sections at higher neutron energy require additional information to calculate the effect of resonance activation (Steinnes, 1971). This equation is most useful for calculating expected activities to aid in planning the irradiation conditions to achieve a desired sensitivity.

The multi-comparator method is commonly used for more precise work. In this method, standards containing known amounts of the elements of interest are irradiated with the samples and the induced activity is measured under the same conditions as the samples. The specific activity (observed count rate per unit mass of element) of a particular nuclide in the sample is then identical to the specific activity in the standard. Hence the mass of the element in the sample can be calculated. This method has the disadvantage of requiring the preparation and measurement of many standards in addition to the samples in each reactor irradiation. This handicap can be largely overcome, however, by mixing standards of the elements of interest to make a single composite standard which is

included with each irradiation. This is particularly applicable to the analysis of rare earths in natural systems where the ratios of elements are not widely variant.

The single comparator method, discussed by Simonits et al. (1975), is often a reasonable compromise between the absolute method and multi-comparator method. In this method, the specific activities of the elements of interest are measured relative to a comparator. In future irradiations, only the comparator is measured and is used to calculate the specific activities of the other elements. This technique can work to advantage when frequent irradiations are required and when the irradiation positions and detector geometries can be closely duplicated. Massart and Hoste (1968) found the single comparator method was advantageous for the determination of rare earths which were separated from each other and counted on NaI(T1) detectors. This method has little advantage where one is measuring rare earths which are not separated from each other since only one mixed rare earth standard needs to be irradiated. If multi-element standards are irradiated each time, the experimenter has the confidence that differences in reactor operation conditions, which are often out of his control, have not yielded differences in relative specific activities that could lead to errors.

3. Irradiation of samples and standards

One of the advantages of neutron activation analysis is that sample preparation requirements are generally minimal. Powdered samples may be weighed into polyethylene or high purity silica tubes and heat sealed, or individual chips may be wrapped Al-foil. Neither polyethylene nor silica produce an appreciable γ-ray activity and often samples can be counted with no further handling after the irradiation. Polyethylene, however, is not suitable for long irradiations at high flux. Aluminum activates to form 2.3 min ^{28}Al and generally has higher levels of impurities, but it can easily be removed before counting.

Errors arise in determinations by neutron activation if the specific activity in the sample is not identical to that in the standard. Two mechanisms can yield activities that are not strictly proportional to the amount of element present: local differences in flux and interfering reactions. Differences in neutron flux between sample and standard can arise from flux gradients which can be as high as several percent per centimeter. Corrections can easily be made, however, by irradiating wires which are later cut into pieces, weighed and counted to determine the flux as a function of position in the irradiation container.

Local flux differences can also arise from attenuation of neutrons in the sample itself. This problem is discussed in detail by Damburg et al. (1971) who show that for a sphere of radius r, the fractional decrease in flux averaged over the entire sphere is $\frac{3}{4}\, r\Sigma N_i\sigma_i$ where σ_i is the neutron absorption cross section and N_i the number of atoms of element i per cm^3. The absorption cross section of an element is not to be confused with the activation cross section, both of which are given in table 37F.2. Many of the rare earths have high absorption

cross sections, but since they are generally measured at trace levels they do not significantly attenuate the neutron flux. The attenuation is usually due to matrix elements. Common elements such as H, C, O, Mg, Al, and Si have cross sections less than one barn; thus in a matrix of these elements, attenuation is negligible for centimeter size samples. Such is not the case, however, for neutron activation of rare earth-rich materials. Gadolinium, for example, has the largest neutron absorption cross section of any element. An average attenuation of 1% occurs in a sphere of Gd_2O_3 which has a 0.12 μm radius and a mass of only 5×10^{-14} g.

Accurate corrections for self-shielding cannot easily be calculated from the cross sections because the attenuation of neutrons may not necessarily occur in the same energy region where activation is important. Precise corrections are better made on an empirical basis, or if possible, a smaller sample can be irradiated to reduce the effect of self-shielding. Empirical corrections can be determined by irradiating standards of the elements sought with various concentrations of the absorbing element to determine the correction factors. Alternatively the sample can be diluted to minimize the self-shielding although this can no longer be considered a non-destructive technique. Massart and Hoste (1968b) analyzed Lu in a 50 mg sample of gadolinite by dissolving the sample and irradiating an aliquot of a chemically separated rare earth solution. Known amounts of Co were added to the solution and the induced ^{60}Co activity was used to monitor self-shielding. Turkstra and Van Droogenbroeck (1975) reduced the effect of self-shielding in rare earth-rich carbonitites by diluting the powdered sample with pure quartz powder. Van den Bergh et al. (1970) found they could irradiate up to 400 μg of mixed rare earths when they were diluted with 200 mg of reactor grade graphite.

The other source of error which may occur in the activation of samples is from interfering reactions forming the indicator nuclide of another element. The more common interferences are presented in table 37F.1. The interference of Yb in Lu determinations is 1.6% and presents no difficulty in natural samples where the Yb/Lu ratio is reasonably constant. In samples with very high Yb/Lu ratios, Lu can be measured via 3.6 h. ^{176m}Lu. The interferences from ^{235}U fission products can often be important and thus require a knowledge of the U content of the sample to make an accurate determination of the light lanthanides. The corrections can be made by irradiating a pure U standard in which the apparent rare earth content is then measured. If U is high relative to the rare earths, it can be removed prior to activation. Alimarin et al. (1970a) and Bächmann and Lieser (1970) have determined rare earths in pure U by this technique and report detection limits down to picograms. Pre-irradiation concentration of the rare earths introduces blanks which are otherwise not important in neutron activation analysis.

The second-order reaction interferences have been calculated by the method of Maenhaut and Op de Beeck (1970). Op de Beeck (1969, 1970) has calculated interferences under different conditions and has included a number of other reactions that contribute interferences of less than a μg/g. The second-order interferences decrease nearly linearly with decreasing flux; hence irradiation

conditions can often be adjusted to eliminate the effect. Under most circumstances, interferences caused by Eu and Dy are the only ones that need to be considered and even these will often be negligible in natural samples. Alimarin et al. (1970b) measured rare earths at the 80–600 ng/g range in pure Eu_2O_3 by pre-irradiation removal of Eu in a Jones reductor. Removal of Eu eliminated both self-shielding and second-order reactions.

The point which needs to be emphasized is that only in rare circumstances are these sources of error important. In most samples the U content will be much lower than the rare earths and the matrix elements are often such that self-shielding is negligible. Because the rare earths are so sensitive, the flux and irradiation times can often be reduced to the point where second-order interferences are also negligible. In the vast majority of cases, the induced activity in the sample will be directly proportional to the amount of element present and will enable very accurate determinations over a wide range of concentration.

4. Measurement of induced activity

The second step in neutron activation analysis is the measurement of the induced radioactivity. A number of different techniques have evolved over the years to keep pace with changes in technology. The techniques can be divided into two groups: radiochemical neutron activation analysis (RNAA), a destructive technique in which various elements are separated after the irradiation, and instrumental neutron activation analysis (INAA), a non-destructive technique in which the activity in the sample is measured directly, relying on differences in γ-ray energy and half-life to discriminate the various nuclides.

4.1. *Radiochemical neutron activation analysis*

The most sensitive means of determining the rare earths is by RNAA. After irradiation the sample is mixed with non-radioactive carriers ($\sim$ 1 mg) of the elements of interest and then dissolved by a suitable means. The elements are then separated from each other and the radioactivity measured without interference from activity due to other elements. The activity can be counted on low background ($\sim$ 0.3 cpm) detectors which can count β particles with an efficiency of $\sim$ 40%. In this way, extremely low detection limits are possible as shown in table 37F.2. It may be noted that 1.6×10^{-17} g of Eu is about 60 000 atoms! The detection limits are, in principle, independent of the matrix in which the element is present if (1) other elements do not interfere in the formation of the nuclide as discussed in the previous section and (2) the element can be isolated in a time comparable to the half-life of the indicating nuclide.

The chemical separation is not required to be quantitative since the amount of carrier recovered can be assayed (e.g. by weighing a precipitate) to determine a chemical yield. Contamination from laboratory reagents will have a negligible

Table 37F. 2
Detection limit and nuclear properties of rare earths.[a]

Element	Absorption cross section (b)	Indicating nuclide	Activation cross section (b)	Isotopic abundance (%)	Half-life	Detection limit[b] separated elements ($\times 10^{-15}$g)	Detection limit[c] group separation ($\times 10^{-12}$g)	γ energies (keV)	γ interferences[d]
Sc	26	^{46}Sc	26	100	83.8 d	2.8	25	889, 1120	
Y	1.2	^{90}Y	1.2	100	64.0 h	6.5	–	–	
La	9.2	^{140}La	9.2	99.91	40.23 h	1.1	11	329, 487, 1596	488^{152}Eu(1.3%)
Ce	0.6	^{141}Ce	0.56	88.5	32.53 d	180	550	145	145^{125}Yb(5.9%)
		^{143}Ce	0.95	11.1	33.0 h	93	580	293	
Pr	11.5	^{142}Pr	11.5	100	19.16 h	0.83	360	1576	
Nd	49	^{147}Nd	1.3	17.2	10.99 d	160	520	91, 531	
		^{149}Nd	2.5	5.7	1.73 h	420	3600	211	211^{171}Er(1.1%)
Sm	5900	^{153}Sm	204	26.7	46.5 h	0.21	1.1	103	103^{153}Gd(73%)
Eu	4500	^{152m}Eu	3200	47.8	9.3 h	0.016	0.24	122, 842	120^{147}Nd(1.5%)
		^{152}Eu	5800	47.8	13. h	5.0	18.	122, 344, 1408	
		^{154}Eu	380	52.2	8.6 y	46	140	123	
Gd	49000	^{153}Gd	100	0.2	241.5 d	3700	9800	98, 103	98^{153}Sm(2.5%); 103^{153}Sm(100%)
		^{159}Gd	2.4	24.7	18.6 h	18	570	363	
Tb	25	^{160}Tb	25	100	72.3 d	9	57	87, 879	
Dy	940	^{165}Dy	2700	28.2	2.35 h	0.05	1.1	94, 546	94^{169}Yb(4%)
Ho	65	^{167}Ho	64	100	26.8 h	0.1	2.3	81	
Er	160	^{171}Er	5.7	15.0	7.52 h	35	160	296	296^{152}Eu(1.4%)
Tm	106	^{170}Tm	106	100	129. d	4.0	35	84	
Yb	37	^{169}Yb	3500	0.14	31. d	22	76	110, 177	
		^{175}Yb	65	31.8	4.10 d	0.96	59	396	398^{147}Nd(3%)
Lu	74	^{176m}Lu	16	97.4	3.69 h	1.6	9.7	88	
		^{177}Lu	2100	2.6	6.71 d	0.52	9.8	208	

[a]Compiled from data of Holden and Walker (1972) and Filby et al. (1970). [b]Assuming flux of 5×10^{14} n · cm^{-2} · s^{-1} for 100 h or saturation, whichever is less. Amount of element to give one disintegration per minute 5 h after irradiation (requires low background detectors). [c]Same irradiation and decay conditions as above but one count per second in the photopeak on a typical Ge(Li) detector with efficiency = 6/Energy (keV). [d]All γ-rays of rare earths with intensities of 1% or greater that occur within 2 × FWHM on a Ge(Li) having a resolution (FWHM) of 0.75 keV at 122 keV and 1.75 keV at 1332 keV.

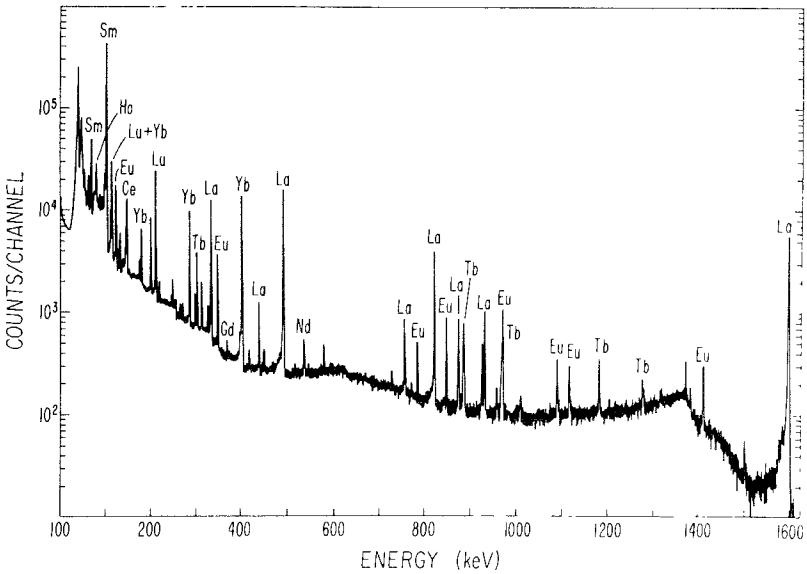

Fig. 37F. 1. Gamma-ray spectrum of neutron activated mixture of lanthanides in chondritic proportions counted 80 h after irradiation. Ten elements can be determined in this spectrum but Gd and Nd are determined with higher precision in counts made at different times in which the remaining four lanthanides can also be determined. The high resolution of Ge(Li) γ-ray detectors has obviated the need for separation of the lathanides from each other in most applications.

effect on the result since milligram quantities of carrier elements are being separated.

Counting of β activity is seldom required because all of the rare earths except Y emit γ-rays which are more conveniently measured. In early work, NaI(T1) scintillation detectors were used to measure γ-ray activity from rare earths which were separated from each other usually with ion exchange columns. Mosen et al. (1961) measured all sixteen rare earths in meteorites by this technique; only Y, Er, and Tm required β counting.

The introduction of the Ge(Li) semiconductor detector has had a tremendous impact on neutron activation. The NaI(T1) detectors typically have an energy resolution of $\sim 7\%$; currently available Ge(Li) detectors have about a factor of 40 better resolution. (See Crouthamel et al. (1970) for a discussion of both NaI(T1) and Ge(Li) detectors.) This improved resolution has allowed the activity of the rare earths to be determined in a group separated from other elements in the sample, but the tedious separation of the rare earths from each other is no longer required. The differences in γ-ray energies and half-lives of the various nuclides are sufficient that all of the rare earths except Y can be measured by this technique.

In Fig. 37F.1 is a Ge(Li) spectrum of a mixture of lanthanides in chondritic proportions counted 80 hours after irradiation. Ten elements can be determined in this single count although ^{159}Gd is usually determined in earlier counts with Pr, Dy and Er, and Nd is determined better in later counts, after La and Sm have decayed away, with Tm and ^{153}Gd. In table 37F.2 are listed the more prominent

γ-ray energies and associated interferences. In a mixture of lanthanides in natural samples most interferences are insignificant or, in the case of the mutual Sm and Gd interference, can be minimized by counting at different times.

The broad continuum is due to Compton scattered γ-rays of higher energy but poses no difficulty in the analysis except to decrease the signal to noise ratio. The Compton plateau can be reduced considerably with an anti-coincidence shield (Cooper and Rancitelli, 1972), but the use of this device does not appear to be widespread. The sensitivities in table 2 for a group separation can only serve as a guide, therefore, because the required count rate will depend on the extent of the Compton plateau due to other elements.

A number of workers have proposed various separation schemes for the rare earths, a number of which are noted in table 37F.3. Generally the group separation schemes separate the lanthanides from Sc because the high energy γ-rays of the latter generate a significant Compton plateau. In most samples, a single group of lanthanides is sufficient to determine all 14 elements. A number of schemes have been devised in which the lanthanides are subdivided into two or three groups which provides greater sensitivity at the expense of greater effort. Stiennes (1974) has devised a novel method to determine Y, without separation from the lanthanides, by β counting with various absorbers.

4.2. *Instrumental neutron activation analysis*

Improvements in γ-ray detectors have considerably improved the ease with which the rare earths may be determined non-destructively. The technique has lower sensitivities and a greater chance of interfering γ-rays than RNAA group separation because of the activity from other elements in the sample. From the INAA studies in table 37F.3, it is apparent, however, that the presence of other nuclides has not prevented the determination of rare earths in a wide variety of samples.

After irradiation, the samples and standards are counted on a Ge(Li) detector at various times over an interval of a month or more. Samples can be loaded into an automatic sample changer (Massoni et al., 1973) and data written onto magnetic tape or into an on-line computer (Webster, 1971) allowing many samples to be analyzed with little operator attention. If a sufficient number of rare earths can be determined for the intended application, INAA is nearly always preferred over RNAA. It has the added advantage that it is essentially non-destructive and it permits the determination of a number of other elements with nearly no additional effort. This advantage is particularly important for very rare samples such as extraterrestrial materials from which the maximum amount of information is desired.

5. Activation with non-thermal neutrons

Samples can be activated with epithermal neutrons, those in the process of being moderated to thermal energies, by irradiating in a Cd container which absorbs the thermal neutrons. Brunfelt and Steinnes (1973) have used epithermal neutron

TABLE 37F.3.
Selected methods and applications of neutron activation of rare earths.

Application	Technique[a]	Comments	References
Various	Various	General review of rare earth activation analysis	Bereznai (1971); Steinnes (1973)
Forensic	Various	Review, various elements	Guinn (1974)
		Rare earths in opium and cannabis	Henke (1976)
Art and archaeology	Various	Review, various elements	Perlman et al. (1972)
Coal and flyash	INAA	Review, various elements	Nadkarni (1975)
	INAA	Interlab comparison, 37 elements, 8 rare earths	Ondov et al. (1975)
Cmde oil	INAA	29 elements, 5 rare earths	Al-Shakristani and Al-Atyia (1973)
Atmospheric pollutants	INAA	Sc, La, Ce, Sm, Eu, Yb, Lu $10^{-4}-10^{-5}$ μg/m^3	Zoller and Gordon (1970)
	INAA	La, Ce, Sm, Dy stable activable tracers added to stack gas	Shum et al. (1974)
Bovine liver	RNAA, g	La, Ce, Pr, Nd, Sm, Eu, Yb La–0.5 ng/g	Gaudry et al. (1976)
Margarine	INAA	La and Sc	Owlya et al. (1974)
Uranium	RNAA, s	Preconcentration, La as low as 1 pg/g	Alimarin et al. (1970a)
	RNAA, s	Preconcentration, all 14 lanthanides	Bächmann and Liesen (1970)
Eu_2O_3	RNAA, s	Preconcentration, sensitivity to 1 ng/g	Alimarin et al. (1970b)
Tb_4O_7, Ho_2O_3, Yb_2O_3	RNAA, s	No preconcentration	Kubota (1974)
Ce	RNAA, g	Ce removed by oxidation	Rouchard and Revel (1973)
Pr_6O_{11}	Various	La only	Dybczynski et al. (1973)
Al	INAA	38 pg/g Sc	Blouri et al. (1973)
Y_2O_3	INAA	Preconcentration, no further processing	Bruijs (1973)
Steel	RNAA,s	La, Ce, Pr, Nd	Dogadkin et al. (1976)
	RNAA, s	La, 17 ng/g	Foldzińska and Dybczyński (1973)
	INAA	La, Ce, Nd, Sm in silicon-cerium alloy steel	Burianová and Frána (1976)
Ti alloys	INAA	Y, Nd, Sm, Tb, Er; 14 MeV 2 seconds/analysis	Broadhead et al. (1965)
Semiconductor materials	RNAA, g	Sc, La, Sm, Eu	Hoste (1974)
Glass	INAA	Sc, Eu, Tb, Yb at 10 ng/g	Kudo et al. (1975)
	RNAA, s	Reverse phase chromatography	McClendon and LaFleur (1973)

TABLE 37F.3. (Cont.)

Application	Technique[a]	Comments	References
Rare earth-rich minerals	RNAA	Preconcentration	Van den Bergh et al. (1970)
	INAA	Y and 12 lanthanides by X-ray counting	Mantel and Amiel (1973)
	INAA		Menon and Cuypers (1965)
Geologic and extraterrestrial materials	Various	Review	Haskin and Korotev (1973)
	INAA	10 lanthanides discusses interfering γ rays	Nadkarni (1976)
	INAA	11 lanthanides with low energy Ge(Li)	Rosenberg and Wilk (1971)
	RNAA, g	14 lanthanides; Tm difficult	Graber et al. (1970)
	RNAA, g	12 lanthanides	Denechaud et al. (1970)
	RNAA, g	Adsorbed on La oxalate	Csajka (1973)
	RNAA, ps	La–Tb, Ho–Lu	Higuchi et al. (1970)
	RNAA, ps	La–Nd, Sm–Tb, Yb–Lu	Brunfelt et al. (1974)
	RNAA, s	Separated by high-voltage electrophoresis, 2–3 h/analysis	Becker et al. (1975)
	RNAA, s	All 16 rare earths, β^- counted Y, Er, Tm	Mosen et al. (1961)
	INAA	Discussion of general considerations for epithermal neutron activation	Steinnes (1971)
	RNAA, g	9 lanthanides by epithermal activation	Brunfelt and Steinnes (1973)
	RNAA, g	Y by β^- counting in the presence of all lanthanides	Steinnes (1974)
	INAA	Y by 14 MeV neutrons, to 4 μg/g	Wänke et al. (1973)

[a]s = separated elements, ps = partial separation, g = single group (usually Sc removed).

activation for the determination of nine lanthanides in rocks by RNAA group separation and found it to be advantageous for Nd, Gd, Ho, Er and Lu. The technique has been discussed extensively by Steinnes (1971) with respect to geologic materials, but much of the information is applicable to other samples as well. The technique allows for the enhancement of some elements over others which may or may not work to advantage depending on the elements of interest.

Activation with fast neutrons from neutron generators has found little application for determination of rare earths because relative to thermal neutron

activation both cross sections and available fluxes are several orders of magnitude lower. It does, however, provide a non-destructive means of determining Y on the order of a few μg/g in lunar samples using 14 MeV neutrons (Broadhead et al. 1965). Wänke et al. (1973) measured Y.

6. Application

The rare earths have been determined in material as diverse as minerals, margarine and marijuana (Table 37F.3). Because many of the rare earths activate so readily, they are probably determined in many samples subjected to INAA even when the rare earth concentrations are not the primary goal of the analysis. It is, therefore, nearly impossible to collect a comprehensive list of all samples in which the rare earths have been determined. In Table 37F.3 procedures typical of those in common use are presented as well as novel applications or techniques.

The rare earths have proven useful in archaeology in determining the provenience of various artifacts (Perlman et al., 1972) and in forensic studies as a "finger print" to relate material found on the suspect with material from the scene of the crime (Guinn, 1974). The rare earths are often measured in air pollution studies at concentrations as low as 10^{-5} μg/m^3 (Zoller and Gordon, 1970), but are indicative of rock dust rather than environmental hazards. Shum et al. (1974) made use of the low toxicity and high sensitivity of the rare earths in an environmental study. They injected mixtures of inactive La, Ce, Sm and Dy into stack gases of various factories, and from INAA of air filter samples collected at various locations, they were able to monitor fallout patterns. Application of rare earths to geochemistry and cosmochemistry are well-known; a new application of RNAA of rare earths is to high temperature inclusions in meteorites in which Tm anomalies are indicative of fractionations between solids and gas in the early history of the solar system (Conard et al., 1975).

7. Summary

Neutron activation analysis is a useful technique for measurement of rare earths particularly at low concentration. All rare earths except Dy and Er activate to nuclides with sufficiently long half-lives that a nuclear reactor on site is not required. In many samples, the rare earths can be determined by INAA which lends itself well to automated procedures and has the additional advantages that many elements can be determined simultaneously and that it is non-destructive. It is inherently free from blanks (assuming pre-irradiation concentration is not required) and is usually free of interferences or matrix effects. The disadvantages are that one may have to work with high levels of radioactivity if maximum sensitivity is required and analyses based on long-lived elements may require several weeks before results are available.

References

Alimarin, I.P., A.Z. Miklishanskii and Yu.V. Yakovlev, 1970a, J. Radioanal. Chem. **4**, 45.

Alimarin, I.P., A.Z. Miklishanskii and Yu.V. Yakovlev, 1970b, J. Radioanal. Chem. **4**, 75.

Allen, R.O., L.A. Haskin, M.R. Anderson, O. Müller, 1970, J. Radioanal. Chem. **6**, 115.

Al-Shahristani, H. and M.J. Al-Atyia, 1973, J. Radioanal. Chem. **41**, 401.

Bächmann, K. and K.H. Lieser, 1970, Z. Anal. Chem. **250**, 172.

Becker, R., K. Buchtela, F. Grass, R. Kittl and G. Müller, 1975, Z. Anal. Chem. **274**, 1.

Bereznai, T., 1971, J. Radioanal. Chem. **9**, 81.

Blouri, J., M. Fedoroff and G. Revel, 1973, J. Radioanal. Chem. **17**, 185.

Broadhead, K.G., D.E. Shanks and H.H. Heady, 1965, Phys. Rev. **139**, B1525.

Bruijs, P.C.M.N., 1973, J. Radioanal. Chem. **16**, 115.

Brunfelt, A.O., I. Roelandts and E. Steinnes, 1974, Analyst **99**, 277.

Brunfelt, A.O. and E. Steinnes, 1973, J. Radioanal. Chem. **13**, 11.

Burianová, M. and J. Frána, 1976, Radiochem. Radioanal. Lett. **24**, 169.

Conard, R.L., R.A. Schmitt and W.V. Boynton, 1975, Meteoritics **10**, 384.

Cooper, J.A. and L.A. Rancitelli, 1972, Nucl. Instrum. Methods **99**, 125.

Crouthamel, C.E., F. Adams and R. Dams, 1970, Applied Gamma-Ray Spectrometry (Pergamon Press, Oxford).

Csajka, M., 1973, Radiochem. Radioanal. Lett. **13**, 151.

Damburg, N.A., L.L. Pelekis and L.F. Protasova, 1971, J. Radioanal. Chem. **9**, 329.

Denechaud, E.B., P.A. Helmke and L.A. Haskin, 1970, J. Radioanal. Chem. **6**, 97.

De Soete, P., R. Gijbels and J. Hoste, 1972, "Neutron Activation Analysis", John Wiley and Sons, New York.

Dogadkin, N.N., O.I. Kychinskaya, V.I. Tustanovsky, Yu.V. Yakovlev, 1976, J. Radioanal. Chem. **29**, 251.

Dybczynski, R., S. Sterlinski and C. Golian, 1973, J. Radioanal. Chem. **16**, 105.

Filby, R.H., A.I. Davis, K.R. Shah, G.G. Wainscott, W.A. Haller and W.A. Cassatt, 1970, Report WSUNRC-97(2), (Washington State University, Pullman, Washington).

Foldzińska, A. and R. Dybczyński, 1973, J. Radioanal. Chem. **229**.

Gaudry, A., B. Maziere, D. Comar and D. Nau, 1976, J. Radioanal. Chem. **29**, 77.

Graber, F.M., H.R. Lukens and J.K. MacKenzie, 1970, J. Radioanal. Chem. **4**, 229.

Guinn, V.P., 1974, Annu. Rev. Nucl. Sci. **24**, 561.

Haskin, L.A. and R.L. Korotev, 1973, in Analysis and Application of Rare Earth Materials, Michelsen, O.B. ed. (Universitetsforlaget, Oslo), pp. 183–211.

Henke, G., 1976, Proceedings of 1976 International Conference: Modern Trends in Activation Analysis, Munich, Germany.

Higuchi, H., K. Tomura and H. Hamaguchi, 1970, J. Radioanal. Chem. **5**, 207.

Holden, N.E. and F.W. Walker, 1972, Chart of the Nuclides, (General Electric Company, Schenectady, New York).

Hoste, J., 1974, J. Radioanal. Chem. **19**, 7.

Kubota, M., 1974, J. Radioanal. Chem. **23**, 73.

Kudo, K., K. Kobayashi and T. Shigematsu, 1975, J. Radioanal. Chem. **27**, 329.

Lukens, H.R., Jr., 1964, Report GA-5073 (Excerpt) (General Atomic, San Diego, CA).

Maenhaut, W. and J.P. Op de Beeck, 1970, J. Radioanal. Chem. **5**, 115.

Mantel, M. and S. Amiel, 1973, J. Radioanal. Chem. **16**, 127.

Massart, D.L. and J. Hoste, 1968a, Anal. Chim. Acta, **42**, 21.

Massart, D.L. and J. Hoste, 1968b, Anal. Chim. Acta, **42**, 15.

Massoni, C.J., R.V. Fones and F.D. Simon, 1973, Rev. Sci. Instrum. **44**, 1350.

McClendon, L.T. and P.D. LaFleur, 1973, J. Radioanal. Chem. **16**, 123.

Menon, M.P. and M.Y. Cuypers, 1965, Anal. Chem. **37**, 1057.

Mosen, A.W., R.A. Schmitt and J. Vasilevskis, 1961, Anal. Chim. Acta **25**, 10.

Nadkarni, R.A., 1975, Radiochem. Radioanal. Lett. **21**, 161.

Nadkarni, R.A., 1976, Radiochem. Radioanal. Lett. **25**, 159.

Ondov, J.M., W.H. Zoller, I. Omez, N.K. Aras, G.E. Gordon, L.A. Rancitelli, K.H. Abel, R.H. Filby, K.R. Shah and R.C. Ragaini, 1975, Anal. Chem. **47**, 1102.

Op de Beeck, J.P., 1970, J. Radioanal. Chem. **4**, 137.

Op de Beeck, J.P., 1969, J. Radioanal. Chem. **3**, 431.

Owlya, A., B. Parsa and F. Fakhruaezi, 1974, Radiochem. Radioanal. Lett. **16**, 355.

Perlman, I., F. Asaro and H.V. Michel, 1972, Annu. Rev. Nucl. Sci. **22**, 393.

Rosenberg, J. and H.B. Wiik, 1971, Radiochem. Radioanal. Lett. **6**, 45.

Rouchaud, J.C. and G. Revel, 1973, J. Radioanal. Chem. **17**, 167.

Shum, Y.S., W.D. Loreland and E.W. Hewson, 1974, Report RLO-2227-T7-28 from Nucl. Sci. Abstr., 1975, **31**, 19608.

Simonits, A., F. De Corte and J. Hoste, 1975, J. Radioanal. Chem. **24**, 31.

Steinnes, E., 1971, in Activation Analysis in Geochemistry and Cosmochemistry, A.O. Brunfelt and E. Steinnes, eds., (Universitetsforlaget, Oslo) pp. 113–128.

Steinnes, E., 1973, in Analysis and Application of Rare Earth Materials, Michelsen, O.B., ed. (Universitetsforlaget, Oslo) pp. 165–181.

Steinnes, E., 1974, Talanta, **21**, 178.

Turkstra, J. and M.A. Van Droogenbroeck, 1975, J.S. Afr. Chem. Inst. **28**, 61.

Vanden Bergh, F., F. Adams and J. Hoste, 1970, J. Radioanal. Chem. **4**, 347.
Wänke, H., H. Baddenhausen, G. Dreibus, E. Jagoutz, H. Kruse, H. Palme, B. Spettel and F. Teschke, 1973, Proc. Lunar Sci. Conf. 4th, 1461.
Webster, R.K., 1971, in Activation Analysis in Geochemistry and Cosmochemistry, A.O. Brunfelt and E. Steinnes, eds., (Universitetsforlaget, Oslo) pp. 183–197.
Zoller, W.H. and G.E. Gordon, 1970, Anal. Chem. **42**, 257.

Handbook on the Physics and Chemistry of Rare Earths, edited by K.A. Gschneidner, Jr. and L. Eyring

Chapter 37G

MASS-SPECTROMETRIC STABLE-ISOTOPE-DILUTION ANALYSIS FOR LANTHANIDES IN GEOCHEMICAL MATERIALS

Shuford SCHUHMANN* and John A. PHILPOTTS*
Laboratory for Extraterrestrial Physics, NASA/Goddard Space Flight Center, Greenbelt, Maryland 20771, USA

Contents

Symbols

e = charge of electron
i_N = atomic abundance of a particular isotope in the sample
i_S = atomic abundance of a particular isotope in the spike
I.P. = first ionization potential (of substance analyzed) (V)
k = Boltzmann's constant
k_N = abundance in sample of isotope enriched in the spike
k_S = abundance in spike of isotope enriched in the spike
n^+ = number of positive ions
n_0 = number of neutral atoms
R_{ik} = resultant ion-current ratio
T = surface temperature (K)
W = surface work function (V)

1. Introduction

Stable isotope dilution mass-spectrometry (MSID) is the most accurate technique for determining lanthanide abundances in geochemical materials. The superior quality of the method may be attributed principally to the inherent sensitivity of mass-spectrometers, and to the use of the "ideal" internal standard, namely, an artificially enriched isotope of each element to be determined. The utilization of isotopic internal standards virtually eliminates such potential analytical problems as quantitative recovery and instrument calibration. The sensitivity of the mass spectrometer is such that the lower limit of measurable abundance is usually controlled by the purity of the reagents used in preparing the sample for analysis.

*Present address: Hawaii Institute of Geophysics, University of Hawaii, Honolulu, Hawaii 96822, USA

We will summarize in this chapter the fundamental theory and scope of the MSID method, describe in some detail the chemical preparation and the mass spectrometry of the samples, and conclude with a brief discussion of data calculation and quality.

2. Theory and scope

Inasmuch as the method depends upon mixing natural and synthetic isotopic compositions, MSID is applicable theoretically to all polyisotopic elements for which an adequate ion current can be generated. Thus all the even Z lanthanides, Ce, Nd, Sm, Gd, Dy, Er and Yb, and the odd Z lanthanides La, Eu, and Lu may be analyzed by this technique. Isotope dilution, theoretically, can be used in determining abundances of the monoisotopic rare earths, Sc, Y, Pr, Tb, Ho, and Tm, by utilizing artificial radioactive (unstable) isotopes; this will not be pursued further in the present chapter.

The technique is based upon measuring mass spectrometrically a mixture containing (a) a known amount of "spike" of the element of interest with known artificially enriched isotopic composition, and (b) the sample with an unknown amount of the element of "natural" (known) isotopic composition. In special cases the "natural" isotopic composition can be determined on a separate aliquant. In most geochemical studies, however, assumption of the natural composition is completely adequate. The isotopic composition of the "spike" is determined mass spectrometrically.

The fundamental MSID equation is:

$$R_{ik} = (i_N + i_S)/(k_N + k_S) \qquad (37G.1)$$

where R_{ik} is the resultant ion-current ratio measured by mass spectrometry, i_N and i_S are the atomic abundances of a particular isotope in the sample and spike respectively, and k_N and k_S are the abundances in the sample and spike respectively of the isotope which is enriched in the spike.

Optimum sensitivity and accuracy in determining the abundance of the element in the sample is obtained when R_{ik} is near the geometric mean of the isotopic ratio in the sample (i_N/k_N) and in the spike (i_S/k_S) (Webster, 1960). This situation can be achieved (if the unknown abundance can be estimated approximately) through judicious choice of sample to spike proportion. When two or more independent ratios can be measured for a particular element then the proportion used will be a compromise. Any loss in determination quality is compensated by having the internal check of independent results. Discrepant results are a sensitive indicator of isobaric interferences.

Equation (37G.1) is an idealization. It is assumed that the ion current ratio measured by the detector is the same as that generated at the source. This is a reasonable assumption in the case of a Faraday-cup detector but less so for an electronmultiplier detector, which is usually mass dependent. It is further assumed that the ion currents from the source identically reflect the isotopic

composition of the mixture being analyzed. This latter assumption is dependent on the characteristics of the ionization process, which we now briefly consider.

Isotope dilution mass-spectrometry for the lanthanides utilizes a surface ionization (thermal emission) source (Inghram and Hayden, 1954; Duckworth, 1960; Webster, 1960; White, 1968; and Chait, 1972). For ionization at a heated metallic surface or filament the ionization efficiency, according to Langmuir and Kingdon (1925), is given by

$$n^+/n^0 \propto \exp\,[e(W - \text{I.P.}/kT]. \tag{37G.2}$$

Inghram and Hayden (1954) describe the behavior predicted by eq. (37G.2) in the following terms:

(1) The ionization potential of the material to be analyzed must be low; i.e. $<$ about 9 V.

(2) The work function of the ionizing surface must be high; and

(3) Substances having ionization potentials higher than the work function should be in refractory form in order to take advantage of the temperature dependence of the efficiency equation. This applies for single filament ion sources where vaporization and ionization are inseparable. It should be noted that the lanthanides can be analyzed acceptably on a single filament, particularly as the oxide. However, use of double or triple filaments provides more control of the vaporization-ionization process and more readily yields strong, stable signals with minimum interference (Inghram and Chupka 1953).

Materials used for filaments in surface ionization are chosen with regard to high value of work function and high burn-out temperature. Rhenium, tungsten and tantalum meet these requirements. Platinum has a higher work function but a lower melting point. Differences in ionization potential and volatility between the lanthanides and their monoxides are used to avoid interelemental interferences and simplify data collection by allowing the measurement of only one or two elements at a given temperature. Differences in ionization potential between the isotopes of an element are negligible. The rate of ionization of a given element or substance can be controlled nearly constant by adjustment of filament temperature(s). Thus, the decay or growth rates of ion currents of all the isotopes of an element follow paths in proportion to their relative abundances. The ionization efficiency for an element (or its monoxide) at a given temperature is not predictable accurately, but the use of the spike provides the requisite internal standardization. It should be noted that surface ionization usually prevents ionization of gases, organic and organometallic compounds. The instrument background is correspondingly free from such interferences.

Although thermal emission sources provide equal ionization efficiency of isotopes of a given element, fractional vaporization may occur. This is one of the several possible sources of mass fractionation in the technique, which must be corrected in order to obtain high quality results. Mass discrimination (relatively constant) and thermal fractionation (variable, at the filament) effects may be minimized by one or more of the following:

(1) By scanning electromagnetically at constant ion accelerating potential.

(2) The use of a triple filament source (instead of a single) because it is much freer from mass discrimination (Palmer, 1956, in Wilson and Daly, 1963) and because its potential for higher sensitivity may obviate the necessity for an electron multiplier detector instead of a Faraday-cup (Inghram and Chupka, 1953).
(3) If scanning electrostatically, by using correction factors derived from analysis of a substance of known isotopic composition, e.g. Dietz et al. (1962).
(4) By reconciling, as a function of mass, different abundance results from two or more independently measured ratios, e.g. Lugmair et al. (1975).
(5) By programmed increase of filament temperatures according to a predetermined minimum fractionation plan, with time integration of individual ion currents in order to measure maximum possible amounts of each isotope.
(6) By conversion to a refractory compound of higher molecular weight, thereby reducing the effects of fractional vaporization from the filament.

Potentially far more troublesome than mass fractionation in the analysis for lanthanide abundances in general, is the problem of interference from adjacent elements or compounds of lighter elements. This problem may be obviated by separating each lanthanide prior to mass-spectrometry. More commonly, the lanthanides are separated into two or more groups, alleviating compound interferences, and the individual spectra are corrected for contributions from adjacent elements.

3. Sample chemistry

A typical analytical procedure for determination of lanthanide abundances (e.g. Thomas et al., 1966; Schnetzler et al., 1967; Masuda , 1966, 1968a, 1968b; 1973; Nakamura and , 1973; 1974; Nagasawa, 1970) consists of these principal steps:
(1) Weighing of sample,
(2) Addition of measured amount of spike,
(3) Acid decomposition, homogenization, concentration,
(4) Partial separation of elements by ion exchange chromatography,
(5) Mass spectrometric analysis.

We now consider in somewhat more detail this typical procedure with occasional mention of possible modifications or alternatives. The first step is the weighing. Generally finely powdered rock samples of 10 to 100 mg provide adequate representation and sensitivity. Then comes addition of the spike. This is commonly measured by a standardized delivery pipette of a few ml volume or gravimetrically (e.g. Loubet et al., 1972a). Inasmuch as a number of lanthanides are to be determined, it is laborious to add spikes element by element. Hooker and co-workers (1975), for example, utilize two spike solutions: La, Ce, Nd, Sm, Eu, and Gd; Dy, Er, Yb, and Lu, Gast and co-workers (1970) used three: La plus Ce, Nd, Sm, Eu, and Gd; and Dy, Er, Yb, and Lu. We have found that a single composite spike solution provides eminently acceptable results over a wide

range of lanthanide sample abundances, both absolute and relative. The isotopic composition of the composite spike is determined by mass spectrometry. The concentrations in the spike are standardized mass spectrometrically against individual solutions each containing a known concentration of a normal lanthanide. In preparing such standard solutions Gast et al. (1970), Masuda et al. (1972) and Hooker et al. (1975) have noted that oxides of the lighter lanthanides La–Eu must be freed of chemisorbed carbon dioxide and water (which may amount to 15% by weight) by heating to constant weight at about 800°C. Nguyen et al. (1973b) have studied in detail lanthanide oxides as used for the preparation of standard solutions. Precise calibration of these solutions is possible using EDTA which has itself been standardized against a zinc chloride solution prepared from 99.999% pure Zn metal. Lanthanide standards and spikes are stable over long periods in 1 N HCl solutions in polyethylene bottles.

Returning to the typical procedure, $HClO_4$ and HF are added to the sample plus spike (which may have been dried) in a platinum or other inert dish, and dissolution proceeds. Because of a more favorable blank, Loubet et al. (1972a) utilize H_2SO_4 instead of $HClO_4$ to oxidize organics and encourage oxide dissolution. Typically, a fraction of a ml of $HClO_4$ is used, and about 10 ml of HF. If the sample is carbonate instead of silicate, then HCl is substituted for HF. Dissolution is speeded by heating, stirring, and further additions of acids or water if required. Silicon is eliminated as the fluoride by evaporation(s) to dryness in a suitable fume hood. The involatile residue is redissolved in 2 N HCl. After further evaporation, the remaining solution is brought up with water to a final volume of about 10 ml for application to an ion exchange column.

The lanthanides are separated from the major elements, from each other groupwise, and are further concentrated by differential elution from an ion exchange column of Dowex 50W-X8 200–400 mesh ion exchange resin. Column dimensions typically range from several mm inside diameter by several cm in length up to an order of magnitude greater. The smaller columns require less volume of elutant and yield lower blanks. Conveniently, the tubing length is made twice the column height to provide free space over the resin to accept portions of elutant liquid (which passes through the column under gravity). Typically, the major elements are eluted with 2 N HCl. The lanthanides are eluted with 6 N HCl as three successive groups in the order heavier, intermediate, light (i.e. decreasing Z). By collecting three fractions, the subsequent mass spectrometry is simplified. The first fraction, bearing chiefly the heavier lanthanides, yields spectra relatively free of compounds of the lighter elements. The second is analyzed for Ce, Nd, Sm and Eu. The third yields GdO+ spectra free of Yb^+ (see below) and check determinations for Ce and Nd. The volume of acid required for group separations is determined empirically. The ionic strength of the eluants may be controlled by accurate measurements of specific gravity with an hydrometer. Finally, the eluted fractions are evaporated to dryness on a steam bath. The plastic beakers containing the separated fractions may be covered and stored until needed for mass spectrometric analysis.

Shimizu (1974) described ion exchange columns and procedures for eight

lanthanides similar to that of Schnetzler et al. (1967). Hooker et al. (1975), Loubet et al. (1972a, 1972b), Masuda (1968b), Nakamura and Masuda (1973), and Nguyen et al. (1973a) describe procedures which include determinations of lanthanum. This element, not measured by us, requires quantitative separation to avoid serious mass spectrometric interference from Ba and Ce. Alternate methods of ion exchange separation of the lanthanides and other R's are listed by Walton (1974). Sisson and Mode (1974) discuss practical aspects of R's separations with emphasis on speed and ease of operation.

4. Mass spectrometry

In preparation for each sample analysis, the mass spectroscopist performs a background scan subtending the lanthanide mass range with source filaments at temperatures near rupture or burn out. The background spectrum decreases with time, usually to negligible, except perhaps for ^{138}Ba. This isobaric interferant for elemental La spectra must be controlled if it or La is included in the analysis. One or more of the following has proved expedient: (1) Lower the filament temperature to reduce or eliminate Ba; do not exceed this temperature in measuring the La or Ba spectra. (2) Before the background run, wash the filament assembly source region and slits with demineralized water and pure acetone and dry with a heat gun. (3) Pre-clean the filaments in a separate apparatus by ion pumping.

Nguyen et al. (1973a) describe analysis of very small samples (<1 mg) without prior separation on columns. They avoid isobaric interferences by using "well defined" filament (single) temperatures to separate and measure "pure M^+ or MO^+ spectra" of each element.

For minimum interference between the elements, the heavier group is analyzed first. The minute residue from the column fraction is dissolved in 2 drops of 2 N HCl (or HNO_3). One drop of this solution is deftly transferred with a quartz micropipette onto the previously cleaned side (sample) filaments of a triple filament, solid source mass spectrometer, (Inghram and Chupka 1953, Roboz 1968, White 1968, and Chait 1972). For this operation, the center or ionizing filament is withdrawn from its normal position to keep it free of sample. The sample is dried on the side filaments by heating each in turn at about 1.5 amps (for rhenium ribbon 0.025×0.76 mm). Completion of drying is conveniently indicated by a sudden drop in filament current corresponding to an increase in resistance with temperature. This is preceded sometimes by the emission of visible fumes.

The filament assembly is re-installed in the source chamber of the mass spectrometer and the chamber and analyzer evacuated to 10^{-6} torr or less. The center or ionizing filament is heated to about 2000°C, marked by a small but measurable signal of ^{185}Re and ^{187}Re. The mass range between ^{138}Ba and ^{185}Re is scanned and rescanned while the operator is progressively increasing the current in the side (sample) filaments. Volatilization-ionization of one or more of the

elements sought is observed by the appearance of ion currents at recognizable mass numbers. In order of increasing temperature (and depending often on the preceding ion-exchange chromatography), the elements may appear in the order: Ba, Eu, Yb, Dy or Sm, Er, Gd, Lu and Hf. The elements measured first are those that vaporize at lower side filament temperatures. Their ion currents should be measured (and re-measured) first, since evaporation will cause them to decay more rapidly. For example, Ba, if present, usually yields a strong signal before Eu appears; Eu may appear and die before Yb, etc.

For each element the rate of ionization is controlled as near constant as possible by adjustments of the heating currents through the sample and ionizing filaments. In general, the most constant signal strength is obtained by low sample currents with highest permissible ionizing filament currents (temperatures). The unavoidable decay or growth of signal intensity with time is compensated for by always pairing an up-mass scan of a spectrum with a down-mass scan measured immediately afterwards. The data may be grouped into as many pairs as desired, for statistical treatment of reproducibility. A dozen pairs of spectra per element is usually adequate. Each scan always includes the ion current from the isotope which is most enriched in the spike and at least one other current engendered principally by a natural isotope of that element. For a lanthanide element with three or more isotopes, interference by compounds of lighter elements is often readily apparent during the run as abnormal ion current ratios of two or more masses expected to be dominated by the natural isotopes of the element. The scans must include a monoelemental mass of any neighboring element that is a potential isobaric interferant to the element determined. The table lists the isotopic weights and natural percentage abundances of the elements to be determined or that may interfere. The analyst will need a similar table of the abundance distributions for the particular spike solutions he employs.

On depletion of the most refractory element, Lu or Gd, the light fraction is introduced to analyze for any lights not yet measured (and for Gd as the monoxide, if the elemental Gd spectra have shown evidence of monoxide interferences from Ce, Pr and Nd at masses 156, 157, 158 and 160, or BaF at 157. (Occasionally, the heavy fraction yields interference-free Gd spectra on initial reheating of the ion source after it has been cooled to ambient.) The light fraction, dissolved in 2N HNO_3, is applied equally to the center and sample filaments (in normal proximity to each other) and air dried by heating each filament in turn. The deposit on the center only is oxidized by further heating at very dull red for 1–2 minutes.

On replacement of the filament assembly in the mass spectrometer, the center filament only is heated to about 1450°C (rhenium) to obtain GdO^+ spectra at masses 171–176 inclusive. Mass 177 is also scanned to permit later calculation of isobaric DyO interferences. With column separations normal, the GdO^+ spectra are much stronger than the Yb spectra and interference is negligible. But if the GdO^+ spectra are too weak for accurate measurement, resort may be had to introducing the intermediate fraction, richer in both Gd and Yb, after the present sample filaments have been analyzed for their contents of the light lanthanides.

To measure the lights, the center is heated to 2000°C to exhaust its load then provide optimum ion yield for the vapors from the side filaments, now heated. Ce determinations often require special care because of a potentially large ^{142}Nd interference. (The natural abundance ratio $^{142}Nd/^{143}Nd > 2$.) Usually, however, Ce is more refractory than Nd; so its spectra persist while the Nd disappears. Also, it is often measurable as the monoxide below the appearance temperatures of Gd elemental spectra. NdO^+ may then coexist and have to be taken into account.

The mass spectrometry of the intermediates for GdO^+ is similar to that for the lights, described above. Gd and Yb should both be present in greater amount than in the lights, but Yb usually disappears preferentially to the more refractory GdO^+. This fraction, too, may be examined for the other lanthanides and spectral measurements made if appropriate.

5. Calculation of results

The spectral data collected as described above are corrected for all the known instrumental biases, discriminations, non-linearities (e.g., mass dependence of an electron multiplier, if used, any significant calibration corrections of the ion measuring system throughout its dynamic range) and for the isobaric inter-elemental interferences. With our instrumental procedure, only the latter correction is significant. It is achieved by subtraction of numbers obtained by ratioing from a monoisotopic ion current of the interfering species to the mass number with which it is interfering. The derived values of monoelemental ion currents and appropriate ratios, "R_{ik}" (see eqs. (37G.1) and (37G.3) are used in all subsequent calculations for the amount of the element.

The atomic abundances in eq. (37G.1) may be written in expanded form in terms of the product of the fraction or percent of the element consisting of the isotope i (similarly, k) in the sample or spike, times the atomic amount of the element in the sample (N) or spike (S) respectively. Equation (37G.1) may then be rewritten:

$$R_{ik} = [N(\%i)_N + S(\%i)_S]/[N(\%k)_N + S(\%k)_S]. \tag{37G.3}$$

Equation (37G.3) may be rearranged to give the atomic ratio of normal to spiked element in the mixture.

$$N/S = [(\%i)_S - R_{ik}(\%K)_S]/[R_{ik}(\%K)_N - (\%i)_N] \tag{37G.4}$$

Subscript N values may be obtained from isotope abundance data (e.g. see table); subscript S values, for the spike, are generally determined empirically. Typically, the amount of the lanthanide in the unknown is given in ppm by weight; so that a factor consisting of the ratio of the atomic weight of normal and spike element must be applied. Hence:

$$\text{ppm by weight} = \frac{N}{S}\frac{\text{(weight factor)(spike ml)}(\mu\text{g/ml of spike})}{\text{(weight of sample in g)}}. \tag{37G.5}$$

The calculations described are simple but lengthy, especially when corrections for interference are required. This tedium may be lessened by the use of automatic data processing. In any case, the values obtained are examined critically for errors and inconsistencies. In particular, if the lanthanide yields polyisotopic results, these are compared, more weight being given to values judged to have the least potential for interference. Likewise, more weight is attached to values derived from the more abundant natural isotopes of the element.

6. Quality of data

It is convenient to discuss the quality of the data obtained in terms of analytical blank, precision and accuracy. The blank arises from lanthanide contamination in the reagents used in the chemistry. We routinely process a blank (i.e. sample free) with every set of samples. Utilizing modest precautions (e.g. reagent HF, once-distilled HCl and H_2O, etc.) blanks may be readily reduced to the nanogram level. Inasmuch as lanthanides in geochemical samples typically are at the microgram level, blank corrections are seldom necessary.

The accuracy of the technique is dependent on the care taken in preparing standard solutions or titrating same. In general, accuracy is expected to be of the same order as precision. In routine geochemical abundance work a precision of several percent is typically achieved. Shimizu (1974), for example considers the method reliable to within 3–5% relative. Hooker et al. (1975) report the accuracy of the method as ±2%, in general. Masuda et al. (1973) estimate relative precision and accuracy for trace lanthanides at better than 1 and 2% respectively. A similar conclusion was reached by Nakamura (1974) in comparing interlaboratory results on standard rock BCR-1. These levels of precision are not intrinsic to the technique but are adequate for most geochemical abundance studies. Recently, however, new demands have arisen in connection with the Sm–Nd age dating technique. Here, abundance accuracies of a tenth of a percent are reported (e.g. Lugmair et al., 1975). Mass spectrometer stable isotope dilution continues to be refined into an ever more exact technique for obtaining lanthanide abundances in geochemical materials.

Appendix

Relative abundances of the isotopes of the polyisotopic lanthanides (and barium, hafnium).

Z	Atomic weights and percentage abundances						
Ba	129.9	131.9	133.9	134.9	135.9	(136.91)	137.90
56	0.101%	0.097%	2.42%	6.59%	7.81%	11.32%	71.66%
La	S137.9	(138.906)					
57	0.089%	99.911%					
Ce	135.9	137.9	(139.91)	S141.91			
58	0.193%	0.250%	88.48%	11.07%			
Nd	141.91	(142.91)	143.91	S144.91	145.91	147.9	149.9
60	27.11%	12.17%	23.85%	8.30%	17.22%	5.73%	5.62%
Sm	143.9	146.91	147.91	S148.92	149.9	151.92	153.92
62	3.09%	14.97%	11.24%	13.83%	7.44%	26.72%	22.71%
Eu	150.92	S152.92					
63	47.82%	52.18%					
Gd	151.9	153.9	S(154.92)	155.92	156.92	157.92	159.93
64	0.200%	2.15%	14.73%	20.47%	15.68%	24.87%	21.90%
Dy	156.0	158.0	159.9	(160.93)	161.93	S162.93	163.93
66	0.052%	0.090%	2.29%	18.88%	25.53%	24.97%	28.18%
Er	161.9	163.9	(165.93)	S166.93	167.93	169.94	
68	0.136%	1.56%	33.41%	22.94%	27.07%	14.88%	
Yb	167.9	169.9	(170.94)	171.94	S172.94	(173.94)	175.94
70	0.135%	3.03%	14.31%	21.82%	16.13%	31.84%	12.73%
Lu	174.94	S175.9					
71	97.41%	2.59%					
Hf	174.0	175.9	(176.94)	177.94	178.95	179.95	
72	0.18%	5.20%	18.50%	27.14%	13.75%	35.24%	

$^{12}C = 12.00000$ A.U.

An "S" preceding an atomic weight indicates the isotope enriched in our spike. The underlined atomic weights are measured mass spectrometrically and are chosen to be relatively free of isobaric interferences from other elements, wherever possible. The masses enclosed in parentheses are measured during the determination of an adjacent lanthanide in order to correct it for isobaric interferences. Barium and Hafnium are listed to permit calculation of their interferences with the isotopes of contiguous lanthanides.

References

Chait, E.M., 1972, Anal. Chem. **44**, 86A.

de Bievre, P.J. and Debus, G.H., 1965, Nucl. Instrum. Methods **32**, 224.

Dietz, L.A., C.F. Pachuki, G.A. Land, 1962, Anal. Chem. **34**, 709.

Gast, P.W., N.J. Hubbard and H. Wiesmann, 1970, "Chemical Composition and Petrogenesis of Basalts from Tranquillity Base", Proc. Apollo 11 Lunar Sci. Conf., Geochim. Cosmochim. Acta Suppl. 1, Vol. **2**, (Pergamon, NY), 1143.

Hooker, P.J., R.K. O'Nions, and R.J. Pankhurst, 1975, Chem. Geol. **16**, 189.

Inghram, M.G., and R.J. Hayden, 1954, Mass Spectroscopy, Nuclear Science Series Rept. No. 14, University Microfilms Ltd., High Wycomb, England, Ann Arbor, Mich., USA, pp. 30.

Inghram, M.G. and W.A. Chupka, 1953, Rev. Sci. Instrum. **24**, 518.

Langmuir, I. and K.H. Kingdon, 1925, Proc. Roy. Soc. (London) **107**, 61.

Loubet, M., J.L. Birck, and C.J. Allegre, 1972a, Earth Planet Sci. Lett., **17** #1, Luna 20 Sect., 19–23.

Loubet, M., M. Bernat, M. Javoy and C.J. Allegre, 1972b, Earth Planet. Sci. Lett. **14**, 226.

Lugmair, G.W., N.B. Scheinin and K. Marti, 1975, "Sm–Nd age and history of Apollo 17 basalt 75075: Evidence for early differentiation of the lunar exterior", Proc. 6th Lunar Sci. Conf., Geochim. Cosmochim. Acta Suppl. 6, Vol. **2** (Pergamon, N.Y.), 1419.

Masuda, A., N. Nakamura and T. Tanaka, 1973, Geochim. Cosmochim. Acta **37**, 239.

Masuda, A., N. Nakamura, H. Kurasawa and T. Tanaka, 1972, "Precise Determination of Rare Earth Elements in Apollo 14 and 15 Samples", Proc. 3rd Lunar Sci. Conf., Geochim. Cosmochim. Acta Suppl. 3, Vol. **2**, (MIT Press, Cambridge), 1307.

Masuda, A., 1968a, Earth Planet. Sci. Lett. **4**, 284.

Masuda A., 1968b, Geochem. J. **2**, 111.

Masuda, A., 1966, Geochem. J. **1**, 11.

Morrison, G.H., 1971, Anal. Chem. 43, 37, 25A.

Nagasawa, H., 1970, Earth Planet. Sci. Lett. **9**, 359.

Nakamura, N., and A. Masuda, 1973, Earth Planet. Sci. Lett. **19**, 429.

Nakamura, N., 1974, Geochim. Cosmochim. Acta **38**, 757.

Nguyen, L.-D., M. de St. Simon, G. Puil, and Y. Yokoyama, (1973a), "Mass Spec. Anal. of R.E. Elements Contained in Very Small Quantities of Lunar Samples", Proc. 10th R.E. Research Conf., (Kevane, C.J., T. Moeller, (eds.), Arizona State Univ., Tempe, USA) 1068.

Nguyen, L.D., M. de St. Simon, M. Foex, J.P. Coutures, P. Gerdanian (1973b) "Analyses of R.E. Oxides Used in the Preparation of Std. Solutions", Proc. 10th R.E. Research Conf., (Kevane, C.J., T. Moeller, eds.), (Arizona State Univ., Tempe, USA) 1056.

Roboz, J., 1968, Mass Spectrometry Instrumentation and Techniques, (Interscience Publishers Div. of John Wiley & Sons, NY, London, Sydney, Toronto) p. 127.

Schnetzler, C.C. and J.A. Philpotts, 1970, Geochim. Cosmochim. Acta **34**, 331.

Schnetzler, C.C., and J.A. Philpotts, 1971, "Alkali, Alkaline E. and R.E. Concentrations in Some Apollo 12 Soils, Rocks, Separated Phases", Proc. 2nd Lunar Sci. Conf. Vol. 2, (MIT Press, Cambridge) p. 1101.

Schnetzler, C.C., H.H. Thomas and J.A. Philpotts, 1967, Anal. Chem. **39**, 1888.

Shimizu, N., 1974, Carnegie Institution Year Bk. **73** (Carnegie Institution, Dept. of Terr. Mag.), 941.

Sisson, D.H., and V.A. Mode, 1974, Proc. 11th R.E. Research Conf., Section B-4, (Traverse City, Mich., USA) 29.

Thomas, H.H., C.C., Schnetzler and J.A. Philpotts, 1966, Trans. Amer. Geophys. Union **47**, 217.

Walton, H.F., 1974, Anal. Chem. **46**, 402R.

Webster, R.K., 1960, "Mass Spectrometric Isotope Dilution Analysis", Methods in Geochemistry, (Smales, A.A., and L.R. Wager, eds.), (Interscience Publishers Inc. NY; Ltd., London) p. 202.

White, F.A., 1968, "Surface Ionization", Mass Spectrometry in Science and Technology, (Wiley, NY, London, Sydney) 62.

Wilson, H.W. and N.R. Daly, 1963, J. Sci. Instrum. **40**, 273.

Handbook on the Physics and Chemistry of Rare Earths, edited by K.A. Gschneidner, Jr. and L. Eyring

Chapter 38

SHIFT REAGENTS AND NMR OF PARAMAGNETIC LANTHANIDE COMPLEXES

Jacques REUBEN* and Gabriel A. ELGAVISH
Isotope Department, The Weizmann Institute of Science, Rehovot, Israel

Contents

Symbols

A = hyperfine coupling constant
g_L = Landé g-factor
$g_\parallel$ = component of g-tensor along axis of symmetry
$g_\perp$ = component of g-tensor perpendicular to axis of symmetry
H_0 = intensity of external magnetic field
J = resultant electronic spin angular momentum
k = Boltzmann's constant
P_b = fractional population in bound state
P_f = fractional population in free state
r = internuclear distance
$\langle S_z \rangle$ = projection of total electronic spin on external magnetic field
T = absolute temperature
T_1 = longitudinal relaxation time
T_{1b} = longitudinal relaxation time in paramagnetic complex (bound state)
T_{1f} = longitudinal relaxation time of free state
T_{1e} = electron spin relaxation time
T_2 = transverse relaxation time
T_{2b} = transverse relaxation time in paramagnetic complex (bound state)
T_{2f} = transverse relaxation time of free state
β = Bohr magneton
γ_N = nuclear magnetogyric ratio
δ = induced shift
Δ_b = chemical shift in paramagnetic complex
Δ_c = contact shift
Δ_d = dipolar shift
ν_0 = resonance frequency
θ = angle between r and principal axis of symmetry
ϕ = angle between projection of r or plane perpendicular to main magnetic axis and one of the axes on this plane
τ_b = mean residence time in bound state
τ_f = mean residence time in free state
ω_0 = nuclear resonance angular frequency

*Present address: Department of Chemistry, University of Houston, Houston, Texas 77004, USA

1. Introduction

The effect of paramagnetic ions or their complexes on the nuclear magnetic resonance (NMR) spectra of ligand molecules has been known since the early days of NMR spectroscopy. However, it was not until the dramatic demonstration by Hinckley (1969), who showed how some paramagnetic lanthanide chelates could be used to induce stereospecific chemical shifts in the NMR spectra of complex organic molecules and thereby to facilitate spectral analysis, that the field of shift reagents was launched. Intensive research in this area ensued and several hundred articles were published in the two year period of 1971–1972. The most appealing features of lanthanide shift reagents are related to the possibility of reducing spectra of great complexity to "first-order" without the loss of resolution and to the definite relationship between the magnitude of lanthanide induced shifts and the details of molecular geometry. These features are due to a number of very special and coexistent magnetic and chemical properties of the trivalent lanthanides, the most important among which seem to be the anisotropy of the magnetic susceptibility, the short electron spin relaxation times, and the lability of lanthanide complexes. Interestingly some of the problems encountered in the application of lanthanide shift reagents stem from some of these very same properties.

Lanthanides can be used as shift reagents both in aqueous solutions and in organic solvents. The tripositive lanthanide ions will form complexes in aqueous solution with negatively charged ligands as well as with neutral molecules containing a favorable arrangement of several polar groups (e.g. polyols). The $R(EDTA)^-$ chelates will often associate with ionized molecules in solution and may serve as shift reagents at higher pH values. The tris-chelates with β-diketonates are readily soluble in organic solvents and form adducts with Lewis bases. The commonly used shift reagents of this type are $R(dpm)_3$ and $R(fod)_3$, where *dpm* stands for dipivaloyl methanate (also known as *thd*: 2,2,6,6-tetramethyl-3,5-heptanedionate) and *fod* denotes 1,1,1,2,2,3,3-heptafluoro-7,7-dimethyl-4,6-octanedionate.

The discovery of lanthanide shift reagents stimulated research on the various aspects of their application as well as on the theory and interpretation of NMR spectra of lanthanide complexes in general. More than ten review articles and chapters have already appeared in the literature. Three of them contain, inter alia, rather extensive coverage of the factual material (Cockerill et al., 1973; Mayo, 1973; Reuben, 1973a). The state of the art in mid-1973 is covered in a series of symposium papers, which along with a complete bibliography, appeared as a book (Sievers, 1973). This chapter is intended to provide a general summary of the theory, experiment, and application of the NMR of paramagnetic lanthanide complexes and shift reagents. The literature coverage is therefore selective rather than extensive. Reference is given only to those articles directly related to our discussion.

2. Chemical shifts in lanthanide complexes: theory and experiment

Nuclei of ligands in paramagnetic complexes are coupled to the electronic spin of the central ion by the electron-nuclear hyperfine interaction. One of the consequences of this interaction is large chemical shifts (relative to the diamagnetic system) in the NMR spectra of the ligands. There are two major independent mechanisms of hyperfine interaction. The *contact* interaction results from a finite probability of finding an unpaired electronic spin on an atomic s orbital. The *dipolar* interaction takes place via space and causes shifts only if the magnetic susceptibility of the central ion is anisotropic. Otherwise it is effectively averaged out and no dipolar shifts are observed. This is the case, e.g., with S-state ions such as Gd^{3+}. Thus the net shift, Δ_b, can be expressed as a sum of two contributions: the contact shift, Δ_c, and the dipolar shift, Δ_d

$$\Delta_b = \Delta_c + \Delta_d. \tag{38.1}$$

2.1. *Contact shifts*

Owing to the similarity in the chemistry and structure of complexes along the lanthanide series it is instructive to investigate NMR spectra of complexes of as many members of the series as possible. The first systematic study of chemical shifts in lanthanide complexes was carried out by Lewis et al. (1962), who measured and interpreted the oxygen-17 shifts of the aquo complexes. The sign variation of the observed shifts along the series suggested that there was no direct overlap between the 4f and the oxygen 2s wave function, but rather a promotion of a bonding electron to an empty antibonding orbital leaving a net spin at the oxygen nucleus. This pathway of contact interaction is referred to as spin polarization in contrast to delocalization or direct overlap. The contact shift (in frequency units) can be expressed as

$$\Delta_c = A\langle S_z \rangle. \tag{38.2}$$

where A is the hyperfine coupling constant (in frequency units) and $\langle S_z \rangle$ is the projection of the total electron spin magnetization of the lanthanide on the direction of the external magnetic field. To a first approximation (and excluding Eu^{3+} and Sm^{3+}) it is given by

$$\langle S_z \rangle = g_L(g_L - 1)J(J + 1)(\beta H_0/3kT) \tag{38.3}$$

where g_L is the Landé g-factor, J is the resultant electronic spin angular momentum (in $\hbar$ units) of the ground level, β is the Bohr magneton, and H_0 is the intensity of the external magnetic field. For Eu^{3+} and Sm^{3+} higher levels have to be included. A tabulation of $\langle S_z \rangle$ values calculated with eq. (38.3) is given in table 38.1. More recently, Golding and Halton (1972) carried out a second-order perturbation treatment which resulted in correction of up to 10% in the $\langle S_z \rangle$ values (at 300 K) with a more complex temperature dependence. Their results, which are also listed in table 38.1, will be used for all the correlations presented

TABLE 38.1
$\langle S_z \rangle$ (in units of $\beta H_0/3kT$) of trivalent lanthanides.

R^{3+}	$\langle S_z \rangle^a$	$\langle S_z \rangle^b$
Pr	−3.200	−2.972
Nd	−4.909	−4.487
Eu	–	10.682
Gd	31.500	31.500
Tb	31.500	31.818
Dy	28.333	28.545
Ho	22.500	22.629
Er	15.300	15.374
Tm	8.167	8.208
Yb	2.571	2.587

[a]Calculated with eq. (38.3). [b]From Golding and Halton (1972).

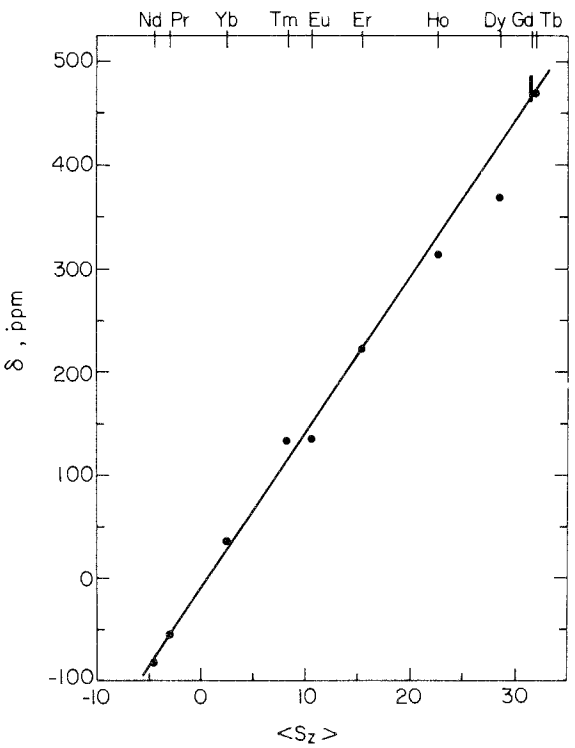

Fig. 38.1. The water oxygen-17 shift in 1 molal $R(ClO_4)_3$ solutions (Reuben and Fiat, 1969a), plotted against the corresponding $\langle S_z \rangle$ value (Golding and Halton, 1972).

in this chapter. The ^{17}O shifts in 1 molal solutions of lanthanide perchlorates are plotted against $\langle S_z \rangle$ in fig. 38.1. The observed relatively good linear correlation means that the hyperfine coupling constant A for the water oxygen in the aquo-complexes does not change appreciably along the series. The temperature dependence of the ^{17}O shifts in aqueous solutions of $Dy(ClO_4)_3$ and of $Ho(ClO_4)_3$ has been shown to conform to the Curie law of eq. (38.3), Reuben and Fiat (1969a). Note that for both Dy^{3+} and Ho^{3+} the corrections resulting from the second-order treatment are small (cf. table 38.1).

2.2. *Dipolar shifts*

The first systematic investigation of proton shifts in aqueous solutions of lanthanide perchlorates showed that the sign variation of the shifts along the series was irregular and definitely different from that observed with the ^{17}O shifts (Reuben and Fiat, 1967a). This observation led to the suggestion that the proton shifts were dominated by dipolar contributions. It was also found that the proton shifts markedly departed from Curie's law (Reuben and Fiat, 1967b). A concise theory of dipolar shifts in lathanide complexes in solution has been presented by Bleaney (1972). Bleaney's theory and its subsequent extension and generalization (Golding and Pyykkö, 1973), provides positive predictions with regard to both the relative dipolar shifts along the lanthanide series and their temperature dependence. There are two cardinal points in this theory. Ignoring for the moment the $4f^5$ and $4f^6$ configurations of Sm^{3+} and Eu^{3+}, respectively, these points can be stated as follows:

(i) In a lanthanide complex the ground state (specified by its quantum number J) of the ion has $2J + 1$ levels split by the ligand field, which may be appreciably populated at room temperature. The magnetic properties of an isolated group of levels may be very anisotropic. However, the lifetime of the ion in any one of them is very short at room temperature. In fact, electron spin relaxation times of the order of 10^{-13} sec have been estimated from nuclear relaxation measurements (vide infra, section 3). Therefore in an NMR experiment only the magnetic moment averaged over a time long compared with the electron spin relaxation time has to be considered since the reorientation time of the complex itself is much longer. This average is composed of the contributions of the $2J + 1$ levels of the ground J manifold, each weighted by the corresponding relative population. As a first approximation it is assumed that at the temperature of the usual NMR experiment $kT \gg \Delta E_J$ where ΔE_J is the energy span of the levels within the manifold. In this case an equal distribution of population is assumed, and the equally-weighted average of the magnetic moments over the entire ground manifold of a lanthanide ion results in an isotropic magnetic susceptibility. Thus, the dipolar shift in this first order approximation vanishes.

(ii) Higher order terms of the level populations take into account the deviation from equal population at a finite temperature. This second order approximation gives a T^{-1} dependent population distribution that serves as weighting factors in

calculating the average magnetic moment. The latter combined with Curie's law results in an *anisotropic*, T^{-2} dependent susceptibility. This second order anisotropic susceptibility is the source of the dipolar nuclear resonance shifts in lanthanide complexes.

For the case of an axially symmetric complex the dipolar shift (in frequency units) can be expressed as a product of several factors:

$$\Delta_d = \frac{\nu_0 \beta^2}{60(kT)^2} \frac{3\cos^2\theta - 1}{r^3} 2A_2^0(r^2)\, g_L{}^2\, J(J+1)\,(2J-1)\,(2J+3)\langle J\|\alpha\|J\rangle \qquad (38.4)$$

where ν_0 is the resonance frequency. The first factor includes the dependence on the inverse square of the absolute temperature. The dependence on molecular structure is included in the second factor where r is the distance between the central ion and a given ligand nucleus and θ is the angle between the vector r and the principal axis of symmetry of the complex. The ligand field coefficients in the third factor are defined according to Abragam and Bleaney (1970) and are assumed to be a constant for a given complex along the lanthanide series. The quantity of the last factor has been calculated by Bleaney (1972). His results (with the inclusion of excited states) scaled to 100 for Dy^{3+} ions are given in table 38.2. For an isostructural series of complexes these will be the relative shifts along the lanthanide series.

It is convenient to express the dipolar shift in the following short hand notation

$$\Delta_d^i = DG_i \qquad (38.5)$$

where $G_i = (3\cos^2\theta_i - 1)/r_i^3$ is the geometrical function specific for a given ligand nucleus, i, and D is a temperature dependent factor characteristic of the lanthanide (cf. table 38.2). We have plotted in Fig. 38.2 the observed shifts versus D for the C_α

TABLE 38.2
Relative dipolar shifts and their ratio to the contact shifts for lanthanide complexes (at 300 K).

R^{3+}	D[a]	$D/\langle S_z\rangle$[b]
Pr	−11.0	3.70
Nd	−4.2	0.94
Eu	4.0	0.37
Gd	0	0
Tb	−86	−2.70
Dy	−100	−3.50
Ho	−39	−1.72
Er	33	2.15
Tm	53	6.46
Yb	22	8.50

[a]From Bleaney et al. (1972). [b]$\langle S_z\rangle$ from Golding and Halton (1972).

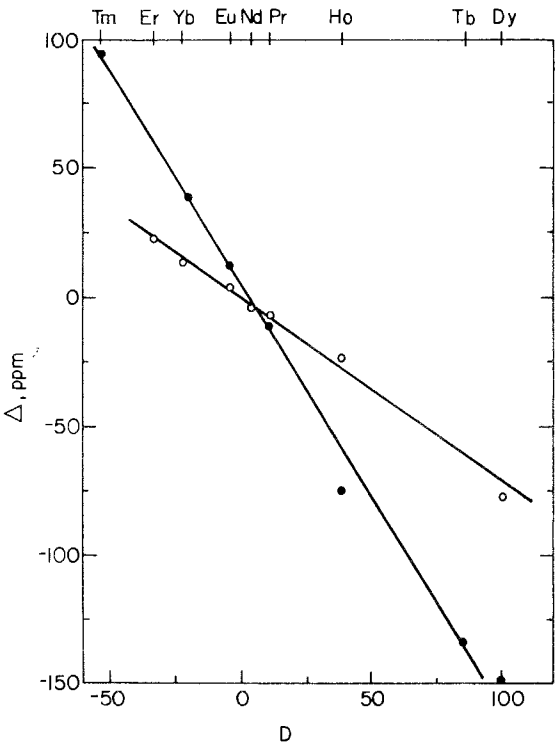

Fig. 38.2. The carbon-13 shift of C_α in $R(DPA)_3$ complexes (filled symbols) (Reilley et al., 1975), and the proton shift of H_7 in quinoline-$R(dpm)_3$ adducts (open symbols) (Chalmers and Pachler, 1974), plotted against the corresponding D value (Bleaney et al., 1972).

of the pyridine-2,6-dicarboxylato (DPA) complexes studied in aqueous solutions, Reilley et al. (1975), and for the H_7 of quinoline in $R(dpm)_3$-quinoline adducts studied in $CDCl_3$ solutions (Chalmers and Pachler, 1974). Excellent correlations are obtained.

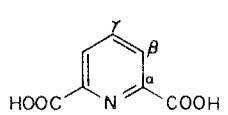

pyridine-2, 6-dicarboxylic acid

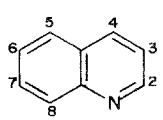

quinoline

Golding and Pyykkö (1973) have generalized Bleaney's treatment to include arbitrary ligand field components and provide ready means by which calculations for any particular case can be carried out. They obtain results that in some cases may differ by as much as 20% from those of Bleaney. Departure from the T^{-2} dependence, in some cases by as much as 10%, is also predicted. For the analysis of NMR results, however, the ligand field parameters have to be known, but since for

most of the systems of interest they are presently unavailable, correlations of experimental data with D as calculated by Bleaney or by Golding and Pyykkö seem to be of similar merit. In the correlations presented in this chapter we elected to use Bleaney's results (table 38.2).

The ground level of Eu^{3+} is diamagnetic. Its paramagnetism arises from the population of higher levels, which have to be included in the calculations. Therefore the temperature dependence of the shifts induced by Eu^{3+} is a rather complex function. It has been analysed in detail, Bleaney (1972), Golding and Pyykkö (1973).

The first theoretical treatment of dipolar shifts in paramagnetic complexes with anisotropic g-tensors has been carried out by McConnell and Robertson (1958). For an axially symmetric lanthanide complex the dipolar shift according to this theory should be

$$\Delta_d = \nu_0\beta^2 J(J+1)G(g_\parallel^2 - g_\perp^2)/9kT \tag{38.6}$$

where $g_\parallel$ and $g_\perp$ are respectively the components of the g-tensor along and perpendicular to the principal axis of symmetry. Since serious objections to Bleaney's theory have been put forward, Horrocks et al. (1973), and are often referred to in the literature, it is important to evaluate the absolute shifts according to eqs. (38.4) and (38.6). For Pr^{3+} and Yb^{3+} and using $\theta = 0$, $r = 5$ Å, $T = 300$ K one obtains -9.4 and 16.9 ppm, respectively, using eq. (38.4), whereas the results obtained using eq. (38.6) with the g-tensor components given by Horrocks et al. (1973) are 177 and 672 ppm, respectively. Referring to fig. 38.2 as well as to other experimental data in the literature one finds that the absolute shifts calculated with eq. (38.4) are well within the range of experimental values, whereas those obtained with eq. (38.6), which are larger by factors of ca. 20 and 40, are outside that range both in their absolute values and relative signs. Even larger deviations are obtained for lanthanides with larger J values.

Obviously, the use of eq. (38.6), which considers only the first term in the expansion of the Boltzmann factors, with g-tensor components weighted by unequal populations of the corresponding levels is a contradiction in terms and as could be anticipated leads to erroneous results. It is thus clear that Bleaney's theory accounts satisfactorily for the dipolar shifts in lanthanide complexes, whereas the criticisms of this theory, Horrocks et al. (1973), seem to be not well founded. We wish to emphasize that the generalized treatment of Golding and Pyykkö (1973) is of course more rigorous.

2.3. *Temperature dependence*

The contact and dipolar contribution to the shift can be incorporated into eq. (38.1) in the following convenient fashion

$$\Delta_b = A\langle S_z\rangle'/T + D'G/T^2 \tag{38.7}$$

where $\langle S_z\rangle' \equiv T\langle S_z\rangle$ and $D' \equiv DT^2$. Thus eq. (38.7) emphasizes the different temperature dependencies of the two contributions. The best way of analyzing the

temperature dependence is to plot the product $\Delta_b T$ against T^{-1}. From the intercept and slope of such plots the relative contact and dipolar contributions can be evaluated according to

$$\Delta_b T = A\langle S_z\rangle' + D'G/T \tag{38.8}$$

This type of plot for the proton shift of acetone induced by $Yb(fod)_3$ is shown in Fig. 38.3. As would be anticipated from the relative $D/\langle S_z\rangle$ ratio (cf. table 38.2) the contact contribution to shifts induced by ytterbium complexes is minimal. Similar behavior has been observed by Desreux and Reilley (1976) for proton shifts in the $Tm(DPA)_3$ and $Yb(DPA)_3$ complexes in aqueous solution. These authors obtained finite intercepts for some of the carbon-13 shifts in $Yb(DPA)_3$. The dipolar shifts obtained from the slopes were in good agreement with those estimated from a geometrical model. One of the reasons for obtaining good temperature correlations with the shifts in ytterbium complexes seems to be the fact that higher J levels are ca. 10 000 cm^{-1} above ground and their contribution to the magnetic moment and its anisotropy is relatively small at the normal temperatures of NMR experiments. This may not be so for other lanthanides. The contribution of excited states will add terms to the contact and dipolar shifts that will be roughly temperature independent for the former, Golding and Halton (1972), and almost linear in T^{-1} for the latter, Golding and Pyykkö (1973).

2.4. *Other shift mechanisms*

Using eq. (38.7) to analyse the temperature dependence of the water proton shifts in aqueous solutions of $Dy(ClO_4)_3$, Granot and Fiat (1975) obtained contact

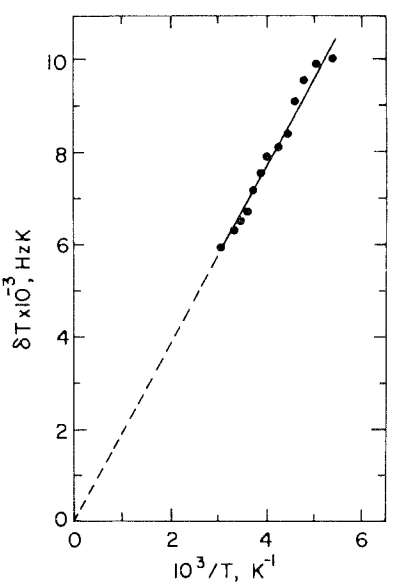

Fig. 38.3. The product of the temperature and the $Yb(fod)_3$ induced proton shift of acetone (in Hz at 90 MHz) plotted against the reciprocal temperature. Reconstructed from the data of Elgavish and Reuben (1974).

contributions that were of opposite sign to the shifts induced by $Gd(ClO_4)_3$. This finding suggests at first sight that a sign reversal in the proton hyperfine coupling constant is taking place along the lanthanide series. Another possibility is the presence of shift contributions that vary with temperature as T^{-1} but which have not been accounted for by the models used to form eq. (38.7). We wish to draw attention to two such contributions that may be of importance for nuclei of atoms in the immediate vicinity of the coordination site of the ligand.

(i) Non-bonding overlap between the 4f orbitals and ligand molecular orbitals will place unpaired electronic spin on atomic s orbitals. This is a major pathway of proton contact shifts in the aquo-complexes of transition metal ions, Chmelnick and Fiat (1972). The relative contribution of this mechanism along the lanthanide series will depend on the population and symmetry of the 4f orbitals. It is likely therefore that the variation of this contribution along the series may not proceed in the same regular manner as that of the spin polarization mechanism discussed in section 2.1.

(ii) Dipolar shifts may also arise from the unpaired spin density distributed over the ligand orbitals, Kurland and McGarvey (1970). Although the quantitative evaluation of this contribution necessitates the detailed knowledge of the spin density distribution for the complex, some general considerations may hint at the relative importance of this mechanism. (a) It is a minute fraction of a spin that will normally be found on the ligand orbital. This fractional density usually decreases with increasing the number of chemical bonds from the central ion. (b) The anisotropy of the spin is now determined by the electronic g-tensor of the corresponding orbital and the shift will follow eq. (38.6), i.e. it is a "first-order" contribution with a T^{-1} dependence. Note that s-orbitals are isotropic and the contribution of spin density centered on hydrogen atoms will practically vanish. (c) The (r^{-3}) factor for contributions of this type will usually be much larger than that of the lanthanide centered dipolar shift. Therefore for nuclei at a short distance from the lanthanide, and for non-hydrogen atoms even further away from the ion, the contribution of this mechanism may be not negligible.

2.5. *Separation of contact and dipolar contributions*

Substitution of eqs. (38.2) and (38.5) into eq. (38.1) gives the following general expression for the shifts in lanthanide complexes

$$\Delta_b^i = A_i\langle S_z\rangle + DG_i \tag{38.9}$$

where i specifies the ligand nucleus. If only a spin polarization mechanism is operative A_i is likely to be constant along the lanthanide series. If in addition the complexes are isostructural so that G_i is also constant, then it is possible to separate the contact and dipolar contributions by a simple graphical method using the following form of eq. (38.9)

$$\Delta_b^i/\langle S_z\rangle = A_i + G_i(D/\langle S_z\rangle). \tag{38.10}$$

The theoretical values of $\langle S_z\rangle$ and $D/\langle S_z\rangle$ are available (cf. table 38.1 and 38.2). A

plot of $\Delta_b^i/\langle S_z\rangle$ against $D/\langle S_z\rangle$ should be linear with a slope of G_i and an intercept on the ordinate of A_i. Departures from the model should be clearly revealed in such plots. Shown on fig. 38.4 are the plots for the carbon-13 shifts of the carboxyl and Cγ of R(DPA)$_3$ complexes in aqueous solutions using the data of Reilley et al. (1975). It is seen that Cγ conforms to the model whereas the carboxyl carbon, which is in an α-position to the coordinating atoms, does not, probably due to contributions from other shift mechanisms. The shifts of most of the other nuclei of DPA or of its γ-methyl derivative conform well to the model. It should be pointed out that maximum sensitivity towards "structural imperfections" along the lanthanide series will be exhibited by nuclei for which $\theta \simeq 45°$ where the derivative of $(3\cos^2\theta - 1)$ has its maximum. This may be another contribution to the behaviour of the carboxyl data. The shifts of H_2 and H_3 of quinoline in its adducts with R(dpm)$_3$ that have been reported by Chalmers and Pachler (1974) are treated in a similar manner and plotted in fig. 38.5. Again a similar picture is obtained where the H_2 proton that is closer to the site of coordination (at β-position) exhibits departures from the model. The shifts of most of the other nuclei of quinoline conform to the model.

The conclusion from the above discussion is that theoretical models of the chemical shifts in lanthanide complexes account satisfactorily for the experi-

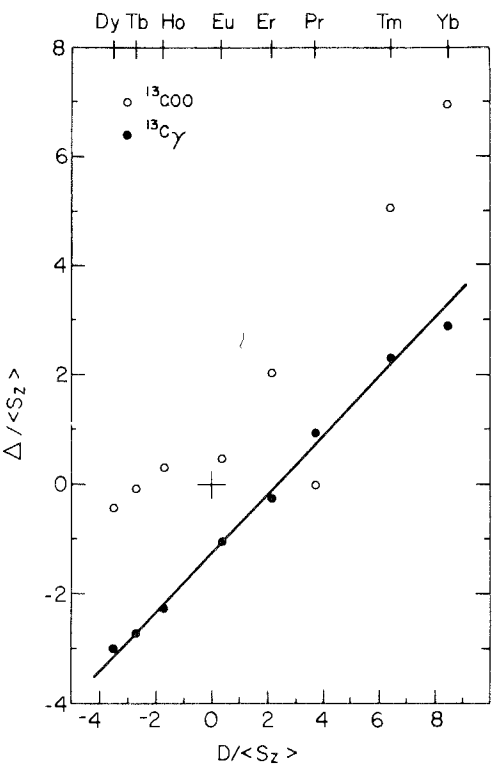

Fig. 38.4. The $\langle S_z\rangle$ normalized carbon-13 shifts of the carboxyl and Cγ in R(DPA)$_3$ complexes (Reilley et al., 1975), plotted against the corresponding $D/\langle S_z\rangle$ ratio.

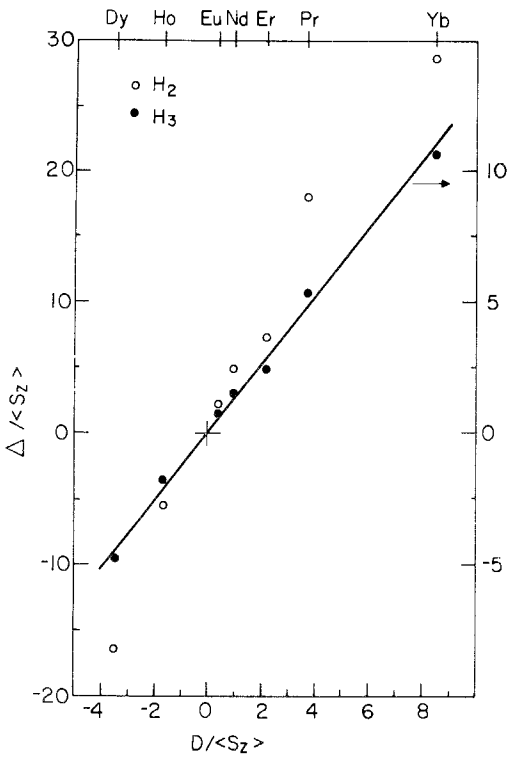

Fig. 38.5. The $\langle S_z \rangle$ normalized proton shifts of H_2 and H_3 in quinoline-R(dpm)$_3$ adducts (Chalmers and Pachler, 1974), plotted against the corresponding $D/\langle S_z \rangle$ ratio.

mental results. However nuclei close to the site of coordination, i.e. at positions α and β to the coordinating atom, may exhibit departures from these models probably due to contributions of other shift mechanisms. Some recommendations based on these conclusions can now be made regarding the application of lanthanide induced shifts for the elucidation of molecular structure. The best way to obtain the relative magnitude of the geometrical function, G for the different ligand nuclei seems to be from the slopes of $\Delta_b^i T$ versus T^{-1} plots. As already pointed out, the temperature dependence of the shifts in ytterbium complexes has been found to conform well to the theoretical model and thus measurements using an ytterbium complex as the sole shift reagent may suffice. There are cases in which the temperature dependence of the shift may be obscured by effects of chemical equilibrium or chemical exchange. In such cases data at room temperature for a number of lanthanides should be obtained in order to permit plots according to eq. (38.10). The lanthanides most suited for such plots in the order of their $D/\langle S_z \rangle$ ratio are Yb, Tm, Pr and Dy. Here, however, isostructurality of the complexes is required and the data for the α and β nuclei should be discarded in the structural fit since they may contain contributions that are unaccounted for by the model.

2.6. *Absence of axial symmetry*

We have so far considered only cases with axial symmetry. However, crystallographic studies have shown that lanthanide shift reagent adducts may be devoid of axial symmetry, (Horrocks et al., 1971; Cramer and Seff, 1972). In such cases the dipolar shift is given by an expression of the general form

$$\Delta_d = r^{-3}[D_1(3\cos^2\theta - 1) + D_2 \sin^2\theta \cos 2\phi] \tag{38.11}$$

where D_1 and D_2 are temperature dependent constants for a given lanthanide and ϕ is the angle between the projection of the vector r on the plane perpendicular to the main magnetic axis of the complex and one of the axes on this plane, (Bleaney, 1972). Non-axial symmetry is most likely to occur with chelating ligands. Thus, e.g., Marinetti et al. (1975) have found that lanthanide complexes with N-acetyl-L-3-nitrotyrosine ethyl ester are non-axial and treated the shifts by an empirical fit of the data to eq. (38.11) using relative distances determined from relaxation measurements on the gadolinium complex. The complexes of the $R(EDTA)^-$ chelates with *o*-nitrophenolate and with the anion of salicylaldehyde have also been shown to be non-axially symmetric, (Reuben, 1976). In the absence of chelation, however, effective axial symmetry is usually observed with regard to the shifts, although the complex or the shift reagent adduct may be devoid of such symmetry. This phenomenon may arise from the following averaging mechanisms. The ligand molecule freely rotates about an axis which passes through the central ion of the complex. This motion will effectively average out the second term of eq. (38.11), (Briggs et al., 1972). Horrocks (1974) has considered the possibility of the lanthanide complex or shift reagent adduct existing in solution as an ensemble of many rapidly interconverting isomers. This is a case equivalent to that of ligand rotation, where the mechanism of achieving the different rotamer states is chemical exchange rather than free rotation in the complex itself.

3. Nuclear relaxation in lanthanide complexes

Nuclear relaxation in paramagnetic complexes is brought by the time dependent terms of the nuclear spin Hamiltonian. The magnitude of the relaxation effect is governed by the intensity of the electron-nuclear interaction and by the rate at which the interaction is interrupted. Thus the relaxation rates of ligand nuclei are determined by the molecular structure and by the molecular dynamics in solution and may in turn be used in studying these factors.

3.1. *Basic equations*

It can be shown, (Guéron, 1975; Vega and Fiat, 1976), that for rapidly tumbling lanthanide complexes, with electron spin relaxation time, T_{1e}, short compared to the rotational reorientation time, τ_r, the electron-nuclear dipolar

interaction will result in nuclear relaxation rates given by the following expression, (Reuben and Fiat, 1969b),

$$1/T_{1b} = 1/T_{2b} = (20/15)\gamma_N^2 g_N^2 \beta^2 J(J+1) r^{-6} T_{1e} \tag{38.12}$$

where T_{1b} and T_{2b} are respectively the longitudinal and transverse relaxation times and γ_N is the nuclear magnetogyric ratio. The contribution of the contact interaction to the nuclear relaxation in lanthanide complexes can be shown to be usually negligible. Note the inverse sixth power dependence on the cation-nuclear distance that allows in favorable cases accurate determinations of relative distances. For Gd^{3+}, for which T_{1e} is relatively large, eq. (38.12) has to be modified by replacing T_{1e} with a function of the correlation time, τ_c, and the resonance frequency, where $1/\tau_c = 1/T_{1e} + 1/\tau_r$. Yet, within a given gadolinium complex the relative relaxation rates for different ligand nuclei will still be proportional to the inverse sixth power of the respective relative distances.

In solutions of many lanthanide complexes chemical exchange between the coordinated ligand molecules and those free in solution is so rapid on the NMR time scale that an average signal is normally observed. The relaxation rates in this case are weighted averages. However the transverse relaxation rate, which when divided by π gives the line-width at half-height, contains an additional contribution arising from the uncertainty due to the chemical shift difference, Δ_b, between the complexed and free states of the ligand molecule. In the presence of this rapid exchange process the relaxation rates are given by

$$1/T_1 = P_f/T_{1f} + P_b/T_{1b} \tag{38.13}$$

$$1/T_2 = P_f/T_{2f} + P_b/T_{2b} + P_f^2 P_b^2(\tau_f - \tau_b)(2\pi\Delta_b)^2 \tag{38.14}$$

where P_f and P_b are respectively the fractional populations in the magnetic environments of the free and bound states ($P_f + P_b = 1$) their mean residence times being τ_f and τ_b, respectively, (Luz and Meiboom, 1964; Gutowsky et al., 1953). If ligand exchange is a first-order process, τ_b may be regarded as a constant characteristic of the system, whereas τ_f will be concentration dependent and at equilibrium, owing to the statistical nature of the exchange process, will be given by

$$\tau_f = \tau_b P_f/P_b \tag{38.15}$$

By substituting eq. (38.15) into (38.14) and setting $P_f = 1 - P_b$, one obtains

$$1/T_2 = (1 - P_b)/T_{2f} + P_b/T_{2b} + P_b(1 - P_b)^2 \tau_b (2\pi\Delta_b)^2 \tag{38.16}$$

This expression may be obtained by a derivation starting with McConnell's equations, (Reuben and Fiat, 1969b).

3.2. *Experimental studies*

The first systematic investigation of longitudinal proton relaxation in aqueous solutions of lanthanide nitrates has been carried out by Conger and Selwood

(1952) in the early days of NMR. A correlation with magnetic moments was attempted, which failed since at that time relaxation processes were not yet well understood. Measurements using the chloride salts have recently been carried out in our laboratory. The results as analyzed according to eqs. (38.13) and (38.12) are summarized in table 38.3. For the calculation of $1/T_{1b}$ a hydration number of 9 was assumed and the T_{1e} values were obtained using 3.1Å for the proton-lanthanide distance. The T_{1e} values as well as those previously estimated from oxygen-17 line-broadenings should be regarded as order of magnitude estimates only. They may depend both on frequency and on temperature, (Granot and Fiat, 1975), and may vary from one complex to another. It is clear, however, that the electron spin relaxation times are of the order of 10^{-13} sec. For the S-state Gd^{3+} ion T_{1e} is much longer, 10^{-9}–10^{-10} sec, and therefore its relaxation effects are stronger, e.g. for the aquo-complex $1/T_{1b} = 90340\ \text{sec}^{-1}$ at 24°C and 35.0 MHz, (Reuben, 1975).

Shortening of longitudinal relaxation times may lead to effective decoupling of spin–spin coupled nuclei resulting in the "washing out" of multiplet structure in the NMR spectra of ligands. Such effects produced by $Eu(dpm)_3$ have been observed in the proton spectrum of quinoline, (Reuben and Leigh, 1972). These authors were also the first to use the lanthanide induced longitudinal relaxation rates for the determination of relative distances.

The lanthanide induced line-broadenings cannot be related to the lanthanide-nuclear distances in a simple way because of the possible contribution of the last term in eq. (38.16). A detailed analysis of results obtained for the $R(fod)_3$ adducts with pinacolone, $(CH_3)_3\ CCOCH_3$, has recently been carried out, Lenkinski and Reuben (1976a). It was found convenient to rearrange eq. (38.16) in the form

$$(1/T_2 - 1/T_{2f})/P_b = (1/T_{2b} - 1/T_{2f}) + 4\pi^2\Delta_b^2\tau_b(1 - P_b)^2 \qquad (38.17)$$

and to plot $(1/T_2 - 1/T_{2f})/P_b$ against $(1 - P_b)^2$. From the intercept on the ordinate of such plots $1/T_{2b}$ is readily obtained and from the slope τ_b can be calculated using the Δ_b value determined from shift measurements. The values of P_b can conveniently be obtained from analysis of the concentration dependence of the shifts (cf. section 5). Results obtained from line-broadening data are summarized in table 38.4. The contribution of the last term in eq. (38.16) has three important

TABLE 38.3
Proton relaxation in aqueous solutions of lanthanides at 21 ± 1°C and 22.1 MHz.

R^{3+}	$1/T_{1b}(\text{sec}^{-1})$	T_{1e}(psec)
Nd	116	0.096
Dy	3309	0.316
Ho	3255	0.313
Er	2467	0.291
Tm	2274	0.430
Yb	382	0.201

TABLE 38.4
Mean life-times and electron spin relaxation times of R(fod)$_3$-pinacolone adducts obtained from line-broadening data at 90 MHz (from Lenkinski and Reuben, 1976a).

R	Temp. (°C)	$\tau_{b\ (msec)}$	$T_{1e\ (psec)}$
Pr	0		0.12
Yb	0	0.22	0.34
Yb	27	0.11	0.22

experimental consequences. (i) Line-broadenings will be larger at higher frequencies due to the frequency dependence of the shift. (ii) Largest broadenings will be observed with $P_b = 1/3$ where the function $P_b(1 - P_b)^2$ has its maximum. Spectral demonstrations of this effect can be found in the literature, (Okigawa and Kawano, 1973; Reuben, 1976). (iii) The ratio between lanthanide induced broadenings for different nuclei within the same ligand may depend both on the lanthanide and on concentration. The different broadening ratios for different lanthanides reported by La Mar and Metz (1974) can thus be rationalized.

4. Kinetic effects

At room temperature, the addition of relatively small amounts of a paramagnetic lanthanide shift reagent to a solution of a potential ligand normally induces chemical shifts in the ligand resonances that at very low lanthanide/ligand ratios are proportional to that ratio. The conditions necessary for the observation of these effects are known in the art as conditions of rapid chemical exchange, i.e. the mean life-time of the complex, τ_b, is much shorter than the reciprocal chemical shift:

$$\tau_b \ll 1/2\pi\Delta_b \tag{38.18}$$

However, as the temperature is lowered, Δ_b will increase according to eq. (38.7) and concomitantly τ_b is likely to increase in an exponential fashion according to Arrhenius' law. Thus, conditions might be reached such that the inequality in eq. (38.18) is reversed or does not hold. This latter case is referred to as slow exchange. Under conditions of slow exchange two separate NMR signals will be observed: one unshifted corresponding to the uncoordinated ligand molecules and another corresponding to the coordinated ligands that is shifted by Δ_b from the former. Evans and Wyatt (1972), (1973), (1974) have shown that conditions of slow exchange can be easily achieved with the R(fod)$_3$ chelates and a number of ligand molecules. From the relative areas of the signals they were able to determine the stoichiometry of the shift reagent adducts. A detailed line-shape analysis of the spectra led to the evaluation of the kinetics in these systems. In

TABLE 38.5.
Mean life-times of 1:2 R(fod)$_3$-hesamethylphosphoramide adducts at 273.2 K (from Evans and Wyatt 1974).

R	τ_b (msec)
Pr	26.32
Eu	15.17
Tb	5.99
Ho	2.35
Er	1.42
Yb	0.39

most of the cases chemical exchange was found to be a first-order process, (Evans and Wyatt, 1974). The results for hexamethylphosphoramide at 273.2K with perdeuterotoluene as the solvent are summarized in table 38.5. A pronounced trend of shorter life-times along the lanthanide series is observed. The kinetic parameters are likely to depend both on the ligand and the solvent, particularly with solvents strongly interacting with the free ligand.

When conditions of slow exchange are approached the chemical shift between the signals corresponding to the free and coordinated states becomes a function of the mean life-time of the complex. Thus the kinetics can be evaluated from shift measurements at different temperatures provided the temperature dependence of Δ_b, the shift in the absence of chemical exchange is known. This approach has been used by Bidzilya et al. (1975) to study the kinetics of exchange of the Pr(fod)$_3$ and Eu(fod)$_3$ adducts with hexamethylphosphoramide chloroform. For the analysis of the results a T^{-2} temperature dependence was assumed for Δ_b of the praseodymium complex and a T^{-1} dependence for the europium one. The enthalpies of activation thus obtained are much lower than those reported by Evans and Wyatt (1974) for the same adducts. It is not clear whether this discrepancy is due to a solvent effect or stems from some of the approximations involved in the data treatment.

The onset of slow exchange may have some rather unexpected effects on the temperature and frequency dependencies of lanthanide induced shifts. The possibility that such effects are present should always be kept in mind particularly when departures from what is believed to be a regular behavior are observed. It can be shown, (Swift and Connick, 1962), that when $\tau_b \ll T_{2b}$ the induced shift δ is given by

$$\delta = P_b \Delta_b / (1 + \omega_0^2 \Delta_b^2 \tau_b^2) \tag{38.19}$$

where the shifts are in frequency independent units and ω_0 is the resonance frequency (in sec^{-1}). It is clear from eq. (38.19) that when $\omega_0^2 \Delta_b^2 \tau_b^2 \simeq 1$ the shift observed at a lower frequency will be greater than that at a higher frequency and

also that the temperature dependence of the observed shift will be different at the two frequencies. Such effects have been demonstrated in a lanthanide shift reagent system, Samitov and Bikeev (1975). It can thus be recommended that, when studying the temperature dependence of chemical shifts in labile lanthanide complexes, the frequency dependence should also be investigated in order to check for possible complications associated with kinetic effects.

5. Equilibria in shift reagent systems

The NMR spectra of most lanthanide shift reagent systems at room temperature are characterized by conditions of rapid chemical exchange. In many cases complexes (or adducts) of a 1:2 stoichiometry are formed, which of course are present in equilibrium with the 1:1 complexes as well as with the free reagent and ligand. This introduces complications in the interpretation of lanthanide induced shifts since the theories discussed in section 2 pertain to the intrinsic shifts of the complex. Therefore there has been a great deal of interest in the literature in analyzing lanthanide induced shifts in terms of intrinsic shifts and equilibrium constants, (Shapiro and Johnston, 1972; Reuben, 1973a, 1973b, 1973c; Porter et al., 1973; Johnston et al., 1975).

Chemical equilibrium in solution has been a problem of long standing interest. Here we will present the procedures and criteria for the characterization of weak molecular complexes, (Deranleau, 1969a, 1969b; Maier and Drago, 1972), as adapted in our laboratory to the problem of shift reagents, Lenkinski, Elgavish and Reuben (1978). The observed lanthanide induced shift, δ, is a sum of two contributions

$$\delta = [RL]\Delta_1/L_t + 2[RL_2]\Delta_2/L_t \tag{38.20}$$

where Δ_1 and Δ_2 are respectively the intrinsic shifts of the RL and RL_2 species, the subscript t denotes total concentration and square brackets equilibrium concentration. This is the observation equation. By rearranging one obtains

$$\frac{[RL]}{L_t\delta} = \frac{1}{\Delta_1} - \frac{2[RL_2]}{L_t\delta}\frac{\Delta_2}{\Delta_1}. \tag{38.21}$$

A plot of $[RL]/L_t\delta$ against $2[RL_2]/L_t\delta$ should be a straight line confined by the axes with intercepts of $1/\Delta_1$ on the ordinate and $1/\Delta_2$ on the abscissa. The analysis of the results (a set of observed shifts and total concentrations) proceeds in the following way. A set of dissociation constants K_1 and K_2 is chosen and equilibrium concentrations calculated. These are used with eq. (38.21) to obtain the intrinsic shifts Δ_1 and Δ_2 from a linear least-squares fit. With the latter, chemical shift values are calculated using eq. (38.20) and compared with the observed δ values to compute the standard deviation. The cycle is repeated varying K_1 and K_2 over a wide range until a minimum in the standard deviation is obtained. The set of parameters (K_1, K_2, Δ_1, Δ_2) corresponding to this minimum is considered to be the best one describing the data. The reliability of

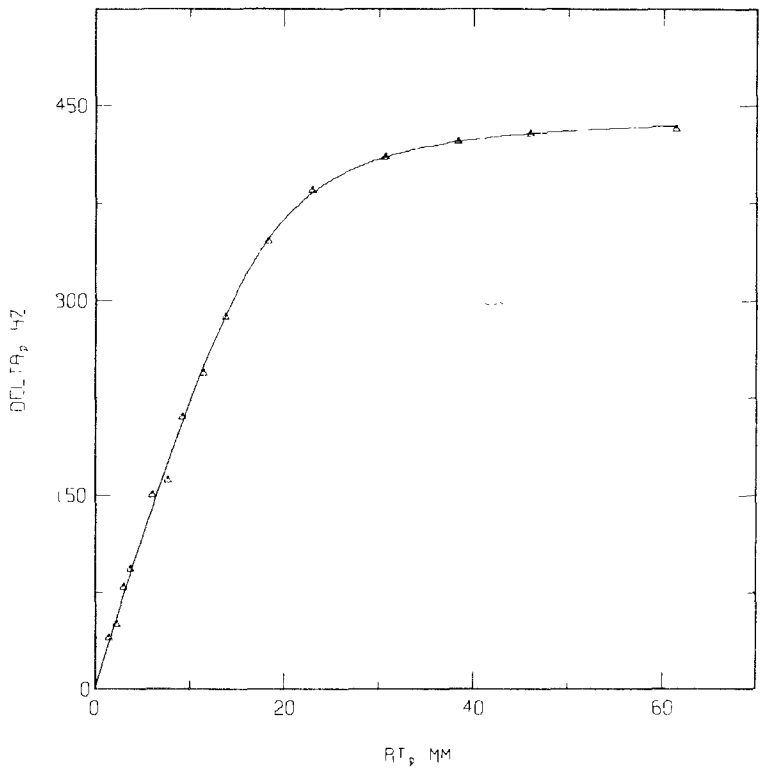

Figure 38.6. Type I titration of the shift induced by $Eu(fod)_3$ (R_t in mM) in the proton resonance of DMSO (20 mM in CCl_4). The curve is calculated with the parameters given in the text (Lenkinski, Elgavish and Reuben, 1978).

the parameters is then judged on the basis of criteria with regard to the relative contribution of each species to the observed shift as well as their respective saturation factors, (Deranleau, 1969a). Normally two types of titrations are carried out: Type I, in which the ligand concentration, L_t, is held constant while R_t is varied and Type II, in which the reagent concentration, R_t is held constant and L_t is varied. Computer simulations of typical cases show that if $4K_1 < K_2$ the Type I titration will enable the accurate determination of K_1 and Δ_1, while from a Type II titration, K_2 will be accurately determined, but, Δ_2 will usually be of lower accuracy. If $4K_1 > K_2$ either of the titrations will permit the accurate determination of K_2 and Δ_2, whereas K_1 and Δ_1 will be much less reliable since the relative contribution of the RL species will be much smaller than that of RL_2. A typical example is the $Eu(fod)_3$-dimethylsulfoxide system in CCl_4. The results of the Type I titration are presented in fig. 38.6 and those of the Type II titration in fig. 38.7. The resulting plot according to eq. (38.21) is shown in fig. 38.8, where the points were calculated with $K_1 = 0.75$ mM and $K_2 = 24.0$ mM. From the intercepts of the best-fit line the intrinsic shifts $\Delta_1 = 447.0$ Hz and $\Delta_2 =$

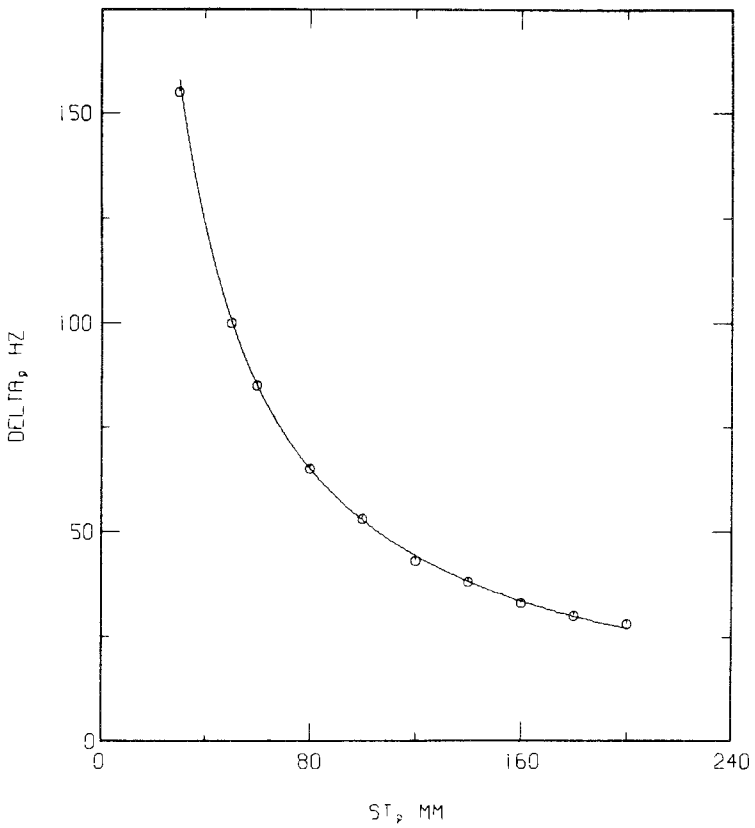

Fig. 38.7. Type II titration of the shift induced by 10 mM $Eu(fod)_3$ in the proton resonance of DMSO (S_t in mM). The curve is calculated with the parameters given in the text (Lenkinski, Elgavish and Reuben, 1978).

275.4 Hz were obtained, which along with the dissociation constants were used to calculate the smooth curves in figs. 38.6 and 38.7. The standard deviation is 4.2 Hz or 2.4% of the average observed shift. Consideration of the criteria for the accuracy in determining the parameters sets their respective error limits and thus the following set is obtained: $K_1 = 0.75 \pm 0.06$ mM, $K_2 = 24.0 \pm 1.7$ mM, $\Delta_1 = 447 \pm 11$ Hz, $\Delta_2 = 275 \pm 65$ Hz. Note the wider error limit for Δ_2. Better accuracy should be expected in a Type II titration carried out at higher R_t.

The above treatment demonstrates the complexity of the problem when intrinsic shifts are desired in systems with 1:2 stoichiometry. Another complication due to 1:2 adduct formation may be encountered with aromatic ligands. There, in addition to the paramagnetic effects of the lanthanide, shifts from ring-current effects arising from the juxtaposition of two aromatic molecules in the 1:2 adduct may also play an important role. Clearly 1:1 systems should be preferred when lanthanide induced shifts are sought for structure deter-

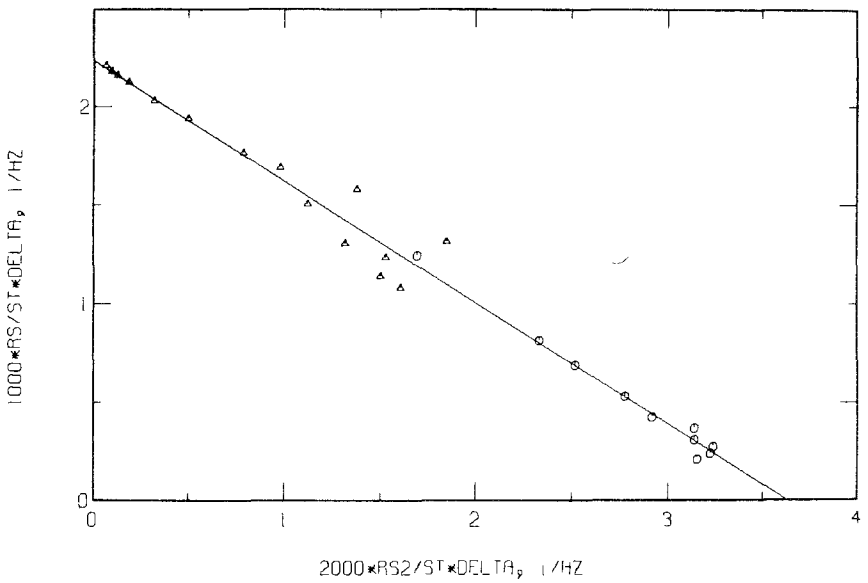

Fig. 38.8. A plot according to eq. (38.21) of the data of figs. 38.6 and 38.7 using values of [RL] and [RL_2] calculated with $K_1 = 0.75$ mM and $K_2 = 24.0$ mM (Lenkinski, Elgavish and Reuben, 1978).

minations. In such systems the relative shifts for the different ligand nuclei should reflect accurately the ratios of the intrinsic shifts. Practically 1:1 stoichiometry is obtained with the following shift reagents: $R(dpm)_3$ chelates in organic solvents, (Catton et al., 1976), $R(fod)_3$ chelates in chloroform (but not in other solvents), (Evans and Wyatt, 1974), $R(EDTA)^-$ chelates in aqueous solution, (Elgavish and Reuben, 1976).

An elegant method of obtaining the relative intrinsic shifts of ligand nuclei in homogeneous systems, where only one type of complex is present, has been developed by Servis and Bowler (1973). It consists of measuring the shifts, δ, relative to an internal standard (e.g. tetramethylsilane for protons in organic solvents) of at least two nuclei at different, but not necessarily known, lanthanide concentrations and plotting one of them against the sum of the two. Considering two nuclei, a and b, their shift is given by

$$\delta^a = \delta_0^a + P_b \Delta_b^a \tag{38.22}$$

$$\delta^b = \delta_0^b + P_b \Delta_b^b \tag{38.23}$$

where δ_0^i is the shift (relative to the standard) in the absence of lanthanide. Evaluating P_b from the sum of eqs. (38.22) and (38.23) and substituting into eq. (38.22) results in

$$\delta^a = \delta_0^a - (\delta_0^a + \delta_0^b)\frac{\Delta_b^a}{\Delta_b^a + \Delta_b^b} + (\delta^a + \delta^b)\frac{\Delta_b^a}{\Delta_b^a + \Delta_b^b} \tag{38.24}$$

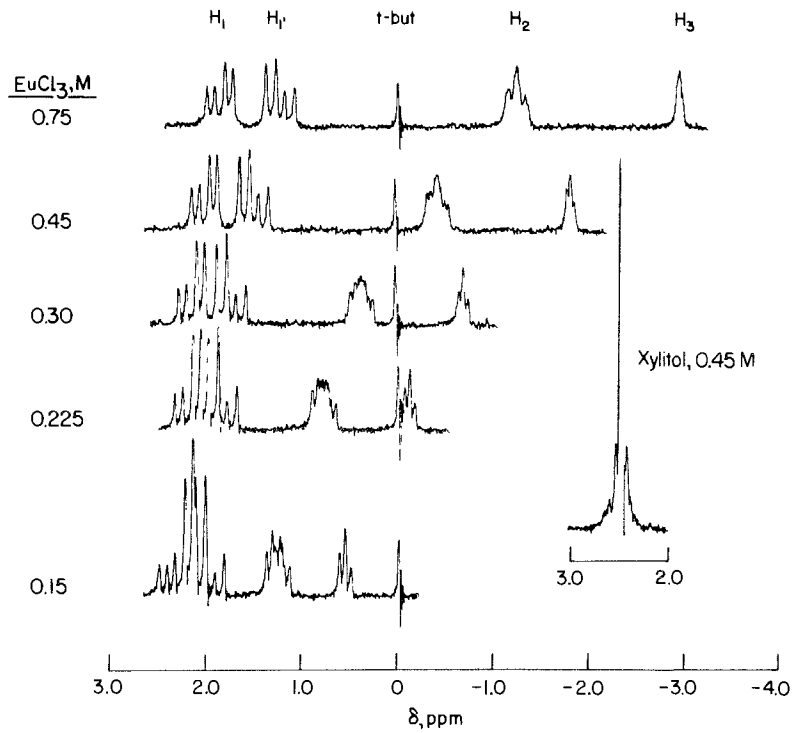

Fig. 38.9. The effect of increasing concentration of $EuCl_3$ on the 60 MHz proton spectrum of xylitol in D_2O solution. The inset on the right is the spectrum in the absence of shift reagent.

A plot of δ^a against $(\delta^a + \delta^b)$ should be linear with a slope of $\Delta^a_b/(\Delta^a_b + \Delta^b_b)$. Thus the relative intrinsic shifts can be obtained even without the knowledge of the shifts in the absence of complexation.

6. Applications

The application of lanthanide shift reagents is intimately related to the general use of NMR spectroscopy in chemistry. The important features of NMR spectra of lanthanide complexes with regard to their applications are enhanced resolution between the spectral lines of ligand nuclei and structural dependence of the shift magnitude. Lanthanide chelates are now routinely used as shift reagents in organic NMR and complete coverage of the large volume of examples is beyond the scope of this chapter. The application of lanthanides to the study of systems of biological interest is covered in chapter 39. In this section we give only a few illustrative examples most of which have appeared since the publication of the earlier reviews of the subject.

6.1. *Spectral resolution and simplification*

Spectral resolution is the most dramatic exhibition of the effect of a paramagnetic lanthanide on the NMR spectra of ligands. This is illustrated in fig. 38.9 by the effect of Eu^{3+} on the proton spectrum of xylitol. An entirely featureless spectrum is transformed into a well resolved one. Angyal et al. (1974) have shown that lanthanides interact with polyols that can achieve an appropriate conformation of three hydroxyl groups on consecutive carbon atoms (cf. ch. 39, section 3.2). Thus, Eu^{3+} forms complexes with xylitol in aqueous solution. As seen in fig. 38.9, the coupling constants between the protons at positions 2 and 3 decrease with increasing the Eu^{3+} concentration indicating that the conformation of xylitol in its complexed form is different from its equilibrium conformation in solution. However, at very low lanthanide concentrations the coupling constants reflect largely the solution conformation. The conformations of a number of cyclic ribonucleotides with different bases have been determined on the basis of coupling constants obtained from the lanthanide resolved spectra (Kainosho and Ajisaka, 1975). In experiments of chemically induced dynamic nuclear polarization many reaction products may occur giving rise to overlapping spectral lines, which can be resolved by the addition of small amounts of lanthanide shift reagents (Bargon, 1973). Deuteron relaxation times are often more readily interpretable than those of other nuclei; however, deuteron chemical shifts (in frequency units) are small and line overlap is a problem. Spectral resolution can be achieved using lanthanide shift reagents. In this case small amounts of the reagent must be employed since at reagent/ligand ratios >0.02 the effect of the reagent on the relaxation times becomes significant (Wooten et al., 1975).

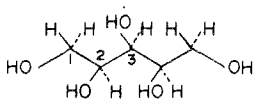

Xylitol

6.2. *Structure elucidation*

The pinnacle of the application of lanthanide shift reagents seemed to be in their assistance in the elucidation of the structure of molecules in solution. It must be borne in mind, however, that the intrinsic dipolar shift, Δ_d, due to the central lanthanide ion is the only part of the observed shift useful in this respect and then only in cases of effective axial symmetry is it readily applicable. Therefore great care should be exercised in the use of lanthanide induced shifts to solve structural problems. Generally the following types of problems may successfully be approached.

(i) Determination of isomeric composition, including *cis–trans* isomerism, rotamers and ring inversions.

(ii) Structure elucidation of molecules containing a rigid moiety of known structure that can serve as a reference frame.

(iii) Determination of the nature and relative position of a coordinating group within a molecule.

Configurational assignments for *cis–trans* pairs of the esters of α,β unsaturated mono- and dicarboxylic acids have successfully been made using $Eu(fod)_3$, Ceder and Beijer (1972), however a similar attempt with a more complex pair has failed. Montaudo et al. (1973) have similarly treated a series of unsaturated aldehydes, ketones, esters and amides. These authors compared data for the pure *cis* and *trans* isomers and then sought the fit of the shifts observed in isomer mixtures with a given population ratio. Lanthanide chlorides were used to assign the configuration of unsaturated carboxylic acids in aqueous solutions (Davoust et al. 1975).

The possibility to discriminate between four isomeric α,β unsaturated sulfones on the basis of the shifts induced by $Eu(fod)_3$ has been investigated by Selling (1975). The minimum in the agreement factor between experimental and calculated shifts was used. This approach, had it been intended to solve the molecular geometry in absolute terms, would have the same shortcomings as in many other cases. However, the more limited aim of devising a procedure by which an isomer could be distinguished on the basis of structural differences as reflected in the induced shifts, was nevertheless achieved. This may serve as an illustration of the kind of structural problems that can be solved by this method. A general outline of the experimental and computational procedures used in conjunction with lanthanide shift reagents in the determination of molecular conformation in solution has recently been presented by Willcott and Davis (1975). Despite their optimistic prognosis, severe limitations to the applicability of this approach can be inferred from the examples given in their article as well as from a more recent analysis of random errors in the coordinates (Hinckley and Brumley, 1976). An iterative computer program capable of handling three sets of shift and relaxation data has been described by Stilbs (1975). He gives general recommendations for averaging procedures to treat cases with conformational equilibria.

The problem of averaging in the case of internal rotations has been discussed by Armitage et al. (1973). Here, as in many other instances, a unique lanthanide position is assumed. In testing this assumption, Chadwick (1974) has concluded that, if the coordinating atom has more than one lone pair of electrons, e.g. a carbonyl oxygen, the assumption may not be valid. A multisite model for lanthanide shift reagent coordination to monofunctional substrates has been developed in our laboratory (Lenkinski and Reuben, 1976b). It treats the two lone pairs of an unsymmetrically substituted ketone, *e.g.* pinacolone, $(CH_3)CCOCH_3$, as two distinct coordination sites. This necessitates the averaging of the effects produced by association at these sites weighted according to their respective populations. Included in the procedure are different methods of averaging over internal rotations. Both chemical shift and line-broadening data are considered. The simultaneous application of both sets of data removes many of the ambiguities present if only one kind of data is

employed. The lanthanide-oxygen distance obtained is in good agreement with crystallographic determinations.

The determination of rotamer populations in 2-alkyl-4-tert-butylcyclohexanones has been elegantly approached by Servis and Bowler (1975). First the ratios of $Yb(dpm)_3$ induced shifts in the ring protons were used to locate the lanthanide atom from the minimum in the agreement factor, thereby establishing the magnetic frame of reference. Then the shift ratios for each of the rotamers of the 2-alkyl group were calculated with the dipolar shift equation for an axially symmetric complex. With at least three side-chain resonances, solutions for the three rotamer populations could be obtained using the observed and calculated shift ratios. It is rather unfortunate that the reliability of the resulting populations depends on the certainty of the lanthanide location, which should be considered to be rather arbitrarily determined in this particular case. The above compounds are unsymmetrically substituted ketones and therefore the multisite model (*vide supra*) had to be employed. Using the data for 4-*tert*-butylcyclohexanones the ring inversion equilibria in 2-alkyl-cyclohexanones complexed to lanthanide shift reagents has also been studied (Servis and Bowler, 1973; Servis et al., 1975). In this case no spatial location of lanthanide is needed and the shift reagent is only used to resolve spectra and induce shifts. The essentially analogous systems of 4-*tert*-butyl-1-methylcyclohexanol and the conformationally mobile 1-methylcyclohexanol have been investigated by Bouquant et al. (1974). They found that the equatorial conformation of the hydroxyl group was preferred for complexation with $Eu(dpm)_3$.

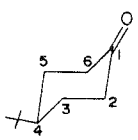

4–*tert*–butylcyclohexanone

We wish to point out that it has been customary in the literature to assume axial symmetry in order to obtain structural information using fitting procedures. This assumption, however, may often be wrong. Thus, e.g., Newman (1974) has shown that for complexes that can exist only in two rotational conformations, the non-axial term of the dipolar shift equation cannot average out (cf. 2.6). In such cases either eq. 38.11 or an equivalent expression, in which the angles are defined relative to the bond between the lanthanide and the coordinating atom, have to be employed. For the $Pr(dpm)_3$-camphor system a better agreement between experimental and calculated shifts is obtained by this method, without any optimization of the lanthanide-oxygen distance.

6.3. *Chiral molecules and shift reagents*

The features of the proton NMR spectrum are closely related to the symmetry properties of the molecule under consideration. Nuclei that are interconvertible by rapid rotation, e.g. the methyl protons, are called equivalent. They are isochronous (resonate at the same frequency) under any circumstances. Nuclei that are interchangeable by reflection in a plane of symmetry are called enantiotopic, e.g. the α-protons of substituted ethanes. They are isochronous in an achiral environment but may become anisochronous in a chiral environment. Nuclei that can be interchanged only by reflections through more than one plane are called diastereotopic, e.g. the β-protons of α-amino acids. They are anisochronous under any circumstances. However, accidental chemical shift degeneracies may occur. For such cases the normal achiral lanthanide shift reagents may be employed. Their effect on the NMR spectrum is tantamount to the application of a much higher external magnetic field. Obviously shift reagents cannot resolve nuclei which are in principle isochronous. Enantiotopic nuclei may be resolved by chiral shift reagents.

Overlooking the above principles a number of authors have reported on "unexpected" effects of shift reagents. In all of the cases, however, the observed effects could be anticipated. Thus, Bose et al. (1972) have found that $Eu(dpm)_3$, $Yb(dpm)_3$, $Eu(fod)_3$ and $Pr(fod)_3$ are capable of resolving the diastereotopic protons of some β-lactames, which display a single peak at 60 MHz. For other compounds of the same type the diastereotopic protons were anisochronous to begin with. The non-equivalence however decreased upon the addition of the downfield shifting reagents $Eu(dpm)_3$ and $Yb(dpm)_3$, but was augmented by the addition of $Pr(fod)_3$, which causes upfield shifts. Mariano and McElroy (1972) have found that the chemical shifts between diastereotopic protons in a series of alcohols are increased by the addition of $Eu(fod)_3$. This increase changes along the chain and is not necessarily maximal for the protons with the largest induced shifts. The authors suggest an unsymmetrical positioning of the lanthanide atom about the C–O bond as a possible mechanism for the observed effects. Their explanation concurs with the multisite model of coordination to monofunctional substrates discussed in section 6.2.

The resolution of mixtures of steroidal diastereomers using $Eu(dpm)_3$ has been reported by Joseph-Nathan et al. (1972). More recently DePuy et al. (1976) demonstrated that $Eu(fod)_3$ resolves not only the diastereomers of 2-methoxy-3-methyl-pentane but also the additional pairs of diastereomers obtained by monodeuteration at position 4. It should be emphasized that spectral resolution of diastereomeric mixtures by achiral shift reagents may occur by two possible mechanisms: different shifts in the adducts and different association constants. If the latter is the dominant mechanism the chemical shift difference induced by the reagent will have a maximum at certain reagent concentration and will decrease with increasing the concentration.

The resolution of enantiomeric mixtures, e.g. L- and D-α-amino acids, is a problem of long standing interest. Enantiomers are pairs of compounds that are

mirror images of each other. A simple approach involving achiral lanthanide shift reagents has recently been introduced by Pirkle and Sikkenga (1975). An enantiomerically pure chiral solvent is used that forms chiral solvates with the compounds of interest. The solvates are now diastereomers and a shift reagent may be used to resolve them. There are several mechanisms that could lead to resolution all of which are discussed in detail by the authors. Another possibility involves the use of shift reagents forming 1:2 adducts, e.g. $Eu(fod)_3$ (Ajisaka and Kainosho, 1975). Since the 1:1 adduct will be chiral, it will in principle differentiate between the enantiomers while forming the 1:2 adduct. In particular the R-LD and the R-LL (or R-DD) adducts will be diastereomeric. Thus maximal resolution is obtained with one of the components in excess. In addition, since this type of chiral recognition is brought about by complex formation, the observed effects will depend on the equilibrium constants and therefore on the concentrations of the reagent and the substrates.

A chiral lanthanide shift reagent can be made by using a chiral β-diketonate, e.g. camphorato derivatives (Goering et al., 1971; Whitesides and Lewis, 1970, 1971). They are used to determine enantiomeric purity by integrating the resolved signals (Goering et al., 1974; Shaath and Saine, 1975). The resolution of *meso* from d- or l-diastereomers has also been demonstrated (Kainosho et al., 1972).

6.4. *Quantitative analysis of mixtures*

As could be inferred from the discussion in the preceding paragraphs lanthanide shift reagents should be useful in the spectral resolution and identification of mixtures of compounds. Integration of the corresponding resonances readily yields a quantitative analysis of the mixture. This analytical approach has successfully been used with a number of systems and illustrations can be found in previous reviews of the field. Recent examples are given here.

Thiocyanates, X-SCN, have usually been distinguished from isothiocyanates, X-NCS, by infra-red spectroscopy, which sometimes provides ambiguous evidence. Anderson and Norbury (1975) have shown that $Eu(fod)_3$ induces substantial shifts in thiocyanates, whereas virtually no shifts are observed with isothiocyanates, since sulfur is practically a non-coordinating atom. Thus mixtures of these two classes of compounds are readily analyzable.

Unsaturated triglycerides are an important constituent of natural fats and oils. For their analysis a time consuming method is usually employed consisting of enzymatic hydrolysis and chromatographic separation. Fronst et al. (1975) have recently shown that $Pr(fod)_3$ can induce chemical shift differences between the fatty acid residues at the α- and β-positions of the triglyceride up to 18 carbon atoms along the chain (at 220 MHz). In this way the fatty acid is not only identified, but also its position determined.

The applicability of $Eu(fod)_3$ as a shift reagent for carboxylic acid and phenols has recently been demonstrated. It has been used in the quantitative analysis of

mixtures of cresol isomers (Werstler and Suman, 1975), and recommended for use in the analysis of mixtures of other derivatives (Shoffner, 1975).

6.5. *Kinetic applications*

The two methyl groups in dimethylformamide are not equivalent. Their signals coalesce into a singlet when the rotation around the C–N bond is faster than the chemical shift between them. If by changing the temperature one could change the conditions from slow to fast exchange, the kinetics of the rotation process could be studied. The larger the chemical shift between the two groups the higher the temperature at which coalescence will occur. Cheng and Gutowsky (1972) have demonstrated the applicability of shift reagents of the $R(fod)_3$ type to increase the chemical shift difference in such kinetic studies. Subsequently, Mannschreck et al. (1973) used a chiral europium shift reagent to split two enantiotopic methyl groups of an aryl-nitrosamine. Coalescence was observed upon raising the temperature thereby permitting the study of the kinetics of rotation around the N-aryl bond.

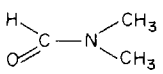

dimethylformamide

7. Chemistry

The *tris* β-diketonates of the lanthanides are soluble in organic solvents and are therefore the compounds most commonly used as shift reagents. The $R(dpm)_3$ series[1] was synthesized and characterized by Eisentraut and Sievers (1965). The $R(dpm)_3$ reagents form 1:1 adducts with Lewis bases in solution (Bouquant and Chuche, 1972; Ghotra et al., 1973; Catton et al., 1976). This is an important feature that may simplify quantitative application (cf. section 5). The $R(fod)_3$ series[2] was synthesized by Springer et al. (1967) and $Eu(fod)_3$ was introduced as a shift reagent by Rondeau and Sievers (1971). The $R(fod)_3$

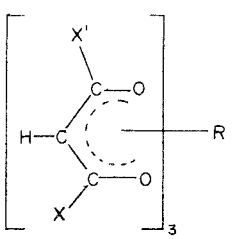

1 $X = -C(CH_3)_3$, $X' = -C(CH_3)_3$
2 $X = -C(CH_3)_3$, $X' = -CF_2CF_2CF_3$
3 $X = -CH_3$, $X' = -CH_3$
4 $X = -CF_2CF_3$, $X' = -CF_2CF_3$

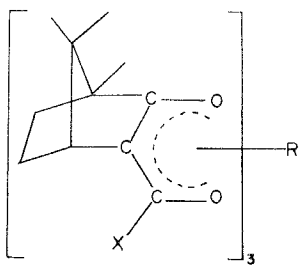

5 $X = -C(CH_3)$
6 $X = -CF_2CF_2CF_3$
7 $X = -CF_3$

reagents are more soluble in organic solvents and are stronger Lewis acids than $R(dpm)_3$. Therefore their application has received wide attention. Unfortunately they form 1:2 adducts, a fact that may lead to complications in quantitative applications. Derivatives with higher fluorination[4] have also been synthesized (Burgett and Warner, 1972), however the expectations that they will induce larger shifts than the $R(fod)_3$ analogues have not been borne out.

Chiral shift reagents are also *tris* β-diketonates based on d-camphor as the chiral moiety. Whitesides and Lewis (1970) introduced the *tris*[3-(*tert*-butyl-hydroxy-methylene)-d-camphorato] europium.[5] It is more soluble in organic solvents than $Eu(dpm)_3$ with otherwise similar chemical properties. Fraser et al. (1971) prepared a fluorinated derivative anticipating advantages similar to those of $R(fod)_3$ relative to $R(dpm)_3$. Indeed their *tris*[3-(heptafluoropropyl hydroxy-methylene)-d-camphorato] europium[6] induces larger chemical shift differences between enantiomers in most of the cases. Even larger differences were obtained with *tris*[3-trifluoromethyl-hydroxymethylene)-d-camphorato] europium[7] (Goering et al., 1971).

A number of investigations of the aggregation properties of lanthanide shift reagents in solution have been carried out. Their results should be of significance regarding the equilibria in shift reagent systems. An extensive gas chromatographic study has been carried out by Feibush et al. (1972). They concluded that substrate coordination occurs with the monomeric species and that reagent dimerization is a concurrent process competing with the substrate. The dimerization process is more prominent for the lighter (and larger) lanthanides. The reagents with bulkier β-diketonates are less affected by the dimerization process. No dimerization for the $R(dpm)_3$ series has been detected by vapor pressure osmometry, whereas for the $R(fod)_3$ dimerization is significant in carbon tetrachloride and n-hexane (Desreux et al., 1972). Dimerization in chloroform or in the presence of strongly coordinating substrates seems to be less significant. Similar studies in benzene as the solvent have shown that dimerization decreases along the lanthanide series (Porter et al., 1973). Analogous results have been obtained in carbon tetrachloride (Bruder et al., 1974). Dimerization of chiral shift reagents with the lighter lanthanides has also been observed, whereas those with the heavier members are practically monomeric (Denning et al., 1973).

The structure of a number of shift reagent adducts has been determined by X-ray crystallography. Similar structures were obtained for $Ho(dpm)_3$. 2(4-methylpyridine)(Horrocks et al., 1971), and for $Eu(dpm)_3 \cdot 2$ pyridine (Cramer and Seff, 1972). The lanthanide coordination sphere can be described as a square antiprism with the pyridine molecules occupying the apices of opposite square faces. For $Lu(dpm)_3 \cdot 3$-methylpyridine a structure that can be described as a capped trigonal prism has been obtained (Wasson et al., 1973). The relevance of these structures for NMR studies in solution is however not well established. A recent fluorescence study has shown that the $Eu(dpm)_3 \cdot 2$ pyridine system retains its solid state structure in solution (Catton et al., 1975). On the other hand considerable configurational lability was observed in the $Eu(dpm)_3$-borneol

system. Catton et al. (1975) suggest that the low symmetry of the borneol molecule imposes no preferences and thus there is a low activation energy for interconversion between a capped octahedral and a face-centered prismatic structure. In this case a time-averaged effective axial symmetry is possible.

The aquo-complexes of the lanthanides are often used as aqueous shift reagents. Their application, however, is restricted to the acidic side of neutral pH due to the precipitation of hydroxides at higher pH values. The use of the $R(EDTA)^-$ chelates at higher pH has been suggested and a characterization study has been carried out in this laboratory, (Elgavish and Reuben, 1976). With carboxylates as substrates the useful pH range is between 6 and 10, confined on the acidic side by the formation of carboxylic acid and on the basic side by the formation of hydroxo complexes of the chelates. The reagent-substrate stoichiometry is practically 1:1.

8. Concluding remarks

The discovery of lanthanide shift reagents has provided a new dimension to the study of molecular structure and dynamics in solution and is responsible for focussing the attention on the chemistry of lanthanide complexes. Lanthanide shift reagents are now routinely used in organic NMR spectroscopy. The great interest in their application led to a number of important theoretical and experimental studies on the NMR of lanthanide complexes. The presently available experimental results seem to conform to current theories. However more data are needed on the temperature dependence of chemical shifts as well as on the crystal field parameters in lanthanide complexes for which NMR data are available. Such data are required for the direct and rigorous comparison between theory and experiment as well as for the separation of contributions due to different shift mechanisms. At the present state of the art there are some doubts regarding the accurate determination of molecular structure on the basis of lanthanide induced shifts alone. Relaxation measurements may be of great help in this respect. The treatment of special and well defined structural problems is however quite feasible particularly in systems with rigid molecular fragments. The magnetic axes determined for a relatively small lanthanide complex may be used in the structure elucidation of more complex molecules containing the same coordinating moiety. Some tentative recommendations regarding the treatment of data obtained in shift reagent studies are given in this chapter. Further developments in the field are likely to result in more clearly cut recipes.

References

Abragam, A. and B. Bleaney, 1970, Electron Paramagnetic Resonance of Transition Ions (Clarendon Press, Oxford) Ch. 5.

Ajisaka, K. and M. Kainosho, 1975, J. Amer. Chem. Soc. **97**, 1761.

Anderson, S.J. and A.H. Norbury, 1975, J.C.S. Chem. Comm., 48.

Angyal, S.J., D. Greeves and V.A. Pickles, 1974, Carbohyd. Res. **35**, 165.

Armitage, I.M., L.D. Hall, A.G. Marshall and L.G. Werbelow, 1973, J. Amer. Chem. Soc. **95**, 1437.

Bargon, J., 1973, J. Amer. Chem. Soc. **95**, 941.

Bidzilya, V.A., N.K. Davidenko, L.P. Golovkova and K.B. Yatsimirskii, 1975, Dokl. Akad. Nauk. SSSR, **225**, 842.

Bleaney, B., 1972, J. Mag. Res. **8**, 91.

Bleaney, B., C.M. Dobson, B.A. Levine, R.B. Martin, R.J.P. Williams and A.V. Xavier, 1972, J.C.S. Chem. Comm., 791.

Bouquant, J. and J. Chuche, 1972, Tetrahed. Lett., 2337.

Bouquant, J., M. Wuilmet, A. Maujean and J. Chuche, 1974, J.C.S. Chem. Comm., 778.

Bose, A.K., B. Dayal, H.P.S. Chawla and M.S. Manhas, 1972, Tetrahed. Lett., 3599.

Briggs, J.M., G.P. Moss, E.W. Randall and K.D. Sales, 1972, J.C.S. Chem. Comm., 1180.

Bruder, A.H., S.R. Tanny, H.A. Rockefeller and C.S. Springer, Jr., 1974, Inorg. Chem. **13**, 880.

Burgett, C.A. and P. Warner, 1972, J. Mag. Res. **8**, 87.

Catton, G.A., F.A. Hart and G.P. Moss, 1975, J.C.S. Dalton, 221.

Catton, G.A., F.A. Hart and G.P. Moss, 1976, J.C.S. Dalton, 208.

Ceder, O. and B. Beijer, 1972, Acta Chem. Scand. **26**, 2977.

Chadwick, D.J., 1974, Tetrahed. Lett., 1375.

Chalmers, A.A. and K.G.R. Pachler, 1974, J.C.S. Perkin II., 748.

Cheng, H.N. and H.S. Gutowsky, 1972, J. Amer. Chem. Soc. **94**, 5506.

Chmelnick, A.M. and D. Fiat, 1972, J. Mag. Res. **7**, 418.

Cockerill, A.F., G.L.O. Davies, R.C. Harden and D.M. Rakham, 1973, Chem. Rev. **73**, 553.

Conger, R.L. and P.W. Selwood, 1952, J. Chem. Phys. **20**, 383.

Cramer, R.E. and K. Seff, 1972, J.C.S. Chem. Comm., 400.

Davoust, D., S. Rebuffat, M. Giraud and D. Molho, 1975, C.R. Acad. Sc. Paris C **280**, 815.

Denning, P.G., F.J.C. Rossotti and P.J. Sellars, 1973, J.C.S. Chem. Comm., 381.

DePuy, C.H., P.C. Fünfschilling and J.M. Olson, 1976, J. Amer. Chem. Soc. **98**, 276.

Deranleau, D.A., 1969a, J. Amer. Chem. Soc. **91**, 4044.

Deranleau, D.A., 1969b, J. Amer. Chem. Soc. **91**, 4050.

Desreux, J.F., L.E. Fox and C.N. Reilley, 1972, Anal. Chem. **44**, 2217.

Desreux, J.F. and C.N. Reilley, 1976, J. Amer. Chem. Soc. **98**, 2105.

Eisentraut, K.J. and R.E. Sievers, 1965, J. Amer. Chem. Soc. **87**, 5254.

Elgavish, G.A. and J. Reuben, 1976, J. Amer. Chem. Soc. **98**, 4755.

Elgavish, G.A. and J. Reuben, 1974, J. Mag. Res. **16**, 360.

Evans, D.F. and M. Wyatt, 1972, J.C.S. Chem. Comm., 312.

Evans, D.F. and M. Wyatt, 1973, J.C.S. Chem. Comm., 339.

Evans, D.F. and M. Wyatt, 1974, J.C.S. Dalton, 765.

Feibush, B., M.F. Richardson, R.E. Sievers and C.S. Springer, Jr., 1972, J. Amer. Chem. Soc. **94**, 6717.

Fraser, R.R., M.A. Petit and J.K. Saunders, 1971, J.C.S. Chem. Comm., 1450.

Frost D.J., J. Bus, R. Kenning and I. Sies, 1975, Chem. Phys. Lipids **14**, 189.

Ghotra, J.S., F.A. Hart, G.P. Moss and M.L. Staniforth, 1973, J.C.S. Chem. Comm., 113.

Goering, H.L., J.N. Eikenberry and G.S. Koermer, 1971, J. Amer. Chem. Soc. **93**, 5913.

Goering, H.L., J.N. Eikenberry, G.S. Koermer and C.J. Lattimer, 1974, J. Amer. Chem. Soc. **96**, 1493.

Golding, R.M. and M.P. Halton, 1972, Aust. J. Chem. **25**, 2577.

Golding, R.M. and P. Pyykkö, 1973, Mol. Phys. **26**, 1389.

Granot, J. and D. Fiat, 1975, J. Mag. Res. **19**, 372.

Gueron, M., 1975, J. Mag. Res. **19**, 58.

Gutowsky, H.S., D.M. McCall and C.P. Slichter, 1953, J. Chem. Phys. **21**, 279.

Hinckley, C.C., 1969, J. Amer. Chem. Soc. **91**, 5160.

Hinckley, C.C. and W.C. Brumley, 1976, J. Amer. Chem. Soc. **98**, 1331.

Horrocks, W. DeW., Jr., J.P. Sipe III and J.R. Luber, 1971, J. Amer. Chem. Soc. **93**, 5258.

Horrocks, W. DeW., Jr., J.P. Sipe III and D.R. Sudnick, 1973, Magnetic Anisotropy and Dipolar Shifts in Shift Reagent Systems, in: Sievers, R.E., ed., Nuclear Magnetic Resonance Shift Reagents (Academic Press, New York and London) pp. 53–86.

Horrocks, W. DeW., Jr., 1974, J. Amer. Chem. Soc. **96**, 3022.

Johnston, M.D., Jr., B.L. Shapiro, M.J. Shapiro, J.W. Proulx, A.D. Godwin and H.L. Pearce, 1975, J. Amer. Chem. Soc. **97**, 542.

Joseph-Nathan, P., J.E. Herz and V.M. Rodriguez, 1972, Canad. J. Chem. **50**, 2788.

Kainosho, M., K. Ajisaka, W.H. Pirkle and S.D. Beare, 1972, J. Amer. Chem. Soc. **94**, 5924.

Kainosho, M. and K. Ajisaka, 1975, J. Amer. Chem. Soc. **97**, 6839.
Kurland, R.J. and B.R. McGarvey, 1970, J. Mag. Res. **2**, 286.
La Mar, G.N. and E.A. Metz, 1974, J. Amer. Chem. Soc. **96**, 5611.
Lenkinski, R.E. and J. Reuben, 1976a, J. Mag. Res. **21**, 47.
Lenkinski, R.E. and J. Reuben, 1976b, J. Amer. Chem. Soc. **98**, 4065.
Lenkinski, R.E., G.A. Elgavish and J. Reuben, 1978, J. Mag. Res., in press.
Lewis, W.B., J.A. Jackson, J.F. Lemons, H. Taube, 1962, J. Chem. Phys. **36**, 694.
Luz, Z. and S. Meiboom, 1964, J. Chem. Phys. **40**, 2686.
Maier, T.O. and R.S. Drago, 1972, Inorg. Chem. **11**, 1861.
Mannschreck, A., V. Jonas and B. Kolb, 1973, Angew. Chem. Internat. Edit. **12**, 909.
Mariano, P.S. and R. McElroy, 1972, Tetrahed. Lett., 5305.
Marinetti, T.D., G.H. Snyder and B.D. Sykes, 1975, J. Amer. Chem. Soc. **97**, 6562.
Mayo, B.C., 1973, Chem. Soc. Rev. **2**, 49.
McConnell, H.M. and R.E. Robertson, 1958, J. Chem. Phys. **29**, 1361.
Montaudo, G., V. Librando, S. Caccamese and P. Maravigna, 1973, J. Amer. Chem. Soc. **95**, 6365.
Newman, R.H., 1974, Tetrahedron **30**, 969.
Okigawa, M. and N. Kawano, 1973, Chemistry and Industry 1, 850.
Pirkle, W.H. and D.L. Sikkenga, 1975, J. Org. Chem. **40**, 3430.
Porter, R., T.J. Marks and D.F. Shriver, 1973, J. Amer. Chem. Soc. **95**, 3548.
Reilley, C.N., B.W. Good and J.F. Desreux, 1975, Anal. Chem. **47**, 2110.
Reuben, J. and D. Fiat, 1967a, J.C.S. Chem. Comm, 729.
Reuben, J. and D. Fiat, 1967b, J. Chem. Phys. **47**, 5440.
Reuben, J. and D. Fiat, 1969a, J. Chem. Phys. **51**, 4909.
Reuben, J. and D. Fiat, 1969b, J. Chem. Phys. **51**, 4918.
Reuben, J. and J.S. Leigh, Jr., 1972, J. Amer. Chem. Soc. **94**, 2789.
Reuben, J., 1973a, Progr. NMR Spectosc. **9**, 1.
Reuben, J., 1973b, J. Amer. Chem. Soc. **95**, 3534.
Reuben J., 1973c, Effects of Chemical Equilibrium and Adduct Stoichiometry in Shift Reagent Studies, in: Sievers, R.E., ed., Nuclear Magnetic Resonance Shift Reagents (Academic Press, New York and London) pp. 341–352.
Reuben, J., 1975, J. Chem. Phys. **63**, 5063.
Reuben, J., 1976, J. Amer. Chem. Soc. **98**, 3726.
Rondeau, R.E. and R.E. Sievers, 1971, J. Amer. Chem. Soc. **93**, 1522.
Samitov, Yu. Yu. and Sh. S. Bikeev, 1975, Org. Mag. Res. **7**, 467.
Selling, H.A., 1975, Tetrahedron **31**, 2543.
Servis, K.L. and D.J. Bowler, 1973, J. Amer. Chem. Soc. **95**, 3392.
Servis, K.L. and D.J. Bowler, 1975, J. Amer. Chem. Soc. **97**, 80.
Servis, K.L., D.J. Bowler and C. Ishii, 1975, J. Amer. Chem. Soc. **97**, 73.
Sievers, R.E., ed., 1973, Nuclear Magnetic Resonance Shift Reagents (Academic Press, New York and London).
Shaath, N.A. and T.O. Soine, 1975, J. Org. Chem. **40**, 1987.
Shapiro, B.L. and M.D. Johnston, Jr., 1972, J. Amer Chem. Soc. **94**, 8185.
Shoffner, J.P., 1975, Anal. Chem. **47**, 341.
Springer, Jr., C.S., D.W. Meek and R.E. Sievers, 1967, Inorg. Chem. **6**, 1105.
Stilbs, P., 1975, Chem. Script. 7, 59.
Swift, T.J. and R.E. Connick 1962, J. Chem. Phys. **37**, 307.
Vega, A.J. and D. Fiat, 1976, Mol. Phys.**11**, 347.
Wasson, S.J.S., D.E. Sands and W.F. Wagner, 1973, Inorg. Chem. **12**, 187.
Werstler, D.D. and P.T. Suman, 1975, Anal. Chem. **47**, 144.
Whitesides, G.M. and D.W. Lewis, 1970, J. Amer. Chem. Soc. **92**, 6979.
Whitesides, G.M. and D.W. Lewis, 1971, J. Amer. Chem. Soc. **93**, 5914.
Willcott, III., M. and R.E. Davies, 1975, Science **190**, 850.
Wooten, J., G.B. Savitsky and J. Jacobus, 1975, J. Amer. Chem. Soc. **97**, 5027.

Handbook on the Physics and Chemistry of Rare Earths, edited by K.A. Gschneidner, Jr. and L. Eyring

Chapter 39

BIOINORGANIC CHEMISTRY: LANTHANIDES AS PROBES IN SYSTEMS OF BIOLOGICAL INTEREST

Jacques REUBEN*
Isotope Department, The Weizmann Institute of Science, Rehovot, Israel

Contents

Symbols

E^* = fluorescence enhancement
ΔG^0 = free energy
ΔH^0 = free enthalpy
K_A = association constant
K_D = dissociation constant
n = hydration number
P_M = fractional population at site M
R = the gas constant
r = internuclear distance
ΔS^0 = free entropy
T_1 = longitudinal relaxation time
T_{1M} = longitudinal relaxation time in a paramagnetic complex
T_{1p} = incremental longitudinal relaxation time
Δ_M = chemical shift in a paramagnetic complex
ε_b = relaxation rate enhancement
λ_{em} = emission wave length
λ_{ex} = excitation wave length
θ = angle between r and principal axis of symmetry
τ_c = correlation time
ω = nuclear resonance angular frequency

1. Introduction

The bioinorganic chemistry of lanthanides is a research subject of the 1970's. It started when several groups reported independently on the use of lanthanides as spectroscopic and magnetic probes in systems of biological interest. Parti-

*Present address: Department of Chemistry, University of Houston, Houston, Texas 77004, USA

cularly encouraging was the finding by Darnall and Birnbaum (1970) that Nd^{3+} could accelerate the rate of an enzymatic reaction. The term Bioinorganic Chemistry in conjunction with lanthanides first appeared in 1972 on the program of the 10th Rare Earth Research Conference chaired by Therald Moeller. At that conference, held in the spring of 1973, researchers actively working on the various aspects of the subject met already for the second time to report on the advances and discuss the problems in this field.

While unusual concentrations of lanthanides have been observed in the leaves of some hickory trees, (Robinson et al., 1958), it seems that the lanthanides are of little biological importance per se. However other metal ions do play important roles in biological systems by being involved in a variety of catalytic and transport processes as well as in serving as triggers and messengers. The cations of sodium, potassium, magnesium, and calcium, which are the most abundant in living systems, are ions with inert-gas closed electronic shells and lack the spectral characteristics that could be used to deduce on their environment. It was in this regard that an Anonymous correspondent (1971) formulated the "Parkinson Law of Biochemistry" stating that the importance of studying a system is inversely proportional to the ease of doing so. The remarkable multitude of spectroscopic and magnetic properties of the tripositive lanthanide ions coupled with the similarity of chemical properties along the series makes them very appealing as probes of the metal ion binding sites of biological macromolecules as well as of the structure, dynamics, and function in these systems. The ionic radius of Ca^{2+} (0.99 Å) is within the range of ionic radii of the lanthanides and the possibility of isomorphous replacement has been emphasized, (Williams, 1970).

Review articles dealing with various aspects of the subject have already appeared in the literature. Glasel (1973) has discussed the chemical shift effects of lanthanides in the nuclear magnetic resonance (NMR) spectra of biological systems with emphasis on nucleotides. Nieboer (1975) has treated the subject vis à vis the coordination chemistry of lanthanides in model systems. Readers of Russian may find interest in an article by Schwarzburd (1975). This chapter is intended to provide a summary of the physical methods that have been employed in studies of biological systems with lanthanides and a comprehensive review of the bioinorganic chemistry of the lanthanides emerging from these studies. Thus section 2 outlines the principles and provides examples of studies utilizing optical absorption, fluorescence, circularly polarized luminescence, nuclear relaxation rates, NMR chemical shifts, NMR of lanthanum-139, electron paramagnetic resonance (EPR) of Gd^{3+}, Mössbauer spectroscopy, and X-ray crystallography. It is followed by a section that reviews the interaction of lanthanides with molecules of biological interest including amino acids, carbohydrates, nucleotides and sugar phosphates, porphyrins, nucleic acids, proteins and enzymes, and phospholipids and membranes. What may be regarded as a résumé of this chapter has been published (Reuben, 1975a).

2. Physical methods

The electronic energy levels of lanthanide aquo-ions are only slightly perturbed upon complex formation. Nevertheless these perturbations, particularly those associated with changes in the ligand-field symmetry, are often spectroscopically discernible. Outstanding are however interactions of the dipole-dipole type that are transmitted through space. Interactions of this kind give rise to such diverse phenomena as intensity enhancement of lanthanide fluorescence and shifts and enhanced relaxation rates in the resonances of ligand nuclei. In this respect macromolecules, in contrast to small ligands, offer the possibility of having close spatial proximity between a lanthanide and a molecule or a molecular fragment without actual association between the two. Another major difference, reflected mainly in nuclear relaxation rates, is the longer molecular tumbling times characteristic of macromolecular complexes. All these properties and phenomena, with the different combinations among them, make possible the application of a rather wide spectrum of physical methods in the study of systems of biological interest using the lanthanides as probes. By some of the techniques a property of the lanthanide ion is observed whereas others detect spectral changes in its environment.

2.1. *Optical absorption*

The lanthanides exhibit typically sharp but complicated absorption spectra in the visible and near-ultraviolet region, which are of relatively low intensity. The spectral features indicate that the f-orbitals are well shielded from the environment. However Karraker (1967) has shown that the spectral lines in the 500–600 nm region associated with the $^4I_{9/2} \rightarrow {}^4G_{5/2}$, $^2G_{7/2}$ transitions of Nd^{3+} are sensitive to complex formation. The use of these "hypersensitive" transitions in studying the interaction of lanthanides with molecules of biological interest was introduced by Birnbaum et al. (1970). These authors have shown that, when a difference spectrum is recorded between two solutions of identical Nd^{3+} concentrations one of which contains bovine serum albumin, distinct features are observed at ca. 520 and 580 nm. The same research group carried out investigations with trypsin and trypsinogen as well as with a number of carboxylic and amino acids (Darnall et al., 1971a; Birnbaum and Darnall, 1973). Typical difference spectra obtained with EDTA and with trypsin as ligands are reconstructed in fig. 39.1. It is seen that the two ligands give rise to rather similar effects. It thus seems that it will be difficult to identify the binding site on a protein from the shape of the difference spectrum alone. However the spectral intensity depends on pH, being a function of the amount of Nd^{3+} bound, and may serve in the determination of the pK's of the protein ligands at the binding site (Birnbaum and Darnall, 1973).

Difference absorption spectra of Nd^{3+} have been observed with staphylococcal nuclease by Williams (1971) and with *E. coli* glutamine synthetase by Wedler and D'Aurora (1974). In the latter case the spectra were used in a qualitative

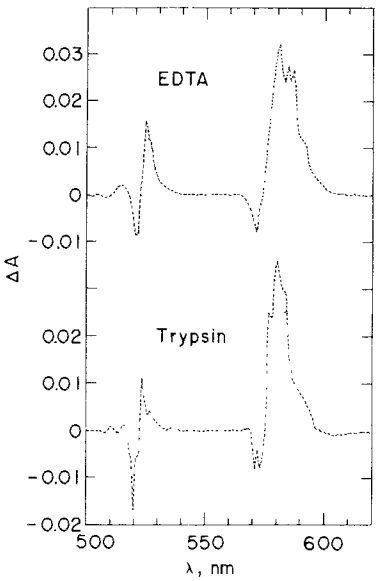

Fig. 39.1. Neodymium (III) difference absorption spectra with EDTA and with trypsin at pH 5.6. Reconstructed from Darnall et al. (1971). Concentrations: Nd^{3+} 3.74 mM, EDTA 87.5 mM, Nd^{3+} 26 mM, trypsin 0.37 mM.

evaluation of the nature of the metal ion environment and its perturbation by small molecules bound to the protein.

The lanthanides perturb the ultraviolet absorption spectra of proteins particularly when aromatic chromophores are at or near the binding site. Luk (1971) observed sharp maxima in the 245 and 295 nm regions of the difference spectrum of transferrin saturated with Tb^{3+} versus that of metal free protein. The shape of the spectrum suggests that the binding of lanthanides modifies the local environment of tyrosine residues. Similar results have been obtained with lactoferrin, which is also an iron-binding protein, (Teuwissen et al., 1972). The intensities of difference spectra can be used to monitor the binding of lanthanides to proteins. Luk (1971) carried out such a study with transferrin and concluded that the protein had two specific but inequivalent binding sites for Eu^{3+}, Tb^{3+}, Ho^{3+}, and Er^{3+} and only one site for the larger Pr^{3+} and Nd^{3+} ions. Protein difference spectra have also been reported for staphylococcal nuclease and some of its mononitrotyrosine derivatives, (Furie et al., 1973). In this case it was shown that Ca^{2+} failed to perturb the protein spectrum.

2.2. *Fluorescence*

Most of the trivalent lanthanides exhibit strong fluorescence either in their crystals or in solution. Weissman (1942) has shown that lanthanide complexes when excited with light absorbed by the ligand give rise to enhanced fluorescence at frequencies similar to those of the aquo-ions. This is due to intramolecular energy transfer from excited energy levels of the ligand to the 4f

levels of the lanthanide ions. Particularly strong emission is observed with complexes in which the ligand has a triplet state lying above the lowest level of the first excited-term multiplet of the ions. Thus both proteins and nucleic acids, by virtue of being abundant in aromatic residues, should be good ligands in this respect. The use of Tb^{3+} as a fluorescent probe in studies of biological macromolecules was introduced by Luk (1971). More recently Luk and Richardson (1974), (1975) investigated and discussed the effects of carboxylic and amino acids on the fluorescence spectra of Tb^{3+} and Eu^{3+} as well as on their circularly polarized luminescence.

The lowest lying level of the first excited-term multiplet of Tb^{3+} is $^5D_4$, which is ca. 20000 cm^{-1} above the lowest lying $^7F_6$ level of the ground-term multiplet, (Carnall et al., 1968a). Transitions between the $^5D_4$ level and the ground term $^7F_6$, $^7F_5$, $^7F_4$, and $^7F_3$ levels usually give rise to an emission spectrum in the 450–650 nm region. Typical spectra of the Tb^{3+} aquo-ion and its complex with porcine trypsin are shown in fig. 39.2. The large enhancement of the fluorescence intensity resulting from the binding of Tb^{3+} to the protein is evident. The maximum enhancement is usually observed for the $^5D_4 \rightarrow {}^7F_5$ transition. It is also found that the enhancement, E^*, strongly depends upon the excitation wavelength, (Epstein et al., 1974). From the value of λ_{ex} leading to maximum E^* the residue involved in energy transfer can often be identified. A summary of fluorescence spectral data for a number of Tb^{3+} complexes with biological macromolecules is given in table 39.1.

The fluorescence enhancement can be used to quantitate the binding of Tb^{3+} to macromolecules. Displacement of bound Tb^{3+} by other cations competing for the

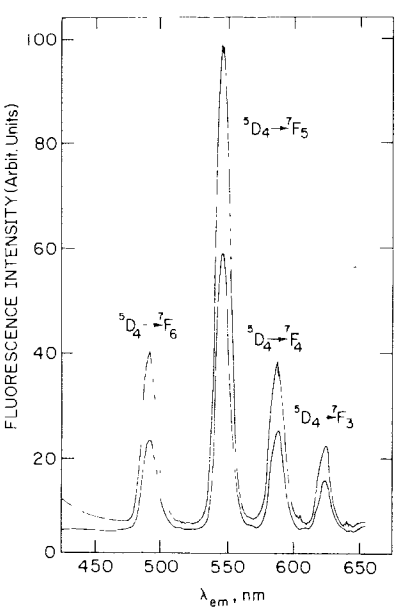

Fig. 39.2. Fluorescence emission spectra with λ_{ex} = 265 nm of 0.1 M $TbCl_3$ in the presence (upper curve) and the absence (lower curve) of 1.25×10^{-5}M porcine trypsin at pH 6.3. Adapted from Epstein et al. (1974).

TABLE 39.1.
Fluorescence spectral data for macromolecular complexes of Tb^{3+}

Ligand	λ_{ex}(nm)	λ_{em}(nm)	E^*	Assignment	Reference
Alk. phosphatase	280	492, 545, 580	–	–	Cottam et al. (1974a)
Concanavalin A	315	492, 545	–	–	Sherry and Cottam (1973)
Bovine factor X	280	490, 545	$\sim 10^4$	Tyr or Trp	Furie and Furie (1975)
Ig G	295	545	$\sim 10^2$	–	Dower et al. (1975)
Parvalbumin	259	545	–	Phe	Donato and Martin (1974)
Thermolysin	280	545	$\sim 7 \times 10^3$	Trp	Berner et al. (1975)
Transferrin	295	550	$\sim 10^5$	Tyr	Luk (1971)
Troponin	275	550	$\sim 10^4$	Tyr	Bunting et al. (1974)
Troponin C	280	545	–	Thr	Miller et al. (1975)
Bovine trypsin	295	545	1.8×10^4	Trp	Epstein et al. (1977)
Porcine trypsin	295	490, 545	$5 \times 10^4, 9 \times 10^4$	Trp	Epstein et al. (1974)
DNA	307	491, 545	–	–	Yonuschot and Mushrush (1975
rRNA	290	488,541	$> 10^3$	–	Barela et al. (1975)
tRNA	285	545	–	–	Formoso (1973)
tRNA	345	545	~ 500	s^4U	Kayne and Cohn (1974)

same site will result in an apparent quenching of the fluorescence, the magnitude of which can be used to monitor the binding of the competing ions, (Epstein et al., 1974).

Because of energy transfer the fluorescence of the protein or the nucleic acid itself is quenched upon binding of Tb^{3+}. Thus, e.g., the fluorescence of porcine trypsin is quenched to the extent of 21% by Tb^{3+} whereas Ca^{2+} produces no quenching, (Epstein et al., 1974). Such effects can be useful in the assignment of residues involved in energy transfer and in fact some of the assignments given in table 2.1 have been made in this way. It is noteworthy that several of the lanthanides can produce quenching effects. Ricci and Kilichowski (1974) report the following order of efficiency to quench indole fluorescence: $Eu^{3+} > Yb^{3+} > Sm^{3+} > Tb^{3+} > Gd^{3+} > Ho^{3+} \approx Dy^{3+}$. They also found that Eu(EDTA) was more efficient in this respect than Eu^{3+}. A likely origin of this effect is that at the pH of the experiments the indole ring is protonated and as a cation it interacts better with the anionic EDTA chelate.

Quenching of Tb^{3+} fluorescence can occur as a result of dipole-dipole interaction with another nearby paramagnetic ion. The magnitude of the effect depends upon the inverse sixth power of the distance between the two ions. This effect was demonstrated by Berner et al. (1975), who used it to determine the distance between a Tb^{3+} ion occupying the "double" calcium site of thermolysin and Co^{2+} replacing the Zn^{2+} ion at the active site of the enzyme. The distance obtained, 13.6 ± 0.5 Å, is in close agreement with X-ray crystallographic determinations. On similar grounds the lack of energy transfer between Tb^{3+} and Fe^{3+} ions bound simultaneously to transferrin led to the conclusion that the respective binding sites are at least 43 Å apart, (Luk, 1971).

Europium can also be a useful fluorescent probe. The lowest lying level of the first excited-term multiplet of Eu^{3+} is $^5D_0$, which is ca. $17000\,cm^{-1}$ above the lowest lying $^7F_0$ level of the ground-term multiplet, (Carnall et al., 1968b). Transitions between the $^5D_0$ level and the ground term $^7F_0$, $^7F_1$, and $^7F_2$ levels usually give rise to an emission spectrum in the 500–700 nm region. Eisinger and Lamola (1971) have shown that the fluorescence is enhanced upon binding of Eu^{3+} to nucleotides. The enhancement was used to probe the excited electronic states and the energy transfer characteristics of nucleotides and polynucleotides in solution, (Lamola and Eisinger, 1971). Kayne and Cohn (1974) found that for the Eu^{3+} – tRNA complex the fluorescence intensity at 585 nm (with $\lambda_{ex} =$ 394 nm) was 300 times as large as that of the aquo-ion. Similar effects were observed by Wolfson and Kearns (1974, 1975), who used the enhancement to monitor the binding of Eu^{3+} to tRNA.

The luminescence of ytterbium-porphyrin complexes has also been investigated and found to be associated with intramolecular energy transfer, (Kachura et al., 1974). Small shifts in the positions as well as some broadening of the emission lines were observed when the potentially coordinating molecules pyridine and quinoline were used as solvents. Spectral sensitivity to axial coordination is an important feature that may allow the use of these complexes as probes of molecular structure in heme proteins.

2.3. *Circular polarization of luminescence*

Although the J levels of the lanthanides are split by ligand fields of low symmetry, splittings are generally not discernible in the fluorescence spectra (*cf.* fig. 39.2). However they are observed in the circularly polarized luminescence (CPL). Thus CPL spectra reflect the asymmetry of the ligand field in the excited electronic state of the ion and may provide detailed information on its binding site. The CPL of Tb^{3+} bound to transferrin and to conalbumin has been studied by Gafni and Steinberg (1974). They found that both the emission and CPL spectra for the two complexes were very similar and concluded that the structure and conformation of the metal ion binding site of the two proteins must be similar. A detailed treatment of the CPL of Eu^{3+} and Tb^{3+} is given by Luk and Richardson (1975) in their study of carboxylic and amino acid complexes. The CPL is expressed by the anisotropy factor, g_{em}, defined as twice the ratio between the intensity of the circularly polarized component of the luminescence and the total luminescence at the same wavelength. A CPL spectrum of Tb^{3+} bound to porcine trypsin that shows the region of the $^5D_4 \rightarrow {}^7F_5$ transition is presented in fig. 39.3. Splitting into at least three components is clearly revealed. It seems at present that a CPL spectrum by itself can provide only qualitative information. However, spectral changes or similarities can form the basis for more quantitative and detailed conclusions.

2.4. *Nuclear relaxation rates*

Paramagnetic ions by virtue of the large magnetic moment associated with their electronic spin greatly enhance the relaxation rates of nuclei in their vicinity through the electron-nuclear hyperfine interaction. Particularly effective and useful in this respect are S-state ions with relatively long electron spin relaxation times. Outstanding in this respect is Gd^{3+} which exerts its influence almost solely through the electron–nuclear *dipolar* interaction. The longitudinal

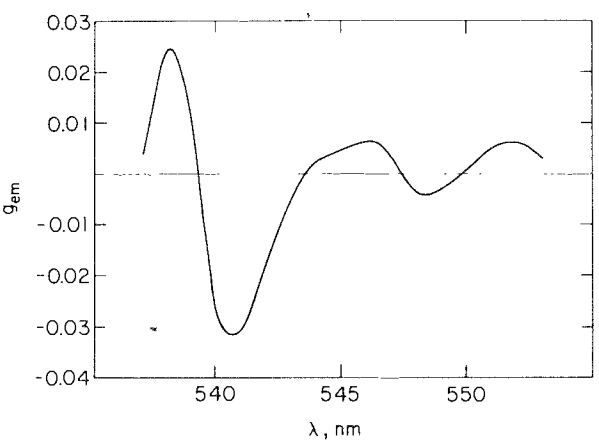

Fig. 39.3. Part of the circularly polarized luminescence spectrum of the Tb^{3+}-porcine trypsin complex showing the $^5D_4 \rightarrow {}^7F_5$ transition. Adapted from Epstein et al. (1977).

relaxation rate of a nucleus due to this interaction may be expressed as

$$1/T_{1M} = Df(\omega,\tau_c)/r^6, \tag{39.1}$$

where D is a constant containing the product of the squares of the interacting magnetic moments, r is the distance between the latter, and $f(\omega,\tau_c)$ is a function of the resonance frequency, ω, and of the correlation time τ_c, characteristic of the process responsible for interruption of the interaction. The book by Dwek (1973b) should be consulted for details not given here. Because of the sixth power dependence on the reciprocal distance, nuclei in close proximity are much more affected than the more distant ones. Thus in aqueous solution the water molecules in the first hydration sphere are those mostly influenced. However, owing to rapid chemical exchange between the coordinated and free water molecules, an average effect is observed in the form of an increment in the relaxation rate. The increment is given by

$$1/T_{1p} = P_M/T_M \tag{39.2}$$

where P_M is the fractional population of the given nuclei in the vicinity of the ion. Thus for water proton relaxation rates (PRR) $P_M = n[M]/55.5$, [M] being the molar concentration of metal ion of hydration number n and 55.5 is the molarity of water. Equation (39.2) assumes rapid chemical exchange with respect to the relaxation T_{1M}, which is the case for aquo-Gd^{3+}, (Reuben, 1975d). Upon binding of Gd^{3+} to proteins part of its water of hydration is substituted by protein ligands. In addition the effective correlation time also changes. While for the aquo-complex it is mainly the molecular tumbling time, which is ca. 7×10^{-11} sec, for macromolecular systems it becomes the electron spin relaxation time, which is of the order of 10^{-9} sec, (Reuben, 1971a, 1971b). As a result a net enhancement of PRR is observed when Gd^{3+} binds to macromolecules. This enhancement, denoted ϵ_b, is a property of the Gd^{3+}-macromolecular complex and depends both on the resonance frequency and on the temperature. A summary of enhancements obtained with proteins is given in table 39.2.

The water PRR enhancement can be used as an analytical method for monitoring the binding of Gd^{3+} to macromolecules. From the detailed interpretation of its frequency and temperature dependence the number of water molecules remaining in the coordination sphere of the bound Gd^{3+} ion may also be obtained. This is an important quantity since it reflects on the number of ligands contributed by the macromolecule and may serve in the identification of the binding site. Relaxation rates of nuclei belonging to small molecules such as substrates or inhibitors of enzymes may be used in mapping their position on the protein relative to the position of a bound Gd^{3+} ion, (Butchard et al., 1972; Furie et al., 1974). In this case particular attention must be paid to the binding phenomena as reflected in the observed relaxation rates in order to avoid possible ambiguities due to heterogeneous binding, (Epstein and Reuben, 1977).

Enhanced relaxation due to dipolar interaction with paramagnetic ions leads to line-broadening in the high resolution NMR spectra of ligands. If a proton NMR spectrum of a protein molecule containing a bound Gd^{3+} ion is subtracted from a

TABLE 39.2.
Water proton relaxation rate enhancement at 24.3 MHz for Gd^{3+}–protein complexes

Ligand	ε_b	Temp. (°C)	Reference
Alk. phosphatase	5.9	25	Cottam et al. (1974a)
α-Amylase	3.4	25	Levitzki and Reuben (1973)
Bovine serum albumin	5.9	35.7	Reuben (1971a)
Concanavalin A	7.1[a]	24	Barber et al. (1975)
Ig G (strong sites)	9.5[b]	19	Dower et al. (1975)
Inorg. pyrophosphatase	9.3	25	Cooperman and Chin (1973)
Lysozyme	11.0[c]	24	Jones et al. (1974)
Phospholipase A_2	16.4	22	Hershberg et al. (1976)
Prophospholipase A_2	5.8	22	Hershberg et al. (1976)
Pyruvate kinase	12.0	28	Valentine and Cottam (1973)
Pyruvate kinase–ATP	9.5	28	Valentine and Cottam (1973)
Trypsin	1.4	25	Epstein et al. (1974)

[a]At 35 MHz. [b]At 20 MHz. [c]At 48 MHz.

spectrum obtained with the diamagnetic La^{3+} ion substituting for Gd^{3+}, a high resolution spectrum will result in which only those resonances will be present that were severely broadened by the Gd^{3+} ion, *i.e.* the resonances of the amino acid residues at the binding site. This approach introduced by Campbell et al. (1973a) can be used both for resolution enhancement and for spectral assignment. In such studies the protein structure as determined by X-ray crystallography serves as a reference frame, (Campbell et al., 1973b). Line-broadenings induced by Gd^{3+} have been used in peptide sequencing and in the assignment of the N-methyl resonances of dimethylated lysine residues of lysozyme, (Bradbury et al., 1974).

2.5. *NMR chemical shifts*

Paramagnetic lanthanides (except for Gd^{3+}) induce large chemical shifts in the NMR absorptions of ligands in their vicinity. One of the main origins of these shifts is the dipolar interaction between the nuclear magnetic moment and the anisotropic magnetic moment of the unpaired 4f electrons. For complexes of axial symmetry the magnitude of the shift may be expressed as

$$\Delta_M = D(3\cos^2\theta - 1)/r^3 \tag{39.3}$$

where D is a temperature dependent constant characteristic of the lanthanide and the complex, r is the distance between the nucleus and the ion, and θ is the angle between the vector $\mathbf{r}$ and the principal axis of symmetry. As may be inferred from eq. (39.3) the shift is a sensitive function of molecular geometry. Based on this shift phenomenon is the application of lanthanides and their complexes as shift reagents in NMR spectroscopy. The subject is discussed in detail in chapter 38 of this Handbook. The lanthanides were introduced as shift

reagents in studies of systems of biological interest by R.J.P. Williams and his coworkers at Oxford. They used relative shifts and line-broadenings in conjunction with eqs. (39.3) and (39.1) in the determination of mononucleotide conformations in solution, (Barry et al., 1971). The Eu^{3+}–lysozyme complex was shown to induce stereospecific shifts in the resonances of β-methyl-*N*-acetylglucoseamine, a substrate analogue of the enzyme, (Morallee et al. 1970). Lanthanide induced shifts in the high resolution spectrum of the lysozyme molecule were interpreted according to eq. (39.3) using the X-ray structure of the enzyme and were instrumental in spectral assignments, (Campbell et al., 1973b). Bystrov et al. (1971, 1972) introduced the use of lanthanides in NMR studies of phospholipid bilayer vesicles. They have shown that upon addition of $EuCl_3$ or $PrCl_3$ to a suspension of vesicles the choline proton resonance as well as the phosphorus-31 resonance split into two peaks: one is shifted and corresponds to the outward pointing groups, whereas the other is unshifted and corresponds to the groups pointing inside the impermeable to lanthanide ions vesicles. Lanthanide induced shifts have also been observed for the hydrogen-bonded protons in the spectrum of tRNA, (Jones and Kearns, 1974a). Thus the lanthanides can be useful as probes for NMR studies of a variety of systems of biological interest.

2.6. *NMR of lanthanum-139*

In many of the spectroscopic and magnetic resonance studies employing lanthanides the diamagnetic spectroscopically "silent" La^{3+} ion serves as a control. Lanthanum-139 however is a nucleus with a spin ($I = \frac{7}{2}$) that can be used in NMR experiments. Such experiments have recently been carried out by this author, (Reuben, 1975b, 1975c). Nuclei of spin $I > \frac{1}{2}$ possess an electric quadrupole moment. The interaction of the latter with intramolecular electric field gradients is responsible for the relaxation of such nuclei. It can be shown that to a good approximation the longitudinal relaxation rate is given by

$$1/T_1 = C\tau_c/(1 + 2.67\omega^2\tau_c^2) \tag{39.4}$$

where C is a constant for a given nucleus and chemical environment, ω is the resonance frequency, and τ_c is the correlation time characteristic of the molecular process modulating the quadrupole interaction, (Reuben and Luz, 1976). As implied by eq. (39.4), measurements of relaxation rates at several frequencies should permit an unequivocal determination of the correlation time. Such measurements have been carried out for the La^{3+}–bovine serum albumin system. It was found that the La^{3+} ions associate with virtually all of the free carboxylates of the protein. Very low protein concentrations (of the order of 1 mg/ml) produced easily measurable and frequency dependent increments in the longitudinal relaxation of ^{139}La in a 0.4 M solution of $LaCl_3$. From the analysis of the results $\tau_c = 3.7 \times 10^{-8}$ sec (at 23°C) was obtained, a value in good agreement with molecular tumbling times determined by other methods, (Reuben and Luz, 1976). Thus ^{139}La can serve as an NMR probe of macromolecular dynamics in solution.

2.7. *EPR of gadolinium (III)*

The EPR spectrum of Gd^{3+} in solution consists of a broad single line. This author has analyzed the temperature and frequency dependence of the line-width of the aquo, cacodylate, and bovine serum albumin complexes of Gd^{3+}, (Reuben, 1971b). Only some tentative conclusions could be reached regarding the symmetry of the macromolecular environment of the ion. The line-width is related to the electron spin relaxation time and EPR data might be useful for the determination of the effective correlation time in PRR experiments.

2.8. *Mössbauer spectroscopy*

Most of the lanthanides have isotopes suitable for Mössbauer spectroscopy, *cf.*, *e.g.*, Wertheim (1964). In such experiments the resonant γ-ray absorption is measured as a function of the relative velocity between the source and the sample. Spectral line shifts and splittings are related to the chemical nature and symmetry of the site of the ion. Spartalian and Oosterhuis (1973) have examined the spectrum of the Eu^{3+}–transferrin complex. A single unshifted line was observed, which by itself offers little information. This is because at the low temperature (4.2 K) at which such experiments are normally carried out, only the ground-singlet level, ^7F_o, of Eu^{3+} is populated and it is hardly affected by the environment. Mössbauer spectra of other members of the lanthanide series should be more informative.

2.9. *X-ray crystallography*

All of the lanthanides give rise to anomalous scattering components of X-ray radiation that may be useful for phase determinations in X-ray crystallographic studies of macromolecules. Particularly large scattering is exhibited by Sm^{3+}, Nd^{3+}, and Eu^{3+}, (Cromer, 1965). The crystals of the protein or the nucleic acid are usually prepared first and soaked in a lanthanide salt solution. The cations diffuse into the crystal and are likely to bind at the strongest binding sites. Table 39.3 gives a listing of biological macromolecules studied using lanthanides for heavy atom derivatives. A description of the lanthanide binding site has been given only for thermolysin, (Matthews and Weaver, 1974), and for lysozyme, (Kurachi et al. 1975).

3. Bioinorganic chemistry

The interaction of lanthanide ions with molecules of biological interest is governed by the same well known principles of lanthanide coordination chemistry, *i.e.* the interactions are largely electrostatic, the bonds formed have a high degree of ionicity, charged oxygen donors are preferred ligands, dehydration of the aquo-ion determines to a large extent the thermodynamics of complex

TABLE 39.3.
Biological macromolecules studied by X-rays using lanthanides for heavy atom derivatives

Macromolecule	Reference
Thermolysin	Colman et al. (1972) Matthews and Weaver (1974)
Lysozyme	Kurachi et al. (1975)
Concanavalin A	Becker et al. (1975)
Ferredoxin	Sieker et al. (1972)
Flavodoxin	Watenpaugh et al. (1972)
tRNA	Kim et al. (1972), Robertus et al. (1974)

formation. Variation in some of these characteristics is observed along the lanthanide series and can be correlated with the ionic radius contraction. In some instances a "gadolinium break" or other division into subgroups is found. Apparent similarities between Ca^{2+} and lanthanides, particularly with regard to ionic radii, ligand exchange rates, and coordination numbers, may be invoked in order to advocate or justify isomorphous replacement in biological macromolecules. Silber (1974) compared the complex formation tendencies of Er^{3+} and Ca^{2+} towards the perchlorate ion in media of different dielectric constant using ultrasonic relaxation techniques and found that inner-sphere lanthanide complexes formed in solutions of low dieletric constant, whereas Ca^{2+} did not form such complexes. He concluded that if the effective environment surrounding the metal ion binding site in a protein is somewhat hydrophobic then a lanthanide ion may not bind. If the site is hydrophilic both R^{3+} and Ca^{2+} can bind and due to the higher charge tighter lanthanide binding may be expected. This of course is a model that awaits experimental verification. While isomorphous replacement of Ca^{2+} (or of other cations) by a lanthanide may indeed take place, the crucial test should be biological activity, *e.g.* enzymatic activity. In this section considerable attention is devoted to these points, since the significance of lanthanide probe studies is undoubtedly related to the extent of chemical and structural perturbation exerted by the probe upon the system of interest.

3.1. *Amino acids, peptides, and related derivatives*

Amino acids are the building blocks of proteins. In aqueous solutions, in the pH range 3–8, they are present in the amphiionic form $^{+}NH_3CH(X)COO^{-}$, where X is a group referred to as the amino acid side chain. Association with lanthanides is expected to take place at the ionized carboxyl group. However, due to the proximity of the positively charged amino group it is likely that complex formation will be weaker than that with simple carboxylates. This effect

is dramatically demonstrated in the Dy^{3+} induced proton shifts in the series of glycine and its homologous peptides, in which the positively charged group is progressively moved away from the complexing carboxyl end, (Nieboer, 1975). The dissociation constants determined for the Eu^{3+} complexes are 0.08 M for glycine and 3.2×10^{-3} M for triglycine, (Nieboer et al., 1973). For comparison, the dissociation constant of the monoacetato complex is 4.9×10^{-3} M, (Kolat and Powell, 1964). Bidentate coordination with histidine, involving the participation of a ring nitrogen, has been suggested by Sherry et al. (1972) on the basis of the pH dependence of Nd^{3+} induced shifts.

Complex formation between lanthanides and carboxylic acids is usually studied by potentiometry. Recently Prados et al. (1974) carried out detailed potentiometric and circular dichroism studies with amino acids and concluded that the main effects observed were associated with lanthanide ion hydrolysis in neutral solutions and that from such measurements no conclusions could be drawn regarding the amino acid complexes of lanthanides. Thus serious doubt is cast on conclusions reached in the previous work of Katzin (1969), Katzin and Gulyas (1968), Jones and Williams (1970, 1971), as well as in the more recent investigations of Lal (1972), Batyaev and Fogileva (1972, 1974), Sekhon and Chopra (1974), Plyushchev et al. (1974). In order to observe by potentiometry complex formation with the amphiionic form of amino acids measurements have to be done starting with the cationic form present in acidified solutions. Such experiments have been carried out by Sherry et al. (1973) and the results obtained are in good agreement with NMR determinations. Their results along with other data from the literature are summarized in table 39.4. While the results obtained by different research groups are in satisfactory agreement, it should be pointed out that amino acids form also 2 : 1 complexes with lanthanides, a fact that not always has been taken into account. Such complexes have been observed by NMR and the following dissociation constants have been evaluated: 1.7 M for the bis-azetidine-2-carboxylato complex of Eu^{3+}, (Inagaki et al., 1975a), 0.55 M for the bis-alaninato complex of Pr^{3+}, (Elgavish and Reuben, 1978). For triglycine and Eu^{3+} $K_2 = 0.04$ M, Nieboer et al., 1973), a value that may be compared with $K_2 = 0.025$ M reported for the bis-acetato complex by Kolat and Powell (1964). It may be of interest to point out that both the amphiionic and anionic forms of amino acids interact with the EDTA chelates of lanthanides, (Elgavish and Reuben, 1978).

Lanthanide induced shifts and line-broadenings have been used in studies of the molecular conformation in solution of the cyclic amino acids *L*-azetidine-2-carboxylic acid, (Inagaki et al., 1975b), hydroxy-*L*-proline, (Inagaki et al., 1976), and a series of penicillins, (Dobson et al., 1975). Lanthanide induced shifts may be used for spectral assignment and sequence determination of peptides. Examining the proton shifts (at 60 MHz) induced by Dy^{3+} in a series of peptides composed of glycyl and alanyl residues Nieboer (1975) found the following Δ_M values (in ppm): 33.3 ± 1.7 for $CH_{\alpha,1}$, 4.17 ± 0.25 for $CH_{\alpha,2}$, 1.38 ± 0.08 for $CH_{\alpha,3}$, 0.55 ± 0.05 for $CH_{\alpha,4}$, 0.17 ± 0.03 for $CH_{\alpha,5}$, 20.8 ± 0.8 for $CH_{\beta,1}$, 1.67 ± 0.08 for $CH_{\beta,2}$ of glycyl, 1.12 ± 0.08 for $CH_{\beta,2}$ of alanyl, and 0.83 ± 0.05 for $CH_{\beta,3}$. Thus it

TABLE 39.4.
Dissociation constants of 1:1 lanthanide-amino acid complexes

R^{3+}	Amino acid	K_D (M)	pH	Temp. (°C)	Method	Reference
La	Sarcosine	0.25	3–8	25	NMR	Kostromina (1971)
Nd	Alanine	0.23	–	22	potent.	Sherry et al. (1973)
Nd	Alanine	0.15	4.0	22	NMR	Sherry et al. (1973)
Nd	Histidine	0.50	4.0	22	NMR	Sherry et al. (1972)
Nd	Serine	0.10	–	22	potent.	Sherry et al. (1973)
Nd	Serine	0.08	4.0	22	NMR	Sherry et al. (1973)
Nd	Threonine	0.13	4.0	22	NMR	Sherry et al. (1973)
Pr	Alanine	0.30	4.6–5.0	39	NMR	Elgavish and Reuben (1978)
Pr	Ampicillin	0.13	4.0–4.6	25	NMR	Dobson et al. (1975)
Eu	Glycine	0.20	3.6	25	partition	Tanner and Choppin (1968)
Eu	Glycine	0.08	3.8	–	NMR	Nieboer et al. (1973)
Eu	Alanine	0.18	3.6–4.5	25	partition	Aziz et al. (1971)
Eu	Azetidine-2-carboxylate	0.28	4.6–5.0	37	NMR	Inagaki et al. (1975a)
Lu	Sarcosine	0.13	3–8	25	NMR	Kostromina (1971)

seems that this method can be used to sequence pentapeptides. With the higher resolution and larger shifts afforded by high frequency NMR spectrometers (e.g. 300 MHz) hexa- or even heptapeptides may also be studied (Anteunis and Gelan, 1973; Anteunis and Callens, 1974). Also useful in this regard should be the shifts induced in the carbon-13 spectra (Bayer and Beyer, 1973).

Using potentiometric titrations and NMR Marinetti et al. (1975) have characterized the interaction of lanthanides with *N*-acetyl-*L*-3-nitrotyrosine ethyl ester. The pK of this compound is 7.09 and R^{3+} ions are chelated by the

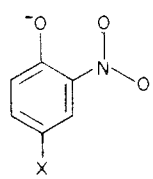

ionized ortho-nitrophenolate moiety. The dissociation constants of the La^{3+}, Eu^{3+}, Pr^{3+}, and Gd^{3+} chelates are respectively 5.1, 2.2, 2.5, and 3.1 mM. Marinetti et al. (1975) have analyzed in detail the lanthanide induced proton shifts and line-broadenings in terms of a non-axial model. Their results should be useful in the analysis of data obtained with proteins containing a nitrotyrosyl group that could serve as a specific lanthanide binding site.

Amino acids react with pyridoxal to form Schiff bases. The luminescence of the Eu^{3+} chelates of the latter have been studied by Zolin et al. (1975), who suggest this approach as a method for identification of the residue at the *N*-terminus of peptides and proteins.

3.2. *Carbohydrates*

The interest in metal ion-sugar complexes has recently been revived by Angyal (1972), who was also the first to use lanthanide ions as shift reagents for carbohydrates in aqueous solution, (Angyal, 1973, 1974). Carbohydrates and polyols in general will bind metal ions if they have three *cis* hydroxyl groups on consecutive carbon atoms that can achieve an *ax–eq–ax* arrangement, (Angyal and Davies, 1971). The tendency of metal ions

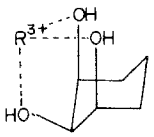

to form complexes with *D*-allose increases in the order $Na^+ < Y^{3+} < Ca^{2+} < La^{3+}$, (Angyal, 1972). Lenkinski and Reuben (1976) have outlined procedures for the analysis of proton NMR data in systems where metal ion-sugar complexation takes place and treated the data obtained for the interaction of Ca^{2+} and La^{3+} with *D*-lyxose and *D*-ribose. Their results are summarized in table 39.5. Substitution of one of the coordinating hydroxyls by a methoxy group does not abolish the binding. Thus Grasdalen et al. (1975a) observed 1 : 1 complex formation between Eu^{3+} and methyl-α-*D*-gulopyranoside.

Angyal et al. (1974) and Kieboom et al. (1975) have investigated the interaction of alditols with the nitrate salts of Eu^{3+} and Pr^{3+}, respectively. They have found that the extent of complex formation depends upon the arrangement and configuration of the hydroxyl groups. The threo-threo

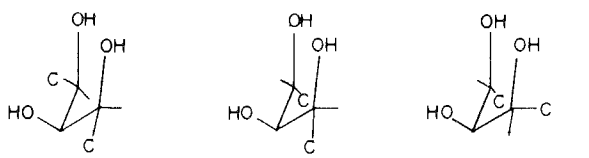

configuration is the most favorable for complex formation, whereas the 1,3-parallel interaction between segments of the carbon chain renders the erythro-erythro configuration unfavorable in this respect. NMR studies by this author have shown that in fact alditols form 2 : 1 complexes with lanthanide chlorides, (Reuben, 1977). The dissociation constants of the xylitol complexes of Pr^{3+}, Nd^{3+} and Eu^{3+} are summarized in table 39.6.

Lanthanide chelation by the anions of *D*-galacturonic acid and its derivatives has been demonstrated by NMR, (Anthonsen et al., 1972, 1973). In this case 3 : 1 complexes are formed, (Grasdalen et al., 1975b). Casu et al. (1975) have shown that Gd^{3+} produces stereospecific relaxation effects in the proton and carbon-13

TABLE 39.5.
Dissociation constants (at 52°C) of Ca^{2+} and La^{3+} complexes with sugars (from Lenkinski and Reuben, 1976)

Sugar	K_D^{Ca}(M)	K_D^{La}(M)
β-D-lyxopyranose	1.25 ± 0.15	1.0 ± 0.1
α-D-ribofuranose	0.45 ± 0.05	0.18 ± 0.01
α-D-ribopyranose	0.71 ± 0.05	0.28 ± 0.01
β-D-ribopyranose	1.45 ± 0.2	1.1 ± 0.1

spectra of uronic acids, suggesting this as a diagnostic method of distinguishing between anomeric forms. Similar conclusions were reached by Hall and Preston (1975), who investigated the effects of Gd^{3+} on the proton relaxation rates of a number of mono- and di-saccharides.

3.3. *Nucleotides*

Nucleotides, in many cases as their metal ion complexes, are involved in a great variety of enzymatic reactions either as substrates or as cofactors. In addition they may be viewed as the monomers of DNA and RNA. Lanthanide complexes of nucleotides have been extensively studied by R.J.P. Williams and his coworkers at Oxford. The interest in these complexes is two fold. The nucleotide conformation in solution can be elucidated by NMR from lanthanide induced chemical shifts and line-broadenings, (Barry et al., 1971). Lanthanide-nucleotide complexes may act as competitive inhibitors in enzymatic reactions, (Tanswell et al., 1974), and can be used as paramagnetic probes in the mapping of their binding site on the enzyme, (Tanswell et al., 1976).

Complex formation between lanthanides and nucleotides has been studied at relatively low pH (ca. 2) by NMR. A summary of dissociation constants is given in table 39.7. Barry et al. (1971) have shown that the phosphate in nucleotide monophosphates acts as a bidentate ligand. In the ATP complex the lanthanide ion interacts with the terminal β and γ phosphates, which act probably as a

TABLE 39.6.
Dissociation constants (at 39°C) of lanthanide complexes with xylitol (from Reuben, 1977).

R^{3+}	K_1(M)	K_2(M)
Pr	0.5 ± 0.1	8 ± 4
Nd	0.25 ± 0.01	2.0 ± 0.1
Eu	0.26 ± 0.04	1.3 ± 0.3

TABLE 39.7.
Dissociation constants (at 25–29°C) of lanthanide–nucleotide complexes at acidic pH (1.5–2.2).

R^{3+}	Ligand	K_D(mM)	Reference
Pr	cytidine 5′-monophosphate	360 ± 30^a	Barry et al. (1974c)
Pr	cyclic adenosine 3′, 5′-phosphate	190 ± 50	Lavallee and Zeltmann (1974)
Eu	adenosine 5′-monophosphate	100 ± 20	Barry et al. (1971)
Eu	thymidine 5′-monophosphate	60 ± 10	Barry et al. (1971)
Eu	nicotinamide mononucleotide	18 ± 2^b	Birdsall et al. (1975)
Eu	guanoside 5′-monophosphate	70	Barry et al. (1972a)
Eu	adenosyl-3′,5′-adenylic acid	250	Barry et al. (1972a)
Eu	adenosyl-3′,5′-cititidylic acid	250	Barry et al. (1972a)
Eu	cytidyl-3′, 5′-adenylic acid	170	Barry et al. (1972a)
Eu	guanyl-3′, 5′-cytidylic acid	250	Barry et al. (1972a)
Eu	cytidyl-3′, 5′-guanylic acid	200	Barry et al. (1972a)
Ho	adenosine 5′-monophosphate	170 ± 60	Barry et al. (1971)
Ho	cyclic adenosine 3′, 5′-phosphate	70 ± 10^c	Lavallee and Zeltmann (1974)

[a] $K_D = 110 \pm 10$ mM at 85°C. [b] At pH 4.4. [c] $K_D = 80 \pm 10$ mM at pH 5.3.

tetradentate ligand, (Tanswell et al., 1975). Complex formation with sugar phosphates has also been reported, (Birdsall et al., 1971; Asso et al., 1975). The dissociation constants of the complexes with glucose-6-phosphate are ca. 15 mM, (Asso et al., 1975). It may be of interest to point out that the $R(EDTA)^-$ chelates interact with mono- as well as with di-nucleotides at higher pH values, (Dobson et al., 1974; Lee and Raszka, 1975).

At pH values above neutrality the nucleotides become fully ionized and complex formation with lanthanides is more favorable. Thus already at pH 5.6 a dissociation constant of the order of 1 mM could be estimated for Tb^{3+} complexes of nucleotide monophosphates from fluorescence measurements, (Formoso, 1973). Using a competitive spectrophotometric technique Ellis and Morrison (1974a) obtained $K_D = 10^{-6}$ M for the Eu^{3+}–ADP complex at pH 7. Gadolinium displaces Mn^{2+} from the Mn^{2+}–ATP complex. By monitoring the free Mn^{2+} by EPR a dissociation constant of 10^{-7} M was obtained for the Gd^{3+}–ATP complex at pH 6.0, (Valentine and Cottam, 1973). The tighter binding at higher pH is reflected in slower ligand exchange rates, (Tanswell et al., 1975).

Lanthanides have been used to afford spectral resolution in NMR studies of cyclic nucleotides, (Kainosho and Ajisaka, 1975). The magnitudes of lanthanide induced chemical shifts and line-broadenings have been analyzed in terms of molecular structure in studies of mononucleotides (Barry et al., 1971, 1972b, 1974a; Birdsall et al. 1975); cyclic nucleotides (Barry et al., 1974b; Lavallee and Zeltmann, 1974; Fazakerley et al., 1975); dinucleotide phosphates (Barry et al., 1972a); and ATP (Tanswell et al., 1975). Interestingly the conformation of AMP in dimethylsulfoxide (DMSO) as established by this method (Barry et al., 1972b), was found to be different than that in water (Barry et al., 1971).

3.4. *Porphyrins*

Metalloporphyrins constitute the prosthetic groups of heme proteins and chlorophyll. The synthesis of lanthanide-acetylacetonato-tetraphenyl-prophyrin [*R*(III)-aca-TPP] complexes and related derivatives has been reported by Wong et al. (1974). The complexes are stable to air and water and are soluble in organic solvents. The proton NMR spectra of the tetra-*p*-tolyl derivatives of the Eu^{3+}, Pr^{3+}, and Yb^{3+} complexes exhibit large dipolar shifts. Horrocks et al. (1975) prepared also the Yb(III)-aca-mesoporphyrin IX complex and inserted it into apomyoglobin to form a lanthanide derivative of a heme protein. The absorption and circular dichroic spectra of the reconstituted material indicate that the lanthanide-porphyrin complex occupies the heme crevice in the protein. Intramolecular energy transfer as reflected in the luminescence spectra of the tetra benzo porphyrin Yb(III)-aca-TBP and Yb(III)-TBP complexes has been investigated and spectral sensitivity towards axial coordination observed (Kachura et al., 1974). These findings indicate that lanthanide-porphyrin complexes have the potential of becoming spectroscopic and magnetic resonance probes in studies of heme proteins.

3.5. *Nucleic acids*

Nucleic acids are responsible for the storage and transcription of genetic information in living cells and are intimately involved in protein synthesis. Being polymers of nucleoside phosphates they are negatively charged in neutral solutions and therefore strongly interact with metal ions. The interaction with metal ions is of importance in maintaining the conformational stability of nucleic acids and in controlling their function. Eichhorn and Butzow (1965) have found that at 64°C polyribonucleotides are rapidly degraded in the presence of La^{3+}. DNA, however, is stable either in its native or heat denatured forms. This supports the suggestion that La^{3+} is chelated between the phosphate and the 2′-hydroxyl group in ribonucleic acids (Bamann et al., 1954).

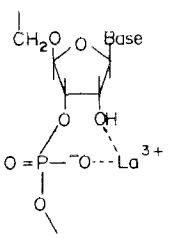

The interaction between DNA and Tb^{3+} in the solid state has been investigated using the terbium fluorescence (Yonuschot and Mushrush, 1975). The fluorescence at 491 and 545 nm upon excitation at 307 nm was monitored as a function

of the Tb^{3+}/DNA ratio. Continuous binding of Tb^{3+} was observed until one cation was present for each phosphate group. With chromatin only 0.48 equivalents were bound per phosphate indicating that more than one half of the phosphates in chromatin were unavailable for cation binding.

The interaction between tRNA and lanthanides has been studied both by fluorescence (Kayne and Cohn, 1974; Wolfson and Kearns, 1974, 1975), and by NMR (Jones and Kearns, 1974a, 1974b). Kayne and Cohn (1974) have found that the fluorescence intensities of Tb^{3+} and of Eu^{3+} are enhanced several hundred fold upon binding to some tRNA molecules from *E. coli*. The major excitation band is at 345 nm corresponding to the uncommon fluorescence base 4-thiouridine (s^4U). This base is located at position *8* in the polynucleotide chain of $tRNA^{Phe}$, $tRNA^{Glu}$, and $tRNA^{fMet}$ from *E. coli*, all of which produce an enhancement in Tb^{3+} fluorescence. Enhancement was not observed with $tRNA^{Phe}$ from yeast, which lacks the s^4U base. The fluorescence enhancement results therefore from energy transfer between the s^4U residue and the bound lanthanide ion. This conclusion is confirmed by the quenching of the s^4U emission that is observed upon the binding of Tb^{3+} or Eu^{3+}. The s^4U emission is enhanced upon the addition of Sm^{3+}, Gd^{3+}, and Yb^{3+} thereby indicating the binding of these cations as well. From the analysis of the fluorescence enhancement it was concluded that there are 4 tight and apparently equivalent binding sites for Eu^{3+} per tRNA molecule (containing *ca.* 80 nucleotides) with an apparent dissociation constant of 6×10^{-6} M (Kayne and Cohn, 1974). The X-ray work of Robertus et al. (1974) also indicates 4 lanthanide binding sites on the $tRNA^{Phe}$ molecule in its crystalline state. One of these sites is in the vicinity of the uridine residue at position *8* of the chain (A. Rich as quoted by Kayne and Cohn, 1974). The fluorescence of Eu^{3+} – tRNA complexes has also been studied by Wolfson and Kearns (1975), who have reached conclusions that are qualitatively similar to those of Kayne and Cohn (1974). The main discrepancy is in the dissociation constant estimated to be 10^{-8} M. It is not clear, however, how could such a small dissociation constant affect the results of experiments carried out with Eu^{3+} and tRNA concentrations that were between 100 and 10 000 times larger than K_D.

The effects of Eu^{3+} on the NMR spectrum of the hydrogen bonded protons of yeast $tRNA^{Phe}$ have been investigated by Jones and Kearns (1974b). Their results indicate that the binding of lanthanides is a sequential process, that chemical exchange of the tRNA molecule between its complexed forms is rapid on the NMR time scale, and that the most shifted resonance belongs to the proton hydrogen bonded between the base pair of an adenine residue and the uridine at position *6*. Upon the addition of ethidium bromide, a dye molecule that may intercalate between base pairs, the lanthanide induced shift reverses sign indicating that binding of the dye drastically affects the symmetry at the metal ion binding site (Jones and Kearns, 1975).

Protein biosynthesis takes place on the ribosomes, which are small organelles composed of proteins and ribosomal RNA (rRNA). The binding of Tb^{3+} to rRNA and ribosomes has been studied by Barela et al. (1975) using equilibrium dialysis

and fluorescence methods. Enhancement of the fluorescence emission at 488 and 541 nm is observed upon excitation at 290 nm. The relative fluorescence is proportional only to the amount of bound Tb^{3+}. The latter however is affected by the ionic strength. Intact ribosomes produce effects similar to those of rRNA suggesting that rRNA is the primary locale for lanthanide binding to ribosomes. The authors conclude that the interaction of ribosomes with Tb^{3+} mimics that of Mg^{2+} and propose that the fluorescence of Tb^{3+} may be useful in studies of the nature and extent of interaction between ribosomes and Mg^{2+}. The effects of Mg^{2+} on the fluorescence of ribosomal complexes of Tb^{3+} should be an important test of this proposal.

3.6. *Proteins and enzymes*

The interaction with proteins is one of the most extensively studied areas of lanthanide bioinorganic chemistry. There are several interrelated aspects of this interaction, paramount among which is the effect on enzymatic activity. The elucidation of this effect should have implications regarding the significance of the results ensuing from the application of the various physical methods based on the spectroscopic and magnetic properties of the lanthanides. Presented in this subsection is a general review of the interaction between lanthanides and proteins, including the effects on enzymatic activity. It is followed by a more detailed description of the findings with some of the systems.

Complex formation between a lanthanide ion and a protein may result in spectral perturbations of the following general types: modification of lanthanide spectrum, alteration of the protein spectrum, and changes in the proton relaxation times of the water of hydration. The magnitudes of such perturbations as well as some common biochemical techniques have been used to quantitate the binding of lanthanides to proteins. A summary is given in table 39.8. The binding to a few other proteins could be inferred from X-ray studies or from enzymatic activities, but its quantitation has been either impractical or not attempted. These ten proteins are listed in table 39.9. The dissociation constants of lanthanide protein complexes span the rather wide range between 2.3×10^{-7} M ($\log K_A = 6.64$) found for the Eu^{3+}-inorganic pyrophosphatase complex and 5.6×10^{-3} M ($\log K_A = 2.26$) determined for the La^{3+}-porcine trypsin complex. It is difficult to rationalize either this range or each individual value without recourse to additional information. Particularly helpful should be thermodynamic data and the constants for a larger number of lanthanides complexed with the same protein. Such information, at least in part, is available for porcine trypsin (Epstein et al. 1974, 1977). Shown on fig. 39.4 is the variation of $\log K_A$ with lanthanide ionic radius of the porcine trypsin and nitrilotriacetate (NTA) complexes. The two sets of data are strikingly parallel although the absolute values of the constants differ by 8–9 orders of magnitude. This parallelism concurs with the spectroscopic evidence presented by Darnall et al. (1971) that lanthanides are coordinated to ionized carboxyl groups of proteins (*cf.* fig. 39.1). Complex

TABLE 39.8.
Stability constants of lanthanide–protein complexes

Protein	R^{3+}	log K_A[a]	pH	Temp. (°C)	Method	Other R^{3+} Measured	Reference
Alk. phosphatase	Gd	4.52(2)	8.0	25	PRR		Cottam et al. (1974a)
α-Amylase	Gd	4.59(2)	4.6	25	PRR		Levitzki and Reuben (1973)
Concanavalin A	Gd	4.40, 3.70	5.6	24	PRR	Tb	Sherry and Cottam (1973)
Factor X, bovine	Gd	6.38(2), 4.82(4)	6.8	25	Rate Dialysis	Sm, Yb	Furie and Furie (1975)
Inorg. pyrophosphatase	Eu	6.64	7.4	30	Fluoresc.		Sperow and Butler (1972)
	Gd	6.10	7.2	25	PRR		Cooperman and Chin (1973)
Immunoglobulin G	Gd	5.22(2), 3.70(4)	5.5	19	PRR	Tb	Dower et al. (1975)
(IgG), Fab	Gd	3.85(2)	5.5	19	PRR		Dower et al. (1975)
(IgG), $(Fab')_2$	Gd	4.00(4)	5.5	19	PRR		Dower et al. (1975)
(IgG), Fc	Gd	5.22(2)	5.5	19	PRR		Dower et al. (1975)
(IgG), pFc'	Gd	5.40	5.5	19	PRR		Dower et al. (1975)
Lysozyme	La	3.30	indepen.	54	NMR		Campbell et al. (1975c)
	Gd	3.44	indepen.	25	Spectr.		Secemeski and Lienhard (1974)
MOPS 315, Fv	Gd	4.52	5.5	19	PRR		Dwek et al. (1975)
Phospholipase A_2	Gd	3.30	5.8	22	PRR		Hershberg et al. (1976)
Prophospholipase A_2	Gd	3.74	5.8	22	PRR		Hershberg et al. (1976)
Pyruvate kinase	Gd	4.19	6.0	28	EPR of Mn^{2+}	La, Nd, Tm	Valentine and Cottam (1973)
Ribonuclease	Nd	4.89	5.6	25	Conductometry	Eu	Geidarova and Antonovskii (1974)
Serum albumin, bovine	Gd	3.89	6.3	27	PRR		Reuben (1971a)
Staph. nuclease	Gd	5.05	7.0	30	Spectr.		Furie et al. (1973)
Troponin	Ce	5.49(2)	7.0	21	Ultrafiltr.	La, Pr, Nd, Sm, Gd, Dy	Fuchs (1974)
	Tb	5.53(2), 3.80(2)	5.5	23	Tb Fluoresc.		Bunting et al. (1974)
Trypsin, bovine	Tb	3.59	6.3	23	Tb Fluoresc.	Gd, Yb	Epstein et al. (1977)
Trypsin, porcine	Tb	2.94	6.3	25	Tb Fluoresc.	series	Epstein et al. (1974)

[a]Number of equivalent sites is given in parantheses.

TABLE 39.9.
Proteins for which lanthanide binding is indicated but not quantitated

Protein	Method	Reference
Aequorin	Enz. act.	Izutsu et al. (1972)
Conalbumin	Tb fluoresc., CPL	Gafni and Steinberg (1974)
Ferredoxin	X-ray	Sieker et al. (1972)
Ferricytochrome C	NMR	Dobson et al. (1975a)
Flavodoxin	X-ray	Watenpaugh et al. (1972)
Glutamine synthetase	Nd spectr., enz. act.	Wedler and D'Aurora (1974)
Lactoferrin	fluoresc.	Teuwissen et al. (1972)
Parvalbumin	Tb fluoresc.	Donato and Martin (1974)
Thermolysin	X-ray	Matthews and Weaver (1974)
Transferrin	Tb fluoresc.	Luk (1971)
Trypsinogen	Enz. act.	Gomez et al. (1974)

formation of lanthanides is usually an entropy driven process (Choppin, 1971). Particularly large entropy changes are observed upon chelation. Thus, chelation by NTA is accompanied by changes of 52.2–63.8 e.u., corresponding to 15.6–19.0 kcal/mole at 25°C, whereas the enthalpy changes are not only small, 0.4–2.6 kcal/mole, but also positive (Moeller and Ferrús, 1962). The differences between the stability constants of the NTA chelates along the lanthanide series are due mainly to the different entropies. The comparison with the results for porcine trypsin suggests that this may hold true for protein complexes as well.

The temperature dependencies of the dissociation constants of the Gd^{3+}

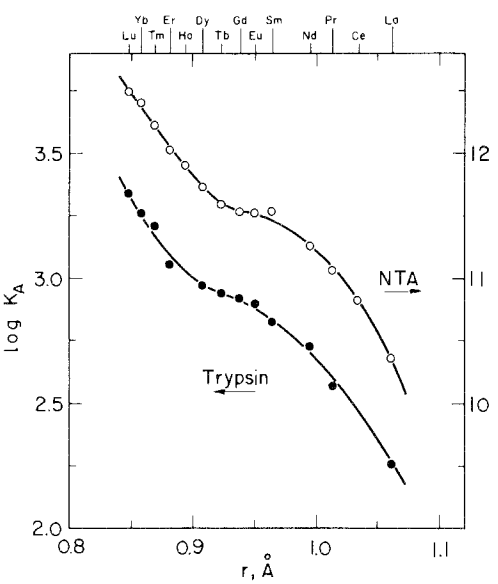

Fig. 39.4. Log of stability constants of lanthanide complexes as a function of ionic radius. Filled circles: porcine trypsin, data from Epstein et al. (1974). Open circles: nitrilotriacetate (NTA), data from Moeller and Ferrús (1962). Crystal ionic radii of R^{3+} from Templeton and Dauben (1954).

complexes with porcine trypsin and with bovine serum albumin (BSA) have been determined (Epstein et al., 1977; Reuben, 1971a). The results are reproduced in fig. 39.5. The dissociation constants decrease with increasing temperature indicating that complex formation is an endothermic process. Endothermic binding has also been observed for lysozyme and Gd^{3+} (Jones et al., 1974), and for glycine and Ce^{3+}, Pm^{3+}, and Eu^{3+} (Tanner and Choppin, 1968). Analysis of the results for BSA and trypsin according to eq. (3.1) shows that indeed the binding process is entropy

$$\ln K_A = -\Delta H^0/RT + \Delta S^0/R \tag{39.5}$$

driven. The thermodynamic parameters are summarized in table 39.10 along with data for the NTA and EDTA chelates. The main difference between the small chelates and the macromolecular complexes is in the large positive enthalpies for the latter. Entropy changes are often attributed to the extensive dehydration accompanying complex formation (Choppin, 1971). The entropy of hydration of Gd^{3+} is 98 e.u. (Bertha and Choppin, 1969). Assuming that the entropies of complexation with proteins are due to dehydration only, one concludes from the results in table 3.7 that the Gd^{3+} ion has lost more than 35% of its water of hydration upon complexation with BSA and more than 70% upon complexation with trypsin. With a hydration number of 8 for the aquo-ion this means that not more than 5.2 and 2.4 water molecules remain in the coordination sphere of a Gd^{3+} ion bound to BSA and trypsin, respectively. An analysis of water PRR data in terms of the number of water molecules, n, has been carried out for trypsin, (Epstein et al., 1977). The value of the water proton–lanthanide distance, r, was estimated from the crystallographic data for the $La(EDTA)^-$ chelate (Hoard et al., 1965) and $r = 3.22$ Å was used with eq. (39.1). The result thus obtained is $n = 2.2$. Using the same value of r with the BSA data of Reuben (1971a) one obtains $2.8 \leqslant n \leqslant 5.5$. Despite the oversimplifications involved, the agreement between the estimates of n obtained from entropy considerations and from the

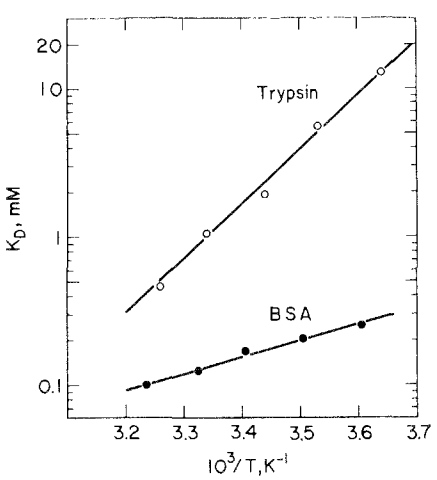

Fig. 39.5. Temperature dependence of the dissociation constants of Gd^{3+} complexes with porcine trypsin (open circles) and bovine serum albumin (BSA, filled circles). Data for trypsin taken from Epstein et al. (1977) and for BSA from Reuben (1971a).

TABLE 39.10.
Thermodynamic parameters for Gd^{3+} complexation with proteins and chelating agents.

Ligand	$\Delta H°$(kcal/mole)	$\Delta S°$(e.u.)	$\Delta G°_{25}$(kcal/mole)	Reference
BSA	5.1	35	−5.33	Reuben (1971a)
Trypsin	16.9	70	−3.96	Epstein et al. (1977)
NTA	1.02	56.2	−15.73	Moeller and Ferrús (1962)
EDTA	−1.73	71.2	−22.95	Mackey et al. (1962)

analysis of PRR data is remarkable. From the above discussions it may be concluded that lanthanide complexation with proteins is an entropy driven process similar to the chelation by smaller ligands. The differences in dissociation constants observed with different lanthanides probably arise from differences both in the entropies and in the enthalpies of complexation. It is now a matter of speculation to suggest that the unfavorable enthalpies will be smaller with more hydrophilic binding sites. Further experiments are likely to throw more light on the tentative interpretations presented here.

Consideration of the tight or specific binding of lanthanides to proteins has led to the general conclusion that chelation plays an important role in this interaction. In addition to it, all of the carboxyl side chains of aspartic and glutamic acid residues in proteins may serve as potential albeit non-specific binding sites. The interaction with the free carboxyl groups of proteins may be expected to be similar to that with acetate and it is likely that the occupancy of these sites will increase at higher lanthanide concentrations. Recent lanthanum-139 NMR studies carried out at 0.1–0.6 M $LaCl_3$ suggest that in this concentration range La^{3+} interacts with virtually all of the free carboxylates of BSA with an apparent dissociation constant of 0.46 M. The dissociation constant for the monoacetato complex is 0.014 M, (Reuben and Luz, 1976). The weaker apparent binding with BSA may be explained with the assumption that the dissociation constant increases with increasing saturation of the binding sites as would be expected for the interaction of cations with negatively charged spherical macromolecules with the net charge spread uniformly over their surface (Scatchard, 1949). Thus in general, a protein molecule may be viewed as a heterogeneous binding domain for lanthanide ions. This heterogeneity may lead to otherwise unexpected spectral effects. Epstein et al. (1977) have found that the CPL of the Tb^{3+}-trypsin complex depends on the concentrations of both cation and protein. Since CPL is a molecular property this fact can be taken as evidence of heterogeneous binding. Ambiguities that may arise from such heterogeneity in NMR mapping studies, in which lanthanides are used as paramagnetic probes, have been pointed out (Epstein and Reuben, 1977). While the binding of lanthanides to proteins could be described within a coherent, albeit tentative, framework, enzyme activity or inhibition in the presence of lanthanides is not yet well understood. This is of no surprise, however, since in most of the cases the mechanism of enzymatic activity in the native state has yet to be elucidated. Most of the studies of the

effects of lanthanides on enzymatic activity or protein function have been carried out on metal ion activated systems. Usually a "yes" or "no" answer has been sought. Enzyme and protein functions activated by lanthanides are listed in table 39.11. With these proteins the lanthanides could safely be used as probes of structure and function since the active conformation of the protein and its substrates is preserved in the lanthanide complex and the lanthanide ion replaces isomorphously the natural metal ion activator. Only for two enzymatic reactions are there sufficient data to allow a comparison between the different lanthanides. Wedler and D'Aurora (1974) have studied the stimulation of the biosynthetic activity of adenylated glutamine synthetase and compared it with that obtained with a similar concentration of the natural activator Mn^{2+}. Their results are plotted against the ionic radius in fig. 39.6. Also given in fig. 39.6 are the results obtained by Gomez et al. (1974) for the conversion of trypsinogen to trypsin. These are the inverse half-lives for reaction at optimal lanthanide concentrations. As seen from fig. 39.6 the two systems exhibit opposing trends. There are several reasons that could underlie such behavior. These include differences in dissociation constants and different function of the metal ion in the enzymatic reaction. It is noteworthy that lanthanides can replace Mg^{2+} and Mn^{2+} as well as Ca^{2+} (cf. table 39.11).

The lanthanides have also been found to inhibit enzymatic activity or protein function. A summary of such cases is given in table 39.12. Here one also finds enzymes that are activated by Ca^{2+}, Mg^{2+}, or Mn^{2+}. With acetylcholine esterase, which is not a metal ion requiring enzyme, the lanthanides are competitive inhibitors towards the substrate suggesting that they bind at the active site. The only generalization that could be attempted is concerned with kinases. These phosphoryl transferring enzymes are normally activated by Mg^{2+} or Mn^{2+} and competitively inhibited by Ca^{2+}. The lanthanide ions seem to mimic the effect of Ca^{2+}. Competitive inhibition indicates that binding probably occurs at the natural metal-ion binding site although the reason for inhibition remains unclear. There are cation binding enzymes the activity of which is unaffected by lanthanides

TABLE 39.11.
Enzyme and protein functions activated by lanthanides.

Protein	Natural activator	Activity with R^{3+}	Reference
Aequorin	Ca^{2+}	$\leq R$	Izutsu et al. (1972)
Concanavalin A	Ca^{2+}	$> R$	Sherry et al. (1975)
Concanavalin A	Mn^{2+}	$> R$	Sherry et al. (1975)
Glutamine Synthetase	Mn^{2+}	$> R$	Wedler and D'Aurora (1974)
Ile-tRNA synthetase	Mg^{2+}	$\leq R$	Kayne and Cohn (1972)
Phospholipase A_2	Ca^{2+}	$> Gd$	Hershberg et al. (1976)
Trypsin acting on trypsinogen	Ca^{2+}	$< R$	Gomez et al. (1974)
Ribonuclease	–	$\leq Eu$	Geidarova and Antonovskii (1974)

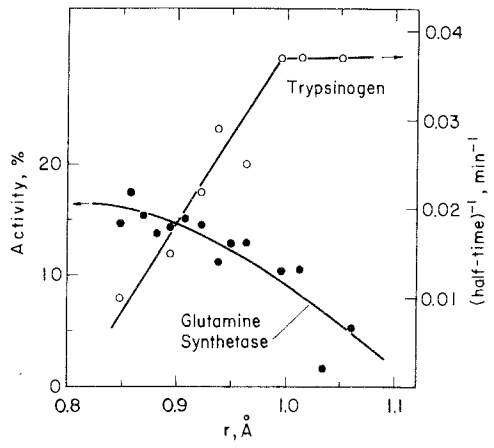

Fig. 39.6. Enzyme activity as a function of lanthanide ionic radius. Filled circles: relative biosynthetic activity of adenylated glutamine synthetase, data from Wedler and D'Aurora (1974). Open circles: reciprocal half-times for the conversion of trypsinogen to trypsin, data from Gomez et al. (1974).

and there are some for which apparently controversial findings have been reported. Details for some of the systems are given in the following paragraphs.

α-Amylase has been the subject of some controversy in the literature. This is a protein of molecular weight (m.w.) 48 000 that binds one Ca^{2+} very tightly: $K_D = 5 \times 10^{-12}$ M. The native pancreatic enzyme does not interact with Gd^{3+} as judged from PRR results (Levitzki and Reuben, 1973). When lanthanides are substituted for Ca^{2+} the enzyme is inactive towards p-nitrophenylmaltoside and two SH groups react with 5,5'(dithio-bis(2-nitrobenzoic) acid. These two groups are protected by Ca^{2+} (Steer and Levitzki, 1973). The enzyme from *Bacillus Subtilis* has two sites for Ca^{2+} and two for Gd^{3+} only one of which is the same for both cations (Levitzki and Reuben, 1973). Smolka et al. (1971) and Darnall and Birnbaum (1973) report that the bacterial enzyme is activated by lanthanides at low concentrations (up to 10^{-4} M) and inhibited at higher concentrations. It should be pointed out that starch was used as the substrate in these studies. In view of the findings of Steer and Levitzki (1973) that starch contains significant amounts of Ca^{2+}, the question of whether the bacterial α-amylase is really activated by lanthanides will remain open until the activation experiments are carried out with a synthetic substrate.

Concanavalin A is a protein existing in solution as a dimer or a tetramer of subunits of m.w. 25 500 each. There is a transition-metal binding site (S1) and Ca^{2+} binding site (S2) and an additional site (S3) to which Gd^{3+} can bind (Barber et al., 1975). The protein binds saccharides when sites S1 and S2 are occupied. Sherry et al. (1975) have found partial activation of this saccharide binding activity when lanthanides are substituted for Ca^{2+} and S1 is occupied by Zn^{2+}. On the other hand the X-ray crystallographic work of Becker et al. (1975) carried out with crystals soaked in either Sm^{3+} or Gd^{3+} solutions showed no change in electron density at the Ca^{2+} site. According to Barber et al. (1975) S3 is composed of Glu-87 of one subunit and Asp-136 of another [cf. also Reeke et al. (1975)]. Also the binding data reported by two groups of investigators (Sherry and Cottam, 1973; Barber et

TABLE 39.12.
Enzyme and protein functions inhibited by lanthanides

Protein	Natural activator	Inhibition by R^{3+}	Reference
Acetylcholinesterase	–	competitive/substrate	Howells and Coult (1971)
Aldolase	Mn^{2+}		Holten et al. (1966)
Creatine kinase	Mg^{2+}		Ellis and Morrison (1974b)
Factor X, bovine	Ca^{2+}	competitive	Furie and Furie (1975)
Inorg. pyrophosphatase	Mg^{2+}	irreversible	Sperow and Butler (1972)
Phosphoglycerate kinase	Mg^{2+}	competitive	Tanswell et al. (1974)
Pyruvate kinase	Mg^{2+}	competitive	Valentine and Cottam (1973)
Staph. nuclease	Ca^{2+}	competitive	Furie et al. (1973)
Dehydrogenases	–		Holten et al. (1966)
Lysozyme	–		Dwek (1973a)

al., 1975), is in disagreement. It seems that minor differences in experimental procedures may result in different findings with this rather complex system.

Pyruvate kinase is a protein composed of four identical subunits with a total m.w. of 237 000. A divalent cation, Mg^{2+} (or Mn^{2+}), and a monovalent cation, K^+, are both required for activity and NMR studies have shown that the two cations are bound in close proximity (Reuben and Kayne, 1971). Gadolinium (III) is a competitive inhibitor towards Mg^{2+} and binds strongly (Valentine and Cottam, 1973). Formation of ternary complexes between Gd^{3+}-pyruvate kinase and the substrate phosphoenolpyruvate (PEP) or the product ATP has been observed by NMR (Cottam et al., 1974b; Cottam and Ward, 1975; Valentine and Cottam, 1973). The dissociation constant for Gd-ATP from the ternary complex is 1.3×10^{-5} M (Valentine and Cottam, 1973). The PRR of water however is unaffected by PEP (Cottam et al., 1974b), and ^{31}P-NMR measurements indicate a Gd-phosphorus distance of 5.2 Å, *i.e.* the phosphate is not coordinated to Gd^{3+} (Cottam and Ward, 1975). It seems however that the binding of the essential monovalent cation to the Gd^{3+}-pyruvate kinase complex has to be investigated before a conclusion can be drawn regarding the mechanism of inhibition.

An ingenious way of using inhibition by lanthanides has been demonstrated in the work of Furie and Furie (1975) on bovine *Factor X*. This is a protein of m.w. 56 000, which participates as a zymogen in an intermediate step of blood coagulation. It is activated by a venom protein in a process exhibiting an absolute requirement for Ca^{2+}. There are two Ca^{2+} binding sites that have an affinity for lanthanides, which is *ca.* 3 orders of magnitude higher than that for Ca^{2+}. Lanthanides act however as competitive inhibitors in the activation process. Taking advantage of these properties Furie and Furie (1975) have purified the venom protein by using a column of Factor X covalently bound to agarose and equilibrated in 10 mM lanthanide chloride solutions.

Trypsin requires no metal ions for its enzymatic activity. However the binding of a Ca^{2+} ion affords protection against autodigestion. Lanthanide ions probably replace Ca^{2+} in an isomorphous fashion. The enzymatic activity is unaffected at low R^{3+} concentrations and the protein is protected. The PRR data and the temperature dependence of the Gd^{3+}-trypsin dissociation constant were analyzed in detail (*vide supra*) and the conclusion was reached that the lanthanide is chelated in a hexadentate manner. Thus it seems likely that several carboxyl side chains form the binding site. Inspection of a molecular model constructed according to crystallographic data suggests that the metal ion binding site is composed of the carboxylates of Glu-70 and Glu-80 and the peptide carbonyl oxygens of Asn-72 and Val-75 (Epstein et al., 1977). This site has independently been identified from X-ray difference maps (Bode and Schwager, 1975a, 1975b). The tryptophan residue responsible for the enhancement of Tb^{3+} fluorescence (Epstein et al., 1974), can now be identified with Trp-141 (Bode and Schwager, 1975a). A different conclusion however has been reached by Abbott et al. (1975). These authors measured Gd^{3+} induced PRR of p-toluamidine, an inhibitor of the enzyme, and using independently determined dissociation constants calculated a distance of 10 Å between the Gd^{3+} and the methyl group of the

inhibitor. With the known position of the inhibitor this places the Gd^{3+} ion at a site composed of the carboxyl side chain of Asp-194 and the hydroxyl of Ser-190. This site is *ca.* 15 Å away from the one mentioned above. The more recent study of Epstein and Reuben (1977) has shown however that the Gd^{3+}-trypsin-inhibitor system is heterogeneous as revealed in the dependence of the water and inhibitor proton NMR line-widths upon both the Gd^{3+} and the enzyme concentrations and in the effects of added Ca^{2+} on the line-widths, implying that in the previous work the distance from a weak rather than from the strong metal ion binding site of trypsin may have been determined.

Trypsinogen is the precursor of trypsin. It is converted to trypsin by the enzymatic hydrolysis of the Lys-6:Ile-7 bond resulting in the cleavage of the hexapeptide Val-$(Asp)_4$-Lys. The enzyme catalysing this hydrolysis is trypsin itself. This was the first enzymatic process shown to be accelerated by a lanthanide ion (Darnall and Birnbaum, 1970). At the 1 mM level Nd^{3+} is *ca.* 10 times as effective as Ca^{2+} in accelerating the reaction. However at higher concentrations, 10–100 mM, an inhibition is observed. Gomez et al. (1974) have studied the acceleration of the trypsinogen conversion by a series of lanthanides (*cf.* fig. 39.6). They found that the concentration required for optimal activity decreased along the series from 5×10^{-4} M for Nd^{3+} to 0.8×10^{-4} M for Lu^{3+}. The maximal velocity of the reaction is unaffected neither by lanthanides nor by Ca^{2+}. The inhibition at high lanthanide concentrations was further investigated and found to be due to the inhibition of trypsin activity. It seems now that this inhibitory effect could result from the weak lanthanide binding at the carboxyl of Asp-194 and the hydroxyl of Ser-190 (*vide supra*), the latter being essential for enzyme specificity. Regarding the acceleration of the trypsinogen conversion Gomez et al. (1974) suggest that cation binding at the carboxylates of the peptide to be cleaved may be responsible for the observed effects. A possible mechanism is charge neutralization accompanied by a conformational change towards the conformation necessary for the formation of an active complex. It may be of interest to point out here that La^{3+} catalysis of amide proton exchange has been observed with aspartylphenylalanine methyl ester and attributed to the inductive effects resulting from cation binding to the carboxyl side chain (Bleich and Glasel, 1975).

Thermolysin (m.w. 37 500) has 4 binding sites for Ca^{2+} denoted for convenience as C1, C2, C3, and C4. It was with this protein that Colman et al. (1972) demonstrated the potential of the lanthanides to serve as isomorphous replacements for Ca^{2+} in protein crystallography. The system has subsequently been studied in greater detail by Matthews and Weaver (1974). It was found that R^{3+} may occupy sites C1, C3, and C4 but not C2 which is only 3.8 Å away from C1. In fact the Ca^{2+} ions at C1 and C2 share some of the carboxyl side chains forming these sites. There is little perturbation of protein structure upon lanthanide substitution, *e.g.* the sites occupied by Eu^{3+} ions differ by only 0.3–0.7 Å from those of the displaced Ca^{2+} ions. Site C1 is composed of the carboxyl side chains of Asp-185, Glu-177, and Glu-190. Site C3 includes the carboxyl side chains of Asp-57 and Asp-59. There is only one carboxyl, that of Asp-200, at C4. Substitution experiments carried out with crystals have shown

that Ca^{2+} is easily displaced by Eu^{3+} from the "double" site, whereas the affinity of C3 and C4 for Ca^{2+} is greater than that for Eu^{3+}. The enzymatic activity is unaffected by lanthanide substitution. Thermal stability however is lower than that of the tetracalcium complex.

Troponin (m.w. 78 000) is a complex composed of at least three functionally distinct proteins involved in muscle contraction, one of which, troponin C (m.w. 17 800), is a Ca^{2+} binding protein. Fuchs (1974) studied the binding of lanthanides to troponin by an ultrafiltration technique and found that the association constants were at least an order of magnitude lower than the one for Ca^{2+}. The Tb^{3+} fluorescence studies of Bunting et al. (1974) indicate the presence of two additional weaker binding sites. Magnesium (II) competes only for these low affinity sites. Miller et al. (1975) have studied the fluorescence and CPL of the Tb^{3+}-troponin C complex and concluded that its association constant is higher than that of the Ca^{2+} complex. A marked change in the symmetry of Tb^{3+} binding site has been observed on going from troponin C to troponin. Thus lanthanides may serve as probes in studying protein-protein interactions as well.

Lysozyme (m.w. 14 500) is a rather basic protein consisting of a single polypeptide chain of 129 amino acid residues. Binding of Gd^{3+} to lysozyme was first demonstrated by PRR (Morallee et al., 1970; Dwek et al., 1971), and further investigated by proton release measurements and protein difference spectroscopy (Secemski and Lienhard, 1974). Recent crystallographic work shows that Gd^{3+} may be bound either to the carboxyl side chain of Glu-35 or to that of Asp-52 (Kurachi et al., 1975). The distance between the two positions is 3.56 Å. In solution it is usually assumed that Gd^{3+} is chelated by both of the carboxylates. Support for this assumption comes from the estimate of the number of water molecules in the coordination sphere of bound Gd^{3+} which is $n \leqslant 4$ (Jones et al., 1974). The two carboxylates involved in cation binding are situated at the active site of the enzyme and indeed it has been found that the enzyme is inhibited by Gd^{3+} (Dwek, 1973a), and that the binding of a transition state analog to the Gd^{3+}-lysozyme complex is 70 times as weak as that to the pure enzyme (Secemski and Lienhard, 1974). In a series of articles Campbell, Dobson and Williams (1975a, 1975b, 1975c, 1975d), have presented the results of extensive and thorough investigations of the high resolution proton NMR spectrum of lysozyme using lanthanides as chemical shift and relaxation probes. Forty resonances were assigned to specific amino acid residues. The analysis of the perturbations of these resonances by lanthanides bound at the single site provides evidence for the close similarity between the solution and crystal structures of the enzyme (Campbell et al., 1975b). Evidence has also been presented for the ability of aromatic rings to flip between equivalent conformations at rates exceeding $10^4\,sec^{-1}$ (Campbell et al., 1975d). These approaches have recently been extended to phosphoglycerate kinase (m.w. 47 000), which is a much larger protein and for which very little structural information is available from other sources. Using perturbations induced by lanthanide-ATP complexes Tanswell et al. (1976) were able to identify amino acid residues in the neighborhood of the active site.

3.7. *Phospholipids and membranes*

Membranes stand on a higher rank on the ladder of molecular organization in biological systems than either of their constituent proteins and phospholipids. It seems likely that the physiological and pharmacological action of lanthanides is associated with their interaction with membranes. Research in this direction started already in the beginning of the century (Mines, 1910, 1911), and was revived more recently following the prediction that La^{3+} should bind strongly at Ca^{2+} binding sites and should serve as a nerve blocking agent (Lettvin et al., 1964). The cellular pharmacology of lanthanum has been comprehensively reviewed by Weiss (1974) and is beyond the scope of this chapter. Only those interactions that have been revealed by spectroscopic methods will be mentioned here.

Lanthanide binding and transport by mitochondria have been studied by Case (1975) using water PRR measurements. Addition of Gd^{3+} to pigeon heart or rat liver mitochondria results in PRR enhancement of 5–6 which decay due to uptake with similar kinetics in both systems. The uptake velocity of Gd^{3+} in rat liver mitochondria is about 1/6 the rate with which Mn^{2+} is transported. Lanthanides diminish the PRR enhancement due to Mn^{2+} and greatly retard its uptake kinetics suggesting that they bind at similar sites. Uncouplers of energy-driven cation uptake depress the PRR enhancements due to Gd^{3+}. Axelrod and Klein (1974) have studied the interaction of lanthanides with the garfish olfactory nerve trunk using the fluorescence of Eu^{3+} and Tb^{3+}. They have found that lanthanides bind to nerve proteins and that most of the observed binding is a slow continuous process of cation uptake into the axoplasm. Permeation through the axon membrane has been suggested as the rate limiting step of this process. The interaction of Tb^{3+} with erythrocyte ghosts produces the appearance of a new excitation peak and an enhancement of the terbium fluorescence accompanied by quenching of tryptophan fluorescence (Mikkelson and Wallach, 1974). Terbium is displaced from the membrane binding sites by excess Ca^{2+}.

Most of the work on the interaction of lanthanides with membranes and on their use as NMR probes has been done using phospholipid bilayer membranes in the form of vesicles (liposomes) obtained by the ultrasonic treatment of lecithin (phosphatidylcholine, PC) dispersions.

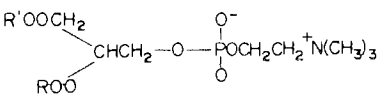

lecithin, R and R' are fatty acid chains

Normally liposomes are impermeable to lanthanides and the interaction is with the outer surface. Bystrov et al. (1971, 1972) have shown that as a result of this interaction the peak due to the choline group in the proton NMR spectrum or that due to the phosphate in the ^{31}P spectrum are split into two components only one of which is shifted. The latter corresponds to the groups on the outer

surface. Kostelnik and Castellano (1972) have shown that subsequent addition of Gd^{3+} causes broadening of the shifted line only. The relative shifting and broadening capabilities of a series of lanthanides have been reported (Andrews et al., 1973). An example of the effect of $PrCl_3$ on the proton NMR spectrum of PC liposomes is shown in fig. 39.7. From the dependence of the peak separation on lanthanide concentration Levine et al. (1973) have estimated that only between 3 and 13% of the outward facing PC molecules are involved in lanthanide binding with affinity constants in the range 120–9 400 M^{-1} at 52°C. Assuming however that all of the surface phosphates are available for binding Hauser et al. (1975) have obtained an apparent binding constant of 30 M^{-1} at 25° and R^{3+} concentrations > 10 mM. From proton and ^{31}P relaxation time measurements in the presence of $GdCl_3$ it has been concluded that the cations bind to the phosphate groups and that this is the only binding site. Indications that cation binding might be accompanied by the association of anions were obtained from proton chemical shifts. It was found that $Eu(NO_3)_3$ induced shifts *ca.* twice as large as those induced by $EuCl_3$, although the same shift ratios between the different groups in the phospholipid molecule were observed in either case (Hauser et al., 1975). Phosphatidylglycerol (PG) lacks the positively charged head group and therefore the interaction with lanthanides is stronger. This has been demonstrated by Michaelson et al. (1973). These authors examined the ^{31}P spectra of PC and PG vesicles and found that while the addition of Eu^{3+} resulted in line-splitting with PC, only broadening was observed with PG, indicating a much lower exchange rate between bound and free Eu^{3+} ions in the latter case. Both broadening and shifting of the ^{31}P resonances have been observed upon the addition of $Eu(NO_3)_3$ to high-density lipoproteins composed of PC and sphingomyelin (Assmann et al., 1974). Carbon-13 NMR spectra usually exhibit better resolution due to larger chemical shifts. Shapiro et al. (1975) were able to identify and assign 19 resonances in the ^{13}C spectrum of PC vesicles of which 6 were split upon the addition of $Pr(NO_3)_3$. The magnitude of the shifts between the "inner" and "outer" signals were found to depend upon

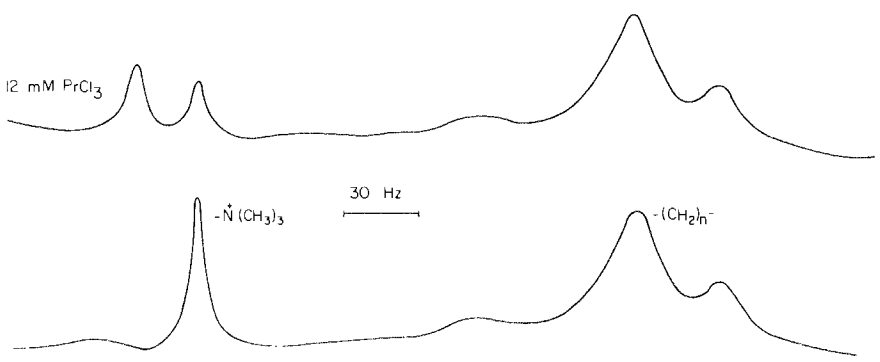

Fig. 39.7. Part of the 90 MHz proton NMR spectrum of a sonicated 5% lecithin dispersion in D_2O in the absence (bottom) and in the presence (top) of 12 mM $PrCl_3$.

the anion present, being larger with CNS^-. Larger shifts were also observed when the vesicles contained a 30% molar fraction of phosphatidylinositol or phosphatidylserine, indicating again that lanthanides bind tighter at negatively charged surfaces.

The mere fact that it is possible to distinguish between the NMR signals due to "inner" and "outer" surfaces, the relative intensities of these signals, as well as the magnitude of the lanthanide induced shifts between them have been instrumental in studies of these model membranes. The analysis of the relative shifts according to eq. (39.3) has led to the conclusion that the phosphorylcholine chain of PC is oriented parallel to the membrane surface (Barsukov et al., 1973). More recently the same group has shown that the lanthanide induced shifts can be used in the quantitative evaluation of the phospholipid composition of vesicles and in studying phospholipid exchange stimulated by soluble proteins from rat liver (Barsukov et al., 1975). The addition of up to 30% cholestrol to lecithin bilayers has little structural effects. However, above a concentration of 30% the "outer" signal increases in intensity at the expense of the "inner" one, indicating an asymmetric distribution of cholestrol in the membrane (Huang et al., 1974). The ability of a number of local anesthetics to displace Pr^{3+} ions away from the membrane surface, as judged by the decrease in the shift magnitude, has been related to the ability of the compounds to interact hydrophobically with the membrane (Fernández and Cerbón, 1973). Ionophores such as the carboxylic acid antibiotic X-537A render the membrane permeable to lanthanides. In this case the doublet due to the "inner" and "outer" groups coalesces but the position of the new signal is shifted (Fernández et al., 1973). Hunt (1975) was able to follow the kinetics of ionophore mediated Pr^{3+} transport across the membrane. Using a similar approach Lan and Chan (1975) have shown that the antibiotic drug alamethicin mediates the fusion of vesicles. The choline resonances shifts but does not split upon the addition of lanthanides unless the vesicles are first annealed at a characteristic temperature (*ca.* 60°C). This indicates that it is the thermal treatment that renders the membrane impermeable to cations (Lawaczeck, 1975).

4. Concluding remarks

This chapter has summarized the present (beginning of 1976) state of the art of lanthanide bioinorganic chemistry and of the application of lanthanides as probes to study systems of biological interest. It is intended to provide the factual background and to hint at the excitement in store for those inorganic chemists, physical chemists, and biochemists who wish to enter this area of research. The gradual but conspicuous changes of chemical properties along the lanthanide series, the great variety of physical methods, and the possibility of studying biological systems of increasing degree of molecular organization seem to be most appealing features of this field. While attempts have been made to draw some generalizations there is need for additional thermodynamic and

systematic studies. Their results will undoubtedly further our understanding not only of the bioinorganic chemistry but of lanthanide chemistry in general.

References

Abbott, F., J.E. Gomez, E.R. Birnbaum and D.W. Darnall, 1975, Biochemistry, **14**, 4935.

Andrews, S.B., J.W. Faller, J.M. Gilliam and R.J. Barnett, 1973, Proc. Nat. Acad. Sci. U.S. **70**, 1814.

Angyal, S.J., 1972, Aust. J. Chem., **25**, 1957.

Angyal, S.J., 1973, Carbohyd. Res., **26**, 271.

Angyal, S.J., 1974, Tetrahedron, **30**, 1695.

Angyal, S.J. and K.P. Davies, 1971, Chem. Commun., 500.

Angyal, S.J., D. Greeves and J.A. Mills, 1974, Aust. J. Chem., **27**, 1447.

Anonymous Correspondent, 1971, Nature, New Biol., **233**, 256.

Anteunis, M. and R. Callens, 1974, J. Magn. Resonance, **15**, 317.

Anteunis, M. and J. Gelan, 1973, J. Amer. Chem. Soc., **95**, 6502.

Anthonsen, T., B. Larsen and O. Smidsrod, 1972, Acta Chem. Scand., **26**, 2988.

Anthonsen, T., B. Larsen and O. Smidsrod, 1973, Acta Chem. Scand., **27**, 2671.

Assmann, G., E.A. Sokoloski and H.B. Brewer, Jr., 1974, Proc. Nat. Acad. Sci., **71**, 549.

Asso, M., J. Mossoyan and D. Benlian, 1975, C.R. Acad. Sci., Paris, Ser. C, **280**, 109.

Axelrod, D. and M.P. Klein, 1974, Biochem. Biophys. Res. Commun., **57**, 927.

Aziz, A., S.J. Lyle and J.E. Newbery, 1971, J. Inorg. Nucl. Chem. **33**, 1757.

Bainann, E., H. Trapmann and F. Fischler, 1954, Biochem. Z., **328**, 89.

Barber, B.H., B. Fuhr and J.P. Carver, 1975, Biochemistry, **14**, 4075.

Barela, T.D., S. Burchett and D.E. Kizer, 1975, Biochemistry, **14**, 4887.

Barry, C.D., A.C.T. North, J.A. Glasel, R.J.P. Williams and A.V. Xavier, 1971, Nature, **232**, 236.

Barry, C.D., J.A. Glasel, A.C.T. North, R.J.P. Williams and A.V. Xavier, 1972a, Biochim. Biophys. Acta, **262**, 101.

Barry, C.D., J.A. Glasel, A.C.T. North, R.J.P. Williams and A.V. Xavier, 1972b, Biochem. Biophys. Res. Commun., **47**, 166.

Barry, C.D., J.A. Glasel, R.J.P. Williams and A.V. Xavier, 1974a, J. Mol. Biol., **84**, 471.

Barry, C.D., D.R. Martin, R.J.P. Williams and A.V. Xavier, 1974b, J. Mol. Biol., **84**, 491.

Barry, C.D., C.M. Dobson, R.J.P. Williams and A.V. Xavier, 1974c, J.C.S. Dalton, 1765.

Barsukov, L.I., Yu.E. Shapiro, A.V. Viktorov, V.F. Bystrov and L.D. Bergelson, 1973, Dokl. Akad. Nauk. SSSR, **208**, 717.

Barsukov, L.I., Yu.E. Shapiro, A.V. Viktorov, V.I. Volkova, V.F. Bystrov and L.D. Bergelson, 1974, Biochem. Biophys. Res. Commun., **60**, 196.

Barsukov, L.I., Yu.E. Shapiro, A.V. Viktorov, V.I. Volkova, V.F. Bystrov and L.D. Bergelson, 1975, Chem. Phys. Lipids, **14**, 211.

Batyaev, I.M. and R.S. Fogileva, 1972, Zh. Neorg. Khim., **17**, 391.

Batyaev, I.M. and R.S. Fogileva, 1974, Zh. Neorg. Khim., **19**, 670.

Bayer, E. and K. Beyer, 1973, Tetrahedron Lett., 1209.

Becker, J.W., G.N. Reeke, Jr., J.L. Wang, B.A. Cunningham and G.M. Edelman, 1975, J. Biol. Chem., **250**, 1513.

Berner, V.G., D.W. Darnall and E.R. Birnbaum, 1975, Biochem. Biophys. Res. Commun., **66**, 763.

Bertha, S.L. and G.R. Choppin, 1969, Inorg. Chem., **8**, 613.

Birdsall, B., J. Feeney, J.A. Glasel, R.J.P. Williams and A.V. Xavier, 1971, Chem. Commun, 1473.

Birdsall, B., N.J.M. Birdsall, J. Feeney and J. Thornton, 1975, J. Amer. Chem. Soc., **97**, 2845.

Birnbaum, E.R. and D.W. Darnall, 1973, Bioinorg. Chem., **3**, 15.

Birnbaum, E.R., J.E. Gomez and D.W. Darnall, 1970, J. Amer. Chem. Soc., **92**, 5287.

Bleich, H.E. and J.A. Glasel, 1975, J. Amer. Chem. Soc., **97**, 6585.

Bode, W. and P. Schwager, 1975a, FEBS Lett., **56**, 139.

Bode, W. and P. Schwager, 1975b, J. Mol. Biol., **98**, 693.

Bradbury, J.H., L.R. Brown, M.W. Crompton and B. Warren, 1974, Pure Appl. Chem., **40**, 83.

Bunting, J.R., A. Cobo-Frenkel and R.M. Dowben, 1974, Binding of Tb^{3+} to the calcium binding site of troponin, in: Haschke, J.M. and H.A. Eick, eds. Proceedings of the 11th Rare Earth Research Conference, Traverse City, Michigan, Vol. 2 (USAEC Technical Information Center, Oak Ridge, Tennessee) pp. 672–681.

Butchard, C.G., R.A. Dwek, S.J. Ferguson, P.W. Kent, R.J.P. Williams and A.V. Xavier, 1972, FEBS Lett., **25**, 91.

Bystrov, V.F., N.I. Dubrovina, L.I. Barsukov and L.D. Bergelson, 1971, Chem. Phys. Lipids, **6**, 343.

Bystrov, V.F., Yu.E. Shapiro, A.V. Viktorov, L.I. Barsukov and L.D. Bergelson, 1972, FEBS Lett., **25**, 337.

Campbell, I.D., C.M. Dobson, R.J.P. Williams, and A.V. Xavier, 1973a, J. Magn. Resonance, **11**, 172.

Campbell, I.D., C.M. Dobson, R.J.P. Williams and A.V. Xavier, 1973b, Ann. N.Y. Acad. Sci., **222**, 163.
Campbell, I.D., C.M. Dobson and R.J.P. Williams, 1975a, Proc. Roy. Soc., Ser. A, **345**, 23.
Campbell, I.D., C.M. Dobson and R.J.P. Williams, 1975b, Proc. Roy. Soc., Ser. A, **345**, 41.
Campbell, I.D., C.M. Dobson and R.J.P. Williams, 1975c, Proc. Roy. Soc., Ser. B, **189**, 485.
Campbell, I.D., C.M. Dobson and R.J.P. Williams, 1975d, Proc. Roy. Soc., Ser. B, **189**, 503.
Carnall, W.T., P.R. Fields and K. Rajnak, 1968a, J. Chem. Phys., **49**, 4447.
Carnall, W.T., P.R. Fields and K. Rajnak, 1968b, J. Chem. Phys., **49**, 4450.
Case, G.D., 1975, Biochem. Biophys. Acta, **375**, 69.
Casu, B., G. Gatti, N. Cyr and A.S. Perlin, 1975, Carbohydr. Res. **41**, C6.
Choppin, G.R., 1971, Pure Appl. Chem. **27**, 23.
Colman, P.M., L.H. Weaver and B.W. Matthews, 1972, Biochem. Biophys. Res. Commun. **46**, 1999.
Cooperman, B.S. and N.Y. Chin, 1973, Biochemistry **12**, 670.
Cottam, G.L. and R.L. Ward, 1975, Biochem. Biophys. Res. Commun. **64**, 797.
Cottam, G.L., A.D. Sherry, and K.M. Valentine, 1974a, Catalytic and spectroscopic properties of the lanthanide ion alkaline phosphatase complex, in: Haschke, J.M. and H.A. Eick, eds., Proceedings of the 11th Rare Earth Research Conference, Traverse City, Michigan, Vol. 1 (USAEC Technical Information Center, Oak Ridge, Tennessee) pp. 204–212.
Cottam, G.L., K.M. Valentine, B.C. Thompson and A.D. Sherry, 1974b, Biochemistry **13**, 3532.
Cromer, D.T., 1965, Acta Crystallogr. **18**, 17.
Darnall, D.W. and E.R. Birnbaum, 1970, J. Biol. Chem. **245**, 6484.
Darnall, D.W., E.R. Birnbaum, 1973, Biochemistry **12**, 3489.
Darnall, D.W., E.R. Birnbaum, J.E. Gomez and G.E. Smolka, 1971, Rare earth metal ions as probes of calcium ion binding sites in proteins, in: Field, P.E., ed., Proceedings of the 9th Rare Earth Research Conference, Blacksburg, Virginia, Vol. 1 (USAEC Technical Information Center, Oak Ridge, Tennessee) pp. 278–291.
Dobson, C.M., R.J.P. Williams and A.V. Xavier, 1974, J.C.S. Dalton 1762.
Dobson, C.M., G.R. Moore and R.J.P. Williams, 1975a, FEBS Lett. **51**, 60.
Dobson, C.M., L.O. Ford, S.E. Summers and R.J.P. Williams, 1975b, J.C.S. Faraday II **71**, 1145.
Donato, H. Jr., and R.B. Martin, 1974, Biochemistry **13**, 4575.
Dower, S.K., R.A. Dwek, A.C. McLaughlin, L.E. Mole, E.M. Press and C.A. Sunderland, 1975, Biochem. J. **149**, 73.
Dwek, R.A., 1973a, Reported at the 10th Rare Earth Res. Conf., Carefree, Ariz.
Dwek, R.A., 1973b, NMR in Biochemistry (Clarendon Press, Oxford).
Dwek, R.A., R.E. Richards, K.G. Morallee, E. Nieboer, R.J.P. Williams and A.V. Xavier, 1971, Eur. J. Biochem. **21**, 204.
Dwek, R.A., J.C.A. Knott, D. Marsh, A.C. McLaughlin, E.M. Press, N.C. Price and A.I. White, 1975, Eur. J. Biochem. **53**, 25.
East, D., E. Nieboer, J.S. Cohen and A.N. Schechter, 1972, Fed. Proc. **31**, 502.
Eichhorn, G.L. and J.J. Butzow, 1965, Biopolymers, **3**, 79.
Eisinger, J. and A.A. Lamola, 1971, Biochim. Biophys. Acta **240**, 299.
Elgavish, G.A. and J. Reuben, 1978, to be published.
Ellis, K.J. and J.F. Morrison, 1974a, Biochim. Biophys. Acta **362**, 201.
Ellis, K.J. and J.F. Morrison, 1974b, Proc. Aust. Biochem. Soc. **7**, 17.
Epstein, M. and J. Reuben, 1977, Biochim. Biophys. Acta, **481**, 164.
Epstein, M., A. Levitzki and J. Reuben, 1974, Biochemistry, **13**, 1777.
Epstein, M., J. Reuben and A. Levitzki, 1977, Biochemistry, **16**, 2449.
Fazakerley, G.V., J.C. Russell and M.A. Wolfe, 1975, J.C.S. Chem. Commun. 527.
Fernández, M.S. and J. Cerbón, 1973, Biochim. Biophys. Acta **298**, 8.
Fernández, M.S., H. Célis and M. Montal, 1973, Biochim. Biophys. Acta **323**, 600.
Formoso, C., 1973, Biochem. Biophys. Res. Commun. **53**, 1084.
Fuchs, F., 1974, Chemical Properties of the calcium receptor site of troponin as determined from binding studies, in: Drabikowski, W., H. Strzelecka-Gclaszewska and E. Carafoli, eds., Calcium Binding Poteins (Elsevier Scientific Publishing Co., Amsterdam) pp. 1–25.
Furie, B.C. and B. Furie, 1975, J. Biol. Chem. **250**, 601.
Furie, B., A. Eastlake, A.N. Schechter and C.B. Anfinsen, 1973, J. Biol. Chem. **248**, 5821.
Furie, B., J.H. Griffin, R.J. Feldmann, E.A. Sokoloski and A.N. Schechter, 1974, Proc. Nat. Acad. Sci. U.S. **71**, 2833.
Gafni, A. and I.Z. Steinberg, 1974, Biochemistry, **13**, 800.
Geidarova, E.T. and V.L. Antonovskii, 1974, Biofizika **19**, 605.
Glasel, J.A., 1973, Lanthanide Ions as Nuclear Magnetic Resonance Chemical Shift Probes in Biological Systems, in: Lippard, S.J., ed., Current Research Topics in Bioinorganic Chemistry (John Wiley and Sons, New York) pp. 383–413.
Gomez, J.E., E.R. Birnbaum and D.W. Darnall, 1974, Biochemistry **13**, 3745.
Grasdalen, H., T. Anthonsen, B. Larsen and O. Smidsrød, 1975a, Acta Chem. Scand. B**29**, 17.

Grasdalen, H., T. Anthonsen, B. Larsen and O. Smidsrod, 1975b, Acta Chem. Scand. B**29**, 99.
Hall, L.D. and C.M. Preston, 1975, Carbohydr. Res. **41**, 53.
Hauser, H., M.C. Phillips, B.A. Levine and R.J.P. Williams, 1975, Eur. J. Biochem. **58**, 133.
Hershberg, R.D., G.H. Reed, A.J. Slotboom and G.H. deHaas, 1976, Biochemistry **15**, 2268.
Hoard, J.L., B. Lee and M.D. Lind, 1965, J. Amer. Chem. Soc. **87**, 1612.
Holten, V.Z., G.C. Kyker and M. Pulliam, 1966, Proc. Soc. Exp. Med. **123**, 913.
Horrocks, W. DeW, Jr., R.F. Venteicher, C.A. Spilburg and B.L. Vallee, 1975, Biochem. Biophys. Res. Commun. **64**, 317.
Howells, D.J. and D.B. Coult, 1971, Biochim Biophys. Acta **244**, 427.
Huang, C.-H., J.P. Sipe, S.T. Chow and R.B. Martin, 1974, Proc. Nat. Acad. Sci. U.S. **71**, 359.
Hunt, G.R.A., 1975, FEBS Lett. **58**, 194.
Inagaki, F., S. Takahashi, M. Tasumi and T. Miyazawa, 1975a, Bull. Chem. Soc. Japan **48**, 853.
Inagaki, F., S. Takahashi, M. Tasumi and T. Miyasawa, 1975b, Bull. Chem. Soc. Japan **48**, 1590.
Inagaki, F., M. Tasumi and T. Miyazawa, 1976, J.C.S. Perkin II, 167.
Izutsu, K.T., S.P. Felton, I.A. Siegel, W.T. Yoda and A.C.N. Chen, 1972, Biochem. Biophys. Res. Commun. **49**, 1034.
Jones, A.D. and D.R. Williams, 1970, J. Chem. Soc., A, 3138.
Jones, A.D. and D.R. Williams, 1971, J. Chem. Soc., A, 3159.
Jones, C.R. and D.R. Kearns, 1974a, J. Amer. Chem. Soc. **96**, 3651.
Jones, C.R. and D.R. Kearns, 1974b, Proc. Nat. Acad. Sci. U.S. **71**, 4237.
Jones, C.R. and D.R. Kearns, 1975, Biochemistry **14**, 2660.
Jones, R., R.A. Dwek and S. Forsén, 1974, Eur. J. Biochem. **47**, 271.
Kachura, T.F., A.N. Sevchenko, K.N. Soloviev and M.P. Zvirko, 1974, Dokl. Akad. Nauk SSSR **217**, 1121.
Kainosho, M. and K. Ajisaka, 1975, J. Amer. Chem. Soc. **97**, 6839.
Karraker, D.G., 1967, Inorg. Chem. **6**, 1863.
Katzin, L.I., 1969, Inorg. Chem. **8**, 1649.
Katzin, L.I. and E. Gulyas, 1968, Inorg. Chem. **7**, 2442.
Kayne, M.S. and M. Cohn, 1972, Biochem. Biophys. Res. Commun. **46**, 1285.
Kayne, M.S. and M. Cohn, 1974, Biochemistry **13**, 4159.
Kieboom, A.P.G., T. Spoormaker, A. Sinnema, J.M. van der Toorn and H. van Bekkum, 1975, Rec. Trav. Chim. Pays-Bas **94**, 53.
Kim, S.H., G.J. Quigley, F.L. Suddath, A. McPherson, D. Sneden, J.J. Kim, J. Weinzierl, P. Blattmann and A. Rich, 1972, Proc. Nat. Acad. Sci. U.S. **69**, 3746.
Kolat, R.S. and J.E. Powell, 1964, Inorg. Chem. **3**, 242.
Kostelnik, R.J. and S.M. Castellano, 1972, J. Magn. Resonance **7**, 219.
Kostromina, N.A., 1971, Zh. Neorg. Khim. **16**, 2966.
Kurachi, K., L.C. Sieker and L.H. Jensen, 1975, J. Biol. Chem. **250**, 7663.
Lal, S., 1972, Aust. J. Chem. **25**, 1571.
Lamola, A.A. and J. Eisinger, 1971, Biochim. Biophys. Acta **240**, 313.
Lau, A.L.Y. and S.I. Chan, 1975, Proc. Nat. Acad. Sci. U.S. **72**, 1975.
Lavallee, D.K. and A.H. Zeltmann, 1974, J. Amer. Chem. Soc., **96**, 5552.
Lawaczeck, R., M. Kainosho, J.-L. Girardet and S.I. Chan, 1975, Nature **256**, 584.
Lee, C.-Y. and M.J. Raszka, 1975, J. Magn. Resonance **17**, 151.
Lenkinski, R.E. and J. Reuben, 1976, J. Amer. Chem. Soc. **98**, 3089.
Lettvin, J.Y., W.F. Pickard, W.S. McCulloch and W. Pitts, 1964, Nature **202**, 1338.
Levine, Y.K., A.G. Lee, N.J.M. Birdsall, J.C. Metcalfe and J.D. Robinson, 1973, Biochim. Biophys. Acta **291**, 592.
Levitzki, A. and J. Reuben, 1973, Biochemistry **12**, 41.
Luk, C.K. 1971, Biochemistry **10**, 2838.
Luk, C.K. and F.S. Richardson, 1974, Chem. Phys. Lett. **25**, 215.
Luk, C.K. and F.S. Richardson, 1975, J. Amer. Chem. Soc. **97**, 6666.
Mackey, J.L., J.E. Powell and F.H. Spedding, 1962, J. Amer. Chem. Soc. **84**, 2047.
Marinetti, T.D., G.H. Snyder and B.D. Sykes, 1975, J. Amer. Chem. Soc. **97**, 6562.
Matthews, B.W. and L.H. Weaver, 1974, Biochemistry **13**, 1719.
Michaelson, D.M., A.F. Horwitz and M.P. Klein, 1973, Biochemistry **12**, 2637.
Mikkelsen, R.B. and D.F.H. Wallach, 1974, Biochim. Biophys. Acta 363, 211.
Miller, T.L., D.J. Nelson, H.G. Brittain, F.S. Richardson, R.B. Martin and C.M. Kay, 1975, FEBS Lett. **58**, 262.
Mines, G.R., 1910, J. Physiol. (London) **40**, 327.
Mines, G.R., 1911, J. Physiol. (London) **42**, 309.
Moeller, T. and R. Ferrús, 1962, Inorg. Chem. **1**, 49.
Morallee, K.G., E. Nieboer, F.J.C. Rossotti, R.J.P. Williams, A.V. Xavier and R.A. Dwek, 1970, Chem. Commun. 1132.
Nieboer, E., 1975, Structure and Bonding, **22**, 1.
Nieboer, E., W.P. Flora, M. Podolski and H. Falter, 1973, The lanthanide cations as NMR probes: a novel approach to organic shift reagent studies and amino acid sequence determination of simple peptides, in: Kevane, C.J. and T. Moeller, eds., Proceedings of the 10th Rare Earth Research Conference, Carefree, Arizona, Vol. 1 (USAEC

Technical Information Center, Oak Ridge, Tennessee) pp. 388–397.
Plyushchev, V.E., G.V. Nadezhdina, G.S. Losseva, V.V. Melnikova and T.S. Parfenova, 1974, Zh. Obshch. Khim. **44**, 2319.
Prados, R., L.G. Stadtherr, H. Donato Jr. and R.B. Martin, 1974, J. Inorg. Nucl. Chem. **36**, 689.
Reeke, G.N., Jr., J.W. Becker and G.M. Edelman, 1975, J. Biol. Chem. **250**, 1525.
Reuben, J. 1971a, Biochemistry **10**, 2834.
Reuben, J., 1971b, J. Phys. Chem. **75**, 3164.
Reuben, J., 1975a, Naturwissenschaften **62**, 172.
Reuben, J., 1975b, J. Phys. Chem. **79**, 2154.
Reuben, J., 1975c, J. Amer. Chem. Soc. **97**, 3823.
Reuben, J., 1975d, J. Chem. Phys. **63**, 5063.
Reuben, J., 1977, J. Amer. Chem. Soc., **99**, 1765.
Reuben, J. and F.J. Kayne, 1971, J. Biol. Chem. **246**, 6227.
Reuben, J. and Z. Luz, 1976, J. Phys. Chem. **80**, 1357.
Ricci, R.W. and K.B. Kilichowski, 1974, J. Phys Chem. **78**, 1953.
Robertus, J.D., J.E. Ladner, J.T. Finch, D. Rhodes, R.S. Brown, B.F.C. Clark and A. Klug, 1974, Nature **250**, 546.
Robinson, W.O., H. Bastron and K.J. Murata, 1958, Geochim. Cosmochim. Acta **14**, 55.
Scatchard, G., 1949, Ann. N.Y. Acad. Sci. **51**, 660.
Schwarzburd, P.M., 1975, Biofizika **20**, 334.
Secemski, I.I. and G.E. Lienhard, 1974, J. Biol. Chem. **249**, 2932.
Sekhon, B.S. and S.L. Chopra, 1974, Israel J. Chem. **12**, 917, and references therein.
Shapiro, Yu.E., A.V. Viktorov, V.I. Volkova, L.I. Barsukov, V.F. Bystrov and L.D. Bergelson, 1975, Chem. Phys. Lipids **14**, 227.
Sherry, A.D. and G.L. Cottam, 1973, Arch. Biochem. Biophys. **156**, 665.
Sherry, A.D., E.R. Birnbaum and D.W. Darnall, 1972, J. Biol. Chem. **247**, 3489.
Sherry, A.D., C. Yoshida, E.R. Birnbaum and D.W. Darnall, 1973, J. Amer. Chem. Soc. **95**, 3011.
Sherry, A.D., A.D. Newman and C.G. Gutz, 1975, Biochemistry **14**, 2191.
Sieker, L.C., E. Adman and L.H. Jensen, 1972, Nature **235**, 40.
Silber, H.B., 1974, FEBS Lett. **41**, 303.
Smolka, G.E., E.R. Birnbaum and D.W. Darnall, 1971, Biochemistry **10**, 4556.
Spartalian, K. and W.T. Oosterhuis, 1973, J. Chem. Phys. **59**, 617.
Sperow, J.W. and L.G. Butler, 1972, Bioinorg. Chem. **2**, 87.
Steer, M.L. and A. Levitzki, 1973, FEBS Lett. **31**, 89.
Tanner, S.P. and G.R. Choppin, 1968, Inorg. Chem. **7**, 2046.
Tanswell, P., E.W. Westhead and R.J.P. Williams, 1974, FEBS Lett. **48**, 60.
Tanswell, P., J.M. Thornton, A.V. Korda and R.J.P. Williams, 1975, Eur. J. Biochem. **57**, 135.
Tanswell, P., E.W. Westhead and R.J.P. Williams, 1976, Eur. J. Biochem **63**, 249.
Templeton, D.H. and C.H. Dauben, 1954, J. Amer. Chem. Soc. **76**, 5237.
Teuwissen, B., P.L. Masson, P. Osinski and J.F. Heremans, 1972, Eur. J. Biochem. **31**, 239.
Valentine, K.M. and G.L. Cottam, 1973, Arch. Biochem. Biophys. **158**, 346.
Watenpaugh, K.D., L.C. Sieker, L.H. Jensen, J. Legall and M. Dubourdieu, 1972, Proc. Nat. Acad. Sci. U.S. **69**, 3185.
Wedler, F.C. and V. D'Aurora, 1974, Biochim. Biophys. Acta **371**, 432.
Weiss, G.B., 1974, Ann. Rev. Pharmacology **14**, 343.
Weissman, S.I., 1942, J. Chem. Phys. **10**, 214.
Wertheim, G.K., 1964, Mössbauer Effect (Academic Press, New York).
Williams, M.N., 1971, Fed. Proc. **30**, 1292.
Williams, R.J.P., 1970, Quart. Rev. (London) **24**, 331.
Wolfson, J.M. and D.R. Kearns, 1974, J. Amer. Chem. Soc. **96**, 3653.
Wolfson, J.M. and D.R. Kearns, 1975, Biochemistry **14**, 1436.
Wong, C.-P., R.F. Venteicher and W. DeW., Horrocks, Jr., 1974, J. Amer. Chem. Soc. **96**, 7149.
Yonuschot, G. and G.W. Mushrush, 1975, Biochemistry **14**, 1677.
Zolin, V.F., L.G. Koreneva and V.I. Zaryuk, 1975, Biofizika **20**, 194.

Handbook on the Physics and Chemistry of Rare Earths, edited by K.A. Gschneidner, Jr. and L. Eyring

Chapter 40

TOXICITY

Thomas J. HALEY
National Center for Toxicological Research, Jefferson, Arkansas 72079, USA

Contents

1. Introduction

With the introduction of ion exchange techniques, the separation of the rare earths from their ores and from one another became practical and new uses were developed. Previous separation difficulties were the result of the ground-state electronic configuration of their atoms and their almost identical chemical reactivity. Moeller (1963) has reviewed the subject in great detail. Prior to the present time, mixtures of the rare earths were used in cigarette lighter flints, in Welsbach mantels for increasing the brightness of gas lights and in Coleman lanterns. Newer uses include control rods for atomic reactors because of their large cross-section capture values for neutrons compared to cadmium (Ransohoff, 1959), the addition of cerium to increase the life of nickel-chrome resistant wire (Spiller, 1960), radiothulium in portable roentgenographic equipment, new types of alloys (Savitskiy, 1960), lasers, masers, microwave devices, phosphours, insulators, capacitors, semiconductors, ferroelectrics and color television (Spedding and Gschneidner, 1964). The wide-spread industrial usage

makes it imperative that more modern and detailed information on the toxicology of the rare earth elements be made available to prevent any possible deleterious effects which might occur during their application to industrial problems. The elements to be considered are listed in table 40.1 (Haley, 1965).

TABLE 40.1.
Rare earth elements

Name	Symbol	At. wt.	At. no.	Abundance (g/metric ton)
Scandium	Sc	44.956	21	5.0
Yttrium	Y	88.905	39	28.10
Lanthanum	La	138.910	57	18.30
Cerium	Ce	140.120	58	46.10
Praseodymium	Pr	140.907	59	5.53
Neodymium	Nd	144.240	60	23.90
Promethium	Pm	147.000	61	ca. 0
Samarium	Sm	150.350	62	6.47
Europium	Eu	151.960	63	1.06
Gadolinium	Gd	157.250	64	6.36
Terbium	Tb	158.924	65	0.91
Dysprosium	Dy	162.500	66	4.47
Holmium	Ho	164.930	67	1.15
Erbium	Er	167.260	68	2.47
Thulium	Tm	168.934	69	0.20
Ytterbium	Yb	173.040	70	2.66
Lutetium	Lu	174.970	71	0.75

From Haley (1965).

2. Toxicity

2.1. *Acute*

The rare earths are considered only slightly toxic according to the Hodge-Sterner classification system (Hodge and Sterner, 1943). The acute lethal dose by various routes of administration are given in table 40.2. The symptoms of toxicity of the rare earth elements including writhing, ataxia, labored respiration, walking on the toes with arched back, and sedation. There is a delayed lethality with the death rate peaking between 48 and 96 hours. A sex difference is apparent with the males being less susceptible than the females. If the animals survive for 30 days, there is generalized peritonitis, adhesions, and hemorrhagic ascitic fluid (Bruce et al., 1963) and also true granulomatous peritonitis and focal hepatic necrosis (Steffee, 1959). Chelating agents, citrate or EDTA, obscure the lethal effects of the rare earths by either decreasing their rate of release or by increasing their lethality by exchanging with other elements such as calcium. The effect of atomic weight on lethality is difficult to assess, but the transition

TABLE 40.2.
Acute lethal doses of the rare earths

Chemical	Species and sex	LD_{50} (mg/kg)	Adm. rt.[b]
Scandium chloride	Mouse ♂	755 (741.7–768.6)	i.p.
	Mouse ♂	4000 (3960–4040)	P.O.
Yttrium chloride	Mouse	88 (67.7–114.4)	i.p.
	Rat	450	i.p.
	Rat	45 (41.1–49.3)	i.p.
nitrate	Frog	350[a]	s.c.
	Mouse	1660	s.c.
	Rat	20–30[a]	i.v.
	Rat	350	i.p.
	Rabbit	500	i.v.
oxide	Rat	500	i.p.
Lanthanum acetate	Rat	10 000	P.O.
	Rat	475	i.p.
ammonium nitrate	Rat	3400	P.O.
	Rat	625	i.p.
citrate chloride	Mouse	78.2 (70.0–100.3)	i.p.
	Guinea pig	60.7 (17.7–207.0)	i.p.
chloride	Frog	about 1000[a]	s.c.
	Mouse	3500[a]	s.c.
	Mouse	3500[a]	s.c.
	Mouse	372.4 (323.6–428.5)	i.p.
	Mouse	>500[a]	s.c.
	Mouse	>160[a]	i.p.
	Rat	106 (91.4–123)	i.p.
	Rat	350	i.p.
	Guinea pig	129.7 (105.4–159.6)	i.p.
	Rat	4200	P.O.
	Rabbit	200–250[a]	i.v.
nitrate	Rat	4500	P.O.
	Rat	450	i.p.
	Mouse ♀	410 (353–475)	i.p.
oxide	Rat	>10,000	P.O.
sulfate	Rat	>5000	P.O.
	Rat	275	i.p.
Cerium chloride	Frog	about 300[a]	s.c.
	Mouse	5000–10 000[a]	s.c.
	Mouse	353.2 (296.5–420.7)	i.p.
	Rat	2000–4000[a]	s.c.
	Rat	50–60[a]	i.v.
	Guinea pig	55.7 (40.1–77.4)	i.p.
citrate chloride	Rat	146.6 (128.6–167.1)	i.p.
	Guinea pig	103.5 (73.1–146.5)	i.p.
nitrate	Mouse ♀	470 (435–508)	i.p.
	Rat ♀	290 (238–354)	i.p.

[a]Minimum lethal dose; [b]s.c., subcutaneous; P.O., oral; i.p., intraperitoneal; i.v., intravenous.
Source: Haley (1965).

TABLE 40.2 (*Contd.*)

Chemical	Species and sex	LD_{50} (mg/kg)	Adm. rt.[b]
	Rat ♀	4200 (3684–4788)	P.O.
	Rat ♀	4.3 (3.4–5.6)	i.v.
	Rat♂	49.6 (32.8–74.4)	i.v.
Praseodymium chloride	Frog	about 1000–1500[a]	s.c.
	Mouse	2500[a]	s.c.
	Mouse	358.9 (297.2–433.5)	i.p.
	Mouse	900–1500[a]	s.c.
	Mouse ♂	600 (552–652)	i.p.
	Mouse ♂	4500 (4054–4995)	P.O.
	Rat	<2000	i.p.
	Guinea pig	125 (78.2–200)	i.p.
	Rabbit	200–250	s.c.
citrate chloride	Mouse	140.6 (126.2–156.7)	i.p.
	Guinea pig	53 (29.9–70.3)	i.p.
nitrate	Mouse ♀	200 (259–325)	i.p.
	Rat ♀	245 (209–287)	i.p.
	Rat ♀	3500 (3017–4060)	P.O.
	Rat ♀	7.4 (5.1–10.8)	i.v.
	Rat♂	77.2 (49.7–119.8)	i.v.
	Rat	10.8–13.9[a]	i.v.
Neodymium chloride	Frog	250[a]	s.c.
	Mouse	4000[a]	s.c.
	Mouse ♂	600 (562.0–640)	i.p.
	Mouse ♂	5250 (4730–5830)	P.O.
	Mouse	348.3(297.2–408.3)	i.p.
	Rat	150–250[a]	i.p.
	Guinea pig	70[a]	i.v.
	Guinea pig	139.6 (99.3–196.3)	i.p.
	Rabbit	200–250[a]	i.v.
citrate chloride	Mouse	138 (94.4–201.8)	i.p.
	Guinea pig	40.5 (4.7–348)	i.p.
nitrate	Mouse ♀	270 (221–329)	i.p.
	Rat ♀	270 (231–316)	i.p.
	Rat ♀	2750 (1896–3988)	P.O.
	Rat ♀	6.4 (5.5–7.3)	i.v.
	Rat♂	66.8 (53.5–83.6)	i.v.
Samarium chloride	Frog	about 150[a]	s.c.
	Mouse ♂	585 (508.7–672.7)	i.p.
	Mouse ♂	>2000	P.O.
	Rat	>2000[a]	s.c.
	Guinea pig	750–1000[a]	s.c.
nitrate	Frog	1600[a]	s.c.
	Mouse♀	315 (258–384)	i.p.
	Rat ♀	285 (254–319)	i.p.

TABLE 40.2 (*Contd.*)

Chemical	Species and sex	LD_{50} (mg/kg)	Adm. rt.[b]
	Rat ♀	2900 (2660–3161)	P.O.
	Rat ♀	8.9 (6.8–11.8)	i.v.
	Rat♂	59.1 (40.5–86.3)	i.v.
	Guinea pig	about 500[a]	s.c.
Europium chloride	Mouse ♂	550 (515.5–586.9)	i.p.
	Mouse ♂	5000 (4505–5500)	i.p.
nitrate	Mouse ♀	320 (294–349)	i.p.
	Rat ♀	210 (172–256)	i.p.
	Rat ♀	>5000	P.O.
Gadolinium chloride	Mouse ♂	550 (495.5–610.5)	i.p.
	Mouse ♂	>2000	P.O.
nitrate	Mouse ♀	300 (261–345)	i.p.
	Rat ♀	230 (204–260)	i.p.
	Rat ♀	>5000	P.O.
Terbium chloride	Mouse ♂	550 (521.3–580.3)	i.p.
	Mouse ♂	5100 (5049.5–5151)	P.O.
nitrate	Mouse ♀	480 (444–518)	i.p.
	Rat ♀	260 (232–291)	i.p.
	Rat ♀	>5000	P.O.
Dysprosium chloride	Mouse ♂	585 (552–620)	i.p.
	Mouse ♂	7650 (7150–8186)	P.O.
nitrate	Mouse ♀	310 (261–369)	i.p.
	Rat ♀	295 (236–369)	i.p.
	Rat ♀	3100 (2870–3348)	P.O.
Holmium chloride	Mouse ♂	560 (541–580)	i.p.
	Mouse ♂	7200 (6667–7776)	P.O.
nitrate	Mouse ♀	320 (302–339)	i.p.
	Rat ♀	270 (237–308)	i.p.
	Rat ♀	3000 (2804–3210)	P.O.
Erbium chloride	Frog	300–400[a]	s.c.
	Mouse ♂	535 (509–562)	i.p.
	Mouse ♂	6200 (5390–7140)	P.O.
nitrate	Mouse ♀	225 (194–261)	i.p.
	Rat	82.8–96.6[a]	i.v.
	Rat ♀	230 (195–271)	i.p.
	Rat ♀	35.8 (27.8–49.9)	i.v.
	Rat ♂	52.4 (37.0–74.5)	i.v.
Thulium chloride	Mouse ♂	485 (466.3–504.4)	i.p.
	Mouse ♂	6250 (5430–7190)	P.O.
nitrate	Mouse ♀	255 (226–288)	i.p.
	Rat ♀	285 (252–322)	i.p.

TABLE 40.2 (*Contd.*)

Chemical	Species and sex	LD_{50} (mg/kg)	Adm. rt.[b]
Ytterbium chloride	Mouse ♂	395 (375–416.7)	i.p.
	Mouse ♂	6700 (6374.9–7041.7)	P.O.
nitrate	Mouse ♀	250 (185–338)	i.p.
	Rat ♀	255 (220–296)	i.p.
	Rat ♀	3100 (2924–3286)	P.O.
Lutetium chloride	Mouse ♂	315 (267–372)	i.p.
	Mouse ♂	7100 (6630–7590)	P.O.
	Mouse ♀	290 (259–325)	i.p.
	Rat ♀	325 (294–382)	i.0.

elements (terbium group) appear to have a lesser toxicity than those above or below them in the periodic table (Haley, 1965). The low oral toxicity is probably related to poor intestinal absorption. Czech investigators reported high mortality at 7 and 16 days following intraperitoneal injection of $ScCl_3$ but their LD_{50} value was only 32 (28.6–35.8) mg/kg which does not agree with value in table 40.2 (Donozal et al., 1966). Intravenous administration of any of the rare earth chlorides to rats followed by local injection of epinephrine causes topical hemorrhagic lesions at the site or in the kidneys. This effect can be blocked by pretreatment with α-adrenergic blocking drugs in the case of $ScCl_3$ (Gabbiani et al., 1966). When given intravenously to mice, the toxicity of rare earth elements increased in the following order: La < Nd < Y. The toxicity of Nd salts increased as follows: chloride < propionate < acetate < 3-sulfoisonicotinate < sulfate < nitrate (Zimakov, 1973). Rats pretreated with polymyxin, then given $GdCl_3$, can be prevented by reticuloendothelial system activators such as zymosan, triolein or BCG, while $CeCl_3$ induced fatty degeneration of the liver can be prevented by reticuloendothelial inhibition with methyl palmitate (Lazar, 1973a). Glucocorticoids plus $GdCl_3$ produce hepatic peliosis in the rat liver (Selye et al., 1972). Oral or intraperitoneal doses of 5 or 10 gm/kg of Dy_2O_3 or Gd_2O_3 had no pathological effects in mice and daily doses of 2 gm/kg were harmless. Rare earth oxides are much less toxic than chlorides or citrates (Mogilevskaya and Roshchina, 1964). Reticuloendothelial system activity in rats was depressed by doses of 0.2 mg/100 gm of $LaCl_3$, $CeCl_3$, $NdCl_3$, $GdCl_3$, $HoCl_3$ or $YbCl_3$ (Lazar, 1973b).

2.2. *Chronic*

Rabbits receiving intravenous injections of various rare earth salts develop degeneration of the spleen and yellow atrophy and central lobular necrosis of the

liver (Fischer and Roeckl, 1938). Considerable changes in hemoglobin, leukocyte count, erythrocyte count and differential count were observed in rabbits receiving single or repeated injections of $LaCl_3$, $CeCl_3$, $PrCl_3$ or $NdCl_3$. Oral doses had no affect on the animals (Oelkers and Vincke, 1938). Oral administration of 2 gm/kg of Gd_2O_3 or Dy_2O_3 for 1.5 months to guinea pigs caused a decrease in weight gain and serum alkaline phosphatase (Mogilevskaya and Roshchina, 1967). Intestinal adhesions but no effect on growth were observed when YCl_3 was administered intraperitoneally for 5 months (Bruce et al., 1963). Perinuclear vacuolization in the liver was produced by feeding $GdCl_3$, $TbCl_3$, $TmCl_3$ and $YbCl_3$ at levels of 0.01, 0.1 and 1% of the diet for 3 months. The other rare earths did not have this effect and none of the elements affected either the hemogram or the growth curve. The liver damage appeared to be sex-linked as it was more prominent in males than females (Haley, 1965). Rare earths accumulate in the Kupfer cells of the liver and spleen pulp cells of mice and rabbits (Vincke and Oelkers, 1938). Feeding 5 ppm of Sc and Y for the life span of mice resulted in significant suppression in growth. Tumors occurred in 27.4% of the Sc mice and 33 per cent of the Y mice; however the significance of the observations is difficult to assess because two control groups had 16.3 and 26.8 per cent tumors respectively (Schroeder and Mitchener, 1971). When Sc, La, Sm, Eu, Dy, Tb, Tm and Yb oxides were fed for three generations, there were no significant changes in growth rate, survival, hematology, morphological development, maturation, reproduction and lactational performance (Hutcheson et al., 1975).

2.3. *Inhalation*

Although there was no pneumonocotic fibrosis produced in guinea pig lungs from inhalation of rare earth fluoride or oxide mixtures, progressive lung retention was observed and it depended on exposure duration (Schepers et al., 1955). Continued investigation of the rare earth oxides revealed a fatal delayed chemical hyperemia and cellular eosinophilia. In those animals surviving 1 year, an isolated cellular vascular granulomata was observed (Schepers, 1955a). Exposure to a mixture with a high fluoride content produced the following lesions: acute transient chemical penumonitis, subacute bronchitis and bronchiolitis, focal hypertropic emphysema and regional bronchiolar stricturing but no granulomatosis (Schepers, 1955b). These rare earth fluoride effects have been confirmed (Roshchin, 1961). Eight months after intratracheal administration of Y_2O_3, Nd_2O_3, or Ce_2O_3 to rats, granulomas were found (Mogilevskaya and Raikhlin, 1963). Intratracheal administration of Dy_2O_2 and Gd_2O_3 in doses of 50 mg. produced numerous cellular foci with large proliferative reactions in the rat lung after 5 months (Mogilevskaya and Roshchina, 1964). Delayed lung fibrosis was observed in mice, rats and guinea pigs after administration of Sm_2O_3 and Eu_2O_3 (Mezentseva, 1967). Intratracheal injection of two doses of 25 mg each of a mixture of Ce_2O_3, La_2O_3, Nd_2O_3, Pr_2O_3, Eu_2O_3 and Sm_2O_3 caused death in 46.1% of the rats, while a single dose of 50 mg of this mixture killed all the animals in one day from pulmonary edema. Other pathological changes included:

erythrocythemia, neutrophilia, hyperhemoglobinemia, hypercoagulability of the blood, massive pneumonia, lung abscesses, pneumosclerosis, ganglion hepatitis and hepatic dystrophy (Arkhangelskaya and Spasskii, 1967). Tracheal instillation of ^{147}Pm in rats resulted in 35 per cent of the isotope being resorbed in 1–2 minutes and elimination of 40 per cent of it within 14 days via the ciliated epithelium (Dobryankova, 1969). Further studies using doses of 0.015 μCi/gm of ^{147}Pm in rats showed lung elimination of isotope to be more rapid in 1 month old animals than in 2.5 month old ones. Liver, spleen and kidney content of the isotope was lower in the younger animals, but the radionuclide caused leukopenia, lymphopenia, metaplasia of the bronchial epithelium and pneumosclerosis. The LD_{50} intracheally of ^{147}Pm was 15 μCi/gm (Burykina et al., 1972). This radionuclide is deposited in the lungs, liver and skeleton after intratracheal administration and diethylenetriamine pentaacetic acid injection will remove 80–90 per cent from the first two organs if given one hour after the isotope (Zhanadilov, 1973).

Inhalation of an aerosol of Nd_2O_3 – particle size 1 μ diameter, concentration 30 mg/M^3 – by mice and guinea pigs for 6 hr/day, 5 days/week for 120 days produced no marked changes but the alveolar macrophages retained the particles (Davison and Ramsey, 1965). A similar study of a Gd_2O_3 aerosol produced the same results and, in addition, impaction of the particles in the tracheobronchial lymph nodes but no acute inflammatory reactions or fibrosis (Talbot et al., 1965). Mice exposed to Gd_2O_3 aerosols for 120 days had increased deaths due to pneumonia, shorter life spans, and pulmonary calcification in the region of the alveolar basement membranes and elastic laminae of small pulmonary vessels (Ball and VanGelder, 1966). Guinea pigs exposed to Gd_2O_3 aerosols for up to 120 days developed decreased lung elasticity, alveolar cell hypertrophy, septal cell thickening, lymphoid hyperplasia, and macrophage formation (Abel and Talbot, 1967). Mice exposed to an aerosol of ^{147}Pm or dusts containing ^{147}Pm showed a biological half-life for ^{147}Pm of 8.4 days in the lungs but the radionuclide readily moved to the liver, cartilage, bone and soft tissues. DPTA and EDTA removed 55–80% of the ^{147}Pm from the lungs and hexametaphosphate removed 77% (Gensicke and Hoelzer, 1972). Luminous masses containing ^{147}Pm, when inhaled in aerosol form, became widely distributed in mouse tissues but by 12 months the nuclide was entirely in the tracheal cartilage (Gensicke et al., 1972). Inhaled $^{147}PmCl_3$ deposited in the mouse lung can be decreased by 75% in 16 days by inhalation or intraperitoneal injection of hexametaphosphate within 24 hours of exposure to the radionuclide (Gensicke et al., 1973). Inhalation of aerosols containing 2–10 μCi of ^{91}Y or ^{144}Ce by rats resulted in only 10–18% being deposited in the lungs while 60% was found in the nose and pharynx. Most pathological changes occurred in the lungs (Semenov et al., 1966). Rats exposed to ^{88}Y with carrier ^{89}Y had a greater fecal excretion of the radionuclide (Wenzel et al., 1969). Aerosols of $^{152-154}Eu_2O_3$ inhaled by rats resulted in traces of the radionuclide at 30 days in the kidney, liver, blood and bone and excretion was almost completely via the gastrointestinal tract (Johnson and Ziemer, 1971). It

has been shown that deposition and retention of inhaled particulates from aerosols of Y, Sc, Ce, Eu and Yb are related to particle size, lung clearance mechanism, organ and tissue distribution, and the elimination route and its magnitude. Other factors include biological response of various organ systems in terms of developing pathology and tumorigenesis, organ function, possible life-span shortening, correlation between body burden and observed deleterious effects and the synergism or potentiation of these effects by concurrent administration of stable and radionuclides (Berke, 1969). Comparison of biological half-lives of ^{91}Y, ^{144}Ce, ^{143}Pr and ^{147}Pm aerosols inhaled by mice gave values of 19, 60, 23 and 21 days respectively for the lower respiratory tract (Gensicke et al., 1966). Guinea pigs exposed to $^{91}YCl_3$ aerosol had an increased renal excretion of ^{91}Y when treated with DTPA (Schmidtke, 1964). Inhalation of $^{140}LaCl_3$ aerosol by rats made it possible to measure the rapidity of phagocytosis of the radionuclide. The decrease in extracellular La was exponential for the first 5 hours post-exposure only (Ducousso and Masse, 1972). Similar studies in monkeys indicated that the chelating agent, DTPA, was unable to chelate ^{140}La at any amount higher than 30 μg (Ducousso et al., 1971). Computer based biological modeling showed that insoluble ^{140}La aerosols would deliver significant radiation doses to lungs and skeleton of Beagle dogs (Cuddihy and Griffith, 1972). Inhalation of $^{144}Ce_2O_3$ by dogs also produced radiation effects but not chemical toxicity (Stuart et al., 1964). Early deposition of ^{140}La-labeled aerosols, particle sizes 0.42 to 6.6 μm, was in the nasopharyngeal, tracheobronchial and pulmonary regions of the respiratory tract of Beagle dogs (Cuddihy et al., 1973). When pulmonary clearance of inhaled ^{90}Y clay particles occurs, gastrointestinal burdens of 18 and 34 mCi are observed, and severe radiation damage to the colon was found (Hahn et al., 1975). Beagle dogs inhaling ^{90}Y, ^{91}Y or ^{144}Ce fused clay particles showed marked pulmonary tissue alteration followed by fibrosis and possibly neoplasia (McClellan et al., 1970). Early deaths from inhaled ^{90}Y and ^{91}Y particles were due to radiation pneumonitis and fibrosis and late deaths from ^{144}Ce particles were due to hemangiosarcomas of endothelial origin (McClellan et al., 1973). Such particulate radiation causes early, transient, subclinical functional pulmonary impairment in the Beagle dog (Mauderly et al., 1973). Exposure of Beagle dogs to ^{90}Y beads which delivered 990 to 55000 rads to the lungs resulted in progressive increase of respiratory rates, abnormal lung sounds on auscultation, progressive weight loss, lymphopenia and eventually cyanosis. Pathological findings included pulmonary and pleural fibrosis, occlusive pulmonary vascular lesions, metaplasia and/or hyperplasia of terminal bronchiole and alveolar epithelium, right heart dilatation and hypertrophy and infarcts of the right atria. This was pure radiation toxicity not associated with chemical toxicity for ^{90}Y (Hobbs et al., 1972). In a sacrifice experiment, the dogs were shown to have radiation damage to the lung, tracheobronchial lymph nodes, skeleton, liver, rib bone marrow and colon (Barnes et al., 1972). A 30 day exposure to Y_2O_3 particles followed by threadmill exercise showed a post-exercise increase in total leukocytes and blood lactic

acid, a decrease in erythrocytes but no change in plasma volume or hemoglobin. The lungs showed hypertrophy, hyperplasia, desquamation of the alveolar epithelium, and leukocyte infiltration. Such toxicity effects apparently only become evident when body systems are subjected to functional stress (Reece et al., 1967).

3. Biochemistry

3.1. *General*

Low doses of $CeCl_3$ and cerium ammonium nitrate stimulate gastric secretion while high doses suppress it (Oda, 1932). Hyperglycemia has been observed in rabbit after intravenous administration of cerium, lanthanum, neodymium and praseodymium salts (Mori, 1931). Administration of 0.5–500 μCi of ^{147}Pm increased liver glucogenolysis and blood glucose levels and decreased muscle glycogen. Liver glycogen was decreased by 20–30% at death (Orlova and Faitelberg, 1973). Doses of 50 to 200 mg/Kg of $NdCl_3$ to rabbits resulted in hypoglycemia and a decrease in the rate of glucogenesis in the isolated rabbit liver (Abdullasev and Guseinov, 1973). Skin irradiation of rats with ^{90}Sr–^{90}Y decreases hepatic glycogen in 24 hours and this effect lasts 15 days. Such changes are ascribed to the phosphorylase enzyme systems. Liver cholesterol is not modified by skin irradiation (Ghircioasiu et al., 1971). Intravenous praseodymium nitrate in fasted rats increased the insulin content in portal vein blood for 48 hours (Oberdisse et al., 1973). Cerium decreases blood glucose while increasing plasma free fatty acids prior to inducing a fatty liver (Snyder and Stephens, 1961). Total liver lipids become similar to adipose tissue before detection of maximum accumulation of fat in hepatic cells (Snyder and Kyker, 1964). The most prominent effect of injected rare earths is the production of a fatty liver within 48 hours. It is characterized by an increase in neutral fat esters and does not occur with oral administration. Only the elements La through Sm induce this change. The effect is more consistent in females and castrated males. Testosterone reduces the fatty infiltration in both intact and ovariectomized females. Adrenalectomy is effective in males and hypophsetomy is effective in both sexes. The condition cannot be prevented by either choline or methionine (Snyder et al., 1959). The rare earth-induced fatty liver is not observed in guinea pigs, chickens or dogs; only occasionally in rabbits; and always in mice, rats and hamsters (Snyder et al., 1960). Cerium nitrate reduced the percentage of stearic acid and increased that of linoleic acid in female rat liver triglycerides while neodymium pyrocatecholdisulfonate had the reverse effect (Lazar et al., 1971).

^{46}Sc binds to erythrocytes and transferrin *in vivo* and is transferred from the latter to ferritin *in vitro* but not *in vivo* (Ford-Hutchinson and Perkins 1972). ^{144}Ce and ^{170}Tm bind not specifically to proteins, the former is bound with proteins into unstable aggregates while the latter is not (Masse et al., 1973).

Lanthanum and other trivalent inner transition metal ions degrade polyribonucleotides of adenylic, cytidylic and uridylic acids at the 5'-phosphate linkages. The reaction with polyinosinic is much slower (Eichhorn and Butzow, 1965). ^{147}Pm binds to the globulin fraction of blood serum (Cupak and Prochazka, 1971). Terbium binds to the calcium binding site of troponin from rabbit psoas muscle (Bunting et al., 1974). Injection of colloidal solutions of ^{90}Y bind to SH-groups of blood, liver, kidney, spleen and testes of rats causing an increase in such groups followed by a decrease on the third day with a return to normal on the fifteenth day (Pavlyushchik et al., 1970). Europium strongly binds to D-galaciuronic acid (Thorleif et al., 1972). $^{144}CeCl_3$ or $^{144}CeEDTA$ localizes in neutral, acid mucopolysaccharides and collagen of the odontoblasts (Beno and Trnovec, 1969). Radioyttrium localizes in the mucopolysaccharides of bone in a similar manner (Lyubashevskii, 1970). Ce and Y bind to bones and incisors of rats for long periods but the molars show the longest retention time (Thomassen and Leicester, 1964). ^{67}Gd and ^{169}Yb are rapidly absorbed by hydroxyapatite in albumin solution and it was suggested that the affinity of isotopes to proteins affects their incorporation into bones (Ando et al., 1974a).

3.2. *Enzyme effects*

Two hours after the administration of an organic neodymium salt, human serum α-amylase, lactic acid dehydrogenase, sorbitol dehydrogenase, and acid and alkaline phosphatase were inhibited but returned to normal in 24 hours (Vincke, 1961). Erythrocyte glucose-6-phosphate dehydrogenase activity was also affected by this compound (Vincke, 1962). Succinic dehydrogenase can be activated by lanthanum and inhibited by yttrium chlorides. Both salts inhibit adenosine triphosphate (Cochran et al., 1950). There is an early decrease in activity of hepatic non-specific esterase and acid phosphatase and a gradual decrease and loss of activity of succinic, lactic and malic dehydrogenases which correlate with hepatic necrosis produced by $LaCl_3$ (Kadas et al., 1974). Lactic, isocitric, malic, glutamic and glucose-6-phosphate dehydrogenases and aldolase activities are inhibited by the chlorides of La, Ce, Pr, Nd, Gd, Dy, Ho, Lu and Y. This is probably a heavy metal effect (Holten et al., 1966). Gd binds to four sites on apo alkaline phosphates from E. coli while Tb apparently only binds to two sites. The luminescence of the enzyme-Tb complex is quenched by the addition of glucose-6-phosphate, phosphoenolypyruvate or inorganic phosphate (Cottam et al., 1974). Membrane bound ATP-ase is inhibited by La in a non-specific manner (Britten and Blank, 1973). Gd, Nd, Tm and La displace Mg from rabbit muscle pyruvate kinase but do not bind to and form a phenolenol-pyruvate-Gd-enzyme ternary complex (Valentine and Cottam, 1973). $Ca^{\#}$ transportation in erythrocytes is inhibited by Ho and Pr as is the membrane ATP-ase and other ATP-ases of the membrane. However, Ho did not inhibit Mg dependent enzyme at high concentration (Schatzmann and Tschabold, 1971). EDTA-induced stromalytic forms of erythrocyte ghosts were abolished by La and Nd

(Pinteric et al., 1975). ADP-induced human platelet aggregation was inhibited in a concentration dependent manner by $LaCl_3$ (Holmsen et al., 1971). Ferroxidase is inhibited by Sc (Huber and Frieden, 1970). Eu and other rare earth ions bind to thermolysin with little perturbation of the protein structure (Matthews and Weaver, 1974). Isoproterenol-induced activation of myocardial phosphosylase is attenuated but not abolished by La (Bockman et al., 1973). Eu binds to yeast inorganic pyrophosphatase but the enzyme becomes inactive (Sperow and Butler, 1973). Nd greatly accelerates the rate of activation of the conversion of trypsinogen to trypsin (Darnall and Birnbaum, 1970). Amino acid complexes of Eu can be used as luminescent markers and those of Nd and Er as magnetic CD markers by replacing Co, Fe or Zn ions in biological structures (Zolin and Koreneva, 1973). *In vitro*, the chlorides of Pr, Nd, Sm, Eu, Gd, Tb and Dy inhibited the thrombin-fibrinogenic and recalcification reactions in blood serum (Anisimova et al., 1972). La, Pr, Nd, Gd, Dy, and Yb competitively inhibit staphylococcal nuclease at the Ca binding site of the enzyme (Furie et al., 1973).

Isolated rat liver RNA polymerase is highly inhibited by La (Novello and Stirpe, 1969). Pr $(NO_3)_3$ inhibited RNA synthesis in liver cell nuclei also RNA polymerase and messenger RNA. In isolated ribosomes, protein synthesis fell 60% in 24 hours and 80% in 48 hours but returned to normal in 96 hours. After 24 hours, polyuridylic acid decreased the inhibition from 60 to 20% (Oberdisse et al., 1974). Eu has been used as a fluorescent probe for transfer RNA (Wolfson and Kearns, 1975). The excitation spectra of Eu and Tb are enhanced by E. coli tRNA; Yb, Sm and Gd resemble Mg in enhancing 4-thiouridine fluorescence (Kayne and Cohn, 1974). The binding of paramagnetic lanthanide ions (Eu, Pr, Dy) to yeast phenylalanine-specific tRNA causes shifts in some of the resonances in the low-field NMR spectrum of this molecule (Jones and Kearns, 1974).

3.3. *Mitochondrial effects*

There is evidence of uncoupling of oxidative phosphorylation in the mitochondria from fatty livers of animals poisoned with Pr (Neubert and Hoffmeister, 1960; Dianzani, 1954). However, the toxic effects of La, Pr, Nd and Sm on the liver do not seem to be related to the synthesis or breakdown of ATP in the mitochondria (Neubert, 1963). The lanthanides produce a small amount of mitochondrial swelling but do not affect respiration (Grabske, 1966). The highest amounts of La bound in the rat myometrium are in the mitochondria (Hodgson et al., 1972). Bovine heart mitochondria bind La in preference to other ions, probably at a lipoprotein site (Jacobus and Brierly, 1969). La binds with a high affinity to membrane associated sites inside and outside the inner membranes of rat liver mitochondria (Reed and Bygrave, 1974). La decreased the swelling of rat liver mitochondria induced by Ca (Pechantikov et al., 1972). Pr inhibits specifically the reaction of Sr, Ba, Ca or Mn ions with the rat liver mitochondrial membrane and their accumulation into the mitochondria (Vainio et al., 1970). Both La and Pr exhibit a competitive effect on the activation of succinate uptake

in rat liver mitochondria (Meisner et al., 1972). The lanthanides can be used to identify and block the divalent cation carrier in rat liver mitochondria (Mela, 1969). Very low concentrations of Pr, Ho, Ce and La inhibit the uptake of Ca in rat liver mitochondria (Chance, 1968). Low concentrations of Pr, which cause little or no mitochondrial swelling, completely inhibit the swelling induced by thyroxine-like compounds (Cash et al., 1967). Using ^{140}La, it has been shown that the specific inhibition of the bivalent ion transport by lanthanides in mitochondria is accompanied by concentration of trivalent ions in the protein fraction but not in the phospholipid fractions (Tashmukhamedov, 1971). In rat liver mitochondria, only the portion of ATP translocation stimulated by Ca is inhibited by $LaCl_3$ (Spencer and Bygrave, 1972).

3.4. *Effects on nutrition*

At this point in time, no rare earth has been shown to be essential for normal growth and development in any species. Studies of the oxides of Sc, La, Sm, Eu, Dy, Tb, Tm and Yb in the diet of mice showed no significant effects on survival, growth, reproduction, lactation, hematology, morphological development and maturation when fed for three generations (Hutcheson *et al.* 1975). Rat feeding studies employing the nitrates of Tb, Ce, Yb and Lu showed a steady state of fecal excretion was obtained in 48–96 hours. The experiments indicated that only Ce was unsuitable for use as an unabsorbed, marker for recovery, passage and indirect apparent digestibility studies (Luckey et al., 1975). Intramammary injection of ^{144}Ce–^{144}Pr mixture resulted in translocation of the nuclides to the liver, spleen, skeleton and mammary lymph gland and a decrease in both milk yield and hay consumption in Jersey cows. These were irradiation-induced changes and not chemical toxicity (Swanson et al., 1970). Radiocolloids of the rare earths are valid flow markers of digesta particulate matter in sheep (Ellis and Huston, 1968). Studies of ^{46}Sc and ^{144}Ce indicated only the former was suitable for a non-absorbed reference material for cattle (Miller and Byrne, 1970). Further studies have shown that the gastrointestinal radiation damage was influenced by the physical form of the radionuclide (Miller et al., 1972). The use of stable rare earths followed by neutron activation analysis of the marker not only eliminated radiation damage but showed that nutritional intake in animals could be accurately predicted (Gray and Vogt, 1974).

4. Metabolism of the rare earths

In general the stable rare earths show very little absorption via the oral route but other routes give great absorption. Older studies of the elements suffered from the lack of a specific analytical method but with the use of neutron activation analysis this has been corrected. The radionuclides of these elements have proven very useful for absorption, fate and excretion studies. Intravenous administration of $^{46,47,48}Sc$ resulted in high concentration in the liver and reti-

culoendothelial system and a low deposition in the skeleton. In four days only 25% was excreted. After intramuscular injection 76.6% remained at the site and the remainder was found in the skeleton, liver, kidney and spleen (Scott et al., 1951). After intravenous injection in rats ^{46}Sc, the blood content was 33.6 and 4.1% at 1 and 24 hours respectively. Body distribution was skeleton, 20%; liver, 15.6%; and muscles, 14.35%. Intratracheal administration results transfer of ^{46}Sc, 70%, to other tissues in 24 hours (Zalikin et al., 1969). Ninety per cent of ^{47}Sc is retained by the rat skeleton (Taylor, 1966). Intravenous ^{46}Sc chelated with nitrilotriacetate slowly leaves the vascular space and is excreted via the intestine in man. ^{46}Sc chelated with EDTA or DTPA rapidly leaves the blood and 82% appears in the urine in 24 hours. The biological half-life of ^{46}Sc NTA in two patients was 1300 and 1557 days respectively (Spencer et al., 1965). Intramuscular administered ^{170}Tm, 16.2%, was still at the injection site 8 months later and of the absorbed nuclide, 44.7% was in the skeleton and 49% appeared in the urine and feces (Scott et al., 1951). The biological distribution of ^{167}Tm EDTA in rabbits showed 70% in the skeleton and the balance was excreted (Chandra et al., 1972). Feeding Sm and Eu to two metabolically different rat strains gave the same nuclide distribution in liver, kidney, pancreas and spleen (Sihvonen, 1972). Intravenous $^{152-154}$Eu rapidly clears the circulation of rats and deposited in the liver, kidney and bone. The bone half-life is 2.7 years and that of soft tissues 40 days. Excretion is mainly via the feces (Berke, 1968; Stepanov, 1970). ^{152}Eu and ^{244}Cm have similar body distribution patterns (Moskalev et al., 1972a). In the isolated perfused rat liver; ^{141}Ce, ^{152}Eu and ^{175}Yb are taken up primarily by the hepatocytes and not the Kupffer cells (Slouka, 1972). In rats intravenous ^{160,161}Tb leaves only 0.64% of the dose in the blood vessels at 6 hours and the balance is found in the skeleton, 40%, liver, 26% and kidneys, 5% (Zalikin and Tronova, 1969). The distribution of ^{140}La, ^{144}Ce and ^{143}Pr was mainly in the liver, $^{160-161}$Tb and ^{169}Yb was 80% in the bone and ^{147}Pm, ^{152}Eu and ^{153}Gd occupied an intermediate position. Excretion from the liver occurred in two phases, 67–86% within four days and 15–33 during days 18 to 37. Bone excretion required three years in the rat (Moskalev et al., 1972b). In rats the lanthanides first complex with bone mucopolysaccharides then attach to the basic bone tissue (Lyubashevskii, 1970). In an accidental exposure of a human to $^{141-144}$Ce, 99.7% of the radionuclide was eliminated via the gastrointestinal tract in four days (Sill et al., 1969). Injection ^{165}Er citrate in rats results in 50% deposition in bone and 25% in the kidneys (Rao et al., 1974). Subcutaneous injection of ^{147}Pm resulted in 56% of the activity being retained at 14 days and 20% at 20 days, mostly in the liver and skeleton of the mice (Gensicke, 1966). After intravenous injection of ^{147}Pm in rats the isotope deposited in the liver and spleen (Grigorescu and Weber, 1969). After intramuscular injection of ^{147}Pm in rats, the nuclide showed liver, kidney and bone accumulation and excretion in the feces and urine (Herman and Clark, 1973). In rabbits, ^{147}Pm locates in the kidney, liver and bone marrow in one hour and at 72 hours it is also found in the pancreas and gastrointestinal tract (Maruka wa, 1970). ^{140}La deposits in the liver, 67.4%, the kidney, 3.85% and the skeleton, 23%. It is also found in the adrenals, bone

marrow, spleen, ovaries and lymph nodes (Moskalev, 1961). Urinary excretion is the main pathway of elimination of ^{140}La-B-glycerophosphate in rats (Anghileri, 1967). Insoluble compounds of ^{46}Sc, ^{90}Y, ^{144}Ce and ^{144}Pr produce extensive radiation damage in sheep and lambs (Bustad et al., 1964; Sasser et al., 1972). Colloidal ^{90}Y silicate accumulates in the blood, liver, spleen, kidneys and gonads of rats and decreases the sulfhydryl content of the liver for 15 days (Pavlyushchik et al., 1970). Intramuscular injection of ^{90}Y in rats gave the usual body distribution but showed that the isotope was not resorbable (Dedenkov and Kiryakov, 1967). Comparison of ingestion with intravenous injection of ^{90}Y in rats showed a very small resorption from the gastrointestinal tract (Krawielitzki, 1967). In beagles the radiation dose from ^{90}Sr–^{90}Y was not uniform due to turnover patterns and bone architecture. The turnover rate of mineral matrix for cancellous bone was ~10-fold that of cortical matrix (Momeni et al., 1975). In goats ^{90}Y concentrations in bone, lung, kidney and spleen remain high 24 hours after administration and although the other organs have decreased levels of the nuclide at 30 days bone does not (Panchenko and Sarapultsev, 1964). In suckling mice, ^{144}Ce had a high intestinal absorption and whole-body retention, 1% on day 1 and 28% at 3 weeks (Matsusaka, 1971). Suckling mice given ^{144}Ce had a higher gastrointestinal absorption than the currently accepted values for adult mice (Naharin et al., 1974). Injection of ^{144}Ce in young rats showed females concentrated the isotope in the liver and males in the skeleton. The opposite sex hormone affected ^{144}Ce content of the liver but only testosterone affected the skeleton. Age increased the retention of ^{144}Ce (Schmautz, 1964). Suckling rats had an initial rapid loss of ^{144}Ce until weaning although their original absorption and retention was higher than adults (Shiraishi and Ichikawa, 1972). ^{144}Ce administered by five different routes showed no differences in urinary excretion up to 15 days but after that time the subcutaneous and intramuscular routes showed 57 and 38% retention respectively at the injection site (Tukada and Fujita, 1972). In beagles, ^{144}Ce has a slow turnover rate and a biological half-life of about 10 years (Richmond and London, 1966). The half-life of ^{144}Ce in lambs is liver, 62.5 days, and skeleton, 118 days, while sheep have values of 94.5 and 219 days respectively (Buldakov and Burov, 1967). In the calf, $^{141-144}$Ce in the rumen decreased from 80% at four hours to 6% at 72 hours and increased in the feces from 0 to 90% in the same time interval (Miller et al., 1971).

4.1. *Autoradiography*

There is a rapid distribution of ^{144}Ce and ^{147}Pm into the liver and skeleton of mice given the isotopes prior to birth. The kidneys, spleen, cartilage and adrenal cortex have a high uptake of ^{144}Ce while ^{147}Pm concentrates in the kidneys and cartilage (Ewaldsson and Magnusson, 1964a). ^{180}Tb and ^{169}Yb are similar to ^{144}Ce, while ^{166}Ho has the same pattern as ^{147}Pm (Ewaldsson and Magnusson, 1946b). ^{147}Pm deposits in the liver Kupfferian star cells and hepatocyte and in the femur, primarily in the organic bone matrix, the osteogenic tissue of the perichondrium and in the primary spongiosa combined with the bone marrow. The nuclide is

also stored in the spleen, pancreas, duodenum, kidney, ovaries, testes and lungs (Holzer and Gensicke, 1966). Autoradiography has also been used to study the distribution of ^{144}Ce in the rat femur (Remy et al., 1965).

5. Pharmacodynamic effects

5.1. *Ocular effects*

Irritation of the conjunctiva but not to the iris and cornea are seen after topical application of the rare earths. The conjunctival ulcers produced by either rare earth crystals or strong solutions require one to three weeks for healing (Haley, 1965). Several hours or days after denudation of the cornea, an opacification of obscure mechanism occurs. This effect is produced by excess deposition of the calcium in the injured area (Haley, 1965).

5.2. *Skin effects*

Physical contact of the rare earths cause no damage to intact skin but cause extensive damage to abraded skin with epilation and scar formation. Such injuries are related to both the acidic portion of the salt and the ability of the metallic portion to combine with tissue constituents, e.g. proteins, lipids, phosphates, etc. (Haley, 1965). The radionuclides of Ce, Y, Pr and Nd distribute in skin structures as follows: insoluble proteins, 82–94%; lipids, 6–12% and water extracts, 2–4% (Shvydko, 1972). Intradermal injection of 0.05 to 0.5 mcg. of rare earth chlorides in guinea pigs produces granulomas (Haley and Upham, 1963). Similar lesions were observed in rabbit skin and they were characterized by macrophages, lymphocytes, plasma cells, multinucleated giant cells and giant cells of the Langhans type (Muroma, 1961). Subcutaneous implantation of metallic pellets of Y, Ce, Pr, Gd, Dy and Yb in male and female mice resulted in granulomas in 556 out of 714 animals and 3 neoplasms (Talbot et al., 1968). Lesions in human skin have been observed in patients injected with rare earths for treatment of sarcoidosis and anthracosilicosis (Shelley et al., 1958). ^{147}Pm contaminates pig skin as a radiocolloid but does not penetrate the underlying skin layers (Tashiro et al., 1966). On the other hand ^{144}Ce readily penetrates the mouse tail skin (Surovezhin, 1967). Skin absorption by rats of ^{90}Y is affected by pH and radiocolloidal ^{90}Y is absorbed with difficulty by normal and injured skin (Takeuchi, 1968).

5.3. *Smooth muscle effects*

There is a loss of contractility and a decreased tonus of the isolated ileum and uterus of rabbits, cats and dogs exposed to La, Nd, Pr and Sm. All of the rare earths have a nonspecific antispasmodic effect against acetylcholine, and increased intraluminal pressure in the ileum and contractility cannot be restored

by washing (Haley, 1965). La inhibits the tone and contractions of the longitudinal smooth muscle layer of the guinea pig ileum. La replaces Ca at superficial binding sites, decreases the mobility of Ca at less superficial binding sites and prevents Ca uptake at various cellular sites (Weiss and Goodman, 1969). La causes a destruction of smooth muscle cells by dislodging Ca from its binding sites (Lohwe, 1974). La appears to bind to collagen fibrils of the mouse cecal mucosa (Henrikson, 1974). La and Pr inhibit the short and long term uptake of Ca by rat duodenal mucosa and the Pr inhibition can be reversed by increasing the Ca concentration (O'Donnell and Smith, 1973). K^+ depolarization resulting in tension development and Ca influx in the guinea pig taenia coli can be prevented by La (Casteels et al., 1972; Mayer et al., 1972). ^{140}La is taken up and tightly bound to the rat myometrium, with the highest concentrations in the mitochondria (Hodgson et al., 1972). K^+ and acetylcholine induced contractions and Ca and Sr uptake by this tissue are inhibited by La (Hodgson and Daniel, 1973). This biphasic effect has been confirmed (Rozza et al., 1975). $LaCl_3$ causes a reversible reduction in the contractions evoked by serosal administration of acetylcholine after a 90 minute delay (Hava and Hurwitz, 1973). Eu and La decreased oxygen consumption by the toad urinary bladder and were more effective after treatment with antidiuretic hormone (Cuthbert and Wong, 1971a,b). La irreversibility inhibits water permeability of the frog urinary bladder only during stimulation by oxytocin or hypertonicity but not those already induced (Weitzebin et al., 1974). La antagonized the contraction of bovine tracheal smooth muscle induced by tetraethylammonium, histamine and acetylcholine (Kirkpatrick, 1974). La blocks the contraction of rabbit thoracic aorta induced by K and both Ca and Ba influxes (Van Breeman, 1969). La, Lu, Eu and Nd all decreased Ca uptake and increased Ca efflux in the vascular smooth muscle. However, histamine contractures were harder to block than those of K or norepinephrine (Weiss and Goodman, 1974). These effects have been confirmed (Freeman and Daniel, 1973, Van Breeman and Lesser, 1971). Hypothyroid rabbit aortic strip responses to norepinephrine were not changed by La but the slope of the dose response curve was increased. The responses to histamine and K were unchanged (Rosenquist and Boreus, 1972). Femoral artery strips from normotensive, renal hypertensive and DCA-hypertensive rats did not contract when exposed to La, but spontaneous hypertensive rat strips did because the tissue was more liable (Holloway and Bohr, 1973). La blocks Ca contracture significantly more than K contracture in bovine coronary artery rings (Fermum and Grisk, 1973). Similar results have been obtained with rabbit anterior mesentericportal veins (Collins et al., 1972).

5.4. *Effects on striated muscle*

Cerium nitrate has a curariform action on frog striated muscle and the decreased muscle contractility depends on the particular rare earth being investigated (Haley, 1965). La has been shown to influence both the pre- and postjunctional membrane receptor processes of the frog sartorius muscle and

increases the conductance change produced by carbamylcholine in both polarized and depolarized fibers (Lambert and Parsons, 1970). La blocks nerve transmission presynaptically by decreasing the quantal content of the end plate potential (De Bassio et al., 1971). La blocks the release of transmitter at the neuromuscular junction, completely depletes the synaptic vesicles and increases coated vesicles, membrane bound tubes and cysternae (Heuser and Miledi, 1971). The other rare earths; Pr, Nd, Sm, Gd, Dy, Er, Tm, Yb and Y; have similar effects on the neuromuscular junction (Bowen, 1972). La decreases the Ca and Na content of frog rectus abdominis muscle and increases the K content (Weiss, 1973). It has been suggested that the increase in miniature end plate potentials frequency caused by La and Pr is due, partially, to interference with mitochondrial Ca sequestration (Alnaes and Rahamimoff, 1974). La desensitization of the post synaptic membrane is not restricted to the receptor level, but also involves the terminal stages of the activation system (Magazanik and Vyskocil, 1970). La also may partially uncouple excitation from contraction by preventing release of a trigger–Ca fraction from its site on the muscle membrane (Parry et al., 1974). La produces no change in the muscle fiber resting potential but causes a graded reduction in the rate of rise, amplitude and rate of fall of the action potential (Andersson and Edman, 1974). Part of these effects appears to be related to penetration of La into the sarcoplasmic reticulum (Sperelakis, 1973). In chronically denervated muscle fibers, La also accelerates receptor desensitization (Parsons et al., 1971). La competitively inhibits Ca binding to the rabbit skeletal muscle sarcoplasmic reticulum similarly to that observed with frog muscle (Butow and Chevallier, 1971).

5.5. *Cardiac effects*

The rare earths are toxic to the isolated frog heart stopping it in diastole. Similar results have been obtained with the isolated rabbit heart and the cat heart-lung preparation. A negative inotropic effect occurs prior to paralysis of the isolated hearts of rats, guinea pigs and rabbits (Haley, 1965). La reduces the contraction of the perfused rabbit interventricular septum by 14.3% (Shine, 1973). La inhibits the K contraction of the helix heart by interacting with Ca-binding sites, and the helix heart is less sensitive than vertebrate hearts (Erdelyi, 1973). La blocks the slow electrical responses and concomitant contractions of the 9 to 19 day old embryonic chick hearts (Shigenobu and Sperelakis, 1972). La inhibits the slow inward current in both pig and sheep ventricular trabeculum preparations, but has no effect on the Na–Ca exchange system in the left guinea pig auricles (Katzung et al., 1973). La and Gd inhibit Ca binding noncompetitively, decreases the velocity of Ca uptake and inhibits the Ca activated Mg-ATPase in isolated dog cardiac sarcoplasmic reticulum (Krasnow, 1972). Rabbit interventricular septal tissue perfused with La has a rapid decline of active tension and an abrupt release of short duration of tissue bound Ca, which returns to normal when the La is removed (Sanborn and Langer, 1970). Perfusion of the sinus node and AV node of open chest dogs with La

resulted in slowed sinus node discharge rate, depressed AV nodal conduction, and lengthening the effective and the functional AV nodal refractory (Zipes and Fischer, 1974). Repeated administration of ^{144}Ce to rats resulted in slight changes in cardiac contraction after 300 days (Seltser, 1967). Sm was found in beef heart RNA by neutron activation analysis (Wester, 1972). Ce, La, Sc and Sm have been found in the conductive tissue of beef hearts, but their significance remains to be determined (Wester, 1965).

5.6. *Nervous system effects*

La antagonizes the inhibitory effect of biogenic amines on rat cerebral cortical neurones but has a potent depressant effect of its own (Phillis et al., 1973). Electrocortical potentials of the cat brain elicited by electrical stimulation can be blocked by La (Garcia Ramos and Ibarra, 1973). La ions inhibit the efflux of Ca ions from the squid giant axon and render it inexcitable (Van Breeman and De Weer, 1970). Both La and Tb cause a shift in membrane surface potential of the isolated frog myelinated nerve fibers (Vogel, 1974). When La is substituted for Ca in the solution bathing the lobster axon, it causes a progressive rise in threshold and a decrease in the height of the action potential as well as in its rates of rise and fall (Takata et al., 1966). La increases adhesion of glial cells and nerve growth cones in culture and reduces glial locomotion, but does not inhibit nerve elongation (Letourneau and Wessells, 1974). Ca uptake in desheathed rabbit vagus nerves is reduced by La and Pr (Kalix, 1971). La is 58 times more active than Ca in inducing a shift of the stationary inactivation curve along the potential axis of the crayfish giant axon (Hartz and Ulbright, 1973). Ce salts have been shown to increase the catecholamine content of the brain, adrenals and heart (Bagirov, 1968). Rare earth salts did not reactivate organophosphate inhibited acetylcholinesterase (Howells and Coult, 1971). Eu and Tb salts bind to nerve proteins, NADH and possibly other sites in the garfish olfactory nerve trunk (Axelrod and Klein, 1974). La depolarizes the frog Ranvier node membrane (Mozhaeya and Naumov, 1973; Khodorov and Peganov, 1969).

5.7. *Blood coagulation effects*

Neodymium 3-sulfoisonicotinate has an anticoagulant effect in guinea pigs and rabbits, inhibiting factors II, VII, IX and X. Factors V and VIII are also inhibited but only at high concentrations of the Nd salt. Thrombin time is not lengthened (Tremblay and Archambault, 1967). Sodium pyrophosphate inhibits the anti-coagulant properties of $NdCl_3$ (Gabbiani et al., 1967). Sc acetate decreases blood coagulation in rabbits (Lakin et al., 1970). Pr, Nd, Sm, Eu, Gd, Tb and Dy chlorides inhibit the thrombin-fibrinogenic and recalcification reactions in blood serum (Anisimova et al., 1973). Pretreatment of thrombin with La, Y or Ce chlorides decreased its enzymic activity in transforming fibrinogen into fibrin (Ducastaing, 1973).

et al.

5.8. *Effects on immunity*

Powdered oxides of La, Ce, Y and Sm, hexaborides of Y, La and Sm, and sulfides of La or Ce administered intratracheally to rats decreased immunological resistance, lysozyme, complement and B-lysine in the blood (Olefin, 1967). ^{144}Ce causes a prolonged circulation of full complement binding autoantibodies in the blood (Shubik, 1972). ^{144}Ce causes a decrease in circulating antibodies (Vikhman, 1968). La or Y propionate increased the number of antibody producing cells in the spleen and hemolysin titers in the serum of CBA mice immunized with sheep erythrocytes (Zimakov and Zimakova, 1971). Total immunological reactivity is most sensitive to ^{144}Ce (Nevstrueva and Kolotvin, 1968). ^{144}Ce causes the appearance of Hoigne antibodies, leukolysins and cytolysins in the blood of rats (Shalnova, 1969). La can inhibit the anaphylactic release of histamine and this can be reversed by eluting the La from the cells. La can also induce the release of histamine in the absence of antigen (Foreman and Mongar, 1973).

5.9. *Carcinogenicity*

Ce, Er, Y and Pr are ineffective in treatment of rat sarcoma or Hyde rat carcinoma (Maxwell and Bischoff, 1931). Subcutaneous implantation of Gd or Yb in CFW mice resulted in 10.2% sarcomas at the site and pulmonary metastes (Ball et al., 1970). La increases the ^{45}Ca uptake by experimental tumors particularly by the mitochondria (Anghileri, 1973). Skin exposure to ^{144}Ce results in papillomas, keratoacanthomas, basaliomas and phanocellulare carcinomas and connective tissue sarcomas (Turosov, 1966). Internally deposited ^{144}Ce or ^{147}Pm causes osteosarcomas, leukemias, liver tumors and pituitary tumors in rats (Moskalev et al., 1969). ^{144}Ce induces intestinal tract tumors, stomach cancer and leiomyosarcoma of the intestines in rats (Moskalev et al., 1966). ^{144}Ce causes the development of proliferative polyps of the large intestines with a tendency towards neoplasia in rats (Lebedeva, 1973). ^{90}Y produces sarcomas at the site of injection (Grat and Lafuma, 1965). Chinese hamsters are resistant to radiation from ^{90}Y but osteosarcomas do develop in a small number of animals (Brooks et al., 1974). ^{90}Y produces osteosarcomas and primitive mesenchymal cell tumors of angiomatous type in mice (Bland et al., 1974). Intratracheal administration of ^{144}Ce induces lung tumors in rabbits and reduces the lung oxidative-reductive enzymes (Kurshakova, 1967). Dusts of the rare earths cause an increased incidence of pulmonary reticulosarcoma (Kikhachev et al., 1972). Radiation fibrosis followed by squamous cell carcinomas of the lungs with metastes to other organs occurred from inhalation of ^{144}Ce by rats (Thomas et al., 1972).

Small fractionated doses of ^{144}Ce give a higher formation of osteosarcomas and polymorphous bone tumors than large doses (Moskalev and Streltsova, 1965). Inhalation of $^{144}CeO_2$ by mice resulted in epidermoid carcinoma (Lundgren et al., 1973). Very small doses of $^{144}CeF_3$ cause lung cancer in rabbits (Ivanov and Gorelchik, 1966). Similar effects are seen in rats with $^{144}CeCl_3$ (Cember and

Stemmer, 1964). Fibrosarcoma and bronchioalveolar carcinoma occurs in beagle dogs after inhalation of ^{144}Ce in fused clay (Hahn et al., 1973). Inhalation of $^{144}CeCl_3$ by beagle dogs resulted in osteosarcoma, maxillary squamous cell carcinoma, hemangioma or myelogenous leukemia (Benjamin et al., 1973). ^{147}Pm produces osteosarcoma and leukosis in rats (Streltsova, 1966). ^{144}Ce produces tumors in mice, rats, dogs and humans (Pesternikov, 1973).

Ehrlich ascites tumor cells accumulate ^{140}La, ^{141}Ce, ^{147}Nd, ^{152}Eu, ^{153}Sm, ^{160}Tb and ^{177}Lu to a greater extent than normal tissues (Higashi et al., 1973a). ^{169}Yb has a greater affinity for Ehrlich tumors and sarcoma 180 in mice and Yoshida sarcoma and Walker sarcoma 256 in rats than in normal tissue (Ando et al., 1975). Radionuclide accumulation in ascites tumor cells at 28 hours was $^{152}Eu \gg {}^{177}Lu \gg {}^{160}Tb$, ^{147}Nd, ^{141}Ce and ^{140}La (Higashi et al., 1972). ^{47}Sc shows a high affinity for bone marrow and Ehrlich solid carcinoma (Hara and Freed, 1973). There is no difference between tumor affinity and hydroxylapatite absorption rate of ^{169}Yb (Orii, 1973). Tm shows a higher affinity towards sarcoma tissue than the other lanthanides (Hisada and Ando, 1972). Ten minutes after intravenous injection ^{67}Gd and ^{169}Yb uptake in sarcoma tissue was 50 and 70% respectively (Ando et al., 1974b). Excretion of ^{169}Yb citrate has a higher rate than $^{169}YbCl_3$ and its accumulation in vertebrae is such that it cannot be used in the diagnosis of cancerous lesions (Higashi et al., 1973b). The heavier lanthanides are more tumor specific than the lighter ones (Sullivan et al., 1975). ^{167}Tm appears to be the best lanthanide for tumor scanning because of its half-life, the energy of its gamma ray and low beta ray emission (Hisada and Ando, 1973). ^{46}Sc has been found in Walker tumor DNA (Andronikashvili et al., 1970). The complex ^{169}Yb-DPTA has a brain to tumor ratio of 1:20 making it a desirable agent for brain scanning (Hosain et al., 1968). ^{169}Yb gave positive scans in 13 of 15 patients with primary lung and liver cancer or lymphosarcoma and various metastatic bone lesions (Hisada et al., 1973).

5.10. *Genetic effects*

^{90}Y increased the double-stroke chromosome aberrations in the somatic cells of Crepis cappillaris (Kaplan et al., 1973). Sprouts of C. capillaris treated with ^{90}Y had chromosome aberrations in radicle meristem metaphases. They were formed during the G_2 and S stages of the first mitotic cycle, were of the chromatid type and occurred in diploid cells. Breaks were seen at the stage of the second mitotis. Twenty-four hours later, 80% tetraploid cells were observed (Shevchenko, 1970). ^{90}Y affects the Atlantic salmon embryo causing chromosome aberrations consisting of single bridges, fragments, multiple bridges, the presence of several fragments in a cell, multipolar mitoses and the formation of micronuclei (Migalovskaya, 1971). Gonads of Misgurnus fossilis larvae exposed to ^{90}Y showed no increase in anaphase-telophases or mitotic index aberrations indicating the lack of effect on the meiotic division of oocytes (Pechkurenkov, 1970). ^{144}Ce causes chromosomal aberrations and changes of the mitotic index of rat small intestine (Zhorno, 1970). Such changes consist of a

decreased number of DNA synthesizing cells, and increased number of karyolytic bodies and aberrant mitoses and a sharp suppression of mitotic activity in the cell population (Ponomareva and Tokin, 1969). Rat thymus and lymph gland lymphocytes are altered by exposure to ^{144}Ce with decreased mitoses and decreased ^{3}H-thymidine labeling of nuclei (Khussar and Lushchikov, 1973). ^{144}Ce also causes chromosomal rearrangements in the rat testicle, tibia, eye and bone marrow (Bikkulov, 1968). ^{90}Y increased the number of chromatid plus isochromatid deletions and the relative frequency of chromosomes in hamster cells (Brooks and McClellan, 1969). In regenerating hamster's liver, ^{144}Ce–^{144}Pr caused a tripling of chromosomal aberrations (Brooks et al., 1972).

5.11. *Teratological effects*

Embryos of sea ruff flounder sustained cytological damage and abnormalities when their roe was exposed to ^{90}Y (Tsytsugina, 1968). The eggs of the loach exposed to ^{90}Y accumulate the isotope beginning at the end of gastrulation and continue until the end of embryogenesis (Shekhanova and Pechkurenkov, 1968). ^{90}Y exposure of khamsa and rock bass spawn resulted in vertebral abnormalities (Polikarpov and Ivanov, 1966). Primordial germ cells of Atlantic salmon were decreased by exposure to ^{90}Y (Migalovskii, 1971b). ^{144}Ce also produces deformed embryos in this species of fish (Migalovskii, 1971a). ^{90}Y damages spawn of perch, crucian carp and tench (Kulikov et al., 1970). Although no morphological changes were observed in the hatching glands of salmon exposed to ^{90}Y, enzymes accumulated in these structures (Kasatkina, 1971). Exposure of Fish roe to ^{90}Y or ^{144}Ce resulted in curvature of the spine, microcephalus, incorrect position of the yolk sac, abnormal pigmentation of the eyes and body and dropsy (Ivanov, 1967). The ovaries of the marine goby are badly damaged by exposure to ^{90}Y (Hyoda-Taguchi et al., 1971). Male embryos of O. latipes exposed to ^{90}Y had an inhibition of multiplication spermatogonia and testes without germ cells and containing oocyte-like cells (Hyodo-Taguchi and Egami, 1970). ^{90}Y and ^{147}Pm administered to hatching chicken eggs resulted in constriction of the center of the long bones resulting in fractures and swollen, hemorrhagic and gangrenous feet (Mraz and Wright, 1964). Administration of ^{144}Ce to pregnant rats resulted in high embryonic resorption rates, embryonic death and ocular damage in survivors (McFee, 1964). Injection of ^{144}Ce into pregnant rats results less isotope in the fetus than in the dam but a significant accumulation in the placenta, fetal membranes and skeleton (Mahlum and Sikov, 1968). Administration of ^{91}Y or ^{144}Ce to the dam rapidly passes to her progeny via the milk (Kulikova, 1970). Injection of chelated ^{144}Ce–^{144}Pr into pregnant rats results in a low fetal body burden (Beno, 1973). ^{144}Ce has a low order of both transplacental and transmammary transfer to offspring of treated dams (Baltrukiewicz et al., 1973).

5.12. *Miscellaneous effects*

Hypotension follows intravenous injection of the rare earths into animals and death occurs from cardiovascular collapse and respiratory paralysis. The ECG

shows slow conduction time, increased height of the P-wave, decreased height of the entire complex, inverted then increased height of the T-wave, transient ventricular fibrillation and 2:1 to 4:1 heart block. The effects were not modified by autonomic drugs (Haley, 1965). The function of rat's adrenal cortex was decreased following a single dose of ^{144}Ce (Truupyld and Tokin, 1969). The P-450 enzyme system of the liver has its oxidative and demethylating functions depressed by $CeCl_3$ (Arvels and Karki, 1971). Phenobarbital protects this enzyme system from the Ce depression (Arvels and Karki, 1972). The administration of γ-tocopherol also protects and inhibits accumulation of liver triglyceride and plasma free fatty acids while enhancing the activation of UDP glucuronyl transferase (Arvels, 1974). Exposure of bovine adrenal glands to La releases catecholamines (Borowitz, 1972). La decreases norepinephrine release from the cat spleen induced by splenic nerve stimulation (Kirpekar et al., 1972). Chlorides of La, Ce, Nd, Gd, Ho and Yb depress the rat reticuloendothelial system (Lazar, 1973b). Rat dextran induced edema is inhibited by Nd pyrocatechol disulfonate (Oyvin et al., 1966). Nd decreases the inflammation of experimental arthritis in the rat (Lorincz et al., 1968). Nd pyrocatechol disulfonate inhibits neurogenic and bradykinin-induced inflammation in rats and rabbits (Jancso-Gabor and Szolcsanyi, 1970). $LaCl_3$ inhibits swimming of sea urchin sperm (Young and Nelson, 1974). $LaCl_3$ or $Y(NO_3)_3$ injected intratesticularly causes progressive calcification of both the seminiferous tubules and interstitium in rats (Sharma et al., 1972) and $LaCl_3$ has the same effect in goats (Sharma et al., 1973).

5.13. *Chelation of lanthanides*

Chelation of Sc, Y, La and Sm with ethylenediaminetetraacetic acid (EDTA) decreased tissue retention and increased urinary excretion while chelation of Sc and Y with nitriloacetic acid (NTA) resulted in high concentrations in bone (Rosoff et al., 1963). EDTA and diethylenetriaminopentaacetate (DPTA) increased urinary excretion of ^{46}Sc in man and the latter was more effective (Spencer and Rosoff, 1965). Triethylenetetraminehexaacetic acid is more effective than DTPA in causing the elimination of ^{144}Ce and ^{91}Y but both chelates cause hydropic degeneration of the kidney tubular epithelium (Catsch, 1963). However, DTPA is an effective chelator (Tarasov et al., 1973). It has been suggested that ^{169}Yb-DTPA injected intracisternally may be useful for the diagnosis of meningitis (Som et al., 1972). It is also useful in cerebrospinal fluid studies (Deland, 1973). DPTA has been shown to decrease liver and bone burdens of ^{88}Y and ^{144}Ce and remove the former but not the latter from an intramuscular injection site (Boemer, 1972). DTPA was compared to desferrioxamine B methanesulfonate in its ability to decrease body burdens of ^{144}Ce and ^{91}Y, the former was more effective (Nigrovic and Catsch, 1965). DTPA is equal to EDTA in increasing urinary excretion of ^{91}Y and can increase fecal excretion of the nuclide when the liver content of ^{91}Y is high (Semenov and Tregubenko, 1966). Excretion of Pm via the urinary and fecal routes was enhanced by DTPA but its effectiveness decreased rapidly when the interval

between administration of Pm and DTPA was lengthened (Palmer et al., 1970). DTPA continues to increase the excretion of ^{140}La even when given 22 days after the isotope (Efimov, 1967). N_2(β-carboxyethyl) diethylenetriaminotetraacetic acid (KETA), N, N, N^1, N^1-tetraacetic acid of 2, 2-diaminodiethyl ester (DEETA) and N, N, N^1, N^1-tetraacetic acid of 2, 2-diaminodiethyl sulfide (DESTA) are effective chelators of ^{91}Y, ^{140}La, ^{141}Ce, ^{143}Pr, ^{147}Nd, and ^{147}Pm decreasing the nuclide body burden (Koval and Kondrashev, 1967). Bone concentrations of ^{152}Eu can be decreased by DPTA (Beno et al., 1964). The ability of iminodiacetate derivatives of hydroxytriphenylmethane to increase the elimination of ^{91}Y and ^{144}Ce increases with the number of iminodiacetate groups in the molecule (Voronina et al., 1970).

6. Clinical applications and toxicity: Radiohypophysectomy

Preliminary experiments in the late 1950's and early 1960's indicated the usefulness of rare earth isotope implantation as a means for treating inoperable pituitary tumors (Haley, 1965). Since that period, stereotaxic techniques for the implantation of ^{90}Y rods have been used successfully to treat brain neoplasms (D'Andrea et al., 1972). Two cases of amenorrhea responded to such treatment with ^{90}Y (Burke et al., 1972). Pituitary implantation of ^{90}Y cylinders in 19 cases of advanced mammary carcinoma, acromegaly or juvenile diabetes mellitus resulted in complete loss of pituitary hormonal activity in 14 cases with no contamination of the surrounding tissues (Notter et al., 1968). Survival varied in 80 mammary carcinomas, 10 seminomas, 4 prostate carcinomas and 3 uterine carcinomas receiving pituitary implants of ^{90}Y (Perez-Modrego et al., 1962). However, early implantation in breast cancer with metastates with suppression of pituitary function may actually be harmful (Stewart et al., 1969). ^{90}Y ablation of the pituitary in 24 patients with prostatic carcinoma resulted in good sympatomatic response in 12 and a partial response in 6 (Steyn et al., 1973).

Pituitary implantation of ^{90}Y in 22 acromegaly patients, while satisfactory, resulted in corticosteroid and/or thyroxine dependence in 9, pituitary absesses in 5, diabetes insipidus in 1, pituitary infections in 8, visual-field defects in 2 and cerebrospinal fluid leaks in 4 (Hartog et al., 1965). Implantation of ^{90}Y in a 14 yr. old boy produced a loss of ACTH, thyrotropin, gonadotropin and prolactin but had no effect on growth hormone secretion (Haigler et al., 1973). In another case, such treatment returned growth hormone to normal levels (Gelinas et al., 1966). ^{90}Y implantation has been shown to be more successful in treating pituitary adenoma than cryosurgery (Conway et al., 1969). Implantation of ^{90}Y in 25 acromeglics resulted in regression of the syndrome in 18 and a return toward normal serum hormone levels in 7 (Lyass and Snigireva, 1972).

Post mortem studies of mammary carcinoma patients indicates that ^{90}Y pituitary ablation is achieved in only three-quarters of the patients (Forrest et al., 1970). However, objective remission of mammary carcinoma was obtained in 30% of 69 patients (Dohn and McCullagh, 1966). ^{90}Y radiobiologic hypophysec-

tomy for advanced and metastic breast cancer was favorable in 50% of cases with a survival of 19 months. There was no correlation between response, patient age and survival (Caldarola et al., 1973). Soft tissue metastastes respond more markedly to such treatment than bone lesions (Blair and Foote, 1965). Implantation of ^{90}Y pellets in the sella turcica does destroy the pituitary and cause remission of mammary carcinoma but it can cause damage to the visual pathways, rhinorrhea and meningitis (Jadresic et al., 1965). ^{90}Y treatment of advanced mammary carcinoma results in survival between 5 and 18 months after implantation (Oproiu, 1973). ^{90}Y ablation of the pituitary is a safe and simple treatment in the late stages of prostate carcinoma with 52% of the patients responding satisfactorily (Morales et al., 1971).

Pituitary ablation with ^{90}Y was successful in 2 of 5 patients with diabetic retinopathy but hyporesponsiveness of the hypophysis to stress caused death in 4 patients (Lomsky et al., 1966). However, such implants can control retinopathy and preserve the patient's sight (Jauregui et al., 1968). The procedure was used in 22 patients with 75% showing distinct improvement but 5 others died of complications (Ray et al., 1968). The cotton wool spots of diabetic retinopathy, when treated by ^{90}Y pituitary implantation, disappear in about 2.3 months but the capillary closure persists (Kohner et al., 1969). New capillaries arise from the optic disc after ^{90}Y implantation but results are better in patients below 40 years of age (Panisset et al., 1971). Such treatment is also beneficial in cases of the thyrotoxic malignant exophthalmos but the patients may develop adrenocortical insufficiency and gonadal hypofunction (Molinatti, 1964).

Intracellar implantation of ^{90}Y in 24 cases of Cushing's disease resulted in a return to normal of the urinary excretion of adrenal steroids and remission of symptoms in 21 cases. Side effects were diabetes insipidus and cerebrospinal rhinorrhea and two deaths from meningoencephalitis (Molinatti et al., 1967). In 5 more such cases, complete and permanent control of the syndrome was obtained with ^{90}Y implantation (McCullagh and Dohn, 1969). Others showed that remission required from 5 to 10 months to become apparent (Arutyunov et al., 1970). Even with ^{90}Y implantation, some patients still require an adrenalectomy or hypophysectomy or both followed by hormone replacement therapy (Burke et al., 1973). There can be no doubt that ^{90}Y implantation can be used to treat Cushing's syndrome successfully. However, it was not suitable in the treatment of 7 patients with cerebral glioma (Fusek, 1972). Stereotaxic administration of colloidal ^{90}Y has been recommended for treatment of craniopharyngioma and 14 cases were successfully treated although residual portions of the tumor required ^{60}Co radiation to completely remove the tumor (Backlund et al., 1972; Backlund, 1973).

Injection of ^{90}Y microspheres gives an internal radiation field which results in ablation of tumors at various sites in the body (Ariel, 1964). This treatment effectively reduced the tumor size in 10 of 32 patients (Blanchard et al., 1964). Microsphere injections have caused tumor regression in 30% of those treated but is only useful in tumors with proven excellent vascularity (Blanchard et al., 1965). Granules of ^{90}Y used in treatment of inoperable tumors at the base of the skull

have produced remissions of 10 months to 5 years (Blagoveshchenskaya et al. 1968). ^{90}Y microspheres have been used in treatment of osteogenic sarcoma of the femur (Simon et al., 1968). Selection of patients with incurable cancer must be done for this type of therapy to be practical and effective (Nolan and Grady, 1969). Lymphangiosarcoma has been successfully treated with ^{90}Y microsphere injection (Herrmann and Ariel, 1967). Chronic rheumatoid effusions of the knee have been successfully treated by intraarticular injection of either ^{90}Y silicate or ^{90}Y resin, the latter is recommended (Prichard et al., 1970). This treatment reduces synovial fluid leukocytes and enzymes also there is leakage of the ^{90}Y into the regional lymph nodes (Oka et al., 1971). Side effects include proliferative synovitis, erosions and degenerated menisci (Oka and Hypen, 1974).

^{169}Yb-DTPA cisternography has been used for diagnosis of basal brain tumors (Matsumoto et al., 1972). ^{169}Yb citrate has been used as a scanning agent in the diagnosis of lung and liver cancer and lymphosarcoma with bone metastases (Hisada et al., 1974). ^{153}Sm-DTPA has been used in brain scanning to detect small superficial tumors (Tarjan et al., 1973). The overall properties of ^{169}Yb-DPTA make it useful for brain scans, cisternography, dynamic renal studies, determination of glomerular filtration rate and measurement of extracellular fluid volume (Everette et al., 1971). ^{169}Yb-DTPA is better than ^{131}I-IHSA for cisternography in cases of suspected hydrocephalus (Harbert et al., 1973). The chelate can be used in myeloscintigraphy, cisternography and ventriculography (Kushelevsky and Oberson, 1974). However, such uses appear to be somewhat dangerous because ^{169}Yb activity persists due to fixation on meningo-encephalic structures (Barbizet et al., 1972). ^{169}Yb citrate is accumulated by malignant but not by benign lung tumors (Tarjan et al., 1974). ^{157}Dy-HEDTA has been used for bone scanning but is not as good as ^{18}F (Yano et al., 1971). However, good concentration of ^{157}Dy in bone fractures plus lower soft tissue and blood concentrations and rapid urinary excretion make it a useful tool in bone studies (Subramanian et al. 1971). More extensive use of Er-HEDTA and Dy-HEDTA in skeletal imaging is only limited by the difficulty of their production (O'Mara and Subramanian, 1972). ^{46}Sc microspheres have been used to measure the distribution of cardiac output in various organs (Van Heerden et al., 1967). ^{169}Yb-DTPA is a safe, effective and inexpensive agent for measuring the glomerular filtration rate. It delivers low radiation doses and thus would not contribute to further renal impairment (Hosain et al., 1969a). ^{169}Yb-EDTA has also been used to study the glomerular rate and gives more reliable results than ^{51}Cr-EDTA (Zubovskii et al., 1971). ^{169}Yb-EDTA has been compared with ^{131}I-hippuran in determining renal function in 100 diabetes mellitus patients. Comparable results were obtained with both agents (Slavnov and Malinkovich, 1973). ^{169}Yb-DPTA can be used to visualize renal structure and function (Hosain et al., 1969b). ^{140}La-DTPA also have been used for renal function studies (Lerson and Delwaide, 1969).

7. Conclusions

The toxicity and usefulness of the rare earths have been extensively reviewed. These elements have a very low acute toxicity. However, the production of skin and lung granulomas after exposure to them requires extensive protection to prevent such exposure. Toxicity from exposure to rare earth radionuclides is related to absorbed radiation dose. The rare earth radionuclides have proven useful clinically in radiohypophysectomy, treatment of mammary and prostatic carcinoma and Cushing's syndrome, diabetic retinopathy and carcinoma in other body tissues and organs. Rare earth chelates have proven useful diagnostic agents in brain, lung and renal scanning and in determining regional blood flow and renal function.

Acknowledgment

The author wishes to thank Miss Helen Warren and Miss Eileen Waters of TIRC, Oak Ridge, Tennessee.

References

Abdullasev, R.A. and D.Ya. Guseinov, 1973, Azerb. Med. Zh. **50**, 53.
Abel, M. and R.B. Talbot, 1967, J. Pharmacol. Exptl. Therap. **157**, 207.
Alnaes, E. and R. Rahamimoff, 1974, Nature **247**, 478.
Andersson, K.E. and K.A.P. Edman, 1974, Acta Physiol. Scand. **90**, 113.
Ando, A., K. Hisada, T. Hiraki, I. Ando and S. Sanada, 1974, Radioisotopes **23**, 52.
Ando, A., K. Hisada, T. Hiraki, I. Ando and S. Sanada, 1974, Radioisotopes **23**, 161.
Ando, A., K. Hisada, T. Hiraki, I. Ando and T. Ujiie, 1975, Radioisotopes **24**, 104.
Andronikashvili, E.L., L.M. Mosulishvili, V.P. Mandzhgaladze, A.I. Belokobylskii, N.E. Kharabadze and E.Yu. Efremova, 1970, Dokl. Acad. Nauk SSSR **195**, 979.
Anghileri, L.J., 1967, Acta Isotop **7**, 281.
Anghileri, J., 1973, Int. J. Clin. Pharmacol. Ther. Toxicol. **8**, 146.
Anisimova, V.P., V.A. Voloshin, V.A. Soroka and P.M. Shvartsburg, 1973, Redkozemel. Metal. Splavy Soedin., Mater. Soveshch. 7th, ed. by Savitskii, E.M., "Nauka", Moscow, USSR, pp. 332–333.
Ariel, I.M., 1964, Arch. Surg. **89**, 244.
Arkhangelskaya, L.N. and S.S. Spasskii, 1967, Nov. Dannye Toksikol. Redk. Metal. Ikh. Soedin., ed. Izraelson, Z.I. Izd. Meditsina, Moscow, pp. 201–207.
Arvels, P. and N.T. Karki, 1971, Experientia **27**, 1189.
Arvels, P. and N.T. Karki, 1972, Acta Pharmacol. **31**, 380.
Arvels, P., 1974, Experientia **30**, 1061.
Arutyunov, A.L., N.S. Blagoveshchenskaya, F.M. Lyass, L.S. Soskin and Z.Z. Tslaf, 1970, Vop. Neirokhir **34**, 25.
Axelrod, D. and M.P. Klein, 1974, Biochem. Biophys. Res. Commun. **57**, 927.
Backlund, E.O., L. Johansson and B. Sarby, 1972, Acta Chir. Scand. **138**, 749.
Backlund, E.O., 1973, Acta Chir. Scand. **139**, 237.
Bagirov, S.N., 1968, Tr. Obshch. Fisol. Azerb. **1**, 17.
Ball, R.A. and G. VanGelder, 1966, Arch. Environ. Health **13**, 601.
Ball, R.A., G. Van Gelder, J.W. Green, Jr. and W.O. Reece, 1970, Proc. Soc. Exp. Biol. Med. **135**, 426.
Baltrukiewicz, Z., J. Derecki and M. Pogorzelaka-Liz, 1973, Acta Physiol. Pol. **24**, 437.
Barbizet, J., P. Duizabo, J. Thomas, P. Galle, J.L. Moretti and R. Pitton, 1972, Nouv. Presse Med. **43**, 2899.
Barnes, J.E., R.O. McClellan, C.H. Hobbs and G.M. Kanapilly, 1972, Radiat. Res. **49**, 416.
Benjamin, S.A., B.B. Boecker, T.L. Chiffelle, F.F. Hahn, C.H. Hobbs, R.K. Jones, R.O. McClellan, J.A. Pickrell and H.C. Redman, 1973, A.E.C. Symp. Ser. **29**, 181.
Beno, M., A. Pleskova, V. Rusek and M. Tatara, 1964, Bratisl. Lek. Listy **44**, 201.
Beno, M. and T. Trnovec, 1969–1970, Int. Symp. Nucl. Med. Proc. 1st, pp. 203–206.
Beno, M., 1973, Health Phys. **25**, 575.
Berke, H.L., 1968, Health Phys. **15**, 301.

Berke, H.L., 1969, USAEC COO-1630-10, pp. 11.
Bikkulov, R.I., 1968, Radiobiologiya **8**, 308.
Blagoveshchenskaya, N.S., E.I. Kandel and F.M. Lyass, 1968, Vestn. Otorinolaringol. **30**, 61.
Blair, D.W. and A.V. Foote, 1965, J. Roy. Coll. Surg. Edin. **11**, 60.
Blanchard, R.J., I. Grotenhuis, J.W. LaFave, C.W. Frye and J.F. Perry, Jr., 1964, Arch. Surg. **89**, 406.
Blanchard, R.J., J.W. LaFave, Y.S. Kim, C.S. Frye, W.P. Ritchie and W.P. Perry, Jr., 1965, Cancer **18**, 375.
Bland, M.R., J.F. Loutit and J.M. Sansom, 1974, Brit. J. Cancer **29**, 206.
Bockman, E.L., R. Rubio and R.M. Berne, 1973, Amer. J. Physiol. **225**, 438.
Boemer, H., 1972, Strahlentherapie **143**, 664.
Borowitz, J.L., 1972, Life Sci. **11**, 959.
Bowen, J.M., 1972, Can. J. Physiol. Pharmacol. **50**, 603.
Britten, J.S. and M. Blank, 1973, J. Colloid Interface Sci. **43**, 564.
Brooks, A.L. and R.O. McClellan, 1969, Int. J. Radiat. Biol. **16**, 545.
Brooks, A.L., R.O. McClellan and S.A. Benjamin, 1972, Radiat. Res. **52**, 481.
Brooks, A.L., S.A. Benjamin and R.O. McClellan, 1974, Radiat. Res. **57**, 471.
Bruce, D.W., B.E. Heitbrink and K.P. DuBois, 1963, Toxicol. Appl. Pharmacol. **5**, 750.
Buldakov, L.A. and N.I. Burov, 1967, Radiobiologiya **7**, 881.
Bunting, J.R., A. Cobo-Frenkel and R.M. Dowben, 1974, Proc. Rare Earth Res. Conf., 11th, 2, 672–681, ed. Haschke, J.M. and H.A. Eick.
Burke, C.W., G.F. Joplin and R. Fraser, 1972, Proc. Roy. Soc. Med. **65**, 486.
Burke, C.W., F.H. Doyle, G.F. Joplin, R.N. Arnot, D.P. Macerlean and T.R. Fraser, 1973, Quart. J. Med. **42**, 693.
Burykina, L.N., L.A. Vasileva, Sh. Zhanadilov, P.P. Lyarskii and V.L. Ponomareva, 1972, Rep. Staatl. Zent. Strahlenschutz DDR, p. 148.
Bustad, L.K., R.O. McClellan and R.J. Gardner, 1964, Pap. Int. Symp. Physiol. Dig. Ruminant, 2nd, Ames, Iowa, pp. 131–146.
Butow, R.A. and J. Chevallier, 1971, Biochemistry **10**, 2733.
Caldarola, L., et al., 1973, Gazz. Med. Ital. **132**, 276.
Cash, W.D., H.E. Carlson, S.W. Cox, A.E. Enobong, J.S. Epstein, S.G. Gabbe and R.M. Sigel, 1967, Endocrinology **81**, 291.
Casteels, R., C. Van Breeman and C.J. Mayer, 1972, Arch. int. Pharmacodyn. **199**, 193.
Catsch, A., 1963, Strahlenschutz Forsch. Praxis **3**, 183.
Cember, H. and K. Stemmer, 1964, Health Phy. **10**, 43.
Chance, B., 1968, Mol. Basis Membrane Funct. Symp., ed. by Tosteson, D.C., Prentice-Hall, Inc., Englewood, N.J., pp. 561–573.
Chandra, R., P. Braunstein and A. Thein, 1972, Int. J. Appl. Radiat. Isotop. **23**, 553.
Cochran, K.W. et al., 1950, Arch. Ind. Hyg. Occ. Med. **1**, 637.
Collins, G.A., M.C. Sutter and J.C. Teiser, 1972, Can. J. Physiol. Pharmacol. **50**, 300.
Conway, L.W., F.T. D'Foghludha and W.F. Collins, 1969, J. Neurol. Neurosurg. Psychiat. **32**, 48.
Cottam, G.L., A.D. Sherry and K.M. Valentine, 1974, Proc. Rare Earth Res. Conf., 11th, ed. by Haschke, J.M. and H.A. Eick, NTIS, Springfield, Va., pp. 204–212.
Cuddihy, R.G. and W.C. Griffith, 1972, Health Phys. **23**, 621.
Cuddihy, R.G., D.G. Brownstein, O.G. Raabe and G.M. Kanapilly, 1973, J. Aerosol Sci. **4**, 35.
Cupak, M. and Z. Prochazka, 1971, Atomkernenergie **17**, 293.
Cuthbert, A.W. and P.Y.D. Wong, 1971a, Biochim. Biophys. Acta **24**, 713.
Cuthbert, A.W. and P.Y.D. Wong, 1971b, J. Physiol. **219**, 39.
D'Andrea, F., E. De Divitis, C.D. Signorelli and A. Cerillo, 1972, Neurochirurgia **15**, 86.
Darnall, D.W. and E.R. Birnbaum, 1970, J. Biol. Chem. **245**, 6484.
Davison, F.C. and F.K. Ramsey, 1965, USAEC. TID No. COO-1170-4, pp. 74.
DeBassio, W.A., R.M. Schnitzler and R.L. Parsons, 1971, J. Neurobiol. **2**, 263.
Dedenkov, A.N. and M.A. Kiryakov, 1967, Radiats. Organizm Sb. Mater. Konf. **2**, 110.
Deland, F.H., 1973, J. Nucl. Med. **14**, 93.
Dianzani, M.U., 1954, Biochem. Biophys. Acta **14**, 514.
Dobryankova, G.V., 1969, Radiobiologiya **9**, 101.
Dohn, D.F. and E.P. McCullagh, 1966, Postgrad. Med. **40**, 402.
Donozal, V., B. Hajek, K. Kacl, I. Manova and F. Petru, 1966, Z. Chem. **6**, 154.
Ducastaing, A., C. Monceyron, J.L. Azanza, P. Creach and J. Raymond, 1973, C.R. soc. biol. **167**, 262.
Ducousso, R., G. Bereziat, G. Perrault and C. Pasquier, 1971, Health Phys. **21**, 21.
Ducousso, R. and R. Masse, 1972, C.R. Hebd. Seances Acad. Sci. Ser. D Sci. Nat. **274**, 3328.
Efimov, V.I., 1967, Radiobiologiya **7**, 90.
Eichhorn, G.L. and J.J. Butzow, 1965, Biopolymers **3**, 79.
Ellis, W.G. and J.E. Huston, 1968, J. Nutr. **95**, 67.
Erdelyi, L., 1973, Acta Biol (Szeged) **19**, 177.
Everette, J.A., Jr., F. Hosain, F.H. DeLand, R.C. Reba and H.N. Wagner, Jr., 1971, J. Canad. Ass. Radiol. **22**, 136.
Ewaldsson, B. and G. Magnusson, 1964a, Acta Radiol. **2**, 65.
Ewaldsson, B. and G. Magnusson, 1964b, Acta Radiol. **2**, 121.
Fermum, R. and A. Grisk, 1973, Acta Biol. Med. Germ. **31**, 583.
Fischler/Ficher, F. and K.W. Roeckl, 1938, Arch. Exptl. Pathol. Pharmakol. **189**, 4.
Ford-Hutchinson, A.W. and D.J. Perkins, 1972, Radiat. Res. **51**, 244.

Foreman, J.C. and J.L. Mongar, 1973, Brit. J. Pharmacol. **48**, 527.
Forrest, A.P.M. et al., 1970, Proc. Roy. Soc. Med. **63**, 616.
Freeman, D.J. and E.E. Daniel, 1973, Can. J. Physiol. Pharmacol. **51**, 900.
Furie, B., A. Eastlake, A.N. Schechter and C.B. Anfinsen, 1973, J. Biol. Chem. **248**, 5821.
Fusek, I., 1972, C. S. Neurol. **35**, 85.
Gabbiani, C., M.L. Jacquin and H. Selye, 1966, J. Pharmacol. Explt. Therap. **152**, 275.
Gabbiani, G., B. Solymoss and R.M. Richard, 1967, Arzneimittel-Frosch. **17**, 505.
Garcia Ramos, J. and B.H. Ibarra, 1973, Acta Physiol. Lat. Amer. **23**, 202.
Gelinas, J.J., E.P. McCullagh and D.F. Dohn, 1966, Cleveland Clin. Quart. **33**, 171.
Gensicke, F., 1966, Naturforsch. **21B**, 567.
Gensicke, F., H.W. Nitschke and F. Hoelzer, 1966, Stud. Biophys. **1**, 347.
Gensicke, F. and F. Hoelzer, 1972, Rep. – Staatl. Zent. Strahlenschutz DDR, pp. 148.
Gensicke, F., F. Hoelzer and H.W. Nitschke, 1972, Health Phys. Probl. Intern. Contam. Proc. IRPA, Eur. Congr. Radiat. Prot. 2nd, ed. E. Bujdoso, Akad. Kiado., Budapest, Hung., 245–248.
Gensicke, F., F. Hoelzer and H.W. Nitschke, 1973, Radibiol. Radiotherap. **14**, 199.
Ghircioasiu, M., E.A. Pora, M. Cadariu, Z. Uray and M. Clichici, 1971, Stud. Univ. Babes-Bolyai Ser. Biol **16**, 131.
Grabske, R., 1966, USAEC, UCRL-50168, pp. 20.
Graf, B. and J. Lafuma, 1965, Bull. Ass. Franc Cancer **52**, 55.
Gray, D.H. and J.R. Vogt, 1974, J. Arg. Food Chem. **22**, 144.
Grigorescu, St. and K.M. Weber, 1969, Atomkernenergie **14**, 147.
Hahn, F.F., S.A. Benjamin, B.B. Boecker, T.L. Chiffelle, C.H. Hobbs, R.K. Jones, R.O. McClellan, J.A. Pickrell and H.C. Redman, 1973, J. Natl. Cancer Inst. **50**, 675.
Hahn, F.F., J.E. Barnes, C.H. Hobbs and J.L. Mauderly, 1975, Radiat. Res. **61**, 444.
Haigler, E.D., J.M. Hershman and C.K. Meador, 1973, Arch. Int. Med. **132**, 588.
Haley, T.J. and H.C. Upham, 1963, Nature **200**, 271.
Haley, T.J., 1965, J. Pharm. Sci **54**, 663.
Hara, T. and B.R. Freed, 1973, Int. J. Appl. Radiat. Isot. **24**, 373.
Harbert, J.C., V. Reed and D.C. McCullough, 1973, J. Nucl. Med. **14**, 765.
Hartog, M., F. Doyle, R. Fraser and G.F. Joplin, 1965, Brit. Med. J. **5428**, 396.
Hartz, T. and W. Ulbright, 1973, Pfluegers Arch. **345**, 281.
Hava, M. and A. Hurwitz, 1973, Eur. J. Pharmacol. **22**, 156.
Henrikson, R.C., 1974, Cell Tissue Res. **148**, 309.
Herman, M.W. and A.J. Clark, 1973, Arch. Environ. Hlth. **26**, 260.
Herrmann, J.B. and I.M. Ariel, 1967, Amer. J. Roentgenol. Radium Ther. Nucl. Med. **99**, 393.
Heuser, J. and R. Miledi, 1971, Proc. Roy. Soc. Lond. B. Biol. Sci. **179**, 247.
Higashi, T., M. Kanno, H. Tobari, K. Tomura and Y. Nakayama, 1972, Igaku No Ayumi **82**, 209.
Higashi, T., K. Ito, H. Tobari and K. Tomura, 1973a, Int. J. Nucl. Med. Biol. **1**, 98.
Higashi, T., T. Fujimura, Y. Nakayama, T. Hisada, K. Tomura, K. Kawai and K. Nakamura, 1973b, Kaku Igaku **10**, 27.
Hisada, K. and A. Ando, 1972, Igaku No Ayumi **82**, 634.
Hisada, K. and A. Ando, 1973, J. Nucl. Med. **14**, 615.
Hisada, K., N. Tonami, T. Hiraki and A. Ando, 1973, J. Nucl. Med. **14**, 772.
Hisada, K., N. Tonami, T. Hiraki and A. Ando, 1974, J. Nucl. Med. **15**, 210.
Hobbs, C.H., J.E. Barnes, R.O. McClellan, T.L. Chiffelle, R.K. Jones, D.L. Lundgren, J.L. Mauderly, J.A. Pickrell and E.W. Rypka, 1972, Radiat. Res. **49**, 430.
Hodge, H.C. and J.H. Sterner, 1943, Am. Ind. Hyg. Assoc. Quart. **10**, 93.
Hodgson, B.J., A.M. Kidwai and E.E. Daniel, 1972, Can. J. Physiol. Pharmacol. **50**, 730.
Hodgson, B.J. and E.E. Daniel, 1973, Can. J. Physiol. Pharmacol. **51**, 914.
Holloway, E.T. and D.F. Bohr, 1973, Circ. Res. **33**, 678.
Holmsen, H., J. Whaun and H.J. Day, 1971, Experientia **27**, 451.
Holten, V.Z., G.C. Kyker and M. Pulliam, 1966, Proc. Soc. Exp. Biol. Med. **123**, 913.
Holzer, F. and F. Gensicke, 1966, Z. Naturforsch. **21B**, 574.
Hosain, F., R.C. Reba and H.N. Wagner, Jr., 1968, Radiology **91**, 1199.
Hosain, F., R.C. Reba and H.N. Wagner, 1969a, Int. J. Appl. Radiat. Isotop. **20**, 517.
Hosain, F., R.C. Reba and H.N. Wagner, Jr., 1969b, Radiology **93**, 1135.
Howells, D.J. and D.B. Coult, 1971, Biochim. Biophys. Acta **244**, 427.
Huber, C.T. and E. Frieden, 1970, J. Biol. Chem. **245**, 3979.
Hutcheson, D.P., D.H. Gray, B. Venugopal and T.D. Luckey, 1975, J. Nutr. **105**, 670.
Hyodo-Taguchi, Y. and N. Egami, 1970, Dobutsagaku Zasshi **79**, 185.
Hyodo-Taguchi, Y., N. Egami and N. Mori, 1971, J. Fac. Sci. Univ. Tokyo, Sect. 4, **12**, 337.
Ivanov, A.E. and K.I. Gorelchik, 1966, Raspredel. Biol. Deistvie Radioaktiv. Izotop. Sb. Statei, 72.
Ivanov, V.N., 1967, Vop. Biookenogr. pp. 185–189.
Jacobus, W.E. and G.P. Brierly, 1969, J. Biol. Chem. **244**, 4995.
Jadresic, V.A., M. Poblete, A. Reid, M. Riera, A. Matus and M. Herreros, 1965, J. Clin Endocrinol. Metab. **25**, 686.
Jancso-Gabor, A. and J. Szolcsanyi, 1970, J. Pharm. Pharmacol. **22**, 366.
Jauregui, G.R., J.C. Scornavachi and O. Betti, 1968, Medicina (Buenos Aires) **27**, 43.

Johnson, R.F., Jr. and P.L. Ziemer, 1971, Health Phys. **20**, 187.
Jones, C.R. and D.R. Kearns, 1974, J. Amer. Chem. Soc. **96**, 3651.
Kadas, I., D. Tanka, M. Keller and K. Jobst, 1974, Acta Morphol. Acad. Sci. Hung. **22**, 35.
Kalix, P., 1971, Pfluegers, Arch. **326**, 1.
Kaplan, I.S., F.A. Tikhomirov and V.V. Khvostova, 1973, Radiobiologiya **13**, 688.
Kasatkina, S.V., 1971, Tr. Polyar. Nauch. Issled. Prockt. Inst. Morsk. Ryb. Khoz. Okeanogr. **29**, 55.
Katzung, B.G., H. Reuter and H. Porzig, 1973, Experientia **29**, 1073.
Kayne, M.S. and M. Cohn, 1974, Biochemistry **13**, 4159.
Khodorov, B.I. and E.M. Peganov, 1969, Biofizika **14**, 474.
Khussar, Yu.P. and E.P. Lushchikov, 1973, Radiobiologiya **13**, 744.
Kikhachev, Yu.P., P.P. Lyarskii and L.T. Elovskaya, 1972, Byull. Eksp. Biol. Med. **74**, 78.
Kirkpatrick, C.T., 1974, J. Physiol. **236**, 28 P.
Kirpekar, S.M., J.C. Prat, M. Puig and A.R. Wakade, 1972, J. Physiol. **221**, 601.
Kohner, E.M., G.T. Dollery and C.J. Bulpitt, 1969, Diabetes **18**, 691.
Koval, Yu.F. and V.M. Kondrashev, 1967, Med. Radiol. **12**, 84.
Krasnow, N., 1972, Biochim. Biophys. Acta **282**, 187.
Krawielitzki, K., 1967, Isotopenpraxis **3**, 383.
Kulikova, V.G., 1970, Tr. Inst. Ekol. Rast. Zhivotn. Ural Filial Akad. Nauk SSSR **68**, 55.
Kulikov, N.V., V.S. Bezel and L.N. Ozhegov, 1970, Radiobiologiya **10**, 792.
Kurshakova, N.N., 1967, Vopr. Onkol. **13**, 81.
Kushelevsky, A. and R. Oberson, 1974, Radiol. Clin. Biol. **43**, 174.
Lakin, K.M., Yu.A. Zimakov, A.A. Menkov, R.I. Bocharova and N.P. Tszyu, 1970, Farmakol. Tokiskol. **33**, 87.
Lambert, D.H. and R.L. Parsons, 1970, J. Gen. Physiol. **56**, 309.
Lazar, G., V. Nikolasev, I. Veresbaranyai and I. Karady, 1971, Kiserl. Orvostud. **23**, 298.
Lazar, G., 1973a, Experientia **29**, 818.
Lazar, G., 1973b, Res. J. Reticuloendothelial Soc. **13**, 231.
Lebedeva, G.A., 1973, Vopr. Onkol. **19**, 47.
Lerson, G. and P. Delwaide, 1969, Proc. 7th Int. Congr. Clin. Chem., ed. by M. Roth, Karger, Basel, Switzerland **3**, 398–404.
Letourneau, P.C. and N.K. Wessells, 1974, J. Cell Biol. **61**, 56.
Lohwe, H., 1974, Acta Biol. Med. Germ. **32**, 219.
Lomsky, R., R. Petr, P. Nadvornik, J. Sverak and K. Dvorak, 1966, Sb. Ved. Pr. Lek. Fak. Karlovy Univ. Hradci. Kralove **9**, 503.
Lorincz, G., G. Balint and G. Gaspardy, 1968, Rheumatol. Balneol. Allerg. **9**, 157.
Luckey, T.D., A. Kotb, J. Vogt and D.P. Hutcheson, 1975, J. Nutr. **105**, 660.
Lundgren, D.L., A. Sanchez, R.L. Thomas, T.L. Chiffelle and R.O. McClellan, 1973, Proc. Soc. Exp. Biol. Med. **144**, 238.
Lyass, F.M. and R.Y. Snigireva, 1972, Med. Radiol. **17**, 41.
Lyubashevskii, N.M., 1970, Tr. Inst. Ekol. Rast. Zhivotn., Ural Filial Akad. Nauk SSSR **68**, 111.
Magazanik, L.G. and F. Vyskocil, 1970, J. Physiol. **210**, 507.
Mahlum, D.D. and M.R. Sikov, 1968, Health Phys. **14**, 127.
Marukawa, M., 1970, Nichidai Igaku Zasshi **29**, 603.
Masse, R., B. Arnoux, I. L'Hullier and J. Lafuma, 1973, Report, CEA-R-441b, pp. 22.
Matsumoto, A., K. Suzuki and H. Nakayama, 1972, Brain Nerve (Tokyo) **24**, 161.
Matsusaka, N., 1971, J. Fac. Agric. Iwate Univ. **10**, 209.
Matthews, B.W. and L.H. Weaver, 1974, Biochemistry **13**, 1719.
Mauderly, J.L., J.A. Pickrell, C.H. Hobbs, S.A. Benjamin, F.F. Hahn, R.K. Jones and J.E. Barnes, 1973, Radiat. Res. **56**, 83.
Maxwell, L.C. and F. Bischoff, 1931, J. Pharmacol. Exper. Therap. **43**, 61.
Mayer, C.J., C. Van Breeman and R. Casteels, 1972, Pfluegers Arch. **337**, 333.
McClellan, R.O., J.E. Barnes, B.B. Boecker, T.L. Chiffelle, C.H. Hobbs, R.K. Jones, J.L. Mauderly, J.A. Pickrell and H.C. Redman, 1970, AEC Symp. Ser. No. 21, 395.
McClellan, R.O., B.B. Boecker, F.F. Hahn, C.H. Hobbs, R.K. Jones and M.B. Snipes, 1973, Proc. Int. Cong. Int. Radiat. Prot. Assoc. 3rd, Sept. 9–14.
McCullagh, E.P. and D.F. Dohn, 1969, Cleveland Clin. Quart. **36**, 163.
McFee, A.F., 1964, Proc. Soc. Exp. Biol. Med. **116**, 712.
Meisner, H., F. Palmieri and E. Quagliariello, 1972, Biochemistry **11**, 949.
Mela, L., 1969, Biochemistry **8**, 2481.
Mezentseva, N.V., 1967, Nov. Dannye Toksikol. Redk. Metal. Ikh. Soedin, ed. Izraelson, Z.I., Izd. Meditsina, Moscow, pp. 207–213.
Migalovskaya, V.N., 1971, Tr. Polyarn Nauchno-Issled Proentn Inst. Morsk Rybn Khoz Okeanogr **29**, 74.
Migalovskii, I.P., 1971a, Tr. Polyar. Nauch. Issled. Prockt. Inst. Morsk. Ryb. Khoz. Okeanogr. **29**, 16.
Migalovskii, I.P., 1971b, Tr. Polyar. Nauch. Issled. Prockt. Inst. Morsk. Ryb. Khoz. Okeanogr. **29**, 32.
Miller, J.K. and W.F. Byrne, 1970, J. Nutr. **100**, 1287.
Miller, J.K., B.R. Moss and W.F. Byrne, 1971, J. Dairy Sci. **54**, 497.
Miller, J.K., W.F. Byrne and W.A. Lyke, 1972, Health Phys. **22**, 461.
Moeller, T., 1963, "The Chemistry of the Lanthanides", Reinhold Publishing Corp., New York, N.Y., p. 117.
Mogilevskaya, O.Ya. and N.T. Raikhlin, 1963, in "Toxicology of Rare Metals", Izraelson, Z.I., ed. Gosudarstyennoe Izdatelstvo Meditsinskoi Literatury, Moscow, pp. 195–208.

Mogilevskaya, O.Ya. and T.A. Roshchina, 1964, Poroshkovaya Met. Akad. Nauk Ukr. SSR **4**, 105.
Mogilevskaya, O.Ya. and T.A. Roshchina, 1967, Nov. Dannye Toxiskol. Redk. Metal. Ikh. Soedin, 213.
Molinatti, G.M., 1964, Acta Isotop. **4**, 400.
Molinatti, G.M., F. Camanni, F. Massara and M. Messina, 1967, J. Clin. Endocrinol. Metab. **27**, 861.
Momeni, M.H., N. Jow and E. Bradley, 1975, Health Phys. **28**, 285.
Morales, A., D.W. Blair and J. Steyn, 1971, Brit. J. Urol. **43**, 520.
Mori, I., 1931, Japan J. Pharmacol. **5**, 13.
Moskalev, Yu.I., 1961, Raspredelenie, Biol. Deisivie i Migratsiya Radioaki. Isotopov. Sb. 40–53.
Moskalev, Yu.I. and V.N. Streltsova, 1965, Med. Radiol. **10**, 40.
Moskalev, Yu.I., L.A. Buldakov, N.A. Koshurnikova, A.P. Nifatov and G.N. Reshetov, 1966, Raspredel. Biol. Deistvie Radioaktiv. Izotop., Sb. Statei, 356.
Moskalev, Yu.I., V.N. Streltsova and L.A. Buldakov, 1969, Delayed Eff. Bone-Seeking Radionuclides, Proc. Int. Symp., Ed. by Mays, C.W. Univ. Utah Press, Salt Lake City, Utah, pp. 489–509.
Moskalev, Yu.I., G.A. Zalikin, V.S. Stepanov and A.I. Semenov, 1972, Radiobiologiya **12**, 730.
Moskalev, Yu.I., G.A. Zalikin and V.S. Stepanov, 1972b, Biol. Deistvie Vnesh. Vnutr. Istochikov Radiats. ed. by Moskalev, Yu.I., "Meditsina", Moscow, USSR, pp. 183–190.
Mozhaeya, G.N. and A.P. Naumov, 1973, Tsitologiya **15**, 1431.
Mraz, F.R. and P.L. Wright, 1964, Proc. Soc. Exp. Biol. Med. **116**, 1114.
Muroma, A., 1961, Ann. Med. Exptl. Biol. Fenniae **39**, 277.
Naharin, A., Y. Feige, E. Lubin and T. Sadeh, 1974, Health Phys. **27**, 207.
Neubert, D. and I. Hoffmeister, 1960, Arch. Exptl. Pathol. Pharmakol. **237**, 519.
Neubert, D., 1963, Biochem. Biophys. Acta **49**, 399.
Nevstrueva, M.A. and V.A. Kolotvin, 1968, Vop. Radiats. Immunol. Tsitomorfol. Ed. by Nevstrueva, M.A., Leningrad, pp. 55–60.
Nigrovic, V. and A. Catsch, 1965, Strahlentherapie **128**, 283.
Nolan, T.R. and E.D. Grady, 1969, Amer. Surg. **35**, 181.
Notter, G., O. Melander and L. Johansson, 1968, Acta Radiol. Ther. Phys. Biol. **7**, 17.
Novello, F. and F. Stirpe, 1969, Biochem. J. **111**, 115.
Oberdisse, E., G. Roehling, W. Losert, R. Schurig and U. Oberdisse, 1973, Naunyn-Schmiedebergs Arch. Pharmakol. **280**, 217.
Oberdisse, E., R. Winkler, O. Grajewski, B. von Lehmann and H.R. Arntz, 1974, Verh. Dtsch. Ges. Inn. Med. **80**, 1556.
Oda, S., 1932, Z. Ges. Exptl. Med. **80**, 6.
O'Donnell, J.M. and M.W. Smith, 1973, J. Physiol. **229**, 733.
Oelkers, H.A. and E. Vincke, 1938, Arch. Exptl. Pathol. Pharmakol. **188**, 53.
Oka, M., A. Rekonen, A. Ruotsi and O. Seppala, 1971, Acta Rheumatol. Scand. **17**, 148.
Oka, M. and M. Hypen, 1974, Acta Rheumatol. Scand. **20**, 33.
Olefin, A.I., 1967, Vrach. Delo **11**, 95.
O'Mara, R.E. and G. Subramanian, 1972, Sem. Nucl. Med. **2**, 38.
Oproiu, A., 1973, Stud. Cercet. Endocrinol. **24**, 125.
Orii, H., 1973, Rinsho Hoshasen **18**, 211.
Orlova, A.V. and V.R. Faitelberg-Blank, 1973, Mater. Vses. Simp. "Teor. Prakt. Aspekty Deistviya Małykh Doz. Ioniz Radiat.", ed. Kudritskii, Yu, K., Akad. Nauk SSSR, Komi Filial Inst. p. 59.
Oyvin, I.A., V.M. Volodin, M.M. Goldshtein and O.Y. Tokarev, 1966, Acta Physiol. Acad. Sci. Hung. **29**, 87.
Palmer, H.E., I.C. Nelson and G.H. Crook, 1970, Health Phys. **18**, 53.
Panchenko, I. Ya. and I.A. Sarapultsev, 1964, Tr. Radiat. Gig. Leningr. Nauch Issled Inst. Radiat. Gig. **2**, 230.
Panisset, A., E.M. Kohner, H. Cheng, and T.R. Fraser, 1971, Diabetes **20**, 826.
Parry, D.J., A. Kover and G.B. Frank, 1974, Can. J. Physiol. Pharmacol. **52**, 1126.
Parsons, R.L., E.W. Johnson and D.H. Lambert, 1971, Amer. J. Physiol. **220**, 401.
Pavlyushchik, A.V., I.A. Golubovich, M.Yu. Makkaveeva and M.P. Stankevich, 1970, Med. Radiol **15**, 54.
Pechantikov, V.A., V.B. Emelyanov and N.D. Bogolyubova, 1972, Biofiz. Zhivoi Kletki **3**, 12.
Pechkurenkov, V.L., 1970, Genetika **6**, 67.
Perez-Modrego, S., J.M. Ortiz Gonzalez, P. Mateo, D. Lasa, J. Sanz-Anton, J.M. Sacristan, F. Galvez and R. Herranz, 1962, Acta Oncol. **1**, 293.
Pesternikov, V.M., 1973, Med. Radiol. **18**, 12.
Phillis, J.W., N. Lake and G. Yarbrough, 1973, Brain Res. **53**, 465.
Pinteric, L., J.F. Manery, I.H. Chaudry and G. Madapallimattam, 1975, Blood **45**, 709.
Polikarpov, G.G. and V.N. Ivanov, 1966. U.K. At. Energy Authority, Reactor Group, TRG. Inform. Ser. **166** (W), 12 pp.
Ponomareva, T.V. and I.B. Tokin, 1969, Biol. Nauk. **12**, 47.
Prichard, H.L., J.F. Bridgman and N.M. Bleehen, 1970, Br J. Radiol. **45**, 466.
Ransohoff, J.A., 1959, Nucleonics **17** (No.7), 80.
Rao, D.V., P.N. Goodwin and F.L. Khalil, 1974, J. Nucl. **15**, 1008.
Ray, B.S., A.G. Pazianos, E. Greenberg, W.L. Peretz and J.M. McLean, 1968, J. Amer. Med. Ass. **203**, 85.
Reed, K.C. and F.L. Bygrave, 1974, Biochem. J. **138**, 239.
Reece, W.O., R.B. Talbot and M.J. Swenson, 1967, Amer. J. Vet. Res. **28**, 979.
Remy, J., P. Nizza, A. Pelser and A. Aeberhardt, 1965, Int. J. Radiat. Biol. **9**, 349.

Richmond, C.R. and J.E. London, 1966, Nature **211**, 1179.
Rosenquist, U. and L.O. Boreus, 1972, Life Sci. **11**, 595.
Roshchin, I.V., 1961, Gig. Truda Prof. Zabol. **7**, 41.
Rosoff, B., E. Siegel, G.L. Williams and H. Spencer, 1963, Intern. J. Appl. Radiation Isotopes **14**, 129.
Rozza, A., L. Favalli, M.C. Chiari and F. Piccinini, 1975, Pharmacol. Res. Commun. **7**, 171.
Sanborn, W.G. and G.A. Langer, 1970, J. Gen. Physiol. **56**, 191.
Sasser, L.B., M.C. Bell and J.L. West, 1972, Health Phys. **22**, 467.
Savitskiy, E.M., 1960, Vestn. Akad. Nauk SSSR **6**, 81.
Schatzmann, H.J. and M. Tschabold, 1971, Experientia **27**, 59.
Schepers, G.W.H., A.B. Delahunt and A.J. Redlin, 1955, AMA Arch. Ind. Health **12**, 297.
Schepers, G.W.H., 1955a, AMA Arch. Ind. Health **12**, 301.
Schepers, G.W.H., 1955b, AMA Arch. Ind. Health **12**, 306.
Schmautz, E., 1964, Strahlentherapie **123**, 267.
Schmidtke, I., 1964, Health Phys. **10**, 1235.
Schroeder, H.A. and M. Mitchener, 1971, J. Nutr. **101**, 1431.
Scott, K.G., J. Crowley and P. Wallace, 1951, UCRL Rept. 1561, Sept.
Seltser, V.K., 1967, Radiobiologiya **7**, 302.
Selye, H., S. Szabo, B. Tuchweber and F. LeFebvre, 1972, Proc. Soc. Exp. Biol. Med. **139**, 887.
Semenov, D.I. and I.P. Tregubenko, 1966, Teor. Vop. Miner. Obmena, Akad. Nauk SSSR, Ural Filial, Inst. Biol. 64.
Semenov, D.I., Yu. I. Moskalev and L.A. Buldakov, 1966, Tr. Inst. Biol. Akad. Nauk SSSR, Ural, Filial No. **46**, 49.
Shalnova, G.A., 1969, Radiobiologiya **9**, 266.
Sharma, S.N., V.P. Kamboj and A.B. Kar, 1972, Exp. Pathol. **7**, 176.
Sharma, S.N., S.N. Chatterjee and V.P. Kamboj, 1973, Indian J. Exp. Biol. **11**, 143.
Shekhanova, I.A. and V.L. Pechkurenkov, 1968, Vop. Ikhtiol. **8**, 689.
Shelley, W.B. et al., 1958, J. Invest. Dermatol. **31**, 301.
Shevchenko, V.V., 1970, Radiobiologiya **10**, 575.
Shigenobu, K. and N. Sperelakis, 1972, Circ. Res. **31**, 932.
Shine, K.I., 1973, Amer. J. Physiol. **224**, 1024.
Shiraishi, Y. and R. Ichikawa, 1972, Health Phys. **22**, 373
Shubik, V.M., 1972, Radiobiologiya **12**, 317.
Shvydko, N.S., L.A. Ilin, R.A. Norets and V.A. Antonova, 1972, Gig. Sanit. **37**, 43.
Sihvonen, M-L., 1972, Ann. Acad. Sci. Fenn. Ser. AII Chem. **168**, 1.
Sill, C.W., L. Voelz, D.G. Olson, and J.I. Anderson, 1969, Health Phys. **16**, 325.
Simon, N., R. Siffert, M.G. Baron, H.A. Mitty and A. Rudavsky, 1968, Cancer **21**, 453.
Slavnov, V.N. and V.D. Malinkovich, 1973, Med. Radiol. **18**, 36.
Slouka, V., 1972, Health Phys. Probl. Intern. Contam., Proc. IRPA Eur. Cong. Radiat. Prot., 2nd, ed. by Bujdoso, E., Akad. Kiado, Budapest, Hung. pp. 357–360.
Snyder, F., E.A. Cress and G.C. Kyker, 1959, J. Lipid Res. **1**, 125.
Snyder, F., E.A. Cress and G.C. Kyker, 1960, Nature **185**, 480.
Snyder, F. and N. Stephens, 1961, Proc. Soc. Exp. Biol. Med. **106**, 202.
Snyder, F. and G.C. Kyker, 1964, Proc. Soc. Exp. Biol. Med. **116**, 890.
Som, P., F. Hosain and H.N. Wagner, 1972, J. Nucl. Med. **13**, 942.
Spedding, F.H. and K.A. Gschneidner, 1964, Jr., Ind. Res. **6**, 20.
Spencer, H. and B. Rosoff, 1965, Health Phys. **11**, 1181.
Spencer, H., S.H. Cohn and E.A. Gusmano, 1965, Int. J. Appl. Radiat. Isotop. **16**, 479.
Spencer, T. and F.L. Bygrave, 1972, FEBS Letts, **26**, 225.
Sperelakis, N., R. Valle, C. Orozco, A. Martinez-Palomo and R. Rubio, 1973, Amer. J. Physiol. **225**, 793.
Sperow, J.W. and L.G. Butler, Bioinorg. Chem. **2**, 87 (1973).
Spiller, R., 1960, Atom Industry **9**, 13.
Steffee, C.H., 1959, AMA Arch. Ind. Health **20**, 414.
Stepanov, V.S., 1970, Radiobiologiya **10**, 475.
Stewart, H.J., A.P.M. Forrest, M.M. Roberts, R.E.A. Chinnock-Jones, V. Jones and H. Campbell, 1969, Lancet **7625**, 816.
Steyn, J., D.W. Blair and A. Morales, 1973, S. Afr. Med. J. **47**, 179.
Streltsova, V.N., 1966, Raspredel. Biol. Deistvie Radioaktiv. Izotop. Sb. Statei, 371.
Stuart, B.O., H.W. Casey and W.J. Bair, 1964, Hanford Symposium, Health Phys. **10**.
Subramanian, G., J.G. McAfee, R.J. Blair, R.E. O'Mara, M.W. Greene and E. Lebowitz, 1971, J. Nucl. Med. **12**, 558.
Sullivan, J.C., A.M. Friedman, G.V.S. Rayudu, E.W. Foreham and P.C. Ramachandran, 1975, Int. J. Nucl. Med. Biol. **2**, 44.
Surovezhin, N.N., 1967, Radial. **12**, 62.
Swanson, E.W., J.K. Miller, and R.G. Cragie, 1970, J. Dairy Sci. **53**, 46.
Takada, K. and M. Fujita, 1972, Hoken Butsuri **7**, 135.
Takata, M., W.F. Pickard, J.Y. Lettvin and J.W. Moore, 1966, J. Gen. Physiol. **50**, 461.
Takeuchi, T., 1968, Hoken Butsuri **3**, 327.
Talbot, R.B., F.C. Davison and W.D. Reece, 1965, USAEC. TID No. C00-1170-6, pp. 23.
Talbot, R.B., F.C. Davison, J.W. Green, Jr., W.O. Reece and G. VanGelder, 1968, Bull. Ga. Acad. Sci. **26**, 1.
Tarasov, N.F., I.N. Tronova, V.I. Levin, V.I. Milko, R.P. Arsenteva, N.D. Kovalchuk, E.A. Tikhomirova, E.N. Pyranishnikova and E.N. Safronov, 1973, Med. Radiol. **18**, 31.
Tarjan, Gy., I. Pal, Zs. Karika, M. Fuzy and I. Szentessy-Szamel, 1973, Izotoptechnika **16**, 440.

Tarjan, Gy., Zs. Karika, I. Pal and O. Schweiger, 1974, Nucl.-Med. **13**, 267.
Tashiro, S., Y. Wadachi and M. Muramatsu, 1966, Radioisotopes **15**, 224.
Tashmukhamedov. B.A., 1971, Ukr. Biokhim. Zh. **43**, 78.
Taylor, D.M., 1966, Brit. J. Radiol. **39**, 620.
Thomas, R.L., J.K. Scott and T.L. Chiffelle, 1972, Radiat. Res. **49**, 589.
Thomassen, P.R. and H.M. Leicester, 1964, J. Dent. Res. **43**, 346.
Thorleif, A., B. Larsen, and O. Smidsrod, 1972, Acta Chem. Scand. **26**, 2968.
Tremblay, J. and A. Archambault, 1967, Rev. Can. Biol. **26**, 1 (1967).
Truúpyld, A. Yu. and I.B. Tokin, 1969, Radiobiologiya **9**, 393.
Tsytsugina, V.G., 1968, Tr. Inst. Ekol. Rast. Zhivoin, Ural Nauch. Tsent. Akad. Nauk SSSR **78**, 154.
Tuchweber, B. and L. Savoie, 1968, Proc. Soc. Exp. Biol. Med. **128**, 475.
Turusov, V.S., 1966, Arkh. Patol. **28**, 36.
Vainio, H., L. Mela and B. Chance, 1970, Eur. J. Biochem. **12**, 387.
Valentine, K.M. and G.L. Cottam, 1973, Arch. Biochem. Biophys. **158**, 346.
Van Breeman, C., 1969, Arch. int. Physiol. Biochim. 77, 710.
Van Breeman, C. and P. DeWeer, 1970, Nature **226**, 760.
Van Breemen, C.A. and P. Lesser, 1971, Microvas. Res. **3**, 113.
Van Heerden, P.D.R., T. Migita, R. Northcutt, V. Lopez-Majano, D.E. Tow and H.N. Wagner, Jr., 1967, J. Nucl. Med. **8**, 275.
Vikhman, A.A. and V.M. Shubik, 1968, Vop. Radiats. Immunol. Tsitomorfol. Ed. by Nevstrueva, M.A., Leningrad, pp. 66–72.
Vincke, E. and H.A. Oelkers, 1938, Arch. Exptl. Pathol. Pharmakol. **188**, 465.
Vincke, E., 1961, Therapie der Gegenwart. **100**, 605.
Vincke, E., 1962, Therapie der Gegenwart. **101**, 276.
Vogel, W., 1974, Pfluegers Arch. **350**, 25.
Voronina, N.N., I.P. Tregubenko, N.I. Latosh, E.I. Sukhacheva and D.I. Semenov, 1970, Tr. Inst. Ekol. Rast. Zhivotn. Ural Filial, Akad. Nauk SSSR **68**, 68.
Weiss, G.B. and F.R. Goodman, 1969, J. Pharmacol. Exper. Therap. **169**, 46.
Weiss, G.B., 1973, J. Pharmacol. Exper. Therap. **185**, 551.
Weiss, G.B. and F.R. Goodman, 1974, Proc. Rare Earth Res. Conf. 11th, Ed. by Haschke, J.M. and H.A. Eick, NTIS, Springfield, Va., pp. 687–694.
Weitzebin, J., Y. Lange, and C.M. Gary-Bobo, 1974, J. Membrane Biol. **17**, 27.
Wenzel, W.J., R.G. Thomas and R.O. McClellan, 1969, Amer. Ind. Hyg. Ass. J. **30**, 630.
Wester, P.O., 1965, Acta Med. Scand. **178**, 789.
Wester, P.O., 1972, Sci. Total Environ. **1**, 97.
Wolfson, J.M. and D.R. Kearns, 1975, Biochemistry **14**, 1436.
Yano, Y., D.C. Van Dyke, T.A. Verdon, Jr. and H.O. Anger, 1971, J. Nucl. Med. **12**, 815.
Young, L.G. and L. Nelson, 1974, J. Reprod. Fertil. **41**, 371.
Zalikin, G.A. and I.N. Tronova, 1969, Radioaktiv. Izotopy Organizm, ed. by Moskalev, Yu. I., Izd. "Meditsina", Moscow. USSR, pp. 103–106.
Zalikin, G.A., I.N. Tronova and I.I. Denisov, 1969, Radioaktiv. Izotopy Organizm, ed. by Moskalev, Yu. I. Izd. "Meditsina", Moscow, pp. 93–102.
Zhanadilov, Sh., 1973, Gig. Truda Prof. Zabol. **17**, 42.
Zhorno, L.Ya., 1970, Radiobiologiya **10**, 122.
Zimakov, Yu.A. and I.E. Zimakova, 1971, Tr. 2nd Mosk. Med. Inst. **3**, 93.
Zimakov, Yu.A., 1973. Mater. Povolzh. Konf. Fisol. Uchastiem Biokhim. Farmakol. Morfol. 6th, **2**, 28.
Zipes, D.P. and J.C. Fischer, 1974, Circ. Res. **34**, 184.
Zolin, V.F. and L.G. Koreneva, 1973, Dokl. Akad. Nauk SSSR **211**, 978.
Zubovskii, G.A., V.Kh. Frenkel and E. Markova, 1971, Radiol. Diagn. **12**, 69.

SUBJECT INDEX